

Climate and frozen ground

3.1 Introduction

The thermal regime in the upper layers of the earth is controlled by exchanges of heat and moisture between the atmosphere and the ground surface, together with the influence of ground thermal properties. The temperature at the ground surface undergoes fluctuations in response to changes in energy transfers, whilst the propagation of these fluctuations downwards depends on the thermal properties of the ground. The major surface temperature variation has a period of one year, corresponding to the annual cycle of solar radiation; there is also a diurnal variation corresponding to the daily cycle of radiation. Superimposed upon these periodic variations are other fluctuations with durations from seconds to years; these have a variety of causes, such as sporadic cloudiness, variations in the weather, and changes in climate.

The mechanisms of energy exchange at the earth's surface in cold regions are the same as those occurring elsewhere on the earth. Their significance springs from the fact that together they determine the surface temperature regime, and whether frozen ground will exist or not. The processes involved in the energy balance comprise the net *exchange of radiation* (represented by Q^*) between the surface and the atmosphere, the *transfer of sensible heat* (Q_H) and *latent heat* (Q_{LE}) by the *turbulent motion* of the air, and the *conduction of heat into the ground* (Q_G). The exact partitioning of the radiative surplus (or deficit) between Q_H , Q_{LE} and Q_G is governed by the nature of the surface and the relative abilities of the ground and the atmosphere to transport heat. Each of the energy transfer terms has an influence on the surface temperature, and the way in which the energy balance is achieved establishes the surface temperature regime (e.g. see Outcalt, 1972).

While the occurrence of ground freezing and permafrost depends basically upon climate, the exact relationship is not simple, since the surface

temperature regime does not depend solely on geographic location. Local surface conditions, for example, type of vegetation or depth of snow cover, have a profound controlling influence on the surface energy regime, being interposed between the atmosphere and the ground. The influence of these conditions on energy exchange, i.e. the interaction of site-specific factors and the atmospheric climate, produces the *microclimate* of a particular locale. It is the microclimate which is ultimately of importance to ground thermal conditions, since a difference in the surface characteristics will cause a change in the exchange of heat energy between the atmosphere and the ground surface, with significant effects for the ground thermal regime (Figure 3.1). Permafrost forms where the mean annual ground surface temperature is maintained below 0 °C, but differences in microclimate affect the near-surface temperature regime, which influences permafrost thickness and the depth of the active layer (or seasonal frost).

3.2 Seasonal frost and permafrost

Freezing conditions in the surface layers of the earth occur not only in the polar regions, but also in temperate zones, and at altitude even in the tropics. The depth of ground freezing depends in some part on the duration and severity of freezing air temperatures. It also depends on the composition and water content of the earth materials, as well as heat flow conditions in the ground. Periods of freezing, and the existence of frozen layers, vary from a few hours in low latitudes to thousands (and even 100 000s) of years in high latitudes. Freezing in tropical and sub-tropical deserts is of relatively little interest since moisture contents of the materials are so low.

For our purposes, we can divide frozen ground into two basic forms: that which thaws annually (i.e. seasonal frost), and that which does not, which we call permafrost. Permafrost terrain itself is characterised by a seasonally 'active' surface layer that thaws each summer, underlain by perennially frozen ground. Throughout this book, however, the term 'seasonal frost' applies to non-permafrost areas. In the northern hemisphere, the areas of seasonally frozen ground and permafrost encompass large parts of Eurasia and North America.

Aspects of seasonal freezing were discussed in Chapters 1 and 2. Let us imagine some change in climatic conditions which causes the mean annual surface temperature to fall to below 0 °C, so that the depth of winter freezing will exceed the depth of the summer thaw. A layer of permafrost would grow downward from the base of the seasonal frost, thickening progressively with each succeeding winter. Were it not for the effect of the

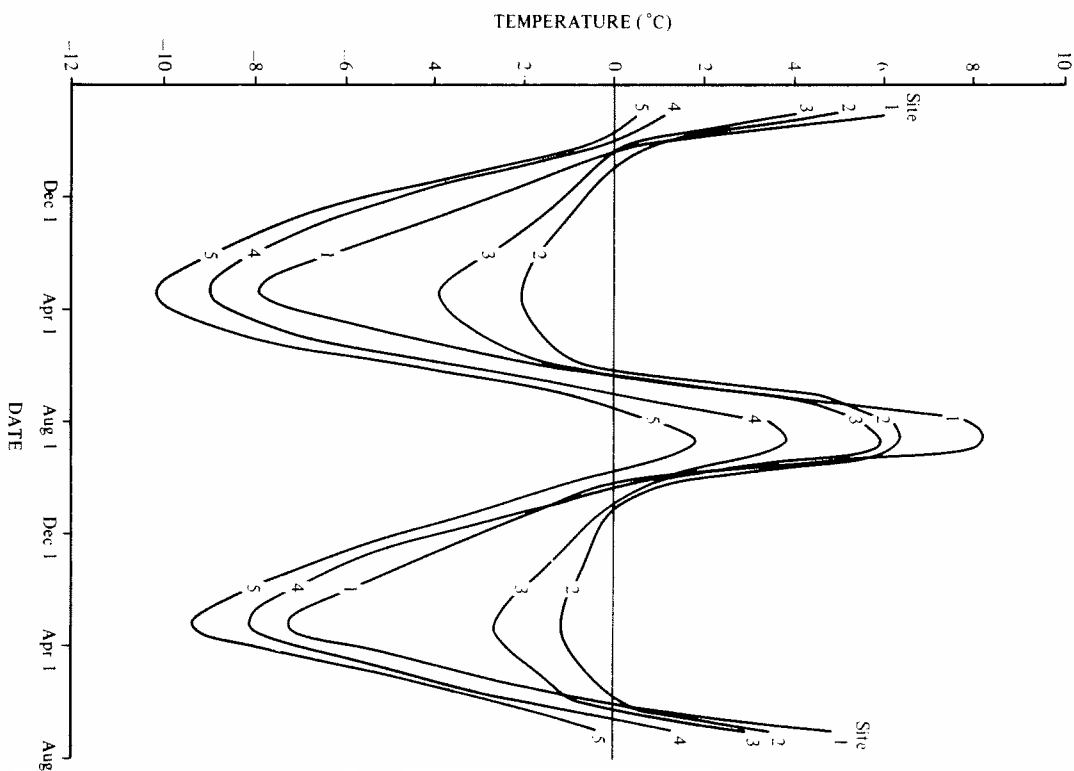


Figure 3.1 The annual temperature regime at a depth of 50 cm for five sites in the Mackenzie Delta, NWT (from Smith, 1975).

heat escaping from the earth's interior, the permafrost would grow to great depths in response to surface temperatures only slightly below 0°C. However, this heat flow from the earth – along the geothermal gradient – results in a temperature increase with depth of about 30 K km⁻¹ (the figure varies with regional geological conditions). Thus the base of permafrost approaches an equilibrium depth where the temperature increase due to the geothermal gradient just offsets the amount by which the surface temperature is below 0°C (see section 4.4.1). However, such an equilibrium configuration might not be attained for thousands of years, and during this time the surface temperature will undoubtedly have changed.

Whereas the bottom of permafrost is determined by the mean 'surface' temperature and geothermal heat flow, through processes that act over long periods of time, the top of the permafrost is controlled by the seasonal fluctuations of temperature about the mean. Temperature variations are experienced with the passage of the seasons at the surface, and extend in a progressively dampened manner to a depth of 10 or 20 metres. Within the layer of annual variation, the maximum and minimum temperatures form an envelope about the mean, and the top of permafrost is that depth where the maximum annual temperature is 0°C (Figures 1.6 and 4.7c). The thickness of seasonal frost corresponds to the depth where the minimum annual temperature is 0°C.

In Figure 1.6, the mean annual temperature profile is shown as extending in a linear fashion right to the ground surface. In reality, this may not be exactly the case. Goodrich (1978) demonstrated that, where there is a marked variation of ground thermal properties with temperature, a deviation characteristically occurs in the equilibrium profile, with mean annual temperatures *increasing* in close proximity to the surface (see Figure 4.15). Burn & Smith (1988) report such offsets in the surface temperature of up to 2°C at field sites near Mayo, Yukon. They noted that the effect terminates near the base of the active layer, where there is relatively little seasonal change in thermal conductivity. Thus it appears that the mean annual temperature at the base of the active layer constitutes a more appropriate thermal boundary condition for permafrost than the ground surface temperature *per se*. However, for the sake of convenience, the term 'surface temperature' will be used throughout the rest of this book, as though the circumstances in Figure 1.6 prevailed. In most practical cases, the surface temperature is determined by simple linear extrapolation of the ground temperature profile at depth.

The analysis of ground temperature conditions is dealt with in Chapter 4, for now, we wish to examine those largely atmospheric (climatic) processes that influence the surface temperature regime.

3.3 Climate and permafrost distribution

Except for a relatively few areas where adequate ground temperature or other observational data exist, maps which show the distribution of permafrost depend on broad extrapolations and some assumed relationship between mean annual air and ground temperatures. For example, in Canada, the 'southern limit' of permafrost is often represented, somewhat misleadingly, as coinciding with the -1°C mean annual air isotherm (R.J.E. Brown, 1978*a*), although localised occurrences of permafrost are known south of this (e.g. Zoltai, 1971). While attempts have been made to regionalise permafrost occurrence on the basis of air temperature, little effort has been made to incorporate the influence of snow cover, other surface characteristics and ground properties into mapping permafrost over large areas in the absence of primary data (but see Nelson & Outcall, 1983).

The general climatic conditions of a place depend on its position (latitude, altitude, aspect and slope angle), since this influences the amount of incoming solar radiation and the air temperature. Since the receipt of solar radiation at the earth's surface decreases consistently with latitude, there is a general corresponding decrease in the mean annual air temperature. However, as a result of the varied physical geographic conditions that can affect the energy exchange between the ground and the atmosphere, the otherwise simple zonal influence of solar radiation upon the temperature regime is much modified. Local factors (i.e. microclimate) commonly override the influence of larger scale macroclimatic factors in the severity of seasonal freezing and the occurrence and distribution of permafrost.

The permafrost map of Canada (R. J. E. Brown, 1978*a*) demarcates three geographical zones – continuous, widespread, and scattered – based on a broad extrapolation using air temperature. In addition, the general decrease in air temperature with altitude results in the occurrence of permafrost at mountain elevations in more temperate regions. This so-called alpine permafrost has been described by Ives (1973) and Harris & Brown (1982), for example. They identify a broad vertical zonation comparable to the general effects of latitude, but stress the significance of microenvironmental factors, such as aspect and snow cover.

Of course, sudden changes in ground thermal conditions do not occur at the borders of permafrost zones. Instead, the zonation really represents the gradual transition from seasonally frozen ground in the temperate regions to the perennially frozen ground of the Arctic. As one moves progressively southward from the far north, where permafrost is present almost everywhere (continuous), the climate ameliorates and permafrost gradually

becomes thinner and less widespread (discontinuous). Where mean annual ground temperatures are close to 0°C, permafrost is present at some sites, where specific local conditions are favourable, while it is absent at other nearby sites. Eventually, permafrost exists only in scattered islands, as in the peatlands of northern Alberta (Lindsay & Odyinsky, 1965; Zoltai, 1971) and the Kenai Lowland of Alaska (Hopkins *et al.*, 1955), but it ultimately disappears altogether.

Whilst they may be of some value in portraying the broad geographical features of permafrost distribution, large-scale maps are of little value to specific studies of a scientific or applied nature. In such cases, original surveys must be carried out, since local environmental factors will always be of some, perhaps great importance.

3.4 The importance of microclimates

While ground thermal (and hydrologic) conditions are linked to the atmospheric climate, this influence is moderated by processes occurring in the boundary layer of vegetation, surface organic material and snow. Because of this, mean annual ground temperatures usually differ by several degrees from mean air temperatures, and the difference is not constant from place-to-place, but varies locally with specific conditions. Under the same boundary conditions, soils of different composition, structure and water content freeze to different depths. On the other hand, the same soil under different boundary conditions also freezes to different depths. Thus even in regions where the mean air temperature is low enough to suggest that permafrost should be present everywhere, this is not necessarily the case since its existence depends on an appropriate combination of climate and local/surface/subsurface conditions. Where ground temperatures are close to 0°C, local factors, such as variations in snow depth, availability of water for evaporation, surface and subsurface materials, etc, can determine whether permafrost is present or not. Consequently, it may occur in a scattered or discontinuous fashion.

Wide variations in ground thermal conditions are known to occur within a small area of uniform climate due to local factors (e.g. R. J. E. Brown, 1973, 1978b; Smith, 1975). Figure 3.1, for example, shows substantial differences in the annual ground temperature regime between neighbouring sites in the Mackenzie Delta, where the mean annual air temperature is close to -10°C (for further details see Smith, 1975). Soil conditions are fairly uniform among the sites, and the temperature differences are due principally to local variations in surface conditions, particularly snow cover, with vegetation shading of secondary importance. The following points can be noted:

1. Site 1 (no vegetation) has the greatest annual range; it is the warmest in summer (high radiation), but cools off the most in winter (least snow cover).
2. Site 4 (open vegetation) is warmer than site 5 (dense vegetation canopy) all year round.
3. Sites 2 and 3 show distinctly different regimes from the others, with a greatly reduced winter cooling wave because of deep snow cover.
4. Ground temperatures during the second winter were everywhere higher than in the previous year, even though monthly air temperatures were 2° to 9°C lower. This was because snow depths were greater at all sites, and, further, snow was on the ground by the end of September, some weeks earlier than normal.

The range in ground thermal conditions observed is equivalent climatically to several degrees of latitude.

Figure 3.2 illustrates the effects of largely lithologic variations on ground temperatures; bedrock has a high thermal diffusivity, because of high density and low water content, and this leads to the deep penetration of summer warming (see also Figure 4.7). R. J. E. Brown (1965) reported large differences in ground temperatures at different sites in the Norman Wells

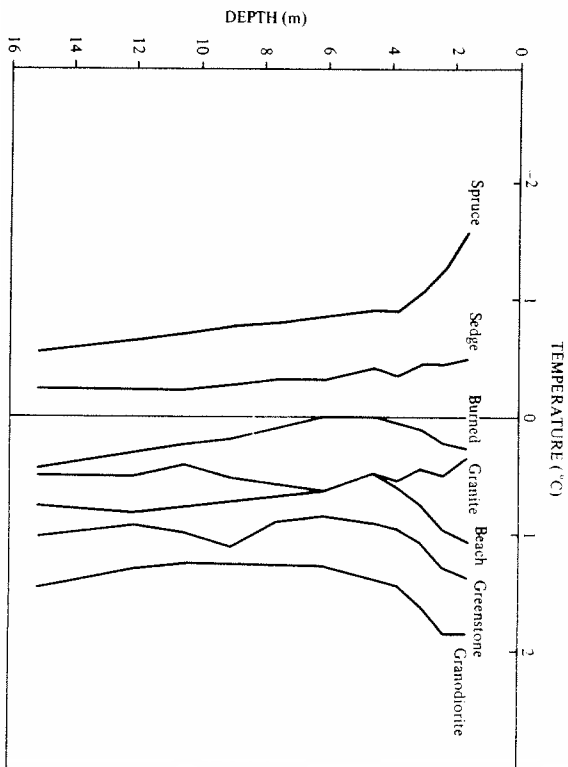


Figure 3.2 Mean annual ground temperature profiles at seven sites near Yellowknife, NWT (from R. J. E. Brown, 1973).

area as a result of the thermal effects of organic matter (see section 4.4.3). There appeared to be a general decrease in temperature with increased moss cover and peat thickness, and temperature amplitudes also decreased in the same order.

Other examples of microclimatic variability can be found in Smith & Riseborough (1983). Together, these observations illustrate the intricacies of the climate-ground temperature relationship, and the need to understand the interaction of climate and local conditions which influences the ground thermal regime. Wright (1981) has commented on two approaches which have been taken in climate-permafrost studies: those based on the spatial association (correlation) of permafrost with vegetation and terrain features, and those relying on energy balance models. In both approaches, the aim is to determine which characteristics of the environment control the ground thermal regime.

There have been numerous studies concerned with the relationship of permafrost to differences in vegetation, topography, hydrology, snow cover, soil conditions, etc. However, interpretations of the effects of site conditions on the details of permafrost distributions are often confused by the high degree of interdependence among these factors. For example, Smith (1975) studying the variation of permafrost along a successional sequence of vegetation in the Mackenzie Delta, found a complex interaction between topography, vegetation and snow cover (see Figure 3.9, also Vierck 1970). Price (1971) found that ground temperatures beneath a north-facing slope were *warmer* than an adjacent southeast-facing slope, which at first seems counter-intuitive. However, the presence of mosses and a thick plant cover on the south-facing slope accounted for the difference. Kudriavtsev (1965, p.17) discusses another example, in which the effect of slope aspect is moderated by the uneven distribution of snow cover. The prevailing winds of the region in question remove snow from south- and west-facing slopes and deposit it on north- and east-facing slopes, which, as a result, remain warmer in winter. In summer, on the other hand, the south- and west-facing slopes receive more solar radiation and are warmer. The net effect is that the two factors compensate, and mean annual soil temperatures are the same for all aspects. Dingman & Kouz, (1974) compared the distribution of permafrost near Fairbanks with the average annual solar radiation, but they found that the relationship was confounded by the effects of vegetation.

Many other such examples could be cited, but it is clear that ultimately we must unravel the interactions of climate, microclimate and lithologic conditions in order to understand the details of the ground thermal regime.

The spatial correlation approach may be a necessary first step, but investigation of the climate-permafrost relationship using a physically based approach allows for more critical examination of which factors are of ultimate significance in determining the ground thermal regime.

3.5 The surface energy balance

The basis for a rational understanding of the variations in ground thermal conditions can be found in terms of the surface energy balance. This may be written:

$$Q^* = Q_H + Q_{LE} + Q_G \quad (3.1)$$

the terms being previously defined. Equation (3.1) can be applied on any time scale, so that we may speak of an hourly, daily, monthly, yearly (or longer) energy budget. In subsequent illustrations, the daily regime is frequently used, although as indicated earlier in this chapter, it is the annual energy regime which is of ultimate importance to us.

Whatever the time-scale chosen, according to the conservation principle, energy cannot simply disappear, and the component fluxes in equation (3.1) must balance at all times:

$$Q^* \pm Q_H \pm Q_{LE} \pm Q_G = 0 \quad (3.2)$$

The chosen sign convention is such that a heat flux towards the surface is deemed positive (an energy input) and a flux away from the surface negative (energy loss). Some difference between the surface temperature and the air temperature is usually inevitable in establishing the balance in equation (3.2), and the difference depends on such variable factors as the amount of radiation absorbed, the degree of air turbulence, the availability of water for evaporation, and the thermal conductivity of the surface ground layer. In winter, the ground will usually be snow covered, and this insulating layer will also contribute to the difference.

The surface energy balance is shown diagrammatically in Figure 3.3(a). In the daytime, Q^* is positive (i.e. more radiation is absorbed than reflected and emitted), and energy is transferred away from the surface by convection of sensible heat (Q_H) and by evaporation (Q_{LE}) into the atmosphere, and by conduction of heat (Q_G) into the ground. The terms K and L refer to fluxes of shortwave and terrestrial (longwave) radiation respectively, the arrows indicating direction. At night Q^* is negative – since no solar radiation is received, but there is a loss of longwave radiation from the earth's surface – and there is a net transfer of energy towards the surface by Q_H , Q_{LE} and Q_G .

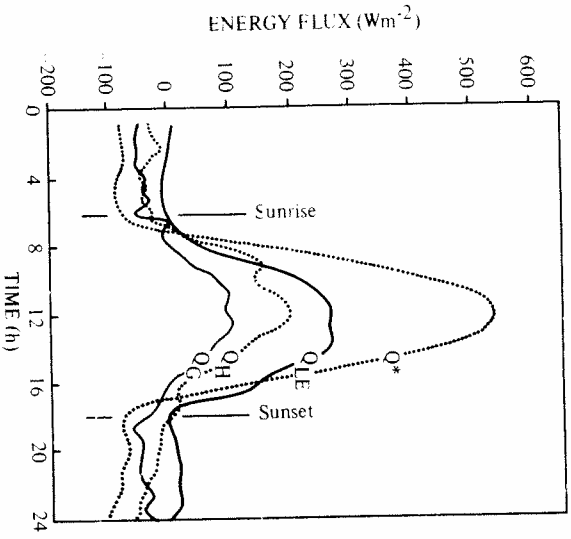
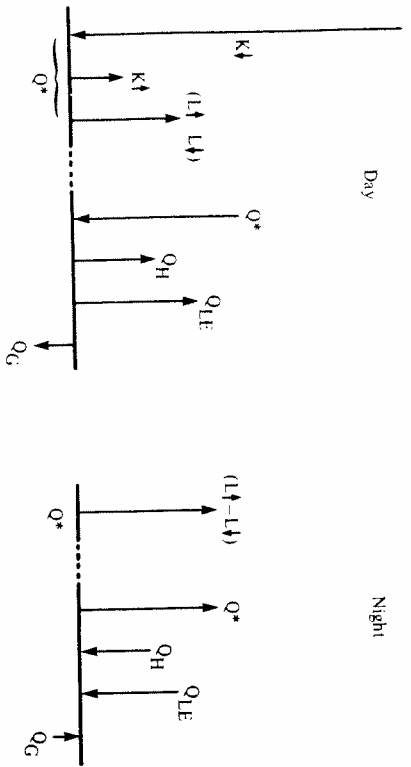


Figure 3.3. (a) Components of the surface energy balance. (b) Diurnal variation of energy balance components (see text for definitions. From Sellers, 1965).

Figure 3.3(b) shows a typical example of the *daily surface energy regime*. (In Figures 3.3(b) and 3.5, although the sign of Q_H , Q_{LE} and Q_G is opposite to Q^* , all values are plotted on the same axis, for convenience.) The net radiation varies systematically through the day, taking on small negative

values from about an hour before sunset until an hour after sunrise. At these times, the small amount of incoming solar radiation just balances the net longwave radiation from the surface. Daytime values of Q^* increase rapidly to a maximum near noon; in northern latitudes in winter, Q^* may be positive for only a few hours, or even not at all. As stated previously, the sensible heat flux, Q_H , is normally directed upward during the day, when the surface is warmer than the air. At night, the surface is likely to be cooler and Q_H is directed downwards. The turbulent transfer of heat is assisted by a decrease of temperature with height (which leads to buoyancy of rising air), and therefore daytime values of sensible heat transfer are much larger than night-time values. The conduction of heat into the ground, Q_G , is often considered small, and this is probably true for daily totals, since the energy gained during the day may be largely lost at night. The heat flow is downward from a little after sunrise until the late afternoon. Over the 24-hour period, Q_G rarely exceeds 10 to 20% of the net radiation, although for bare ground it can be up to 30%.

The term Q_G may be neglected in the *annual energy balance*, since heat stored in the ground during spring and summer is all released in the fall and winter, except insofar as the earth may be warming or cooling on a longer time-scale (see sections 3.5.3 and 3.6). Thus equation (3.1) becomes:

$$Q^* = Q_H + Q_{LE}$$

The net radiation increases more-or-less uniformly from a minimum in winter to a maximum in summer, with the winter minimum being negative poleward of 40° (Sellers, 1965, p.105). At high latitudes in summer, the net radiation is favoured by long daylength, but limited by the low sun angle and the high reflectivity of snow- and ice-covered surfaces. In the more humid regions Q_{LE} is mainly a function of the available radiative energy, and the annual course of evaporation is similar to that of the net radiation, with a summer maximum and winter minimum (Sellers, 1965, p.109).

The energy exchanges mentioned above can be described in terms of standard micrometeorological relationships. For a discussion of these and the methods and instrumentation used to measure energy balance terms the reader is referred to Oke (1978) or Rosenberg, Blad & Verma (1983).

The relative magnitude of the different energy balance components, then, varies greatly from place to place, and from one time period to another. For example, the net radiation depends on the albedo and cloud conditions; evaporation depends upon the net radiation and the availability of water; the transfer of sensible heat depends on the windspeed and the surface

roughness, which increases air turbulence; and the ground heat flux depends on the conductivity of the ground. This interplay between climatic factors and the site-specific aerodynamic, radiative, thermal and hydrologic properties that affect energy exchange, is known as the microclimate.

Figure 3.4 provides an overview of the interactions occurring in the surface boundary layer that affect ground temperatures. The interplay between climatic conditions, site-specific factors and soil conditions determines the surface temperature, which, together with the influence of the soil thermal properties, drives the ground thermal regime. The soil properties will vary with the moisture content and the temperature of the soil (see section 4.3).

3.5.1 The nature of surface interactions

Lockwood (1979) provides a useful scheme for exploring the nature and significance of these surface interactions, and this is used as a basis for the following brief discussion.

DRY SURFACE WITH NO ATMOSPHERE

While not actually occurring on earth, a surface of this nature would assume a very simple energy balance:

$$Q^* = K \downarrow (1 - \alpha) - L \uparrow = Q_G$$

or,

$$K \downarrow (1 - \alpha) - ekT_s^4 = Q_G \quad (3.3)$$

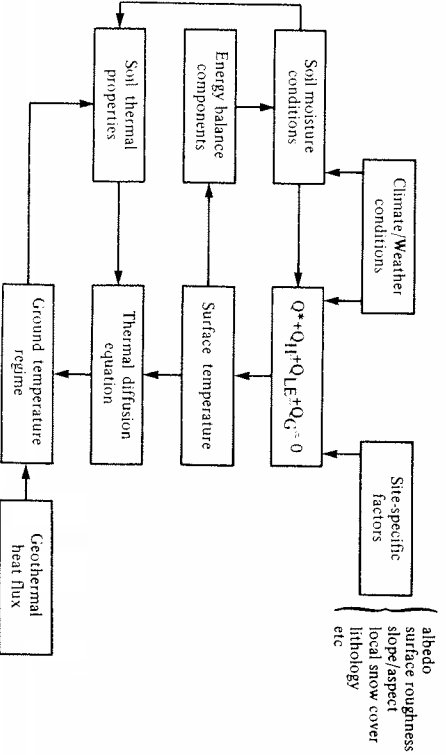


Figure 3.4 A flow diagram of climate-ground thermal interaction.

As mentioned, the net radiation consists of fluxes of *shortwave* (K), and *longwave/infrared* (L) radiation (W m^{-2}), whose sources are *solar* and *terrestrial* respectively. α is the *albedo* (reflectivity) of the surface, T_s is the surface temperature, e is the surface *emissivity* and k is a constant ($5.67 \times 10^{-8} \text{ W m}^{-2} \text{ K}^{-4}$).

As mentioned previously, Q_G is generally very small compared to the other terms, and the surface temperature will change in close accordance with the variations in incoming radiation – from day to night, summer to winter. From equation (3.3) we can see that the surface temperature for a given value of incoming radiation will depend on the albedo, the infrared emissivity and the thermal conductivity of the surface material (i.e. site-specific factors). The higher the albedo, the more radiation is reflected and the lower the surface temperature will be. A surface with a relatively low emissivity will lose heat by longwave radiation more slowly; to compensate for this, the surface temperature will have to rise. Finally, if the thermal conductivity is high (as in most rocks), heat is transferred into and out of the ground more easily, and surface temperature variations are moderated. Conversely, if the thermal conductivity is low (e.g. dry soil), surface temperatures will be higher by day (and in summer) and lower by night (and in winter). Thus, the radiative and conductive properties of the surface materials of the ground can impart significant modulations to the surface temperature regime.

DRY SURFACE WITH ATMOSPHERE PRESENT

The surface energy balance equation now becomes:

$$Q^* = K \downarrow (1 - \alpha) - ekT_s^4 + L \downarrow (1 - \epsilon) = Q_H + Q_G \quad (3.4)$$

In addition to convecting sensible heat, the atmosphere will also modify the incoming radiation by reflection, scattering and absorption (climatic effects). Further, since the atmosphere also absorbs and radiates infrared (longwave) radiation, there is an infrared flux towards the surface ($L \downarrow$) as well as away from it. The magnitude of this flux depends largely on air mass and cloud cover conditions (climatic factors).

Equation (3.4) reveals the influence of both atmospheric (climatic) and site-specific (microclimatic) factors on the net radiation:

$K \downarrow$ is primarily a climatic factor, depending on latitude, time of year (and day), and weather conditions (cloudiness). However, the receipt of solar radiation at the earth's surface is also affected by the local topography (slope angle and aspect – e.g. see Oke, 1978). In addition, $K \downarrow$ at the ground surface may be reduced by the shading effects of vegetation (a site-specific property).

Table 3.1. Albedo values for various surfaces

Water/lake	< 0.10
Wet tundra	0.11
Recent burn	0.07-0.12
Tundra	0.17-0.20
Lichen heath	0.19
Lichen woodland	0.20
Stoney plain	0.24
Dry sandy plain	0.36
Snow cover	0.80

Compiled from various sources

α (the albedo) is a site-specific property, and can vary widely (some typical values are given in Table 3.1).

$L \downarrow$ is a climatic factor, depending largely on cloud conditions and atmospheric humidity.

ϵ (the infrared emissivity) is a site-specific property, but does not vary as much as the albedo.

The convective transfer of sensible heat into the air may be expressed by:

$$Q_H = -\rho c_p K_H (dT/dz) \quad (3.5)$$

or, in finite form:

$$Q_H = -\rho c_p K_H (T_s - T_1)/(z_2 - z_1)$$

where T is measured at two levels in the air. ρ is the density and c_p the mass heat capacity of air. The turbulent transfer coefficient, K_H , depends on the windspeed (a largely climatic factor) and the *surface roughness* (a site-specific property). Alternatively, Q_H may be expressed in the height-integrated form:

$$Q_H = \frac{\rho c_p}{r_a} (T_s - T_a) \quad (3.6)$$

where T_a is the temperature at some height in the air and r_a is an aerodynamic resistance term (an inverse form of K_H). Since the flux of sensible heat into the air depends on the windspeed and the aerodynamic roughness of the surface, rougher surfaces, such as forests, will tend to be cooler, other things being equal (e.g. Rouse, 1984).

WET SURFACE WITH ATMOSPHERE PRESENT

A wet surface is one from which evaporation can take place, and it is the most common type of surface found in nature. The energy balance

becomes that in equation (3.1). Evaporation is the change of water or ice to vapour, and it proceeds continuously from water, soil, snow and ice surfaces. In addition, soil water is extracted by plant roots, passed upward through the plant and discharged as vapour into the air. This is known as transpiration, and the combined process of evaporation and transpiration is called evapotranspiration. Globally, evaporation accounts for about 80% of the energy transfer from the earth's surface (Sellers, 1965, p.103), and variations in evaporation are a principal cause of microclimatic differences.

The rate of evaporation depends on prevailing weather and climatic conditions (radiation, temperature, windspeed, humidity) and on the availability of water at the surface. If profile measurements of humidity and windspeed are available, the evaporative energy flux may be determined from:

$$Q_{LE} = -\rho L_v K_v (q_s - q_1)/(z_2 - z_1) \quad (3.7)$$

where q is specific humidity and K_v is the turbulent transfer coefficient for water vapour (cf. equation (3.5)) and L_v is the latent heat of vaporisation. When the surface is wet, the surface specific humidity may be assumed to be the saturation value (q^*) for the surface temperature, i.e.

$$q_s = q^*(T_s) \quad (3.8)$$

This allows a functional approximation, first introduced by Penman (1948), which eliminates the need for measurements of humidity, temperature and windspeed at two levels, as in the profile and energy balance methods (e.g. see Oke, 1978). Measurements at one level suffice. A discussion of Penman's method, and various derivations from it, can be found in Brutsaert (1982).

When a surface is saturated, evaporation proceeds at the potential rate, the maximum rate at which water vapour can be added to the atmosphere under the given climatic conditions. As the surface or ground dries, however, remaining moisture is held under an increasing suction and eventually the evaporation will fall below the potential value. Whatever the relationship chosen for this, it is included in Figure 3.4 under '*soil moisture conditions*', which, as shown, serve to influence the disposition of energy at the surface.

Figure 3.5 illustrates the diurnal energy regimes at two adjacent sites which differ significantly only in terms of moisture availability - site 1 has saturated conditions at the surface whereas site 2 is drier. With the greater moisture availability, evaporation is much higher at site 1, and as a result of this cooling it experiences lower daily surface (and subsurface) temperatures. Figure 3.6 shows how this difference increases with higher daily

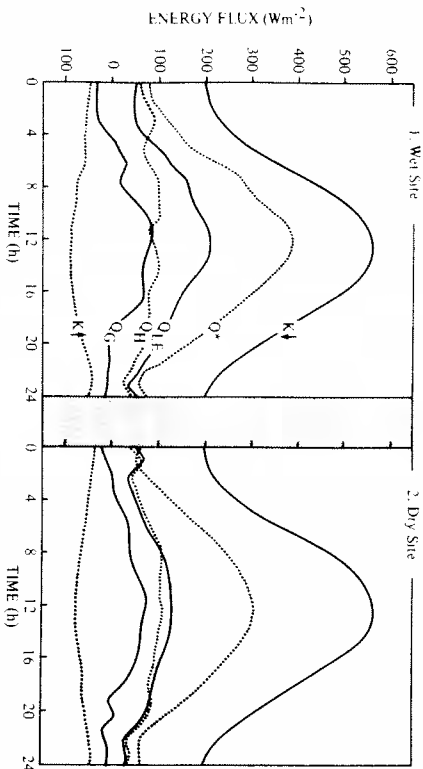


Figure 3.5 Diurnal energy regimes at adjacent tundra sites (from Smith, 1977).

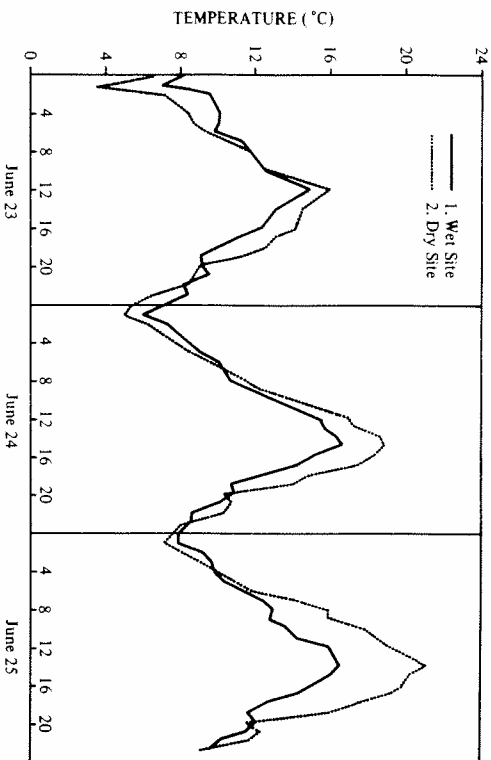


Figure 3.6 Diurnal patterns of surface temperature at the same sites as Figure 3.5 (from Smith, 1977).

amounts of incoming solar radiation. Interestingly, while $K \downarrow$ is similar at both sites (i.e. the albedo is similar), the net radiation at 1 is higher – this is due to the lower surface temperatures there which reduce the outgoing longwave radiation (as shown in equation (3.3)).

3.5.2 A buffer layer model

In terms of their significance to the ground thermal regime, Luthin & Guymon (1974) visualised these boundary layer interactions in terms of a buffer layer model, comprising the vegetation canopy, ground cover and snow cover, interposed between the atmosphere and the ground (Figure 3.7). Atmospheric mass and energy flows together with the geothermal heat flux constitute the boundary conditions, with the vegetation canopy, snow cover (when present) and surface organic layer acting as buffers between the atmosphere (climate) and the ground. In areas of little vegetation or snow-cover – such as can be found in the Canadian Arctic Islands, for example – the linkage between air temperatures and ground temperatures is more direct.

In Figure 3.4, the influence of the buffer layer is described in terms of

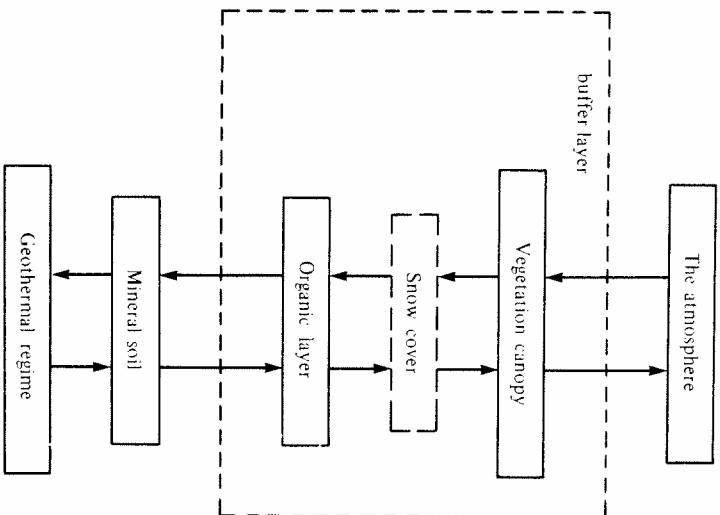


Figure 3.7 A conceptual model of the climate-permafrost relationship (based on Luthin & Guymon, 1974).

various site-specific factors, which depend on vegetation, topography and snow cover. The exact partitioning of the radiative surplus or deficit (Q^*) between Q_H , Q_{LE} and Q_G is governed by the nature of the surface (albedo, roughness, soil moisture, etc) and the relative abilities of the atmosphere (turbulence) and the ground (thermal conductivity) to transport heat.

The primary influences of the vegetation canopy are the reduction of solar radiation reaching the ground surface and the variable effects on the depth and persistence of snow cover (e.g. Luthin & Guymon, 1974; Rouse, 1982). In addition, interception of precipitation and transpiration by the canopy influence the ground thermal regime through the water balance (Risborough, 1985). The role of the vegetation canopy has been investigated by comparative observational studies. For example, Rouse (1984) found that summer soil temperatures beneath an open spruce forest were lower than adjacent tundra, presumably as a result of radiation interception by the canopy, higher evaporation from the wetter surface and the large aerodynamic roughness of the forest producing greater turbulent exchange with the atmosphere. Annersten (1964) concluded, however, that the direct effect of vegetation *per se* was far less important than its role as a snow accumulator – a view supported by the results of Smith (1975) and those of Rouse (1984). Figure 3.8 shows that, although cooler in summer, the near-surface forest soils are considerably warmer than in the nearby tundra in winter, due to the forest acting as a snow fence and trapping a deep blanket of snow. As a result, the forest soil temperatures are more than 3 °C warmer on an annual basis.

Snow is a very important factor to the ground thermal regime, since it presents a barrier to heat loss from the ground to the air in winter (see section 4.4.3). In the Schefferville area Nicholson & Granberg (1973) found the variation in mean annual ground temperatures to be determined primarily by the snow depth, with variations in summertime conditions being less important. Smith (1975), in a study of ground temperature variations in the Mackenzie Delta, found that the warmest sites were so because of higher minimum (winter) temperatures, as influenced by snow cover. In some locations the mean annual ground temperature was raised above 0 °C because of snow accumulation (Figure 3.9). Calculations showed that the outflow of heat from the ground at these sites during the winter was only one-fifth to one-tenth of that at a site with only 25 cm of snow, and that permafrost was actively degrading as a new, higher surface temperature became established.

Near the southern fringes of permafrost distribution, snow cover alone

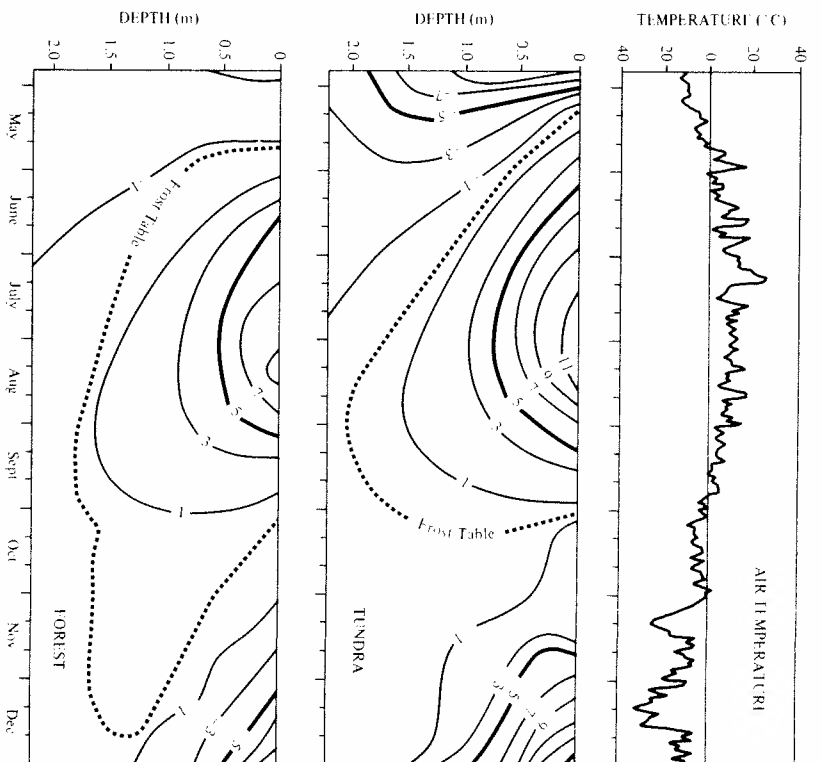


Figure 3.8 The ground thermal regime at a tundra and a forest site (from Rouse, 1984).

may be the critical local factor determining whether permafrost is present or not. In the colder regions of more widespread permafrost, it influences the depth of the active layer. Also, in regions of heavy snowfall, lake and river ice will not be so thick, so that even shallow water bodies may not freeze through. Such is the case in the Mackenzie Delta, where this has an important effect on the local distribution of permafrost (Smith, 1976).

Finally, the influence of organic material on the ground thermal regime in permafrost areas is well documented in the literature (see section 4.4.3). Generally, its presence leads to lower mean annual temperatures, which is attributed mainly to:

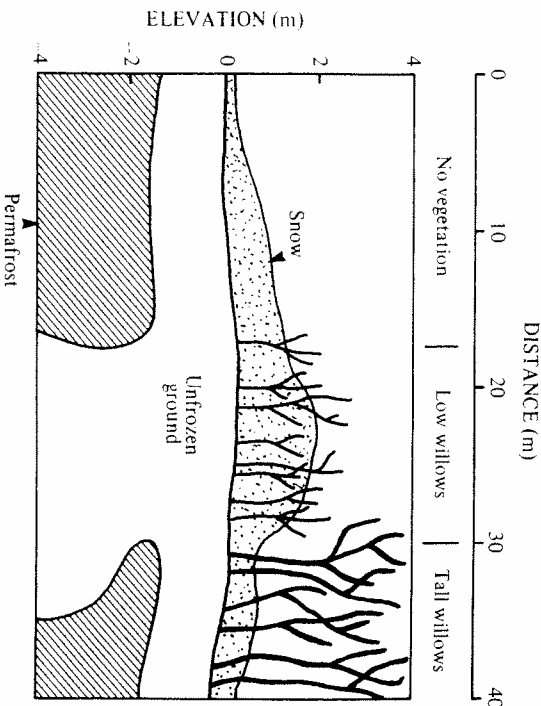


Figure 3.9 Details of permafrost configuration beneath a perennial snowbank (from Smith, 1975).

1. the seasonal variation in conductivity (low in summer, high in winter);
2. the evaporative regime, which promotes cool summer temperatures.

In addition, the results of Nelson *et al.* (1985) indicate that non-conductive modes of heat transfer may be important in the thermal buffering effect of organic material, which keeps ground temperatures low in summertime.

R. J. E. Brown (1963) reported ground temperature data from the Norman Wells area that reveal a decrease in temperature with increasing thickness of moss and peat. In a later paper (R. J. E. Brown, 1965), he concluded that variations in the vegetation canopy *per se* were a relatively minor influence on the ground thermal regime compared to the surface organic layer (see also Riseborough, 1985).

3.5.3 *Effects of surface changes*

It should be apparent that changes in the thermal regime of the ground, such as associated with degradation and formation of permafrost, can result from changes in the surface conditions as well as from fluctuations in climate. Most documented instances of disturbance to the natural environment are associated with human activities, but natural events such

as fire are also important. Any removal, damage or compaction of surface materials (vegetation, peat, soil) will alter the balance of surface energy transfers: in general this will lead to an increase in the mean summer surface temperature (Figure 3.10). This increase will eventually be accompanied by melting in the upper layer of permafrost. For example, Mackay (1970) describes the example of an experimental farm site at Inuvik that was cleared of spruce and birch in 1956. The depth of thaw prior to clearing was about 36 cm, but by 1962 the active layer had deepened to 183 cm.

In winter, changes in snow cover accumulation, as might result from barriers, structures and depressions, can lead to significant warming (or cooling) of the ground. Figure 3.11 shows how the erection of snow fences had an immediate effect on ground temperatures and how the warming was maintained even against natural cooling trends.

Figure 3.12 shows the progressive degradation of permafrost as a result of (controlled) surface disturbance, over a 26-year period. Throughout the period, mean climatic conditions remained more-or-less constant, as revealed by the stability of permafrost conditions in the undisturbed area. The surface treatments in the cleared and stripped areas altered both the summer and winter surface temperature regimes. The bare surface would be the warmest in summer, but because of lower snow accumulation it would cool off more in winter (cf. Figure 3.1). The net result is that while perma-

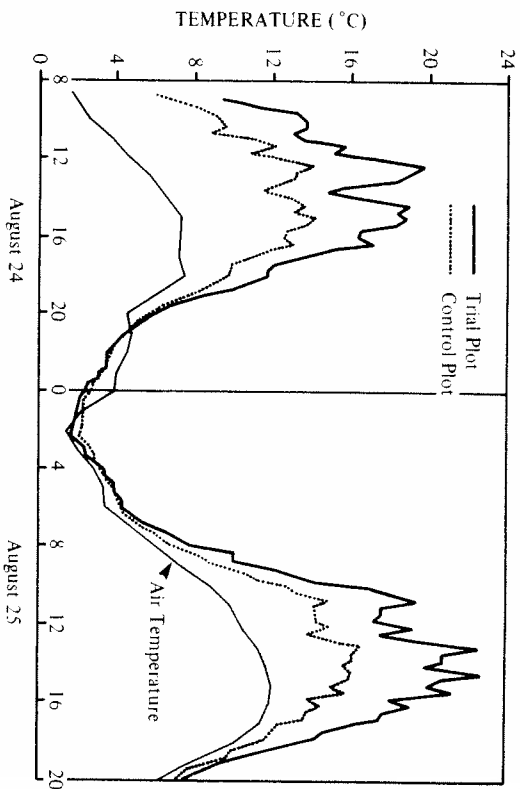


Figure 3.10 Surface temperatures at a disturbed and a control plot (from Nicholson, 1978). The vegetation was removed from the disturbed plot.

subsidence and erosion, particularly where fire lines have been cleared with bulldozers (Heginbottom 1973).

Rouse (1976) compiled a time sequence of the microclimatic changes resulting from forest fire. The most obvious effect of fire is on the tree canopy, but a more significant effect may be the partial or complete destruction of the organic layer at the soil surface. Both the canopy and the organic layer serve to insulate the mineral soil from the heat of summer, the net result being a lower mean annual soil temperature. Destruction of these by fire causes an increase in soil temperature.

Figure 3.14 shows a decrease in net radiation following a fire, even though the albedo is reduced. This is a result of the increase in the surface temperature (as shown in equation (3.3)), which itself is due to the substantial reduction in evapotranspiration (cf. Figures 3.5 and 3.6). All this leads ultimately to an increase in soil temperature – *the important consequence for*

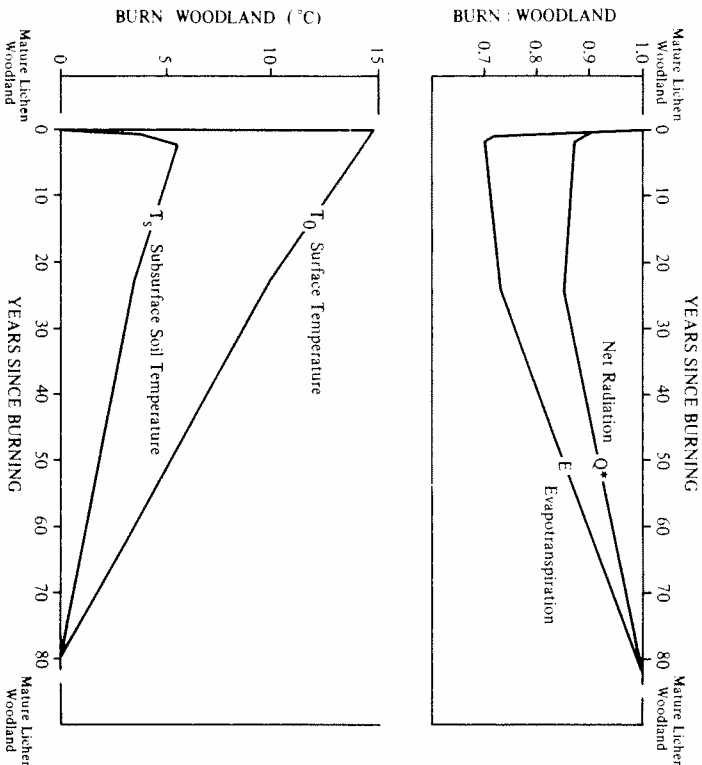


Figure 3.14 A time sequence of microclimatic changes following fire (from Rouse, 1976).

ground thermal conditions thus being the surface temperature at which the new balance of energy transfers is achieved. The heat of the fire, as such, is largely inconsequential to ground warming. The example in Figure 3.14 shows that all the terms gradually return to their original values as the vegetation is restored with time. However, if thermokarst processes are active, some of the changes will be irreversible.

While the foregoing examples all deal with ground warming and permafrost degradation, there are occasions where surface changes bring about ground cooling. For example, permafrost is absent, or lies at great depth, beneath many of the lakes, ponds and rivers in the north. Lake drainage or river shifting will expose these unfrozen sediments to freezing air temperatures, leading to ground freezing and the growth of permafrost (e.g. Smith, 1976; Mackay, 1979). In practical terms, where highways and airfields are built, the clearance of snow in winter may serve to stabilise the thermal condition of the permafrost, perhaps resulting even in some aggradation. Unfortunately, this may also lead to icing problems on highways (see section 2.2.4).

3.6 Possible effects of climatic change

Since permafrost is a thermal ('climatic') condition, it is potentially sensitive to climatic change. Currently, there is growing interest in the impact of human activity on the levels of CO₂ and other radiatively active trace gases in the atmosphere, and their likely effect on climate. Climatologists have shown that air temperatures would increase because of the so-called 'greenhouse effect', although it is not clear by how much. Studies demonstrate, however, almost universal agreement on a warming concentrated in the polar regions, along with increased precipitation there; for a doubling of the atmospheric CO₂ content, some models predict that annual air temperatures throughout the Arctic could increase by 3° to 6°C, and perhaps even more in some areas (Harvey, 1982; Hansen *et al.*, 1984). However, this would undoubtedly take many decades, at least.

While such a trend has not yet been clearly identified in the meteorological record (e.g. see Weller, 1984), the magnitude of such changes in climate would produce serious and far-reaching environmental and engineering problems in permafrost regions, and for the arctic environment as a whole (McBeath, 1984; French, 1986; Goodwin *et al.*, 1984). However, it is difficult to deal with this question in any precise way yet, since most of the inter-relationships are poorly known.

Permafrost is unique in earth material terms, since it exists close to its melting point. Most discontinuous permafrost is either relict, or in such

delicate balance that climatic or other environmental changes can have drastic disequilibrium effects. Tens of thousands of square kilometres of permafrost are warmer than -3°C , and we can expect that most of it would eventually disappear under the climatic warming predicted, although complete degradation would certainly take many centuries. This (1974) reported a decrease in the areal extent of permafrost from 60 to 15% over the past several centuries in the discontinuous permafrost region of Manitoba. Suslov (1961) wrote that the permafrost at Mezen (NE of Archangel) has retreated northward at an average rate of 400 m/yr since 1837, and according to Bird (1967), Sumgin, in 1934, wrote that in the USSR generally, the southern limit of permafrost was probably receding, as a result of climatic amelioration.

In the zone of continuous permafrost, ground temperatures, which may be many degrees below 0°C , would rise with a climatic warming, but perhaps no major changes in regional distribution of permafrost would occur. Meanwhile, however, we could expect progressive deepening of the active layer with the melting of shallow ground ice and ensuing thaw subsidence. In some areas, this would undoubtedly create severe maintenance and repair problems for roads, airports, buildings, pipelines, etc. Greater depths of gravel padding would be needed to preserve permafrost under roads and structures.

In addition to permafrost degradation *per se*, any change in the temperature could cause a major change in the strength and deformation properties of frozen ground, *even without thaw*. The effect of temperature is important not only because of its influence on the deformational mechanisms in the ice but also as it determines the amount of unfrozen water in frozen soil (Chapter 9). There could be problems with the bearing capacity of piles, which are widely used in northern construction, as permafrost warms and adhesion forces decline. As well, the creep rates of (ice-rich) permafrost slopes would increase and slope stability would be decreased.

It is important to realise that climatic changes would also affect various earth surface processes which are characteristic of the permafrost environment, such as ice wedge cracking, frost heave, mass movements and creep. This may not be easy to determine, however, since according to Washburn (1980) the climatic relationships of permafrost processes are poorly known. This aspect has been reviewed briefly by Smith (1986). It has been hypothesised that thaw lakes in the western Arctic expanded during periods of warmer climatic conditions (Carson, 1968; Rampton, 1973). However, the sensitivity of thaw lakes to climate (change) is not well understood, although careful observations of lakes over a 10- to 20-year period might

yield valuable information on growth patterns as a function of climatic variation.

Consideration of climatic change should not be confined to temperature alone, nor simply to a change in mean annual conditions. According to Hansen *et al.* (1984), while the mean annual temperature in northwestern North America could be 7°C higher in a $2 \times \text{CO}_2$ world, increases in winter temperatures (up to 11°C) would be 3- or 4-times greater than for summer (2 to 3°C). In addition, there will be changes in precipitation (10 to 50% higher in summer, 60% higher in winter). Various earth surface processes in the permafrost environment could be affected by *increased rainfall*, but more importantly, perhaps, changes in *snow cover* would complicate the effect of climatic warming on ground thermal conditions. While increased snow depths would partly offset any adjustment in ground thermal conditions to higher winter air temperatures, calculations made by Goodrich (1982b) showed that a doubling of snow cover *per se* from 25 to 50 cm increased the minimum ground surface temperature by about 7°C and the mean annual surface temperature by 3.5°C (see section 4.4.3). In terms of ground temperatures, variations in snow cover are most critical at shallow depths, and the precipitation increases of as much as 60% in fall and early winter, predicted in the Hansen model, could be a significant factor in permafrost degradation, particularly in marginal areas.

Caution must be exercised in simply extrapolating a warming trend in the atmosphere to the ground, however. As discussed in section 3.5, permafrost conditions are affected by the nature of vegetation, soil and snow conditions, as well as climate. Riseborough (1985) concluded that the ground thermal regime in the boreal forest, where a surface organic layer is present, could be considerably shielded from the effects of climatic change. The interception effects of the forest canopy, but, more importantly, the thermal resistance of the moss and peat, serve to isolate the ground from the atmosphere. Ground thermal conditions, therefore, may be highly buffered from atmospheric (climatic) changes, so that any response in the permafrost conditions may be very slow to develop. In addition, ground thermal conditions will certainly be further affected as vegetation itself changes in response to climatic change. Finally, the thermal stability of permafrost is aided by the widespread occurrence of ice-rich ground near the present permafrost table. These considerations indicate the difficulty in assessing the sensitivity of local permafrost conditions to climatic change on a regional scale (see Smith & Riseborough, 1983). Nevertheless, Lachenbruch & Marshall (1986) have reported that throughout much of the 100 000 km² region of northernmost Alaska the temperature in the upper

two metres of permafrost has generally increased about 2°C or more during the last several decades to a century.

Finally, we must recognise that since more than simply climatic conditions determine the surface temperature regime, ground thermal conditions can change for a variety of other reasons.

3.7 Summary

Climate sets the stage for ground thermal conditions over the earth, but other factors complicate any otherwise simple relationship. The physical conditions at the earth's surface intervene to buffer the effects of the atmosphere on the ground, and serve to influence the surface temperature regime. Such conditions can change dramatically over quite short distances, and therefore it is the *microclimate* which is of ultimate importance to particular, local ground thermal conditions. Additionally, the thermal properties of the ground materials determine the pattern of variation in ground temperatures; together with the influence of the local geothermal heat flux. Apart from introducing considerable spatial variation in ground thermal conditions, changes in surface conditions arising from natural or human factors can lead to the degradation or formation of frozen ground. Finally, since permafrost is ultimately a 'climatic' condition, it is potentially sensitive to climatic change, surface buffering effects notwithstanding. There is evidence of this occurring in the past and we may anticipate further changes in the future, especially if the predictions of CO₂-induced warming are fulfilled.

4

The ground thermal regime

4.1 Introduction

The previous chapter discussed how the surface temperature is governed by climatic and microclimatic conditions. In turn, the surface regime is the major factor affecting the ground thermal regime. Once the surface temperature regime is known, the thermal regime of the ground may generally be analysed without further reference to climate. However, ground thermal properties and, at greater depths, the heat flowing from the earth's interior, serve to modify the effects of surface temperature (Figure 3.4).

The behaviour of soils in cold regions is strongly influenced by temperature and therefore the analysis of ground thermal regimes is of importance in many problems of scientific interest. In addition, the thermal interaction of engineering structures with frozen ground must be understood to allow for their proper design. While cold is generally seen as the singular feature of high latitudes, it is often the problems resulting from thaw that are of vital concern to engineering design. The problem of thaw settlement is not purely thermal, however. When soils thaw, meltwater is produced at a rate controlled by thermal processes, whereas the dissipation of this water depends on the discharge capacity of the soil (e.g. Nixon & Ladanyi, 1978).

Ground temperatures are, for the most part, determined by *conductive heat transfer*, although localised circulation of groundwater can occur particularly in areas of seasonal frost and discontinuous permafrost. In general, therefore, ground temperatures can be analysed in terms of *heat conduction theory*. The ground is not a simple solid, however, but comprises different layers whose thermal properties vary with mineral composition, organic content, density, moisture content and temperature (see Farouki, 1981). Moisture may occur as vapour, ice and unfrozen water.

Under freezing and thawing conditions the analysis of temperature

changes in the ground is further complicated by the phase change relations of water. Changes in temperature alter the phase composition of soil moisture and can cause dramatic changes in thermal properties. In particular, the heat capacity is dominated by the *latent heat of fusion*. When dealing with short-term transient problems these phase change effects must be included, or the rate of ground thermal changes may be greatly over estimated.

It is not the aim of this chapter to review the range of techniques used for analysing specific ground thermal problems; for this, the reader is referred to treatments by Carstlaw & Jaeger (1959), Junniks (1977), Goodrich & Gold (1981), Lunardini (1981) and Goodrich (1982a), among others. Rather, this chapter applies heat conduction theory to understanding the significant features of the ground thermal regime in cold regions (cf. Gold & Lachenbruch, 1973).

Even though much insight and practical value can be gained from the application of heat conduction theory to ground thermal conditions, this overlooks the true complexity of soil freezing, which arises from the fact that frozen soils can contain appreciable amounts of unfrozen water at temperatures down to several degrees below 0°C (see Chapter 7). As a result, a temperature gradient in frozen soil establishes a gradient of water potential which will induce water movements. A comprehensive analysis of soil freezing must ultimately deal with this coupling of heat and moisture flows, and these aspects are discussed in Chapter 8.

4.2 Heat flow in the ground

The basic traits of the ground thermal regime can be understood by considering the ground as a homogeneous medium in which heat flows by conduction in the vertical direction only. The amount of heat that flows by conduction is given by:

$$Q_G = -K(dT/dz) \quad (4.1)$$

where the 'constant' of proportionality, $K(\text{W m}^{-1} \text{K}^{-1})$ is the *thermal conductivity* (see section 4.3). (In reality, in the presence of a temperature gradient in moist soil, whether frozen or not, some heat transfer takes place by mass flow and hence K is really an effective thermal conductivity.) The negative sign in equation (4.1) indicates that the heat flow is in the direction of decreasing temperature. Equation (4.1) also indicates that for a given temperature gradient, more heat will flow through a material of higher conductivity (or, for a given value of heat flux, the temperature gradient must increase as the thermal conductivity of the material decreases).

Under steady-state conditions, dT/dz is constant if K is constant - i.e. the temperature profile is linear with depth - and equation (4.1) can be integrated to give an expression for the temperature at any depth, z , as follows:

$$T_s = T_0 + (Q_G/K)z \quad (4.2)$$

where T_s is the surface temperature.

In reality, the process of heat conduction in the ground is more complex than this, partly because steady states are rarely achieved, since the surface temperature is continually changing, and partly because the natural variations in soil conditions leads to variations in thermal properties. In addition, the thermal properties of frozen soils change significantly with temperature. The main limitation of heat conduction models is the degree to which such natural conditions can be represented.

4.2.1 The heat conduction equation

While the *rate* of heat transfer depends on the thermal conductivity, the temperature change experienced by the soil as a result depends upon the *volumetric heat capacity*, $C(\text{J m}^{-3} \text{K}^{-1})$. When a unit volume of a substance changes temperature by dT , the change in heat content is simply the product (CdT). We assume, for now, that C itself does not vary with temperature (but see section 4.3.2).

With expressions for heat flow (equation (4.1)) and heat content in hand, we may write the equation for the heat balance of a soil layer, of unit cross-sectional area, and thickness dz . The heat flowing into the layer must be balanced by the heat flowing out and the change in heat content of the layer:

$$\text{Rate of heat flow in} = \text{Rate of heat flow out} + \text{Rate of change of heat storage}$$

or:

$$K(dT/dz)_0 = K(dT/dz)_z + C(dT/dt)dz \quad (4.3)$$

where t is time. Rearranging equation (4.3) leads to:

$$dT/dt = (K/C)(1/dz)((dT/dz)_0 - (dT/dz)_z) \quad (4.4)$$

which, in differential form, is the heat conduction equation:

$$\frac{\partial T}{\partial t} = \kappa \frac{\partial^2 T}{\partial z^2} \quad (4.5)$$

where $\kappa (= K/C)$ is the *thermal diffusivity* ($\text{m}^2 \text{s}^{-1}$) - i.e. the coefficient of

heat diffusion. A high value for thermal diffusivity implies rapid and large changes in temperature. Equation (4.5) expresses the fact that the rate of change of temperature at any depth is proportional to the divergence of heat flow (as expressed by the curvature of the temperature profile at that depth). In other words, where there is a curved profile in the ground, the temperature will change most rapidly (largest $\partial T/\partial t$) at the depth where the curvature ($\partial^2 T/\partial z^2$) is greatest. In the case of steady-state conditions ($\partial T/\partial t = 0$), the equation reduces to the form in equation (4.1).

Equation (4.5) furnishes a general solution to determining the temperature variations, $T(z, t)$, in a solid body and the solution of any particular problem in heat conduction must satisfy this equation, or some form of it. In addition, T must satisfy not only equation (4.5) but also the particular initial and boundary conditions of the problem.

Analytical (i.e. mathematically exact) solutions to equation (4.5) are available for a wide variety of initial and boundary conditions and are described in standard texts (e.g. Ingersoll, Zobel & Ingersoll, 1954; Carslaw & Jaeger, 1959; Lunardini, 1981). However, their applicability is restricted to problems of limited complexity, and where transient effects may be neglected or are unimportant.

In its simplest application, the heat conduction equation assumes the ground is entirely uniform, and thus a single value only for the thermal diffusivity is required. This condition is rarely met, if ever, in nature, since soil thermal properties normally vary with depth, moisture conditions and temperature. In particular, the assumption is not acceptable for freezing and thawing problems over short (engineering) time scales, where the transient effects of phase change are important. For problems such as these, numerical solution methods must generally be used. In this case, the differential terms are replaced by small finite differences, Δz and ΔT , and a series of simultaneous solutions formed and solved by computer. Complex initial and boundary conditions, and complex problem geometries can also be accommodated in numerical models. Lunardini (1981) and Goodrich (1982*a*) provide an introduction to these methods, and can refer the reader to many specialised texts that are available.

Since many natural processes occur very slowly, problems of a long-term (geomorphological) nature can often be analysed adequately without phase change considerations, using simple analytical solutions to the heat conduction equation (e.g. Lachenbruch, 1957*a, b*, 1959; Mackay, 1963; W. G. Brown *et al.*, 1964; Smith, 1976). Furthermore, even simpler steady-state solutions may be adequate in some situations, when dT/dt is very small.

4.3 Thermal properties

A knowledge of thermal properties is required for the proper interpretation and analysis of thermal conditions in the ground, and for carrying out thermal calculations. For steady-state conduction problems (i.e. no change of temperature with time), only the thermal conductivity, K ($\text{W m}^{-1} \text{K}^{-1}$), need be considered. This is a measure of the quantity of heat that will flow through a unit area of the substance per unit time, under a unit temperature gradient – i.e. $\text{J s}^{-1} \text{m}^{-2} (\text{K m}^{-1})^{-1}$, or $\text{W m}^{-1} \text{K}^{-1}$. Thus it determines the rate of heat transfer. In transient problems, the thermal diffusivity, κ , arises, but in situations where phase change occurs, the latent heat of fusion, L_f (MJ kg^{-1}) dominates.

The presence of ice and water close to their transition temperature has a dominant effect on the thermal properties of frozen soils. When water changes to ice, its conductivity increases four-fold, its mass heat capacity decreases by half, and it releases heat equivalent to that required to raise the temperature of an equal volume of rock by about 150° (Gold & Lachenbruch, 1973). The situation is made more complex by the unfrozen water content relationship of frozen soils. Since the volume fractions of ice and unfrozen water in a soil are temperature dependent, the thermal properties of soils can change significantly with small changes in temperature below 0°C. Because of these effects, soil moisture content plays a decisive role in the thermal conditions of frozen earth materials.

In addition to the special circumstances associated with freezing, the generally variable nature of soil conditions precludes the unique specification of the thermal properties for an entire profile or soil formation, and the dependence on soil type, density, and water content, as well as temperature must be considered. These relationships are generally determined by laboratory experimentation, although the complex nature of frozen materials presents some unique problems. The methods in use were initially developed for unfrozen soils or less complex materials such as metals, and modifications and limitations become necessary.

Unfortunately, there is little published information available on the temperature-dependency of soil thermal properties in the range between 0 to –3°C, although for many practical situations this is the range of greatest concern. In many cases, therefore, estimates and approximations must be used. Various methods for calculating the thermal conductivity of frozen materials are available, and these have been reviewed by Farouki (1981, 1982). In addition, Smith & Riseborough (1985) analysed the errors that can occur in thermal calculations as a result of simplifying assumptions about soil thermal properties.

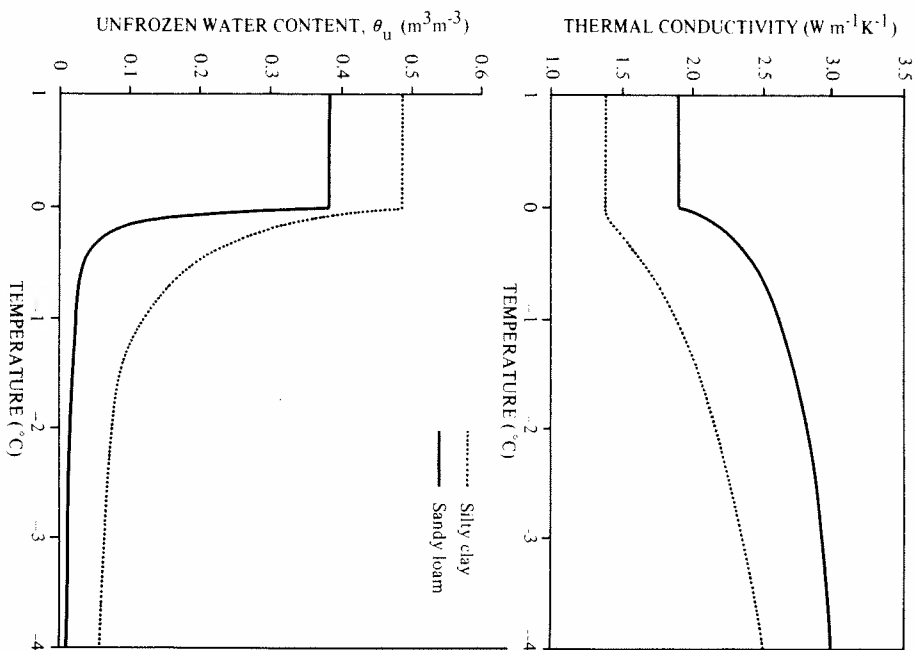


Figure 4.1 (a) Variation of thermal conductivity with temperature for a sandy loam and a silty clay. (b) Unfrozen water content characteristics for the same soils.

4.3.1 Thermal conductivity

Since the conductivity of ice is higher than for water, frozen soils have higher thermal conductivities than unfrozen soils. However, since the volume fractions of ice and water are temperature-dependent, there can be no single value for the thermal conductivity of a frozen soil (provided it contains water). Figure 4.1 shows the variation of thermal conductivity with negative temperature for a silt and a clay soil, together with the unfrozen water content curve for each. In the case of the silt, most of the water freezes by about $-1^\circ C$, and the conductivity increases quite abruptly over this range. Below about $-2^\circ C$, the conductivity is relatively constant, since as Figure 4.1(b) shows, the unfrozen water content changes very little below this temperature. The change in unfrozen water content is more gradual for the clay, and this is reflected in the conductivity curve. These examples illustrate the importance of the unfrozen water content characteristics of the soil to the thermal properties.

Figure 4.1 also illustrates the importance of soil mineralogy. The thermal conductivity of quartz is much higher than for other soil minerals (Table 4.1), and the higher quartz content in the case of the silt leads to higher conductivity values overall.

The first comprehensive testing of the thermal conductivity of soils in the frozen and unfrozen states was that of Kersten (1949). This work predated much research into the behaviour of water in soil materials, so that some of the results are now seen to be questionable. Specifically, the values were obtained using a steady-state method, which we now know is not suitable for thermal conductivity tests on fine-grained materials at freezing temperatures.

There are three basic conductivity test procedures for use on earth materials: they are known as the Guarded Hot Plate (GHP), Divided Bar (DB), and Thermal Probe (TP) methods (see Farouki, 1981). Each method involves heating the test material in some way, which raises unique problems in the case of frozen materials containing water – i.e. the latent heat release associated with temperature change, and variations in thermal properties associated with temperature-dependent phase composition. Thus steady state methods requiring prolonged and/or substantial heating of the specimen (GHP and DB) will cause a change in the properties being measured. In addition, the potentials which develop in unfrozen water films (or gradients in vapour pressure at low water contents) can result in the redistribution of moisture when a temperature gradient is present, leading to complications in heat transfer and inhomogeneity in the sample. When the effects of liquid and vapour transport are present in a test, one can then only determine an apparent conductivity (e.g. see Kay *et al.*, 1981).

Table 4.1. Thermal properties of soils and their constituents

	Density (kg m ⁻³)	Mass Heat Capacity (J kg ⁻¹ K ⁻¹)	Thermal Conductivity (W m ⁻¹ K ⁻¹)	Thermal Diffusivity (× 10 ⁻⁶ m ² s ⁻¹)
(a) Soil constituents				
Quartz	2660	800	8.80	4.14
Clay minerals	2650	900	2.92	1.22
Organic matter	1300	1920	0.25	0.10
Water (0°C)	1000	4180	0.56	0.13
Ice (0°C)	917	2100	2.24	1.16
Air	1.2	1010	0.025	20.63
(b) Unfrozen Soils				
Water				
Content (m ³ m ⁻³)				
Sandy soil	0.0	1600	0.30	0.24
(40% porosity)	0.2	1800	1.80	0.85
	0.4	2000	1.480	2.20
Clay soil	0.0	1600	0.25	0.18
(40% porosity)	0.2	1800	1.18	0.53
	0.4	2000	1.58	0.51
Peat soil	0.0	300	1920	0.06
(80% porosity)	0.4	700	3300	0.29
	0.8	1100	3650	0.50

Compiled from Monteith (1973) and other sources.

In thermal conductivity determinations, then, the duration of the test will affect the results, and as a general rule the test should be kept as short as possible, although the limits depend on the moisture content of the sample. For example, steady state methods are likely to induce substantial moisture migration in wet fine-grained soils near 0°C, although they are suitable for dry materials, those with low porosity, or for fine-grained soils at low temperatures where most of the moisture is immobilised as ice. The effect of moisture redistribution is less in transient state tests, since these are short enough to limit the amount of redistribution which can occur. According to Lachenbruch (1957c) the time of the test should be kept short when liquid water is present in the specimen. Risborough *et al.* (1983) have developed a method for determining the thermal properties of frozen soils at temperatures close to 0°C, using a thermal probe, while E. Penner (1970) presents a variety of results for lower temperatures.

Where certain physical data are available, it is possible to substitute a

calculation method for the direct determination of thermal conductivity. Various methods exist, but that developed by Johansen (1972, 1973, 1977) is the most useful. It is applicable to frozen, mineral soils containing ice and water, and requires information on the physical properties, phase composition and quartz content of the material. The latter is important because, as stated, quartz has a higher thermal conductivity than other soil-forming minerals (Table 4.1).

4.3.2 Heat capacity

In order to describe the heat content of a substance, we need to know its heat capacity, expressed on either a mass or volume basis. The mass heat capacity, c (J kg⁻¹ K⁻¹), is the amount of heat required to change the temperature of 1 kg of the substance by 1 K. For a given amount of heat supplied, changes in temperature will be greater in a material with a low heat capacity. If we multiply the mass heat capacity by the density of the substance, ρ , we obtain the volumetric heat capacity, C , (J m⁻³ K⁻¹). In changing its temperature by an amount dT , a unit volume of substance will experience a change in heat content of (CdT).

In the case of composite materials such as soils, a weighted average value for heat capacity must be used:

$$C_s = X_m C_m + X_o C_o + X_w C_w \quad (4.6)$$

where X is the volume fraction of soil minerals, organic material and water respectively (the influence of air content being negligible). The thermal properties of soil constituents are given in Table 4.1. Quartz, feldspar and clay minerals, the main solid constituents of most soils, have similar heat capacity values. Organic matter has a higher specific heat, but being much less dense has a volumetric heat capacity that is similar to the mineral components. As a result, most dry soils have a heat capacity in the range 1.0 to 1.5 MJ m⁻³ K⁻¹ near 0°C. Since the heat capacity of water is 4.2 MJ m⁻³ K⁻¹ (at 0°C), the heat capacity of a soil increases substantially when it is wet, the increase being linear with the increase in water content. In frozen soils, the temperature dependence of the unfrozen water content means that changes in heat storage are dominated by latent heat effects, especially within a few degrees below 0°C. The complete change in heat storage is then given by:

$$\Delta H = \int_{T_1}^{T_2} C dT + L_f \quad (4.7)$$

(Lunardini, 1981), where the first term refers to the (sensible) heat capacity of the soil and the second term is the latent heat capacity of the soil. As a

consequence of the unfrozen water content relationship (such as shown in Figure 4.1(b)) latent heat of fusion is released over a range of negative temperature, such that equation (4.7) becomes:

$$\Delta H = \int_{T_1}^{T_2} C_d T + \int_{T_1}^{T_2} \rho_w L_f d\theta_u \quad (4.8)$$

where $d\theta_u$ is the change in the unfrozen water content between T_1 and T_2 . Thus changes in heat storage in the soil will include a large latent heat component over the entire range of temperature where there is a significant slope ($d\theta_u/dT$) to the unfrozen water content curve. In clays, for example, this range can extend to many degrees below 0°C. Once again, this illustrates the importance of the unfrozen water content characteristics of the soil.

The latent heat effect is often described in terms of an 'apparent heat capacity' for the soil. An example will explain this. Let us consider 1 m³ of moist clay soil at an initial temperature of 1°C and with a heat capacity of 3 MJ m⁻³ K⁻¹ in the unfrozen state. To change its temperature to 0°C, we must remove 3 MJ of heat. If it is further cooled to some temperature below 0°C, an amount of latent heat is released corresponding to the volume of soil water that freezes over the particular range of negative temperature. In the case of the clay soil shown in Figure 4.1(b), this would amount to some 63.5 MJ m⁻³ over the temperature range from 0° to -1°C. This heat tends to warm the soil, and it must therefore be removed if the soil is to cool further. In this way the heat capacity *appears* to be much larger than would be the case in the absence of any phase change. On the other hand, the apparent diffusivity is very much smaller. If phase change effects are ignored in thermal analyses, the sequence of ground thermal changes will be distorted.

Since the rate at which soil water turns into ice is temperature dependent, the apparent volumetric heat capacity of the soil varies with temperature, as follows:

$$C_g(T) = C_s(T) + \rho_w L_f (d\theta_u/dT)_T \quad (4.9)$$

As indicated, the volumetric heat capacity of frozen soil, $C_g(T)$, also varies with temperature and the change in the volume fractions of ice and water. However, its influence is quite minor compared to the second term, which can be evaluated by taking the slope of the unfrozen water content curve at temperature T (Figure 4.2(a); compare Figure 4.1(b)).

Heat capacity values for any frozen material can be determined using the equations described in this section. Phase composition data are required to calculate heat capacity values for materials containing ice and water. Smith

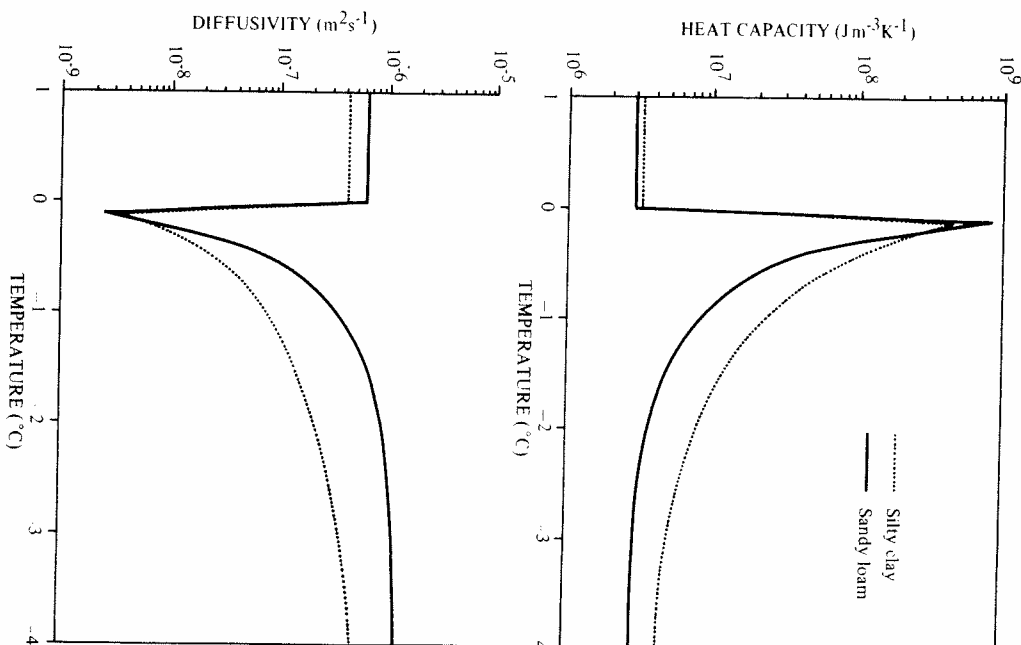


Figure 4.2 (a) Heat capacity for the soils in Figure 4.1. (b) Apparent thermal diffusivity for the same two soils.

& Riseborough (1985) have illustrated the importance of accurate heat capacity values to thermal calculations.

4.3.3 Thermal diffusivity

Since the thermal diffusivity is equal to the ratio (K/C), its variation with water content and temperature depends on the interplay of these two defining properties. When water is added to dry, unfrozen soil, the conductivity increases more rapidly than the heat capacity, so that the diffusivity also increases with water content. At high water contents, however, the increase in conductivity levels off while the heat capacity continues to increase at a constant rate. As a result, the diffusivity may start to decrease (Table 4.1.) Thus the diffusion of heat may be impeded at low water contents by the low thermal conductivity of the soil, and at high water contents by the large heat capacity.

The thermal diffusivity of frozen soils is highly temperature dependent and is dominated by the heat capacity term, especially within the range 0° to -3°C. For example, Figure 4.1(a) shows that the conductivity of the clay soil increases by a factor of almost two between -0.05 and -3°C. Over the same temperature range, the apparent heat capacity decreases by a factor of 75, with the result that the apparent thermal diffusivity, κ_a , increases by two orders of magnitude (Figure 4.2(b)). With decreasing temperature, the effect of increasing conductivity and decreasing apparent heat capacity results in an increasing diffusivity. A noteworthy feature of Figure 4.2(b) is the change of κ_a over a wide temperature range for the clay, indicating continuing phase change.

4.4 Ground thermal conditions

4.4.1 Geothermal heat flow and permafrost thickness

A simple application of equation (4.1) can be made to the case of the steady-state one-dimensional flow of heat from the earth's interior to the surface. Under uniform ground conditions, this can be written as:

$$\dot{Q}_G = K G g \tag{4.10}$$

where Gg is called the *geothermal gradient* ($K \text{ km}^{-1}$). The temperature at any depth in the ground, z , is simply given by:

$$T(z) = T_s + Gg z \tag{4.11}$$

(cf. equation (4.2)). Where the long-term mean surface temperature, T_s , is below 0°C, permafrost will be present, with an equilibrium depth (z_p) at

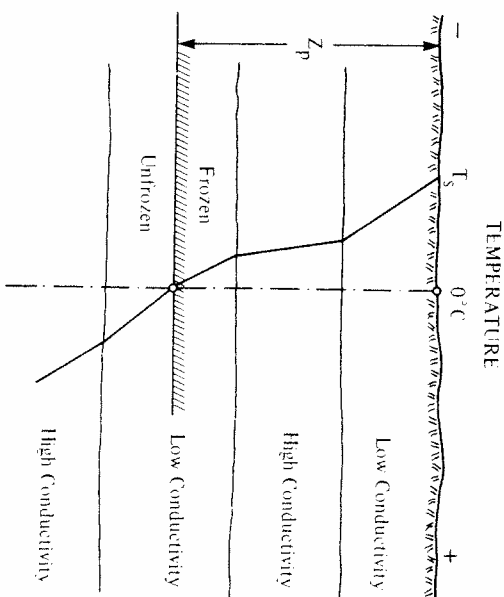


Figure 4.3 Influence of thermal conductivity on the geothermal gradient (from Terzaghi, 1952).

which the temperature increase due to the geothermal gradient just offsets the amount by which 0°C exceeds T_s :

$$z_p = (0^\circ - T_s) / Gg \tag{4.12}$$

In this case it should be noted that, because of the high pore pressures existing at substantial depths in the ground, there will be a temperature difference between the base of *ice-bearing* permafrost and the 0°C isotherm. If we assume that the pore pressure is hydrostatic, then at a depth of 600 m the freezing point depression is about -0.44°C (Osterkamp & Payne, 1981). A freezing point depression can also result from the presence of solutes in the pore water and soil particle effects (see section 7.1.2).

In nature, the thermal conductivity normally varies with depth at any location, as soil and rock materials change. Thus the geothermal gradient also varies, and the change in the slope of the temperature profile affects the permafrost thickness (Figure 4.3). From equation (4.10) we have:

$$Gg = \dot{Q}_G / K \tag{4.13}$$

and equation (4.12) then becomes:

$$z_p = T_s K / \dot{Q}_G \tag{4.14}$$

taking the absolute value of T_s . Equation (4.14) expresses the important

Table 4.2. Variation in permafrost thickness with T_s and K

T_s (°C)	Q_G ($W m^{-2}$)	K ($W m^{-1} K^{-1}$)	z_p (m)
-2	0.04	1.5	75
-1.5	0.04	1.5	56.3
-1	0.04	1.5	37.5
-0.5	0.04	1.5	18.8
0	0.04	1.5	0
-2	0.04	2.5	125
-1.5	0.04	2.5	93.8
-1	0.04	2.5	62.5
-0.5	0.04	2.5	31.3
0	0.04	2.5	0
-2	0.04	4.0	200
-1.5	0.04	4.0	150
-1	0.04	4.0	100
-0.5	0.04	4.0	50
0	0.04	4.0	0

fact that the thickness of permafrost is equally sensitive to the thermal conductivity and geothermal heat flux, as it is to the surface temperature. If K is large, then G_g will be small, and permafrost will be thick; in materials with a low conductivity, permafrost will be thinner.

In this simplified picture it is apparent that the thickest permafrost will occur under a combination of low surface temperature, low heat flow and relatively high thermal conductivity. For a mean surface temperature, T_s , of $-5^\circ C$, Judge (1973) calculated a range of 100 to 550 m in the thickness of permafrost, for variations in G_g . Where T_s is $-10^\circ C$, the equivalent values are doubled (200 to 1100 m).

Variations in surface temperature and the geothermal gradient may be particularly important in the marginal areas of permafrost. For example, for a mean surface temperature of $-1^\circ C$ and a local variation of $\pm 1^\circ C$, a heat flux of $0.04 W m^{-2}$ and thermal conductivity values of 1.5, 2.5 and $4 W m^{-1} K^{-1}$ the thickness of permafrost could vary from 0 to 200 metres (Table 4.2). For northern Canada, Judge (1973) calculated that permafrost is thickest beneath the pre-Cambrian rocks of northern Baffin Island, Boothia Peninsula and Victoria Island, where it reaches 1000 metres or more; in general, however, values of around 500 metres apply. It should be appreciated that the development of permafrost to such great thicknesses involves geological time. According to Kudriavtsev (1965), the occurrence of permafrost up to 700 m thick in western Siberia indicates that it has probably existed during the entire Quaternary period. In contrast, in the

formerly glaciated areas of the western Canadian Arctic, for example, permafrost is much thinner and is only a few thousand years old. Washburn (1979, pp.37-40) presents a table of permafrost thickness data for many locations throughout the Arctic.

Lachenbruch *et al.* (1982) have explained the variations in permafrost thickness along the Arctic coast of Alaska, where the heat flux is fairly uniform, by differences in T_s and the thermal conductivity of the ground materials. At Prudhoe Bay (T_s about $-11^\circ C$) permafrost is about 650 metres thick, whereas at Barrow ($T_s = -12^\circ C$) it is only about 400 metres thick, because of a lower thermal conductivity. At Cape Thompson, where T_s is only $-7^\circ C$, permafrost is still about 360 metres thick, because of the relatively high conductivity of the ground materials there.

Where the ground is not homogeneous with depth, the problem outlined above can still be solved quite easily for steady-state conditions (see Lunardini, 1981; Lachenbruch *et al.*, 1982).

4.4.2 *Effects of climatic change*

Under steady-state conditions, the mean annual ground temperature profile is linear with depth (assuming that thermal conductivity is constant). A conspicuous feature of temperature profiles observed in many northern boreholes, however, is a distinct *inversion* in the upper 100 metres or so, with near-surface temperatures being significantly warmer than those obtained by simple upward extrapolation (Figure 4.4). Widespread 'deviations' in near-surface temperatures such as this can be explained by climatic change, although similar effects can be produced locally by changes in surface conditions, such as a forest fire, or submergence, for example.

Using a heat conduction model, Lachenbruch & Marshall (1969) analysed borehole temperature data from Alaska, and concluded that the mean annual surface temperature had increased in the range of 2 to $4^\circ C$ during the last few decades to a century. If maintained, such a change would eventually lead to a decrease in permafrost thickness (Figure 4.4), and in the marginal areas some permafrost could well disappear. As the envelope of seasonal temperature fluctuation (see section 4.4.3) shifts to warmer values, the active layer will deepen. At the same time, permafrost thins from below due to the melting by geothermal heat.

Suppose that a change in the climate results in a shift of the mean annual surface temperature from some initial, stable value, T_{s0} , to a new value ($T_{s0} + \Delta T_s$). After thermal equilibrium is re-established in the permafrost, the new temperature profile will be (after Gold & Lachenbruch, 1973):

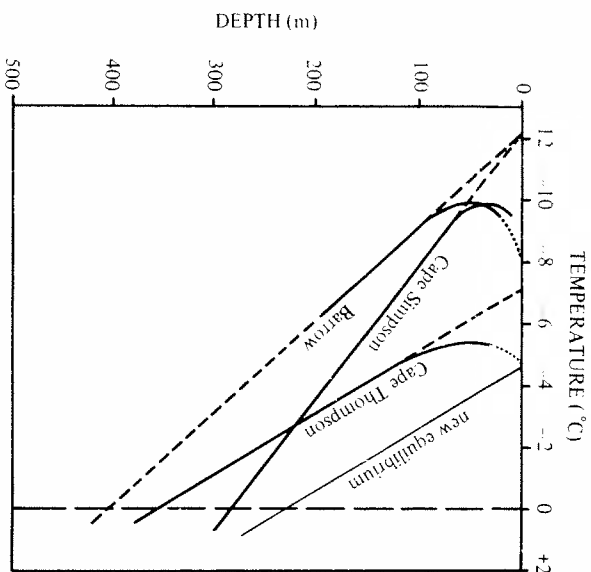


Figure 4.4 Temperature borehole profiles from the arctic coast of Alaska (from Lachenbruch *et al.*, 1982).

$$T(z) = T_s + Gg \cdot z + \Delta T_s \tag{4.15}$$

and the permafrost will have thinned from the bottom by $(\Delta T_s / Gg)$. For $Gg = 20 \text{ K km}^{-1}$, and $\Delta T_s = 4^\circ\text{C}$, this would amount to 200 m. However, as Lunardini (1981, pp.138-142) demonstrates, the time required for this new equilibrium to be reached is very long – maybe as much as 10 000 years or more, depending on the thermal diffusivity and depth. He calculates that surface temperature fluctuations of short period (a century or less) will not affect the thickness of permafrost significantly. Indeed, Lachenbruch *et al.* (1982) calculated that the climatic warming of the last 100 years or so has been sufficient to melt a total of only 0.8 m at the bottom of permafrost during the period. The main destabilising effects of short-term climatic change will be those resulting from the melting of shallow ground ice as the surface temperature change(s), will propagate into the ground. The transient temperature profile is given by:

During the transition towards a new steady-state condition, the effects of surface temperature change(s), will propagate into the ground. The transient temperature profile is given by:

$$T(z, t) = T_s + Gg \cdot z + \Delta T_s(t) \tag{4.16}$$

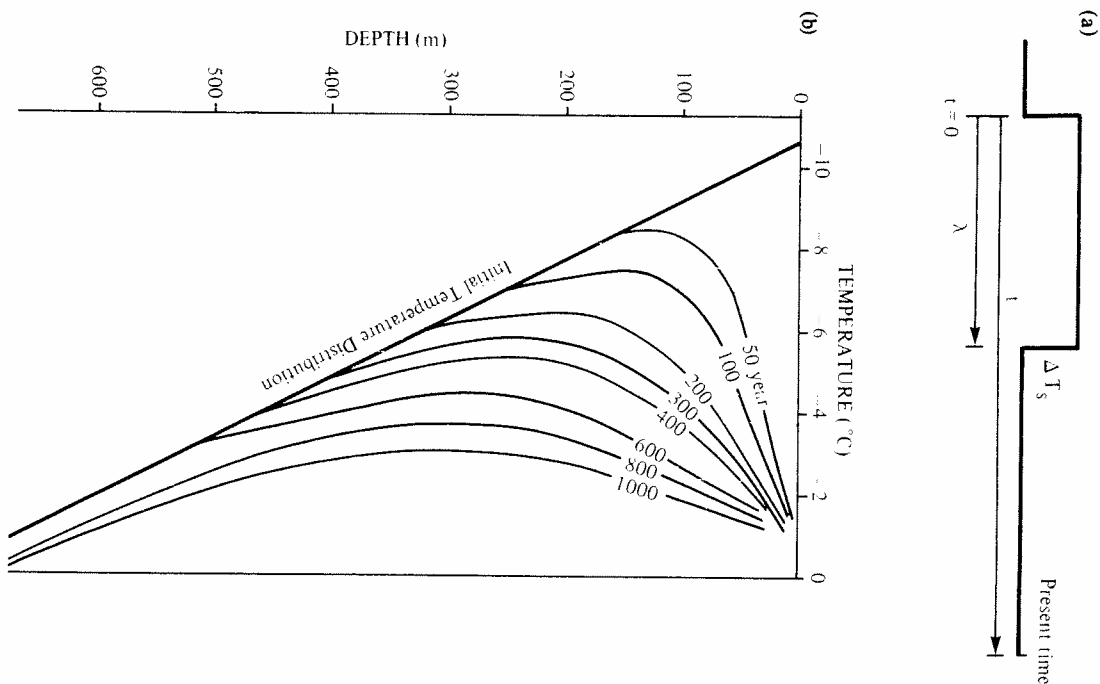


Figure 4.5 (a) Illustration of a step change model for climatic change. (b) Sequence of geothermal response to a surface temperature step change (from Molochuskin, 1973).

Where temperatures remain quite cold (say below -2°C or so), the transient departure of the temperature profile from equilibrium can be analysed quite adequately without reference to phase change complications. Birch (1948) developed a general formulation for the problem of climatic change in terms of simple step functions applied as the boundary condition to equation (4.5). In the case of a single episode as illustrated in Figure 4.5(a), the term $\Delta T(z, t)$ in equation (4.16) is given by:

$$\Delta T(z, t) = \Delta T_0 \left[\operatorname{erf} \left(\frac{z}{(4\kappa t - \lambda)^{1/2}} \right) - \operatorname{erf} \left(\frac{z}{(4\kappa t)^{1/2}} \right) \right] \quad (4.17)$$

where $\operatorname{erf}()$ is the error function and λ is defined in Figure 4.5(a). Equation (4.17) expresses the fact that ground temperatures respond to surface changes according to the thermal diffusivity, the depth in the ground and the elapsed time since the surface change (Figure 4.5(b)). If we refer back to Figure 4.4, we see that the effects of the recent climatic warming have penetrated most deeply at Cape Thompson (highest diffusivity) and least at Cape Simpson (lowest diffusivity).

By superimposing the results for different episodes the effects of arbitrary changes in surface temperature on ground thermal conditions can be calculated. Thus a variety of past climatic changes can be represented in differential fashion throughout the ground temperature profile.

In principle, a detailed analysis of the present temperature record with depth can be used to examine hypotheses concerning past climatic patterns, although local environmental effects can distort or obscure the climatic 'memory' of the ground. For example, Cermak (1971) describes a method which analyses the departure of the temperature gradient from the equilibrium condition. Very precise values for temperature (to within a few millidegrees) and thermal diffusivity are required. He applied his method to estimate the magnitude and duration of the post-Glacial climatic optimum in Central Canada, and illustrated how different models of past climatic change can be examined using temperature borehole data (see also Gold & Lachenbruch, 1973; Lachenbruch & Marshall, 1986).

4.4.3 Seasonal temperature variations

Whereas the position of the bottom of permafrost is determined by T_s , K and Q_0 , under processes that act over long periods of time, the position of the top of permafrost (the depth of the active layer) is controlled by the seasonal fluctuation of temperature about the mean annual value, specifically by the warmest temperatures of the year. The seasonal fluctuation about the annual mean also determines the depth of winter freezing in the more temperate zones.

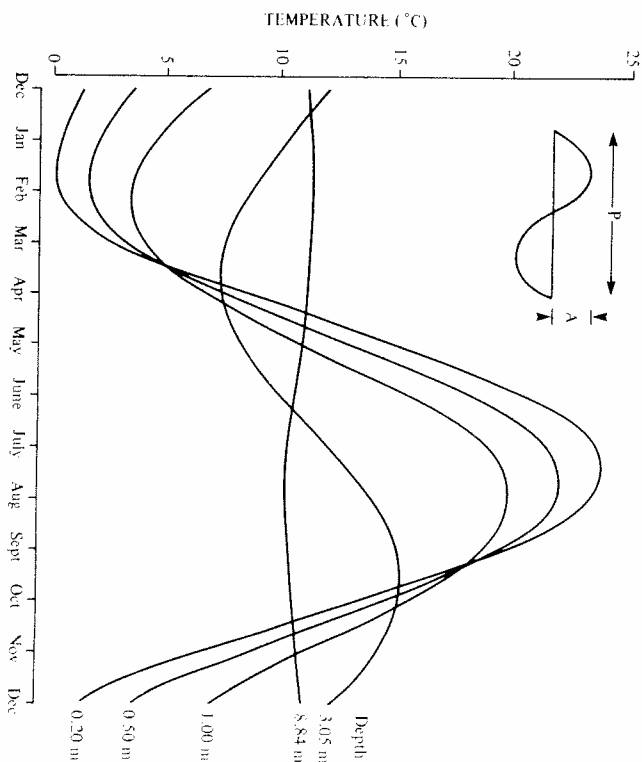


Figure 4.6 Annual temperature variations in unfrozen soil (from Carson & Moses, 1963).

The systematic seasonal fluctuation of solar radiation and air temperature imparts a temperature wave to the ground surface that propagates downward into the earth. The temperature at depth oscillates with the same (annual) frequency as the surface temperature, but with an amplitude that diminishes and a phase lag that increases with depth (Figure 4.6). Eventually, a point is reached where the temperature remains essentially constant, except for any long-term drift related to climatic change, for example, the depth of 'zero' annual amplitude may be 10 to 15 metres in soils, but can be much deeper in rock.

The top of permafrost coincides with the depth where the maximum annual temperature is 0°C . In addition, the seasonal variations of temperature are responsible for periodic thermal stresses in the surface ground layers that cause them to crack, with important geomorphological consequences such as ice-wedge development (Chapter 6). Periodic temperature changes may also be important to creep activity in surface layers of the ground (Chapter 9).

The general features of the thermal regime in the layer of annual variations – such as the exponential *attenuation* of the seasonal wave with *depth*, and the *lag in phase* – can be analysed using the heat conduction equation (4.5) with a sinusoidal surface temperature variation. In this case, the temperature at any depth, z , is given by (Ingersoll, Zobel & Ingersoll 1954, pp.45–57):

$$T(z, t) = \bar{T}_z + A_s e^{-z(\omega/2\kappa)^{1/2}} \sin \left[\omega t - \left(\frac{\omega}{2\kappa} \right)^{1/2} z \right] \quad (4.18)$$

where $\omega = 2\pi/P$, P is the period of the wave (one year), and A_s is the amplitude of the surface temperature wave (Figure 4.6). Time t is counted from the date in spring when the surface temperature wave passes through its mean annual value. The expression:

$$A_z = A_s e^{-z(\omega/2\kappa)^{1/2}} = A_s e^{-z(\pi\kappa/P)^{1/2}} \quad (4.19)$$

represents the amplitude of the temperature wave at depth z , and the term:

$$t = z \left(\frac{1}{2\kappa\omega} \right)^{1/2} = \frac{z}{2} \left(\frac{P}{\pi\kappa} \right)^{1/2} \quad (4.20)$$

is the lag of the wave with depth. From equation (4.19), we see that the depth of zero temperature change (i.e. where $A_z = 0$) technically occurs at $z = \infty$. Normally, we take an operational definition for the depth of 'zero' annual amplitude as that where the change is less than 0.1° , say. Alternatively, we can take the depth where the annual wave is delayed by exactly one year from that at the surface. This is given by:

$$z = (\pi\kappa P)^{1/2} \quad (4.21)$$

The effect of the thermal diffusivity on seasonal fluctuations in ground temperatures can be illustrated by applying equation (4.18) with different annual wave at depths of 1 and 3 m

κ (m ² day ⁻¹)	A_1/A_s	A_3/A_s	t_1 (days)	t_3 (days)
0.010	0.40	0.06	54	162 (snow, peat)
0.025	0.56	0.17	34	102
0.045	0.65	0.27	25	76
0.065	0.69	0.34	21	63
0.085	0.73	0.38	18	55 (frozen soil)
0.110	0.76	0.43	16	49 (rock)

values for κ . This is equivalent to imposing the same surface temperature variation on different lithologies. The result (shown in Figures 4.7(a) and (b)) reveals greater damping of variations for the low diffusivity case; at a depth of 8 metres, the annual amplitude is virtually zero. (In these examples, a mean annual surface temperature of -5°C was assumed, and the geothermal gradient was ignored.) Figure 4.7(c) shows the envelope of annual temperature variation for the same two cases. The seasonal range is greatly reduced in case 1, and a much greater active layer depth results in case 2, under the identical surface temperature conditions.

The dependence of the amplitude reduction and phase lag on the thermal diffusivity is illustrated further in Table 4.3. Temperature waves are attenuated less and suffer a shorter lag in materials with high diffusivity, such as rocks.

Conversely, if seasonal ground temperature data are available, they can be used to determine the thermal diffusivity. If we take the ratio of the amplitudes at two depths, z_1 and z_2 , we have:

$$\frac{A_2}{A_1} = e^{-(z_2 - z_1) \left(\frac{P}{4\pi\kappa} \right)^{1/2}} \quad (4.22)$$

from which κ can be calculated as follows:

$$\kappa = \frac{\pi}{P} \left(\frac{z_2 - z_1}{\ln(A_1/A_2)} \right)^2 \quad (4.23)$$

Alternatively, we can compare the lag at two depths:

$$t_2 - t_1 = (z_2 - z_1) \left(\frac{P}{4\pi\kappa} \right)^{1/2} \quad (4.24)$$

from which κ can again be calculated:

$$\kappa = \frac{(z_2 - z_1)^2}{(t_2 - t_1)^2} \cdot \frac{P}{4\pi} \quad (4.25)$$

These equations have been widely used, and a review of these and other methods can be found in Horton, Wierenga & Nielsen (1983).

The results of the periodic (annual) temperature model have been discussed widely in the literature. They apply equally to other variations, such as diurnal for example, although, as the equations describe, the period of temperature variation affects the depth of propagation and the variation at any depth. Ultimately, the practical value of the relationships presented depends on the extent to which the surface temperature regime can be

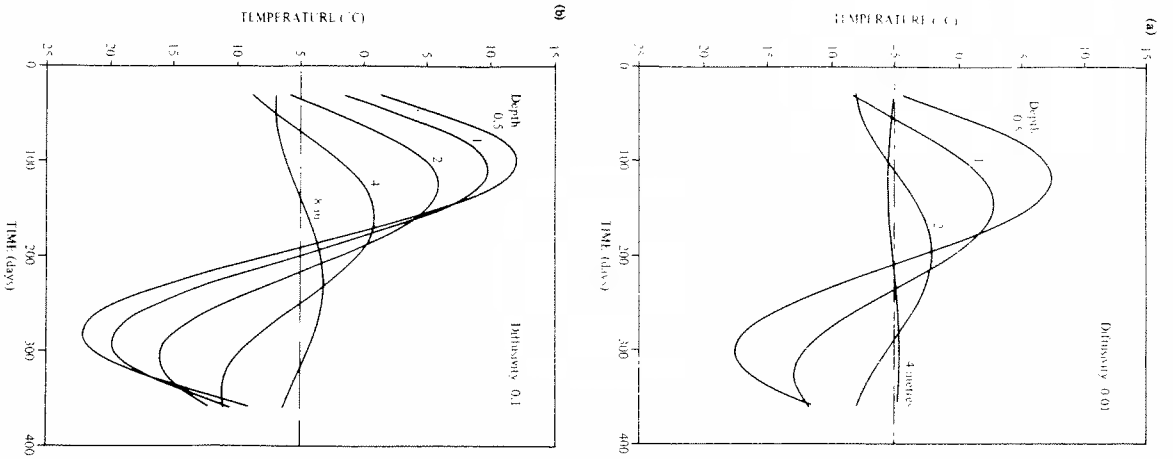


Figure 4.7 Influence of thermal diffusivity on annual ground temperature variations.

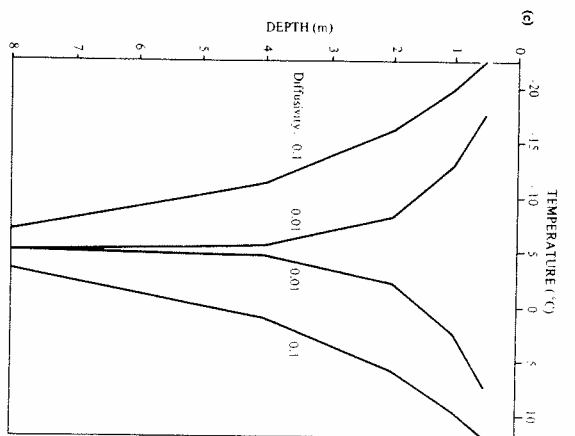


Figure 4.7 (cont.)

represented by a simple sine wave. For diurnal temperatures especially, this is often far from the case. However, the relationships can provide valuable insights into the nature and significance of periodic variations in ground thermal conditions.

An important departure from the simple temperature model described above arises from the effects of periodic freezing and thawing in the surface layer of the ground. In the autumn, the surface temperature drops sharply below 0 °C, and temperatures throughout the active layer fall to near 0 °C shortly after this. Subsequently, however, ground temperatures may fall slowly for a prolonged period, because large amounts of latent heat originating from the freezing of water within the active layer must be removed from the ground. The result is that the ground temperature remains near 0 °C for some period. This is terminated when most of the water is frozen, and rapid cooling then ensues. This effect, termed the 'zero curtain', is more prolonged in soils with high water contents. Sometimes one can note a prolongation of the zero curtain to lower temperatures, indicating that appreciable amounts of soil water have freezing points below 0 °C (see section 7.1.2).

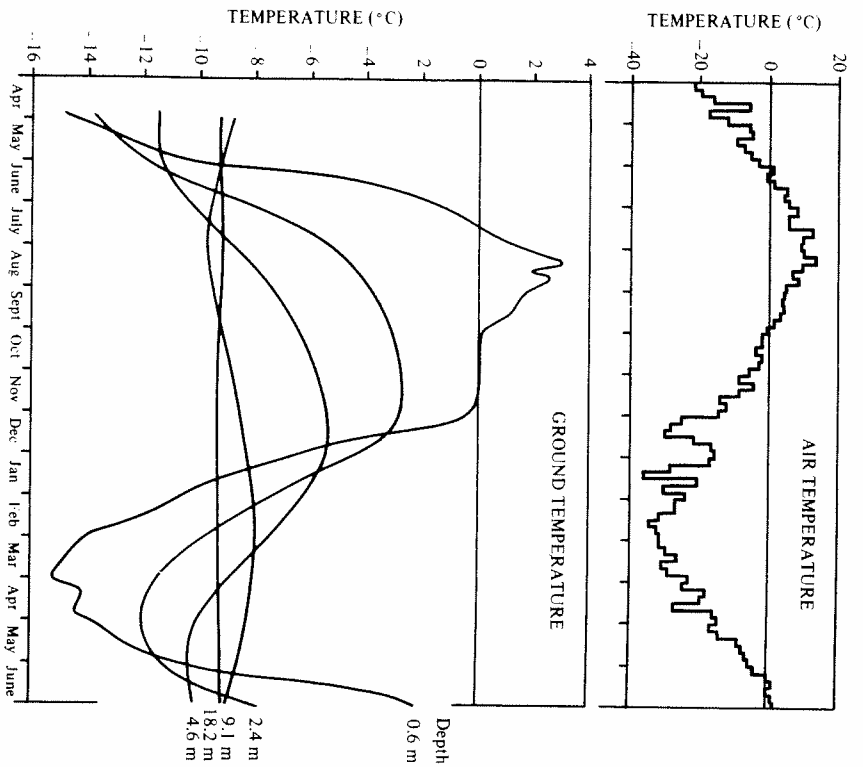


Figure 4.8 Typical air and ground temperatures at Barrow, Alaska (after Lachenbruch *et al.*, 1962).

The zero curtain effect produces some asymmetry in ground temperature curves, although this vanishes, along with high frequency fluctuations due to weather (noticeable in the air temperature record), at increasing depths (Figure 4.8). In Figure 4.8, the annual temperature range also decreases from 18° at 0.6 m to 0.1° at 18.2 m. The figure also shows that the minimum temperature at 4.6 m occurs in the spring, and at 9.1 m in mid-summer. This phase lag can sometimes result in the spring and summer freeze-up of wells and buried conduits in regions of discontinuous permafrost (Lachenbruch *et al.*, 1962).

Where substantial phase change is involved, use of equations (4.23) and (4.25) may not be useful for determining the thermal diffusivity, κ from ground temperature data, but another approach is possible using the heat conduction equation (4.5). By evaluating $(\partial T/\partial t)$ and $(\partial^2 T/\partial z^2)$ at a particular time and depth, and by taking the ratio of these terms, the apparent thermal diffusivity, κ_a , is determined (see Takagi, 1971, McGaw *et al.*, 1978). This approach incorporates the effects of latent heat, and can provide estimates of κ_a as a function of temperature. It can also be used to reveal whether non-conductive forms of heat transfer are operative in the ground (e.g. Nelson *et al.*, 1985).

THE ROLE OF PEAT AND SNOWCOVER

The importance of snow cover and peat to ground thermal conditions is widely recognised. Their influence can be explained with reference to the pattern of seasonal temperature variation. Snow is an *insulator* compared to other natural materials, and is a leading factor in protecting the ground from heat loss in winter. Its net effect is to raise mean annual ground temperatures; Gold (1963) concluded that snow cover was the principal reason why annual average ground temperatures can be many degrees warmer than the mean air temperature in cold regions. Snow amelioration measures were widely used in the north-eastern USSR to mitigate ground freezing in agriculture, as well as in open pit mining (Klyukin, 1963). Where temperatures are close to 0°C, snow cover can be responsible for the absence of permafrost in certain locations (e.g. see Smith, 1975). Conversely, peat, which also acts as an insulator, is commonly associated with the *existence* of permafrost at certain locations in marginal areas. Unlike snow cover, of course, a peat layer is present the year round, but its conductivity varies seasonally with moisture conditions. When it is dry, as it frequently is in the summer, the conductivity is low and thus the soil beneath is shielded from the heat of summer. Consequently, the mean annual ground temperatures are lower than otherwise. Even if the peat remains wet during the summer, the resulting predominance of evaporation in the energy regime will lead to lower surface, and hence subsurface, temperatures (see section 3.5.1).

The snow cover interposes a layer of low thermal diffusivity between the air and the ground, serving to isolate the ground from the extreme temperature changes of the air (compare the two sites in Figure 4.9). Since heat exchange takes place at the snow surface rather than the ground surface, the range of annual ground surface variation is reduced and ground temperatures are higher, not only in winter, but also on an annual basis. In Figure 4.10, an increasing divergence between the air and ground surface tempera-

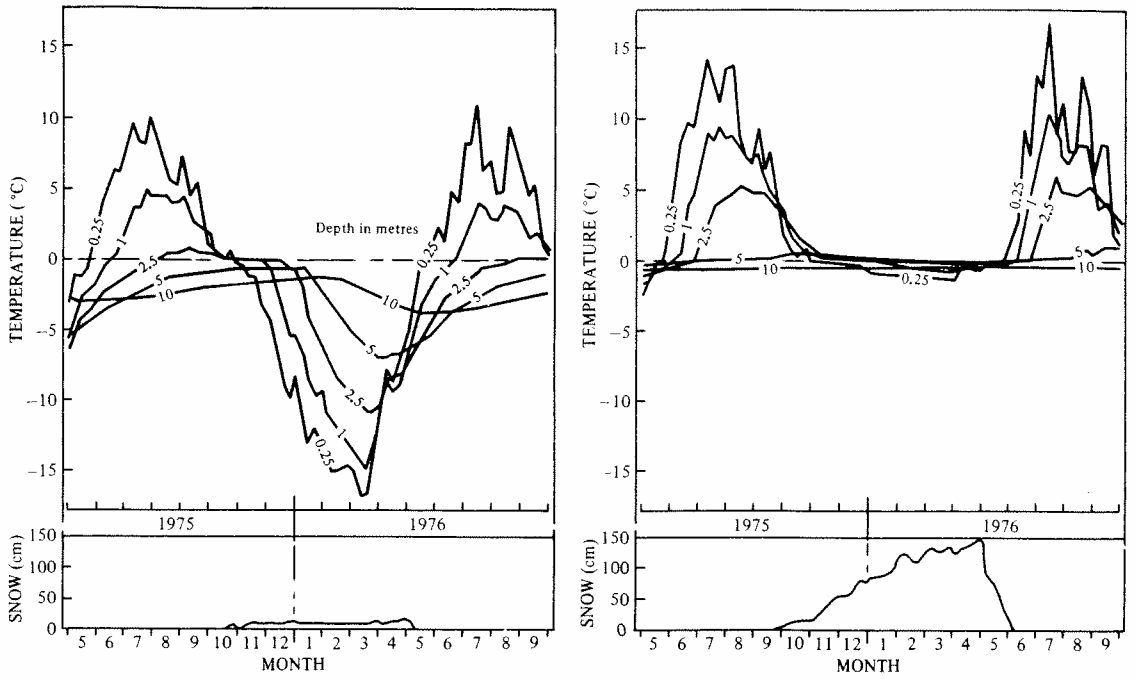


Figure 4.9 Annual temperature variations at two sites of contrasting snow cover conditions (from Nicholson, 1978). The deep snowcover of the trial plot held the temperatures close to 0°C.

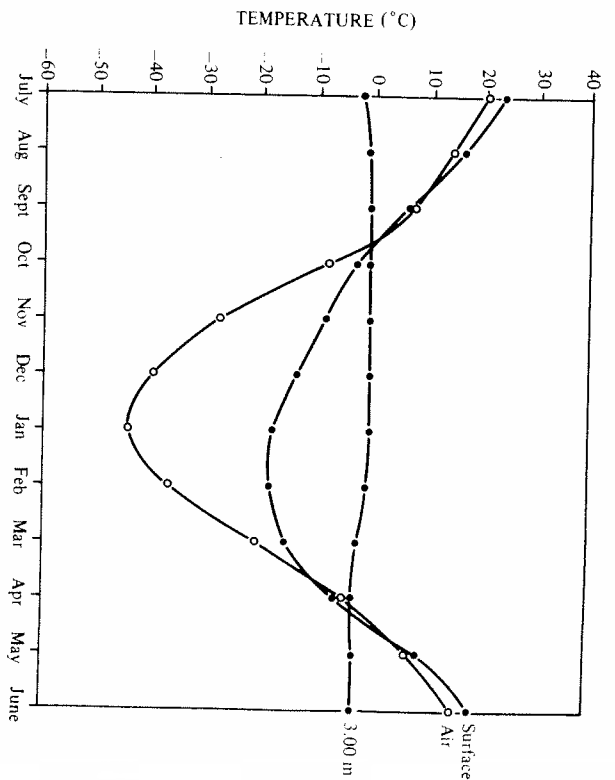


Figure 4.10 Air, surface and ground temperature regimes for Yakutsk (data from Pavlov, 1973).

tures occurs through the winter with the seasonal build up in snow depth. The large difference between the air and ground surface temperatures in winter (20° or more) contrasts with their closeness in summer, when heat exchange takes place at the ground surface. As a result, there is virtually no cooling evident at a depth of 3 m in the ground. In the Mackenzie Delta, where the mean daily air temperature is below -20°C for almost 6 months in winter, the 1-metre ground temperature beneath 120 cm of snow did not fall below -0.2°C (Smith, 1975).

This effect of snow results from its very low thermal conductivity, which in turn depends on the density. For the density range 100 to 400 kg m⁻³, the relationship shown in Figure 4.11 can be used. At a density of 200 kg m⁻³, the snow has a conductivity of 0.11 W m⁻¹ K⁻¹, which compares to values of 2 to 3 for frozen soil. The heat capacity of the snow (applying equation 4.6) would be 0.42 MJ m⁻³ K⁻¹, and the diffusivity 0.01 m² day⁻¹. This compares to values up to 0.1 m² day⁻¹ for frozen soil. Referring to Table 4.3, we see that the annual surface temperature wave would be reduced to 40% beneath 1 m of snow. For snow of higher density, the damping effect would be less.

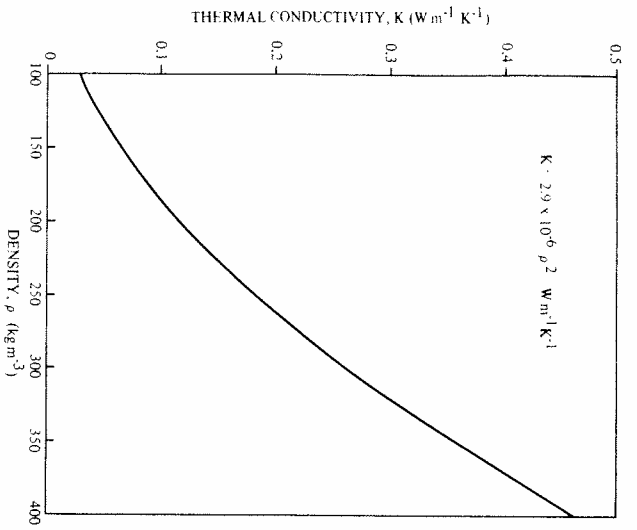


Figure 4.11 Relationship between the thermal conductivity and density of snow (based on a relationship in Goodrich, 1982b).

Smith (1975) measured ground surface temperatures in mid-winter in the Mackenzie Delta, and found a relationship with snow depth (Figure 4.12). The range in temperatures shown – about 20°C – is twice as great as the maximum variation observed in summer (which result from differences in vegetation). Figure 4.12 indicates that increases in snow cover become less effective above 50 or 60 cm. Figure 4.13 shows snow and ground temperature profiles on a typical day in early winter at two sites near Schefferville, Quebec. There is a characteristically steep temperature gradient immediately below the snow surface, with a marked inflection at a depth of 50 to 60 cm, below which temperatures are fairly uniform. Together, Figures 4.12 and 4.13 imply that variations in snow depth are more critical for ground temperatures where the snow cover is thin.

Goodrich (1982b) analysed the general features of snow cover/ground thermal interactions, using a heat conduction model. He concluded that mean annual ground temperatures are most strongly influenced by an accumulation of snow in autumn and early winter, and by the maximum

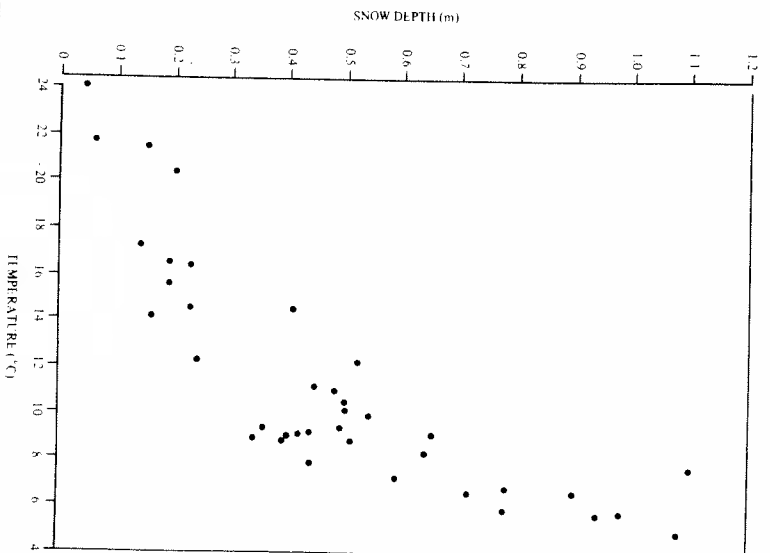


Figure 4.12 Effect of snow depth on ground surface temperature (from Smith, 1975).

depth attained over the winter. In his calculations, a doubling of the snow cover from 25 to 50 cm increased the minimum ground surface temperature by about 7° (from -19.7° to -12.3°C), and the mean annual surface temperature by 3.5° (from -7° to -3.4°C). If the 50 cm of snow built up within 30 days in autumn, the minimum temperature would be only -2.8°C , the mean annual temperature would be $+1.1^{\circ}\text{C}$, and permafrost would degrade.

Finally, Mackay (1984b) has shown that snow depth plays an important role in ice-wedge cracking. A rapid drop in the ground temperature is necessary to cause cracking, and this is impeded by the insulating properties of a deep snow cover. He found that a depth of 60 cm was sufficient to prevent ice-wedge cracking in an area of active ice wedges on Garry Island, NWT.

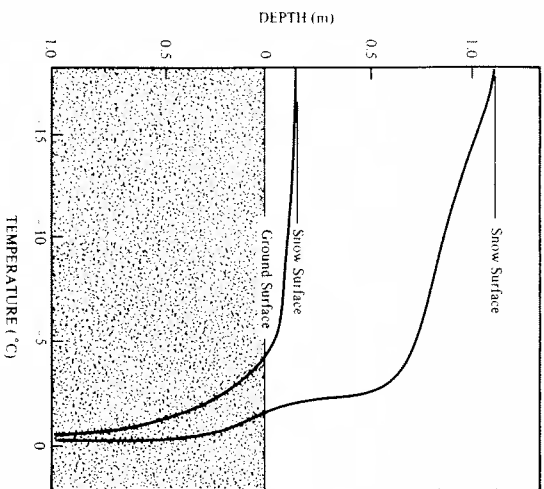


Figure 4.13 Mean snow and ground temperatures at two sites for a typical day in winter (from Nicholson & Granberg, 1973).

The influence of the organic layer on ground thermal conditions has also been well documented in the literature (e.g. Nakano & Brown, 1972, Luthin & Guymon, 1974, Zoltai & Tarnocai, 1975, Fitzgibbon, 1981), and the presence of permafrost in marginal areas is frequently associated with peat. For example, R. J. E. Brown (1973) reports that in the Yellowknife area, the greatest local extent of permafrost is in peatlands, and that the mean annual temperature at a depth of 15 m ranges from about 2 °C in granite to -1.0 °C in spruce peatland (see Figure 3.2). This effect arises because of the *marked seasonal variation in the thermal properties* of peat, which imparts an asymmetry to the pattern of seasonal temperature variations. In summer, when the surface layer is usually dry (because of evaporation), the thermal conductivity is very low and warming of the ground is inhibited. However, in the fall the peat becomes quite moist, because of the much reduced evaporation rate. Further, when it freezes the conductivity becomes even higher and the ground can cool rapidly. The net effect, in contrast to snow, is that mean annual ground temperatures under peat are (much) lower than under adjacent areas without peat.

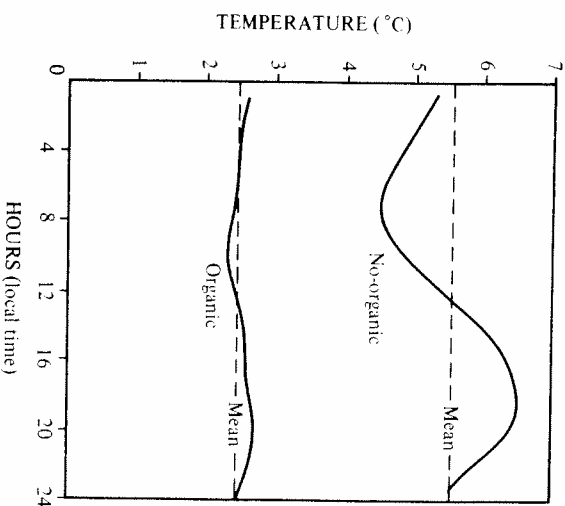


Figure 4.14 Mean diurnal 10-cm ground temperature regimes at adjacent sites in the Mackenzie Delta (from Smith, 1975).

Figure 4.14 shows the temperatures measured at a depth of 10 cm over the summer at two sites only 1 m apart, in a spruce forest in the Mackenzie Delta. At one site there was a 10-cm layer of organic material at the surface, whilst at the other there was simply bare mineral soil. The mean daily temperature is 3 °C warmer at the bare site and the diurnal range 5 times greater. R. J. E. Brown (1963) writes that after removal of the moss and peat from the ground surface, in the arctic region of the Yenisey River valley, the depth of thaw increased by 1.5 to 2.5 times.

Goodrich (1978) used a heat conduction model to demonstrate the significance of temperature-dependent thermal properties – with peat providing an extreme case – to ground thermal conditions. He showed that an offset occurs in the mean annual temperature profile as a result of the seasonal change in the thermal conductivity. When the frozen conductivity is higher, the mean annual temperature profile shifts to colder values down to the depth to which the property change takes place (Figure 4.15(a)). The effect is seen to increase as the ratio of frozen to thawed conductivities increases. R. J. E. Brown & Péwé (1973) point out that the conductivity of peat can also change throughout the year as a function of the water

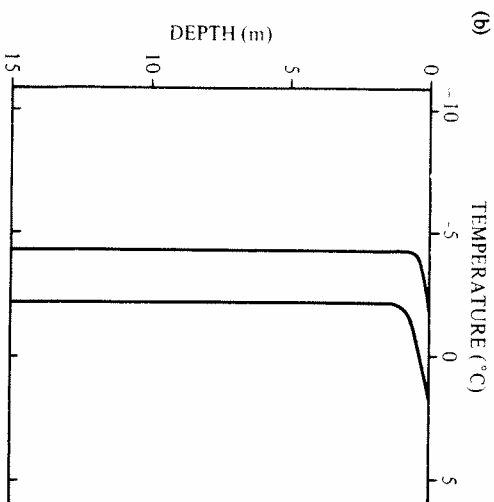
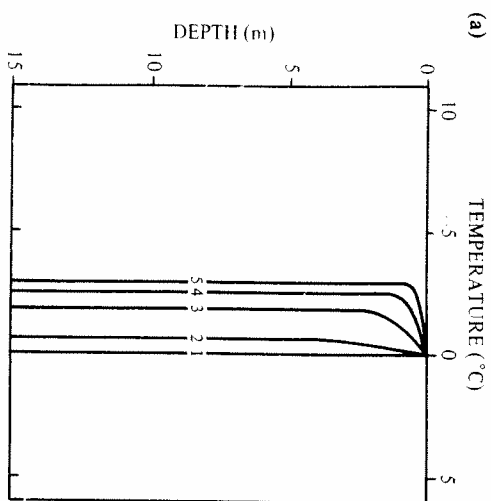


Figure 4.15 (a) Mean annual temperature profiles in relation to the ratio of frozen to unfrozen thermal conductivity; (b) Significance of the thermal offset near 0°C. (From Goodrich, 1978). Profiles are shown without the influence of the geothermal gradient.

balance: the ratio of wet to dry thermal conductivity is about 30 for peat (Fitzgibbon, 1981). Since this seasonal trend is generally the same as for the frozen/thawed variation, the effect mentioned above is reinforced. Recently, Nelson *et al.* (1985) have demonstrated that non-purely conductive processes of heat transfer (i.e. vapour transport) may be responsible for the thermal buffering effect of peat layers in summertime.

Overall, these effects can lead to the existence of permafrost in locations where the mean annual *surface* temperature is actually above 0°C (Figure 4.15(b)); see also Lindsay & Odynsky, 1965; Zoltai, 1971, for example).

In concluding this section, the reader is reminded that it is rare that any single factor alone can explain local ground thermal conditions. As discussed in Chapter 3, the ground thermal regime results from the interaction of climatic, surface and subsurface factors, and this is ultimately responsible for the (considerable) variations in ground temperatures which occur locally.

4.5 Lateral variations in ground temperatures

Until this point, we have considered only how ground temperature varies one-dimensionally with depth beneath the surface. This view would be quite adequate if it happened that the earth's surface temperature was uniform over large areas. In Chapter 3, however, it was emphasised that natural variations in microclimatic and terrain conditions introduce significant variations to the surface temperature regime within even a small area.

An important problem, therefore, both from a scientific and practical (engineering) viewpoint, is to determine the 'disturbance' of ground temperatures that result when the temperature within some finite boundary differs from that of the surrounding area. Such conditions could pertain to the presence of natural features such as shorelines, lakes and rivers, or to modifications of the surface as a result of vegetation removal, buildings, or highways. At geomorphological time-scales, when conditions approach the steady state, the purely transient effects of latent heat become negligible and such problems can be analysed by means of simple heat conduction models. However, as stated previously, detailed engineering analyses of transient problems, for time-scales measured in decades, generally require more complex numerical approaches.

The theoretical aspects of three-dimensional heat conduction in a semi-infinite medium disturbed by surface effects, have been treated by Lachenbruch (1957*a, b*) and Carslaw & Jaeger (1959), while W. G. Brown (1963) and Lunardini (1981) present a number of worked examples.

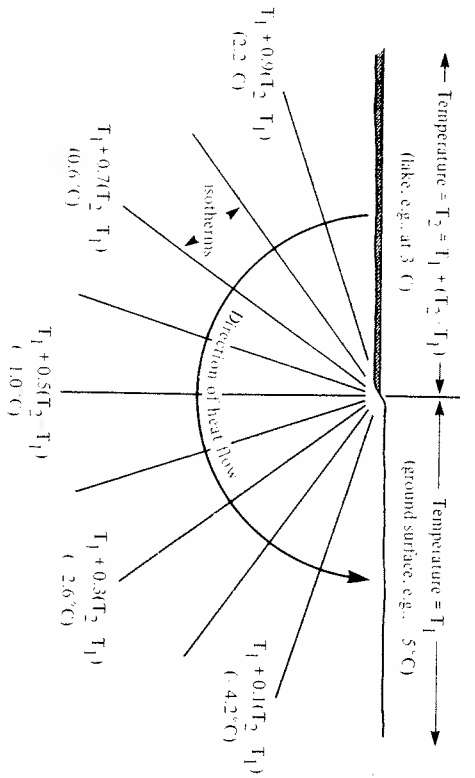


Figure 4.16 Steady-state temperatures beneath the shoreline of a large lake (from W. G. Brown, 1963).

4.5.1 Influence of water bodies

In high latitudes, bodies of water that do not freeze to the bottom in winter have a marked effect upon ground temperatures and the local configuration of permafrost. This arises from the fact that the mean annual bottom temperature must be greater than 0°C, whereas the temperature of the neighbouring land surface may be -5°C or lower. The presence of a water body thus constitutes a heat source, giving rise to anomalous heat flow and temperature conditions in the ground (Figure 4.16). According to the results of Brewer (1958a, b), Johnson & Brown (1964) and Smith (1976), where the mean annual air temperature is as low as -10° to -15°C, even relatively shallow lakes do not freeze to the bottom. This is especially so where the snow cover on top of the ice is sufficient to limit downward freezing. Wherever water bodies remain unfrozen at depth, permafrost is affected (Figure 4.17). The size and temperature of the water body are important factors (see below). Hopkins *et al.* (1955) reported that permafrost is absent or lies at great depths beneath lakes and ponds throughout Alaska. The thermal effects of water bodies constitute the greatest local departures of ground temperatures from any systematic geographical patterns determined by climate.

Under steady-state conditions, the normal geothermal temperature

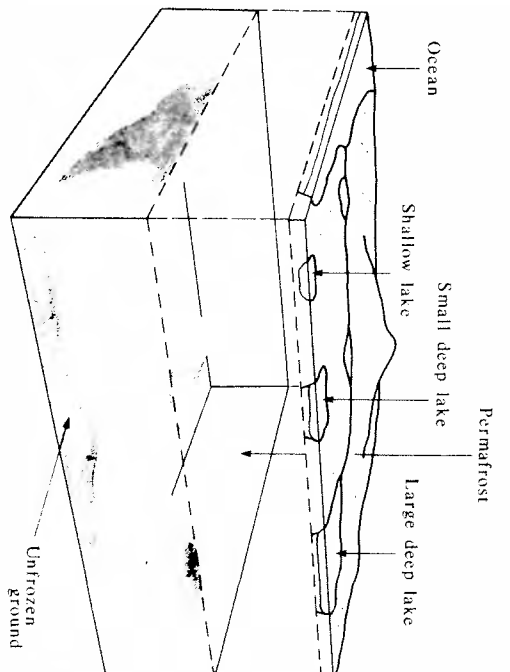


Figure 4.17 Schematic representation of permafrost configuration beneath water bodies (from Gold & Lachenbruch, 1973).

profile (equation (4.11)) is modified in the vicinity of a water body as follows:

$$T(z) = (T_s + Ggz) + (T_w - T_s) \cdot \Phi(x, y, z) \tag{4.26}$$

where the second term on the right-hand side is the thermal disturbance at the point (x, y, z) in the ground due to the water body, or water bodies nearby (as illustrated in Figure 4.16). This term can be calculated for any arbitrarily-shaped area, by dividing it into sectors of a circle, θ (Figure 4.18(a)), and summing the effects. In this case:

$$\Phi(x, y, z) = \sum \frac{\theta}{360} \left[1 - \frac{z}{(z^2 + R^2)^{1/2}} \right] \tag{4.27}$$

(Lachenbruch 1957a). By repeating the procedure for various (x, y, z)s, a complete picture of the temperature field created by the disturbance can be compiled. For locations lying outside the boundary of the feature, the disturbance is obtained by subtracting the effects due to sectors of radii R_1 from those with radii R_2 (Figure 4.18(b)). The method is easily extended to more complex areas (Figure 4.18(c)). Lachenbruch (1957b) has described special solutions for estimating the thermal effects of rivers and ocean shorelines.

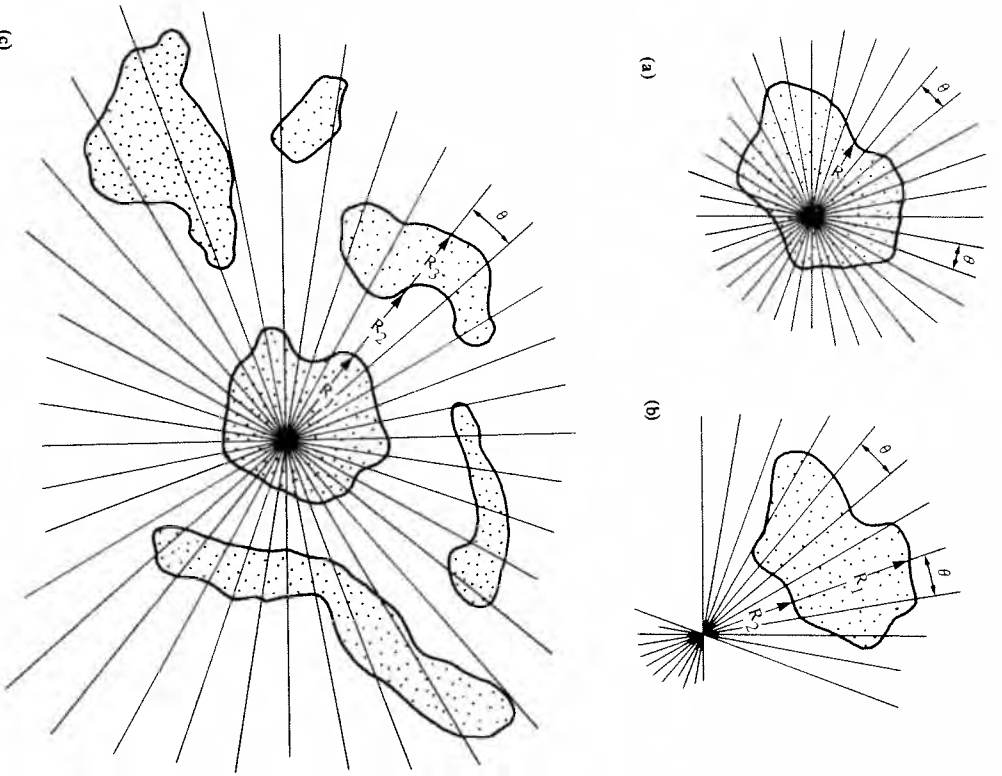


Figure 4.18 Method of dividing a given surface area into sectors of circles (from W. G. Brown, 1963).

Using the approach outlined above, Smith (1976) calculated ground temperatures and permafrost configuration within an area of the Mackenzie Delta (Figure 4.19). In this example, permafrost shows a steeply plunging surface at the edge of the river and the large lake. Beneath the

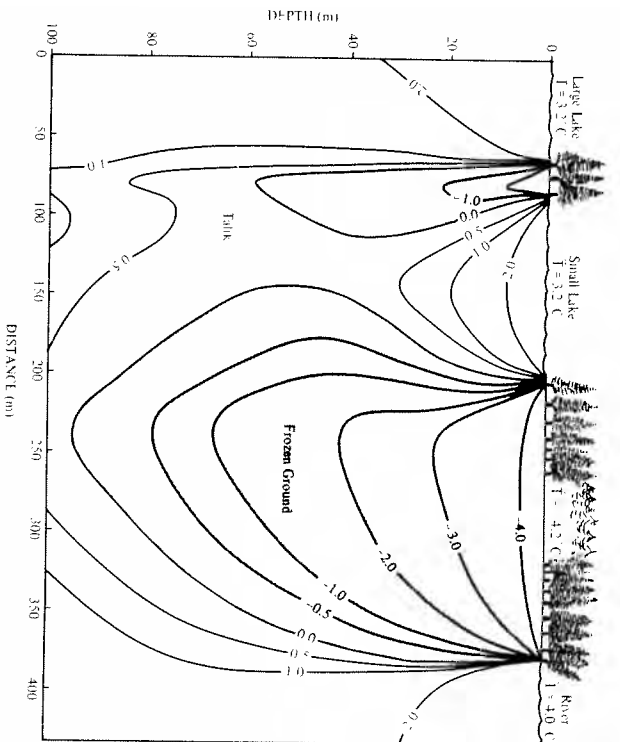


Figure 4.19 Calculated temperatures and permafrost configuration (from Smith, 1976).

small lake, the thermal effect is sufficient only to form an hour-glass-shaped *talik*. The maximum permafrost thickness is 95 m, but beneath the narrow isthmus it is only 60 m. Equations (4.26) and (4.27) were used by W. G. Brown *et al.* (1964) to calculate the ground temperatures beneath a small lake in permafrost, and Mackay (1963) used the simplified form for a circular lake, in his explanation of pingo formation.

In the case of a circular lake, of radius R , the steady-state thermal disturbance beneath the centre can be calculated from:

$$\Phi(z) = \left[1 - \frac{z}{(z^2 + R^2)^{1/2}} \right] \quad (4.28)$$

This expression is plotted in Figure 4.20. Using this, we may calculate the ground temperature disturbance at a depth of 20 m below the centre of a circular lake which has a radius of 100 m. R/z is equal to 5 and from Figure 4.20, Φ is equal to 0.8. If we assume that the mean lake bottom temperature, T_w , is 3°C, and that for the surrounding land area, T_s , is -7°C, then:

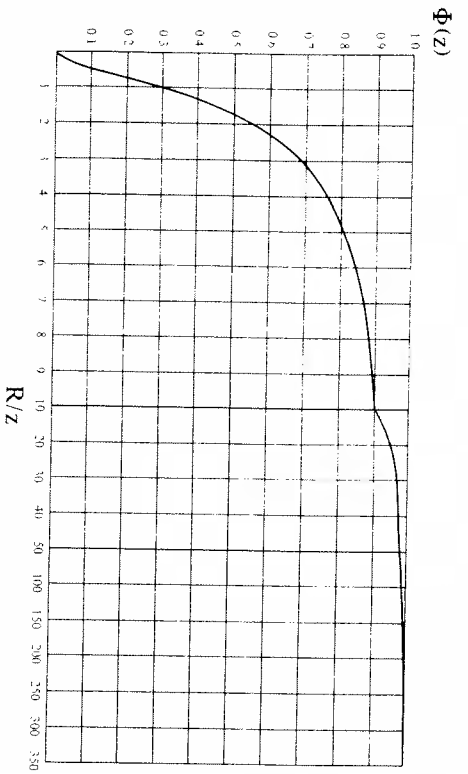


Figure 4.20 Function for the steady-state temperature disturbance of a circular lake (from W. G. Brown, 1963).

$$\Phi(T_a - T_s) = (0.8) \cdot (10^\circ\text{C}) = 8^\circ\text{C}$$

That is, the ground at this location is 8° warmer than it would be in the absence of the lake. The actual temperature can be calculated from equation (4.26). Assuming a geothermal gradient of 20 K km^{-1} , the temperature would be:

$$T_{30} = (-7 + 20 \times 0.02) + 8 = 1.4^\circ\text{C}$$

and thus the ground at this point would be unfrozen.

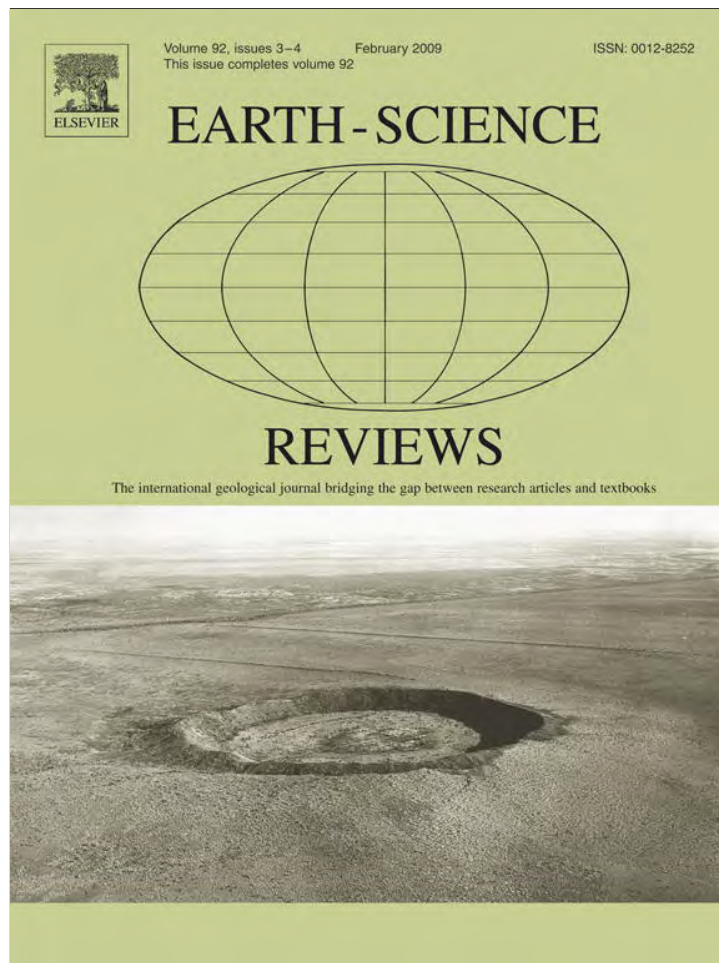
4.6 Summary

In summary, the thermal conditions in the ground can be viewed as the combined outcome of a number of effects. First, the flow of heat from the earth's interior, together with the thermal conductivity of earth materials, establishes a steady state profile (increase) of temperature with depth. Superimposed upon this are the seasonal (periodic) variations of temperature in the upper 10 to 20 metres of the ground induced by the annual regime of climate and modified by snow cover and ground thermal properties. Where the thermal properties are strongly temperature dependent, the seasonal fluctuation may impart a characteristic offset to the mean temperature profile. Superimposed upon this long-term steady state picture are the transient effects associated with shifts in the surface temperature

regime as a result of climatic change, vegetation change, submergence or geomorphic activity for example. A number of such effects, operating at different time scales, may be present simultaneously. Finally, lateral variations in surface temperature, as a result of terrain and/or hydrological conditions, or microclimatic differences, produce distinct spatial variations in ground thermal conditions.

Each of these effects can be considered in terms of heat conduction theory. Together, the expressions presented in this chapter provide insights into understanding the relationship between the temperature of the ground and the dynamic climatological and geomorphic processes that modify the surface terrain and energy regime.

Provided for non-commercial research and education use.
Not for reproduction, distribution or commercial use.



This article appeared in a journal published by Elsevier. The attached copy is furnished to the author for internal non-commercial research and education use, including for instruction at the authors institution and sharing with colleagues.

Other uses, including reproduction and distribution, or selling or licensing copies, or posting to personal, institutional or third party websites are prohibited.

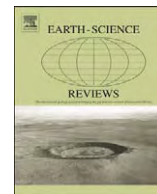
In most cases authors are permitted to post their version of the article (e.g. in Word or Tex form) to their personal website or institutional repository. Authors requiring further information regarding Elsevier's archiving and manuscript policies are encouraged to visit:

<http://www.elsevier.com/copyright>



Contents lists available at ScienceDirect

Earth-Science Reviews

journal homepage: www.elsevier.com/locate/earscirev

Permafrost and climate in Europe: Monitoring and modelling thermal, geomorphological and geotechnical responses

Charles Harris^{a,*}, Lukas U. Arenson^b, Hanne H. Christiansen^c, Bernd Etzelmüller^d, Regula Frauenfelder^d, Stephan Gruber^e, Wilfried Haeberli^e, Christian Hauck^f, Martin Hölzle^e, Ole Humlum^d, Ketil Isaksen^g, Andreas Kääh^d, Martina A. Kern-Lütschg^a, Michael Lehning^h, Norikazu Matsuokaⁱ, Julian B. Murton^j, Jeanette Nötzli^e, Marcia Phillips^h, Neil Ross^k, Matti Seppälä^l, Sarah M. Springman^m, Daniel Vonder Mühllⁿ

^a School of Earth and Ocean Sciences, Cardiff University, CF10 3YE, UK

^b Department of Civil and Environmental Engineering, University of Alberta, Edmonton, Alberta, Canada T6G 2W2

^c Department of Geology, The University Centre in Svalbard, 9171 Longyearbyen, Norway

^d Department of Geosciences, University of Oslo, Blindern, NO-0316 Oslo, Norway

^e Department of Geography, University of Zurich, CH-8057 Zurich, Switzerland

^f Institute for Meteorology and Climate Research, Karlsruhe Institute of Technology, 76131 Karlsruhe, Germany

^g The Norwegian Meteorological Institute, Blindern, 0313 Oslo, Norway

^h WSL, Swiss Federal Institute for Snow and Avalanche Research, SLF Davos, CH-7260 Davos Dorf, Switzerland

ⁱ Graduate School of Life and Environmental Sciences, University of Tsukuba, Ibaraki 305-8572, Japan

^j Department of Geography, University of Sussex, Brighton, BN1 9SJ, UK

^k School of Geosciences, University of Edinburgh, West Mains Road, Edinburgh EH9 3JW, UK

^l Department of Geography, University of Helsinki, Helsinki, FIN-00014, Finland

^m Geotechnical Institute, ETH Zurich, CH-8093 Zürich, Switzerland

ⁿ The Swiss Initiative in Systems Biology, ETH-Zürich, CH-8092 Zürich, Switzerland

ARTICLE INFO

Article history:

Received 13 July 2007

Accepted 5 December 2008

Available online 24 December 2008

Keywords:

European permafrost
climate change
geothermal monitoring
geothermal modelling
geophysics
slope stability
permafrost hazards
permafrost engineering

ABSTRACT

We present a review of the changing state of European permafrost within a spatial zone that includes the continuous high latitude arctic permafrost of Svalbard and the discontinuous high altitude mountain permafrost of Iceland, Fennoscandia and the Alps. The paper focuses on methodological developments and data collection over the last decade or so, including research associated with the continent-scale network of instrumented permafrost boreholes established between 1998 and 2001 under the European Union PACE project. Data indicate recent warming trends, with greatest warming at higher latitudes. Equally important are the impacts of shorter-term extreme climatic events, most immediately reflected in changes in active layer thickness. A large number of complex variables, including altitude, topography, insolation and snow distribution, determine permafrost temperatures. The development of regionally calibrated empirical-statistical models, and physically based process-oriented models, is described, and it is shown that, though more complex and data dependent, process-oriented approaches are better suited to estimating transient effects of climate change in complex mountain topography. Mapping and characterisation of permafrost depth and distribution requires integrated multiple geophysical approaches and recent advances are discussed. We report on recent research into ground ice formation, including ice segregation within bedrock and vein ice formation within ice wedge systems. The potential impacts of climate change on rock weathering, permafrost creep, landslides, rock falls, debris flows and slow mass movements are also discussed. Recent engineering responses to the potentially damaging effects of climate warming are outlined, and risk assessment strategies to minimise geological hazards are described. We conclude that forecasting changes in hazard occurrence, magnitude and frequency is likely to depend on process-based modelling, demanding improved understanding of geomorphological process-response systems and their impacts on human activity.

© 2008 Published by Elsevier B.V.

* Corresponding author. School of Earth and Ocean Sciences, Cardiff University, Main Building, Park Place, Cardiff CF10 3YE, UK. Tel.: +44 2920 874336; fax: +44 2920 874326. E-mail address: harrisc@cardiff.ac.uk (C. Harris).

Contents

1.	Introduction	119
2.	Holocene climate and permafrost evolution	119
2.1.	Context	119
2.2.	The Western Arctic and Sub Arctic Maritime Zone: Iceland	121
2.3.	The Eastern Arctic and Sub Arctic Maritime Zone: Svalbard	121
2.4.	Northern Continental Europe	122
2.5.	Central Europe	122
2.6.	European climate during the 20th century	122
3.	Monitoring permafrost temperatures and active layer thickness	124
3.1.	Geothermal conditions in mountain permafrost	124
3.2.	The European mountain permafrost borehole network	126
3.3.	Active layer thickness	126
3.4.	Permafrost temperature profiles	127
3.5.	Recent trends in permafrost temperatures	128
4.	Modelling mountain permafrost thermal condition and spatial distribution	130
4.1.	Modelling approaches	130
4.2.	Spatial and temporal scales of permafrost distribution modelling	131
4.3.	Recent developments	131
4.4.	Regional-scale modelling	132
4.5.	Local-scale modelling	132
4.6.	The significance of snow	134
4.7.	Validation	134
4.8.	Perspectives on mountain permafrost modelling	135
5.	Geophysical characterisation of frozen ground	135
5.1.	Geophysical properties	135
5.2.	Resistivity surveys	136
5.3.	Electromagnetic induction mapping	138
5.4.	Ground Penetrating Radar (GPR)	138
5.5.	Refraction seismic techniques	139
5.6.	Crosshole methods	139
5.7.	Combined geophysical measurements	139
5.8.	Monitoring permafrost change	140
6.	Rock weathering	141
6.1.	Ice segregation in frozen bedrock: laboratory and field evidence	142
6.2.	Temporal scales of frost weathering	143
7.	Rockfalls and rockslides	143
7.1.	Field monitoring of annual debris production from rock walls	143
7.2.	The role of permafrost in the initiation of rockfall events	144
7.3.	Mechanisms leading to rock fall	144
7.4.	Modelling near-surface rock temperature response to changing boundary conditions	145
7.5.	The significance of scale in a warming climate	146
8.	Creeping permafrost: rock glaciers and climate	146
8.1.	Rock glacier thermal condition	146
8.2.	Rock glacier dynamics	146
8.3.	Geotechnical properties of coarse frozen soils in relation to permafrost creep	147
8.4.	Measurement of rock glacier creep	147
8.5.	Observed creep rates	148
8.6.	Spatial modelling of rock glacier distribution and its response to changing climate	148
8.7.	Environmental change and rock glacier dynamics	148
9.	Thaw-related mass movement processes: solifluction and debris flows	149
9.1.	Slow mass movements (solifluction)	149
9.2.	Field and laboratory studies of solifluction processes	150
9.3.	Debris flows and related phenomena on thawing soil-covered slopes	151
10.	Ground ice phenomena	152
10.1.	Ice wedge formation and climate	152
10.1.1.	Thermal conditions for present-day ice wedge activity in Svalbard	152
10.1.2.	Ice wedge formation and decay in relation to climate change	153
10.2.	Palsa formation in relation to climate	154
11.	Permafrost engineering in a changing climate	155
11.1.	Introduction	155
11.2.	Characteristics of alpine permafrost soils	156
11.3.	Accounting for climate change	156
11.3.1.	Assessing ground conditions	156
11.4.	Modification of ground thermal conditions	157
11.5.	Technical solutions	157
11.6.	Long term monitoring of structures and substrates in mountain permafrost	157
11.7.	Engineering in mountain permafrost: the challenge of climate change	157
12.	Permafrost hazards	158
12.1.	Creeping frozen debris	158
12.2.	Warming permafrost on soil-covered slopes	158

12.3.	Warming permafrost in rock walls	158
12.4.	Glacier-permafrost interactions	159
12.5.	Emerging methodologies and challenges	159
12.6.	Mapping	160
12.7.	Modelling.	160
12.8.	Ground-based methodologies	160
12.9.	Challenges	160
13.	Conclusions	160
	Acknowledgements	162
	References.	162

1. Introduction

Permafrost (perennially frozen ground) forms a major element of the global cryosphere and since it is thermally defined as ground that remains below 0 °C for at least two years (Permafrost Subcommittee NRC Canada, 1988), is particularly sensitive to climate change (Haeberli and Hohmann, 2008). The relationship between mean ground temperatures and mean air temperatures reflects complex interaction between a range of variables including aspect, surface cover, soil moisture status and winter snow depth (Burn, 2007). As a result, mean annual ground surface temperatures may vary by many degrees within a given region. In addition, the higher thermal conductivity of the frozen active layer in winter than the thawed active layer in summer results in mean annual temperature at the permafrost table somewhat lower than mean annual ground surface temperature (the difference is known as the “thermal offset”). This thermal offset is strongly influenced by moisture status. Thus ground temperatures may be spatially variable, and permafrost is frequently discontinuous in the sub arctic and in mid-latitude high mountains.

In this paper we review the current status of European permafrost, its response to past, present and likely future climate change, the likely impact this will have on periglacial landforms and processes, and potential consequences regarding hazard and risk to human infrastructure. A major stimulus for this research was the international project “Permafrost and Climate in Europe” (PACE) that commenced in 1997 (see Harris et al., 2001a), funded by the European Union, and subsequently the PACE21 programme (2003–2006) sponsored by the European Science Foundation. The present paper includes reference to earlier research and to parallel studies, but its focus is on the progress made in this last decade of European research. A number of national and international programmes continue to develop permafrost research in Europe and elsewhere; many under the auspices of the International Polar Year (see Brown et al., 2008; Romanovsk et al., 2008).

The geographical area considered here is the European sector, defined approximately by lines of longitude 30°E to 25°W, including Svalbard, Iceland, Fennoscandia and the Alps, but excluding Greenland and Russia (Fig. 1). In this zone, permafrost occurs largely in mountainous regions, in bedrock, superficial sediments, and sometimes in association with glaciers. The major regional contrast is between the Arctic Archipelago of Svalbard, and the lower latitude higher altitude mountains of Scandinavia and the Alps. In Svalbard, permafrost is continuous outside the glacier covered areas, and glaciers are polythermal, with permafrost extending beneath their margins. Interaction between glacier and permafrost therefore leads to distinctive depositional processes and landform assemblages (see Etzelmüller and Hagen, 2005). In lower latitude mountains, permafrost is discontinuous or sporadic (Brown et al., 1997) (Fig. 1), and glaciers are generally warm-based, though at higher elevations permafrost may well extend to cold-based glacier margins (Haeberli, 2005; Kneisel, 2003). In the high mountains, permafrost is strongly influenced by altitude and aspect (e.g. Hoelzle et al., 2001; Etzelmüller et al., 2001a), and recent progress in mapping and modelling permafrost distribution is discussed. In many cases, ground tempera-

tures are only a few degrees below zero, so that European mountain permafrost is highly sensitive to projected climate changes in the 21st century. Literature on the distribution and character of discontinuous and sporadic permafrost in European mountains was reviewed by King and Åkerman (1993), who included reference to permafrost occurrences in the Pyrenees, Carpathians and parts of European Russia, areas that are not discussed in the present paper.

A major goal of the PACE Project was to establish a continental scale north-south transect of permafrost monitoring stations, and this was achieved through drilling six deep (>100 m) boreholes in frozen bedrock (Fig. 1) over the period 1998 to 2001. Data from a borehole drilled through ice-rich frozen debris in 1987 at Murtèl–Corvatsch, Switzerland, have also been included, and are discussed in this paper. The PACE borehole network provides a regional framework for long-term European permafrost monitoring within the context of the worldwide monitoring network of WMO, ICSU and other international organisations (Global Terrestrial Network on Permafrost, GTN-P, contributing to GCOS/GTOS, see for instance, Cihlar et al., 1997, Harris et al., 2001a). This network corresponds to Tier 1 (Large Transect) in the global hierarchical observing strategy (GHOST) of GTN-P (Harris and Haeberli, 2003), and is the basis for the present discussion on the current thermal status of European permafrost. Details of each borehole are given in Table 1. Further European networks of shallow boreholes are currently being established in order that local variability in permafrost thermal regime and detailed changes in permafrost distribution may be established (see for instance, Vonder Mühl et al., 2007, 2008).

The sensitivity of permafrost terrain to global warming has recently been emphasised (e.g. Nelson et al., 2001, 2002; Jorgenson et al., 2006) but attention has mainly been paid to arctic regions. The present thermal status of European permafrost reflects not only the prevailing environmental conditions, but also past climate cycles, since the response to perturbations in the upper boundary (ground surface) thermal condition are often of longer duration than that of the forcing climate signals. In the longer term, permafrost has evolved under the major climatic cycles of the Pleistocene. However the focus here is on responses to 20th and early 21st Century climate change, for which more recent and less extreme Holocene climate fluctuations provide the main context, and these are therefore briefly reviewed before we discuss the current and potential future status of European permafrost.

2. Holocene climate and permafrost evolution

2.1. Context

In the Northern Hemisphere, summer insolation peaked at 10–9 ka BP, when the last remnants of the large ice sheets retreated rapidly. Incoming solar radiation was approximately 40 W/m² higher than now (Berger and Loutre 1991). Since then the Northern Hemisphere summers have seen gradually decreasing incoming solar radiation. This has been important, especially for high latitudes during summer when daylight persists for 24 h (Bradley 1990). The late Holocene was punctuated by a number of 400–800 yr periods with either relatively warm or cold climate, such as the Medieval Warm Period (MWP; c. AD

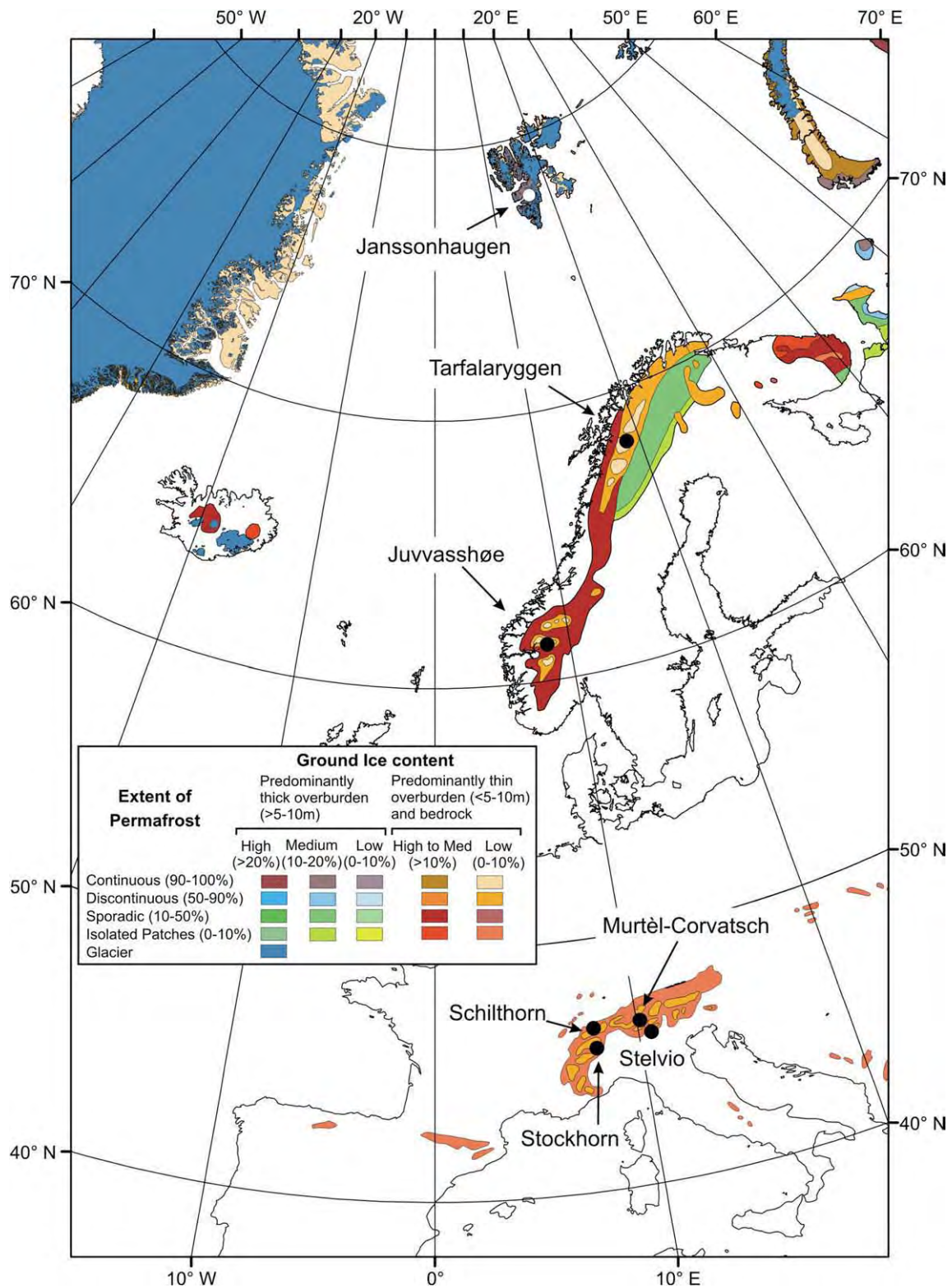


Fig. 1. Distribution of permafrost in the European sector according to the IPA Circum-Polar Map of Permafrost (Brown et al., 1997). The location of PACE boreholes is shown.

800–1200) or the Little Ice Age (LIA; c. AD 1300–1900). This overall Holocene climatic development is reflected in many regions of Europe, but to varying degrees.

A number of attempts have been made to develop dynamic regional and global time series temperature reconstructions for the last 1000 years (Mann et al., 1999; Shaopeng et al., 2000; Briffa et al., 2001; Moberg et al., 2005). With few exceptions, these are based on

annually resolved proxies, particularly tree-rings, effectively limiting such studies to the last millennia when annual archives are widely available (Bradley, 1999). Observational evidence and numerical models suggest that climatic variability in large parts of Europe is closely linked to changes in the North Atlantic atmospheric and thermohaline circulation (for a recent overview, see Meincke 2002). The intensity of North Atlantic oceanic circulation governs energy

Table 1
Details of the PACE permafrost monitoring network

PACE boreholes and test sites		Janssonhaugen Svalbard Norway	Tarfalaryggen Lapland Sweden	Juvvashøe Jotunheimen Norway	Schiltthorn Bernese Oberland, Switzerland	Stelvio Pass Lombardia, Italy	Murtèl-Corvatsch Oberengadin Switzerland	Stockhorn Plateau Wallis Switzerland
Site description	Latitude	78°10'45" N	67°55' N	61°40'32" N	46°33'34" N	46°30'59" N	46°26' N	45°59'17" N
	Longitude	16°28'15" E	18°38' E	08°22'04" E	07°50'10" E	10°28'35" E	09°49'30" E	07°40'31" E
	Elevation a.s.l.	275 m	1540 m	1894 m	2909 m	3000 m	2670 m	3410 m
	Topography	Hill	Ridge	Plateau	Slope	Summit,	Rock glacier	Plateau on crest
	MAAT	-8 °C (estimated)	-6 °C (Estimated)	-4.5 °C (Estimated)	-4.3 °C	-3.7 °C (Sep 98–Sep 99)	-3 °C	-5.5 °C (Estimated)
1st borehole	Drilling date	April 1998	March 2000	April 1999	August 2000	1998	May/June 1987	July 2000
	Depth	102 m	100 m	129 m	101 m	100.3 m	62 m	100.7 m
	Chain length	(Vertical) 100 m	(Vertical) 100 m	(Vertical) 100+129 m	(Vertical) 100 m	(Vertical) 100 m	(Vertical) 58 m	(Vertical) 100 m
2nd borehole	Thermistor depths	PACE standard	PACE standard	PACE standard	PACE standard	24 (0.02–100 m)	52 (0.6–58 m)	PACE standard
	Drilling date	May 1998	March 2000	August 1999	October 1998			August .2000
	Depth	15 m	15 m	20 m	14 m			31 m
	Chain length	(Vertical)	(Vertical)	(Vertical)	(Vertical)			(Vertical)
	Thermistor	15 m	15 m	15 m	13.7 m			17 m
Depths	PACE Standard	PACE Standard	PACE Standard	PACE Standard			PACE Standard	

transfer to the atmosphere and regulates regional atmospheric pressure differences over Europe on timescales ranging from millennial to interannual (Hurrell 1995; Rodwell et al., 1999).

Climatic evolution is conveniently summarised by geographical subdivision into Arctic and Sub Arctic Maritime Europe, Northern Europe, and Central Europe, the latter two being roughly divided by the 55°N parallel. All dates quoted below are calibrated ages (calendar years).

2.2. The Western Arctic and Sub Arctic Maritime Zone: Iceland

In Iceland the early Holocene was characterized by progressive warming, rapidly retreating glaciers and development of a vegetation cover (e.g., Hallsdóttir, 1995; Ingólfsson et al., 1997). The Icelandic Holocene temperature maximum occurred between 8 and 4 ka BP, with summer temperatures 2–3 °C higher than present (Fig. 2) and extensive birch woodlands covering most of the lowlands (Einarsson, 1975; Hallsdóttir, 1995). The onset of colder and wetter climate began around 5 ka BP, and was marked by lowering of the mountain tree line and birch woods being replaced by heath and peatlands. By 4 ka BP

glaciers were expanding, but did not reach their Holocene maximum until the LIA in the later part of the 19th century (Gudmundsson, 1997). Given the high geothermal gradients that prevail in Iceland, much pre-existing permafrost probably disappeared rapidly during the mid Holocene climatic optimum, so that most of the present day Icelandic permafrost and associated landforms (palsas, rock glaciers and ice-cored moraines) were probably initiated during the onset of the late Holocene cooling c. 5 ka BP (Wangenstein et al., 2006), culminating in the Little Ice Age (Hamilton and Whalley, 1995).

2.3. The Eastern Arctic and Sub Arctic Maritime Zone: Svalbard

Sediment cores from the Nordic Seas near Svalbard indicate the first half of the Holocene to have been the warmest period during the last 13.4 ka (Koç et al., 1993) and in the Barents Sea, south of Svalbard, $\delta^{18}\text{O}$ data show early Holocene warming culminating between 9 and 6.5 ka BP (e.g., Ivanova et al., 2002). MAAT was 3–5 °C higher than today until c. 5 ka BP (e.g., Birks, 1991; Hjort, 1997; Salvigsen, 2002) (Fig. 2). Glacier margins on Svalbard and Franz Josef Land lay within the present ice limits until the Late Holocene, with high summer

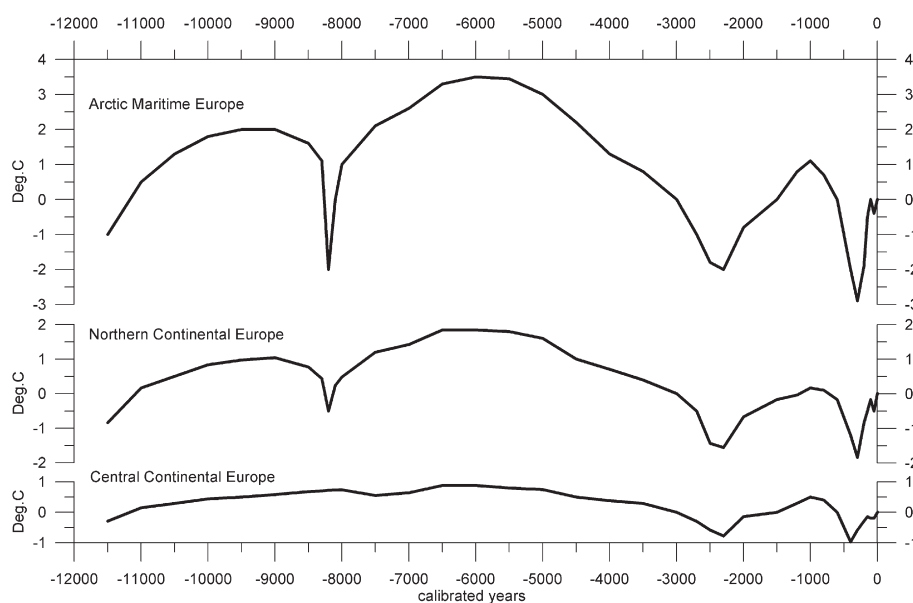


Fig. 2. Estimated Holocene air temperature changes in Arctic Maritime Europe, Northern Continental Europe and Central Continental Europe. Temperature units (vertical axes) approximate degrees Celsius, time axis in calibrated years. Modern temperature (late 20th century) is baseline for temperatures shown.

temperatures dominating glacier budgets (Svendsen and Mangerud 1997; Lubinski et al., 1999). After 5–4 ka BP the surface waters along western Svalbard cooled and air temperatures fell as the influence of Atlantic Water decreased (e.g. Koç and Jansen, 1994). Glacier expansion began in western Svalbard around 5–4 ka BP (Svendsen and Magerud, 1997), glaciers reaching a maximum around 2.3 ka BP and their Holocene maximum during the Little Ice Age (Furrer, 1994; Humlum et al., 2005). The long composite meteorological record from Svalbard indicates that MAAT during periods of the Little Ice Age was 4–6 °C below late 20th century values (Fig. 2).

Permafrost in many coastal locations probably disappeared in the early Holocene warm period, and was discontinuous to altitudes of 300–400 m (Humlum et al., 2003; Humlum, 2005). In the main trunk valleys, permafrost was presumably eliminated by warm-based Weichselian glaciers (Humlum et al., 2003). Permafrost development was apparently controlled by Holocene cooling after around 3 ka BP (e.g. Büdel, 1977; Svensson, 1971; Jeppesen, 2001). Below the early Holocene marine limit (c.70–80 m asl.), permafrost evolution has been partly controlled by emergence totalling 15–30 m in eastern Svalbard and 5–10 m in western and central areas since 5 ka BP (Forman et al., 2004).

2.4. Northern Continental Europe

Holocene temperature variations in Northern Europe were apparently greatest in the NE and decreased towards the SW. Early Holocene summer temperatures were similar to today in Northern Scandinavia (e.g., Seppä and Birks, 2001) and Western Norway, (e.g., Karlén, 1998; Lauritzen and Lundberg, 1999) and the tree-line appears to have been close to its present position (e.g., Dahl and Nesje, 1996). Warming by 9.5–9 ka BP led to migration of pine forests and reduction in glaciers (Hyvärinen 1975; Karlén, 1988; Eronen and Zetterberg, 1996; Barnekow and Sandgren, 2001; Seierstad et al., 2002) and between 8 and 5.8 ka BP, MAAT rose to 2.5 °C, some 3 °C higher than today (e.g. Kultti et al., 2006), and glaciers in southern Norway virtually disappeared (Nesje and Kvamme, 1991; Nesje et al., 2000). Cooling, glacier expansion and tree line retreat followed (e.g., Korhola et al., 2002; Nesje et al., 2001; Matthews et al., 2005), with the periods 4.35–3.35 ka BP and post 1.35 ka BP having the severest winters during the entire Holocene (Blikra and Selvik, 1998).

During the succeeding Medieval Warm Period between AD 980 and 1250, winter air temperatures in Finland were up to 2 °C warmer than today (Tiljander et al., 2003) (see Fig. 2) although July temperatures were only marginally warmer (Seppä and Birks, 2002). Subsequent cooling in the Little Ice Age of the 18th–19th centuries saw glaciers in Norway reach their greatest Neoglacial extent (Nesje, 1992), with summer temperatures 0.5 to 1.6 °C lower than the reference period 1949–1963 (Matthews, 1976).

The mid-Holocene altitudinal limit for permafrost in Northern Europe probably lay around 150–300 m higher than today though local changes in snow cover duration and timing may have reduced or enhanced this altitudinal difference. The period from 5 ka BP to the Little Ice Age was characterised by lowering of permafrost altitudinal limits, though during the Medieval Warm Period the trend would have been reversed. Thermal inertia arising from latent heat effects would have limited complete permafrost degradation to marginal zones of ice-poor bedrock, and it is likely that present day permafrost distribution is currently adjusting to the warmer 20th century climate but still largely reflects that of the Little Ice Age (Juliussen and Humlum, 2008).

2.5. Central Europe

Generally, climate reconstructions from Central Europe do not show the large and coherent Holocene warming and cooling trends that characterise Northern Europe. On the basis of plant macrofossil and pollen evidence, Haas et al. (1998) suggest summer temperatures 0.7–0.9 °C above present values in the early Holocene. Following this period, temperature fluctuations within 1.0 °C of modern values have been reported (e.g. Haas et al., 1998; Davis et al., 2003) and alpine glaciers have responded periodically to such fluctuations (Hormes et al., 2001). The mid-Holocene thermal maximum at around 6 ka BP was more clearly defined in the west than in the east (Davis et al., 2003), and saw tree lines at their maximum altitudes (Haas et al., 1998; Wick and Tinner, 1997) though in NW Italy, the timberline was 100–200 m higher than today (Burga, 1991), corresponding to summer temperatures 1.5–3.0 °C above present day. Following the Holocene thermal maximum, summer temperatures declined in the west, although winter temperatures continued to increase (Davis et al., 2003). Alpine timberlines retreated (Tinner et al., 1996), and after 4.5 ka BP, bog surfaces were wetter (Barber et al., 1994).

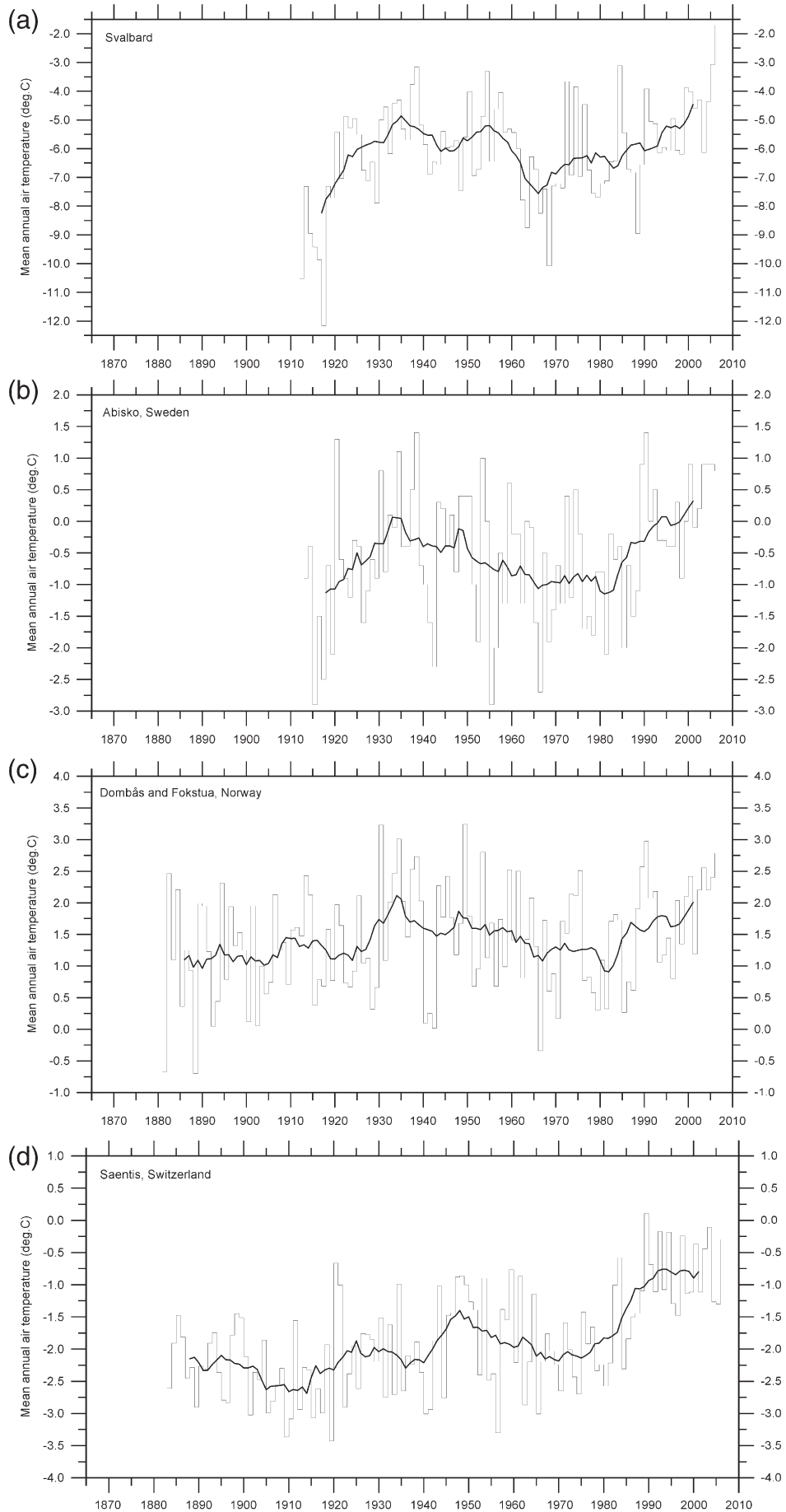
The Medieval Warm Period, between AD 800 and 1100, led to glacier retreat in Switzerland (Holzhauser et al., 2005) and was followed by transition to the Little Ice Age. MAAT fell by about 1.5 °C (Filippi et al., 1999) culminating around AD 1850–1860 when Alpine glaciers reached their late Holocene maximum. Fluctuation in the permafrost altitudinal limits in Central Europe were probably less marked than in Northern Europe and would have been strongly modulated by variations in snow depth and duration. Permafrost advance during cooling would probably have been more rapid than permafrost retreat during warming, due to the thermal inertia associated with latent heat. In the highest Alpine peaks, that penetrated the Weichselian glaciers as nunataqs, permafrost may have survived from the last glaciation.

2.6. European climate during the 20th century

It is generally agreed that European climate during the 20th century has been characterised by warming. Slonosky et al. (2000, 2001) investigated the variability of the surface atmospheric circulation over Europe from 1774 to 1995 and found that records suggest episodes of more intense meridional circulation from 1822 to 1870, and stronger zonal westerlies from 1947 to 1995. The zonal flow appears to have been considerably more variable with more extreme values in the late 18th and early 19th centuries than in the 20th century. Luterbacher et al. (2004) investigated European seasonal and annual temperature variability, trends, and extremes since 1500, using multiproxy reconstructions of monthly and seasonal surface temperature fields. They found that the late 20th- and early 21st-century European climate is likely to be warmer than that of any time during the past 500 years. In central and western Europe from 1901 to 1999, the dominant trend has been for increasing winter precipitation intensity and frequency of moderately extreme events (Moberg and Jones, 2005). The length of dry spells in summer generally increased during the 20th century. Both the warm and cold tails of the temperature distribution in winter rose over the entire 20th century but notably low values in the cold tail for daily maximum temperatures (Tmax) and daily minimum temperatures (Tmin) occurred in the early 1940s.

To provide a geographical overview of 20th century temperature changes within Europe, monthly meteorological data from 318

Fig. 3. Mean Annual Air Temperatures observed at selected meteorological stations in Europe, near PACE boreholes. Heavy lines show the 11 years unweighted running average. (a) Svalbard, (b) Abisko, Sweden, (c) Dombås and Fokstugu, Norway and (d) Saentis, Switzerland. Note that in (c) a constant of 1.3 °C has been added to the Fokstugu data (stippled), in order to simulate modern continuation of the old Dombås data series. Data sources: the Norwegian Meteorological Institute, the Abisko Research Station, and NASA Goddard Institute for Space Studies (GISS).



meteorological stations have been analysed. Data are largely derived from a database at the NASA Goddard Institute (GISS). All data have been homogenized, i.e. corrected for environmental change in the surroundings of the measuring instrument, and for errors arising at the point of measurement (known equipment or procedural faults, change of measuring site, change of surroundings, change of averaging method, etc.), before inclusion in the GISS database. However, some unknown inhomogeneities may still remain in the data set for some stations. A few series with missing data were encountered. In such cases, missing data were generated by comparison with the two nearest meteorological stations having continuous data for the months in question. Meteorological observations from 1880 to December 2005 have been used in the analysis.

Interannual temperature variations are known to be substantial, especially at high latitudes during winter. Both the global and the European mean annual air temperatures are characterised by 2–5 year oscillations which most likely are associated with oceanographic and volcanic effects. To reduce the influence of such short-term variations, the spatial pattern of change of 11 years unweighted running means was analysed, highlighting variability over longer time periods. Fig. 3 shows the mean annual air temperature (MAAT) record from selected meteorological stations. Several, but not all, display rising temperatures during the first 30–40 years of the 20th century, and then falling temperatures until 1970–1975, when a renewed temperature increase occurred. Thus, the climatic development within Europe during the observational period has not been uniform and in general, temperature variations (interannual, decadal or multi-decadal) tend to increase with latitude.

Selected time windows, centred on start and end year of the period considered, have been analysed to explore the spatial variability of climate trends. The calculated changes were spatially interpolated across the entire European continent between 32°N and 72°N (for mapping reasons Svalbard was omitted), using a standard kriging algorithm. This interpolation procedure is widely considered one of the more flexible interpolation methods, producing a smooth map with few “bulls' eyes”. The method is suitable for gridding almost any type of data set, especially those with a heterogeneous point distribution, such as the present meteorological data set (Polyak, 1996). The results of the spatial surface temperature analyses are shown in Fig. 4.

Between 1900 and 1940, MAAT increased in western and northern Europe (including Iceland), while most of the remaining part of Europe experienced only small changes. Due to their geographical locations, most of the PACE borehole sites experienced increasing air temperatures during this period, especially the two northernmost boreholes (Svalbard and Sweden). The period from 1940 to 1975 was one of widespread cooling in the Arctic, affecting Iceland and Svalbard (Fig. 4), but in continental Europe cooling was confined to the northern and western regions. At the same time, regions in Eastern Europe experienced slight warming and Central and Southern Europe experienced relatively minor changes.

Most of the PACE borehole sites in this period experienced relatively small changes in MAAT, again with the exception of the boreholes in Sweden and Svalbard (Figs. 3 and 4). Widespread climate warming has been recorded in Europe in the period 1975 to 2000. On an annual basis, this has been most pronounced in SW Europe and in central Scandinavia (Fig. 4). Seasonally, however, there are large regional deviations from these overall annual trends. Winters (Fig. 4, lower right panel, DJF) have been characterised by rising temperatures in western and northern Europe, especially within a region stretching from central Scandinavia to southern Russia. Spring (Fig. 4, lower right

panel, MAM) has been characterised by increasing temperatures over most of Europe, but most pronounced in the central and southwestern regions. Summers (Fig. 4, lower right panel, JJA) have warmed everywhere, but especially in southern Europe, and autumn temperatures (Fig. 4, lower right panel, SON) have been characterised by spatial variability.

All PACE borehole sites have been exposed to atmospheric warming in all seasons since 1975. The warming has been especially pronounced during the autumn and winter for the northernmost boreholes. For boreholes in central Europe the warming has been greatest during spring and summer. The response of near-surface permafrost temperatures to changes in air temperature are very strongly modulated by snow thickness and duration, and since the seasonal trends identified above also correspond to changes in snow regime, any attempt to model impacts of climate change on permafrost temperatures cannot be based simply on mean annual air temperatures and precipitation, but must also consider seasonal changes, with particular emphasis on snow cover thickness and duration.

3. Monitoring permafrost temperatures and active layer thickness

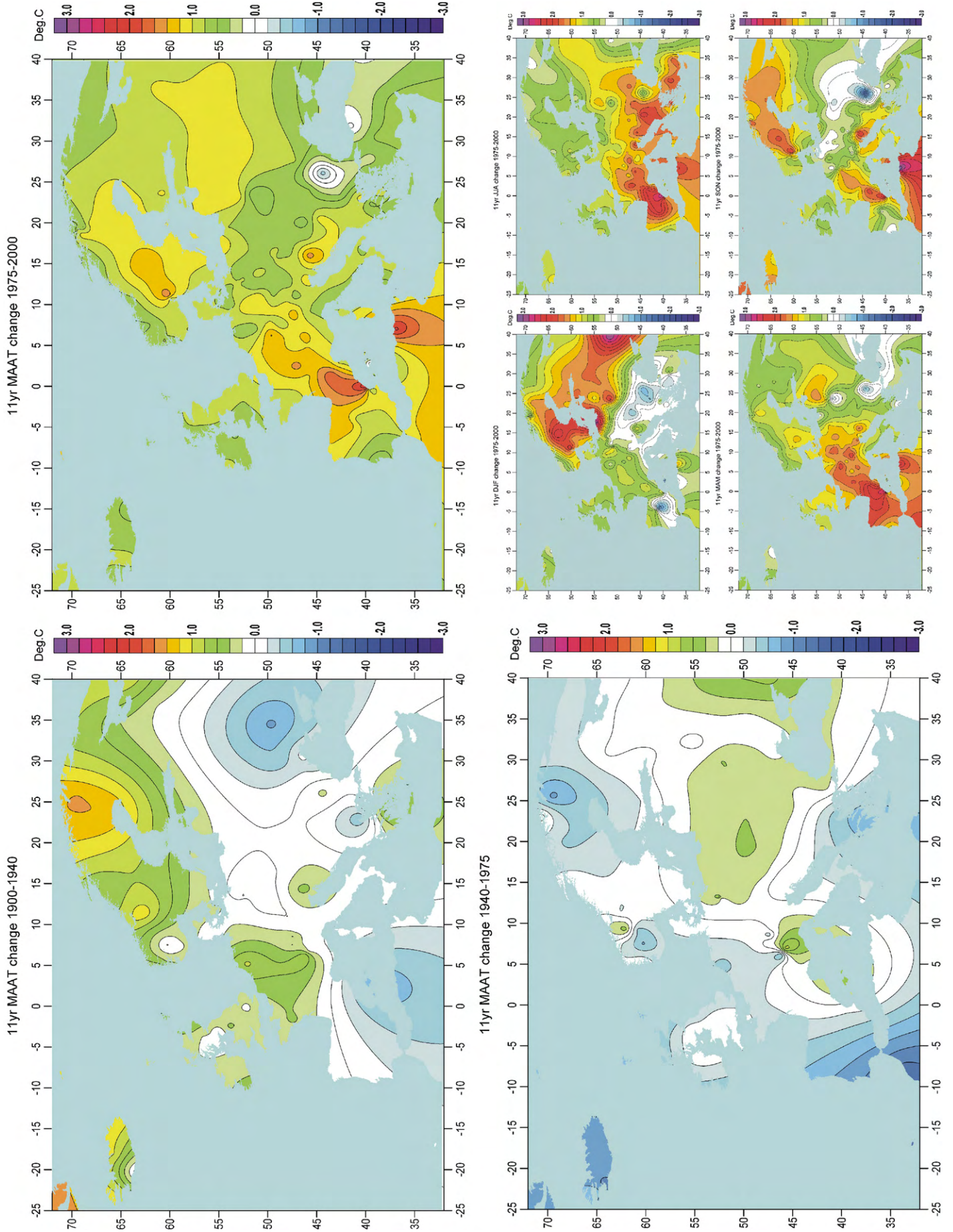
3.1. Geothermal conditions in mountain permafrost

The geothermal regime of mountain permafrost is strongly influenced by the nature of the ground surface (especially the temporal and spatial variability of snow cover, together with local topography), the nature of the substrate (spatial and depth variation in lithology and ice content) and the regional geothermal heat flux (see for instance Harris et al., 2003a,b). At lower elevations, local hydrology might also be significant. Time scales of climatically-forced cycles of ground surface temperature range from daily, through seasonal, annual, decadal, century to millennial, with corresponding differences in magnitude. Thus, geothermal profiles are generally in a transient state, continually adjusting to changes in the upper boundary temperature that propagate downwards into the ground (e.g. Beltrami and Harris, 2001).

Ground temperature data from permafrost boreholes are particularly well suited to the detection of changes in the surface boundary condition that can be interpreted as climate signals (e.g. Lachenbruch and Marshall, 1986), mainly because heat advection by ground water or air circulation is often negligible. The geothermal profile is, therefore, primarily a function of heat conduction, depending on heat flux from the Earth's interior and heat flux arising from the energy exchanges that occur at the ground surface. Downward propagation of temperature changes at the permafrost table may take considerable time, and is accompanied by progressive attenuation. The annual thermal cycle generally penetrates to a depth of 15–20 m, but larger perturbations in surface temperature of longer periodicity may penetrate much deeper and take much longer to do so. Thus, changes in the subsurface thermal gradient provide a record of the recent ground surface temperatures.

Geothermal time series obtained from monitoring of permafrost represent a systematic running mean that filters the higher frequency signal at the ground surface and preserves only the low frequency, long-term signals (cf. Lachenbruch and Marshall, 1986). Thus, records of ground temperatures below the depth of zero annual amplitude may provide direct evidence of thermal trends at the permafrost table during recent decades (e.g., Osterkamp and Romanovsky, 1999; Osterkamp, 2008; Cermak et al., 2000; Romanovsky and Osterkamp, 1995).

Fig. 4. Spatial distribution of changes in surface mean annual air temperature 1900–1940, 1040–1975 and 1975–2000, based on 11-year unweighted running temperature means, comparing unweighted averages for the periods 1895–1905, 1935–1945, 1970–1980 and 1995–2005. Temperature interval 0.2 °C. Lower right panel shows seasonal changes for the period 1975–2000. DJF = December, January, February, MAM = March, April, May, JJA = June, July, August, SON = September, October, November. Data sources the Norwegian Meteorological Institute, the Abisko Research Station, and NASA Goddard Institute (GISS).



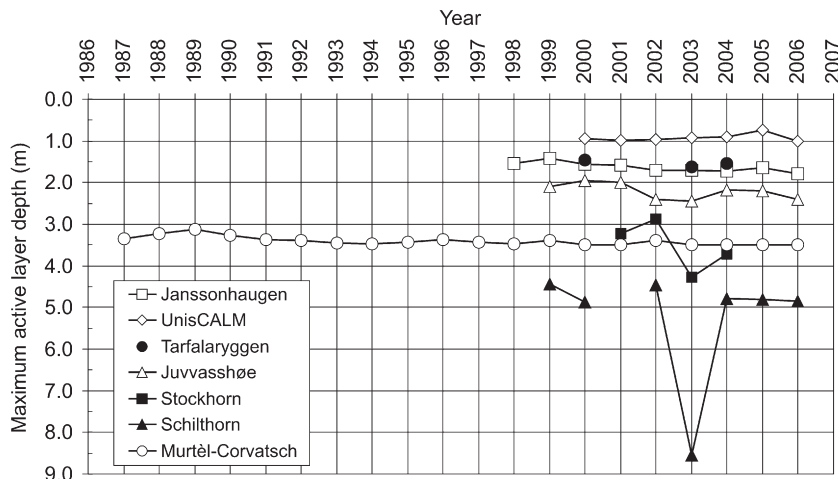


Fig. 5. Maximum annual active layer depth. The thickness of the active layer during each thaw season is estimated using an exponential best-fit between all thermistors in the boreholes. Daily temperature records are used. At Janssonhaugen and Juvvasshøe, data series were obtained from nearby 15–20 m deep control boreholes (Isaksen et al., 2001 see Table 1).

In the Arctic, the mean annual ground temperature and the thermal response of the surface to the passage of the seasons can vary significantly as one passes from, for instance, dry to wet habitats, gravel beaches, ponds, lakes and rivers (Gold and Lachenbruch, 1973). In addition, variable snow cover, especially in early winter, exerts an important influence on ground temperatures, causing strong lateral variations (e.g., Goodrich, 1982; Vonder Mühl et al., 1998; Zhang, 2005). In mountain permafrost, the problem of 3-dimensionality of the thermal field is complicated further by the often complex surface geometry and by strong spatial heterogeneity of the surface conditions and temperatures (Gruber et al., 2004c). Circulation of water and air within coarse blocks in typical steep slopes may result in highly variable and sometimes extreme thermal offsets (e.g., Hoelzle et al., 2001). Thus, permafrost ground temperatures may integrate effects of several processes involved in the heat transfer regime of the air-ground boundary. This integration modulates the thermal signal conducted downwards into the permafrost below. Therefore, interpretation of measured temperature profiles should be undertaken carefully, with particular attention being paid to the strong 3-dimensional effects of rugged alpine topography (Kohl, 1999; Gruber et al., 2004c) (see Section 7).

3.2. The European mountain permafrost borehole network

Currently seven boreholes form the core network of the PACE permafrost monitoring network (Fig. 1, Table 1) (Harris et al., 2003a,b). In the Alps, bedrock boreholes have been drilled and instrumented at Schilthorn (Vonder Mühl et al., 2000; Harris et al., 2001a, 2003a,b; Harris and Isaksen, 2008) and Stockhorn (Gruber et al., 2004c) in Switzerland and at the Stelvio Pass in Italy (Guglielmin et al., 2001). At Schilthorn an additional oblique 100 m borehole was drilled to study the influence of topography on the thermal regime (Vonder Mühl et al., 2004). In Scandinavia and Svalbard, boreholes have been installed at Juvvasshøe, Jotunheimen (Norway), Tarfalaryggen (Sweden) and Janssonhaugen (Svalbard) (Sollid et al., 2000; Isaksen et al., 2001). The boreholes extend to a depth of 100 m or more.

Borehole casing, sensors and data logging equipment were assembled according to guidelines provided by the PACE project in order to standardise procedures and ensure comparability between sites (Harris et al., 2001a). This also ensured reliability and serviceability. Periodic recalibration of the installed thermistors is possible and the holes remain accessible for other probes in future. Borehole temperatures were measured with negative temperature coefficient (NTC) thermistors, namely Yellow Spring Instruments YSI 44006

with a resistance of about $2.95 \times 10^4 \Omega$ at 0 °C, with a temperature coefficient of about 5% per °C. The absolute accuracy is estimated at ± 0.05 °C and the relative accuracy at ± 0.02 °C. Depths of thermistors followed the general instructions for the PACE boreholes and levels were: 0.2 m, 0.4 m, 0.8 m, 1.2 m, 1.6 m, 2.0 m, 2.5 m, 3.0 m, 5.0 m, 7.0 m, 9.0 m, 10.0 m, 13.0 m, 15.0 m, 20.0 m, 25.0 m, 30.0 m and 10 m spacing to 80.0 m, and then denser again to 100.0 m. The measurement interval of the thermistors in the upper 15 m of the control borehole is every 6 h. Temperatures of the thermistors below 5 m in the main boreholes are taken once every 24 h. For more details on borehole instrumentation, see Isaksen et al. (2001). In addition, time series data from the Murtèl–Corvatsch borehole (Switzerland), drilled in 1987 to a depth of 58 m in creeping frozen ice-rich rock debris are available (Vonder Mühl and Haerberli, 1990; Hoelzle et al., 2002).

3.3. Active layer thickness

Summer surface temperatures at the Scandinavian and Svalbard borehole sites are significantly lower than those in the Alps, so that active layers are shallower in the former than in the latter (Harris et al., 2003a,b). Fig. 5 shows the maximum annual active layer depth at each PACE borehole, together with data from the UNISCALM site in Adventdalen, Svalbard where the substrate is frozen silt (this forms part of the Circumpolar Active Layer Monitoring (CALM) network of the GTN-P, (Christiansen and Humlum, 2008)). The UNISCALM site is less than 15 km from Janssonhaugen. Maximum and minimum active layer thickness recorded in each time series is given in Table 2. The Alpine boreholes, plus the Scandinavian sites at Juvvasshøe and Tarfalaryggen showed maximum active layer depths in 2003, while in Svalbard maximum summer thaw penetration occurred in 2006.

Table 2 Maximum and minimum active layer depths recorded at European PACE boreholes

Site	Minimum thickness (m)	Year with minimum thickness	Maximum thickness (m)	Year with maximum thickness
Janssonhaugen, Svalbard	1.42	1999	1.80	2006
UNISCALM, Svalbard	0.75	2005	1.00	2006
Tarfalaryggen, Sweden	1.45	2000	1.63	2003
Juvvasshøe, Norway	1.95	2000	2.45	2003
Schilthorn, Switzerland	4.43	1999	8.55	2003
Stockhorn, Switzerland	2.88	2002	4.27	2003
Murtèl–Corvatsch, Switzerland	3.12	1999	3.5	2003, 2004, 2005

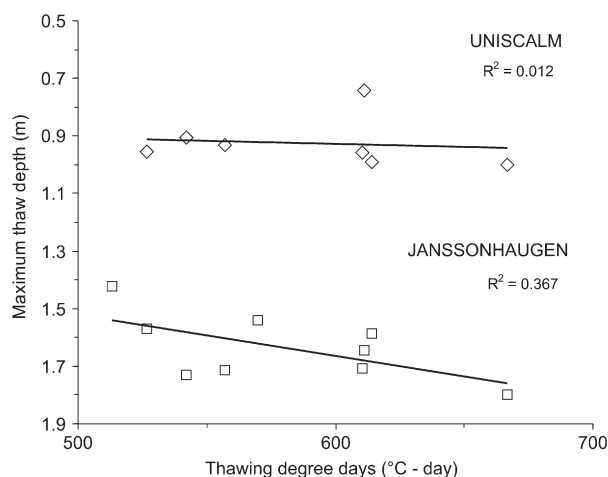


Fig. 6. Relationship between cumulative above zero degree days and active layer thickness, Janssonhaugen and the Longyearbyen CALM site, Svalbard.

On Svalbard, the mean air temperature in December–May 2005–2006 was as high as -4.8 °C, which is 8.2 °C above the 1961–1990 average. This is 2.8 °C higher than the previous record from 1954, amounting to an offset of 3.7 standard deviations from the mean (Isaksen et al., 2007a). In southern Norway, the summers of 2002 and 2003 were among the warmest recorded, and in the Alps, summer 2003 saw sustained record temperatures, in Switzerland approximately 3 °C higher than the 1961–1990 average for the three month period June, July and August (Schär et al., 2004). Active layer responses depended largely on the composition and ice content of the ground, with higher ice contents limiting thaw penetration because of greater latent heat demand (see Murtèl–Corvatsch (Switzerland) in Table 2).

On Janssonhaugen, where permafrost comprises ice-poor bedrock, the extreme 2005–2006 winter temperature, coupled with summer 2006 air temperatures ~ 2 °C above the 1961–1990 normal, resulted in the earliest commencement of thawing during spring 2006 in the 8-year borehole record, and in late summer 2006 the active layer thickness exceeded previous years by 0.18 m (Isaksen et al., 2007b). At Juvvasshøe, southern Norway, again in ice-poor bedrock, active layer depths were 20% greater in the 2003, 2004 and 2006 summers than in previous years. Snow cover at Janssonhaugen and Juvvasshøe is usually thin or absent, surfaces are normally dry and water content in the ground is low, so that active layer thickness is well correlated with local summer air temperatures on an inter-annual basis.

At the UNISCALM site, where winter snow thickness is generally less than 0.3 – 0.4 m and ground cooling in winter is sufficient to promote thermal contraction cracking, the average active layer depth was 0.93 m over the period 2000–2006, with a minimum of 0.74 m recorded in 2005 and a maximum of 1.0 m in 2006. Thus, the 2006 active layer thickness was 0.07 m greater than average, though only slightly greater than that recorded in 2001. It is possible that ice contents increase in the permafrost immediately below the active layer at this site, reducing thaw penetration during extreme years. The active layer, however, is less ice-rich, as evidenced by the 2006 thaw depth exceeding that in 2005 by as much as 0.26 m (Christiansen and Humlum, 2008).

In the Alpine boreholes, the response to the extreme summer of 2003 varied considerably. At Murtèl–Corvatsch in the Swiss Alps, active-layer thickness ranged between 3.1 and 3.5 m within the 19-year observation period, with a trend towards increasing depths (Fig. 5). In the ice-rich frozen debris at Murtèl–Corvatsch, the large latent heat requirement restricted active layer thickening in 2003, though the active-layer was deeper than had previously been recorded (Fig. 5). In the two Swiss bedrock boreholes, Stockhorn and Schilthorn, minimum recorded active layer thickness over the past 5–6 years was just less than 3 m at Stockhorn and just less than

4.5 m at Schilthorn. The depth of thaw penetration in the extreme summer of 2003 at Schilthorn was around twice the average of the previous years, and at Stockhorn it increased by around 30%, indicating strong heat conduction coupled with possible convective heat transfer by water (e.g. Gruber et al., 2004b).

Plotting maximum active layer depths against the summer accumulated above zero degree days for Janssonhaugen with a frozen bedrock substrate and the UNISCALM site, with a frozen silt substrate, demonstrates that active layer thawing is largely driven by summer air temperatures (Fig. 6). Scatter within the plots results from several factors, including the degree of cooling in the previous winter and the duration of spring snow cover, while differences in the coefficients largely reflect contrasting active layer and permafrost ice contents (and hence latent heat) between sites. The presence of an ice-rich “transient layer” in the transition zone between the active layer and the permafrost in non-bedrock locations such as Adventdalen acts as a thermal buffer, slowing active layer thickening during warmer than average summers (Shur et al., 2005).

3.4. Permafrost temperature profiles

The greater altitudinal range and steeper topographic gradients in the Alps leads to considerably greater ground temperature variability among the Swiss boreholes than among those in Scandinavia (Harris et al., 2003a,b, Harris and Isaksen, 2008). In Svalbard, in the continuous permafrost zone, spatial variation is considerably less than in the Alps. Fig. 7 shows updated ground temperature profiles from all the sites, recorded in April 2005. Seasonal temperature variations influence the upper 15–20 m and data from this zone are less useful in analysing interannual to decadal variations in ground temperatures than the thermal gradients recorded at greater depths.

The smooth profile at Janssonhaugen on Svalbard suggests little geothermal disturbance by non-climate sources (cf. Isaksen et al., 2000b). Here the temperature gradient at 25 m is 0.010 °C m $^{-1}$ and this increases to 0.037 – 0.038 °C m $^{-1}$ at 95 m. At Tarfalaryggen and Juvvasshøe the thermal gradients in the upper 40–50 m of bedrock are negative (temperatures increasing with depth), the temperature gradient changing from -0.015 °C m $^{-1}$ at 25 m to 0.010 – 0.011 °C m $^{-1}$ at 95 m in the Tarfalaryggen borehole and -0.011 °C m $^{-1}$ at 25 m to 0.010 – 0.011 °C m $^{-1}$ at 126.5 m in Juvvasshøe. Large-scale topographic influence may partly explain the low geothermal gradients at Tarfalaryggen and Juvvasshøe since adjacent valleys extend ~ 400

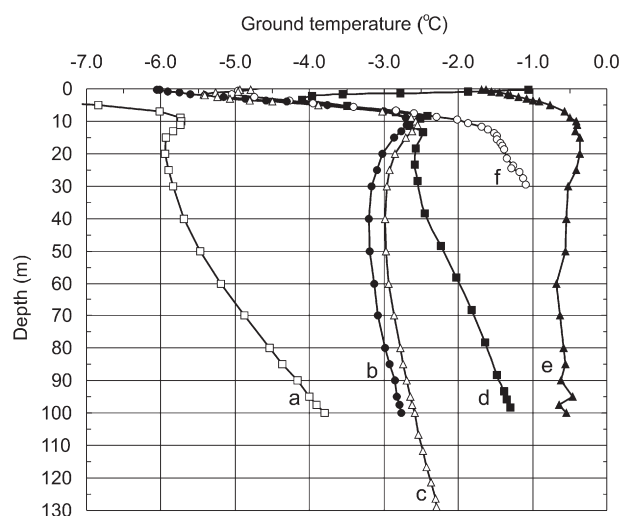


Fig. 7. Ground temperature profiles in permafrost at (a) Janssonhaugen, (b) Tarfalaryggen, (c) Juvvasshøe, (d) Stockhorn, (e) Schilthorn and (f) Murtèl–Corvatsch. Data recorded 22nd April 2005 (temperature profile at Juvvasshøe below 100 m depth recorded manually 1st October 2000). The upper 15–20 m of the boreholes are influenced by the annual temperature fluctuations.

and ~1100 m respectively below the ground surface altitudes of the two boreholes. To obtain undisturbed vertical heat flow values, the boreholes should probably be at least 5 to 10 times deeper (Isaksen et al., 2007a).

In the Alps, the temperature profiles are highly disturbed by topography (Gruber et al., 2004c). The position of the Stockhorn borehole on the Stockhorn plateau has a major influence on its temperatures and temperature gradients at depth. This effect was demonstrated by Gruber et al. (2004c) in a simple model experiment showing the coexistence of both positive (temperature increasing with depth) and negative near-surface geothermal gradients in adjacent vertical profiles, even under steady state conditions. At Schilthorn, permafrost temperatures are close to 0 °C. Analyses of data series indicate that the permafrost temperature is influenced by latent heat effects and convective heat transfer by water. In combination with topographical effects this makes the interpretation of transient signals contained in the temperature profile on Schilthorn an extremely complex problem (Gruber et al., 2004c).

The three boreholes in Svalbard and Scandinavia are located on plateaux or ridges with minor topographic relief within a radius of 100–200 m, smooth ground surfaces, and uniform snow conditions. This ensures little disturbance from small-scale 3-dimensional thermal effects in the upper parts of the boreholes (Isaksen et al., 2007a), as opposed to possible effects of the larger scale relief at greater depths. All three boreholes show a significant warm-side deviation in their thermal profiles to 70 m depth (Fig. 7), that is most likely associated with surface warming during the last few decades, with the greatest change occurring in the northernmost borehole in Svalbard (cf. Harris et al., 2003b; Isaksen et al., 2001). Upward extrapolation to the surface of the temperature gradient between 30–20 m depths indicates surface temperature changes with a magnitude of ~1.4 °C, ~1.1 °C and ~1.0 °C for Janssonhaugen, Tarfalaryggen and Juvvasshøe respectively (Isaksen et al., 2007a). There is no evidence that the observed anomalies in the upper part of the thermal profiles reflect factors other than past changes in ground surface temperatures. In addition, the similarity of the two thermal profiles from Tarfalaryggen and Juvvasshøe suggest a general common effect, that is, a warming of the upper permafrost surface.

3.5. Recent trends in permafrost temperatures

On Murtèl–Corvatsch, temperatures have been measured since 1987 in the 58 m deep borehole. Between 1987 and 1994, the uppermost 25 m warmed rapidly (Vonder Mühl and Haerberli, 1990; Vonder Mühl et al., 1998). At 11.6 m below the surface, the temperature rose by approximately 1.0 °C during this period (Fig. 8). Mean annual surface temperature is estimated to have increased from –3.3 °C (1988) to –2.3 °C (1994), and probably exceeded previous maximum temperatures during the 20th century (Hoelzle et al., 2002). During the following two years (1994–1996), winter snowfall was low, resulting in intense cooling of the ground and permafrost temperatures returning to values similar to those in 1987 (Fig. 8). Since 1996, interannual variations in permafrost temperatures have increased slightly. In 2000/2001 snow came very early and in some places reached maximum values in early winter. During winter 2001/2002 a new period of intense cooling occurred due to exceptionally late snow fall. Since 2002 temperatures have been rising. Overall, permafrost warming during the 18 years of observations at Murtèl–Corvatsch was about 0.5 °C at 11.6 m (Fig. 8) and 0.3 °C at 21.6 m (Fig. 9). At 21.6 m the temperature in 2005 was –1.3 °C, the highest since readings began. Winter snow thickness, coupled with its date of arrival and disappearance, clearly plays a critical role in interannual ground temperature fluctuations.

On Stockhorn and Schilthorn, the episode of intensive cooling found in the Murtèl–Corvatsch series during winter 2001/2002 is also clearly visible at 13.3 m and 13.0 m depth respectively (Fig. 8), but data

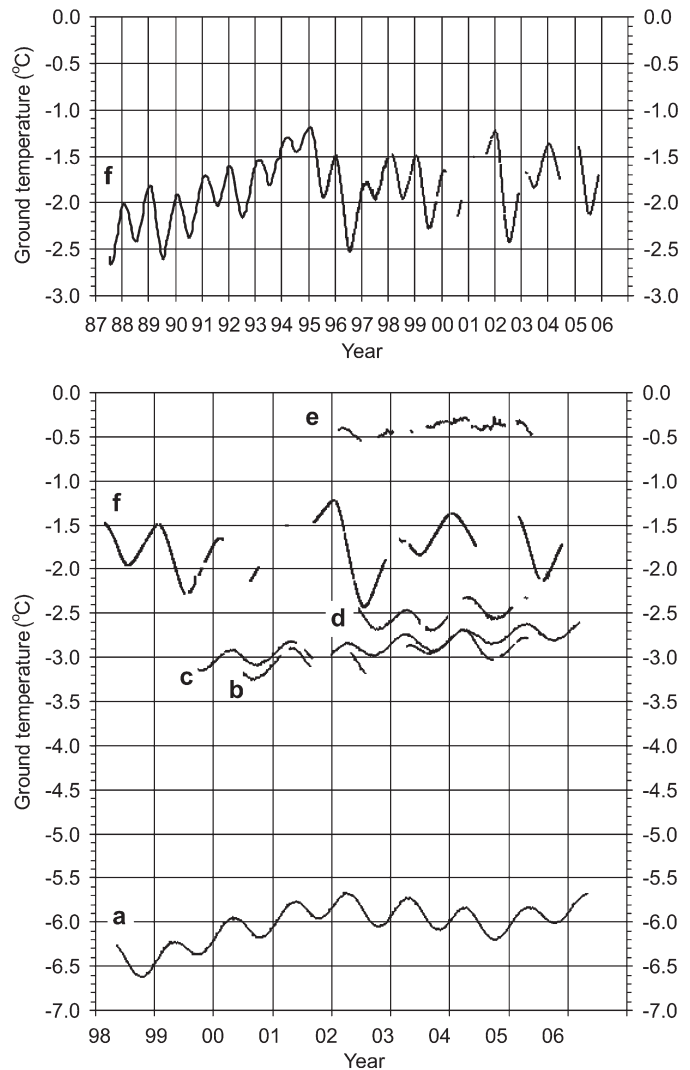


Fig. 8. Observed ground temperatures at the depth where seasonal fluctuations are less than, 0.5 °C. (a) Janssonhaugen (13.0 m), (b) Tarfalaryggen (13.0 m), (c) Juvvasshøe (13.0 m), (d) Stockhorn (13.3 m), (e) Schilthorn (13.0 m) and (f) Murtèl–Corvatsch (11.6 m). At Schilthorn data were smoothed and filtered due to some errors in the data logger and periods of refreezing of meltwater in the bedrock.

series are too short to draw conclusions on longer term temperature changes. It is concluded that interpretation of ground temperature series from the Alps must take account of the complex relationship between the ground surface and atmospheric temperatures, particularly the strong modulating affect of snow conditions (see below; Harris et al., 2003a,b). The significance of the interaction between snow cover and ground surface/subsurface characteristics in influencing ground surface temperature offsets from air temperature has been emphasised by Hoelzle and Gruber (2008) using data from the Murtèl–Corvatsch and Schilthorn borehole sites. At the Nordic sites of Janssonhaugen, Tarfalaryggen and Juvvasshøe, wind action maintains relatively snow-free conditions in winter, and the relationship between air-, ground surface- and ground temperatures is much stronger, resulting in a climate signal that penetrates the permafrost with no large perturbations caused by changing near-surface and surface conditions (Isaksen et al., 2007b).

Continuous ground temperature monitoring just below the depth of zero annual amplitude over periods from five to seven years on Janssonhaugen, Tarfalaryggen and Juvvasshøe show that the ground temperature has increased by 0.36 °C, 0.27 °C and 0.24 °C respectively at 20 m depth (Fig. 9). Observed warming is statistically significant to

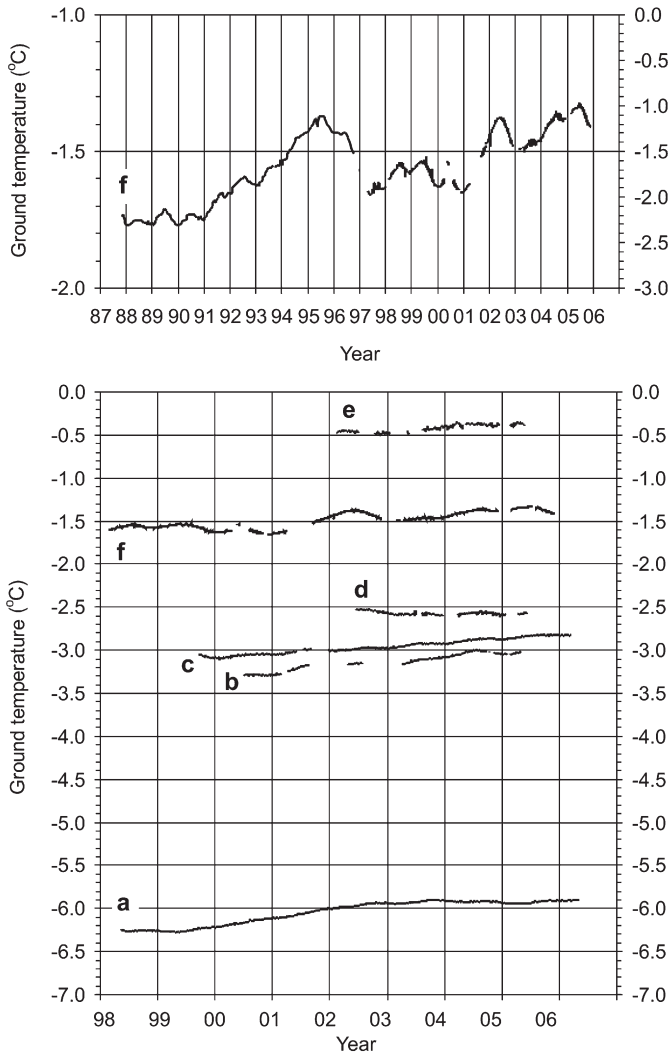


Fig. 9. Observed ground temperatures at the depth where annual amplitude is less than 0.1 °C, that is just below the approximate depth of zero annual amplitude. (a) Janssonhaugen (20.0 m), (b) Tarfalaryggen (20.0 m), (c) Juvvasshøe (20.0 m), (d) Stockhorn (23.3 m), (e) Schilthorn (20.0 m) and (f) Murtèl-Corvatsch (21.6 m). At Schilthorn data were smoothed and filtered due to some errors in data logger and periods of refreezing of meltwater in the bedrock.

60 m depth at all three Nordic sites (Isaksen et al., 2007a). This strongly supports previous interpretation by Isaksen et al. (2001) and Harris et al. (2003b) that most of the anomalies observed in the geothermal profiles (cf. Fig. 7) are associated with surface warming.

In all boreholes the temperature signal below a depth of 20 m is free of any response to annual or shorter-term temperature variations. At these depths, any recorded systematic temperature time variations must correspond to a longer period of several years and it is possible to calculate the actual rate of temperature change as a function of depth (Fig. 10). Below 50–60 m depth, longer time-series than those currently available are required to identify thermal trends. Calculated warming rates over the past several decades based on the recorded temperature trends at a depth of between 40 and 50 m correspond with present decadal warming rates at the permafrost table, in the order of 0.04–0.07 °C yr⁻¹, the highest rates being on Janssonhaugen and Tarfalaryggen (Isaksen et al., 2007a). Higher rates of permafrost warming are reported in northern Alaska, rates tending to increase with increasing latitude (Osterkamp, 2008) while observed permafrost warming rates over the past 30 years in Siberia are somewhat lower (Romanovsky et al. 2008).

If the thermal responses observed within the PACE mountain borehole network are indicative of longer term trends, major changes in permafrost distribution may be anticipated through the 21st Century. It is also clear that on a seasonal time scale, extreme summer temperatures may lead to large increases in bedrock active layer depths, and are likely to increase the scale and frequency of mountain slope instability (see Section 8.2). The PACE boreholes provide a regional framework for monitoring European mountain permafrost geothermal responses to climate change, and additional networks of shallow (up to 20 m) boreholes in both the Alps and the Nordic countries (e.g. Vonder Mühl et al., 2004; Sollid et al., 2003; Ødegård et al., 2008) provide more detailed information on local variability.

Of particular importance in this respect are three permafrost monitoring boreholes installed in central and northeastern Iceland in 2004 (Farbrot et al., 2007; Etzelmüller et al., 2007, 2008), at altitudes of between 890–930 m a.s.l. (Fig. 11). All are shallow (12–22 m deep), and penetrate thin sediment into basaltic bedrock. Observed permafrost temperatures below the depth of seasonal temperature fluctuation were between -1 °C and 0 °C, and at the Snæfell and Gagnheiði boreholes, permafrost thickness was estimated to be 30–35 m, with active layers around 2 m and 4 m respectively. At Hágöngur, permafrost was thin, temperatures were close to zero and the active layer was around 6 m deep. Meteorological data indicate that mean annual ground surface temperatures for the past few years in Iceland have been 0.5–1 °C higher than those for the 1961–90 period (Etzelmüller et al., 2007). At the Gagnheiði and Snæfell boreholes, temperature profiles show warm-side deviation from steady state, suggesting recent rises in the upper boundary temperature (Fabrot et al., 2007).

One-dimensional thermal modelling suggests that increases in mean daily surface air temperatures of (a) 0.01 °C a⁻¹ and (b) 0.03 °C a⁻¹ would cause permafrost to disappear in 160 and 100 years respectively at Snæfell, and 125 and 75 years respectively at Gagnheiði (Farbrot et al., 2007; Etzelmüller et al., 2008). Higher ice contents explain the slower response at Snæfell than at Gagnheiði. The influence of snow cover on the ground thermal regime at these sites was quantified by Etzelmüller et al. (2008), by damping the winter air temperatures by a nival factor

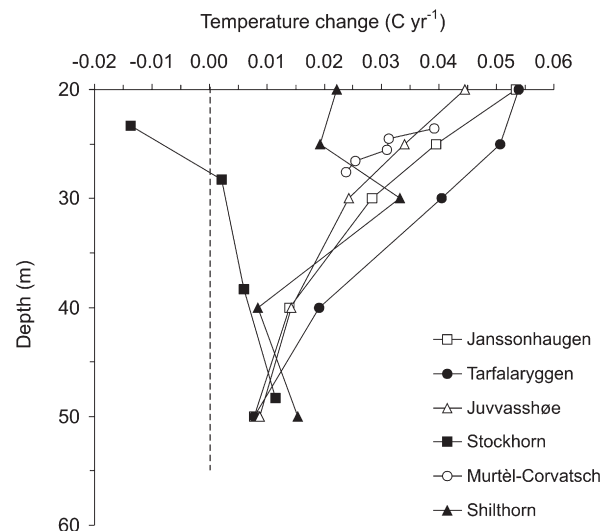


Fig. 10. Observed present-day temperature change as a function of depth below the depth of annual amplitude. Time series generally start one year or more after establishment of the boreholes to minimise influence from borehole drilling. In addition, analyses of the data series are based on whole years (3–7 years) to reduce any systematic errors in the dataloggers and measurements. Data periods are at Janssonhaugen 26.04.1999–25.04.2006, Tarfalaryggen 20.04.2001–19.04.2005, Juvvasshøe 26.02.2000–25.02.2006, Stockhorn 15.06.2002–31.05.2005 and Schilthorn 20.05.2002–19.05.2005.

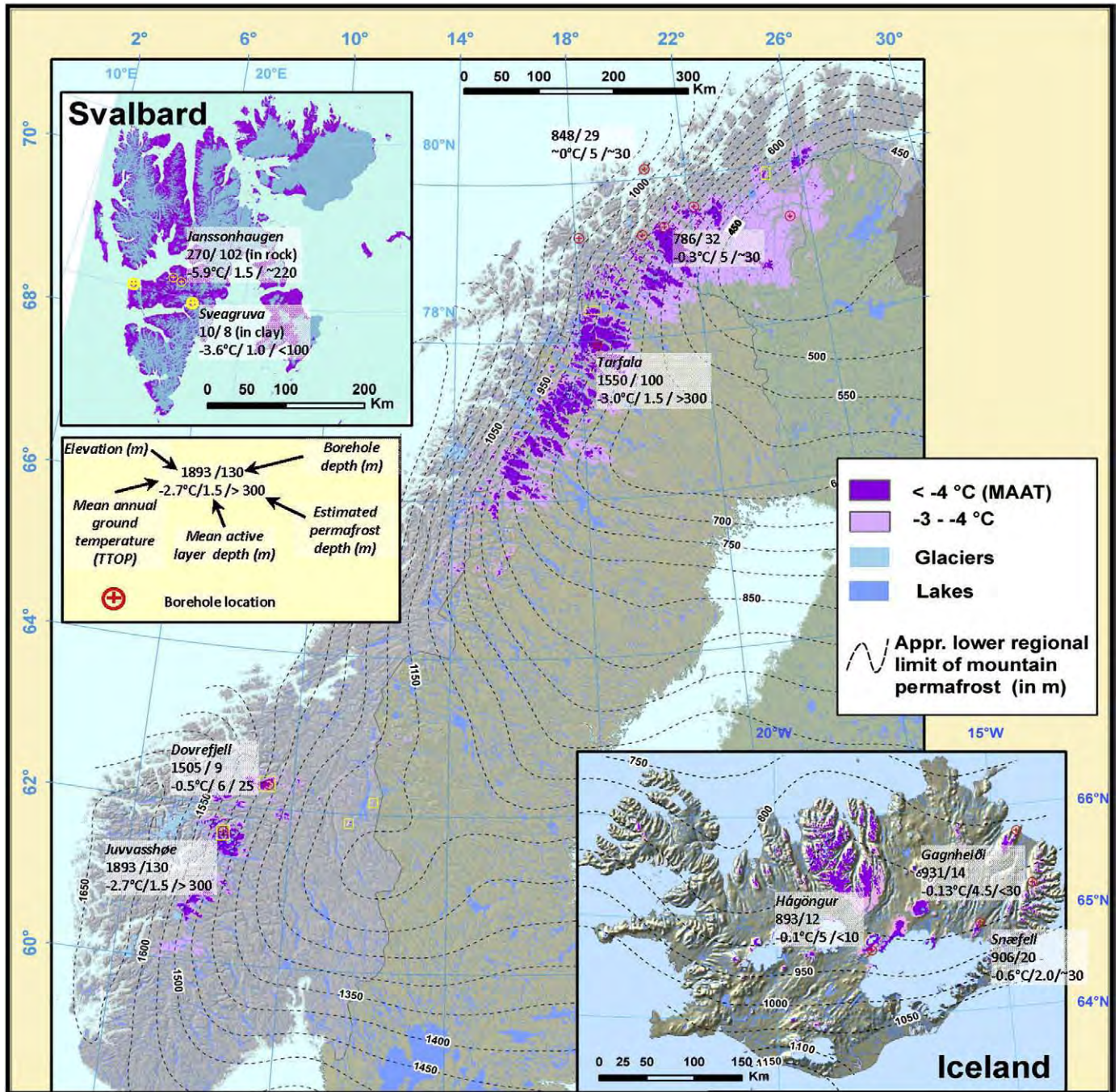


Fig. 11. Permafrost map of the Nordic countries. The approach selected here is based on a relation between gridded air temperature data and permafrost existence not considering snow and topographic heterogeneity. The dashed contour lines indicate the regional lower limit of discontinuous mountain permafrost. Existing shallow boreholes in Scandinavia are shown, including key thermal parameters and average active layer thickness. On most sites, several boreholes are drilled in different topographic positions and with varying depths. The map is compiled at the University of Oslo (UiO), Norway, based on data provided by UiO, met.no, UNIS and NGU.

(between 0 and 1), following equilibrium modelling approaches (see Riseborough et al., 2008). The study indicated critical snow cover thresholds, where permafrost is stable, aggrading or degrading for different snow cover scenarios. Modelled temperature evolution since 1955 suggested that the present-day permafrost thicknesses reflect cooling in the late 1960s/early 1970s. This rapid permafrost thermal response is in part a reflection of the shallowness of the permafrost layer, but also the influence of high geothermal heat fluxes that at Snæfell are around 150 mW m^{-2} , approximately five times the values at the Scandinavian PACE borehole sites (cf. Isaksen et al., 2001).

4. Modelling mountain permafrost thermal condition and spatial distribution

4.1. Modelling approaches

Unlike the other cryospheric phenomena such as glaciers or sea ice, permafrost is a largely invisible phenomenon. Therefore, modelling based on thorough process understanding is the best method for estimating permafrost spatial distribution patterns in the past, present and future. In recent years, several attempts have been made to

develop and improve spatial modelling of mountain permafrost distribution (Etzelmüller et al., 2001a; Hoelzle et al., 2005). Appropriate models are useful to a wide range of permafrost-related environmental issues, including the evaluation of climate-change scenarios, large- and local-scale mapping, surface process studies, and environmental concerns such as natural hazards and ground engineering.

Modelling capability for mountain areas has progressively improved over the past decade, not least as a result of the EU-funded PACE-project (Harris et al. 2001a, Riseborough et al., 2008). The selection of a particular methodology often depends on the objectives, the scale and the application for which the models are developed. On a more local-scale, process-oriented numerical approaches and sensitivity studies with respect to process interactions and feedbacks within the mountain permafrost system have received more attention, focusing on the interface between atmosphere and ground surface as well as within the uppermost layers of the ground. On a larger regional scale, empirical–statistical models have been developed and applied. For mountain areas in Europe in general, the preferred modelling methodology is now changing from more stochastic and empirical to more numerical approaches.

In this section, we review the currently available typology of models at various levels of sophistication and spatio-temporal scales, and we present new data and results relating to permafrost modelling in mountainous regions.

4.2. Spatial and temporal scales of permafrost distribution modelling

A simplified conceptual distinction between the influence of 'Climate', 'Topography' and 'Ground Condition' can be made on the basis of scale (Gruber, 2005). Latitude plus large-scale atmospheric/oceanic circulation patterns mainly determines weather and climate patterns on a global and continental scale. At a regional to local scale (areas covering several square kilometres) topography strongly overprints weather and climate. Terrain geometry controls air temperature by elevation, orographic precipitation, and solar radiation via the insolation angle and shading. Locally, surface and subsurface properties further influence the translation of the "climatic" signal into ground temperatures. Factors such as snow cover, air or water movement and ground surface characteristics influence different (often non-conductive) thermal processes that have an important overall influence on the total energy and mass exchange of the system. Thus, many process models are applicable only at regional to local scales in which complex models are able to simulate transient 3D-temperature fields with some restrictions (see below). A major problem exists in bridging continental and local scales, and this is particularly important for the application of climate scenarios when the outputs from Regional Climate Models (RCMs) have to be downscaled to meet the needs of local scale permafrost models.

The coarse resolution of certain models is in most cases appropriate for overview maps and long-term predictive models. However, many applied and scientific applications are concerned with the identification of more local distribution patterns of forms, processes and potential slope instability (Harris et al., 2001a), demanding refined models with higher resolutions. Such models need an increasing number of input parameters and better calibration but are essential for a better process understanding and for transient extrapolations into the future within complex three-dimensional mountain topography.

As permafrost is a thermal system with slow response to climate forcing, the present state of permafrost is in part a function of former climatic conditions and present day climate changes will in turn affect the future thermal state of permafrost. The response time of permafrost depends mainly on the thermal conductivity, the ice content and the thickness of the frozen ground. Empirical models neglect important feedback mechanisms such as atmo-

sphere/snow/permafrost-interactions and do not take into consideration transient conditions at depth. Even in relatively warm and thin discontinuous mountain permafrost, propagation of a warming trend through the entire permafrost thickness is typically measured in decades to centuries. PACE-borehole thermal data support the contention that alpine permafrost thickness and its distribution in marginal areas most probably still reflect maximum Holocene cooling during the Little Ice Age that culminated in the 19th century (see Section 2).

4.3. Recent developments

Today, mountain permafrost distribution models combine stochastic with deterministic elements and include two main types; regionally calibrated empirical–statistical models, and more physically based numerical models (Etzelmüller et al., 2001a,b, Hoelzle et al., 2001, Riseborough et al., 2008). Several model approaches calculate the main energy exchange processes in one dimension (Goodrich, 1978; Stähli et al., 1996; Zhang et al., 2001; Riseborough, 2002; Gruber et al., 2004b; Farbrøt et al., 2007; Etzelmüller et al., 2008). More recently, attempts have been made to apply equilibrium models such as the TTOP-approach (Riseborough, 2002) in European mountain environments (Juliussen and Humlum, 2007; Etzelmüller et al., 2008). Both transient and the equilibrium approaches have been applied, though only at specific locations; spatial modelling remains a future task.

Empirical–statistical distributed permafrost models directly relate documented permafrost occurrences to topoclimatic factors (altitude, slope and aspect, mean air temperature, solar radiation), that can easily be measured or computed (Jorgenson and Kreig, 1988; Hoelzle and Haeblerli, 1995; Hoelzle, 1996; Imhof, 1996; King and Kalisch, 1998; Li et al., 1998; Etzelmüller et al., 2001b; Kneisel et al., 2000a; Gruber and Hoelzle, 2001; Lugon and Delaloye, 2001; Tanarro et al., 2001; Duchesne et al., 2003; Mustafa et al., 2003; Wright et al., 2003; Heggem et al., 2005; Nyenhuis et al., 2005). In some studies this model type is also used for paleo-reconstructions and simulating future scenarios (Frauenfelder and Käb, 2000; Lambiel and Reynard, 2001; Frauenfelder et al., 2001; Janke, 2005). In these models, the energy and mass exchange processes at the surface and within the active layer are not treated explicitly. Therefore, these models can be seen as a grey box with topoclimatic factors being selected according to their relative influence in the total energy balance exchange. This simplification results in advantages and disadvantages: empirical–statistical permafrost distribution models are easily applied, need only limited input parameters and are quite reliable if well calibrated locally or regionally. They are, however, yes/no-functions about the presence or absence of permafrost, primarily applicable to certain areas. They assume steady-state conditions and neglect the influence of the complex heat fluxes within the three dimensional topography. Extrapolations in time and space may lead to uncertain or even misleading results.

Process-oriented models focus on more detailed understanding of the energy fluxes between the atmosphere and the permafrost (Romanovsky et al., 1997; Wegmann et al., 1998; Kukkonen and Safanda, 2001; Marchenko, 2001; Riseborough, 2002; Stocker-Mittaz et al., 2002; Isaksen et al., 2003; Kasymkaya et al., 2003; Oelke and Zhang, 2003; Gruber et al., 2004b; Ling and Zhang, 2004). They explicitly parameterise solar radiation, turbulent heat fluxes, surface albedo, heat conduction, etc., are often complex and need a correspondingly large amount of precisely measured or computed data. Such approaches allow for spatio-temporal extrapolation and are especially well suited for sensitivity studies with respect to interactions and feedbacks involved with climate-change scenarios (Salzmänn et al., 2007a,b). They enable surface temperatures to be computed and, hence, thermal conditions at depth and transient effects in complex topography to be estimated (Noetzli et al., 2007).

However, the proper investigation of uncertainties is an important element of the application of this type of model.

4.4. Regional-scale modelling

Regional-scale modelling operates on a ground resolution of 100 m or more, depending on the heterogeneity and size of the area modelled. Such regional models aim to give a first indication of permafrost distribution, with limited accuracy demands, identifying the areas of permafrost abundance. A simple climate-permafrost model based on the relationship between gridded Mean Annual Air Temperature (1961–90, MAAT) values (Tveito et al., 2001) to permafrost existence has been used to generate a permafrost map of the Nordic countries (Fig. 11). However, the approach does not consider snow conditions and topographic heterogeneity. A MAAT map was generated by reducing air temperatures at official climate stations to sea level, interpolating between the stations, and subsequently estimating the air temperatures for real elevations using a constant lapse rate. For studies in southern Norway it has been shown that an annual air temperature of -3 to -4 °C is a good estimate for the regional limit of the lower mountain permafrost boundary (e.g. King, 1986; Ødegård et al., 1996; Etzelmüller et al., 2003). For Iceland, a value of -3 °C was derived, based on ground surface temperature (GST) measurements in different sites in northern and eastern Iceland (Etzelmüller et al., 2007). This approach is justified by the fact that most areas of permafrost in the Nordic countries have more gentle topography than the Alps (Etzelmüller et al., 2003), where large topographic effects strongly influence permafrost distribution.

Predicted permafrost distribution was compared with observations in different regions, including southern Norway (Heggen et al., 2005; Isaksen et al., 2002), northern Norway (Farbrot et al., 2008; Isaksen et al., 2008) and Iceland (Etzelmüller et al., 2007; Farbrot et al., 2007). All validation indicated that the general permafrost pattern is well reproduced and shows a decrease in the lower permafrost limit from west to east in Scandinavia though local variations are not represented. In Iceland, the predicted southwards increase in altitude of the permafrost limit is due to more maritime and snow-rich

conditions in Southeastern Iceland. In Scandinavia, mountain permafrost distribution clearly exceeds the glacier coverage, while in Iceland it seems to be in the same order of magnitude.

A regional map of potential permafrost distribution at a scale of 1:50,000 for the Swiss Alps has recently been published by the Swiss Federal Office for the Environment (Map realization: Geotest, GEO7, Academia Engiadina). The map is based on two different approaches. The empirical model uses as input the digital elevation model of the Federal Office of Topography (DHM25, swisstopo). The potential permafrost calculation distinguishes three different high alpine ground surface characteristics with a) coarse debris, b) bedrock and c) glaciers and water (see Fig. 12). For the calculation, a permafrost index was generated based on the topographic parameters. For all calculations of permafrost distribution in non-bedrock and non-glaciated areas, the well-known 'rules of thumb' developed by (Haerberli, 1975) and implemented in a GIS by (Keller, 1992) were used. For bedrock, an index was developed, based on energy balance models and on field validations (Gruber et al., 2003a,b, 2004b). For glaciers and water surfaces no calculations were performed. This index approach to estimate permafrost distribution is only very approximate, and the resulting map contains considerable uncertainties relating to the influence of topography on a variety of heat transfer mechanisms.

4.5. Local-scale modelling

During the PACE project, a distributed energy balance model was developed with the aim of investigating and simulating the interactions between the ground, the snow cover and the atmosphere (Mittaz et al., 2002; Stocker-Mittaz et al., 2002; Gruber, 2005). Progress has been made in modelling the major energy fluxes, but there remain many challenges. Firstly, the model is still not able to produce a sufficiently accurate estimation of snow cover and secondly, the coupling between atmosphere and ground where ground cover comprises coarse debris (non-conductive heat transfer) is not satisfactorily included. Therefore, as a first approach, more simple systems have been selected for detailed process modelling to avoid complex

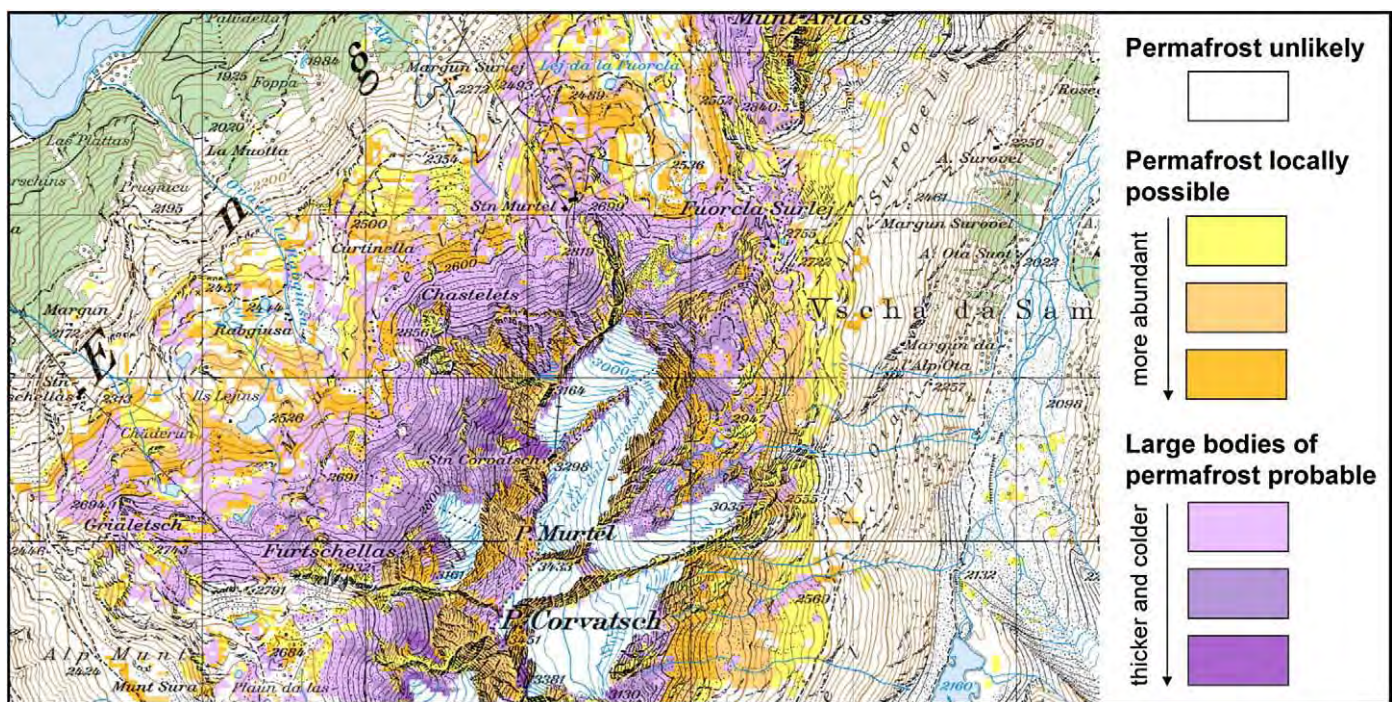


Fig. 12. Potential permafrost distribution as shown by the new Swiss Permafrost Map 1:50,000 (subsection of map sheet "Julierpass") published by the Swiss Federal Office for the Environment (FOEN) and realized by Geotest, GEO7 and Academia Engiadina.

interactions with snow cover or complex materials such as coarse debris. Steep alpine rock walls represent such a system and allow more straightforward modelling with better estimation of uncertainties. The model was validated by several rock temperature loggers placed in steep rock walls at different altitudes with different aspects (Gruber et al., 2003a,b, 2004a,b).

In many areas with limited coverage of meteorological stations, statistical-empirical modelling is still in use. Most common is the bottom temperature of snow (BTS) method (Haeberli, 1973), where field data are related to topo-climatic factors, establishing a statistical relationship between BTS temperatures and these factors (Hoelzle & Haeberli 1995; Hoelzle 1996). Recently, more sophisticated statistical methods such as logistic regression have been utilised, simulating permafrost probability in a region (Brenning et al., 2005; Lewkowicz and Ednie, 2004; Heggem et al., 2005; Lewkowicz and Bonnaventure, 2008). The most important topo-climatic factors are the altitude and potential incoming radiation, while the potential topographic wetness in a region also seems to play a significant role (Heggem et al., 2005). These models do not explain the heat transfer processes, but result in an easily obtainable map of permafrost occurrence and distribution in a region, and thus have an applied value.

Multi-criteria approaches within a GIS framework have been applied to generate maps of “permafrost favourability” in regions

where meteorological data is restricted. Here, scores are derived for single factors (elevation, topographic wetness, potential solar radiation, vegetation) based on simple logistic regression or basic process understanding, and the sum of the derived probabilities is used as a measure of permafrost favourability in a given location within the framework of a multi criteria analysis (Etzelmüller et al., 2006; Fig. 13). The index maps are in this case the map layers representing the spatially distributed attributes that are found to contribute to the favourability (f) of permafrost existence, ranging between 0 and 1. The f -values obtained were statistically related both to measured ground surface temperatures and ground resistivities obtained by DC electrical resistivity. The approach is well suited for both local and regional surveys of permafrost distribution, but less applicable for studies of the impact of climate change.

In general, DEM-derived topographic parameters coupled with satellite-image derived information offers the potential for more accurate permafrost distribution modelling in remote areas (e.g. Etzelmüller et al., 2001a,b). For instance, Heggem et al. (2006) estimated the spatial distribution of annual Ground Surface Temperature (GST) based on measured GST in different landscape categories defined by a classification of topographic parameters (elevation, potential solar radiation, wetness index) and satellite-image derived factors (forest and grass cover). A sine-function was adapted to the

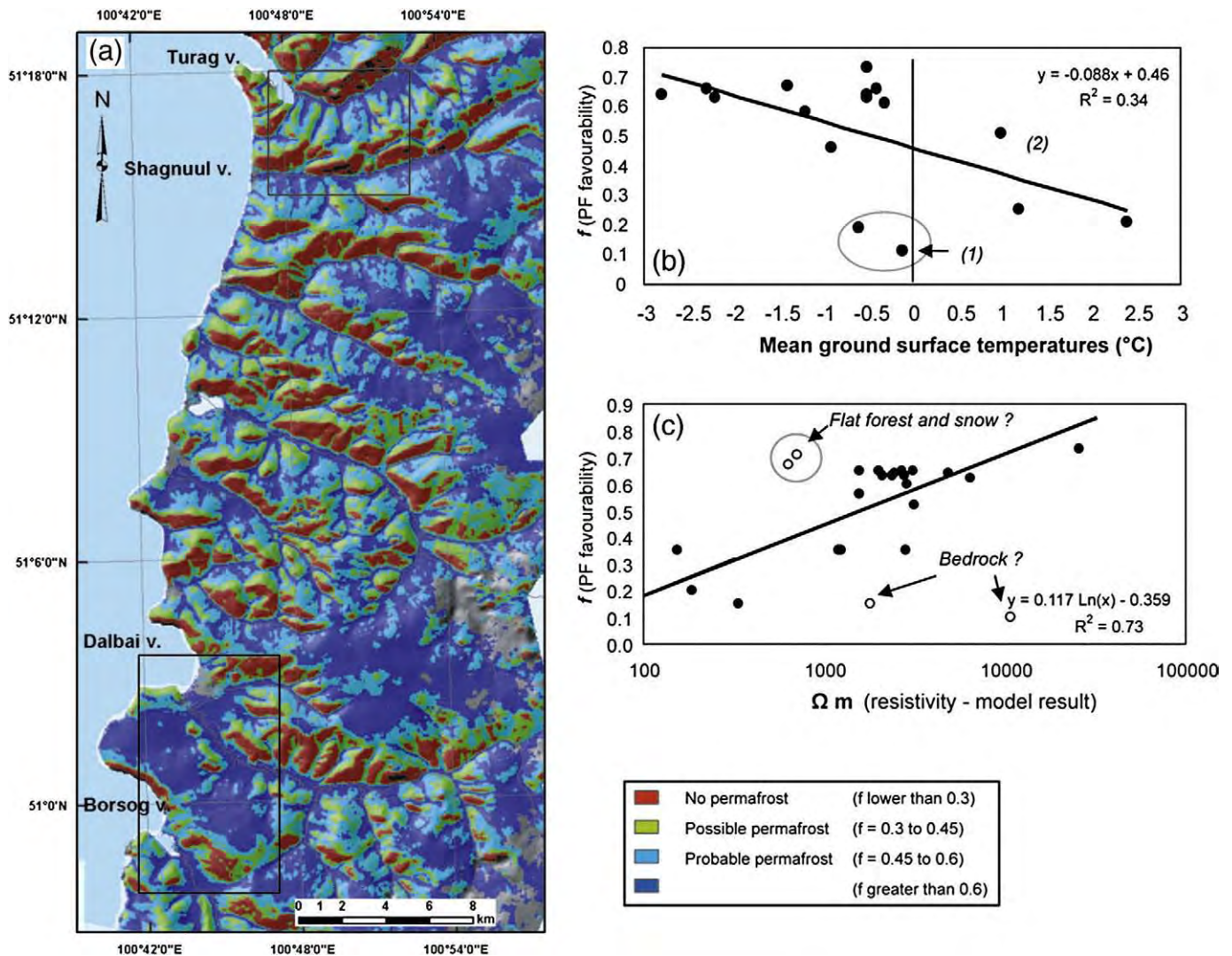


Fig. 13. Permafrost favourability mapping based on multi-criteria approaches within a GIS framework. (a) Permafrost favourability map (reproduced after Etzelmüller et al., 2006). (b) Plot of ground surface temperature against permafrost favourability. (c) Plot of modelled resistivity at 8 m depth vs. permafrost favourability. The regression equation was developed without including the marked outliers (from Etzelmüller et al., 2006).

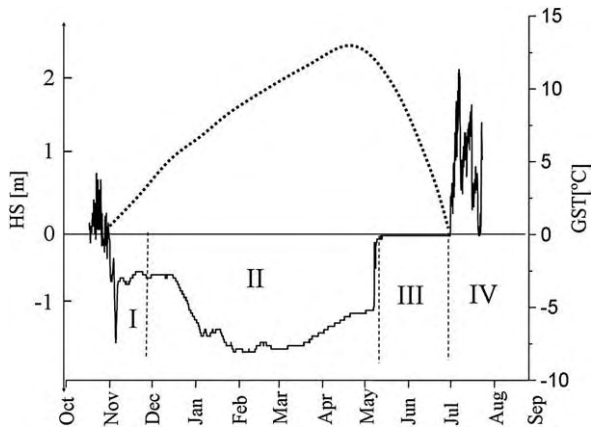


Fig. 14. The interaction between seasonal snow cover (i.e. snow depth (HS), dotted line) and ground surface temperature (GST, solid line) can be divided into four stages reflecting different thermal effect of the snow cover: I) the ground cooling non-insulating early snow cover, II) the ground warming, insulating snow cover in winter III) the snow-melt season in spring and IV) the snow-free stage in summer.

measured GST curves, parameterised with the temperature amplitude and mean annual temperature. This allowed the simulation of the GST field for changing temperature or snow cover (amplitude).

4.6. The significance of snow

The importance of snow cover arises largely from its low thermal conductivity (depending on density and microstructure (Fierz and Lehning, 2001; Luetsch and Haeberli, 2005)), its high surface albedo, and the energy sink provided by latent heat demand during snowmelt (Mellor, 1977; Sturm et al., 1997; Zhang, 2005). Ground under a snow depth greater than 60–80 cm can be regarded as effectively thermally insulated from the atmosphere (Keller and Gubler, 1993; Hanson and Hoelzle, 2004). Typically, the role of snow cover changes through the year over four distinct time periods (Fig. 14) and the timing and duration of these periods can have a considerable influence on mean annual ground temperatures (Goodrich, 1982; Harris and Corte, 1992; Keller, 1994; Seppälä, 1994; Luetsch et al., 2004). In autumn and early winter, an absence of snow or the presence of a thin cover, allows conduction of heat from the ground surface, and if thin snow is present, additional ground cooling arises from the high albedo of the snow surface. Increasing snow thickness then effectively insulates the ground surface from air temperature variation. During the spring thaw, melt-water percolation results in constant ground surface temperatures close to zero, this period lasting up to one or two weeks in the Arctic and Sub-Arctic (Zhang, 2005), but up to several months at the foot of steep avalanche slopes in mountain areas (e.g. Luetsch, 2005). Finally, during the summer snow-free season, ground surface temperatures reflect daily air temperature and radiation fluctuations.

Modelling approaches show differences in emphasis between arctic permafrost regions and mid-latitude mountains. In the Arctic, 1-D modelling generally includes complex hydrothermal processes associated with the freezing and thawing of a fine-grained and water rich active layer, but the thermal effect of seasonal snow cover is often simplified (e.g. Goodrich, 1982). Zhang and Stamnes (1998) and Zhang et al. (2001) using a one-dimensional heat flux model concluded that in high latitude permafrost, ground temperatures are most strongly affected by air temperatures, though soil moisture and the onset date of snow cover and the snow thickness were also shown to be critical for the persistence of marginal permafrost.

Corresponding modelling of mid-latitude mountain permafrost places greater emphasis on the complexities of seasonal snow cover, but generally treats the substrate as a less humid, coarse-grained non-frost susceptible soil in which conductive heat fluxes dominate. An

example is a three-year simulation of the ground temperature evolution of a 16 m thick dry, coarse blocky ground layer (Luetsch, 2005). Simulations utilised the SNOWPACK model (Lehning et al., 1999; Bartelt and Lehning, 2002), which allows significant temporal changes in snow properties to be included, and was extended to incorporate underlying soil layers (Luetsch et al., 2003). The snow and soil are simulated respectively as three-component (air, water and ice) and four-component (air, water, ice and soil grains) materials (Fierz and Lehning, 2001; Lehning et al., 2002a,b). Mass and energy transport and phase change processes are treated in the same way in the snow and soil layers. For gravitational water transport, a bucket water transport algorithm is applied that for some soil layers is a crude approximation (Lehning et al., 2002a). The four stages in the role of snow cover with respect to ground thermal conditions outlined earlier are clearly indicated (Fig. 15). More recently, the model has been developed into a distributed model system to simulate Alpine surface processes in general, including snow redistribution by wind, terrain influences on the surface energy balance, snow-soil-vegetation interactions and runoff (Lehning et al., 2006, 2008).

4.7. Validation

Validation of permafrost modelling against measured data must be an integral part of the model development process. As permafrost is thermally defined, the most secure validation data are derived from boreholes instrumented to measure ground temperatures. The PACE borehole network provided initial European data sets, but since then numerous additional borehole networks have been established. Measurements of the bottom temperature of the winter snow cover (BTS) combined with selected ground temperature loggers, are suitable for validation purposes for broader areas, e.g. for validation of regional empirical or energy balance models. Geophysical methods, such as DC resistivity tomography and seismic soundings are especially useful for detection of ice rich permafrost grounds in a local scale (see Section 6). Geoelectrical soundings have proved to be very useful, clearly mapping the transition zones between permafrost and no permafrost, allowing relationships to altitudinal or surface cover effects to be established (Hauck et al., 2004; Isaksen et al., 2002, Etzelmüller et al., 2006). On specific sites, where meteorological stations are available, other important variables, such as measured air

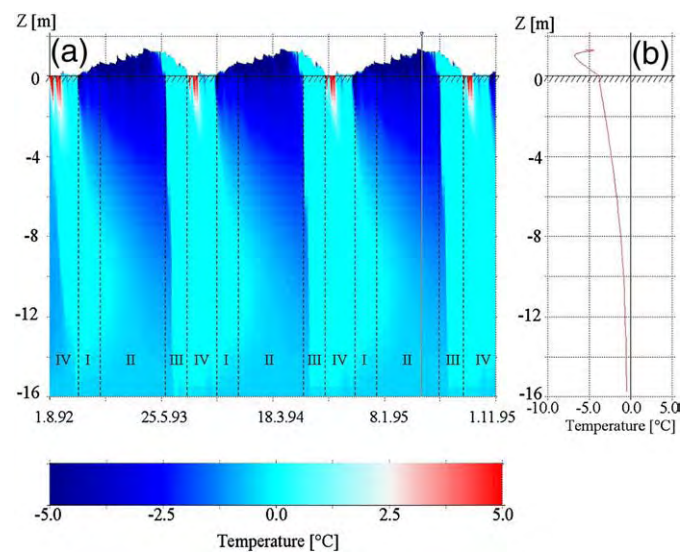


Fig. 15. (a) SNOWPACK three-year simulation run of the ground temperature evolution with time and depth for a 16 m thick dry, coarse blocky soil, including the influence of the seasonal snow cover. (b) Winter temperature profile through the soil and snow layers.

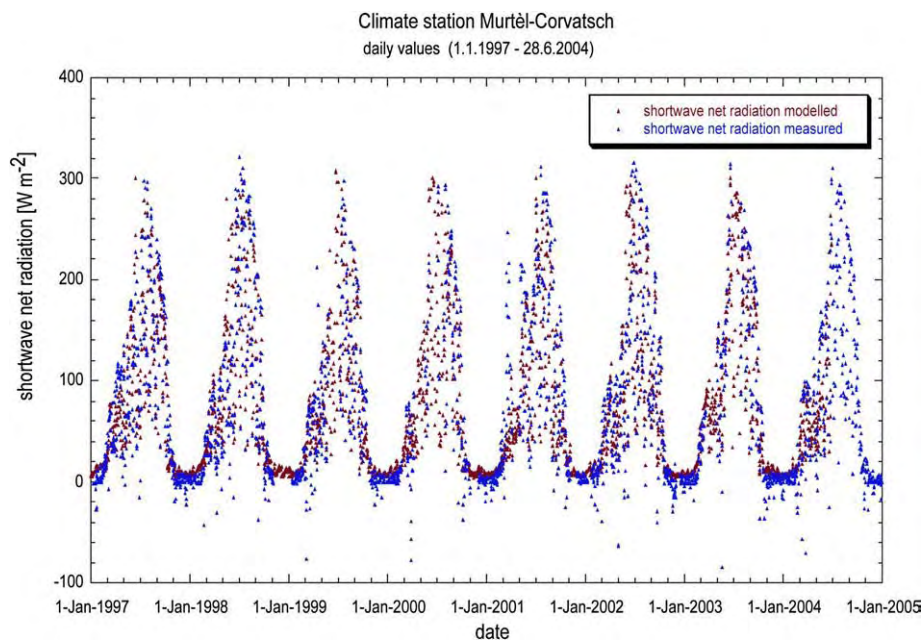


Fig. 16. Modelled and measured Shortwave net radiation in Wm^{-2} at the climate station Corvatsch–Murtèl, Upper Engadin, Switzerland.

or ground temperatures, thickness of snow cover, or radiation can be used as validation for the modelled variables (e.g. Fig. 16), especially when applying physical models.

4.8. Perspectives on mountain permafrost modelling

The main challenges for the development of more sophisticated and reliable permafrost distribution models can be summarised as follows. Firstly, there remains a need for field measurement and numerical modelling of processes within the main types of ground material such as bedrock, fine-grained debris and coarse, ice-rich debris. Several factors strongly influence the ground thermal regime in these materials and many of these are still poorly understood. Of particular importance is the influence of snow cover, and the need to model the spatial variability of snow thickness and duration. In addition, more accurate modelling of the role of ice within bedrock and fine and coarse debris, heat transfer by percolating water, and the effects of general local inhomogeneities is required. Secondly, validation of models should include the application of modern measurement technology using appropriate sensors. This requires collaborative research between a numbers of specialists. Thirdly, improved evaluation of uncertainties and uncertainty propagation within measurements and models is required. Fourthly, scaling issues between different models and between models and validation data need to be addressed, and finally, the modelling sequence Global Circulation Models–Regional Circulation Models–Energy Balance Models–Heat Transfer Models within three-dimensional topography should be further improved. The focus should be modelling transient effects, which requires coupling of time-dependent surface and subsurface ground thermal conditions. This is a prerequisite for realistic modelling of impacts of potential future climate-change scenarios in relation to possible permafrost degradation or aggradation.

5. Geophysical characterisation of frozen ground

One of the main problems in assessing future permafrost response to climate change is a lack of 3-dimensional information relating to subsurface composition, ice content and structure. Since a number of geophysical properties alter significantly when phase change of water occurs, surface based geophysical methods represent a cost-effective approach to permafrost mapping and characterisation, and when

repeated through time, monitoring of changing ground conditions. Measurements are largely non-invasive, making geophysical methods very suitable for monitoring purposes. An earlier review of geophysical and geomorphological methods of detecting and mapping mountain permafrost is provided by King et al. (1992). Scott et al. (1990) have discussed geophysical investigations in arctic regions and Vonder Mühll et al. (2001) and Hauck and Vonder Mühll (2003a) described mountain permafrost applications. Recent overviews of geophysical methods for the application in periglacial environments are provided in Hauck and Kneisel (2008) and Kneisel et al. (2008).

5.1. Geophysical properties

In permafrost studies, key properties of interest are temperature and ice content. Without a borehole, these properties cannot be observed directly, and borehole data may not be representative of a larger area of complex terrain. The detection and characterisation of permafrost from the surface depends on those characteristics that differentiate it from surrounding non-cryotic (temperature above zero) ground. These are mainly related to differences in physical properties of earth materials containing either frozen or unfrozen water. The degree of variation depends on water/ice content, pore size, pore water chemistry, ground temperature and pressure on the material (Scott et al., 1990). Three commonly used geophysical parameters for differentiating between frozen and unfrozen material are:

- electrical resistivity, which in moist porous rocks and soils increases markedly at the freezing point, and in fine-grained soils continues to increase exponentially until most of the pore water is frozen (e.g. King et al., 1988; McGinnis et al., 1973; Daniels et al., 1976; Pearson et al., 1983; Hauck, 2002);
- dielectric permittivity, which governs the propagation speed of georadar waves, also changes significantly between frozen and unfrozen material, with the dielectric constant having values of 3–4 for ice, around 6 for frozen sediment, around 25 for unfrozen sediment and 80 for fresh water (Moorman et al., 2003); and
- seismic compressional- and shear-wave velocities that increase sharply on freezing in most moist porous materials, the increase being more pronounced as porosity increases (McGinnis et al., 1973).

The presence of saline pore waters leads to freezing point depression, and significantly affects all three of the above geophysical properties (Pandit and King, 1978). Geoelectrical approaches are sensitive even to small changes in unfrozen water at sub-zero temperatures, but seismic energy is transmitted primarily through the solid matrix, so once the pore volume is largely ice filled, further changes in unfrozen water content produce only negligible changes in velocity (Pearson et al., 1983). In permafrost terrain, the effects of topography, high electrical contact resistance and scattering of georadar by boulders may also cause difficulties. The use of capacitive-coupled resistivity systems (Timofeev et al., 1994; Hauck and Kneisel, 2006; de Pascale et al., 2008) or electromagnetic induction methods (e.g. Harada et al., 2000; Hauck et al., 2001; Bucki et al., 2004, Yoshikawa et al., 2006) have proved effective in overcoming problems of high contact resistance.

5.2. Resistivity surveys

Most geophysical case studies of mountain permafrost reported in the literature have involved applications of sounding methods that

provide 1-D distributions of physical properties as functions of depth and/or lateral mapping methods that supply information on the horizontal variations of physical properties over a narrow depth range (e.g. Ikeda, 2006). Only recently have applications of 2-D imaging (tomographic inversion) techniques to mountain permafrost been published. These imaging techniques provide more reliable and more complete information than the sounding and lateral mapping methods by generating a 2-D ground model.

Electrical Resistivity Tomography (ERT) has been successfully applied to map and characterise different permafrost structures in mountain terrain (e.g. Kneisel et al., 2000b; Ishikawa et al., 2001; Vonder Mühl et al., 2001; Hauck and Vonder Mühl, 2003b; Marescot et al., 2003; Kneisel, 2004; Heggem et al., 2005; Krautblatter and Hauck 2007). In winter, however, it may be impossible to use ERT surveys as a dry snow cover acts as an electrical insulator. To overcome this problem, de Pascale et al. (2008) used a capacitive-coupled ERT system, the so-called OhmMapper instrument, that allows standard ERT measurements without the need for galvanic contact. For monitoring purposes, measurements are repeated at certain time intervals using a permanently installed electrode array. The fixed-

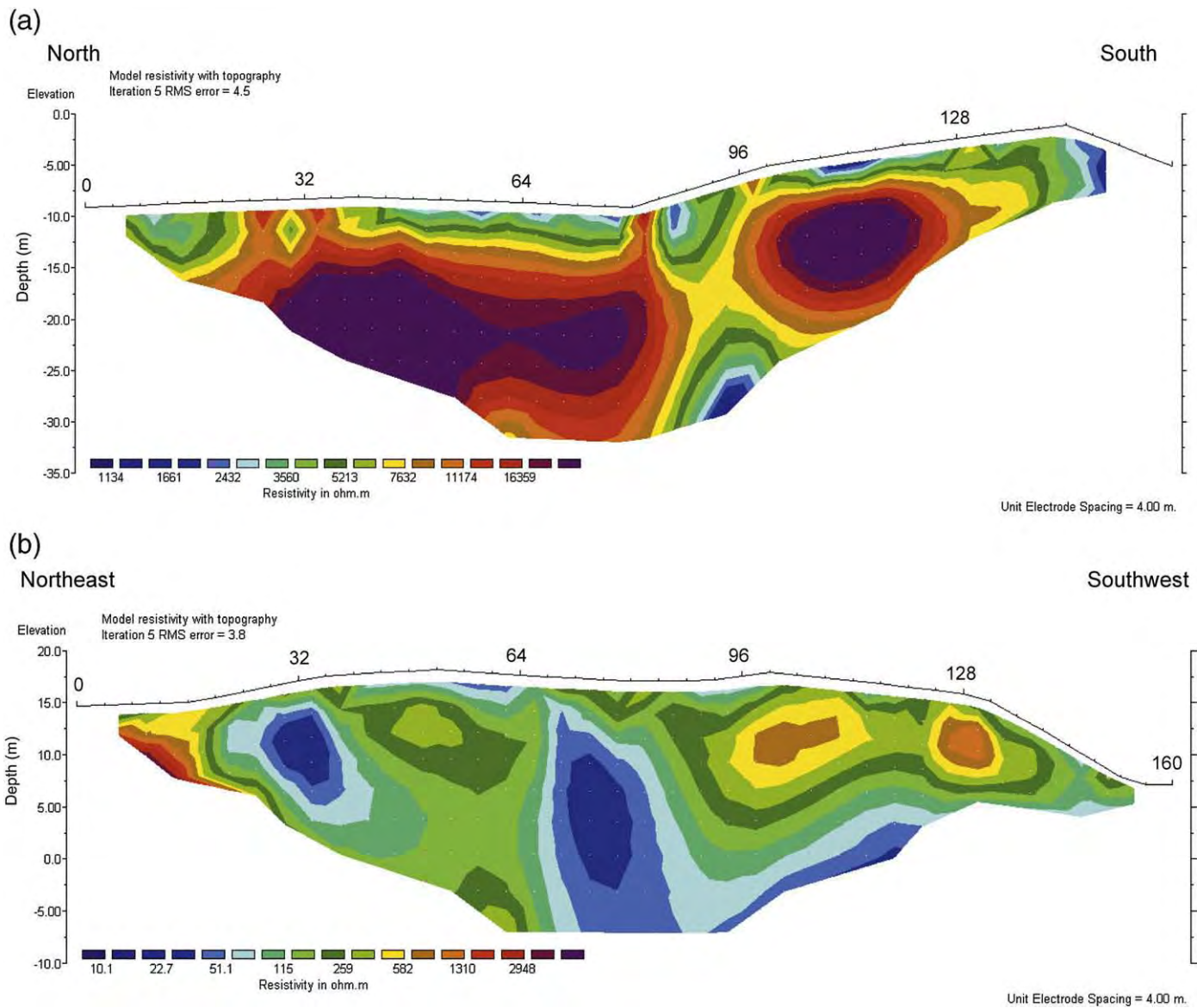


Fig. 17. Electrical resistivity tomograms through contrasting pingo types in Svalbard. (a) Innerhytte pingo, Adventdalen, above the marine limit. (b) Longyear pingo, Adventdalen, below the marine limit.

electrode array effectively filters resistivity variations due to variable electrode contacts or geological background variations, as mainly temporal resistivity changes are determined (Hauck, 2002; Hilbich et al., 2008a).

An example of the application of ERT surveys to investigate the nature and distribution of ground ice is provided by a recent study of the internal structure of open system pingos in Svalbard by Ross et al. (2007). At Innerhytte Pingo, located above the marine limit in Adventdalen, electrical resistivity tomography surveys identified a 3–4 m thick layer of relatively low to intermediate resistivity (1500–

6000 Ω m), and a zone of high resistivity (6000–30,000 Ω m) that extends to depths in excess of 20–25 m below the ground (Fig. 17a) and likely corresponds to a complex core of injection ice. These data are in accordance with resistivity values of pingo ice in Alaska (4500–18,000 Ω m) (Yoshikawa et al., 2006). In contrast, exceptionally low resistivity values (predominantly 10–400 Ω m, but up to 4000 Ω m) characterise the internal structure of Longyear Pingo (Fig. 17b), a younger and smaller open system pingo located below the marine limit in Adventdalen. This suggests that its core is dominated by segregation ice within a fine matrix of saline marine sediments.

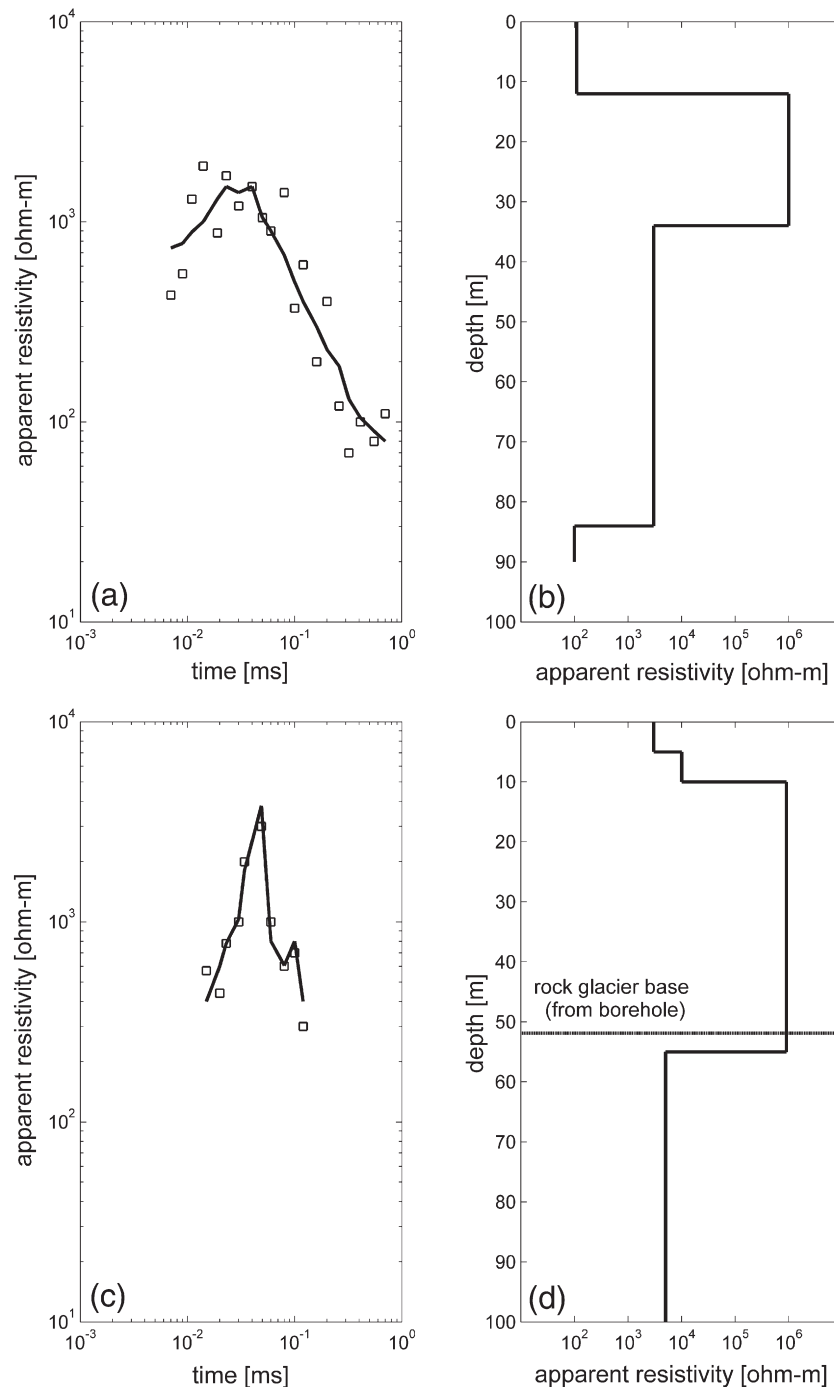


Fig. 18. Offset transient electromagnetic sounding data. (a) Measured (square symbols) and modelled (solid line) apparent resistivity values Muragl Rock Glacier, Swiss Alps. (b) Derived resistivity model, Muragl Rock Glacier, Swiss Alps. (c) Measured (square symbols) and modelled (solid line) apparent resistivity values Murtèl Rock Glacier, Swiss Alps. (d) Derived resistivity model, Murtèl/Rock Glacier, Swiss Alps. Depth of rock glacier base is marked by the horizontal line. In both field sites the high-resistive zones correspond to massive ground ice in the rock glacier core.

5.3. Electromagnetic induction mapping

Electromagnetic (EM) induction techniques measure the electrical conductivity ($1/\text{resistivity}$). A wire loop carrying an electrical current produces a primary magnetic dipole field, and this dipole field is varied either by using an alternating current operating in the frequency-domain (FEM method) or by terminating it (transient methods operating in the time-domain (TEM)). This time-varying magnetic field induces very small eddy currents in the Earth. The eddy currents generate a secondary magnetic field, that may be sensed by a receiver loop at the surface. The more conductive the subsurface, the larger are the eddy currents and the larger is the measured secondary field, which in turn allows the ground conductivity to be determined by a simple proportional relation (McNeill, 1980). In the case of FEM, further data processing is required, and the lateral variability of the bulk conductivity of the uppermost subsurface layer is determined, but with no or limited depth information (e.g. Hauck et al., 2001; Cannone et al., 2003). However, EM induction sounding allows the determination of vertical conductivity variations, and commonly utilises transient electromagnetic systems (TEM), measuring the induced secondary magnetic field in the transmitter-off periods, when the primary magnetic is terminated. The response of the subsurface in terms of the decaying amplitude of the secondary magnetic field is measured as a function of time and therefore of depth.

To illustrate the effectiveness of this approach, results of a recent assessment of permafrost status in the rock glaciers Muragl and Murtèl, Swiss Alps (Musil et al., 2002; Maurer and Hauck, 2007) are presented in Fig. 18. Voltages measured during offset TEM sounding were transformed into apparent resistivities (Fig. 18a and c) and finally inverted to yield a specific resistivity model with depth (Fig. 18b and d). The results indicate an approximately 10 m thick unfrozen surface layer ($\rho < 1 \text{ K}\Omega\text{m}$), which is slightly overestimated by the TEM, and a 20 m (Muragl) and 40 m (Murtèl) thick frozen layer ($\rho > 500 \text{ K}\Omega\text{m}$) above the assumed bedrock layer ($\rho < 10 \text{ K}\Omega\text{m}$), which is in good agreement with complementary geophysical and borehole data (Maurer and Hauck, 2007).

5.4. Ground Penetrating Radar (GPR)

Ground Penetrating Radar (GPR) has been successfully used to study permafrost distribution and structure in the Arctic and Antarctica for many years (e.g. Arcone et al., 1998a,b; Moorman et al., 2003; Munroe et al., 2007; Dallimore and Davis, 1987). Attenuation is highest (and therefore penetration lowest) in low-resistive earth materials (usually having a high liquid water content, particularly where pore water is saline) and in fine-grained sediments (even when frozen), where penetration depths can be less than 1 m. GPR is therefore best suited to investigating the unfrozen active layer in summer, and ice-rich permafrost. GPR surveys in mountain permafrost can be more difficult due to the low signal-to-noise ratio that arises from complex reflections within blocky layers, and can mask the true layer horizons. For high-resolution investigations, antennae with dominant frequencies between 20 and 100 MHz have proved to be suitable (Lehmann and Green, 2000; Isaksen et al., 2000a; Berthling et al., 2000) and adequate coupling of the antennae to the ground is extremely important. Data processing can include amplitude scaling to enhance later arriving events, and frequency filtering in the time and space domains to remove system noise and improve the coherency of reflected signals (Gross et al., 2003). If reliable velocity information is available, migration may be used to convert the processed time sections to equivalent depth sections. To account for the effects of strong topographic relief, special purpose topographic migration algorithms may be applied (Lehmann and Green, 2000).

In an arctic setting, GPR survey has recently been applied to investigate the internal structure of the open system pingo known as Riverbed pingo, located above the marine limit in Adventdalen (Ross et al., 2005, 2007). Reflections 0–7.5 m below the ground surface dipping sub-parallel to the surface (Fig. 19) were interpreted on the basis of geological evidence (Yoshikawa, 1993) as interbedded units of ground-ice and frozen partially disaggregated shale bedrock. The lack of basal reflections and poor signal penetration suggest attenuation of

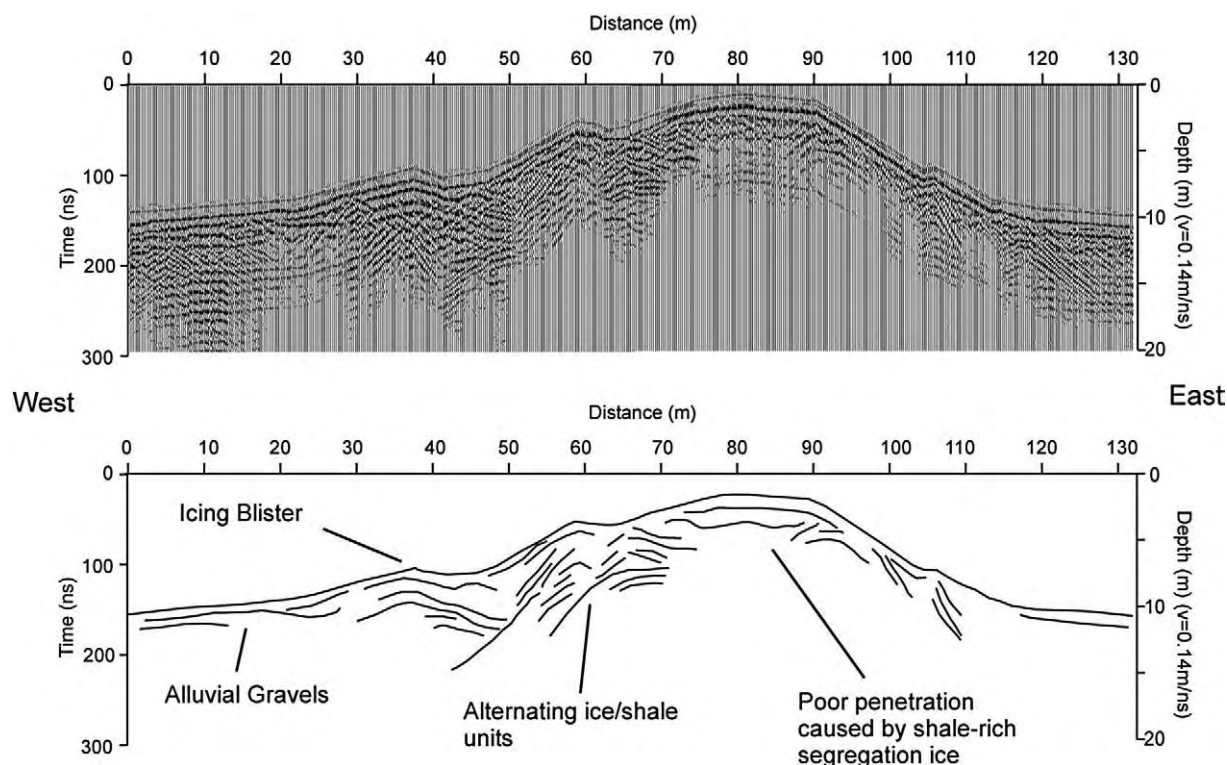


Fig. 19. Ground penetrating radar profile (100 MHz), Riverbed pingo, Adventdalen, Svalbard.

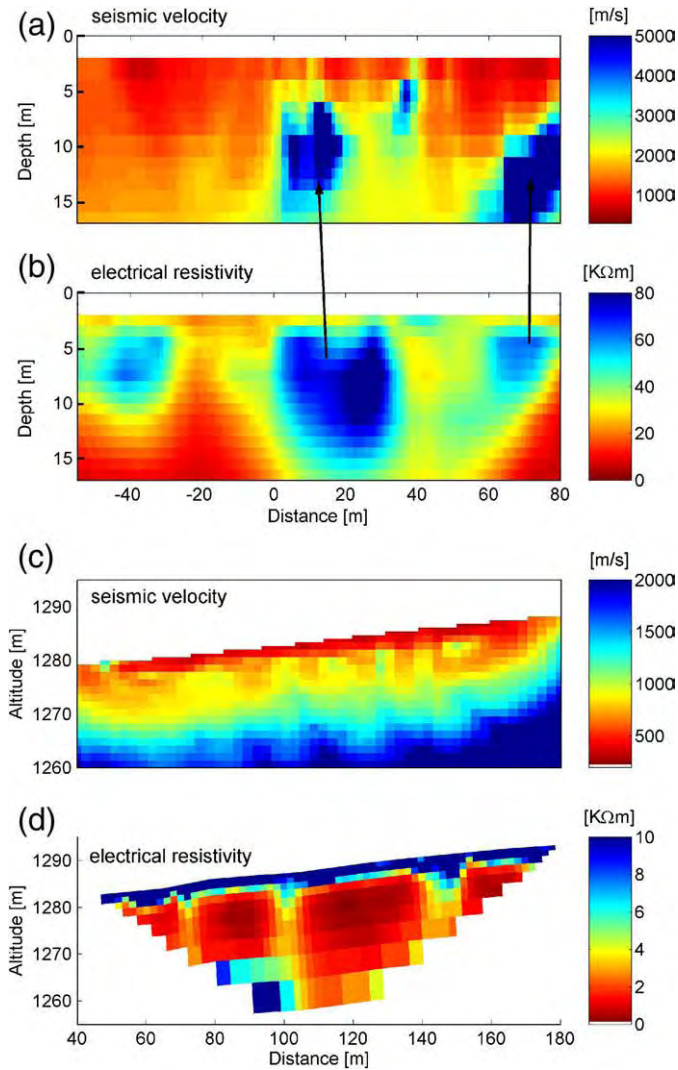


Fig. 20. Refraction seismic and DC resistivity inversion results for two field sites. (a) refraction seismics Val Bever, Switzerland. (b) DC resistivity Val Bever. (c) refraction seismics Juvvasshoe, Norway. (d) DC resistivity Juvvasshoe. The high-velocity anomalies (2500–4500 m/s, marked with the solid lines) in (a) indicate buried ice occurrences and the very low velocities (<500 m/s) in the uppermost 1–2 m in (c) indicate the presence of air-filled cavities (taken from Hauck and Vonder Mühl, 2003b).

the EM signal by the bedrock, and possibly a pingo core rich in segregation ice rather than massive intrusive ice.

5.5. Refraction seismic techniques

Refraction seismics has a long tradition in permafrost studies (e.g. Timur, 1968; Zimmerman and King, 1986; King et al., 1988; Ikeda, 2006). The P-wave velocity distribution can be used as a complementary indicator to resistivity for the presence of frozen material. The method is especially useful for differentiation between the presence of subsurface ice and air, and to determine the top of the permafrost layer, as the contrast for the P-wave velocity between the unfrozen top layer (= active layer, 400–1500 m/s) and the permafrost body (2000–4000 m/s) is usually large. For most permafrost applications using a sledgehammer as seismic source, depth penetration is slightly smaller than the corresponding penetration depth of resistivity surveys with similar horizontal survey lengths. Interpretation techniques are often based on layered models, but this may be of limited use for very heterogeneous ground conditions in mountainous environments. As with the ERT technique, tomographic inversion

schemes can be used for more reliable 2D interpretation (Musil et al., 2002; Hauck et al., 2004; Maurer and Hauck, 2007).

5.6. Crosshole methods

Conceptually, most geophysical techniques can also be applied by placing the sources in one borehole and receivers in another. Crosshole tomography provides detailed 2D information in the plane containing the two boreholes. The multiple illumination of subsurface targets provided by crosshole geometries results in more reliable and higher resolution than can be provided by most surface-based techniques. Ideally, the borehole separation should be about half the borehole depth. To date, crosshole methods have been used only where very detailed subsurface information is needed and boreholes are already present (e.g. Delisle et al., 2003; Musil et al., 2006) and since measurements are confined to the plane between the two boreholes, they are best combined with additional surface-based geophysical measurements (Maurer and Hauck, 2007).

5.7. Combined geophysical measurements

Since the environmental effects of permafrost degradation in a future changing climate depend largely on ground ice content, the similarity in resistivity between ice, air and certain rock types may present a problem in the interpretation of resistivity data. In such cases,

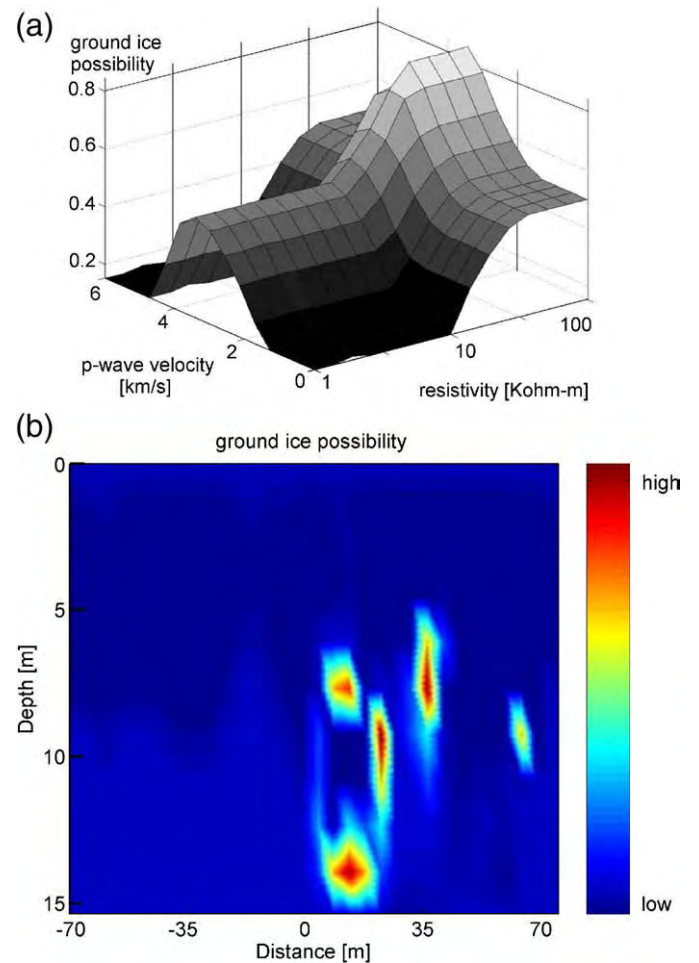


Fig. 21. (a) Decision surface for the fuzzy inference system for ground ice detection. Each value of seismic velocity (in km/s) and electrical resistivity (in Kohm-m) is associated with a degree of possibility for ground ice (z-axis). (b) Degree of possibility for ground ice for an example from Val Bever, Switzerland (based on data in Fig. 20 (a) and (b)).

it is necessary to use more than one geophysical method to improve interpretation in terms of permafrost delineation, ice content or stratigraphy. Complementary methods include (a) refraction seismics and ERT (Fig. 20), since the former differentiates between ice and water and the latter between ice and air, and (b) ERT and GPR, since ERT identifies the presence or absence of ice, whilst structural information is provided by GPR (e.g. Hauck and Vonder Mühll, 2003b; Farbroth et al., 2005; Otto and Sass, 2006). Other combinations, such as ERT, FEM and seismics (Hauck et al., 2004), TEM, seismics and GPR (Bucki et al., 2004), ERT, seismics, GPR and TEM (Maurer and Hauck, 2007) or even ERT, GPR, seismics and three different EM methods (Yoshikawa et al., 2006) may also be applied.

Newer approaches combine information from several geophysical data sets in a quantitative way. Hauck and Wagner (2003) used a fuzzy-logic approach to delineate those regions where the occurrence of ground ice was most likely. The input data were derived from ERT and refraction seismic surveys, the output indicated the “degree of ice content” (but not the ice content itself), that is the possibility of ground-ice occurrence. The fuzzy inference system used is based on nine rules, all linking low, medium and high resistivity and velocity values to a corresponding output (low, medium and high ice content). A practical view of the rule system is shown as a decision surface showing the likelihood of ground ice at Val Bever in Switzerland (Fig. 21a), where each pair of velocity (Fig. 20a) and resistivity (Fig. 20b) data points is associated with a possibility of ground-ice occurrence (Fig. 21b).

Another possibility is the so-called 4-phase model (Hauck et al., 2005, 2008), which is based on two well-known geophysical mixing rules for electrical resistivity (Archie, 1942) and seismic P-wave velocity (Timur, 1968). Due to the presence of four phases within the frozen material (rock/soil matrix, unfrozen water, ice and air), the respective volumetric fractions of the phases in the subsurface cannot be quantified by using one method alone. Using the above mixing

rules and a combination of electric and seismic data sets, the respective volumetric fractions of each phase (e.g. the ice content) can be approximated.

5.8. Monitoring permafrost change

In principle, all the above methods can be used to monitor changes by repeated measurements using the same survey geometry. ERT is possibly the most effective for monitoring ice content, and GPR for active layer thickness. A fixed 30 electrode array along a 58 m survey line was permanently installed at Schilthorn in September 1999 (Hauck, 2002). Resistivity surveys were made by connecting a standard 4-channel resistivity meter to a manual switchbox for each of the selected electrode configurations. Since September 1999 monitoring has included daily, seasonal and annual time scale studies (Hauck, 2002; Schudel, 2003; Völsch, 2004; Scherler, 2006; Hilbich et al., 2008a; Noetzi et al., 2008) confirming the effectiveness of the approach. Fig. 22 shows an example from 1999–2004, where the annual variation of the resistivity in the uppermost 10 m was determined. Instead of analysing the resulting resistivity tomograms in terms of absolute values, the resistivity change based on the first September measurement in 1999 are shown. Whereas the annual resistivity changes at greater depths were in the order of 10% until 2002, the anomalously warm summer of 2003 in the Alps caused a resistivity decrease of more than 30%, indicating substantial melting of permafrost. This coincides with a deepening of the active layer from 5 m to 9 m, as measured in a nearby borehole (Hilbich et al., 2008a).

Monitoring programmes at permafrost sites considered particularly sensitive to warming, such as potential debris flow source areas with high ground ice contents, or sites with structures sensitive to ground settlement, may in future incorporate such geophysical monitoring, coupled with ground temperature measurements, as an effective method of obtaining early indications of changes in ice

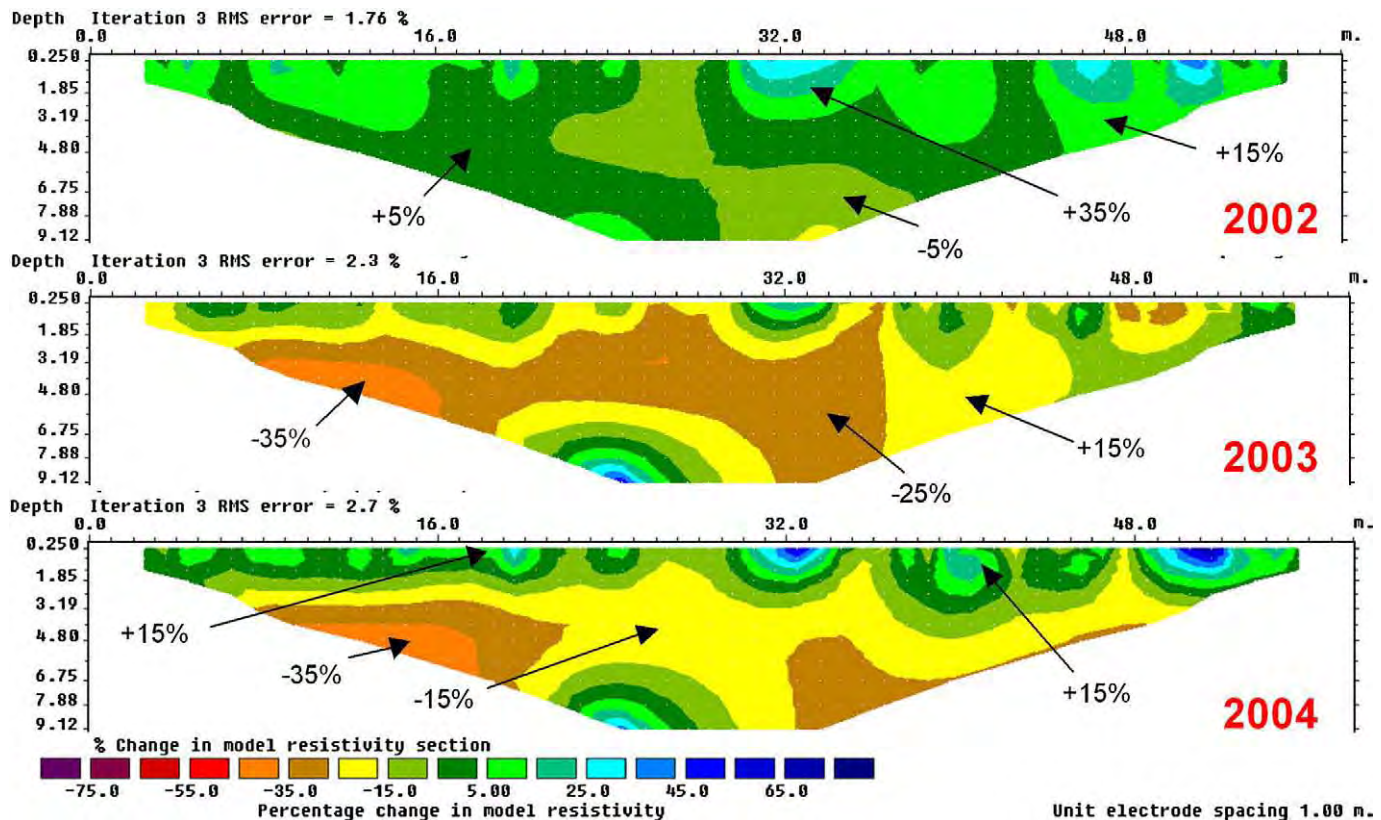


Fig. 22. Relative change in resistivity calculated for 3 ERT profiles in time-lapse mode for the years 2002–2004, each related to the baseline year 1999. Orange colours indicate regions with decreased resistivities due to thaw processes.

content or active-layer thickness. As a first step, long-term geophysical monitoring has now been included in the Swiss PERMOS network including the three PACE monitoring sites Murtél, Stockhorn and Schilthorn (Hilbich et al., 2008b; Noetzi et al., 2008).

6. Rock weathering

Climate-related changes in permafrost geothermal regime may lead to changes in the nature, intensity and the frequency of occurrence of many geomorphic processes. Changes in process intensity and type are associated with thawing (and sometimes simply warming) of permafrost and may lead to significant landscape response. Frequently such processes depend fundamentally on the nature and volume of ice formed during ground freezing and lost during ground thawing. Bedrock weathering in permafrost regions includes a number of physical and chemical processes, their nature and intensity varying both spatially and temporally according to environmental and geological conditions. Rock freezing and thawing may occur over a range of time scales, in the longer term as permafrost aggrades and degrades in response to climate change, seasonally as active layers

thaw and refreeze and seasonal frost penetrates then thaws, or over diurnal or shorter time scales, when frost is likely to penetrate into the near surface only (Fig. 23).

The change in phase of water from liquid to solid and vice versa within bedrock plays a critical role in reducing rock strength and eventually breaking the rock down (e.g. Rapp, 1960; Sass, 2005a; Stoffel et al., 2005). The 9% volumetric expansion accompanying phase change has traditionally been considered the main causal mechanism of frost weathering, though recently the role of ice segregation within certain bedrock lithologies has been recognised as potentially of greater significance. The main difference between the two is that the former arises from *in situ* freezing of water, while the latter involves water migration within freezing or frozen ground. Volumetric expansion occurs at the freezing point of the water occupying pores or cracks and requires a high saturation level (>90%) of the rock. In contrast, ice segregation can occur in unsaturated rocks. The presence of capillary and adsorbed water with a freezing point below 0 °C allows unfrozen pore water to migrate through partially frozen rock to supply progressive growth of ice lenses. The resulting rock fracture can occur at temperatures considerably below 0 °C (e.g. Walder and

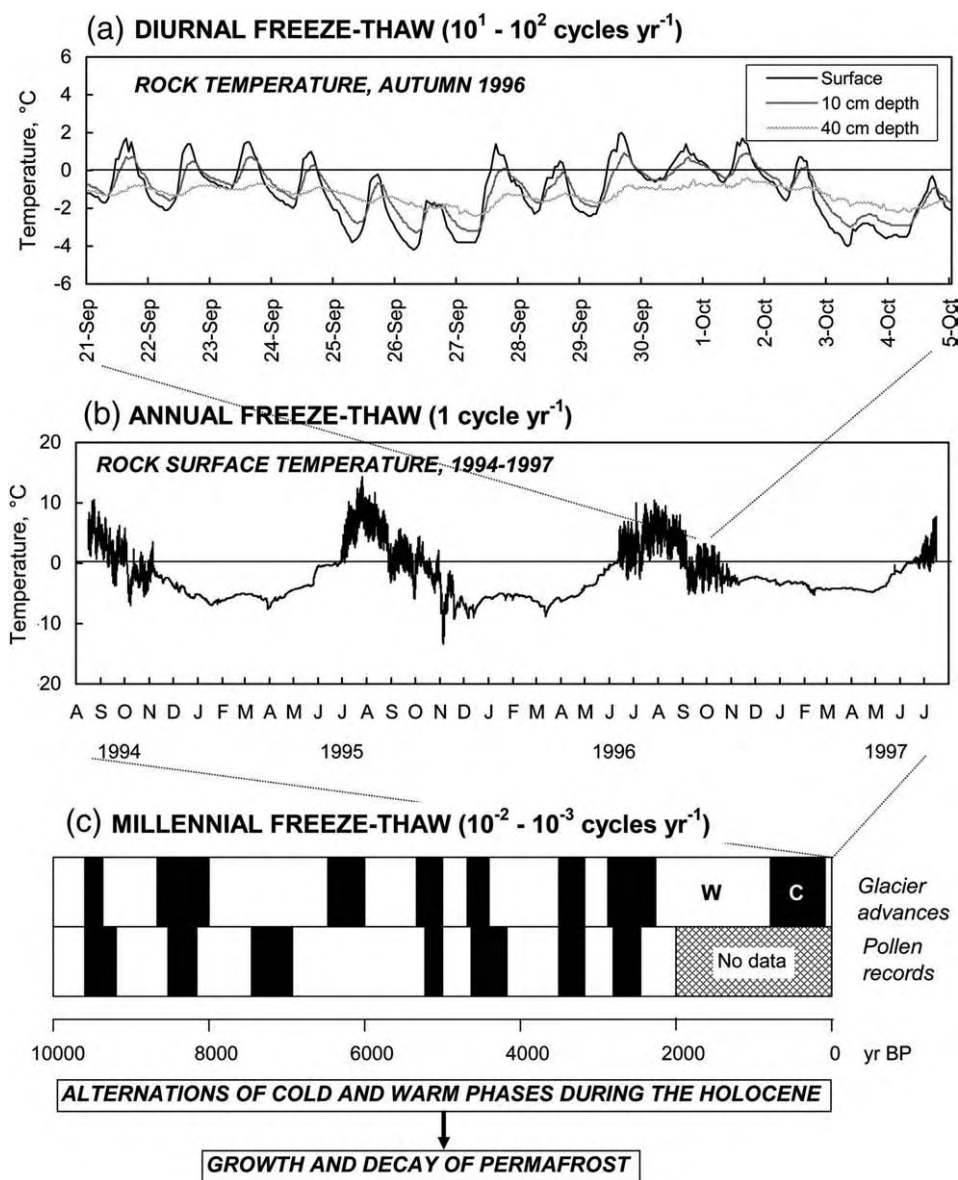


Fig. 23. Diurnal, annual and millennial freeze-thaw cycles in the Alps. A and B are based on data from Murtél-Corvatsch Southern Swiss Alps. C is compiled and simplified from Gamper (1993) and Burga (1993).

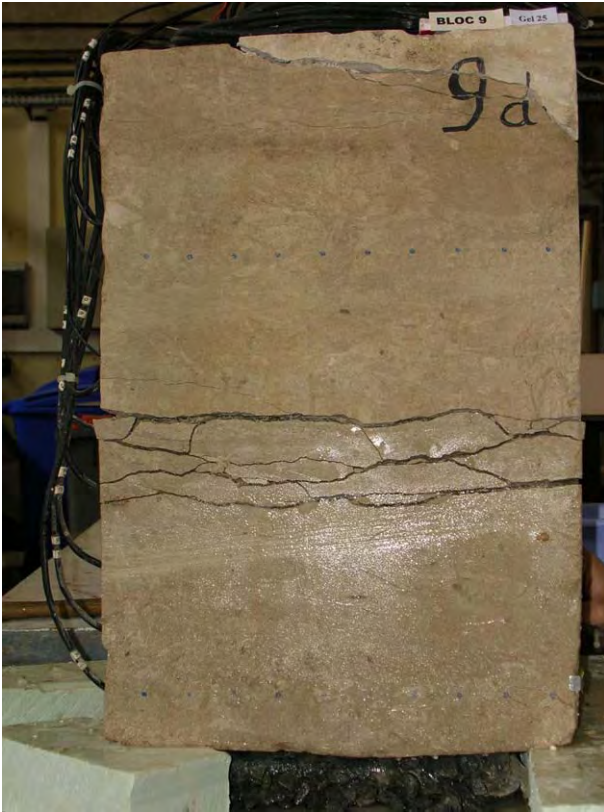


Fig. 24. Fractures formed by ice segregation in near-surface permafrost and the base of the active layer in moist chalk. The fractures are filled with segregated ice. The block of chalk is 450 mm high and 300 mm wide, and at the start of the experiment was unweathered and lacked visible fractures. The upper half of the block was subjected to 24 cycles of active-layer freezing and thawing, while the lower half remained as permafrost. The mean active-layer depth was 240 mm (SD±36 mm).

Hallet, 1985; Akagawa and Fukuda, 1991; Hallet et al., 1991; Murton et al., 2001), depending partly on the pore structure (e.g. Matsuoka, 2001a). Recent summaries of weathering processes, rates and products in cold regions are given by Hall et al. (2002), Murton et al. (2006) and Matsuoka and Murton (2008).

6.1. Ice segregation in frozen bedrock: laboratory and field evidence

In frost-susceptible soils, migration of water downwards from the active layer to the underlying permafrost leads to ice segregation and formation of an ice-rich zone, directly beneath the active layer, that thaws only during infrequent extreme summer events (Cheng, 1983; Schur, 1988; Shur et al., 2005). Field observations of fine-grained porous bedrock in the Arctic reveal a similar layer of ice-rich, fractured rock within the upper few metres of permafrost. Büdel (1982) observed an ice-rich layer, which he termed the “ice rind”, within a variety of sedimentary rocks (e.g. Triassic marly limestones, shales and arkoses) in the continuous permafrost zone of southwest Barents Island, Svalbard. Büdel attributed the ice rind to thermal contraction cracking and infilling of fractures with hoar frost. Subsequent Canadian observations from Melville Island (French et al., 1986), Ellesmere Island (Hodgson et al., 1991) and the Western Arctic Coast (Mackay, 1999) indicate a similar layer in the upper layer of permafrost within Mesozoic sedimentary rocks. In these cases, the ice was interpreted as segregated ice.

It has been unclear until recently if ice can fracture intact bedrock subject to natural freezing regimes, or whether it simply enlarges existing fractures or does both. This question is important, because if ice segregation in bedrock permafrost is widespread, then there may be considerable potential for significantly increased rock slope

instability associated with rising ground temperatures and thickening active layers in a period of climate warming. Laboratory modelling has now begun to elucidate the process of ice segregation in bedrock.

If freezing processes in porous rock are fundamentally the same as those in frost-susceptible soils (Walder and Hallet, 1986), then ice lenses will concentrate in wet rock just beneath the top of the permafrost and in the base of the active layer, leading to pervasive fracturing at these depths. To test this hypothesis, an experimental methodology was developed and systematic experiments were carried out to simulate a bedrock active layer above permafrost that in winter freezes from the ground surface downwards and from the permafrost table upwards (Murton et al., 2000, 2001, 2006). The experiments clearly demonstrated that ice segregation fractures the upper layer of permafrost and the base of the active layer in moist chalk (a porous limestone). At the beginning of the experiments the chalk was unweathered and lacked visible fractures. But after repeated cycles of active-layer freezing and thawing, fractures filled with segregated ice had formed in the uppermost permafrost and in the lower part of the active layer.

Fig. 24 shows an example of an experimental block 450 mm high in which net heave of the rock surface was almost 13 mm over the course of 24 seasonal cycles. The dominant fractures are more or less horizontal, which is expected because the isotherms were parallel to the permafrost table. The permafrost table determines the depth of ice segregation. Heave data indicate that ice segregation and fracture occur not only during upward freezing (early winter) of the active layer but also during the late stages of thaw cycles (late summer) as water migrates down below the base of the active layer and into the underlying permafrost (Fig. 25), as occurs in summer in Arctic permafrost soils (Mackay, 1983). In summary, the experiments showed that moist, porous rock behaves remarkably like moist, frost-susceptible soil, with both substrates experiencing ice enrichment and fracture/fissuring of near-surface permafrost. It appears that significant concentrations of segregated ice are most likely in the transition zone between the active layer and the permafrost, as a result of downward migration of water in summer and upward advance of freezing at the beginning of the winter (Murton et al., 2001, 2006; Sass, 2005b).

Laboratory modelling discussed above indicates clearly that given adequate water supply, ice segregation produces a zone of ice-bonded fractured bedrock immediately below the permafrost table. In general,

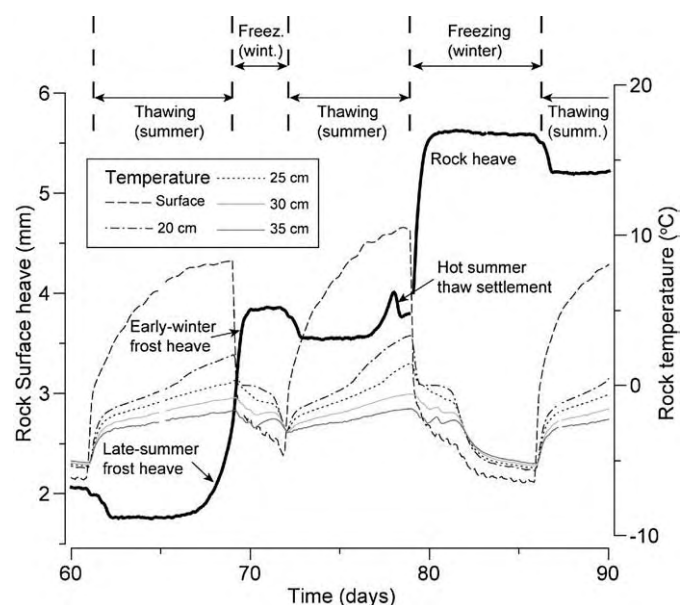


Fig. 25. Temperatures and frost heave during laboratory simulation of three annual cycles of active layer freezing and thawing in chalk bedrock.

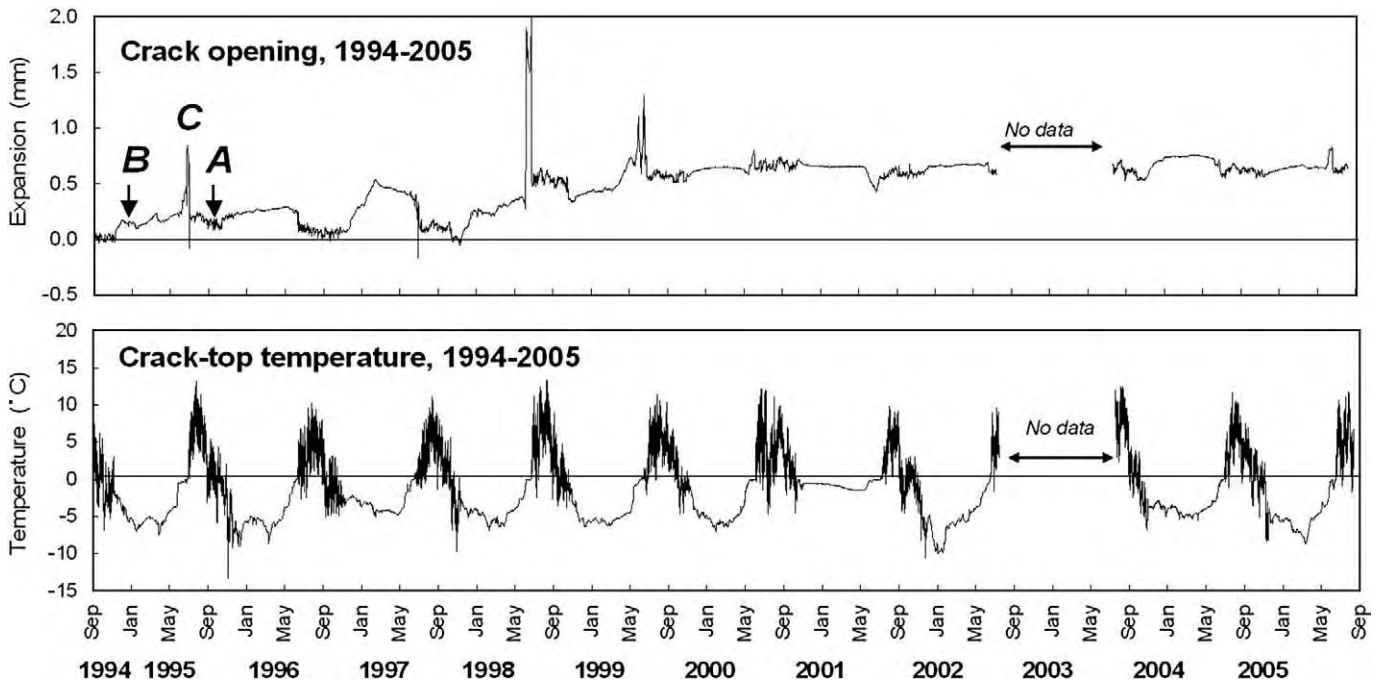


Fig. 26. Monitoring frost wedging at MW site (Murtèl–Corvatsch). Three types of movements (Types A–C) are identified. Note significant permanent opening from 1997 to 1999.

the importance of ice segregation relative to in-situ volume expansion increases with decreasing thermal gradients and increasing duration of freezing (Powers and Helmuth, 1953; Walder and Hallet, 1985). Rempel and co-workers (2004) suggest that the maximum possible disjoining pressure is governed by the temperature depression below the bulk-melting point, even in the absence of large temperature gradients, and therefore slow ice segregation in bedrock may be possible at greater depths where the frozen permeability of rock limits the actual amount of heave produced. Thus, over long timescales, ice segregation may be highly significant in frozen steep bedrock slopes where the presence of ice-rich fractured bedrock may be critically important in releasing rock falls and rock slides during climate-induced warming and permafrost degradation (see Section 7 of this paper).

6.2. Temporal scales of frost weathering

A high frequency of frost cycles is likely to be most effective within the outermost decimetre of bedrock, leading to the spalling off of relatively small (up to pebble size) rock fragments (Matsuoka, 1994) though lack of moisture may considerably reduce the number of effective freeze-thaw cycles (e.g. Prick, 2003). Seasonal freezing progresses much more slowly – over a period of a few months – but penetrates deeper into the bedrock. The annual freezing and thawing depth varies with the surface freezing or thawing index, thermal conductivity and moisture content of the rock, but may reach several metres (Matsuoka, 1994; Wegmann and Gudmundsson, 1999; Gruber et al., 2004a).

The roles of diurnal and annual freeze-thaw cycles in rock weathering have recently been evaluated through long-term field measurements of near-surface rock temperatures and rock joint widening at rockwalls near the altitudinal boundary between the permafrost zone and seasonal frost zone in the Engadine, Swiss Alps (Matsuoka et al., 1997, 1998, 2003; Matsuoka, 2008). Here three types of rock joint widening were distinguished (Fig. 26): repetitive and frequent opening and closing of the order of 10^{-2} mm during diurnal freeze-thaw cycles in autumn and in early summer (type A); widening of 0.1–0.5 mm that accompanied seasonal freezing in early winter (type B); and finally, widening (often exceeding 0.5 mm) at the onset of seasonal thawing, probably resulting from refreezing of snow melt

entering the rock joint at a subfreezing temperature (type C). At Murtèl–Corvatsch, these events resulted in permanent widening of the joint at a rate of 0.06 mm a^{-1} over 11 years (1994–2005), with most change associated with significant type C events.

The rate of surficial rock weathering resulting from diurnal freezing and thawing may be significantly affected by climate changes through an increase or decrease in cycle frequency, or through modification of ground surface insulation arising from changes in vegetation or snow-cover. An increase in mean annual air temperature is also likely to deepen the active layer by thawing of the uppermost part of the permafrost, and hence increase the potential thickness of rock fall material.

7. Rockfalls and rockslides

7.1. Field monitoring of annual debris production from rock walls

In the Swiss Alps, production of pebble-sized (and smaller) rock debris has been observed annually by collecting recently fallen rock

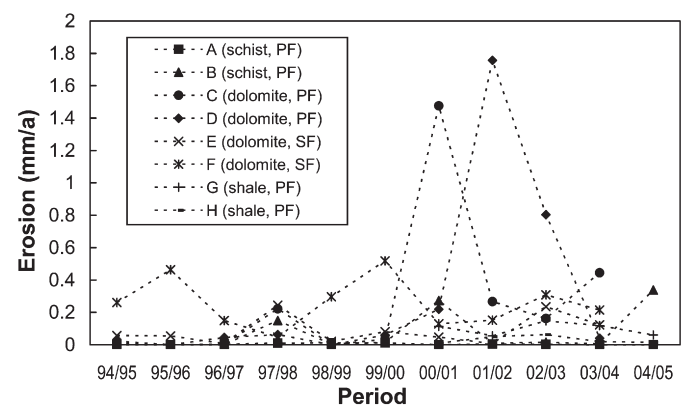


Fig. 27. Inter-annual variations in the annual rockwall retreat computed from the volume of rock debris released from painted quadrangles. PF: Bedrock underlain by permafrost. SF: Bedrock subjected to seasonal frost.

fragments released from painted quadrangles 50 cm × 50 cm wide at sites in the Engadine, (Matsuoka et al., 2003; Matsuoka, 2008). For each quadrangle, the total volume of fragments was converted to the annual rockwall erosion. The observed rockwall erosion rates were about 0.1 mm a⁻¹ on average, although this was increased by sporadic occurrences of extreme rates (1.5–1.8 mm a⁻¹) (Fig. 27). The interannual variability of the debris production rate is likely to depend mainly on the freeze-thaw cycle frequency, snow-cover and moisture availability (Sass, 2005a,b).

Average rockwall retreat rates calculated on the basis of these measurements were much lower than the long-term rates estimated from the volume and age of talus rock glaciers in the Alps (e.g. 1–2 mm a⁻¹: Haeberli et al., 2001). This indicates that falls of pebble-sized and smaller rock fragments only account for up to 10% of the long-term rockwall retreat. In other words, seasonal or episodic larger scale boulder falls govern the long-term evolution of these alpine rockwalls. One such boulder fall, equivalent to about 100 m³ in total volume (or around 2.5 mm of rockwall retreat), was recorded at Murtèl–Corvatsch in mid June 1997 (Matsuoka, 2008). Rockfalls comprising large boulders tend to occur in summer in response to progressive seasonal thaw penetration and/or refreezing of meltwater (e.g. Rapp, 1960; Matsuoka and Sakai, 1999; Stoffel et al., 2005). An increase in scale and frequency of such rockfall events would, therefore, contribute to a significant increase in the overall rate of rockwall retreat (see below).

7.2. The role of permafrost in the initiation of rockfall events

Atmospheric and ground temperatures are strongly coupled on steep mountain bedrock slopes due to the absence of an insulating interface of snow, vegetation and soil material. Climatically-driven permafrost degradation can lead to increased instability leading to a serious increase in hazard and risk (c.f. Varnes 1984 for definitions of hazard and risk). A large number of rock fall events that most likely originated in permafrost areas have been inventoried for the Alps (Deline, 2002; Noetzli et al., 2003). In glacial environments in particular, rock falls have the potential to trigger down-slope cascades of hazardous events (Huggel et al., 2004) with especially long runout distances (Evans and Clague, 1988; Noetzli et al., 2006). An example that illustrates the potential scale of such events was the rock/ice avalanche of 2002 at Kolka/Karmadon (Haerberli et al., 2004; Huggel et al., 2005) that travelled 19 km down a sparsely populated valley in the Russian Caucasus and claimed the lives of 140 (see Section 12).

Research into relationships between permafrost and the stability of Alpine rock faces was initiated in the 1990s (Haerberli et al., 1997; Wegmann, 1998; Wegmann et al., 1998) and renewed impetus has come from improved measurement strategies and technology in combination with more sophisticated models (Gruber et al., 2003a,b; Gruber et al., 2004a). The extreme summer in 2003, when the months of June, July and August were the hottest on record in the Alps (Schär et al., 2004), led to significantly deeper active layers than normal (see Section 3.3) and greatly increased rock fall activity (Schiermeier, 2003; Gruber et al., 2004b). Measurements (Fig. 5) and model experiments (Gruber et al., 2004b) confirmed the extraordinary response in active layer thickening during 2003. Careful observation of detachment surfaces located within the permafrost zone immediately following failure often revealed the presence of ice that formerly occupied, and probably cemented, the discontinuities along which failure occurred (Fig. 28).

In steep, cold mountain ranges such as the European Alps, where permafrost in bedrock slopes makes up a large proportion of the total permafrost area, the presence of ice-bonded discontinuities is likely to be a decisive factor in the stability of rock faces (Haerberli and Gruber, 2008). Unlike slope geometry, structure and rock mass properties, the presence of permafrost constitutes a transient element that responds rapidly to climate change or human disturbance. Recently Gruber and

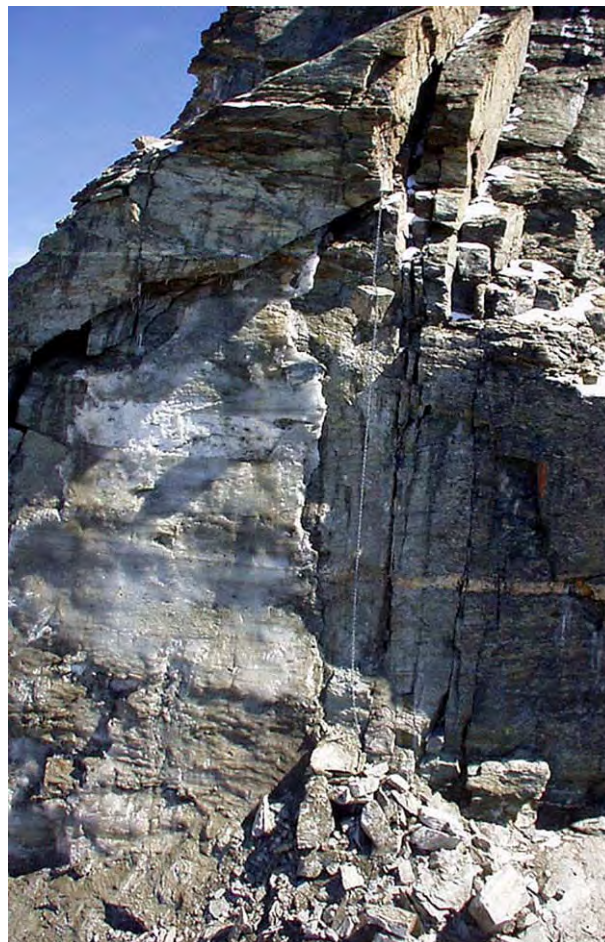


Fig. 28. Ice-covered detachment surface exposed by release of a rock fall in 2003 on the Matterhorn Lion ridge. Photo: L. Trucco.

Haerberli (2007) have provided an overview of warming-induced destabilization in steep bedrock and highlighted the following evidence for the importance of permafrost:

- a) the high proportion of rock fall events originating in permafrost areas;
- b) ice observed on fresh detachment surfaces immediately after several events;
- c) the presence of wide ice-filled fissures in bedrock;
- d) the potential temperature-dependent loss of stability in permafrost (see below);
- e) recent research demonstrating physical processes that actively widen frozen rock joints; and
- f) observed warming of both atmospheric and rock temperatures.

7.3. Mechanisms leading to rock fall

Permafrost rock walls in general only present a hazard when they are jointed. Loss of strength of ice-bonded joints during warming or thaw is likely to be related to changes in ice/rock interlocking (Davies et al., 2001), ice-rock adhesion (Ryzhkin and Petrenko, 1997), pore water pressure, ice crystal geometry (Voytkovskiy and Golubev, 1973) and presence of impurities (Hooke et al., 1972; Paterson, 1994). It is well known that the shear strength of ice is usually higher at lower temperatures and decreases toward the bulk-melting temperature (e.g. Fish and Zaretsky, 1997). This has been demonstrated in laboratory direct shear tests and centrifuge experiments (Davies et al., 2001, 2003) where the shearing resistance of a frozen ice-bonded bedrock slope was shown to fall during warming. Direct shear

tests and centrifuge modelling of ice-filled joints in an instrumented model rock slope imply that where the direction of dip of the joint planes is appropriate, the stability of a steep, jointed rock slope may be maintained by the ice (Davies et al., 2000, Davies et al., 2001). In all cases, the factor of safety reduces when the temperature increases.

Thus, many processes (operating at different temperatures and time scales) may translate warming or thaw of permafrost into reduced rock slope stability. In view of current understanding and results of laboratory experiments (see Section 6.1), it appears plausible that very slow growth of segregation ice over a long period during permafrost aggradation and stability might actively widen joints in their frozen state and thus contribute to a reduction in stability when permafrost subsequently warms and thaws (Gruber and Haeblerli, 2007). Warming may result from changes in snow and ice cover ice during the retreat of glaciers (c.f. Fischer et al., 2006), as well as the direct effects of atmospheric temperatures.

7.4. Modelling near-surface rock temperature response to changing boundary conditions

Surface temperatures are mainly controlled by the surface energy balance that depends on climatologic variables, topographical factors and surface characteristics (see Section 4) (Hoelzle et al., 2001; Mittaz et al., 2000). Since snow and soil cover are sparse or absent, the surface temperatures of steep rock walls mainly change with aspect (short-wave radiation), altitude (sensible heat and longwave incoming radiation) and lithology. In complex high mountain topography these factors can change significantly over very short distances leading to spatially highly variable surface temperatures.

Several researchers report rock surface or near-surface temperature measurements (e.g. Coutard and Francou, 1989; Hall, 1997; Matsuoka et al., 1997; Wegmann, 1998; Matsuoka and Sakai, 1999; Hall and André, 2001; Lewkowicz, 2001) but a coherent spatial pattern can usually not be deduced. A combination of systematic measurements and modelling was used by Gruber et al. (2003a,b, 2004a) to investigate spatial (mainly related to topography), regional (related to climate) and temporal variations in rock surface temperatures. Fourteen time series of daily near-surface rock temperatures from rock faces in the Alps between 2500 and 4500 m a.s.l., with different exposure to solar radiation (aspect) were used to further develop and validate an energy-balance model that simulates surface temperatures over alpine topography. The validated model was then used to perform 21-year forward model runs based on meteorological data (Fig. 29). The high temporal and spatial variability of simulated mean annual ground temperatures during those 21 years demonstrated the importance of a combination of measurements and modelling. Surface conditions such as the presence of snow or ice in the rock wall can have a strong effect on surface temperatures, but currently little is known of their influence.

Salzmann et al. (2007a,b) have assessed a possible range of changes in ground surface temperatures in steep rock. Surface temperature scenarios were calculated based on an energy balance model and climate time series that were downscaled from output of Regional Climate Models (RCM). In order to account for the uncertainties associated with RCM output, a set of 12 different scenario climate time series were applied to simulate the average change in ground surface temperatures for 36 different topographical situations. Results show a significant influence of topography on the temperature changes because it modifies the amount of solar radiation received at the surface. In addition, north-facing surfaces show a higher sensitivity to the climate scenario used while the uncertainty for south-facing surfaces is generally higher.

In alpine environments, most topographic features such as mountain peaks or steep ridges are 3-dimensional in nature and geothermal responses to change in ground surface temperatures are similarly strongly three dimensional. Such three dimensional complexity in the ground thermal field influences the heat flow density and generates strong lateral heat fluxes (Wegmann, 1998; Gruber et al., 2004c). In order to describe these effects, Noetzli et al. (2007) conducted a series of numerical experiments using idealised test cases. Subsurface temperatures were calculated for simplified ridges, peaks and spurs that were identified as the most typical topographic features found in high mountains. For this purpose, a modelling chain that combines the processes in the atmosphere (climate), at the surface (energy balance) and in the subsurface (heat conduction) has been developed. Surface temperatures were calculated using an energy balance model driven by climate time series. These were then used as upper boundary conditions in a numerical 3D heat conduction scheme that determines temperatures at depth. Climate time series gained from RCMs and generated in the scope of a study by Salzmann et al. (2007a,b) were used for time-dependent model runs.

Results indicate complex 3-dimensional patterns of temperature distribution and heat flow density below mountainous topography for equilibrium conditions, that are additionally perturbed by transient effects. The steady state temperature field below complex topography is basically controlled by the spatially varying surface temperature of different mountain sides and is little influenced by the geothermal heat flux (Fig. 30). Isotherms are nearly vertical and a strong heat flux is directed from the warmer to the colder sides of a mountain. This leads to permafrost occurrence at many locations where temperatures at the surface do not indicate it, e.g., on the south face of ridges or below the edges of a peak. Permafrost degradation in steep topography takes places from different sides, affecting both the permafrost table and the permafrost base leading to an increase in the pace of permafrost degradation as compared to flat terrain, where warming penetrates vertically into the ground. For the investigation of permafrost occurrence in complex terrain and its response to climate forcing, it is therefore important to account for 3-dimensional effects

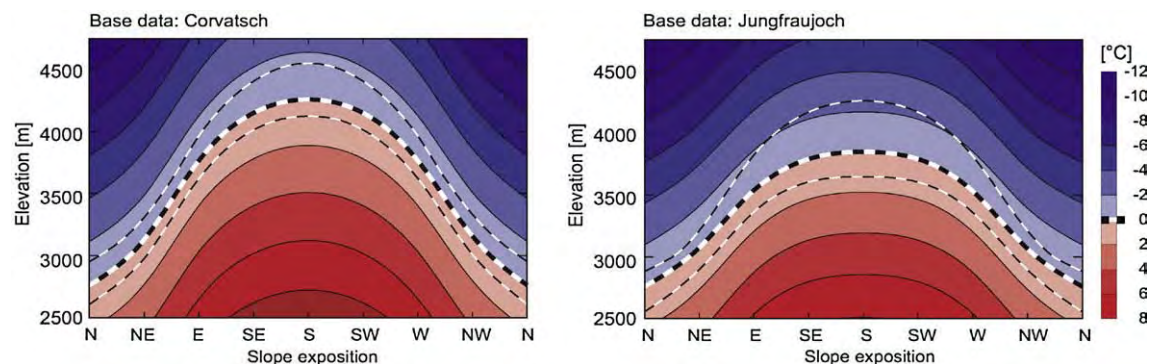


Fig. 29. Mean simulated annual rock surface temperature for 70° slope steepness and two locations, 1982–2002. The thick dashed line indicates the elevation of the mean 0 °C isotherm during this period. The thin dashed lines indicate the highest and lowest positions of the mean annual 0 °C isotherm. From Gruber et al. (2004b).

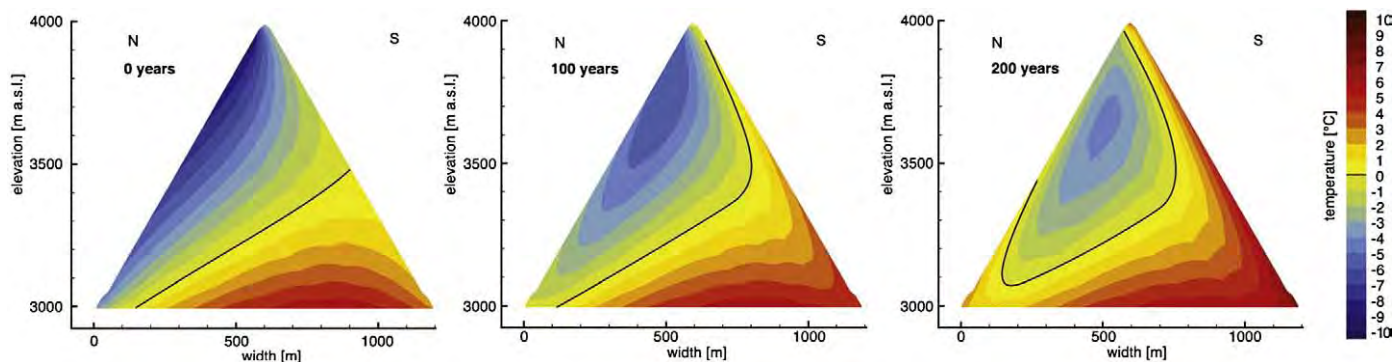


Fig. 30. Distribution and evolution of subsurface temperatures in a simplified ridge with a gradient of 60° for steady state (0 years) and after time periods of 100 and 200 years. The warming at the surface was set to +3.5 °C for north slopes, +2.5 °C for south slopes and +3 °C for east and west slopes over a time period of 100 years. The black line corresponds to the 0 °C.

(caused by geometry and variable surface temperatures) and transient effects (Noetzli et al., 2007). This type of artificial geometry is suitable for the investigation and understanding of thermal effects at depth, and the modelling chain applied in Fig. 30 (Noetzli et al., 2007; Salzmann et al., 2007a,b) can easily be applied to study the distribution and evolution of mountain permafrost temperatures in response to extreme events (e.g., warmer than average summer periods), or to investigate transient states of thermal fields in real topography.

7.5. The significance of scale in a warming climate

The thermal response of permafrost to atmospheric warming generally takes place at different scales of time and depth (Haeblerli et al., 1997; Haeblerli and Beniston, 1998; Lunardini, 1996), that correspond to frequency and magnitude of potential rock slope destabilisation (Fig. 31). Following increases in surface temperature, with a delay of only months or years, the active layer thickens, and thus, new volumes of rock will be subject to critical temperature ranges or thaw. This rapid and immediate response corresponds to events observed in the hot summer of 2003. A longer timescale response relates to the temperature profile within the permafrost, which is displaced towards the warmer side as the warming propagates downwards (See Section 3.4). Eventually, the lower permafrost boundary (up to several hundred metres depth) will rise, potentially causing large and deep-seated instabilities delayed by decades or centuries. The Brenva Glacier rock avalanche (Deline, 2002) that occurred in January 1997 in the Mont Blanc East face, Italy, may be related to such deep-reaching and long-term changes of the subsurface thermal conditions. Ice content additionally influences the response time by the uptake of latent heat (Wegmann, 1998; Noetzli et al., 2007) and can influence the time scales of permafrost degradation by about an order of magnitude. Clearly, the assessment of hazard and risk arising from future climate-related changes in rock fall magnitude and frequency must take account of the complex transient thermal fields within high mountain permafrost.

8. Creeping permafrost: rock glaciers and climate

8.1. Rock glacier thermal condition

Creeping perennially frozen debris streams, or rock glaciers (Fig. 32) are widely reported in cold mountains (e.g. Barsch, 1992) and are fundamentally characterised by their thermal state (Haeblerli, 2000). The rock glacier surface layer consists of debris with typical diameters ranging from several centimetres, decimetres, to metres, depending on the geological setting, weathering conditions, and processes of debris reworking. If this layer is at least as thick as the local active layer, summer thawing cannot reach the underlying

ground-ice containing permafrost body, which therefore persists. The difference between rock glaciers, dead glacier ice, and debris-covered glaciers can thus be defined by the thermal state of the material, since rock glaciers by definition require the presence of permafrost. The debris on and within rock glaciers may be derived from periglacial and glacial processes, and the rock glacier ice content may originate from refreezing rain and meltwater, glacier ice, buried ice, avalanche snow, and snow patches, etc., or combinations thereof (Haeblerli and Von der Mühll, 1996; Humlum et al., 2007). Temporal transformations and spatial transitions between rock glaciers, debris-covered glaciers or dead ice, ice-cored moraines, etc., are certainly possible, and indeed often found in nature.

Rock glaciers provide a clear topographic expression of the presence of perennially frozen ground. Rock glaciers may, however, end above the regional permafrost limit due to topographic conditions, the lack of sufficient material supply, or insufficient time to fully develop. On the other hand, the coarse debris cover on top of a rock glacier favours ground cooling due to enhanced heat transfer to the atmosphere and rock glaciers may therefore extend below the regional permafrost limit when the surrounding terrain cover causes relatively higher ground temperatures.

8.2. Rock glacier dynamics

The basic concept of mass transport within a rock glacier can be derived from the characteristic thermal and kinematic conditions. Frozen ice-rich debris is transported down-slope by gravitational creep, with the highest rates at the surface. The advected surface material then falls over the steep rock glacier front. The grain-size

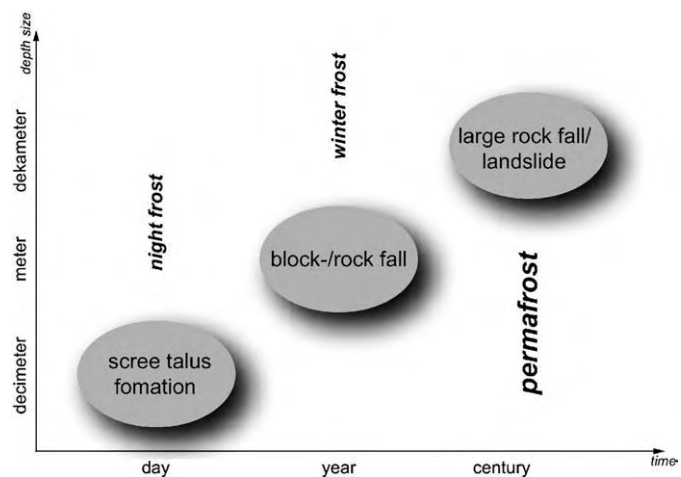


Fig. 31. Time and depth scales involved in slope stabilities in high-mountain areas.



Fig. 32. Muragl rock glacier, Upper Engadine, Swiss Alps.

sorting along the frontal slope occurring during this process leads to the typical appearance of rock glacier fronts. The surface debris that accumulates at the front is then overridden by the advancing rock glacier and again incorporated into its base (“caterpillar” or “conveyor belt” effect) (Kääb and Reichmuth, 2005).

In the case of a total cessation of mass supply, a rock glacier would continue to advance as long as sufficient ice is present, and shear stresses are sufficient to make creep possible. Loss of interstitial ice would lead to stagnation of the rock glacier, but not retreat. The main process of mass loss is the melt-out of ice at the rock glacier front where the thermally protecting debris cover becomes thinner than the thaw depth due to frontal erosion. In addition, the frontal grain-size sorting leads to smaller grain sizes in the upper part of the front, reducing the insulation effect in comparison to the coarser debris at the rock glacier surface. Due to the melt-out of ice, the potential loss of solids, and the decrease of horizontal speeds with depth, the advance rate of rock glaciers is significantly smaller than their surface speed. Advance rates measured so far range from a few centimetres to decimetres per year (Kääb, 2005).

8.3. Geotechnical properties of coarse frozen soils in relation to permafrost creep

Arenson et al. (2007) present a detailed overview of the geotechnical properties of coarse frozen soils, characterised by high ice and air content. The behaviour of frozen finer-grained soils is discussed by Andersland and Ladanyi (2004) and Esch (2004). The strength and the deformation behaviour of frozen soils is mainly a function of i) ice and air content, ii) temperature, iii) loading rate (Goughnour and Andersland, 1968; Ting, 1983; Arenson et al., 2003a; Arenson and Springman, 2005a). Laboratory investigations suggest that dispersed soil particles within dirty ice change the failure mechanism, so that strength is slightly lower than in pure ice (e.g. Hooke et al., 1972; Yasufuku et al., 2003; Arenson and Springman, 2005a). As the volumetric ice content decreases, structural hindrance between the solid particles develops and dilation occurs, increasing the strength and reducing creep deformation significantly.

At high relative soil densities, the ice cements the matrix, and the resulting increase in strength over the same soil in its unfrozen state may be quantified as cohesion at zero stress (e.g. Arenson et al., 2004). However, at large strains, ice-bonding fails, destroying the cohesive

effect and the large strain strength of the frozen material is tending towards a similar strength to that of the equivalent unfrozen soil. In other words, the thawed large strain strength can be considered as a lower boundary for the frozen state. Since the strength of ice decreases as the temperature increases, so does the strength of the frozen soil.

8.4. Measurement of rock glacier creep

Technological advances have resulted in the rapid introduction of new methods for quantifying small-scale ground movements and today a range of ground-based, airborne and spaceborne methods are applied in monitoring temporal and spatial trends in rock glacier creep rates. Terrestrial surveying techniques such as polar survey and global navigation satellite system (Zick, 1996; Berthling et al., 1998; Kääb et al., 2003b; Kääb and Weber, 2004; Lambiel and Delaloye, 2004) have provided time series of rock glacier movement with comparable high temporal resolution and thus revealed inter-annual and seasonal speed variations (Schneider and Schneider, 2001; Kääb et al., 2005a,b). Terrestrial laserscanning (Bauer et al., 2003) and perhaps also terrestrial radar interferometry are likely to become increasingly important in resolving small spatio-temporal variations of rock glacier surfaces.

Photogrammetry, based on repeat optical data (mostly air-photos), has been used to measure entire surface velocity fields on rock glaciers or groups of rock glaciers, and also to measure spatio-temporal variations of rock glacier velocity (Kääb and Vollmer, 2000; Kaufmann and Ladstädter, 2003; Kääb and Weber, 2004; Roer et al., 2005) (Fig. 33). Repeat airborne laserscanning, though not yet applied to rock glaciers, has a large potential to measure rock glacier volume changes and, to some extent, horizontal displacements (Geist and Stötter, 2003). Spaceborne radar interferometry is being applied to detect and quantify rock glacier surface deformation over large areas (Rott and Siegel, 1999; Rignot et al., 2002; Kenyi and Kaufmann, 2003; Strozzini et al., 2004). Due to the millimetre-accuracy of this technique even small displacements can be detected.

More traditional approaches to rock glacier movement monitoring have included repeat slope indicator measurements in boreholes to investigate the vertical variation of velocities within rock glaciers (Arenson et al., 2002) and occasionally, ground-based mechanical techniques designed to measure surface deformation (Haeberli, 1985; White, 1987). Finally, qualitative investigation of rock glacier creep has

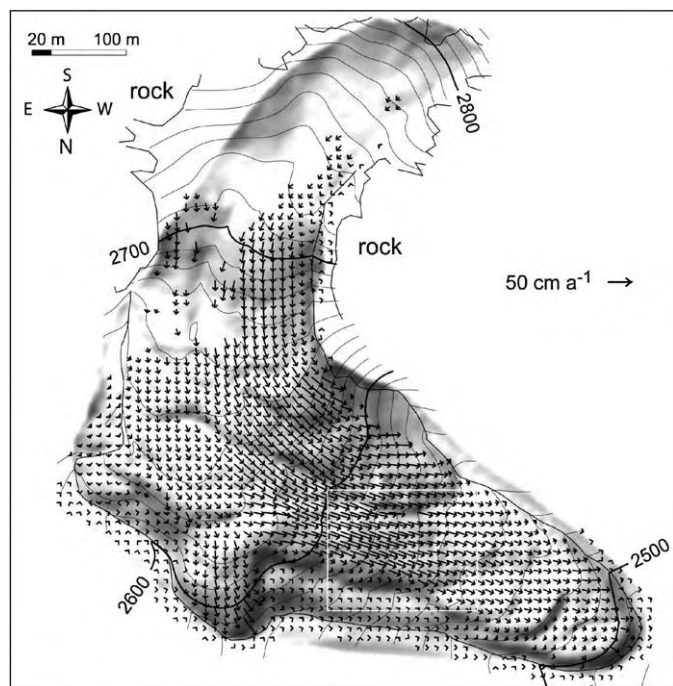


Fig. 33. Average horizontal surface velocities on Muragl rock glacier measured from aerial photography of 1981 and 1994. The white rectangle marks the section shown in Fig. 36.

been attempted through absolute and relative dating methods, geomorphodynamic indicators, vegetation mapping, etc. (e.g. Strozzini et al., 2004).

8.5. Observed creep rates

Surface creep rates of up to several metres per year are common in rock glaciers (Kaufmann and Ladstädter, 2002; Käab et al., 2003b; Haeblerli et al., 2006), transporting talus or glacial debris downslope. Permafrost creep within the high mountain context is localised by the distribution of sufficient ground ice to promote creep movements. In high arctic lowlands, where ground ice is often more extensive within the continuous permafrost, creep is generally much slower (e.g. Dallimore et al., 1996; Foriero et al., 1998), and does not generate such clear surface landforms as in mountain terrain.

Rock glacier creep rates depend among other things on surface slope, composition and internal structure, thickness of the ice-rich body, and ground temperature (Haeblerli, 1985). The observation of minimum surface speeds is limited by the detection level of available measurement techniques (see above). A coherent ice content within rock glaciers leads to the lateral transfer of stresses, and thus to a coherent velocity field (Figs. 33 and 36). A number of factors, including the distribution of stress, the effects of lateral friction, and variations in shear modulus, usually result in the highest downslope creep rates on a rock glacier being along its centreline. In the few rock glacier boreholes available, the downslope deformation was concentrated in sub-horizontal layers some decimetres to metres in thickness, rather than being distributed through the body of the rock glacier with a parabolic variation in creep rate with depth, as is found for glacier ice (Arenson et al., 2002).

8.6. Spatial modelling of rock glacier distribution and its response to changing climate

It is generally accepted that several conditions must be fulfilled in order for a rock glacier to form. There must exist (a) a headwall composed of weathering-susceptible rock, (b) a relief permitting the accumulation of talus, (c) a climate cold enough to allow the build-up

and preservation of ground ice (super-saturation) over typical time scales of millennia and dry enough to inhibit the formation of glaciers, (d) hydrological and lithological preconditions that allow the formation of a cohesive debris-ice matrix, and (e) angle and thickness of accumulated talus sufficient to generate sufficient shear stress to cause deformation. To enable the further development, ground temperatures must remain in a range enabling creep, and talus thickness must be maintained by continuous debris supply to allow mass conservation. Stabilisation and formation of relict rock glaciers results either from climatic or dynamic inactivation processes.

Statistical modelling by Brenning (2004, 2005) in the Chilean Andes suggested key factors in rock glacier formation include slope profile, elevation, convergence index, and vertical extent of the contributing area, plus the ratio of potential solar radiation to global radiation, the 'northexposedness' (the cosine of terrain aspect), and their interaction. Studies by Morris (1981) in the Sangre de Cristo Mountains, Southern Colorado and Frauenfelder et al. (2003) in the Eastern Swiss Alps showed interaction between altitude, radiation and rock wall jointing, rather than additive independent effects, determined the development of rock glaciers. The relation between rock-wall extent and rock glacier size was complex, involving factors such as cliff recession rates and subsequent talus input variations. Flow rates apparently respond predominantly to non-linear thermal influences on strain rates rather than effects from stress-related geometry (slope-dependent thickness).

Recent dynamic modelling of rock glacier evolution (Frauenfelder et al., 2008) considers both external and internal processes in the spatial and temporal domain. Climate inputs are key external variables, together with rock-debris accumulation, hydrology, and glacier extent. The internal processes considered are creep initiation, advance rate, and creep termination. Field validation shows that the dynamic model enables the simulation of spatio-temporal creep processes on a regional scale, but that the model is highly dependent on the accuracy of the relevant input parameters.

8.7. Environmental change and rock glacier dynamics

The altitudinal belts where active, inactive and relict rock glaciers are found, suggest that atmospheric and ground temperatures are important drivers of rock glacier activity through their influence on debris supply from rockfalls and rock glacier ground ice (Olyphant,

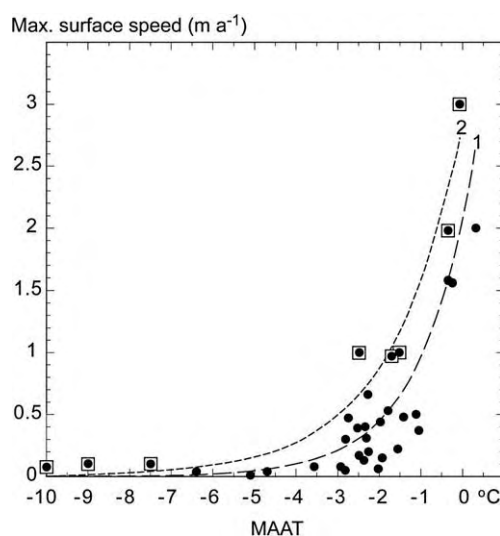


Fig. 34. Maximum surface speed of a global sample of rock glaciers as a function of mean annual air temperature (MAAT) at the rock glacier front (black dots). For data sources see Frauenfelder et al. (2003). Curve 1 is an exponential fit through all points, curve 2 an exponential fit through the upper maximum points only (points marked with rectangles). (For details see also Käab et al., 2007).

1987; Frauenfelder et al., 2001; Frauenfelder, 2005). Warming trends since the end of the Little Ice Age may be largely responsible for recent reduction in activity of rock glaciers in certain areas. Significantly less well investigated, but potentially of similar importance, is the influence of long-term changes in precipitation, especially snow cover, on mass supply and ground temperatures. Climate change may also lead to overriding of rock glaciers by expanding glaciers, or initiation of rock glaciers in locations vacated by retreating glaciers (Maisch et al., 2003; Käab and Kneisel, 2005).

Geostatistical investigations of surface velocity measurements and climatic parameters, together with laboratory data and numerical modelling show that the deformation rate of a rock glacier with a given slope, composition, or thickness, is largely dependent on the ground temperature. The increase of rock glacier surface speed with ground temperature seems to be approximately exponential (Frauenfelder et al., 2003; Käab et al., 2007) (Fig. 34). Consequently, ground temperature warming due to rising air temperatures or changes in snow cover, is expected to increase rock glacier deformation, especially in rock glaciers with ground temperatures of close to 0 °C. Indeed, early investigations confirm a significant recent acceleration of many rock glaciers in the European Alps, where an air temperature increase of close to +1 °C was observed since the 1980s (Käab et al., 2007) (Figs. 35 and 36). However, once mean ground temperatures begin to rise above 0 °C, decline in creep activity is likely, so that the response of rock glaciers to prolonged warming might be an initial acceleration, followed eventually by stagnation.

The high thermal responsiveness of permafrost creep rates at ground temperatures close to 0 °C has apparently led to increased sensitivity to short-term seasonal temperature cycles, ground water influences, impacts from snow cover variations, etc. and in some locations may lead to the initiation of permafrost creep (Käab et al., 2007; Ikeda et al., 2008).

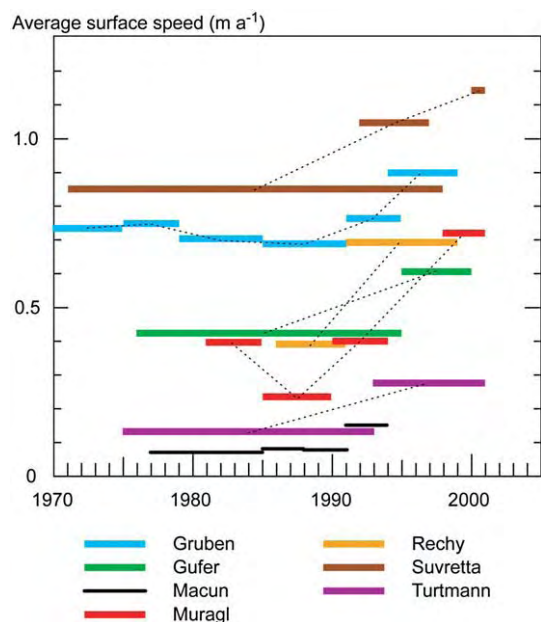


Fig. 35. Average rock glacier surface speeds in the Swiss Alps as measured for different periods since 1970. Most of the data are from photogrammetry, some from geodesy. The Macun data are from Zick (1996), all other data from Käab et al., 2007. All horizontal bars represent average speeds over the individual measurement periods. The measurement periods for Suvretta overlap because they refer to different methods (photogrammetry vs. terrestrial survey). The dotted lines connect the average values for individual rock glaciers and measurement periods for better readability. Due to the very different time periods compared these dotted lines do not necessarily indicate the actual changes in surface speed.

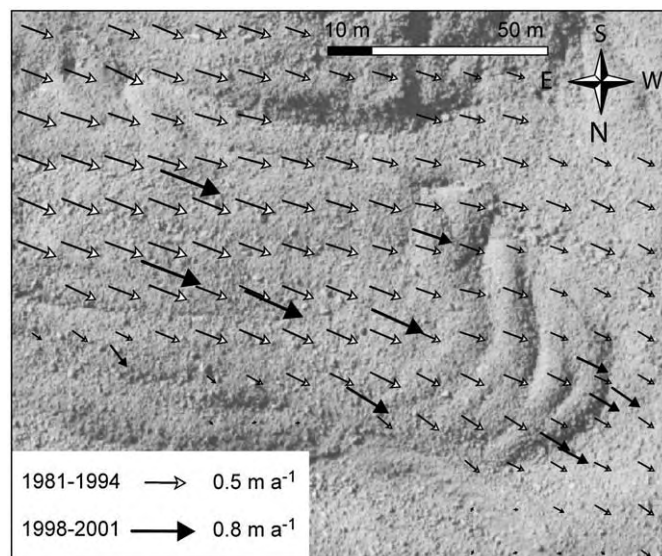


Fig. 36. Horizontal surface velocities on Muragl rock glacier (see Fig. 33). The vectors 1981–1994 represent average velocities derived from airphotos of 7.9.1981 and 23.8.1994. The bold vectors are average velocities between 24.10.1998 and 21.9.2001 derived from repeat terrestrial survey of a set of surface markers. Speed seems to have nearly doubled for 1998–2001 compared to 1981–1994. It is, however, important to keep in mind that Muragl rock glacier showed significant seasonal and pluriannual (Fig. 35) speed variations (Käab et al., 2007).

9. Thaw-related mass movement processes: solifluction and debris flows

European permafrost areas are generally characterised by a landscape assemblage of steep bedrock slopes, coarse-grained scree slopes with gradients close to the angle of repose where rock glaciers are often initiated, and lower gradient footslopes mantled by finer-grained sediments. Scree and coarser sandy soils are not frost susceptible and where such materials contain significant ice it is likely to have accrued through burial of snow, freezing of groundwater or possibly the burial of residual cold glacial ice (see section 8). Although susceptible to creep when frozen, ice-rich coarse-grained frozen soils will drain rapidly on thawing, so that raised pore pressures leading to large-scale slope failures are unlikely. However, thawing of ice-rich fine-grained soils causes thaw consolidation, raised pore pressures, reduced effective stresses, and in consequence, lowered soil shear strength (e.g. Morgenstern and Nixon, 1971; Harris, 2007). As a result of this, mass movement processes are particularly important.

Periglacial mass movements include slow perennial solifluction (e.g. Washburn 1967, 1999; Harris, 1981; Matsuoka, 2001b) and more localised shallow translational landslides and debris flows. Shallow slope failures may occur when soil thawing is rapid and soil ice content is high or when heavy rainfall leads to rapid saturation of shallow active layers. Thus, many soil-covered periglacial slopes consist of a slowly moving solifluction mantle that from place to place and from time to time is disrupted by rapid mass movement events.

9.1. Slow mass movements (solifluction)

Two processes have been identified as contributing to slow downslope active-layer movement; frost creep, the downslope settlement of near-surface soil particles disturbed by frost action, and gelifluction, the slow gravitational shear deformation of a thawing active layer (Washburn, 1967; Harris, 1981, 2007). Since both frost creep and gelifluction are associated with frost heaving and thaw settlement, in practice they are often impossible to differentiate in field measurements and the term solifluction is commonly used to include all such processes contributing to slow (several mm to several

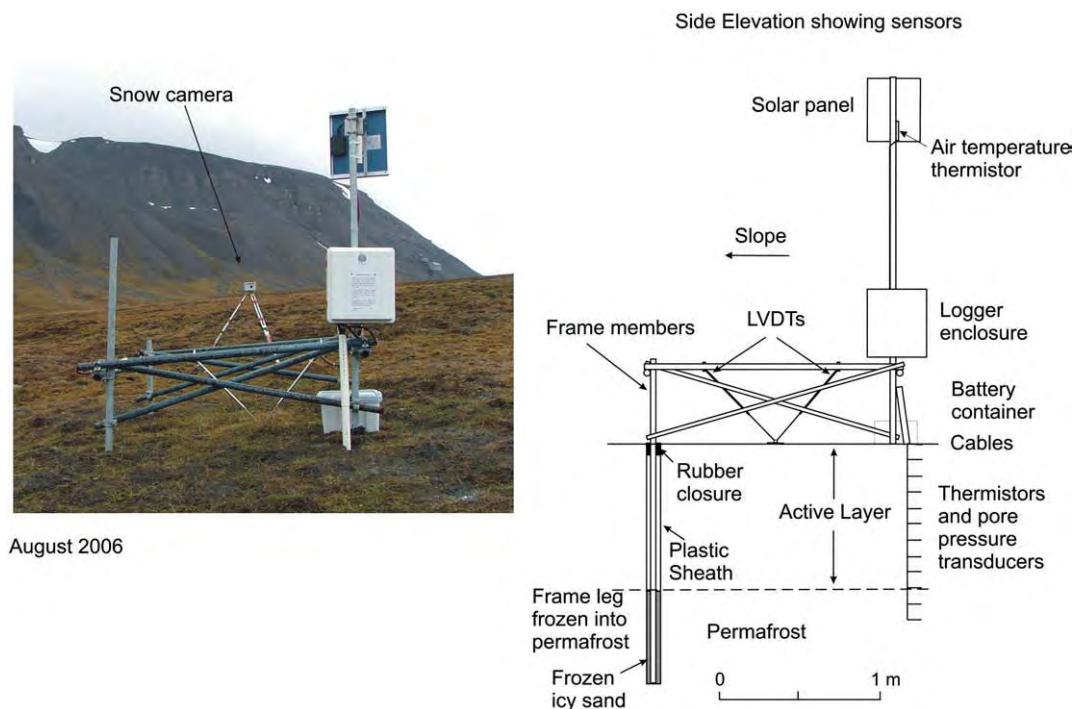


Fig. 37. Solifluction measurement station installed in Endalen, Svalbard in August 2005.

cm per annum) periglacial mass wasting (e.g. Ballantyne and Harris, 1994). The process is commonly the dominant mechanism of sediment transport on periglacial slopes (Matsuoka, 2001b) and occurs both in permafrost areas and in non-permafrost areas with deep seasonal ground freezing.

9.2. Field and laboratory studies of solifluction processes

Recent field studies have focused on continuous monitoring of environmental conditions (air and soil temperatures, snow fall, soil moisture status, frost heave, thaw settlement, and downslope soil movements). Field measurements of slope movements (frost heave, thaw settlement and downslope displacements) require a stable reference datum, and this is often provided by a metal frame anchored in a stable substrate (e.g. Lewkowicz, 1992; Matsuoka 1994; Matsuoka et al., 1997; Jaesche et al., 2003) although technological advances are now allowing surface motion to be resolved at high spatial and temporal resolution using carrier-phase differential GPS (Berthling et al., 2000). Continual measurement of soil temperatures, pore water pressures and ground surface movements was developed by Harris et al. (1997, 2008a) during laboratory simulations of solifluction processes using thermistors, pore pressure transducers, and pairs of linear variable differential transformers (LVDTs), and this instrument package has recently been transferred from the laboratory to two field sites, one in southern Norway and the second in Svalbard (Fig. 37) (Harris et al., 2007, 2008c), allowing direct comparisons to be made between observations in the field and in laboratory simulations.

In Alpine, non-permafrost sites, freezing and thawing is from the surface downwards and ice segregation and soil movement rates are greatest near the surface and decrease with depth (Matsuoka, 2001b; Harris, 2007). Drier steeper slopes are often dominated by frost creep associated with short-term freeze-thaw cycles (Matsuoka, 2005; Matsuoka et al., 1997), while gelifluction is generally more important than frost creep at snow-rich sites with deep seasonal ground freezing (Jaesche et al., 2003; Harris et al., 2008c).

In permafrost regions, the active layer is likely to freeze from the surface downwards and the permafrost table upwards. The upward

advance of a freezing front from the permafrost table causes water migration towards it from the unfrozen soil above, leading to enhanced ice segregation in the lowermost parts of the active layer. In many cases a particularly ice-rich transition zone, termed the “transient layer” (Shur et al., 2005), is present within the lowest parts of the active layer the upper one or two metres of permafrost (Fig. 38). Here ice segregation is enhanced by downward percolation and refreezing of meltwater during active-layer thaw (Mackay, 1983). During two-sided freezing, the active layer may become effectively a hydraulically closed system, so that migration of water towards the advancing freezing fronts leaves the central zone relatively dry and ice poor. During active layer thaw, thaw-settlement and associated solifluction occurs early in the thaw period as near-surface ice-rich soil thaws, and then again later in the summer when the ice-rich basal zone begins to thaw. In late summer, therefore, the active layer above moves down slope en-masse across a soft deforming basal layer



Fig. 38. Borehole core sample taken from within the uppermost 0.5 m of permafrost in Endalen, Svalbard. Thick lenses of segregation ice indicate a volumetric ice content of between 40 and 50%. Photograph F.W. Smith.

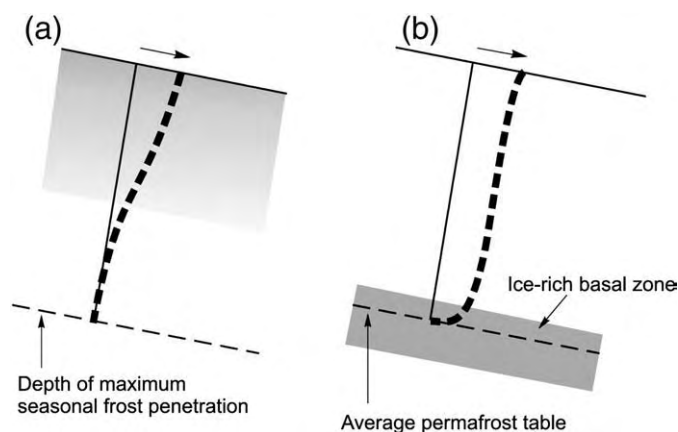


Fig. 39. Distribution of segregation ice and associated solifluction profiles in (a) seasonally frozen ground with one-sided freezing, and (b) permafrost, with two-sided active layer freezing.

(Fig. 39) where thaw consolidation is concentrated (Matsuoka and Hirakawa, 2000; Lewkowicz and Clark, 1998; Mackay, 1981).

In Svalbard, Matsuoka and Hirakawa (2000) emphasized the importance of ice distribution within the active layer. They observed no ice-rich zone at the base of the active layer in a solifluction sheet at Kapp Linné, due to the absence of two-sided freezing at this relatively warm site (mean annual temperature -4.9°) and the presence of non-frost susceptible marine sands beneath the solifluction sheet. Summer thawing was associated with solifluction in the upper 10–50 cm only, with no soil deformation at depth. In contrast, at a site in Adventdalen (mean annual air temperature -7° to -8° C), continuous monitoring throughout an annual cycle in 2005–2006 at a site with frost susceptible soil revealed two-sided freezing with soil deformation during summer thaw concentrated within the basal ice-rich zone, giving plug-like active layer movement (Harris et al., 2006).

The influence of climate change is likely to differ markedly between the alpine non-permafrost environments with deep seasonal ground freezing, and colder regions (higher altitudes or higher latitudes) with ice-rich permafrost. In the former, the link between atmospheric temperatures and the near-surface thermal regime may be weak, depending largely on the depth and duration of snow and its date of arrival and clearance. Sediment transport by solifluction, reflecting rates of surface movement and the profile of soil movement with depth, is therefore likely to respond in a complex and site-specific manner to changes in snowfall regime that may accompany future climate change. In permafrost areas, particularly the continuous permafrost of high latitudes, warming air temperatures and an increase in frequency of warm years are likely to cause increasing active layer depths and increasing frequency of extreme thaw events, leading to thawing of the ice-rich zone at the base of the active layer and in the upper layers of permafrost. The consequence is likely to be a marked increase in both rates of solifluction and the volume of sediment transported annually (Matsuoka, 2001b).

Long-term (1973–2003) monitoring of annual surface displacement rates at Kapp Linné, Svalbard by Åkerman (2005) appears to illustrate such trends. Summer mean air temperatures are shown to have increased fairly consistently from around $+3.5^{\circ}$ C in the early 1980s to around 5.5° C in 2004, and this has been accompanied by increasing values of degree days thaw and increasing active layer depth. A highly significant correlation between average annual surface movement rates of solifluction sheets and the depth of active-layer thawing can be demonstrated (Fig. 40).

The advantages of laboratory physical modelling in, which soil properties and boundary conditions are well-controlled, have recently been exploited in full-scale modelling (e.g. Harris et al., 1997; 2008a;

Harris and Davies, 2000) and reduced scale geotechnical centrifuge modelling (Harris et al., 2003a, 2008b, Kern-Luetschg et al., 2008) of solifluction processes. Harris et al. (2003a,b) demonstrated that gelifluction is the elasto-plastic deformation of saturated thawing soils in, which shear strengths are reduced by high pore pressures, rather than viscosity-controlled flow as was suggested in some early definitions of the process. Both full-scale modelling and scaled centrifuge modelling have established a clear relationship between the amount of frost heave (and hence thaw settlement) and the observed rate of solifluction (e.g. Harris and Smith, 2003).

9.3. Debris flows and related phenomena on thawing soil-covered slopes

Extreme events such as deeper than normal thaw penetration during very warm summers, or intense summer rainstorms that rapidly saturate the active layer, may cause high pore water pressures sufficient to release rapid slope failures (e.g. Larsson, 1982; Chandler, 1972; Harris and Lewkowicz, 2000; Lewkowicz and Harris, 2005a,b). On steep mountain slopes, by far the most common mode of failure is debris flow. The mechanisms of debris flow initiation and displacement were reviewed by Iverson et al. (1997), who showed that most are triggered by high pore pressures often associated with transient very high groundwater levels. Initial slope failure is followed by soil liquefaction as the soil fabric is disturbed during movement. At this stage, a pore-pressure induced upward component of seepage enhances the potential for debris flow mobilisation. Mechanisms of thaw-related mass movement, including mudflows, flow-slides and detachment slides, were recently simulated in scaled centrifuge experiments by Harris et al. (2008b) who showed that initial instability arose from thaw consolidation of ice-rich soils giving excess pore pressures and upward seepage away from the thaw front, the subsequent displacement process (flow or slide) depending largely on soil properties.

A well-documented example of debris flow initiation in permafrost is from the Longyear Valley, Svalbard, where 30.8 mm rainfall fell in a 12 h period in July 1972 and caused some 80 debris flows and slides (Larsson, 1982). Many debris flows were initiated as translational slides over the permafrost table and developed into debris flows as water contents and slope gradients increased. Clearly climate change associated with an increase in frequency of extreme summer rainfall events would lead to greater debris flow activity. A lack of long-term

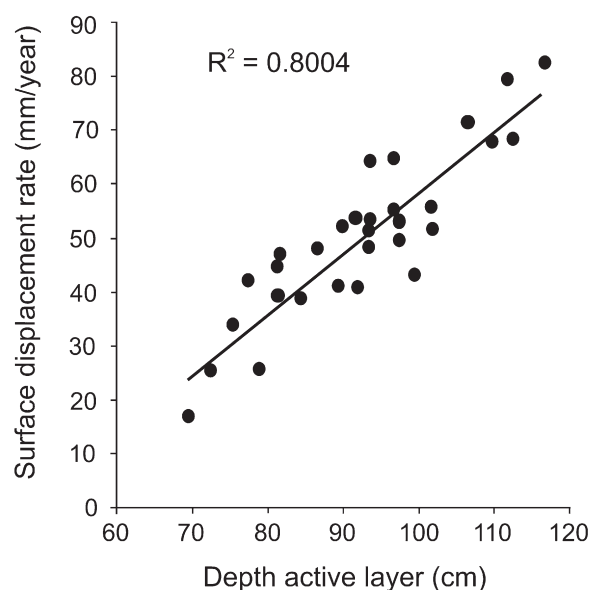


Fig. 40. Relationship between average surface movement rates and average active layer depths at Kapp Linné over the period 1973 to 2003. Data from Åkerman (2005).

data makes accurate assessment of recurrence intervals difficult, but there is evidence for increasing annual precipitation in Svalbard through the latter part of the 20th century (Larsson, 1982). Debris flows elsewhere also result from intense summer rainfall. In Northern Sweden, for instance, debris flow initiation by extreme rainfall has been described by Jonasson and Nyberg (1999) and Beylich and Sandberg (2005). In the latter study, a rainstorm in the Abisko region in July 2004 was shown to have initiated debris flows, shallow translational landslides and fluvial erosion that generated sediment transfers in one day that exceeded average annual sediment transfers by several times.

In the Swiss Alps, evidence has been presented that the number of extreme rainfall events capable of triggering debris flows in summer has increased. Analysis of climatic data for the last decades of the 20th century in the region of Ritigraben, Valais, Switzerland, suggested an increasing frequency of such events (Rebetez et al., 1997). The rise in atmospheric temperatures observed through the latter part of the 20th Century, and the early years of the 21st Century (see Section 2) is associated with permafrost degradation and glacier retreat, both factors tending to increase the sediment supply during debris flow events (Zimmermann and Haeblerli, 1992; Haeblerli, 1992, 1994; Rikenmann and Zimmermann, 1993). However, a longer-term perspective on debris flow activity in the Ritigraben Valley based on tree ring analysis (Stoffel et al., 2005) showed that debris flows actually occurred more frequently in the nineteenth century than they do today.

Jomelli et al., (2004) have demonstrated that in the French Alps the frequency of debris flows has decreased significantly at low altitudes (<2200 m) since the 1950s, whereas no significant variation has been observed at high altitude (>2200 m). The zone from, which debris flows are triggered also appears to have moved toward higher elevations. Over this period, air temperatures have risen and the number of freezing days fallen, and there has been a significant increase in summer rains higher than 30 mm/d. Jomelli et al. (2004) suggested that climate changes may have reduced the rate of sediment production at lower altitudes, so that debris flow transport may be limited by sediment supply rather than rainstorm frequency.

The limitation of debris flow activity by debris supply rather than the frequency of extreme rainfall events was also emphasised in the context of hazard assessment by Glade (2005) in a study of debris flow frequency in the Westfjords of Iceland. Here supply rates by rock weathering and solifluction were less than potential debris flow transport rates by a factor of 6.2–8.5, so that replenishment of debris storage was not always fast enough to supply the next potential debris flow triggering rainfall event. Thus debris flow initiation may depend as much on the stochastic variation in timing of extreme rainfall events as the overall statistical recurrence interval.

10. Ground ice phenomena

This section reviews the geomorphological significance of ground ice in the arctic and sub-arctic zones of Europe (Svalbard, Iceland and Fennoscandia) in the context of changing climate. Thus, the focus is on lowland areas rather than the mountain permafrost realm. Ground ice is classified according to its principal transfer process (Mackay, 1972) into wedge ice, intrusive ice and segregated ice.

10.1. Ice wedge formation and climate

It is likely that ice wedges are the most widespread periglacial landform in lowland continuous permafrost areas. Settlements located in arctic lowlands or valleys must take account of the likely presence of ice wedges within the substrate. Svalbard airport, Longyearbyen, for example, is located on a raised marine terrace with a large-scale polygonal network of ice wedges. Since its opening in 1975, the runway has suffered from unevenness of the surface due to thaw settlement in the spring/summer, and frost-heave during

autumn/winter causing significant maintenance problems and costs (Humlum et al., 2003).

Pleistocene distribution of permafrost in Europe has been mapped largely through identification of ice wedge casts (e.g. Svensson, 1988, Huijzer and Vandenberghe, 1998; Huissteden et al., 2003). The presence of ice wedge casts has been interpreted as indicating maximum mean annual air temperature at the time of formation of -6°C in Alaska (Péwé, 1966), -4°C in Yukon (Burn, 1990) and up to -2.5°C in Siberia if formed in clay (Romanovskii, 1985). Péwé also concluded that periodic winter cooling of the permafrost down to -15°C to -20°C is necessary. In the Canadian arctic, Mackay (1993) demonstrated that sharp falls in air temperature lasting for at least 4 days, with a cooling rate of $1.8^{\circ}\text{C}/\text{day}$, were necessary to cause ice wedge cracking, and this was prevented by snow depths above 60 cm (Mackay, 1986). Cooling rates of -0.5°C to $-0.9^{\circ}\text{C}/\text{day}$ at the surface and -0.1°C to $-0.4^{\circ}\text{C}/\text{day}$ at the permafrost table were reported by Mackay (1993) and similar threshold conditions were reported by Fortier and Allard (2005) and Allard and Kasper (1998). In temperate southern Sweden, Svensson (1996) showed that in the winter of 1966 a rapid fall in air temperature of $3\text{--}4^{\circ}\text{C}/\text{h}$ to -15°C to -20°C caused opening of thermal contraction fissures and associated ground shaking.

The use of ice wedge casts to reconstruct palaeotemperatures was questioned by Murton and Kolstrup (2003) because of the limited knowledge of the frequency of ice wedge cracking in modern permafrost environments, the lack of understanding of the natural controls on cracking, the difference between former mid latitude permafrost environments and modern high latitude permafrost environments, and the limited understanding of ice wedge casting.

10.1.1. Thermal conditions for present-day ice wedge activity in Svalbard

The modern high arctic continuous permafrost landscape in Svalbard (Fig. 41) provides the opportunity to study the frequency of ice wedge cracking, and its climatic controls in a maritime climatic setting that may differ only a little from much of central Europe during the last glacial maximum. Investigations have included morphology, isotope variation, age and process (e.g. Christiansen, 2005; Svensson, 1969a,b, 1976). The year-round field access from the University Centre in Svalbard, UNIS, has enabled continuous or high frequency ice wedge process monitoring since 2002, including cracking events recorded by miniature shock recorders, at a field site in Adventdalen, 10 km east of Longyearbyen (Christiansen, 2005). Some initial results of the first three years are presented below. A more detailed analysis is presented in Matsuoka and Christiansen (2008).

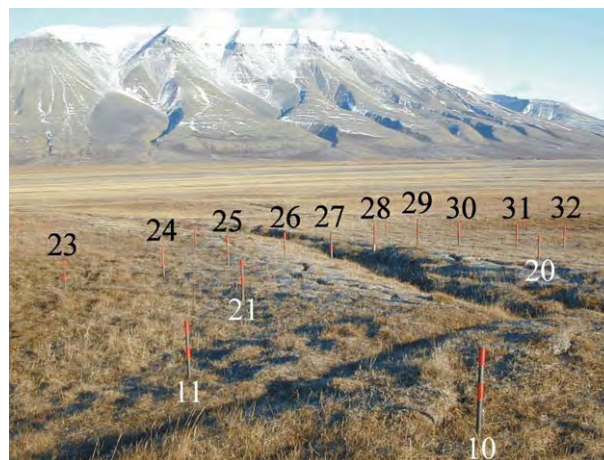


Fig. 41. Ice wedge research site in Adventdalen, Svalbard, September 2003. In the foreground, benchmark poles on the ramparts each side of ice wedge troughs are numbered below the poles. In the background benchmark poles, numbered above the poles, cross a first order ice wedge through and ramparts. Photo Hanne H. Christiansen.

The mean annual air temperature measured at the official meteorological station closest to the field site ranged from -5.1 to -3.7 °C for the period 2002–2005. Winter air temperature was below -30 °C for shorter or longer periods each year. In the centre of the ice wedge, below the deepest part of the ice wedge trough, and also in the ice wedge periphery below the rampart, temperatures at the top of the permafrost were below -15 °C for a period each winter. Ice wedge polygon ramparts were mainly blown free of snow, with only up to 5 cm snow accumulating for short periods, while the troughs contained up to 35 cm snow each winter.

The relationship between air and ground temperature and the incidence of ice wedge cracking has been investigated through thermal measurements and the installation of one-dimensional miniature accelerators with dataloggers (Tinytag Plus High Sensitivity Shock (0–5 g) and Sensitivity Shock (0–120 g)). These record hourly maximum ground acceleration and are placed in the ground surface, measuring acceleration perpendicular to the ice wedge orientation. In the winter of 2004–2005, nine such shock loggers were distributed around an ice wedge polygon in Adventdalen. Fig. 42 shows data from four of these shock loggers located along a 6.5 m section of the large ice wedge in the polygon seen in Fig. 41. Ground acceleration was only registered shortly after or during significant temperature falls. The largest acceleration of 6.3 m/s² occurred at the end of a 20 °C fall in air temperature on 14 January 2005, when all the nine loggers registered acceleration during the same hour. When the air temperature dropped from $+1$ °C to -24 °C from 23 to 27 February, and again when the air temperature dropped further from -16 °C to -31 °C from 7 to 9 March, small-scale ground accelerations of up to 2 m/s² were recorded over a period of several days. It was not until the end of this last period of activity that the permafrost temperature fell to -15 °C and the vertical temperature gradient reached -15 °C/m. The maximum cooling rate of -0.4 °C/h occurred just after this period (Fig. 43).

Excavation of snow profiles across the ice wedge troughs on 20 February 2005 revealed no open cracks in the ground surface. Cracks were present in the snow cover over a short distance in the ice wedge trough and in the top of the ramparts on 9 March. Seven snow pits were dug at shock logger locations on 16 April 2005, and open cracks were found in only two of them. During early July 2005, no cracks were seen along the 5.6 m section of the ice wedge where the shock loggers had registered small-scale movement (Fig. 42). However, open cracks were found in most of the ice wedge troughs elsewhere in the polygon, where shock loggers registered acceleration maxima of 4–5 m/s², significantly above the level recorded by the loggers in Fig. 42. Thus the data presented in Figs. 42 and 43 are thought to lie close to the thermal limit for ground thermal contraction cracking to occur.

10.1.2. Ice wedge formation and decay in relation to climate change

From the data reported above it is clear that ice wedge cracking depends on the occurrence of significantly cold winter periods, with rapid cooling of the near-surface permafrost to below -15 °C, as suggested by Mackay (1993, 2000). In Svalbard, such cold periods occur during high pressure conditions. The data from Svalbard also demonstrate that cracking can occur at MAAT up to -3.7 °C in this maritime area, where the substrate comprises fine-grained silt-rich frozen sediments. In contrast, it has been suggested that frozen sand and gravel require a maximum MAAT of -6 °C for cracking to occur (e.g. Murton and Kolstrup, 2003).

Climate warming leading to thicker active layers will cause degradation of ice wedges in the upper permafrost. In most cases, ice wedges thaw from above (Harry and Gozdzik, 1988) due to increasing active layer thickness or because of local geomorphological activity such as alar lake development. Since ice wedge growth and decay are slow, little is known of the nature of the thaw transformation process both in different materials, geomorphological settings

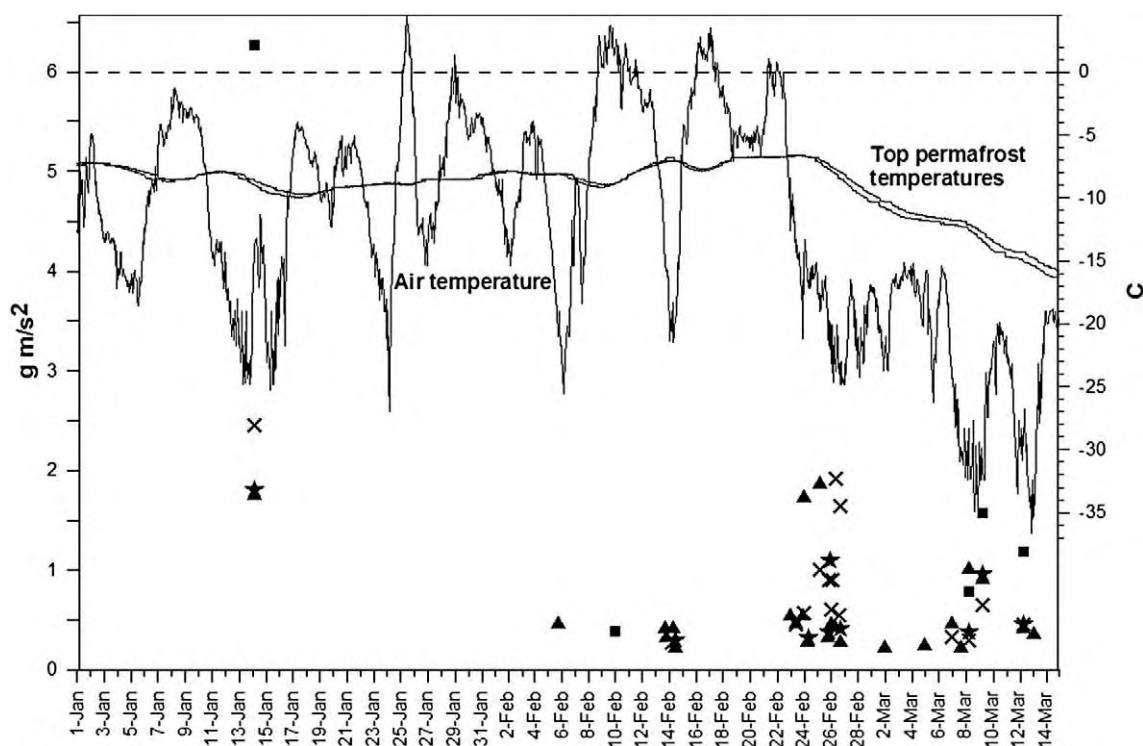


Fig. 42. Air and ground temperatures plotted with ground acceleration data measured in the top of the active layer at three places along a 6.5 m section of a first order ice wedge trough during winter 2005. The ground temperature graphs are from 68 cm depth below the centre of the ice wedge trough, at the top of the ice wedge, and from the permafrost table 100 cm below the rampart crest, adjacent to the ice wedge trough. Ground acceleration is measured by 3 High Sensitivity Shock loggers (0–5 g) and one Sensitivity logger (0–120 g), each represented by a different symbol.

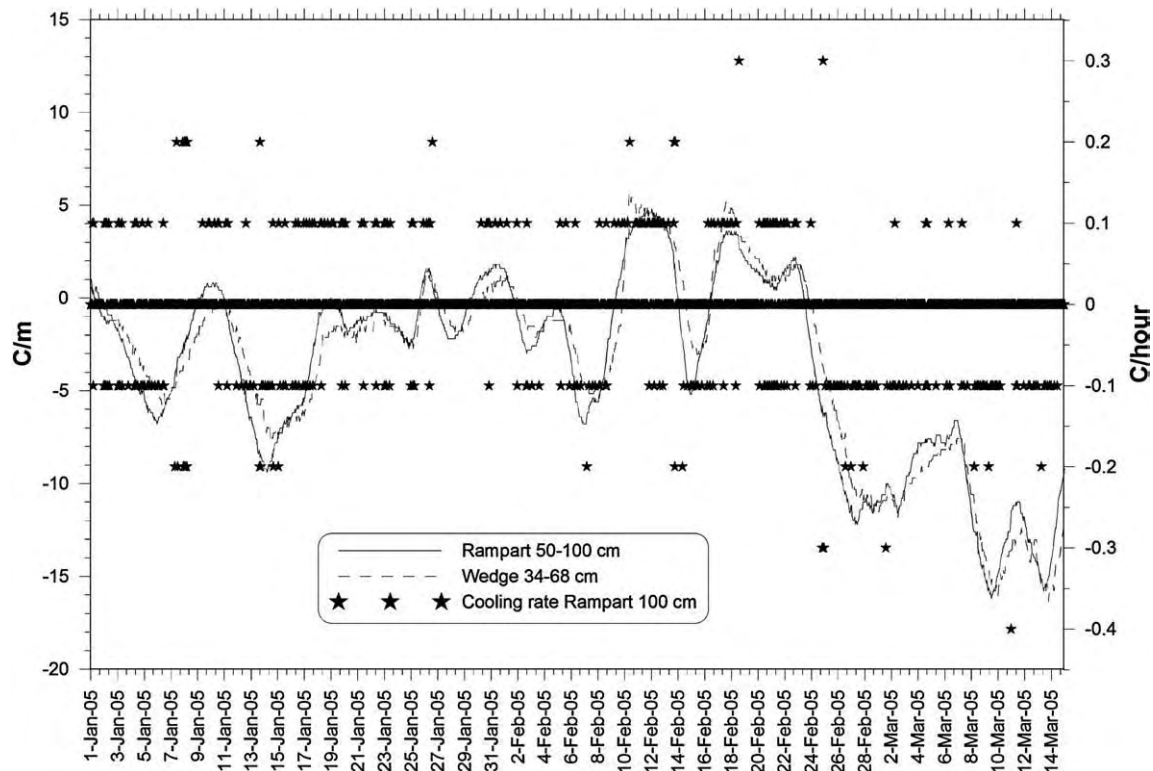


Fig. 43. Vertical temperature gradients ($^{\circ}\text{C}/\text{m}$) in the lower half of the active layer of the rampart and ice wedge trough during winter 2005 (lines). Cooling (negative) and warming (positive) rates ($^{\circ}\text{C}/\text{h}$) for the permafrost table below the rampart is also shown (stars).

and relationships to climatic change. Most studies of partial thaw of ice wedges are based on stratigraphical sections (Harry and Gozdzik, 1988), and they indicate small-scale faulting with subsidence and slumping in the thawed zone above the ice wedge, affecting the stability of the terrain surface. This situation can lead to development of thermokarst terrain. Rapid backwards niveo-fluvial erosion of ice wedges has been demonstrated to create small valleys or large gullies in polygonal terrain (Svensson, 1982, 1988; Harry and Gozdzik, 1988). In Svalbard such small valleys are up to 20–30 m long and 4–5 m deep and have developed relatively rapidly in sediments deposited during the last 3000 years.

Harris and Murton (2005) modelled ice wedge thawing and found that the degree of deformation during casting increases as the host sediments become finer-grained and more ice-rich. Thus, well-preserved ice wedge casts that replicate the original ice wedge form are common in coarse-grained ice-poor sediments, but in silts and clays, casts may be poorly preserved and significantly smaller than the original ice wedges. Temperature reconstructions where casts in coarser sediments are over-represented may therefore be on the cold side (Harris and Murton, 2005).

10.2. Palsa formation in relation to climate

Palsas are peat covered permafrost mounds containing segregation ice, surrounded by wet mires in, which permafrost is absent (French, 1996). Palsas develop where the dry surface peat layer provides sufficient insulation to preserve the frozen palsa core during summer, but is moist enough and has a sufficiently high thermal conductivity in winter to allow deep frost penetration. Winter snow is generally thin, so that mean annual air temperature and mean annual ground surface temperatures are closely coupled. Because of the special combination of vegetation and snow cover, palsa mires may fall beyond the limits of discontinuous mountain permafrost predicted by spatial modelling (see Section 4). However, the location of palsa mires in areas close to

the limits of permafrost development makes them highly sensitive to climatic fluctuations (e.g. Seppälä, 1988). The limiting MAAT for palsa formation is between 0°C and -1.5°C , though the ideal areas for palsa formation have mean annual air temperature between -3° and -5°C and low annual precipitation ($<450\text{ mm}$) (Luoto et al., 2004b).

Both aggradation and degradation of palsas has been shown to occur contemporaneously on the same mires (Seppälä, 1986; Matthews et al., 1997), due to cyclic palsa development. Frost heave caused by ice segregation raises the palsa surface above the mire, but cracking eventually releases peat blocks, that slide from the edges of the mound into the surrounding mire. In this way the frozen core loses its insulation (Seppälä, 1988). In winter, the insulating peat layer becomes thinner as wind abrades the surface, again leading to palsa degradation. During the last few years, wind erosion associated with winter storms in northern Finland has caused heavy abrasion of palsas (Seppälä, 2003b).

In Fennoscandia, palsas are mainly located north of $68^{\circ} 30' \text{ N}$ latitude, but on the high fells of Norway palsas occur north of about 62°N (Fig. 44). From Fennoscandia the palsa area continues to the central Kola Peninsula north of the Arctic Circle, and towards northern Russia also south of the Arctic Circle (Oksanen, 2005). Palsas are particularly abundant in northern Finland at altitudes between 180 m and 390 m asl (Luoto & Seppälä, 2002b) where peat thicknesses are in excess of 40–50 cm. In Scandinavia, the extent of subarctic palsa mires appears to be decreasing (e.g. Luoto and Seppälä, 2003; Luoto et al., 2004a), but some expansion of areas with palsa formation has been reported in Finnish Lapland (Seppälä, 1998; Luoto and Seppälä, 2002a). Degradation of palsas in southern Norway and in northern Sweden may be related to rising air temperatures (Sollid and Sørbel, 1998; Zuidhoff and Kolstrup, 2000), but new permafrost formation observed in places in Finland might be due to stronger winter deflation of snow (Seppälä, 2003b, 2004). In the winter 1992–93, frost penetration was deeper than normal, and in places the ground was

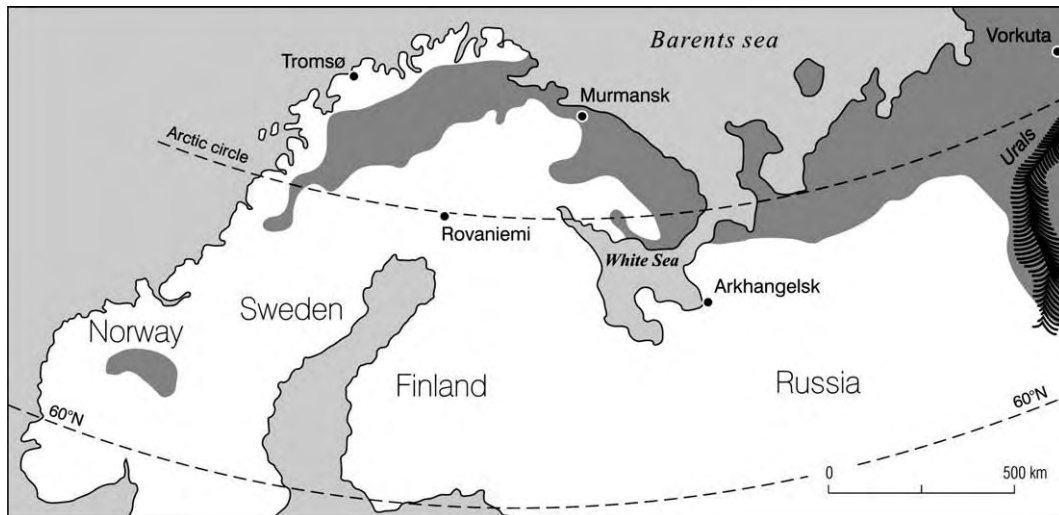


Fig. 44. The area of permafrost with palsas in northern Europe compiled from different sources (based on Oksanen, 2005).

still frozen in September 2005, with new small palsas between 2 and 6 m in diameter, and elevation 20–30 cm above the wet mire surface. The active layer of these new features was around 30 cm in September 2005.

Measurements in Finnish Lapland since 1974 (Seppälä, 1983; Rönkkö & Seppälä, 2003) indicate active layer thickness on palsas to range from 30–75 cm, tending to be thickest where palsa relief is greatest and beneath lichen-covered surfaces, and thinnest under low shrubs such as *Betula nana* (dwarf birch). Recent very warm summers have caused drying of surface peat, leading to greater insulation of the soil below and no increase in active layer thickness. In contrast, during wet summers, the surface peat stays wetter and its thermal conductivity is higher, leading to increasing active layer thicknesses.

Removal of snow from a mire surface several times during three winters between 1976–78 caused the depth of frost penetration to almost double, and a frozen layer to survive for several subsequent thawing seasons (Seppälä, 1982). Conversely, artificial thickening of snow cover by approximately 50 cm between 1997 and 2002, raised mid-winter ground surface temperatures by several degrees (Seppälä, 2003a), but summer thaw penetration was slower. In August 1999 the experimental active layer was 10 to 13 cm thinner than in an adjacent

control palsa but by 2002, the active layers were essentially the same (Seppälä, 2003a). Thus, changes in snow cover may have complex impacts on palsa thermal regime, causing surface warming in winter but slowing summer active layer thaw. The date of arrival and duration of snow may be as important as changes in snow thickness.

Radiocarbon dating of the more xerophilous peat layer that develops on palsa mounds above the general palsa mire surface allows investigation of the timing of palsa initiation (e.g. Vorren, 1972; Vorren and Vorren, 1975; Seppälä, 1988). However, wind abrasion may make precise dating more problematic (Seppälä, 2004). In Fennoscandia, palsa mires seem to have developed to approximately their present extent by about 2000 yr BP, though most modern palsas are less than 1000 years old (Seppälä, 2005).

11. Permafrost engineering in a changing climate

11.1. Introduction

Construction and maintenance of mountain infrastructure in permafrost terrain is an engineering challenge. Ground ice is the main problem directly affecting infrastructure, with its susceptibility

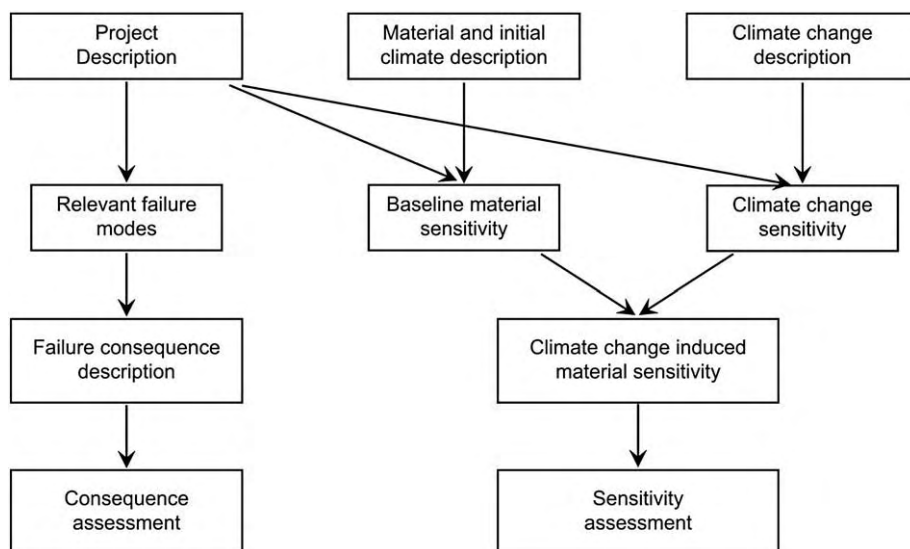


Fig. 45. Schematic of climate change screening process (PERD, 1998).

to creep, accrete and melt. Specially adapted construction and maintenance techniques are necessary in this environment, to ensure the longevity of the infrastructure. Climate change may lead to progressive modification of the permafrost thermal regime, and hence its physical properties and distribution. The rates and magnitudes of changes are difficult to predict, but since the stability and serviceability of structures may be compromised, the impacts of future climate change must be taken into account in the design of infrastructure (Instanes et al., 2005; Springman and Arenson, 2008).

In contrast to arctic regions, where infrastructure in permafrost includes entire communities (Instanes et al., 2005), there are no large permanently inhabited settlements constructed on European mountain permafrost. However, densely populated settlements and transportation routes at lower altitudes may be severely affected by processes occurring in permafrost terrain (see Section 12), requiring engineering solutions such as retention dams (Keller et al., 2002) and the establishment of hazard maps for improved land-use management (Götz and Raetz, 2002, and see Bommer et al., 2008; Springman and Arenson, 2008). Much of the infrastructure located directly on or in mountain permafrost pertains either to tourism, communication or power-related industries and is of high economic and social significance.

11.2. Characteristics of alpine permafrost soils

Typically alpine soils are coarse, though glacial tills and rock glaciers often show well graded grain size distributions (Barsch, 1996; Arenson, 2002; Arenson et al., 2002; Springman et al., 2003; Nater et al., 2008). The characteristics of the soil particles and their distribution affect the strength and deformation response of the frozen soil and its frost susceptibility. Although permafrost is defined by temperature, geotechnical properties are a function of both temperature and ice content. The mineralogy, particle size and pore water chemistry may change the freezing point and the unfrozen water content, so that even at temperatures some degrees below 0 °C, part of the pore water may not be frozen (e.g. Williams, 1967a,b; Anderson and Tice, 1972; Fish, 1985). Alpine permafrost may consist of solid rock with ice-filled joints, fine grained soils containing segregation ice, ice supersaturated gravels, where not all particles are in contact, or dirty ice with some dispersed solid particles distributed within the ice. Recent sampling from triple cored, air cooled drilling has shown that air contents of over 20% by volume can exist (Arenson and Springman, 2005b). The geotechnical properties and stress–strain relationships in frozen coarse grained alpine soils are discussed in section 8.3 of this paper.

11.3. Accounting for climate change

Current engineering practice demands the consideration of climate variability to ensure long-term project reliability. Global climate change adds an additional uncertainty to the design. However, statistical approaches based on historical data to predict future magnitudes and frequency of climatically-driven extreme events are no longer reliable (e.g. Bourque and Simonet, 2006; Guillaud, 2006). In 1998, the Canadian Panel on Energy Research and Development published guidelines for permafrost design affected by climate change (PERD, 1998). The report describes a screening process to account for these uncertainties. This process assesses the sensitivity of the project to climate change as well as the consequences associated with failure in a systematic way (Fig. 45). It concludes that the effort required accounting for climate change effects will not exceed what would normally be undertaken, and may possibly be incorporated into an existing design process with little modification. Fig. 46 shows a flow diagram with the questions that need to be addressed regarding climate change when constructing in alpine permafrost. The figure has been adopted and modified from the recommendations made by Instanes et al. (2005) for Arctic environments.

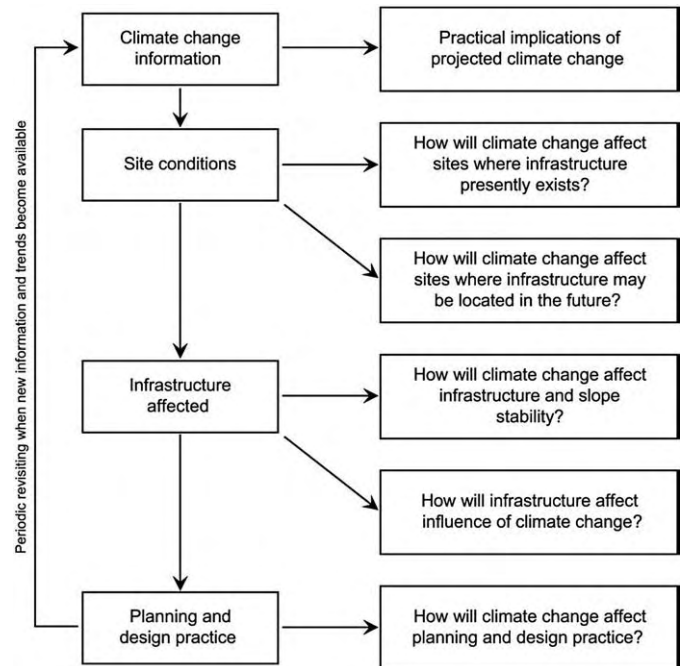


Fig. 46. Flow chart for the design of engineered structures regarding climate change (adapted from Instanes et al., 2005).

In contrast to other regions, the design life of a structure built in a permafrost environment should be planned to be 30 to 50 years, rather than 100 years. In addition, monitoring and adaptation strategies have to be implemented, that will later permit modifications to be made to the structure, as required. Since future climatic trends are difficult to predict, sensitive structures have to be re-assessed on a regular basis, as new trends and better models become available.

11.3.1. Assessing ground conditions

Laboratory and field investigations are essential in order to determine the thermal and geotechnical properties of a particular permafrost soil, in particular its ground ice content and susceptibility to thaw consolidation. The conventional approach is to drill boreholes, generating core material for testing. It is important to test the soil at the boundary conditions that are to be expected in the field. A range of testing procedures is available, such as:

- thermal needle probe measurements for thermal conductivity (ASTM, 2005).
- uniaxial compression tests for creep or strength parameters (ASTM, 2001, 2006).
- triaxial compression tests for deformation and failure mechanisms (e.g. Arenson et al., 2004).
- direct shear tests for strength characteristics of shear interfaces, in the laboratory (Davies et al., 2000, 2001; Yasufuku et al., 2003; Arnold et al., 2005) or in the field (Springman et al., 2003).
- pressuremeter tests for creep properties (Ladanyi, 1993; Arenson et al., 2003b).
- centrifuge modelling for deformation and failure mechanisms (e.g. Davies et al., 2003; Harris et al., 2007).

Clearly information derived from boreholes is specific to each sampling location, and if ground conditions are likely to vary across the site it may be advisable to investigate permafrost characteristics and sensitivity through geophysical approaches (see Section 6 of this paper), using borehole information to calibrate the resulting models.

11.4. Modification of ground thermal conditions

The challenges of construction in permafrost are generally related to thawing of ground ice, and start with a change in the ground thermal regime during or after construction (e.g. Wegmann, 1998; Dätwyler, 2004), or through climatic changes. Excavation of trenches for foundations and removal of surface vegetation may modify the energy balance, and exposure of ground ice can lead to rapid thaw. Thermal disturbance is also possible from frictional heat and water used for flushing during borehole drilling (Haeberli, 1992; Vonder Mühll et al., 2003). Tunnels can also have a disturbing effect, as air or water can warm adjacent frozen rock zones, as was observed during the drilling of access tunnels in Chli Titlis (Haeberli et al., 1997), Klein Matterhorn (Rieder et al., 1980) and in the Jungfrau east ridge (Wegmann, 1998). Measurements below steel snow-supporting structures in Switzerland, however, have shown that despite strong diurnal above ground warming, no discernable heat was conducted into the ground (Phillips et al., 2000; Phillips 2006). The main problem affecting such structures are temperature- and water dependent creep movements of the ice rich permafrost soils in, which they are anchored (Rieder et al., 1980; Phillips et al., 2003a).

Hydration heat generated during curing of concrete or grout can melt large quantities of permafrost ice. For instance, during construction of the midway station for a chairlift in Grächen (Swiss Alps) in 1997 at 2450 m a.s.l., severe permafrost ice degradation occurred, with, as a consequence, settlement, cracking of the concrete and pronounced creep of the structure, that had to be replaced completely in 2003 (Phillips et al., 2007). Subzero ground temperatures can also cause freezing of concrete or grout, impairing the curing process before the appropriate bearing capacity is attained. Anti-freeze additives (Moser, 1999) or warm water (SLF/BUWAL, 2000; Thalparpan, 2000) may be used to delay freezing and ensure that the curing process can be achieved successfully but will disturb the thermal regime of the permafrost. These aspects must therefore be considered carefully in terms of the effect on the ice content and long term stability of the ground.

Infrastructure in snowy, windy areas, including avalanche defence structures, may modify snow cover distribution (Hestnes, 2000; Thiis and Jaedicke, 2000) and thus affect the thermal regime of the ground. The use of technical snow in modern ski piste preparation can lead to long-term lowering of ground temperature due to the higher density and thermal conductivity of technical snow (Fauve et al., 2002). Indeed, Rixen et al. (2004) suggest that at Alpine sites where mean ground temperature is close to 0 °C, the additional temperature reduction may suffice to induce permafrost formation.

11.5. Technical solutions

In order to reduce the risk of failure of a structure or a slope in a permafrost environment, thermal stability of the ground has to be the main goal. Even during pre-construction activities, thermal disturbances should be minimised through the use of insulation materials (Thalparpan 2000) and drilling using chilled air flushing rather than fluids (Arenson, 2002; Vonder Mühll et al., 2003). Passive cooling systems such as thermosyphons, thermoprobes, air-duct cooling systems and gravity-driven air convection offer another possibility (Smith et al., 1991; McKenna and Biggar, 1998; Goering et al., 2000; Goering, 1998; Cheng, 2005; Wen et al., 2005; Arenson et al., 2006; Ma et al., 2006), but their efficiency in alpine environments is still to be tested.

Adaptable systems that have no stiff connection to their foundations, or structures on point bearings, are designed to accommodate terrain movements such as creep and settlement since their geometry can be subsequently corrected (Phillips et al., 2003b). The new chairlift midway station in Grächen, Switzerland, is an example of this type of structure: the two concrete supports are carried by a T-shaped girder

with three point bearings (two upslope and one downslope), all of which can slide horizontally to enable the entire midway station to find its optimal equilibrium position (Phillips et al., 2007). Adaptable systems need to be monitored at regular intervals to allow timely geometrical corrections to be made.

11.6. Long term monitoring of structures and substrates in mountain permafrost

Thermal monitoring is an essential contribution toward the longevity of infrastructure in mountain permafrost. If the thermal regime of the undisturbed site is known in advance in combination with its geotechnical characteristics, the impact of construction activities and climate can be predicted more precisely (Haeberli et al., 1997; Delaloye et al., 2000) and ground deformations foreseen (Steiner et al., 1996). Thermal monitoring should extend through pre-construction (providing baseline data), construction and operational phases at various depths on the site and in the surrounding terrain. Failure to carry out adequate thermal analysis can have serious consequences, such as complete structure replacement after a few years (Phillips et al., 2007). Post construction instrumentation is possible, but the effects of earlier construction activity cannot be construed and it may also be difficult to drill boreholes near or under existing infrastructure. During construction, thermistors can be installed between the structure and the ground, in intermediate insulating materials or air spaces and within the structure itself. Mobile miniature data loggers can be placed in strategic positions and moved whenever necessary (Hoelzle et al., 1999).

Monitoring ground and structural deformation is also crucial for the serviceability of any structure in an alpine permafrost environment. Adaptation strategies have to be designed in advance and have to be applied as critical deformation thresholds are reached. Ground based surveying is the easiest approach to detecting surface deformation, but a range monitoring techniques is available, depending on the structure and situation. Measurement of borehole deformation using inclinometers and extensimeters allow monitoring of ground movements (e.g. Arenson et al., 2002). Time domain reflectometry (TDR) can be used to locate shear zones at depth with more precision than inclinometers (Kane et al., 1996; Arenson, 2002), but the direction and magnitude of strain can only be estimated. Seasonal and long-term changes in pore water pressure have a fundamental effect on the shear strength of soil and measurements of water pressures and moisture contents within the active layer using TDR technologies (O'Connor and Dowding, 1999) or pore pressure transducers (Harris et al., 2008b), allow potential ground deformation processes to be recognised in a timely fashion.

11.7. Engineering in mountain permafrost: the challenge of climate change

In future, infrastructure design, construction methods and monitoring systems in mountain permafrost regions must be adapted to observed trends in climate. Designs should therefore allow for such future adaptations. Before optimum construction techniques can be achieved, further knowledge about the thermo-mechanical behaviour of ice-rich permafrost in response to warming (natural or artificial) is needed. There is a particularly urgent need for the development of guidelines that include risk assessment procedures and economic impact analyses for the construction and maintenance of infrastructure in mountain permafrost. Geotechnical risk assessment requires input from geothermal modelling of permafrost distribution in a changing climate, and from geomorphological process studies that may improve prediction of the nature, magnitude and frequency of permafrost related geohazards. Not only are the structures in mountain permafrost environments endangered, but also those buildings and infrastructure located below any permafrost occurrences. Rock falls,

debris flows and other forms of slope instabilities triggered within the permafrost environment may have severe consequences on infrastructure situated at lower altitudes. Periodic risk assessment and re-evaluation of existing hazard zoning have to be carried out, while incorporating knowledge and understanding of all the diverse but interconnected aspects of climate impact on permafrost.

12. Permafrost hazards

A key issue regarding the assessment of mountain permafrost hazards is the degree to which climate change may influence the future magnitude and probability of potentially hazardous events. Permafrost hazards generally arise from thawing of ice-bonded frozen debris and rock walls (Harris et al., 2001c), and pose a risk to people and infrastructure. Construction works may be damaged by thaw settlement and slope failures (debris flows, landslides or rockfalls), and serviceability of installations on creeping permafrost may also be compromised (see Section 11). A greater frequency of extreme summers, such as that experienced in Europe in 2003, is likely to lead to significant increases in seasonal thaw depths (see Section 3.3) and problems related to permafrost may become an increasing cost factor in the maintenance or construction of high-mountain infrastructure (Kääb et al., 2005a).

12.1. Creeping frozen debris

Rock glaciers are able to displace debris volumes of the order of 10^3 to 10^4 m³ per millennium, and the current trend towards higher ground temperatures may be responsible for an apparent increase in creep rates in many Alpine rock glaciers (see Section 8.7). Structures, such as cableways constructed where permafrost creep is active, clearly run the risk of increased maintenance costs and in the absence of appropriate engineering solutions (see Section 11.5) may eventually become unserviceable.

Rock glaciers also act as reservoirs of potentially unstable debris within debris flow initiation zones (Holzle et al., 1998; Frauenfelder, 2006; Roer et al., 2008). An analysis by Arnold et al. (2005) of the stability of the active layer of a rock glacier in Switzerland showed that interlocking in the coarse, elongated and angular particles causes significant dilatancy and hence generates extremely high shear strength parameters. However, sliding over a possible massive ice layer at the permafrost table might be of concern if the interface angle of friction reduces to about half the peak internal angle of friction of the rock glacier materials. Field data relating to hydrothermal processes developing within the active layer (ground temperatures, water contents and deformation rates) have confirmed this concern (Rist and Phillips, 2005).

Ground temperatures have been shown to increase rapidly during snow melt because of convective heat fluxes, and latent heat release during refreezing of water onto the permafrost table. Meltwater seepage will also tend to reduce the effective stresses, while refreezing enhances the ice layer, providing a potential sliding surface. Where a rock glacier has advanced onto steeper ground, debris falls along the steep rock glacier front (Bauer et al., 2003; Kääb and Reichmuth, 2005) may increase the local hazard, and if the ground falls steeply away below the rock glacier, slides and debris flows may affect much greater areas (Kaufmann and Ladstädter, 2003; Kääb et al., 2007; Roer et al., 2005, 2008).

12.2. Warming permafrost on soil-covered slopes

Increasing ground temperatures in ice-rich permafrost is likely to cause extensive thaw settlement and thermokarst processes in arctic lowlands, and thaw-related slope instability in both arctic and lower latitude mountain areas (Harris et al., 2001b; Nelson et al., 2001; Haeberli and Burn, 2002) (see Section 9.3). The latent heat effects of an



Fig. 47. Debris flow source area in the front of a frozen debris body. Here, groundwater concentration and active layer thickening provide an important trigger. Photo: W. Haeberli, 1987.

ice-rich transient layer immediately below the permafrost table reduces thaw penetration (Shur et al., 2005) but also increases the volume of meltwater released, increasing the risk of landsliding in areas with finer-grained soils. Greater active layer thicknesses associated with climate change will also tend to increase the likelihood of slope failure (e.g. Lewkowicz and Harris, 2005b) and increase the volume of displaced material, while the loss of cementing ground ice is likely to increase retrogressive erosion caused by debris flows (Fig. 47) (Haeberli, 1992; Zimmermann and Haeberli, 1992).

In cold mountainous regions, ground thermal conditions in moraines are often a crucial factor in the damming of moraine lakes (see below). Permafrost or near-permafrost conditions support the long-term preservation of dead ice bodies, but ice melting may leave cavities (Richardson and Reynolds, 2000). Sudden release of meltwater stored in such cavities may lead to significant hazard. Differential thaw settlement is frequently associated with the formation of thermokarst lakes that continue to develop through positive feedback mechanisms of water convection and latent heat effects, leading to further ground ice melt (Kääb and Haeberli, 2001). In such unstable terrain, sudden lake drainage is likely. Glaciers and permafrost often coexist in close spatio-temporal proximity. For instance, permafrost may aggrade in recently deglaciated glacier forefields, thereby altering the thermal, hydrological and dynamic conditions of glacial deposits, and influencing related hazards. These effects are of increasing importance in the light of the current pronounced worldwide glacier retreat.

12.3. Warming permafrost in rock walls

The significance of warming permafrost to the stability of rock walls is reported in detail in Section 7 of this paper, but the role of partially glacierised alpine rock faces where complex thermo-mechanical conditions are found (Kääb et al., 2004; Fischer et al., 2006) has not been discussed. Through advection of temperate firn, steep glaciers may not be frozen to their beds for much of their lengths, but enhanced heat flux near the lower margin leads to cold frontal sections that have a stabilising influence. Though little understood, it is clear that changes in surface temperatures can cause complicated feedback mechanisms and chain reactions both for rock and glacier stability. In that context, the retreat of steep glaciers and the resulting exposure of rock surfaces might have even more drastic and rapid consequences than a rise in mean annual air temperature itself. Beside the thermally-governed impacts, retreat of steep glaciers leads to de-stressing of the underlying and surrounding

rock wall. It appears that increasing rockfall activity and a number of large rock avalanche disasters might have been influenced by thermo-mechanical changes.

12.4. Glacier-permafrost interactions

Widespread melting of glaciers and rising permafrost temperatures provide an early indication of the environmental and societal significance of global warming (Haerberli and Beniston, 1998; Reiersen, 2005). In both high latitude and high altitude mountains, glaciers commonly interact with permafrost, leading to potentially hazardous geomorphological processes at the temporal and spatial interface between them. A dramatic example, though geographically peripheral to the European sphere of mountain permafrost, was on the north-northeast face of Dzhimarai–Khokh (4780 m a.s.l.), North Ossetia, Russian Caucasus, where on 20 September 2002, 10 million m³ of rock and ice broke away, falling onto the underlying Kolka glacier, which in turn sheared off (Fig. 48). As a result, a sledge-like rock-ice avalanche with a volume of about 100 million m³ and speeds of up to 300 km/h overran parts of the village of Karmadon. Subsequently, the moving mass was blocked by the narrow Genaldon gorge, damming rivers and ejecting a mudflow with devastating effects (Fig. 49). The catastrophic event travelled over a total distance of 33 km, leaving over 100 people killed, and buildings and the main access roads in the valley completely destroyed (Haerberli et al., 2004; Kotlyakov et al., 2004). The resulting damage added up to a total of nearly 20 million EURO. Subsequent risk assessment was based on an integral approach for hazard analysis that implies the reconstruction of the event and all processes involved (cf. Petak and Atkisson, 1982).

Bedrock surface temperatures in the detachment zone were estimated at about -5 to -10 °C (Haerberli et al., 2003, 2004), indicating permafrost within the source area of the rockfall that triggered the event (Haerberli et al., 2003; Frauenfelder et al., 2005).



Fig. 48. Starting zone of the devastating 20 September 2002 rock-ice avalanche in Kolka–Karmadon, Caucasus (North Ossetia, Russia). The rock-ice avalanche broke off the north-northeast face of Dzhimarai–Khokh, a rock face with complex thermal and mechanical interactions between steep glaciers and frozen rock. Photo: Igor Galushkin, 25.09.2002.

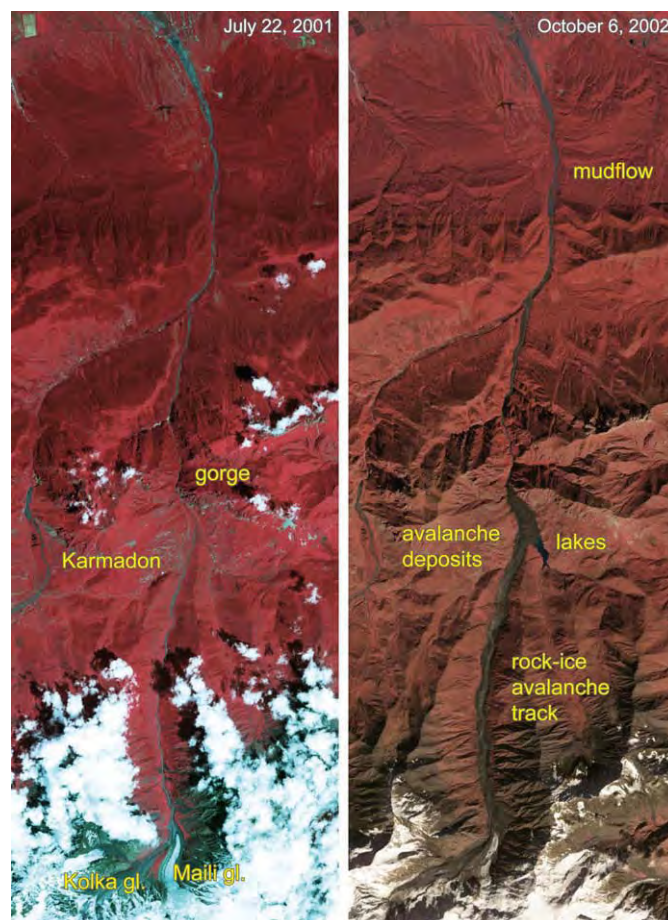


Fig. 49. ASTER false colour imagery from before (left) and after (right) the 20 September 2002 Kolka–Karmadon disaster. A large rock/ice avalanche from the north face of the Dzhimarai–Khokh peak (bottom) sheared off the entire Kolka glacier tongue. The rock-ice mass filled the valley of Genaldon from the Kolka glacier cirque (lower left) to the gorge of Karmadon (centre). The debris swept through the Genaldon river valley and backed up at the entrance of the narrow gorge of Karmadon (centre), leading to the creation of several large lakes in upstream direction and the ejection of a mudflow through the gorge far into the lowlands (top). Images: ASTER data.

Prior to the rock fall, the slope had been covered by hanging glaciers that introduced deep-seated thermal anomalies within the bedrock (Haerberli et al., 1997). It is likely, therefore, that the detachment zone at Dzhimarai–Khokh was thermally complex with relatively cold and thick permafrost adjacent to much warmer, if not unfrozen, bedrock within, which meltwater could flow (Haerberli, 2005). Though similar events have apparently occurred in the region before (e.g. Kolka Glacier ice avalanches in 1902), it is not clear whether permafrost–glacier interactions had also played a role in these earlier events. The large run-out distance of the event and the difficult access made spaceborne remote sensing an important tool in assessing the damage (Kääb et al., 2003a,b; Huggel et al., 2005).

12.5. Emerging methodologies and challenges

The assessment of glacier and permafrost hazards requires systematic and integrative approaches. Historical data can be used to test spatial models based on new earth observation and geoinformatics techniques. Such modern methodologies provide powerful tools to assist hazard assessments in complex mountain systems that are experiencing increasing change and divergence from equilibrium conditions (Kääb et al., 2005a). Currently, the most successful strategy is based on the combination of remote sensing, modelling with Geographical Information Systems (GIS), geophysical soundings and other local field surveys and intrusive sampling

techniques. These methods are best structured in a downscaling approach from area-wide first-order assessments for systematically detecting hazard potentials (i.e. the domain of space-borne remote sensing and GIS-techniques) to detailed ground-based or airborne local investigations in high-risk areas (i.e. the domain of geophysics, surveying, and air-borne and close-range remote sensing) (Kääb et al., 2005a).

12.6. Mapping

A pre-condition for precise hazard mapping is the availability of up-to-date and accurate topographic maps. Since such publicly available data are lacking in many areas, air- and space-borne optical imagery (e.g. Corona, Landsat series, Aster, Ikonos, QuickBird) and microwave data (e.g. ERS, Radarsat, Envisat, Shuttle Radar Topography Mission) can be used instead. Such data can be used to inventory and classify glaciers, lakes, areas prone to mass movements, and debris and other terrain types relevant to glacier and permafrost hazards (e.g. Leber et al., 1999; Kääb et al., 2005b, Kääb 2008). Remotely sensed data can also be used to derive digital elevation models (DEM), a fundamental prerequisite for analysing hazard potential in high-mountains and for related GIS-modelling (Huggel et al., 2003; Kääb et al., 2005b). Even ice flow and terrain displacements can be measured with high accuracy from repeated remote sensing data (Kääb et al., 2005b, Kääb 2008). Using these methods, terrain cover, geometry and dynamics of an area can be investigated without direct access.

12.7. Modelling

A further step towards an integrative hazard assessment consists in the application of GIS and other numerical models for simulating complex processes that are undetectable by remote monitoring. Glacier lake outburst floods, ice avalanches or debris flows can be modelled with a GIS (e.g. Huggel et al., 2003, Kneisel et al., 2007; Salzmann et al., 2004). Also, permafrost distribution, approximate ground-, firn- and ice-temperatures, or various other terrain parameters that have an impact on natural hazards can be computed. Integration of remote sensing results and numerical process models provides a particularly promising basis for the assessment of hazard potential (e.g. Huggel et al., 2003; Kääb et al., 2005b).

12.8. Ground-based methodologies

A more detailed analysis of the hazard sources detected by remote sensing often involves ground-based methods. Geophysical investigations, employing electrical resistivity tomography and ground penetrating radar (see Section 5.2 of this paper), in particular, have been used to develop three-dimensional ground models and have provided information on potential causes of instability such as buried ice bodies within moraine dams that could lead to breaches in the dam if the ice were to melt (Richardson and Reynolds 2000; Pant and Reynolds, 2000). High spatial and temporal resolution of terrain dynamics also demands detailed terrestrial surveying using laser technology or Global Navigation Satellite Systems (GNSS).

12.9. Challenges

Climatically-driven changes in the thermal status and spatial distribution of glaciers and permafrost are leading to perturbation of their dynamic equilibria, with transient conditions shifting hazard zones beyond the range of variability documented in historical archives. For instance, modelling suggests that the lower boundary of permafrost distribution in the Swiss Alps rose at an average vertical rate of 1 to 2 m per year between 1850 and the present (Frauenfelder et al., 2001). Current temperature observations in the Alps suggest the

rate is now close to 2 m per year. If, in fact, environmental conditions in high-mountain regions were to evolve beyond the range of Holocene and historical variability, hazard assessments may become increasingly difficult because estimates of hazard potential based on empirical data from the past (historical documents, statistics, geomorphological evidence) will not be directly applicable under new conditions. In future, prediction of hazard and risk is likely to depend on process-based modelling, especially with respect to slope stability problems. The potential of coupling remote sensing with numerical modelling should be fully exploited, and knowledge transferred to vulnerable regions in the second and third world. Downscaling approaches from initial regional-scale assessments of hazard potentials towards high resolution and high precision site-scale observations and simulations are needed as a response to the current environmental changes (Salzmann et al., 2007a,b).

Magnitude-frequency relations of catastrophic events are one of the key parameters required for risk assessment and the design of engineering solutions. Such relationships are particularly difficult to estimate for permafrost and glacier hazards in mountains due to the complex chain reactions involved. In many cases, large magnitude events occur in remote mountain areas, and are often unnoticed and undocumented. This leads to highly non-uniform and incomplete global event documentation, further complicating the estimation of magnitude-frequency relations. Past (e.g. Lateglacial to Holocene) and historic (e.g. end of Little Ice Age) transitions in permafrost and glacier conditions suggest that adjustments in thermal conditions towards a warmer phase are accompanied by intensified mass movement events. For a number of periglacial and glacial processes, both the event frequency and magnitude might temporarily increase until the corresponding sediment reservoir is exhausted and/or new equilibrium conditions are reached (e.g. Ballantyne, 2002; Curry et al., 2006).

13. Conclusions

This paper provides an overview of the status of permafrost within the European sector, from the discontinuous high mountain permafrost zone in the Alps, to the continuous permafrost of Arctic Svalbard. Much of the research in the last decade originated from the European Union PACE project. Assessment of the impacts of climate change in the sensitive permafrost domain requires an infrastructure for monitoring, and this has been a major achievement over the past decade. In addition, new geophysical methods of permafrost characterisation and mapping have been developed, modelling protocols are being refined to allow impact assessments of future climate scenarios, geomorphologic studies have improved understanding of processes and their likely responses to climate change, and research outcomes have been integrated to provide better understanding of potential permafrost-related hazards and engineering solutions in the context of a changing climate. Data arising from this on-going research will become increasingly valuable as time series become longer, and we report here a snapshot of one decade of progress. The major conclusions to be drawn may be summarised as follows.

1. Palaeoclimate reconstructions provide a critical context for assessing current trends and their potential impacts in permafrost regions. In Europe, Holocene climate fluctuations apparently increased in amplitude with increasing latitude, so that during the climatic optimum, mean annual air temperatures in the Alps were only a degree or so higher than the late 20th Century, while in northern Scandinavia the difference was up to 2 °C and in the arctic archipelago of Svalbard, temperatures between 3–4 °C higher than recent norms. Similarly, during the Little Ice Age in Svalbard, mean annual air temperatures are inferred to have been 4–6 °C below late 20th century values, and in the Arctic Maritime Zone generally, around 3 °C cooler, while in the Alps the difference was less than one degree Celsius.
2. During the 20th Century, air temperatures have tended to increase across mainland Europe, though with greater warming in

- Scandinavia than elsewhere during the early part of the century. Since 1975 warming has been more marked during autumn and winter in Scandinavia, but greatest in spring and summer in central Europe.
- Change in active-layer thickness is a key response of permafrost to climate forcing. In the PACE bedrock boreholes, maximum inter-annual variation has been 20% at Janssonhaugen (Svalbard) and Juvvasshøe (southern Norway), 30% at Stockhorn and 100% at Schilthorn (Swiss Alps). This contrasts with the ice-rich Murtèl–Corvatsch borehole (Swiss Alps) where although the active-layer has increased in thickness by around 16% since 1987, inter-annual variations are less than 4%. Latent heat exchanges dominate the thermal response at Murtèl–Corvatsch, while heat conduction is dominant in the bedrock examples.
 - The extreme summer of 2003 led to warming of near-surface permafrost and thaw penetrating some 4.5 m deeper than in previous years on Schilthorn, and around 1 m deeper on Stockhorn. Across steep Alpine slopes containing ice-bonded discontinuities, this scale of active-layer thickening significantly increased the risk of rockfall events.
 - Consistent warm-side deviations are observed in all the PACE borehole thermal profiles, but in the Alps, the complex topography and variable ground surface interface makes derivation of the climate signal from a given thermal profile a very difficult problem. In contrast, the three boreholes in Svalbard and Scandinavia are located in subdued topography, and permafrost temperatures are strongly coupled to atmospheric temperatures. Here thermal profiles have been interpreted as indicating surface warming of ~ 1.4 °C, ~ 1.1 °C and ~ 1.0 °C over the past few decades at Janssonhaugen (Svalbard), Tarfalaryggen (northern Sweden) and Juvvasshøe (southern Norway) respectively (Isaksen et al., 2007a,b).
 - Time series data from the three northernmost PACE boreholes suggest rapid recent warming, rates at the permafrost table being estimated as 0.04 – 0.07 °C yr⁻¹, warming being greater at Janssonhaugen and Tarfalaryggen than at Juvvasshøe. In the Swiss Alpine bedrock boreholes time series are shorter and strongly affected by short term seasonal extremes such as the cold winter of 2001–2002 and the hot summer of 2003. However, at depth there is evidence for warming, at Stockhorn, for instance, rates are around 0.01 °C yr⁻¹ at 48.3 m depth, and at Schilthorn, similar or slightly higher warming rates are indicated. Trends observed in the ice-rich frozen debris at Murtèl–Corvatsch indicate significant warming over the past 20 years, but the record is dominated by the influence of snow depth and duration rather than atmospheric temperatures.
 - Mapping permafrost distribution and forecasting change is generally based on numerical modelling. The scale of the modelling is critically important, with atmospheric/oceanic circulation patterns and latitude dominating at a global and continental scale, topography appearing as a major factor at regional and local scales, and surface and subsurface properties becoming increasingly important at finer resolutions. A major problem remains in bridging between continental and local scales and this is particularly important when the outputs from Regional Climate Models (RCMs) are downscaled to meet the needs of local scale permafrost models.
 - Two permafrost modelling approaches have been developed, firstly, regionally calibrated empirical-statistical models, and secondly, more physically based process-oriented models. The former may not be applicable in other regions, are limited by assumptions of steady-state conditions, and neglect complex three dimensional topographic effects. Since process-oriented approaches compute surface temperatures and thermal conditions at depth, they are better suited to estimating transient effects in complex topography.
 - The modelling sequence Global Circulation Models–Regional Circulation Models–Energy Balance Models–Heat Transfer Models within three-dimensional topography is identified as a key approach in future, with emphasis on transient effects that require coupling of time-dependent surface and subsurface ground thermal conditions.
 - Three geophysical properties; electrical resistivity, the dielectric permittivity and the seismic compressional wave velocity, are sensitive to permafrost temperature and ice content. Diffusive electromagnetic, geoelectric, seismic and ground-penetrating radar (georadar) techniques have therefore proved most suitable for determining the distribution and internal structure of frozen ground, and through use of fixed electrode arrays, monitoring of changing permafrost conditions. However, in all cases, accurate calibration of geophysical models against borehole information is required.
 - Recent developments have included the combination of information from several geophysical data sets, using for instance, a fuzzy-logic approach to delineate areas where the occurrence of ground ice is most likely, or the so-called 4-phase model to estimate volumetric fractions of rock, soil matrix, unfrozen water, ice, and air within the ground.
 - The distinctive suite of permafrost geomorphologic processes are intimately related to the presence of, or changes in, ground ice. Understanding these processes is a critical element in formulating adequate assessments of geological hazards and risks in permafrost regions, and to the development of suitable engineering strategies.
 - Monitoring has shown that near-surface freeze-thaw rock weathering is limited by the availability of water, but is responsible for generation of small-scale rock debris. Laboratory studies have emphasised the potential for ice-segregation to occur in porous rocks, and shown that ice volume and frequency of cracking are highest in the upper parts of the permafrost profile. Ice lenses and their bedrock discontinuities form parallel to the isotherms, which are generally parallel to the ground surface. Thus, ice segregation may play a key role in generating rock masses that are susceptible to major rock falls during permafrost warming and active layer thickening.
 - In the Alps the rapid increase in active layer thickness during the extreme summer of 2003 was associated with greatly increased rock fall activity within the permafrost zone and many detachment surfaces revealed ice that formerly cemented the discontinuities along, which failure occurred. Thus, there is good circumstantial evidence that warming and melting of near-surface permafrost during such extreme events will generate a significant increase rockfall frequency.
 - Over much longer timescales, permafrost warming may lead to a rise in the lower permafrost boundary, decreasing permafrost thickness by bottom-upward thawing, and hence increasing the risk of large, deep-seated landslides. The Brenva Glacier rock avalanche (Deline, 2002) that occurred in January 1997, may be related to such deep-reaching and long-term changes of the subsurface thermal conditions. Thus, the probability of large-scale rock falls (millions of cubic meters and more) is likely to increase with time in a period of climate warming.
 - Rock glaciers develop due to permafrost creep where ground ice content in frozen debris is high. Since creep is largely dependent on the ground temperature, warming is expected to increase rock glacier deformation, especially where ground temperatures are close to 0 °C. Investigations confirm a significant recent acceleration of many rock glaciers in the European Alps, where an air temperature increases of close to +1 °C have occurred since the 1980s.
 - Seasonal thawing of ice-rich fine-grained soils leads to solifluction and shallow debris flows or landslides. In Alpine regions, changes in solifluction rates in response to future changes in atmospheric thermal conditions and snow fall regime are likely to be complex and site specific. In the continuous permafrost terrain of Svalbard, however, rising air temperatures and an increase in frequency of warm years are likely to cause greater active layer depths and a marked increase in both rates of solifluction and the volume of sediment transported annually.

18. Debris flows require an unfrozen sediment source area, and are usually triggered by high intensity summer rainfall events. Recent evidence suggests that in the Alps, debris flow starting zones are migrating to higher elevations, but there is no clear indication of increased debris flow activity in these zones, despite the likely increase in potentially unstable sediment as glaciers retreat and permafrost degrades.
19. In the continuous permafrost of Svalbard, monitoring of thermal contraction cracking and formation of vein ice has suggested that the thermal limit for significant cracking to occur corresponds to a fall in winter air temperatures of at least 15–25 °C over one or two days. Climate warming might therefore reduce the frequency of cracking, and through active layer thickening, lead to an overall reduction in the volume vein ice by reducing the length of existing ice wedges.
20. Palsas occur across subarctic Europe, from Iceland, across Scandinavia to Russia, and represent outliers of sporadic permafrost that form isolated lenses in peat-covered mires. Deflation of snow is critical for their formation. Changes in winter snow regime therefore strongly modulate the effects of atmospheric warming, but there is evidence that palsa mires are shrinking across northern Europe.
21. Just as many of the geomorphological processes specific to permafrost regions relate to ground ice, so ground ice is the main problem directly affecting engineering and infrastructure. Thus, detailed ground investigations of the site and its hinterland prior to any construction work should focus not only on geotechnical characteristics, but also on establishing ground ice content and composition and ground thermal conditions. Ground ice is susceptible to creep and may accrete or melt, all of, which may adversely affect the longevity of engineering structures. Frost heaving, thaw settlement, and on sloping ground, thaw-induced slope instability may directly affect structural integrity. An additional threat is at lower elevations that lie within the run-out zones of rock falls, landslides and debris flows.
22. A range of engineering solutions are available, but the importance of monitoring should not be forgotten, and in view of uncertainties relating to future climate impacts, design lifetimes of no more than 30–50 years may be appropriate for many structures in permafrost areas.
23. Permafrost hazards generally arise from ground instability caused by thawing of ice-bonded frozen debris and rock walls, and pose a risk to people and infrastructure. Instability of rock walls is considered in conclusions 14 and 15, above, but in addition to permafrost effects, hazardous ground conditions may also arise from glacier-permafrost interactions. Rapid decay of glacier ice on steep bedrock slopes may lead to ice falls, complex geothermal conditions in bedrock may trigger unforeseen rock fall events, and decay of buried ground ice may cause catastrophic proglacial lake drainage.
24. Assessment of permafrost hazard in the context of changing climate should be based on the combination of remote sensing, modelling with Geographical Information Systems (GIS), and field investigations using geophysics and intrusive sampling approaches. Area-wide first-order assessments to detect hazard potentials (i.e. the domain of space-borne remote sensing and GIS-techniques) should be followed by progressively more detailed ground-based or airborne local investigations in high-risk areas, including permafrost modelling approaches to assess potential change, and the establishment of monitoring strategies to provide early warnings.
25. Finally, risk assessment strategies require accurate information on the future magnitude and frequency of hazardous events. Data may be derived from forecasting changes in occurrence and intensity of extreme climatic events, but information on hazard occurrence, magnitude and frequency may be difficult to acquire in remote and sparsely populated regions. For this reason, prediction of hazard and risk is likely to depend on process-based modelling, demanding a better understanding of geomorphological process-response systems. Thus there remains a need for continued integrative research in permafrost regions between atmospheric

scientists, permafrost scientists, geomorphologists and geotechnical engineers.

Acknowledgements

The research discussed in this paper was initiated and partly funded by the European Union PACE project (Contract ENV4-CT97-0492). Support is also acknowledged from the European Science Foundation (NW.GC/24 Network 112).

References

- Akagawa, S., Fukuda, M., 1991. Frost heave mechanism in welded tuff. *Permafrost and Periglacial Processes* 2, 301–309.
- Åkerman, H.J., 2005. Relations between slow slope processes and active-layer thickness 1972–2002. *Kapp Linné, Svalbard Norsk Geografisk Tidsskrift* 59, 116–128.
- Allard, M., Kasper, J.N., 1998. Temperature conditions for ice-wedge cracking: field measurements from Salluit, Northern Quebec. In: Lewkowicz, A.G., Allard, M. (Eds.), *Permafrost, Proceedings, 7th International Conference, Yellowknife, Canada, Centre d'études nordiques, Université Laval, Collection Nordicana* 57, Quebec, pp. 5–11.
- Andersland, O.B., Ladanyi, B., 2004. *An introduction to frozen ground engineering*. John Wiley & Sons, Inc., Hoboken, New Jersey, xii, 363 pp.
- Anderson, D.M., Tice, A.R., 1972. Predicting unfrozen water content in frozen soils from surface area measurements. No. 393. *Highway Research Record*.
- Archie, G.E., 1942. The electrical resistivity log as an aid in determining some reservoir characteristics. *American Institute of Mining and Metallurgical Engineers*, pp. 55–62.
- Arcone, S., Lawson, D., Delaney, A., Strasser, J.C., Strasser, J.D., 1998a. Ground-penetrating radar reflection profiling of groundwater and bedrock in an area of discontinuous permafrost. *Geophysics* 63 (5), 1573–1584.
- Arcone, S.A., Lawson, D.E., Delaney, A.J., Strasser, J.C., Strasser, J.D., 1998b. Ground-penetrating radar reflection profiling of groundwater and bedrock in an area of discontinuous permafrost. *Geophysics* 63, 1573–1584.
- Arenson, L.U. 2002. Unstable alpine permafrost: a potentially important natural hazard. Ph.D. dissertation, Institute for Geotechnical Engineering ETH, Zurich. Available from <http://e-collection.ethbib.ethz.ch/show?type=diss&nr=14801>.
- Arenson, L.U., Springman, S.M., 2005a. Mathematical description for the behaviour of ice-rich frozen soils at temperatures close to zero centigrade. *Canadian Geotechnical Journal* 42 (2), 431–442.
- Arenson, L.U., Springman, S.M., 2005b. Triaxial constant stress and constant strain rate tests on ice-rich permafrost samples. *Canadian Geotechnical Journal* 42 (2), 412–430.
- Arenson, L., Hoelzle, M., Springman, S., 2002. Borehole deformation measurements and internal structure of some rock glaciers in Switzerland. *Permafrost and Periglacial Processes* 13 (2), 117–135.
- Arenson, L.U., Almasi, N., Springman, S.M., 2003a. Shearing response of ice-rich rock glacier material. In: Phillips, M., Springman, S.M., Arenson, L.U. (Eds.), *Eighth International Conference on Permafrost*. A.A. Balkema, Zurich, Switzerland, pp. 39–44.
- Arenson, L.U., Springman, S.M., Hawkins, P.G., 2003b. Pressuremeter tests within an active rock glacier in the Swiss Alps. In: Phillips, M., Springman, S.M., Arenson, L.U. (Eds.), *Eighth International Conference on Permafrost*. A.A. Balkema, Zurich, Switzerland, pp. 33–38.
- Arenson, L.U., Johansen, M.M., Springman, S.M., 2004. Effects of volumetric ice content and strain rate on shear strength under triaxial conditions for frozen soil samples. *Permafrost and Periglacial Processes* 15 (3), 261–271.
- Arenson, L.U., Segó, D.C., Newman, G., 2006. The use of a convective heat flow model in road designs for Northern regions. *Climate Change Technology Conference*, Ottawa, Ontario, Canada. CD-ROM.
- Arenson, L.U., Springman, S.M., Segó, D.C., 2007. The rheology of frozen soils. *Applied Rheology* 17 (1), 12147–1–12147–14.
- Arnold, A., Thielen, A., Springman, S.M., 2005. On the stability of active layers in alpine permafrost. 11th International Conference and Field Trip on Landslides (ICFL). Taylor & Francis, Netherlands, Trondheim, Norway, pp. 19–25.
- ASTM, 2001. D 5520, Standard test method for laboratory determination of creep properties of frozen soil samples by uniaxial compression.
- ASTM, 2005. D 5334, Standard test method for determination of thermal conductivity of soil and soft rock by thermal needle probe procedure.
- ASTM, 2006. WK10696, New standard test method for laboratory determination of strength properties of frozen soil at a constant rate of strain.
- Ballantyne, C.K., 2002. Paraglacial geomorphology. *Quaternary Science Reviews* 21 (18–19), 1935–2017.
- Ballantyne, C.K., Harris, C., 1994. *The Periglaciation of Great Britain*. Cambridge University Press, Cambridge. 330p.
- Barber, K.E., Chambers, F.M., Maddy, D., Stoneman, R., Brew, J.S., 1994. A sensitive high resolution record of late Holocene climatic change from a raised bog in northern England. *The Holocene* 4, 198–205.
- Barnekow, L., Sandgren, P., 2001. Palaeoclimate and tree-line changes during the Holocene based on pollen and plant macrofossil records from six lakes at different altitudes in northern Sweden. *Review of Palaeobotany and Palynology* 117, 109–118.
- Barsch, D., 1992. Permafrost creep and rockglaciers. *Permafrost and Periglacial Processes* 3, 175–188.
- Barsch, D., 1996. *Rockglaciers: indicators for the present and former geocology in high mountain environments*. Springer Series in Physical Environment, vol. 16. New York, Springer. 331 pp.
- Bartelt, P., Lehning, M., 2002. A physical SNOWPACK model for the Swiss avalanche warning. Part I: numerical model. *Cold Regions Science and Technology* 35 (3), 123–145.

- Bauer, A., Paar, G., Kaufmann, V., 2003. Terrestrial laser scanning for rock glacier monitoring. In: Phillips, M., Springman, S., Arenson, L. (Eds.), 8th International Conference on Permafrost, Proceedings 1. Zurich. Swets & Zeitlinger, Lisse, pp. 55–60.
- Beltrami, H., Harris, R.N. (Eds.), 2001. Inference of climate change from geothermal data. *Global and Planetary Change*, vol. 29, pp. 149–348 (Special Issue).
- Berger, A., Loutre, M.F., 1991. Insolation values for the climate of the last 10 million years. *Quaternary Science Reviews* 10, 297–317.
- Berthling, I., Eitzelmüller, B., Eiken, T., Sollid, J.L., 1998. Rock glaciers on Prins Karls Forland, Svalbard, I: internal structure, flow velocity and morphology. *Permafrost and Periglacial Processes* 9 (2), 135–145.
- Berthling, I., Eitzelmüller, B., Isaksen, K., Sollid, J.L., 2000. Rock glaciers on Prins Karls Forland. II: GPR soundings and the development of internal structures. *Permafrost and Periglacial Processes* 11 (4), 357–369.
- Beylich, A.A., Sandberg, O., 2005. Geomorphic effects of the extreme rainfall event of 20–21 July, 2004 in the Latnjavagge catchment, northern Swedish Lapland. *Geografiska Annaler* 87 A, 409–419.
- Birks, H.H., 1991. Holocene vegetational history and climatic change in West Spitsbergen based on plant macrofossils from Skardtjørna. *The Holocene* 1, 209–218.
- Blikra, L.H., Selvik, S.F., 1998. Climate signals recorded in snow avalanche-dominated colluvium in western Norway: depositional facies successions and pollen records. *The Holocene* 8, 631–658.
- Bommer, C., Keusen, H.R., Phillips, M., 2008. Engineering solutions for foundations and anchors in mountain permafrost. In: Kane, D.L., Hinkel, K.M. (Eds.), Ninth International Conference on Permafrost, Fairbanks, Fairbanks Alaska, 29 June–3 July 2008, vol. 1. Institute of Northern Engineering, University of Alaska, pp. 159–163.
- Bourque, A., Simonet, G., 2006. Impacts of climate change on infrastructures and implications on engineering. EIC Climate Change Technology Conference, Ottawa, ON Canada. CD-ROM.
- Bradley, R.S., 1990. Holocene paleoclimatology of the Queen Elizabeth Islands, Canadian high Arctic. *Quaternary Science Reviews* 9, 365–384.
- Bradley, R.S., 1999. Paleoclimatology: Reconstructing climates of the Quaternary. Academic Press, San Diego, CA. 613 p.
- Brenning, A., 2004. Statistical estimation and logistic regression modelling of rock glacier distribution in the Andes of Santiago, Central Chile. European Geosciences Union 2004, Nice, France. SRef-ID: 1607-7962/gra/EGU04-A-01032.
- Brenning, A., 2005. Climatic and geomorphological controls of rock glaciers in the Andes of Central Chile – combining statistical modelling and field mapping. PhD Thesis, Humboldt-Universität zu Berlin, Berlin, 137 pp.
- Brenning, A., Gruber, S., Hoelzle, M., 2005. Sampling and statistical analysis of BTS measurements. *Permafrost and Periglacial Processes* 16 (3), 231–240.
- Briffa, K.R., Osborn, T.J., Schweingruber, F.H., Harris, I.C., Jones, P.D., Shiyatov, S.G., Vaganov, E.A., 2001. Low-frequency temperature variations from a northern tree ring density network. *Journal of Geophysical Research* 106 (d3), 2929–2941.
- Brown, J., Ferrians, O., Heginbottom, J.A. and Melnikov, E.S. 1997. Circum-arctic map of permafrost and ground-ice conditions. 1:10,000,000 Map CP-45. Circum-Pacific map series, USGS.
- Brown, J., French, H.M., Cheng, G., 2008. The International Permafrost Association: 1983–2008. In: Kane, D.L., Hinkel, K.M. (Eds.), Ninth International Conference on Permafrost, University of Alaska Fairbanks, 29 June–3 July 2008. Institute of Northern Engineering, University of Alaska Fairbanks, pp. 199–204.
- Bucki, A.K., Echelmeyer, K.A., MacInnes, S., 2004. The thickness and internal structure of Fireweed rock glacier, Alaska, U.S.A., as determined by geophysical methods. *Journal of Glaciology* 50 (168), 67–75.
- Büdel, J., 1977. Klima-Geomorphologie. Gebrüder Borntraeger, Berlin. 304 pp.
- Büdel, J., 1982. Climatic Geomorphology. Princeton University Press, Princeton.
- Burga, C.A., 1991. Vegetation history and paleoclimatology of the middle Holocene – pollen analysis of Alpine peat bog sediments, covered formerly by the Rutor Glacier, 2510 m Aosta Valley, Italy. *Global Ecology and Biogeography Letters* 1 (5), 143–150.
- Burga, C.A., 1993. Swiss alpine palaeoclimate during the Holocene: pollen analytical evidence and general features. In: Frenzel, B. (Ed.), Solifluction and Climatic Variation in the Holocene. European Science Foundation, Verlag, Stuttgart, pp. 11–22.
- Burn, C.R., 1990. Implications for palaeoenvironmental reconstruction of recent ice-wedge development at Mayo, Yukon Territory. *Permafrost and Periglacial Processes* 1, 3–14.
- Burn, C.R., 2007. Permafrost. In: Elias, S.A. (Ed.), *Encyclopedia of Quaternary Science*, vol. 3. Elsevier, Oxford. 2191–2199.
- Cannone, N., Guglielmin, M., Hauck, C., Vonder Mühll, D., 2003. The impact of recent glacier fluctuation and human activities on the permafrost distribution: a case study from Stelvio Pass (Italian Central-Eastern Alps). In: Phillips, Springman, Arenson (Eds.), *Permafrost*. Swets & Zeitlinger, Lisse, pp. 125–130.
- Cermak, V., Safanda, J., Kresl, M., Dedecek, P., Bodri, L., 2000. Recent climate warming: surface air temperature series and geothermal evidence. *Studia geophysica et geodaetica* 44, 430–441.
- Chandler, R.J., 1972. Periglacial mudslides in Vestspitsbergen and their bearing on the origin of fossil “solifluction” shears in low angled clay slopes. *Quarterly Journal of Engineering Geology* 5, 223–241.
- Cheng, G.D., 2005. A roadbed cooling approach for the construction of Qinghai–Tibet Railway. *Cold Regions Science and Technology* 42 (2), 169–176.
- Cheng, G., 1983. The mechanism of repeated segregation for the formation of thick-layered ground ice. *Cold Regions Science and Technology* 8, 57–66.
- Christiansen, H.H., 2005. Thermal regime of ice-wedge cracking in Adventdalen, Svalbard. *Permafrost and Periglacial Processes* 16, 87–98.
- Christiansen, H.H., Humlum, O., 2008. Interannual variations in active layer thickness in Svalbard. In: Kane, D.L., Hinkel, K.M. (Eds.), *Proceedings Ninth International Conference on Permafrost*, June 29–July 3, Fairbanks Alaska, vol. 1. Institute of Northern Engineering, University of Alaska Fairbanks, pp. 257–262.
- Cihlar, J., Barry, T.G., Ortega Gil, E., Haerberli, W., Kuma, K., Landwehr, J.M., Norse, D., Running, S., Scholes, R., Solomon, A.M., Zhao, S., 1997. GCOS/GTOS plan for terrestrial climate related observation.
- Coutard, J.P., Francou, B., 1989. Rock temperature measurements in two alpine environments: implications for frost shattering. *Arctic and Alpine Research* 21 (4), 399–416.
- Curry, A.M., Cleasby, V., Zukowkyj, P., 2006. Paraglacial response of steep, sediment-mantled slopes to post-‘Little Ice Age’ glacier recession in the central Swiss Alps. *Journal of Quaternary Science* 21 (3), 211–225.
- Dahl, S.O., Nesje, A., 1996. A new approach to calculating Holocene winter precipitation by combining glacier equilibrium line altitudes and pine-tree limits: a case study from Hardangerjøkulen, central south Norway. *The Holocene* 6, 381–398.
- Dallimore, S.R., Davis, J.L., 1987. Ground probing radar investigations of massive ground ice and near surface geology in continuous permafrost. Geological Survey of Canada, Paper 87–1A, 913–918.
- Dallimore, S.R., Nixon, F.M., Eggington, P.A., Bisson, J.G., 1996. Deep-seated creep of massive ground ice, Tuktoyaktuk, N.W.T., Canada. *Permafrost and Periglacial Processes* 7, 337–347.
- Daniels, J.J., Keller, G.V., Jacobson, J.J., 1976. Computer-assisted interpretation of geomagnetic soundings over a permafrost section. *Geophysics* 41, 752–765.
- Dätwyler, T., 2004. SAC-Hütten und Jahrhundertssommer 2003. *Die Alpen*, vol. 1. Stämpfli, Bern, pp. 46–49.
- Davies, M.C.R., Hamza, O., Lumsden, B.W., Harris, C., 2000. Laboratory measurements of the shear strength of ice-filled rock joints. *Annals of Glaciology* 31, 463–467.
- Davies, M.C.R., Hamza, O., Harris, C., 2001. The effect of rise in mean annual temperature on the stability of rock slopes containing ice-filled discontinuities. *Permafrost and Periglacial Processes*, 12, 137–144.
- Davies, M.C.R., Hamza, O., Harris, C., 2003. Physical modelling of permafrost warming in rock slopes. In: Phillips, M., Springman, S.M., Arenson, L.U. (Eds.), *Proceedings of the 8th International Conference on Permafrost*, Zurich. Lisse, Netherlands, Balkema, pp. 169–173.
- Davis, B.A.S., Brewer, S., Stevenson, A.C., Guiot, J., data contributors, 2003. The temperature of Europe during the Holocene reconstructed from pollen data. *Quaternary Science Reviews* 22, 1701–1716.
- de Pascale, G.P., Williams, K.K., Pollard, W.H. 2008. Geophysical mapping of ground ice using a combination of capacitive coupled resistivity and ground penetrating radar, NWT, Canada. *Journal of Geophysical Research – Earth Surface*, in press.
- Delaloye, R., Reynard, E., Lambiel, C., 2000. Pergélisol et construction de remontées mécaniques: l'exemple des Lapires (Mont-Gelé, Valais). Publication de la Société Suisse de Mécanique des Sols et des Roches, Le gel en géotechnique, Réunion d'automne, 10 novembre 2000, pp. 103–113.
- Deline, P. 2002. Etude géomorphologique des interactions écoulement rocheux/glaciales dans la haute montagne alpine (versant sud-est du massif Mont Blanc), PhD thesis, Savoie, Savoie.
- Delisle, G., Allard, M., Fortier, R., Calmels, F., Larrivé, É., 2003. Umiujaq, Northern Québec: innovative techniques to monitor the decay of a lithalsa in response to climate change. *Permafrost and Periglacial Processes* 14, 375–385.
- Duchesne, C., Wright, J.F., Côté, M.M., Nixon, F.M., 2003. An enhanced vegetation classification for permafrost modelling, NWT, Canada. In: Phillips, M., Springman, S.M., Arenson, L. (Eds.), *Proceedings 8th International Conference on Permafrost*. Swets and Zeitlinger, Lisse, pp. 217–221.
- Einarsson, T.H., 1975. Um myndunarsögu íslensks myrlendis. In: Gardarso, A. (Ed.), *Votlendi*. Reykjavík, Landvernd, pp. 15–21.
- Eronen, M., Zetterberg, P., 1996. Climatic changes in Northern Europe since late glacial times, with special reference to dendroclimatological studies in northern Finnish Lapland. *Geophysica* 2, 35–60.
- Esch, D.C. (Ed.), 2004. Thermal analysis, construction, and monitoring methods for frozen ground. Technical Council on Cold Regions Engineering monograph. American Society of Civil Engineers, Reston, VA. 492 pp.
- Eitzelmüller, B., Hagen, J.O., 2005. Glacier-permafrost interaction in Arctic and alpine mountain environments with examples from southern Norway and Svalbard. In: Harris, C., Murton, J.M. (Eds.), *Cryospheric Systems: Glaciers and Permafrost*. Geological Society of London Special Publication, vol. 242, pp. 11–28.
- Eitzelmüller, B., Berthling, I., Sollid, J.L., 1998b. The distribution of permafrost in Southern Norway; a GIS approach. In: Lewkowicz, A.G., Allard, M. (Eds.), *Seventh International Conference on Permafrost*, Proceedings. Collection Nordicana. Centre d'Etudes Nordiques, Université Laval, Québec, PQ, Canada, pp. 251–257.
- Eitzelmüller, B., Berthling, I., Sollid, J.L., 2003. Aspects and concepts on the geomorphological significance of Holocene permafrost in southern Norway. *Geomorphology* 52, 87–104.
- Eitzelmüller, B., Hoelzle, M., Heggem, E.S.F., Isaksen, K., Mittaz, C., Vonder Mühll, D., Ødegård, R.S., Haerberli, W., Sollid, J.L., 2001a. Mapping and modelling the occurrence and distribution of mountain permafrost. *Norwegian Journal of Geography* 55, 186–194.
- Eitzelmüller, B., Ødegård, R.S., Berthling, I., Sollid, J.L., 2001b. Terrain parameters and remote sensing data in the analysis of permafrost distribution and periglacial processes: principles and examples from Southern Norway. *Permafrost and Periglacial Processes* 12 (1), 79–92.
- Eitzelmüller, B., Heggem, E.S.F., Sharkhuu, N., Frauenfelder, R., Käab, A., Goulden, C.E., 2006. Mountain permafrost distribution modelling using a multi-criteria approach in the Hövsgöl area, Northern Mongolia. *Permafrost and Periglacial Processes* 17, 91–104.
- Eitzelmüller, B., Farbrøt, H., Guðmundsson, Á., Humlum, O., Tveit, O.E., Björnsen, H., 2007. The regional distribution of mountain permafrost in Iceland. *Permafrost and Periglacial Processes* 18, 185–199.
- Eitzelmüller, B., Schuler, T.V., Farbrøt, H., Guðmundsson, A., 2008. Permafrost in Iceland – distribution, ground temperatures and climate change impact. In: Kane, D.L., Hinkel, K.M. (Eds.), *Proceedings Ninth International Conference on Permafrost*,

- June 29–July 3, Fairbanks Alaska, vol. 1. Institute of Northern Engineering, University of Alaska Fairbanks, pp. 421–426.
- Evans, S.G., Clague, J.J., 1988. Catastrophic rock avalanches in glacial environment. Proceedings of the fifth International Symposium on Landslides, Lausanne, 10–15 July 1988, vol. 2, pp. 1153–1158.
- Farbrot, H., Isaksen, K., Eiken, T., Kääb, A., Sollid, J.L., 2005. Composition and internal structures of a rock glacier on the strandflat of western Spitsbergen, Svalbard. *Norsk Geografisk Tidsskrift* 59 (2), 139–148.
- Farbrot, H., Eitzelmüller, B., Gudmundsson, A., Schuler, T.V., Eiken, T., Humlum, O., Björnsson, H., 2007. Thermal characteristics and impact of climatic change on mountain permafrost in Iceland. *Journal of Geophysical Research* 112. doi:10.1029/2006JF000541.
- Farbrot, H., Isaksen, K., Eitzelmüller, B., 2008. Present and past distribution of mountain permafrost in Gaissane Mountains, Northern Norway. In: Kane, D.L., Hinkel, K.M. (Eds.), Proceedings volume 1, Ninth International Conference on Permafrost, University of Alaska Fairbanks, 29 June–3 July 2008. Institute of Northern Engineering, University of Alaska Fairbanks, pp. 427–432.
- Fauve, M., Rhyner, H., Schneebeli, M., 2002. Pistenpräparation und Pistenpflege: Das Handbuch für den Praktiker. Davos, Eidg. Institut für Schnee- und Lawinenforschung.
- Fierz, C., Lehning, M., 2001. Assessment of the microstructure-based snow-cover model SNOWPACK: thermal and mechanical properties. *Cold Regions Science and Technology* 33, 123–131.
- Filippi, M.L., Lambert, P., Hunziker, J., Kubler, B., Bernasconi, S., 1999. Climatic and anthropogenic influence on the stable isotope record from bulk carbonates and ostracodes in Lake Neuchâtel, Switzerland, during the last two millennia. *Journal of Paleolimnology* 21, 19–34.
- Fischer, L., Kääb, A., Huggel, C., Nötzli, J., 2006. Geology, glacier retreat and permafrost degradation as controlling factors of slope instabilities in a high-mountain rock wall: the Monte Rosa east face. *Natural Hazards and Earth System Sciences* 6, 761–772. www.nat-hazards-earth-syst-sci.net/6/761/2006/.
- Fish, A.M., 1985. Creep strength, strain rate, temperature and unfrozen water relationship in frozen soil. In: Kinoshita, S., Fukuda, M. (Eds.), Fourth International Symposium on Ground Freezing. A.A. Balkema, Rotterdam, Sapporo, pp. 29–36.
- Fish, A.M., Zaretsky, Y.K., 1997. Ice strength as a function of hydrostatic pressure and temperature. Cold Regions Research and Engineering Laboratory (CRREL), Hanover NH, USA. 14pp.
- Foriere, A., Ladanyi, B., Dallimore, S.R., Egginton, P.A., Nixon, F.M., 1998. Modelling of deep seated hill slope creep in permafrost. *Canadian Geotechnical Journal* 35, 560–578.
- Forman, S.L., Lubinski, D.J., Ingolfsson, O., Zeeberg, J.J., Snyder, J.A., Siegert, M.J., Matishov, G.G., 2004. A review of postglacial emergence on Svalbard, Franz Josef Land and Novaya Zemlya, northern Eurasia. *Quaternary Science Reviews* 23 (11–13), 1391–1434.
- Fortier, D., Allard, M., 2005. Frost-cracking Conditions, Bylot Island, Eastern Canadian Arctic Archipelago. *Permafrost and Periglacial Processes* 16, 145–161.
- Frauenfelder, R., 2005. Regional-scale modeling of the occurrence and dynamics of rockglaciers and the distribution of paleopermafrost. Department of Geography, University of Zurich, Physical Geography Series. 45, 70 p. plus Annex. ISBN 3 85543 241 4.
- Frauenfelder, R., 2006. Debris transport by rockglacier – a quantitative estimate for an Alpine study site. NGF - Abstracts and Proceedings of the Geological Society of Norway 4, 40–41.
- Frauenfelder, R., Kääb, A., 2000. Towards a palaeoclimatic model of rock glacier formation in the Swiss Alps. *Annals of Glaciology* 31, 281–286.
- Frauenfelder, R., Haerberli, W., Hoelzle, M., Maisch, M., 2001. Using relict rockglaciers in GIS-based modelling to reconstruct younger dryas permafrost distribution patterns in the Err-Julier area, Swiss Alps. *Norwegian Journal of Geography* 55 (4), 195–202.
- Frauenfelder, R., Haerberli, W., Hoelzle, M., 2003. Rockglacier occurrence and related terrain parameters in a study area of the Eastern Swiss Alps. In: Phillips, M., Springman, S.M., Arenson, L.U. (Eds.), Proceedings 8th International Conference on Permafrost. Swets and Zeitlinger, Lisse, pp. 253–258.
- Frauenfelder, R., Zraggen-Oswald, S., Huggel, C., Kääb, A., Haerberli, W., Galushkin, I., Polkvoy, A., 2005. Permafrost distribution assessments in the North-Osetian Caucasus: first results. *Geophysical Research Abstracts*, vol. 7. 01619, SRef-ID: 1607-7962/gra/EGU05-A-01619.
- Frauenfelder, R., Schneider, B., Kääb, A., 2008. Using dynamic modelling to simulate the distribution of rockglaciers. *Geomorphology* 93, 130–143.
- French, H.M., 1996. The Periglacial Environment. Longman, Harlow, 341pp.
- French, H.M., Bennett, L., Hayley, D.W., 1986. Ground ice conditions near Rea Point and on Sabine Peninsula, eastern Melville Island. *Canadian Journal of Earth Sciences* 23, 1389–1400.
- Furrer, G., 1994. Zur Gletschergeschichte des Liefdefjords/NW-Spizbergen. *Zeitschrift für Geomorphologie*, N.F., Suppl.-Bd. 97, 43–47.
- Gamper M.W., 1993. Holocene solifluction in the Swiss Alps: dating and climatic implications. In: Frenzel, B. (Ed.), Solifluction and Climatic Variation in the Holocene. European Science Foundation, Verlag, Stuttgart, pp. 1–10.
- Geist, T., Stötter, H., 2003. First results of airborne laser scanning technology as a tool for the quantification of glacier mass balance. *EARSEL eProceedings* 2 (1), 8–14.
- Glade, T., 2005. Linking debris-flow hazard assessments with geomorphology. *Geomorphology* 66, 189–213.
- Goering, D.J., 1998. Experimental investigation of air convection embankments for permafrost-resistant roadway design. In: Lewkowicz, A.G., Allard, M. (Eds.), Seventh International Conference on Permafrost. Collection Nordicana, vol. 57. Yellowknife, NWT, Canada, pp. 319–326.
- Goering, D.J., Instanes, A., Knudsen, S., 2000. Convective heat transfer in railway embankment ballast. International Symposium on Ground Freezing and Frost Action in Soils. Louvain-la-Neuve, Belgium, pp. 31–36.
- Gold, L.W., Lachenbruch, A.H., 1973. Thermal conditions in permafrost – a review of North American literature. Permafrost: The North American Contribution to the Second International Conference, 13–28 July 1973, Yakutsk, U.S.S.R. National Academy of Science, Washington, DC, pp. 3–25.
- Goodrich, L.E., 1978. Efficient numerical technique for the one-dimensional thermal problems with phase change. *International Journal of Heat and Mass Transfer* 21, 615–621.
- Goodrich, L.E., 1982. The influence of snow cover on ground thermal regime. *Canadian Geotechnical Journal* 19, 421–432.
- Götz, A., Raetz, H., 2002. Permafrost – mit dem Risiko umgehen. *TEC* 21 (17), 7–10.
- Gross, R., Green, A.G., Horstmeyer, H., Holliger, K., Baldwin, J., 2003. 3-D georadar images of an active fault: efficient data acquisition, processing and interpretation strategies. *Subsurface Sensing Technique and Application* 4 (1), 19–40.
- Goughnour, R.R., Andersland, O.B., 1968. Mechanical properties of a sand-ice system. *Journal of the soil mechanics and foundations division. ASCE* 94 (SM 4), 923–950.
- Gruber, S., 2005. Mountain Permafrost: Transient spatial modelling, model verification and the use of remote sensing. PhD Thesis, Universität Zürich, Zürich, 121 pp.
- Gruber, S., Hoelzle, M., 2001. Statistical modelling of mountain permafrost distribution: local calibration and incorporation of remotely sensed data. *Permafrost and Periglacial Processes* 12 (1), 69–77.
- Gruber, S., Haerberli, W., 2007. Permafrost in steep bedrock slopes and its temperature-related destabilization following climatic change. *Journal of Geophysical Research* 112, F02S18. doi:10.1029/2006JF000547.
- Gruber, S., Peter, M., Hoelzle, M., Woodhatch, I., Haerberli, W., 2003a. Surface temperatures in steep alpine rock faces – a strategy for regional-scale measurement and modelling. In: Phillips, M., Springman, S.M., Arenson, L.U. (Eds.), Proceedings 8th International Conference on Permafrost. Swets and Zeitlinger, Lisse, pp. 325–330.
- Gruber, S., Peter, M., Hoelzle, M., Woodhatch, I., Haerberli, W., 2003b. Surface temperatures in steep alpine rock faces – a strategy for regional-scale measurement and modelling. In: Phillips, M., Springman, S.M., Arenson, L.U. (Eds.), Proceedings of the 8th International Conference on Permafrost, vol. 1. Swets & Zeitlinger, Lisse, pp. 325–330.
- Gruber, S., Hoelzle, M., Haerberli, W., 2004a. Rock-wall temperatures in the Alps: modelling their topographic distribution and regional differences. *Permafrost and Periglacial Processes* 15, 299–307.
- Gruber, S., Hölzle, M., Haerberli, W., 2004b. Permafrost thaw and destabilization of Alpine rock walls in the hot summer of 2003. *Geophysical Research Letters* 31, L13504. doi:10.1029/2004GL020051.
- Gruber, S., King, L., Kohl, T., Herz, T., Haerberli, W., Hoelzle, M., 2004c. Interpretation of geothermal profiles perturbed by topography: the Alpine permafrost boreholes at Stockhorn Plateau, Switzerland. *Permafrost and Periglacial Processes* 15, 349–357.
- Gudmundsson, H., 1997. A review of the Holocene environmental history of Iceland. *Quaternary Science Reviews* 16, 81–92.
- Guglielmin, M., Cannone, N., Dramis, F., 2001. Permafrost – glacial evolution during the Holocene in the Italian Central Alps. *Permafrost and Periglacial Processes* 12 (1), 111–124.
- Guillaud, C., 2006. Coping with uncertainty in the design of hydraulic structures: climate change is but one more uncertain parameter. EIC Climate Change Technology Conference, Ottawa, ON Canada. CD-ROM.
- Haas, J.N., Risch, J., Tinner, W., Wick, L., 1998. Synchronous Holocene climatic oscillations recorded on the Swiss Plateau and at the timberline in the Alps. *The Holocene* 8 (3), 301–309.
- Haerberli, W., 1973. Die Basis-Temperatur der winterlichen Schneedecke als möglicher Indikator für die Verbreitung von Permafrost in den Alpen. *Zeitschrift für Gletscherkunde und Glazialgeologie. Universitätsverlag Wagner - Innsbruck*, pp. 221–227.
- Haerberli, W., 1975. Untersuchungen zur Verbreitung von Permafrost zwischen Flüelapass und Piz Grialetsch (Graubünden). Mitteilung der Versuchsanstalt für Wasserbau, Hydrologie und Glaziologie der ETH Zürich 17, 221.
- Haerberli, W., 1985. Creep of mountain permafrost. Mitteilungen der Versuchsanstalt für Wasserbau, Hydrologie und Glaziologie der ETH Zürich 77.
- Haerberli, W., 1992. Construction, environmental problems and natural hazards in periglacial mountain belts. *Permafrost and Periglacial Processes* 3 (2), 111–124.
- Haerberli, W., 1994. Accelerated glacier and permafrost changes in the Alps. In: Beniston, M. (Ed.), Mountain Environments in Changing Climates. Routledge Publishing Company, London and New York, pp. 91–107.
- Haerberli, W., 2000. Modern research perspectives relating to permafrost creep and rock glaciers. *Permafrost and Periglacial Processes* 11, 290–293.
- Haerberli, W., 2005. Investigating glacier/permafrost-relations in high-mountain areas: historical background, selected examples and research needs. In: Harris, C., Murton, J.B. (Eds.), Cryospheric Systems: Glaciers and Permafrost, 242. Geological Society, London, Special Publications, pp. 29–37.
- Haerberli, W., Vonder Mühll, D., 1996. On the characteristics and possible origins of ice in rock glacier permafrost. *Zeitschrift für Geomorphologie* 104, 43–57.
- Haerberli, W., Wegmann, M., Vonder Mühll, D., 1997. Slope stability problems related to glacier shrinkage and permafrost degradation in the Alps. *Eclogae Geologicae Helvetiae* 90, 407–414.
- Haerberli, W., Beniston, M., 1998. Climate change and its impacts on glaciers and permafrost in the Alps. *Ambio* 27 (4), 258–265.
- Haerberli, W., Burn, C., 2002. Natural hazards in forests – glacier and permafrost effects as related to climate changes. In: Sidle, R.C. (Ed.), Environmental Change and Geomorphic Hazards in Forests. IUFRO Research Series, 9, pp. 167–202.
- Haerberli, W., Gruber, S., 2008. Research challenges for permafrost in steep and cold terrain: an Alpine perspective. Plenary paper. In: Kane, D.L., Hinkel, K.M. (Eds.), Proceedings Ninth International Conference on Permafrost, June 29–July 3, Fairbanks Alaska, vol. 1. Institute of Northern Engineering, University of Alaska Fairbanks, pp. 597–605.
- Haerberli, W., Hohmann, R., 2008. Climate, glaciers and permafrost in the Swiss Alps 2050: scenarios, consequences and recommendations. In: Kane, D.L., Hinkel, K.M.

- (Eds.), Proceedings Ninth International Conference on Permafrost, vol. 1. Institute of Northern Engineering, University of Alaska Fairbanks, pp. 607–612.
- Haerberli, W., Kääh, A., Vonder Mühl, D., Teyseire, Ph., 2001. Prevention of outburst floods from periglacial lakes at Grubengletscher, Valais, Swiss Alps. *Journal of Glaciology* 47 (156), 111–122.
- Haerberli, W., Huggel, C., Kääh, A., Polkvoj, A., Zotikov, I., Osokin, N., 2003. Permafrost conditions in the starting zone of the Kolka–Karmadon rock/ice slide of 20 September 2002 in North Osetia (Russian Caucasus). In: Haerberli, W., Brandova, D. (Eds.), 8th International Conference on Permafrost, Extended Abstracts, Zurich, pp. 49–50.
- Haerberli, W., Huggel, C., Kääh, A., Zraggen-Oswald, S., Polkvoj, A., Galushkin, I., Zotikov, I., Osokin, N., 2004. The Kolka–Karmadon rock/ice slide of 20 September 2002: an extraordinary event of historical dimensions in North Ossetia, Russian Caucasus. *Journal of Glaciology* 50, 533–546.
- Haerberli, W., Hallet, B., Arenson, L., Elconin, R., Humlum, O., Kääh, A., Kaufmann, V., Ladanyi, B., Matsuoka, N., Springman, S., Vonder Mühl, D., 2006. Permafrost creep and rock glacier dynamics. *Permafrost and Periglacial Processes* 17 (3), 189–214.
- Hall, K., 1997. Rock temperatures and implications for cold region weathering I: New data from Viking Valley, Alexander Island, Antarctica. *Permafrost and Periglacial Processes* 8, 69–90.
- Hall, K., André, M.-F., 2001. New insights into rock weathering as deduced from high-frequency rock temperature data: an Antarctic study. *Geomorphology* 41, 23–35.
- Hall, K., Thorn, C.E., Matsuoka, N., Prick, A., 2002. Weathering in cold regions: some thoughts and perspectives. *Progress in Physical Geography* 26, 577–603.
- Hallet, B., Walder, J.S., Stubbs, C.W., 1991. Weathering by segregation ice growth in microcracks at sustained sub-zero temperatures: verification from an experimental study using acoustic emissions. *Permafrost and Periglacial Processes* 2, 283–300.
- Hallsdóttir, M., 1995. On the pre-settlement history of Icelandic vegetation. *Icelandic Agricultural Science* 9, 17–29.
- Hamilton, S.J., Whalley, W.B., 1995. Preliminary results from the lichenometric study of Hanson S., Hoelzle M. 2004. The thermal regime of the active layer at the Murtèl rock glacier based on data from 2002. *Permafrost and Periglacial Processes* 15, 273–282.
- Harada, K., Wada, K., Fukuda, M., 2000. Permafrost mapping by the transient electromagnetic method. *Permafrost and Periglacial Processes* 11, 71–84 2000.
- Harris, C., 1981. Periglacial mass-wasting: a review of research. BGR Research Monograph, 204. Geobooks, Norwich.
- Harris, C., 2007. Slope deposits and forms. In: Elias, S.A. (Ed.), *Encyclopedia of Quaternary Science*, vol. 3. Elsevier, Amsterdam, pp. 2207–2216.
- Harris, C., Davies, M.C.R., 2000. Gelifluction: observations from large-scale laboratory simulations. *Arctic, Antarctic and Alpine Research* 32 (2), 202–207.
- Harris, C., Lewkowicz, A.G., 2000. An analysis of the stability of thawing slopes, Ellesmere Island, Nunavut, Canada. *Canadian Geotechnical Journal* 37 (2), 465–478.
- Harris, C., Haerberli, W., 2003. Warming permafrost in the mountains of Europe. *WMO Bulletin* 52/3, 252–257.
- Harris, C., Smith, J.S., 2003. Modelling gelifluction processes: the significance of frost heave and slope gradient. In: Phillips, M., Springman, S.M., Arenson, L.G. (Eds.), Proceedings 8th International Conference on Permafrost, Zurich. Swets and Zeitlinger, Lisse, pp. 355–360.
- Harris, C., Murton, J.B., 2005. Experimental simulation of ice-wedge casting: processes, products and palaeoenvironmental significance. In: Harris, C., Murton, J.B. (Eds.), *Cryospheric Systems: Glaciers and Permafrost*. Geological Society, London, Special Publication, vol. 242, pp. 131–143.
- Harris, C., Isaksen, K., 2008. Recent warming of European permafrost: evidence from borehole monitoring. In: Kane, D.L., Hinkel, K.M. (Eds.), Proceedings vol. 1, Ninth International Conference on Permafrost, University of Alaska Fairbanks, 29 June–3 July 2008. Institute of Northern Engineering, University of Alaska Fairbanks, pp. 655–661.
- Harris, C., Davies, M.C.R., Coutard, J.-P., 1997. Rates and processes of periglacial solifluction: an experimental approach. *Earth Surface Processes and Landforms* 22, 849–868.
- Harris, C., Haerberli, W., Vonder Mühl, D., King, L., 2001a. Permafrost monitoring in the high mountains of Europe: the PACE project in its global context. *Permafrost and Periglacial Processes* 12 (1), 3–11.
- Harris, C., Rea, B., Davies, M.C.R., 2001b. Scaled physical modelling of mass movement processes on thawing slopes. *Permafrost and Periglacial Processes* 12 (1), 125–136.
- Harris, C., Davies, M.C.R., Eitzelmüller, B., 2001c. The assessment of potential geotechnical hazards associated with mountain permafrost in a warming global climate. *Permafrost and Periglacial Processes* 12 (1), 145–156.
- Harris, C., Davies, M.C.R., Rea, B.R., 2003a. Gelifluction: viscous flow or plastic creep? *Earth Surface Processes and Landforms* 28, 1289–1301.
- Harris, C., Vonder Mühl, D., Isaksen, K., Haerberli, W., Sollid, J.L., King, L., Holmlund, P., Dramis, F., Guglielmin, M., Palacios, D., 2003b. Warming permafrost in European mountains. *Global and Planetary Change* 39, 215–225.
- Harris, C., Luetsch, M., Murton, B., Smith, F.W., Davies, M.C.R., Christiansen, H.H., Ertlen-Font, M., 2006. Solifluction processes in Arctic permafrost: results of laboratory and field experiments. *Eos Trans. AGU* 87 (52) Fall Meeting Supplement, Abstract C43A-03.
- Harris, C., Luetsch, M.A., Davies, M.C.R., Smith, F.W., 2007. Field instrumentation for real-time monitoring of periglacial solifluction. *Permafrost and Periglacial Processes* 18 (1), 105–114.
- Harris, C., Kern-Luetsch, M., Murton, J.B., Font, M., Davies, M.C.R., Smith, F.W., 2008a. In: Kane, D.L., Hinkel, K.M. (Eds.), Full-scale physical modelling of solifluction processes associated with one-sided and two-sided active layer freezing. Proceedings Ninth International Conference on Permafrost, June 29–July 3, Fairbanks Alaska, vol. 1. Institute of Northern Engineering, University of Alaska Fairbanks, pp. 663–668.
- Harris, C., Smith, J.S., Davies, M.C.R., Rea, B., 2008b. An investigation of periglacial slope stability in relation to soil properties based on physical modelling in the geotechnical centrifuge. *Geomorphology* 93, 437–459. doi:10.1016/j.geomorph.2007.03.009.
- Harris, C., Kern-Luetsch, M.A., Smith, F.W., Isaksen, K., 2008c. Solifluction processes in an area of seasonal ground freezing, Dovrefjell, Norway. *Permafrost and Periglacial Processes* 19, 31–47. doi:10.1002/ppp.609.
- Harris, S.A., Corte, A.E., 1992. Interactions and relations between mountain permafrost, glaciers, snow and water. *Permafrost and Periglacial Processes* 3, 103–110.
- Harry, D.G., Gozdzik, J.S., 1988. Ice wedges: growth, thaw transformation, and palaeoenvironmental significance. *Journal of Quaternary Science* 3, 39–55.
- Hauck, C., 2002. Frozen ground monitoring using DC resistivity tomography. *Geophysical Research Letters* 29 (21), 2016.
- Hauck, C., Guglielmin, M., Isaksen, K., Vonder Mühl, D., 2001. Applicability of frequency-domain and time-domain electromagnetic methods for mountain permafrost studies. *Permafrost and Periglacial Processes* 12 (1), 39–52.
- Hauck, C., Vonder Mühl, D., 2003a. Evaluation of geophysical techniques for application in mountain permafrost studies. *Z. Geomorph.* vol. 132, 159–188 N.F., Suppl.-
- Hauck, C., Vonder Mühl, D., 2003b. Inversion and interpretation of 2-dimensional geoelectrical measurements for detecting permafrost in mountainous regions. *Permafrost and Periglacial Processes* 14 (4), 305–318.
- Hauck, C., Wagner, U., 2003. Combining and interpreting geoelectric and seismic tomographies in permafrost studies using fuzzy logic. Extended abstract, 8th Int. Conf. on Permafrost, Zurich 2003, pp. 57–58.
- Hauck, C., Kneisel, C., 2006. Application of capacitively-coupled and DC electrical resistivity imaging for mountain permafrost studies. *Permafrost and Periglacial Processes* 17 (2), 169–177.
- Hauck, C., Kneisel, C. (Eds.), 2008. *Applied geophysics in periglacial environments*. Cambridge University Press.
- Hauck, C., Isaksen, K., Vonder Mühl, D., Sollid, J.L., 2004. Geophysical surveys designed to delineate the altitudinal limit of mountain permafrost: an example from Jotunheimen, Norway. *Permafrost and Periglacial Processes* 15 (3), 191–205.
- Hauck, C., Vonder Mühl, D., Hoelzle, M., 2005. Permafrost monitoring in high mountain areas using a coupled geophysical and meteorological approach. In: de Jong, C., Collins, D., Ranzi R. (Eds.), *Climate and Hydrology of Mountain Areas*. Wiley, London, pp. 59–71.
- Hauck, C., Bach, M., Hilbich, C., 2008. A 4-phase model to quantify subsurface ice and water content in permafrost regions based on geophysical data sets. In: Kane, D.L., Hinkel, K.M. (Eds.), Proceedings Ninth International Conference on Permafrost, June 29–July 3, Fairbanks Alaska, vol. 1. Institute of Northern Engineering, University of Alaska Fairbanks, pp. 675–680.
- Heggem, E., Juliussen, H., Eitzelmüller, B., 2005. Mountain permafrost in Central-Eastern Norway. *Norsk Geografisk Tidsskrift* 59 (2), 94–108.
- Heggem, E.S.F., Eitzelmüller, B., Sharkhuu, N., Goulden, C.E., Nandinseteg, B., 2006. Spatial empirical modelling of ground surface temperature in the Hövsgöl area, Northern Mongolia. *Permafrost and Periglacial Processes* 17 (4), 357–369.
- Hestnes, E. 2000. Impact of rapid mass movement and drifting snow on the infrastructure and development of Longyearbyen, Svalbard. Proceedings of the International Workshop on Permafrost Engineering, 259–282, Longyearbyen, Svalbard, Norway, 18–21 June 2000. Ed. K. Senneset.
- Hilbich, C., Hauck, C., Hoelzle, M., Scherler, M., Schudel, L., Völsch, L., Vonder Mühl, D., Mäusbacher, R., 2008a. Monitoring mountain permafrost evolution using electrical resistivity tomography: a 7-year study of seasonal, annual, and long-term variations at Schilthorn, Swiss Alps. *J. Geophys. Res.* 113, F01S90. doi:10.1029/2007JF000799.
- Hilbich, C., Hauck, C., Delaloye, R., Hoelzle, M., 2008b. A geoelectric monitoring network and resistivity-temperature relationships of different mountain permafrost sites in the Swiss Alps. In: Kane, D.L., Hinkel, K.M. (Eds.), Proceedings Ninth International Conference on Permafrost, June 29–July 3, Fairbanks Alaska, vol. 1. Institute of Northern Engineering, University of Alaska Fairbanks, pp. 699–704.
- Hjort, C., 1997. Glaciation, climate history, changing marine levels and the evolution of the Northeast Water Polynia. *Journal of Marine Systems* 10, 23–33.
- Hodgson, D.A., St-Onge, D.A., Edlund, S.A., 1991. Surficial materials of Hot Weather Creek basin, Ellesmere Island, Northwest Territories. *Current Research, Part E: Geological Survey of Canada, Paper 91-1E*, pp. 157–163.
- Hoelzle, M., 1996. Mapping and modelling of mountain permafrost distribution in the Alps. *Norwegian Journal of Geography* 50, 11–15.
- Hoelzle, M., Haerberli, W., 1995. Simulating the effects of mean annual air temperature changes on permafrost distribution and glacier size. An example from the Upper Engadin, Swiss Alps. *Annals of Glaciology* 21, 400–405.
- Hoelzle, M., Wegmann, M., Krummenacher, B., 1999. Miniature temperature data loggers for mapping and monitoring of permafrost in high mountain areas: first experience from the Swiss Alps. *Permafrost and Periglacial Processes* 10, 113–124.
- Hoelzle, M., Mittaz, C., Eitzelmüller, B., Haerberli, W., 2001. Surface energy fluxes and distribution models of permafrost in European mountain areas: an overview of current developments. *Permafrost and Periglacial Processes* 12 (1), 53–68.
- Hoelzle, M., Vonder Mühl, D., Haerberli, W., 2002. Thirty years of permafrost research in the Corvatsch-Furtschellas area, Eastern Swiss Alps: a review. *Norwegian Journal of Geography* 56 (2), 137–145.
- Hoelzle, M., Paul, F., Gruber, S., Frauenfelder, R., 2005. Glacier and Permafrost in Mountain areas: different modelling approaches. Projecting Global Change Impact and Sustainable Land use and Natural Resource Management in Mountain Biosphere Reserves (GLOCHAMORE). *Global Change Impacts in Mountain Biosphere Reserves*. UNESCO, Paris, pp. 28–39.
- Hoelzle, M., Gruber, S., 2008. Borehole and ground surface temperatures and their relationship to meteorological conditions in the Swiss Alps. In: Kane, D.L., Hinkel, K.M. (Eds.), Proceedings Ninth International Conference on Permafrost, June 29–July 3, Fairbanks Alaska, vol. 1. Institute of Northern Engineering, University of Alaska Fairbanks, pp. 723–728.
- Holzhauser, H., Magny, M., Zumbühl, H.J., 2005. Glacier and lake-level variations in west-central Europe over the last 3500 years. *The Holocene* 15, 789–801.

- Hooke, R.I., Dahlin, B.B., Kauper, M.T., 1972. Creep of ice containing dispersed fine sand. *Journal of Glaciology* 11, 327–336.
- Hormes, A., Müller, B.U., Schlüchter, C., 2001. The Alps with little ice: evidence for eight Holocene phases of reduced glacier extent in the Central Swiss Alps. *The Holocene* 11 (3), 255–265.
- Huggel, C., Käab, A., Haeberli, W., Krummenacher, B., 2003. Regional-scale GIS-models for assessment of hazards from glacier lake outbursts: evaluation and application in the Swiss Alps. *Natural Hazards and Earth System Science* 3 (6), 647–662.
- Huggel, C., Käab, A., Salzmann, N., 2004. GIS-based modeling of glacial hazards and their interactions using Landsat-TM and IKONOS imagery. *Norwegian Journal of Geography* 61–73.
- Huggel, C., Zraggen-Oswald, S., Haeberli, W., Kaab, A., Polkvoj, A., Galushkin, I., Evans, S.G., 2005. The 2002 rock/ice avalanche at Kolka/Karmadon, Russian Caucasus: assessment of extraordinary avalanche formation and mobility, and application of QuickBird satellite imagery. *Natural Hazards and Earth System Sciences* 5, 173–187.
- Huijzer, B., Vandenbergh, J., 1998. Climatic reconstruction of the Weichselian Pleniglacial in northwestern and central Europe. *Journal of Quaternary Science* 13, 391–417.
- Huissteden, K.V., Vandenbergh, J., Pollard, D., 2003. Palaeotemperature reconstructions of the European permafrost zone during marine oxygen isotope Stage 3 compared with climate model results. *Journal of Quaternary Science* 18, 453–464.
- Humlum, O., 2005. Holocene permafrost aggradation in Svalbard. In: Harris, C., Murton, J.B. (Eds.), *Cryospheric Systems: Glaciers and Permafrost*. Special Publication, 242. Geological Society, London, pp. 119–130.
- Humlum, O., Instanes, A., Sollid, J.L., 2003. Permafrost in Svalbard: a review of research history, climatic background and engineering challenges. *Polar Research* 22, 191–225.
- Humlum, O., Elberling, B., Hormes, A., Fjordheim, K., Hansen, O.H., Heinemeier, J., 2005. Late Holocene glacier growth in Svalbard, documented by subglacial relict vegetation and living soil microbes. *The Holocene* 15 (3), 396–407.
- Humlum, O., Christiansen, H.H., Juliussen, H., 2007. Avalanche derived rock glaciers in Svalbard. *Permafrost and Periglacial Processes* 18, 75–88.
- Hurrell, J.W., 1995. Decadal trends in the North Atlantic Oscillation: regional temperatures and precipitation. *Science* 269, 676–679.
- Hyvärinen, H., 1975. Absolute and relative pollen diagrams from northernmost Fennoscandia. *Fennia* 142, 1–23.
- Ikeda, A., 2006. Combination of conventional geophysical methods for sounding the composition of rock glaciers in the Swiss Alps. *Permafrost and Periglacial Processes* 17, 35–48. doi:10.1002/ppp.550.
- Ikeda, A., Matsuoka, N., Käab, A., 2008. Fast deformation of perennially frozen debris in a warm rock glacier in the Swiss Alps: an effect of liquid water. *Journal of Geophysical Research-Earth Surface* 113, F01021.
- Imhof, M., 1996. Modelling and verification of the permafrost distribution in the Bernese Alps (Western Switzerland). *Permafrost and Periglacial Processes* 7, 267–280.
- Ingólfsson, Ó., Björck, S., Hafliðason, H., Rundgren, M., 1997. Glacial and climatic events in Iceland reflecting regional North Atlantic climatic shifts during the Pleistocene–Holocene transition. *Quaternary Science Reviews* 16, 1135–1144.
- Instanes, A., Anisimov, O., Brigham, L., Goering, D., Khrustalev, L., Ladanyi, B., Larsen, J.O., 2005. Arctic climate impact assessment, chapter 16: infrastructure: buildings. Support Systems, and Industrial Facilities. Cambridge University Press, pp. 908–944.
- Isaksen, K., Oedegaard, R.S., Eiken, T., Sollid, J.L., 2000a. Composition, flow and development of two tongue-shaped rock glaciers in the permafrost of Svalbard. *Permafrost Periglacial Processes* 11 (3), 241–257.
- Isaksen, K., Vonder Mühl, D., Gubler, H., Kohl, T., Sollid, J.L., 2000b. Ground surface temperature reconstruction based on data from a deep borehole in permafrost at Janssonhaugen, Svalbard. *Annals of Glaciology* 31, 287–294.
- Isaksen, K., Holmlund, P., Sollid, J.L., Harris, C., 2001. Three deep alpine-permafrost boreholes in Svalbard and Scandinavia. *Permafrost and Periglacial Processes* 12, 13–25.
- Isaksen, K., Hauck, C., Gudevang, E., Ødegård, R.S., Sollid, J.L., 2002. Mountain permafrost distribution in Dovrefjell and Jotunheimen, southern Norway, based on BTS and DC resistivity tomography data. *Norwegian Journal of Geography* 56 (2), 122–136.
- Isaksen, K., Bakkehøi, S., Ødegård, Eiken, T., Eitzmüller, B., Sollid, J.L., 2003. Mountain permafrost and energy balance on Juvvasshøe, southern Norway. In: Phillips, M., Springman, S., Arenson, L. (Eds.), 8th International Conference on Permafrost, Proceedings. Swets & Zeitlinger, Lisse, Zurich, Switzerland, pp. 467–472.
- Isaksen, K., Benestad, R.E., Harris, C., Sollid, J.L., 2007a. Recent extreme near-surface permafrost temperatures on Svalbard in relation to future climate scenarios. *Geophysical Research Letters* 34, L17502. doi:10.1029/2007GL031002 2007.
- Isaksen, K., Sollid, J.L., Holmlund, P., Harris, C., 2007b. Recent warming of mountain permafrost in Svalbard and Scandinavia. *Journal of Geophysical Research* 112, F02S04. doi:10.1029/2006JF000522.
- Isaksen, K., Farbro, H., Blikra, L.H., Johansen, B., Sollid, J.L., Eiken, T., 2008. Five year ground surface temperature measurements in Finnmark, Northern Norway. In: Kane, D.L., Hinkel, K.M. (Eds.), *Proceedings Volume 1, Ninth International Conference on Permafrost*, University of Alaska Fairbanks, 29 June–3 July 2008. Institute of Northern Engineering, University of Alaska Fairbanks, pp. 789–794.
- Ishikawa, M., Watanabe, T., Nakamura, N., 2001. Genetic difference of rock glaciers and the discontinuous mountain permafrost zone in Kanchanjunga Himal, Eastern Nepal. *Permafrost and Periglacial Process* 12 (3), 243–253.
- Ivanova, E.V., Murdmaa, I.O., Duplessy, J.-C., Paterne, M., 2002. Late Weichselian to Holocene paleoenvironments in the Barents Sea. *Global and Planetary Change* 34, 209–218.
- Iverson, R.M., Reid, M.E., LaHusen, R.G., 1997. Debris-flow mobilization from landslides. *Annual Review Earth and Planetary Science* 25, 85–138 1997.
- Jaesche, P., Veit, H., Huwe, B., 2003. Snow cover and soil moisture controls on solifluction in an area of seasonal frost, eastern Alps. *Permafrost and Periglacial Processes* 14, 399–410.
- Janke, J.R., 2005. Modeling past and future alpine permafrost distribution in the Colorado Front Range. *Earth Surface Processes and Landforms* 30 (12), 1495–1508.
- Jepesen, J.W., 2001. Palæoklimatiske indikatorer for central Spitsbergen, Svalbard. Eksemplificeret ved studier af iskiler og deres værtssedimenter. M.Sc. thesis, The University Center in Svalbard (UNIS), 101 pp.
- Jomelli, V., Pech, V.P., Chochillon, C., Brunstein, D., 2004. Geomorphic variations of debris flows and recent climatic change in the French Alps. *Climatic Change* 64, 77–102.
- Jonasson, C., Nyberg, R., 1999. The rainstorm of August 1998 in the Abisko area, northern Sweden: preliminary report on observations of erosion and sediment transport. *Geografiska Annaler* 81A (3), 387–390.
- Jorgenson, M.T., Kreig, R.A., 1988. A model for mapping permafrost distribution based on landscape component maps and climatic variables. In: Senneset, K. (Ed.), 5th International Conference on Permafrost. Proceedings. Tapir Publishers, Trondheim, Trondheim, Norway, pp. 176–182.
- Jorgenson, M.T., Shur, Y.L., Pullman, E.R., 2006. Abrupt increase in permafrost degradation in Arctic Alaska. *Geophysical Research Letters* 33, L02503. doi:10.1029/2005GL024960.
- Juliussen, H., Humlum, O., 2007. Towards a TTOP ground temperature model for mountainous terrain in central-eastern Norway. *Permafrost and Periglacial Processes* 18, 161–184.
- Juliussen, H., Humlum, O., 2008. Thermal regime of openwork block fields on the Mountains Elgähogna and Sølen, Central-eastern Norway. *Permafrost and Periglacial Processes* 19, 1–18.
- Käab, A., 2005. Remote sensing of mountain glaciers and permafrost creep. *Schriftenreihe Physische Geographie. Glaziologie und Geomorphodynamik*, vol. 48. University of Zurich.
- Käab, A., 2008. Remote sensing of permafrost-related problems and hazards. *Permafrost and Periglacial Processes* 19, 107–136. doi:10.1002/ppp.619.
- Käab, A., Vollmer, M., 2000. Surface geometry, thickness changes and flow fields on creeping mountain permafrost: automatic extraction by digital image analysis. *Permafrost and Periglacial Processes* 11 (4), 315–326.
- Käab, A., Haeberli, W., 2001. Evolution of a high-mountain thermokarst lake in the Swiss Alps. *Arctic, Antarctic, and Alpine Research* 33 (4), 385–390.
- Käab, A., Kneisel, C., 2005. Permafrost creep within a recently deglaciated glacier forefield: Muragl, Swiss Alps. *Permafrost and Periglacial Processes* 17 (1), 79–85.
- Käab, A., Weber, M., 2004. Development of transverse ridges on rockglaciers. Field measurements and laboratory experiments. *Permafrost and Periglacial Processes* 15 (4), 379–391.
- Käab, A., Reichmuth, T., 2005. Advance mechanisms of rockglaciers. *Permafrost and Periglacial Processes* 16 (2), 187–193.
- Käab, A., Wessels, R., Haeberli, W., Huggel, C., Kargel, J., Khalsa, S.J.S., 2003a. Rapid ASTER imaging facilitates timely assessment of glacier hazards and disasters. *EOS Transactions, American Geophysical Union* 84 (13), 117–121.
- Käab, A., Kaufmann, V., Ladstädter, R., Eiken, T., 2003b. Rock glacier dynamics: implications from high-resolution measurements of surface velocity fields. Eighth International Conference on Permafrost, vol. 1. Balkema, pp. 501–506.
- Käab, A., Huggel, C., Barbero, S., Chiarle, M., Cordola, M., Epifani, F., Haeberli, W., Mortara, G., Semino, P., Tamburini, A., Viazzo, G., 2004. Glacier hazards at Belvedere Glacier and the Monte Rosa east face, Italian Alps: processes and mitigation. *Interpraevent* 1, 67–78.
- Käab, A., Reynolds, J.M., Haeberli, W., 2005a. Glacier and permafrost hazards in high mountains. In: Huber, U.M., Bugmann, H.K.M., Reasoner, M.A. (Eds.), *Global Change and Mountain Regions (A State of Knowledge Overview)*. Advances in Global Change Research. Springer, Dordrecht, pp. 225–234.
- Käab, A., Huggel, C., Fischer, L., Guex, S., Paul, F., Roer, I., Salzmann, N., Schlaefli, S., Schmutz, K., Schneider, D., Strozzi, T., Weidmann, W., 2005b. Remote sensing of glacier- and permafrost-related hazards in high mountains: an overview. *Natural Hazards and Earth System Sciences* 5, 527–554.
- Käab, A., Frauenfelder, R., Roer, I., 2007. On the reaction of rockglacier creep to surface temperature variations. *Global and Planetary Change* 56, 172–187.
- Kane, W.F.B., Anderson, T.J., Perez, N.O., Hernan, 1996. Remote monitoring of unstable slopes using time domain reflectometry. Proceedings, 11th Thematic Conference and Workshops on Applied Geologic Remote Sensing, p. 431.
- Karlén, W., 1988. Scandinavian glacial climatic fluctuations during the Holocene. *Quaternary Science Reviews* 7, 199–209.
- Karlén, W., 1998. Climate variations and the enhanced greenhouse effect. *Ambio* 27, 270–274.
- Kasymyskaya, M., Sergueev, D., Romanovskii, N., 2003. Evolution of Alpine permafrost under the impact of climatic fluctuations (the results of numerical modeling). In: Haeberli, W., Brandova, D. (Eds.), 8th International Conference on Permafrost, Extended Abstracts. University of Zurich, Zürich, pp. 73–74.
- Kaufmann, V., Ladstädter, R., 2002. Spatio-temporal analysis of the dynamic behaviour of the Hochebenkar rock glaciers (Oetztal Alps, Austria) by means of digital photogrammetric methods. *Grazer Schriften der Geographie und Raumforschung* 37, 119–140.
- Kaufmann, V., Ladstädter, R., 2003. Quantitative analysis of rock glacier creep by means of digital photogrammetry using multi-temporal aerial photographs: two case studies in the Austrian Alps. In: Phillips, M., Springman, S., Arenson, L. (Eds.), 8th International Conference on Permafrost. Proceedings, vol. 1. Swets & Zeitlinger, Lisse, pp. 525–530.
- Keller, F., 1992. Automated mapping of mountain permafrost using the program PERMAKART within the geographical information system ARC/INFO. *Permafrost and Periglacial Processes* 3 (2), 133–138.
- Keller, F., Gubler, H.U., 1993. Interaction between snow cover and high mountain permafrost at Murtèl/Corvatsch, Swiss Alps. The 6th International Conference on Permafrost, Beijing, China, pp. 332–337.
- Keller, F., Haeberli, W., Rickenmann, D., Rigendinger, H., 2002. Dämme gegen Naturgefahren: Bau von Schutzdämmen gegen Rufen und Lawinen in Pontresina. *TEC* 21 (17), 13–17.

- Kenyi, L.W., Kaufmann, V., 2003. Measuring rock glacier surface deformation using SAR interferometry. Eighth International Conference on Permafrost, vol. 1. Balkema, pp. 537–541.
- Kern-Luetsch, M., Harris, C., Cleall, P., Li, Y., Thomas, H., 2008. Scaled centrifuge modelling of solifluction in permafrost and seasonally frozen soils. In: Kane, D.L., Hinkel, K.M. (Eds.), Proceedings Ninth International Conference on Permafrost, June 29–July 3, Fairbanks Alaska, vol. 1. Institute of Northern Engineering, University of Alaska Fairbanks, pp. 919–924.
- King, L., 1986. Zonation and ecology of high mountain permafrost in Scandinavia. *Geografisk Annaler* 68 A, 131–139.
- King, M.S., Zimmerman, R.W., Corwin, R.F., 1988. Seismic and electrical properties of unconsolidated permafrost. *Geophysical Prospecting* 36, 349–364.
- King, L., Gorbunov, A.P., Evin, M., 1992. Prospecting and mapping of mountain permafrost and associated phenomena. *Permafrost and Periglacial Processes* 3 (2), 73–81.
- King, L., Åkerman, J., 1993. Mountain permafrost in Europe. Proceedings of the Sixth International Conference on Permafrost, July 5–9, Beijing, vol. 2. South China University of Technology Press, pp. 1022–1027.
- King, L., Kalisch, A., 1998. Permafrost distribution and implications for construction in the Zermatt area, Swiss Alps. In: Lewkowicz, A.G., Allard, M. (Eds.), 7th International Conference on Permafrost. Proceedings. Collection Nordica. Centre d'Études Nordiques, Université Laval, Yellowknife, Canada, pp. 569–574.
- Kneisel, C., 2003. Permafrost in recently deglaciated forefields – measurements and observations in the eastern Swiss Alps and northern Sweden. *Zeitschrift für Geomorphologie* 47 (3), 289–305.
- Kneisel, C., 2004. New insights into mountain permafrost occurrence and characteristics in glacier forefields at high altitude through the application of 2D resistivity imaging. *Permafrost and Periglacial Processes* 15, 221–227.
- Kneisel, C., Haerberli, W., Baumhauer, R., 2000a. Comparison of spatial modelling and field evidence of glacier/permafrost relations in an Alpine permafrost environment. *Annals of Glaciology* 31, 269–274.
- Kneisel, C., Hauck, C., Vonder Mühll, D., 2000b. Permafrost below the timberline confirmed and characterized by geoelectrical resistivity measurements, Bever Valley, eastern Swiss Alps. *Permafrost and Periglacial Processes* 11, 295–304.
- Kneisel, C., Rothenbühler, C., Keller, F., Haerberli, W., 2007. Hazard assessment of potential periglacial debris flows based on GIS-based spatial modelling and geophysical field surveys: a case study in the Swiss Alps. *Permafrost and Periglacial Processes* 18, 259–268. doi:10.1002/ppp.593.
- Kneisel, C., Hauck, C., Fortier, R., Moorman, B., 2008. Advances in geophysical methods of permafrost investigations. *Permafrost and Periglacial Processes* 19, 157–178. doi:10.1002/ppp.616.
- Koç, N., Jansen, E., Haffidason, H., 1993. Paleocceanographic reconstructions of surface ocean conditions in the Greenland, Iceland and Norwegian seas through the last 14 ka based on diatoms. *Quaternary Science Reviews* 12, 115–140.
- Koç, N., Jansen, J., 1994. Response of the high-latitude Northern Hemisphere to orbital climate forcing: evidence from the Nordic Seas. *Geology* 22, 523–526.
- Kohl, T., 1999. Transient thermal effects of complex topographies. *Tectonophysics* 306, 311–324.
- Korhola, A., Vasko, K., Toivonen, H.T.T., Olander, H., 2002. Holocene temperature changes in northern Fennoscandia reconstructed from chironomids using Bayesian modelling. *Quaternary Science Reviews* 21 (16–17), 1841–1860.
- Kotlyakov, V.M., Rototava, O.V., Nosenko, G.A., 2004. The September 2002 Kolka glacier catastrophe in North Ossetia, Russian Federation. evidence and analysis. *Mountain Research and Development* 24 (1), 78–83.
- Krautblatter, M., Hauck, C., 2007. Electrical resistivity tomography monitoring of permafrost in solid rockwalls. *Journal of Geophysical Research* 112, F02S20. doi:10.1029/2006JF000546.
- Kukkonen, I.T., Safanda, J., 2001. Numerical modelling of permafrost in bedrock in northern Fennoscandia during the Holocene. *Global and Planetary Change* 29, 259–274.
- Kultti, S., Mikkola, K., Virtanen, T., Timonen, M., Eronen, M., 2006. Past changes in the Scots pine forest line and climate in Finnish Lapland: a study based on megafossils, lake sediments, and GIS-based vegetation and climate data. *Holocene* 16 (3), 381–391.
- Lachenbruch, A.H., Marshall, B.V., 1986. Changing climate: geothermal evidence from permafrost in the Alaskan Arctic. *Science* 234, 689–696.
- Ladanyi, B.M., 1993. Determination of creep properties of frozen soils by means of the borehole stress relaxation test. *Canadian Geotechnical Journal* 30, 170.
- Lambiel, C., Reynard, E., 2001. Regional modelling of present, past and future potential distribution of discontinuous permafrost based on a rock glacier inventory in the Bagnes–Hérémence area (Western Swiss Alps). *Norwegian Journal of Geography* 55 (4), 219–223.
- Lambiel, C., Delaloye, R., 2004. Contribution of real-time kinematic GPS in the study of creeping mountain permafrost: examples from the Western Swiss Alps. *Permafrost and Periglacial Processes* 15 (3), 229–241.
- Larsson, S., 1982. Geomorphologica effects on the slopes of Longyear Valley, Spitsbergen, after a heavy rainstorm in July 1972. *Geografiska Annaler* 64A, 105–125.
- Lauritzen, S.-E., Lundberg, J., 1999. Calibration of the speleothem delta function: an absolute temperature record for the Holocene in northern Norway. *The Holocene* 9 (6), 659–669.
- Leber, D., Häusler, H., Morawetz, R., Schreilechner, M., Wangda, D., 1999. GLOF risk assessment in the Northwestern Bhutanese Himalayas based on remote sensing sustained geo-hazard mapping and engineering geophysical methods. *Journal of Nepal Geological Society* 20, 141–142.
- Lehmann, F., Green, A.G., 2000. Topographic migration of georadar data: implications for acquisition and processing. *Geophysics* 65, 836–848.
- Lehning, M., Bartelt, P., Brown, B., Russi, T., Stöckli, U., Zimmerli, M., 1999. SNOWPACK model calculation for avalanche warning based upon a new network of weather and snow stations. *Cold Regions Science and Technology* 30 (1–3), 145–157.
- Lehning, M., Bartelt, P., Brown, B., Fierz, C., Satyawali, P., 2002a. A physical SNOWPACK model for Swiss avalanche warning. Part II. Snow microstructure. *Cold Regions Science and Technology* 35 (3), 147–167.
- Lehning, M., Bartelt, P., Brown, B., Fierz, C., 2002b. A physical SNOWPACK model for Swiss avalanche warning. Part III: meteorological forcing, thin layer formation and evaluation. *Cold Regions Science and Technology* 35 (3), 169–184.
- Lehning, M., Völkisch, I., Gustafsson, D., Nguyen, T.A., Stähli, M., Zappa, M., 2006. ALPINE3D: a detailed model of mountain surface processes and its application to snow hydrology. *Hydrological Processes* 20, 2111–2128.
- Lehning, M., Löwe, H., Ryser, M., Raderschall, N., 2008. Inhomogeneous precipitation distribution and snow transport in steep terrain. *Water Resources Research*. doi:10.1029/2007WR006545.
- Lewkowicz, A.G., 1992. A solifluction meter for permafrost sites. *Permafrost and Periglacial Processes* 3, 11–18.
- Lewkowicz, A.G., 2001. Temperature regime of a small sandstone tor, latitude 80°N, Ellesmere Island, Nunavut, Canada. *Permafrost and Periglacial Processes* 12, 351–366.
- Lewkowicz, A.G., Clark, S., 1998. Late summer solifluction and active-layer depths, Fosheim Peninsula, Ellesmere Island, Canada. In: Lewkowicz, A.G., Allard, M. (Eds.), Proceedings of the 6th International Conference on Permafrost. Centre d'études nordiques, Université Laval, pp. 641–666.
- Lewkowicz, A.G., Ednie, M., 2004. Probability mapping of mountain permafrost using the BTS method, Wolf Creek, Yukon Territory, Canada. *Permafrost and Periglacial Processes* 15 (1), 67–80.
- Lewkowicz, A.G., Harris, C., 2005a. Frequency and magnitude of active-layer detachment failures in discontinuous and continuous permafrost, northern Canada. *Permafrost and Periglacial Processes* 16 (1), 115–130.
- Lewkowicz, A.G., Harris, C., 2005b. Morphology and geotechnique of active-layer detachment failures in discontinuous and continuous permafrost, northern Canada. *Geomorphology* 69, 275–297.
- Lewkowicz, A.G., Bonnaventure, P.P., 2008. Interchangeability of mountain permafrost probability models, northwest Canada. *Permafrost and Periglacial Processes* 19, 49–62. doi:10.1002/ppp.612.
- Li, X., Cheng, G., Chen, X., 1998. Response of permafrost to global change on the Qinghai–Xizang plateau – a GIS-aided model. In: Lewkowicz, A.G., Allard, M. (Eds.), 7th International Conference on Permafrost. Proceedings. Collection Nordica. Centre d'Études Nordiques, Université Laval, Yellowknife, Canada, pp. 657–661.
- Ling, F., Zhang, T., 2004. A numerical Q81 model for surface energy balance and thermal regime of the active layer and permafrost containing unfrozen water. *Cold Regions Science and Technology* 38, 1–15. doi:10.1016/S0165-232X(03)00057-0.
- Lubinski, D.J., Forman, S.L., Miller, G.H., 1999. Holocene glacier and climate fluctuations on Franz Josef Land, Arctic Russia, 80°N. *Quaternary Science Reviews* 18, 85–108.
- Luetsch, M.A., 2005. A model and field analysis of the interaction between snow cover and Alpine permafrost. *Schriftenreihe Physische Geographie. Glaziologie und Geomorphologie*, vol. 47, 204pp.
- Luetsch, M.A., Bartelt, P., Stoekli, V., Lehning, M., Haerberli, W., 2003. Numerical simulation of the interaction processes between snow cover and alpine permafrost. In: Phillips, M., Springman, S., Arenson, L. (Eds.), 8th International Conference on Permafrost. Proceedings. Swets & Zeitlinger, Lisse, Zürich, pp. 697–702.
- Luetsch, M.A., Stoekli, V., Lehning, M., Haerberli, W., 2004. Temperature studies in two boreholes at Fluella Pass, Eastern Swiss Alps: the effect of snow redistribution on permafrost distribution patterns in high mountain areas. *Permafrost and Periglacial Processes* 15, 283–297.
- Luetsch, M.A., Haerberli, W., 2005. Permafrost evolution in the Swiss Alps in a changing climate and the role of the snow cover. *Norwegian Journal of Geography* 59 (2), 77–83.
- Lugon, R., Delaloye, R., 2001. Modelling alpine permafrost distribution. Val de Rechy, Valais Alps (Switzerland). *Norsk Geografisk Tidsskrift* 55 (4), 224–229.
- Lunardini, V.J., 1996. Climatic warming and the degradation of warm permafrost. *Permafrost and Periglacial Processes* 7, 311–320.
- Luoto, M., Seppälä, M., 2002a. Characteristics of earth hummocks (pounus) with and without permafrost in Finnish Lapland. *Geografiska Annaler* 84A (2), 127–136.
- Luoto, M., Seppälä, M., 2002b. Modelling the distribution of palsas in Finnish Lapland with logistic regression and GIS. *Permafrost and Periglacial Processes* 13, 17–28.
- Luoto, M., Seppälä, M., 2003. Thermokarst ponds indicating former distribution of palsas in Finnish Lapland. *Permafrost and Periglacial Processes* 14, 19–27.
- Luoto, M., Heikkilä, R.K., Carter, T.R., 2004a. Loss of palsa mires in Europe and biological consequences. *Environmental Conservation* 31, 30–37.
- Luoto, M., Fronzek, S., Zuidhoff, F.S., 2004b. Spatial modelling of palsa mires in relation to climate in northern Europe. *Earth Surface Processes and Landforms* 29, 1373–1387.
- Luterbacher, J., Dietrich, D., Xoplaki, E., Grosjean, M., Wanner, H., 2004. European seasonal and annual temperature variability, trends, and extremes since 1500. *Science* 303, 1499–1503.
- Ma, W., Shi, C.-H., Wu, Q.-B., Zhang, L.-X., Wu, Z.-J., 2006. Monitoring study on technology of the cooling roadbed in permafrost region of Qinghai–Tibet plateau. *Cold Regions Science and Technology* 44 (1), 1–11.
- Mackay, J.R., 1972. The world of underground ice. *Annals, Association of American Geographers* 62, 1–22.
- Mackay, J.R., 1981. Active layer slope movement in a continuous permafrost environment, Garry Island, Northwest Territories, Canada. *Canadian Journal of Earth Sciences* 18, 1666–1680.
- Mackay, J.R., 1983. Downward water movement into frozen ground, western Arctic coast, Canada. *Canadian Journal of Earth Sciences* 20, 120–134.
- Mackay, J.R., 1986. The first 7 years (1978–1985) of ice wedge growth, Illisarvik experimental drained lake site, western Arctic coast. *Canadian Journal of Earth Sciences* 23, 1782–1795.
- Mackay, J.R., 1993. Air temperature, snow cover, creep of frozen ground, and the time of ice-wedge cracking, western Arctic coast. *Canadian Journal of Earth Sciences* 30, 1720–1729.

- Mackay, J.R., 1999. Cold-climate shattering (1974–1993) of 200 glacial erratics on the exposed bottom of a recently drained arctic lake, Western Arctic Coast, Canada. *Permafrost and Periglacial Processes* 10, 125–136.
- Mackay, J.R., 2000. Thermally induced movements in ice-wedge polygons, western arctic coast: a long-term study. *Geographie physique et Quaternaire* 54, 41–68.
- Maisch, M., Haeblerli, W., Frauenfelder, R., Käab, A., 2003. Lateglacial and Holocene evolution of glaciers and permafrost in the Val Muragl, Upper Engadine, Swiss Alps. In: Phillips, M., Springman, S.M., Arenson, L.U. (Eds.), *Proceedings of the 8th International Conference on Permafrost*, vol. 2. Swets & Zeitlinger, Lisse, Zürich, pp. 717–722.
- Mann, M.E., Bradley, R.S., Hughes, M.K., 1999. Northern Hemisphere temperatures during the last millennium: inferences, uncertainties and limitations. *Geophysical Research Letters* 26, 759–762.
- Marchenko, S.S., 2001. A model of permafrost formation and occurrences in the intracontinental mountains. *Norwegian Journal of Geography* 55 (4), 230–234.
- Marescot, L., Loke, M.H., Chapellier, D., Delaloye, R., Lambiel, C., Reynard, E., 2003. Assessing reliability of 2D resistivity imaging in permafrost and rock glacier studies using the depth of investigation index method. *Near Surface Geophysics* 1 (2), 57–67.
- Matsuoka, N., 1994. Diurnal freeze-thaw depth in rockwalls: field measurements and theoretical considerations. *Earth Surface Processes and Landforms* 19, 423–435.
- Matsuoka, N., 2001a. Microgelivation versus macrogelivation: towards bridging the gap between laboratory and field frost weathering. *Permafrost and Periglacial Processes* 12, 299–313.
- Matsuoka, N., 2001b. Solifluction rates, processes and landforms: a global review. *Earth-Science Reviews* 55, 107–133.
- Matsuoka, N., 2005. Temporal and spatial variations in periglacial soil movements on alpine crest slopes. *Earth Surface Processes and Landforms* 30, 41–58.
- Matsuoka, N., 2008. Frost weathering and rockwall erosion in the eastern Swiss Alps: long-term (1994–2006) observations. *Geomorphology* 99, 353–368.
- Matsuoka, N., Hirakawa, K., 2000. Solifluction resulting from one-sided and two-sided freezing: field data from Svalbard. *Polar Geoscience* 13, 187–201.
- Matsuoka, N., Christiansen, H.H., 2008. Ice wedge dynamics in Svalbard: high resolution monitoring by multiple techniques. In: Kane, D.L., Hinkel, K.M. (Eds.), *Proceedings Ninth International Conference on Permafrost*, Fairbanks Alaska, 29 June–3 July 2008. Institute of Northern Engineering, University of Alaska Fairbanks, pp. 1149–1154.
- Matsuoka, N., Murton, J., 2008. Frost weathering: recent advances and future directions. *Permafrost and Periglacial Processes* 19, 195–210.
- Matsuoka, N., Sakai, H., 1999. Rockfall activity from an alpine cliff during thawing periods. *Geomorphology* 28, 309–328.
- Matsuoka, N., Hirakawa, K., Watanabe, T., Moriwaki, K., 1997. Monitoring of periglacial slope processes in the Swiss Alps: the first two years of frost shattering, heave and creep. *Permafrost and Periglacial Processes* 8, 155–177.
- Matsuoka, N., Hirakawa, K., Watanabe, T., Haeblerli, W., Keller, F., 1998. The role of diurnal, annual and millennial freeze-thaw cycles in controlling alpine slope stability. In: Lewkowicz, A.G., Allard, M. (Eds.), *Proceedings of the Seventh International Conference on Permafrost*. Centre d'études nordiques, Université Laval, pp. 711–718.
- Matsuoka, N., Ikeda, A., Hirakawa, K., Watanabe, T., 2003. Contemporary periglacial processes in the Swiss Alps: seasonal, inter-annual and long-term variations. In: Phillips, M. (Ed.), *Proceedings of the Eighth International Conference on Permafrost*, vol. 2. Balkema, Lisse, pp. 735–740.
- Matthews, J.A., 1976. 'Little Ice Age' paleotemperatures from high altitude tree growth in S. Norway. *Nature* 264, 243–245.
- Matthews, J.A., Dahl, S.-O., Berrisford, M.S., Nesje, A., 1997. Cyclic development and thermokarstic degradation of palsas in the mid-alpine zone at Leipullan, Dovrefjell, southern Norway. *Permafrost and Periglacial Processes* 8, 107–122.
- Matthews, J.A., Berrisford, M.S., Dresser, Q.P., Nesje, A., Dahl, S.O., Bjune, A.E., Bakke, J., John, H., Birks, B., Lie, Ø., Dumayne-Peaty, L., Barnett, C., 2005. Holocene glacier history of Bjornbreen and climatic reconstruction in central Jotunheimen, Norway, based on proximal glaciofluvial stream-bank mires. *Quaternary Science Reviews* 24, 67–90.
- Maurer, H., Hauck, C., 2007. Geophysical imaging of alpine rock glaciers. *Journal of Glaciology* 53 (180), 110–120.
- McGinnis, L.D., Nakao, K., Clark, C.C., 1973. Geophysical identification of frozen and unfrozen ground, Antarctica. *Proceedings 2nd International Conference on Permafrost*. Yakutsk, Russia, pp. 136–146.
- McKenna, J.K., Biggar, K.W., 1998. The rehabilitation of a passive-ventilated slab on grade foundation using horizontal thermosyphons. *Canadian Geotechnical Journal* 35, 684–691.
- McNeill, J.D., 1980. Electromagnetic terrain conductivity measurements at low induction numbers.- Technical Note, TN-6. Geonics Ltd.
- Meincke, J., 2002. Climate dynamics of the North Atlantic and NW Europe: an observation-based overview. In: Wefer, G., Berger, W., Behre, K.-E., Jansen, E. (Eds.), *Climate development and history of the North Atlantic realm*. Springer-Verlag, Berlin, Heidelberg, pp. 25–40.
- Mellor, M., 1977. Engineering properties of snow. *Journal of Glaciology* 19 (81), 15–66.
- Mittaz, C., Hoelzle, M., Haeblerli, W., 2000. First results and interpretation of energy-flux measurements of Alpine permafrost. *Annals of Glaciology* 31, 275–280.
- Mittaz, C., Imhof, M., Hoelzle, M., Haeblerli, W., 2002. Snowmelt evolution mapping using an energy balance approach over an alpine terrain. *Arctic, Antarctic and Alpine Research* 34 (3), 264–281.
- Moberg, A., Jones, P.D., 2005. Trends in indices for extremes in daily temperature and precipitation in central and western Europe, 1901–99. *International Journal of Climatology* 25, 1149–1171.
- Moberg, A., Sonechkin, D.M., Holmgren, K., Datsenko, N.M., Karlén, W., 2005. Highly variable Northern Hemisphere temperatures reconstructed from low- and high-resolution proxy data. *Nature* 433, 613–617.
- Moorman, B.J., Robinson, S.D., Burgess, M.M., 2003. Imaging periglacial conditions with ground-penetrating radar. *Permafrost and Periglacial Processes* 14, 319–329.
- Morgenstern, N.R., Nixon, J.F., 1971. One-dimensional consolidation of thawing soils. *Canadian Geotechnical Journal* 8, 558–565.
- Morris, S.E., 1981. Topoclimatic factors and the development of rock glacier facies, Sangre de Cristo Mountains, Southern Colorado. *Arctic and Alpine Research* 13 (3), 329–338.
- Moser, K., 1999. Ankermörtel im Permafrost. EMPA (Swiss Federal Laboratories for Materials Testing and Research). Technical Report no. 200229.
- Munroe, J.S., Doolittle, J.A., Kanevsky, M.Z., Hinkel, K.M., Nelson, F.E., Jones, B.M., Shur, Y., Kimble, J.M., 2007. Application of ground-penetrating radar imagery for three-dimensional visualization of near-surface structures in ice-rich permafrost, Barrow, Alaska. *Permafrost and Periglacial Processes*, 18 (4), 309–321.
- Murton, J.B., Kolstrup, E., 2003. Ice-wedge casts as indicators of palaeotemperatures: precise proxy or wishful thinking? *Progress in Physical Geography* 27, 155–170.
- Murton, J.B., Coutard, J.-P., Ozouf, J.-C., Lautridou, J.-P., Robinson, D.A., Williams, R.B.G., Guillemet, G., Simmons, P., 2000. Experimental design for a pilot study on bedrock weathering near the permafrost table. *Earth Surface Processes and Landforms* 25, 1281–1294.
- Murton, J.B., Coutard, J.P., Lautridou, J.P., Ozouf, J.C., Robinson, D.A., Williams, R.B.G., 2001. Physical modelling of bedrock brecciation by ice segregation in permafrost. *Permafrost and Periglacial Processes* 12, 255–266.
- Murton, J.B., Peterson, R., Ozouf, J.-C., 2006. Bedrock fracture by ice segregation in cold regions. *Science* 314, 1127–1129. doi:10.1126/science.1132127.
- Musil, M., Maurer, H., Green, A.G., Horstmeyer, H., Nitsche, F., Vonder Mühl, D., Springman, S., 2002. Shallow seismic surveying of an Alpine rock glacier. *Geophysics* 67 (6), 1701–1710.
- Musil, M., Maurer, H., Hollinger, K., Green, A.G., 2006. Internal structure of an alpine rock glacier based on crosshole georadar traveltimes and amplitudes. *Geophysical Prospecting* 54 (3), 273–285.
- Mustafa, O., Gude, M., Hoelzle, M., 2003. Modeling permafrost distribution in the northern Alps using global radiation. In: Haeblerli, W., Brandova, D. (Eds.), *8th International Conference on Permafrost*, Extended Abstracts. University of Zurich, Zürich, pp. 111–112.
- Nater, P., Arenson, L.U., Springman, S.M., 2008. Choosing geotechnical parameters for slope stability assessments in alpine permafrost soils. In: Kane, D.L., Hinkel, K.M. (Eds.), *Ninth International Conference on Permafrost*, University of Alaska Fairbanks, 29 June–3 July 2008. *Proceedings*, vol. 2. Institute of Northern Engineering, University of Alaska Fairbanks, pp. 1261–1266.
- Nelson, F.E., Anisimov, O.A., Shiklomanov, N.I., 2001. Subsidence risk from thawing permafrost – the treat to man-made structures across regions in the far north can be monitored. *Nature* 410, 889–890.
- Nelson, F.E., Anisimov, O.A., Shiklomanov, N.I., 2002. Climate change and hazard zonation in the Circum-Arctic permafrost regions. *Natural Hazards* 26, 203–225.
- Nesje, A., 1992. Younger Dryas and Holocene glacier fluctuations and equilibrium-line altitude variations in the Jostedalbreen region, western Norway. *Climate Dynamics* 63 (3–4), 221–227.
- Nesje, A., Dahl, O.S., Andersson, C., Matthews, J.A., 2000. The lacustrine sedimentary sequence in Sygneskardvatnet, western Norway: a continuous, high-resolution record of the Jostedalbreen ice cap during the Holocene. *Quaternary Science Reviews* 19, 1047–1065.
- Nesje, A., Kvamme, M., 1991. Holocene glacier and climate variations in western Norway: evidence for early Holocene glacier demise and multiple Neoglacial events. *Geology* 19, 610–612.
- Nesje, A., Matthews, J.A., Olaf Dahl, S., Berrisford, M.S., Andersson, C., 2001. Holocene glacier fluctuations of Flatebreen and winter precipitation changes in the Jostedalbreen region, western Norway, based on glaciolacustrine sediment records. *The Holocene* 11 (3), 267–280.
- Noetzli, J., Hoelzle, M., Haeblerli, W., 2003. Mountain permafrost and recent Alpine rock-fall events: a GIS-based approach to determine critical factors. In: Phillips, M., Springman, S.M., Arenson, L.U. (Eds.), *Proceedings of the 8th International Conference on Permafrost*, vol. 2. Swets & Zeitlinger, Lisse, Zürich, pp. 827–832.
- Noetzli, J., Huggel, C., Hoelzle, M., Haeblerli, W., 2006. GIS-based modelling of rock/ice avalanches from Alpine permafrost areas. *Computational Geosciences* 10, 161–178.
- Noetzli, J., Gruber, S., Kohl, T., Salzmann, N., Haeblerli, W., 2007. Three-dimensional distribution and evolution of permafrost temperatures in idealized high-mountain topography. *Journal of Geophysical Research* 112, F02S13. doi:10.1029/2006JF000545.
- Noetzli, J., Hilbich, C., Hauck, C., Hoelzle, M., Gruber, S., 2008. Comparison of simulated 2D temperature profiles with time-lapse electrical resistivity data at the Schilthorn crest, Switzerland. In: Kane, D.L., Hinkel, K.M. (Eds.), *Ninth International Conference on Permafrost*, University of Alaska Fairbanks, 29 June–3 July 2008. *Proceedings*, vol. 2. Institute of Northern Engineering, University of Alaska Fairbanks, pp. 1293–1298.
- Nyenhuis, M., Hoelzle, M., Dikau, R., 2005. Rock glacier mapping and permafrost distribution modelling in the Turtmanntal, Valais, Switzerland. *Zeitschrift für Geomorphologie* 49 (3), 275–292.
- O'Connor, K.M., Dowding, C.H., 1999. Geomeasurements by pulsing TDR cables and probes. *CRC Press*. 402 pp.
- Ødegård, R.S., Hoelzle, M., Johansen, K.V., Sollid, J.L., 1996. Permafrost mapping and prospecting in southern Norway. *Norsk geografisk Tidsskrift* 50, 41–54.
- Ødegård, R.S., Isaksen, K., Eiken, T., Sollid, J.L., 2008. MAGST in Mountain Permafrost, Dovrefjell, Southern Norway, 2001–2006. In: Kane, D.L., Hinkel, K.M. (Eds.), *Ninth International Conference on Permafrost*, University of Alaska Fairbanks, 29 June–3 July 2008. *Proceedings*, vol. 2. Institute of Northern Engineering, University of Alaska Fairbanks, pp. 1311–1315.
- Oelke, C., Zhang, T., 2003. Comparing thaw depth measured at CALM field sites with estimates from a medium-resolution hemispheric heat conduction model. In:

- Haeblerli, W., Brandova, D. (Eds.), 8th International Conference on Permafrost, Extended Abstracts. University of Zurich, Zürich, pp. 117–118.
- Oksanen, P.O., 2005. Development of palsa mires on the northern European continent in relation to Holocene climatic and environmental changes. *Acta Universitatis Ouluensis A446*, 50 p + 6 appending papers.
- Olyphant, G.A., 1987. Rock glacier response to abrupt changes in talus production. In: Giardino, J.R., Shroder, J.F., Vitek, J.D. (Eds.), *Rock Glaciers*. Allen & Unwin, pp. 55–64.
- Osterkamp, T.E., Romanovsky, V.E., 1999. Evidence for warming and thawing of discontinuous permafrost in Alaska. *Permafrost and Periglacial Processes* 10, 17–37.
- Osterkamp, T.E., 2008. Thermal state of permafrost in Alaska during the fourth quarter of the twentieth century. In: Kane, D.L., Hinkel, K.M. (Eds.), *Ninth International Conference on Permafrost*, University of Alaska Fairbanks, 29 June–3 July 2008. Proceedings, vol. 2. Institute of Northern Engineering, University of Alaska Fairbanks, pp. 1333–1338.
- Otto, J.C., Sass, O., 2006. Comparing geophysical methods for talus slope investigations in the Turtmann valley (Swiss Alps). *Geomorphology* 76 (3–4), 257–272.
- Pandit, B.I., King, M.S., 1978. Influence of pore fluid salinity on seismic and electrical properties of rocks at permafrost temperatures. *Proc. 3rd Int. Conf. on Permafrost*, vol. 1. Edmonton, Canada, pp. 553–566.
- Pant, S.R., Reynolds, J.M., 2000. Application of electrical imaging techniques for the investigation of natural dams: an example from Thulagi Glacier Lake, Nepal. *Journal of Nepal Geological Society* 22, 211–218.
- Paterson, W.S.B., 1994. *The Physics of Glaciers*. Pergamon Press Ltd, 380 pp.
- Pearson, C., Murphy, J., Halleck, P., Hermes, R., Mathews, M., 1983. Sonic and resistivity measurements on Berea sandstone containing tetrahydrofuran hydrates: a possible analog to natural gas hydrate deposits. *Proceedings 4th International Conference on Permafrost*, Fairbanks, Alaska, pp. 973–978.
- PERD, 1998. Climate change impacts on permafrost engineering design. Panel on Energy Research and Development, Environment Canada, Ottawa ON, Canada. 42p.
- Permafrost Subcommittee, National Research Council of Canada, 1988. *Glossary of Permafrost and Related Ground-ice Terms*, National Research Council of Canada Technical Memorandum No. 142. 156pp.
- Petak, W.J., Atkisson, A.A., 1982. Natural hazard risk assessment and public policy: anticipating the unexpected. Springer, New York.
- Péwé, T.L., 1966. Ice wedges in Alaska – classification, distribution and climatic significance. *Proceedings, 1st International Conference on Permafrost*, vol. 1287. National Academy of Science: National Research Council of Canada, Publication, pp. 76–81.
- Phillips, M., 2006. Avalanche defence strategies and monitoring of two sites in mountain permafrost terrain, Pontresina, Eastern Swiss Alps. *Natural Hazards* 39, 353–379.
- Phillips, M., Bartelt, P., Christen, M., 2000. Anchor temperatures of avalanche defence snow-supporting structures in frozen ground. In: Hjorth-Hansen, E., Holand, I., Løset, S., Norem, H. (Eds.), *Proceedings of the Fourth International Conference on Snow Engineering*, Trondheim, Norway, 19–21 June 2000. Balkema, pp. 245–250.
- Phillips, M., Margreth, S., Ammann, W.J., 2003a. Creep of snow-supporting structures in alpine permafrost. In: Phillips, Springman, Arenson (Eds.), *Proceedings of the Eighth International Conference on Permafrost*, 21–25 July, Zurich. A.A. Balkema, Zurich, Switzerland, pp. 891–896.
- Phillips, M., Margreth, S., Stoffel, L., Ammann, W.J., 2003b. Development of Swiss Guidelines for the construction of snow-supporting structures in creeping Alpine permafrost terrain. In: Culligan, P.J., Einstein, H.H., Whittle, A.J. (Eds.), *Proceedings of the 12th Panamerican Conference on Soil Mechanics and Geotechnical Engineering – Soil and Rock America 2003*, vol. 2. MIT, Verlag Glückauf, pp. 2603–2610.
- Phillips, M., Ladner, F., Müller, M., Sambeth, U., Sorg, J., Teyssie, P., 2007. Monitoring and reconstruction of a chairlift midway station in creeping permafrost terrain, Grächen, Swiss Alps. *Cold Regions Science and Technology* 47 (1), 32–42.
- Polyak, I., 1996. *Computational Statistics in Climatology*. Oxford University Press, New York and Oxford. 358 pp.
- Powers, T.C., Helmuth, R.A., 1953. Theory of volume changes in hardened Portland cement paste during freezing, paper presented at Highway Research Board Proceedings. In: Press, F., Hamilton, R.M. (Eds.), *Mitigating natural disasters*. Science, vol. 284, p. 1927.
- Prick, A., 2003. Frost weathering and rock fall in an arctic environment, Longyearbyen, Svalbard. In: Phillips, M., et al. (Ed.), *Proceedings of the Eighth International Conference on Permafrost*, vol. 2. Balkema, Lisse, pp. 907–912.
- Rapp, A., 1960. Recent development of mountain slopes in Kärvevagge and surroundings, Northern Scandinavia. *Geografiska Annaler* 42A, 65–200.
- Rebetez, M., Lugon, R., Baeriswyl, P.-A., 1997. Climatic change and debris flows in high mountain regions: the case study of the Ritigraben Torrent (Swiss Alps). *Climatic Change* 36, 3–4.
- Rieder, U., Keusen, H.R., Amiguet, J.L., 1980. Geotechnische Probleme beim Bau der Luftseilbahn Trockener Steg–Klein Matterhorn. *Schweizer Ingenieur und Architekt* 18, 428–431.
- Reiersen, L.-O., 2005. Impacts of a warming Arctic. *European Geosciences Union, General Assembly 2005*, Vienna. EGU05-A-07268 (CD-ROM).
- Rempel, A.W., Wettlaufer, J.S., Worster, M.G., 2004. Premelting dynamics in a continuum model of frost heave. *Journal of Fluid Mechanics* 498, 227–244.
- Richardson, S.D., Reynolds, J.M., 2000. Degradation of ice-cored moraine dams: implications for hazard development, debris covered Glaciers. *IAHS Publication* 264, 187–197.
- Riseborough, D.W., 2002. The mean annual temperature at the top of permafrost, the TTOP model, and the effect of unfrozen water. *Permafrost and Periglacial Processes* 13, 137–143.
- Riseborough, D., Shiklamanov, N.I., Etzelmüller, B., Gruber, S., Marchengo, S., 2008. Recent advances in permafrost modeling. *Permafrost and Periglacial Processes* 19 (2), 137–156.
- Rignot, E., Hallet, B., Fountain, A., 2002. Rock glacier surface motion in Beacon Valley, Antarctica, from synthetic-aperture radar interferometry. *Geophysical Research Letters* 29 (12), 1607.
- Rikenmann, D., Zimmermann, M., 1993. The 1987 debris flows in Switzerland: documentation and analysis. *Geomorphology* 8, 175–189.
- Rist, A., Phillips, M., 2005. First results of investigations on hydrothermal processes within the active layer above alpine permafrost in steep terrain. *Norwegian Journal of Geography* 59, 177–183.
- Rixen, C., Haeblerli, W., Stoeckli, V., 2004. Ground temperature under ski pistes with artificial and natural snow. *Arctic, Antarctic and Alpine Research* 36 (4), 419–427.
- Rodwell, M.J., Rowell, D.P., Folland, C.K., 1999. Oceanic forcing of the wintertime North Atlantic Oscillation and European climate. *Nature* 398, 320–323.
- Roer, I., Käbb, A., Dikau, R., 2005. Rockglacier kinematics derived from small-scale aerial photography and digital airborne pushbroom imagery. *Zeitschrift für Geomorphologie* 49 (1), 73–87.
- Roer, I., Haeblerli, W., Avian, M., Kaufmann, V., Delaloye, R., Lambiel, C., Käbb, A., 2008. Observations and considerations on destabilizing active rock glaciers in the European Alps. In: Kane, D.L., Hinkel, K.M. (Eds.), *Ninth International Conference on Permafrost*, vol. 2. Institute of Northern Engineering, University of Alaska Fairbanks, pp. 1505–1510.
- Romanovskii, N.N., 1985. Distribution of recently active ice and soil wedges in the USSR. In: Church, M., Slaymaker, O. (Eds.), *Field and theory; lectures in geocryology*. University of British Columbia Press, Vancouver, pp. 154–165.
- Romanovsky, V.E., Osterkamp, T.E., 1995. Interannual variation of the thermal regime of the active layer and near surface permafrost in northern Alaska. *Permafrost and Periglacial Processes* 6, 313–335.
- Romanovsky, V.E., Osterkamp, T.E., Duxbury, N.S., 1997. An evaluation of three numerical models used in simulations of the active layer and permafrost temperature regime. *Cold Regions Science and Technology* 26, 195–203.
- Romanovsk, V.E., Kholodov, A.L., Marchenko, S.S., Oberman, N.G., Drozdov, D.S., Malkova, G.V., Moskalenko, N.G., Vasiliev, A.A., Sergeev, D.O., Zheleznyak, M.N., 2008. Thermal state and fate of permafrost in Russia: first results of IPY. In: Kane, D.L., Hinkel, K.M. (Eds.), *Ninth International Conference on Permafrost*, University of Alaska Fairbanks, 29 June–3 July 2008. Proceedings, vol. 2. Institute of Northern Engineering, University of Alaska Fairbanks, pp. 1511–1518.
- Rönkkö, M., Seppälä, M., 2003. Surface characteristics affecting active layer formation in palsas, Finnish Lapland. In: Phillips, M., Springman, S.M., Arenson, L.U. (Eds.), *Permafrost: Proceedings of the Eighth International Conference on Permafrost*. Swets and Zeitlinger, Lisse, pp. 995–1000.
- Ross, N., Harris, C., Christiansen, H.H., Brabham, P.J., 2005. Ground-penetrating radar investigations of open system pingos, Adventdalen, Svalbard. *Norwegian Journal of Geography* 59, 129–138.
- Ross, N., Brabham, P.J., Harris, C., Christiansen, H.H., 2007. Internal structure of open system pingos, Adventdalen, Svalbard: the use of resistivity tomography to assess ground-ice conditions. *Journal of Environmental and Engineering Geophysics* 12, 113–126.
- Rott, H., Siegel, A., 1999. Analysis of mass movement in alpine terrain by means of SAR interferometry. *IEEE Geoscience and Remote Sensing Symposium*, pp. 1933–1936. IGARSS'99.
- Ryzhkin, I.A., Petrenko, V.F., 1997. Physical mechanisms responsible for ice adhesion. *Journal of Physical Chemistry B* 101, 6267–6270.
- Salvigsen, O., 2002. Radiocarbon-dated *Mytilus edulis* and *Modiolus modiolus* from northern Svalbard: climatic implications. *Norwegian Journal of Geography* 56, 56–61.
- Salzmann, N., Käbb, A., Huggel, C., Allgöwer, B., Haeblerli, W., 2004. Assessment of the hazard potential of ice avalanches using remote sensing and GIS-modelling. *Norwegian Journal of Geography* 58, 74–84.
- Salzmann, N., Nötzli, J., Hauck, C., Gruber, S., Hoelzle, M., Haeblerli, W., 2007a. Ground surface temperature scenarios in complex high-mountain topography based on regional climate model results. *Journal of Geophysical Research* 112 (No. F2), F02S12. doi:10.1029/2006JF000527.
- Salzmann, N., Frei, C., Vidale, P.-L., Hoelzle, M., 2007b. The application of Regional Climate Model output for the simulation of high-mountain permafrost scenarios. *Global and Planetary Change* 56, 188–202.
- Sass, O., 2005a. Spatial patterns of rockfall intensity in the northern Alps. *Zeitschrift für Geomorphologie* 138, 51–65 N.F., Suppl.-Bd.
- Sass, O., 2005b. Rock moisture measurements: techniques, results, and implications for weathering. *Earth Surface Processes and Landforms* 30, 359–374.
- Schär, C., Vidale, P.L., Luthi, D., Frei, C., Haberli, C., Liniger, M.A., Appenzeller, C., 2004. The role of increasing temperature variability in European summer heatwaves. *Nature* 427, 332–336.
- Scherler, M., 2006. Messung und Modellierung konvektiver Wärmetransportprozesse in der Auftauschicht von Gebirgspermafrost am Beispiel des Schilthorns. *Diploma thesis Geographical Institute Zürich*, University of Zürich, Switzerland.
- Schiermeier, Q., 2003. Alpine thaw breaks ice over permafrost's role. *Nature* 424, 712.
- Schneider, B., Schneider, H., 2001. Zur jährigen Messreihe der kurzfristigen Geschwindigkeitsschwankungen am Blockgletscher im Äusseren Hochebenkar, Ötztal Alps, Tirol. *Zeitschrift für Gletscherkunde und Glazialgeologie*, 37 (1), 1–33.
- Schudel, L., 2003. *Permafrost Monitoring auf dem Schilthorn mit geophysikalischen Methoden und meteorologischen Daten*. Diploma thesis Geographical Institute Zürich, University of Zürich, Switzerland.
- Scott, W., Sellmann, P., Hunter, J., 1990. *Geophysics in the study of permafrost*. In: Ward, S. (Ed.), *Geotechnical and Environmental Geophysics*. Society of Exploration Geophysics Tulsa, pp. 355–384.
- Seierstad, J., Nesje, A., Dahl, S.O., Simonsen, J.R., 2002. Holocene glacier fluctuations of Grovabreen and Holocene snow-avalanche activity reconstructed from lake sediments in Groningstolsvatnet, western Norway. *The Holocene* 12 (2), 211–222.

- Seppä, H., Birks, H.J.B., 2001. July mean temperature and annual precipitation trends during the Holocene in the Fennoscandian tree-line area: pollen-based climate reconstructions. *The Holocene* 11 (5), 527–539.
- Seppä, H., Birks, H.J.B., 2002. Holocene climate reconstructions from the Fennoscandian tree-line area based on pollen data from Toskaljavri. *Quaternary Research* 57, 191–199.
- Seppälä, M., 1983. Seasonal thawing of palsas in Finnish Lapland. *Permafrost: Fourth International Conference. Proceedings. National Academy Press, Washington, D.C.*, pp. 1127–1132.
- Seppälä, M., 1986. The origin of palsas. *Geografiska Annaler* 68A, 141–147.
- Seppälä, M., 1988. Palsas and related forms. In: Clark, M.J. (Ed.), *Advances in Periglacial Geomorphology*. John Wiley & Sons Ltd, Chichester, pp. 247–278.
- Seppälä, M., 1994. Snow depth controls palsa growth. *Permafrost and Periglacial Processes* 5, 283–288.
- Seppälä, M., 1998. New permafrost formed in peat hummocks (pounus), Finnish Lapland. *Permafrost and Periglacial Processes* 9, 367–373.
- Seppälä, M., 2003a. An experimental climate change study of the effect of increasing snow cover on active layer formation of a palsa, Finnish Lapland. In: Phillips, M., Springman, S.M., Arenson, L.U. (Eds.), *Proceedings of the Eighth International Conference on Permafrost*, vol. 2. Swets & Zeitlinger, Lisse, pp. 1013–1016.
- Seppälä, M., 2003b. Surface abrasion of palsas by wind action in Finnish Lapland. *Geomorphology* 52, 141–148.
- Seppälä, M., 2004. Wind as a geomorphic agent in cold climates. Cambridge University Press, Cambridge. 358 pp.
- Seppälä, M., 2005. Dating of palsas. In: Ojala, A.E.K. (Ed.), *Quaternary studies in the northern and Arctic regions of Finland*. Geological Survey of Finland, Special Paper, vol. 40, pp. 79–84.
- Seppälä, M., 1982. An experimental study of the formation of palsas. The Roger J.E. Brown Memorial Volume. *Proceedings Fourth Canadian Permafrost Conference*, Calgary, Alberta. National Research Council of Canada, pp. 36–42.
- Shaopeng, H., Pollack, H.N., Po-Yu, S., 2000. Temperature trends over the past five centuries reconstructed from borehole temperatures. *Nature* 403 (6771), 756–758.
- Schur, Y.I., 1988. The upper horizon of permafrost soils. In: Senneset, K. (Ed.), *Proceedings of the Fifth International Conference on Permafrost*. Tapir, Trondheim, pp. 867–871.
- Shur, Y., Hinkel, K.M., Nelson, F.E., 2005. The transient layer: implications for geocryology and climate-change science. *Permafrost and Periglacial Process* 16, 5–17.
- SLF/BUWAL, 2000. Richtlinien für den Lawinverbau im Anbruchgebiet. EDMZ, Bern.
- Slonosky, V.C., Jones, P.D., Davies, T.D., 2000. Variability of the surface atmospheric circulation over Europe, 1774–1995. *International Journal of Climatology* 20, 1875–1897.
- Slonosky, V.C., Jones, P.D., Davies, T.D., 2001. Atmospheric circulation and surface temperature in Europe from the 18th century to 1995. *International Journal of Climatology* 21, 63–75.
- Smith, L.B., Graham, J.P., Nixon, J.F., Washuta, A.S., 1991. Thermal-analysis of forced-air and thermosiphon cooling systems for the Inuvik Airport expansion. *Canadian Geotechnical Journal* 28 (3), 399–409.
- Sollid, J.L., Sørbel, L., 1998. Palsa bogs as a climatic indicator – examples from Dovrefjell, southern Norway. *Ambio* 27, 287–291.
- Sollid, J.L., Holmlund, P., Isaksen, K., Harris, C., 2000. Deep permafrost boreholes in western Svalbard, northern Sweden and southern Norway. *Norwegian Journal of Geography* 54, 186–191.
- Sollid, J.L., Isaksen, K., Eiken, T., Ødegård, R.S., 2003. The transition zone of mountain permafrost on Dovrefjell, southern Norway. In: Phillips, M., Springman, S.M., Arenson, L.U. (Eds.), *Proceedings Volume 2, Eight International Conference on Permafrost*, Zurich, Switzerland, 21–25 July. Swets & Zeitlinger, Lisse, pp. 1085–1090.
- Springman, S.M., Jommi, C., Teyssie, P., 2003. Instabilities on moraine slopes induced by loss of suction: a case history. *Géotechnique* 53 (1), 3–10.
- Springman, S.M., Arenson, L.U., 2008. Recent advances in permafrost geotechnics. *Proceedings ninth international conference on permafrost*, volume 2, university of Alaska Fairbanks, 29 June–3 July 2008. In: Kane, D.L., Hinkel, K.M. (Eds.), *Institute of Northern Engineering, University of Alaska Fairbanks*, pp. 1685–1694.
- Ståhli, M., Jansson, P.E., Lundin, L.C., 1996. Preferential water flow in a frozen soil – a two domain model approach. *Hydrological Processes* 10, 1305–1316.
- Steiner, W., Keusen, H.-R., Graber, U., 1996. Construction in Rock at 3550 meters elevation (Jungfraujoeh, Switzerland). *Proceedings Eurock*.
- Stocker-Mittaz, C., Hoelzle, M., Haeberli, W., 2002. Permafrost distribution modeling based on energy-balance data: a first step. *Permafrost and Periglacial Processes* 13 (4), 271–282.
- Stoffel, M., Lièvre, I., Conus, D., Griching, M.A., Raetz, H., Gärtner, H.W., Monbaron, M., 2005. 400 years of debris-flow activity and triggering weather conditions: Ritigraben, Valais, Switzerland. *Arctic, Antarctic, and Alpine Research*, vol. 37, No. 3, pp. 387–395.
- Strozzi, T., Käab, A., Frauenfelder, R., 2004. Detecting and quantifying mountain permafrost creep from in-situ, airborne and spaceborne remote sensing methods. *International Journal of Remote Sensing* 25 (15), 2919–2931.
- Sturm, M., Holmgren, J., König, M., Morris, K., 1997. The thermal conductivity of seasonal snow. *Journal of Glaciology* 43, 26–41.
- Svendsen, J.L., Mangerud, J., 1997. Holocene glacial and climatic variations on Spitsbergen, Svalbard. *The Holocene* 7, 45–57.
- Svensson, H., 1969a. Open fissures in a polygonal net on the Norwegian arctic coast. *Biuletyn Peryglacjalny* 19, 389–398.
- Svensson, H., 1969b. Permafrost på Spetsbergen. *Forskning och Framsteg* 8, 20 (in Swedish).
- Svensson, H., 1971. Pingos i yttre delen av Adventdalen. *Norsk Polarinstittut Årbok* 1969, 168–174.
- Svensson, H., 1976. Iskilar som Klimatindikator. *Meddelanden från Lunds Universitets Geografiska Institutionen*, No. 547, *Svensk Geografisk Årsbok* (Swedish Geographical Yearbook), 52, pp. 46–57 (in Swedish).
- Svensson, H., 1982. Valley formation initiated by ice-wedge polygonal nets in terrace surfaces. *Biuletyn Peryglacjalny* 29, 139–142.
- Svensson, H., 1988. Ice-wedge casts and relict polygonal patterns in Scandinavia. *Journal of Quaternary Science* 3, 57–67.
- Svensson, H., 1996. Weather extremes – geomorphology. *Svensk Geografisk Årsbok* (Swedish Geographical Yearbook), pp. 173–179 (In Swedish).
- Tanarro, L.M., et al., 2001. Permafrost distribution modelling in the mountains of the Mediterranean: Corral del Veleta, Sierra Nevada, Spain. *Norwegian Journal of Geography* 55 (4), 253–260.
- Thalparpan, P., 2000. Lawinverbauungen im Permafrost. Eidg. Institut für Schnee- und Lawinenforschung, Davos.
- Thiis, T.K., Jaedicke, C., 2000. Changes in the snowdrift pattern caused by a building extension – investigations through scale modelling and numerical simulations. *Proceedings of the Fourth International Conference on Snow Engineering*, Trondheim, Norway, 19–21 June 2000, 363–375. Eds. E. Hjorth-Hansen, I. Holand, S. Løset, H. Norem. Balkema.
- Tiljander, M., Saarnisto, M., Ojala, A.E.K., Saarinen, T., 2003. A 3000-year palaeoenvironmental record from annually laminated sediment of Lake Korttajarvi, central Finland. *Boreas* 26, 566–577.
- Timofeev, V.M., Rogozinski, A.W., Hunter, J.A., Douma, M., 1994. A new ground resistivity method for engineering and environmental geophysics. *Proceedings of the Symposium on the application of geophysics to engineering and environmental problems*. EEGS, pp. 701–715.
- Timur, A., 1968. Velocity of compressional waves in porous media at permafrost temperatures. *Geophysics* 33 (4), 584–595.
- Tinner, W., Ammann, B., Germann, P., 1996. Treeline fluctuations recorded for 12,500 years by soil profiles, pollen and plant macrofossils in the Central Swiss Alps. *Arctic and Alpine Research* 28 (2), 131–147.
- Ting, J.M., 1983. Tertiary creep model for frozen sands. *Journal of Geotechnical Engineering* 109 (7), 932–945.
- Tveito, O.E., et al., 2001. Nordic climate maps. Report No. 06/01. DNMI, Oslo.
- Varnes, D., 1984. *Landslide hazard zonation: A review of principles and practice*. UNESCO, Paris. 63 pp.
- Völksch, I., 2004. *Untersuchung und Modellierung kleinräumiger Unterschiede im Verhalten von Gebirgspermafrost*. Diploma thesis, Departement Earth Sciences, ETH Zürich, Switzerland.
- Vonder Mühl, D., Haeberli, W., 1990. Thermal characteristics of the permafrost within an active rock glacier (Murtèl/Corvatsch, Grisons, Swiss Alps). *Journal of Glaciology* 36 (123), 151–158.
- Vonder Mühl, D., Stucki, T., Haeberli, W., 1998. Borehole temperatures in Alpine permafrost: a ten years series. In: Lewkowicz, A.G., Allard, M. (Eds.), *Proceedings Seventh International Conference on Permafrost*, Yellowknife, Canada, 23–27 June 1998. Centre d'Etudes Nordiques, Université Laval, pp. 1089–1095. Collection Nordicana 57.
- Vonder Mühl, D., Hauck, C., Lehmann, F., 2000. Verification of geophysical models in Alpine permafrost using borehole information. *Annals of Glaciology* 31, 300–306.
- Vonder Mühl, D., Hauck, C., Gubler, H., McDonald, R., Russill, N., 2001. New geophysical methods of investigating the nature and distribution of mountain permafrost with special reference to radiometry techniques. *Permafrost and Periglacial Process* 12 (1), 27–38.
- Vonder Mühl, D.S., Arenson, L.U., Springman, S.M., 2003. Temperature conditions in two Alpine rock glaciers. In: Phillips, M., Springman, S.M., Arenson, L.U. (Eds.), *Proceedings of the Eighth International Conference on Permafrost*, 21–25 July, Zurich. A.A. Balkema, Zurich, Switzerland, pp. 1195–1200.
- Vonder Mühl, D., Nötzli, J., Makowski, K., Delaloye, R., 2004. Permafrost in Switzerland 2000/2001 and 2001/2002. *Glaciological report (permafrost)*. vol. 2/3. 86 pp.
- Vonder Mühl, D., Noetzi, J., Roer, I., Makowski, K., Delaloye, R., 2007. Permafrost in Switzerland 2000/2003 and 2003/2004. *Glaciological Report (Permafrost) No. 4/5 of the Glaciological Commission (GC) of the Swiss Academy of Sciences (SAS) and the Department of Geography, University of Zurich*, 107pp.
- Vonder Mühl, D., Noetzi, J., Roer, I., 2008. PERMOS – a comprehensive monitoring network of mountain permafrost in the Swiss Alps. 1869–1874. In: Kane, D.L., Hinkel, K.M. (Eds.), *Proceedings Ninth International Conference on Permafrost*, Volume 2, University of Alaska Fairbanks, 29 June–3 July 2008. Institute of Northern Engineering, University of Alaska Fairbanks, pp. 1869–1874.
- Vorren, K.-D., 1972. Stratigraphical investigations of a palsa bog in northern Norway. *Astarte* 5, 39–71.
- Vorren, K.-D., Vorren, B., 1975. The problem of dating a palsa. Two attempts involving pollen diagrams, determination of moss subfossils, and C14-datings. *Astarte* 8, 73–81.
- Voytkovskiy, K.F., Golubev, V.N., 1973. Mechanical properties of ice as a function of the conditions of its formation. Paper presented at 2nd International Conference on Permafrost. *Proceedings, National Academy of Sciences, Washington D.C.*
- Walder, J., Hallet, B., 1985. A theoretical model of the fracture of rock during freezing. *Geological Society of America, Bull.* 96 (3), 336–346.
- Walder, J.S., Hallet, B., 1986. The physical basis of frost weathering: toward a more fundamental and unified perspective. *Arctic and Alpine Research* 18, 27–32.
- Wangenstein, B., Guðmundsson, Á., Eiken, T., Käab, A., Farbrøt, H., Etzelmüller, B., 2006. Surface displacements and surface age estimates for creeping slope landforms in northern and eastern Iceland using digital photogrammetry. *Geomorphology* 80, 59–79.
- Washburn, A.L., 1967. Instrumental observations of mass-wasting in the Mesters Vig district, Northeast Greenland. *Meddelelser om Grønland*. vol. 166. 318 pp.
- Washburn, A.L., 1999. A high arctic frost creep/geifluction slope, 1981–1989: Resolute Bay, Cornwallis Island, Northwest territories, Canada. *Permafrost and Periglacial Processes* 10, 163–186.

- Wegmann, M., 1998. Frostdynamik in hochalpinen Felswänden am Beispiel der Region Jungfrau-Aletsch, PhD thesis, 144 pp, ETH Zürich, Zürich.
- Wegmann, M., Gudmundsson, G.H., 1999. Thermally induced temporal strain variations in rock walls observed at subzero temperatures. In: Hutter, K., Wang, Y., Beer, H. (Eds.), *Advances in Cold-Region Thermal Engineering and Sciences*. Springer, Berlin, pp. 511–518.
- Wegmann, M., Gudmundsson, G.H., Haeberli, W., 1998. Permafrost changes in rock walls and the retreat of alpine glaciers: a thermal modelling approach. *Permafrost and Periglacial Processes* 9 (1), 23–33.
- Wen, Z., Sheng, Y., Ma, W., Qi, J.L., Wu, J.C., 2005. Analysis on effect of permafrost protection by two-phase closed thermosyphon and insulation jointly in permafrost regions. *Cold Regions Science and Technology* 43 (3), 150–163.
- White, S.E., 1987. Differential movement across ridges on Arapaho rock glaciers, Colorado Front Range, US. *Rock glaciers*. Allen and Unwin, London, pp. 145–149.
- Wick, L., Tinner, W., 1997. Vegetation changes and timberline fluctuations in the central alps as indicators of Holocene climatic oscillations. *Arctic and Alpine Research* 29, 445–458.
- Williams, P.J., 1967a. Suction and its effects on unfrozen water of frozen soils. *Publications of the Norwegian Geotechnical Institute* 72, 27–35.
- Williams, P.J., 1967b. Unfrozen water in frozen soils. *Publications of the Norwegian Geotechnical Institute* 72, 37–48.
- Wright, J.F., Duchesne, C., Côté, M.M., 2003. Regional-scale permafrost mapping using the TTOP ground temperature model. In: Phillips, M., Springman, S.M., Arenson, L. (Eds.), *Proceedings 8th International Conference on Permafrost*. Swets and Zeitlinger, Lisse, pp. 1241–1246.
- Yasufuku, N., Springman, S.M., Arenson, L.U., Ramholt, T., 2003. Stress-dilatancy behaviour of frozen sand in direct shear. *8th International Conference on Permafrost*, Zurich. Balkema, Rotterdam, pp. 1253–1258 (2).
- Yoshikawa, K., 1993. Notes on open-system pingo ice, Adventdalen, Spitsbergen. *Permafrost and Periglacial Processes* 4, 327–334.
- Yoshikawa, K., Leuschen, C., Ikeda, A., Harada, K., Gogineni, P., Hoekstra, P., Hinzman, L., Sawada, Y., Matsuoka, N., 2006. Comparison of geophysical investigations for detection of massive ground ice (pingo ice). *Journal of Geophysical Research* 111, E06S19.
- Zhang, T., Stamnes, K., 1998. Impact of climatic factors on the active layer and permafrost at Barrow, Alaska. *Permafrost and Periglacial Processes* 9 (3), 229–246.
- Zhang, T., 2005. Influence of the seasonal snow cover on the ground thermal regime: an overview. *Reviews of Geophysics* 43, RG4002. doi:10.1029/2004RG000157.
- Zhang, T., Barry, R.G., Haeberli, W., 2001. Numerical simulations of the influence of the seasonal snow cover on the occurrence of permafrost at high latitudes. *Norwegian Journal of Geography* 55, 261–266.
- Zick, W., 1996. Bewegungsmessungen 1965–1994 am Blockgletscher Macun I (Unterengadin/Schweiz) – neue Ergebnisse. *Zeitschrift für Geomorphologie N.F., Supplement-Band* 104, 59–71.
- Zimmerman, R.W., King, M.S., 1986. The effect of freezing on seismic velocities in unconsolidated permafrost. *Geophysics* 51, 1285–1290.
- Zimmermann, M., Haeberli, W., 1992. Climatic change and debris flow activity in high-mountain areas – a case study in the Swiss Alps. In: Boer, M., Koster, E. (Eds.), *Catena Supplement* 22, 59–72.
- Zuidhoff, F.S., Kolstrup, E., 2000. Changes in palsa distribution in relation to climate change in Laivadalén, northern Sweden, especially 1960–1997. *Permafrost and Periglacial Processes* 11, 55–69.

Elevated erosion surfaces in central West Greenland and southern Norway: their significance in integrated studies of passive margin development

Johan M. Bonow, Karna Lidmar-Bergström, Peter Japsen, James A. Chalmers & Paul F. Green.

Bonow, J.M., Lidmar-Bergström, K., Japsen, P., Chalmers, J.A. and Green, P.F.: Elevated erosion surfaces in central West Greenland and southern Norway: their significance in integrated studies of passive margin development. *Norwegian Journal of Geology*, Vol. 87, pp. 197-206. Trondheim 2007. ISSN 029-196X.

Elevated erosion surfaces were used as an independent data set in an integrated study of the landscape development in central West Greenland. The study resulted in a time-constrained model describing multiple episodes of post-rift uplift, erosion and burial on a passive margin. The model is based on full integration of three data sets: analysis of large-scale landforms, apatite fission track analysis (AFTA) of samples from outcrops and deep boreholes, and the geological record. These data are equally important as they record specific and unique parts of the landscape history. The relative chronology obtained from the landform record is constrained by geology, which gives the maximum age of an erosion surface, and AFTA that records the cooling history of the subsurface rock. This combined approach validates the interpretation of erosion surface as having been governed by different base levels in the past, and shows that erosion surfaces can be used to reconstruct tectonic events. Geomorphological key observations for the landscapes of southern Norway are presented and the similarities with landscapes in central West Greenland emphasised, especially the elevated plateaux and the Mesozoic etch surfaces. This similarity suggests that it may be possible to construct a time-constrained model for the landscape development of southern Norway based on our West Greenland approach.

Johan M. Bonow, Peter Japsen, James A. Chalmers, Geological Survey of Denmark and Greenland (GEUS), DK-1350, Copenhagen K, Denmark. E-mail: jbon@geus.dk. Karna Lidmar-Bergström, Department of Physical Geography and Quaternary Geology, Stockholm University, SE-10691, Stockholm, Sweden. Paul F. Green, Geotrack International, 37 Melville Road, West Brunswick, Victoria 3055, Australia.

Introduction

Passive continental margins are in many cases characterised by mountains with near planar erosion surfaces at high elevation (Ollier 1985), while similar landscapes also occur along the rims of the northern North Atlantic (e.g. Bonow et al. 2006a, b). In early studies, conclusions based on landscape analysis led geomorphologists to interpret these planar surfaces as representing true erosion surfaces formed near former base levels (the sea) and reflecting late Cenozoic uplift events, for example in Scandinavia (Reusch 1901; Ahlmann 1919). The relevance of such erosion surfaces for tectonic conclusions was doubted in the 1960s (e.g. Chorley 1965) and landform analysis went out of fashion. The use of landforms is still rejected by some authors (e.g. Summerfield 2005), but this paradigm is beginning to change due to close integration of data from different disciplines (e.g. Kuhle-mann et al. 2005). There is still a lack of understanding of the processes that have controlled passive margin development (Mosar 2003) and as yet there is no consensus on when and how the highly elevated margins around the North Atlantic arose (Japsen & Chalmers 2000; Olesen et al. 2002; Japsen et al. 2006; Fig. 1). A major and controversial issue globally is whether these erosion surfaces

are the remnants of uplifted rift shoulders, implying that they have been high ever since the original rifting (e.g. Gallagher et al. 1995; Brown et al. 2000; Persano et al. 2005), or if the surfaces have been uplifted and the relief rejuvenated long after continental break up (e.g. King 1976; Lidmar-Bergström et al. 2000; Bonow et al. 2006a).

The formation and development of the passive margins have been studied by a number of disparate methods, e.g. fission track analysis showing palaeo-temperatures and cooling events, sonic velocity data showing maximum burial of sediments, seismic data offshore combined with borehole data showing timing for sediment supply, tilting and truncation of sedimentary sequences and erosion surfaces which give the relative timing of uplift and erosional events (cf. Doré et al. 2002). Much of the controversy in interpretations of the landscape development in earlier studies is due to the use of single disciplines alone, lack of full integration of data and, maybe most important, lack of understanding of the possibilities and limitations within the different methods, and misunderstanding in the language and technical terms used in the different scientific fields. In this paper we describe an integrated post-rift model of tectonism, with uplift and burial connected to phases of erosion and landscape

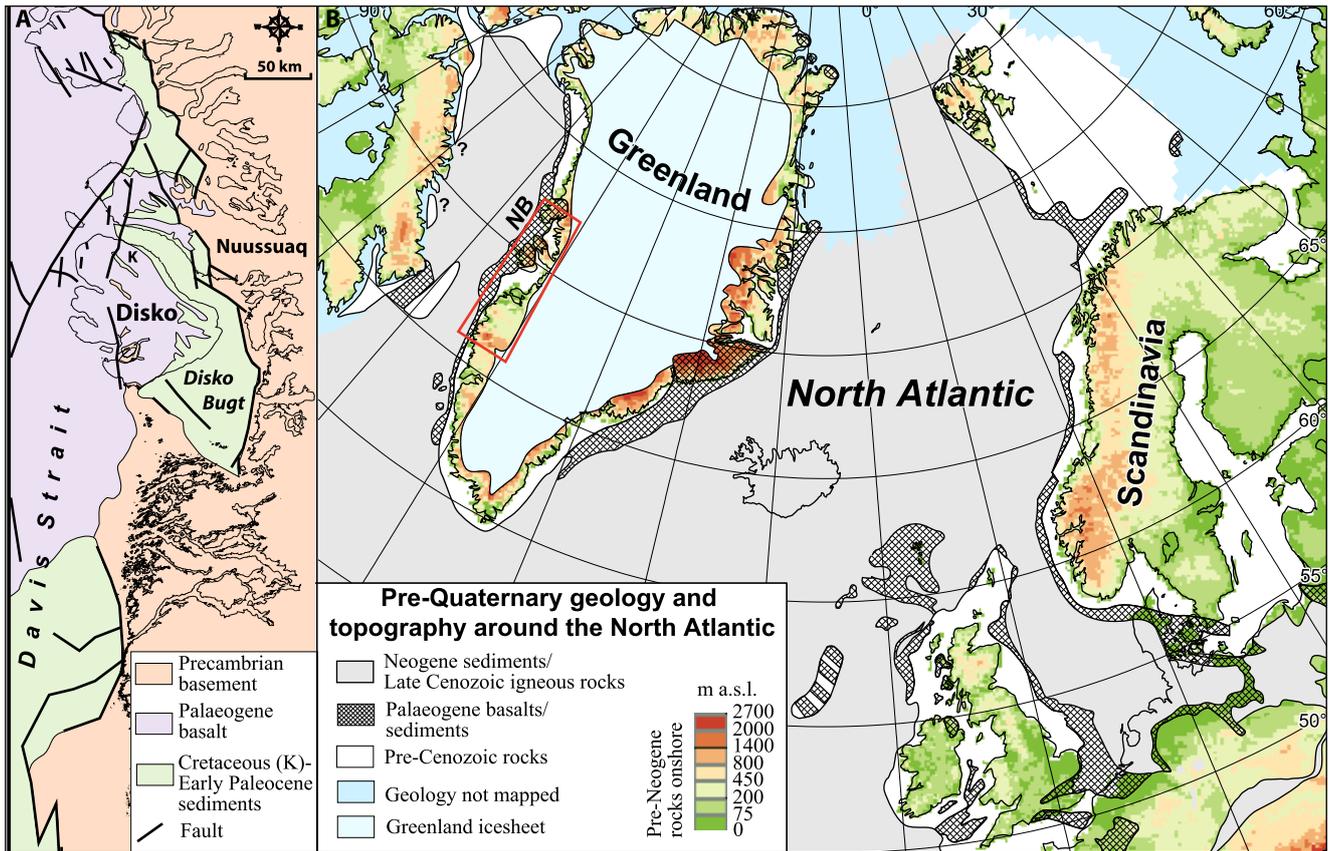


Fig. 1. A: Geology of central West Greenland (area indicated by red box in B). Note the Cretaceous-Palaeogene cover on the Precambrian basement. B: Topography and offshore geology around the North Atlantic. The age of the pre-Quaternary sediments increases in age towards the coasts, where the hinterland is often elevated. This configuration of the sedimentary sequences is consistent with Neogene uplift of the continents. Geology after Jackson et al. (1992), Wheeler et al. (1996), Chalmers et al. (1999) and Japsen & Chalmers (2000). Topography from ETOPO-2. NB: Nuussuaq Basin. Modified from Bonow et al. (2006a, b).

development of the well studied West Greenland margin (Mathiesen 1998; Chalmers et al. 1999; Chalmers 2000; Chalmers & Pulvertaft 2001; Bonow 2005; Japsen et al. 2005; 2006 Bonow et al. 2006a, b; Pedersen et al. 2006). We then compare style and the appearance of events with the less time-constrained margin of southern Norway (Fig. 1) and formulate the relevant questions. Finally we discuss the usefulness of our integrated method for providing answers to these questions.

Methods

We combine the conclusions from three techniques:

- 1) *Landform analysis* of long-term landscape development, based on relationships between geomorphology and geology (Lidmar-Bergström 1982; 1989, 1995, 1996, 1999; Lidmar-Bergström et al. 2000; Bonow et al. 2003, 2006a, b; Bonow 2004, 2005).
- 2) *Apatite fission track analysis (AFTA)* (Green et al. 1989, 2002).
- 3) *Analysis of seismic data and deep drill-cores* (Chalmers et al. 1999; Chalmers & Pulvertaft 2001 and references therein) and *vertical geological sections onshore* (Pedersen et al. 2006 and references therein).

The major advance in understanding the landscape development in West Greenland was achieved by constraining the development of palaeosurfaces not only by the geology, but also with the thermochronological record from outcrop and borehole samples (Fig. 2) (Japsen et al. 2006). The relative timing of tectonic events defined from landform analysis was translated to geological timescales by AFTA data. AFTA gives the timing for the onset of cooling from a palaeothermal peak, resulting either from exhumation or from change in heat-flow. Formation of a palaeosurface subsequent to a cooling event indicates that the cooling was a starting point for erosion of the landmass, rather than only a change in heat flow.

The characteristics of a re-exposed palaeosurface can be ascertained at the contacts with cover rocks. Its final age of formation is constrained by remnants of datable cover rocks, thereby defining a relative chronology (Fig 2a, b). If cover rocks are missing, the distinct character and shape of a surface indicates the climate/environment in which it was formed and give some hint of its age. The relationships between a tilted re-exposed surface and a truncating higher, more horizontal surface also give the relative age of the higher surface (younger) (Fig. 2a).

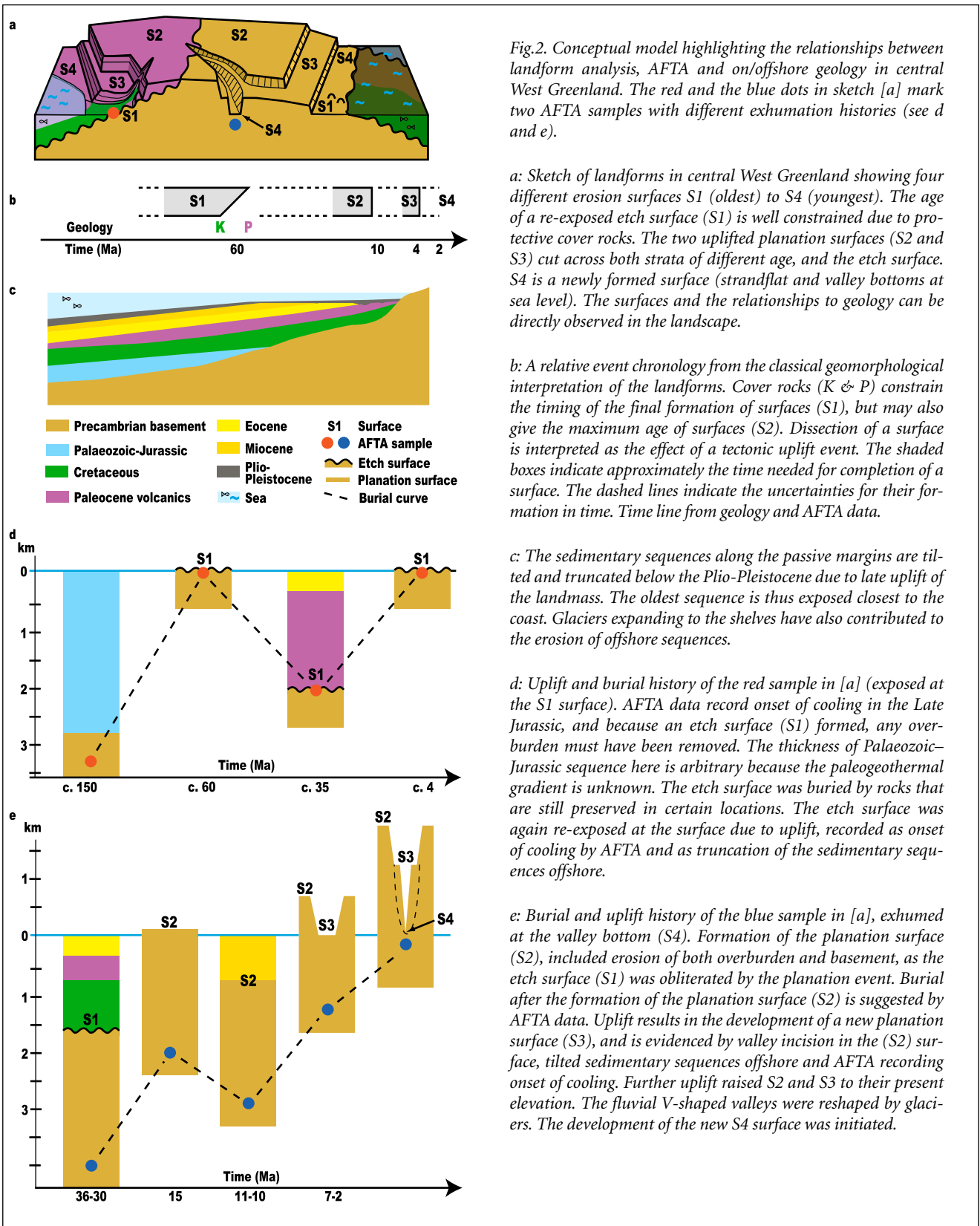


Fig.2. Conceptual model highlighting the relationships between landform analysis, AFTA and on/offshore geology in central West Greenland. The red and the blue dots in sketch [a] mark two AFTA samples with different exhumation histories (see d and e).

a: Sketch of landforms in central West Greenland showing four different erosion surfaces S1 (oldest) to S4 (youngest). The age of a re-exposed etch surface (S1) is well constrained due to protective cover rocks. The two uplifted planation surfaces (S2 and S3) cut across both strata of different age, and the etch surface. S4 is a newly formed surface (strandflat and valley bottoms at sea level). The surfaces and the relationships to geology can be directly observed in the landscape.

b: A relative event chronology from the classical geomorphological interpretation of the landforms. Cover rocks (K & P) constrain the timing of the final formation of surfaces (S1), but may also give the maximum age of surfaces (S2). Dissection of a surface is interpreted as the effect of a tectonic uplift event. The shaded boxes indicate approximately the time needed for completion of a surface. The surfaces and the relationships to geology can be directly observed in the landscape. Time line from geology and AFTA data.

c: The sedimentary sequences along the passive margins are tilted and truncated below the Plio-Pleistocene due to late uplift of the landmass. The oldest sequence is thus exposed closest to the coast. Glaciers expanding to the shelves have also contributed to the erosion of offshore sequences.

d: Uplift and burial history of the red sample in [a] (exposed at the S1 surface). AFTA data record onset of cooling in the Late Jurassic, and because an etch surface (S1) formed, any overburden must have been removed. The thickness of Palaeozoic–Jurassic sequence here is arbitrary because the paleogeothermal gradient is unknown. The etch surface was buried by rocks that are still preserved in certain locations. The etch surface was again re-exposed at the surface due to uplift, recorded as onset of cooling by AFTA and as truncation of the sedimentary sequences offshore.

e: Burial and uplift history of the blue sample in [a], exhumed at the valley bottom (S4). Formation of the planation surface (S2), included erosion of both overburden and basement, as the etch surface (S1) was obliterated by the planation event. Burial after the formation of the planation surface (S2) is suggested by AFTA data. Uplift results in the development of a new planation surface (S3), and is evidenced by valley incision in the (S2) surface, tilted sedimentary sequences offshore and AFTA recording onset of cooling. Further uplift raised S2 and S3 to their present elevation. The fluvial V-shaped valleys were reshaped by glaciers. The development of the new S4 surface was initiated.

Tilted sedimentary sequences may indicate either uplift or subsidence (Fig. 2c). Truncation of a sequence gives a maximum age for the erosional event. Deposition and later removal of sedimentary sequences are almost impossible to identify from the geological record, but the sedimentary cover causes additional heating that can

be recorded by AFTA and vitrinite reflectance data (Fig. 2d, e). By integrating these independent data, we have obtained a closely time-constrained model for the tectonic development of the passive margin of Central West Greenland (Fig. 2).

Phanerozoic development of central West Greenland

Geology

Central West Greenland consists of a Precambrian shield (Henriksen et al. 2000). Sedimentary basins formed during the Early Cretaceous due to rifting and the shield was separated from Canada by sea floor spreading in the Early Tertiary (Chalmers & Pulvertaft 2001). Cretaceous to lower Paleocene sediments of the Nuussuaq Basin were later partly covered by upper Paleocene–Eocene basaltic rocks from volcanoes in the west (Clark & Pedersen 1976; Chalmers et al. 1999). The Precambrian basement is deeply weathered to a kaolinitic saprolite at the contact with Cretaceous and Palaeogene strata (Pulvertaft 1979; Bonow 2005). The Nuussuaq Basin was subjected to several episodes of uplift, erosion and subsidence in the Maastrichtian to early Paleocene, evidenced by deeply incised valleys in the older succession with infill of younger sediments (Dam et al. 1998; Chalmers et al. 1999). Subsequent eruption of submarine lavas shows that subsidence kept pace with the volcanic fill and ultimately the volcanism became sub-aerial (Pedersen et al. 2002), but marine sediments within the sub-aerial volcanic pile (Piasecki et al. 1992) show that subsidence continued. The post-rift subsidence was more than 1 km and all occurred in the Paleocene. The major phase of volcanism was in the Paleocene (Storey et al. 1998), but resumed in the early Eocene and in the mid-Eocene (Schmidt et al. 2005). In the mid-Eocene the basalts were transgressed and a succession of strata up to 3 km thick deposited (Skaarup 2002). This mid-Eocene seaward-dipping sedimentary section became truncated at a late date, and in the seismic lines the truncation can be identified either by the sea bed or by a shallow unconformity (the 'base Quaternary') (Chalmers 2000).

Apatite fission-track analysis (AFTA)

The timing of cooling events has been constrained by apatite fission track data supported by vitrinite reflectance data (Mathiesen 1998, Japsen et al. 2005). Access to sub-surface data from a 3 km deep well in the Meso-

zoic sedimentary basin was significant for resolving the details of the very late Cenozoic erosional history (exhumation) in West Greenland. AFTA data from outcrop and samples from two boreholes showed three distinct cooling episodes, beginning between 40 and 30 Ma, 11 and 10 Ma, and 7 and 2 Ma. Japsen et al. (2005) concluded that the two last episodes must have included erosion of the landmass and not only a change of the palaeothermal gradient. However, the integration with geomorphology showed that the first cooling episode was also a major erosional event (Japsen et al. 2006).

Geomorphology

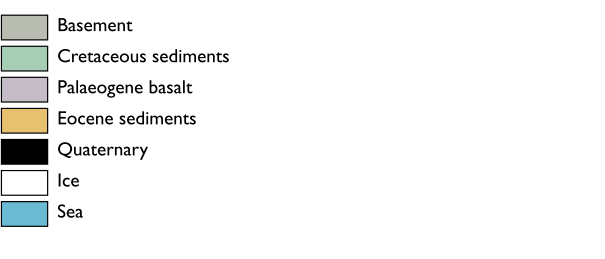
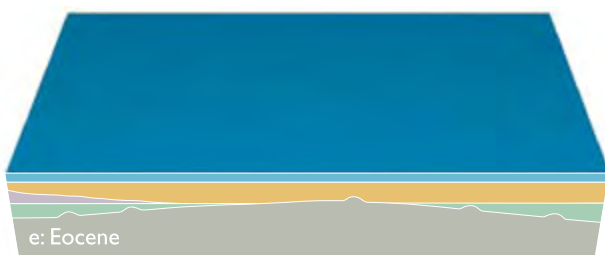
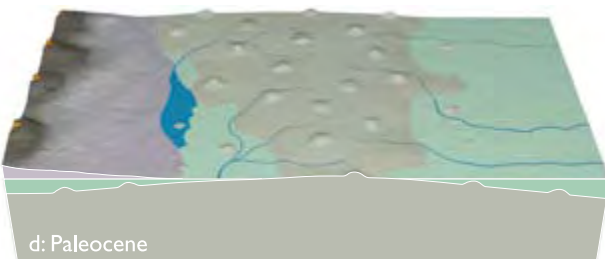
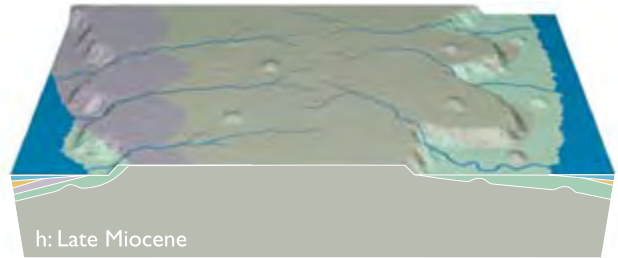
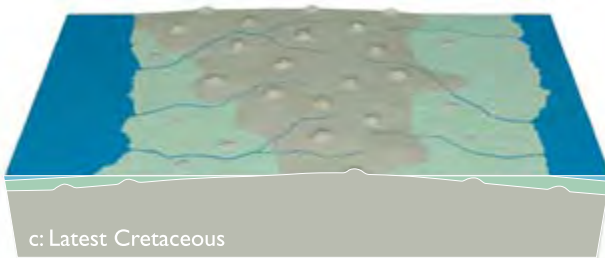
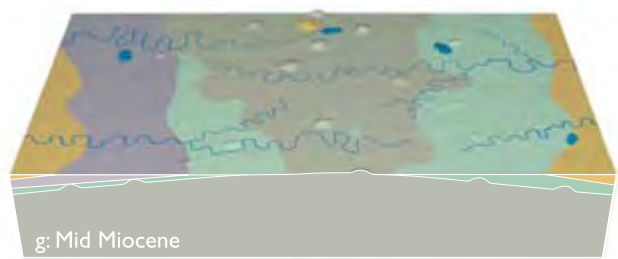
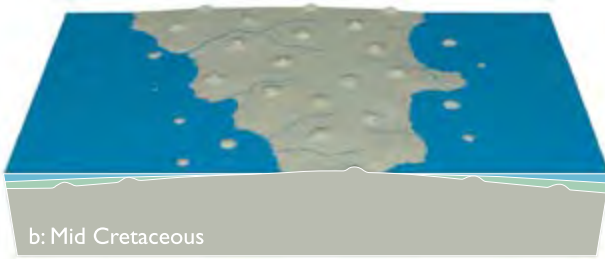
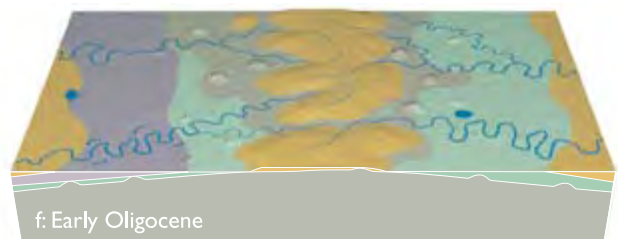
West Greenland is mainly characterised by high plateaus with summits reaching above 2000 m above sea level (a.s.l.) and bordered by an escarpment. The appearance is thus indistinguishable from a so-called 'classic' rift margin. The plateaus are partly dissected by deeply incised valleys. Two types of erosion surfaces in the Precambrian basement have been identified in West Greenland, namely

- a re-exposed etch surface (Bonow 2005; Bonow et al. 2006a) and
- two uplifted planation surfaces, an upper planation surface (UPS) and a lower planation surface (LPS) (Bonow et al. 2006a, b).

The etch surface was formed by deep weathering and subsequent stripping of kaolinitic saprolites, and today it forms characteristic landscapes with an undulating topography and a relative relief of about 100 m, a hilly relief surface. In areas where the hilly relief surface is well preserved it means that the surface has recently emerged from beneath its protective cover rocks of Cretaceous–Paleocene age due to erosion, e.g. on southern Disko and in the area south of Disko Bugt (Bonow 2005; Fig. 1). The cover rocks confirm the minimum age of this surface.

The etch surface has been cut off by the regionally developed UPS. This planation surface also cuts the youngest volcanics in the Nuussuaq Basin as well as older rocks and must therefore have developed after the mid-Eocene. The LPS is younger and has only been partially developed as an incised generation. Both these surfaces have developed sub-horizontally and close to the general base-level,

Fig. 3. Block diagrams generalising the landscape development in central West Greenland, for a volcanic and non-volcanic settings. The front of each block diagram is approximately 350 km. a: Early Cretaceous: Development of hilly relief. b: Mid Cretaceous: Transgression and burial of the hilly relief. c: Latest Cretaceous: Large land areas are covered by Cretaceous strata as the sea regresses. d: Paleocene. Basalt flows on-lap both the basement with hilly relief and the Cretaceous strata. e: Eocene. Transgression accompanied by subsidence. f: Early Oligocene: Uplift resulting in erosion and initial planation. g: Mid Miocene: The end result of planation: a fairly flat surface where geology and structures are of limited importance (the upper planation surface, -UPS). h: Late Miocene: Uplift of the UPS triggering valley incision and the formation of a lower planation surface (LPS). i: Latest Miocene-Pliocene: Uplift and rejuvenation of the relief resulting in a stepped landscape. The valleys incise headwards and widen by scarp retreat. The steps between surfaces are kept mainly intact as the base level for surfaces away from the valleys are unchanged. The steepness of slope will depend on the resistance of the bedrock. Uplift causes erosion of cover rocks, re-exposing the hilly relief. Offshore, the sediments are being truncated. j: Quaternary: Pre-glacial fluvial valleys are exploited by valley glaciers and reshaped in various degrees. Surfaces in a low position are destroyed by the glaciers. Sediments are transported offshore and older offshore sediments are eroded by the expanding ice-sheets. k: Present: The general appearance of the landscape, with stepped surfaces more than 2 km above sea level and deeply incised valleys, is mainly a result of the fluvio-tectonic landscape development. Fjords and new as well as old fluvial valleys occur together in the landscape.



- Basement
- Cretaceous sediments
- Palaeogene basalt
- Eocene sediments
- Quaternary
- Ice
- Sea

because even a minor tilt of a surface will cause fluvial systems to incise and the relief to rejuvenate (Rudberg 1970; Bonow et al. 2006b fig. 6). Both UPS and LPS are situated at high elevations and are therefore undergoing destruction. As the UPS was identified as a tilted surface from a maximum elevation at c. 2 km a.s.l. and with a variance in elevation of c. 1.7 km across the area, it was concluded that tectonism caused the uplift and tilt. The difference in elevation between the UPS and LPS was also found to vary and thus the second uplift event also had a tectonic component. As the surfaces have developed close to sea level they could be used as a reference for estimating the amount of uplift. Thus, the two planation surfaces represent two phases of uplift, the first with an amount between 500 and 1000 m and the second between 700 and 1000 m. The last uplift event initiated erosion of the cover rocks, re-exposing the etch surface (Bonow et al. 2006a).

Time-constrained, post-rift passive margin model of central West Greenland

As an example for the interpretation of other elevated margins we present an empirical model developed for the passive margin of central West Greenland (Chalmers et al. 1999; Chalmers 2000; Bonow 2004, 2005; Bonow et al. 2006a, b; Japsen et al. 2005, 2006; Pedersen et al. 2006). The landscape development is described from the Late Mesozoic to the present based on integration of geomorphology, thermochronology, and onshore and offshore geological data (Fig. 3). The figure is a composite of the development in central West Greenland reflecting the development in both the volcanic and non-volcanic settings.

Figure 3a: A Cretaceous etch surface formed in Precambrian basement rocks. Palaeozoic rocks were present in West Greenland up to the Jurassic (see Bonow et al. 2006a), but this cover was eroded prior to the Cretaceous, as Cretaceous strata now rest directly on basement (cf. Fig. 3b). The etch surface characterised by hilly relief was formed by deep weathering and subsequent stripping of kaolinitic saprolites. This exhumation history is constrained by AFTA data, which show a regional cooling episode starting between 160 and 150 Ma and resulting in formation of this etch surface.

Figure 3b: Transgression in the mid Cretaceous. The mid Cretaceous was characterised by very high sea-levels worldwide (Frakes et al. 1992). In West Greenland the transgression was further enhanced by subsidence of the landmass, resulting in deposition of a several km thick sedimentary sequence.

Figure 3c: Regression and erosion of cover rocks. The Cretaceous cover was partly eroded from basement areas in West Greenland as evidenced by later Paleocene basalt flows lying directly on top of the basement. The erosion was related to uplift during the rifting.

Figure 3d: Palaeocene rifting, sea-floor spreading and volcanism. The landmass was subjected to km-scale uplift and subsidence within a few million years. These movements has been suggested to be related to the impact of the Iceland Plume (Dam et al. 1998). Prograding Palaeocene delta sediments offshore show that the rivers flowing from the east towards this area were turned towards the south. The change was probably caused by uplift of the landmass in the west in connection with basaltic volcanism.

Figure 3e: Post-volcanic subsidence and burial during the Eocene. A transgression is recorded in the offshore sedimentary sequences, and additional onshore burial is also required to explain the AFTA data (Japsen et al. 2005).

Figure 3f: Mid-Cenozoic uplift, erosion of cover rocks and initiation of planation. The erosion in the mid-Cenozoic was subaerial as shown by the occurrence of a 39 Ma subaerial basalt (Schmidt et al. 2005), but also by the AFTA data that record onset of a regional cooling event in West Greenland between 36 and 30 Ma (Japsen et al. 2006). The most probable cause of this cooling event was uplift and subsequent erosion (Bonow et al. 2006b), although some of this cooling also involved a decrease in heat flow (Japsen et al. 2005). This event cannot be associated with any known rifting activity in West Greenland.

Figure 3g: Oligocene-Miocene: formation of a preserved regional surface. The Oligocene hiatus offshore West Greenland (Rolle 1985; Chalmers 2000; Sørensen 2006) is consistent with a regionally developed planation surface onshore, which is of low relief and was formed close to sea level (the upper planation surface -UPS). In central West Greenland the end result was a flat surface, cutting across mid-Eocene strata and older rocks as well as the sub-Cretaceous etch surface. This planation surface (the UPS) developed until interruption by an uplift event in the late Neogene (Fig. 3h).

Figure 3h: First Neogene tectonic uplift event. An uplift event triggered valley incision with consequent headward erosion, causing the dissection of the older surface (the UPS). Over time the initially narrow V-shaped valleys were widened forming a new lower planation surface (the LPS). Surface formation took place in preglacial times and this timing is consistent with the cooling event beginning between 11 and 10 Ma recorded by AFTA data (Japsen et al. 2005). Uplift exposed cover rocks for erosion, causing re-exposure of the basement with its ancient hilly relief and subsequent reshaping (cf. 3a).

Figure 3i: Second Neogene uplift event. The relief was rejuvenated and adjusted to the new base level after a second uplift event, followed by valley widening. Ultimately a stepped landscape was formed as a consequence of incision along the main valleys to give a valley-in-valley pattern. The erosional conditions for the surfaces away from the valleys were unchanged, as they were not affected directly by the changed base level. The hilly relief was subjected to continued re-exposure and destruction.

Figure 3j: Late Cenozoic glaciations and reshaping of the relief. Ice-sheets in highly elevated areas were probably cold-based and non-erosive during long periods (e.g. Kleman & Hättestrand 1999; Bonow et al. 2006a), therefore leaving the uplifted pre-glacial relief without any major reshaping. Significant erosion of cover rocks occurred on the shelf and also affected onshore areas to some extent. Ice sheets were responsible for transportation of sediments from onshore areas, removing older sediments from offshore areas close to the coasts and then re-depositing them in the oceans. Glacial erosion along the valleys and other low areas was locally substantial, resulting in the formation of deep fjords and the destruction of low-lying parts of the tilted erosion surfaces.

Figure 3k: The present landscape. The stepped landscapes are a result of tectonic-fluvial development and have kept their overall appearance intact despite the late Cenozoic glaciations. The originally V-shaped valleys have been reshaped to different degrees. Hilly relief etch surfaces are only well preserved where they have been covered until recent times.

Landscapes of southern Norway: general geomorphological patterns and scientific frontiers

Overviews of the geomorphology of southern Norway have described the landscape as a result of a marginal bulge (Peulvast 1985) or a dome-like uplift (Lidmar-Bergström et al. 2000). Central southern Norway is characterised by high undulating plateaux with erosion surfaces at distinct levels similar to West Greenland. In Norway these plateaux are referred to as the Palaeic surface or Palaeic relief which is clearly different from the deeply incised valleys (Reusch 1901, Lidmar-Bergström et al. 2000, Bonow et al. 2003). Analysis of the major landforms in southern Norway has shown four major planation surfaces in stepped sequence, following the major valleys (Lidmar-Bergström et al. 2000) and it is suggested that the planation surfaces developed after early tectonic uplift events, possibly since the Early Cretaceous, while deeply incised valleys, on the other hand, might reflect late tectonic uplift events (Lidmar-Bergström et al. 2000; Lidmar-Bergström & Näslund 2002). The late incisions apparently occurred stepwise as indicated by remnants of valley benches (at c. 600 and 500 m a.s.l.) along Gudbrandsdalen, one of the major valleys in southern Norway (Bonow et al. 2003). The timing of uplift movements cannot be determined using erosion surfaces alone, as southern Norway consists solely of Caledonian basement with reworked Palaeozoic or older rocks (Sigmond 1992), apart for some minor remnants of down-faulted Mesozoic rocks (e.g. Fossen et al. 1997; Sommeruga & Bøe 2002).

The eastern flank of the southern Scandes (southeast Norway) has a characteristic hilly relief with occurrences of kaolinised zones. The area has therefore been

interpreted to be a Mesozoic etch surface, re-exposed by erosion of protective cover rocks due to uplift in the Neogene (Reusch 1903; Lidmar-Bergström 1995, 1999). It is analogous to the proven sub-Jurassic and sub-Cretaceous etch surfaces in southern Scandinavia (Lidmar-Bergström 1988, 1989) and the sub-Cretaceous and sub-Paleocene etch surfaces in central West Greenland (Pulvertaft 1979; Bonow 2005).

Here we have presented some key observations for understanding the landscape development in southern Norway and emphasized that important aspects of the landscape are similar to those of West Greenland, in particular the elevated plateaux and the Mesozoic etch surfaces. However, whereas the timing for the formation of the Cenozoic planation surfaces in West Greenland is now known, the history of the Norwegian landscapes is poorly time-constrained. Important questions to be answered are: To what extent do re-exposed erosion surfaces exist in southern Norway and how old are they? When and for how long was southern Norway covered by sediments? When did the formation and uplift of the erosion surfaces occur? What conclusions can the erosion surfaces reveal about uplift style?

For example, it has been suggested that southern Norway was transgressed during the late Mesozoic (Jensen & Schmidt 1992, 1993; Riis 1996), but how thick that sequence was is unknown. Similarly, southern Norway may have been submerged in the Middle–Late Eocene (Jordt et al. 1995), and integration between landforms and AFTA data may give some hint about how long an assumed cover lasted and what was its thickness. The offshore record based on seismic and well data must also be included. Studies of sedimentary input have, for example, argued for increased relief of Scandinavia through the Miocene and Pliocene (e.g. Spjeldnæs 1975; Clausen et al. 1999; Japsen et al. 2002) and the seaward-dipping sedimentary sections have their deepest truncations towards the margin. This is also interpreted as a consequence of late uplift and subsidence of the basin (Doré 1992; Jensen & Schmidt 1993; Osmundsen et al. 2002).

Future uplift studies in southern Norway

The landscape development in central West Greenland could be deciphered because it is well documented regarding 1) Landforms 2) AFTA and 3) Onshore and offshore geology. However, the development in southern Norway is only well documented as regards the onshore and offshore geology (e.g. Jordt et al. 1995; Mosar 2003), while the regional extent of stepped erosion surfaces is only very briefly mapped (Lidmar-Bergström et al. 2000), and because the results from fission track studies in Norway and southern Scandinavia remain inconclusive (Rohrman et al. 1995; Hendriks & Redfield 2005; Söderlund et al. 2005; Green & Duddy 2006; Larsson et al.

2006). An inherent advantage for the study of the landscape development in West Greenland is the presence of a thick Palaeogene sequence onshore – this advantage can of course not be applied to southern Norway.

To be able to solve the questions above, single disciplines cannot stand alone. Each dataset from either landforms, AFTA or geology records specific parts of the event chronology and are equally important to constrain the history of landscape development. Therefore it is vital to acknowledge all available data to get a consistent tectonic model, and also to understand the possibilities and difficulties inherent in each method. In order to do this for southern Norway, some new data are required.

It is necessary to map in detail both re-exposed and new erosion surfaces in southern Norway, because this will reveal the relative chronology for the landscape development. Furthermore, it is important to acquire new apatite fission-track data and to integrate these with those of the landscape analysis, because this may lead to absolute timing of the onset of erosional events as the West Greenland example has shown. AFTA data from vertical profiles are important for assessing palaeogeothermal gradients and the magnitude of sections removed during episodes of exhumation. Results from such AFTA profiles in Norway are currently under way (Japsen et al. 2007). In West Greenland, AFTA of rock samples from a deep borehole located at the mouth of a deeply incised valley made it possible to constrain the timing of even the most recent cooling episodes. Only drilling of a deep borehole in a similar setting in central Norway, can provide the necessary data for revealing the time when the mountains of Norway reached their present altitude.

Conclusions

Conclusions obtained from geomorphological analysis, apatite fission-track analysis and geology have been closely integrated in our study of central West Greenland. These made it possible to constrain the time for surface formation, to identify the mode and timing of uplift events, and to separate the spatial distribution in time and space of erosion, deposition and subsidence. The approach used in West Greenland may also be applied to southern Norway for the purpose of investigating the extent to which palaeosurfaces of similar appearance in the two areas share a similar history and for constructing a time-constrained landscape development model.

Acknowledgements: This study benefited from financial support by the Carlsberg Foundation, the Swedish Research Council and the Danish Natural Science Research Council. We thank J. Kuhlemann and F. Riis for a constructive review. Stefan Sølberg prepared figure 3 from hand made drawings. The paper is published with permission of the Geological Survey of Denmark and Greenland.

References

- Ahlmann, H.W. 1919: Geomorphological studies in Norway. *Geografiska Annaler* 1, 3–320.
- Bonow, J.M. 2004: Palaeosurfaces and palaeovalleys on North Atlantic previously glaciated passive margins - reference forms for conclusions on uplift and erosion. *PhD thesis. Dissertation No. 30.* The Department of Physical Geography and Quaternary Geology, Stockholm University.
- Bonow, J.M. 2005: Re-exposed basement landforms in the Disko region, West Greenland – disregarded data for estimation of glacial erosion and uplift modelling. *Geomorphology* 72, 106–127.
- Bonow, J.M., Lidmar-Bergström, K. & Näslund, J.-O. 2003: Palaeosurfaces and major valleys in the area of the Kjølén Mountains, southern Norway – consequences of uplift and climatic change. *Norsk Geografisk Tidsskrift – Norwegian Journal of Geography* 57, 83–101.
- Bonow, J.M., Lidmar-Bergström, K. & Japsen, P. 2006a: Palaeosurfaces in central West Greenland as reference for identification of tectonic movements and estimations of erosion. *Global and Planetary Change* 50, 161–183.
- Bonow, J.M., Japsen, P., Lidmar-Bergström, K., Chalmers, J.A. & Pedersen, A.K. 2006b: Cenozoic uplift of Nuussuaq and Disko, West Greenland - elevated erosion surfaces as uplift markers of a passive margin. *Geomorphology* 80, 325–337.
- Brown, R.W., Gallagher, K., Gleadow, A.J.W. & Summerfield, M.A. 2000: Morphotectonic evolution of the South Atlantic margins of Africa and South America. In Summerfield, M.A. (ed.): *Geomorphology and global tectonics*, 255–281. Wiley, Chichester.
- Chalmers, J.A. 2000: Offshore evidence for Neogene uplift in central West Greenland. *Global and Planetary Change* 24, 311–318.
- Chalmers, J.A. & Pulvertaft, T.C.R. 2001: Development of the continental margins of the Labrador Sea: a review. In Wilson, R.C.L., Whitmarsh, R.B., Taylor, B. & Froitzheim, N. (eds.): *Non-volcanic rifting of continental margins: A comparison of evidence from land and sea*, 77–105. Geological Society, London, Special Publications 187.
- Chalmers, J.A., Pulvertaft, C., Marcussen, C. & Pedersen, A.K. 1999: New insight into the structure of the Nuussuaq Basin, central West Greenland. *Marine and Petroleum Geology* 16, 197–224.
- Chorley, R.J., 1965: A re-evaluation of the geomorphic system of W.M. Davis. In Chorley, R.J. & Haggett, P. (eds.): *Frontiers in geographical teaching*, 21–38. Methuen, London.
- Clark, D.B. & Pedersen, A.K. 1976: Tertiary volcanic province of West Greenland. In Escher, A. & Watt, W.S. (eds.): *Geology of Greenland*, 364–385. Geological Survey of Greenland.
- Clausen, J.A., Gabrielsen, R.H., Reksnes, P.A. & Nysæther, E. 1999: Development of intraformational (Oligocene–Miocene) faults in the northern North Sea: influence of remote stresses and doming of Fennoscandia. *Journal of Structural Geology* 21, 1457–1475.
- Dam, G., Larsen, M. & Sønderholm, M. 1998: Sedimentary response to mantle plumes: implications from Paleocene onshore successions, West and East Greenland. *Geology* 26, 207–210.
- Doré, A.G. 1992: The Base Tertiary Surface of southern Norway and the northern North Sea. *Norsk Geologisk Tidsskrift* 72, 259–265.
- Doré, A.G., Cartwright, J.A., Stoker, M.S., Turner, J.P. & White, N.J. 2002: Exhumation of the North Atlantic margin: introduction and background. In Doré, A.G., Cartwright, J.A., Stoker, M.S., Turner, J.P. & White, N. (eds.): *Exhumation of the North Atlantic Margin: Timing, Mechanisms and Implications for Petroleum Exploration*, 1–12. Geological Society, London, Special Publications 196.
- Fossen, H., Mangerud, G., Hesthammer, J., Bugge, T. & Gabrielsen, R.H. 1997: The Bjørøy Formation: a newly discovered occurrence of Jurassic sediments in the Bergen Arc System. *Norsk Geologisk Tidsskrift* 77, 269–287.
- Frakes, L.A., Francis, J.E. & Syktus, J.I. 1992: *Climate modes of the Phanerozoic: the history of the earth's climate over the past 600 million years*, 274pp. Cambridge University Press, Cambridge, 274 pp.

- Gallagher, K., Hawkesworth C.J. & Mantovani, M.S.M. 1995: Denudation, fission track analysis and the long-term evolution of passive margin topography: application to the southeast Brazilian margin. *Journal of South American Earth Sciences* 8, 65–77.
- Green, P.F., Duddy, I.R., Gleadow, A.J.W. & Lovering, J.F. 1989: Apatite Fission Track Analysis as a palaeotemperature indicator for hydrocarbon exploration. In Naeser, N.D. & McCulloh, T. (eds.): *Thermal history of sedimentary basins - methods and case histories*, 181–195. Springer-Verlag, New York.
- Green, P.F., Duddy, I.R. & Hegarty, K.A. 2002: Quantifying exhumation from apatite fission-track analysis and vitrinite reflectance data: precision, accuracy and latest results from the Atlantic margin of NW Europe. In Doré, A.G., Cartwright, J.A., Stoker, M.S., Turner, J.P. & White, N. (eds.): *Exhumation of the North Atlantic Margin: Timing, Mechanisms and Implications for Petroleum Exploration*, 331–354. Geological Society, London, Special Publications, 196.
- Green, P.F. & Duddy, I.R. 2006: Interpretation of apatite (U–Th)/He ages and fission track ages from cratons. *Earth and Planetary Science Letters* 244, 541–547.
- Henriksen, N., Higgins, A.K., Kalsbeek, F. & Pulvertaft, T.C.R. 2000: Greenland from Archaean to Quaternary. Descriptive text to the Geological map of Greenland, 1:2500000. *Geology of Greenland Survey Bulletin* 185, 93 pp.
- Hendriks, B.W.H. & Redfield, T.F. 2005: Apatite fission track and (U–Th)/He data from Fennoscandia: An example of underestimation of fission track annealing in apatite. *Earth and Planetary Science Letters* 236, 443–458.
- Jackson, H.R., Dickie, K. & Marillier, F. 1992: A seismic reflection study of the northern Baffin Bay: implication for the tectonic evolution. *Canadian Journal of Earth Science* 29, 2353–2369.
- Japsen, P. & Chalmers, J.A. 2000: Neogene uplift and tectonics around the North Atlantic: Overview. *Global and Planetary Change* 24, 165–173.
- Japsen, P., Bidstrup, T. & Lidmar-Bergström, K. 2002: Neogene uplift and erosion of southern Scandinavia induced by the rise of the South Swedish Dome. In Doré, A.G., Cartwright, J.A., Stoker, M.S., Turner, J.P. & White, N. (eds.): *Exhumation of the North Atlantic Margin: Timing, Mechanisms and Implications for Petroleum Exploration*, 183–207. Geological Society, London, Special Publications, 196.
- Japsen, P., Green, P.F. & Chalmers, J.A. 2005: Separation of Palaeogene and Neogene uplift on Nuussuaq, West Greenland. *Journal of the Geological Society, London* 162, 299–314.
- Japsen, P., Bonow, J.M., Green, P.F., Chalmers, J.A. & Lidmar-Bergström, K. 2006: Elevated, passive continental margins: Long-term highs or Neogene uplifts? New evidence from West Greenland. *Earth and Planetary Science Letters* 248, 315–324.
- Japsen, P., Green, P.F., Bonow, J.M., & Chalmers, J.A. 2007: New apatite fission-track data from Jotunheim-Sognefjord, Norway EGU General Assembly, Vienna, Austria, Geophysical Research Abstract 9 (EGU2007-A-07327).
- Jensen, L.N. & Schmidt, B.J. 1992: Late Tertiary uplift and erosion in the Skagerrak area: magnitude and consequences. *Norsk Geologisk Tidsskrift* 72, 275–279.
- Jensen, L.N. & Schmidt, B.J. 1993: Neogene uplift in the northeastern North Sea; magnitude and consequences for hydrocarbon exploration in the Farsund Basin. In Spencer, A.M. (ed.): *Generation, Accumulation and Production of Europe's Hydrocarbons*, European Association of Petroleum Geologists Special Publication, 79–88, Florence.
- Jordt, H., Faleide, J.I., Bjørlykke, K. & Ibrahim, M.T. 1995: Cenozoic sequence stratigraphy of the central and northern North Sea Basin: tectonic development, sediment distribution and provenance areas. *Marine and Petroleum Geology* 12, 845–879.
- King, L.C. 1976: Planation remnants upon high lands. *Zeitschrift für Geomorphologie N.F.* 20, 133–148.
- Kleman, J. & Hättestrand, C. 1999: Frozen-bed Fennoscandian and Laurentide ice sheets during the last glacial maximum. *Nature* 402, 63–66.
- Kuhlemann, J., Székely, B., Frisch, W., Danišik, M., Dunkl, I., Molnár, G. & Timár, G. 2005: DEM analysis of mountainous relief in a crystalline basement block: Cenozoic relief generations in Corsica (France). *Zeitschrift für Geomorphologie N.F.* 49, 1–21.
- Larson, S.Å., Cederbom, C.E., Tullborg, E.-L. & Stiberg, J.-P. 2006: Comment on “Apatite fission track and (U–Th)/He data from Fennoscandia: An example of underestimation of fission track annealing in apatite” by Hendriks & Redfield [Earth and Planetary Science Letters 236 (443–458)]. *Earth and Planetary Science Letters* 248, 560–567.
- Lidmar-Bergström, K. 1982: Pre-Quaternary geomorphological evolution in southern Fennoscandia. *Sveriges Geologiska Undersökning* 75(6), series C785, 202 pp.
- Lidmar-Bergström, K. 1989: Exhumed Cretaceous landforms in south Sweden. *Zeitschrift für Geomorphologie N.F. Supplementband* 72, 21–40.
- Lidmar-Bergström, K. 1995: Relief and saprolites through time on the Baltic Shield. *Geomorphology* 12, 45–61.
- Lidmar-Bergström, K. 1996: Long term morphotectonic evolution in Sweden. *Geomorphology* 16, 33–59.
- Lidmar-Bergström, K. 1999: Uplift histories revealed by landforms of the Scandinavian domes. In Smith, B.J., Whalley, W.B. & Warke, P.A. (eds.): *Uplift, Erosion and Stability: Perspectives on Long-term Landscape Development*, 85–91. Geological Society, London, Special Publications 162.
- Lidmar-Bergström, K. & Näslund, J.-O. 2002: Landforms and uplift in Scandinavia. In Doré, A.G., Cartwright, J.A., Stoker, M.S., Turner, J.P. & White, N. (eds.): *Exhumation of the North Atlantic Margin: Timing, Mechanisms and Implications for Petroleum Exploration*, 103–116. Geological Society, London, Special Publications 196.
- Lidmar-Bergström, K., Sulebak, J.R. & Ollier, C.D. 2000: Landforms and uplift history of southern Norway. *Global and Planetary Change* 24, 211–231.
- Mathiesen, A. 1998: Modelling uplift history from maturity and fission track data, Nuussuaq, West Greenland. *Danmarks og Grønlands Geologiske Undersøgelse Rapport* 1998/87, 90pp.
- Mosar, J. 2003: Scandinavia's North Atlantic passive margin. *Journal of Geophysical Research* 108, B8, 2360, doi:10.1029/2002JB002134.
- Olesen, O., Lundin, E., Nordgulen, Ø., Osmundsen, P.T., Skilbrei, J.R., Smethurst, M.A., Solli, A., Bugge, T. & Fichler, C. 2002: Bridging the gap between the onshore and offshore geology in Nordland, northern Norway. *Norwegian Journal of Geology* 82, 243–262.
- Ollier, C.D. 1985: Morphotectonics of passive continental margins: Introduction. *Zeitschrift für Geomorphologie, N.F. Supplementband* 54, 1–9.
- Osmundsen, P.T., Sommaruga, A., Skilbrei, J.R. & Olesen, O. 2002: Deep structure of the Norwegian Sea area, NE Atlantic margin. *Norwegian Journal of Geology* 82, 205–224.
- Pedersen, A.K., Larsen, L.M., Riisager, P. & Dueholm, K.S. 2002: Rates of volcanic deposition, facies changes and movements in a dynamic basin: the Nuussuaq Basin, West Greenland, around the C27n–C26R transition. In Jolley, D.W. & Bell, B.R. (eds.): *The North Atlantic Igneous Province: Stratigraphy, Tectonic, Volcanic and Magmatic Processes*, 157–181. Geological Society, London, Special Publications 197.
- Pedersen, A.K., Larsen, L.M., Pedersen, G.K. & Dueholm, K.S. 2006: Five slices through the Nuussuaq Basin, West Greenland. *Geological Survey of Denmark and Greenland Bulletin* 10, 53–56.
- Peulvast, J.P. 1985: Post-orogenic morphotectonic evolution of the Scandinavian Caledonides during the Mesozoic and Cenozoic. In Gee, D.G. & Sturt, B.A. (eds.): *The Caledonide Orogen; Scandinavia and related areas*, 979–995. John Wiley & Sons, Chichester.
- Persano, C., Stuart, F.M., Bishop, P. & Dempster, T.J. 2005: Deciphering continental breakup in eastern Australia using low-temperature thermochronometers. *Journal of Geophysical Research* 110, B12405, doi:10.1029/2004JB003325.

- Piasecki, S., Larsen, L.M., Pedersen, A.K. & Pedersen, G.K. 1992: Paly-nostratigraphy of the Lower Tertiary volcanics and marine clastic sediments in the southern part of the West Greenland Basin: implications for the timing and duration of the volcanism. *Rapport Grønlands Geologiske Undersøgelse* 154, 31pp.
- Pulvertaft, T.C.R. 1979: Lower Cretaceous fluvial-deltaic sediments at Kùk, Nùgssuaq, West Greenland. *Bulletin of the Geological Society of Denmark* 28, 57–72.
- Reusch, H. 1901: Nogle bidrag till forstaaelsen af hvorledes Norges dale og fjelde er blevene til. *Norges geologiske undersøgelse* 32, 124–263.
- Reusch, H. 1903: Glommens boining ved Kongsvinger. *Norske Geografiske Selskape, Aarbok* 14, 96–102.
- Riis, F. 1996: Quantification of Cenozoic vertical movements of Scandinavia by correlation of morphological surfaces with offshore data. *Global and Planetary Change* 12, 331–357.
- Rohrman, M., van der Beek, P., Andriessen, P. & Cloetingh, S. 1995: Meso-Cenozoic morphotectonic evolution of southern Norway: Neogene domal uplift inferred from apatite fission track thermochronology. *Tectonics* 14, 704–718.
- Rolle, F. 1985: Late Cretaceous-Tertiary sediments offshore central West Greenland: lithostratigraphy, sedimentary evolution, and petroleum potential. *Canadian Journal of Earth Sciences* 22, 1001–1019.
- Rudberg, S. 1970: The sub-Cambrian peneplain in Sweden and its slope gradient. *Zeitschrift für Geomorphologie, Supplementband* 9, 157–167.
- Schmidt, A.G., Riisager, P., Abrahamsen, N., Riisager, J., Pedersen, A.K. & van der Voe, R. 2005: Palaeomagnetism of Eocene Talerua Member lavas on Hareøen, West Greenland. *Bulletin of the Geological Society of Denmark* 52, 27–39.
- Skaarup, N. 2002: Evidence for continental crust in the offshore Palaeogene volcanic province, central West Greenland. *Geology of Greenland Survey Bulletin* 191, 97–102.
- Sigmond, E.M.O. 1992: Berggrunnskart, Norge med havområder. Målestokk 1:3 millioner, *Norges geologiske undersøgelse*, Trondheim.
- Sommeruga, A. & Bøe, R. 2002: Geometry and subcrop maps of shallow Jurassic basins along the Mid-Norway coast. *Marine and Petroleum Geology* 19, 1029–1042.
- Söderlund, P., Juez-Larre, J., Page, L.M. & Dunai T.J. 2005: Extending the time range of (U-Th)/He thermochronometry in slowly cooled terranes: Paleozoic to Cenozoic exhumation history of southeast Sweden. *Earth and Planetary Science Letters* 239, 266–275.
- Sørensen, A.B. 2006: Stratigraphy, structure and petroleum potential of the Lady Franklin and Maniitooq Basins, offshore southern West Greenland. *Petroleum Geoscience* 12, 221–234.
- Spjeldnæs, N. 1975: Paleogeography and facies distribution in the Tertiary of Denmark and surrounding areas. *Norges geologiske undersøgelse* 316, 289–311.
- Storey, M., Duncan, R.A., Pedersen, A.K., Larsen, L.M. & Larsen, H.C. 1998: ⁴⁰Ar/³⁹Ar geochronology of the West Greenland Tertiary volcanic province. *Earth and Planetary Science Letters* 160, 569–586.
- Summerfield, M.A. 2005: The changing landscape of geomorphology. *Earth Surface Processes and Landforms* 30, 779–781.
- Wheeler, J.O., Hoffman, P.F., Card, K.D., Davidson, A., Sanford, B.V., Okulitch, A.V. & Roest, W.R. (compilers) 1996: *Geological Map of Canada 1860A*, scale 1: 5000000. Geological Survey of Canada.



Aspects and concepts on the geomorphological significance of Holocene permafrost in southern Norway

Bernd Etzelmüller^{a,*}, Ivar Berthling^b, Johan Ludvig Sollid^a

^a*Department of Physical Geography, University of Oslo, P.O. Box 1042 Blindern, N-0316 Oslo, Norway*

^b*Norwegian Water Resources and Energy Directorate, P.O. Box 5091 Majorstua, N-0301 Oslo, Norway*

Received 14 December 2001; received in revised form 8 May 2002; accepted 14 August 2002

Abstract

This review paper aims at discussing aspects and concepts of the significance of the spatial and temporal distribution of permafrost on glacial and gravitational processes in southern Norway. The study first reviews the distribution of mountain permafrost in southern Norway in comparison with high-relief alpine areas like the Alps, and then discusses the influence of permafrost on gravitational and glacial–geomorphological processes. The basis for the paper is a regional-scale distribution model of mountain permafrost in southern Norway, which is analysed in relation to topographic variations within the same area. The model allows a crude extrapolation to past and future permafrost distribution, which is discussed in relation to geomorphic processes.

© 2002 Elsevier Science B.V. All rights reserved.

Keywords: Permafrost; Slope forms; Glaciers; Scandinavia; Norway; Sediment transport

1. Introduction

The presence of permafrost influences a majority of the surface processes taking place in mountainous environments and is therefore an important regulating factor for the geomorphological process pattern in these environments. Another regulating factor is the topography. Topography varies with space but is, in the time perspective considered here, relatively time invariant. Permafrost distribution varies with both time and space. The types of processes taking place and their relative importance will change with changes in the

permafrost distribution, but one may expect that the morphological signal of permafrost is dependent also on the type of topographic shape of the mountain region the permafrost is covering. Compared with lower latitude mountain regions, e.g. the Swiss Alps, high-mountain permafrost areas in southern Norway display an almost absence of permafrost creep features such as rock glaciers (Sollid and Sørbel, 1992).

The basis for the study is a digital elevation model (DEM) with 500-m ground resolution (©Norwegian Mapping Authorities), and a regional empirical model of permafrost distribution (Etzelmüller et al., 1998; Hoelzle et al., 2001) describing the lower limits of mountain permafrost in southern Norway with 1000-m ground resolution. The model uses a digital map of mean annual air temperature (MAAT) derived by Tveito and Førland (1999) to construct a quadratic

* Corresponding author. Department of Physical Geography, University of Oslo, P.O. Box 1042 Blindern, N-0316 Oslo, Norway.

E-mail address: bernd.etzelmuller@geografi.uio.no (B. Etzelmüller).

trend surface through altitude points showing MAAT of about $-4\text{ }^{\circ}\text{C}$. The use of MAAT as a major modelling variable is justified by site investigations in the Jotunheimen and Dovrefjell area of southern Norway (Fig. 1), showing that radiation plays only a minor role on permafrost distribution (e.g. Ødegård et al., 1996, 1999; Isaksen et al., 2002) in these locations. With this assumption, the trend surface could be shifted for simulation of warming or cooling trends of the MAAT. The results were validated by Bottom Temperature of

winter Snow cover (BTS, Haerberli, 1973) measurements and DC-resistivity soundings in various locations in southern Norway. Varying snow conditions are not considered in the model, which certainly introduces an error. However, within the accuracy and scale of this model (ground surface resolution of 1000 m and altitude accuracy of $\pm 80\text{ m}$; Etzelmüller et al., 1998), the results are assumed to reflect the main pattern of permafrost distribution, both at present and during periods of higher or lower MAAT.

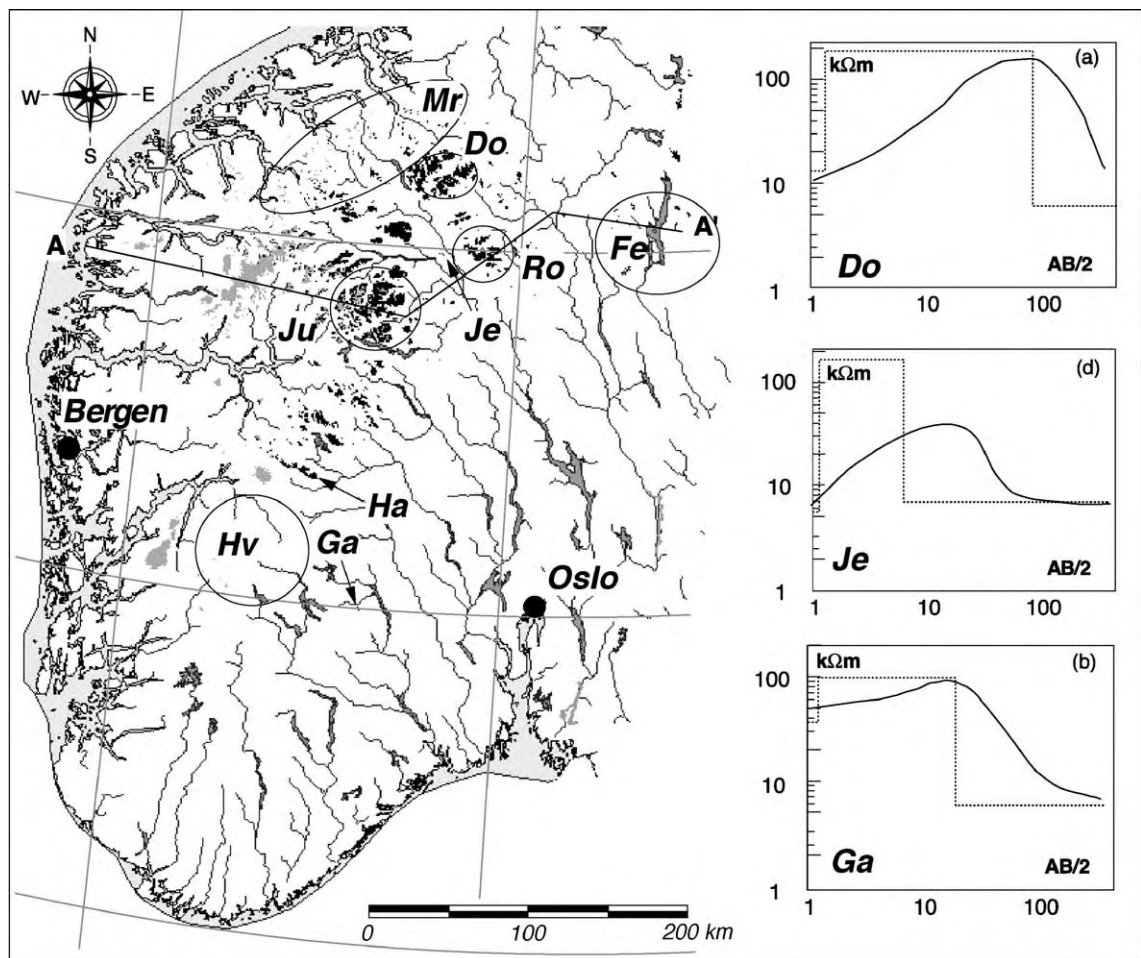


Fig. 1. The distribution of alpine permafrost in southern Norway. Probable permafrost area in dark shading, recent glacier coverage in grey shading. The solid line shows the profile line displayed in Fig. 3. The method of deriving permafrost areas used for southern Norway is described in Etzelmüller et al. (1998). Ju = Juvvass/Galhøpiggen, Je = Jetta mountain, Ga = Gaustatoppen, Do = Dovrefjell, Fe = Femund–Sølen, Ha = Hallingskarvet, MR = Møre and Romsdal, Hv = Hardangevidda. The diagrams show selected one-dimensional DC-resistivity soundings on different locations, indicating permafrost sites. The dashed line in the diagram shows a probable interpretation of the curves, resulting in a three-layer model defining thickness and resistivity of the subsurface.

The objective of the paper is to review and discuss the significance of permafrost on glacial and gravitational processes in high-latitude areas of southern Norway on a regional scale. The influence of permafrost on these processes is related to the presence of permafrost relative to the glacier equilibrium line, and to the topographic shape of the landforms. This paper aims to quantify these relationships and partly compare the results to high-relief alpine areas. The aim is reached by combining the modelled permafrost areas with topographic information and the glacier areas, all on a regional scale. This allowed the analysis of permafrost distribution in relation to changing climatic conditions, glacier equilibrium line altitudes and topographic regions in southern Norway. The analysis was expected to result in a better understanding of geomorphological process and landform pattern connected to mountain permafrost distribution.

2. Permafrost limits and relict permafrost in southern Norway

Alpine permafrost in Norway has been recognised since the turn of the last century. Reusch (1901) found permafrost in Lyngen in northern Norway at 750 m a.s.l. and recognised permafrost as being a normal phenomena at high altitudes in northern Norway. He also suggested that the inner parts of the Finnmarkvidda were underlain by permafrost. During the 1950s, deep permafrost was discovered on Gaustatoppen (1883 m a.s.l.), southern Norway, during construction work of a military radio station (Dons, personal communication 1995). Williams (1959) suggested that a MAAT of about $-4\text{ }^{\circ}\text{C}$ was necessary under Scandinavian conditions for widespread permafrost. Liestøl (1965) reported of sporadic permafrost patches as low as 300 m a.s.l. in blocky material near Otta in Gudbrandsdalen valley east of Jotunheimen, southern Norway. First, quantitative mapping approaches were carried out by Barsch and Treter (1976), King (1983, 1986) and Harris and Cook (1988) in the Jotunheimen and Rondane area, using BTS measurements, seismic refraction and DC-resistivity soundings. Both King (1984) and later Ødegård et al. (1996) presented permafrost maps, based on a proposed boundary of $\text{MAAT} = -4\text{ }^{\circ}\text{C}$ as the lower altitude limit of alpine permafrost. In the Dovrefjell and Jotunheimen areas,

southern Norway, Ødegård et al. (1996, 1999), Sætre (1997) and Isaksen et al. (2002) showed that BTS values could possibly be explained mainly on the basis of altitude, while radiation is of minor importance. This is in contrast to the situation in the Alps where radiation is considered to be more important (Hoelzle, 1992, 1996; Gruber and Hoelzle, 2001).

Recent studies about permafrost (e.g. within the Permafrost and Climate in Europe, PACE, project, Harris, 2001; Harris et al., 2001) have provided increased knowledge of permafrost thickness and spatial distribution in southern Norway (Isaksen et al., 2001) and Svalbard (Isaksen et al., 2000). In Jotunheimen, southern Norway (borehole depth 129 m), and at the Tarfalaryggen, northern Sweden (borehole depth 100 m), permafrost thickness seems to be more than 300 m at 1890 and 1600 m a.s.l., respectively (Sollid et al., 2000; Isaksen et al., 2001). These boreholes showed low-temperature gradients, indicating a severe warming of the permafrost during the last decades (Isaksen et al., 2001). Comparable boreholes in the Alps displayed a similar trend (Harris et al., 2001). In southern Norway, permafrost depth is known from the construction of an elevator inside Gaustatoppen (1883 m a.s.l.). Ice-rich permafrost was discovered above 1600 m a.s.l., and DC-resistivity soundings indicate permafrost below 1500 m a.s.l. on the slopes of this mountain. The permafrost thickness is about 250 m, with a present MAAT on the top of the mountain of $-4\text{ }^{\circ}\text{C}$. Together with the results from the PACE-drillings in permafrost, this indicates much thicker permafrost in European

Table 1
Area of permafrost in southern Norway according to the map published by Etzelmüller et al. (1998)

	Probable permafrost (km ²)	Glacier area (km ²)
Present situation according to model	2800	1600
One degree cooling of MAAT ("LIA situation")	6600	>2000
One degree warming of MAAT ("climate warming situation")	1000	?

The estimates are conservative and do not include areas with patchy permafrost distribution, permafrost under snow patches or permafrost related to palsa mires. The glacier area is estimated based on the N1000-map published by the Norwegian Mapping Authorities. The glacier area for the LIA situation is a crude estimate based on the fact that many glaciers in southern Norway have been reduced in size by about 30% since the LIA maximum.

mountains, in general, than assumed earlier (cf. Ødegård et al., 1992).

Mountain permafrost in southern Norway is mainly concentrated in a 50–100-km-wide zone between Hallingskarvet in the south (Fig. 1) and the Dovrefjell mountains in the north (Fig. 1). According to the model, only small areas east and west of this zone have permafrost. On the western side, glaciers normally cover high-mountain areas. Furthermore, the lower permafrost limit rises to over 1600 m a.s.l. due to increasing maritime influence. Thus, there are few areas where permafrost can exist. On the eastern side of this zone, only small mountain areas or single peaks reach altitudes above 1400 m a.s.l. In the eastern areas, these peaks seem to have permafrost. Preliminary results of a permafrost-distribution modelling applied

for the whole Scandinavia and new field investigations indicate even lower alpine permafrost limits down to below 1200 m a.s.l. in the Femund–Sølen area (Fig. 1). The lower limit increases again towards east, possibly due to the climate influence of the Botnian Sea. Recent permafrost field mapping seems to confirm that pattern (Heggem et al., in press). The transition zone of the mountain permafrost might be broad. At Snøhetta/Dovrefjell the zone is located between 1480–1340 m a.s.l. (Sollid et al., in press).

The present extent of highly probable permafrost areas is approximately twice that of the glaciated area (Table 1). Assuming a 1 °C colder situation, the area of probable permafrost was more than doubled during the Little Ice Age (LIA) (Fig. 2a, Table 1). Large areas have probably been subjected to permafrost thaw since the

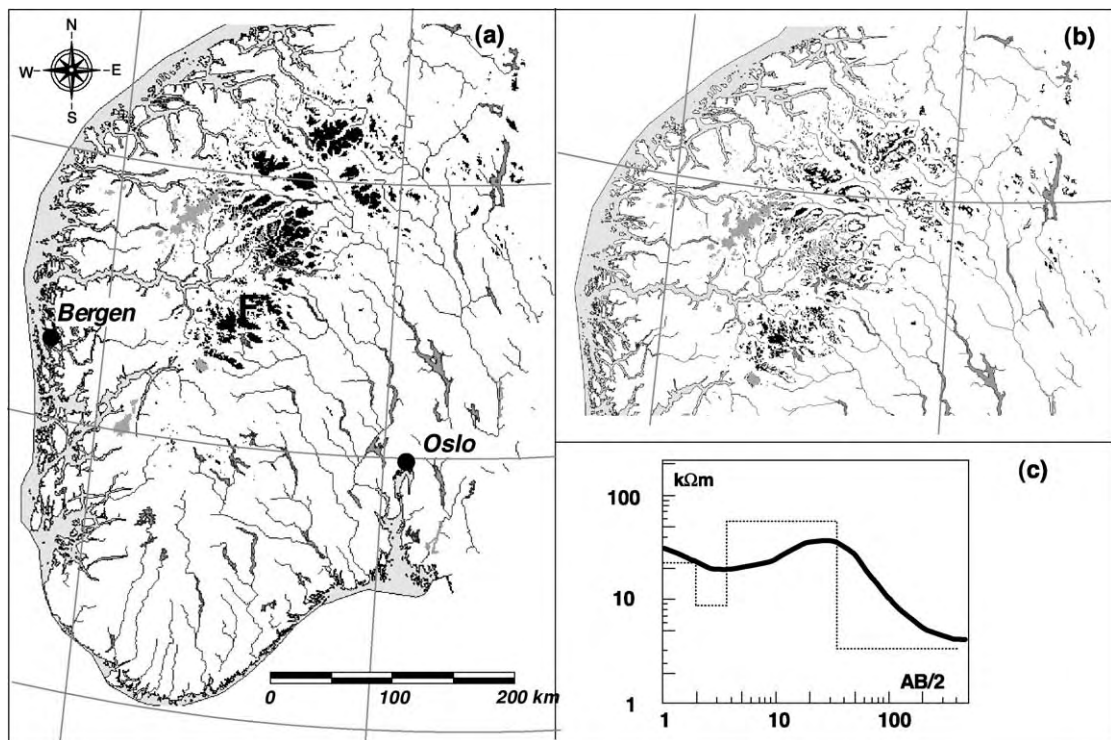


Fig. 2. (a) Estimated distribution of alpine permafrost for a 1 °C cooler scenario, which may have prevailed during the Little Ice Age (LIA) (dark shading in the map). The trend surface was here shifted down slope with 150 m. This number is in accordance with numerical modelling from other areas in Fennoscandia (e.g. Kukkonen and Safanda, 2001). (b) Areas, which are modelled to have been in the permafrost zone during the LIA-scenario, and are not supposed to lie in the permafrost zone during present climate conditions (black shading in the map). These areas are believed to be under permafrost degradation, and may contain considerable areas with relict permafrost. Grey shading denotes recent glacier coverage in both maps. The DC-resistivity diagram (c) show an example from the western Jotunheimen Mountains (Hurrungane). The dashed line in the diagram shows a probable interpretation of the curves, resulting in a four-layer model defining thickness and resistivity of the subsurface.

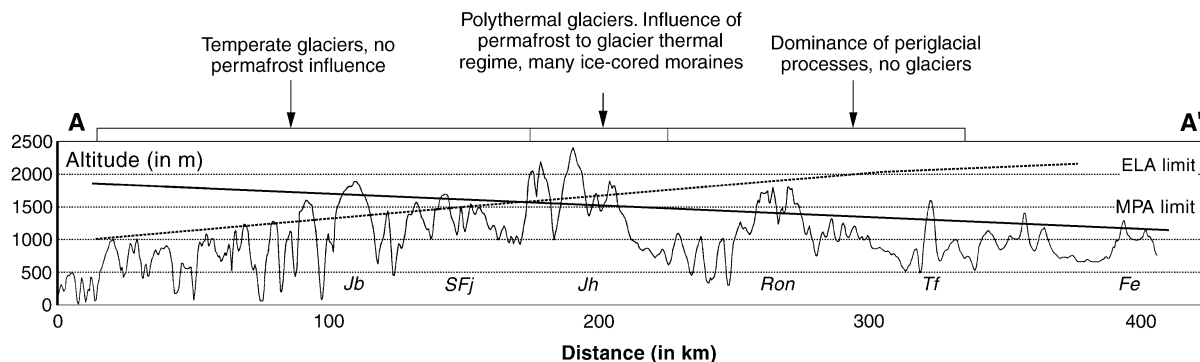


Fig. 3. Profile through southern Norway (A–A', Fig. 1) including the lower altitude of mountain permafrost (MPA) according to the model published by [Etzelmüller et al. \(1998\)](#) and the limits of the ELA. A spatial distribution of the ELA in southern Norway was generated based on an ELA contour map published in [Liestøl \(1994\)](#). The map was digitised and a DEM was constructed using [Hutchinson \(1989\)](#) interpolation algorithm. The profile is interpreted to distinguish three major morphogenetic zones in relation to glacial and periglacial processes. Jb = Jostedalsgreen glacier, SFj = Sognefjellet mountains, Jh = Jotunheimen, Ron = Rondane mountains, Tf = Tron mountain, Fe = Femund mountains.

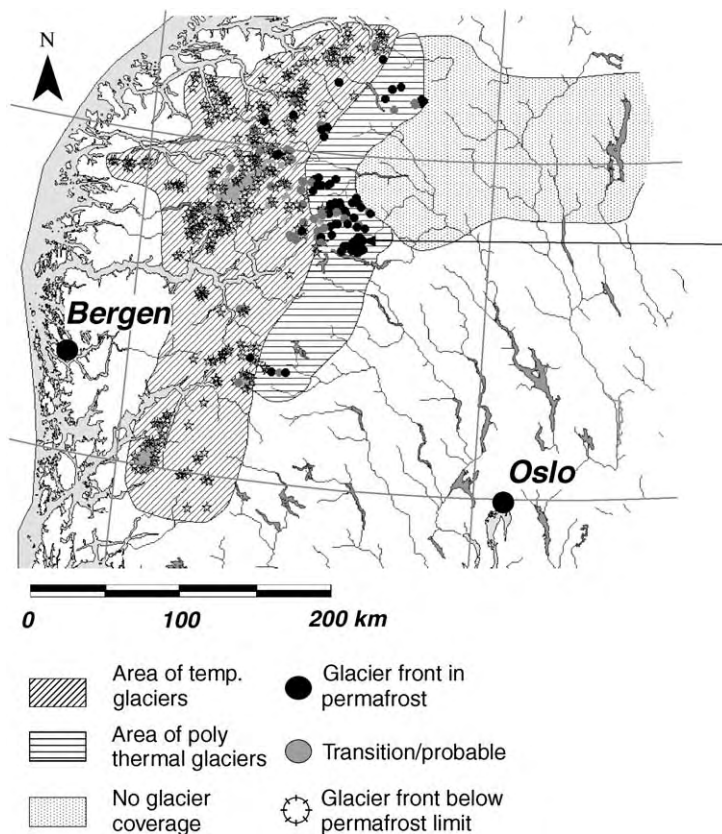


Fig. 4. The possible areal extent of the morphogenetic zones defined in Fig. 3. The point labels denotes the position of recent end moraines in southern Norway. The label signature indicates whether the moraines are situated within the permafrost zone or not, according to the MAAT-based permafrost distribution model. The area signature indicates the morphogenetic regions. The spatial difference was calculated on a cell-by-cell basis using a data set containing the lower altitude of mountain permafrost (MPA) and a data set of the ELA. In the western areas, $MPA - ELA > -50$, the central areas, $MPA - ELA \in [-50 - 300]$ and in the eastern areas, $MPA - ELA < -300$.

LIA (Fig. 2b). As the change of ground temperatures and the eventual melt-out is a slow process due to the damping and delay of surface temperature signals and latent heat effects (Lachenbruch et al., 1988; Williams and Smith, 1989), we can assume relict permafrost in parts of these areas. Several DC-resistivity soundings in this zone (Department of Physical Geography, University of Oslo, unpublished data) indicate thick low-resistivity layers over high-resistivity layers, which are interpreted as possible degrading permafrost (Fig. 2b,c). Ødegård et al. (1996) suggest relict permafrost to exist in Jotunheimen based on resistivity measurements. Isaksen et al. (2002) found signals of upper ground warming in permafrost by temperature measurements in a borehole in Jotunheimen and by resistivity measurements on Dovrefjell.

3. Permafrost limits and equilibrium line altitudes of glaciers

In southern Norway, the lower limit of mountain permafrost altitude (MPA) decreases towards east, while the equilibrium line altitude (ELA) of the glaciers increases in the same direction (Fig. 3), a pattern already proposed by King (1986). We can distinguish here a transition from predominance of glacial processes to predominance of permafrost-related processes (Fig. 4).

In the near and high-altitude regions of the western coast, the ELA is lower or close to the MPA. In these areas, the temperate glaciers are situated (Østrem and Haakensen, 1993). Permafrost may exist on slopes around the accumulation area of the glaciers; however, many of the glaciers are plateau glaciers (Østrem and Haakensen, 1993) where permafrost thus have limited influence. The glacier tongues always end below the MPA. Cold firn areas like those known from high areas in the Alps (cf Suter et al., 2001) probably do not exist in the western parts of southern Norway.

In an intermediate, relative narrow zone ranging from central Dovrefjell to central Jotunheimen, the MPA lies well-below the ELA (Figs. 3 and 4). Here, glaciers and permafrost coexist and most likely affect the temperature regime of the snout of many glaciers. In this area, the ice-cored moraines early studied by Østrem (1964) are situated, indicating

the presence of permafrost at the glacier front altitudes. Further east, the ELA is above most of the mountain peaks, and thus permafrost dominates at high altitudes.

4. Permafrost limits and topographic regions

4.1. Spatial distribution

The quantification of elevation data is included within the field of geomorphometry (Pike, 1995), and based on the quantitative analysis of topographic parameters. The topographic parameters related to this concept are normally estimated on the basis of altitude matrixes. In our case, a digital elevation model with a 500-m ground resolution was used. In this part of the study, point parameters are calculated for a single location based on its nearest neighbours. The basic parameters are the *altitude* itself, *slope/aspect* and

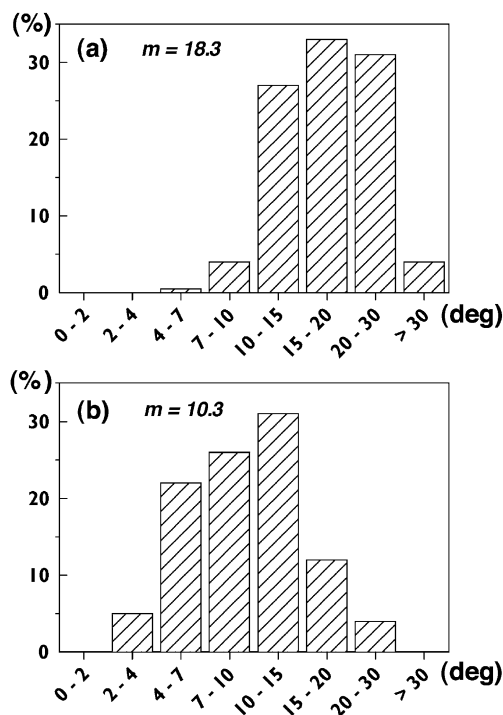


Fig. 5. Slope distribution in permafrost areas for Switzerland (a) and southern Norway (b). The permafrost information from Switzerland is based on Keller et al. (1998).

curvature. The latter is the first and second derivatives of *altitude*, respectively. From these, other parameters are derived, such as statistical measures (e.g. *altitude skew*), relief and hypsographic measures (Evans, 1972; Mark, 1975).

For comparative reasons, the same set of parameters were calculated for southern Norway and the

Swiss Alps. In the first step, the frequency distribution of topographic slope within probable permafrost regions was analysed for these areas (Fig. 5). There are clear differences between the situation in Switzerland and southern Norway. This pattern displays the abundance of low-relief (“paleic”) mountains and plains in the Scandinavian Mountains (e.g. Reusch,

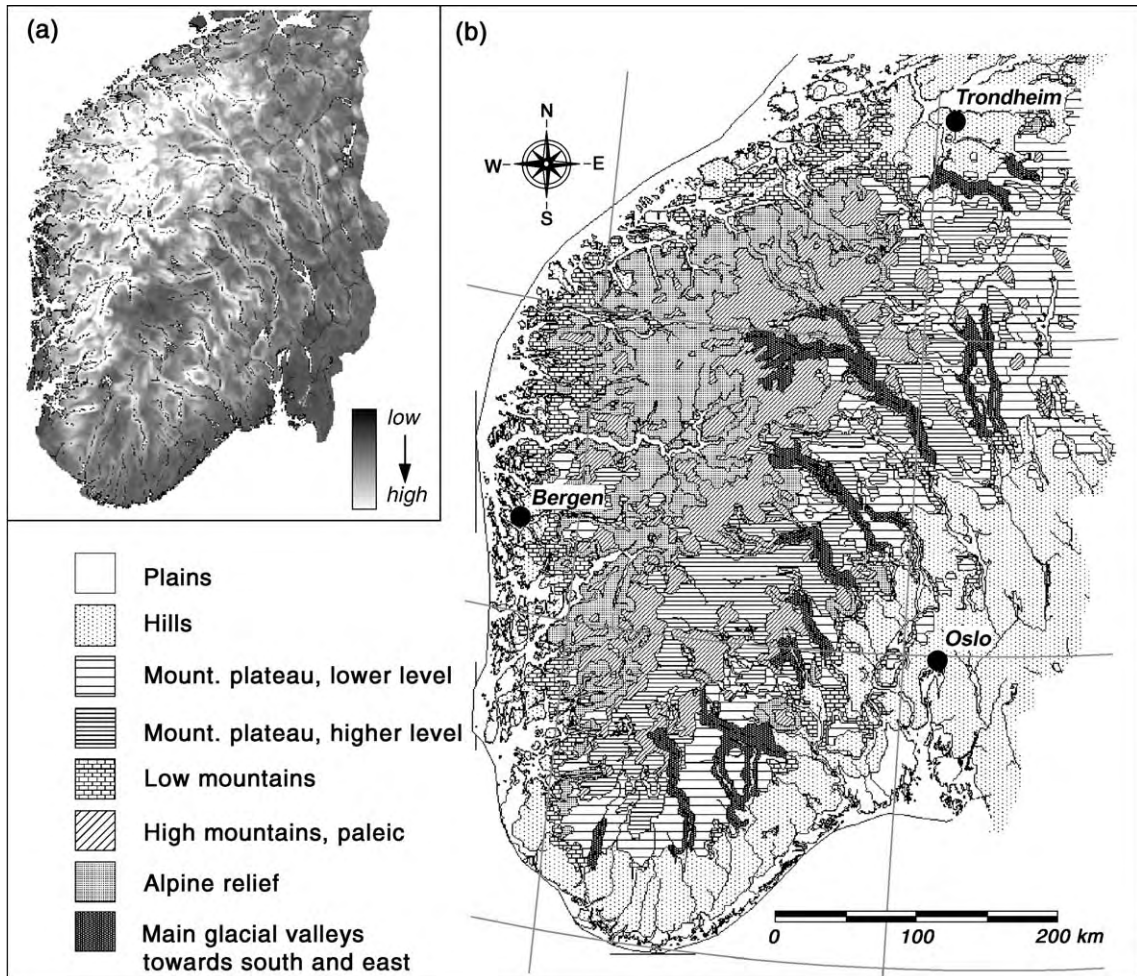


Fig. 6. (a) Distribution of topographic roughness in southern Norway. The topographic roughness map is produced using a digital moving window technique. For each cell position of the DEM, the standard deviation of altitude within a circular window kernel with a 5-km radius is calculated. (b) Topographic regions of southern Norway established based on an automatic, multivariable regional relief classification. The classification is based on a combination of altitude, surface roughness and altitude mass distribution. These are the first three moments of altitude (mean, standard deviation and skewness), which describes the regional aspect of topography. The parameters were calculated as a moving window operation, where the circular window had a radius of 5 km. First, a contextual classification was performed. The contextual classification (cf. Friedrich, 1996) merges classes in the spatial domain using their attribute characteristics. The algorithm starts with as much classes as cells within the study area. Classes are then merged based on similarities of neighbouring cells within the attribute domain. An ISO-cluster algorithm then merges these classes to larger entities.

1901; Gjessing, 1967). In general, really steep alpine topographic settings are rare within the permafrost realm in southern Norway. Only in the Møre Romsdal area of the northwestern part of southern Norway, a fully developed alpine relief exists. However, the terrain is above the lower mountain permafrost boundary only in few locations.

A relief classification was carried out with the parameters *altitude*, *altitude standard deviation* and *elevation–relief ratio*. From this classification, eight major topographic regions were identified (Fig. 6), showing the areal predominance of medium- to low-relief topography in the central and eastern

parts of southern Norway. Comparing these results with the modelled permafrost distribution, high-alpine relief represents only 17% of the total permafrost area. Based on these considerations, four major types of permafrost regions were identified (Fig. 7):

4.1.1. The northwestern part of southern Norway

This area consists of alpine landforms with a pronounced relief. The highest peaks reach altitudes of 1800 m. Permafrost patches do exist in some top areas and covers approximately 4% of the modelled permafrost area.

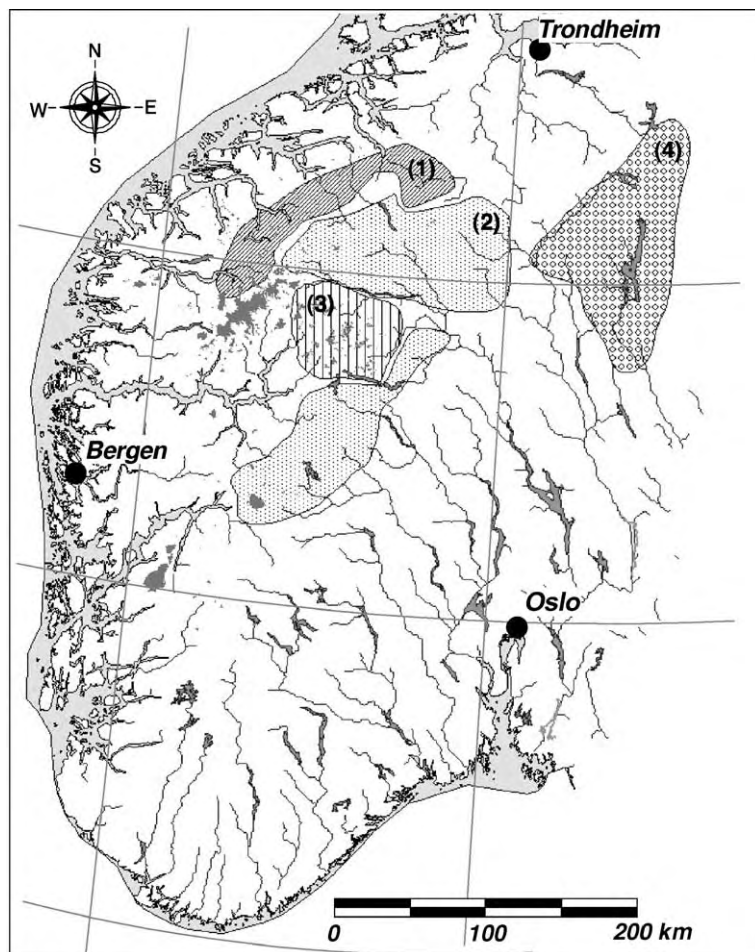


Fig. 7. The major permafrost regions in southern Norway. (1) The northwestern part of southern Norway, (2) the central high-mountain area, (3) the central glacierized high-mountain area of Jotunheimen and Breheimen, and (4) the mountain plateaux.

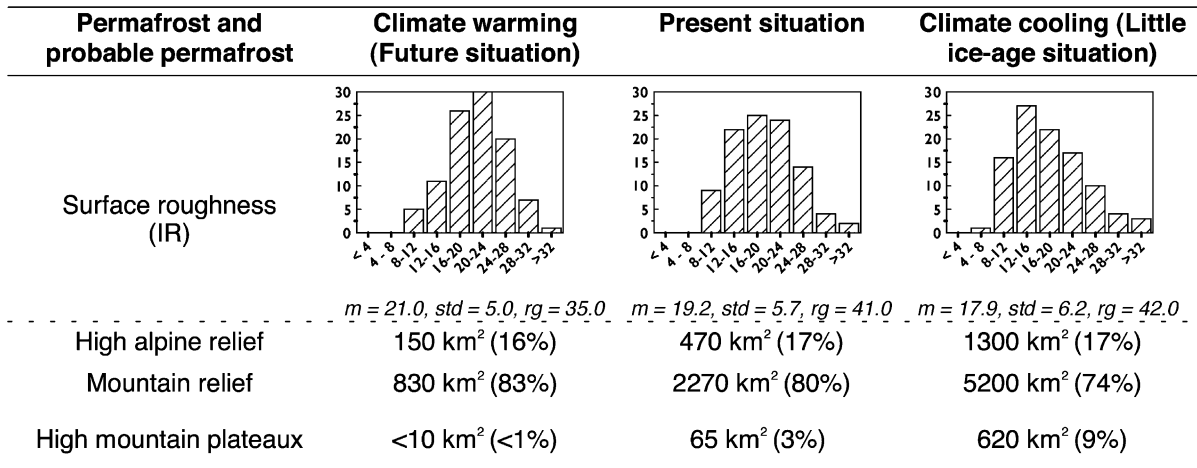


Fig. 8. Probable mountain permafrost areas seen in relation to topographic surface roughness and topographic regions according to the relief classification shown in Fig. 6b. IR is the roughness index, defined as $R = \sqrt{(\sum X_i)^2 + (\sum Y_i)^2 + (\sum Z_i)^2}$ and $IR = 1 - \frac{R}{n}$ with $X = -\sin y \sin a$, $Y = \cos y \sin a$ and $Z = \sin a$, with y and a being *aspect* and *slope*, respectively. n is the number of samples in the calculation. m = mean, st = standard deviation, rg = range.

4.1.2. The central glacierised high-mountain area of Jotunheimen and Breheimen

In this area, both alpine relief forms and larger areas with paleic surfaces are present. Permafrost is widespread both in top areas and in smaller intermountain plateaux. In this area, glaciers and permafrost coexist. This region covers approximately 35% of the total permafrost area.

4.1.3. The central high-mountain area

This area is dominated by paleic relief forms and covers the mountain areas of Dovrefjell, Rondane, Kjølénfjellet and Hallingskarvet. The mountains have larger mountain plateaux, medium relief and are dissected by deep glacial valleys draining towards east. The area is partly influenced by present or former cirque glaciation, and the region covers approximately 56% of the total modelled permafrost area.

4.1.4. The mountain plateaux

This area is dominated by flat mountain plateaux, containing scattered mountain massifs. It is found mainly in the eastern part of southern Norway, but includes also the southern rim of Hardangervidda. Permafrost is found on top of these scattered mountain massifs, such as Gaustatoppen. Scattered degra-

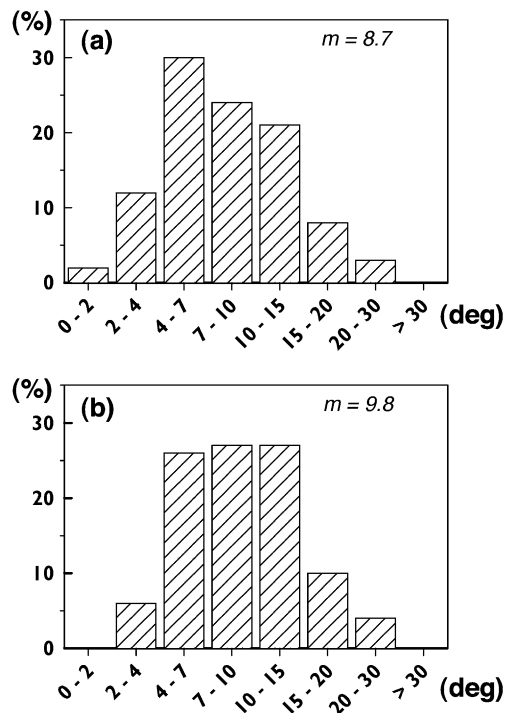


Fig. 9. Slope distribution for areas potentially under degradation since the LIA (a) and potential future degradation due to climatic warming (b). The graph axes denotes slope in degree and percentage of total area. m = mean value of slope (in degree).

ciated cirques are found. Permafrost coverage in relation to the total permafrost area is estimated at 4%.

4.2. Effect of climate change

The distribution of topographic characteristics for the permafrost areas modelled for different climatic settings were analysed (Figs. 8 and 9), only considering MAAT variation. According to this approach, much possible degradation of permafrost has taken place in low-relief areas. Permafrost recently covering flat mountain plateaux may degrade completely during further climatic warming. This means that permafrost has become more restricted to higher-relief areas since the LIA. The exception to this pattern is the alpine areas in the northwestern part of southern Norway (Møre og Romsdal, Fig. 1). In this high-relief alpine area, permafrost always has been restricted to steep slope settings, comparable to the conditions described, for, e.g. the Swiss Alps.

5. Implications of the permafrost distribution on geomorphological processes—a discussion

5.1. Glacial processes

5.1.1. Spatial pattern

Glacier tongues ending on land in a permafrost environment are most probably cold-based, and these glaciers normally have a cold or polythermal temperature regime (cf. Liestøl, 1969, 1977). Polythermal glaciers display a frontal ice-compression zone with shear planes due to the rapid decrease of glacier velocity caused by the reduction of basal sliding towards the glacier front (cf. Weertman, 1961; Boulton, 1972; Hooke, 1973). Cooler ice reduces surface velocities and mass flux, and the restricted basal sliding reduces the influence of subglacial erosion. This results in a characteristic process pattern at the glacier front, with respect to debris entrainment and sedimentation (Fig. 10). In many valley and cirque glacier settings, there is an increased relative importance of external

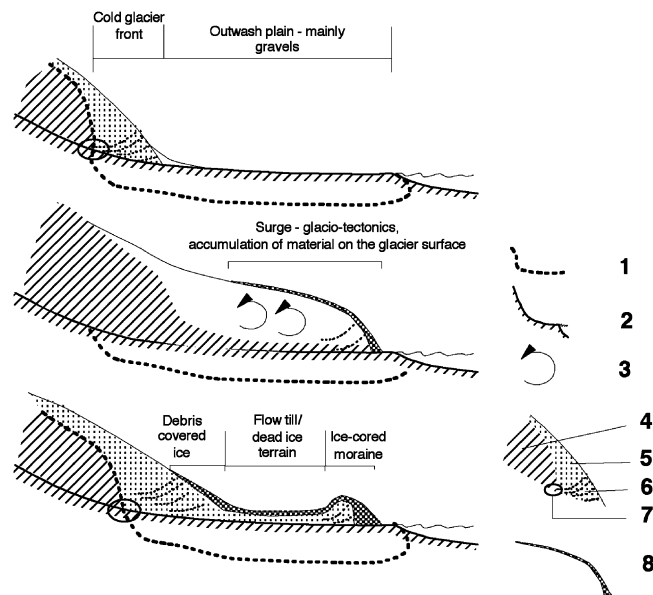


Fig. 10. Principle development of glacier marginal landforms (ice-cored moraines) in permafrost as observed on Svalbard (from Etzelmüller et al., 1996) under the condition of an advance of the glacier over bedrock or frictional, nondeformable sediments. (1) Base of permafrost. (2) Bedrock. (3) Deformed ice during an advance/surge, glacio-tectonical processes. (4) Temperate ice, at the pressure melting point. (5) Cold ice. (6) Shear zone and/or englacial material bands. (7) Transition zone between net melting and net freezing in the sense of Weertman (1961) and Boulton (1972). In this zone, onfreezing of subglacial sediments may take place. Transport of material towards the surface. (8) Debris covered glacier front, material cover preserving underlying glacier ice.

debris input in relation to subglacial material production. In addition, the transition between temperate and cold-based ice favours onfreezing of subglacial sediments, and englacial transport processes relative towards the ice surface in connection to the ice-compression zone (Weertman, 1961; Boulton, 1972). This process causes accumulation of often coarse-grained or even sorted debris in and on the glacier tongue, and leads to the buildup of ice-cored moraines due to accumulation of debris. During glacier advances, stresses from the glacier can be transmitted in the permafrost package over longer distances, resulting in large-scale push moraines (composite ridges) in the glacier marginal distal zone (cf. discussion in Bennett, 2001). Contemporary long retreat phases result in partly down-wasting of ice-underlain glacier marginal zones, resulting in thermokarst features (Sollid and Sørbel, 1988; Etzelmüller, 2000; Lyså and Lønne, 2001).

This pattern is mainly described from polythermal glaciers in the high-Arctic like on Svalbard (Sollid and Sørbel, 1988; Etzelmüller et al., 1996; Hart and Watts, 1997; Boulton et al., 1999; Lyså and Lønne, 2001) and the Canadian Islands (Kälin, 1971; King and Hell, 1993; Bennett, 2001). However, also in southern Norway, a different moraine morphology is described for glaciers ending at higher altitudes than for the temperate western glaciers (Østrem, 1964; Haeberli, 1979). An example is Midtdalsbreen in the Finse area of southern Norway, a temperate outlet glacier of the Hardangerjøkulen ice cap (Sollid and Bjørkenes, 1977). Here, geomorphological indications and thermistor measurements have shown that the lowermost, up to 20 m thick, area of the glacier front is cold-based (Liestøl and Sollid, 1980; Bø, 1992; Konnestad, 1996). Annual moraines built up since the 1960s show clear melt-out of frozen subglacial layers, and an asymmetric moraine morphology (Andersen and Sollid, 1971). Matthews et al. (1995) describe a similar process in front of Styggedalsbreen, western Jotunheimen.

In southern Norway, the large-scale ice-cored moraines are frequent, especially in the Jotunheimen area (Østrem, 1964) and around the Snøhetta massif in Dovrefjell, indicating permafrost conditions in these areas. To the authors' knowledge, no recent special studies do exist so far explicitly relating the glacial thermal regime to moraine morphology in southern Norway.

5.1.2. Temporal pattern

During the cooler LIA period, more permafrost were probably present (Fig. 2a); however, also the glacier tongues were larger, reaching further down slope. Recent studies estimate the decrease of the ELA in different regions of southern Norway, with numbers varying from more than 100 m on Hardangerjøkulen, western Norway (Dahl and Nesje, 1996), to 70 and 25 m at Storbreen and Leirbreen, respectively, in Jotunheimen (Matthews et al., 2000).

With glacier retreat due to climatic warming or changing winter precipitation pattern, the thermal regime of a glacier may change, resulting in a different glacial–geomorphological process pattern. Originally, temperate glaciers retreating into the marginal permafrost zone will develop partly cold glacier tongues. An example is again Midtdalsbreen, displaying a different moraine morphology between recent moraines and LIA moraines (Andersen and Sollid, 1971; Sollid and Bjørkenes, 1977). Polythermal glaciers that are thinning may become cold-based. Examples of this pattern are reported from Svalbard (Hodsen, 1994; Björnsson et al., 1996).

In many areas, permafrost may have been built up in the glacier marginal zones during glacier retreat. The larger glaciers in Jotunheimen ended below the permafrost limit during the LIA, and do now retreat into the permafrost zone. This leads to the buildup of new permafrost in the marginal zone of formerly temperate glaciers. An example is the glacier Memurubreen in central Jotunheimen, where a detailed geomorphologic map exists (Erikstad and Sollid, 1990). The map shows that fluted surface is found up to 1700 m a.s.l., indicating temperate subglacial conditions. Today, these areas lie in the zone of highly probable permafrost, and ice-cored moraines are present at the glacier margins. This process pattern has been observed and mapped in glacier marginal areas by Kneisel (1999). Permafrost aggregation in recently deglaciated terrain changes the process pattern and the geotechnical properties in the area.

5.2. Slope processes

The topographic analysis in relation to modelled permafrost distribution indicates a dominance of relatively low-relief areas affected by permafrost in southern Norway. These patterns are obviously in

contrast to high-relief alpine areas, affecting the pattern of permafrost-related slope processes and, thus, landscape development in southern Norway.

5.2.1. Spatial pattern

Rockfall is a commonplace process in Norway, influencing most areas and causing distinct problems with respect to damages on transport infrastructure. Regional maps of geomorphology and Quaternary geology (Sollid and Kristiansen, 1982; Kristiansen and Sollid, 1985; Sollid and Trollvik, 1991) as well as detailed maps (Sollid and Carlson, 1979; Sollid and Sørbel, 1979b; Sollid et al., 1980) indicate that taluses are not particularly well-developed in the main areas of permafrost distribution in southern Norway. In the northwestern part of southern Norway, the areas of talus accumulation are mainly below the permafrost distribution, while steep mountain walls in the Jotunheimen–Breheimen areas mostly are associated with present cirque or valley glaciers. It must be anticipated that the extraglacial material input from slope processes constitutes an important part of the total sediment production within alpine glacier catchments. Effects of snow avalanches often modify the talus slopes found in this area. The main areas for talus development within permafrost in southern Norway are thus deglaciated cirques in the central high-mountain area and structurally determined mountain walls such as along the edges of nappes that overlie softer rocks. The Rondane area is an example of the first situation, and the slopes along the Hallingskarvet mountain massif of the second. To the authors' knowledge, there is no consensus on how permafrost influences rockfall activity. The potential for frost weathering should generally increase, as long as water is available at the surface (Hallet, 1983; Ødegård and Sollid, 1993; Ødegård et al., 1995).

Debris flows are generally a common phenomenon in southern Norway, especially in the western areas (Blikra and Nemeč, 1998). Within the permafrost regions, however, they are not particularly usual. In Jotunheimen, they seem to develop beneath the regional permafrost limit. A study from the valley Visdalen in central Jotunheimen indicates that the starting zone of the debris flows in the area seems to be situated close to the permafrost limit (Sørli, 2002). The lack of debris flows on permafrost may be attributed to the generally thin or lacking material

cover on the steeper slopes in these areas. Also, in terrain positions where debris flows normally would tend to develop, slush flows are very common and probably dominant with respect to frequency, local form development and sediment transfer. Sandersen (1997) notes that in the continental parts of Norway, debris flows are either caused by intense snowmelt on unfrozen ground or by convective rainstorms. Thus, conditions leading to debris flows elsewhere might induce slush flows on permafrost. This is due both to a low potential for meltwater infiltration into soil, and to refreezing of meltwater within the snow pack and at the snow/ground interface, which retains water on permafrost slopes until late in the melt season when rapid melting can be expected.

Rock glaciers in the sense of creeping permafrost (Haeberli, 2000) are not common in southern Norway (Sollid and Sørbel, 1992). Although a few examples of smaller permafrost creep features generally can be found (e.g. Sollid and Kristiansen, 1984), rock glaciers are only common in the Rondane area (Barsch and Treter, 1976), where also talus slopes are best developed.

Large rock avalanches and rockslides have been mapped at a large number of locations both in northern and southern Norway (Blikra and Anda, 1997). A number of these have originated in areas where permafrost may have been present. Jonasson et al. (1997) suggest that many such incidents in the north Swedish and the Norwegian mountains may have been triggered in late glacial times. Although such events generally have a complex origin, permafrost may be one of several important factors for their release by its influence or control on rock joint shear strength (Davis et al., 2001). The rock avalanche deposits are sometimes difficult to distinguish from rock glaciers, especially where they are deposited on permafrost (Barsch and Treter, 1976; Dawson et al., 1986).

The described pattern of slope forms that can be related to permafrost presence or degradation seems to reflect the topographical setting and the abundance of permafrost in low-relief mountain areas. A further reason is displayed in the spatial distribution of surficial deposits in the high-mountain areas of southern Norway. The oldest cover deposits are probably the *blockfields* (cf. Sollid and Sørbel 1979a; Sollid and Kristiansen, 1982; Nesje et al., 1988; Sollid and Trollvik, 1991; Dahl, 1992; Follestad, 1995). A pre-

glacial age of these deposits has been suggested, based on vegetation successions (Dahl, 1956); warm-climate, clay-weathering remnants (Dahl, 1954; Roaldset et al., 1982; Rea et al., 1996); and a regional distribution above glacial trimlines in west coastal areas (Sollid and Sørbel, 1979a; Sollid and Reite, 1983; Nesje et al., 1988) or in areas of possible landscape preservation beneath cold-based part of the inland ice sheet (Sollid and Sørbel, 1982, 1994; Nesje et al., 1988). Apart from the blockfields in top areas and colluvium found on scree slopes and talus, the cover deposits seem to be mainly thin and discontinuous in high-relief permafrost regions (Sollid et al., 1980; Sollid and Kristiansen, 1982; Kristiansen and Sollid, 1985; Sollid and Trollvik, 1991).

5.2.2. Temporal pattern

The effect of the variation of permafrost distribution and thickness during time on slope processes must be addressed at different time scales. We consider here only the Holocene, which did become gradually cooler from the warm Atlanticum towards the LIA, with a clear warming trend during the last century (e.g. Dahl and Nesje, 1994; Nesje et al., 2000).

One of the prime concerns regarding the probable mountain permafrost degradation under climatic warming is the potential for slope stability problems in bedrock and nonconsolidated sediments (Haerberli, 1992). Although climatic warming has been going on since the LIA, the rate of temperature changes has been much faster during the recent decades (e.g. Jones et al., 1999). Nevertheless, the period of general warming since the LIA could provide an analogue for the processes likely to take place under possible future climatic warming. No tendency for enhanced debris flow activity can be noted for this period. Increased debris flow activity in Scandinavia is rather associated with colder periods (Nesje et al., 1994; Matthews et al., 1997). The lack of effect of a warming situation is quite probably caused by the dominance of debris flows below the regional limit of permafrost. On the other hand, much degradation of permafrost since the LIA has probably taken place on low-relief areas. It is likely that new starting zones for debris flows may develop, higher up on mountain slopes, as active layer thickness increase. The most important effect of climate change on debris flow

activity will nevertheless probably be the anticipated increase in magnitude of precipitation events (Frei et al., 1998).

The only area where permafrost degradation since the LIA has mainly involved steep slopes is the northwestern permafrost region. In this area, large rock avalanches represent a threat to human life and constructions (cf. Blikra and Anda, 1997). The frequency of large rock avalanches is too low to conclude on a relationship to climate. The analyses connected to the permafrost-distribution model presented in this study might offer indications that high-altitude peaks in the northwestern part of southern Norway are subject to permafrost degradation.

5.3. The sediment transport system

The processes within the permafrost zone in high-mountain areas are highly heterogeneous. They should be treated as a sediment cascade system of material transport and sedimentation, where the factor-governing processes, activity states and reaction time on changing constraints will vary in time and space (Caine, 1974, 1986; Barsch and Caine, 1984; Caine and Swanson, 1989). The sediment cascades in high-mountain environments are schematically shown in Fig. 11a. In this concept, the processes are parted in a fine sediment system, a coarse sediment system and a glacier system (Caine, 1974; Barsch and Caine, 1984), where, e.g. talus cones, rock glaciers and moraine ridges are important sediment magazines. These sediment magazines store material and may release considerable amounts of debris during changing environmental conditions, as for instance due to permafrost degradation or during a glacial cycle.

Permafrost seems to be an important regulator of this system as described by e.g. Etzelmüller (2000). In temperate glacier catchments, there is a close relationship between the amount and type of sediments (fluxes) and the existence and size of glaciers within the catchment. Most of the sediments produced in the glacier are evacuated by the meltwater, and the amount of sediments during summer decreases despite of increasing discharge (Liestøl, 1967; Østrem, 1975; Collins, 1979; Repp, 1979; Lawsen, 1993). Thus, there is a close relationship between the existence and size of a temperate glacier and sediment flux (Fig. 11b). In permafrost areas, the glaciers are polythermal,

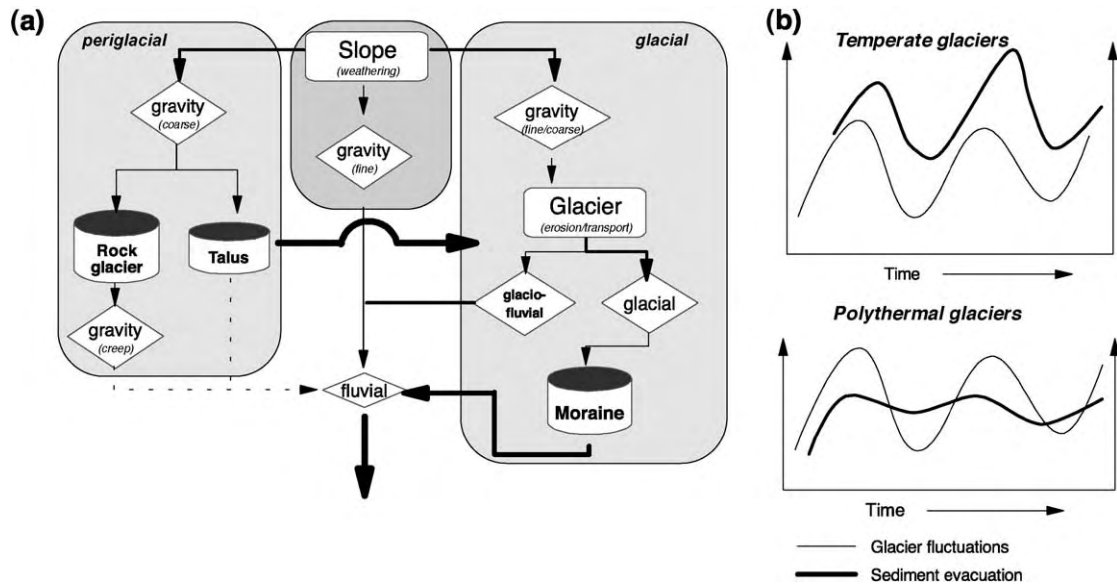


Fig. 11. (a) Conceptual flow chart of the glacial and periglacial particulate material transfer system in arctic glacierized mountains and alpine permafrost areas. The glacial system is an effective transport system, transferring material from the slope to the moraines, which act as sediment magazines. The periglacial slope system is producing sediment magazines, which store material over very long time periods (e.g. rock glaciers). However, coupled with a glacier system, material is effectively removed from the slopes and coupled with the fluvial system. (b) Conceptual illustration of the relationship between glacier variations in time and correspondent particulate material evacuation out of a glacier-dominated catchment. Temperate glaciers show high correspondence between sediment evacuation and glacier activity. In permafrost areas with dominating polythermal and cold glaciers, this signal may be lower and damped.

meltwater discharge is lower, and much erodable material is accumulated under the glacier or in form of ice-cored moraines (Vatne et al., 1995; Hodkins, 1997; Hodsen et al., 1997; Hodsen, 1999; Etzelmüller et al., 2000) and act as a sediment magazine, releasing material also during glacier retreat. Hence, the above-mentioned relationship is locally damped or maybe even reversed in special situations (Fig. 11b). Especially ice-cored moraines play an important role. Material release there is dependent on the removal of material protecting the ice-core. Climate warming increases ice-core melting and thus material release increases from these sediment magazines, while when the glacier retreats and erodes, material production decreases. Thus, glacier variation must not necessarily be in phase with variations in sediment fluxes in permafrost-dominated areas. Actually, small cirque glaciers enhance the periglacial mass-transport system by capturing and transporting material, keeping the slopes steep and active. Even with low erosional potential, cirque and valley glaciers in cold environments have relatively high material transport and

long-term erosion rates measured by meltwater evacuation of solids (Hodsen, 1994; Hallet et al., 1996; Hodkins, 1997). In many cases, the production of the material is predominantly periglacial in a permafrost environment (Etzelmüller et al., 2000).

In previous studies on lake sediments in southern Norway, e.g. on Finse and around Jostedalbreen, the sediment signal in the lake cores indicate very good correspondence between glacier existence and size and the sediment record (Dahl and Nesje, 1994, 1996; Nesje et al., 2000). These glaciers are temperate, such as Midtdalsbreen (Liestøl and Sollid, 1980), and the lake cores allowed a detailed reconstruction of Holocene glacier and thus climate history.

Permafrost seems to conserve sediment magazines in high-alpine environments over longer time periods, affecting sediment output of permafrost-dominated catchments. Sediment magazines are mobilised during permafrost degradation. On the other hand, coarse-material production on slopes due to frost weathering may be enhanced during colder periods (Blikra and Nemeč, 1998; McCarroll et al., 1998, 2001).

6. Concluding remarks

This study reviewed the distribution of mountain permafrost in relation to the topographic setting in southern Norway. On that basis, glacier type and slope-distribution patterns are discussed in relation to permafrost occurrence and its temporal change. From this discussion, the following main conclusions can be drawn:

- Permafrost is predominantly found in non-alpine topography in southern Norway.
- Exceptions are the high-alpine areas of Møre and Romsdal. To the authors knowledge explicit permafrost mapping do not exist in that area so far.
- Sparse sediment cover on steep slopes suggests low permafrost-induced hazards, except for the speculative relationship between large rockslide events and permafrost degradation.

The pattern of increasing ELA and decreasing MPA towards east is assumed to cause a distinct influence of permafrost on sediment transport and thermal regime of glaciers in the central mountain areas.

Acknowledgements

This paper is written based on a presentation held at the 5th International Conference on Geomorphology in Tokyo, Japan, 23–28 August 2001. Parts of the results and observations presented are from the EU-funded PACE project (Permafrost and Climate in Europe, coordinated by Professor C. Harris, Cardiff), headed by Professor J.L. Sollid at the Department of Physical Geography, University of Oslo. Late Professor em. Olav Liestøl (shared professorship) from the same department early realised the importance of permafrost on glacial–geological processes, and his work as glaciologist at the Norwegian Polar Institute (NPI) and teaching at the Department has inspired this paper. Two anonymous reviewers gave constructive comments to an earlier version of the paper. The GIS-work was carried out at the Laboratory for Remote Sensing and GIT at the same department. The temperature and topographic map data were provided by the Norwegian Meteorological Institute (DNMI) and the Norwegian Mapping Authorities (Statens

Kartverk), respectively. We want to thank all contributing persons and institutions.

References

- Andersen, J.L., Sollid, J.L., 1971. Glacial chronology and glacial geomorphology in the marginal zones of the glaciers Midtdalsbreen and Nigardsbreen, Southern Norway. *Nor. Geogr. Tidsskr.* 25, 1–38.
- Barsch, D., Caine, N., 1984. The nature of mountain geomorphology. *Mt. Res. Dev.* 4 (4), 287–298.
- Barsch, D., Treter, U., 1976. Zur Verbreitung der Periglazialphänomenen in Rondane/Norwegen. *Geogr. Ann.* 58A (1–2), 83–93.
- Bennett, M., 2001. The morphology, structural evolution and significance of push moraines. *Earth-Sci. Rev.* 53 (3–4), 197–236.
- Björnsson, H., Gjessing, Y., Hamran, S.-E., Hagen, J.O., Liestøl, O., Pálsson, F., Erlingsson, B., 1996. The thermal regime of sub-polar glaciers mapped by multi-frequency radio-echo sounding. *J. Glaciol.* 42 (140), 23–32.
- Blikra, L.H., Anda, E., 1997. Large rock avalanches in Møre and Romsdal, western Norway. *Bull.-Nor. Geol. Unders.*, 44–45.
- Blikra, L.H., Nemeč, W., 1998. Postglacial colluvium in western Norway: depositional processes, facies and palaeoclimatic record. *Sedimentology* 45 (5), 909–959.
- Bø, P.H., 1992. Materialtransport i Midtdalsbreen, Sør-Noreg, og Vestre Lovénbreen og Erikbreen, Svalbard. *Cand. scient. Thesis*, University of Oslo, Oslo, 83 pp.
- Boulton, G.S., 1972. The role of thermal regime in glacial sedimentation. *Spec. Publ.-Inst. Br. Geogr.* 4, 1–19.
- Boulton, G.S., van der Meer, J.J.M., Beets, D.J., Hart, J.K., Ruegg, G.H.J., 1999. The sedimentary and structural evolution of a recent push moraine complex: Holmstrømbreen, Spitsbergen. *Quat. Sci. Rev.* 18, 339–371.
- Caine, N., 1974. The geomorphic process of the alpine environment. In: Ives, J.D., Berry, R.G. (Eds.), *Arctic and Alpine Environments*. Methuen, London, pp. 721–748.
- Caine, N., 1986. Sediment movement and storage on alpine slopes in the Colorado Rocky Mountains. In: Abrahams, A.D. (Ed.), *Hillslope Processes*. Allen & Unwin, London, pp. 115–137.
- Caine, N., Swanson, F.J., 1989. Geomorphic coupling of hillslope and channels systems in two small mountain basins. *Z. Geomorphol.*, NF 33 (2), 189–203.
- Collins, D.N., 1979. Sediment concentration in melt waters as an indicator of erosion processes beneath an alpine glacier. *J. Glaciol.* 89, 247–256.
- Dahl, E., 1954. Weathered gneisses at the island of Runde, Sunnmøre, western Norway, and their geological interpretation. *Nytt Mag. Bot.* 3, 5–23.
- Dahl, E., 1956. Biogeographic and geologic indications of unglaciated areas in Scandinavia during the glacial ages. *Bull. Geol. Soc. Am.* 66, 1499–1519.
- Dahl, E., 1992. Nunatakteori: IV. Hvor fantes isfrie områder og hva slags planter kunne leve på dem. *Blyttia* 1, 23–36.
- Dahl, S.O., Nesje, A., 1994. Holocene glacier fluctuations at Hardangerjøkulen, central southern Norway: a high-resolution com-

- posite chronology from lacustrine and terrestrial deposits. *Holocene* 4, 269–277.
- Dahl, S.O., Nesje, A., 1996. A new approach of calculating Holocene winter precipitation by combining glacier equilibrium-line altitudes and pine-tree limits: a case study from Hardangerjøkulen, central southern Norway. *Holocene* 6, 381–398.
- Davis, M.C.R., Hamza, O., Harris, C., 2001. The effect of rise in mean annual temperature on the stability of rock slopes containing ice-filled discontinuities. *Permafr. Periglac. Process.* 12 (1), 137–144.
- Dawson, A.G., Matthews, J.A., Shakesby, R.A., 1986. A catastrophic landslide (Sturzstrom) in Verkilsdalen, Rondane National Park, Southern Norway. *Geogr. Ann.* 68A (1–2), 77–87.
- Erikstad, L., Sollid, J.L., 1990. Memurubreen, Jotunheimen—glacialgeomorfologi 1:6500, Norsk Institutt for Naturforskning/Geografisk institutt, UiO, Oslo.
- Etzelmüller, B., 2000. Quantification of thermo-erosion in pro-glacial areas—examples from Spitsbergen. *Z. Geomorphol.*, NF 44 (3), 343–361.
- Etzelmüller, B., Hagen, J.O., Vatne, G., Ødegård, R.S., Sollid, J.L., 1996. Glacier debris accumulation and sediment deformation influenced by permafrost, examples from Svalbard. *Ann. Glaciol.* 22, 53–62.
- Etzelmüller, B., Berthling, I., Sollid, J.L., 1998. The distribution of permafrost in Southern Norway; a GIS approach. In: Lewkowicz, A.G., Allard, M. (Eds.), *Seventh International Conference on Permafrost, Proceedings. Collection Nordicana. Centre d'Etudes Nordiques, Université Laval, Québec, PQ, Canada*, pp. 251–257.
- Etzelmüller, B., Ødegård, R.S., Vatne, G., Mysterud, R.S., Tønning, T., Sollid, J.L., 2000. Glacier characteristic and sediment transfer systems of Longyearbyen and Larsbreen, western Spitsbergen. *Nor. Geogr. Tidsskr.* 54 (4), 157–168.
- Evans, I.S., 1972. General geomorphometry, derivatives of altitude, and descriptive statistics. In: Chorley, R.J. (Ed.), *Spatial Analysis in Geomorphology*. Methuen & Co, London, pp. 17–92.
- Follestad, B.A., 1995. Møre og Romsdal fylke—kvartærgeologisk kart 1:250000, Norges geologiske undersøkelse (Norwegian Geological Survey), Trondheim.
- Frei, C., Schar, C., Luthi, D., Davies, H.C., 1998. Heavy precipitation processes in a warmer climate. *Geophys. Res. Lett.* 25 (9), 1431–1434.
- Friedrich, K., 1996. Digitale Reliefgliederungsverfahren zur Ableitung bodenkundlich relevanter Flächeneinheiten Frankfurter Geowissenschaftliche Arbeiten, vol. 21. Universität Frankfurt, Frankfurt. 258 pp.
- Gjessing, J., 1967. Norway's paleic surface. *Nor. Geogr. Tidsskr.* 15, 69–132.
- Gruber, S., Hoelzle, M., 2001. Statistical modelling of mountain permafrost distribution: local calibration and incorporation of remotely sensed data. *Permafr. Periglac. Process.* 12 (1), 69–78.
- Haeberli, W., 1973. Die Basis Temperatur der winterlichen Schneedecke als möglicher Indikator für die Verbreitung von Permafrost. *Z. Gletsch.kd. Glazialgeol.* 9 (1–2), 221–227.
- Haeberli, W., 1979. Holocene push-moraines in alpine permafrost. *Geogr. Ann.* 61A, 43–48.
- Haeberli, W., 1992. Construction, environmental problems and natural hazards in periglacial mountain belts. *Permafr. Periglac. Process.* 3, 111–124.
- Haeberli, W., 2000. Modern Research Perspectives relating to permafrost creep and rock glaciers: a discussion. *Permafr. Periglac. Process.* 11, 290–293.
- Hallet, B., 1983. The breakdown of rock due to freezing: a theoretical model. 4th International Conference on Permafrost, Proceedings. National Academy Press, Washington, DC, pp. 433–438.
- Hallet, B., Hunter, L., Bogen, J., 1996. Rates of erosion and sediment evacuation by glaciers: a review of field data and their implications. *Glob. Planet. Change* 12, 213–235.
- Harris, C., 2001. Permafrost and Climate in Europe (PACE). *Permafr. Periglac. Process.* 12 (1), 156.
- Harris, C., Cook, J.D., 1988. Micromorphology and microfabrics of sorted circles, Jotunheimen, Southern Norway. 5th International Permafrost Conference, Proceedings. Tapir, Trondheim, Norway, pp. 776–783.
- Harris, C., Haeberli, W., Vonder Mühl, D., King, L., 2001. Permafrost monitoring in the high-mountains of Europe: the PACE project in its global context. *Permafr. Periglac. Process.* 12 (1), 3–12.
- Hart, J.K., Watts, R.J., 1997. A comparison of the styles of deformation associated with two recent push moraines, south Van Keulenfjorden, Svalbard. *Earth Surf. Processes Landf.* 22, 1089–1107.
- Heggen, E.S.F., Juliussen, H., Etzelmüller, B., in press. Mountain permafrost in the Sølen massif, central-eastern Norway. Eight International Conference of Permafrost, Proceedings, Zurich, Switzerland.
- Hodkins, R., 1997. Glacier hydrology in Svalbard, Norwegian High Arctic. *Quat. Sci. Rev.* 16, 957–973.
- Hodsen, A., 1994. Climate, hydrology and sediment transfer process interactions in a sub-polar glacier basin. PhD Thesis, University of Southampton, Southampton.
- Hodsen, A.J., 1999. Glacio-fluvial sediment and solute transfer in high Arctic basins: examples from Svalbard. *Glacial Geol. Geomorphol.* RP10/1999, <http://www.ggg.qub.ac.uk/ggg/papers/full/1999/rp101999/rp10.html>.
- Hodsen, A.J., Tranter, M., Dowdeswell, J.A., Gurnell, A.M., Hagen, J.O., 1997. Glacier thermal regime and suspended-sediment yield: a comparison of two high-Arctic glaciers. *Ann. Glaciol.* 24, 32–37.
- Hoelzle, M., 1992. Permafrost occurrence from BTS measurements and climatic parameters in the eastern Swiss Alps. *Permafr. Periglac. Process.* 3 (2), 143–147.
- Hoelzle, M., 1996. Mapping and modelling of mountain permafrost distribution in the Alps. *Nor. Geogr. Tidsskr.* 50 (1), 11–16.
- Hoelzle, M., Mittaz, C., Etzelmüller, B., Haeberli, W., 2001. Surface energy fluxes and distribution models relating to permafrost in European Mountain areas: an overview of current developments. *Permafr. Periglac. Process.* 12 (1), 53–68.
- Hooke, R.L., 1973. Flow near the margin of the Barnes Ice Cap, and the development of ice-cored moraine. *Geol. Soc. Amer. Bull.* 84, 3929–3948.
- Hutchinson, M.F., 1989. A new procedure for gridding elevation and stream line data with automatic removal of spurious pits. *J. Hydrol.* 106, 211–232.

- Isaksen, K., Vonder Mühl, D., Gubler, H., Kohl, T., Sollid, J.L., 2000. Ground surface temperature reconstruction based on data from a deep borehole in permafrost at Janssonshaugen, Svalbard. *Ann. Glaciol.* 31, 287–294.
- Isaksen, K., Holmlund, P., Sollid, J.L., Harris, C., 2001. Three deep alpine permafrost boreholes in Svalbard and Scandinavia. *Permafrost. Periglac. Process.* 12 (1), 13–26.
- Isaksen, K., Hauck, C., Gudevang, E., Ødegård, R.S., Sollid, J.L., 2002. Mountain permafrost distribution on Dovrefjell and Jotunheimen, southern Norway, based on BTS and DC resistivity topography data. *Nor. Geogr. Tidsskr.* 56 (2), 122–136.
- Jonasson, C., Nyberg, R., Rapp, A., 1997. Dating of rapid mass movements in Scandinavia: talus rockfalls, large rockslides, debris flows and slush avalanches. In: Matthews, J.A., Brunsden, D., Frenzel, B., Gläser, B., Weiss, M.M. (Eds.), *Rapid Mass Movement as a Source of Climatic Evidence for the Holocene*. *Palaoklimaforschung* 19 (12), 321–332 (Special Issue, Gustav Fischer Verlag, Stuttgart).
- Jones, P.D., Parker, D.E., Martin, S., Rigor, I.G., 1999. Surface air temperature and its changes over the past 150 years. *Rev. Geophys.* 37 (2), 173–199.
- Kälin, M., 1971. The active push moraine of the Thompson Glacier, Axel Heiberg Island, Canadian Arctic Archipelago, Canada. PhD Thesis, ETH, Zürich, 61 pp.
- Keller, F., Frauenfelder, R., Gardaz, J.-M., Hoelzle, M., Kneisel, C., Lugon, R., Philips, M., Reynard, E., Wenker, L., 1998. Permafrost map of Switzerland. In: Lewkowicz, A.G., Allard, M. (Eds.), *Seventh International Conference on Permafrost, Proceedings*. Collection Nordicana. Centre d'Etudes Nordiques, Université Laval, Québec, PQ, Canada, pp. 557–562.
- King, L., 1983. High mountain permafrost in Scandinavia. 4th International Conference on Permafrost, Proceedings. National Academy Press, Washington, DC, pp. 612–617.
- King, L., 1984. Permafrost in Skandinavien. Untersuchungsergebnisse aus Lappland, Jotunheimen und Dovre/Rondane. *Heidelb. Geogr. Arb.* 76, 174.
- King, L., 1986. Zonation and ecology of high mountain permafrost in Scandinavia. *Geogr. Ann.* 68A, 131–139.
- King, L., Hell, G., 1993. Photogrammetry and geomorphology of high arctic push moraines, examples from Ellesmere Island, Canadian Arctic, and Spitsbergen, Svalbard Archipelago. *Z. Geomorphol., Suppl.* 92, 21–38.
- Kneisel, C., 1999. Permafrost in Gletschervorfeldern—Eine vergleichende Untersuchung in den Ostschweizer Alpen und Nordschweden. *Trierer Geogr. Stud.* 22, 156 pp.
- Konnestad, H., 1996. Moreneformer i fronten av Midtdalsbreen. Cand. Scient. Thesis, University of Oslo, Oslo, 99 pp.
- Kristiansen, K., Sollid, J.L., 1985. Buskerud Fylke, Kvartærgeologi og Geomorfologi 1:250000. Department of Physical Geography, University of Oslo, Oslo.
- Kukkonen, I.T., Safanda, J., 2001. Numerical modelling of permafrost in bedrock in northern Fennoscandia during the Holocene. *Glob. Planet. Change* 29, 259–273.
- Lachenbruch, A., Cladouhos, T.T., Saltus, R.W., 1988. Permafrost temperatures and the changing climate. 5th International Conference on Permafrost, Proceedings. Tapir, Trondheim, Norway, pp. 9–17.
- Lawsen, D.E., 1993. Glaciohydrologic and glaciohydraulic effects on runoff and sediment yield in glacierized basins. US Army Corps of Engineers, Cold Region Research and Engineering Laboratory (CRREL), 93-2, 108 pp.
- Liestøl, O., 1965. Lokalt område med permafrost i Gudbrandsdalen. *Årb.-Nor. Polarinst.* 1965, 129–133.
- Liestøl, O., 1967. Storbreen glacier in Jotunheimen, Norway. *Skr.-Nor. Polarinst.* 141, 63 pp.
- Liestøl, O., 1969. Glacier surges in West Spitsbergen. *Can. J. Earth Sci.* 6, 895–897.
- Liestøl, O., 1977. Pingos, springs, and permafrost in Spitsbergen. *Årb.-Nor. Polarinst.* 1975, 7–29.
- Liestøl, O., 1994. *Compendium i Glasiologi* Geografisk Institutt, Universitetet i Oslo, Oslo.
- Liestøl, O., Sollid, J.L., 1980. Glacier erosion and sedimentation at Hardangerjøkulen and Omnsbreen. In: Orheim, O. (Ed.), *Symposium on Processes of Glacier Erosion and Sedimentation, Field Guide to Excursion*. Norsk Polarinstittutt, Oslo, pp. 1–22.
- Lyså, A., Lønne, I., 2001. Moraine development at a small High-Arctic valley glacier: Rieperbreen, Svalbard. *J. Quat. Sci.* 16 (6), 519–529.
- Mark, D.M., 1975. Geomorphometric parameters: a review and evaluation. *Geogr. Ann.* 57A, 165–177.
- Matthews, J.A., McCarroll, D., Shakesby, R.A., 1995. Contemporary terminal-moraine ridge formation at a temperate glacier—Styggedalsbreen, Jotunheimen, Southern Norway. *Boreas* 24 (2), 129–139.
- Matthews, J.A., Dahl, S.O., Berrisford, M.S., Nesje, A., Dresser, P.Q., Dumayne Peaty, L., 1997. A preliminary history of Holocene colluvial (debris-flow) activity, Leirdalen, Jotunheimen, Norway. *J. Quat. Sci.* 12 (2), 117–129.
- Matthews, J., Dahl, S., Nesje, A., Berrisford, M., Andersson, C., 2000. Holocene glacier variations in central Jotunheimen, southern Norway based on distal glaciolacustrine sediment cores. *Quat. Sci. Rev.* 19 (16), 1625–1647.
- McCarroll, D., Shakesby, R., Matthews, J., 1998. Spatial and temporal patterns of late Holocene rockfall activity on a Norwegian talus slope: a lichenometric and simulation-modeling approach. *Arct. Alp. Res.* 30 (1), 51–60.
- McCarroll, D., Shakesby, R., Matthews, J., 2001. Enhanced rockfall activity during the Little Ice Age: further lichenometric evidence from a Norwegian talus. *Permafrost. Periglac. Process.* 12 (2), 157–164.
- Nesje, A., Dahl, S.O., Anda, E., Rye, N., 1988. Blockfield in southern Norway. Significance for the Weichselian ice sheet. *Nor. Geol. Tidsskr.* 68, 149–169.
- Nesje, A., Blikra, L.H., Anda, E., 1994. Dating rockfall–avalanche deposits from degree of rock-surface weathering by Schmidt–Hammer tests—a study from Norangsdalen, Sunnmøre, Norway. *Nor. Geol. Tidsskr.* 74 (2), 108–113.
- Nesje, A., Dahl, S.O., Andersson, C., Matthews, J.A., 2000. The lacustrine sedimentary sequence in Syngneskardvatnet, western Norway: a continuous, high-resolution record of the Jostedal-breen ice cap during the Holocene. *Quat. Sci. Rev.* 19, 1047–1065.
- Ødegård, R., Sollid, J.L., 1993. Coastal cliff temperatures related to the potential for cryogenic weathering processes, western Spitsbergen, Svalbard. *Polar Res.* 12 (1), 95–106.

- Ødegård, R.S., Sollid, J.L., Liestøl, O., 1992. Ground temperature measurements in mountain permafrost, Jotunheimen, southern Norway. *Permafrost Periglacial Process.* 3, 231–234.
- Ødegård, R., Etzelmüller, B., Vatne, G., Sollid, J.L., 1995. Near-surface spring temperatures in an Arctic coastal rock cliff: possible implications for rock breakdown. In: Slaymaker, O. (Ed.), *Steepland Geomorphology*. Wiley, Chichester, pp. 89–102.
- Ødegård, R.S., Hoelzle, M., Johansen, K.V., Sollid, J.L., 1996. Permafrost mapping and prospecting in southern Norway. *Nor. Geogr. Tidsskr.* 50, 41–54.
- Ødegård, R.S., Isaksen, K., Mastervik, M., Billdal, L., Engler, M., Sollid, J.L., 1999. Comparison of BTS and Landsat TM data from Jotunheimen, southern Norway. *Nor. Geogr. Tidsskr.* 53, 226–233.
- Østrem, G., 1964. Ice-cored moraines in Scandinavia. *Geogr. Ann.* 46A, 282–337.
- Østrem, G., 1975. Sediment transport in glacial meltwater streams. In: Jopling, A.V., McDonald, B.C. (Eds.), *Glaciofluvial and Glaciolacustrine Sedimentation*. Society of Economic Paleontologists, Tulsa, OK, pp. 101–122.
- Østrem, G., Haakensen, N., 1993. Glaciers of Europe—glaciers of Norway. In: Williams, R.S., Ferrigno, J.G. (Eds.), *Satellite Image Atlas of Glaciers of the World*. US Geological Survey Professional Paper 1386-E. US Geological Survey, Washington, pp. E63–E109.
- Pike, R.J., 1995. Geomorphometry—process practice and prospect. *Z. Geomorphol., Suppl.* 101, 221–238.
- Rea, B.R., Whalley, W.B., Rainey, M.M., Gordon, J.E., 1996. Blockfields, old or new? Evidence and implications from some plateaus in northern Norway. *Geomorphology* 15, 109–121.
- Repp, K., 1979. Breerosjon, glasio-hydrologi og materialtransport i et høyarktisk miljø, Brøggerbreene, Vest-Spitsbergen. Cand.real. Thesis, University of Oslo, Oslo, 136 pp.
- Reusch, H., 1901. Nogle bidrag til forstaaelsen af hvorledes Norges dale og fjelde er blevne til. *Årb.-Nor. Geol. Unders.* 32, 124–263.
- Roaldset, E., Pettersen, E., Longva, O., Mangerud, J., 1982. Remnants of preglacial weathering in western Norway. *Nor. Geol. Tidsskr.* 62, 169–178.
- Sandersen, F., 1997. The influence of meteorological factors on the initiation of debris flows in Norway. In: Matthews, J.A., Brunson, D., Frenzel, B., Gläser, B., Weiss, M.M. (Eds.), *Rapid Mass Movement as a Source of Climatic Evidence for the Holocene*. Paläoklimaforschung 19 (12), 321–332 (Special Issue, Gustav Fischer Verlag, Stuttgart).
- Sollid, J.L., Bjørkenes, A., 1977. *Glacial Geology of Midtdalsbreen*. 1:5000. Norges Geografiske Oppmåling, Oslo.
- Sollid, J.L., Carlson, A.B., 1979. *Folldal kvartærgeologisk kart 1:50000 1519II*. Department of Physical Geography, University of Oslo, Oslo.
- Sollid, J.L., Kristiansen, K., 1982. *Hedmark Fylke, Kvartærgeologi og geomorfologi 1:250000*. Department of Physical Geography, University of Oslo, Oslo.
- Sollid, J.L., Kristiansen, K., 1984. *Raumavassdraget. Kvartærgeologi og geomorfologi 1:80000*. Department of Physical Geography, University of Oslo, Oslo.
- Sollid, J.L., Reite, A., 1983. Central Norway, glaciation and deglaciation. In: Ehlers, J. (Ed.), *Glacial Deposits in North-West Europe*. Balkema, Rotterdam, pp. 41–59.
- Sollid, J.L., Sørbel, L., 1979a. Deglaciation of western central Norway. *Boreas* 8, 233–239.
- Sollid, J.L., Sørbel, L., 1979b. *Einunna Kvartærgeologisk kart 1:50000 1519I*. Department of Physical Geography, University of Oslo, Oslo.
- Sollid, J.L., Sørbel, L., 1982. Indikasjoner på kald bre (cold based ice) under avsmeltingen av innlandsisen i sentrale Øst-Norge. *Geolognytt*, 17.
- Sollid, J.L., Sørbel, L., 1988. Influence of temperature conditions in formation of end moraines in Fennoscandia and Svalbard. *Boreas* 17, 553–558.
- Sollid, J.L., Sørbel, L., 1992. Rock glaciers in Svalbard and Norway. *Permafrost Periglacial Process.* 3, 215–220.
- Sollid, J.L., Sørbel, L., 1994. Distribution of glacial landforms in southern Norway in relation to the thermal regime of the last continental ice-sheet. *Geogr. Ann.* 76A (1–2), 25–35.
- Sollid, J.L., Trollvik, J.A., 1991. *Oppland Fylke, Kvartærgeologi og geomorfologi 1:250000*. Department of Physical Geography, University of Oslo, Oslo.
- Sollid, J.L., Carlson, A.B., Torp, B., 1980. *Trollheimen–Sunnalsfjella–Oppdal, Kvartærgeologisk kart 1:1000000*. Department of Physical Geography, University of Oslo, Oslo.
- Sollid, J.L., Holmlund, P., Isaksen, K., Harris, C., 2000. Deep permafrost boreholes in western Svalbard, northern Sweden and southern Norway. *Nor. Geogr. Tidsskr.* 54 (4), 186–191.
- Sollid, J.L., Isaksen, K., Eiken, T., Ødegård, R.S., in press. The transition zone of mountain permafrost on Dovrefjell, southern Norway. *Eight International Conference on Permafrost, Proceedings, Zurich, Switzerland*.
- Suter, S., Laternser, M., Haeberli, W., Frauenfelder, R., Hoelzle, M., 2001. Cold firn and ice of high-altitude glaciers in the Alps: measurements and distribution modelling. *J. Glaciol.* 47 (156), 85–96.
- Sætre, S., 1997. *Undersøkelser av Permafrost i Snøhettaområdet, Dovrefjell, Sør-Norge*. Rapportserie i Naturgeografi, Geografisk institutt, Universitetet i Oslo 9, 64 pp.
- Sørli, H., 2002. *Fordeling av hurtige massebevegelser innenfor kartblad Galdhøpiggen—en analyse av fordelingsmønster*. Cand.scient. Thesis, University of Oslo, Oslo, 70 pp.
- Tveito, O.E., Førland, E.J., 1999. Mapping temperatures in Norway applying terrain information, geostatistics and GIS. *Nor. Geogr. Tidsskr.* 53 (4), 202–212.
- Vatne, G., Etzelmüller, B., Ødegård, R., Sollid, J.L., 1995. Subglacial drainage and sediment evacuation at Erikbreen, northern Spitsbergen. *Nord. Hydrol.* 26, 169–190.
- Weertman, J., 1961. Mechanism for the formation of inner moraines found near the edge of cold ice caps and ice sheets. *J. Glaciol.* 3, 965–978.
- Williams, P.J., 1959. Solifluction and patterned ground in Rondane. *Det Norske Videnskaps-Akademi i Oslo. Skrifter I. Mat.-Naturv. Klasse 2*.
- Williams, P.J.S., Smith, M.W., 1989. *The Frozen Earth: Fundamentals of Geocryology*. Cambridge Univ. Press, Cambridge. 300 pp.

Comparison of the meteorology and surface energy balance at Storbreen and Midtdalsbreen, two glaciers in southern Norway

R. H. Giesen¹, L. M. Andreassen^{2,3}, M. R. van den Broeke¹, and J. Oerlemans¹

¹Institute for Marine and Atmospheric research Utrecht, Utrecht University, Princetonplein 5, 3584 CC Utrecht, The Netherlands

²Section for Glaciers, Snow and Ice, Norwegian Water Resources and Energy Directorate, P.O. Box 5091 Majorstua, 0316 Oslo, Norway

³Department of Geosciences, University of Oslo, P.O. Box 1047 Blindern, 0316 Oslo, Norway

Received: 13 October 2008 – Published in The Cryosphere Discuss.: 17 December 2008

Revised: 5 March 2009 – Accepted: 11 March 2009 – Published: 20 March 2009

Abstract. We compare 5 years of meteorological records from automatic weather stations (AWSs) on Storbreen and Midtdalsbreen, two glaciers in southern Norway, located approximately 120 km apart. The records are obtained from identical AWSs with an altitude difference of 120 m and cover the period September 2001 to September 2006. Air temperature at the AWS locations is found to be highly correlated, even with the seasonal cycle removed. The most striking difference between the two sites is the difference in wind climate. Midtdalsbreen is much more under influence of the large-scale circulation with wind speeds on average a factor 1.75 higher. On Storbreen, weaker katabatic winds are dominant. The main melt season is from May to September at both locations. During the melt season, incoming and net solar radiation are larger on Midtdalsbreen, whereas incoming and net longwave radiation are larger on Storbreen, primarily caused by thicker clouds on the latter. The turbulent fluxes are a factor 1.7 larger on Midtdalsbreen, mainly due to the higher wind speeds. Inter-daily fluctuations in the surface energy fluxes are very similar at the AWS sites. On average, melt energy is a factor 1.3 larger on Midtdalsbreen, a result of both larger net radiation and larger turbulent fluxes. The relative contribution of net radiation to surface melt is larger on Storbreen (76%) than on Midtdalsbreen (66%). As winter snow depth at the two locations is comparable in most years, the larger amount of melt energy results in an earlier disappearance of the snowpack on Midtdalsbreen and 70% more ice melt than on Storbreen. We compare the relative and absolute values of the energy fluxes on Storbreen and Midtdalsbreen with reported values for glaciers at similar

latitudes. Furthermore, a comparison is made with meteorological variables measured at two nearby weather stations, showing that on-site measurements are essential for an accurate calculation of the surface energy balance and melt rate.

1 Introduction

The climate in southern Norway shows a strong precipitation gradient from west to east, with a maritime climate at the western coast and a more continental climate east of the main watershed, located less than 150 km from the coast (Fig. 1, Green and Harding, 1980). The glaciers of southern Norway are found in the areas with the largest annual snow amount; areas characterized by a combination of low temperatures due to topography and sufficient precipitation (Figs. 1 and 2). The annual mass balance turnover (the summed absolute values of the area-averaged winter and summer balance divided by two) on glaciers in southern Norway reflects the precipitation gradient, ranging from 3.7 m water equivalent (w.e.) at Ålfotbreen near the coast to 0.92 m w.e. on Gråsubreen in eastern Jotunheimen, further inland. On Ålfotbreen, interannual fluctuations in the net mass balance are primarily determined by variations in the winter balance, while summer-balance variations dominate interannual variability at the more continental glaciers (Andreassen et al., 2005).

Climate maps reveal large-scale patterns in meteorological variables, giving a first indication where conditions are favourable for glaciers. At smaller spatial scales, large deviations from these numbers occur due to differences in the altitude and terrain exposure. Accumulation and ablation on glaciers are not only related to the local air temperature and winter precipitation, but are also influenced by other



Correspondence to: R. H. Giesen
(r.h.giesen@uu.nl)

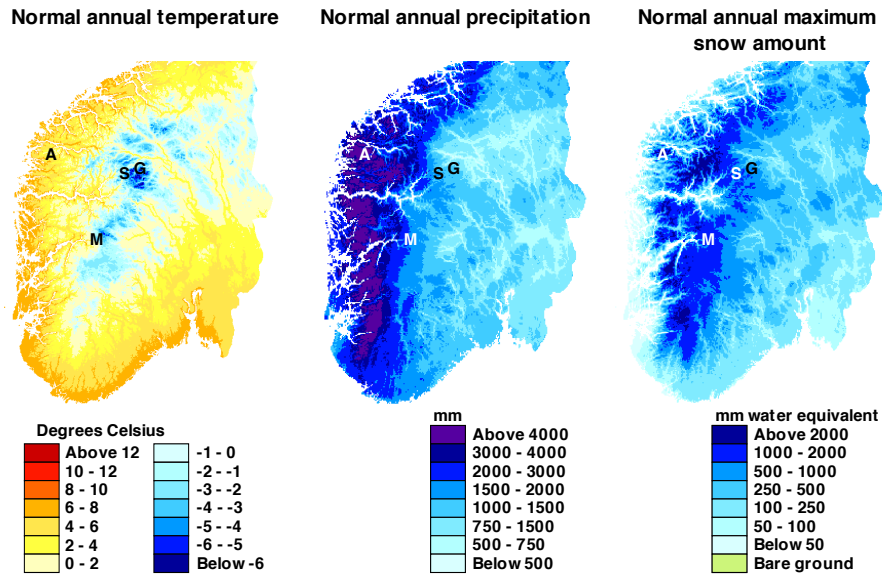


Fig. 1. Annual mean air temperature, precipitation and maximum snow amount in southern Norway over the normal period 1971–2000. Note the non-linear scale. The maps are downloaded from seNorge.no, an initiative of the Norwegian Meteorological Institute, the Norwegian Water Resources and Energy Directorate and the Norwegian Mapping Authority. The locations of Storbreen (S), Midtdalsbreen (M), Ålfotbreen (A) and Gråsubreen (G) are indicated on each map.

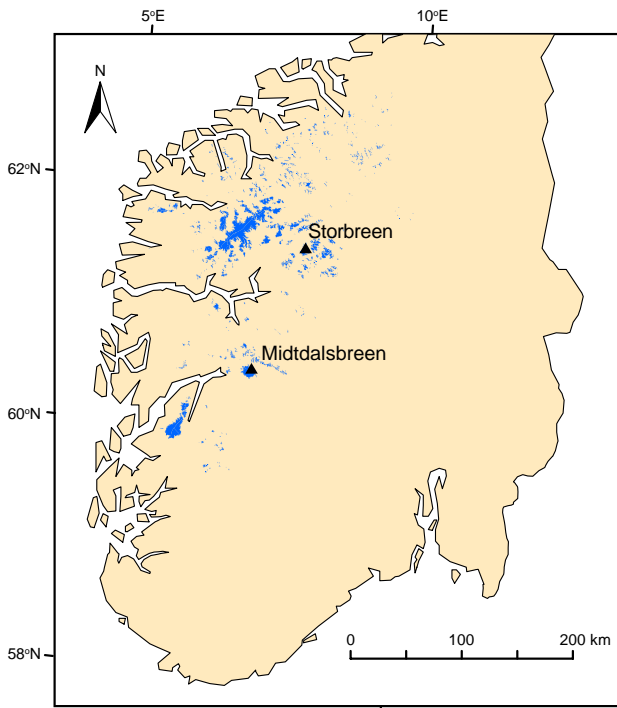


Fig. 2. Glaciers in southern Norway (in blue) and the location of Storbreen and Midtdalsbreen. The source for this map is the Statens Kartverk 1:250 000 map series and includes perennial snow fields.

variables and factors, for example wind speed, cloudiness and surface properties. Therefore, detailed knowledge of the relation between meteorological quantities and the mass and energy exchange at the glacier surface can only be obtained from meteorological studies on glaciers. Between 1954 and 1981, glacio-meteorological experiments have been carried out on a number of glaciers in southern Norway (e.g., Liestøl, 1967; Klemsdal, 1970; Messel, 1971). The combined results from these studies reveal that the relative importance of radiative fluxes compared to turbulent fluxes for surface melt increases from glaciers near the coast to the glaciers further inland (Messel, 1985). However, a detailed comparison could not be made as the studies were conducted in different years and for different periods during the summer season.

In this paper, we compare meteorological records from two identical AWSs on Midtdalsbreen and Storbreen, two glaciers in southern Norway, 120 km apart (Fig. 2). Both glaciers are located in the transitional zone between the maritime climate at the coast and the more continental inland climate. We use meteorological data collected over 5 years, from September 2001 until September 2006. The AWS data sets comprise all quantities needed to determine the atmospheric energy fluxes, including the four radiation fluxes. Apart from a 19-day data gap in the summer of 2004 for Storbreen and a 39-day gap in the Midtdalsbreen record for the summer of 2005, the records are continuous. Analyses of the time series have shed light on the local meteorology and the surface energy and mass balance at the AWS sites (Andreassen et al., 2008; Giesen et al., 2008). Here, we analyse similarities and differences between meteorological variables

Table 1. The main characteristics of Storbreen and Midtdalsbreen and the AWS sites on the two glaciers. Values are derived from a digital terrain model (DTM) for Storbreen from 1997 (Andreassen, 1999) and a DTM for Hardangerjøkulen from 1995 derived from the 25 m resolution digital terrain model (DTM25) of Norway by the Norwegian mapping authorities (Statens Kartverk, <http://www.statkart.no>).

	Storbreen	Midtdalsbreen
General characteristics		
Latitude (° N)	61.60	60.57
Longitude (° E)	8.13	7.47
Area (km ²)	5.4	6.7
Lowest altitude (m a.s.l.)	1390	1380
Highest altitude (m a.s.l.)	2090	1865
AWS location		
Altitude (m a.s.l.)	1570	1450
Distance from the snout (m)	900	400
Surface slope (°)	6	7
Surface aspect	NE	NE

measured on the two glaciers and discuss their influence on the surface energy balance. In line with previous studies we compare the relative contribution of the surface energy fluxes to melt. The absolute and relative values of the surface energy fluxes are compared with values found for glaciers at similar latitudes, for which we provide a summary which complements earlier overviews (e.g., Ohmura, 2001; Willis et al., 2002; Hock, 2005). To investigate whether similarities and differences found for meteorological variables on Storbreen and Midtdalsbreen are also observed outside the glacier boundary-layer, we compare our data with records from two nearby weather stations.

2 Setting and AWS description

Storbreen and Midtdalsbreen are located in southern Norway, 120 km apart (Figs. 2 and 3). Storbreen is a valley glacier in the western part of the Jotunheimen mountain massif. Midtdalsbreen is an outlet glacier of Hardangerjøkulen, an ice cap situated at the north-western border of the Hardangervidda plateau. Both glaciers are facing north-east, cover a similar altitudinal range and are of comparable size (Table 1). Storbreen has had a mass deficit since annual mass balance measurements started in 1949 (Andreassen et al., 2005). No long-term mass balance series are available for Midtdalsbreen, but annual measurements were initiated in 1963 on Rembesdalsskåka, another outlet glacier from Hardangerjøkulen. They show an approximate equilibrium until the late 1980s and a subsequent mass surplus. After 2000, net mass balances were mainly negative; the net balance of the year 2006 was the lowest ever measured on both Storbreen and Rembesdalsskåka (Kjøllmoen et al., 2007). The net retreat over

the period 1982–2006, when length change was measured at both glaciers, was 80 m at Storbreen and 25 m at Midtdalsbreen.

The AWSs on Midtdalsbreen and Storbreen (Fig. 3) are operated by the Institute of Marine and Atmospheric research Utrecht (IMAU). The AWS on Midtdalsbreen was placed in October 2000, the AWS on Storbreen in September 2001. The stations are of identical design and are both located in the ablation zones of the respective glaciers. The mast rests on the ice surface. Air temperature and humidity, wind speed and wind direction are measured at two levels. Temperature and humidity sensors (Vaisala HMP45C) are mounted on the arms at approximately 2.4 and 5.7 m above the ice surface, the measurement level of the wind speed and wind direction sensors (Young 05103) is 0.35 m higher. In addition, the upper arm carries a radiation sensor (Kipp & Zonen CNR1), measuring the four components of the radiation balance (incoming and reflected solar radiation, incoming and outgoing longwave radiation), and a sonic ranger (Campbell SR50), measuring the distance to the surface. A second sonic ranger is mounted on a tripod, which is drilled into the ice (Fig. 3). This sonic ranger registers both ice melt and snow accumulation. The sonic ranger in the mast ensures a continuous record when the other sensor is buried by snow. Readings at one to four ablation stakes around the AWS are used as a reference for the sonic ranger measurements and enable continuation of the surface height record when data from the sonic rangers is missing. Air pressure (Vaisala PTB101B) is recorded inside the box containing the electronics. Sample time varies per sensor, every 30 min (average) values are stored on a data logger (Campbell CR10X). Power is supplied by lithium batteries, the solar panel generates energy to ventilate the temperature sensors.

3 Methods

3.1 Data treatment

In this section we give an overview of the necessary corrections to the data. More detailed descriptions are given in Andreassen et al. (2008) and Giesen et al. (2008).

- Air temperature was corrected for radiation errors at times when the sensor was not aspirated using expressions that give the excess temperature as a function of wind speed and the sum of incoming and reflected solar radiation.
- Relative humidity measured at temperatures below the melting point was corrected by multiplying with the ratio of the saturated water vapour pressures over water and over ice, using an expression by Curry and Webster (1999). Specific humidity has been calculated from the measurements of relative humidity, air temperature and air pressure.

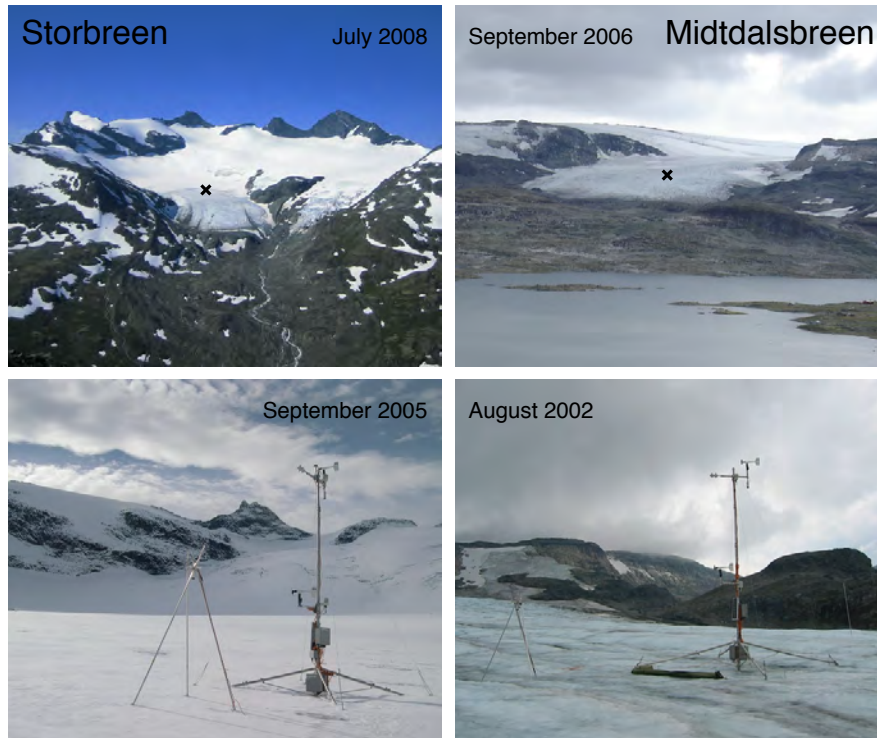


Fig. 3. The location of the AWSs (×) on Storbreven (left) and Midtdalsbreen (right) and a close-up of the AWS sites. The tripod with a sonic ranger is seen to the left of the mast.

- The sonic ranger uses the speed of sound at 0°C to determine the distance to the surface. As the speed of sound is a function of air density and hence temperature, the record was corrected by multiplying with the ratio of the actual speed of sound and the speed of sound at 0°C.
- The tilt of the masts was estimated from tilt angles measured during maintenance visits, combined with data from a tilt sensor in the mast, which did not function properly. On Midtdalsbreen the estimated tilt of the mast is often large enough to significantly affect the absolute value of the incoming solar radiation. The tilt only affects the direct solar beam, hence we applied a tilt correction dependent on cloudiness. A tilted mast also influences the reflected solar radiation measurements, but the correction was found to be smaller than uncertainties associated with the poor tilt estimates and was therefore not applied. Tilt values recorded on Storbreven are smaller and do not seem to influence daily mean values of incoming solar radiation significantly. Hence, no tilt correction was applied to the incoming solar radiation on Storbreven.
- Half-hourly values of net shortwave radiation were calculated using the accumulated albedo method (Van den Broeke et al., 2004) to remove the effects of a poor cosine response of the radiation sensor at low sun angles and a possible phase shift due to tilting of the sensor on the daily cycle of incoming solar radiation. As we only use daily averaged values in this analysis, the effect of this correction on net shortwave radiation is negligible.
- Due to the opening of a crevasse, the mast on Storbreven fell down in the summer of 2004. The same happened on Midtdalsbreen in 2005. As the data measured during these periods cannot be used in the analysis, the series from Storbreven contains a 19-day gap from 30 July to 17 August 2004. The series from Midtdalsbreen has 39 days without useful data from 18 July to 25 August 2005. Motivated by the observation that the records of all variables on Storbreven and Midtdalsbreen generally display similar and simultaneous fluctuations, we used measurements from Midtdalsbreen to create a data set to fill the gap on Storbreven. For the data gap on Midtdalsbreen, we used measurements from an AWS at the summit of Hardangerjøkulen, except for relative humidity and incoming longwave radiation where data from Storbreven were used.
- The sonic rangers on the tripods were buried by the snowpack during several winter seasons and melted out at the end of several summer periods. In addition to this, sonic ranger data are missing for shorter periods during the rest of the year, for various reasons. Small gaps in the surface height record were filled by linear interpolation between surrounding values, for larger gaps in

the melt season we used melt values calculated from the surface energy balance, combined with stake readings. For Storbreen, measurements from both sonic rangiers are lacking during the accumulation season of 2002–2003. For this period, precipitation data from the nearby Norwegian Meteorological Institute (NMI) weather station Bråtå (664 m a.s.l.) were used to create a continuous record.

3.2 Cloud fraction and effective cloud optical depth

Information about clouds can be obtained from both incoming shortwave and incoming longwave radiation. Fractional cloud cover was estimated from incoming longwave radiation (Van den Broeke et al., 2008a). Cloud optical thickness was determined from incoming solar radiation using an expression by Fitzpatrick et al. (2004), resulting in effective cloud optical depth values representative for a uniform cloud cover consisting of cloud droplets with a standard effective radius of 8.6 μm . However, this expression can only be applied to daytime measurements without shading by the topography. For all days with more than 20 half-hourly values for the cloud optical thickness, we calculated daily averages and regressed these values against the cloud fraction. For both locations, an exponential function fitted the data well (linear correlation r of 0.81) and was used to obtain year-round daily values for cloud optical depth.

3.3 Surface energy balance

The energy balance at the glacier surface can be described by

$$Q = S_{\text{in}} + S_{\text{out}} + L_{\text{in}} + L_{\text{out}} + H_{\text{sen}} + H_{\text{lat}} + G \quad (1)$$

$$= S_{\text{net}} + L_{\text{net}} + H_{\text{sen}} + H_{\text{lat}} + G, \quad (2)$$

where Q is melt energy ($Q=0$ if the surface temperature is below the melting point), S_{in} and S_{out} are incoming and reflected solar radiation, L_{in} and L_{out} are incoming and outgoing longwave radiation, H_{sen} and H_{lat} are the sensible and latent heat fluxes and G is the subsurface heat flux. Net solar radiation and net longwave radiation are written as S_{net} and L_{net} . All fluxes are defined positive when directed towards the surface. Heat supplied by rain is neglected, which is justified on glaciers with a considerable mass turnover (Oerlemans, 2001). Penetration of shortwave radiation is not included either. Compared to the other fluxes its contribution to the energy balance is expected to be small and it has been shown not to affect total melt (Van den Broeke et al., 2008b).

3.3.1 Model description

We have used an energy balance model that solves Eq. (1) for a skin layer without heat capacity, which is described in more detail by Van den Broeke et al. (2005, 2006). S_{in} , S_{out} and L_{in} are taken from the (corrected) measurements,

the other fluxes are written as functions of the surface temperature T_s . The model time-step is 10 min, to obtain model input for every time-step, the AWS data are linearly interpolated between half-hourly values. Using an iterative procedure, the surface energy balance is solved for the surface temperature T_s . If T_s found by the model is higher than the melting point temperature, T_s is set back to 0°C and the excess energy is used for melting. The amount of melt M in meters water equivalent (m w.e.) is calculated by dividing Q by the latent heat of fusion ($3.34 \times 10^5 \text{ J kg}^{-1}$) and the density of water (1000 kg m^{-3}).

The turbulent fluxes are computed with the bulk method, based on differences in temperature, humidity and wind speed between the measurement level and the surface. We use measurements from the upper level, the records from the lower level sensors contain several data gaps. Following Van den Broeke et al. (2005), stability correction functions by Holtslag and De Bruin (1988) and Dyer (1974) are applied for stable and unstable conditions, respectively. A comparison of turbulent fluxes calculated with data from either the upper or the lower measurement level revealed that when using wind speed measurements from the upper level, turbulent fluxes are underestimated, mainly on days with low wind speeds. At both AWS sites, the ratio of wind speeds measured at the upper and lower level is always larger than unity for wind speeds above 6 m s^{-1} ; for lower wind speeds this ratio is smaller than unity about 20% of the time. On days with a wind speed maximum below the upper level, the wind is always directed down-slope. Moreover, the temperature difference between the air and the surface is mostly larger than 5 K, suggesting the presence of katabatically driven flow. Although wind speeds are relatively low in these circumstances, turbulent fluxes are underestimated considerably by using the upper level measurements, because the temperature difference between the air and the surface is large. To obtain good agreement between turbulent fluxes calculated with the upper or lower level measurements, we limited the turbulent flux reduction by the stability correction to one third when using the upper level data. For the surface roughness length for momentum (z_{0v}) we use constant values of 0.13 mm for snow surfaces and 0.75 mm for ice surfaces at both AWS sites. Whether the surface is ice or snow is determined from a snow depth record constructed from the sonic ranger measurements. The roughness length values are median values, derived from wind speed differences between the AWS upper and lower measurement levels at near-neutral atmospheric conditions. We used the derived roughness lengths for Midtdalsbreen, as only few datapoints remained for near-neutral conditions at Storbreen and these were mainly found in mid-winter, biasing z_{0v} towards low values. Using roughness lengths from Midtdalsbreen on Storbreen will not likely introduce a large error, because derived values are similar during the periods they could be calculated for both glaciers and the surface characteristics at the AWS sites are comparable. Sensitivity tests with the energy balance model using data

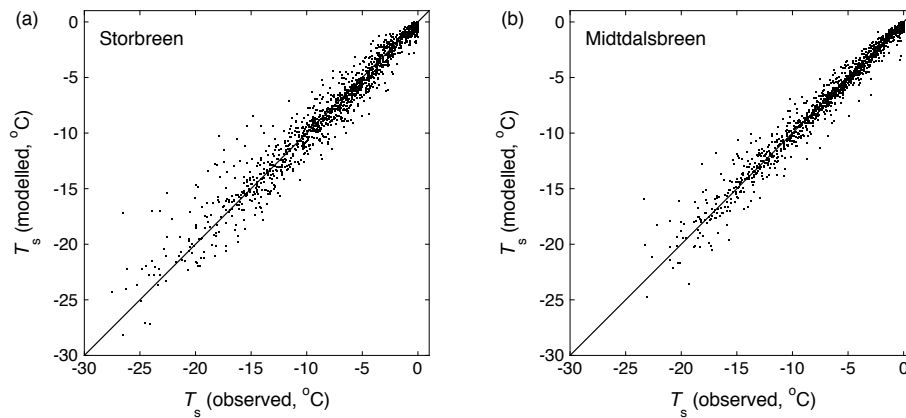


Fig. 4. Modelled versus observed surface temperature (daily mean values) for (a) Storbreen and (b) Midtdalsbreen.

from Midtdalsbreen, have shown that an order-of-magnitude change in z_{0v} roughly affects the sum of the turbulent fluxes by 15%, while removing the stability correction increases the summed turbulent fluxes by 20%, on average (Giesen et al., 2008). The roughness lengths for heat and moisture are calculated from expressions by Andreas (1987).

Subsurface heat conduction is computed from the one-dimensional heat-transfer equation for 0.04 m thick layers down to a depth of 20 m. The temperature at the lowest level is assumed to remain stable. The initial temperature profile is generated by continuously running the model over the measurement period until the 20 m temperature is stable within 0.01°C. The number of snow layers is determined by dividing the observed snow depth by the model layer thickness. Snow density has a constant value of 500 kg m⁻³, based on measurements in snow pits around the AWSs. Meltwater percolates vertically through the snowpack and refreezes where snow temperatures are below the melting point. When the snowpack is saturated with melt water, the remaining melt water is assumed to run off. Note that in our approach, the changing snow depth is prescribed from the sonic ranger record and not calculated by the model. This ensures that the snow cover appears and disappears at the right moment. When the snow has disappeared, input from the height sensor is not needed anymore and model and measurements are independent. For this snow-free period, the melt M computed by the model can be compared with the surface lowering registered by the sonic ranger and the ablation stakes by dividing M by 0.9, the ratio of the ice and water densities used in this study.

3.3.2 Model performance

A comparison of the modelled and observed surface temperature (from measured L_{out} , assuming a surface with unit emissivity) gives an indication of the model performance. Figure 4 shows modelled versus observed daily average surface

temperatures for Storbreen and Midtdalsbreen. The overall agreement is good, although surface temperatures are somewhat overestimated on clear-sky winter days. This cannot be attributed to the limited stability correction, removing the limit only slightly reduces the temperature difference on these days. Riming of the sky-facing longwave radiation sensor is a plausible cause. For Storbreen, the mean difference between modelled and observed surface temperature is +0.07°C, with a root-mean-square error (RMSE) of 1.3°C. For Midtdalsbreen, the mean difference is +0.14°C with a RMSE of 1.1°C. Given the uncertainties in both the measurements and the energy balance model, this is a good result. For both locations, the match between modelled and measured surface melt is generally good (Andreassen et al., 2008; Giesen et al., 2008), which indicates that all relevant processes are included in the model and the calculated energy balance is robust.

4 Results

For the main atmospheric quantities and the surface energy fluxes, mean values over the five years (7 September 2001 to 6 September 2006) were computed, as well as averages over all 30-min intervals when the surface was melting ($Q > 0$). We used measurements made at the upper level for the analysis, since the records from the lower level sensors have several data gaps. Correlation coefficients (r) between variables on Storbreen and Midtdalsbreen were computed for both half-hourly and daily mean values. The periods with data missing for one of the locations were excluded from the calculation of r . The mean values and linear correlations are listed in Table 2.

4.1 Air temperature and humidity

Annual mean air temperature is 0.7°C higher on Midtdalsbreen (Table 2), reflecting the lower altitude of the

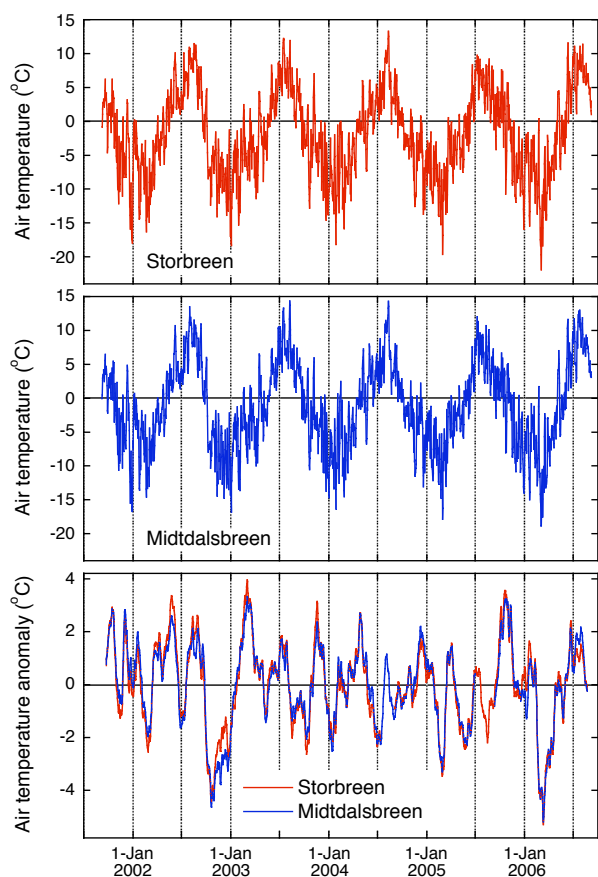


Fig. 5. Daily mean air temperature on Storbreen and Midtdalsbreen and 31-day moving average of daily air temperature anomalies on Storbreen and Midtdalsbreen. The temperature anomalies were calculated by subtracting the monthly mean temperature at both locations.

AWS location. The mean and most frequent temperature lapse rate calculated from the two temperature records is $6.0^{\circ}\text{C km}^{-1}$. The temperature difference is smaller during melt ($4.3^{\circ}\text{C km}^{-1}$), when the air above the glaciers is cooled by the melting surface. Daily mean air temperatures for the AWS sites on Storbreen and Midtdalsbreen have an almost perfect resemblance, in both inter-daily fluctuations and annual amplitude (Fig. 5). The correlation coefficient of daily mean air temperatures on the two glaciers is 0.98 (Table 2). To eliminate the correlation due to the seasonal cycle, we calculated daily mean temperature anomalies by subtracting the monthly mean temperature, including all months with measurements available from both AWSs. After the removal of the seasonal cycle the linear correlation is still 0.95. Computed daily temperature anomalies with a moving average of 31 days, show that the winters 2000–2001, 2002–2003 and 2005–2006 were relatively cold, while the major part of the summer of 2002 was warmer than the other summers in the record (Fig. 5, third panel). In 2003, temperatures in spring were relatively high and 2005 had a very warm autumn.

At both glaciers the air is humid, with an average relative humidity around 80% (Table 2). Relative and specific humidity are generally slightly lower on Storbreen. This could indicate a more continental climate than at Midtdalsbreen, but can also be the result of a different boundary-layer structure at the two sites. As the local free-atmosphere humidity is not measured, we cannot distinguish whether the lower humidity values on Storbreen are a local or a regional feature. At both AWS sites, specific humidity averaged over the melt season is higher than the annual average, as warmer air can contain more water vapour. The mean relative humidity is also slightly higher in summer than in winter, because the free atmosphere air is cooled near the cold glacier surface, increasing the relative humidity.

4.2 Wind speed and wind direction

The most striking difference between the two glaciers is that wind speeds are on average 1.75 times larger on Midtdalsbreen (Table 2). This ratio is almost constant through the year, from October to December values are slightly higher. A similar ratio is found for wind speeds at the lower level, using all available simultaneous wind speed measurements from both locations. The linear correlation between wind speeds at Storbreen and Midtdalsbreen is nonetheless relatively high ($r=0.74$ for daily means).

The dominant wind directions on the two glaciers (Fig. 6) are related to the local topography. Two wind directions are imposed by the orientation of the valleys in which the glaciers are situated. Midtdalsbreen flows into the valley Finsedalen, which has an approximate west-east orientation, seen as winds from directions 130° and 280° . Northerly winds seldomly occur on Midtdalsbreen. Storbreen is situated in the almost north-south oriented Leirdalen, resulting in winds from 355° and 165° . Winds with the directions 225° on Midtdalsbreen and 200° on Storbreen are down-slope winds along the glacier length axis, commonly known as katabatic or glacier winds. Although the glacier slopes are similar (Table 1), katabatic winds occur more frequently on Storbreen and impose the dominant wind direction, while westerly winds are dominant on Midtdalsbreen. Westerly winds are also common on Storbreen and are likely large-scale winds, as they generally occur simultaneously with westerly winds on Midtdalsbreen. While the highest wind speeds on Midtdalsbreen are recorded during westerly flow, westerly winds on Storbreen are much weaker. Storbreen is surrounded by higher mountains than Midtdalsbreen, which shelter the glacier from the large-scale circulation. The large differences in wind regimes suggest that on Midtdalsbreen the development of a katabatic flow is often suppressed by the strong large-scale circulation and is thereby limited to calm days, while on Storbreen katabatic winds can develop more frequently.

Table 2. Mean values of meteorological quantities and energy fluxes for Storbreen (S) and Midtdalsbreen (M) over the period 7 September 2001–6 September 2006, for the entire period and periods when the surface was melting. The absolute accuracy is given for daily and annual mean values. Linear correlations r between variables on Storbreen and Midtdalsbreen are shown for half-hourly and daily mean values.

	Annual mean		Melt period mean		Accuracy		Correlation	
	S	M	S	M	day	year	30 min	day
<i>Meteorological quantities</i>								
Air temperature ($^{\circ}\text{C}$)	-1.9	-1.2	4.9	5.3	0.3	0.1	0.97	0.98
Relative humidity (%)	77.9	81.9	78.2	80.8	3	1.0	0.72	0.83
Specific humidity (g kg^{-1})	3.4	3.6	5.1	5.3	0.2	0.1	0.95	0.98
Wind speed (m s^{-1})	3.8	6.6	3.3	6.0	0.4	0.1	0.53	0.74
Air pressure (hPa)	834.0	848.5	838.3	852.4	0.4	0.1	1.00	1.00
Cloud fraction	0.62	0.60	0.69	0.64	0.05	0.02	0.67	0.83
Effective cloud optical depth	16.0	11.9	–	–	10	3	–	0.72
Surface albedo	0.73	0.68	0.52	0.47	0.05	0.02	–	0.91
<i>Surface energy fluxes (W m^{-2})</i>								
Shortwave in	108	126	220	242	20	5	0.92	0.96
Shortwave out	-70	-76	-125	-126	10	2	0.93	0.96
Longwave in	272	270	311	304	10	2	0.79	0.91
Longwave out	-292	-295	-316	-316	5	2	0.95	0.97
Sensible heat flux	15	24	20	39	10	5	0.66	0.81
Latent heat flux	1	4	9	16	10	5	0.75	0.88
Subsurface heat flux	3	3	-2	-2	5	2	0.61	0.81

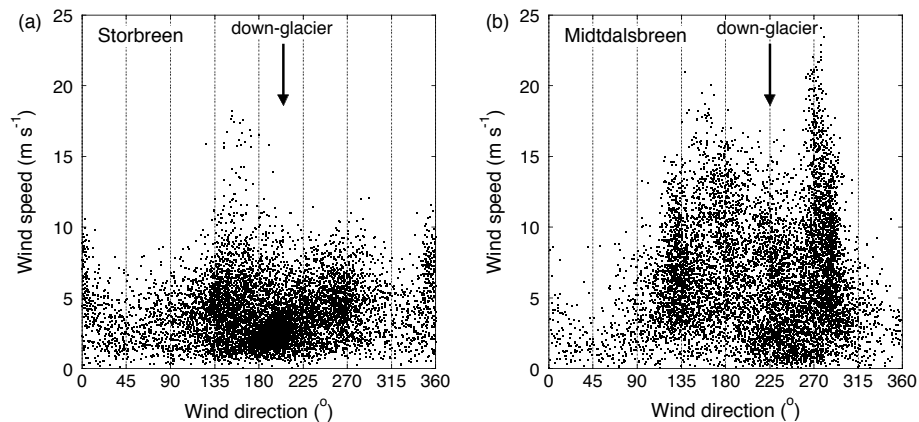


Fig. 6. Half-hourly wind speed versus wind direction on (a) Storbreen and (b) Midtdalsbreen. Measurements are shown at hourly intervals for the period September 2005 to September 2006.

4.3 Incoming solar radiation and cloudiness

Incoming shortwave radiation is significantly larger on Midtdalsbreen, both in the annual mean value as in periods with surface melt (Table 2). The annual mean top-of-the-atmosphere incoming solar radiation is only 5 W m^{-2} higher at Midtdalsbreen, hence the lower latitude of Midtdalsbreen cannot explain this difference. Figure 7a shows that monthly mean atmospheric transmissivity at the AWS site on Midtdalsbreen is always higher than on Storbreen. On both glaciers, the atmospheric transmissivity is maximum in spring and gradually decreases during summer. The lower atmospheric transmissivity at Storbreen could be caused by

more frequent shading of the AWS site or differences in cloud characteristics. In winter, shading by the surrounding topography reduces the amount of S_{in} considerably, an effect which is larger on Storbreen. In summer, the solar zenith angle is much smaller and the influence of shading on S_{in} is small. For this period, the cloud fraction (Table 2) and the effective cloud optical depth (Fig. 7b) are larger for Storbreen, hence the smaller S_{in} in summer is mainly resulting from thicker clouds. We investigated possible relations between the difference in cloudiness and other measured variables or differences in variables between the two locations, but no dependencies were found. Since most meteorological

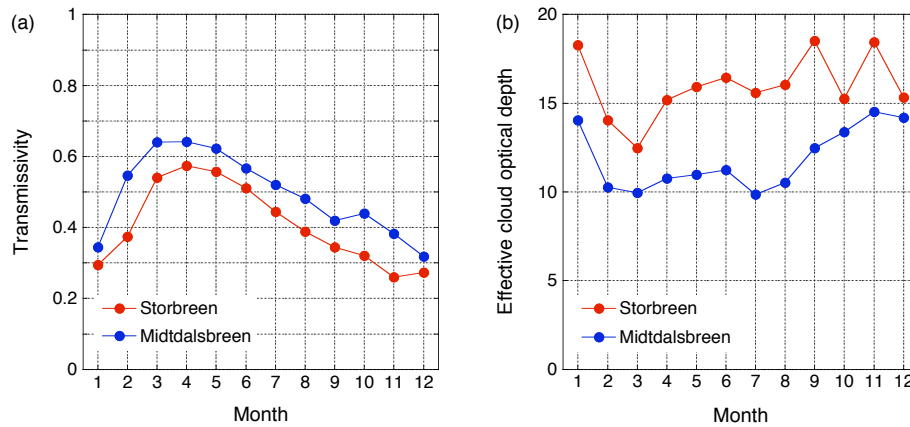


Fig. 7. Monthly mean values of (a) atmospheric transmissivity and (b) effective cloud optical depth on Storbreen and Midtdalsbreen.

variables on Storbreen and Midtdalsbreen, including S_{in} , are highly correlated, the larger cloud fractions found for Storbreen are likely associated with local factors affecting cloud properties and not with different synoptic situations at the two glaciers.

4.4 Reflected shortwave radiation and surface albedo

Figure 8 presents the daily mean surface albedo for Storbreen and Midtdalsbreen for two winter and summer seasons. These years were selected because the data are continuous and cover two complete seasons. Snow generally starts to accumulate at the AWS sites between the end of September and the end of October. The albedo fluctuations in winter are very similar on the two glaciers. In summer, most precipitation falls as rain at the AWS sites, but occasional snow-fall events can be recognised by a simultaneous increase in albedo at both locations. In all years, the snow disappears earlier in summer at the AWS site on Midtdalsbreen than on Storbreen. The time difference in ice reappearance at the two locations varies between 11 days (2003) and 35 days (2002) and is weakly related to the maximum snow depth and the difference in total snow accumulation at the two locations. In the winter 2001–2002, Midtdalsbreen received considerably less snow than Storbreen, leading to the largest difference in ice reappearance dates. Ice albedo on Midtdalsbreen remained rather high during the summer of 2002 for unknown reasons. In general, ice albedo has a value around 0.3 at both locations, but can get as low as 0.22.

Annual mean reflected shortwave radiation is slightly larger on Midtdalsbreen ($+6 \text{ W m}^{-2}$), due to more incoming solar radiation (Table 2). For the period with surface melt, the difference between the two glaciers becomes very small ($+1 \text{ W m}^{-2}$), mainly a result of the earlier disappearance of the snowpack on Midtdalsbreen. As the difference between absolute S_{out} at the two locations is small, S_{net} is larger on Midtdalsbreen (Fig. 9).

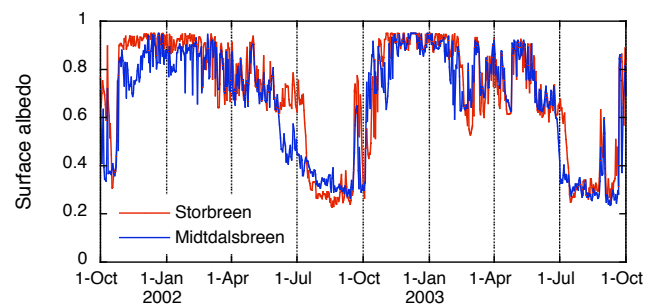


Fig. 8. Daily mean surface albedo on Storbreen and Midtdalsbreen from October 2001 to October 2003.

4.5 Longwave radiation

Annual mean incoming longwave radiation is comparable at the two AWS locations (Table 2). However, in summer monthly averaged L_{in} is 4 to 6 W m^{-2} larger on Storbreen, while during the winter season L_{in} is often larger on Midtdalsbreen. In summer, thicker clouds on Storbreen result in larger L_{in} than on Midtdalsbreen (Fig. 7b), as was already discussed in Sect. 4.3. The larger L_{in} for Midtdalsbreen during the winter months is a result of occasional multi-day periods with substantially more humid and cloudier weather than on Storbreen.

Outgoing longwave radiation is similar at the two locations, values are slightly higher on Midtdalsbreen, as surface temperatures are higher due to more positive energy fluxes towards the surface. During the melt season, the surface is almost continuously at the melting point and L_{out} is approximately equal at the AWS sites. The combination of higher L_{in} and lower L_{out} on Storbreen compared to Midtdalsbreen, results in less negative L_{net} on Storbreen (Fig. 9).

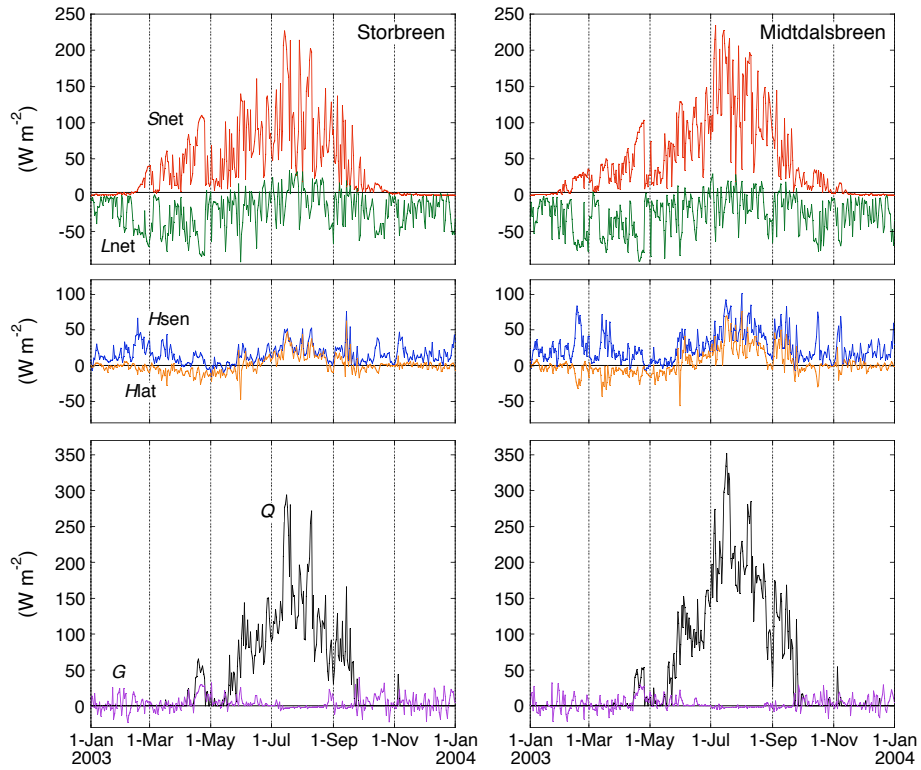


Fig. 9. Daily mean surface energy fluxes on Storbreen and Midtdalsbreen in 2003.

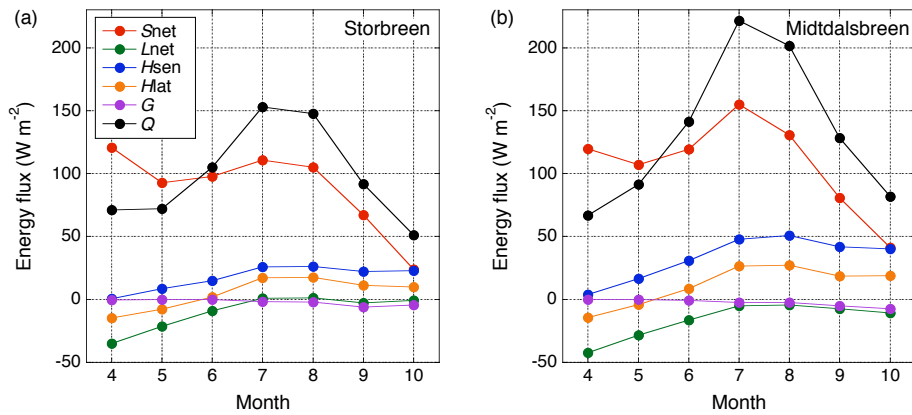


Fig. 10. Monthly mean values of the surface energy fluxes during melt for (a) Storbreen and (b) Midtdalsbreen.

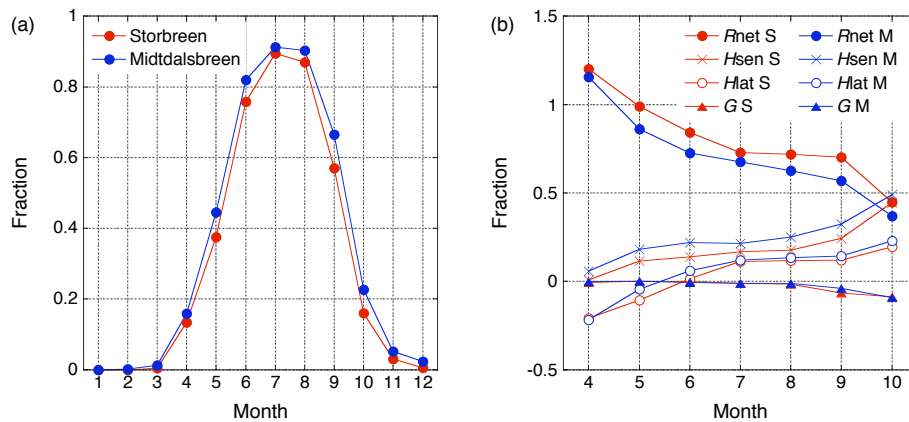


Fig. 11. Monthly values of (a) the fraction of time with melt and (b) the contribution of the energy fluxes to surface melt on Storbreen (S) and Midtdalsbreen (M).

4.6 Turbulent fluxes

On both glaciers, the daily mean sensible heat flux is almost permanently positive (Fig. 9), as the daily average surface temperature is seldom higher than the air temperature. The sensible heat flux is generally larger on Midtdalsbreen, especially in summer, which is a result of the higher air temperatures and higher wind speeds.

The latent heat flux is mainly negative and partly balances the sensible heat flux (Fig. 9). Again, the absolute values of H_{lat} are generally larger on Midtdalsbreen, because of the more humid and windier conditions. During summer, both H_{sen} and H_{lat} are positive and contribute substantially to the energy available for melting (Fig. 10).

4.7 Subsurface heat flux

The subsurface heat flux warms or cools the surface depending on the sign of the sum of the atmospheric energy fluxes. Daily mean values only occasionally exceed 20 W m^{-2} and are small compared to the other energy fluxes (Fig. 9). The subsurface heat fluxes are similar in magnitude and inter-daily fluctuations at the two AWS sites. In the early melt season, when the surface consists of snow, G is generally zero or positive as the entire snowpack is at the melting point temperature. As soon as the snow has disappeared, G becomes slightly negative. The glacier ice is still cold because it was isolated by the snowpack during spring; all through the melt season a small amount of energy is used to warm the ice. The model does not include penetration of shortwave radiation, but in reality the near-surface ice is likely heated by penetrating shortwave radiation during the day. This process creates an isothermal layer causing G to vanish.

4.8 Melting energy

The energy available for melting is, on average, a factor 1.3 larger on Midtdalsbreen. Net radiation R_{net} , the sum of the shortwave and longwave radiative fluxes, is 1.2 times larger

than on Storbreen, the turbulent fluxes are almost twice as large (factor 1.9). On both Storbreen and Midtdalsbreen, the surface is melting almost continuously during July and August (Fig. 11a). The main melt season is between May and October, when S_{net} dominates over L_{net} and the sum of H_{sen} and H_{lat} is positive (Fig. 9). In the winter months, melt occurs sporadically. During the five years considered in this study, the glacier surface at the AWS site on Storbreen was melting 32% of the time, on Midtdalsbreen this percentage is 35%. The relative contribution of the energy fluxes to the surface melt for the months between April to October is illustrated in Fig. 11b. Note that only periods with melt are included in this calculation. In early spring, the contribution of R_{net} to surface melt is larger than unity, to balance the negative H_{lat} . In fact, S_{net} needs to compensate H_{lat} and L_{net} which are both negative (Fig. 10), implying that large S_{in} is required for melt in spring. The relative importance of R_{net} decreases during the melt season, when top-of-the-atmosphere solar irradiance becomes smaller, cloudiness increases and the turbulent fluxes increase due to higher wind speeds. In October, S_{net} and H_{sen} contribute equally to the melt energy and the turbulent fluxes together dominate the surface energy balance (Figs. 10 and 11b). The largest melt fluxes occur on Midtdalsbreen in July, on Storbreen the amount of melt in July is significantly lower and comparable to melt in August. The main cause for this difference is the earlier disappearance of the snowpack on Midtdalsbreen, which happens in June or early July. The lower ice albedo enhances the amount of energy supplied by S_{net} . Net radiation dominates the surface energy balance at both AWS sites, but its relative contribution is larger on Storbreen. Over the entire period with melt its fraction of the total melt energy is 0.76 on Storbreen and 0.66 on Midtdalsbreen.

4.9 Accumulation and ablation

Snow accumulation is highly variable from year to year, but generally similar in timing and magnitude at the two

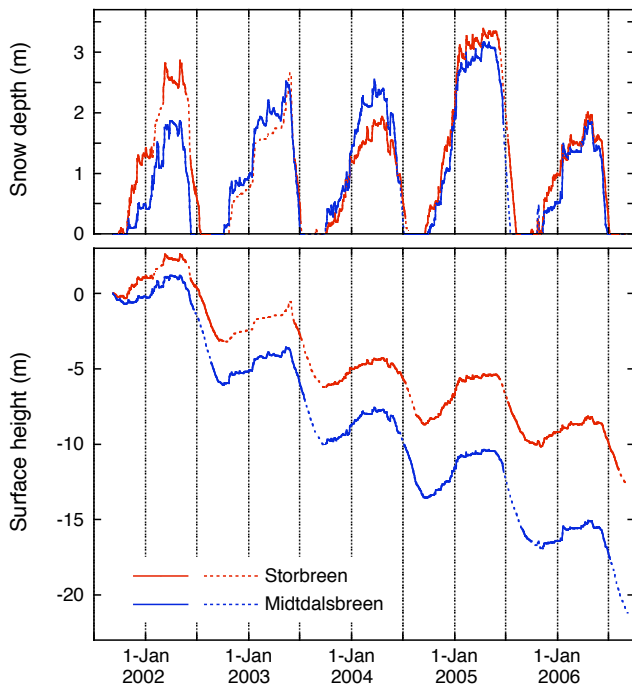


Fig. 12. Daily values of (a) snow depth and (b) cumulative surface height at the AWS sites on Storbreen and Midtdalsbreen for the entire period. Direct measurements from the sonic ranger are shown as solid lines, accumulation estimated from precipitation data and ablation computed with the energy balance model are drawn with dashed lines.

AWS sites (Fig. 12a). The similarity between the snow depth records indicates that the two glaciers are situated in a similar precipitation regime, even though Fig. 1 suggests a slightly more maritime climate on Midtdalsbreen. The largest differences between the two records occur when a heavy snowfall event takes place at only one of the two locations. To determine whether these occasional events are related to local or large-scale wind directions, we selected the periods with large differences in snow accumulation. For these periods, we examined both the wind direction measured at the AWS sites as well as the wind direction at the 850 hPa level from (re-)analyses by the European Centre for Medium-Range Weather Forecasts (ECMWF), but no relation was found. On several days with more snowfall on Storbreen, wind speeds were higher than 10 m s^{-1} on Midtdalsbreen, pointing towards fresh snow removal by snowdrift and sublimation. However, during other windy periods on Midtdalsbreen snow accumulation was similar or higher than on Storbreen, hence no common cause for the snowfall differences could be established.

The larger energy fluxes on Midtdalsbreen lead to a higher ablation rate than on Storbreen. The snowpack on Midtdalsbreen melts away more quickly in spring, resulting in a longer period with ice at the surface. For the five years considered in this study, the surface became snow-free be-

tween 10 June (in 2002) and 17 July (in 2005) on Midtdalsbreen, while on Storbreen the ice reappeared between 4 July (in 2006) and 12 August (in 2005). Over the entire period, the cumulative ice melt is 1.7 times larger on Midtdalsbreen (Fig. 12b). To quantify the effect of the earlier disappearance of the snowpack on Midtdalsbreen on the total ice melt, we compared the amount of ice melted in the periods with a snow-free surface at both locations. For these periods, cumulative ice melt on Midtdalsbreen is 30% larger than on Storbreen, entirely the result of the larger energy fluxes on Midtdalsbreen. Hence the effect of the earlier reappearance of the ice surface on Midtdalsbreen in the five summers considered, is as large as 40%.

5 Discussion

5.1 Uncertainties in measurements and calculations

Meteorological quantities measured on Storbreen and Midtdalsbreen were found to be generally highly correlated, while absolute differences can be considerable. The identical design of the AWSs minimizes uncertainties due to different instruments, sample intervals or measurement heights. Besides uncertainties due to measurement errors, the results from the energy balance model depend on the values chosen for the model parameters. By applying the same model to both data sets, we exclude uncertainties introduced by different model equations or computation methods. We estimated the accuracy of the measured and modelled variables, considering random and systematic measurement errors as well as uncertainties arising from processing steps and the model design (Table 2). In this section, we discuss the largest error sources and implications for the energy balance calculations.

Incoming solar radiation has the largest uncertainty of the measured variables. The instrument accuracy given by the manufacturers is $\pm 10\%$ for daily totals (Andreassen et al., 2008), suggesting large potential errors in daily values when solar irradiance is large. However, these random errors are considerably reduced when averaging over longer periods. Tilting of the mast is a possible source for systematic errors. We were able to reduce the systematic error in S_{in} with a tilt correction, but because only the approximate tilt angle is known, large uncertainties remain. Daily mean values for the tilt corrections applied to the solar radiation data from Midtdalsbreen rarely exceed $\pm 10 \text{ W m}^{-2}$. We investigated the effect of the tilt correction on the energy balance by recalculating the S_{in} values reported in Table 2 for Midtdalsbreen with uncorrected solar radiation measurements. The resulting annual and melt period mean values are 1 and 8 W m^{-2} higher, respectively; the contribution of net radiation to melt slightly increases from 66% to 68%. We assume that the applied tilt correction has reduced the errors in S_{in} , hence the remaining uncertainty is expected to be smaller than the values presented above.

The effective cloud optical depth calculated from the AWS measurements also has a large uncertainty (Table 2). The parameterization requires solar incoming radiation measurements for an unshaded site and can therefore only be determined during daytime when the solar zenith angle is large enough. An exponential relation with daily mean cloud fraction values was used to obtain the effective cloud optical depth for all days (Sect. 3.2), including winter days with all-day shading of the AWS site. Although the fitted function describes the relation between cloud fraction and cloud optical depth well, large uncertainties are associated with the computed values for individual days.

The largest model uncertainties result from the calculation of the turbulent fluxes, as the available data only provide estimates for the stability correction and the surface roughness length, due to the limited number of usable data and the highly variable nature of the surface and the boundary-layer. Giesen et al. (2008) investigated the sensitivity of the turbulent fluxes and modelled melt to changes in the roughness length for momentum and the stability correction. When z_{0v} on Midtdalsbreen is increased to 5 mm, the sum of the mean turbulent fluxes during melt becomes 9 W m^{-2} higher, while the contribution of the turbulent fluxes to melt increases by 4%. Omitting the stability correction has a similar effect on the results; applying the full stability correction reduces the absolute and relative contributions to melt by the turbulent fluxes by a comparable magnitude. As the values for z_{0v} and the stability correction used in this study have been derived from local observations, we expect that these sensitivity tests give the upper limit of uncertainties associated with the turbulent fluxes on Midtdalsbreen. Uncertainties in the turbulent fluxes will have a smaller effect on the energy balance at Storbreen, where the turbulent fluxes are less important than on Midtdalsbreen.

Although the uncertainties in the results introduced by measurement errors and model uncertainties are considerable (Table 2), they are mostly smaller than the observed differences in meteorological quantities between the two locations. Hence, it is unlikely that these differences result from measurement or model uncertainties.

5.2 Comparison to other glaciers

To compare the surface energy fluxes on Storbreen and Midtdalsbreen with values on other glaciers, we selected a number of energy balance studies conducted on glaciers at comparable latitudes, between 50° and 70° on both hemispheres. Table 3 lists the absolute values for the energy fluxes found in these studies and their contribution to the energy balance. The reported values are mostly averages over the measurement period and not specifically for a melting surface. However, most studies are conducted during the main melt season and the surface is often assumed or found to be melting continuously. The mean air temperature T_a and wind speed v at the study sites are also listed in Table 3, when reported. Hu-

midity is not included because it is less often reported and cannot be compared directly as some studies report relative and others absolute humidity values.

The mean absolute and relative values for the energy fluxes on Storbreen found in this study are higher than those reported for Storbreen for the summer of 1955 (Liestøl, 1967), but the numbers reported for 1955 are within the range of the annual values reported for the period 2001–2006 (Andreassen et al., 2008). Energy fluxes at the AWS site on Storbreen compare both in absolute and relative numbers to McCall Glacier (Klok et al., 2005). The total melt energy is also comparable to values reported for Storglaciären (Hock and Holmgren, 1996), Nordbogletscher (Braithwaite and Olesen, 1990) and Omnsbreen (Messel, 1971), but at those locations turbulent fluxes are more important. In fact, Storbreen has the highest contribution by net radiation of all the selected studies. A probable explanation is that many of the glaciers in this latitude range are situated in more maritime climates than Storbreen, but the surface albedo on Storbreen may also be lower. In relative numbers, the values found for Midtdalsbreen in this study compare well to those reported for Storglaciären, Qamanârssûp sermia (Braithwaite and Olesen, 1990), Ecology Glacier (Bintanja, 1995) and the measurements at 2300 m a.s.l. on Peyto Glacier (Munro, 1990), which were obtained above an ice surface. The absolute values for net radiation and total melt energy on Midtdalsbreen are similar to those measured on Qamanârssûp sermia and Peyto Glacier as well, although the values for the separate turbulent fluxes are different. The melting energy on Midtdalsbreen is considerably larger than on Omnsbreen, a small glacier located approximately 11 km north of Midtdalsbreen. The values for the turbulent fluxes measured on the two glaciers are comparable, but net radiation is much smaller on Omnsbreen. During the investigation period in 1968, Omnsbreen remained snow-covered, in 1969 the ice was not exposed before 21 July (Messel, 1971). The higher surface albedo on Omnsbreen resulted in smaller net radiation than during melt periods on Midtdalsbreen.

The magnitude of the energy fluxes on Storbreen and Midtdalsbreen lies in between numbers reported for other glaciers at comparable latitudes. However, no simple dependencies of the absolute or relative energy fluxes on latitude, altitude, air temperature or wind speed could be found for the studies listed in Table 3. There are several reasons why a thorough comparison between these studies cannot be made. First, the measurements were obtained in different years and interannual variability can be large. Second, at the latitudes considered here, the absolute values and relative contributions of the energy fluxes change significantly during the melt season (Figs. 9 and 11b), hence the period of measurement largely influences the results. Furthermore, measurements are made over different surface types (snow and/or ice) and the range in altitudes is large, influencing the absolute values of the energy fluxes and their relative contribution to the energy balance. Moreover, in the selected studies various

Table 3. Mean values of the energy fluxes (W m^{-2}) and relative contribution to the surface energy balance (%; boldface numbers) from several energy balance studies. Values are rounded to the nearest integer. H_r is heat supplied by rain. The total melt energy Q is the sum of the individual energy fluxes, not measured ablation as these are not always equal. When reported, the surface type (snow/firn/ice), altitude (m a.s.l.), mean air temperature T_a ($^{\circ}\text{C}$) and wind speed v (m s^{-1}) at the study site are also listed.

Location Reference	Latitude	Period	Surface Altitude	T_a v	R_{net}	H_{sen}	H_{lat}	H_r	G	Q
McCall Glacier, Alaska (Klok et al., 2005)	69° N	15 Jun–20 Aug 2004	snow/ice 1715	5.3 3.1	93 74	31 25	6 5	– –4	–5	125
Storglaciären, Sweden (Hock and Holmgren, 1996)	68° N	19 Jul–27 Aug 1994	snow/ice 1370	5.4 2.5	73 66	33 30	5 5	– –3	–3	110
Qamanârssûp sermia, Greenland (Braithwaite and Olesen, 1990)	64° N	1 Jun–31 Aug 1980–1986	ice 790	– –	103 64	62 39	–6 –4	– –	–	161
West Gulkana Glacier, Alaska (Brazel et al., 1992)	63° N	21 Jun–19 Jul 1986	snow/ice 1520	– –	79 57	49 35	11 8	1 0	–	139
Ecology Glacier, King George Island (Bintanja, 1995)	62° S	17 Dec–16 Jan 1990–1991	snow/ice 100	1.9 5.7	61 64	27 29	7 7	– –	–	96
Storbreen, Norway (Liestøl, 1967)	62° N	6 Jul–8 Sep 1955	snow/ice 1600	– –	73 56	40 31	17 13	– –	–	130
Storbreen, Norway (this study)	62° N	7 Sep–6 Sep 2001–2006	snow/ice 1570	4.9 3.3	89 76	20 17	9 8	– –2	–2	117
Nordbogletscher, Greenland (Braithwaite and Olesen, 1990)	61° N	1 Jun–31 Aug 1979–1983	ice 880	– –	79 71	32 29	2 2	– –	–	111
Worthington Glacier, Alaska (Streten and Wendler, 1968)	61° N	16 Jul–1 Aug 1967	ice ± 850	9.6 2.1	127 51	68 29	47 20	– –	–	242
Omnsbreen, Norway (Messel, 1971)	60° N	3 Jun–8 Sep 1968–1969	snow/ice 1540	– –	57 52	35 32	16 15	– –	–	108
Midtdalsbreen, Norway (this study)	60° N	7 Sep–6 Sep 2001–2006	snow/ice 1450	5.3 6.0	104 66	39 25	16 11	– –2	–2	157
Lemon Creek Glacier, Alaska (Wendler and Streten, 1969)	58° N	5 Aug–20 Aug 1968	firn 1200	7.6 1.5	41 48	36 43	8 9	– –	–	84
Koryto Glacier, Russia (Konya et al., 2004)	55° N	7 Aug–12 Sep 2000	snow 810	7.6 2.4	43 33	59 44	31 23	– –	–	133
Hodges Glacier, South Georgia (Hogg et al., 1982)	54° S	1 Nov–4 Apr 1973–1974	snow/ice 375	– 3.8	47 55	41 48	–2 –3	– –	–	86
Glaciar Lengua, Chile (Schneider et al., 2007)	53° S	28 Feb–12 Apr 2000	ice 450	5.9 4.1	57 35	86 54	12 7	7 4	–	162
Peyto Glacier, Canada (Munro, 1990)	52° N	17 Jun–6 Jul 1988	ice 2300	– –	108 65	57 34	2 1	– –	–	166
		21 Jun–5 Jul 1988	snow 2500	– –	39 51	32 42	5 7	– –	–	76
Tyndall Glacier, Chile (Takeuchi et al., 1995a,b)	51° S	9 Dec–17 Dec 1993	ice 700	5.1 6.6	137 51	111 42	19 7	– –	–	266
Moreno Glacier, Chile (Takeuchi et al., 1995a,b)	50° S	12 Nov–27 Nov 1993	ice 330	7.9 4.9	139 54	126 49	–9 –4	– –	–	256

methods are applied to calculate the turbulent fluxes and the contribution of the fluxes to surface melt, which should as well be considered when comparing results. The values reported in Table 3 for Storbreen and Midtdalsbreen are averages over half-hourly periods with surface melt, as given by the energy balance model. Changing to hourly instead of half-hourly intervals reduced the reported fluxes by 1 to 2%, whereas the relative contributions to melt did not change notably. Although the surface on Storbreen and Midtdals-

breen was always melting during the day in July and August, the surface temperature dropped below the melting point on clear-sky nights. If we had included the periods without melt in our calculation, the average values for net radiation in July and August had been 13% (Midtdalsbreen) and 18% (Storbreen) lower. The turbulent fluxes and the subsurface heat flux at the two AWS locations were found to be less sensitive to including periods without melt, as they have a smaller daily cycle. The contribution to melt by the different fluxes

Table 4. Mean values and linear correlations of daily mean values of meteorological quantities for Storbreen (S), Sognefjellhytta (So), Midtdalsbreen (M) and Finsevatn (F) over the period 7 September 2001–6 September 2006, for all days with data available for all stations.

Variable	Number of days	Coverage (%)	Mean				Correlation				
			S	M	So	F	S–So	S–F	M–So	M–F	So–F
Air temperature (°C)	1518	83	−2.4	−1.7	−2.1	−1.4	0.98	0.92	0.98	0.94	0.97
Relative humidity (%)	927	51	76.4	80.6	83.6	88.3	0.80	0.52	0.78	0.66	0.76
Specific humidity (g kg ^{−1})	805	44	3.0	3.2	3.3	3.6	0.99	0.98	0.98	0.99	0.99
Wind speed (m s ^{−1})	1549	85	3.8	6.6	3.9	5.2	0.70	0.71	0.72	0.90	0.75
Air pressure (hPa)	1305	71	834.0	848.5	850.5	872.9	1.00	0.99	1.00	1.00	1.00

changed by only 1–3% when periods without melt in July and August were included. We conclude that a thorough comparison between energy fluxes at two different locations can only be made when the period of measurement and the methods applied to determine the turbulent fluxes and the contribution to melt are identical, as they are in the present study.

5.3 Comparison to nearby weather stations

As glacio-meteorological records are only available for a limited number of glaciers, mass and energy balance models are mostly driven by meteorological data measured at a distance from the glacier of interest. Although air temperature and air pressure are generally correlated over relatively large distances, variables like wind speed and cloudiness depend on small-scale topography and other local conditions. In this section we compare the records from Storbreen and Midtdalsbreen with measurements from two NMI weather stations located close to the respective glaciers. Sognefjellhytta (1413 m a.s.l.) is situated 8 km south-west from Storbreen, Finsevatn (1210 m a.s.l.) is located 4 km north-east from the AWS on Midtdalsbreen. Both stations are automatic weather stations with hourly measurements of air temperature, relative humidity, air pressure, wind speed and wind direction. Precipitation is measured at Finsevatn, but is excluded from the comparison as these measurements are very uncertain at automatic weather stations and only snow accumulation is recorded at the AWSs on Storbreen and Midtdalsbreen. Relative humidity measurements were corrected for temperatures below 0°C (Sect. 3.1). Specific humidity has been calculated from air temperature, relative humidity and air pressure when these three variables were available. Mean values and linear correlations (r) have been computed for all days with measurements from all four stations (Table 4) and are not annual mean values. The relative humidity record from Finsevatn contains large data gaps, hence the number of days included for relative and specific humidity is much smaller than for the other variables.

Daily mean air temperatures at Storbreen, Midtdalsbreen and Sognefjellhytta are highly correlated, while correlations with air temperatures at Finsevatn are considerably lower. On clear-sky days, the diurnal temperature cycle is much

stronger at Sognefjellhytta and Finsevatn than at the glacier sites (Fig. 13). On such days, low wind speeds are recorded outside the glaciers, promoting heating of the near-surface air during the day and strong cooling at night. On the sloping glacier surface, wind speeds are higher and the air is better mixed. Since especially the clear-sky nights are colder outside the glaciers, mean air temperatures for Sognefjellhytta and Finsevatn are lower than expected from an extrapolation of the mean air temperatures at the glacier sites.

The highest wind speeds are measured on Midtdalsbreen and are well correlated with wind speeds at Finsevatn, while the correlation of wind speeds at other locations is significantly lower. Wind directions at Sognefjellhytta and Finsevatn have two very pronounced directions (Fig. 14), on Midtdalsbreen and Storbreen wind directions are more variable. Although the dominant wind directions at Sognefjellhytta and Finsevatn differ, westerly or south-easterly winds occur at the same time, hence the measured wind direction is likely a large-scale wind direction modified by local topography. These large-scale winds are often recorded on Midtdalsbreen, while on Storbreen down-glacier winds are dominant and large-scale wind directions only occur occasionally. The comparison with Sognefjellhytta and Finsevatn supports the supposition (Sect. 4.2) that wind characteristics at Midtdalsbreen are generally determined by the large-scale circulation and that wind speeds on Storbreen are often of a local nature.

To investigate how a change in meteorological input data affects the calculated energy balance for Storbreen and Midtdalsbreen, we performed additional model runs with air temperature, relative humidity or wind speed taken from a different location. The only melt season with these three variables available for all four AWSs, is the summer of 2006. To capture the entire melt season, the model was run from 1 March to 8 September 2006, the end of the records from Storbreen and Midtdalsbreen. We applied a lapse rate of 6.0°C km^{−1} to extrapolate air temperatures to the glacier AWS altitudes. We estimated the change in incoming longwave radiation from the new air temperature and cloud cover by inverting the method by Van den Broeke et al. (2006), which is normally used to estimate fractional cloud cover from incoming longwave radiation and air temperature. Relative humidity and wind speed data were used without alterations. Snow

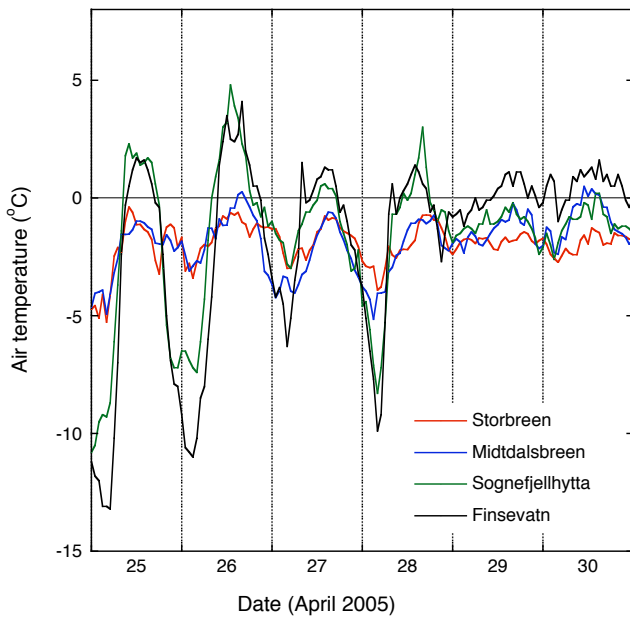


Fig. 13. Hourly air temperatures at Storbreen, Midtdalsbreen, Sognefjellhytta and Finsevatn on six days in April 2005.

depth and surface albedo are taken from the measurements, hence the positive feedback process of a possible change in ice reappearance date on net solar radiation is not included. The model has been run for Storbreen with data from Midtdalsbreen and Sognefjellhytta, for Midtdalsbreen we used data from Storbreen and Finsevatn.

Using relative humidity data from another location affects the modelled melt by less than 2%. Applying air temperatures from the other glacier AWS also has a small effect. However, air temperatures extrapolated from Sognefjellhytta result in 11% more melt on Storbreen and using air temperatures from Finsevatn lead to an 8% increase in modelled melt on Midtdalsbreen. In spring, applying a different temperature record does not notably affect modelled melt, despite the large differences in the daily cycle. In summer, air temperatures on the glaciers are almost continuously overestimated using air temperatures from Sognefjellhytta and Finsevatn. The air above the glaciers is cooled by the relatively cold glacier surface and variable lapse rates should be applied. Using wind speeds measured on Midtdalsbreen in the energy balance calculations for Storbreen and vice versa induces the largest changes in modelled melt: a 17% increase on Storbreen and a 13% decrease on Midtdalsbreen. Wind speeds from Sognefjellhytta affect the melt on Storbreen by less than 1%, while wind speeds from Finsevatn reduce melt on Midtdalsbreen by 9%. Hence, on glaciers where the turbulent fluxes contribute significantly to the total melt, local wind speed and air temperature measurements are required for an accurate calculation of the surface energy balance. Energy balance models driven with data from outside the

glacier boundary-layer need to be calibrated with measurements made on the glacier. Alternatively, an energy balance model including glacier boundary-layer processes could be applied (e.g. Denby, 1999).

6 Conclusions

We compared measurements made with two identical AWSs on Storbreen and Midtdalsbreen, two glaciers in southern Norway, 120 km apart. Except for wind speed and wind direction, daily mean values of all recorded variables exhibit simultaneous fluctuations of comparable magnitude. Especially daily mean air temperature is highly correlated ($r=0.98$); the good correlation persists when the seasonal cycle is removed ($r=0.95$). The average wind speed is a factor 1.75 higher on Midtdalsbreen than on Storbreen. The wind climate on Midtdalsbreen is mainly dominated by the large-scale circulation. On Storbreen, a katabatic wind develops regularly and determines the dominant wind direction. Katabatic winds are also observed on Midtdalsbreen, but less frequently, as wind speeds associated with the large-scale circulation are much higher. On Midtdalsbreen, westerly winds are dominant.

Incoming and net solar radiation are larger on Midtdalsbreen, due to a higher atmospheric transmissivity and an earlier disappearance of the snowpack than on Storbreen. In spring and summer, thicker clouds on Storbreen result in more positive incoming and net longwave radiation than on Midtdalsbreen. The turbulent fluxes are a factor 1.9 larger on Midtdalsbreen, mainly due to the larger wind speeds, but secondly because the air is slightly warmer and more humid.

On both glaciers net radiation is the largest contributor to surface melt, its relative contribution is larger on Storbreen (76%) than on Midtdalsbreen (66%). The importance of net radiation decreases over the melt season, while the turbulent fluxes become more important. Recorded snow depth at the two AWS sites generally shows simultaneous snowfall events of comparable magnitude. The larger surface energy fluxes on Midtdalsbreen result in a larger ablation rate and an earlier reappearance of the ice surface. The consequent drop in albedo further enhances the difference in ablation at the two glaciers; annual ice melt is 70% larger on Midtdalsbreen.

The absolute values and relative contributions of the surface energy fluxes to surface melt found for Storbreen and Midtdalsbreen lie within the range of values reported from energy balance studies performed on glaciers at comparable latitudes, although the contribution of net radiation for Storbreen is relatively large.

Recalculating the energy balance with meteorological variables measured outside the glacier boundary-layer shows that large errors originate when differences in variables caused by the glacier environment are not accounted for. Hence, an energy model driven with meteorological data measured outside the glacier needs to be calibrated with

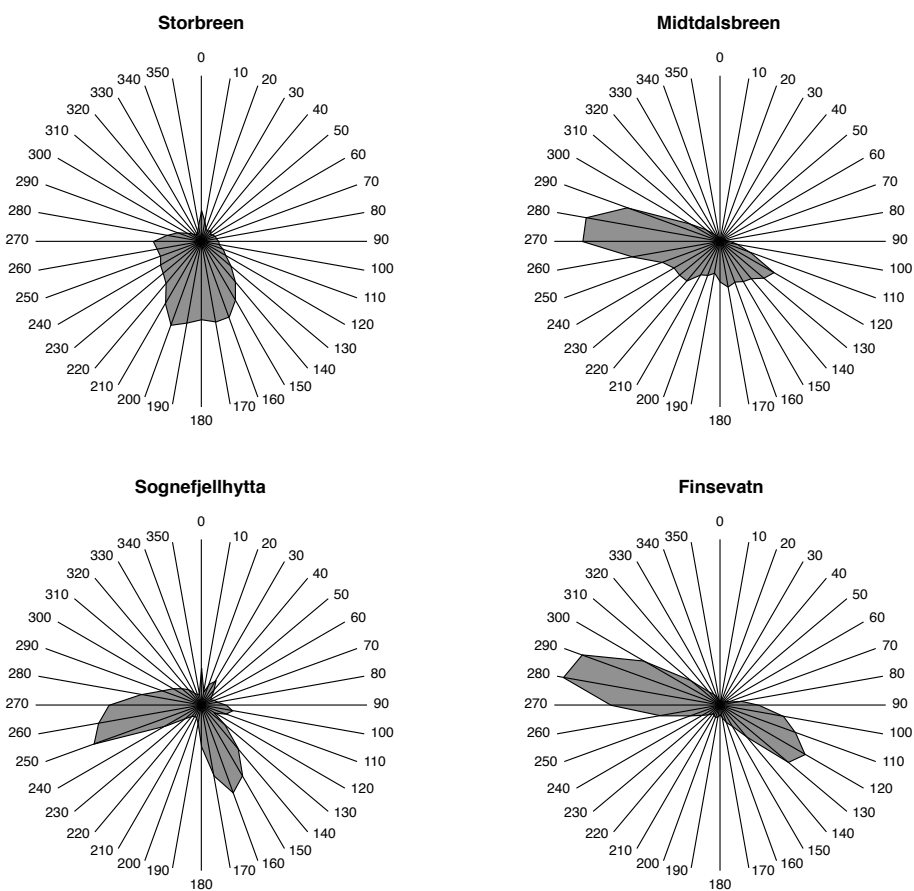


Fig. 14. Wind direction frequency distributions for Storbreen, Midtdalsbreen, Sognefjellhytta and Finsevatn, where all hourly intervals with measurements at all four stations are included (63% of all hourly intervals).

measurements made on the glacier or should include a glacier-boundary layer model.

Acknowledgements. We thank the IMAU technicians, in particular Wim Boot, for the dedicated maintenance of the AWSs and several colleagues for their assistance in the field. The Norwegian Meteorological Institute is thanked for access to and use of their meteorological database eKlima. ECMWF ERA-40 and operational data used in this study have been provided by ECMWF. This project has been supported by NWO (Netherlands Organisation for Scientific Research) through the Spinoza-grant to J. Oerlemans.

References

- Andreas, E. L.: A theory for the scalar roughness and the scalar transfer coefficients over snow and sea ice, *Bound.-Lay. Meteorol.*, 38, 159–184, 1987.
- Andreassen, L. M.: Comparing traditional mass balance measurements with long-term volume change extracted from topographical maps: a case study of Storbreen glacier in Jotunheimen, Norway, for the period 1940–1997, *Geogr. Ann. A*, 81, 467–476, 1999.
- Andreassen, L. M., Elvehøy, H., Kjöllmoen, B., Engeset, R. V., and Haakensen, N.: Glacier mass-balance and length variation in Norway, *Ann. Glaciol.*, 42, 317–325, 2005.
- Andreassen, L. M., Van den Broeke, M. R., Giesen, R. H., and Oerlemans, J.: A 5 year record of surface energy and mass balance from the ablation zone of Storbreen, Norway, *J. Glaciol.*, 54, 245–258, 2008.
- Bintanja, R.: The local surface energy balance of the Ecology Glacier, King George Island, Antarctica: measurements and modelling, *Antarct. Sci.*, 7, 315–325, 1995.
- Braithwaite, R. J. and Olesen, O. B.: A simple energy-balance model to calculate ice ablation at the margin of the Greenland ice sheet, *J. Glaciol.*, 36, 222–228, 1990.
- Brazel, A. J., Tempe, F. B., Chambers, D., and Kalkstein, L. S.: Summer energy balance on West Gulkana Glacier, Alaska, and linkages to a temporal synoptic index, *Z. Geomorphol. Suppl. Band*, 86, 15–34, 1992.
- Curry, J. A. and Webster, P. J.: *Thermodynamics of atmospheres and oceans*, Academic Press, San Diego, 1999.
- Denby, B.: Second-order modelling of turbulence in katabatic flows, *Bound.-Lay. Meteorol.*, 92, 65–98, 1999.
- Dyer, A. J.: A review of flux-profile relationships, *Bound.-Lay. Meteorol.*, 7, 363–372, 1974.
- Fitzpatrick, M. F., Brandt, R. E., and Warren, S. G.: Transmission

- of solar radiation by clouds over snow and ice surfaces: a parameterization in terms of optical depth, solar zenith angle, and surface albedo, *J. Climate*, 17, 266–275, 2004.
- Giesen, R. H., Van den Broeke, M. R., Oerlemans, J., and Andreassen, L. M.: The surface energy balance in the ablation zone of Midtdalsbreen, a glacier in southern Norway: Interannual variability and the effect of clouds, *J. Geophys. Res.*, 113, D21111, doi:10.1029/2008JD010390, 2008.
- Green, F. H. W. and Harding, R. J.: The altitudinal gradients of air temperature in southern Norway, *Geogr. Ann. A*, 62, 29–36, 1980.
- Hock, R.: Glacier melt: a review of processes and their modelling, *Prog. Phys. Geog.*, 29, 362–391, 2005.
- Hock, R. and Holmgren, B.: Some aspects of energy balance and ablation of Storglaciären, Northern Sweden, *Geogr. Ann. A*, 78, 121–131, 1996.
- Hogg, I. G. G., Paren, J. G., and Timmis, R. J.: Summer heat and ice balances on Hodges Glacier, South Georgia, Falkland Islands Dependencies, *J. Glaciol.*, 28, 221–238, 1982.
- Holtslag, A. A. M. and De Bruin, H. A. R.: Applied modeling of the nighttime surface energy balance over land, *J. Appl. Meteorol.*, 27, 689–704, 1988.
- Kjøllmoen, B., Andreassen, L. M., Elvehøy, H., Jackson, M., Tvede, A. M., Laumann, T., and Giesen, R. H.: Glaciological investigations in Norway in 2006, NVE Report No 1, Norwegian Water Resources and Energy Directorate, Oslo, 99 pp., 2007.
- Klemsdal, T.: A glacio-meteorological study of Gråsubreen, Jotunheimen, in: *Norsk Polarinstittutt – Årbok 1968*, Norsk Polarinstittutt, Oslo, Norway, 58–74, 1970.
- Klok, E. J., Nolan, M., and Van den Broeke, M. R.: Analysis of meteorological data and the surface energy balance of McCall Glacier, Alaska, USA, *J. Glaciol.*, 51, 451–461, 2005.
- Konya, K., Matsumoto, T., and Naruse, R.: Surface heat balance and spatially distributed ablation modelling at Koryto Glacier, Kamchatka peninsula, Russia, *Geogr. Ann. A*, 86A, 337–348, 2004.
- Liestøl, O.: Storbreen Glacier in Jotunheimen, Norway, *Norsk Polarinstittutt Skrifter Nr. 141*, Norsk Polarinstittutt, Oslo, Norway, 63 pp., 1967.
- Messel, S.: Mass and heat balance of Omnsbreen – a climatically dead glacier in southern Norway, *Norsk Polarinstittutt Skrifter No. 156*, Norsk Polarinstittutt, Oslo, Norway, 43 pp., 1971.
- Messel, S.: Energibalansundersøkelser på breer i Norge 1954–1981, in: *Glasiologiske undersøkelser i Norge 1982*, NVE rapport Nr. 1–85, edited by Roland, E. and Haakensen, N., Norwegian Water Resources and Energy Directorate, Oslo, Norway, 45–59, 1985.
- Munro, D. S.: Comparison of melt energy computations and ablatometer measurements on melting ice and snow, *Arctic Alpine Res.*, 22, 153–162, 1990.
- Oerlemans, J.: *Glaciers and Climate Change*, Balkema, Lisse, 2001.
- Ohmura, A.: Physical basis for the temperature-based melt-index method, *J. Appl. Meteorol.*, 40, 753–761, 2001.
- Schneider, C., Kilian, R., and Glaser, M.: Energy balance in the ablation zone during the summer season at the Gran Campo Nevado Ice Cap in the Southern Andes, *Global Planet. Change*, 59, 175–188, 2007.
- Streten, N. A. and Wendler, G.: The midsummer heat balance of an Alaskan maritime glacier, *J. Glaciol.*, 7, 431–440, 1968.
- Takeuchi, Y., Naruse, R., and Satow, K.: Characteristics of heat balance and ablation on Moreno and Tyndall glaciers, Patagonia, in the summer 1993/94, *Bull. Glacier Res.*, 13, 45–56, 1995a.
- Takeuchi, Y., Satow, K., Naruse, R., Ibarzabal, T., Nishida, K., and Matsuoka, K.: Meteorological features at Moreno and Tyndall glaciers, Patagonia, in the summer 1993/94, *Bull. Glacier Res.*, 13, 35–44, 1995b.
- Van den Broeke, M. R., Reijmer, C. H., and Van de Wal, R. S. W.: Assessing and improving the quality of unattended radiation observations in Antarctica, *J. Atmos. Ocean. Tech.*, 21, 1417–1431, 2004.
- Van den Broeke, M. R., Reijmer, C. H., Van As, D., Van de Wal, R. S. W., and Oerlemans, J.: Seasonal cycles of Antarctic surface energy balance from automatic weather stations, *Ann. Glaciol.*, 41, 131–139, 2005.
- Van den Broeke, M. R., Reijmer, C. H., Van As, D., and Boot, W.: Daily cycle of the surface energy balance in Antarctica and the influence of clouds, *Int. J. Climatol.*, 26, 1587–1605, 2006.
- Van den Broeke, M. R., Smeets, P., Ettema, J., and Kuipers Munneke, P.: Surface radiation balance in the ablation zone of the west Greenland ice sheet, *J. Geophys. Res.*, 113, doi: 10.1029/2007JD009283, 2008a.
- Van den Broeke, M., Smeets, P., Ettema, J., Van der Veen, C., Van de Wal, R., and Oerlemans, J.: Partitioning of melt energy and meltwater fluxes in the ablation zone of the west Greenland ice sheet, *The Cryosphere*, 2, 179–189, 2008b.
- Wendler, G. and Streten, N. A.: A short term heat balance study on a coast range glacier, *Pure Appl. Geophys.*, 77, 68–77, 1969.
- Willis, I. C., Arnold, N. S., and Brock, B. W.: Effect of snowpack removal on energy balance, melt and runoff in a small supraglacial catchment, *Hydrol. Process.*, 16, 2721–2749, 2002.



ELSEVIER

Available online at www.sciencedirect.com

SCIENCE @ DIRECT®

Global and Planetary Change 39 (2003) 215–225

GLOBAL AND PLANETARY
CHANGE

www.elsevier.com/locate/gloplacha

Warming permafrost in European mountains

Charles Harris^{a,*}, Daniel Vonder Mühll^b, Ketil Isaksen^c, Wilfried Haeberli^d,
Johan Ludvig Sollid^e, Lorenz King^f, Per Holmlund^g, Francesco Dramis^h,
Mauro Guglielminⁱ, David Palacios^j

^aDepartment of Earth Sciences, Cardiff University, P.O. Box 914, Cardiff CF10 3YE, UK

^bUniversity of Basel, Petergraben 35/3, CH-4051 Basel, Switzerland

^cNorwegian Meteorological Institute, P.O. Box 43 Blindern, N-0313 Oslo, Norway

^dDepartment of Geography, University of Zürich, Winterthurerstrasse 190, CH-8057 Zürich, Switzerland

^eDepartment of Physical Geography, University of Oslo, P.O. Box 1042, Blindern, N-0316 Oslo, Norway

^fGeographical Institute, Justus Liebig University, Senckenbergstrasse 1, Giessen D35390, Germany

^gDepartment of Physical Geography, Stockholm University, S-10591 Stockholm, Sweden

^hDepartment of Geological Sciences, Third University of Rome, Largo San Leonardo Murialdo, I-00146 Rome, Italy

ⁱGeological Survey of Lombardy, Milan, Italy

^jDepartamento de AGR y Geografía Física, Universidad Complutense, Madrid 28040, Spain

Received 4 July 2002; accepted 23 April 2003

Abstract

Here we present the first systematic measurements of European mountain permafrost temperatures from a latitudinal transect of six boreholes extending from the Alps, through Scandinavia to Svalbard. Boreholes were drilled in bedrock to depths of at least 100 m between May 1998 and September 2000. Geothermal profiles provide evidence for regional-scale secular warming, since all are nonlinear, with near-surface warm-side temperature deviations from the deeper thermal gradient. Topographic effects lead to variability between Alpine sites. First approximation estimates, based on curvature within the borehole thermal profiles, indicate a maximum ground surface warming of +1 °C in Svalbard, considered to relate to thermal changes in the last 100 years. In addition, a 15-year time series of thermal data from the 58-m-deep Murtèl–Corvatsch permafrost borehole in Switzerland, drilled in creeping frozen ice-rich rock debris, shows an overall warming trend, but with high-amplitude interannual fluctuations that reflect early winter snow cover more strongly than air temperatures. Thus interpretation of the deeper borehole thermal histories must clearly take account of the potential effects of changing snow cover in addition to atmospheric temperatures.

© 2003 Elsevier B.V. All rights reserved.

Keywords: Permafrost; Global warming; Borehole temperatures; European mountains

1. Introduction

Initial measurements of geothermal profiles from a series of six recently drilled boreholes in the high-elevation mountain permafrost zone of Europe are reported in this paper. All boreholes were drilled by

* Corresponding author. Tel.: +44-2920-874336; fax: +44-2920-874326.

E-mail address: harrisc@cardiff.ac.uk (C. Harris).

the EU-funded Permafrost and Climate in Europe (PACE) Project (Harris et al., 2001a,b) between May 1998 and September 2000. The locations of the PACE boreholes discussed here are shown in Fig. 1, and include the Schilthorn and Stockhorn Mountains (Switzerland), Stelvio Pass (Italy) Juvvasshøe, Jotunheimen (Norway), Tarfalaryggen (Sweden) and Janssonhaugen (Svalbard). At the Valeta Peak (Sierra Nevada, Spain), permafrost was not encountered. Here, lateral heat flux from an adjacent steep south-facing mountainside leads to ground temperatures close to $+2\text{ }^{\circ}\text{C}$. The PACE borehole at this site is therefore excluded from the analysis. However, shallow geothermal measurements on the north-facing slope of Valeta Peak indicate the presence of patchy permafrost in favoured localities (Gomez et al., 2001). All PACE boreholes extend to a depth of

100 m or more, and apart from Valeta, are in frozen bedrock (Table 1). The network forms a new European long-term permafrost monitoring facility. Time series data from the Murtèl–Corvatsch borehole (Switzerland), drilled in 1987 to a depth of 58 m in creeping frozen ice-rich rock debris (Haerberli et al., 1988), are also presented in this paper to illustrate the significant role of snow cover in buffering the near-surface geothermal response to atmospheric thermal changes.

Permafrost has been identified as one of six cryospheric indicators of global climate change within the monitoring framework of the WMO Global Climate Observing System (GCOS) (Cihlar et al., 1997; Burgess et al., 2000; Harris et al., 2001a,b). Permafrost reacts sensitively to changes in atmospheric temperature (e.g. Anisimov and Nelson, 1996; Jin et al., 2000), and it is predicted that degradation will lead to extensive thaw subsidence in the arctic (Nelson et al., 2001) and increased slope instability in lower latitude mountains (Haerberli, 1992; Haerberli et al., 1997; Haerberli and Beniston, 1998; Dramis et al., 1995; Harris et al., 2001a,b). Environmental implications of on-going climate change may therefore be significant. In Switzerland, for instance, permafrost underlies about 5% of the country (equivalent to twice the currently glacierized area) (Keller et al., 1998).

A rise in ground surface temperature is associated with responses at three time and depth scales in permafrost (Haerberli et al., 1993; Haerberli and Beniston, 1998); (a) thickening and warming of the surface active layer within one to several years (Anisimov et al., 1997), (b) development of a nonlinear temperature profile at depths of several tens to hundreds of metres over periods of many decades (Lachenbruch and Marshall, 1986), and (c) permafrost thinning due to thawing at the base, within tens of decades, centuries or thousands of years, depending on ground ice content and the initial permafrost thickness. In many arctic permafrost boreholes, for example in Alaska, ground temperatures in the upper 50–100 m show marked warm-side deviation from the deeper thermal gradient (Lachenbruch and Marshall, 1986; Lachenbruch et al., 1988; Pavlov, 1994; Osterkamp, 1983; Osterkamp and Romanovsky, 1999) and suggest surface warming over the past century of between $+2$ and $4\text{ }^{\circ}\text{C}$.

Inversion modelling offers the potential for estimating the evolution of former changes in surface

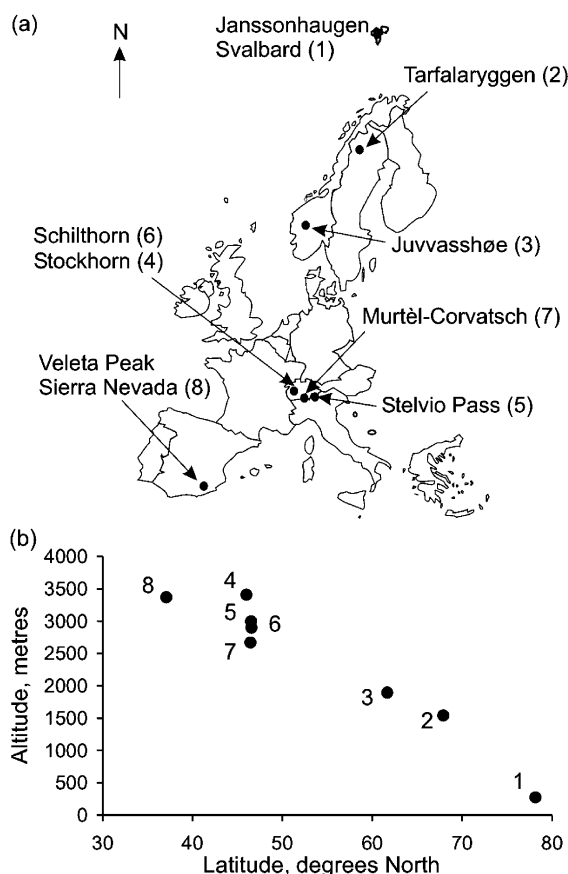


Fig. 1. PACE permafrost borehole network: (a) geographical distribution, (b) altitudinal distribution.

Table 1
Summary of PACE borehole sites. MAAT is the Mean Annual Air Temperature

Borehole name and depth	Date drilled	Altitude (m a.s.l.)	Topography	Bedrock	MAAT (°C)	Ground cover
Janssonhaugen Adventdalen, Svalbard, 102 m	May 1998	275	Small rise in valley floor	Fine-grained sandstone	− 8	Thin weathered rock, little vegetation
Tarfalaryggen, Sweden, 100 m	March 2000	1540	Mountain ridge	Massive amphibolite	− 7	ca. 4 m weathered bedrock
Juvvasshøe, Jotunheimen, Norway, 129 m	August 1999	1894	Mountain plateau	Gneiss	− 4	3–4 m weathered bedrock
Schilthorn Berner Oberland, Switzerland, 101 m	August 2000	2900	Slope beneath mountain summit	Calcareous schist	− 3.5	Thin weathered bedrock
Stockhorn plateau, Wallis, Switzerland, 100.7 m	July 2000	3410	Crest plateau	Albite–muscovite schist	− 5.5	Weathered bedrock
Stelvio Pass, Lombardia, Italy, 100.3 m	May 1998	3000	Rounded summit	Dolomitic limestone	− 3.7	Weathered bedrock
Murtèl–Corvatsch, 58 m	June 1987	2670	Rock glacier	Ice-rich boulders and scree	− 3.5	Boulders

temperature from observed geothermal profiles (e.g. Shen and Beck, 1991; Beltrami and Mareschal, 1995; Beltrami and Harris, 2001) and since heat advection by groundwater flow can be excluded in ice-bearing permafrost, inversion modelling is particularly appropriate. However, in the European mountains, topographic influences on the upper thermal boundary must be considered, and at lower latitudes the significance of aspect may be considerable, so that three-dimensional analysis of the geothermal fields is a critical component of inversion modelling. This analysis is currently in progress, and results are not yet available. It is important to stress, therefore, that the current paper presents only a first approximation of likely surface warming at the PACE borehole sites interpreted from the observed near-surface geothermal profiles.

2. The monitoring network

The six PACE boreholes discussed in this paper form a latitudinal transect extending from 46°31' N to 78°10' N from the Alps through the Scandinavian mountains to Svalbard (Table 1). During drilling, boreholes were flushed with chilled compressed air, and no liquids were used. The northernmost borehole at Janssonhaugen, Svalbard (Fig. 1) lies above the Holocene marine limit, in an area with no mining history. In all cases bedrock lithology, observed from rock chippings produced during drilling, was reported to be approxi-

mately uniform, although during drilling of the Stelvio borehole, a few metres of icier frozen bedrock were encountered at depths around 42 and 90 m. Standardized instrumentation procedures included installation of 30 individually calibrated thermistors with absolute accuracy better than ± 0.05 °C, at increasing down-hole depth intervals (Harris et al., 2001b). Boreholes were lined with plastic tubing to allow periodic recalibration of thermistors. No fluid such as oil was introduced inside the borehole liner. Data are recorded every 6 h in the uppermost 5 m, and every 24 h at greater depths. Long-term monitoring will contribute data to the Global Terrestrial Network for Permafrost (GTN-P) of the Global Climate Observing System (GCOS). At all sites permafrost thickness exceeded expectations on the basis of atmospheric temperatures. In all cases, the depth of penetration of the seasonal thermal signal was around 20 m.

3. Permafrost thermal profiles

Permafrost temperature profiles show near-surface warm-side deviation from linear, with thermal gradients increasing with depth. In the case of Schilthorn, Juvvasshøe and Tarfalaryggen, the thermal gradient is negative (decreasing with depth) to between 30 and 40 m (Table 2, Fig. 2). Borehole thermal gradients may be influenced by four major factors; regional geothermal heat flux, variation in lithology with depth, ground surface topography (governing the shape of the

Table 2

Geothermal gradients observed from depths of 100 to 70 m and 30 to 20 m in PACE permafrost boreholes, temperature anomalies from the projected 100–70 m gradient, and surface mean temperatures indicated by projection of thermal gradients at depths of 100–70 m and 30–20 m

PACE borehole site	Thermal gradient between 30 and 20 m depth ($^{\circ}\text{C m}^{-1}$)	Thermal gradient between 100 and 70 m depth ($^{\circ}\text{C m}^{-1}$)	Temperature deviation at 20 m depth from the projected geothermal gradient between 100 and 70 m ($^{\circ}\text{C}$)	Temperature deviation at 40 m depth from the projected geothermal gradient between 100 and 70 m ($^{\circ}\text{C}$)	Mean surface temperature extrapolated from the geothermal gradient between 70 and 100 m ($^{\circ}\text{C}$)	Mean surface temperature extrapolated from the geothermal gradient between 30 and 20 m ($^{\circ}\text{C}$)	Apparent secular warming trend (difference) ($^{\circ}\text{C}$)
Janssonhaugen, Svalbard	0.017	0.036	0.51	0.21	-7.4	-6.4	+1.0
Tarfalaryggen, Sweden	-0.004	0.011	0.35	0.15	-3.8	-3.2	+0.6
Juvvasshøe, Norway	-0.0015	0.009	0.29	0.12	-3.5	-3.0	+0.5
Schilthorn, Switzerland	-0.0055	0.0046	0.40	0.13	-1.0	-0.2	+0.8
Stockhorn, Switzerland	0.0045	0.0183	0.10	-0.07	-3.1	-2.6	+0.5
Stelvio, Italy	0.0065	0.011	0.34	0.13	-2.2	-1.5	+0.7

local upper thermal boundary), and past changes in ground surface temperatures. Heat flow at Janssonhaugen, Svalbard is estimated to be 67 mW m^{-2} (Isaksen et al., 2001) but in the metamorphic rocks of Scandinavia low flux rates are reported, averaging 46 mW m^{-2} (Eriksson and Malmqvist, 1979; Parasnis,

1982), and this may in part explain the low thermal gradients observed at Juvvasshøe and Tarfalaryggen. In the Alps, the high relief results in heat flow less than the Swiss average of 85 mW m^{-2} (Bodmer and Rybach, 1984). Bedrock lithology influences thermal diffusivity, but in all PACE boreholes, little

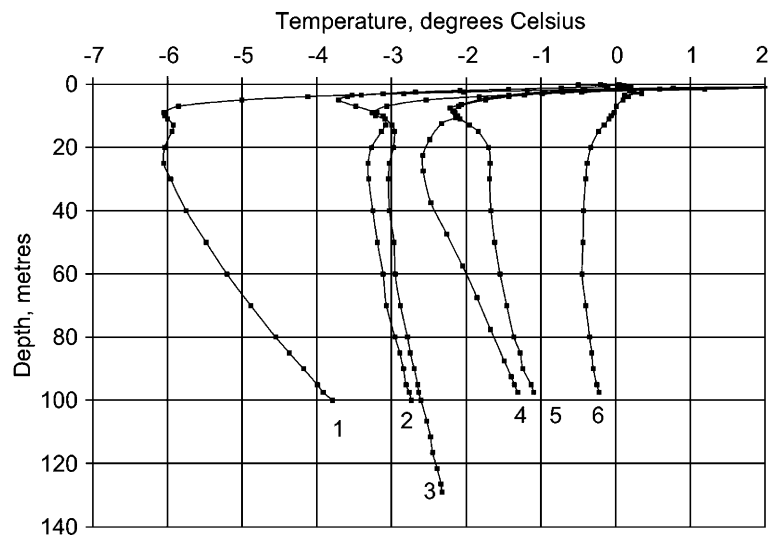


Fig. 2. Geothermal profiles measured in the PACE permafrost borehole network. (1) Janssonhaugen, Svalbard, August 2001; (2) Tarfalaryggen, Sweden, June 2000; (3) Juvvasshøe, Norway, August 2001; (4) Stockhorn, Switzerland, January 2001; (5) Stelvio Pass, Italy, July 2000; (6) Schilthorn, Switzerland, January 2001.

variation in lithology was observed during drilling. Three-dimensional modelling of the temperature field is necessary to assess the influence of topography. However, initial data suggest that at the

PACE permafrost borehole sites, the final factor, past changes in ground surface temperature, is highly significant with respect to depth-related changes in the thermal gradient.

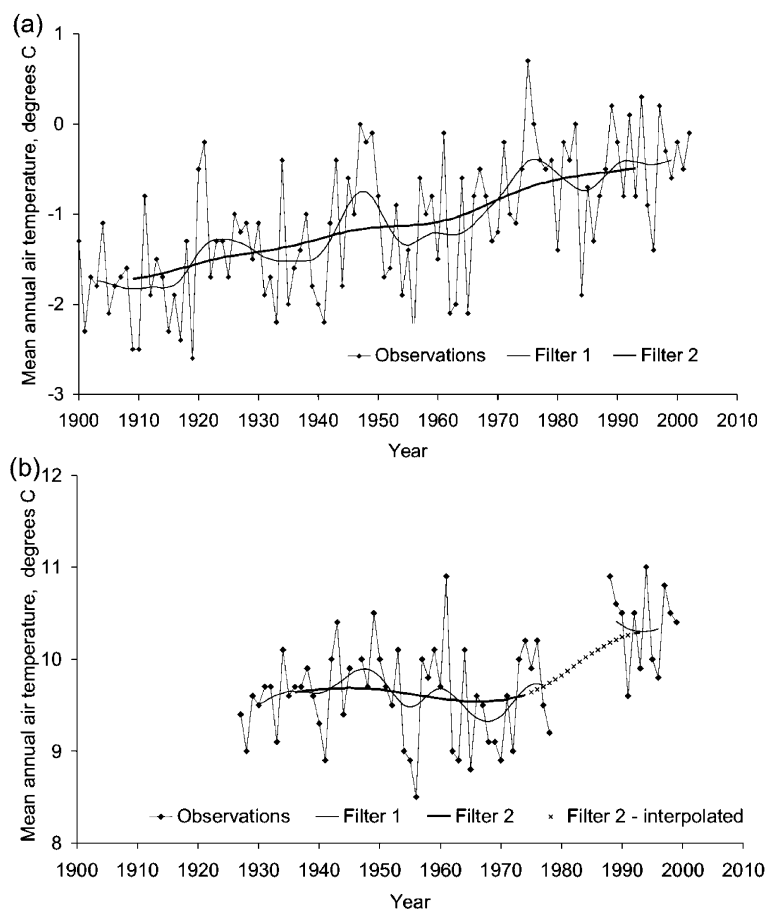
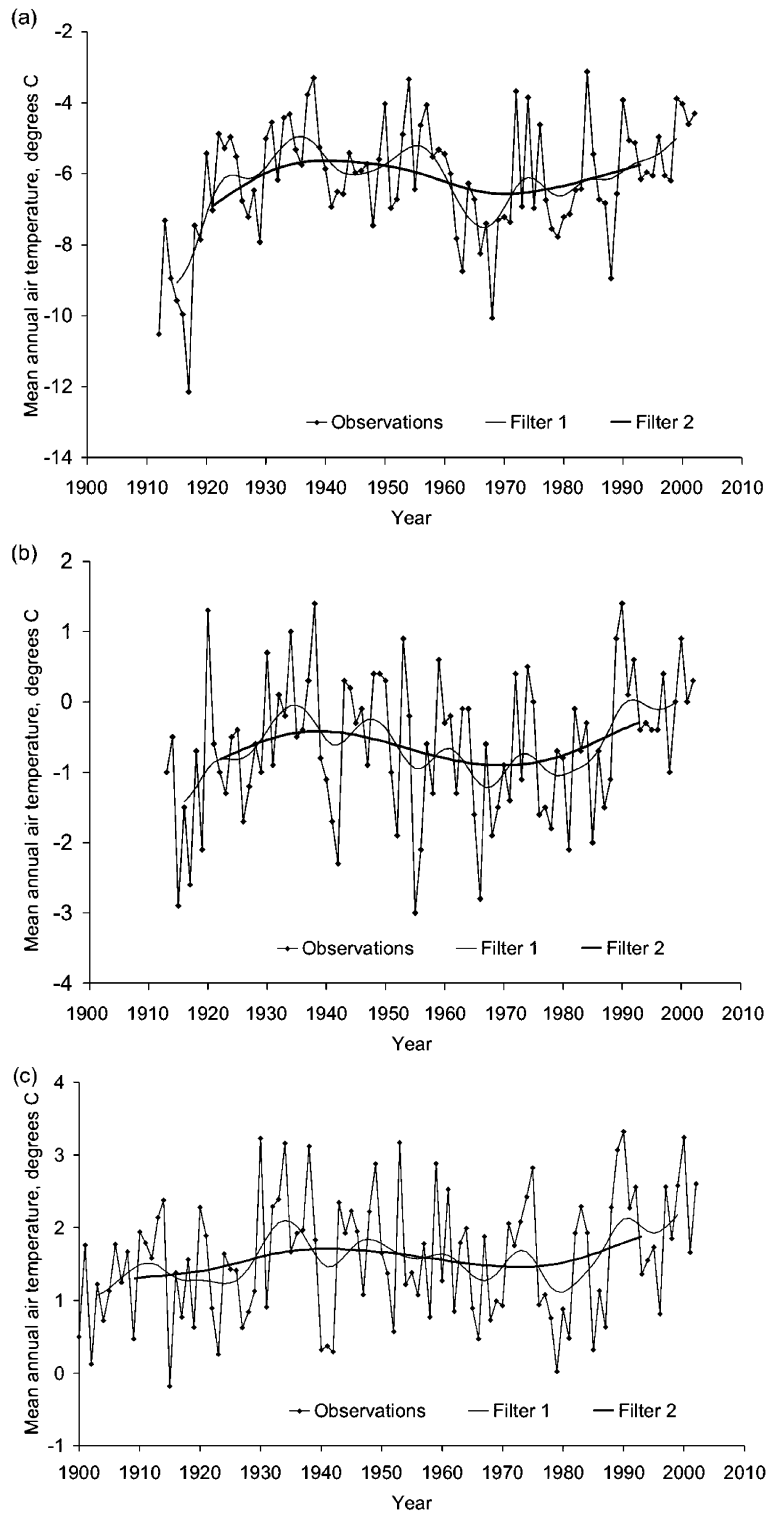


Fig. 3. 20th Century air temperature data from meteorological stations adjacent to boreholes within the PACE borehole transect. (a) Grand St. Bernard, Switzerland ($45^{\circ}87' 00''\text{N}$, $7^{\circ}18' 00''\text{E}$; 2472 m a.s.l.) (Boehm et al., 2001); (b) Silandro, Italy ($46^{\circ}38' 09''$, $10^{\circ}43' 49''$; 720 m a.s.l.). Note: the filtering techniques used in this study are based on methods described by Førland et al. (1997). Time series of scattered individual values often give a rather chaotic impression. To identify local maxima and minima as well as trends, a low pass Gaussian filter may smooth the series. The weighting coefficient in year j , G_j is given by:

$$G_j = \frac{\sum_{i=1}^n w_{ij} x_i}{\sum_{i=1}^n w_{ij}} \quad w_{ij} = e^{-\frac{(i-j)^2}{2\sigma^2}}$$

where the x_i is the original series which consists of n years, and σ is the standard deviation in the Gaussian distribution. For the present paper, filters with $\sigma=3$ (Filter 1) and $\sigma=9$ years (Filter 2) are chosen. These filters are favourable for studying variations on decadal and 30 years time scales.



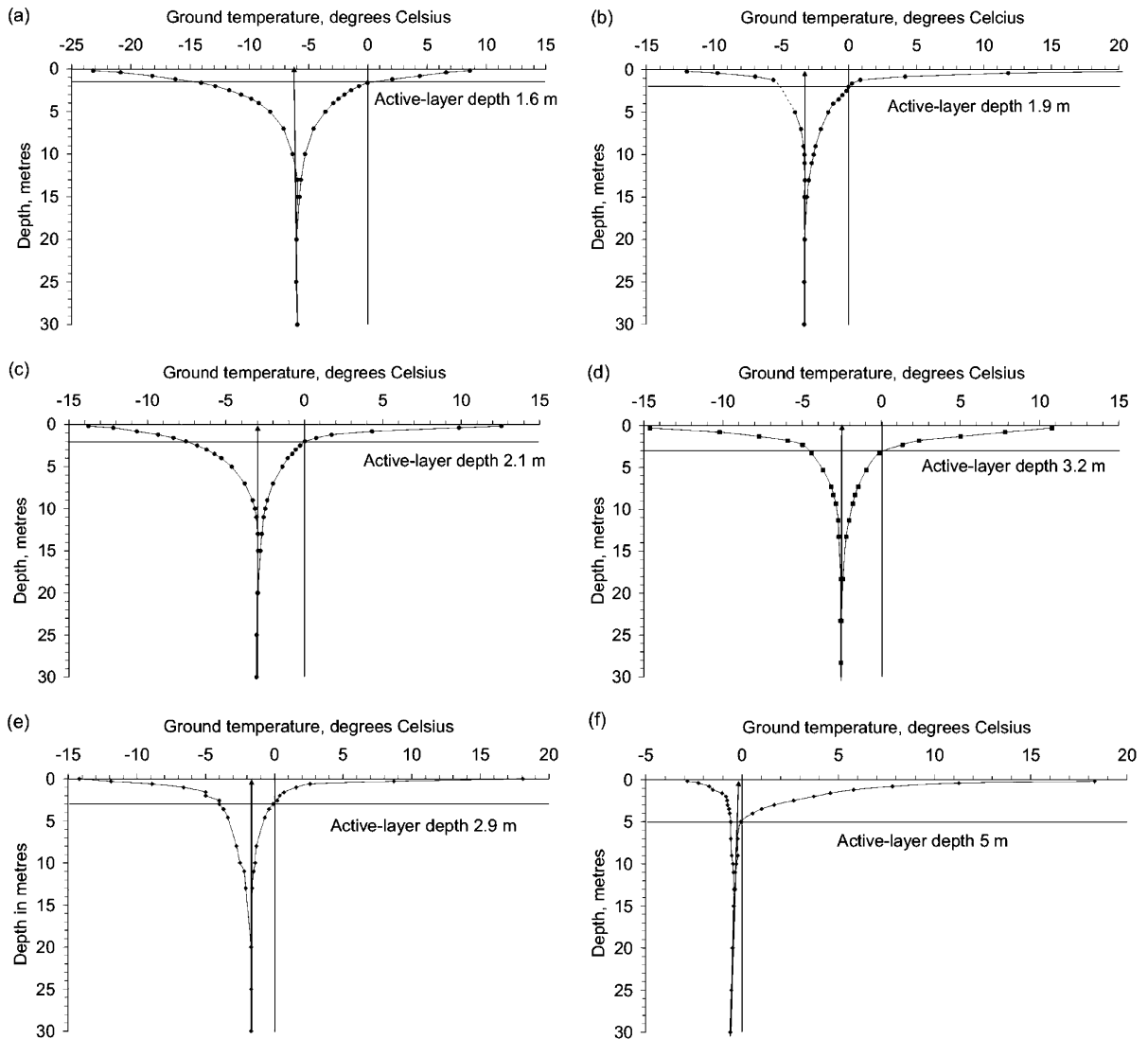


Fig. 5. Seasonal ground temperature variations within the PACE boreholes. Note the projected geothermal gradients between 30 and 20 m and predicted ground surface mean temperatures. (a) Janssonhaugen, Svalbard: (b) Tarfalaryggen, Sweden: (c) Juvasshøe, Norway: (d) Stockhorn, Switzerland: (e) Stelvio Pass, Italy: (f) Schilthorn, Switzerland.

The highest warm-side deviation of the 20 m depth permafrost temperature from a linear extrapolation of the deeper geothermal gradient (observed between 70 and 100 m) is $0.51\text{ }^{\circ}\text{C}$ at the most northerly location (Janssonhaugen, Svalbard) (Table 1). In the mainland

Scandinavian boreholes the deviation decreases southwards, being $0.35\text{ }^{\circ}\text{C}$ at Tarfalaryggen, Sweden and $0.29\text{ }^{\circ}\text{C}$ at Juvasshøe, Norway. The steeper topography and greater influence of aspect in the Alps is reflected in greater variation in observed thermal

Fig. 4. 20th Century temperature data from meteorological stations adjacent to boreholes within the PACE borehole transect. Filtering technique is as described in Fig. 3. (a) Svalbard Airport Svalbard ($78^{\circ}15'00''\text{N}$, $15^{\circ}28'00''\text{E}$; 28 m a.s.l.); (b) Abisko, Sweden ($68^{\circ}21'\text{N}$, $18^{\circ}49'\text{E}$; 388 m a.s.l.). Data courtesy of the Swedish Meteorological and Hydrological Institute (SMHI); (c) Kjoeremsgrenda, Norway ($62^{\circ}05'63''\text{N}$, $9^{\circ}02'76''\text{E}$; 626 m a.s.l.).

profiles, with warm-side 20 m temperature deviations from the projected deep thermal gradient ranging from 0.10 °C at Stockhorn, Switzerland to 0.40 °C at nearby Schilthorn (Table 1). At 40 m, the warm-side deviations from the extrapolated deep thermal gradients are 0.21 °C at Janssonhaugen; 0.15 °C at Tarfalaryggen Sweden; 0.12 °C at Juvvasshøe, Norway; and 0.13 °C at both Schilthorn (Swiss Alps) and Stelvio (Italian Alps). The thermal profile at Stockhorn, Switzerland shows a slight cold-side anomaly at 40 m.

Under equilibrium conditions, providing the thermal properties of the substrate are constant with depth, projection to the ground surface of the permafrost geothermal gradient measured below the depth of seasonal temperature variation, indicates the prevailing Mean Annual Surface Temperature (MAST) (Gold and Lachenbruch, 1973). Assuming uniform geothermal properties with depth in each borehole, the projected deeper thermal gradients (100–70 m) give an indication of earlier MAST, and these may be compared with the MAST indicated by a similar upward projection of the geothermal gradients nearer the surface (30–20 m) (see Fig. 5). Differences provide a first approximation of the secular trend, since the time lag of the thermal response at a depth of 100 m to warming of the upper boundary is likely to be many decades (Lachenbruch and Marshall, 1986).

In all PACE permafrost boreholes, the MAST predicted by the 30–20 m thermal gradient is higher than that predicted by the 100–70 m gradient, the difference ranging from 0.5 to 1 °C (Table 1). Greatest variability is observed in the steep-sided alpine mountain sites. Meteorological stations such as St. Bernhard 2472 m (Switzerland) and Silandro at 720 m (Valtellina, Italy) indicate significant increases in 20th century atmospheric temperatures at high elevations within the Alps (Fig. 3). At the more northern localities where relief is less extreme, warming of some 0.5 °C is indicated at Juvvasshøe, Norway and Tarfalaryggen, Sweden, but in the arctic borehole at Janssonhaugen (Svalbard) the warming is double this value, at 1.0 °C. Mean annual air temperature data recorded at stations close to the two Scandinavian boreholes and on Svalbard show pronounced fluctuations and large interannual variability, making identification of longer term trends more difficult (Fig. 4). The 9-year Gaussian filter (Fig. 4) indicates three distinct periods. Firstly, a warming trend through to the late 1930s; secondly, temperatures

decreased from the 1930s to the 1960s; and finally, from the 1960s to the present day, temperatures have increased significantly with an apparent accelerating trend. It must be emphasized that three-dimensional analysis of the geothermal fields, taking account of thermal properties, is necessary before more precise inversion modelling of near-surface permafrost temperature changes can be undertaken for comparison with the air temperature records.

4. Seasonal and interannual variations

Details of near-surface thermal regimes measured in the deep PACE boreholes are given in Fig. 5, where the seasonal ranges and thermal gradients between 20 and 30 m are shown. Clearly summer surface temperatures are significantly higher in the Alps than in Scandinavia and Svalbard, and active-layer depths are therefore greater (Fig. 6).

The longest continuous series of temperature measurements within European mountain permafrost is from the 58 m deep borehole at Murtèl–Corvatsch (Engadin, Switzerland) which was drilled in 1987 through slowly creeping ice-rich debris (Vonder Mühl et al., 1998; Haeblerli et al., 1988; Vonder Mühl, 2001). Rapid warming of the uppermost 25 m of permafrost was observed between 1987 and 1994 (Fig. 7). The mean annual ground surface temperature is estimated to have increased from –3.3 °C (1988) to –2.3 °C (1994). However, low snowfall in December and January in the winter of 1994–1995, followed by

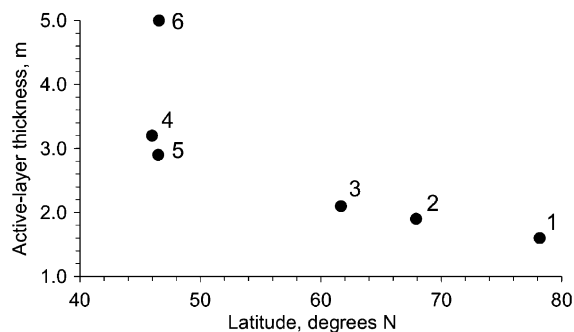


Fig. 6. Active-layer depth at PACE borehole sites in relation to latitude. (1) Janssonhaugen, Svalbard; (2) Tarfalaryggen, Sweden; (3) Juvvasshøe, Norway; (4) Stockhorn, Switzerland; (5) Stelvio Pass, Italy; (6) Schilthorn, Switzerland.

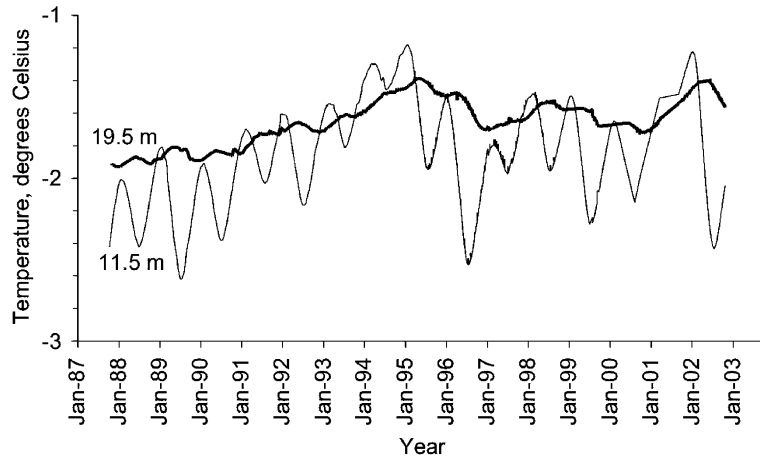


Fig. 7. Permafrost temperatures (a) at 11.6 m and (b) 19.5 m depths, Murtèl–Corvatsch (Engadin, Swiss Alps), 1987–2002.

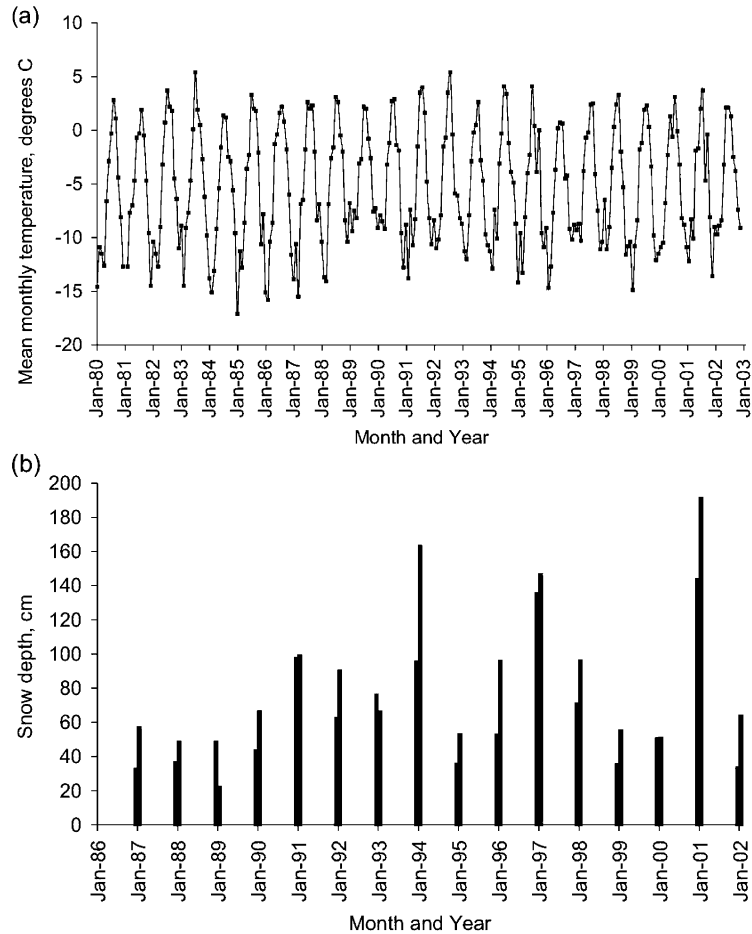


Fig. 8. Murtèl–Corvatsch Borehole (Engadin, Swiss Alps): (a) air temperatures 1980–2002 from the Murtèl–Corvatsch station (3295 a.s.l.). (b) Snow depths in December and January, 1987–2002. ©2003SLF-Messdaten, SLF.

moderate snow fall in 1995–1996 (Fig. 8) caused intense cooling of the ground and permafrost temperatures returned to values similar to those in 1987. Early winter snow was thin in 1998–1999 and winter ground temperatures remained low in 1999, 2000 and 2001. Mean permafrost temperature at a depth of 11 m rose and fell by 1.0 °C and at 20 m by 0.4 °C during the 15-year observation period, the dominant variable being snow cover rather than mean atmospheric temperatures (Fig. 8). Thus, interpretation of inversion modelling based on the PACE borehole profiles must take account of the complex relationship between the ground surface and atmospheric temperatures, particularly the strong modulating affect of snow conditions. Overall, permafrost warming during the 15 years of observation at Murtèl–Corvatsch was about 0.6 °C at 11.6 m (within the depth range of strong seasonal temperature variability) and 0.2 °C at 20 m (below the depth of seasonal variation), indicating continued if not accelerated warming in recent years.

5. Conclusions

The PACE mountain permafrost borehole network offers the prospect of long-term monitoring as part of the Global Terrestrial Network for Permafrost (GTN-P). The first data sets presented here show thermal gradients consistent with 20th century surface warming. Relief and aspect lead to greater variability between the Swiss and Italian Alpine boreholes than between those in Scandinavia and Svalbard. Observed warm-side deviation of ground temperatures at both 20 and 40 m is greater in the polar latitude Svalbard borehole than the more southerly boreholes in the network, suggesting greater warming at higher latitudes, as predicted by Global Climate Models (Houghton et al., 1996). First approximations of surface warming range from 0.5 °C at Stockhorn, Switzerland and Juvvasshøe, Norway to 1.0 °C at Janssonhaugen in Svalbard. A 15-year record of permafrost temperatures from the 58 m deep Murtèl–Corvatsch in Switzerland shows a warming trend, but with large amplitude interannual variations that reflect early winter snow thickness and duration rather than mean air temperatures. The significance of snow cover to the thermal regime of the upper permafrost boundary must therefore be carefully considered in interpret-

ing future thermal inversion modelling of the permafrost geothermal profiles.

Acknowledgements

This research was funded by the European Community through the 4th Framework Permafrost and Climate in Europe (PACE) Project; Contract ENV4-CT97-0492.

References

- Anisimov, O.A., Nelson, F.E., 1996. Permafrost distribution in the Northern Hemisphere under scenarios of climate change. *Global and Planetary Change* 14, 59–72.
- Anisimov, O.A., Shiklomanov, N.I., Nelson, F.E., 1997. Global warming and active-layer thickness: results from transient general circulation models. *Global and Planetary Change* 15, 61–77.
- Beltrami, H., Harris, R.N. (Eds.), 2001. Inference of Climate Change from Geothermal Data. *Global and Planetary Change*, vol. 29, pp. 149–348 (Special issue).
- Beltrami, H., Mareschal, J.-C., 1995. Resolution of ground temperature histories inverted from borehole temperature data. *Global and Planetary Change* 11, 57–70.
- Bodmer, Ph., Rybach, L., 1984. Geothermal map of Switzerland (heat flow density). Commission Suisse de Géophysique. *Materiaux pour la géologie de la Suisse*, vol. 22. Kümmerli and Frey, Bern, p. 47.
- Boehm, R., Auer, R.I., Brunetti, M., Maugeri, M., Nanni, T., Scoehner, W., 2001. Regional temperature variability in the European Alps 1760–1998 from homogenised instrumental time series. *International Journal of Climatology* 21, 1779–1801.
- Burgess, M.M., Smith, S.L., Brown, J., Romanovsky, V., Hinkel, K., 2000. Global Terrestrial Network for Permafrost (GTNet-P): permafrost monitoring contributing to global climate observations. *Geological Survey of Canada, Current Research*, 1–8 (2000-E14).
- Cihlar, J., Barry, T.G., Ortega Gil, E., Haeberli, W., Kuma, K., Landwehr, J.M., Norse, D., Running, S., Scholes, R., Solomon, A.M., Zhao, S., 1997. GCOS/GTOS plan for terrestrial climate-related observation. GCOS 32, version 2.0, WMO/TD-796, UNEP/DEIA/TR, 97-7.
- Dramis, F., Govi, M., Guglielmin, M., Mortara, G., 1995. Mountain permafrost and slope instability in the Italian Alps. The Val Pola landslide. *Permafrost and Periglacial Processes* 6, 73–81.
- Eriksson, K.G., Malmqvist, D., 1979. A review of the past and present investigations of heat flow in Sweden. In: Cemak, V., Rybach, L. (Eds.), *Terrestrial Heat Flow in Europe*. Springer, Berlin, pp. 267–277.
- Førland, E.J., Hanssen-Bauer, I., Nordli, P.Ø., 1997. Climate statistics and long term series of temperature and precipitation at Svalbard and Jan Mayen. Norwegian Meteorological Institute. Report No. 21/97 KLIMA23. 54 pp.

- Gold, L.W., Lachenbruch, A.H., 1973. Thermal conditions in permafrost—a review of North American literature. *Proceedings Second International Conference on Permafrost, Yakutsk, U.S.S.R., North American Contribution*. National Academy of Sciences, Washington, U.S., pp. 3–25.
- Gomez, A., Palacios, D., Ramos, M., Tanarro, L.M., Schulte, L., Salvador, F., 2001. Location of permafrost in marginal regions: Corral del Valeta, Sierra Nevada, Spain. *Permafrost and Periglacial Processes* 12, 93–110.
- Haeblerli, W., 1992. Construction, environmental problems and natural hazards in periglacial mountain belts. *Permafrost and Periglacial Processes* 3, 111–124.
- Haeblerli, W., Beniston, M., 1998. Climate change and its impacts on glaciers and permafrost in the Alps. *Ambio* 27, 258–265.
- Haeblerli, W., Huder, J., Keusen, H.-R., Pica, J., Röthlisberger, H., 1988. Core drilling through rock–glacier permafrost. *Proceedings of the Fifth International Conference on Permafrost*. Tapir, Trondheim, pp. 937–942.
- Haeblerli, W., Hölzle, M., Keller, F., Schmid, W., Vonder Mühll, D., Wagner, S., 1993. Monitoring the long-term evolution of mountain permafrost in the Swiss Alps. *Proceedings of the Sixth International Conference on Permafrost, South China*. University of Technology Press, Beijing, pp. 214–219.
- Haeblerli, W., Wegmann, M., Vonder Mühll, D., 1997. Slope stability problems related to glacier shrinkage and permafrost degradation in the Alps. *Ecologae Geologicae Helveticae* 90, 407–414.
- Harris, C., Davies, M.C.R., Etzelmüller, B., 2001a. The assessment of potential geotechnical hazards associated with mountain permafrost in a warming global climate. *Permafrost and Periglacial Processes* 12, 145–156.
- Harris, C., Haeblerli, W., Vonder Mühll, D., King, L., 2001b. Permafrost monitoring in the high mountains of Europe: the PACE Project in its global context. *Permafrost and Periglacial Processes* 12, 3–11.
- Houghton, J.T., Meira Filho, L.G., Callander, B.A., Harris, N., Kattenberg, A., Maskell, K., 1996. *Climate Change 1995: the Science of Climate Change*, Intergovernmental Panel on Climate Change (IPCC). Cambridge Univ. Press, Cambridge. 572 pp.
- Isaksen, K., Holmlund, P., Sollid, J.L., Harris, C., 2001. Three deep alpine-permafrost boreholes in Svalbard and Scandinavia. *Permafrost and Periglacial Processes* 12, 13–25.
- Jin, H., Shuxun, L., Guodong, C., Shaoling, W., Li, X., 2000. Permafrost and climatic change in China. *Global and Planetary Change* 26, 387–404.
- Keller, F., Frauenfelder, R., Gardaz, J.M., Hölzle, M., Kneisel, C., Lugon, R., Philips, M., Reynard, E., Wenker, L., 1998. Permafrost map of Switzerland. In: Lewkowicz, A.G., Allard, M. (Eds.), *Proceedings, 7th International Conference on Permafrost*. Collection Nordicana, vol. 57. Université Laval, Quebec, pp. 557–562.
- Lachenbruch, A.H., Marshall, B.V., 1986. Changing climate: geothermal evidence from permafrost in the Alaskan Arctic. *Science* 234, 689–696.
- Lachenbruch, A.H., Cladouhos, T.T., Saltus, R.W., 1988. Permafrost temperature and the changing climate. *Proceedings of the Fifth International Conference on Permafrost*, vol. 3. Tapir, Trondheim, pp. 9–17.
- Nelson, F.E., Anisimov, O.E., Shiklomonov, O.I., 2001. Subsidence risk from thawing permafrost. *Nature* 410, 889–890.
- Osterkamp, T.E., 1983. Response of Alaskan permafrost to climate. *4th International Conference on Permafrost*. National Academy Press, Washington, pp. 145–152.
- Osterkamp, T.E., Romanovsky, V.E., 1999. Evidence for warming and thawing of discontinuous permafrost in Alaska. *Permafrost and Periglacial Processes* 10, 17–37.
- Parasnis, D.S., 1982. Temperature phenomena and heat flow estimates in two Precambrian ore-bearing areas in north Sweden. *Geophysical Journal of the Royal Astronomical Society* 143, 531–544.
- Pavlov, A.V., 1994. Current changes of climate and permafrost in the Arctic and sub-Arctic of Russia. *Permafrost and Periglacial Processes* 5, 101–110.
- Shen, P.Y., Beck, A.E., 1991. Least squares inversion of borehole temperature measurements in functional space. *Journal of Geophysical Research* 96, 19965–19979.
- Vonder Mühll, D., 2001. Thermal variations of mountain permafrost: an example of measurements since 1987 in the Swiss Alps. In: Visconti, G., Beniston, M., Iannorelli, E.D., Barba, D. (Eds.), *Global Change in Protected Areas*. Kluwer Academic Publishing, Dordrecht, pp. 83–95.
- Vonder Mühll, D., Stucki, T., Haeblerli, W., 1998. Borehole temperatures in alpine permafrost: a ten year series. In: Lewkowicz, A.G., Allard, M. (Eds.), *Proceedings of the Seventh International Conference on Permafrost*. Collection Nordicana, vol. 57. Université Laval, Quebec, pp. 1089–1095.

Surface Energy Fluxes and Distribution Models of Permafrost in European Mountain Areas: an Overview of Current Developments

Martin Hoelzle,^{1*} Catherine Mittaz,¹ Bernd Etzelmüller² and Wilfried Haeberli¹

¹ Department of Geography, Glaciology and Geomorphodynamics Group, University of Zurich, Zurich, Switzerland

² Department of Physical Geography, University of Oslo, Oslo, Norway

ABSTRACT

In recent years successful attempts have been made to develop and improve spatial modelling of mountain permafrost distribution. Work package 4 of the PACE project (Permafrost and Climate in Europe) sought to provide the essential basis not only of present-day modelling capability, but also of future enhancements in modelling methodology. This paper briefly outlines the currently available typology of models, which involve various levels of sophistication at different spatio-temporal scales. Appropriate models may be applied to a range of environmental issues in cold mountain areas, including engineering applications, climate-change scenarios, large-scale mapping, studies of surface processes or environmental concerns. Special emphasis is given here to aspects of energy exchange at the surface and within the active layer. Such energy fluxes remain poorly understood but play an essential role in process-oriented research and sensitivity studies with respect to complex interactions and feedbacks within the system. In contrast to relatively flat permafrost areas in polar and subpolar lowlands, circulation of water and air can cause important lateral fluxes of matter and energy within coarse blocks on steep slopes and result in highly variable and sometimes extreme thermal offsets between the ground surface and the permafrost table. Measuring and numerically modelling such fluxes together with coupling time-dependent surface and subsurface ground thermal conditions in characteristic materials (bedrock, ice-rich debris, fine-grained deposits) constitute the main challenge for research in the near future. Copyright © 2001 John Wiley & Sons, Ltd.

RÉSUMÉ

Dans ces dernières années, des essais ont, avec succès, développé et amélioré les modélisations spatiales de la distribution du pergélisol de montagne. La quatrième partie du programme PACE (Pergélisol et Climat en Europe) a cherché à établir les bases essentielles, non seulement des possibilités actuelles de modélisation, mais aussi les améliorations méthodologique futures. Le présent article souligne brièvement la typologie couramment disponible des modèles qui comprennent plusieurs niveaux de sophistication à différentes échelles spatio-temporelles. Des modèles appropriés peuvent être appliqués à de nombreux problèmes environnementaux, entre autres à des applications des ingénieurs, des scénarios de changement de climat, des cartographies à grande échelle, et des études des processus de surface ou environnementaux. Une attention spéciale est accordée ici aux échanges d'énergie à la surface et dans la couche active. De tels flux d'énergie restent mal compris

*Correspondence to: Dr M. Hoelzle, University of Zurich, Department of Geography, Glaciology and Geomorphodynamics Group, Winterthurerstrasse 190, CH-8057 Zurich, Switzerland. E-mail: hoelzle@geo.unizh.ch

Contract grant/sponsor: EU Environment and Climate Research Programme; Contract grant/number: ENV4-CT97-0492; BBW 97.0054-2.

bien qu'ils jouent un rôle essentiel dans la recherche des processus et dans le domaine des interactions complexes et rétroactives du système. Par opposition à ce qui se passe dans les basses terres polaires et subpolaires, les circulations de l'eau et de l'air peuvent causer des flux importants de matières et d'énergie au sein des blocs grossiers accumulés sur des pentes raides; il en résulte des échanges très variables et parfois extrêmement importants entre la surface du sol et la table du pergélisol.

Mesurer et établir des modèles numériques de flux semblables dans des conditions variables de matériaux (roche en place, débris riches en glace, dépôts de granulométrie fine) et en tenant compte des conditions variables dans le temps de la température de surface et du sol, constitue le principal challenge pour la recherche dans le proche avenir Copyright © 2001 John Wiley & Sons, Ltd.

KEY WORDS: Energy balance; mountain permafrost; spatial permafrost modelling

INTRODUCTION

The sensitivity of the upper permafrost layers (10–50 m) with respect to decadal climatic changes and the potential impact of permafrost evolution on surface processes, landscape dynamics and natural hazards in high-alpine environments makes knowledge about the spatial distribution patterns of mountain permafrost fundamentally important. With increasing activity in cold mountain areas for tourism, communication networks and hydropower production, knowledge about the distribution patterns of mountain permafrost helps reduce installation/maintenance costs and leads to more safety for people living in such areas (Haeberli, 1992). Model calculations allowing estimations of permafrost distribution patterns are especially useful during the planning stages of hazard mitigation measures such as flood and avalanche protection work, or any other construction activity (Ives and Bovis, 1978; Haeberli *et al.*, in press; Keusen and Haeberli, 1983; Phillips, 2000; Thalparpan *et al.*, 1998; Wegmann and Keusen, 1998). Mountain permafrost differs considerably from lowland permafrost at high latitudes owing to strong topographic and microclimatic variability. Patchy or discontinuous permafrost is therefore present in many periglacial belts between the timberline and glaciers (Cheng, 1983; Cheng and Dramis, 1992). Various efforts have been made in recent years to develop and improve spatial modelling of mountain permafrost distribution. At the International Conference on Permafrost in Yellowknife (1998), the International Permafrost Association (IPA) established a Task Force on 'Mapping and Distribution Modelling of Mountain Permafrost'. At the same time, spatial modelling together with permafrost mapping and geophysical prospecting is applied to assessing the representativeness of long-term borehole monitoring at tier 4 of the newly established

global climate-related Terrestrial Network for Permafrost (GTN-P: cf. Burgess *et al.*, 2000; Harris *et al.*, 2001, this issue). These programmes show the high priority attributed at international level to the development of the topic. This was reflected in research by the PACE project, where the main objectives were:

- (1) to measure near-surface energy exchange processes at selected high-mountain permafrost sites in the Alps, the Sierra Nevada and Scandinavia
- (2) to develop an advanced understanding of energy fluxes and cryotic processes involved with permafrost development and decay, particularly regarding surface-cover characteristics and lateral/advective mass/energy transfer in the active layer
- (3) to improve modelling and simulation of spatial permafrost distribution patterns in different mountain regions and for various climatic scenarios based on energy balance data.

The primary goal is to build up a hierarchy of models at various levels of sophistication and scale, in order to deal with a range of problems and databases. These models are especially suited for planning of engineering applications, simulating climate-change scenarios, large-scale mapping, studies of surface processes or environmental concerns in cold mountain areas all over the world. This paper briefly reviews basic aspects of the spatio-temporal scales and model typology underpinning current techniques. It then summarizes the most important results from first PACE energy-flux measurements, illustrates approaches to regional- and local-scale modelling and outlines possibilities of model validation. Finally, it discusses some important aspects concerning future modelling steps.

SPATIO-TEMPORAL SCALES

Earth surface processes can be seen as acting in a wide range of spatial and temporal scales (Ahnert, 1994; De Boer, 1992). The relative importance of factors influencing processes normally differs depending on the scale considered. In relation to distributed modelling, such as hydrological models, processes are mainly observed and measured over short time intervals and in small areas. Thus, many process theories are valid only at small *spatial* scales. Much effort has been made in upscaling information, e.g. within hydrology, to meet the scale used in GCMs (Hallidin *et al.*, 1999). In the opposite direction, downscaling of outputs from GCMs is necessary for application of future climate scenarios with respect to small-scale surface processes (Dehn and Buma, 1999; Dehn *et al.*, 2000). In modelling of permafrost distribution similar problems exist. Permafrost is thermally defined and thus depends on the energy balance at the ground surface, the snow cover thickness and duration and the characteristics of surface material. At increasingly large scales, such factors governing small-scale variations decrease in importance, while factors such as mean annual air temperature (MAAT) give a good approximation of permafrost distribution. Within the PACE project, two basic spatial scale ranges have been proposed related to end-user products of permafrost maps and slope-activity maps: a micro or patch scale with a spatial resolution of ≤ 25 m, and a meso scale with a resolution > 25 m and up to 200 m, covering more regional aspects of landform and process distribution. Regions covered by a resolution > 250 m are defined as the macro scale: the coarse resolution is appropriate for overview maps and long-term predictive models. For many applied and scientific applications, the identification of a regional distribution pattern of forms, processes and potential instabilities on slopes is demanded (cf. Harris *et al.*, 2001, this issue). Higher resolution requires refined models, an increasing amount of input parameters and better calibration.

Permafrost is a *thermal* system with slow response to climate forcing. Thus, the present state of permafrost is influenced by former climatic conditions and affects future developments. The response time of permafrost depends on the thermal conductivity, the ice content and the thickness of the frozen ground (Osterkamp, 1983). Empirical models not only neglect potentially important feedback mechanisms relating, for instance, to atmosphere/snow/permafrost interactions, but also disregard non-stationary transitions at depth. However, even relatively warm

and thin discontinuous mountain permafrost has a response time which is typically measured in decades to centuries (Haeberli, 1990). In fact, the thickness and some marginal occurrences of alpine permafrost most probably still reflect maximum Holocene cooling during the Little Ice Age, which culminated in the nineteenth century. Temperature profiles observed in the PACE boreholes (Isaksen *et al.*, 2001, this issue; in press; Vonder Mühl *et al.*, 1998) prove permafrost thicknesses in excess of values expected from present-day mean annual ground temperature (MAGT). Moreover, low thermal gradients at depths between 40 and about 100 m (Isaksen *et al.*, 2001, this issue) can be interpreted as a thermal adjustment to ground surface temperatures increasing at high if not accelerating rates. Such non-stationary conditions at depth should be included for realistic modelling of impacts from potential future climate-change scenarios related to possible permafrost degradation or aggradation.

MODEL TYPOLOGY

Today, permafrost distribution models combine stochastic with deterministic elements and can be divided into two main types: regionally calibrated empirical-statistical models and more physically based process-oriented models.

Empirical-statistical models directly relate documented permafrost occurrences to topoclimatic factors (altitude, slope and aspect, mean air temperature, solar radiation) which can easily be measured or computed (e.g. Keller, 1992). The complex energy exchange processes at the surface and within the active layer are not treated explicitly but rather as a grey box with topoclimatic factors being selected according to their relative influence in the energy balance equation. This simplification gives advantages and disadvantages. Empirical-statistical permafrost distribution models can be easily applied, have a limited need for input parameters and are quite reliable if well calibrated locally or regionally. They are, however, yes/no functions about the presence or absence of permafrost, primarily applicable to certain areas, and assume steady-state conditions. Extrapolations in time and space may lead to uncertain or even misleading results.

Process-oriented models focus on more detailed understanding of the energy fluxes between the atmosphere and the permafrost. They explicitly parameterize solar radiation, sensible heat, surface albedo, heat conduction etc., are often complex and need a correspondingly large amount of precisely

measured or computed data. Such approaches allow for spatio-temporal extrapolation and are especially well suited for sensitivity studies with respect to interactions and feedbacks involved with climate-change scenarios. They enable surface temperatures to be computed and, hence, thermal conditions at depth and transient effects to be estimated. As a first step towards the development of such approaches, detailed energy balance measurements have to be carried out at high-mountain permafrost sites. This task involves numerous and difficult problems and was undertaken in a coordinated regional study for the first time in the PACE project.

PRELIMINARY RESULTS FROM ENERGY BALANCE MEASUREMENTS

Microclimatological studies are in progress at all PACE borehole locations (Harris *et al.*, 2001, this issue) for model development and calibration. These measurements provide data on heat fluxes between the atmosphere and the active layer, and between the active layer and the underlying permafrost (Mittaz, 1998; Mittaz *et al.*, 2000a,b). The processes involved in the *energy balance* comprise the net exchange of radiation between the atmosphere and the earth surface, the transfer of sensible and latent heat by turbulent motion of the air, and conduction of heat into the ground. The nature of the earth surface and the relative abilities of the ground and the atmosphere to transport heat govern the exact partitioning between the components of the radiative and heat balances. Advective energy fluxes were not measured. The sum of all measured energy fluxes indeed will give a hint on the order of magnitude of lateral fluxes (cf. below).

In order to enhance the understanding of these energy exchange processes, a complete energy balance data set has been obtained since 1997 on creeping permafrost at a high mountain site (the Murtèl–Corvatsch rock glacier, Upper Engadin, Switzerland; Mittaz *et al.*, 2000b). These measurements help to identify the most important climatic and site-specific factors for determining local and regional permafrost distribution patterns (Hoelzle, 1996).

The results obtained during 1997 and 1998 are shown in Figure 1. Among all energy exchange processes, net radiation and snow cover appear to play the determining role for the existence of mountain permafrost. Net radiation is negative during winter (up to -46 W m^{-2} in February 1998), but reaches monthly values as high as 151 W m^{-2} in July 1998. Snow cover strongly

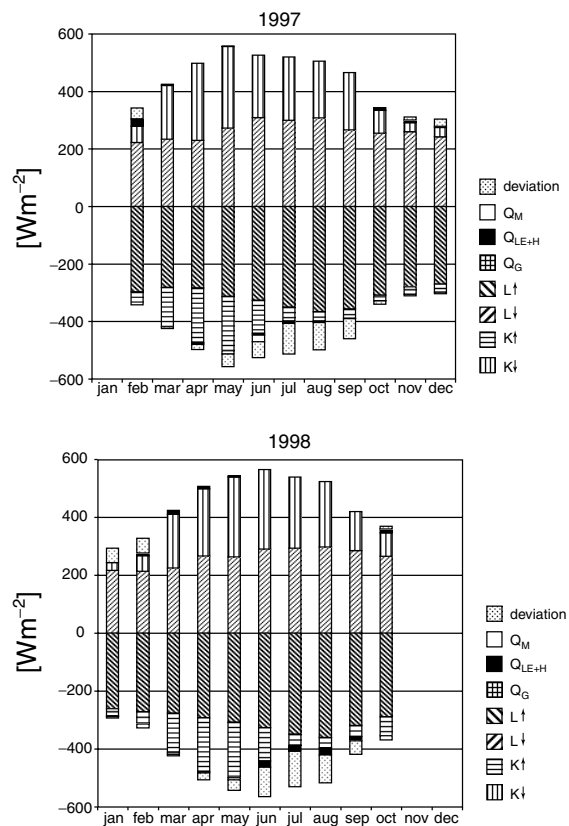


Figure 1 Energy balance measured during the years 1997 and 1998 at a creeping permafrost site, Corvatsch–Murtèl, Upper Engadin, Switzerland (Mittaz *et al.*, 2000b). Net radiation controls most of the energy exchange processes. The surface consists of coarse rocks, which are a typical and widespread surface characteristic in mountain permafrost areas. $K \downarrow$ = short-wave incoming radiation, $K \uparrow$ = short-wave reflected radiation, $L \downarrow$ = long-wave incoming radiation, $L \uparrow$ = long-wave emitted radiation, Q_{LE+H} = turbulent heat fluxes (sensible and latent), Q_M = latent melt energy, Q_G = ground heat flux, deviation = imbalance to a zero energy balance.

influences surface characteristics such as albedo, aerodynamic roughness length defined after Oke (1987) and emissivity, and insulates the ground from atmospheric conditions. Thus, ground heat flux remains small during winter (-1 W m^{-2}), whereas heat transport during summer is higher (8 W m^{-2} in July 1998). Monthly values for turbulent heat exchange are within -20 and $+20 \text{ W m}^{-2}$. Ground heat flux, latent melt energy (during the snowmelt season) and turbulent fluxes during summer all vary within the same order of magnitude, but are much smaller than the radiation fluxes.

The sum of all measured components indicates a non-zero energy budget, with a positive deviation of up to 78 W m^{-2} in winter and a negative deviation up to -130 W m^{-2} in summer. It is proposed that this overall imbalance of the energy exchange fluxes could be explained by unmeasured advective energy fluxes that occur within the layer of large boulder and blocks at the top of the permafrost (Mittaz *et al.*, 2000b). The mean annual ground surface temperature was determined as the average of the 0.6 m borehole temperature during winter 1997 ($\pm 0.02^\circ\text{C}$), and the temperature at the ground surface as measured with miniature temperature loggers ($\pm 0.25^\circ\text{C}$) during winter 1997–98 (Hoelzle *et al.*, 1999). For the snow-free period, the surface temperature was calculated from long-wave radiation measurements. To obtain more information on the processes taking place within the active layer, mean annual ground surface temperature and mean annual ground temperature were compared (Figure 2). The difference between these two temperatures is a key parameter for modelling permafrost–climate relationships and essentially contributes to the so-called thermal offset (see below). The mean temperature differences are around 16°C during both summers of 1997 and 1998, when the surface was much warmer than the underlying ground. The difference was only less than 2°C and negative during the winter months (Figure 2). The large temperature difference during the summer months cannot only be explained through heat conduction from the surface towards depth or vice versa, but probably

originates from unmeasured advective heat fluxes within the blocky surface layer and corresponds to the observed non-zero energy budget (Mittaz *et al.*, 2000b).

The progress and current status of spatial mountain permafrost modelling in the light of these first results from energy balance measurements are now considered.

PROGRESS AND CURRENT STATUS OF SPATIAL MOUNTAIN-PERMAFROST MODELLING

The first *empirical model*, called rules of thumb, was developed by Haerberli (1975) in the early 1970s for describing mountain permafrost distribution in the Eastern Swiss Alps. Since the 1990s, models combining similar approaches with digital elevation models (DEMs) and modern GIS techniques (Delaloye and Morand, 1998a; Etzelmüller *et al.*, 1998; 2001, this issue; Gruber and Hoelzle, 2001, this issue; Imhof, 1996; Jensen, 1999; Keller, 1992; Keller *et al.*, 1998; King and Kalisch, 1998; Li *et al.*, 1998; Ødegård *et al.*, 1996) were frequently applied to various mountain areas. The parameterizations of these models are based on proxy variables of selected energy balance factors, which reflect a simplified relation between climate and permafrost distribution. Air temperature, solar radiation, snow and surface characteristics are considered to be the most important factors influencing mountain permafrost distribution.

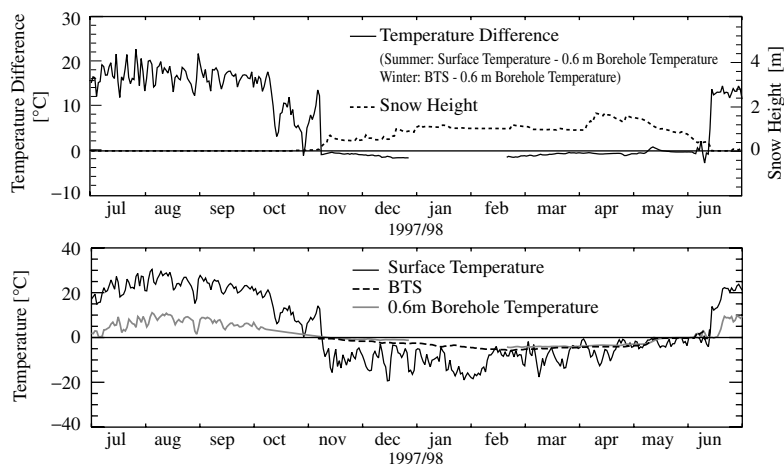


Figure 2 Thermal offset measured at Murtèl–Corvatsch site. The lower figure shows the measured temperature at the surface, the 0.6 m borehole temperature and the BTS. The upper figure shows the temperature difference between surface temperature and the 0.6 m borehole temperature for the summer months and the temperature difference between BTS and 0.6 m borehole temperature for the winter months.

Altitudinal limits are determined based on latitude, slope, aspect and topology. These types of models are now frequently applied for scientific as well as practical purposes and appear to work quite successfully (Frauenfelder *et al.*, 1998; Kneisel, 1998; Lieb, 1998a).

Empirical-statistical models allow for rough simulations of past and future surface conditions as described by Hoelzle and Haerberli (1995). They were first developed for regions outside mountain permafrost (Jorgensen and Kreig, 1988; Nelson and Outcalt, 1987) and use different kinds of calculated or measured climatic factors as proxy, i.e. freezing or thawing indices, potential direct solar radiation and mean annual air temperature (MAAT). Several types of topographic radiation balance models have been developed for mountain areas. The programme SRAD (Gallant and Wilson, 1996; Moore, 1992), for instance, was applied in the Jotunheimen and Dovrefjell mountains of southern Norway (Heggem, 1999) as well as in the Alps (Gruber, 2000; Gruber and Hoelzle, 2001, this issue). A comparable model described by Funk and Hoelzle (1992) was calibrated and used at different locations in the Alps (Hoelzle, 1996; Hoelzle and Haerberli, 1995; Hoelzle *et al.*, 1993).

The development of a *process-oriented permafrost distribution model for mountain areas* is the main

goal to be achieved within work package 4 of the PACE project. Figure 3 shows the principles in the form of a flow chart. The model contains two main components, an energy balance model and a thermal offset model. The energy balance provides ground surface temperatures which are then used as input for simulating ground heat flux.

The *energy balance model* is based on a description of the main energy exchange processes between the atmosphere and the surface. It includes calculations of short-wave net radiation, long-wave incoming radiation and turbulent fluxes as well as of snow distribution. As a physical model, the energy balance module requires an extensive set of input data describing meteorological conditions, ground surface characteristics (albedo, surface roughness, emissivity) and topography. The most important database is a DEM with a grid-cell size of 25 m. The data set of meteorological variables needs single values of air temperature, vapour pressure, air pressure, wind speed and direction, cloud cover, radiation at the top of atmosphere, precipitation and global radiation for each day. Available data sets from the Swiss Meteorological Service (MeteoSwiss) are used exclusively.

As a first step, the meteorological input data are extrapolated from the meteorological station to the investigated area. Subsequently different

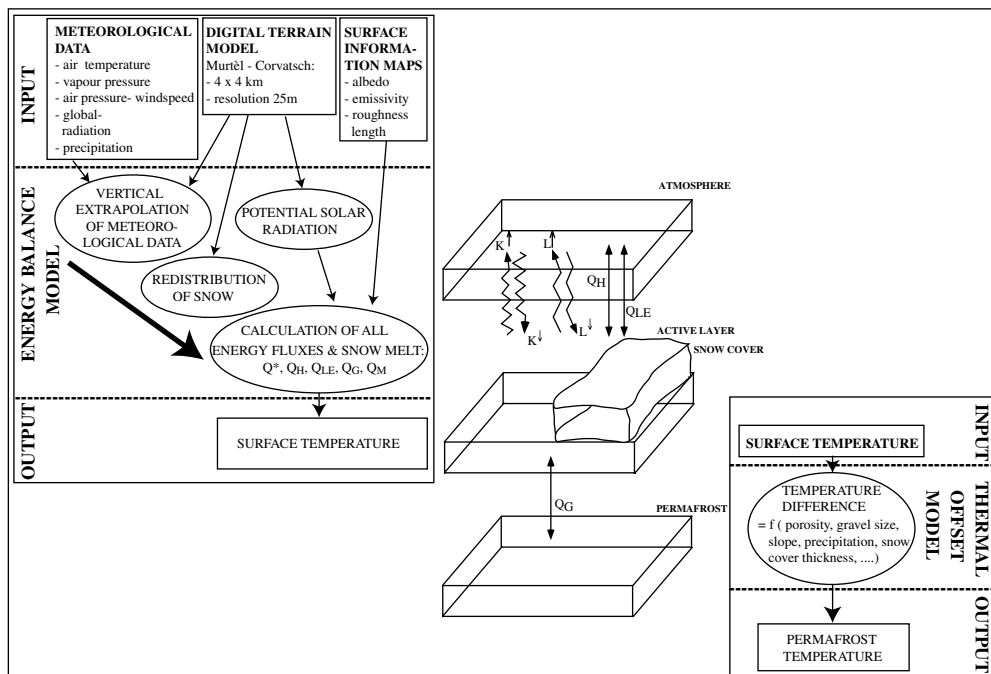


Figure 3 Schematic model description of the energy balance and the thermal offset models as developed in the PACE project.

climatological data like the albedo of snow are determined depending on the input data. These extrapolated meteorological variables provide the necessary input parameters for the calculation—in daily time steps—of energy fluxes at each gridpoint. Only forest-free areas are modelled.

Modelling the evolution of the snow cover is one of the main components within the energy balance model. Snow cover influences the energy budget as a crucial parameter, on the one hand by insulating the ground from the cold atmosphere in winter and from the warm air in summer, and on the other hand by changing the surface albedo and therefore influencing net radiation. Calculation of all energy fluxes allows determination of the amount of snow melt during winter and spring and thus calculation of the melt-out day of each pixel. As soon as the duration of the snow-free period is known, the sum of all energy fluxes is used for determination of the emitted long-wave radiation and thus the ground surface temperatures (see Figures 4 and 9). Figure 4 shows the measured surface temperature at the Murtèl–Corvatsch site, which is compared with the modelled surface temperature using the energy balance model at this site. The modelled surface temperatures can then be used as input for thermal offset modelling.

The *thermal offset* (Burn and Smith, 1988; Goodrich, 1982; Romanovsky and Osterkamp, 1995) is defined as the difference between mean annual ground surface temperature (MAGT) and mean annual permafrost temperature (MAPT) at the permafrost table and constitutes a key parameter for modelling permafrost–climate relationships (Smith and Riseborough, 1996). To date, most investigations of the thermal offset have been in high-latitude lowlands rather than in low-latitude mountains. Equations derived by Romanovsky and Osterkamp (1995) from analyses of conductive heat transfer

within the active layer are useful for cold permafrost but of rather limited applicability in discontinuous, warm permafrost (Burn, 1998). Various approaches based on climate statistics, soil and surface conditions or locally calibrated numerical applications working at different scales have been used by other authors (Nelson and Outcalt, 1987; Riseborough and Smith, 1998; Romanovsky *et al.*, 1997; Smith, 1975; Smith and Riseborough, 1996) to model the impact of climate change on permafrost distribution. The limitations of such ‘lowland’ concepts for mountain areas with warm discontinuous permafrost on slopes are obvious where rough topography leads to pronounced small-scale variability in microclimatic conditions and surface characteristics. Severe problems exist, especially where the active layer consists of coarse debris with intensive horizontal heat exchange (for example the Balch effect: cf. Harris and Pedersen, 1998; Hoelzle *et al.*, 1999; Humlum, 1998; Wakonigg, 1996). Detailed investigation of this topic constitutes one of the main challenges for the coming years.

MODEL APPLICATIONS

Examples of regional- and local-scale modelling given below illustrate modern applications relating to European mountains.

In southern Norway, temperature measurements from the Juvasshøe area, Jotunheimen, have shown a linear relationship between mean annual ground temperature (MAGT) and MAAT (Ødegård *et al.*, 1996). Similarly, unpublished field data from the Department of Physical Geography, University of Oslo indicate that BTS values in the Dovrefjell and in the Juvasshøe areas can be mainly explained on the basis of altitude, while radiation is of minor importance. These findings justify the use

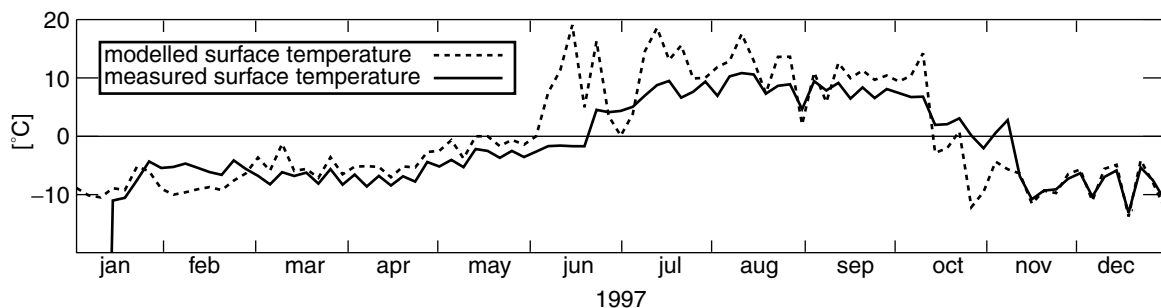


Figure 4 Comparison of measured and modelled surface temperature. The dashed line represents the modelled and the solid line the measured temperatures. The surface temperature data are averaged over four days.

of MAAT values as a good approximation for estimating permafrost distribution at a *regional scale* (Figure 5). In this case, a grid-based temperature map produced at the Norwegian Meteorological Institute with a grid-cell size of 1000 m (DNMI: Tveito and Førland, 1999) together with spatial analysis of the relationship between permafrost occurrence and MAAT were used to estimate the lower limit of discontinuous permafrost distribution in southern Norway. To achieve this goal, the lower limit of discontinuous permafrost at several locations was estimated in the field using BTS measurements, DC resistivity soundings and geomorphologic indicators (Etzelmüller *et al.*, 1998). In most of these areas,

the lower limit of discontinuous permafrost was at MAAT approx. -4°C . All cells of the MAAT map with values of -4°C were used to fit a quadratic trend surface to the corresponding altitudes. With this approach, a goodness of fit of $r^2 = 0.9$ and a RMS error of 85 m were obtained in relation to the $<-4^{\circ}\text{C}$ boundary. The choice of a trend surface is justified because of the regional smoothing pattern of the macroclimatic relationship assumed in this study. According to these results, the altitude of the lower limit of permafrost distribution decreases from above 1700 m ASL in the western part of southern Norway down to about 1200 m ASL in its eastern part. Comparison with large-scale mapping

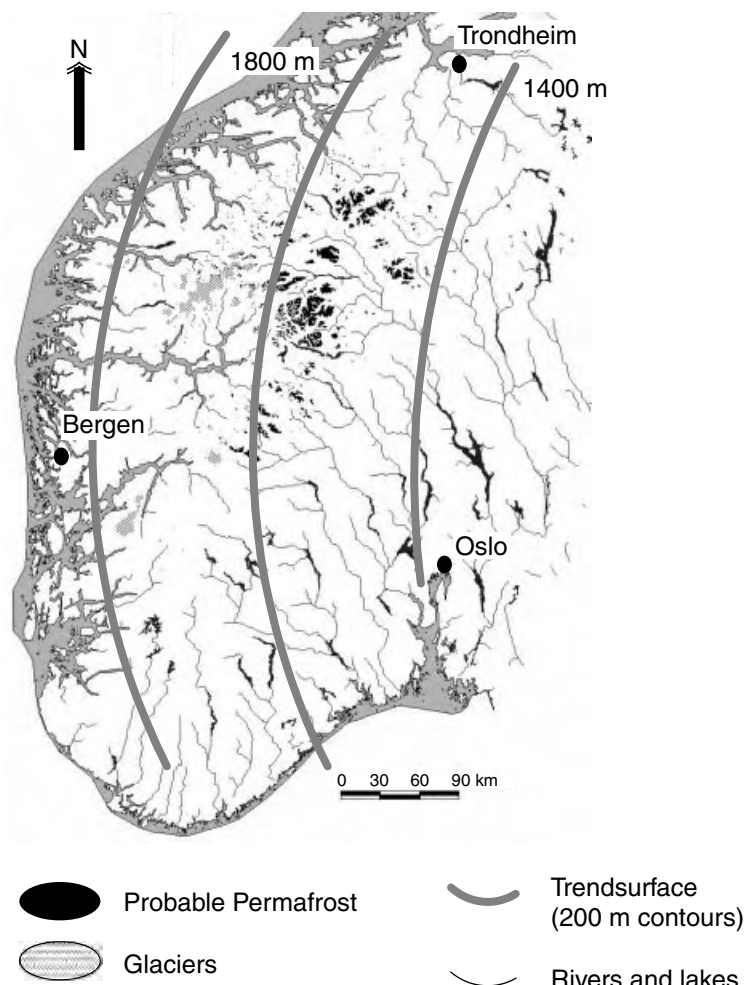


Figure 5 Permafrost distribution modelled according to the model described by Etzelmüller *et al.* (1998) on a regional scale in southern Norway. The model has a grid-cell size of 1000 m. The dark shaded areas denote the lower boundary of discontinuous permafrost. The three contour lines describe the second-order trend surface describing this lower boundary. Sporadic permafrost exists at lower altitudes as shown in the figure, usually connected to palsas.

(Ødegård *et al.*, 1999) and geomorphologic mapping and geophysical soundings (Barsch and Treter, 1976; King, 1986) showed quite good agreement with the regional model.

Three different *local-scale models* are presented for the Corvatsch–Furtschellas area in the Upper Engadin, Swiss Alps (Figures 6–9). Comparison of the model results confirms that all approaches provide a generally accurate picture of the permafrost distribution pattern as documented by several hundred BTS measurements in this area (Figure 6). In detail, however, differences occur which can mainly be explained by the characteristics of the individual models. The model PERMAKART (Figure 7: Keller, 1992), for instance, is based on the ‘rules of thumb’ originally developed for analogue maps, distinguishes foot-of-slope from slope cases and indicates permafrost at typical sites with spring-avalanche deposits. The model PERMAP (Figure 8: Hoelzle and Haeberli, 1995) uses potential solar radiation and MAAT and does not consider the effects of snow redistribution by avalanches, but is able to map small permafrost patches in extreme shadow. The third approach (Figure 9) is based on energy balance considerations and provides ground surface temperatures as described above, which must later be complemented with thermal offset corrections in order to reflect permafrost conditions.

MODEL VALIDATION

Information from remote sensing, geomorphological mapping, geophysical soundings, borehole observations and micrometeorological measurements can be used not only to develop and calibrate but also to validate models. Different methods of model validation can be used, depending on the model types. Most promising for model validation at a local scale are geophysical methods. In particular, BTS measurements are quite useful for validation (Keller *et al.*, 1998; Frauenfelder *et al.*, 1998; Imhof *et al.*, 2000a; Riedlinger and Kneisel, 2000). Other geophysical methods are mostly limited to areas where a clear difference between material with and without ice is present (Hauck *et al.*, 2001, this issue). Remote sensing is not so suitable for validation, because thermal surface information cannot be directly used. Geomorphologic mapping for model validation involves landforms that are indicative of permafrost occurrence (Lewkowicz and Duguay, 1999). Most of these methods for validation are based on point (e.g. BTS measurements), line (e.g. geophysical

soundings) or restricted polygon (e.g. geomorphologic mapping) information, which implies the use of interpolation methods for comparison with the models. Debris bodies with a well-organized viscous appearance are evidence of cumulative creep deformation due to the present-day or former long-term existence of ground ice in various forms (Haeberli *et al.*, 1998; Konrad *et al.*, 1999). Today, corresponding flow fields can be measured effectively and over large areas using digital photogrammetry (Kääb and Vollmer, 2000). In the European Alps, rock glacier inventories exist in Switzerland (Delaloye and Morand, 1998b; Frauenfelder, 1998; Hoelzle, 1998; Imhof, 1998; Phillips *et al.*, 1998; Reynard *et al.*, 1998; Schoeneich, 1998), Austria (Lieb, 1998b), Spain (Martinez de Pisón *et al.*, 1998), Italy (Guglielmin, 1998), Norway (Sollid, 1998), Poland (Dobinski, 1998; Kotarba, 1992) and Romania (Urdea, 1992; 1993). These inventories are most suitable for estimating lower limits of permafrost occurrence during recent or past time periods (Barsch, 1996; Frauenfelder and Kääb, 2000; Urdea, 1998).

Another landform specifically related to perennially frozen ground are push moraines (Boulton *et al.*, 1999; Etzelmüller *et al.*, 1996) or composite ridges (Benn and Evans, 1998). Here, an advancing glacier front deforms and thrusts proglacial sediments far from the glacier front by transmitting a stress field through ductile ice-rich frozen ground. Such moraines have been known for some time from Arctic Canada (Kälin, 1971), Svalbard (Boulton *et al.*, 1999; Croot, 1988; Etzelmüller *et al.*, 1996; Hagen, 1987; Hambrey *et al.*, 1996), and indicate permafrost for the Scandinavian mountains and the Alps (Haeberli, 1979). Under permafrost conditions, large ice-cored moraines can exist for extended time periods as described in Scandinavia (Østrem, 1964) or Svalbard (Boulton *et al.*, 1999; Etzelmüller *et al.*, 1996; Sollid and Sørbel, 1988). Such long-term buried ice within frozen ground may creep on steep slopes and result in landforms which are transitional between moraines and rock glaciers. Their areal restriction makes these forms indicators in areas where glaciers and permafrost coexist. Palsas are abundant in northern Scandinavia, and have been mapped as indicators of sporadic permafrost patches (Rapp, 1982; Seppälä, 1997; Sollid and Sørbel, 1998). They need special topographic, botanical and hydrological conditions for their development and are thus rare in high-alpine environments. In a similar way, active ice-wedges or pingos can seldom be expected in rugged mountain topography (Liestøl, 1976).

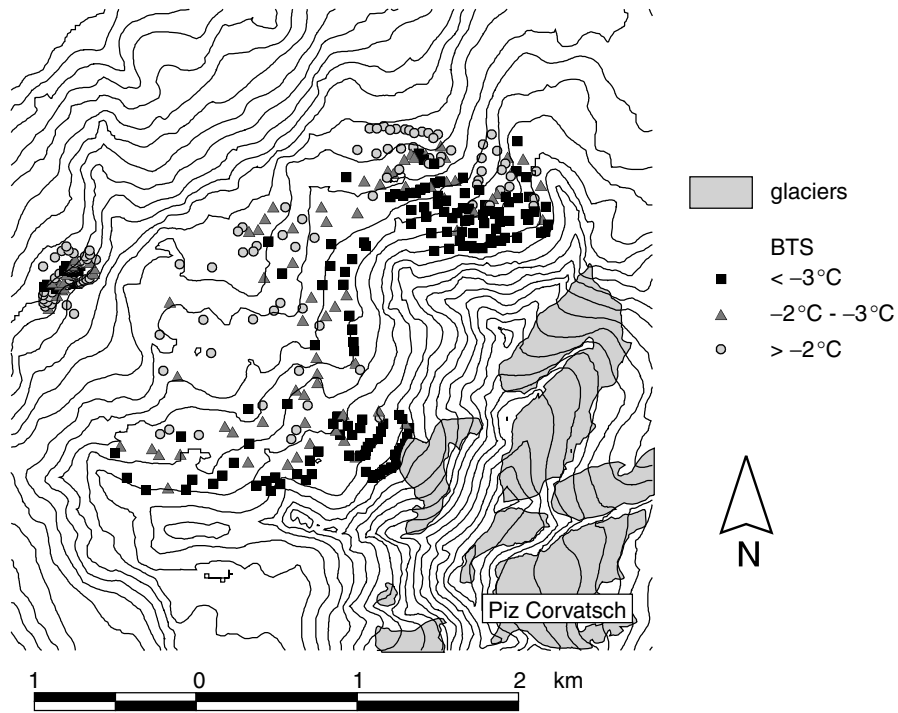


Figure 6 Measured permafrost distribution with the BTS method on a local scale in the Corvatsch–Furtschellas area, Upper Engadin, Switzerland. The BTS values could be used as an indicator of the present permafrost distribution in this area and also as a validation tool for the models.

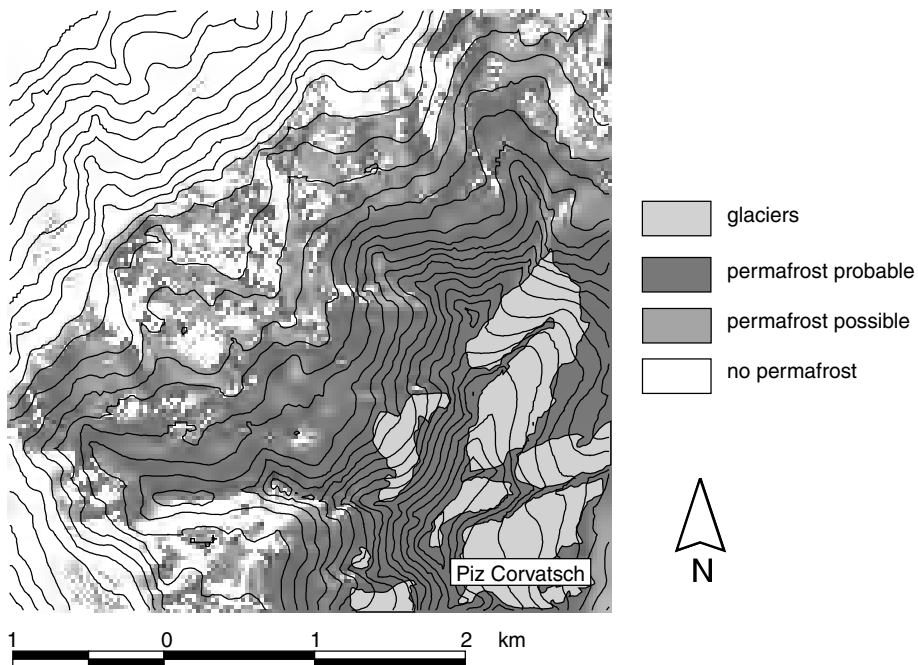


Figure 7 Permafrost distribution modelled with the programme PERMAKART developed by Keller (1992) on a local scale in the Corvatsch–Furtschellas area, Upper Engadin, Switzerland.

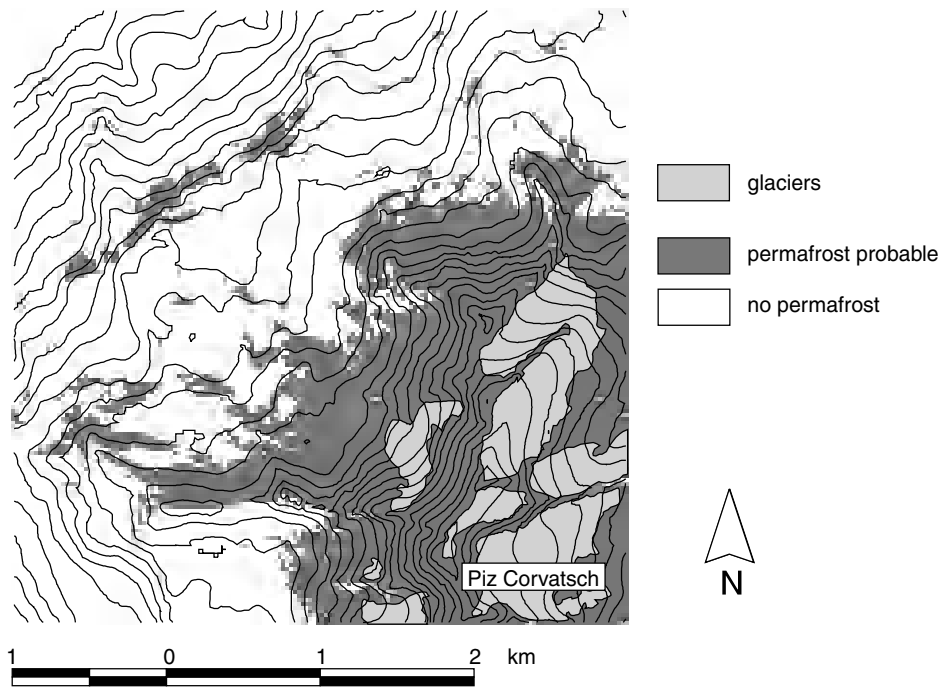


Figure 8 Permafrost distribution modelled with the programme PERMAMAP developed by Hoelzle and Haerberli (1995) on a local scale in the Corvatsch–Furtschellas area, Upper Engadin, Switzerland.

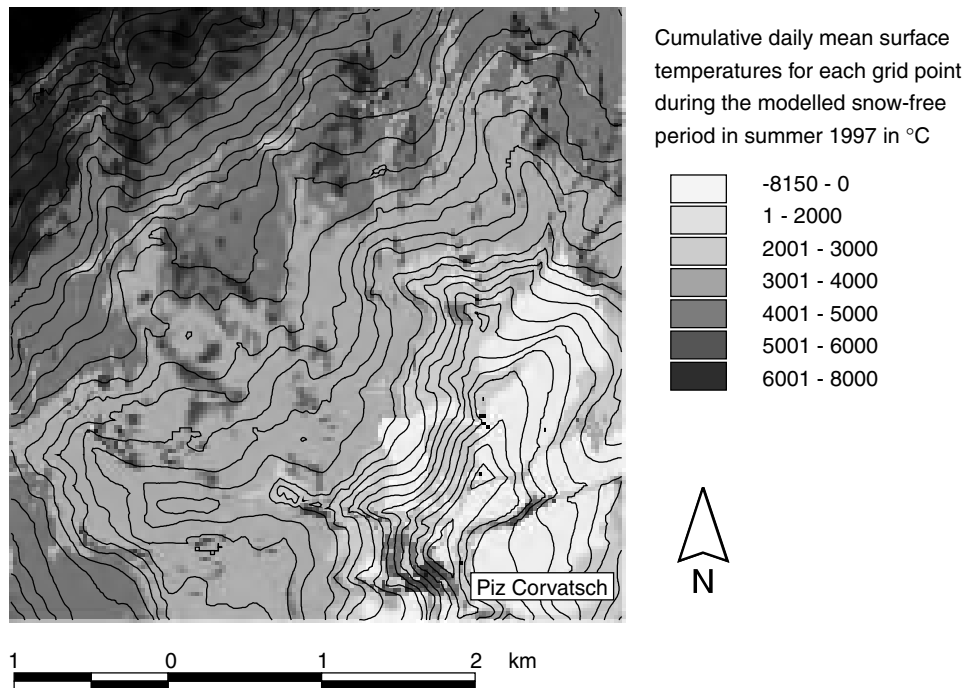


Figure 9 Results from an energy balance model expressed as cumulative daily mean surface temperatures during the snow-free period on a local scale in the Corvatsch–Furtschellas area, Upper Engadin, Switzerland.

SUMMARY AND PERSPECTIVES FOR THE FUTURE

Since the 1970s and especially during the last ten years, considerable progress has been achieved in the development of distribution modelling of mountain permafrost. A variety of GIS-based empirical-statistical approaches with correspondingly differing strengths and weaknesses exist today for predicting the presence or absence of permafrost in terms of yes/no functions on the basis of digital terrain information. This variety not only enables quite realistic distribution patterns to be estimated for extended mountain areas but also permits degrees of certainty/uncertainty to be assessed from intercomparison of different model calculations. The main potential for future improvement and development of a new modelling philosophy lies in the inclusion of surface energy fluxes and temperatures in physically based algorithms. It is in this area that the major contribution of the PACE project work package 4 has been made.

First results from detailed energy balance measurements at alpine permafrost sites confirm that the grey-box approaches used for selecting key variables in the existing empirical-statistical models effectively reflect the importance of the governing physical processes. However, these results also clearly demonstrate the importance of active layer processes specifically related to mountain conditions, especially advective fluxes of matter and energy in highly porous slope deposits. Scientific research concerning such processes is in its infancy. Two strategies appear promising:

- (a) The use of continued energy balance observations for empirically calibrating thermal offset values characterizing variable materials (coarse/fine debris, bedrock) and slopes (steep, flat). The relatively constant mean winter and summer differences between ground surface temperatures and active layer temperatures as observed at the Murtèl site suggest that this approach may provide useful results. Information gained from boreholes drilled by the PACE project and distributed in a large N–S transect may also provide valuable data.
- (b) A detailed analysis of high-frequency variations of measured thermal offset with respect to possible heat-exchange mechanisms. Special attention must thereby be paid to the uncertainties of the measurements and calculations as introduced by extremely difficult terrain conditions.

A major problem with atmosphere/lithosphere coupling is the integration of snow (Imhof *et al.*, 2000b) and its redistribution by wind and avalanches. Snow has a very complex influence on the ground thermal regime in mountain areas (Stähli, 1997; Phillips, 2000). In general, snow is a poor heat conductor and short-term variations of air temperature and radiation rarely reach the snow-covered ground, because they are damped as long as the snow cover is thick enough. A thick early winter snow cover prevents cooling of the ground. In contrast, a thin snow cover in fall effectively conducts heat out of the underlying ground by intensifying the emission of long-wave radiation (Keller and Gubler, 1993). In spring, a long-lasting snow cover prevents the ground from heating up despite the large radiation income during this period (Bernhard *et al.*, 1998). As a consequence, temperature distribution, phase changes, energy and mass flux have to be modelled within the snow cover as well as the underlying active layer and permafrost using well-tested numerical snow models (Bader and Weilenmann, 1992; Gubler, 1999; Morris *et al.*, 1997; Zhang *et al.*, 1996).

The energy balance model currently under development enables sensitivity studies to be undertaken to investigate individual factors and aspects of the complex exchange processes between the atmosphere and the permafrost. This is especially interesting in the context of past and possible future climate change. The ultimate goal is, in fact, to establish a chain linking climate data, global circulation models, regional climate models, regional GIS models, local GIS models and site observations or simulations coupled with time-dependent ground thermal conditions.

ACKNOWLEDGEMENTS

This work was funded by the Federal Office for Education and Sciences (contract 97.0054-2) within the EU programme Permafrost and Climate (PACE, contract ENV4-CT97-0492). We would like to acknowledge the comments of Dr Charles Harris and an unknown reviewer which improved the paper.

REFERENCES

- Ahnert F. 1994. Equilibrium, scale and inheritance in geomorphology. *Geomorphology* **11**: 125–140.
- Bader HP, Weilenmann P. 1992. Modeling temperature distribution, energy and mass flow in a (phase changing) snowpack. Model and case studies. *Cold Regions Science and Technology* **20**: 157–181.
- Barsch D. 1996. *Rockglaciers*. Springer: Berlin.

- Barsch D, Treter U. 1976. Zur Verbreitung der Periglazialphänomene in Rondane/Norwegen. *Geografiska Annaler* **58**: 83–93.
- Benn DI, Evans DJA. 1998. *Glaciers and Glaciations*. Arnold: London.
- Bernhard L, Sutter F, Haeberli W, Keller F. 1998. Processes of snow/permafrost-interactions at a high-mountain site, Murtèl/Corvatsch, Eastern Swiss Alps. In *Proceedings of the 7th International Conference on Permafrost, Yellowknife, Canada*. Nordicana, 57, 35–41.
- Boulton GS, van der Meer JJM, Beets DJ, Hart JK, Ruegg GHJ. 1999. The sedimentary and structural evolution of a recent push moraine complex: Holmstrømbreen, Spitsbergen. *Quaternary Science Review* **18**: 339–371.
- Burgess MM, Smith SL, Brown J, Romanowsky V, Hinkel K. 2000. Global Terrestrial Network for Permafrost (GTN-P): permafrost monitoring contributing to global climate observations. *Current Research 2000-E14, Geological Survey of Canada*, 1–8.
- Burn CR. 1998. Field investigations of permafrost and climatic change in Northwest North America. In *Proceedings of the 7th International Conference on Permafrost, Yellowknife, Canada*. Nordicana, 57, 107–120.
- Burn CR, Smith CAS. 1988. Observations of the 'thermal offset' in near-surface mean annual ground temperatures at several sites near Mayo, Yukon Territory Canada. *Arctic* **41**: 99–104.
- Cheng G. 1983. Vertical and horizontal zonation of high-altitude permafrost. In *Proceedings of the 4th International Conference on Permafrost, Fairbanks, Alaska*. National Academy Press; 136–141.
- Cheng G, Dramis F. 1992. Distribution of mountain permafrost. *Permafrost and Periglacial Processes* **3**: 83–91.
- Croot DG. 1988. Morphological, structural and mechanical analysis of neoglaciated ridges in Iceland. In *Glaciotectonics: Forms and processes*. Balkema: Rotterdam; 33–48.
- De Boer DH. 1992. Hierarchies and spatial scale in process geomorphology: a review. *Geomorphology* **4**: 303–318.
- Dehn M, Buma J. 1999. Modelling future landslide activity based on general circulation models. *Geomorphology* **30**: 175–187.
- Dehn M, Burger G, Buma J, Gasparetto P. 2000. Impact of climate change on slope stability using expanded downscaling. *Engineering Geology* **55**: 193–204.
- Delaloye R, Morand S. 1998a. Les glaciers rocheux de la région d'Entremont (Alpes Valaisannes): inventaire et analyse spatiale à l'aide d'un SIG. In *Beiträge aus der Gebirgs-Geomorphologie*. Mitteilungen der Versuchsanstalt für Wasserbau, Hydrologie und Glaziologie, 158, ETH-Zürich, 75–86.
- Delaloye R, Morand S. 1998b. Rock glaciers, Entremont, Valais, Switzerland. International Permafrost Association, Data and Information Working Group, NSIDC, University of Colorado at Boulder 1.0, CD-ROM.
- Dobinski W. 1998. Permafrost occurrence in the alpine zone of the Tatra Mountains, Poland. In *Proceedings of the 7th International Conference on Permafrost, Yellowknife, Canada*. Nordicana, 57, 231–237.
- Etzelmüller B, Hagen JO, Vatne G, Ødegård RS, Sollid JL. 1996. Glacier debris accumulation and sediment deformation influenced by permafrost, examples from Svalbard. *Annals of Glaciology* **22**: 53–62.
- Etzelmüller B, Berthling I, Sollid JL. 1998. The distribution of permafrost in southern Norway—a GIS approach. In *Proceedings of the 7th International Conference on Permafrost, Yellowknife, Canada*. Nordicana, 57, 251–257.
- Etzelmüller B, Ødegård RS, Berthling I, Sollid JL. 2001. Terrain parameters and remote sensing data in the analysis of permafrost distribution and periglacial processes: principles and examples from Southern Norway. *Permafrost and Periglacial Processes* **12**: 00–00.
- Frauenfelder R. 1998. Rock glaciers, Fletschhorn Area, Valais, Switzerland. International Permafrost Association, Data and Information Working Group, NSIDC, University of Colorado at Boulder 1.0, CD-ROM.
- Frauenfelder R, Kääh A. 2000. Towards a palaeoclimatic model of rock glacier formation in the Swiss Alps. *Annals of Glaciology* **31**: 281–286.
- Frauenfelder R, Allgöwer B, Haeberli W, Hoelzle M. 1998. Permafrost investigations with GIS—a case study in the Fletschhorn area, Wallis, Swiss Alps. In *Proceedings of the 7th International Conference on Permafrost, Yellowknife, Canada*. Nordicana, 57, 291–295.
- Funk M, Hoelzle M. 1992. Application of a potential direct solar radiation model for investigating occurrences of mountain permafrost. *Permafrost and Periglacial Processes* **3**: 139–142.
- Gallant JC, Wilson JP. 1996. TAPES-G: a grid-based terrain analysis program for the environmental sciences. *Computer and Geosciences* **22**: 713–722.
- Goodrich LE. 1982. The influence of snow cover on the ground thermal regime. *Canadian Geotechnical Journal* **19**: 421–432.
- Gruber S. 2000. Slope instability and permafrost: a spatial analysis in the Matter Valley, Switzerland. Master thesis, Justus Liebig University of Giessen.
- Gruber S, Hoelzle M. 2001. Statistical modelling of mountain permafrost distribution: local calibration and incorporation of remotely sensed data. *Permafrost and Periglacial Processes* **12**: 69–77.
- Gubler H. 1999. A model to determine snow surface properties from remote measurements. In *Proceedings of ISSW 991, Sunriver, Oregon, USA*. 35–48.
- Guglielmin M. 1998. Rock glaciers, Lombardy, Italy. International Permafrost Association, Data and Information Working Group, NSIDC, University of Colorado at Boulder 1.0, CD-ROM.
- Haeberli W. 1975. *Untersuchungen zur Verbreitung von Permafrost zwischen Flüelapass und Piz Grialetsch (Graubünden)*. Mitteilungen der Versuchsanstalt für Wasserbau, Hydrologie und Glaziologie, 17, ETH Zürich.
- Haeberli W. 1979. Holocene push-moraines in alpine permafrost. *Geografiska Annaler* **61A**: 43–48.
- Haeberli W. 1990. Glacier and permafrost signals of the 20th-century warming. *Annals of Glaciology* **14**: 99–101.

- Haerberli W. 1992. Construction, environmental problems and natural hazards in periglacial mountain belts. *Permafrost and Periglacial Processes* **3**: 111–124.
- Haerberli W, Kääh A, Wagner S, Vonder Mühl D, Geissler P, Haas JN, Glatzel-Mattheier H, Wagenbach D. 1998. Pollen analysis and C14-age of moss remains in a permafrost core recovered from the active rock glacier Murtèl/Corvatsch, Swiss Alps: geomorphological and glaciological implications. *Journal of Glaciology* **45**: 1–8.
- Haerberli W, Kääh A, Vonder Mühl D, Teyssseire P. in press. Prevention of outburst floods from periglacial lakes at Gruben Glacier, Valais, Swiss Alps. *Journal of Glaciology*.
- Hagen JO. 1987. Glacier surge at Usherbreen, Svalbard. *Polar Research* **5**: 239–252.
- Halldin S, Gottschalk L, Gryning SE, Jochum AA, Lundin LC, Van de Griend AA. 1999. Energy, water and carbon exchanges in a boreal forest—Nopex experiences. *Journal of Agricultural and Forest Meteorology* **98/99**, 75–102.
- Hambrey MJ, Dowdeswell JA, Murray T, Porter PR. 1996. Thrusting and debris entrainment in a surging glacier: Bakaninbreen, Svalbard. *Annals of Glaciology* **22**: 241–248.
- Harris C, Haerberli W, Vonder Mühl D, King L. 2001. Permafrost monitoring in the high mountains of Europe: the PACE project in its global context. *Permafrost and Periglacial Processes* **12**: 3–11.
- Harris SA, Pedersen DE. 1998. Thermal regimes beneath coarse blocky material. *Permafrost and Periglacial Processes* **9**: 107–120.
- Hauck C, Guglielmin M, Isaksen K, Vonder Mühl D. 2001. Applicability of frequency-domain and time-domain electromagnetic methods for mountain permafrost studies. *Permafrost and Periglacial Processes* **12**: 39–52.
- Heggem ESF. 1999. Adaptation, sensitivity tests and application of a spatially distributed radiation balance model (SRAD) (in Norwegian). Oslo, University of Oslo.
- Hoelzle M. 1996. Mapping and modelling of mountain permafrost distribution in the Alps. *Norsk Geografisk Tidsskrift* **50**: 11–15.
- Hoelzle M. 1998. Rock glaciers, Upper Engadin, Switzerland. International Permafrost Association, Data and Information Working Group, NSIDC, University of Colorado at Boulder 1.0, CD-ROM.
- Hoelzle M, Haerberli W. 1995. Simulating the effects of mean annual air temperature changes on permafrost distribution and glacier size. An example from the Upper Engadin, Swiss Alps. *Annals of Glaciology* **21**: 400–405.
- Hoelzle M, Haerberli W, Keller F. 1993. Application of BTS measurements for modelling permafrost distribution in the Swiss Alps. In *6th International Conference on Permafrost, Beijing, China*. South China University Technology Press: 272–277.
- Hoelzle M, Wegmann M, Krummenacher B. 1999. Miniature temperature dataloggers for mapping and monitoring of permafrost in high mountain areas: first experiences from the Swiss Alps. *Permafrost and Periglacial Processes* **10**: 113–124.
- Humlum O. 1998. The climatic significance of rock glaciers. *Permafrost and Periglacial Processes* **9**: 375–395.
- Imhof M. 1996. Modelling and verification of the permafrost distribution in the Bernese Alps (Western Switzerland). *Permafrost and Periglacial Processes* **7**: 267–280.
- Imhof M. 1998. Rock glaciers, Bernese Alps, western Switzerland. International Permafrost Association, Data and Information Working Group, NSIDC, University of Colorado at Boulder 1.0, CD-ROM.
- Imhof M, Mittaz C, Hoelzle M, Haerberli W. 2000a. Snow-melt evolution—a new parameter for the simulation of alpine permafrost distribution. European Geophysical Society, 25th General Assembly, Vol. 2. Geophysical Research Abstracts, Nice, CD-ROM.
- Imhof M, Pierrehumbert G, Haerberli W, Kienholz H. 2000b. Permafrost investigation in the Schilthorn massif, Bernese Alps, Switzerland. *Permafrost and Periglacial Processes* **11**: 189–206.
- Isaksen K, Vonder Mühl D, Gubler H, Kohl T, Sollid JL. in press. Ground surface temperature reconstruction based on data from a deep borehole in permafrost at Janssonhaugen, Svalbard. *Annals of Glaciology* **31**.
- Isaksen K, Holmlund P, Sollid JL, Harris C. 2001. Three deep alpine—permafrost boreholes in Svalbard and Scandinavia. *Permafrost and Periglacial Processes* **12**: 00–00.
- Ives JD, Bovis MJ. 1978. Natural hazards maps for land-use planning, San Juan Mountains, Colorado, USA. *Arctic and Alpine Research* **10**: 185–212.
- Jensen J. 1999. An analysis of permafrost distribution on Plateau Mountain, Alberta using the Geographic Information System ARC/INFO. Calgary, University of Calgary.
- Jorgensen MT, Kreig RA. 1988. A model for mapping permafrost distribution based on landscape component maps and climatic variables. In *5th International Conference on Permafrost, Trondheim, Norway*. 176–182.
- Kääh A, Völlmer M. 2000. Monitoring landslides by digital photogrammetry. European Geophysical Society, 25th General Assembly, Vol. 2. Geophysical Research Abstracts, Nice, CD-ROM.
- Kälin M. 1971. The active push moraine of the Thompson Glacier, Axel Heiberg Island, Canadian Arctic Archipelago, Canada. PhD thesis, Zürich, ETH.
- Keller F. 1992. Automated mapping of mountain permafrost using the program PERMAKART within the geographical information system ARC/INFO. *Permafrost and Periglacial Processes* **3**: 133–138.
- Keller F, Gubler HU. 1993. Interaction between snow cover and high mountain permafrost, Murtèl–Corvatsch, Swiss Alps. In *6th International Conference on Permafrost, Beijing, China*. South China University of Technology Press; 332–337.
- Keller F, Frauenfelder R, Gardaz JM, Hoelzle M, Kneisel C, Lugon R, Philips M, Reynard E, Wenker L. 1998. Permafrost map of Switzerland. In *7th International*

- Conference on Permafrost, Yellowknife, Canada*. Nordicana, 57, 557–562.
- Keusen HR, Haeberli W. 1983. Site investigation and foundation design aspects of cable car construction in Alpine permafrost at the 'Chli Matterhorn', Wallis, Swiss Alps. In *4th International Conference on Permafrost, Fairbanks, Alaska, USA*. 601–605.
- King L. 1986. Zonation and ecology of high mountain permafrost in Scandinavia. *Geografiska Annaler* **68**: 131–139.
- King L, Kalisch A. 1998. Permafrost distribution and implications for construction in the Zermatt area, Swiss Alps. In *7th International Conference on Permafrost, Yellowknife, Canada*. Nordicana, 57, 569–574.
- Kneisel C. 1998. Occurrence of surface ice and ground ice/permafrost in recently deglaciated glacier forefields, St Moritz area, Eastern Swiss Alps. In *7th International Conference on Permafrost, Yellowknife, Canada*. Nordicana, 57, 575–581.
- Konrad S, Humphrey NF, Steig EJ, Clark DH, Potter NJ, Pfeffer WT. 1999. Rock glacier dynamics and paleoclimatic implications. *Geology* **27**: 1131–1134.
- Kotarba A. 1992. Natural environment and landform dynamics of the Tatra Mountains. *Mountain Research and Development* **12**: 105–129.
- Lewkowicz AG, Duguay CR. 1999. Detection of permafrost features using SPOT panchromatic imagery, Fosheim Peninsula, Ellesmere Island, N.W.T. *Canadian Journal of Remote Sensing* **25**: 34–44.
- Li X, Cheng G, Chen X. 1998. Response of permafrost to global change on the Qinghai–Xizang plateau—a GIS-aided model. In *7th International Conference on Permafrost, Yellowknife, Canada*. Nordicana, 57, 657–661.
- Lieb GK. 1998a. High-mountain permafrost in the Austrian Alps (Europe). In *7th International Conference on Permafrost, Yellowknife, Canada*. Nordicana, 57, 663–668.
- Lieb GK. 1998b. Rock glaciers, Austria. International Permafrost Association, Data and Information Working Group, NSIDC, University of Colorado at Boulder 1.0, CD-ROM.
- Liestøl O. 1976. Pingos, springs and permafrost in Spitsbergen. *Norsk Polarinstitutt Arbok* 7–29.
- Martinez de Pison E, Serrano E, Agudo C, Arenillas M, Cantarino I, Garcia F, Martinez R, Navarro J, Pedrero A. 1998. Rock glaciers in the Pyrenees, Spain and France. International Permafrost Association, Data and Information Working Group, NSIDC, University of Colorado at Boulder 1.0, CD-ROM.
- Mittaz C. 1998. Energiebilanz über alpinem Permafrost. In *Beiträge aus der Gebirgs-Geomorphologie, Samedan, Schweiz*. VAW/ETH Zürich 158, 152–167.
- Mittaz C, Hoelzle M, Haeberli W. 2000a. First steps towards a mountain permafrost distribution model with energy balance data. *European Geophysical Society, 25th General Assembly*, Vol. 2. Geophysical Research Abstracts, Nice, CD-ROM.
- Mittaz C, Hoelzle M, Haeberli W. 2000b. First results and interpretation of energy-flux measurements of Alpine permafrost. *Annals of Glaciology* **31**: 275–280.
- Moore ID. 1992. SRAD: direct, diffuse, reflected short wave radiation, and the effects of topographic shading. Terrain analysis programs for the environmental sciences (TAPES) radiation program documentation. Canberra, Centre for Resource and Environmental Studies, Australian National University.
- Morris EM, Bader HP, Weilenmann P. 1997. Modeling temperature variations in polar snow using DAISY. *Journal of Glaciology* **48**: 180–191.
- Nelson FE, Outcalt SI. 1987. A computational method for prediction and regionalization of permafrost. *Arctic and Alpine Research* **19**: 279–288.
- Ødegård R, Hoelzle M, Johansen KV, Sollid JL. 1996. Permafrost mapping and prospecting in southern Norway. *Norsk Geografisk Tidsskrift* **50**: 41–54.
- Ødegård RS, Isaksen K, Mastervik M, Billdal L, Engler M, Sollid JL. 1999. Comparison of BTS and Landsat TM data from Jotunheimen, southern Norway. *Norsk Geografisk Tidsskrift* **53**.
- Oke TR. 1987. *Boundary Layer Climates*. Cambridge University Press: Cambridge.
- Osterkamp TE. 1983. Response of Alaskan permafrost to climate. In *4th International Conference on Permafrost, Fairbanks, Alaska, USA*. 145–152.
- Østrem G. 1964. Ice-cored moraines in Scandinavia. *Geografisk Annaler* **46A**: 282–337.
- Phillips M. 2000. *Influences of Snow Supporting Structures on the Thermal Regime of the Ground in Alpine Permafrost*. Eidgenössische Forschungsanstalt WSL: Davos.
- Phillips M, Reynard E, Wenker L. 1998. Rock glacier inventory, Haute Alpes Calcaires, Switzerland. International Permafrost Association, Data and Information Working Group, NSIDC, University of Colorado at Boulder 1.0, CD-ROM.
- Rapp A. 1982. Zonation of permafrost indicators in Swedish Lapland. *Norsk Geografisk Tidsskrift* **82**: 37–38.
- Reynard E, Lambiel C, Wenker L. 1998. Rock glaciers, Printse Valley, Valais, Switzerland. International Permafrost Association, Data and Information Working Group, NSIDC, University of Colorado at Boulder 1.0, CD-ROM.
- Riedlinger T, Kneisel C. 2000. Interaktionen von Permafrost und Ausaperung im Gletschervorfeld des Vadret da Rosatsch, Oberengadin, Schweiz. *Trierer Geographische Studien* **23**: 147–164.
- Riseborough DW, Smith MW. 1998. Exploring the limits of permafrost. In *7th International Conference on Permafrost, Yellowknife, Canada*. Nordicana, 57, 935–941.
- Romanovsky VE, Osterkamp TE. 1995. Interannual variations of the thermal regime of the active layer and near surface permafrost in northern Alaska. *Permafrost and Periglacial Processes* **6**: 313–335.
- Romanovsky VE, Osterkamp TE, Duxbury NS. 1997. An evaluation of three numerical models used in simulations of the active layer and permafrost temperature regimes. *Cold Regions Science and Technology* **26**: 195–203.
- Schoeneich P. 1998. Rock glaciers of the Prealps, Vaud, Switzerland. International Permafrost Association, Data

- and Information Working Group, NSIDC, University of Colorado at Boulder 1.0, CD-ROM.
- Seppälä M. 1997. Distribution of permafrost in Finland. *Bulletin of the Geological Society of Finland* **69**: 87–96.
- Smith MW. 1975. Microclimatic influences on ground temperatures and permafrost distribution, Mackenzie Delta. *Canadian Journal of Earth Science* **12**: 1421–1438.
- Smith MW, Riseborough DW. 1996. Ground temperature monitoring and detection of climate change. *Permafrost and Periglacial Processes* **7**: 301–310.
- Sollid JL. 1998. Rock glaciers in mainland Norway and Svalbard. International Permafrost Association, Data and Information Working Group, NSIDC, University of Colorado at Boulder 1.0, CD-ROM.
- Sollid JL, Sørbel L. 1988. Influence of temperature conditions in formation of end moraines in Fennoscandia and Svalbard. *Boreas* **17**: 553–558.
- Sollid JL, Sørbel L. 1998. Palsa bogs as a climate indicator—examples from Dovrefjell, Southern Norway. *Ambio* **27**: 287–291.
- Stähli M. 1997. Heat and water transfer in the frozen soil environment. PhD thesis, Uppsala, Swedish University of Agricultural Sciences.
- Thalparpan P, Phillips M, Amman W. 1998. Snow supporting structures in steep permafrost terrain in the Swiss Alps. In *7th International Conference on Permafrost, Yellowknife, Canada*. Nordicana, 57, 1049–1056.
- Tveito OE, Førland EJ. 1999. Mapping temperatures in Norway applying terrain information, geostatistics and GIS. *Norsk geografisk Tidsskrift* **53**: 202–212.
- Urdea P. 1992. Rock glaciers and periglacial phenomena in the Southern Carpathians. *Permafrost and Periglacial Processes* **3**: 267–273.
- Urdea P. 1993. Permafrost and periglacial forms in the Romanian Carpathians. In *6th International Conference on Permafrost, Beijing, China*. South China University Technology Press; 631–637.
- Urdea P. 1998. Rock glaciers and permafrost reconstruction in the southern Carpathian Mountains, Romania. In *7th International Conference on Permafrost, Yellowknife, Canada*. Nordicana, 57, 1063–1069.
- Vonder Mühl D, Stucki T, Haerberli W. 1998. Borehole temperatures in alpine permafrost: a ten year series. In *7th International Conference on Permafrost, Yellowknife, Canada*. Nordicana, 57, 1089–1095.
- Vonder Mühl D, Hauck C, Gubler H, McDonald R, Russill N. 2001. New geophysical methods of investigating the nature and distribution of mountain permafrost with special reference to radiometry techniques. *Permafrost and Periglacial Processes* **12**: 27–38.
- Wakonigg H. 1996. Unterkühlte Schutthalden. In *Arbeiten aus dem Institut für Geographie der Karl-Franzens Universität*, Vol. 33, Graz, 209–223.
- Wegmann M, Keusen HR. 1998. Recent geophysical investigations at a high alpine permafrost construction site in Switzerland. In *7th International Conference on Permafrost, Yellowknife, Canada*. Nordicana, 57, 1119–1123.
- Zhang T, Osterkamp TE, Stamres K. 1996. Influence of the depth hoar layer of the seasonal snow cover on the ground thermal regime. *Water Resources Research* **32**: 2075–2086.

Thermal Regime of Openwork Block Fields on the Mountains Elgåhogna and Sølén, Central-eastern Norway

Håvard Juliussen^{1*} and Ole Humlum²

¹ Department of Geology, University Centre in Svalbard, N-9170 Longyearbyen, Norway

² Department of Physical Geography, Institute of Geosciences, University of Oslo, P.O. Box 1042 Blindern, N-0316 Oslo, Norway

ABSTRACT

Ground temperatures in openwork blocky debris are frequently lower than in bedrock or regolith with a matrix of fine sediment, creating a negative temperature anomaly. Two years of temperature measurements in seven 1-m-deep profiles located in central-eastern Norway showed that mean annual ground temperatures were 1.3–2.0°C lower in block fields (felsenmeer) compared with till and bedrock. These data suggest that mountain permafrost can be present in block fields several hundred metres lower than in bedrock and till, providing other conditions remain the same. Better thermal coupling of the ground and the air in winter was responsible for the observed anomaly, probably caused by enhanced conduction through blocks protruding into and through the snow and thereby acting as efficient heat bridges. Convection in the blocky debris, which has been used previously as an explanation of the negative thermal anomaly, was less important than initially presumed. Copyright © 2008 John Wiley & Sons, Ltd.

KEY WORDS: block field; thermal anomaly; convection; surface offset; central-eastern Norway

INTRODUCTION

The prevalence of lower temperatures in openwork blocky debris as compared with adjacent bedrock and regolith with a matrix of finer sediment, termed a negative thermal anomaly, has been recognised for many years (Balch, 1900; Liestøl, 1965). In the past decade, a number of studies have focused on this anomaly and the underlying heat transfer mechanisms. For example, Harris and Pedersen (1998) reported a negative temperature anomaly of 4–7°C in blocky debris as compared with adjacent mineral soil, based on data from Plateau Mountain, Canada and the Kunlun Mountains, China. Understanding such anomalies is important in order to improve permafrost

distribution modelling and to obtain better insight into periglacial processes in blocky debris. Most of the existing work has been conducted on specific landforms, such as rock glaciers (Humlum, 1997; Bernhard *et al.*, 1998; Hoelzle *et al.*, 1999; Hanson and Hoelzle, 2004) or talus slopes (Delaloye and Lambiel, 2005) or where blocky debris provides extrazonal occurrences of permafrost (Delaloye *et al.*, 2003; Gude *et al.*, 2003; Sawada *et al.*, 2003; Gorbunov *et al.*, 2004; Zacharda *et al.*, 2007). There is a paucity of studies on typical block fields (felsenmeer) and block slopes that dominate the ground surface in many mountain regions (Harris and Pedersen, 1998; Hanson and Hoelzle, 2005).

This paper presents a two-year temperature time series from seven 1-m-deep profiles in block fields, till and bedrock from the mountains Elgåhogna and Sølén in central-eastern Norway (Figure 1). The aims are (1) to quantify the thermal regime of block fields in this

* Correspondence to: Håvard Juliussen, Department of Geology, University Centre in Svalbard, N-9170 Longyearbyen, Norway. E-mail: havard.juliussen@unis.no

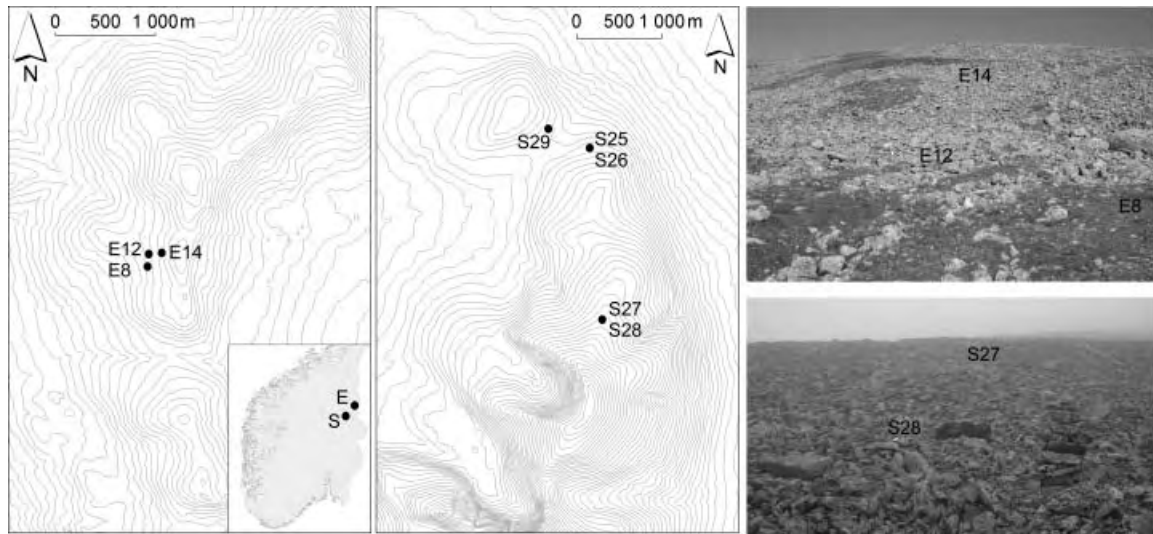


Figure 1 Key maps and photographs. Left panel: map of the sites on Elgåhogna (E8, E12 and E14). Inset map shows the positions of Elgåhogna (E) and Sølén (S) in southern Norway. Middle panel: map of the sites on Sølén (S25, S26, S27, S28, S29). Upper right panel: photograph showing the sites on Elgåhogna. Lower right panel: photograph showing the sites S27 and S28 on Sølén (block field sites). The cairn in which air temperature was monitored can be seen on the right.

area, and (2) to identify the heat transfer processes associated with thermal anomalies in block fields.

Heat Transfer in Openwork Blocky Debris

Several hypotheses have been put forward to explain the negative thermal anomaly in openwork blocky debris. Harris and Pedersen (1998) summarised and discussed four of these.

1. *The Balch effect.* This concept is based on cold air being denser than warm air so that it tends to displace warmer air in the pore-spaces of openwork blocky debris. The result is that openwork blocky debris acts as a thermal filter allowing cold air to enter and tending to keep warmer air out.
2. *The chimney effect.* This hypothesis is also based on density differences, but is attributed to lateral air advection within openwork blocky slopes (talus slopes, rock glaciers, etc.). In winter, cold air enters the blocky slope wherever there are holes in the snow cover and is advected downslope due to its relatively high density. The warmer and less dense air is displaced upslope before eventually escaping through funnels. The result is a positive thermal anomaly in the upper part of the slope and a negative thermal anomaly in the lower part.
3. *Summer evaporation/sublimation of water/ice in the blocky debris.* Evaporation and sublimation

of water and ice in the summer may cool the blocky debris, depending on the amount of latent heat removed from the system.

4. *Continuous air exchange with the atmosphere.* This is a simple extension of the chimney effect in areas without a continuous winter snow cover. Since there is nothing to stop a continuous air exchange with the atmosphere along the bare surface of the block field, this results in almost instantaneous warming and cooling of the blocky deposit to a considerable depth in response to changes in the air temperature. The process is most effective in windy situations on steep slopes.

Three of the four hypotheses include air movement within the pore spaces of the blocky debris. However, the terms used in hypotheses 1, 2 and 4 are not informative with respect to the common process operating: heat transfer by circulating pore space air. The subdivision has probably developed due to site-specific factors (e.g. snow depth, topography) influencing the process pattern. We prefer to use the terms *convection* (Nield and Bejan, 1992) when there is a movement of the pore air mainly between the top and base of the blocky debris layer and *advection* when there is a significant component of movement parallel to the surface.

Movement of pore air can be induced by free or forced convection (Kane *et al.*, 2001). Free convection

occurs as a result of temperature-induced variations in air density, and forced convection is driven by pressure gradients in the air, such as those induced by high wind speeds. Blocky debris pore air experiences free convection if a critical Rayleigh number is exceeded (Nield and Bejan, 1992; Goering, 2002). The Rayleigh number determines if heat transfer in a fluid is predominantly by convection or conduction, and is given by (Goering, 2002):

$$Ra = \frac{C\beta gKH\Delta T}{\nu k}$$

where C , β and ν are the volumetric heat capacity, expansion coefficient and kinematic viscosity of the pore fluid (in this case air), g is gravitational acceleration, K is the intrinsic permeability of the blocky debris layer, H is the thickness of the layer, ΔT is the temperature difference between the top and bottom of the layer (warmer boundary below) and k is the effective thermal conductivity. In this study, a conservative value was estimated for intrinsic permeability using the approach of Fair and Hatch (1933) (see also Goering, 2002). As a result, the Rayleigh number estimate is also conservative. The effective thermal conductivity was estimated from a correlation with porosity (Johansen, 1975).

Free convection can be expected if the Rayleigh number exceeds a critical value. In the case of closed upper and lower boundaries, such as a continuous snow cover and the base of the openwork layer, respectively, this critical value is $4\pi^2$, i.e. ≈ 40 (Nield and Bejan, 1992). When there is no snow and the pore volume is open to the atmosphere (open boundary), the critical value is 27 (Serkitjits and Hagentoft, 1998).

Harris and Pedersen's third hypothesis, regarding evaporation and sublimation of water and ice in the pore volume of the blocky debris in the summer, may be important in windy areas where the air is dry in the summer (Harris and Pedersen, 1998) and water or ice is available.

SETTING

The mountains Elg hogna (62  09'N, 11  57'E, 1460 m a.s.l.) and S len (61  55'N, 11  31'E, 1755 m a.s.l.) are located on a plateau (600–1000 m a.s.l.) in the Femunden area in central-eastern Norway (Figure 1). Openwork block fields dominate the ground surface above 1100–1200 m a.s.l. (Juliussen and Humlum, 2007).

The climate is continental with 12 C amplitude of the mean monthly temperatures and precipitation amounts of 450–740 mm year⁻¹ (data from The Norwegian Meteorological Institute). The 0 C isotherm for the 1961–990 normal period is at 750 m a.s.l. Snow depths are greater on Elg hogna than on S len.

According to Heggem *et al.* (2005), permafrost is probable above 1300–1350 m a.s.l. on Elg hogna and 1100–1200 m a.s.l. on S len. The main controlling factor for the permafrost distribution is elevation, whereas solar radiation and surface wetness influence the distribution locally on S len and Elg hogna, respectively. Measurements of the Bottom Temperature of Snow (BTS) (H eberli, 1973; Hoelzle *et al.*, 1993) have demonstrated lower temperatures on block fields than on vegetated ground (Juliussen, 2007).

Miniature temperature dataloggers (MTDs) were installed in July and August 2004 in two profiles to approximately 1 m depth on Elg hogna and five profiles on S len (Table 1). The sites were chosen to represent a range of ground materials, snow depths and topographic positions. The MTDs were installed at three or four levels. In blocky debris, the MTDs measured the temperature in the pore air between the blocks. The uppermost MTD was installed beneath a rock to avoid direct solar radiation on the sensor. The thickness of this rock determines the depth of the upper MTD. It should be noted that in such an environment the surface is highly irregular and difficult to define. Air temperature was measured at 1 m height at each site in naturally ventilated stone

Table 1 Site characteristics.

Site	Elevation (m a.s.l.)	Material	Topographic position	Miniature temperature datalogger depths (m)
E8	1316	Till	Lower slope	0.30, 0.60, 0.95
E12	1316	Blocky debris	Lower slope	0.20, 0.35, 0.56, 1.00
E14	1335	Blocky debris	Upper slope	0.20
S25	1071	Till	Ridge	0.02, 0.20, 0.50, 1.00
S26	1070	Till	Depression	0.02, 0.20, 0.50, 0.95
S27	1420	Blocky debris	Upper slope	0.05, 0.30, 0.60, 0.90
S28	1418	Blocky debris	Lower slope	0.10, 0.30, 0.65, 0.90
S29	1043	Bedrock	Outcrop	0.17, 0.67, 0.95

cairns (Figure 1, lower right panel). TinyTag-loggers with a precision of 0.2°C were used to record data at 1 h intervals.

Information on snow depth was acquired by attaching MTDs to sticks standing above the ground surface. Snow coverage of the MTDs was determined by a damped temperature signal. The MTDs were mounted at 0.1 m, 0.3 m and 0.7 m. In this way, it could be determined if and when the snow depth at the stick exceeded these levels. As the snow depth increases, the snow is assumed to cover increasingly larger fractions of the heterogeneous surface of the block fields.

The two profiles from Elg hogna were located 35 m apart in the lower part of the permafrost transition zone according to Heggem *et al.* (2005) (Figure 1). Geoelectrical resistivity soundings at the site have suggested permafrost lenses at depth that are not in equilibrium with the present climate (unpublished field data). One of the temperature profiles was located in the lower end of an openwork block slope (E12) and the other in nearby vegetated till (E8), permitting quantification of a potential thermal anomaly in the blocky debris. Winter snow depth was thick ($>1\text{ m}$) at both sites. The blocky debris fined downwards, and typical clast-sizes were 10–25 cm at the surface and 3–5 cm at 1 m depth. The base of the blocky debris was not reached, due to the difficulties of digging in such materials. To identify possible pore air advection in the block slope, one MTD (E14) was installed in the upper end of the block slope (1335 m a.s.l., at 0.2 m depth) (Figure 1). The block slope is approximately 40 m long and has a gradient of $16\text{--}20^{\circ}$.

Two of the profiles on S len (S27 and S28) were installed in a block field, two were installed in till (S25 and S26) and one was drilled in bedrock (S29) (Figure 1 and Table 1). The two profiles in the block field were located in the upper (S27) and lower end (S28) of a small slope at 1420 m a.s.l., about 10 m apart (Figure 1, lower right panel, see also Figure 10), so potential pore air advection along the slope could be identified. These sites are probably underlain by permafrost (Heggem *et al.*, 2005), but the permafrost table was not reached during installation of the MTDs. The sites were located on a wind-exposed ridge so a thick snow cover did not develop. Block diameters at S27 were a maximum of 30–40 cm at the surface and fined downwards to gravel size at 0.9 m depth. At S28 the blocks were larger, up to 50–60 cm at the surface and typically a few centimetres at the base of the blocky layer at 0.9 m depth. Thus the potential influence of clast size on pore air convection could be examined. At S28 the openwork blocky layer was

penetrated, and the 0.9 m MTD was located 2 cm within silty material.

The two profiles in till were located at 1070 m a.s.l., and less than 10 m apart. This was just below the predicted altitudinal limit of permafrost (Heggem *et al.*, 2005), and geoelectrical resistivity soundings suggested no permafrost at the site (unpublished field data). Site S25 was located on a wind-exposed ridge that experiences only sporadic snow cover in the winter, whereas S26 was located in an adjacent depression where wind-blown snow accumulates and forms a $>2\text{ m}$ thick cover by mid-winter. In addition to the MTDs mounted on a stick (only at S26), snow accumulation was monitored at S25 and S26 with daily automatic digital photography (see Christiansen, 2001).

The bedrock profile was drilled to 0.95 m at 1043 m a.s.l. The bedrock consisted of red sandstone belonging to the Rendalen Formation, Osen-R a Nappe Complex (Nystuen, 1982). Permafrost at this site is not probable (Heggem *et al.*, 2005), but no geophysical soundings have been performed here to test this. The profile was located on an outcrop that probably experienced only sporadic snow cover, but snow depth was not monitored.

RESULTS

Thermal Anomaly

Mean annual temperatures in block fields typical of the mountains of central-eastern Norway were indeed lower than in nearby till and bedrock (Figure 2). The difference was $1.3\text{--}2.0^{\circ}\text{C}$ on Elg hogna (Figure 2a) and $2.6\text{--}4.2^{\circ}\text{C}$ on S len (Figure 2b), although the last must partly be due to the 350 m elevation difference between the sites in blocky debris and those in till or bedrock (Table 1). Our data indicated no significant thermal offset, i.e. decreasing temperature with depth (e.g. Burn and Smith, 1988), in any of the materials.

Figure 3 shows the annual extreme temperature range for the same sites. On Elg hogna, a greater range was present in the blocky debris than in the till (Figure 3a). This wider temperature range mainly related to winter conditions (lower minimum values in the blocky debris). Maximum temperatures were higher in the blocky debris than in till down to the 0.56 m depth, but became lower at a depth of 1.0 m. Similarly, the maximum temperatures in the blocky debris on S len were significantly lower below 0.6 m compared with till and bedrock (Figure 3b). Minimum temperatures in blocky debris on S len were similar or lower than in bedrock and till. Thus, the thermal

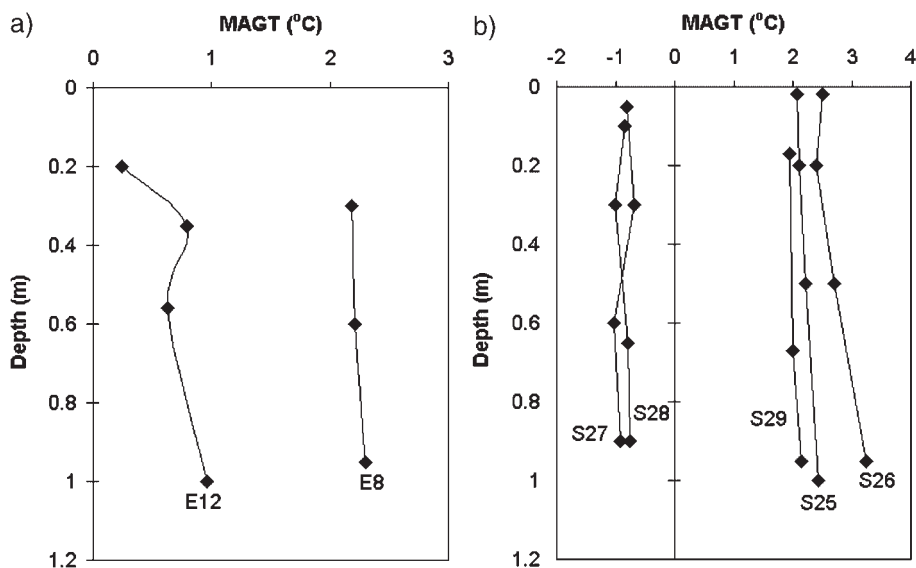


Figure 2 Mean annual ground temperatures July 2005 to June 2006 in (a) till (E8) and blocky debris (E12) on Elgåhogna, and (b) till (S25, S26), blocky debris (S27, S28) and bedrock (S29) on Sølen.

anomaly in the investigated blocky debris was related to both summer and winter conditions. Integrated over the year, the freezing degree-days (FDD) at 0.95–1.0 m depth on Elgåhogna totalled 142°C days in blocky debris (E12) and 17°C days in till (E8). Thawing degree-days (TDD) at the same depth totalled 496°C days (E12) and 857°C days (E8).

Based on previous studies on heat transfer in openwork blocky debris (e.g. Goering, 2002), the following hypothesis to explain the observed negative thermal anomaly in the block fields was explored:

The negative thermal anomaly in the blocky debris is due to efficient buoyancy-induced free

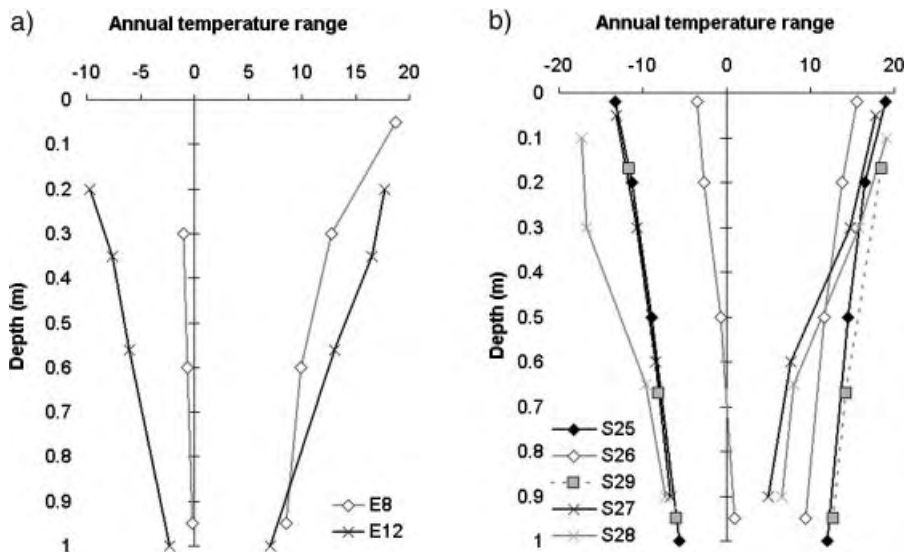


Figure 3 Annual extreme temperature range (daily values) July 2005 to June 2006 in (a) till (E8) and blocky debris (E12) on Elgåhogna, and (b) till (S25, S26), blocky debris (S27, S28) and bedrock (S29) on Sølen.

pore air convection operating in the winter when the pore air density gradients are unstable. In summer, pore air density gradients are stable and the slower process of thermal conduction is the primary mode of heat transfer.

The alternative hypothesis is that convection of the pore air is less efficient in winter, and heat transfer in the blocky debris is by conduction. Different thermal (effective thermal conductivity) and environmental properties (snow depth and coverage) of the blocky debris as compared with till and bedrock would then be required to explain the observed thermal anomaly.

Our observations and data are presented and discussed below in light of the proposed hypothesis, and its alternative.

Convection?

Elgåhogna.

Large, intricate networks of ice crystals were observed in the upper 0.3 m of the blocky debris at E12 on the 7 June 2006 (Figure 4). Such amounts of crystals probably take significant time to develop and thus suggest a steady supply of saturated air towards the developing crystal network, either by air convection or water vapour diffusion (Smith and Burn, 1987). Vigorous air convection would presumably destroy the delicate structure. Hence, if convection is operating,

the ice crystal network suggests slow, but stable convection.

Figure 5 shows daily air temperature (at 1 m height) and ground temperatures at four levels in the lower end of the block slope (E12) and at three levels (a fourth sensor at 0.05 m malfunctioned) in nearby till (E8) on Elgåhogna for the period 13 August 2004 to 23 July 2006. The sensors at 0.60 m and 0.95 m in till malfunctioned until 30 June 2005. Temperature gradients from 0.35 m to 1.00 m in the blocky debris (E12) and from 0.30 m to 0.95 m in till (E8) are also shown, together with the estimated Rayleigh number in the blocky debris (E12).

The difference in winter conditions between till and blocky debris indicated in Figure 3a is apparent. The temperature in the till remained at or just below 0°C through both winters, even in the autumn when snow was thinner than 0.3 m. This can be attributed to the combined effect of the insulating snow and vegetation, and to the soil moisture content being higher than in the highly permeable blocky debris. The temperature in the blocky debris showed considerable fluctuations in accordance with the air temperature until January the first winter and February the second winter before stabilising (−4 to −5°C at 0.2 m depth). At that time, snow cover at the snow monitoring stick was at least 0.7 m thick, and the nearby air temperature sensor at 1 m height was covered with snow. Thus, whereas 0.3 m deep snow is able to insulate the underlying ground at the till site, a thicker snow cover is required



Figure 4 Network of ice crystals on the bottom side of a block (turned upside down) in the blocky debris at E12. Such crystals were observed filling up the pore volume of the upper 30 cm of the blocky debris. Ruler for scale (cm). The photograph was taken on 7 June 2006.

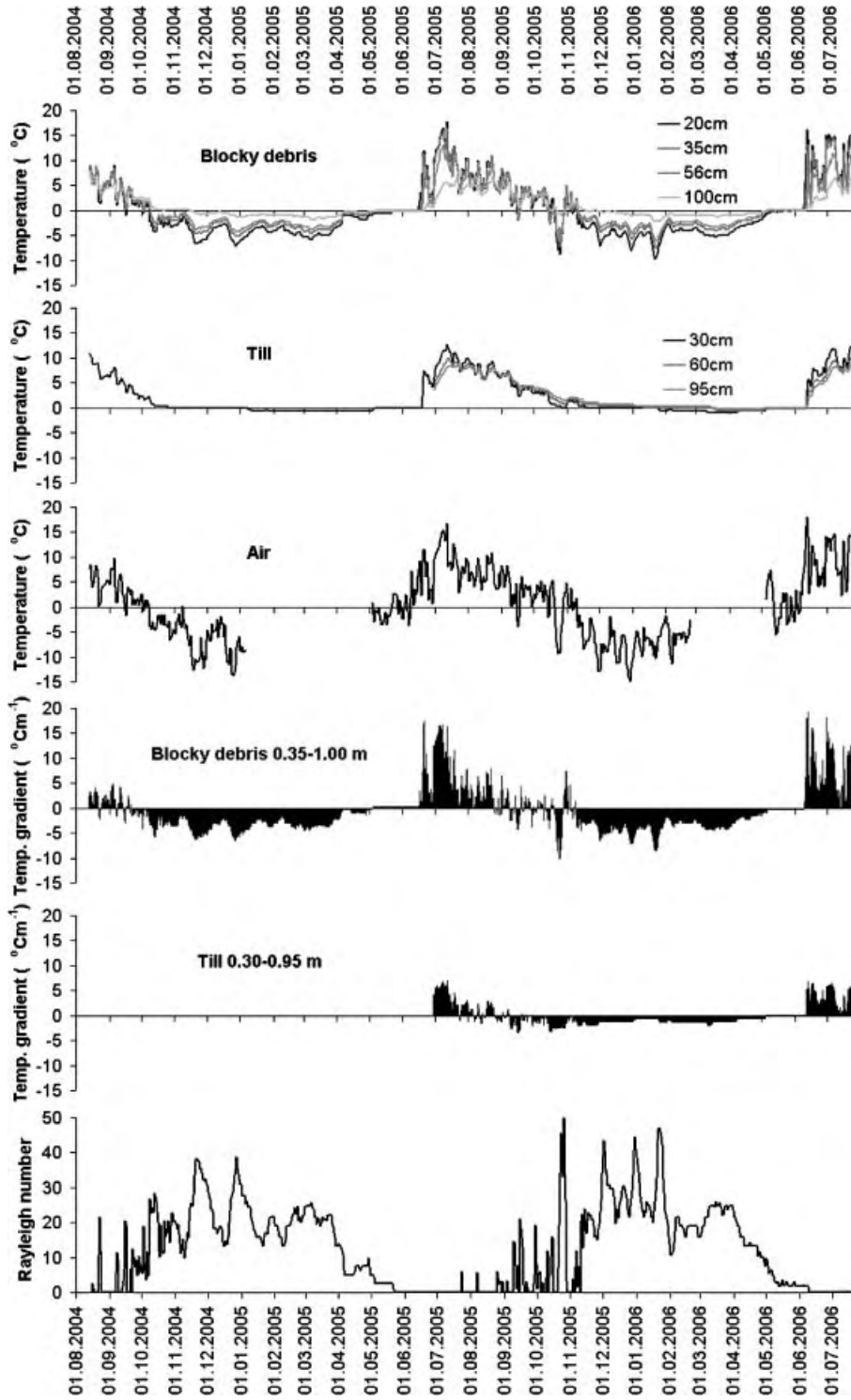


Figure 5 Temperatures and temperature gradients in blocky debris (E12) and till (E8) on Elgähogna for the period August 2004 to July 2006. Air temperature at the site and Rayleigh number at E12 are also given. Two of the three miniature temperature dataloggers at E8 malfunctioned until June 2005. Air temperature is omitted for periods when the air temperature sensor was snow-covered.

to insulate the ground at the blocky debris site, probably because only thick snow entirely covers the blocky debris. The site was visited on 5 March 2005 and 16 March 2006, and no visible connections in the form of funnels through the snow or snow-free blocky ground, in which efficient heat exchange could occur, were observed. Snow depths on these dates were 1.4–1.7 m and 0.9–1.7 m, respectively, with the highest values on the blocky debris.

The insulating effect of the snow above the till led to low winter temperature gradients (typically -0.6 to $-2.5^{\circ}\text{C m}^{-1}$). Winter temperature gradients in the blocky debris were more variable and in the range of -10 to 0°C m^{-1} .

Unstable air stratification and potential free convection as indicated by the Rayleigh number were clearly controlled by low ambient air temperature. The Rayleigh number exceeded the critical value on four to eight occasions, depending on the boundary conditions used, indicating a potential for convection in the blocky debris at these times.

Visual inspection of the temperature curves (at 1 h resolution) was also undertaken to identify possible convection events. Convection or advection was inferred when the temperature changed more rapidly at depth than close to the surface or when the temperature change at depth was the opposite of that close to the surface (see below, Figure 9). No convection events were identified at E12. However, advection along the block slope (the chimney effect) could possibly explain an observed temperature increase at the upper end (E14) in the two first weeks

of March 2006, when the air temperature remained low and ground temperatures at the lower end (E12) actually decreased (Figure 6). Snow temperature data indicate that the decrease in temperature at the lower end was due to conduction through snow and not accumulation of advected cold air. However, the increase in temperature at the upper end may indicate advection in certain parts of the slope. No other occurrences of possible pore air advection along the slope were inferred.

In summer, the pore air density stratification in the blocky debris was stable and convection could not occur (Figure 5). Heat transfer was thus primarily by conduction. Although temperatures in the upper 0.5 m of the blocky debris frequently were higher than in till, the temperature at 1.0 m depth was always lower than at 0.95 m in till (see also Figure 3a). As a result, the summer temperature gradient was up to three times higher in blocky debris, indicating a low effective thermal conductivity and a high thermal resistance.

Sølen.

Daily temperatures at four levels in the blocky debris (S27 and S28) and at 1 m height in the air, and temperature gradients and estimated Rayleigh numbers in the blocky debris for the period 7 July 2004 to 25 August 2006 are shown in Figure 7. Figure 8 gives daily ground temperatures and temperature gradients in till (S25 and S26) and bedrock (S29) on Sølen for the same period.

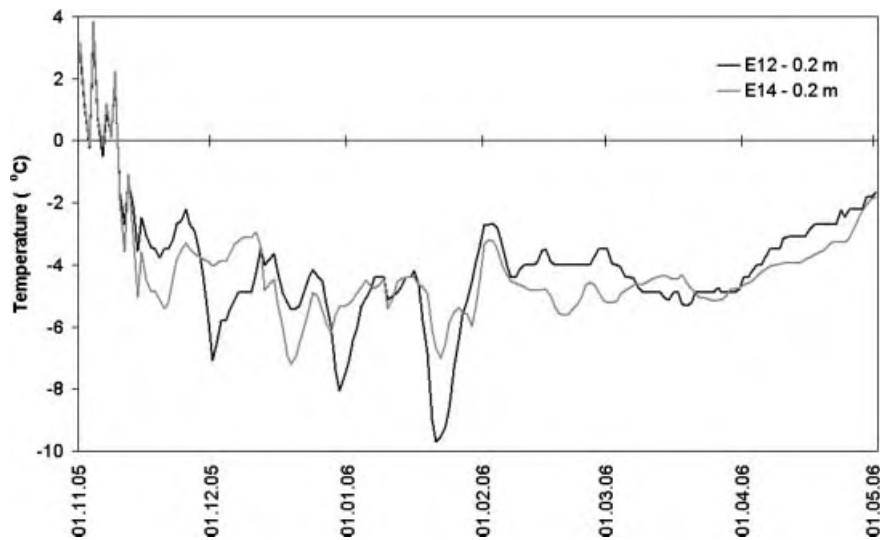


Figure 6 Daily average temperature at 0.2 m depth in the lower (E12) and upper end (E14) of the block slope on Elgåhogna for the period November 2005 to May 2006.

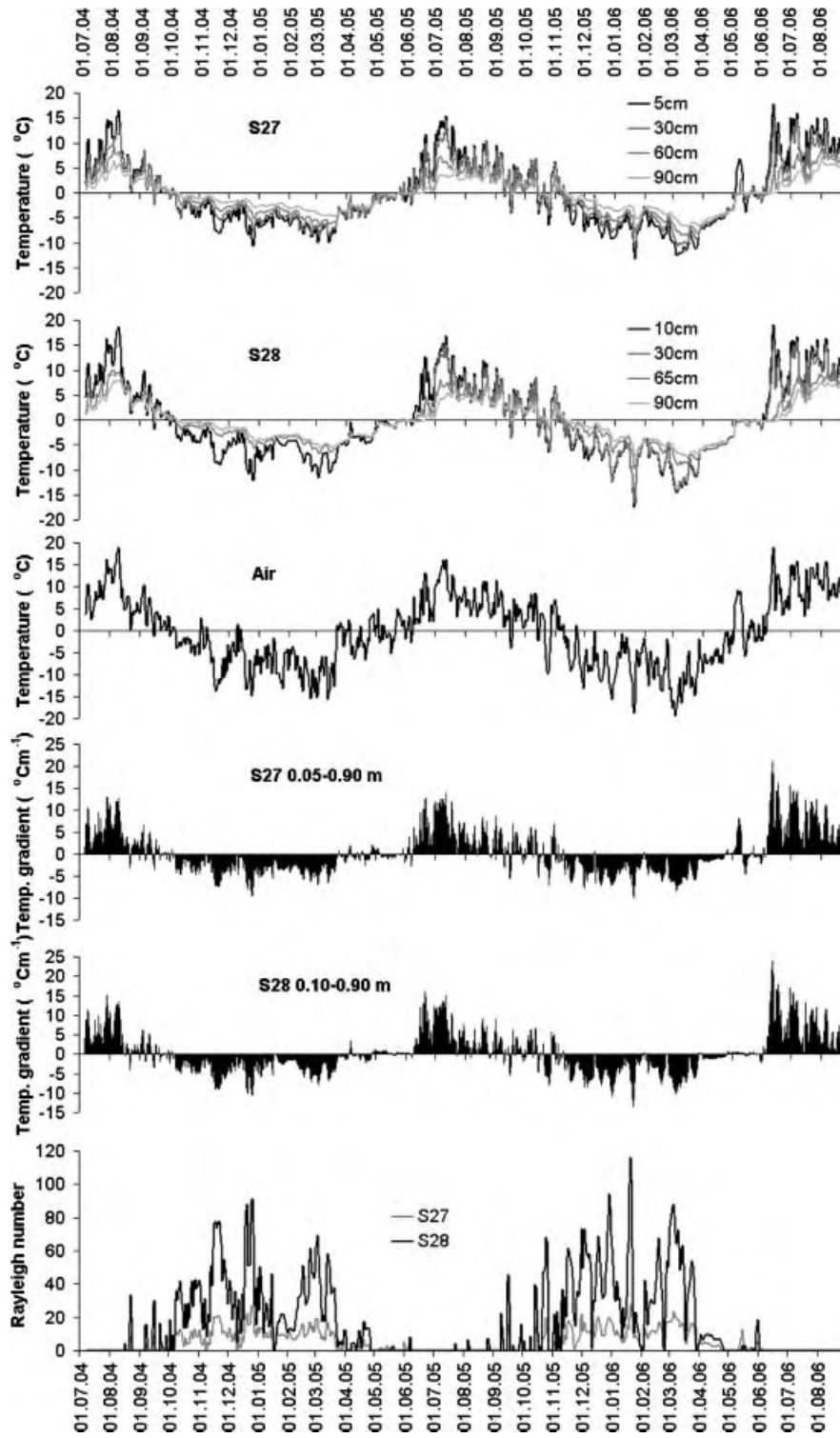


Figure 7 Temperatures, temperature gradients and Rayleigh number in blocky debris (S27 and S28), and air temperature, on Sølen for the period July 2004 to August 2006. The miniature temperature datalogger at the 0.30 m level malfunctioned until June 2005.

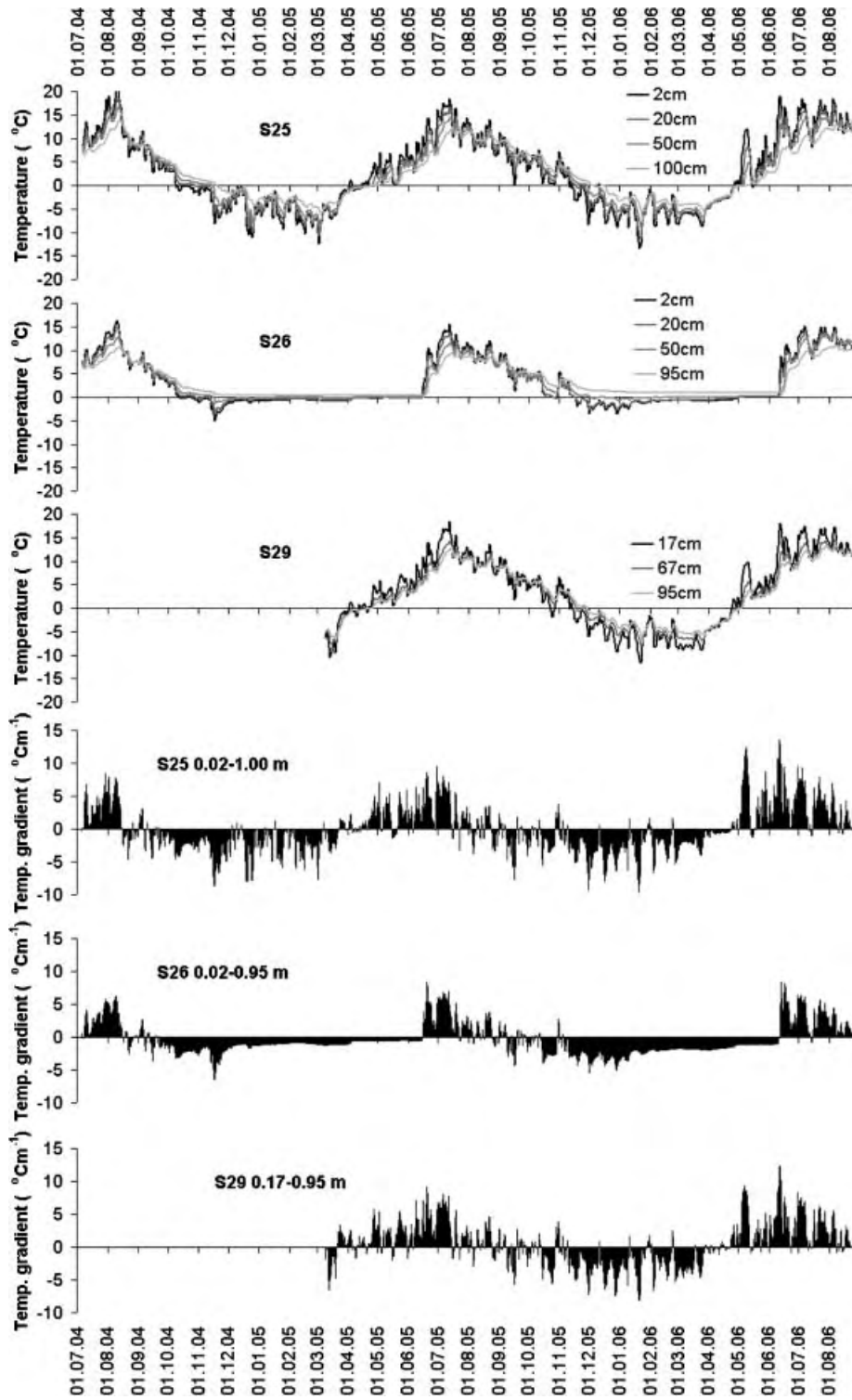


Figure 8 Temperatures and temperature gradients in till (S25 and S26) and bedrock (S29) on Sølén for the period July 2004 to August 2006. Temperature monitoring at S29 started in March 2005.

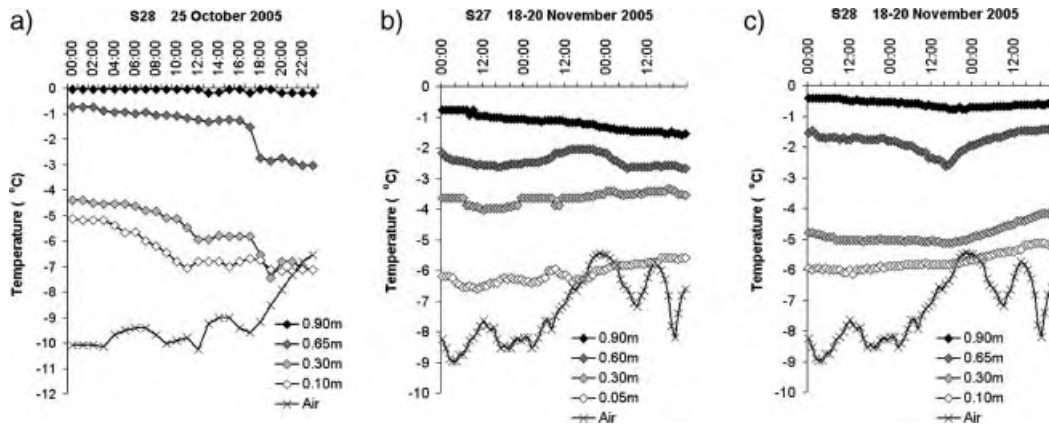


Figure 9 Convection and advection events revealed by visual inspection of the temperature curves. (a) 25 October 2005 at S28. (b) 18–20 November 2005 at S27. (c) 18–20 November 2005 at S28.

Temperatures in the blocky debris (Figure 7) varied in tandem with air temperatures throughout the winter, indicating an efficient heat exchange with the atmosphere. The snow depth at the stick at S28 was between 0.3 m and 0.7 m from mid-January to late May 2005 and late March to early May 2006. The snow depth at S27 (no measurements) was presumably somewhat lower as this site was more exposed to wind. Field observations on 9 March 2005 and 14 March 2006 showed 25–50 cm thick snow on the first visit and 5–20 cm on the second. In both years, the snow

cover was discontinuous and individual boulders protruded through the snow surface. Temperatures in the blocky debris varied somewhat less beneath the snow cover, but unlike the Elgåhogna site (E12), stable values never developed. The steepest winter temperature gradients in the blocky debris were $-9.9^{\circ}\text{C m}^{-1}$ at S27 and $-13.3^{\circ}\text{C m}^{-1}$ at S28.

Winter temperatures in till and bedrock also varied with the air temperature where the snow was thin or sporadic (S25 and S29) (Figure 8). Winter temperature gradients at these sites were similar to or less steep



Figure 10 Typical winter situation at the sites in blocky debris on Sølén. S27 was located at the upper end of the slope, and the location of S28 below the snow is marked with the stick. The cairn in which air temperature was measured is in the foreground. The photograph was taken on 9 March 2005.

than those in the blocky debris (median values: S25, $-2.0^{\circ}\text{C m}^{-1}$; S27, $-3.0^{\circ}\text{C m}^{-1}$; S28, $-3.3^{\circ}\text{C m}^{-1}$; S29, $-2.3^{\circ}\text{C m}^{-1}$), indicating equally efficient or even more efficient heat transfer in till and bedrock compared with blocky debris in winter. Since heat transfer in till and bedrock is governed mainly by conduction, the stronger temperature gradients in blocky debris also suggest heat transfer predominantly by conduction, with a lower effective thermal conductivity than for bedrock and till.

At S26, a thick snow cover developed in December of the first winter and in January during the second. Before the development of the thick snow cover, ground temperatures fluctuated with the air temperature. Once a thick snow cover had developed, ground temperatures stabilised at -1 to 1°C . The ground did not freeze at the 0.95 m depth. The thick snow allowed only low temperature gradients to develop.

The Rayleigh number in blocky debris at S27, with the lower permeability, never exceeded the critical value (Figure 7), suggesting heat transfer primarily by conduction. Keeping in mind that the estimate of the Rayleigh number was conservative, however, free convection cannot be excluded. Also, free convection may be induced at lower Rayleigh numbers in sloping terrain (Goering, 2002). On the other hand, at S28 with the higher permeability, the Rayleigh number was frequently above the critical value (Figure 7), indicating a potential for heat transfer by free convection.

Visual inspection of the temperature curves revealed several obvious convection events (Figure 9). These events were not identified for all periods through the winter with a high Rayleigh number, but occurred for some situations early in the season. On 25 October 2005, a convection event was identified at S28 by a temperature decrease of more than 1°C at the 0.30 m and 0.65 m levels when temperature change was small or non-existent at the 0.10 m and 0.90 m levels (Figure 9a). This temperature decrease must have been due to an internal convection process. As the event occurred at sub-zero temperatures, convection by water is not likely. Further, since the temperature decrease at the 0.10 m level was slight compared with that at the 0.30 m and 0.65 m levels, wind-forced convection is unlikely, and therefore free pore air convection appears to be the most probable process. The estimated Rayleigh number was between 69 and 96. The event shown in Figure 9a was also identified at S27 on the same date, but at a different time of the day. Identification of the convection events at both S27 and S28 indicates that clast size was not a limiting factor.

On 19 November 2005, the temperature at 0.60 m depth at the upper end of the slope (S27) temporarily increased by *c.* 0.5°C (Figure 9b) while that at 0.65 m

depth at the lower end (S28) decreased by *c.* 0.9°C (Figure 9c). Temperatures at the other depths were unaffected. The event lasted for about 24 h. and may be an example of advection of pore air (chimney effect), operating at *c.* 0.60 m depth within the blocky slope. The slope was covered by a thin, discontinuous layer of snow at the time, and the temperature difference (at 0.60 m to 0.65 m depth) between S27 and S28 at the onset of the possible advection event was 0.8 to 0.9°C .

In summer, the pore air density stratification in the blocky debris was stable and no free convection could occur (Figure 7). Summer heat transfer was thus dominated by conduction, as at Elgåhögna. Summer temperatures at depth in the blocky debris (S27 and S28) were lower than in till (S25 and S26) and bedrock (S29), resulting in higher temperature gradients in the blocky debris (Figures 7 and 8), particularly during the warmest periods (10 – $25^{\circ}\text{C m}^{-1}$). Thus, the blocky debris provided a high thermal resistance in summer, protecting the underlying permafrost.

In summary, the hypothesis concerning air convection in the pore volume of the blocky debris as the process responsible for the temperature anomaly can be rejected. Although there is potential for convection in at least two of the sites, there is little evidence of convection as the main operating process. The alternative hypothesis in which different thermal (effective thermal conductivity) and environmental (effect of snow) properties of blocky debris compared with till and bedrock are responsible for the negative thermal anomaly, seems more appropriate. The effect of snow on the thermal regime in the different materials is discussed further below.

Coupling to Air Temperature

Good thermal coupling to the air temperature is characteristic of the block field sites. Table 2 lists the mean annual air temperature, the mean annual temperatures for the uppermost MTD in the ground (see Table 1 for depth), and the difference between them, termed the surface offset (Smith and Riseborough, 1996). Surface offset in blocky debris was much less than that in till, indicating more efficient heat exchange between the atmosphere and the ground. It follows that in blocky debris the insulating effect of snow is effectively reduced, enabling efficient winter cooling of the substrate.

The close coupling between the atmosphere and the blocky debris is probably due to conduction through boulders protruding into and through the snow cover (Figure 10). Since the boulders have a much higher

Table 2 Mean annual temperature at the uppermost miniature temperature datalogger in the ground (MAGT) and in the air (MAAT), and the difference between them (surface offset).

Site	MAGT	MAAT	Surface offset
E8	2.2	-0.8	3.0
E12	0.2	-0.8	1.0
S25	2.1	0.9	1.2
S26	2.5	0.9	1.6
S27	-0.8	-1.1	0.3
S28	-0.9	-1.1	0.2
S29	1.9	0.9	1.0

thermal conductivity than the snow, they provide bridges for efficient heat transfer through the snow.

The Effect of Wind

Wind-forced convection in the blocky debris is a possibility for exposed sites such as those examined here. Tables 3 and 4 give median winter and summer temperature gradients, respectively, for each depth interval at all sites. In blocky debris, with the exception of E12 in winter, the steepest gradient and thus the highest thermal resistance occurred at mid-depth (0.3–0.6 m), suggesting a more effective heat transfer near the surface than at depth. This was in contrast to sites in bedrock or till. The reason for this may be wind-forced convection within the near-surface blocky layer. Also, the accumulation of ice between the blocks in winter may increase the effective thermal conductivity, resulting in more efficient heat transfer by conduction. Site E12 was covered by thick snow and consequently the wind could not have affected the heat transfer there (Table 3). In the bottom part of the measured profiles, temperature gradients decreased, possibly due to a

Table 3 Median winter temperature gradients through the substrate ($^{\circ}\text{C m}^{-1}$).

Site	Upper part ^a	Middle part ^a	Bottom part ^a
E8	NA	-1.7	-1.1
E12	-5.1	-2.4	-3.4
S25	-3.5	-2.1	-2.0
S26	-1.0	-1.3	-1.6
S27	-2.6	-3.2	-2.8
S28	-1.4	-4.5	-2.5
S29	NA	-2.3	-2.5

^aSee Table 1 for sensor depths.
NA = not available.

Table 4 Median summer temperature gradients through the substrate ($^{\circ}\text{C/m}$).

Site	Upper part ^a	Middle part ^a	Bottom part ^a
E8	NA	4.0	1.3
E12	3.7	4.0	3.1
S25	4.8	2.4	2.8
S26	2.5	2.7	3.1
S27	2.3	4.7	3.8
S28	1.6	6.1	2.8
S29	NA	2.4	2.0

^aSee Table 1 for sensor depths.
NA = not available.

higher effective thermal conductivity caused by increased contact area between individual clasts as the grading fines with depth (Farouki, 1981) and/or higher moisture contents.

In order to investigate wind-forced convection further, hourly temperature gradients in the blocky debris at S27 and S28 were plotted against wind speed measured at 2 m height at S29 (Figure 1) for the period 30 June 2005 to 30 September 2005 (Figure 11). This is the only period when local wind data are available. At S27, the temperature gradient from 0.05 m to 0.30 m plotted around zero when wind speed was high (Figure 11a, left panel), suggesting efficient heat transfer by wind. The critical wind speed seemed to be between 5 and 10 m s^{-1} . The temperature gradient from 0.30 m to 0.60 m, on the other hand, was generally positive when wind speed was high (Figure 11a, right panel), indicating heat conduction into the ground along the temperature gradient. Thus, wind-forced convection at S27 probably did not extend down to 0.60 m depth. At S28, the temperature gradient from 0.10 m to 0.30 m showed a larger spread than at S27 when wind speeds were high (Figure 11b, left panel), suggesting that wind-forced convection was less effective here. It follows that wind-forced convection was not important at depth either (Figure 11b, right panel). The efficiency of wind-forced convection at S27 compared with S28, located only a few metres apart, can be explained in terms of their respective exposed and sheltered topographic positions.

The effect of wind-forced convection can also be highlighted by estimating the apparent thermal diffusivity from the temperature data. The thermal diffusivity was estimated from the 0.1 m to 0.3 m levels, 0.3 m to 0.6 m levels and 0.6 m to 0.9 m levels using the classic amplitude method. This method assumes a sinusoidal temperature pattern and no phase

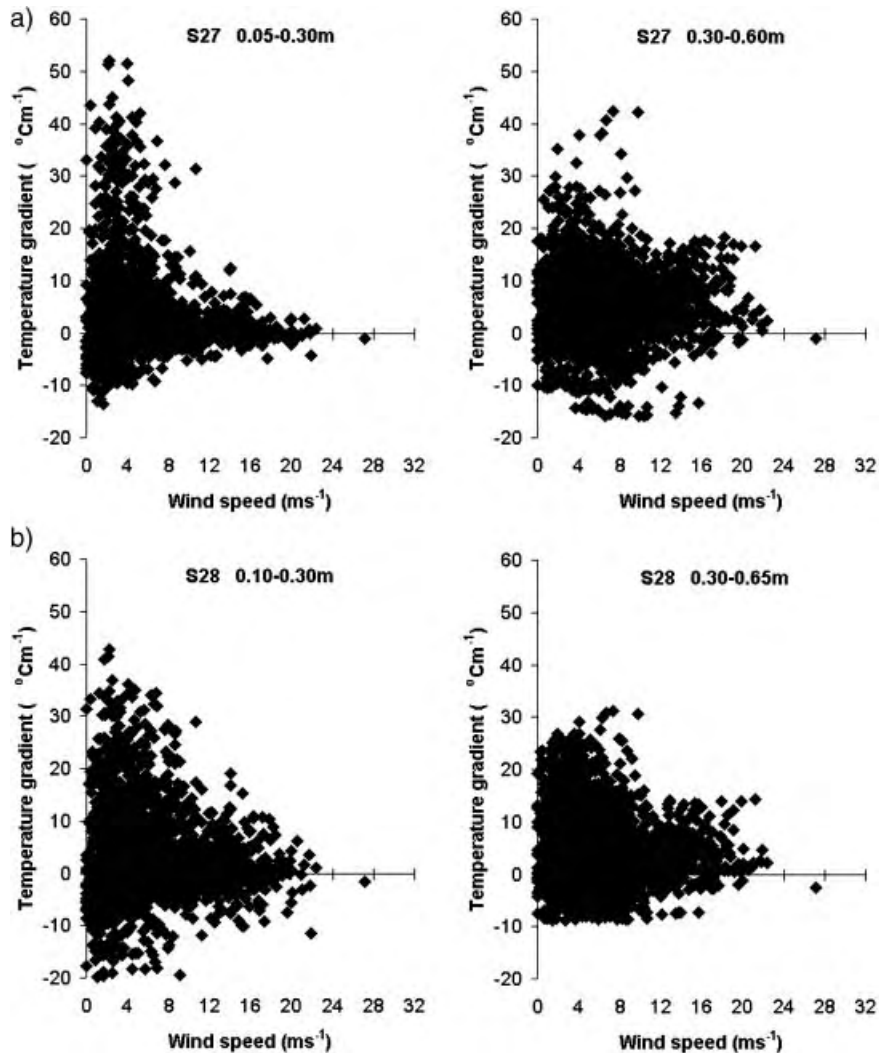


Figure 11 (a) Wind speed (measured at S29) plotted against the temperature gradient 0.05–0.30 m (left panel) and 0.30–0.60 m (right panel) at S27 for the period 30 June to 30 September 2005. (b) Wind speed (measured at S29) plotted against the temperature gradient 0.10–0.30 m (left panel) and 0.30–0.65 m (right panel) at S28 for the period 30 June to 30 September 2005.

change, so only a limited number of days were suitable for analysis. Figure 12 shows the apparent thermal diffusivities for the period 29 June to 10 July 2005, together with wind speed measured at S29. At S27, the apparent diffusivity was typically $0.5\text{--}2.0 \times 10^{-5} \text{ m}^2 \text{ s}^{-1}$ at all depths (Figure 12a). This is the diffusivity related to conduction in the blocky debris. On 2 July, however, a peak in diffusivity of $7 \times 10^{-5} \text{ m}^2 \text{ s}^{-1}$ in the upper part was clearly too high to be due to conduction alone. This corresponded to a day with 5 m s^{-1} winds blowing towards the slope and we believe that the high rate of heat transfer in the upper 0.3 m was due to wind-forced convection. Stronger winds on the following days did not produce similar

effects, but a change in wind direction meant that the slope was then in the lee of the winds. At S28, which was located in the lower end of the slope and was less exposed to wind, there were no major peaks in the diffusivity and the values of $0.5\text{--}2.4 \times 10^{-5} \text{ m}^2 \text{ s}^{-1}$ probably reflected heat transfer by conduction at all depths in the blocky debris (Figure 12b).

DISCUSSION

Our results show negative temperature anomalies in the investigated blocky debris of $1.3\text{--}2.0^\circ\text{C}$, values that are less than those reported previously

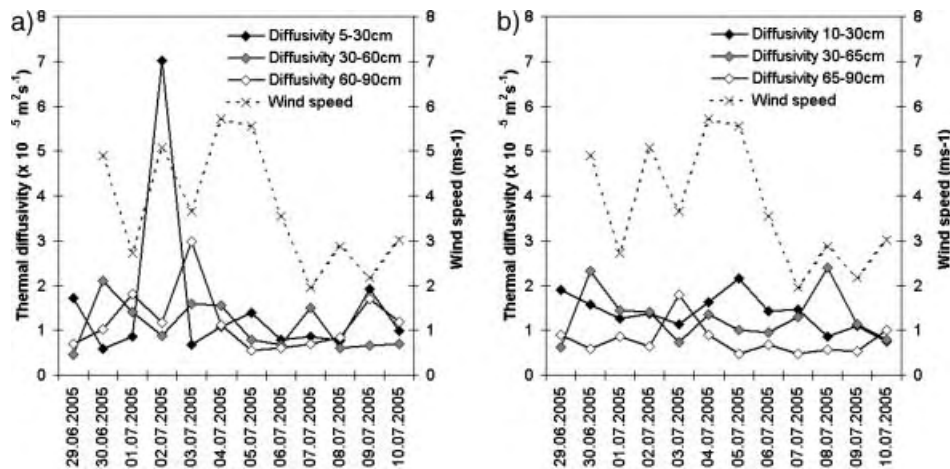


Figure 12 Apparent thermal diffusivity and wind speed (measured at S29) for the period 29 June to 10 July 2005 at (a) S27 and (b) S28.

(e.g. the 4–7°C difference of Harris and Pedersen, 1998). Our sampling strategy was to cover typical situations with different topographical situations and different snow depths. Thus, we believe that our data reflect the characteristic thermal regimes of openwork block fields (felsenmeer) in the mountains of central-eastern Norway and conclude that as a geomorphological unit, block fields provide a negative temperature anomaly that is favourable for permafrost. It is therefore important to include their thermal effects in permafrost distribution modelling (Etzelmüller *et al.*, 2001; Hoelzle *et al.*, 2001). However, this study represents only two years of data from three locations in blocky debris, so further work is required to evaluate the spatial and temporal variation of the thermal anomaly in block fields. The magnitude of the anomaly suggests that permafrost may be present in blocky debris at elevations several hundred metres lower than in bedrock and till.

Convection in the pore volume appears to have been less important than initially presumed and we had to reject our hypothesis of convection as the process responsible for the temperature anomaly. More subtle convection was suggested by the observed large network of ice crystals (Figure 4), but could not be validated with the present approach. Methodological refinement with, for example, wind sensors (M. Oswald, personal communication) and higher precision temperature sensors would be required to gain more information on this. The existence of funnels through the snow cover (Heggem *et al.*, 2005) indicated localised convection in the blocky debris (Keller and Gubler, 1993; Bernhard *et al.*, 1998), but the thermal effect of these may have been restricted to the surface layer.

Instead of convection, we suggest that the negative thermal anomalies are caused primarily by a significantly higher effective thermal conductivity of the snow cover above block fields, caused by rocks protruding into and through the snow cover (the alternative hypothesis). Further, accumulation of ice in the pore volume of the blocky debris in the winter demonstrated by visual observations near the surface, and a zero curtain of up to one month in spring (Figure 7), must have increased the effective thermal conductivity of the blocky layer in the winter compared with the summer. This is the traditional explanation for thermal offsets in fine-grained materials (Goodrich, 1978; Burn and Smith, 1988). Another important factor is the soil moisture content, which probably is higher in the till than in the highly permeable blocky debris, reducing ground freezing in till by liberating latent heat.

An important question is why only a few of the situations identified by the Rayleigh number actually showed signs of convection. Conservative values of the Rayleigh numbers were used, so inaccurate estimation of these should have had limited effect on the interpretation. The probable answer lies again in the accumulation of ice in the pore volume in the winter, which would have reduced the permeability of the material. The observed convection and advection events (Figure 9) occurred in autumn, probably before most of the ice had formed.

Although convection may be of limited importance for the overall thermal regime of the block fields, a few events were observed. Free convection events occurred on the same date, but at different times of the day (see Figure 9a), suggesting that the ambient air temperature is the main, external forcing factor and that local factors

trigger the process. Both convection and advection events were identified at the same sites, but at different times. The advection event on Sølén occurred when the temperature at S27 at the upper end of the slope was lower than at S28 at the lower end of the slope, facilitating buoyancy-driven free convection parallel to the slope. The temperature distribution in the slope, being responsible for the density-differences, is itself controlled by external factors such as air temperature and snow distribution along the slope. It is interesting to note that the advection event occurred on a much smaller scale than previously reported (e.g. Delaloye *et al.*, 2003; Gude *et al.*, 2003) over horizontal and vertical distances of about 10 m and not more than 3 m, respectively (Figure 1).

In summer, the low effective thermal conductivity of the air–rock mixture provides a high thermal resistance protecting the lower temperatures in the subsurface. Wind-forced convection may be effective in transporting summer heat into the blocky debris at exposed sites, but probably to not much deeper than 30 cm. Wind-forced convection is therefore less effective here than reported from a wind-exposed rock glacier in Greenland by Humlum (1997), where wind pumped through the entire active layer of 175 cm. The ground surface roughness length may control the depth of wind action (Kane *et al.*, 2001). Since wind-forced convection was more important at S27, with a lower permeability than at S28 with a higher permeability, it can be concluded that clast size was not the limiting factor for wind-forced convection, but rather exposure to winds. This is in agreement with laboratory tests (Zhang *et al.*, 2006).

The hypothesis of summer evaporation and sublimation of water and ice in the pore volume cooling the blocky debris (Harris and Pedersen, 1998), could not be addressed as humidity gradients in the pore air were not measured. A qualitative guess is that this process may locally be important at the study sites. Excavations in blocky debris revealed surfaces that were usually dry down to a few decimetres depth, but were always wet at depth, suggesting that evaporation is restricted to the surface layer. However, our temperature data showed that the low summer temperatures in the blocky debris occurred below 0.6 m and not near the surface, suggesting that summer evaporation had limited importance on the deeper thermal regime.

CONCLUSIONS

Based on two years of thermal monitoring in blocky debris, till and bedrock in the mountains of

central-eastern Norway, the following conclusions could be drawn.

- Block field sites produce a negative temperature anomaly of 1.3–2.0°C.
- The temperature anomaly was largely a result of enhanced heat transfer by conduction through the winter snow cover, due to blocks protruding into and through the snow. An increase in effective thermal conductivity of the blocky layer in the winter due to accumulation of ice in the pore volume may also have contributed. Convection in the blocky debris was less important than initially presumed.
- In the summer, the high thermal resistance of the blocky debris helped maintain low temperatures at depth. Wind-forced convection may have been important, but only in the uppermost 0.3–0.6 m at exposed sites.
- Reduced permeability of the blocky debris in winter by accumulation of ice must be taken into account when using the Rayleigh number to characterise convection in a field situation.
- More sophisticated instrumentation is needed to fully evaluate the significance of convection on the temperature regime in the block fields on Elgåhogna and Sølén.

ACKNOWLEDGEMENTS

The installation of the miniature temperature dataloggers was assisted by J. Fjellanger, E.S.F. Heggem, M. Avian and M. Nutz. Assistance during geophysical field campaigns was given by H. Farbrot, M. Bagge-Lund and A. Kellerer-Pirklbauer. Comments given by two anonymous reviewers and editor Professor A. Lewkowicz improved the manuscript significantly.

REFERENCES

- Balch ES. 1900. *Glacières or Freezing Caverns*. Allen, Lane and Scott: Philadelphia; 337 pp.
- Bernhard L, Sutter F, Haerberli W, Keller F. 1998. Processes of snow/permafrost-interactions at a high-mountain site, Murtel/Corvatsch, eastern Swiss Alps. *Seventh International Conference on Permafrost (Yellowknife, Canada)*. Collection Nordicana: 35–41.
- Burn CR, Smith CAS. 1988. Observation of the ‘thermal offset’ in near-surface mean annual ground temperatures at several sites near Mayo, Yukon Territory, Canada. *Arctic* **41**: 99–104.

- Christiansen HH. 2001. Snow-cover depth, distribution and duration data from northeast Greenland obtained by continuous automatic digital photography. *Annals of Glaciology* **32**: 102–108.
- Delaloye R, Lambiel C. 2005. Evidence of winter ascending air circulation throughout talus slopes and rock glaciers situated in the lower belt of alpine discontinuous permafrost (Swiss Alps). *Norsk Geografisk Tidsskrift* **59**: 194–203. DOI 10.1080/00291950510020673
- Delaloye R, Reynard E, Lambiel C, Maescot L, Monnet R. 2003. Thermal anomaly in a cold scree slope (Creux du Van, Switzerland). *Eighth International Conference on Permafrost (Zürich)*. A.A. Balkema: Rotterdam; 175–180.
- Etzel Müller B, Hoelzle M, Heggem ESF, *et al.* 2001. Mapping and modelling the occurrence and distribution of mountain permafrost. *Norsk Geografisk Tidsskrift* **55**: 186–194.
- Fair GM, Hatch LP. 1933. Fundamental factors governing the streamline flow of water through sand. *Journal of the American Water Works Association* **25**: 1551–1565.
- Farouki OT. 1981. *Thermal Properties of Soils*. CRREL Monograph 81-1, US Army Cold Regions Research and Engineering Laboratory; Hanover, NH; 136 pp.
- Goering DJ. 2002. Convective cooling in open rock embankments. *11th International Conference on Cold Regions Engineering*, Anchorage, Alaska, 20–22 May; 629–644.
- Goodrich LE. 1978. Some results of a numerical study of ground thermal regimes. *Third International Conference on Permafrost*, Edmonton, Canada; 30–34.
- Gorbunov AP, Marchenko SS, Seversky EV. 2004. The thermal environment of blocky materials in the mountains of central Asia. *Permafrost and Periglacial Processes* **15**: 95–98. DOI: 10.1002/ppp.478
- Gude M, Dietrich S, Mäusbacher R, *et al.* 2003. Probable occurrence of sporadic permafrost in nonalpine scree slopes in central Europe. *Eighth International Conference on Permafrost (Zürich)*. A.A. Balkema: Rotterdam; 331–336.
- Haerberli W. 1973. Die Basis-Temperatur der winterlichen Schneedecke als möglicher Indikator für die Verbreitung von Permafrost in den Alpen. *Zeitschrift für Gletscherkunde und Glazialgeologie* **4**: 221–227.
- Hanson S, Hoelzle M. 2004. The thermal regime of the active layer at the Murtèl rock glacier based on data from 2002. *Permafrost and Periglacial Processes* **15**: 273–282.
- Hanson S, Hoelzle M. 2005. Installation of a shallow borehole network and monitoring of the ground thermal regime of a high alpine discontinuous permafrost environment, Eastern Swiss Alps. *Norsk Geografisk Tidsskrift* **59**: 84–93.
- Harris SA, Pedersen DE. 1998. Thermal regimes beneath coarse blocky materials. *Permafrost and Periglacial Processes* **9**: 107–120.
- Heggem ESF, Juliussen H, Etzel Müller B. 2005. Mountain permafrost in central-eastern Norway. *Norsk Geografisk Tidsskrift* **59**: 94–108. DOI: 10.1080/00291950510038377
- Hoelzle M, Haerberli W, Keller F. 1993. Application of BTS-measurements for modelling mountain permafrost distribution. *Sixth International Conference on Permafrost (Beijing)*. University of South China Technology Press: Guangzhou; 272–277.
- Hoelzle M, Wegmann M, Krummenacher B. 1999. Miniature temperature dataloggers for mapping and monitoring of permafrost in high mountain areas: first experience from the Swiss Alps. *Permafrost and Periglacial Processes* **10**: 113–124. DOI: 10.1002/(SICI)1099-1530(199904/06)10:2<113::AID-PPP317>3.0.CO;2-A
- Hoelzle M, Mittaz C, Etzel Müller B, Haerberli W. 2001. Surface energy fluxes and distribution models of permafrost in European mountain areas: An overview of current developments. *Permafrost and Periglacial Processes* **12**: 53–68. DOI: 10.1002/ppp.385
- Humlum O. 1997. Active layer thermal regime at three rock glaciers in Greenland. *Permafrost and Periglacial Processes* **8**: 383–408.
- Johansen O. 1975. *Thermal Conductivity of Soils*. Unpublished PhD thesis, Trondheim.
- Juliussen H. 2007. *Near-surface Ground Thermal Regime in Permafrost Areas of Norway and Svalbard: processes and geomorphic implications*. Unpublished PhD thesis, University of Oslo; 88 pp.
- Juliussen H, Humlum O. 2007. Preservation of block fields beneath Pleistocene ice sheets on Sølén and Elgåhognå, central-eastern Norway. *Zeitschrift für Geomorphologie. Supplementband* **51**(2): 113–138.
- Kane DL, Hinkel KM, Goering DJ, Hinzman LD, Outcalt SI. 2001. Non-conductive heat transfer associated with frozen soils. *Global and Planetary Change* **29**: 275–292.
- Keller F, Gubler H. 1993. Interaction between snow cover and high mountain permafrost, Murtel-Corvatsch, Swiss Alps. *Sixth International Conference on Permafrost (Beijing)*. University of South China Technology Press: Guangzhou; 332–337.
- Liestøl O. 1965. Local area with permafrost in the Gudbrandsdalen valley (Lokalt område med permafrost i Gudbrandsdalen). *Norwegian Polar Institute Yearbook* **1965**: 129–133.
- Nield DA, Bejan A. 1992. *Convection in Porous Media*. Springer: New York; 408 pp.
- Nystuen JP. 1982. Late Proterozoic basin evolution on the Baltoscandian craton: the Hedmark group, southern Norway. *NGU Bulletin* **67**. *Norges Geologiske Undersøkelse* **375**: 1–74.
- Sawada Y, Ishikawa M, Ono Y. 2003. Thermal regime of sporadic permafrost in a block slope on Mt. Nishinupukaushinupuri, Hokkaido Island, Northern Japan. *Geomorphology* **52**: 121–130.
- Serkitjij M, Hagentoft CE. 1998. The influence of natural convection on heat transfer in an air filled porous medium bounded by an air layer. *Nordic Journal of Building Physics* **1**: 1–24.

- Smith MW, Burn CR. 1987. Outward flux of vapour from frozen soils at Mayo, Yukon, Canada: results and interpretation. *Cold Regions Science and Technology* **13**: 143–152.
- Smith MW, Riseborough DW. 1996. Permafrost monitoring and detection of climate change. *Permafrost and Periglacial Processes* **7**: 301–309. DOI: 10.1002/(SICI)1099-1530(199610)7:4<301::AID-PPP231>3.0.CO;2-R
- Zacharda M, Gude M, Ruzicka V. 2007. Thermal regime of three low elevation scree slopes in central Europe. *Permafrost and Periglacial Processes* **18**: 301–308. DOI: 10.1002/ppp.598.
- Zhang M, Lai Y, Li S, Zhang S. 2006. Laboratory investigation on cooling effect of sloped crushed-rock revetment in permafrost regions. *Cold Regions Science and Technology* **46**: 27–35. DOI: 10.1016/j.coldregions.2006.06.003



The lacustrine sedimentary sequence in Syngneskardvatnet, western Norway: a continuous, high-resolution record of the Jostedalsbreen ice cap during the Holocene

Atle Nesje^{a,*}, Svein Olaf Dahl^b, Carin Andersson^a, John A. Matthews^c

^aDepartment of Geology, University of Bergen, Allégt. 41, N-5007 Bergen, Norway

^bDepartment of Geography, University of Bergen, Breiviksveien 40, N-5045 Bergen, Norway

^cHolocene Research Group Department of Geography, University of Wales at Swansea, Singleton Park, Swansea SA2 8PP, Wales, UK

Abstract

Two lacustrine sediment cores from Syngneskardvatnet, Sunndalen, confirm that at least the northern part of the Jostedalsbreen ice cap melted away during the Atlantic Chronozone between 6475 and 5300 ¹⁴C yr BP (7340 and 6150 cal. BP), possibly interrupted for short intervals of glacier activity around 6000 and 5800 ¹⁴C yr BP (6900 and 6700 cal. BP). Prior to this, periods of glacier expansion culminated at ca. 8500, 8400, 8200, 7750, 7600, and 7400 cal. BP. The 8400/8200 cal. BP advances are correlated with the widespread '8200 event' ('Finse event') recorded in Greenland ice cores, lacustrine and proglacial sites, and marine sediments. During the early part of the Holocene, periods of glacier contraction culminated at ca. 8450, 8300, 7900, 7500, and 6250 cal. BP, of which the last represents climatic optimum conditions (lowest supply of minerogenic sediments and/or highest organic production). The sedimentary record also shows that the ice cap has existed continuously since 5300 ¹⁴C yr BP (6150 cal. BP). Neoglaciation involved three main phases (1: 6150–4500 cal. BP, 2: 4500–2700 cal. BP, 3: 2700 cal. BP to the present) and a series of low-amplitude glacier advances which occurred at 6000, 5800–5700, 5600, 5500, 5200, 5100, 4900, 4800, 4700–4550, 4450, 4300, 4200, 4150, 4050, 4000, 3900, 3800, 3550, 3300, 2550, 2450, 2350, 2250, 2150, 2000, 1800, 1700, 1600, 1400, 1300, 1150, 1050, and the 1000 cal. BP (including "the Little Ice Age"). Loss-on-ignition analyses indicate, however, that episodes of less glacier activity occurred during the mid- and late Holocene at around 5900–5800, 5550, 5450–5300, 5050, 4850, 4750, 4500, 4400, 4100, 3950, 3700, 3450, 3100, 2650, 2500, 2400, 2300, 2200, 1850, 1700, 1550, 1350, 1250, 1050–1000 cal. BP, and during the twentieth century. Altogether, the lacustrine record from Syngneskardvatnet indicates that the Holocene has been interrupted by 41 periods of increased glacier activity (mean return period of ca. 150 years) and by 36 events of glacier contraction (mean return period of 210 years). Spectral analysis of the LOI data show peaks at periods of about 50, 85, 110, 250–285, 500, and 2000 calendar years. The mean time resolution in core Syngneskardvatnet-2 is ca. 20 yr cm⁻¹, while the mean sedimentation rate is 0.5 mm yr⁻¹. © 2000 Elsevier Science Ltd. All rights reserved.

1. Introduction

Holocene climate has traditionally been considered as relatively stable with none of the abrupt variations that characterised the Weichselian climate (e.g. Dansgaard et al., 1993). Recent terrestrial, marine, and ice-core data indicate, however, several rapid Holocene climate oscillations. These palaeoclimate records suggest that the Holocene was punctuated by millennial-scale cooling events (Karlén et al., 1995; O'Brien et al., 1995; Alley et al., 1997; Bond et al., 1997; Campbell et al., 1998 Bianchi and

McCave, 1999). Historical data indicate that the 'Little Ice Age' cooling was 1–2°C (e.g. Grove, 1988), while the early- to mid-Holocene climatic optimum experienced temperatures about 2°C higher than at present in Scandinavia (e.g. Nesje and Kvamme, 1991; Matthews and Karlén, 1992; Karlén, 1998), giving a Holocene temperature amplitude of 3–4°C. Thus, Holocene climate is now considered to have been more variable than previously thought, although the details and precise timing of the Holocene climatic variations are poorly understood (e.g. Nesje and Johannessen, 1992; Karlén and Kuylenstierna, 1996).

Holocene glacier and climate variations in southern Norway have been reconstructed using evidence from, among others, historical data (e.g. Grove, 1988),

* Corresponding author. Tel.: 0047-555-83502; fax: 0047-555-89417.

E-mail address: atle.nesje@geol.uib.no (A. Nesje).

lichenometry (e.g. Erikstad and Sollid, 1986; Bickerton and Matthews, 1993; Matthews, 1994), rock-surface weathering from Schmidt-hammer rebound values (e.g. Matthews and Shakesby, 1984; McCarroll, 1989a, b, 1994), palaeosols and palynology (e.g. Matthews and Dresser, 1983; Matthews and Caseldine, 1987a, b; Matthews, 1991), and stratigraphic evidence from proglacial sites characterised by glaciofluvial and glaciolacustrine sediments intercalated with gyttja and peat (e.g. Nesje and Dahl, 1991a, b; Karlén and Matthews, 1992; Matthews and Karlén, 1992; Dahl and Nesje, 1994, 1996). Due to extensive glaciers during the 'Little Ice Age', almost all terrestrial evidence from the period subsequent to the deglaciation was erased by Neoglacial activity in the vicinity of the present glaciers. However, records from continuous lacustrine sedimentary sequences in downstream glacial lakes are considered to produce reliable evidence about former glacier activity from variations in the minerogenic content (see below). However, lacustrine sedimentary records from steep, alpine regions are commonly complicated by such processes as floods, snow avalanches, debris flows and turbidity currents of non-glacial origin. Lacustrine sedimentary records therefore need to be carefully evaluated, taking into account both climatic factors and local geomorphological conditions (e.g. Nesje et al., 1991, 1995; Karlén and Matthews, 1992; Dahl and Nesje, 1996).

In this paper, we present lacustrine sediment studies from Sygneskardvatnet in, Sunndalen, draining the NW part of Jostedalsbreen (487 km²) (Fig. 1), the largest ice cap in mainland Europe. The results report a continuous, high-resolution record from this major ice cap since about 8000 ¹⁴C yr BP (9000 calendar yr BP). Particular attention is paid to: (a) testing the view that Jostedalsbreen melted away during the early Holocene (Nesje et al., 1991; Nesje and Kvamme, 1991); and (b) refining the history of short-term glacier variations during the Holocene.

2. Study site

In the upper part of Sunndalen, two lakes, named Øvre (upper) and Nedre (lower) Sygneskardvatnet (664 and 662 m a.s.l., respectively), receive meltwater from Sygneskardbreen, a minor outlet glacier at the NW part of Jostedalsbreen (Fig. 2 and 3). From the lower of the two lakes, hereafter called Sygneskardvatnet, two sediment cores were retrieved. The lake is located 3.3 km downstream from the glacier and approximately 2 km beyond the 'Little Ice Age' maximum position of Sygneskardbreen. The part of Jostedalsbreen which drains to the lake covers an area of 7 km² and is 4.7 km long with an altitudinal range of 570 m (1810–1240 m) (Østrem et al., 1988). The western valley side along the two lakes is steep and covered by avalanche deposits. Annual snow ava-

lanches are, however, only recorded along the southern (upper) lake (Fig. 3).

The present equilibrium-line altitude (ELA) has been calculated as 1570 m using an accumulation area ratio (AAR) of 0.6 (Fig. 4). Marginal moraines, and a significant change in vegetation cover at about 900 m, delimit the maximum 'Little Ice Age' position of Sygneskardbreen about 1.2 km beyond its present terminus (Fig. 2). At that time the glacier covered an area of 8.23 km² (18% larger than at present). The AAR approach gives a 'Little Ice Age' ELA of 1530 m, a lowering of 40 m compared to the modern ELA. This is 40 m less than the mean "Little Ice Age" ELA lowering of 80 m calculated for the outlet glaciers from Jostedalsbreen (Torsnes et al., 1993). An ice-marginal deposit at the outlet of Sygneskardvatnet (Fig. 3) most probably represents the Erdalen event moraine, dated at other sites around Jostedalsbreen at 9100 ± 200 ¹⁴C yr BP (Nesje and Kvamme, 1991; Nesje et al., 1991).

3. Methods

3.1. Lacustrine archives

One of the best archives of palaeoclimatic information in Scandinavia are lake sediments. Annual and decadal climatic shifts influence sediment production and deposition in the lakes. During the winter, lakes in the mountainous regions are normally frozen, strongly reducing the sediment input to the lakes. Terrigenous silts and clays, deposited in the lakes from upstream glaciers and surface runoff from rainfall and snow melt settle out of suspension throughout the summer. This seasonal alternation of depositional regimes may result in the annual production of laminae/varves. Commonly, lakes are characterised by continuous and relatively high sedimentation and thereby high time resolution. The sediments may, however, be disturbed by several factors, such as (a) river floods and mass movements (landslides, turbidites, avalanches or debris flow from adjacent valley sides), (b) erosion by currents or lake ice, (c) biological or physical mixing (bioturbation, resuspension), (d) diagenetic reactions combined with diffusional migration of soluble components, and (e) human activity in the lake catchment.

3.2. Lake coring

The coring equipment was flown to the lake by helicopter. Coring was carried out from lake ice during the spring of 1996. Two cores were retrieved 25 m apart from the central, deepest and flat-bottomed part of the lake where water depth was 12 m. Cores were retrieved by means of a piston corer with diameter 110 mm constructed to obtain up to 6 m of sediments from deep water

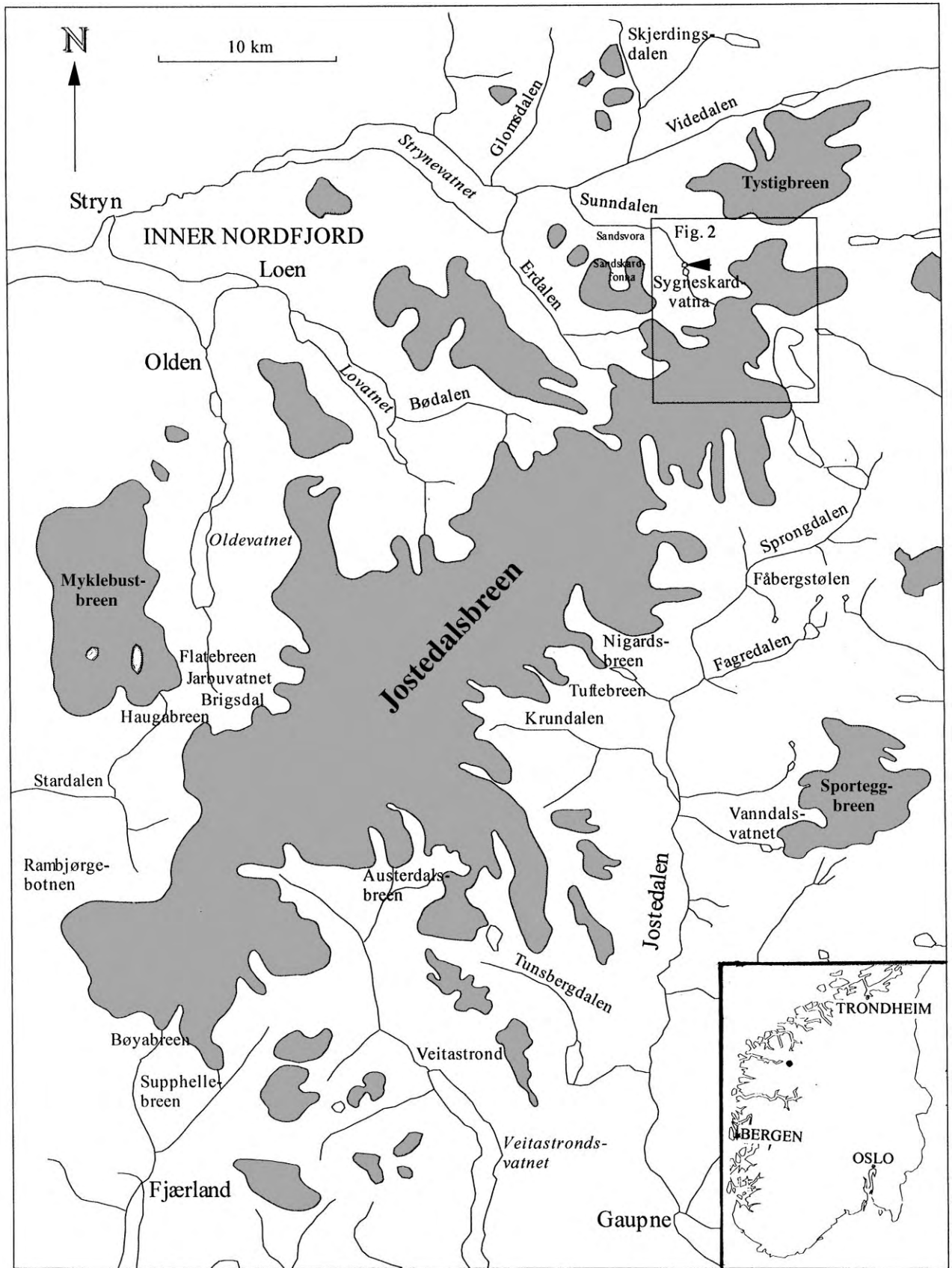


Fig. 1. Map of the Jostedalsglaciären region (present glaciers in dark shading). The area of Fig. 2 framed. The arrow indicates Syngeskardvatnet (the coring site).

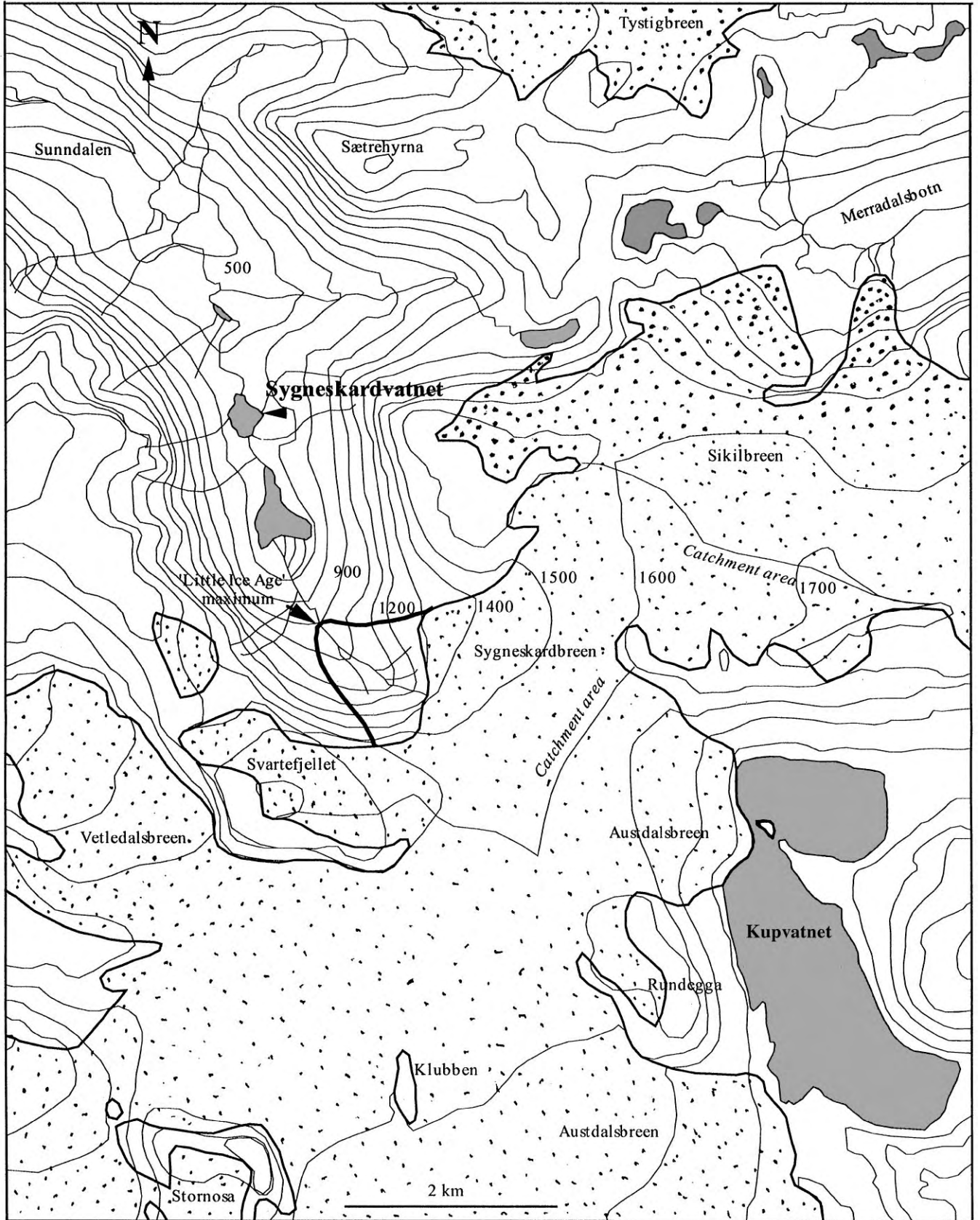


Fig. 2. Location map of the study area. Contour interval 100 m. Present glaciers are stippled and lakes are shown by light shading.



Fig. 3. Oblique air photograph of Syngneskardvatna. The cores were retrieved from the central part of the lower lake. The arrow indicates the ice-marginal deposit (possible Erdalen event moraine) at the outlet of the lake. Photograph: Fjellanger-Widerøe AS.

(Nesje, 1992) and stored in a cold room at 4°C until opened. After opening, the upper layer closest to the tube was removed and the sediment surface was cleaned carefully. Visual lithofacies, structures and texture were logged before the cores were split into 1 cm discs and stored in plastic bags.

3.3. Weight loss-on-ignition

The amount of organic carbon in lake sediments is a fundamental property that is a function of autochthonous and allochthonous organic production and clastic sediment input. Weight loss-on-ignition (LOI) is a simple method for determining the organic content of lacustrine sediments. The samples (normally 1–3 g dry sample) were dried overnight at 105°C in ceramic crucibles before the dry weight was measured. The samples were then subject to gradually rising temperatures for

$\frac{1}{2}$ h and ignited at 550°C for 1 h (Dean, 1974). After ignition, the samples were put into a desiccator and weighed at room temperature (18–20°C). The weight loss after ignition was calculated as percent dry weight. Snowball and Sandgren (1996) found a close relationship between total organic carbon (TOC) and LOI, where the latter yielded approximately 2% higher values, most probably as a result of evaporation of crystalline water.

3.4. Magnetic susceptibility

Down-core magnetic susceptibility variations of lacustrine sediments have received considerable attention as an indicator of erosion and transport in lake catchments (e.g. Snowball and Thompson, 1990). Magnetic susceptibility commonly reflects the concentration of magnetic minerals (e.g. Thompson and Oldfield, 1986) and have

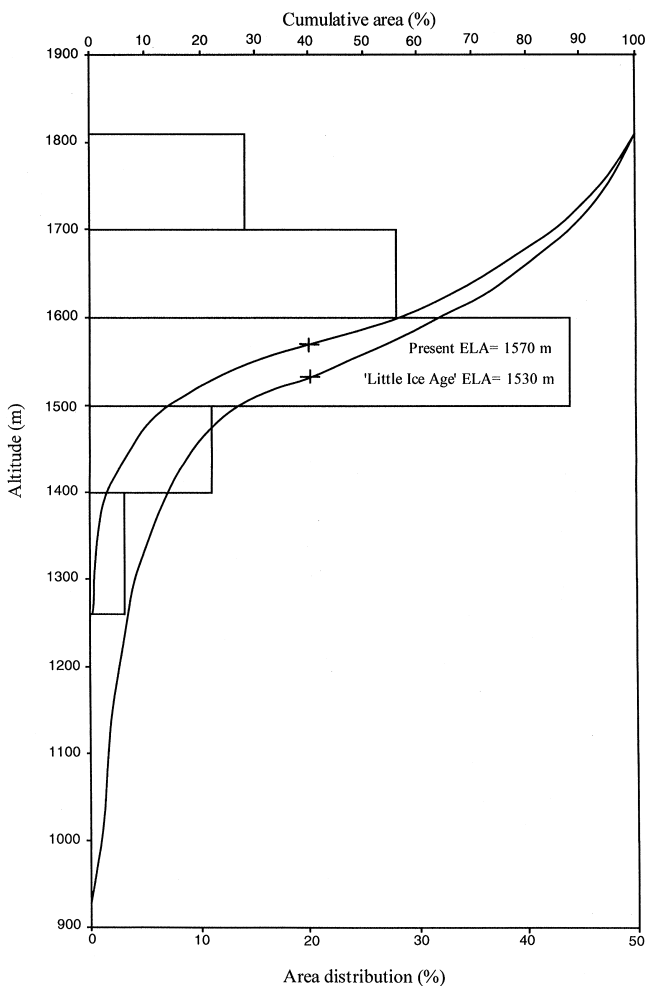


Fig. 4. Area distribution of the present glacier (horizontal bars) and the present and 'Little Ice Age' equilibrium-line altitude (ELA) calculated by means of an accumulation area ratio (AAR) of 0.6.

been widely used in Scandinavia to infer variations in glacier activity (Sandgren and Risberg, 1990; Nesje et al., 1991, 1994; Matthews and Karlén, 1992; Snowball, 1993; Dahl and Nesje, 1994; Snowball and Sandgren, 1996; Sohlenius, 1996). During periods when glacier activity increases in the lake catchment, increased erosion and input of clastic sediments cause higher minerogenic content, as seen from the LOI analysis. Periods of insignificant or reduced glacier activity in the lake catchment are characterised by lower production of glacial sediments. Increased magnetic susceptibility tends therefore to be related directly to the amount of allochthonous clastic material transported into the lake (e.g. Thompson et al., 1975) and magnetic susceptibility of lacustrine sediments can be used as a valuable lithoparameter for further interpretation of past environmental changes. Since magnetic susceptibility measurements commonly show parallel variations from core to core within the same lake or in lakes within the same catchment, they also provide a valuable basis for correlation, especially where litho-

stratigraphic variations are not visually distinguishable. Whole core, pass through, volume susceptibility with a resolution of 2 cm was carried out on the core Sygne-skardvatnet-2 using a Bartington MS2B sensor.

3.5. Radiocarbon dating

The radiocarbon dates (Table 1) were carried out at Beta Analytic Inc, Florida, USA, and at University of Utrecht, The Netherlands, according to standard procedures for accelerator mass spectrometry (AMS) radiocarbon dating. The radiocarbon ages are corrected for isotopic fractionation ($\delta^{13}\text{C}$) and have been calibrated using the program of Stuiver and Reimer (1993).

3.6. Reconstruction of glacier activity and ELAs

Clastic sediments deposited in proglacial lakes are generally considered to reflect the glacier activity in the lake catchment (e.g. Karlén, 1976, 1981, 1998). However, care must be taken to avoid or separate glacially derived sediments deposited in proglacial lakes from material supplied by surface runoff during rainfall, floods, and mass movements (snow avalanches and debris flows) from adjacent valley sides (e.g. Karlén and Matthews, 1992; Nesje et al., 1995). The organic carbon content in glacial lakes with negligible input from other sediment sources is mainly a function of autochthonous (lake productivity) and allochthonous (lake catchment) organic production. Thus, the weight-loss-on-ignition in such a setting is considered to represent a proxy for the glacier activity upstream from the glacier. Similarly, magnetic susceptibility, being a reflection of the concentration of magnetic minerals, is an index of the erosion and transport in the lake catchment. Thus, magnetic susceptibility and LOI are commonly inversely correlated. In addition, a study of sediment yield from nine Norwegian glaciers (Roland and Haakensen, 1985) shows a positive correlation ($R^2 = 0.74$) between glacier size and calculated sediment transport in proglacial rivers, which further strengthens this approach to reconstructing glacier variations.

Variations in glacier size are mainly determined by variations in equilibrium-line altitude (ELA). The main climatic factors contributing to variations in the ELA are winter accumulation and summer ablation. On Nigardsbreen (Fig. 1) (observation period 1962–1997) the cumulative net balance has increased 16.59 m (water equivalents) during the observation period, most of which was due to increased winter accumulation in the late 1980s and early 1990s (Kjøllmoen, 1998). Regression of ELA on net balance predicts that the steady-state ELA (net balance = 0) on Nigardsbreen is ca. 1560 m. A correlation between winter balance versus net balance and summer balance versus net balance on Nigardsbreen shows that the two mass balance parameters are of

Table 1
Radiocarbon dates from core Syngeskardvatnet-2. The two radiocarbon dates at 57–60 cm and 373 cm (in italics) are not used to calculate time resolution and sedimentation rates

Depth (m)	Dated material	Lab.no.	¹⁴ C-date BP	Calibrated age		δ ¹³ C
				Intercept (BP)	1 sigma (BP)	
<i>57–60</i>	<i>Salix twig</i>	<i>Beta-102074</i>	<i>300 ± 60</i>	<i>310</i>	<i>445–290</i>	– 27.1
63–66	Gyttja	Beta-102075	1160 ± 60	1065	1150–975	– 28.0
90	Gyttja	Beta-102076	1300 ± 60	1255	1285–1165	– 28.8
181	Gyttja	Beta-102077	2240 ± 40	2230	2325–2155	– 27.1
256–260	Gyttja	Beta-102078	3180 ± 60	3380	3455–3350	– 28.3
311–313	Gyttja	Beta-102079	4060 ± 50	4530	4560–4440	– 28.2
371–372	Gyttja	Beta-102080	5320 ± 50	6150	6185–6005	– 28.4
<i>373</i>	<i>Gyttja</i>	<i>UtC-6573</i>	<i>5175 ± 45</i>	<i>5925</i>	<i>5980–5905</i>	– 28.4
383–383.5	Gyttja	Beta-102081	5940 ± 50	6765	6845–6730	– 28.3
399	Gyttja	UtC-6574	6475 ± 50	7340	7390–7280	– 29.2
402	Gyttja	UtC-6575	6600 ± 45	7470	7520–7395	– 29.1
410	Gyttja	UtC-6576	7190 ± 60	7945	8055–7915	– 28.0
412–415	Gyttja	Beta-102082	7410 ± 50	8150	8185–8125	– 27.4
418	Gyttja	UtC-6577	7560 ± 50	8335	8370–8315	– 27.0
426	Gyttja	UtC-6578	7760 ± 50	8495	8550–8420	– 27.0
430–433	Gyttja	Beta-102083	7840 ± 50	8560	8600–8520	– 27.0

almost equal importance for the annual net balance ($R^2 = 0.71$ and 0.69 , respectively).

A similar mass balance record from Austdalsbreen (Kjøllmoen, 1998) E/SE of the Syngeskardbreen catchment (Fig. 1) covers the period 1988–1997. Between 1988 and 1995 the glacier mass increased. However, in 1996 and 1997 the net balance was slightly negative. The steady-state ELA at Austdalsbreen is 1430 m, which is 140 m lower than calculated by means of the AAR (AAR = 0.6) method on Syngeskardbreen. If real, this difference may reflect extra lee-ward accumulation of dry snow on Austdalsbreen from westerly and northwesterly winds. Correlation between winter balance and net balance, and between summer balance and net balance shows that the winter balance is the more important mass balance factor ($R^2 = 0.60$ and 0.37 , respectively).

4. Previous palynological investigations in Syngeskardet

Investigations of the vegetation succession in Syngeskardet have been carried out on a limnic sequence 680 m a.s.l. east of Syngeskardvatnet (Kvamme, 1984). A basal radiocarbon date of 9280 ± 130 ¹⁴C yr BP [10,250 (10,380–10,040) cal. BP] is considered to give a close minimum date of the deglaciation of the upper Sunddalen area. The pioneer vegetation was dominated by *Betula nana* with some *Hippophaë*. *Betula* and *Pinus* established around 8500 ¹⁴C yr BP (9500 cal. BP), while *Alnus* arrived around 7750 ¹⁴C yr BP (8600 cal. BP). Between 6500 and 5000 ¹⁴C yr BP (7400 and 5800 cal.

BP), *Ulmus* and some *Corylus* were present at the site. Kvamme (1984), Nesje and Kvamme (1991), and Nesje et al. (1991) concluded that these species indicated a summer temperature ca. 2°C higher than at present and that the glacier above the site (Syngeskardbreen) and possibly most of the northern Jostedalsbreen ice cap was melted at that time. The palynological investigations in Syngeskardet suggested that a climatic deterioration occurred approximately 5000 ¹⁴C yr BP (5800 cal. BP) and that the thermophilous (warmth-demanding) trees disappeared shortly afterwards as a response to katabatic winds from the ice cap formed on the mountains above the site. *Pinus* was present in Syngeskardet up to 2000–3000 ¹⁴C yr BP (1900–3300 cal. BP) (Kvamme, 1984).

5. Results: Sediment cores from Syngeskardvatnet

Two sediment cores were retrieved from Syngeskardvatnet.

5.1. Core Syngeskardvatnet-1

The lacustrine sequence of core Syngeskardvatnet-1 has been divided into nine sedimentary units (Units A-I) (Fig. 5). The core consists of clastic sediments [silty sand (Unit A, H), sandy silt (Unit B, C, E, G) and sand (Unit I)], and two closely spaced thin layers of light brown gyttja (Unit D and F). The upper and middle part of Unit C and F contain macroscopic plant remains and two distinct organic layers are present in the upper part of the core.

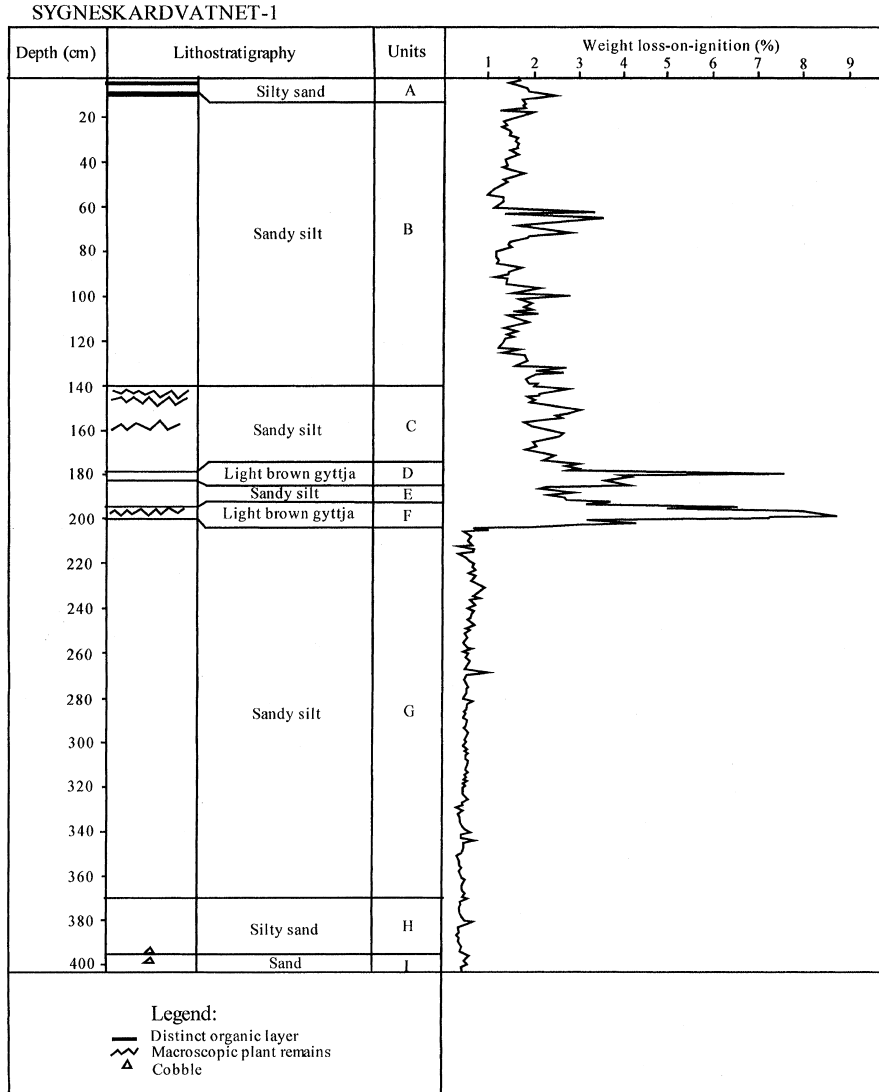


Fig. 5. Lithostratigraphy and weight loss-on-ignition in the Sygneskardvatnet-1 core.

The weight loss-on-ignition (LOI) is < 1% below 200 cm in the core, rising abruptly to a maximum of 8.7% at 198 cm. The second highest LOI value of 7.5% is at 179 cm. Above this level, the organic content is much lower. Although there are variations in the upper part of the core, LOI values are consistently > 1%.

5.2. Core Sygneskardvatnet-2

The lacustrine sequence in core Sygneskardvatnet-2 has been divided into 11 sedimentary units (Units A-K) (Fig. 6). The core consists mainly of clastic sediments (clay, silt, and sand), intercalated with eighth thin, but distinct organic layers. The LOI is generally highest in the lower part of the core, reaching a maximum of 9.0% at 370 cm depth. There is an irregular decline in LOI values between 370 and about 180 cm with a more dis-

tinct drop to values generally less than 2% above 180 cm. Since core Sygneskardvatnet-2 has the longest post-deglaciation record (see Figs. 5 and 6) and thus highest time resolution, this core was chosen for detailed magnetic susceptibility analysis and radiocarbon dating. The magnetic susceptibility record is largely a mirror image (inversely correlated) but with more marked variations in the upper part of the core of the 5-point-running mean LOI record (Fig. 7).

5.3. Dating, time resolution and sedimentation rate

Altogether 16 AMS dates, six from Utrecht University and ten from Beta Analytic Inc, were obtained from core Sygneskardvatnet-2 (Table 1). The upper date at 57–60 cm (Beta-102074) obtained on a *Salix* twig may reflect sinking into the sediments, giving a younger date

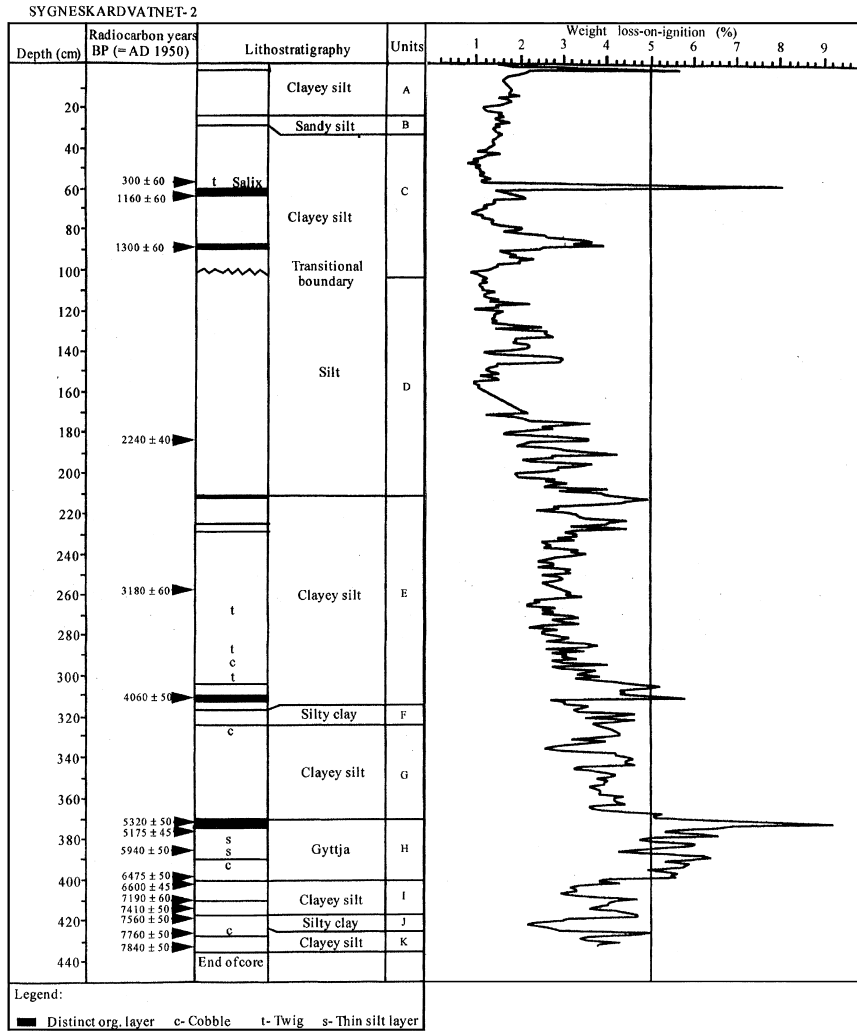


Fig. 6. Lithostratigraphy, radiocarbon dates, and weight loss-on-ignition in the Sygneskardvatnet-2 core. The vertical line at 5% on the weight loss-on-ignition panel marks the value above which the sediments were brown-coloured.

than the stratigraphic position should indicate. Except for the date of 5175 ± 45 ^{14}C yr BP (UtC-6573), the radiocarbon dates become progressively older with depth (Table 1, Fig. 8), indicating generally undisturbed sedimentation since about 8560 cal. BP.

Intercept calendar dates from core Sygneskardvatnet-2 (except Beta-102074 and UtC-6573 at 57–60 and 373 cm, respectively) have been used to calculate the time resolution and sedimentation rate. The relationship between the two parameters is shown in Fig. 9. Time resolution (yr cm^{-1}) of the 1-cm interval LOI analyses ranges from 7 (interval 64–90 cm) to 68 yr cm^{-1} in the depth interval 410–413 cm (Fig. 10, Table 2). The mean time resolution in core Sygneskardvatnet-2 is ca. 20 yr cm^{-1} .

According to the age/depth relationship obtained from core Sygneskardvatnet-2 (Fig. 8), the sedimentation rates vary between 0.15 and 1.37 mm yr^{-1} (Fig. 10, Table 2), with a mean sedimentation rate of 0.50 mm yr^{-1} .

6. Inferred glacier development

The glacier development in the lake catchment is based on two assumptions. Firstly, at LOI values $> 5\%$ the sediments are brown coloured indicating very low or no glacier activity in the catchment upstream from the lake. At LOI values $< 5\%$, on the other hand, the sediments are bluish grey in colour typical of glacial meltwater drainage systems. Secondly, oscillations below the 5% level are interpreted as variations in glacier activity. Measurements of modern sediment transport in Norwegian glacier meltwater streams seem to justify such an interpretation (Østrem, 1975; Roland and Haakensen, 1985). It is, however, difficult to evaluate how representative the LOI signal is as a reflection of glacier activity. Since the lake is located in a short distance downstream from the glacier, the LOI signal is, however, considered to strongly reflect the glacier activity in the lake

catchment. To reduce the possibilities of “noise” in the LOI record, the overall Holocene glacier development of Sygneskardbreen is presented as 5-point-running mean weight loss-on-ignition (LOI) values in core Sygneskardvatnet-2 (Fig. 11, middle panel).

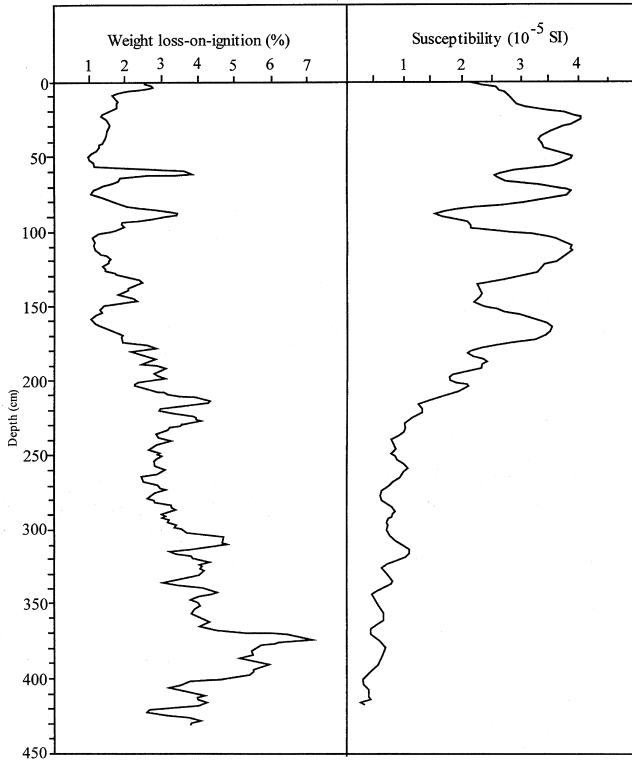


Fig. 7. Five-point-running mean of the loss-on-ignition values in core Sygneskardvatnet-2 (left panel) and the 2-cm-interval magnetic susceptibility values in the same core.

The basal radiocarbon date of 9280 ± 130 ^{14}C yr BP [10,250 (10,380–10,040) cal. BP] at a palynological site east of Sygneskardbreen demonstrates that the upper part of Sunndalen was deglaciated during the late Pre-boreal Chronozone (Kvamme, 1984). This date is in close agreement with other deglaciation dates obtained from the Jostedalsbreen region (Rye et al., 1997). According to the sediment texture and LOI values, a glacier (‘Sygneskardbreen’) existed in the catchment until around 6475 ± 50 yr BP [7340 (7390–7280)] cal. BP (395 cm in core 2). Before this, the sediment texture and LOI curve indicate increases in glacier activity around 8500, 8400, 8200, 7750, 7600, and 7400 cal. BP. Periods of reduced

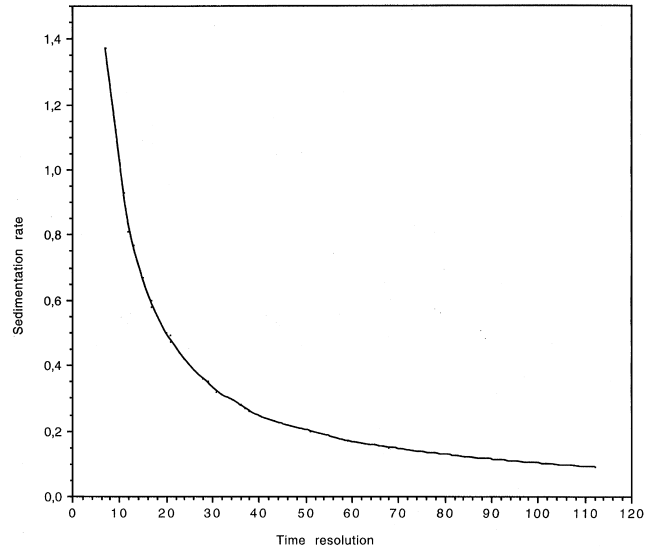


Fig. 9. The relationship between time resolution (yr cm^{-1}) and sedimentation rate (mm yr^{-1}).

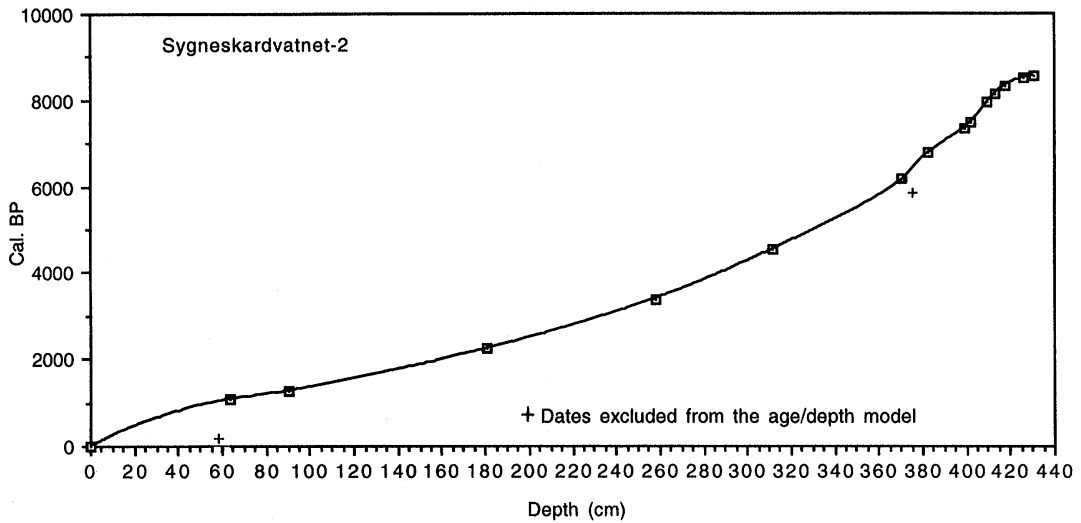


Fig. 8. Intercept calendar dates used to construct an age/depth curve for core Sygneskardvatnet-2. The two radiocarbon dates at 57–60 and 373 cm in Fig. 6 and Table 1 are not used in constructing the curve.

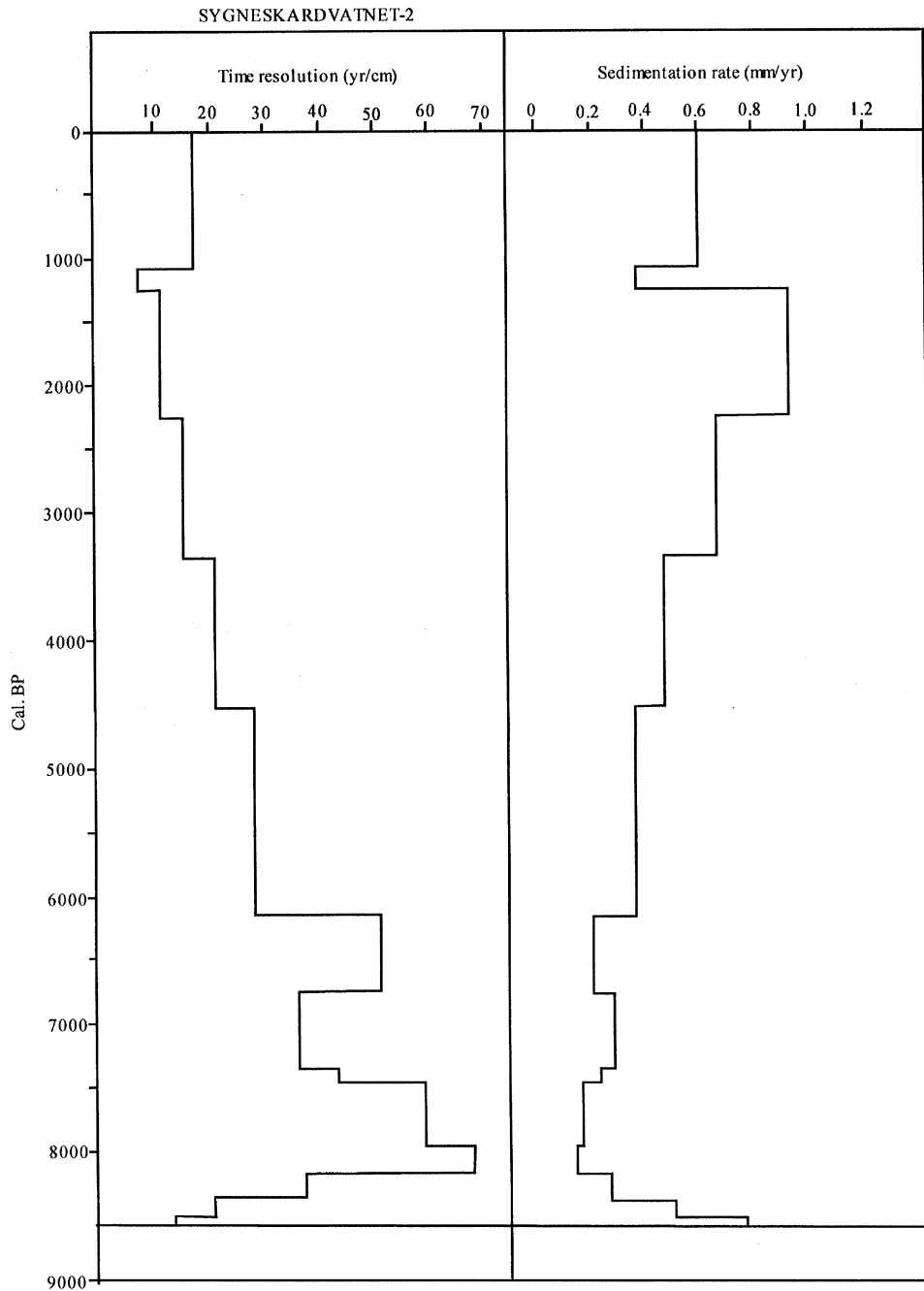


Fig. 10. Time resolution and sedimentation rate as a function of age [cal. BP (BP = AD 1950)] between the dated levels in core Sygneskarvatnet-2.

glacier activity occurred around 8450, 8300, 7900, and 7500 cal. BP (Fig. 11).

Between 6475 ± 50 [7340 (7390–7280) cal. BP] and 5320 ± 50 yr BP [6150 (6185–6005) cal. BP], the glacier is interpreted as having melted away, except possibly for short intervals around 6000 and 5800 ^{14}C yr BP (6900 and 6700 cal. BP). Deposition of gyttja in the lake indicates no glacier activity in the lake catchment for over a thousand years, with periods of high organic produc-

tion around 7100, 7000, 6800 and 6550 cal. BP. Accordingly, the ELA must have been at least 240 m higher than at present during that time interval. The highest LOI values in the whole core occurred at 5500 ^{14}C yr BP (6250 cal. BP), indicating climatically favourable conditions (low input of minerogenic sediments and/or high organic production) at that time.

The post-thermal optimum glacier development (Neoglaciation) seems to have occurred in three major

Table 2

Time resolution and sedimentation rates inferred from the radiocarbon dates (intercept calendar dates) in core Sygneskardvatnet-2. The two radiocarbon dates at 57–60 cm and 373 cm in Table 1 are not used in the calculations of time resolution and sedimentation rates.

Depth in core (cm)	Time resolution (yr cm ⁻¹)	Sedimentation rate (mm yr ⁻¹)
0–64	17	0.60
64–90	7	1.37
90–181	11	0.93
181–258	15	0.67
258–312	21	0.47
312–371	28	0.36
371–383	51	0.20
383–399	36	0.28
399–402	43	0.23
402–410	59	0.17
410–413	68	0.15
413–418	37	0.27
418–426	20	0.50
426–431	13	0.77

phases. During the first phase, a series of events with increasing glacier extent occurred at about 6000, 5800–5700, 5600, 5500, 5200, 5100, 4900, 4800, and 4700–4550 cal. BP. Periods of reduced glacier activity (higher LOI values) seem to have occurred around 5900–5800, 5550, 5450–5300, 5050, 4850, and 4750 cal. BP (Fig. 11).

During the second phase, further events of progressively increasing glacier activity occurred at 4450, 4300, 4200, 4150, 4050, 4000, 3900, 3800, 3550, and 3300 cal. BP. Glacier activity remained high, with possible minor increases around 3350, 3200, 3050, and 2800 cal. BP. Periods of reduced glacier activity occurred around 4500, 4400, 4100, 3950, 3700, 3450, and 3100 cal. BP. Two periods of significantly relatively reduced glacier activity during the second phase occurred at 3000–2850 and around 2700 cal. BP.

Finally, during the most recent, third phase, episodes of increased glacier activity occurred at around 2550, 2450, 2350, 2250, 2150, 2000, 1800, 1700, 1600, 1400, 1300, 1150, 1050, and during the last 1000 cal. yr BP (including the “Little Ice Age”). Higher LOI values indicating somewhat less glacier activity during the third phase occurred at approximately 2650, 2500, 2400, 2300, 2200, 1850, 1750, 1550, 1350, 1250, 1050–1000 cal. BP, and during the 20th century (Fig. 11).

The lacustrine sequence obtained in Sygneskardvatnet indicates that the Holocene has been interrupted by altogether 41 periods of increased glacier activity and by 36 episodes of reduced glacier activity, with mean return periods of 150 ± 10 and 210 ± 15 yr, respectively (± 1 standard error).

7. Spectral analysis of the loss-on-ignition data

There is growing evidence of millennial-scale variability of Holocene climate at periodicities of approximately 2500 and 950 yr possibly caused by changes in solar flux (Röthlisberger, 1986; O’Brien et al., 1995) and at about 1500 years possibly related to an internal oscillation of the climate system (Bond et al., 1997; Campbell et al., 1998; Bianchi and McCave, 1999). Shorter, quasi-periodic oscillations of 120, ~ 135 , and ~ 200 yr have been observed in the Northern Hemisphere. Possible forcing mechanisms for these oscillations include solar variability (Stuiver and Brazunias, 1989, 1993) and lunar tidal effects (Burroughs, 1992).

To investigate the variability of the LOI data in the frequency-domain, spectral analysis was carried out. Spectral estimates were calculated using two different methods (Fig. 12). A major problem with analysing palaeoclimatic data using many of the most widely used methods for spectral analysis, is the need for regularly spaced time series (Yiou et al., 1996; Schultz and Stettger, 1997). This criterion is fairly easily met in palaeoclimatic time series originating from environments with only minor variations in sedimentation rates. However, there are environments in which changes in sedimentation rate are accompanied by changes in the climatic proxy/parameter of interest. This is commonly the case with glacier-fed lakes, such as Sygneskardvatnet, in which a decrease in sedimentation rate generally correlates to an increase in organic content (as reflected in the LOI records). In such cases, even densely sampled cores will be unevenly spaced in the time domain. Interpolation is widely used, but interpolation of unevenly spaced time series may not only artificially reduce or increase the number of data points of a time series, but it has been shown that interpolation leads to an underestimation of high-frequency components in a spectrum (Schultz and Stettger, 1997).

The spectral estimates for the time series of LOI from Sygneskardvatnet (Fig. 11), were calculated using a technique based on the Lomb–Scargle Fourier transform in combination with a Welch-Overlapped-Segment-Averaging procedure (SPECTRUM software; see Schultz and Stettger, 1997 and references therein) in which unevenly spaced time series can be directly analysed. The resulting spectral estimates were compared with the widely used Blackman–Tukey (BT) method (Blackman and Tukey, 1958) one of many methods which requires evenly spaced data. The estimates obtained using “SPECTRUM” show discrete peaks at several frequencies; at periods about 50, 85, 110, 250–285, 500 and 2000 yr. The longest period of 2000 yr must be interpreted with caution. It is doubtful that a period of 2000 yr can be estimated with confidence in a time series only 8500 calendar years long. Such long periods could very well be

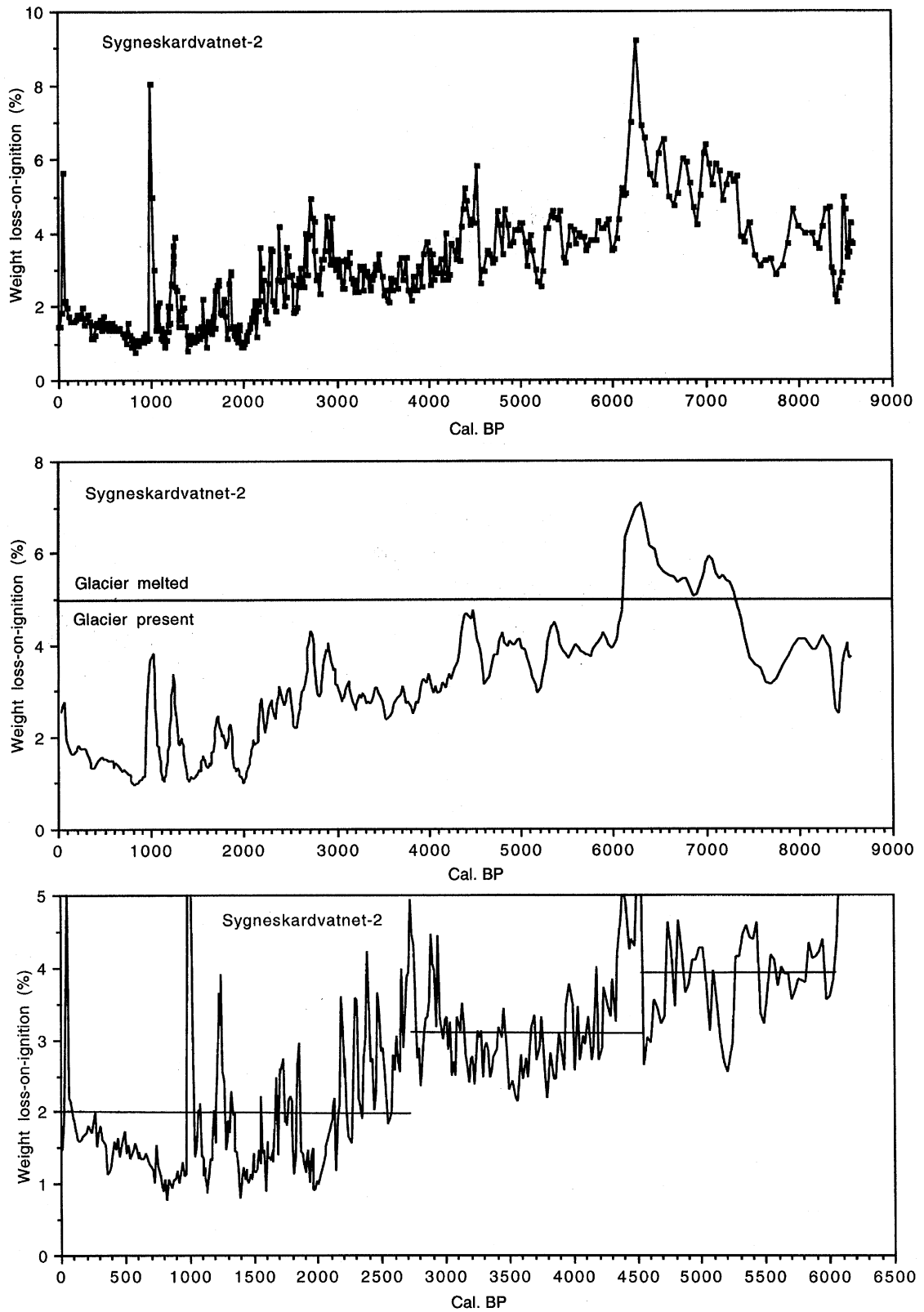


Fig. 11. Weight loss-on-ignition (LOI) values at 1-cm-intervals (upper panel) and 5-point-running mean weight loss-on-ignition (LOI) values (middle panel) in the Syngneskardvatnet-2 core from 9000 cal. BP up to the present based on the age/depth curve in Fig. 9. The horizontal line at 5% LOI marks the level above which the glacier in the catchment is interpreted to have melted away. The lower panel shows the weight loss-on-ignition record from Syngneskardvatnet-2 put into a calendar BP time scale from 6500 cal. BP up to the present visualising the three episodes of progressively increasing glacier activity from 6000 cal. BP up to the present.

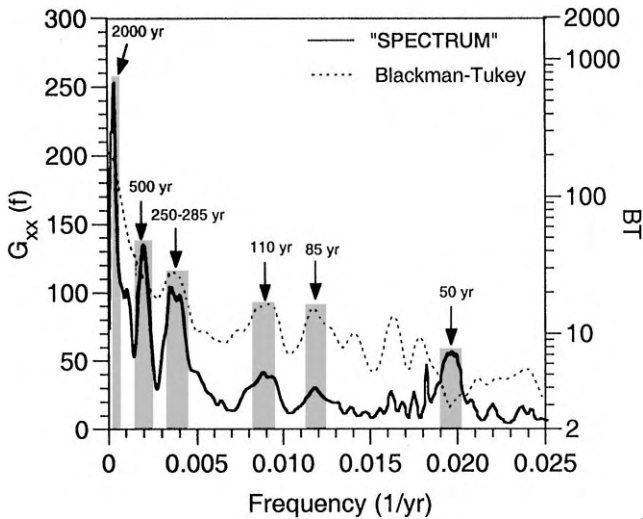


Fig. 12. Spectral estimates of LOI data. Autospectrum of the LOI data using the SPECTRUM software (Schultz and Stattegger, 1997) (OFAC = 6; HIFAC = 1; $N_{\text{seg}} = 6$; Hanning-window, $N = 434$) and the Blackman–Tukey autospectra of the LOI data based on an interpolated time series. Parameters for the Blackman–Tukey estimates were set to $m = 60$, $\Delta t = 20$ yr, $N = 430$, pre-widening = 0.5. Dominant frequencies are indicated.

the effect of harmonics or aliasing. The main difference between the “SPECTRUM”-estimates and the BT spectra, i.e. the inability of the BT method to produce reliable information of the high-frequency end, is most likely the result of the input time series being interpolated. With an average sampling interval of about 20 yr the resulting Nyquist frequency ($\frac{1}{2}\Delta t$) of 40^{-1} yr effectively limits the possibility to obtain information about periods shorter than 40 yr. In practice though, for short periods to be estimated with high confidence the Nyquist frequency should be decreased. Some of the shifts seen at the upper boundary of the BT estimates could be the result of aliasing of under-sampled high-frequency signals.

8. Comparison of the Syngneskardvatnet glacier record with other terrestrial and marine records

In Fig. 13, the Holocene record of glacier fluctuations obtained from the lacustrine sediment investigations in Syngneskardvatnet (B) is compared with the history of glacier and climate variations put together from several sites adjacent to Jostedalsbreen (A) Nesje et al., 1991; Nesje and Kvamme, 1991 with a record of glacier variations at the northern part of Hardangerjøkulen (C) (Dahl and Nesje, 1994, 1996), a reconstruction of Holocene climate in northern Sweden (D) (Karlén et al., 1995), and a Holocene deep-sea record of ice rafting from core VM 29-191 in the North Atlantic ocean (E) (Bond et al., 1997).

The reconstruction of glacier and climatic fluctuations in the Jostedalsbreen region (Nesje et al., 1991; Nesje and Kvamme, 1991 with some minor later modifications, Fig. 13A) is based upon palynological records from Syngneskardet (Kvamme, 1984), Sprongdalen (Kvamme, 1989), Rambjørgebotnen (Torske, 1996), and the Haugabreen foreland (Matthews and Caseldine, 1987b), from peat deposits with distal glaciofluvial sediments in Rambjørgebotnen, Bevringsdalen (Nesje and Dahl, 1991b), Tunsbergdalen (Mottershead et al., 1974; Mottershead and Collin, 1976), Glomsdalen (Nesje et al., 1991), and Sandsvora (Nesje and Rye, 1993), and finally from proglacial lake sediments in Vanndalsvatnet, draining Spørteggbreen east of Jostedalen (Nesje et al., 1991). That the ‘Little Ice Age’ advance represented the maximum Neoglacial extent of Jostedalsbreen is well established from moraine stratigraphic evidence (e.g. Matthews and Dresser, 1983; Matthews, 1991), historic evidence (Grove and Battagel, 1983; Grove, 1988) and lichenometry (Andersen and Sollid, 1971; Erikstad and Sollid, 1986; Bickerton and Matthews, 1993). The early Holocene event (“Erdalen event”) in the reconstruction relates to the advance of outlet glaciers from the Jostedalsbreen Plateau at 9100 ± 200 ^{14}C yr BP, forming terminal moraines up to 1 km beyond the ‘Little Ice Age’ moraines. In addition, they suggested that at least the northern part of the glacier melted away during the early Holocene, and that the glacier was reformed around 5300 ^{14}C yr BP.

Holocene glacier fluctuations at the northern sector of Hardangerjøkulen (Fig. 13C) were reconstructed from four radiocarbon-dated lake and terrestrial sites in the Finse region, providing a detailed record concerning the number, age, and magnitude of early Holocene glacier variations (Dahl and Nesje, 1994, 1996). The main findings of their study were that the glacier expanded at 7600 ^{14}C yr BP (8300 cal. BP) (“Finse event”), after which the glacier disappeared completely between 7500 and 6300 ^{14}C yr BP (8200–7200 cal. BP) and from 5300 to 4800 ^{14}C yr BP (6100–5600 cal. BP). The period from 4800 to 3800 ^{14}C yr BP (5600–4200 cal. BP) was characterised by high-frequency glacier variations. Since 3800 ^{14}C yr BP (4200 cal. BP), the glacier has existed continuously up to the present.

The history of climatic variations in northern Sweden (e.g. Karlén et al., 1995; Fig. 13D) was reconstructed from proglacial lacustrine sediment records and tree-limit (mainly pine tree) variations. Numerous glacier advances are indicated during the last 9000 yr.

Bond et al. (1997) showed evidence from deep sea cores in the North Atlantic of abrupt shifts, advecting cool, ice-bearing waters as far south as the latitude of Great Britain during distinct events throughout the Holocene (Fig. 13E). In core VM 29-191 in the North Atlantic events of increased ice rafting during the last 11,000 cal. BP peaked at 1400, 2800, 4300, 5900, 8200, 9500, and

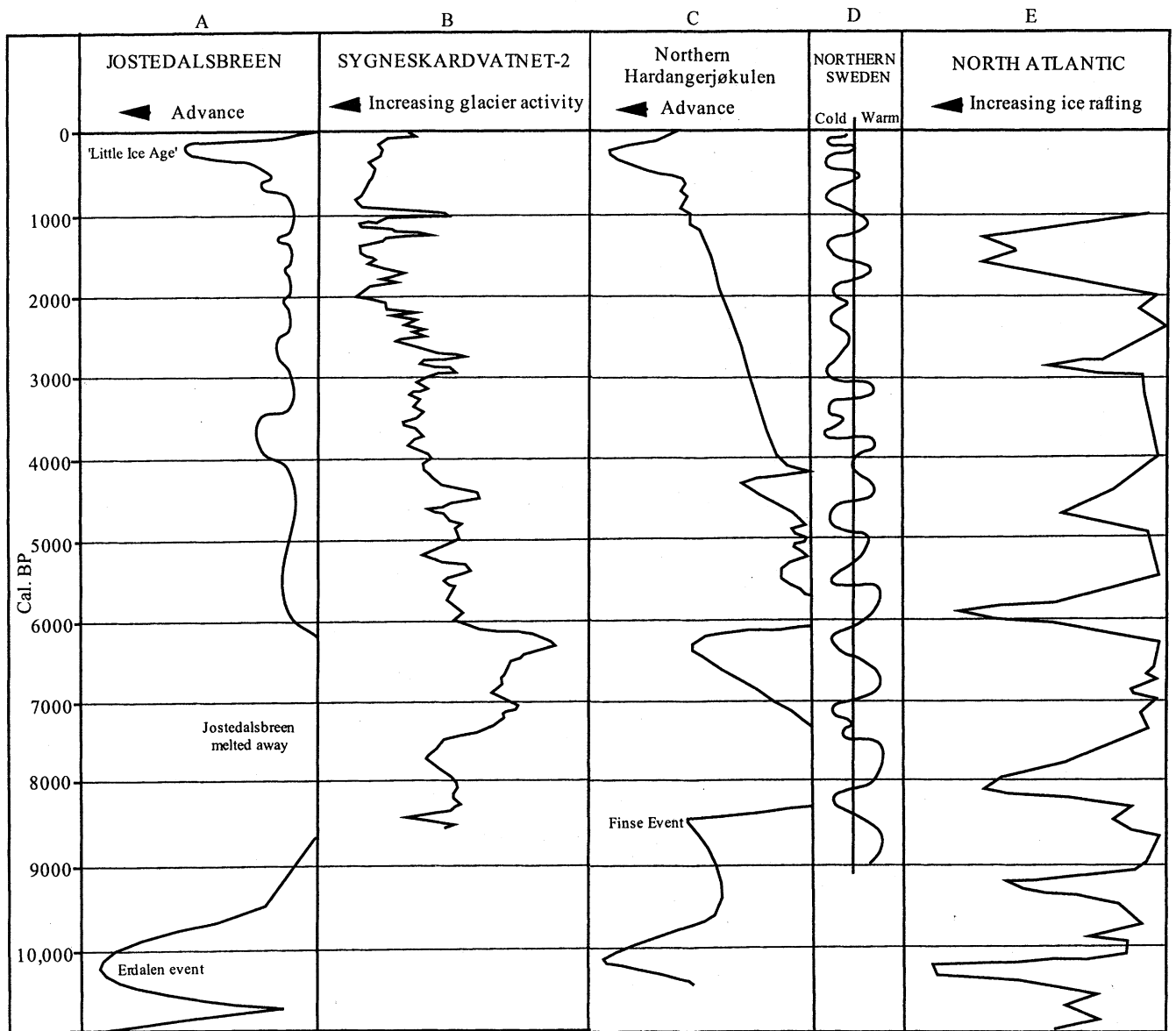


Fig. 13. Records of (A) glacier variations at Jostedalsbreen (Nesje et al., 1991; Nesje and Kvamme, 1991), (B) glacier activity in the Sygneskardet catchment (this paper), (C) glacier fluctuations at the northern part of Hardangerjøkulen (Dahl and Nesje, 1994, 1996), (D) climate variations in northern Sweden (Karlén, 1995), and (E) frequency of increased ice rafting in core VM 29-191 in the North Atlantic (Bond et al., 1997).

10,300 cal. BP. The mean time resolution in the core is, however, rather poor (approximately 100 yr cm^{-1}); the last 11,000 cal. yr being represented by 109 cm of sediments and by 64 data points.

The Finse event (Fig. 13A) is recorded both in the Hardangerjøkulen and the North Atlantic regions (Fig. 13C and E). The 8400 event in the Sygneskardvatnet sequence is the same event as the Finse event (Fig. 13C) and also correlates with a cold episode in northern Sweden (Fig. 13D) and the spike of increased ice rafting in the North Atlantic (Fig. 13E). The period of the highest LOI values in the Sygneskardvatnet record coincides

with reduced ice rafting in the North Atlantic, but with expanded glaciers probably caused by increased winter precipitation at the northern part of Hardangerjøkulen.

During the early Holocene, six episodes of glacier expansion are recorded in Sygneskardet at ca. 8500, 8400, 8200, 7750, 7600, and 7400 cal. BP (Fig. 11). Surely, the 8400 episode appears to belong to the same widespread event as recorded in Greenland ice cores, in lacustrine and proglacial sites, and marine sediments. In both the GRIP and GISP2 Greenland ice cores (Fig. 14), as well as in lacustrine sequences (Karlén, 1976; Grafenstein et al., 1998) and marine records (Bond et al., 1997;

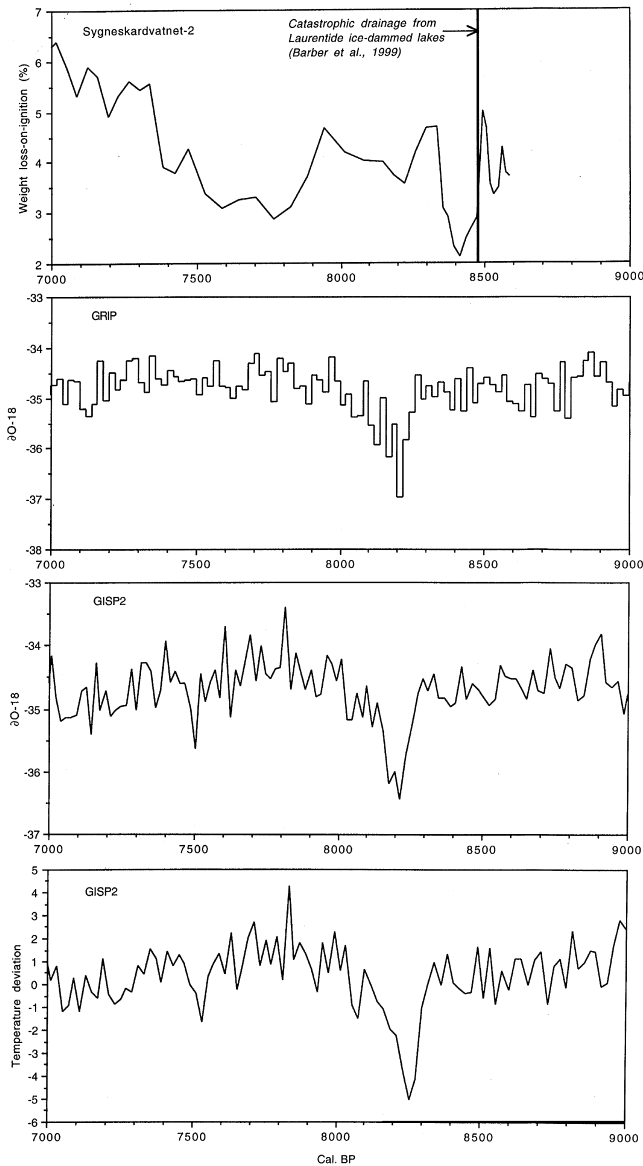


Fig. 14. Weight loss-on-ignition (%) in Syngneskardvatnet-2 (this paper) compared with $\delta^{18}\text{O}$ in the GRIP (Dansgaard et al., 1993) and GISP2 ice cores (Grootes et al., 1993), and with temperature deviations from the mean over the last 2000 years (Stuiver et al., 1995) between 7000 and 9000 cal. BP. The vertical line in the upper panel marks the timing (~ 8470 cal. BP) of a catastrophic drainage event from the glacier-dammed lakes Agassiz and Ojibway at the margin of the Laurentide ice sheet.

Klitgaard-Kristensen et al., 1998), this widespread event has been dated to between 8400 and 8000 cal. BP [centred around 8200 cal. BP (7600 ^{14}C yr BP)] (e.g. Alley et al., 1997). In central south Norway (Hardangerjøkulen) it has been termed the Finse event by Dahl and Nesje (1994, 1996). The episode of reduced LOI values in the lake sediments peaks at 8410 cal. BP (upper panel of Fig. 14), which is about 200 years prior to the ice core records (Fig. 14). Barber et al. (1999) suggested that this “8200

event” was triggered by a drainage episode from the glacial lakes Agassiz and Ojibway (dammed by a remnant of the Laurentide ice sheet) around 8470 cal. BP. As evident from Fig. 14 (upper panel), the drop in LOI values in the core occurred immediately after this meltwater drainage event.

The evidence from Syngneskardvatnet that at least the northern part of Jostedalbreen melted away between 7340 and 615 cal. BP (possibly with two short interruptions at approximately 6900 and 6700 cal. BP) and the re-establishment around 5300 ^{14}C yr BP (6100 cal. BP) is in good agreement with the pollen evidence presented from the Jostedalbreen region (Kvamme, 1984, 1989; Nesje and Kvamme, 1991). In the North Atlantic, this episode is recorded as a period of low ice rafting. The two records from Hardangerjøkulen and northern Sweden indicate no glaciers and warm climate, respectively. Likewise, a significant episode of increased glacier activity in the Syngneskardvatnet catchment at 5200 cal. BP is not recorded at Hardangerjøkulen; neither in northern Sweden, nor in the North Atlantic. These discrepancies, which may relate to imprecision of dating or regional patterns in climate change, will need to be resolved by future research.

Between 2800 cal. BP and the Medieval warm period, the Medieval in Syngneskardvatnet recorded as low minerogenic input at 1350, 1250, and 1050–1000 cal. BP, the activity of Syngneskardbreen increased significantly. A similar development is recorded at the northern part of Hardangerjøkulen. In northern Sweden, a series of four episodes of colder climate is recorded during the same time span. In the North Atlantic, a significant peak of ice rafting occurred just prior to the Medieval warm period, centred around 1400 cal. BP. Subsequent to the latter of the Medieval episodes of reduced glacier activity, a significant increase in glacier activity occurred during the last millennium (including the “Little Ice Age”). This is in accordance with other relevant records and historical evidence (e.g. Grove, 1988). In this paper, the record of glacier variations at the NW part of Jostedalbreen has not been converted into summer temperature and winter precipitation variations (e.g. Dahl and Nesje, 1996). This will be presented in a later paper (Nesje et al., 1999).

9. Conclusions

1. The sediment texture and LOI values indicate that ‘Syngneskardbreen’ was present from deglaciation until 6475 ± 50 yr BP [7340 (7390–7280)] cal. BP. During this time interval, increased glacier activity occurred around 8500, 8400, 8200, 7750, 7600, and 7400 cal. BP. The 8400 cal. BP glacier episode recorded in the Syngneskardvatnet-2 core clearly relates to a widespread event in the North Atlantic region, which took place

- between 8400 and 8000 cal. BP [centred around 8200 cal. BP (7600 ^{14}C yr BP)] (e.g. Alley et al., 1997). This event was probably triggered by a meltwater release from ice-dammed lakes at the margin of the Laurentide ice sheet (Barber et al., 1999). In central south Norway this oscillation has been termed the Finse event by Dahl and Nesje (1994, 1996).
2. Between 6475 ± 50 yr BP [7340 (7390–7280) cal. BP] and 5320 ± 50 yr BP [6150 (6185–6005) cal. BP], gyttja was deposited in the lake, indicating that the glacier was melted away. At 6900 and 6700 cal. BP, however, two short episodes of glacier activity are indicated. When the glacier was melted, the ELA must have been at least 240 m higher than at present. The highest LOI values in the whole core occurred at 6250 cal. BP, indicating climate optimum conditions at that time. The results confirm and refine the earlier conclusions by Nesje et al. (1991) and Nesje and Kvamme (1991), based largely on palynological evidence (Kvamme, 1984, 1989), that Jostedalsbreen melted away during the early Holocene and that the glacier was formed 5200 ^{14}C yr BP (6000 cal. BP).
 3. Glacier growth subsequent to the thermal optimum seems to have occurred in three phases: (1) from 5200 to 4000 ^{14}C yr BP (6000 to 4500 cal. BP); (2) from 4000 to 2500 ^{14}C yr BP (4500 to 2700 cal. BP); and (3) after 2700 cal. BP. During the first phase (6000–4500 cal. BP), a series of events with increased glacier activity occurred at about 6000, 5800–5700, 5600, 5500, 5200, 5100, 4900, 4800, and 4700–4550 cal. BP. Periods of reduced glacier activity (higher LOI values) seem to have occurred around 5900–5800, 5550, 5450–5300, 5050, 4850, and 4750 cal. BP.
 4. During the second phase (4500–2700 cal. BP), episodes of increased glacier activity occurred at 4450, 4300, 4200, 4150, 4050, 4000, 3900, 3800, 3550, and 3300 cal. BP. Glacier activity remained high with minor increases around 3350, 3200, 3050, and 2800 cal. BP. Reduced glacier activity occurred around 4500, 4400, 4100, 3950, 3700, 3450, 3100, 3000–2850, and 2700 cal. BP.
 5. During the third phase, between 2700 cal. BP and the present, episodes of increased glacier activity occurred at 2550, 2450, 2350, 2250, 2150, 2000, 1800, 1700, 1600, 1400, 1300, 1150, and 1050 cal. BP, and during the last millennium. Higher LOI values indicating somewhat less glacier activity occurred approximately 2650, 2500, 2400, 2300, 2200, 1850, 1750, 1550, 1350, 1250, and 1050–1000 cal. BP, and during the 20th century.
 6. The lacustrine sequence obtained in Sygneskardvatnet indicates that the Holocene has been interrupted by altogether 41 periods of increased glacier activity and by 36 episodes of reduced glacier activity, with mean return periods of 150 ± 10 and 210 ± 15 yr, respectively (± 1 standard error).

7. Spectral analysis of the loss-on-ignition data show discrete peaks at several frequencies at periods about 50, 85, 110, 250–285, 500, and 2000 calendar years.

Acknowledgements

The project was supported financially by the Norwegian Science Foundation (NFR) and the British Natural Environmental Research Council (Grant GR 3/9691). The paper represents Jotunheimen Research Expeditions, Contribution No. 137. J. Bakke, Ø. Lie and S. Sandvold assisted with the lake coring. M.S. Berrisford helped with laboratory work. The palaeomagnetic analyses were carried out in R. Løvlie's laboratory at the University of Bergen. Permission to land with helicopter in the Jostedalsbreen National Park was given by Stat-skog. The helicopter transport was carried out by Helitransport. The radiocarbon analyses were carried out at Beta Analytic Inc., Florida, USA and at the University of Utrecht, The Netherlands. Mons Kvamme read the manuscript critically and suggested improvements. To these persons and institutions we offer our sincere thanks.

References

- Alley, R.B., Mayewski, P.A., Sowers, T., Stuiver, M., Taylor, K.C., Clark, P.U., 1997. Holocene climate instability: A prominent, widespread event 8200 yr ago. *Geology* 25, 483–486.
- Andersen, J.L., Sollid, J.L., 1971. Glacial chronology and glacial morphology in the marginal zones of the glaciers Midtdalsbreen and Nigardsbreen, South Norway. *Norsk geografisk Tidsskrift* 25, 1–38.
- Barber, D.C., Dyke, A., Hillaire-Marcel, C., Jennings, A.E., Andrews, J.T., Kerwin, M.W., Bilodeau, G., McNeely, R., Southon, J., Morehead, M.D., Gagnon, J.-M., 1999. Forcing of the cold event of 8,200 years ago by catastrophic drainage of Laurentide lakes. *Nature* 400, 344–348.
- Bianchi, G.G., McCave, N., 1999. Holocene periodicity in North Atlantic climate and deep-ocean flow south of Iceland. *Nature* 397, 515–517.
- Bickerton, R.W., Matthews, J.A., 1993. 'Little Ice Age' variations of outlet glaciers from the Jostedalsbreen ice cap, southern Norway: a regional lichenometric-dating study of ice-marginal moraine sequences and their climatic significance. *Journal of Quaternary Science* 8, 45–66.
- Blackman, R.B., Tukey, J.W., 1958. *The Measurement of Power Spectra From The Point of View of Communication Engineering*. Dover, New York.
- Bond, G., Showers, W., Cheseby, M., Lotti, R., Almasi, P., deMenocal, P., Priore, P., Cullen, H., Hajadas, I., Bonani, G., 1997. A pervasive millennial-scale cycle in North Atlantic Holocene and glacial climates. *Science* 278, 1257–1266.
- Burroughs, W.J., 1992. *Weather Cycles, Real or Imaginary*. Cambridge University Press, Cambridge.
- Campbell, I.D., Campbell, C., Apps, M.J., Rutter, N.W., Bush, A.B.G., 1998. Late Holocene ~ 1500 yr climatic periodicities and their implications. *Geology* 26, 471–473.
- Dahl, S.O., Nesje, A., 1994. Holocene glacier fluctuations at Hardangerjøkulen, central-southern Norway: a high resolution composite

- chronology from lacustrine and terrestrial deposits. *The Holocene* 4, 269–277.
- Dahl, S.O., Nesje, A., 1996. A new approach to calculating Holocene winter precipitation by combining glacier equilibrium-line altitudes and pine-tree limits: a case study from Hardangerjøkulen, central southern Norway. *The Holocene* 6, 381–398.
- Dansgaard, W., Johnsen, S.J., Clausen, H.B., Dahl-Jensen, D., Gundestrup, N.S., Hammer, C.U., Hvidberg, C.S., Steffensen, J.P., Sveinbjörnsdóttir, A.E., Jouzel, J., Bond, G., 1993. Evidence for general instability of past climate from a 250-kyr ice-core record. *Nature* 364, 218–220.
- Dean, W.E., 1974. Determination of carbonate and organic matter in calcareous sediments and sedimentary rocks by loss on ignition: comparison with other methods. *Journal of Sediment Petrology* 44, 242–248.
- Erikstad, L., Sollid, J.L., 1986. Neoglaciation in South Norway using lichenometric methods. *Norsk geografisk Tidsskrift* 40, 85–105.
- Grafenstein, U. von, Erlenkeuser, H., Müller, J., Jouzel, J., Johnsen, S., 1998. The cold event 8200 years ago documented in oxygen isotope records of precipitation in Europe and Greenland. *Climate Dynamics* 14, 73–81.
- Groote, P.M., Stuiver, M., White, J.W.C., Johnsen, J., Jouzel, J., 1993. Comparison of oxygen isotope records from the GISP2 and GRIP Greenland ice cores. *Nature* 366, 552–554.
- Grove, J.M., 1988. *The Little Ice Age*. Methuen, London.
- Grove, J.M., Battagel, A., 1983. Tax records from western Norway as an index of Little Ice Age environmental and economic deterioration. *Climatic Change* 5, 265–282.
- Karlén, W., 1976. Lacustrine sediments and tree-limit variations as indicators of Holocene climatic fluctuations in Lapland: Northern Sweden. *Geografiska Annaler* 58A, 1–34.
- Karlén, W., 1981. Lacustrine sediment studies. *Geografiska Annaler* 63A, 273–281.
- Karlén, W., 1998. Climate variations and the enhanced greenhouse effect. *Ambio* 27, 270–274.
- Karlén, W., Bodin, A., Kuylenstierna, J., Näslund, J.-O., 1995. Climate of northern Sweden during the Holocene. In: Finkl jr., C.W. (Ed.), *Holocene Cycles. Climate, Sea Levels, and Sedimentation*. *Journal of Coastal Research* 17, 49–54.
- Karlén, W., Kuylenstierna, J., 1996. On solar forcing of Holocene climate: evidence from Scandinavia. *The Holocene* 6, 359–365.
- Karlén, W., Matthews, J.A., 1992. Reconstructing Holocene glacier variations from glacial lake sediments: studies from Nordvestlandet and Jostedalbreen-Jotunheimen, southern Norway. *Geografiska Annaler* 74, 327–348.
- Kjøllmoen, B., 1998. *Glasiologiske undersøkelser i Norge 1996 og 1997. Rapport 20, 1998, Norges vassdrags- og energiverk*. 134 pp.
- Klitgaard-Kristensen, D., Sejrup, H.-P., Hafliðason, H., Johnsen, S., Spurk, M., 1998. A regional 8200 cal. yr BP cooling event in northwest Europe, induced by final stages of the Laurentide ice-sheet deglaciation? *Journal of Quaternary Science* 13, 165–169.
- Kvamme, M., 1984. Vegetasjonshistoriske undersøkelser. In: Berge Meyer, O. (Ed.), *Breheimen-Stryn. Konesjonsavgjørende botaniske undersøkelser*. Botanical Institute, University of Bergen Report, Vol. 34, pp. 238–275.
- Kvamme, M., 1989. Vegetasjonshistoriske undersøkelser i Sprongdalen. In: Odland, A., Aarrestad, P.A., Kvamme, M. (Eds.), *Botaniske undersøkelser i forbindelse med vassdragsregulering i Jostedalen, Sogn og Fjordane*. Botanical Institute, University of Bergen Report, Vol. 47, pp. 166–202.
- Matthews, J.A., 1991. The late Neoglacial ('Little Ice Age') glacier maximum in southern Norway: new ¹⁴C dating evidence and climatic implications. *The Holocene* 1, 219–233.
- Matthews, J.A., 1994. Lichenometric dating: a review with particular reference to 'Little Ice Age' moraines in southern Norway. In: Beck, C. (Ed.), *Dating in Exposed and Surface Contexts*. University of New Mexico Press, Albuquerque, pp. 185–212.
- Matthews, J.A., Caseldine, C.J., 1987a. Arctic-alpine brown soils as a source of palaeoenvironmental information: further ¹⁴C dating and palynological evidence from Vestre Memurubreen, Jotunheimen, Norway. *Journal of Quaternary Science* 2, 59–71.
- Matthews, J.A., Caseldine, C.J., 1987b. Podzol development, vegetation change and glacier variations at Haugabreen, South Norway. *Boreas* 16, 215–230.
- Matthews, J.A., Dresser, P.Q., 1983. Intensive ¹⁴C dating of a buried palaeosol horizon. *Geologiska Föreningen i Stockholm, Förhandlingar* 105, 59–63.
- Matthews, J.A., Karlén, W., 1992. Asynchronous Neoglaciation and Holocene climatic change reconstructed from Norwegian glaciolacustrine sedimentary sequences. *Geology* 20, 991–994.
- Matthews, J.A., Shakesby, R.A., 1984. The status of the 'Little Ice Age' in southern Norway: relative age-dating of Neoglacial moraines with Schmidt hammer and lichenometry. *Boreas* 13, 333–346.
- McCarroll, D., 1989a. Potential and limitations of the Schmidt hammer for relative-age dating: field tests on Neoglacial moraines. Jotunheimen, southern Norway. *Arctic and Alpine Research* 21, 268–275.
- McCarroll, D., 1989b. Schmidt hammer relative-age evaluation of a possible pre-'Little Ice Age' Neoglacial moraine. Leirbreen, southern Norway. *Norsk Geologisk Tidsskrift* 69, 125–130.
- McCarroll, D., 1994. A new approach to lichenometry: dating single-age and diachronous surfaces. *The Holocene* 4, 383–396.
- Mottershead, D.N., Collin, R.L., 1976. A study of Flandrian glacier fluctuations in Tunsbergdalen, southern Norway. *Norsk geografisk Tidsskrift* 56, 413–436.
- Mottershead, D.N., Collin, R.L., White, I.D., 1974. Two radiocarbon dates from Tunsbergdal. *Norsk Geologisk Tidsskrift* 54, 131–134.
- Nesje, A., 1992. A piston corer for lacustrine and marine sediments. *Arctic and Alpine Research* 24, 257–259.
- Nesje, A., Dahl, S.O., 1991a. Holocene glacier variations of Blåisen. Hardangerjøkulen, central southern Norway. *Quaternary Research* 35, 25–40.
- Nesje, A., Dahl, S.O., 1991b. Late Holocene glacier fluctuations in Bevringsdalen, Jostedalbreen region, western Norway (ca 3200–1400 BP). *The Holocene* 1, 1–7.
- Nesje, A., Johannessen, T., 1992. What were the primary forcing mechanisms of high-frequency Holocene climate and glacier variations?. *The Holocene* 2, 79–84.
- Nesje, A., Kvamme, M., 1991. Holocene glacier and climate variations in western Norway: Evidence for early Holocene glacier demise and multiple Neoglacial events. *Geology* 19, 610–612.
- Nesje, A., Rye, N., 1993. Late Holocene glacier activity at Sandskardfonna. Jostedalbreen area, western Norway. *Norsk geografisk Tidsskrift* 47, 21–28.
- Nesje, A., Dahl, S.O., Løvlie, R., 1995. Late Holocene glacier and avalanche activity in the Alfoten area, western Norway: evidence from a lacustrine sedimentary record. *Norsk Geologisk Tidsskrift* 75, 120–126.
- Nesje, A., Kvamme, M., Rye, N., Løvlie, R., 1991. Holocene glacial and climate history of the Jostedalbreen region, western Norway; evidence from lake sediments and terrestrial deposits. *Quaternary Science Reviews* 10, 87–114.
- Nesje, A., Matthews, J.A., Dahl, S.O., Berrisford, M.S., Karlén, W., 1999. The lacustrine sedimentary succession in Jarbuvatnet: a continuous, high-resolution record of the Holocene glacier history of Flatebreen, SW Jostedalbreen area, western Norway, in preparation.
- O'Brien, S.R., Mayewski, P.A., Meeker, L.D., Meese, D.A., Twickler, M.S., Whitlow, S.I., 1995. Complexity of Holocene climate as reconstructed from a Greenland ice core. *Science* 270, 1962–1964.

- Roland, E., Haakensen, N., 1985. Glasiologiske undersøkelser i Norge 1982. Norges vassdrags- og elektrisitetsvesen, Vassdragsdirektoratet, Hydrologisk avdeling. Rapport nr. 1–85, 102 pp.
- Rye, N., Nesje, A., Lien, R., Blikra, L.H., Eikenæs, O., Hole, P.A., Torsnes, I., 1997. Glacial geology and deglaciation chronology of the area between inner Nordfjord and Jostedalbreen - Strynefjellet, western Norway. *Norsk Geologisk Tidsskrift* 77, 51–63.
- Röthlisberger, F., 1986. 10,000 Jahre Gletschergeschichte der Erde. Sauerländer, Aarau.
- Sandgren, P., Risberg, J., 1990. Magnetic mineralogy of the lakes in lake Ådran, eastern Sweden, and an interpretation of early Holocene water level changes. *Boreas* 19, 57–68.
- Schultz, M., Statterger, K., 1997. SPECTRUM: Spectral analysis of unevenly spaced paleoclimatic time series. *Computers and Geosciences* 23, 929–945.
- Snowball, I., 1993. Mineral magnetic properties of Holocene lake sediments and soils from the Kårsa valley, Lappland, Sweden, and their relevance to palaeomagnetic reconstruction. *Terra Nova* 5, 258–270.
- Snowball, I., Sandgren, P., 1996. Lake sediment studies of Holocene glacial activity in the Kårsa valley, northern Sweden: contrast in interpretation. *The Holocene* 6, 367–372.
- Snowball, I., Thompson, R., 1990. A mineral magnetic study of Holocene sedimentation in Lough Catherine, Northern Ireland. *Boreas* 19, 127–146.
- Sohlenius, G., 1996. Mineral magnetic properties of Late Weichselian-Holocene sediments from the northwestern Baltic Proper. *Boreas* 25, 79–88.
- Stuiver, M., Brazunias, T.F., 1989. Atmospheric ^{14}C and century-scale solar oscillations. *Nature* 338, 405–408.
- Stuiver, M., Brazunias, T.F., 1993. Sun, ocean, climate and atmospheric $^{14}\text{CO}_2$: an evaluation and spectral relationships. *The Holocene* 3, 289–305.
- Stuiver, M., Reimer, P.J., 1993. Extended ^{14}C data base and revised CALIB 3.0 ^{14}C age calibration program. *Radiocarbon* 35, 215–230.
- Stuiver, M., Grootes, P.M., Brazunias, T.F., 1995. The GISP2 $\delta^{18}\text{O}$ record of the past 16,500 years and the role of the Sun, ocean, and volcanoes. *Quaternary Research* 44, 341–354.
- Thompson, R., Oldfield, F., 1986. Environmental magnetism. George Allen & Unwin, London.
- Thompson, R., Batterbee, R.W., O'Sullivan, P.E., Oldfield, F., 1975. Magnetic susceptibility of lake sediments. *Limnology and Oceanography* 20, 687–698.
- Torske, N., 1996. Holocene vegetation, climate and glacier histories in the Jostedalbreen region, western Norway – palaeoecological interpretations from an alpine peat deposit. *Palaeoclimate Research* 20, 215–232.
- Torsnes, I., Rye, N., Nesje, A., 1993. Modern and Little Ice Age equilibrium-line altitudes on outlet valley glaciers from Jostedalbreen, western Norway: an evaluation of different approaches to their calculation. *Arctic and Alpine Research* 25, 106–116.
- Yiou, P., Baert, E., Loutre, M.F., 1996. Spectral analysis of climate data. *Surveys in Geophysics* 17, 619–663.
- Østrem, G., 1975. Sediment transport in glacial meltwater streams. In: Joplin, A.V., Macdonald, B.C. (Eds.), *Glaciofluvial and Glaciolacustrine Sedimentation*. Society of Economic Palaeontologists and Mineralogists Special Publication 23, pp. 101–122.
- Østrem, G., Dale Selvig, K., Tandberg, K., 1988. Atlas over breer i Sør-Norge. Norges vassdrags- og energiverk, Vassdragsdirektoratet. Meddelelse nr. 61 fra Hydrologisk avdeling.

Sediment fluxes from creep processes at Jomfrunet, southern Norway

IVAR BERTHLING, BERND ETZELMÜLLER, CHRISTINE KIELLAND LARSEN & KNUT NORDAHL



Berthling, I., Etzelmüller, B., Kielland Larsen, C. & Nordahl, K. 2002. Sediment fluxes from creep processes at Jomfrunet, southern Norway. *Norsk Geografisk Tidsskrift–Norwegian Journal of Geography* Vol. 56, 67–73. Oslo. ISSN 0029-1951.

Based on velocity measurements of surface and subsurface creep, sediment flux due to solifluction and ploughing boulder activity were estimated in a mid-alpine site in southern Norway (Finse, UTM185198). The results indicate geomorphic work performed by solifluction of approximately $9 \text{ Mjkm}^{-2} \text{ a}^{-1}$ and imply that sediment flux rates by solifluction under favourable conditions may be comparable to or exceed those of rapid mass movement obtained in more alpine environments.

Keywords: *Finse, ploughing boulder, sediment flux, solifluction, southern Norway*

I. Berthling & C. Kielland Larsen, Norwegian Water Resources and Energy Directorate, P.O. Box 5091 Majorstua, NO-0301 Oslo, Norway; B. Etzelmüller, Department of Physical Geography, University of Oslo, P.O. Box 1042 Blindern, NO-0316 Oslo, Norway; K. Nordahl, Statkraft Grøner AS, P.O. Box 400 Lysaker, NO-1327 Lysaker, Norway

Introduction

There are two debris transport systems in mountainous terrain: the fine sediment system and the coarse debris system (Caine 1974). On slopes, the fine sediment and coarse debris systems are essentially closed, with surficial material mainly redistributed and stored within the system. Exceptions are episodic events such as slushflows, debris flows, etc., which are capable of transporting debris directly to the valley bottom, where fluvial processes may transport parts of the delivered material out of the catchment boundaries. Creep processes are found within both the fine system (e.g. solifluction) and the coarse system (permafrost creep). In earlier studies of sediment budgets in alpine catchments, the fine sediment creep processes account for only a limited amount of total sediment transport (Rapp 1960; Caine 1976, 1986). However, this would depend on the scale of investigation and the relief of the landscape. In areas of less pronounced relief, and few free cliff faces and talus accumulations, creep can be expected to be relatively more important.

There are many field studies of solifluction process rates, particularly from alpine environments (Harris 1981), but there is potential bias in many of them if used to infer sediment transport rates. First, they are conducted mainly on solifluction lobes, and no information is given on movement rates outside such landforms or on slopes where solifluction lobes are less well developed (Harris 1981). Second, solifluction lobes form a system where displacement is normally largest in the rear or middle part of the lobe, along the length axis (e.g. Benedict 1970), so the exact position of measurement points may be important. Third, long-term studies (e.g. Gamper 1983; Veit et al. 1995) indicate large year-to-year variability in recorded displacement rates.

The objective of this article is to estimate the sediment transport rates from slow mass-wasting processes at a small site where solifluction is widely distributed and active. We chose a mid-alpine site at Finse, southern Norway, where morphological expressions of the solifluction process are dominant small-scale landforms (Larsen 1999). In addition, ploughing boulders, a phenomenon closely related to

solifluction (e.g. Ballantyne 2001), are widespread (Berthling et al. 2001a, b). In this article, we aim to evaluate the role of these features in the sediment transport system.

Setting

Our study was undertaken on the small mountain Jomfrunet at Finse, southern Norway. Finse is situated along the Oslo–Bergen railway line at the northern margin of the Hardangervidda mountain plateau (UTM MN185198, Fig. 1). The valley bottom lies at an altitude of about 1200 m a.s.l. and the surrounding mountains reach altitudes of above 1800 m a.s.l. The bedrock in the lower part of the valley consists of Finse granite on the northern side and of gneiss on the central and southern parts of the valley (Sigmond et al. 1984). Both belong to the Precambrian basement rocks, which were eroded down to a peneplain at the end of the Precambrian. This geological peneplain is today partly exhumed, and can be seen as a bench on both sides of the valley at about 1350 m. The basement rocks are overlain by phyllite originating from Cambrium–Silurian sedimentary rocks modified during the Caledonian orogenesis.

Mean annual temperature for the period 1969–1990 was -2.0°C , while mean yearly precipitation (1970–1992) was 1027 mm (DNMI). Snow cover, which usually starts accumulating in October and lasts until June or early July, has a high spatial variability because of snowdrifting. Permafrost is found above about 1600 m a.s.l. and, in connection with perennial snow banks, also well below this level (Etzelmüller et al. 1998).

Our study site is the mountain Jomfrunet rising to 1470 m a.s.l. (Fig. 1). Total relief is about 250 m on the southern side, but considerably less to the north. Vegetation cover on the southern and western slopes is continuous, except where bedrock outcrops and in areas of semi-perennial snow banks. On the southern side of the mountain, the subcambrian peneplain is an important dividing line. The peneplain itself forms a wide platform along part of the slope. Beneath it, there are distinct but mainly small granitic cliffs. Surface boulders are common, deriving partly from weathering of the

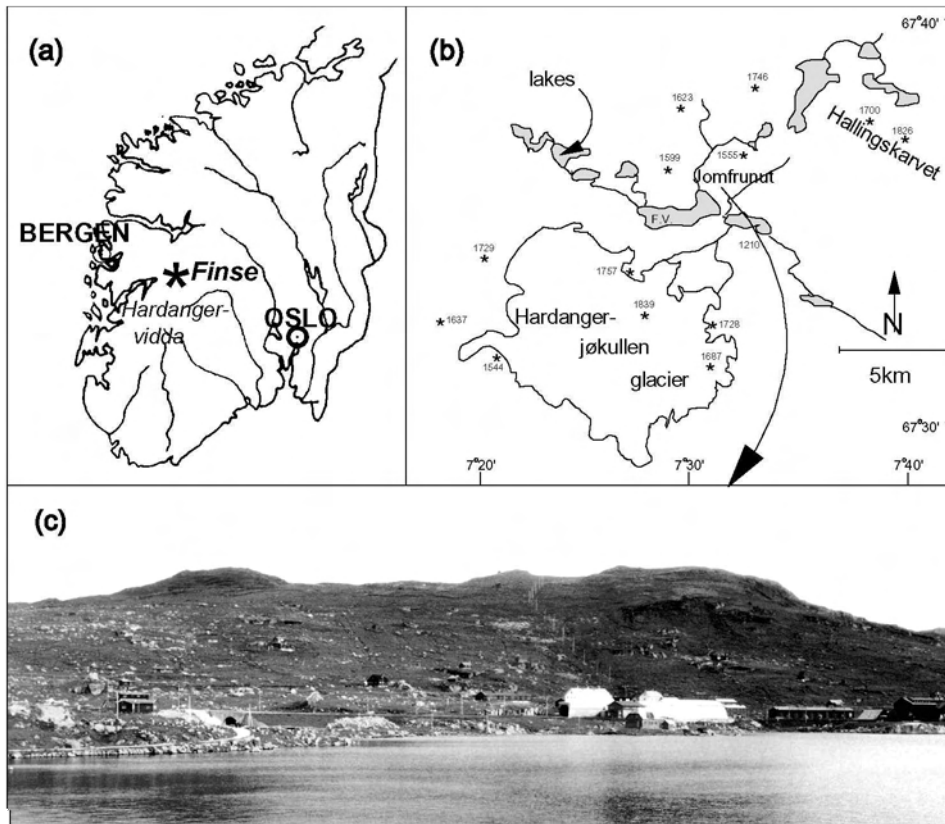


Fig. 1. Key map with picture showing the southwestern slope of Jomfrunut. The railway station in the foreground is located 1222 m a.s.l., while the top of Jomfrunut is 1471 m a.s.l.

cliffs. Above the peneplain, there are rugged cliff walls up to 30 m in height on the southern and southeastern sides of the mountain. Smaller bedrock exposures and outcrops are common, especially towards the top. There are few surface boulders above the peneplain. Extensive, mainly perennial, snow patches dominate the eastern and northern sides of Jomfrunut.

The sediment transport system at Jomfrunut

Scree slopes on Jomfrunut are rare, and with respect to mass transport the main importance of the coarse debris system is probably the delivery of boulders from weathering on granite outcrops, which develop into ploughing boulders. In the strict sense of Caine (1974), the ploughing boulders themselves belong to the coarse debris system. Nevertheless, because of the close connection between ploughing boulders and solifluction features (cf. Ballantyne 2001, Berthling et al. 2001a, b), we prefer to treat them as part of the fine sediment system. No permanent streams are found, and ephemeral streams during snowmelt and rainstorms commonly drain on top of a vegetation cover, inhibiting surface erosion. An exception is found in the large areas of more or less perennial snow banks on the northern and eastern sides of Jomfrunut, where lack of vegetation sometimes leads to local erosion. This is the case particularly where upslope streams melt a channel underneath a snow patch. However, qualitative observations, according to quantitative studies elsewhere,

suggest that much of the eroded material is redeposited within the system. Thus, fluvial processes are considered of minor importance for sediment export, but redistribution of material may be expected in years of large snowmelt. There are some geomorphological signs of relict earth slides on the south slopes of Jomfrunut, but their vegetation cover suggests that these are rare. In May 1996, a heavy rainstorm on still partly frozen ground triggered several earth slides in the area, five of which took place on Jomfrunut. This provided an opportunity to estimate the debris transport involved in rapid mass movements, although the frequency of such events is difficult to assess. Five years after the event, no vegetation cover has developed in the affected areas.

Methods and measurement programme

Transport rates for the creep processes and rapid mass movements were established from measurements of surface displacement and subsurface displacement profiles. Some extrapolation procedure had to be adopted to assign appropriate creep rates to different parts of the slope. Surface displacements as a result of solifluction are generally expected to vary along a broad range in response to differences in frost penetration, water availability, frost susceptibility of sediments, slope and vegetation cover. Surface markers were therefore established in as wide a range of site characteristics as possible. A total of 71 targets were measured in the period 1997 to 1998. An additional 21

targets were measured from 1973 to 1975 and re-measured in 1996, 1997 and 1998. Data on soil characteristics, soil moisture, slope and vegetation cover were collected in each of these areas. Further data were gathered from existing geomorphological maps (Knudsen 1986; Pedersen 1989).

A relatively large number of surface markers were required, while expected year-to-year displacements were just a few centimetres or less. Tape measurements were used to achieve both high accuracy and speed of measurement. The benchmarks for these measurements were hooks drilled into bedrock – the hook ensuring a rigid connection between benchmark and tape, and enabling measurements to be carried out by one person only. Anchor screws for gypsum walls served as surface targets; these were inserted through plastic plates and into the ground. When the screws are fastened, the anchor folds out within the soil, thus ensuring a firm position of the target, especially where there is vegetation. The cross for the screwdriver serves as the point for measurement, so it was possible to achieve a reading below millimetre level. Each surface target was measured from two benchmarks, the coordinates of which were found using GPS or traditional surveying. By considering the target movement to be along a plane defined by the two benchmarks and the target position, the target displacement vector could be found from tape measurements on different dates. Using a steel tape, measurements were performed using a fixed drag force and corrected for temperature. The method is sensitive to wind conditions and requires a large number of bedrock outcrops where benchmarks can be established close to the desired target points. The old measurement series of surface boulder displacements was performed with tape measurements from one bedrock benchmark to painted crosses on the boulder. The ploughing boulders were investigated using traditional surveying from two benchmarks in bedrock and differential carrier-phase GPS (Berthling et al. 2001b).

Existing data on vertical displacement profiles from Jomfrunut, collected by re-excavating inserted Rudberg columns (Østensen 1977), were utilised and a few new columns were inserted and re-excavated.

Concerning rapid mass movements, the dimensions of each slide were measured and the volume of the slide scar and the accumulation area (where possible) were calculated. Where the accumulation had a well-defined centre of mass, the mean travel distance was calculated as half the length of the slide scar plus the distance from the starting point of the accumulation to the centre of mass. In the other cases, travel distance was estimated based on length of both slide scar and accumulation area. The angle of the slide scar provided a basis for conversion to vertical transport.

Results

Surface sediments and site characteristics

The sediments are generally frost susceptible, belonging to Beskow class (1932) 2 or 3. Soil samples from each area were dried and the weight difference used as a measure of soil moisture status. According to assumed effect on soil movement, the vegetation was classified within three classes on a scale from 4 (high restriction on movement) to 2 (little restriction on movement). Bare ground has no restriction on movement and was classified as class 1. Surface slope was measured at all locations where displacement measurements were performed, and varied between 5° and 48°, with a mean of about 20°.

Surface and subsurface solifluction displacements

Targets for surface displacement measurements were located in 15 different areas (Nordahl 1999); most of the areas chosen were those where no or only minor and irregular solifluction features were found. Only areas J and K represent solifluction features (Table 1). K is a well-defined medium-sized solifluction lobe and J is a large solifluction terrace. Despite similar surface characteristics, a large variability in surface movement was recorded within each area (Table 1). Furthermore, no correlation between average surface movements and the corresponding parameters describing soil and

Table 1. Measured solifluction displacement in mm from 1997–1998, mean slope and number of measurements in the different areas.

Area	Slope (gon)	Displacement (mm)			N	Standard deviation	Morphology
		Average	Max.	Min.			
A	34	11.0	21	2	5	7	No
C	40	16.3	26	4	6	8	No
E	21	14.2	21	2	5	7	Small, irregular lobes
F	48	18.5	23	15	4	3	No
G	20	6.0	10	2	4	4	No
H	11	7.8	11	4	5	4	No
I	10	21.2	67	3	5	26	Snow patch
J	18	39.9	93	0	27	21	Snow patch / lobe
K	20	38.5	62	9	4	26	Lobe
L	20	15.2	26	5	5	9	Small, irregular lobes
N	10	6.0	11	1	4	4	No
O	14	29.5	38	2	4	8	Snow patch
P	27	6.5	11	2	2	6	No
Q	5	6.8	9	5	4	2	No
R	29	5.3	9	3	4	3	No

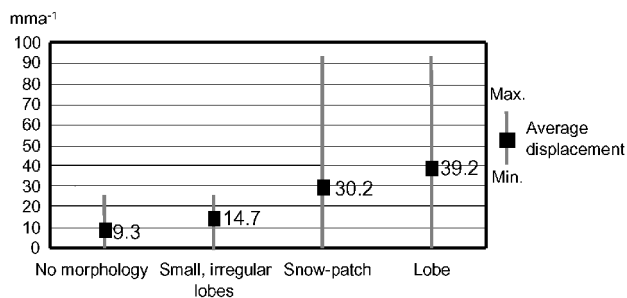


Fig. 2. Mean displacement and range of values for targets grouped according to surface characteristic.

surface conditions was found. However, it was apparent that markers associated with solifluction lobes and/or snow patches were moving faster than those with no association to any lobe form (Fig. 2). The limited number of areas associated with lobes and snow patches reduces the reliability of this result, but the values are nevertheless within the range expected from published results elsewhere (e.g. Harris 1981).

The surface boulders measured in the period 1973 to 1975 were mainly located in area J. Re-measured in 1996, 1997 and 1998 (Fig. 3), the boulders showed a large year-to-year variability in displacement rates. Thirteen Rudberg columns dug out in 1975 (Østensen 1977) and three in 1998, each inserted for 2 years, gave an average displacement depth of 0.35 m.

Solifluction sediment fluxes

A general problem in studies of sediment fluxes as a result of creep processes is how to extrapolate a limited number of point measurements to cover the area of investigation. One approach has been to take an average of data for dry areas, moist areas and solifluction features and multiply by the corresponding areas (Caine 1986). Our results indicate that creep displacements can be highly variable even within areas of homogeneous surface characteristics, so extrapolations based on limited sets of data can yield erroneous results. We therefore used the relationship shown in Fig. 2 and assigned a mean value for each fractional area of solifluction features and areas of snow patches. The ‘no morphology’ and ‘small, irregular lobes’ classes were merged with respect to both displacement and areas. The area of solifluction features was found from a map of periglacial landforms on Jomfrunet (Knudsen 1986). Included was an upslope area corresponding to an arbitrary ‘catchment’ of each or a complex of features. The rationale for this originated from observations at Jomfrunet of extending flow above a solifluction lobe, and compressive flow on the lobe itself, showing that the solifluction form is a consequence of sediment deposition. The area of perennial snow patches was found from the same map; the remaining areas were classified as lacking morphology or with small, irregular solifluction lobes. Flat areas and areas of exposed bedrock are considered insignificant.

The volume involved in solifluction displacement was calculated by considering a generalized depth profile, so that across unit width the flux is $Q = 0.5 \times 0.35 \times v$. Here, 0.35 is

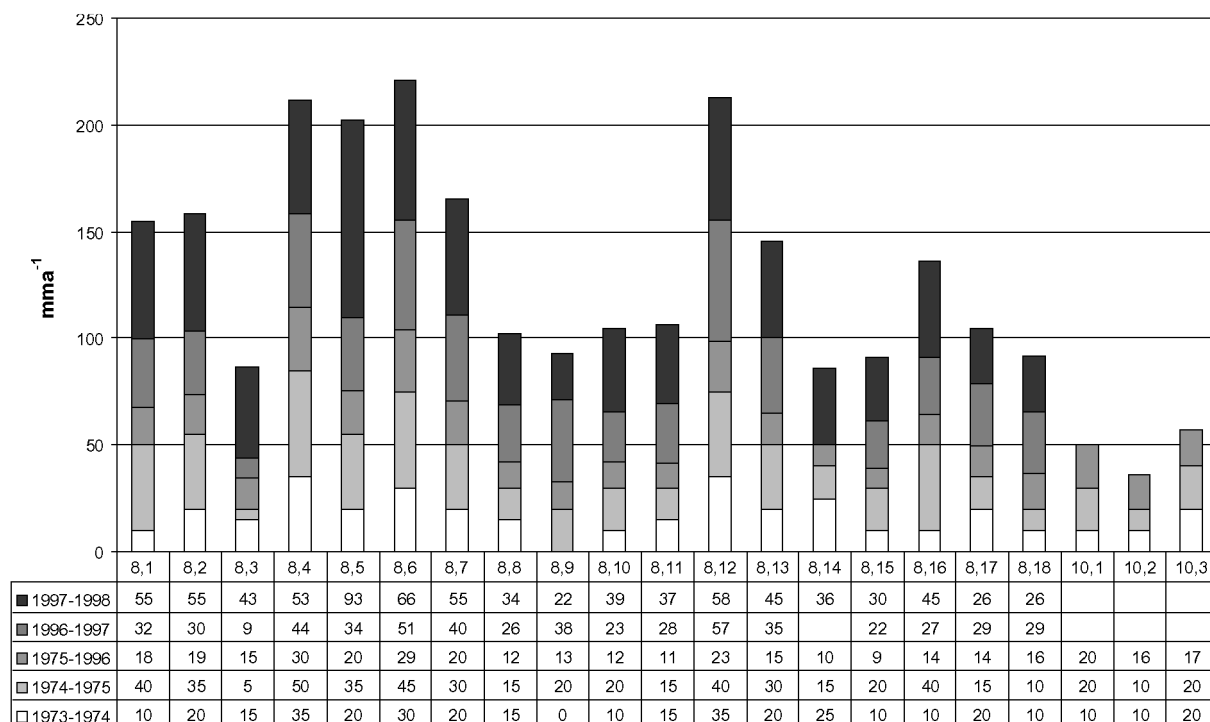


Fig. 3. Displacement in mma^{-1} for painted boulders during five measurement periods.

Table 2. Geomorphic work performed by solifluction, calculated as $\Delta E = V\rho g(d \sin\theta)$, where V is volume, ρ is density, g is the acceleration of gravity, d is slope distance and θ is slope angle. The dry weight density of the soil was set to 1640 kgm^{-3} .

	Solifluction	Snow patches	No or small irregular lobes	Sum
Velocity (ma^{-1})	0.039	0.03	0.012	
Area (km^2)	0.057	0.12	0.87	1.05
Slope (gon)	17	10	13	
Work ($\text{MJkm}^{-2} \text{a}^{-1}$)	1.54	1.72	5.81	9.07

the mean depth of movement (m) and v is the velocity (ma^{-1}) for each fractional area. Each of the three final classes was also assigned a mean slope for conversion to vertical transport. The total specific transport is expressed in Table 2 as geomorphic work ($\text{Jkm}^{-2} \text{a}^{-1}$) (Caine 1976). On Jomfrunet, total geomorphic work from solifluction is about $9 \text{ MJkm}^{-2} \text{a}^{-1}$. Solifluction lobes account for only 17% of the work, while areas of no morphology or small irregular lobes contribute most (64%).

The displacements recorded in 1997–1998 were above average for the period 1973–1998 (Fig. 3). It might therefore be necessary to scale down the final results. On the other hand, using data from Rudberg columns recording displacements during 1996–1998, the ratio of sediment flux into a large solifluction lobe and a conservative estimate of its volume gave an approximate age for the lobe of 5000 years (Berthling 2001). Considering past environmental conditions at this site, a higher age for the lobe is unlikely; the higher rates may therefore be more correct for long-term conditions.

Ploughing boulder mass transfer

The velocity values for the three measurement periods (1989–1993, 1993–1994 and 1994–2000) were not consistent, showing much higher values in 1993–1994 (Berthling et al. 2001a, b). When estimating the ploughing boulder mass transfer, we used the average yearly displacement values for the period 1989–1994, as this is the most complete series and the average displacements during this period are not much different from corresponding values for 1989–2000.

All boulders visible within 5 selected $100 \times 100 \text{ m}$ squares on a detailed map of the ploughing boulders (Fig. 2 in Berthling et al. 2001b) were counted per size class to find the total volume of boulders. The size class corresponds to their representation on this map (dot, circle or traced circumference). The boulders investigated for annual displacement were classified according to these size classes, and the mean displacement for each category was calculated (Table 3). The classes show differences in mean velocity, with larger boulders giving higher velocities, but the absolute differences are small. Furthermore, the number of monitored boulders in each size class is small, and any size–velocity relation is therefore not well documented. It is supported, however, by a possible correlation between boulder displacement and height of the boulder (Berthling et al. 2001b), which is probably physically justified because of the influence of snow cover on frost penetration.

Table 3. Measured ploughing boulder velocities for the period 1989–1994, categorised in size classes. Only boulders showing a downslope trend were chosen. Boulders associated with ploughing boulder mounds were also excluded. Length, width and height refer to field measured boulder size (in metres), where available.

Pl. b. no.	Velocity (mma^{-1})			Dimensions (m)		
	Size 1	Size 2	Size 3	Length	Width	Height
1			8.6	2.8	1.9	1.3
2		4.0				
3			10.0	2.1	2.0	0.9
4			9.4			
5			8.4	1.8	2.5	0.8
6		5.6				
7		19.0				
8	9.8					
9	5.6					
11			12.0			
13	5.4			1.0	0.6	0.3
15	5.0			1.1	0.55	0.3
16		3.4				
17	7.6					
22			15.0			
26		7.0				
27		5.2		1.6	1.3	0.7
28		9.8				
29		8.6		1.2	0.7	0.3
32			11.2	4.5	4.0	2.5
34		5.8		1.4	0.7	0.6
Mean	6.7	7.6	10.7			

The volume of the boulders was calculated as $V = \pi R_b^2 h_b$, where R_b is boulder radius and h_b is boulder height (Table 4). Density of the ploughing boulders was set to 2700 kgm^{-3} , and the dry density of soil in the ploughing boulder mound, as for soliflucted soils, to 1640 kgm^{-3} . Vertical velocity was found from a mean slope angle of 15° . Total volume of ploughing boulder mounds was calculated as $V = \frac{1}{2}\pi(R_m^2 - R_b^2)h_m n$, where $R_m = 4R_b/3$, $h_m = R_m/2$ and n is the number of boulders in size classes 2 and 3, respectively (Table 4). The velocity of the ploughing boulder mound was set equal to that of the boulder. Size class 1 was omitted from this calculation because these boulders mainly have small, even lacking, signs of ploughing.

The area investigated for ploughing boulder movement does not coincide with that of the solifluction movement. However, as all the boulders considered are not necessarily ploughing boulders and the number of boulders on this site is

Table 4. Parameter values and estimates of ploughing boulder sediment transfer. The calculations are explained in the text. Number of boulders, their total volume and specific geomorphic work refer to an investigated area of $50,000 \text{ m}^2$. The density of the boulders was set to $2,700 \text{ kgm}^{-3}$ and the dry weight density of the ploughing boulder mounds to 1640 kgm^{-3} .

	Size 1	Size 2	Size 3	SUM
Radius (m)	0.25	0.7	1.5	
Height (m)	0.33	0.5	1.2	
No. of boulders	548	368	70	986
Total volume (m^3)	36	283	594	913
Volume boulder mound (m^3)		103	192	295
Work boulders ($\text{MJkm}^{-2} \text{a}^{-1}$)	0.03	0.31	0.90	1.24
Work incl. mound	0.03	0.37	1.08	1.48

Table 5. Calculation of vertical debris transport resulting from rapid mass movements in May 1996. The vertical velocity is calculated based on the slope of the slide scar area. Mass transport is calculated from the dry density of the soil of $1,640 \text{ kg m}^{-3}$. Specific transport calculated from a total area of 1.05 km^2 (corresponding to the investigated area for solifluction displacement, Table 2).

Slide no.	Slope (gon)		Volume (m^3)		Along-slope travel distance	Geomorphic work (MJ)
	Scar	Accumulation	Scar	Accumulation		
1a	41	29	22	23	7.5	1.45
1b	37	23	245	247	20.5	40.1
2	40	26	53	54	14.5	6.66
3	37	32	11	Not measurable	10	0.85
4	40	31	9	Not measurable	6	0.44
5	33	21	12	Not measurable	15	1.29
SUM (specific value – MJ km^{-2})						48.3
SUM (specific value – $\text{MJ km}^{-2} \text{ a}^{-1}$)*						0.97

* Based on a suggested approximate return period of 50 years.

large, the results are a probable maximum value for the role of ploughing boulder mass transfer in this environment. The geomorphic work of the ploughing boulders is about $1.5 \text{ MJ km}^{-2} \text{ a}^{-1}$, of which the ploughing boulder mounds account for 16%.

Rapid mass movements

Key parameters for the investigated shallow slides and estimated mass transport are given in Table 5. The specific geomorphic work as a result of rapid mass movements in 1996 was about 48 MJ km^{-2} . Such an event probably requires combinations of a heavy rainstorm and still partly frozen ground free of snow. The return period of such events is difficult to assess, but we know of no other reports on earth slides here; this area was regularly employed for scientific investigations and education in physical geography in the 1960s. A frequency of about 50 years is suggested as an approximation, but this is speculative. Nevertheless, it implies that sediment transport due to rapid mass movements is low at Jomfrunet in comparison with solifluction.

Discussion

Of the investigated mass wasting processes on Jomfrunet, solifluction is dominant with respect to geomorphic work. Despite the great number of both small and large ploughing boulders in parts of the investigated area, the work done by the ploughing boulders is almost an order of magnitude less than that of solifluction. The geomorphic work performed by the earth slides is below that of the ploughing boulders if the return period of such events has not been overestimated.

The site chosen for these investigations may be considered especially favourable for solifluction processes. The phylitic bedrock is broken down, either from glacial processes or weathering, to a frost-susceptible residual with individual flake-like fragments. A generally wet environment provides a high groundwater level when the soil starts to freeze in autumn, while the deep snow cover leads to low temperature gradients, slow frost penetration and probably promote substantial frost heaving. Thaw consolidation in excess of

10 cm was reported from a solifluction lobe underneath a thick snow patch at this site by Berthling et al. (2000), while the depth of frozen ground measured during thawing was only 35 cm. The results presented are therefore generally not representative of a mid-alpine environment. Instead, they are indicative of the upper range of sediment transport by solifluction.

The specific solifluction sediment fluxes on Jomfrunet are about 2.5 times larger than in Kärkevagge, (Rapp 1960; corresponding values in $\text{MJ km}^{-2} \text{ a}^{-1}$ from Barsch & Caine 1984) and in Williams Lake Basin (Caine 1976). This is not too surprising, considering the fact that solifluction takes place all over Jomfrunet but is restricted to smaller areas in the studies referred to above. However, compared to the rapid mass movements reported in these studies, only the mudflow values from Kärkevagge are very much larger than the solifluction sediment fluxes reported here. In regions of moderate relief and slope, and under favourable conditions, not only may solifluction be a relatively more important process for sediment transfer than rapid mass movements, it may also cause sediment fluxes comparable to those from rapid mass wasting processes in more alpine environments. The results presented here may therefore be important for understanding long-term evolution of gentle slopes in present and former periglacial areas.

Conclusions

The following conclusions can be drawn from our study:

- The geomorphic work performed by solifluction is about $9 \text{ MJ km}^{-2} \text{ a}^{-1}$ at our site.
- The geomorphic work performed by ploughing boulders and earth slides is much less, but still a significant contribution to sediment transfer.
- Solifluction may give sediment fluxes comparable to rapid mass wasting processes in more alpine environments.

Acknowledgements.—This article is based on I. Berthling's PhD study supervised by Professor J. L. Sollid, to whom it is dedicated in honour of his work in glacial and periglacial geomorphology. We thank T. Eiken for

help with setting up the measurement programme and L. Sørbel at the Department of Physical Geography, University of Oslo for valuable discussions and field data from the area. E. Leslie at the Alpine Research Station at Finse was always helpful during our visits to Finse.

Manuscript submitted 20 January 2002; accepted 8 April 2002

References

- Ballantyne, C. K. 2001. Measurement and theory of ploughing boulder movement. *Permafrost and Periglacial Processes* 12, 267–288.
- Barsch, D. & Caine, N. T. 1984. The nature of mountain geomorphology. *Mountain Research and Development* 4, 287–298.
- Benedict, J. B. 1970. Downslope soil movement in a Colorado Alpine region: rates, processes and climatic significance. *Arctic and Alpine Research* 2, 165–226.
- Berthling, I. 2001. Slow periglacial mass-wasting processes and geomorphological impact. Case studies from Finse, southern Norway and Prins Karls Forland, Svalbard. PhD thesis. Series of dissertations submitted to the Faculty of Mathematics and Natural Sciences, University of Oslo, No. 113.
- Berthling, I., Eiken, T. & Sollid, J. L. 2001a. Frost heave and thaw consolidation of ploughing boulders in a mid-alpine environment, Finse, southern Norway. *Permafrost and Periglacial Processes* 12, 165–177.
- Berthling, I., Eiken, T., Madsen, H. & Sollid, J. L. 2001b. Downslope displacement rates of ploughing boulders in a mid-alpine environment: Finse, southern Norway. *Geografiska Annaler* 83 A, 103–116.
- Beskow, G. 1935. Tjälbildningen og tjällyftningen med särskild hänsyn til vägar og järnvägar. *Sveriges Geologiska Undersökning, Arsbok* 26, Ser. C, No. 375.
- Caine, N. 1974. The geomorphic processes of the alpine environment. Ives, J. D. & Barry, R. G. (eds.) *Arctic and Alpine Environments*, 721–748. Methuen, London.
- Caine, N. 1976. A uniform measure of subaerial erosion. *Geological Society of America Bulletin* 87, 137–140.
- Caine, N. 1986. Sediment movement and storage on alpine slopes in the Colorado Rocky Mountains. Abrahams, A. D. (ed.) *Hillslope Processes*, 115–137. Allen & Unwin, London.
- Etzelmüller, B., Berthling, I. & Sollid, J. L. 1998. The distribution of permafrost in Southern Norway – a GIS approach. *7th International Conference on Permafrost (Yellowknife, 23–27 June 1998)*, Collection Nordicana 57, 251–257. Centre d'études nordiques, Université Laval, Québec.
- Gamper, M. 1983. Controls and rates of movement of solifluction lobes in the Eastern Swiss Alps. *Proceedings, Fourth International Conference on Permafrost*, 328–333.
- Harris, C. 1981. *Periglacial Mass-Wasting. A Review of Research*. Geo Abstracts, Norwich. 204 pp.
- Knudsen, C. 1986. Frostjordsformer på Jomfrunut. Hovedoppgave (Master's thesis, in Norwegian). Department of Physical Geography, University of Oslo.
- Larsen, C. K. 1999. Digital terrengeanalyse som verktøy for å analysere relasjoner mellom periglasielle former, overflatematerial og topografi. Eksempel fra Jomfrunut, Finse. Hovedoppgave (Master's thesis, in Norwegian). Department of Physical Geography, University of Oslo.
- Nordahl, K. 1999. Solifluksjon på Jomfrunut, Finse. Hovedoppgave (Master's thesis, in Norwegian). Department of Physical Geography, University of Oslo.
- Pedersen, A. E. 1989. En studie av sibebløkker på Finse, med vekt på bevegelsesmålinger. Hovedoppgave (Master's thesis, in Norwegian). Department of Physical Geography, University of Oslo.
- Rapp, A. 1960. Recent development of mountain slopes in Kärkevagge and surroundings, Northern Scandinavia. *Geografiska Annaler* 42, 1–200.
- Sigmond, E., Gustavson, M. & Roberts, D. 1984. Berggrunnskart over Norge – 1:1000000 (Bedrock Geology of Norway). Geological Survey of Norway (NGU), Trondheim.
- Veit, H., Stügl, H., Emmerich, K.-H. & John, B. 1995. Zeitliche und räumliche Variabilität solifluidaler Prozesse und ihre Ursachen – Eine Zwischenbilanz nach acht Jahren Solifluktionmessungen (1985–1993) an der Messstation 'Glorer Hütte', Hohe Tauern, Österreich. *Z. Geomorph. N.F. Suppl. Bd.*, 99, 107–122.
- Østensen, U. E. S. 1977. Frostjordsformer på Jomfrunut, Finse. Hovedoppgave (Master's thesis, in Norwegian). Department of Physical Geography, University of Oslo.

Mountain permafrost distribution in Dovrefjell and Jotunheimen, southern Norway, based on BTS and DC resistivity tomography data

KETIL ISAKSEN, CHRISTIAN HAUCK, ESPEN GUDEVANG, RUNE S. ØDEGÅRD & JOHAN LUDVIG SOLLID



Isaksen, K., Hauck, C., Gudevang, E., Ødegård, R. S. & Sollid, J. L. 2002. Mountain permafrost distribution in Dovrefjell and Jotunheimen, southern Norway, based on BTS and DC resistivity tomography data. *Norsk Geografisk Tidsskrift—Norwegian Journal of Geography* Vol. 56, 122–136. Oslo. ISSN 0029-1951.

The influence of climate and topography on the distribution of permafrost within the Dovrefjell and Jotunheimen areas, southern Norway, is analysed. A dataset of 972 BTS (bottom temperature of winter snow) measurements was analysed in relation to altitude, potential direct incoming radiation, aspect, snow depth, curvature and slope. To confirm and characterise permafrost-transition zones indicated from the BTS measurements, miniature temperature data-loggers, borehole temperatures, one-dimensional DC resistivity soundings and two-dimensional DC resistivity tomography were used. In addition, small-scale variance analyses upon the BTS values were performed using spatial-statistical methods. Results confirm that BTS values are highly correlated with altitude. Based on analysis of BTS data, the lower limit of possible permafrost is 1490 m a.s.l. on Dovrefjell and 1460 m a.s.l. in Jotunheimen. The relation between altitude and BTS suggests that the climate conditions on Dovrefjell and in Jotunheimen are similar with respect to permafrost distribution. Potential direct incoming radiation (PR) has a minor influence on BTS. A significant correlation between both surface moisture and surface type conditions in summer and BTS measurements were found. The results from Jotunheimen suggest that 20–45% of the variance in BTS results that are not explained by altitude are explained by small-scale spatial variance within a 20–30 m range. The results from the BTS measurements and the two-dimensional DC resistivity tomography were highly consistent.

Keywords: *BTS, DC resistivity tomography, permafrost distribution*

Ketil Isaksen, Norwegian Meteorological Institute, P.O. Box 43 Blindern, NO-0313 Oslo, Norway. E-mail: ketil.isaksen@dnmi.no. Christian Hauck, Graduiertenkolleg Natural Disasters, University of Karlsruhe, Am Fasanengarten, DE-76128 Karlsruhe, Germany. E-mail: hauck@imb.uni-karlsruhe.de. Espen Gudevang, Norwegian Mapping Authority, Sogn og Fjordane County-department, P.O. Box 9, NO-6861 Leikanger, Norway. E-mail: espen.gudevang@statkart.no. Rune S. Ødegård, Gjøvik University College, P.O. Box 191, NO-2802 Gjøvik, Norway. E-mail: rune.oedegaard@hig.no. Johan Ludvig Sollid, Department of Physical Geography, University of Oslo, P.O. Box 1042 Blindern, NO-0316 Oslo, Norway. E-mail: j.l.sollid@geogra.uio.no

Introduction

The term ‘mountain permafrost’ is increasingly being used to define both *alpine permafrost* (traditionally referred to permafrost existing at high altitudes in middle and low altitudes) and *polar mountain permafrost*, which has not conventionally been regarded as ‘alpine permafrost’ (French 1996). Permafrost occurrences in the world mountain ranges are widespread, but scientific investigation only started during the past few decades (Haeberli et al. 1993). Because mountain permafrost is thermally defined, it is very sensitive to climate changes. Degradation of permafrost may lead to thaw settlement and reduction in the stability of mountain slopes (e.g. Harris et al. 2001a). Where buildings and other installations are underlain by permafrost, their foundations may be directly affected by ground thawing (Haeberli 1992, Haeberli et al. 1993). Slow thaw of deeper subsurface materials may provoke larger-scale instability on steeper slopes in areas previously considered stable (Dramis et al. 1995). It is therefore important to investigate the marginal permafrost areas in relation to variation in both space and time. Equally important is an understanding of the dominant processes for permafrost development and degradation.

Measurement of the bottom temperature of winter snow (BTS) has been used as a well-established method during the past 30 years for mapping of mountain permafrost distribution in the Alps (e.g. Haeberli 1973, Haeberli & Patzelt 1982, Hoelzle 1992, Imhof et al. 2000). An empirical relation has been found to exist between the BTS and mountain

permafrost based on three temperature classes (cf. Hoelzle 1992).

The spatial distribution of BTS measurements means that there is a potential to analyse permafrost distribution in relation to terrain parameters and remotely sensed data. Predictive models of BTS can, in this way, be used indirectly to develop permafrost distribution models (e.g. Hoelzle et al. 2001, Eitzelmüller et al. 2001, Gruber & Hoelzle 2001).

Geophysical methods have long been recognised as suitable tools for mapping and characterising permafrost (for a review, see Scott et al. 1990). In the European Alps, application of the two-dimensional DC resistivity tomography method has developed only recently. The method relies on the fact that the resistivity of frozen debris or bedrock is higher than that of the same material in the unfrozen state. The method has been used in the European Alps with excellent results (e.g. Hauck & Vonder Muhl 1999a, 1999b, Kneisel et al. 2000, Vonder Muhl et al. 2000).

The main aim of this paper is to better understand the influence of climate and topography on the distribution of permafrost within the Dovrefjell and Jotunheimen areas, southern Norway (Fig. 1). Earlier studies in Jotunheimen (King 1982, 1983, 1984, Harris & Cook 1986, Ødegård et al. 1992, 1996, Isaksen et al. 2001) show that permafrost is widespread at high altitudes. Ødegård et al. (1996) suggested that BTS depends more on altitude and less on exposure and slope in contrast to results from the Swiss Alps (e.g. Hoelzle 1992). However, more measurements were needed to draw general conclusions. The dataset used in the present study

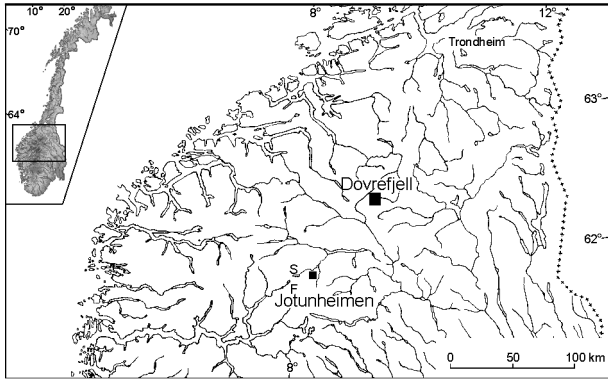


Fig. 1. Location map, showing the two study areas (black quadrangles) on Dovrefjell (62°20'N, 9°20'E; 75 km²) and in Jotunheimen (61°40'N, 8°25'E; 38 km²). The letters S and F refers to locations of the meteorological stations at Sognefjell and Fannaråken, respectively.

consists of a total of 972 BTS measurements carried out in different exposures and altitudes in the two study areas. In addition, results from miniature temperature data-loggers, borehole temperatures, one-dimensional DC resistivity soundings and two-dimensional DC resistivity tomography are used to confirm and characterise the mountain-permafrost transition zones indicated by the BTS analyses. The dependence of permafrost based on differences in small-scale surface characteristics, such as snow cover, type of

superficial material and the moisture conditions, are also presented. The BTS measurements on Dovrefjell and in Jotunheimen were performed over 7 and 3 winter seasons, respectively, in the 1990s. The resistivity measurements were performed in summers 1998–2001.

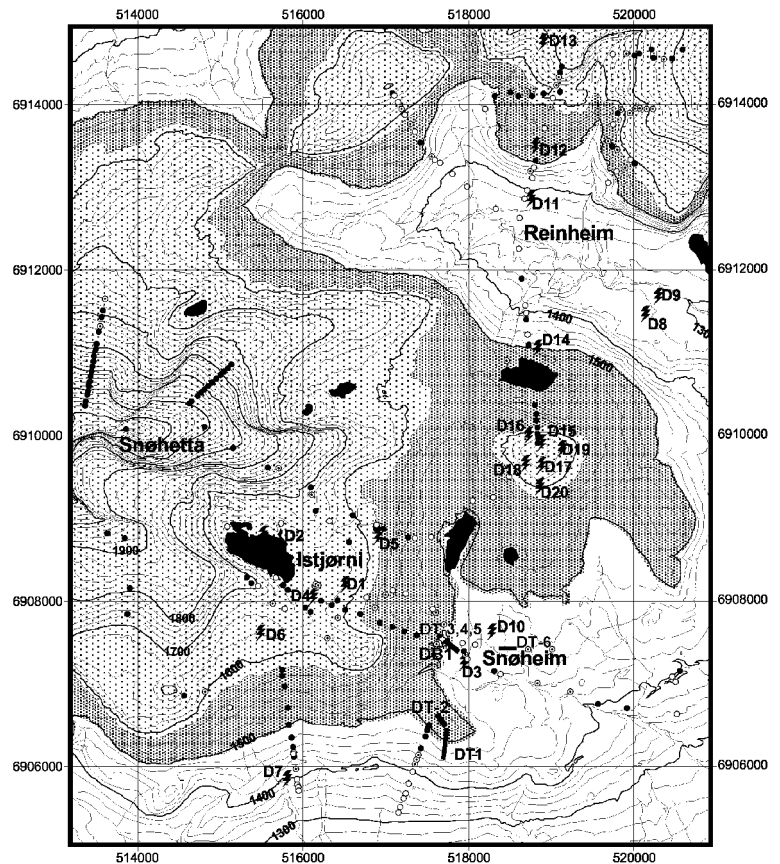
Study area

Dovrefjell

Climate. – A mean air-temperature lapse rate for the area was calculated based on background measurements from 18 climate stations in the vicinity (Aune 1993). In addition, measurements from the meteorological stations at Sognefjell (1413 m a.s.l.) and Fannaråken (2068 m a.s.l.) were used, since their elevation is comparable to that of the field site (see Fig. 1). Regression indicates that the 0°C isotherm is located at 910 m a.s.l. The mean temperature lapse rate is $-0.44^{\circ}\text{C}/100\text{ m}$. The average yearly precipitation at Istjørni at the base of the mountain Snøhetta (2286 m a.s.l., Fig. 2), according to Østrem et al. (1988) is 600 mm. Unstable and stormy weather are common in winter and the dominant wind direction is from the south-west.

Soil, geomorphology and bedrock. – The study area is primarily covered by till deposited at the end of the Weichselian period. On the valley floor the main sediment types are glaciofluvial, deposited during the Preboreal

Fig. 2. The study area on Dovrefjell. The BTS measurements are coded according to probability of permafrost; black dots are probable permafrost (BTS $<-3^{\circ}\text{C}$), white dots with small black dots inside are possible permafrost (BTS between -2°C and -3°C) and white dots are permafrost-free sites (BTS $<-2^{\circ}\text{C}$). The dark shaded and light shaded areas represent possible and probable permafrost occurrence, respectively, based on a linear correlation of the BTS classes (see Fig. 5). The positions of the resistivity measurements are shown. 'DT-1 to DT-6' is two-dimensional DC resistivity tomography profiles. DT-7 is located 1 km outside the right-bottom corner of the map. 'D1 to D20' are the locations of one-dimensional resistivity soundings. DB1 is a 10 m deep borehole, located at the tomography profiles DT-3, DT-4 and DT-5 (Fig. 14a).



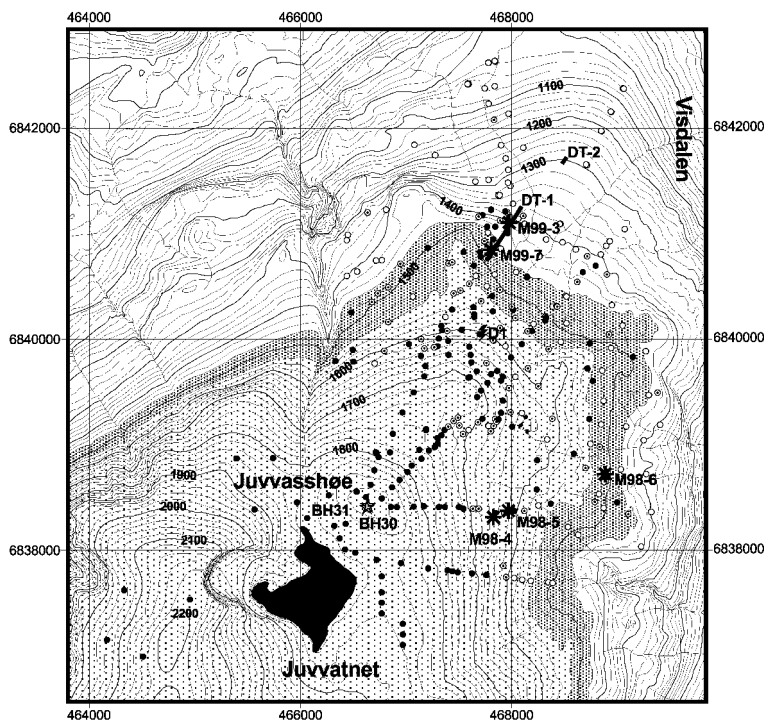


Fig. 3. The study area in Jotunheimen. The BTS measurements and areal symbols as in Fig. 2. The two permafrost boreholes on Juvvasshøe (BH30 (129 m deep) and BH31 (20 m deep)) are marked with a star. Miniature loggers from winter season 1998/1999 are marked M98-4, M98-5 and M98-6. The positions of the resistivity measurements are shown. 'DT-1' and 'DT-2' are two-dimensional DC resistivity tomography profiles (Figs. 14b and 14c) and 'D1' is a one-dimensional resistivity sounding made by Ødegård et al. (1996). Along DT-1 there are two miniature data loggers, M99-7 and M99-3.

period (Sollid & Sørbel 1984, 1997). The cirques in the Snøhetta massif are characterized by ice-cored moraines, formed during the Little Ice Age (Østrem 1964). The slope surfaces near Snøhetta are dominated by frost-weathered blocks of pre-Weichselian age thought to have been preserved under a cold-based ice-age glacier (Sollid & Sørbel 1994, 1997). The study area is characterized by frost sorting, especially in the area around Snøheim (Fig. 2). The bedrock in the investigated area is a Late Precambrian metamorphosed sandstone of the Snøfjellet nappe (Krill 1987).

Jotunheimen

Climate. – The mean air-temperature lapse rate for Jotunheimen was calculated with data from 16 climate stations in the vicinity (Aune 1993). Based on these data, the 0°C isotherm is found at 930 m a.s.l., and the mean temperature lapse rate is $-0.42^{\circ}\text{C}/100\text{ m}$. Bruun (1957) concluded that the global lapse rate of $-0.65^{\circ}\text{C}/100\text{ m}$ was not representative of annual mean temperatures in Norway. The lapse rate varied with season and location. The low lapse rates reported in the present study are due to strong temperature inversions in the valleys during calm periods in winter. Mean annual air temperature on Juvvasshøe (Fig. 3), year 2000, was -3.4°C (Fig. 4). The study area in the surroundings of Juvvasshøe receives slightly more precipitation than at Dovrefjell. The average yearly precipitation at Juvvasshøe according to Østrem et al. (1988) is 800 mm. Prevailing wind is from the west and south-west. During the winter season 1999–2000 a total of 70% of the wind

direction was from south to west on Juvvasshøe (Fig. 4). At flat and convex areas exposed to strong winds, snow cover is thin ($<0.2\text{ m}$) or absent until March and April, with a maximum snow cover of less than 0.5 m in May (Ødegård et al. 1992). A borehole was drilled at Juvvasshøe (Fig. 3) in the summer of 1999 (Sollid et al. 2000). Initial geothermal monitoring indicates an active layer thickness in the summers of 1999 and 2000 to be c. $\sim 2.2\text{ m}$. Mean annual ground surface temperature for the year 2000 was -2.4°C (Isaksen 2001). Permafrost thickness at Juvvasshøe is estimated as c. 380 m (Isaksen et al. 2001).

Soil type, geomorphology and bedrock. – Juvvasshøe is mantled by weathered material with blocks generally up to 1 m in size. The weathered mountain-top detritus material has a more block-rich surface than the till material on the lower terrain (Ødegård 1986). The terminal moraine that lies in front of Veslejuv glacier is ice-cored (Østrem 1964). In the study area, especially in the eastern and south-eastern surroundings of Juvvatnet (Fig. 3), there are well-developed, sorted periglacial features. Sorted stone circles dominate where the terrain is flat, while sorted stripes are prevalent in sloping terrain (Ødegård et al. 1988).

The Jotunheimen mountains lie in the central part of the Caledonian mountain chain (Battay 1960). The bedrock is part of the Jotun nappe. The Juvvasshøe area, which belongs to the northern part of the Jotun nappe, consists of crystalline rocks comprised of mainly quartz monzonite (Kvartsjotunnitt) (Isaksen et al. 2001). The slopes down to Bøverdalen consist of gabbroic rocks and in the lower lying areas, phyllite (Battay 1960).

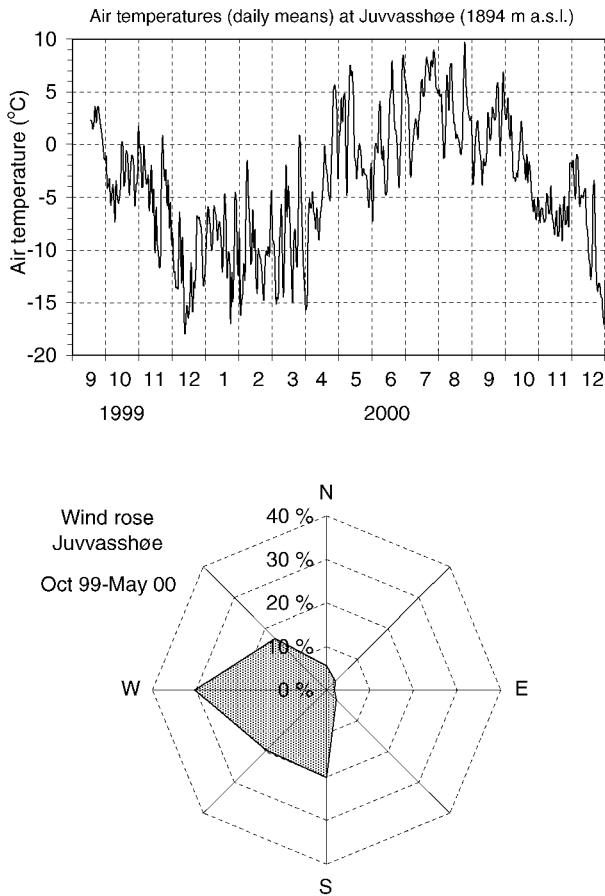


Fig. 4. Air temperatures (daily means) 1999–2000 and wind rose during winter season at Juvvasshøe (1894 m a.s.l.) drill site (Fig. 3). Air temperatures are extrapolated from nearby meteorological stations during the first week of March 2000 due to data loss. The meteorological station at Juvvasshøe drill site was established in September 1999.

Methods

BTS

Under a thick snow cover with low thermal conductivity the temperature will mainly be controlled by heat transfer from the underlying surface, which is largely governed by the presence or absence of permafrost (Haerberli 1973, Hoelzle 1992). A minimum snow thickness of 0.8–1.0 m is necessary to diminish the effect from short-lived variations in the snow surface energy balance. The measurements are made late in the winter when the temperature at the bottom of the snow pack has stabilized and melting has not yet started.

The precision of well-calibrated thermistors is $\pm 0.1^\circ\text{C}$ absolute value and $\pm 0.05^\circ\text{C}$ relative value (Vonder Muhl et al. 1998). Based on earlier experiments from Jotunheimen and Dovrefjell (cf. Ødegård et al. 1996), the standard deviations of the BTS measurements caused by sensor calibration and time-dependent stabilisation to ambient temperatures were set to $\pm 0.1^\circ\text{C}$ and $\pm 0.2^\circ\text{C}$, respectively.

Positioning of the BTS data was conducted using handheld GPS receivers or using a compass and an altimeter. The positional accuracy was estimated to be *c.* ± 50 m. Along the

two-dimensional DC resistivity tomography profiles in Jotunheimen and Dovrefjell, differential carrier-phase GPS was used in positioning of the profiles. The system gives 3D-position accuracy better than ± 0.1 m. The system was also used for positioning of the BTS points along DT-1 in Jotunheimen (Figs. 3 and 14b). The BTS points were re-found in summer and surface conditions at each BTS point could be analysed (see Table 1).

Continuous bottom temperature measurements of the snow cover

9 UTL-1 miniature temperature loggers (University of Bern, Department of Geography) were used, 5 were buried at the surface (*c.* 0.05 m depth) and 4 were used to monitor the temperature envelope through a snow pack. The miniloggers were installed in early autumn at selected sites in Jotunheimen (Fig. 3). The thermistors in the miniature loggers are of the type TMC-1T, with accuracy better than 0.27°C given by the manufacturer (Hoelzle et al. 1999). In contrast to the BTS soundings, these loggers can be programmed to record the temperature at the base of the snow cover during the whole winter. This makes it possible to determine the damping of the short-term fluctuations through the snow (reflecting the development and thickness of a sufficient snow cover), timing of the temperature stabilisation (confirming the reliability of the respective BTS campaign), and to document the time when melting occurs at the bottom of the snow pack (reflecting the end of the BTS season). In combination with other geophysical information, the mini temperature loggers give important additional information concerning the presence or absence of permafrost at the site.

Borehole monitoring

A 10 m deep borehole in debris (DB1) was drilled on Dovrefjell (1505 m a.s.l.) in September 2001. The borehole was located in the supposed permafrost transition zone, indicated from the BTS measurements (Fig. 2). Borehole casing, sensors and data-logging equipment were assembled according to guidelines provided by the PACE (Permafrost and Climate in Europe) project (Harris et al. 2001b). Eleven thermistors from 0.2 m to 6.7 m were installed. The measurement interval is every 6 h. No measurements were performed below 7 m due to an obstacle in the borehole.

Resistivity measurements

The ABEM Lund (Sweden) multi-electrode, high-resolution two-dimensional resistivity system was used. The system used consisted of 61 electrodes with a standard spacing of 2 m, giving a maximum penetration depth of *c.* 25 m. The system automatically measures the apparent resistivities for all particular electrode combinations for a given array and all possible spacings. Each measurement was repeated up to 16 times, depending on the variance of the results. 2D model interpretation was performed using the software package RES2DINV, which performs smoothness-constrained inver-

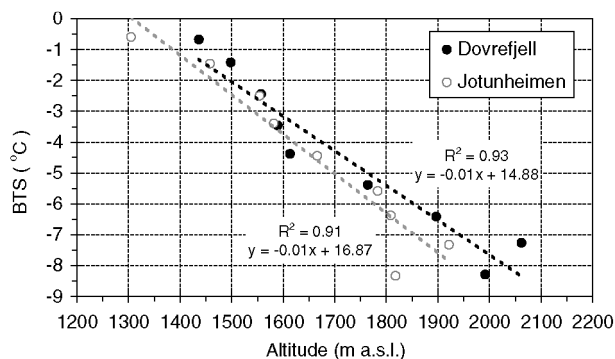


Fig. 5. Relation between BTS and altitude according to BTS classes (see text) on Dovrefjell and in Jotunheimen.

sion using finite difference forward modelling and quasi-Newton techniques (Loke & Barker 1995). Hereby, the specific resistivities for a number of model blocks in a two-dimensional grid are determined by minimising the difference between the observed and modelled apparent resistivities for each model block.

Earlier published results of one-dimensional DC resistivity soundings (Ødegård et al. 1996, Sætre 1997) on Dovrefjell (D1-D10) and Jotunheimen (D1) were used for comparison and validation of typical resistivity values for permafrost in the investigated areas. In addition, 10 one-dimensional DC resistivity soundings (D11-D20) on Dovrefjell were performed. The investigations were done using an ABEM Terrameter SAS 300 C (ABEM, Sweden) using Wenner and Schlumberger configurations. The profiles were interpreted using the software RESIX plus (Interpex Ltd., Colorado, USA). A 2-layer model was used for one-dimensional data inversion.

Elevation and radiation models

An elevation model (DTM, Digital Terrain Model) in raster form with a cell size of 50 m was made for the field areas in Dovrefjell and Jotunheimen. The database was digitised from a 1:50,000 map. The terrain parameters aspect, slope and curvature were calculated based on the DTM.

The average daily potential, short-wave radiation (PR) was calculated for the period July, August, September and October using the radiation model SRAD developed by Moore et al. (1993) and adjusted to Norwegian climate conditions by Heggem et al. (2001). From November to June, most of the investigated area is covered by snow and the influence of direct solar radiation upon the ground is small (cf. Hoelzle 1992). The radiation model applied uses terrain parameters derived from the DTM.

Results and interpretations

BTS data

On a large scale, the respective BTS values were analysed in relation to altitude, potential direct incoming radiation (PR),

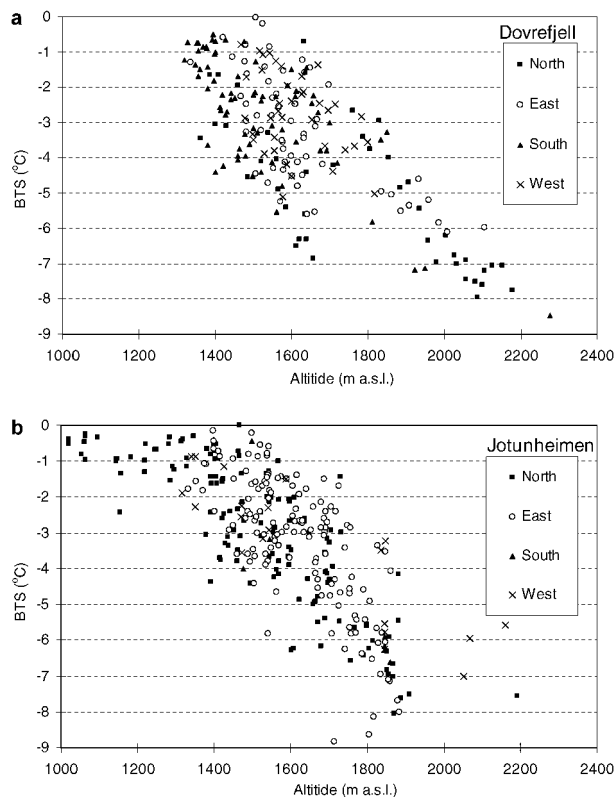


Fig. 6. Scatter plots of BTS and altitude for different aspects on Dovrefjell (a) and Jotunheimen (b). The BTS values are averaged for all locations with more than one measurement (mostly parallel) and total number of measurements is reduced from 531 to 214 on Dovrefjell and from 357 to 314 BTS values in Jotunheimen.

aspect, snow depth and the terrain parameters curvature and slope. The results and analyses are based on a total of 888 BTS measurements. (The last 84 measurements are related to small-scale analyses along the two-dimensional DC resistivity profile in Jotunheimen.) The measurements were averaged for all locations with more than one measurement in order to slightly smooth out local scatter of BTS. In this way the total number of measurements was reduced from 531 BTS values to 214 BTS values in Dovrefjell. In Jotunheimen, fewer parallel measurements were taken, 357 individual measurements were reduced to 314 BTS values. The measurements are considered representative of areas with a stable snow cover of 1–2 m in flat areas and moderate slopes. The main problem concerning the representativeness of the data for all aspects and curvatures in the two investigated areas is the lack of areas facing west and south-west in Jotunheimen and the absence of sufficient snow cover on exposed flat or slightly convex areas at both places. These limitations of the measurement sites introduce a bias in the dataset.

On a small scale, the BTS measurements were analysed with respect to the surface parameters: snow depth, block cover, vegetation cover and surface wetness. In addition to the dataset mentioned, a set of 84 BTS measurements along a two-dimensional DC resistivity tomography profile in Jotunheimen (DT-1) was used.

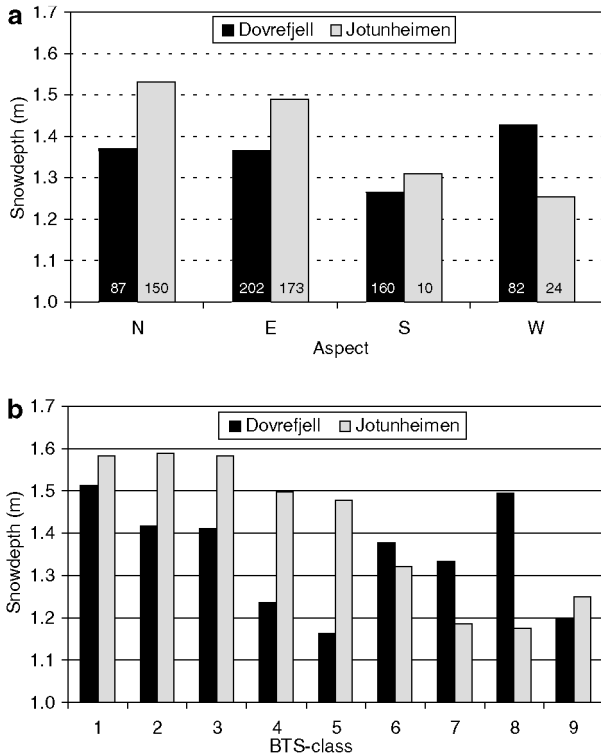


Fig. 7. (a) Average snow depths for the BTS measurements in different aspects on Dovrefjell and in Jotunheimen. The values in the columns show the number of BTS measurements within each aspect. Especially on south-facing slopes, the snow depths represent higher values than snow depth in general in the same aspect. This is due to the general absence of sufficient snow cover and subsequent need for selections of sites where the snow cover exceeds 0.8–1.0 m. (b) Average snow depths for BTS classes (see text) on Dovrefjell and in Jotunheimen.

Large-scale BTS measurements in Dovrefjell and Jotunheimen. – A simple linear regression, with altitude as the dependent variable, explains 55% and 60% of the variance in BTS on Dovrefjell and Jotunheimen, respectively. At low altitudes, especially in Jotunheimen, there is an indication of non-linearity. The reason is that the measurements are extended at low altitude where BTS values approach 0°C. Therefore a linear regression cannot be applied safely to the low altitude BTS measurements.

A possible solution is to analyse the results with respect to BTS classes (cf. Hoelzle 1992). In each BTS class (1 = 0°C > BTS > -1°C, 2 = -1°C > BTS > -2°C, etc.) altitudes are normalised by subtracting the mean value of each class. A grouping introduces a suitable weighting of the data and the influence of extreme values is modified (Hoelzle 1992). The analyses suggest that altitude explains 93% and 91% of the variance in the BTS classes on Dovrefjell and in Jotunheimen, respectively (Fig. 5). A linear correlation suggests that the limits for possible and probable permafrost according to BTS classes are 1490 m a.s.l. and 1580 m a.s.l. on Dovrefjell, and 1460 m a.s.l. and 1540 m a.s.l. in Jotunheimen. These values were used in the permafrost distribution maps (Figs. 2 and 3).

The influence of potential direct incoming radiation (PR) was analysed by plotting PR against the altitude deviations in

each BTS class. A simple linear regression explains only 20% of the variance within the BTS classes in Jotunheimen. Moreover, the Jotunheimen data set has very few measurements towards south and west and must be treated with care. On Dovrefjell, no significant trend was found in the dataset.

The influence of aspect was analysed in different ways. The first step was by dividing the BTS measurements into north-, east-, south- and west-facing sites and analysing each in relation to altitude (Fig. 6). In addition, the altitude deviations in each BTS class were also plotted against aspect. The results indicate no significant correlation in the data set from Dovrefjell. A low correlation was found in Jotunheimen, with slight indications of warmer BTS values in slopes towards the east-facing compared to north-facing slopes.

As an indication of how snow distribution affects the BTS measurements at large scale on Dovrefjell and in Jotunheimen, the average snow depths for the BTS measurements at sites with different aspects (Fig. 7a) and BTS classes (Fig. 7b) were plotted. The results suggest a 10–15% reduction in snow cover thickness in south-facing slopes compared to the north-facing slopes on both Dovrefjell and in Jotunheimen (Fig. 7a). This reduction is suggested to be a minimum due to the general absence of sufficient snow cover at especially southern exposures. Another clear trend is seen from the snow depth for the different BTS classes (Fig. 7b). The general trend is a decreasing snow depth with colder BTS

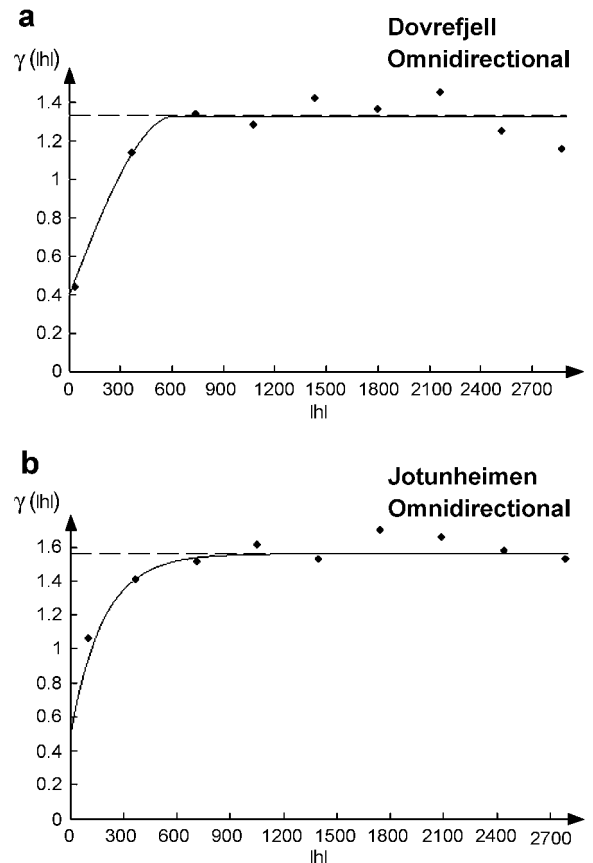


Fig. 8. Geostatistical models fitted to BTS measurements on Dovrefjell (a) and in Jotunheimen (b). See text for details.

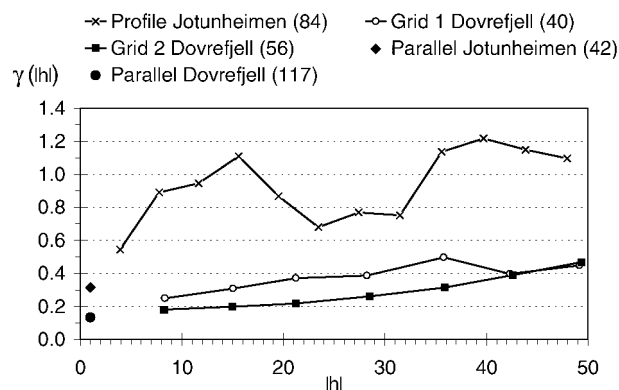


Fig. 9. Experimental variograms calculated from BTS measurements within a range of 50 m. Numbers given in parentheses are the total number of measurements at each site (see text for details). The parallel measurements are made with 1 m distance. The sample variances for the Jotunheimen and Dovrefjell data set are 1.56 and 1.34, when the dependency on altitude is removed by a linear regression. The calculations suggest that the small-scale variance of BTS measurements in Jotunheimen is about twice the variance from Dovrefjell. The variance on a scale of 20–30 m is c. 0.3–0.7 corresponding to 20–45% of the sample variance.

classes. This trend is most evident in Jotunheimen. On Dovrefjell, low snow depths are also found in BTS classes 4 and 5, which generally correspond to BTS points located between 1400 m a.s.l. and 1600 m a.s.l. This area is dominated by flat and open terrain, which is exposed to strong winds.

The analyses of curvature and slope gave no significant correlation with BTS in the scale used in this study.

Small-scale spatial and temporal variability of BTS data. – BTS data are spatially correlated, which means that ordinary statistical methods assuming independent samples must be handled with care. The spatial correlation can be investigated using methods from spatial statistics (Cressie 1993). In Fig. 8, geostatistical models have been applied based on the experimental variogram of the BTS data from Dovrefjell and Jotunheimen. The altitude dependency in the data has been removed by a linear regression. The Dovrefjell data has been fitted to a spherical model with a range of 610 m, a nugget value of 0.41 and a sill

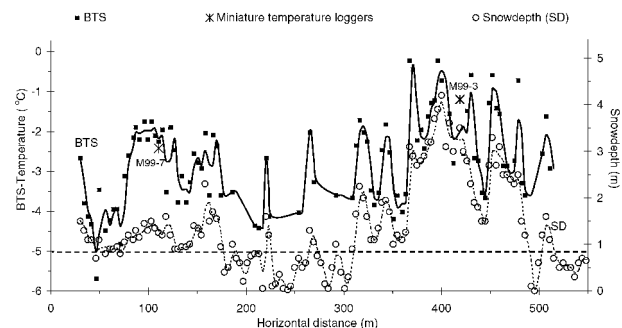


Fig. 10. BTS values (black dots and two periods moving average (bold line)) and snow depths (open circles and two periods moving average (dotted line)) along a two-dimensional DC resistivity tomography profile (DT-1) in Jotunheimen.

corresponding to the sample variance of 1.34. The Jotunheimen data are fitted to an exponential model with a range of 560 m, nugget value of 0.51 and a sill corresponding to the sample variance of 1.56. The range corresponds to the distance at which samples become independent of one another. The nugget value is a constant raising the theoretical variogram. This value can be considered as a random component related to measurement errors and very small-scale spatial variation.

To get an impression of how these small-scale differences in surface material influence BTS in the investigated area on Dovrefjell and in Jotunheimen, two measurements were made at many of the BTS measurement sites with generally 1 m spacing between the measurements. The close spacing ensured no significant difference in snow depth between the measurements. The calculated variance for 1 m lag is shown in Fig. 9 for Dovrefjell (117 measurements) and Jotunheimen (42 measurements).

Sætre (1997) undertook similar investigations within two defined areas on Dovrefjell, which were homogeneous with respect to slope, aspect and PR. The first area (~2700 m²) was located at a plain surface, with the centre in DC resistivity sounding D4 (Fig. 2). The second area (~2000 m²) was located at a gentle slope towards east, with the centre in DC resistivity sounding D5 (Fig. 2). At both places a BTS grid system was performed by uniform distribution of BTS measurements with 7 m spacing between each of the measurements for both axes, resulting in 56 (7 × 8) and 40 (5 × 8) BTS measurements respectively within the two defined areas. The spatial variance at these two sites is shown in Fig. 9. At both areas, snow depth varied in the range of 1–2 m, with an average of 1.3 m for both places. The small-scale spatial variance of the BTS data is calculated for the 84 measurements along DT-1 in Jotunheimen. The results from Jotunheimen show a higher small-scale spatial variance compared to Dovrefjell.

There is an additional source of variance caused by seasonal variation and interannual variations between the different campaigns in this study. The small-scale variance presented in Fig. 9 is based on measurements made the same day. Concerning the seasonal variations, field measurements in Jotunheimen in winter 1998 and 1999 were made in stable periods, as highlighted from the results of the mini temperature loggers (see Fig. 11). In addition, some of the data used in this study originate from earlier BTS campaigns performed in the same period (March). From permafrost investigations in the Alps, Imhof et al. (2000) concluded that significant interannual variations of the BTS may occur. The main controlling parameters for the evolution of BTS in late winter are the depth of snowfall and the pattern of air temperatures during the preceding months (e.g. Goodrich 1982, Vonder Muhl et al. 1998, Imhof et al. 2000) (Fig. 12).

BTS measurement and surface-material analysis in relation to the two-dimensional resistivity tomography profile in Jotunheimen (DT-1). – Eighty-four BTS measurements were made at 4 m intervals along the 2D-resistivity tomography profile (DT-1) in Jotunheimen, including BTS, late winter snow depths and a visual classification of surface conditions in late summer. The results of the 84 BTS measure-

Fig. 11. Ground temperatures obtained at five locations (for miniature loggers M98-4, M98-5, M98-6, M99-7, M99-3) in Jotunheimen during winter 1998–99 and 1999–2000. The arrows mark the date when respective BTS campaigns were performed. The circles denote the onset of melting, corresponding to the end of the ‘BTS season’.

Logger M98-4 was located at 1650 m a.s.l. The ground has a patchy grass cover and is dominated by a block cover of weathered till. Snow depth and BTS were measured at the site on 9 March 1999 and were 1.1 m and -3.7°C , respectively. The strong fluctuations of the ground surface temperature until mid-February point to only a thin snow cover during the first half of the winter. During the last half of February and throughout March the temperatures are more stable and clearly suggest permafrost at the site.

Logger M98-5 (1615 m a.s.l.) was installed in a local depression with a more developed vegetation cover, consisting of grass species. The block cover was only scattered and fine material dominated the soil. Snow depth and BTS were measured at the site on 10 March 1999. Two BTS measurements were made, both c. 1 m away from the miniature logger and showed temperatures of -3.2°C and -2.8°C . Snow depth was 1.25 m. The logger shows a different temperature pattern through the winter compared to all the others in this study. The most striking is the absence of short-term temperature fluctuations in both autumn and winter. The reason for this pattern is probably a combination of an early build-up of snow cover combined with a high-water content in the soil. This is supported by the type of surface material at the site and the temperatures, which show a slow progressive cooling of the ground during the whole winter. The miniature logger temperature at the end of the BTS season shows clear indications of a cooling trend and has still not stabilised. Based on the two BTS measurements and the pattern of the temperature curve from the logger, it is suggested that permafrost is present.

Logger M98-6 (1520 m a.s.l.) was located at ground dominated by a dry lichen cover with only scattered blocks. Snow depth and two BTS measurements were done on the site on 18 March 1999. Values were 1.2 m, and -3.0°C and -2.7°C , respectively. Similar to M98-4, significant fluctuations of the ground surface temperature are seen until mid-February. This suggests a thin snow cover over the first half of the winter. During the last half of February and throughout March the temperatures are stable, with ground surface temperatures suggesting permafrost at the site. The lower two graphs show ground temperatures for miniature loggers M99-7 and M99-3 at two sites along the two-dimensional DC resistivity tomography profile DT-1 (Fig. 14b) in Jotunheimen during winter 1999–2000. At M99-3 snow temperatures (ST) are shown for 0.5 m, 1.0 m and 1.5 m height over ground surface.

Logger M99-7 (1480 m a.s.l.) was located in the higher part along DT-1 in Jotunheimen. The ground was similar to the location of M98-6, dominated by a dry grass and lichen cover with no blocks at the surface. Snow depth and BTS was measured on the site on 7 March 2000 and were 1.25 m and -2.3°C , respectively. Note the large fluctuations of the ground surface temperature until mid-January before a sufficient snow cover developed and temperatures stabilised in mid-March. The stabilised ground surface temperature suggests that permafrost is probable at the site.

Logger M99-3 (1410 m a.s.l.) was located in the lower part along DT-1 in Jotunheimen. At this site, the ground surface was generally dry and covered with blocks of till material, with only some small patches of lichen in between. Snow depth was measured on both 9 December 1999 and 8 March 2000 and was 0.4 m and 3.5 m, respectively. BTS measurement 2 m downslope gave a temperature of -1.2°C on 8 March 2000. The short-term fluctuations of the ground surface temperature ends in beginning of January and temperatures are stable the whole winter. The temperatures and results from DT-1 and additional geophysical soundings prove an absence of permafrost at this site.

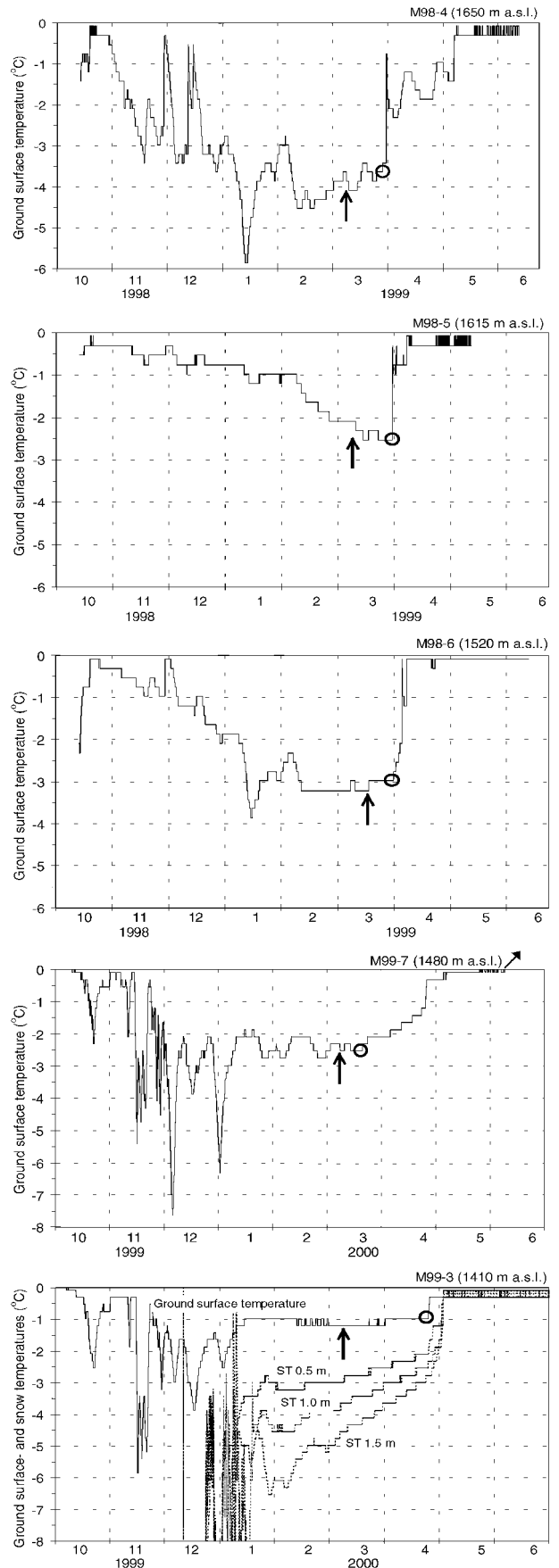


Table 1. Statistical analyses of BTS measurements and ground surface characteristic along the two-dimensional tomography line (DT-1) in Jotunheimen. Unclassified points are mainly related to an old road crossing the profile. The 'BTS deviation' is the deviation from a linear regression line between BTS and snow cover. Negative values indicate lower BTS values than expected relative to the linear regression.

Type of surface	No. of measurements	Total (not classified)	Average BTS	Average snow depth	Average BTS-deviation	T-stat BTS-deviation
Surface covered with blocks	23	84 (0)	-1.87	2.81	-0.21	0.9-2.1
Medium block cover	34		-2.71	1.64	-0.052	
No blocks or scattered blocks	27		-2.80	1.20	0.23	
Grass or moss-cover (wet)	24	70 (14)	-2.51	1.27	0.47	3.9
Lichen-cover (dry)	46		-2.65	1.85	-0.16	
Moist surface	8	82 (2)	-1.74	1.88	0.73	2.3-3.7
Medium moist	24		-2.16	1.99	0.20	
Dry surface	50		-2.82	1.69	-0.21	

ments are presented in Figs. 10 and 14b. Where snow depths were less than 0.8 m, no BTS measurements were performed.

There is a general warming from the upper to the lower ends of the profile. A linear correlation indicates mean BTS value of -3.4°C at the upper end of the profile and -1.9°C at the lower end. According to 'BTS theory', these values suggest that the upper end of the profile begins in an area

where permafrost is possible and ends in a non-permafrost area. In between, permafrost is probable.

The BTS values show high variability along the profile with temperature differences of up to 4°C within 10-20 m (Fig. 10). BTS values are correlated with snow depths (linear correlation coefficient 0.57). The average BTS for different classes is given in Table 1. A general increase in snow depth in downslope direction is due to wind-drift of snow and subsequent accumulation on the steeper slopes. Boulder tongues are common in the area (Ødegård 1988) and are clearly visible along profile DT-1 in Fig. 14b (e.g. on stations 86, 232, 304, 390, 440). The elevated boulder tongues create significant small-scale variations in snow depths and conse-

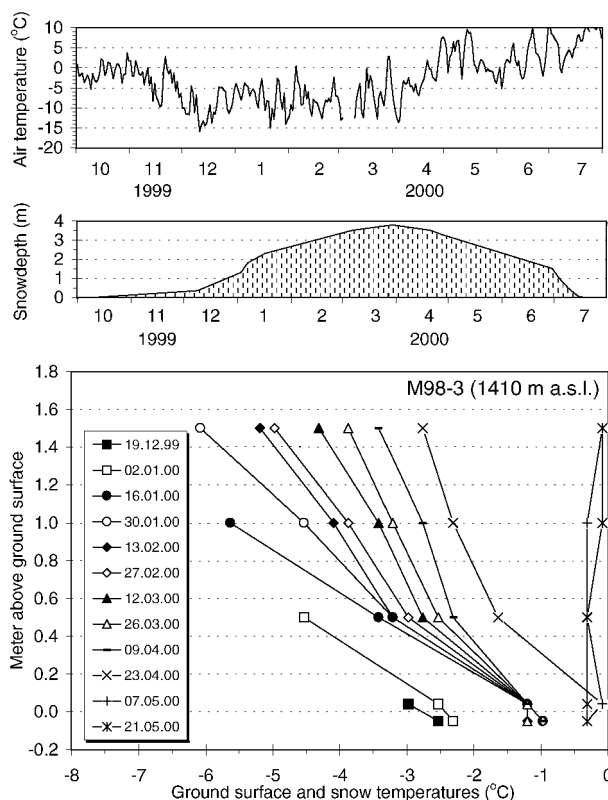


Fig. 12. Air-, snow- and ground temperatures measured at the location of miniature logger M99-3. The snow-ground interface is taken as depth 0. Air temperatures were extrapolated from the meteorological station at Juvvasshøe, based on the mean annual air temperature gradient in the area. A build-up of snow and snow depth during winter is shown, based on two control measurements of snow depth and a simple heat conduction assessment of the temperature amplitude decrease and phase lag within the snow.

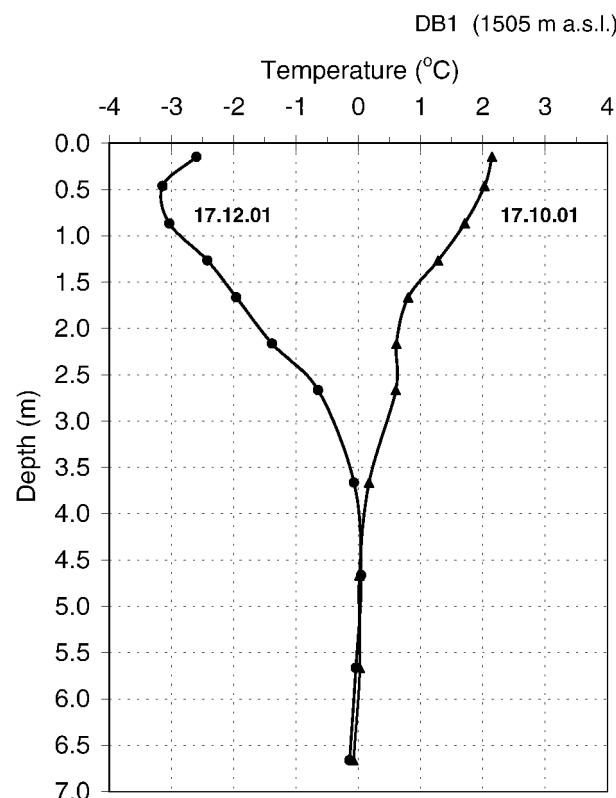


Fig. 13. Two selected ground temperature profiles from borehole DB1 (1505 m a.s.l.), Dovrefjell. DB1 was drilled on 5 September 2001.

Table 2. Interpretation of two-dimensional DC resistivity tomography profiles and one-dimensional vertical electrical sounding results (Schlumberger and Wenner configuration) at different altitudes on Dovrefjell. The different measurements are sorted by altitude. D1-D3 is from Ødegård et al. (1996). D4-D10 is from Sætre (1997).

	Altitude (m a.s.l.)	Layer 1	Layer 2			
2D-tomography		ρ (k Ω m)	h (m)	ρ (k Ω m)	<i>Interpretation layer 2</i>	
DT-1	1527–1484	50–150	3–9	3–20	Sporadic pf., bedrock	
DT-2	1527–1520	50–100	2–3	10–20	Frozen bedrock	
DT-3	1505–1500	30–100	2–4	20–100	Frozen debris (~0°C*)	
DT-4	1505–1496	30–100	2–4	20–150	Frozen debris (~0°C*)	
DT-5	1505–1485	50–200	1–4	5–150	Sporadic pf., debris (~0°C*)	
DT-6	1481–1467	70–150	4–6	5–50	Sporadic pf., debris (~0°C*)	
DT-7	1178–1177	30–150	2–4	1–5	Unfrozen bedrock (>2°C*)	
Schlumberger (1D)		ρ (k Ω m)	h (m)	ρ (k Ω m)	h (m)	<i>Interpretation layer 2</i>
D1, D2, D4	1620–1640	20–80	1–5	>200	30–100	Frozen debris and bedrock
D5, D6	1570, 1620	20–90	2–3	100–200	10–20	Frozen debris
D10	1480	50–150	5–9	5–15	20–30	Unfrozen debris
D3	1480	20–30	5–7	10–30	20–35	Marginal permafrost, debris
D7	1400	20	10	2–4	>30	Unfrozen bedrock
D8, D9	1320, 1340	40–100	1–5	10–20	10–30	Unfrozen debris
Wenner (1D)		ρ (k Ω m)	h (m)	ρ (k Ω m)		<i>Interpretation layer 2</i>
D13, D15	1675, 1660	10–20	2–4	30–80		Frozen bedrock
D12	1520	15–20	1–2	5–10		Marginal permafrost, bedrock
D14	1500	15–20	3–5	40–60		Frozen bedrock
D11	1380	10	3–5	5–10		Unfrozen debris

* Ground temperatures obtained from boreholes.
pf. = permafrost.

quently BTS. A generally thin snow cover (1.0–1.5 m) and cold BTS (e.g. < -3°C) are found on the top surface and close to the front of the boulder tongues, while snow accumulates on and below the boulder tongues front slopes, resulting in warmer BTS.

Results from the visual classification of the surface conditions in late summer are given in Table 1. The classification of surface moisture conditions is poorly correlated with snow depth. The results show that the difference in average BTS values at dry and moist surfaces is 0.9°C (T-test 2.9). This difference is highly significant, assuming independent observations. This assumption is not strictly valid, which could lead to inflated T-values.

To improve the interpretation of the relation between BTS and ground cover, the dependence of the BTS on snow cover was removed by a linear regression (Table 1). As expected, the classes of surface moisture conditions, which are poorly correlated with snow depth, show approximately the same results as averaging the original BTS measurements. The difference between grass/moss vegetation and lichen-cover is the most significant when the dependency on snow depth is removed (Table 1).

Table 3. Interpretation of vertical electrical sounding results (Wenner configuration) in different aspects around a small mountain top (Brunkollen (1665 m a.s.l.)).

	Altitude	Aspect	Layer 1	Layer 2	
Wenner			ρ (k Ω m)	ρ (k Ω m)	<i>Interpretation layer 2</i>
D16	1615	NW	15	30	Frozen bedrock
D19	1635	E	15	35	Frozen bedrock
D17	1645	S	30	75	Frozen bedrock
D20	1600	S	20	45	Frozen bedrock
D18	1630	SW	20	55	Frozen bedrock

Continuous bottom temperature measurements of the snow cover

The miniature data loggers (Fig. 11) gave valuable data about the ground surface temperature evolution below the snow cover at some selected sites in Jotunheimen. Temperature data obtained from the loggers showed that the BTS campaigns in both winters 1998 and 1999 were completed at suitable and representative times and that the BTS season ended around end of March in both years. The miniature data loggers were installed in mid-October in 1998 ('M98-loggers') and in July 1999 ('M99-loggers'). The loggers were located at different altitudes and at representative locations within the area. A total of 6 loggers were installed in 1998 and 11 loggers in 1999. In this paper, the focus is on some selected loggers that were installed at low altitudes, close to or in the permafrost transition area.

Fig. 11 shows three different ground surface temperature patterns, all indicating permafrost, on different sites in Jotunheimen during winter 1998–1999. The ground surface temperatures are all colder than -2.5°C at the end of the representative BTS season that year.

Ground surface temperatures for two locations below 1500 m a.s.l., along the two-dimensional DC resistivity tomography profile (DT-1, Fig. 14b), are shown in Fig. 11. Temperatures from the uppermost data logger (M99-7) indicate that permafrost is probable. Ground surface temperatures from the lowermost data logger (M99-3) prove an absence of permafrost at the site. The results from the data loggers are supported by the results from DT-1, which indicate a clear transition from patchy-permafrost in the upper part to non-permafrost at the end of the profile (Fig. 14b).

Continuous temperature measurements within the snow, at

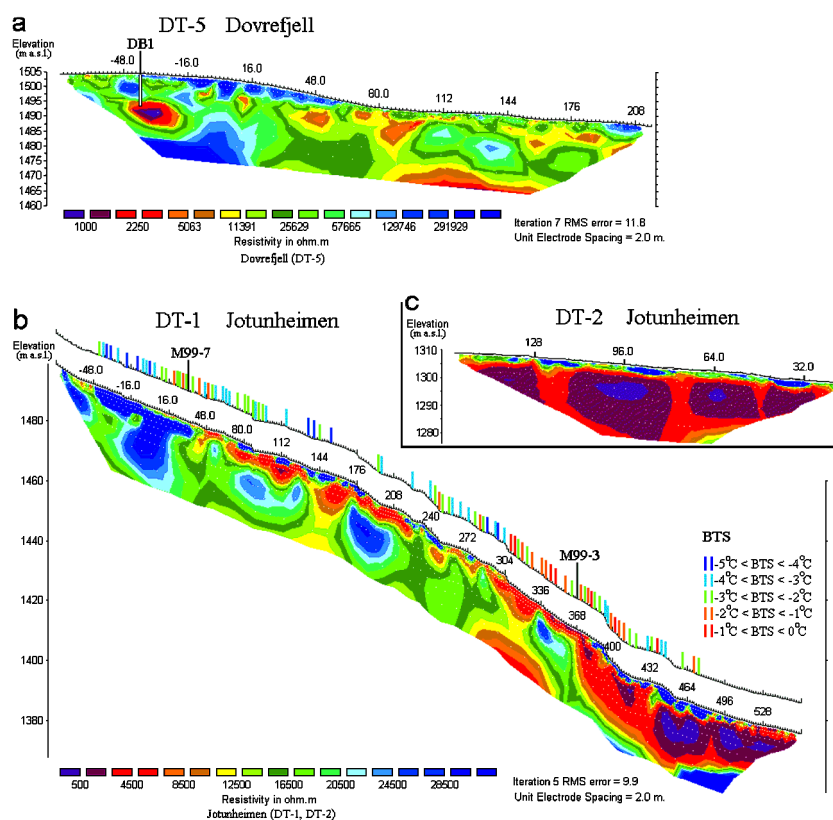


Fig. 14. Tomography model results for the two-dimensional DC resistivity tomography profiles on Dovrefjell (a) and in Jotunheimen (b, c). (a) The tomography model results for DT-5 show high resistivities at the upper end of the profile, interpreted as frozen debris. From station 20 to the lower end of the profile, the resistivity values are lower and permafrost is likely to be absent or only marginally present. Between stations 100 and 150 there are areas of higher resistivities, which are likely to be permafrost remnants, or patches with a slightly higher ice content. The location of borehole DB1 (Fig. 13) is marked. Disturbance (from heat and water) from the drilling, resulting in a melted patch, is clearly seen as an isolated low resistivity area below the borehole in downslope direction. (b) Two-dimensional DC resistivity tomography results and BTS results for DT-1. Resistivity values along DT-1 indicate a clear transition from permafrost in the upper part to non-permafrost at the end of the profile. In between, high-resistive patches suggest isolated frozen bodies. Low-resistive zones at shallow depth are caused by rills and water flow above the permafrost layer. BTS are divided into five BTS classes. Locations without BTS are due to insufficient snow cover (<0.8 m) and make open intervals along the profile. The locations of the miniature loggers M99-7 and M99-3 are marked. (c) On DT-2, resistivities are generally between 1 and 5 k Ω m, indicating no permafrost.

different levels above ground, revealed interesting indications about ground thermal conditions at a permafrost-free site, where mean annual ground surface temperatures probably are close to 0°C (Figs. 11 and 12). The temperature gradients in the first 0.5 m of the snow pack above ground were significantly different from snow layers above. In the basal snow layers (≤ 0.5 m), temperature gradient in early winter was *c.* $4.4^{\circ}\text{C m}^{-1}$ and in late winter before melting *c.* $2.4^{\circ}\text{C m}^{-1}$. This is in contrast to situations in permafrost, where temperature gradients and heat flux are greatly reduced in basal snow layers over permafrost and might even be negative in late winter (Keller & Gubler 1993).

Borehole temperatures on Dovrefjell

Two selected temperature profiles (42 days and 103 days after drilling) from borehole DB1 are presented in Fig. 13. Below 4.5 m, temperatures are 0°C or slightly below. For the two lowermost thermistors (5.7 m and 6.7 m), temperatures show a slight cooling trend of 0.1°C during the two months of measurements. The initial ground temperature monitoring indicates an active layer thickness of at least 4 m.

DC resistivity results on Dovrefjell

The interpretations of all DC resistivity soundings on Dovrefjell are presented in Tables 2 and 3. The DC resistivity soundings on Dovrefjell show high resistivity values in the

upper surface layer. This is typical for debris-covered surfaces and may be misinterpreted for permafrost occurrences (e.g. Hauck 2001). Field observations and other data show that the debris cover on Dovrefjell is thick, sometimes several tens of metres. In the interpretation of the resistivity data it is distinguished between bedrock and debris (Tables 2 and 3).

One selected tomography profile, DT-5 (1505–1485 m a.s.l.), is presented in Fig. 14a. High resistivities (60–150 k Ω m, blue colours) dominate at depth between stations -80 to 20 at the upper end of the profile. The high resistivities indicate frozen debris. This is confirmed by the borehole measurements (DB1), which show ground temperatures slightly below 0°C (Fig. 13).

The profile (DT-5) cross borehole DB1 at station -40 . The tomography measurements were performed a few days after drilling of DB1. Disturbance (from heat and water) from the drilling of borehole DB1 is clearly seen as an isolated low resistivity area (3–10 k Ω m) below the borehole in downslope direction. This area is suggested to be a melted patch due to the drilling disturbance.

From station 20 to the lower end of the profile, the resistivity values are lower compared to the upper part and there are several areas similar to the low resistivity area below the borehole. Here, permafrost is likely to be absent or only marginally present. Between stations 100 and 150 there are areas of higher resistivities (30–100 k Ω m), which are likely to be permafrost remnants or patches with a slightly higher ice content.

In the Schlumberger results from above 1570 m a.s.l. (D1, D2, D4, D5, D6 (Fig. 15), D13 and D15), the resistivities below the surface layer were high (Table 2), definitely indicating permafrost conditions. In D3, D7, D8, D9, D10 and D11 (below 1500 m), the resistivities were low (≤ 20 k Ω m, Table 2) throughout the uppermost 30 m, except for the surface layer, where high values were encountered, most probably due to the presence of air caverns in the till and glaciofluvial debris.

From the resistivity data, a permafrost-altitude profile can be summarised as follows:

- Definite permafrost occurrence at altitudes 1600–1640 m a.s.l. with frozen debris values generally more than 100–200 k Ω m and permafrost thickness of at least 30–100 m.
- Decreasing permafrost thickness at altitudes below 1570–1600 m a.s.l.
- Sporadic or marginal permafrost from *c.* 1525 m a.s.l. downwards.

DC resistivity soundings (D15–D20) around a small mountain-top (Brunkollen) yielded information regarding the influence of aspect on resistivity values, performed at about the same altitudes in bedrock (Table 3). All profiles suggest frozen bedrock with resistivities generally between 30 and 75 k Ω m (Table 3). The resistivity measurements gave no clear indications on aspect dependency, despite a possible difference in PR of 30–40% between north-facing and south-facing slopes. The soundings located on south-facing (D17, D20) and south-west-facing (D18) surfaces indicate a slightly higher resistivity than the other soundings on east-facing and north-west-facing surfaces (D19 and D16). In addition, resistivity values are closer to what can be expected for marginal permafrost on the north-west (D16) and east (D19) facing slopes of Brunkollen.

DC resistivity results in Jotunheimen

Fig. 14b shows the inversion model results from DT-1 in Jotunheimen. The low resistivities (1–5 k Ω m, deep red and mauve colours) at the lower altitude end of the profile (~ 1370 m a.s.l.) are in good agreement with the results from DT-2 (Fig. 14c), which is a non-permafrost site (Hauck et al. 2000, Hauck 2001). This shows that permafrost cannot be present at the lower part of the DT-1 profile. The high resistivities (> 20 k Ω m, blue colours) at the upper end (~ 1500 m a.s.l.) are due to permafrost (in weathered material and bedrock) underneath a ~ 4 m thick unfrozen coarse-grained active layer. This was confirmed by refraction seismic measurements along the same profile line yielding seismic P-wave velocities between 3000 and 6000 m s $^{-1}$ for the high-resistive regions (Hauck 2001, Hauck et al. 2000). In between, the distribution of high-resistive patches is irregular, pointing to frozen bodies or even ice lenses occurring in the transition zone between permafrost and non-permafrost. The high-resistive patches at the surface are due to air voids between medium size rocks, with alternating occurrences of boulders, fine-grained material, vegetation and even small creeks.

The location of the interpreted permafrost transition area is

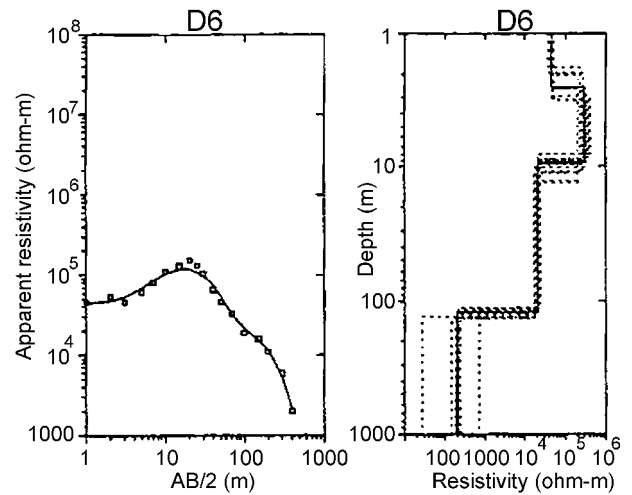


Fig. 15. Interpretation of vertical electrical sounding results (Schlumberger configuration) for one selected sounding in permafrost on Dovrefjell, with the best fit model (left) and corresponding equivalence model (right). Interpretation in a 4-layer model corresponds to an upper active layer (1–3 m thick), a frozen debris layer (100–200 k Ω m, 10–15 m thick), a frozen bedrock layer (10–30 k Ω m, *c.* 100 m thick) and unfrozen bedrock (0.1–1 k Ω m) below the permafrost base (modified after Sætre, 1997). Interpretations of all vertical electrical soundings conducted on Dovrefjell are listed in Tables 2 and 3.

in very good agreement with the results from the BTS measurements and the findings from other geophysical surveys (Hauck et al. 2000). Comparing the two-dimensional DC resistivity tomography data with the BTS data (Fig. 14b), it is quite apparent why permafrost exists at some isolated patches along the profile while not at others. In general terms, in those zones that have only a thin snow cover or remain snow-free (where no BTS measurements were performed; see Fig. 14b) permafrost may persist more easily, as no insulation snow cover prohibits the penetration of cold winter temperatures into the subsurface (e.g. Haeberli 1973, Smith 1975). Variations in resistivity within a few metres along the profile are generally detectable on the BTS measurements (Fig. 14b) and the absolute values are consistent.

The results from a one-dimensional sounding (D1) located at 1600 m a.s.l. (taken from Ødegård et al. 1996) are in good agreement with the results from DT-1. On D1, a 10–15 m thick high resistivity layer (30–100 k Ω m), interpreted as frozen debris, is found beneath the active layer.

Discussion

Spatial variation of BTS – large-scale

The variations of BTS in relation to altitude indicate that altitude is the most important factor for the distribution of permafrost on Dovrefjell and in Jotunheimen (cf. Ødegård et al. 1996). This is in contrast to the Alps, where altitude is of less importance in relation to BTS compared to other factors (Haeberli & Patzelt 1982, Hoelzle 1992). Interpretation of the results from Dovrefjell and Jotunheimen shows that the altitudinal zonation of permafrost is similar, which is

expected from the meteorological record of air temperatures and observations of snow cover distribution. BTS correlated with altitude yields a gradient of *c.* -1.1°C per 100 m altitude (Fig. 5). The mean annual air temperature lapse rate is not sufficient to explain the high BTS gradient. Effects of differences in snow distribution and evolution are the most evident explanation for the high gradient (see Fig. 7). A snow cover presents a barrier to heat loss from the ground to the air in winter (e.g. Hoelzle 1992, Keller & Gubler 1993). Because of increasing wind speed with altitude (Barry 1992), the density of snow will increase with altitude (Smith 1975). This results in a higher heat loss from the ground at higher altitudes for the same snow thickness. In addition, heat loss may be large at higher altitudes on Dovrefjell and in Jotunheimen owing to a thin or absent snow cover until March and April, caused by strong winds. On Dovrefjell, large wide-open and flat areas are exposed to strong winds at altitudes between 1400 m a.s.l. and 1600 m a.s.l., corresponding mainly to BTS classes 4 and 5. These classes exhibit low values due to lower snow depths (Fig. 7b) and deviate from the linear trend in BTS classes with altitude (Fig. 5).

The short-wave incoming radiation (PR) depends on horizon, slope and aspect (Hoelzle 1992). The results from Dovrefjell and Jotunheimen indicate that PR has a minor influence on BTS and suggests that BTS values are not significantly different for the different aspects (Fig. 6). On Dovrefjell, no significant correlation between PR and BTS was found. This was supported by the results from the one-dimensional resistivity measurements. In Jotunheimen, the analysis explains *c.* 20% of the variance in PR within the BTS classes. The reported results from this study show a different pattern compared to the Swiss Alps, where PR explains more than 90% of the variance within the BTS classes (Hoelzle 1992). Terrain differences, with steeper slopes in the Alps, may explain some of the differences. Moreover, they can be explained by differences in total incoming radiation due to latitude. In October, the Swiss Alps receive about twice the total amount of incoming radiation compared to the investigated sites in southern Norway (cf. Hartmann 1994).

The more continental the climate, the larger is the influence of radiation because of the reduced cloud cover and air humidity. Results from two synoptic stations (held by the Norwegian Meteorological Institute) nearby the study sites in Dovrefjell and Jotunheimen (Fokstua and Elveseter, respectively) show a low frequency of clear days, and that clouds dominate during July, August, September and October.

Wind drift strongly influences the snow accumulation pattern in Dovrefjell and Jotunheimen. The prevailing south-westerly winds (Fig. 4) redistribute the snow and deposit a larger amount of it on north-facing and east-facing slopes (Fig. 7), which as a result remain warmer in winter. In summer, on the other hand, the south-facing and west-facing mountain slopes receive more solar radiation. The net effect is that the two factors compensate.

The geostatistical analyses show that BTS data are spatially dependent within a range of 500–600 m when the dependence on altitude is removed. The spatial dependency

on the scale from 20–30 m to 500–600 m might be related to snow cover, exposure to prevailing winds and variations in direct radiation. The ‘black-box’ character of statistical analysis makes it difficult to discuss BTS data related to energy balance components.

The positional accuracy was estimated to *c.* ± 50 m for the large-scale BTS data. This might explain why no correlation was found between BTS and slope and curvature. In addition, the elevation model used here, with a 50 m grid, will smooth out the local small-scale terrain variations.

Data obtained by the miniature temperature logger’s complement the set of conventional BTS values and showed that the BTS campaigns in Jotunheimen in both 1999 and 2000 generally were performed when the temperatures at the bottom of the snow cover were stabilised. The results indicate that future BTS campaigns should be performed at the beginning of March, similar to this study.

Spatial variation of BTS – small-scale

The investigations of small-scale variance of BTS show a higher variance in Jotunheimen as compared to Dovre. The sample variance when the dependency on altitude is removed is also higher in Jotunheimen. Small-scale permafrost mapping is generally performed on spatial scales of 20–30 m. The results from Jotunheimen suggest that as much as 20–45% of the variance not explained by altitude can be explained by small-scale spatial variance in the range of 20–30 m (Fig. 9). The results show that any single factor alone can explain local ground thermal conditions. The ground thermal regime results from the interaction of climatic, surface and subsurface factors, and this is ultimately responsible for the considerable small-scale variations in ground temperatures observed in this study.

Permafrost distribution on Dovrefjell and in Jotunheimen

Based on the analyses from Dovrefjell and Jotunheimen, the strong correlation between BTS and altitude suggests that air temperature causes most of the variance in BTS on larger scales. In the investigated areas on Dovrefjell and in Jotunheimen, all BTS measurements above ~ 1800 m a.s.l. and ~ 1700 m a.s.l., respectively, were classified as good indicators of permafrost. Based on analysis of BTS data, the lower limit of mountain permafrost in the investigated areas on Dovrefjell and in Jotunheimen is estimated to be 1490 m a.s.l. and 1460 m a.s.l., respectively. These findings are representative in flat areas and moderate slopes with a stable winter snow cover of 1–2 m. Sporadic permafrost is probably found at lower altitudes on convex and flat sites, which are exposed to strong winds during winter. The lowest altitude of probable permafrost on Dovrefjell and in Jotunheimen according to BTS was found at *c.* 1350 m a.s.l. at both places. On Dovrefjell, sporadic permafrost forms associated with bogs (palsa bogs) and marshy areas, are found down to *c.* 1000 m a.s.l. (Sollid & Sørbel 1998).

In the study area, the long-term trends from recent decades show an overall increase in annual air temperature, where an

increase in the winter months is especially pronounced (Førland et al. 2000). A ground surface warming of 0.5–1.0°C during the last decades is interpreted from the borehole on Juvvasshøe in Jotunheimen (Isaksen et al. 2001). On Juvvasshøe, the coldest ground temperatures are found at 30–40 m depth. Similar signals of an upper ground warming are found from the resistivity measurements. At some measurements located inside the permafrost transition zone, the highest resistivities are found in the deepest part of the tomography profiles (e.g. DT-2, DT-3, DT-4 and DT-5 on Dovrefjell). From resistivity measurement D1 in Jotunheimen, Ødegård et al. (1996) suggested a possible relict permafrost layer below ~30 m depth.

In response to the observed warming the lower limits of mountain permafrost on Dovrefjell and in Jotunheimen must rise c. 100–150 m in altitude. The present ground temperatures in borehole DB1 on Dovrefjell at 1505 m a.s.l. are slightly below 0°C. Ground temperature monitoring from DB1 and additional permafrost boreholes in southern Norway will provide important thermal data and probable evidence of enhanced melting of mountain permafrost in the future due to the predicted climatic amelioration.

Conclusions

BTS is highly correlated with altitude in the investigated part of Dovrefjell and Jotunheimen. Based on the BTS results, the lower limits of possible permafrost are 1490 m a.s.l. and 1460 m a.s.l., respectively. The results suggest that the lower limit of mountain permafrost on Dovrefjell and in Jotunheimen correspond to mean annual air temperatures (MAAT) between –2°C and –3°C, and that mountain permafrost occurrences at MAAT warmer than –2°C are rare and only found on exposed sites.

Potential radiation (PR) has a minor influence on BTS on Dovrefjell and in Jotunheimen. The Dovrefjell dataset is clearly the best to investigate aspect dependency of the BTS data and shows no clear relation between aspect and BTS. Low relief, low total amount incoming radiation and high frequency of clouds explain some of the low relation between PR and BTS. Last, but not least, the effect of aspect is moderated by the uneven distribution of snow cover in winter and masks any influence of PR.

The application of two-dimensional DC resistivity tomography has been proven to be a useful tool for mapping and characterising mountain permafrost transition zones and isolated permafrost occurrences on a small scale in southern Norway. The results from the resistivity measurements, miniature data loggers, borehole temperatures and the BTS measurements on Dovrefjell and in Jotunheimen are highly consistent. Indications of an upper ground warming are found from the resistivity measurements.

Small-scale variances of BTS show a higher variance in Jotunheimen compared to Dovre. The results from Jotunheimen suggest that 20–45% of the variance not explained by altitude can be explained by small-scale spatial variance on the range of 20–30 m. The relation between measured BTS values in late winter and surface conditions in late summer suggests that surface moisture conditions, block cover and

vegetation type should be further investigated as proxy data in detailed permafrost mapping. Similar measurements should be made at other sites to see if these findings can be generalised to larger areas.

Acknowledgements.—This study, led by Professor J. L. Sollid at the Department of Physical Geography, University of Oslo (UoO), is part of the EU project PACE (Permafrost and Climate in Europe) and was performed in cooperation with ETH-Zurich by Dr D. Vonder Muhl, who took part in the DT-1 and DT-2 measurements in Jotunheimen and the DT-1 measurements on Dovrefjell.

In Jotunheimen, the fieldwork was supported by: Dr B. Etzelmueller, Dr K. Melvold, S. T. Haagensen and H. Sørli, all from UoO, N. Russill (Terradat Ltd, Cardiff, UK), K. V. Johansen (Gausdal College), T. Th. Reichel (Friedrich-Alexander-University Erlangen-Nürnberg) and K. Giesa (University of Zurich). H. Farbro, S. T. Haagensen and A. Kallhovd, all from UoO and H. P. Olstad (Norwegian Defence Construction Service (FBT)), participated in fieldwork on Dovrefjell.

T. Eiken (UoO) did the carrier-phase differential GPS positioning and calculations. E. S. F. Heggem (UoO) calculated potential radiation for all BTS points. P.-E. Olsson (ABEM, Sweden) corrected the topography of the DT-5 profile on Dovrefjell. S. Bakkehøi (Norwegian Geotechnical Institute (NGI)), was responsible for the establishment of the meteorological station on Juvvasshøe, Jotunheimen. F. Sivertsvik (Norwegian Geological Survey (NGU)), performed the drilling (of borehole DB1) on Dovrefjell. The Norwegian Mapping Authority contributed with altitude base maps.

Professor W. Haeberli (University of Zurich), Professor H. French (University of Ottawa), Dr S. Gruber (University of Zurich) and one anonymous referee carefully read the manuscript and gave advice and constructive comments. Professor C. Harris (Cardiff University) corrected the English.

The study was financed by the PACE-project (Contract no. ENV4-CT97-0492 and BBW no. 97.0054-1), the Norwegian Research Council (NFR; Contract no. 12052/720), the FBT (Contract no. 325 01) and the Department of Physical Geography, UoO. The Norwegian Meteorological Institute (DNMI), by B. Aune, financially supported the meteorological station on Juvvasshøe. NGU, by B. A. Follestad, financially supported borehole DB1 on Dovrefjell. FBT, by O.-E. Martinsen, financed the DB1 borehole instrumentation.

The above-mentioned persons and institutions are all gratefully acknowledged.

Manuscript submitted 10 May 2001; accepted 31 January 2002

References

- Aune, B. 1993. Temperaturnormaler, normalperiode 1961–1990. *DNMI. Report 2/93 KLIMA*. 63 pp.
- Barry, R. G. 1992. *Mountain Weather and Climate*. London, New York. 402 pp.
- Batthey, M. H. 1960. Geological factors in the development of Veslgjuv-botn and Vesl-Skautbotn. *Royal Geographical Society (R.G.S.) Research Series* 4, 5–10.
- Bruun, I. 1957. *Lufttemperaturer i Norge 1861–1955*, Bind I. Norwegian Meteorological Institute, Oslo.
- Cressie, N. 1993. *Statistics of Spatial Data*. Wiley, New York.
- Dramis, F., Govi, M., Guglielmin, M. & Mortara, G. 1995. Mountain permafrost and slope instability in the Italian Alps: the Val Pola Landslide. *Permafrost and Periglacial Processes* 6, 73–81.
- Etzelmueller, B., Hoelzle, M., Heggem, E. S. F., Isaksen, K., Stocker-Mittaz, C., Ødegård, R. S., Haeberli, W., Sollid, J. L. et al., 2001. Mapping and modelling the occurrence and distribution of mountain permafrost. *Norsk Geografisk Tidsskrift—Norwegian Journal of Geography* 55(4), 186–194.
- Førland, E., Roald, L. A., Tveito, O. E. & Hanssen-Bauer, I. 2000. Past and future variations in climate and runoff in Norway. *Norwegian Meteorological Institute, Report 19/00*.
- French, H. M. 1996. *The Periglacial Environment*. Longmans, London.
- Goodrich, L. E. 1982. The influence on snow cover on the ground thermal regime. *Canadian Geotechnical Journal* 19, 421–432.

- Gruber, S. & Hoelzle, M. 2001. Statistical modelling of mountain permafrost distribution: local calibration and incorporation of remotely sensed data. *Permafrost and Periglacial Processes* 12(1), 69–78.
- Haerberli, W. 1973. Die Basis Temperatur der winterlichen Schneedecke als möglicher Indikator für die Verbreitung von Permafrost. *Zeitschrift für Gletscherkunde und Glazialgeologie* 9, 221–227.
- Haerberli, W. 1992. Construction, environmental problems and natural hazards in periglacial mountain belts. *Permafrost and Periglacial Processes* 3, 111–124.
- Haerberli, W. & Patzelt, G. 1982. Permafrostkartierung im Gebiet der Hochebenkar – Blockgletscher, Obergurgl, Ötztaler Alpen. *Zeitschrift für Gletscherkunde und Glazialgeologie* 18, 127–150.
- Haerberli, W., Guodong, C., Gorbunov, A. P. & Harris, S. A. 1993. Mountain permafrost and climate change. *Permafrost and Periglacial Processes* 4, 165–174.
- Harris, C. & Cook, J. D. 1986. The detection of high altitude permafrost in Jotunheimen, Norway, using seismic refraction techniques: an assessment. *Arctic and Alpine Research* 18, 19–26.
- Harris, C., Davies, M. C. R. & Etzelmüller, B. 2001a. The assessment of potential geotechnical hazards associated with mountain permafrost in a warming global climate. *Permafrost and Periglacial Processes* 12, 145–156.
- Harris, C., Haerberli, W., Vonder Mühll, D. & King, L. 2001b. Permafrost monitoring in the high mountains of Europe: the PACE project in its global context. *Permafrost and Periglacial Processes* 12, 3–12.
- Hartmann, D. L. 1994. Global Physical Climatology. *International Geophysics Series* Vol. 56. Academic Press. 411 pp.
- Hauck, C. 2001. Geophysical methods for detecting permafrost in high mountains. Ph.D. thesis, VAW-ETH Zurich, *Mitteilungen* Nr. 171. 204 pp.
- Hauck, C. & Vonder Mühll, D. 1999a. Using DC resistivity tomography to detect and characterise mountain permafrost. *61st European Association of Geoscientists and Engineers (EAGE) Conference, Proceedings (Helsinki, 7–11 June 1999)*, 2–15.
- Hauck, C. & Vonder Mühll, D. 1999b. Detecting Alpine permafrost using electro-magnetic methods. Hutter, K., Wang, Y. & Beer, H. (eds.) *Advances in Cold Regions Thermal Engineering and Sciences*, 475–482. Springer Verlag, Heidelberg.
- Hauck, C., Vonder Mühll, D., Russil, N. & Isaksen, K. 2000. An integrated geophysical study to map mountain permafrost: a case study from Norway. *6th EEGS Conference, Proceedings (Bochum, 3–6 September 2000)*. Extended Abstracts, CH01. 4 pp.
- Heggen, E. S. F., Etzelmüller, B. & Berthling, I. 2001. Topographic radiation balance models: sensitivity and application in periglacial geomorphology. *Norsk Geografisk Tidsskrift–Norwegian Journal of Geography* 55(4), 203–211.
- Hoelzle, M. 1992. Permafrost occurrence from BTS measurements and climatic parameters in the Eastern Swiss Alps. *Permafrost and Periglacial Processes* 3, 143–147.
- Hoelzle, M., Wegmann, M. & Kruppenacher, B. 1999. Miniature temperature dataloggers for mapping and monitoring of permafrost in high mountain areas – first experience from the Swiss Alps. *Permafrost and Periglacial Processes* 10, 113–124.
- Hoelzle, M., Mittaz, C., Etzelmüller, B. & Haerberli, W. 2001. Surface energy fluxes and distribution models relating to permafrost in European Mountain areas: an overview of current developments. *Permafrost and Periglacial Processes* 12(1), 53–68.
- Imhof, M., Pierrehumbert, G., Haerberli, W. & Kienholz, H. 2000. Permafrost investigation in the Schilthorn Massif, Bernese Alps, Switzerland. *Permafrost and Periglacial Processes* 11, 189–206.
- Isaksen, K. 2001. Past and present ground thermal regime, distribution and creep of permafrost – case studies in Svalbard, Sweden and Norway. *Series of dissertations submitted to the Faculty of Mathematics and Natural Sciences, University of Oslo*. No. 144. Unipub forlag, Oslo.
- Isaksen, K., Holmlund, P., Sollid, J. L. & Harris, C. 2001. Three deep alpine permafrost boreholes in Svalbard and Scandinavia. *Permafrost and Periglacial Processes* 12, 13–16.
- Keller, F. & Gubler, H. 1993. Interaction between snow cover and high mountain permafrost Murtél/Corvatsch, Swiss Alps. *6th International Conference on Permafrost (Beijing, 23–27 June 1998)*, Collection Nordicana 57, 332–337. Centre d'études nordiques, Université Laval, Québec.
- King, L. 1982. Qualitative and quantitative Erfassung von Permafrost in Tarfala (Schwedisch-Lappland) und Jotunheimen (Norwegen) mit Hilfe geoelektrischer Sondierungen. *Zeitschrift für Geomorphologie, N.F. Suppl.-Bd.* 43, 139–160.
- King, L. 1983. High mountain permafrost in Scandinavia. *4th International Conference on Permafrost, (Edmonton), Proceedings*, 612–617.
- King, L. 1984. Permafrost in Scandinavia, results from Lapland, Jotunheimen and Dovre/Rondane. *Heidelberger Geographische Arbeiten* 76. 174 pp.
- Kneisel, C., Hauck, C. & Vonder Mühll, D. 2000. Permafrost below the timberline confirmed and characterized by geoelectrical resistivity measurements, Bever Valley, eastern Swiss Alps. *Permafrost and Periglacial Processes* 11, 295–304.
- Krill, A. G. 1987. *Snøhetta berggrunnskart 1519 IV, 1:50000. Preliminary printed map, The Geological Survey of Norway (NGU)*.
- Loke, M. H. & Barker, R. D. 1995. Rapid least-squares inversion of apparent resistivity pseudosections using a quasi-Newton method. *Geophysical Prospecting* 44, 131–152.
- Moore, I. D., Norton, T. W. & Williams, J. E. 1993. Modelling environmental heterogeneity in forested landscapes. *Journal of Hydrology* 150, 717–747.
- Ødegård, R. S. 1986. Periglasiale former og permafrost ved Juvvasshytta i Jotunheimen. Master's thesis (Cand. Sci.), Department of Physical Geography, University of Oslo. 89 pp.
- Ødegård, R. S., Liestøl, O. & Sollid, J. L. 1988. Periglacial forms related to terrain parameters in Jotunheimen, southern Norway. *5th International Conference on Permafrost (Trondheim)*, Vol. 3, 59–61. Tapir Publishers, Trondheim.
- Ødegård, R. S., Sollid, J. L. & Liestøl, O. 1992. Ground temperature measurements in mountain permafrost, Jotunheimen, southern Norway. *Permafrost and Periglacial Processes* 3, 231–234.
- Ødegård, R. S., Hoelzle, M., Johansen, K. V. & Sollid, J. L. 1996. Permafrost mapping and prospecting in southern Norway. *Norsk Geografisk Tidsskrift* 50, 41–53.
- Østrem, G. 1964. Ice-cored moraines in Scandinavia. *Geografiska Annaler* 3, 282–337.
- Østrem, G., Dale Selvig, K. & Tandberg, K. 1988. *Atlas over breer in Sør-Norge*. Meddelser nr. 61 fra Hydrologisk avdeling. Norwegian Water Resources and Energy Directorate (NVE). Oslo. 45 pp.
- Sætre, S. 1997. Undersøkelser av permafrost i Snøhetta-området, Dovrefjell, Sør-Norge. 63 pp. Master's thesis (Cand. Sci.), Department of Geography, University of Oslo. *Rapportserie i naturgeografi, Universitetet i Oslo, Report 9*. 64 pp.
- Scott, W., Sellmann, P. & Hunter, J. 1990. Geophysics in the study of permafrost. Ward, S. (ed.) *Geotechnical and Environmental Geophysics*, 355–384. Society of Exploring Geophysics, Tulsa.
- Smith, M. W. 1975. Microclimatic influences on ground temperatures and permafrost distribution, Mackenzie Delta, Northwest Territories. *Canadian Journal of Earth Sciences* 12, 1421–1438.
- Sollid, J. L. & Sørbel, L. 1984. Einunna. Beskrivelse til kvartærgeologisk kart 1:50000 (1519 I). *Norsk Geografisk Tidsskrift* 38, 43–68.
- Sollid, J. L. & Sørbel, L. 1994. Distribution of glacial landforms in southern Norway in relation to the thermal regime of the last continental ice sheet. *Geografiska Annaler* 76A, 25–35.
- Sollid, J. L. & Sørbel, L. 1997. *Geomorfologien på Dovrefjell*. Fylkesmannen i Hedmark, Miljøvernavdelingen, Report 13/97. 39 pp.
- Sollid, J. L. & Sørbel, L. 1998. Palsa bogs as a climate indicator – examples from Dovrefjell, southern Norway. *Ambio* 27, 287–291.
- Sollid, J. L., Holmlund, P., Isaksen, K. & Harris, C. 2000. Deep permafrost boreholes in western Svalbard, northern Sweden and southern Norway. *Norsk Geografisk Tidsskrift–Norwegian Journal of Geography* 54(4), 186–191.
- Vonder Mühll, D., Stucki, T. & Haerberli, W. 1998. Borehole temperatures in Alpine permafrost: a ten years series. *7th International Conference on Permafrost (Yellowknife, 23–27 June 1998)*, Collection Nordicana 57, 1089–1095. Centre d'études nordiques, Université Laval, Québec.
- Vonder Mühll, D., Hauck, C. & Lehmann, F. 2000. Verification of geophysical models in Alpine permafrost using borehole information. *Annals of Glaciology* 31, 300–306.

Mountain Permafrost Distribution Modelling using a Multi-criteria Approach in the Hövsgöl Area, Northern Mongolia[†]

Bernd Etzelmüller,^{1*} Eva S. Flo Heggem,¹ N. Sharkhuu,² Regula Frauenfelder,³ Andreas Käüb¹ and Clyde Goulden⁴

¹ Department of Geosciences, Physical Geography, University of Oslo, Oslo, Norway

² Hövsgöl GEF Project, Institute of Geo-Ecology, Mongolian Academy of Sciences, Ulaanbaatar, Mongolia

³ Department of Geography, University of Zürich, Zürich, Switzerland

⁴ Institute of Mongolian Biodiversity and Ecological Studies, Academy of Natural Sciences, Philadelphia, Pennsylvania, USA

ABSTRACT

Lake Hövsgöl is located on the southern fringe of the continuous permafrost zone in northern Mongolia. This paper describes a GIS-based empirical permafrost model that is calibrated with ground temperature observations, and utilises a multi-criteria approach to derive zones of permafrost favourability based on terrain parameters and land cover information. The scores are derived either by logistic regression or from satellite image information. The model is validated by DC resistivity tomography measurements. The overall permafrost distribution in the study area is well-described and the method appears to be a valid approach for mapping permafrost at both local and regional scales in mountain areas with low data coverage. Copyright © 2006 John Wiley & Sons, Ltd.

KEY WORDS: permafrost; Mongolia; DC resistivity tomography; permafrost modelling; GIS

INTRODUCTION AND BACKGROUND

The distribution of permafrost in Mongolia is known from numerous studies carried out by Russian (e.g. Gravis *et al.*, 1978; Gravis, 2001; Zabolotnik, 2001) and Mongolian scientists (e.g. Sharkhuu, 1993, 1998, 2001b; Tumurbataar and Mijiddorj, 2006). Starkel (1998) published a transect of environmental parameters in the region from Tibet to Siberia at a continental scale. Bohner and Lehmkuhl (2005) recently modelled the forest, glacier and permafrost

spatial distribution based on empirical relationships in Central Asia for past and future climate scenarios, and anticipated a severe decrease of both glacier cover and permafrost extent. Most studies of present-day permafrost in Mongolia are based on borehole temperatures, with the measurement locations representing typical landscape settings, such as certain topographic aspects or vegetation cover types. This knowledge has been used to create permafrost maps at a variety of scales (e.g. Sharkhuu, 2001a). As mountain permafrost in Mongolia delineates the southern fringe of the continuous Siberian permafrost zone, it is vulnerable to climate change. During the last few decades a substantial warming has been observed, both in measurements at climate stations (e.g. Dagvadorj *et al.*, 2001; Namkhajantsan, 2006) and in borehole temperatures (e.g. Sharkhuu, 1998).

In the arid, high-mountain Hövsgöl area in northern Mongolia (c. 50°N, 100°E) an interdisciplinary pro-

* Correspondence to: Bernd Etzelmüller, Department of Geosciences, Physical Geography, University of Oslo, PO Box 1047, Blindern, N—0316 Oslo, Norway.
E-mail: bernde@geo.uio.no

[†]The study was financially supported by a grant from the Global Environment Facility (GEF), implemented by the World Bank and awarded to the GeoEcology Institute of the Mongolian Academy of Sciences.

ject has been examining the relationship between permafrost, ecosystems and anthropogenic land use (nomadism). Records of ground surface temperature based on temperature data-loggers and ground temperature readings from shallow boreholes give a general indication of the permafrost thermal structure. The main aim of this study was to model the spatial distribution of permafrost. In heterogeneous mountain areas, models must be used that include topographically related effects and surface characteristics (e.g. Hoelzle *et al.*, 2001). Such models are either *empirical* or *process-oriented*. Process-oriented models assess the energy regime directly, based on high-resolution inputs of measured climatic parameters. However, the extensive input of meteorological information needed for model calibration is seldom available for remote areas. Therefore, the aim of this study was to derive an empirical permafrost distribution model using the relation between certain topo-climatic factors and permafrost existence. A Geographical Information System (GIS)-based methodology was used, derived from a limited number of ground surface temperature records and digital elevation model (DEM)-derived parameters (e.g. Etzelmüller *et al.*, 2001), and employing a multi-criteria approach. DC resistivity tomography was used to validate the results.

SETTING

The study area encompasses the eastern side of Lake Hövsgöl (Figure 1). The lake is situated at 1650 m a.s.l., is 135 km long, between 20 and 40 km wide, and has a maximum depth of approximately 260 m. While the western side of the lake is dominated by alpine relief above 3000 m a.s.l., the eastern side has more gentle topography with mountain peaks up to 2300 m a.s.l. Morphologically, the eastern shore is dissected by a series of east-west oriented valleys, including the valleys of Borsog, Dalbay, Shagnuul and Turag (Figure 1), which are the main field sites of this study. Devonian dolomites and olivine basalts dominate the lithology of the area. During humid phases in the Pleistocene, the lake level fluctuated up to 100 m (e.g. Goulden *et al.*, 2006; Krivonogov 2006). This resulted in sand-rich lacustrine valley fills and lake terraces along the valley slopes.

Siberian larch forest exists on the hills but is virtually absent on the valley floors and on steeper south-facing slopes. The forest in this area forms the southern edge of the Siberian taiga and defines the southern fringe of continuous permafrost in Central Asia (Figure 1). This environment is therefore highly

sensitive to climate variations. The nearest climate station is at Hatgal, about 65 km south of the main study area. The present climate conditions are characterised by cold, dry winters with little snow, and by mild, wetter summers. The mean annual air temperature (MAAT) in Hatgal is -4.5°C . Average precipitation is between 300 and 350 mm a⁻¹, and is mainly related to convective rain storms which are concentrated from mid-June to early August. In Hatgal, and at the neighbouring climate stations, an increase of MAAT of more than 1.5°C has been measured during the last few decades (Namkhajantsan, 2006). The snow cover in the area is thin, normally less than 10 to 20 cm, but higher in flat forest stands. Sublimation is common on south-facing slopes, often keeping them snow-free during the winter.

According to Sharkhuu (1998), permafrost exists both close to the lake shore and in the mountains except on south-facing slopes. Above approximately 2200 m a.s.l., permafrost seems to be continuous, even on south-facing slopes. It is assumed that this elevation is lower on the eastern shore due to a more gentle relief. According to borehole records permafrost thickness at the elevation of the lake is in the order of tens of metres, increasing to more than 200 m in the high mountains.

The non-forested valley bottoms and steppe areas are used to varying degrees for grazing by nomad livestock. While there is little or no pasture use in the southern valleys of Borsog and Dalbay, the northerly valleys of Shagnuul and Turag are characterised by more intensive grazing. This leads to an altered vegetation cover which is expected to affect the permafrost.

METHODS

Temperature Measurements and Data Basis

Ground surface temperatures were monitored continuously at 18 locations (2002–04) using UTL-1 miniature temperature loggers, which were buried in the ground at depths of 5 to 10 cm (Table 1). The thermistors in these loggers are of the TMC-1T type, with an accuracy of $\pm 0.13^{\circ}\text{C}$ (c.f. Hoelzle *et al.*, 1999). Information was also obtained from shallow boreholes (<10 m). Temperatures in the boreholes were read manually using a movable thermistor string or monitored using UTL1 or Onset Hobo data-loggers. Based on the temperature measurements on the surface and in the boreholes it was decided whether a site had permafrost or not, and a binary variable was formed ($n = 30$).

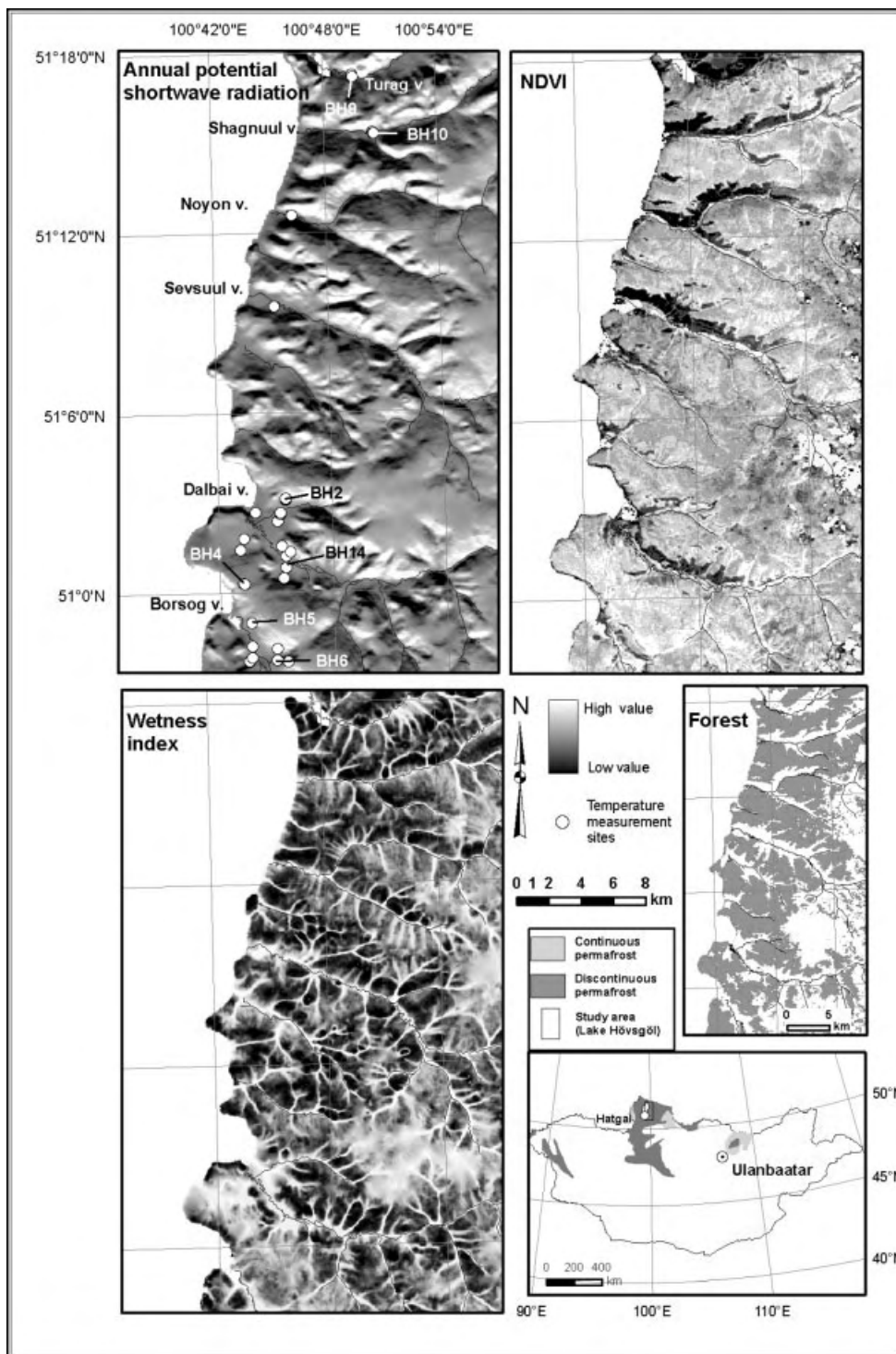


Figure 1 Derived terrain parameters and NDVI. The inset map for the study site shows regional permafrost distribution based on Brown *et al.* (1995). The solid circles denote the data points used in the study (miniature data logger positions and boreholes). The numbers refer to the borehole numbering.

Table 1 Ground surface temperature data.

Temperature measurement site	Elevation	TDD FDD	MGST FN	WI	PR year W/m ²	Surface cover	Permafrost favourability (<i>f</i>)	Permafrost (yes/no)
M27	1806	1116	-0.9	8	185	Forest	0.46	Yes
Borsog		-1471	0.53					
M26	1667	306	-1.2	10	194	Forest	0.58	Yes
Borsog		-744	0.61					
M12	1719	2378	2.4	9	232	Dry Grass	0.21	No
Borsog		-1483	0.44					
BHAL	1659	1255	-0.5	13	199	Grass	0.64	Yes
Borsog		-1526	0.52					
BH6	1691	1643	1.0	10	188	Grass	0.51	Yes
Borsog		-1314	0.46					
BH5	1708	1405	-0.6	9	232	Forest	0.19	No
Borsog		-1713	0.52					
BH4	1799			12	205	Forest	0.69	Yes
Borsog								
BH3	1705	1123	-0.5	10	191	Forest	0.73	Yes
Borsog		-1328	0.52					
M21	1675	507	-2.8	11	193	Wet Grass	0.64	Yes
Dalbaj		-1557	0.64					
M15	1680	1670	-0.5	10	196	Grass	0.63	Yes
Dalbaj		-1834	0.51					
M08	1727	1469		8	222	Dry Grass	0.17	No
Dalbaj		-1905						
M06	1697	1886	1.2	8	230	Dry Grass	0.25	No
Dalbaj		-1491	0.47					
M04	1722	1145	-1.4	11	180	Grass	0.67	Yes
Dalbaj		-1706	0.55					
BH2	1735	1407	-0.1	7	219	Forest	0.11	No
Dalbaj		-1511	0.51					
BH1	1656	1461	-0.3	10	197	Grass	0.61	Yes
Dalbaj		-1664	0.52					
M03	1678			10	198	Wet Grass	0.64	Yes
Dalbaj								
M28	1707	1743	-0.4	12	207	Grass	0.66	Yes
Shagnuul		-1903	0.51					
M22	1706	1044	-2.3	13	203	Grass/Forest	0.66	Yes
Shagnuul		-1896	0.57					
M16	1670	1914	-2.2	15	198	Grass	0.63	Yes
Turag		-2709	0.54					

BH = loggers attached to boreholes; M = loggers placed outside borehole location; MGST = mean ground surface temperature; FN = frost number, calculated using $FN = FDD^{1/2} / (FDD^{1/2} + TDD^{1/2})$, where FDD = freezing degree days and TDD = thawing degree days (Nelson and Outcalt, 1987), FN > 0.5 indicates permafrost; WI = wetness index, calculated after Beven and Kirkby (1979); PR = potential incoming direct solar radiation, calculated after Wilson and Gallant (2000); *f* = permafrost favourability obtained from the permafrost model described in this study. The parameters are sampled from the DEM-derived maps.

Generation of a DEM and Derivation of Relief Parameters

A 50 m DEM, was generated from digitised contour lines (at 20-m intervals) derived from analogue Russian maps published in 1942 and re-printed in 1962,

originally at a scale of 1:100 000. The absolute accuracy of these maps is not known. A gridding algorithm implemented in the GIS-software ArcGIS (®ESRI, USA) based on Hutchinson's (1989) ANUDEM algorithm was applied (version 4.6.3). The contour line elevations were used for interpolation while the

digitised river network served as break lines. The algorithm is based on a minimum curvature (or spline) interpolation, which often smooths out surfaces and sharp edges, an effect that is not necessarily advantageous for steep mountain areas. However, the field area has fairly smooth relief and small topographic features are not represented on the contour map, so the interpolation algorithm is expected to represent topography satisfactorily within the limits of the resolution and the original quality of the contour line map. Visual inspection of the DEM was performed to identify and correct larger errors. Absolute accuracy of the DEM could not be established because of the lack of reliable GPS benchmarks. However, the DEM is within the accuracy range of handheld GPS-derived elevations, or some tens of metres.

The DEM was used to calculate the topographic point-parameters *slope*, *curvature*, *potential radiation* and *wetness index* (Figure 1). *Slope*, *aspect* and *curvature* were calculated following the procedures described in Zevenberge and Thorne (1987). The spatial distribution of potential solar radiation was estimated using the 'SRAD' topographic model (see Wilson and Gallant, 2000). In our study no adjustment was made for surface characteristics such as albedo or emissivity. The topographic *wetness index* is defined as the quotient of the specific upstream area and the surface slope (Beven and Kirkby, 1979) (Figure 1). For calculating the *specific upstream area*, an algorithm allowing diverting flow was used (e.g. Wilson and Gallant, 2000). Transmissivity values were not included in the calculation because of a lack of reliable spatial data on this factor. The index as used, therefore, describes a form of potential wetness due to topographic and not sub-surface conditions. The index is widely employed as a soil moisture substitute, and several studies exist relating it to measured soil moisture (e.g. Sulebak *et al.*, 2000; Hugget and Cheesman, 2002). For each binary data point the topographic parameters were obtained for further statistical analysis. Considering interpolation smoothing effects and DEM resolution these values represent topographic conditions in a wider neighbourhood than at a particular point, enhancing the regional characteristics of this study.

Satellite Image Classification

A Landsat TM mosaic image (ground resolution 30 m) and an ASTER scene (ground resolution 15 m, from 27 August 2001) were used for vegetation index calculation (e.g. Jensen, 2005) and land cover classification. The vegetation index ($NDVI = \text{Normal difference vegetation index}$) was derived from the

Landsat image using the formula $NDVI = (NIR - Red)/(NIR + Red)$ (e.g. Jensen, 2005). Both images were subsequently classified using standard supervised classification routines with the ERDAS Imagine (8) software. Five classes were selected: forest, open forest, grassland, dry grassland and sand. Areas such as exposed bedrock (revealed using *NDVI* and photos from the field), scattered clouds or haze and open water were excluded from the classification. Due to a lack of real ground-truthing coverage (aerial photos or up-dated topographic maps) the classified result was only qualitatively compared to field observations and photographs. The forest classification results were compared to scanned topographic maps containing a forest layer. Deviations were found on small mountain peaks. The topographic map showed forest at these sites whereas the classification results did not. The lower forest border corresponds well with the border displayed on the maps. Considering the simplicity of the land cover classes, the application scale and areal extent of the study region, this classification was considered to be sufficient.

DC Resistivity Soundings

The principle of the DC resistivity method is that different types of material have different abilities to conduct electricity (e.g. Reynolds, 1997). The application of resistivity soundings in permafrost mapping is justified through the large contrast between water resistivity ($\sim 10^1$ to $10^2 \Omega\text{m}$) and permafrost with ground ice ($\sim 10^3$ to $10^6 \Omega\text{m}$). Therefore, the method allows for the identification of ground ice, and hence permafrost in water-containing material (e.g. Vonder Mühl *et al.*, 2002). For two-dimensional (2D) resistivity tomography, an ABEM Lund (®ABEM Sweden) multi-electrode, high-resolution 2D resistivity system was used. This system is based on cables with a standard spacing of 2 m, and can measure a length of 160 m during one survey. We used the Wenner configuration (see Reynolds, 1997), which gives a maximum electrode distance of 48 m and a maximum penetration depth of approximately 25 m for our setup. The length of a section can be increased by moving individual cables from one end to the other, allowing flexible profile lengths. The system automatically measures the resistance for a given electrode combination with varying spacing and calculates resistivity. 2D-model interpretation was undertaken using the software package RES2DINV, which performs smoothness-constrained inversions using finite difference forward modelling (Loke and Barker, 1995). Profiles were topographically corrected before inversion.

Statistical Analyses

Descriptive statistics, non-parametric (Spearman) correlations and logistic regression parameters were calculated using the statistical programme package SPSS (©SPSS Inc., v. 12). Logistic regression modelling was used to estimate the spatial permafrost probability based on single independent variables, an approach recently introduced in mountain permafrost research (Lewkowicz and Ednie, 2004; Brenning *et al.*, 2005). The logistic regression estimates the probability of a certain condition occurring (here 'permafrost' or 'no permafrost') by calculating changes in the log odds of the dependent variable. The logistic regression model solves this problem:

$$\ln \left[\frac{p}{1-p} \right] = A + Bx + Cy \dots \quad (1)$$

where p is the probability of permafrost existence, A is the regression constant, B and C are regression coefficients and x and y are the independent variables. The logistic regression is thus a non-linear transformation of the linear regression, describing an S-shaped distribution function. The distribution is constrained by the estimated probabilities between 0 and 1, and takes the form:

$$p = \frac{1}{1 + \exp(-A - Bx - Cy \dots)} \quad (2)$$

EMPIRICAL MODELLING AND VALIDATION

Basic Data

Freezing and thawing indices were established for different sites using the near-surface temperature logger data (Table 1). During the measurement period (2002–04) freezing indexes varied between -1400 and -2700°C d , while thawing indexes were between 300 and 2300°C d . Loggers in forest and wet grass influenced by shading and water refreezing effects generally showed lower thawing degree day totals than those in drier and open settings. Mean ground surface temperatures (MGST) were mostly around

-1°C or above, except in wet grass settings in the riparian zone (M21) or in the northerly valleys of Turag and Shagnuul, which appear to be cooler than other sites during winter. This is also indicated by automatic climate station measurements in the valleys of Dalbai and Turag (Namkhajantsan, 2006). The sites in dry grass or steppe vegetation exhibit annual mean temperatures above 0°C and show no permafrost. However, there are cases which are not straightforward, such as the loggers BH2 or BH6 (Table 1). The former is located on a southerly slope in open forest and has no permafrost according to borehole measurements. The latter is on the edge between dry and wet grass and there is some permafrost in the adjacent borehole. The ground temperatures measured in the boreholes indicate a thin permafrost layer with temperatures near 0°C for locations outside the wet, grass-covered valley bottoms. In wet, grass-covered parts of the valley bottoms, ground temperatures at 10 m depth are between -1.5 and -2°C . Active layer thicknesses in the boreholes are around 1–2 m in wet valley settings, increasing up to 4–5 m in drier settings both in grassland and forest. In general, the temperature pattern confirms that vegetation, wetness conditions and aspect are major variables for determining permafrost distribution in the area.

Relation and Statistics

We first related the binomial existence of permafrost derived from the field observations to topographic parameters (Table 2). Significant relations were established in spite of the limited data. Permafrost existence has a strong positive correlation to the *wetness index*, and some weaker negative correlations to *curvature* and *potential solar radiation*. The parameters *wetness index* and *curvature* are strongly inter-correlated, especially *plan curvature* which displays water-converging topographic conditions. The *NDVI* and the elevation are not significantly correlated to permafrost. Concerning elevation, the range of the data is small. In general, a greater probability of permafrost is expected at higher elevations due to negative lapse rates but the range of data is too limited to demonstrate this. Concerning vege-

Table 2 Non-parametric (Spearman's rho) correlation for terrain parameters and binary permafrost probability (Perm).

Perm	ELEV	CURV	PLAN	PROF	NDVI	WI	PR	PRSUM	SLOPE	PRWI	Perm
1.000	-0.347	-0.443 (*)	-0.616 (**)	-0.010	0.279	0.704 (**)	-0.588 (**)	-0.588 (**)	-0.616 (**)	-0.589 (**)	Perm

*Correlation is significant at the 0.05 level (two-tailed). **Correlation is significant at the 0.01 level (two-tailed). N = 30. ELEV = elevation (m); CURV = total curvature; PLAN = plan curvature; PROF = profile curvature; NDVI = vegetation index; WI = wetness index; SLOPE = surface slope; PRSUM, PR and PRWI = potential solar radiation averaged over summer, year and winter, respectively.

tation biomass, the *NDVI* shows a positive, but non-significant relation to permafrost existence. This is probably due to the low number of quantitative data points and the relatively coarse resolution of the data. The average *NDVI* was 0.42 in forest, 0.35 for grass and 0.21 for dry grass, indicating that the calculated *NDVI* does not reflect the vegetation distribution.

Permafrost Distribution Map

From our field observations and other investigations (e.g. Sharkhuu, 2006; Heggem, 2005) it is evident that vegetation cover (especially forest), topographic wetness, potential radiation and partly elevation are the main factors governing permafrost distribution in the area. The available measurement points (distributed spatially over a limited area) are certainly too weak a basis for an overall multi-dimensional quantitative probabilistic approach such as those derived between topo-climatic factors and mountain permafrost indi-

cators like *BTS* (basal temperature of snow) in various high mountain areas (e.g. Lewkowicz and Ednie, 2004; Brenning *et al.*, 2005). Therefore, scores were derived for single factors based on simple logistic regression (Figure 2), and then the sum of the derived probabilities was used as a measure of permafrost favourability in a given location within the framework of a multi-criteria analysis (e.g. Eastman, 1999). The index maps are in this case the map layers which represent the spatially distributed attributes that are found to contribute to the favourability (f) of permafrost existence. The combination of assigned weights (w) for each of the index maps (M) and a given score (X) can be expressed as:

$$f = \sum_M w_M X_M \quad (3)$$

Scores based on logistic probabilities were derived between permafrost presence and *potential radiation* and *wetness index*, respectively (Figure 2). The relations are weak, with low significance values for the constants and coefficients (0.1–0.3), but reproduce the data points quite well (90% correctly classified, $r^2 > 0.7$). For the *elevation* factor a satisfactory statistical relationship could not be derived because of a limited range of field data. Furthermore, at lower elevations there is no straightforward relationship between permafrost and elevation. Assuming cooling-with elevation on an annual basis an s-shaped function centred around 1900 m a.s.l. was constructed (Figure 2). This value was chosen based on the average tree line elevation in the study area and on many years of observations by one of the authors. Vegetation was included as a fourth factor, using the *NDVI* to define the scores, but distinguishing between inside and outside the forest. High *NDVI* within the forest denotes dense trees or dense under-storey vegetation, both of which favour permafrost. High *NDVI* outside forest denotes dense and/or wet grass cover, and in addition *NDVI* averages in wetlands are higher than those in dry grassland. All four data sets now had scores defined between 0 and 1.

As a last step the weights for these factors were chosen, a process that is highly subjective. At lower elevations, permafrost distribution can be satisfactorily described by *potential radiation*, *wetness index* and *forest existence*. Also the statistical analyses (Table 2) gave quite similar correlation values for the topographic parameters, so we gave the same weight (0.25) to each of these factors. To account for conditions at high elevation and for densely vegetated but not necessarily very wet sites, we used the factors *elevation* and *NDVI* outside the forest. However, we assigned them the same weight com-

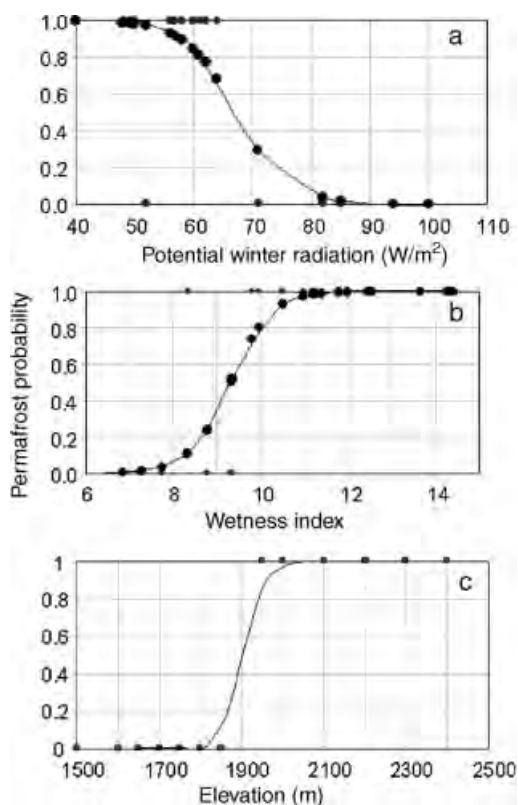


Figure 2 (a) Logistic regression between *winter solar radiation* and permafrost probability. (b) Logistic regression between *wetness index* and permafrost probability. (c) *Elevation* factor used to model increased favourability of permafrost above 1900 m a.s.l.

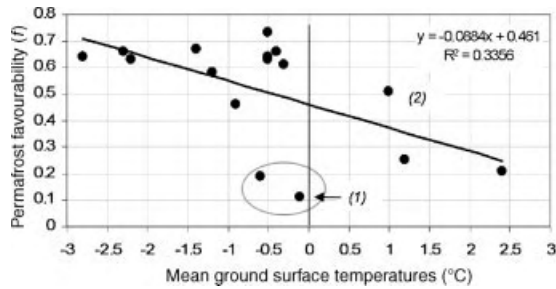


Figure 3 Plot of surface temperature against permafrost favourability. Outlier points: (1) Forest shading on southerly slopes at borehole 2; (2) Borsog valley bottom in transitional area with warm and shallow (<10 m) permafrost at borehole 6 (see Figure 1 and Plate 2).

bined as each of the other three. The reason for this was that *NDVI* outside forest and *wetness index* together would over-estimate the permafrost favourability. In addition *elevation* appears to be a major factor only at higher values, but we have no definitive quantitative data to demonstrate this.

The procedure resulted in a set of four data layers, each having values which indicate whether permafrost can be expected or not. The sum of these values represents an indicator of permafrost favourability (f) and ranges between 0 and 1. Plotting mean surface temperatures against f reveals a weak linear relation, showing $f=0.45$ at 0°C for the particular years of measurement (Figure 3). However, there is no straightforward relation between surface temperature and permafrost existence because of varying thermal offsets (e.g. Burn and Smith, 1988; Williams and Smith, 1989) in different materials. In addition the inter-annual variability of ground surface temperatures in the area is high. Forested southerly slopes show negative mean annual temperatures while boreholes indicate no permafrost. Conversely, dry surfaces in the transition between riparian zones and southerly slopes with thin permafrost show temperatures $>0^{\circ}\text{C}$ during this particular measurement period (Figure 3). Average f -values can be calculated for the land cover zones: forested and grass-covered areas show an average of $f=0.5$ or above, while dry steppe shows an average of less than $f=0.3$. The highest qualitative favourability is achieved in the wet valley bottoms of the riparian zone ($f>0.6$) and in north-facing, forest-covered slopes with high biomass ($f>0.7$). South-facing slopes have the lowest values ($f<0.2$). Intermediate areas comprise vegetated south-facing slopes and transitional areas between valley bottom and southerly slopes. Convex, water-diverging surface areas, even under forest cover on northerly slopes,

show reduced favourability due to low potential surface wetness, but still have f -values above 0.5.

Based on these investigations, we determined that areas with $f<0.3$ are unlikely to have permafrost, while those with $f>0.45$ are probably underlain by permafrost (Table 1). A transitional zone exists between these two thresholds where permafrost is possible (Figure 4). The nomenclature of the permafrost distribution as *possible* and *probable* is purely qualitative and avoids *continuous* or *discontinuous* permafrost, which is widely used in literature. This is in contrast to Lewkowicz and Ednie (2004), who defined the latter terms quantitatively based on statistically-derived probabilities derived from a large field data set.

Validation

2D resistivity tomography measurements were carried out at 22 sites in 2002 and 2005. The inversion procedure applied to the measured data resulted in low Root Mean Square (RMS)-errors, mostly below 10%. The results show varying resistivity patterns depending on aspect, vegetation cover and wetness. Good contrast in resistivities between frozen and unfrozen ground was present at most sites. To interpret profiles the transition between the active layer and the permafrost table was first obtained for selected locations based on ground temperature information from boreholes. In areas with thick sediment cover, mainly in the grass-covered valleys, the transition appears to be between $600\ \Omega\text{m}$ and $900\ \Omega\text{m}$ (Plate 1). In cold forest stands and under relatively dry soil it was not possible to distinguish clearly between the active layer and the permafrost. Based on the borehole measurements, active layer thickness varied between $c. 1\text{--}2\ \text{m}$ in wet sites in the riparian zone to more than $4\ \text{m}$ on drier well-drained sites. These values were well reproduced in the geophysical soundings (Plate 1). From the profile interpretations three main general patterns could be distinguished:

Grass-covered Sites in Valleys. The valley floors, especially in the riparian zone, indicate relatively high-resistivity permafrost ($>1500\ \Omega\text{m}$) for the areas studied (Plate 2, RT2, 6, 3b), overlain by an active layer with much lower resistivities. These areas show permafrost favourability values of between 0.5 and 0.7. The exceptions are profiles obtained in the northerly valleys of Turag and Shagnuul. While having a similar topographic setting as some of the Borsog and Dalbay valley profiles (north-facing gentle slopes close to the flat valley bottoms), the profiles in Turag and Shagnuul showed markedly higher resistivities near the surface (Plate 2, RT9, 10). These are

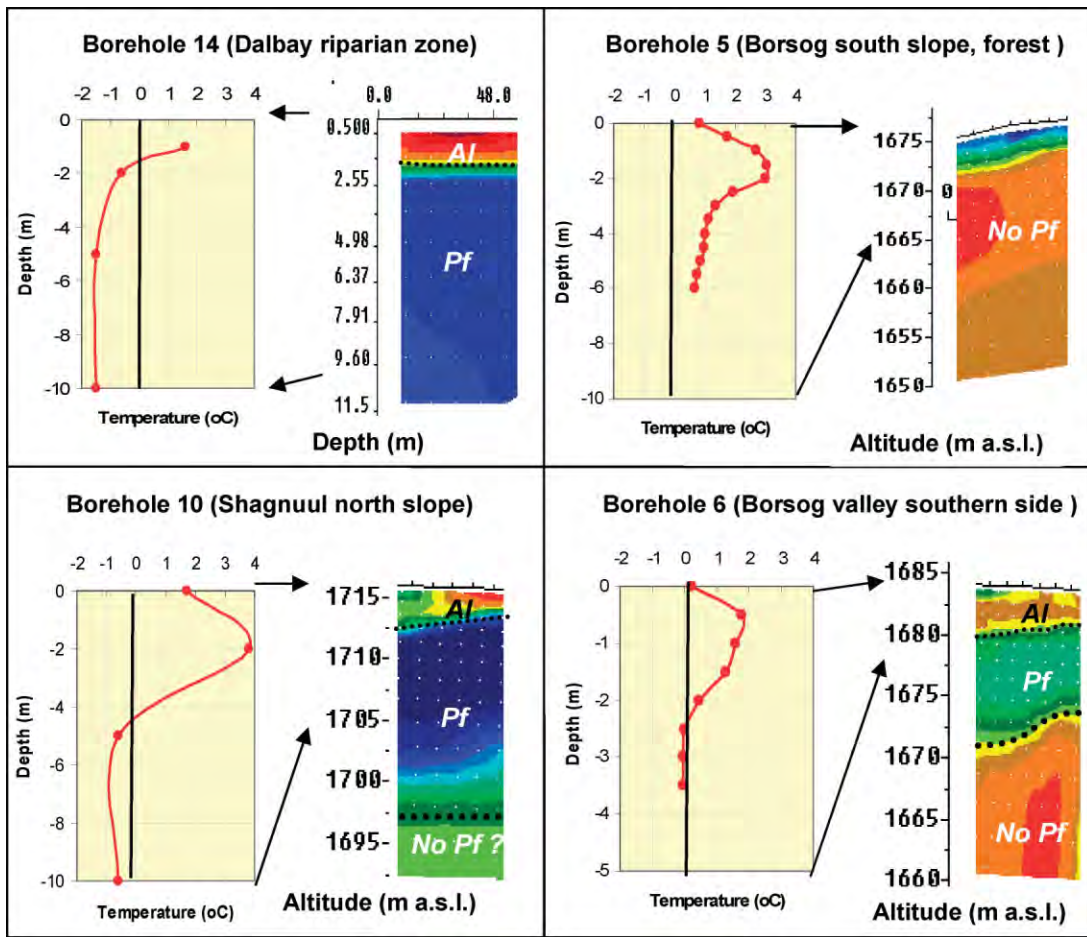


Plate 1 Ground temperatures and resistivities at selected boreholes. For colour scale, see Plate 2.

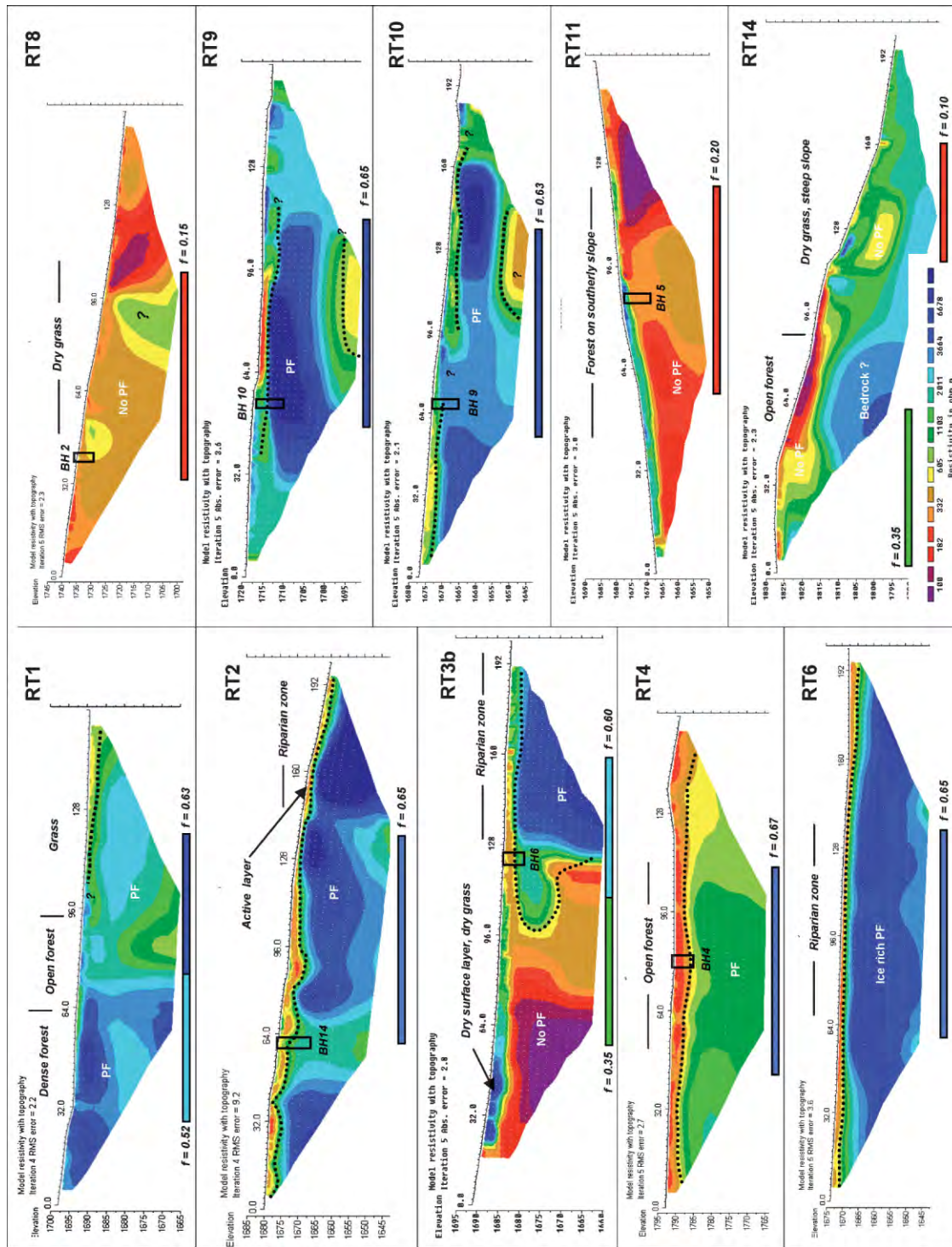


Plate 2 Selected resistivity profiles. Positions are given in Figure 4. The colour code is the same for all profiles. Red to yellow indicates resistivities below 700 kΩ m, a value that seems to define the border between the active layer and permafrost outside forested sites. Bluish colours indicate ice-rich permafrost or very dry conditions. Boreholes are indicated in the profiles and the dashed lines show the possible active layer thickness at the time of the resistivity soundings (late August 2002 and 2005).

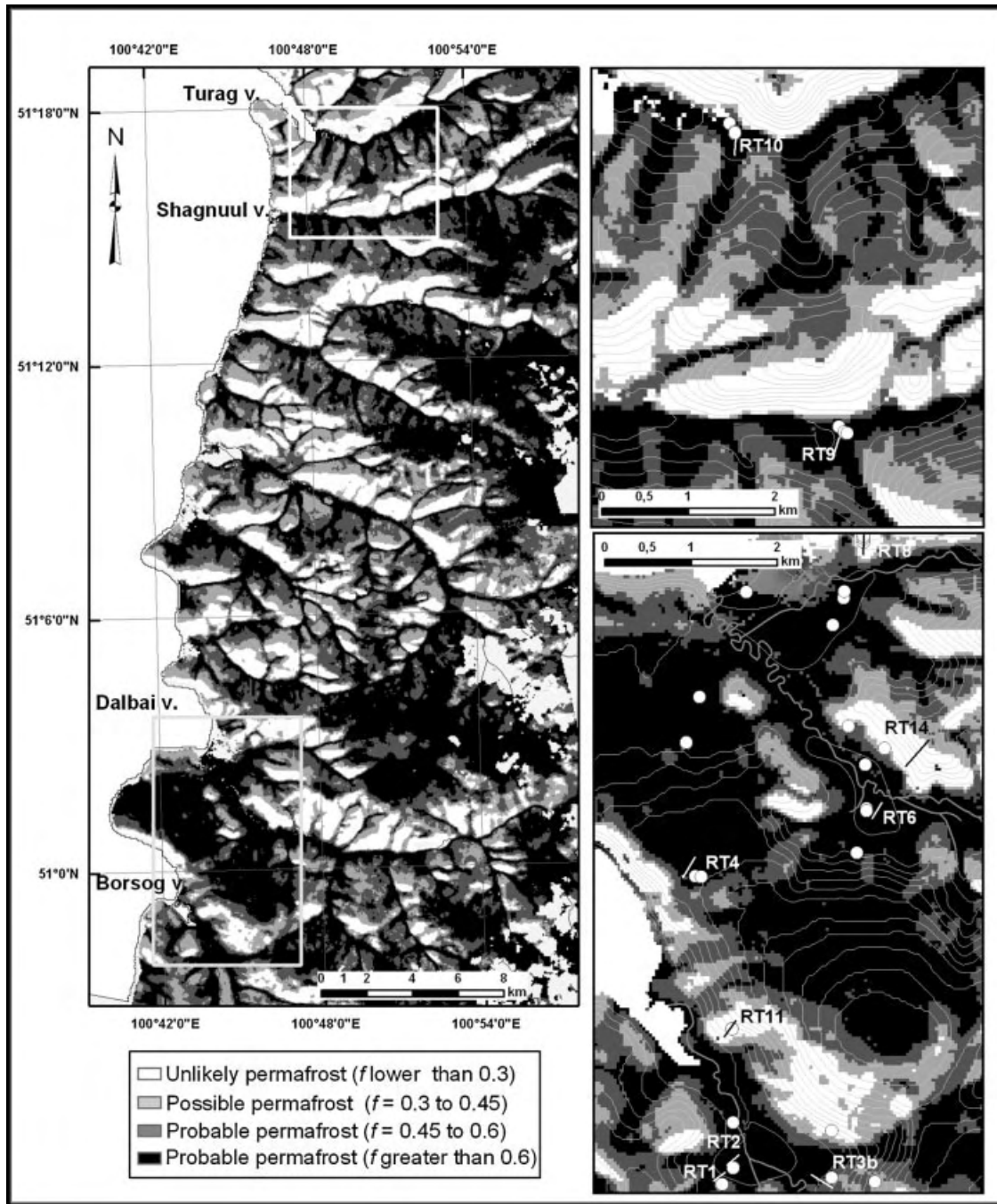


Figure 4 Regional permafrost favourability map. The inset map areas are enlargements of the main study areas containing the positions of the DC resistivity profiles used for validation (see Plate 2).

attributed to the grazing impacts of the large number of livestock in these valleys which result in a thinner vegetation cover. This in turn leads to drier near-surface soil conditions, a thicker active layer

(Goulden *et al.*, 2005) and thus higher resistivity values in the first layer of the model interpretation. This variability is not reproduced by the permafrost modelling approach.

South-facing Slopes. Permafrost is absent on south-facing slopes such as in the Dalbay (grass and open forest) and Borsog (forest) valleys (Plate 2, RT8, 11, 3b), and resistivity values are typically less than $500 \Omega\text{m}$ throughout the profile. At the surface, higher values can be obtained, which are normally attributable to dry surface soil conditions (e.g. Plate 2, RT3b, 11). The calculated permafrost favourability values are well below 0.3. The exceptions are steep southerly slopes with low surface sediment or regolith cover where relatively higher resistivities were measured at depth, probably due to solid and dry bedrock (Plate 2, RT14). At such sites there is no correspondence between resistivity values and estimated permafrost favourability.

Forested Slopes. Forested slopes, which mainly have northerly aspects, show the highest resistivities at depth (Plate 2, RT1), and these areas also exhibit the highest permafrost favourability values (>0.65). In northerly-exposed forest stands it was not possible to distinguish the active layer from the underlying permafrost. This may be due to low active layer thickness or the tree root system, which may cause larger air-filled voids. The exceptions here were flat forested areas, for example, in the pass between the Borsog and Dalbayn valleys, where the ground temperatures indicate a thick active layer and permafrost temperatures close to 0°C at 6 m depth. The resistivities obtained were relatively low (Plate 2, RT4), with values below $1000 \Omega\text{m}$, while the permafrost map displayed favourability values of $f \sim 0.7$. A possible explanation is snow cover, which in the forest is considerably thicker than in the valleys. Snow will effectively buffer the winter cold penetration and therefore leads to warmer ground temperatures. Another reason may be the presence of temperature inversions during winter, which are known to occur but were not quantitatively validated during this study. These factors are not considered during the permafrost map compilation procedure.

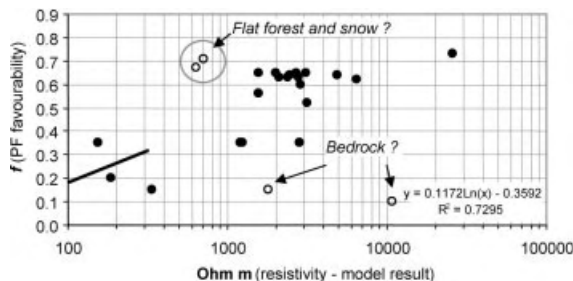


Figure 5 Plot of modelled resistivity at 8 m depth vs. permafrost favourability. The regression equation was developed without including the marked outliers.

For validation purposes we plotted apparent resistivity and modelled resistivity (Figure 5) obtained for 8 m depth against permafrost favourability obtained by the multi-criteria approach for 20 locations. When ignoring the outliers produced by either dry bedrock in southerly slopes or possible thick snow cover in flat, forested sites (Figure 5, open circles), a significant log-linear relation could be obtained, with a R^2 of ~ 0.73 (Figure 5). Thus, the tomography results appear to confirm the overall permafrost distribution calculated by the empirical model for a major part of the land cover setting in the study area.

DISCUSSION

The Permafrost Model. Scale is a major issue within the framework of permafrost distribution mapping and modelling (see also Heginbottom, 2002). At regional or continental scales (ground resolution >100 m), simple relations between topography and climate or precipitation parameters are sufficient to produce an overall picture (Nelson and Outcalt, 1987; Keller, 1992; Li and Cheng, 1999; Etzelmüller *et al.*, 2003; Bohner and Lehmkühl, 2005). For lowland areas, sophisticated numerical models can be applied, addressing large-scale climate impact on permafrost distribution (Anisimov and Nelson, 1996). For more local applications in mountains (local scale or ground resolution of between 25–100 m), permafrost indicators such as temperature measurements under a stable snow cover (BTS) or landforms (e.g. rock glaciers) may be suitable (Hoelzle *et al.*, 2001). In areas where these measurements are possible or the landforms are abundant, multi-dimensional statistical relationships between permafrost existence and topographically or remotely-sensed parameters can be obtained. These analyses lead to quite detailed and accurate permafrost maps, with 50 m or better ground resolution. Most of them relate BTS to elevation and potential radiation (e.g. Isaksen *et al.*, 2002; Lewkowicz and Ednie, 2004) or the wetness index (Heggem *et al.*, 2005), while some include satellite image-derived parameters like albedo measures or NDVI (Ødegård *et al.*, 1999; Gruber and Hoelzle, 2001). The rock glacier distribution is often used to validate the results.

The study presented here is at the upper boundary of the local scale, where simple meteorological- and land-cover- derived relationships may not reflect permafrost distribution satisfactorily, while the data density is too low for more objective statistical investigations. A major drawback is the lack of data from higher elevations, and the spatial clustering of the measurement spots. In addition, unlike high

mountain areas such as the Alps or the Scandinavian mountains, vegetation cover and type are important factors for permafrost existence. These are nominal data which are not easily included, and in addition to the topographic variability make it more challenging to develop valid permafrost models. Therefore, a multi-criteria approach was chosen, which combined univariate analyses and logical criteria, to define the required scores. This type of approach is well-known where the allocation of spatial entities is based on physically non-comparable variables (Burrough and McDonald, 1998; DeMers, 2000). The major criticism of this approach is related to the often subjective assignment of scores and weights in the modelling process. However, especially in landslide risk studies, this deficiency has been addressed by introducing statistical methods for score estimation (see Eastman, 1999; Guzzetti *et al.*, 1999). In permafrost research, Janke (2005) recently derived a logistic model based on the relation of rock glaciers and topography, combined with criteria weights based on land cover. In our study, scores for two of the factors (potential solar radiation and wetness index) were calculated using statistical relations and thus were justified in relation to the field measurements. In general, the model results give a coherent picture of permafrost distribution, but do not reproduce active layer depth or the permafrost thickness. The approach is thus not very useful for evaluating the impact of climate change on permafrost distribution in the area. However, the effects of changes of land cover, for example, due to frequent forest fires (e.g. Yoshikawa *et al.*, 2002) or forest cutting, on permafrost favourability could potentially be evaluated within such a model.

Validation of the Model. In this study the resistivity soundings proved to be extremely useful. The actual resistivity values for permafrost layers were, however, one or two orders of magnitudes lower than those reported from the Alps or Scandinavia (e.g. Isaksen *et al.*, 2002; Hauck *et al.*, 2004; Heggem *et al.*, 2005). Since it is probable that the origin of the ice is due to the same processes, namely ice-segregation and re-freezing of surface melt water at the permafrost table, the differences may be attributed to ice content, lithology and type of surficial material. The generally coarser blocky morainic and weathered materials in the high mountains of Europe likely produce a higher ice-content than at the Mongolian sites. Moreover, most of the measurements in European mountains are conducted in crystalline rocks, which often show higher electrical resistance than younger volcanic rocks due to their mineralogical composition. This is also indicated by initial results from DC resistivity measurements at permafrost boreholes on Iceland,

where comparable values to those in Mongolia were obtained in basaltic material (e.g. Farbrot *et al.*, 2005). Furthermore, similar resistivity values have been observed elsewhere in warm permafrost in Mongolia (e.g. Ishikawa *et al.*, 2005). However, the range of observed resistivities here is wide (see e.g. Reynolds, 1997), and clear conclusions cannot be drawn without detailed bedrock investigations. Dry bedrock and possible thicker snow cover in topographic forest stands were identified as major problems. This shows that resistivity sounding must be used with care for permafrost mapping purposes and that good thermal ground control is required.

Quality and Errors: The main issues here are DEM quality, land use classification and ground truthing points, which were addressed earlier in this paper. The DEM used is certainly not an optimal one; it contains some elevation errors and inaccurate contours on the valley bottoms, which were edited manually. These particularly affect calculations of the *wetness index*. These factors are, however, a matter of scale. For an approach aiming to reproduce major spatial patterns, the quality appears sufficient as the major permafrost distribution was displayed satisfactorily. For more local-scale studies, for example, within a single valley catchment, a higher accuracy DEM derived from air photos or high-resolution satellite-based sources would be needed. The major drawback of this study is the limited number of measurement points which precludes a complete statistical assessment.

General Permafrost Distribution Pattern. The results confirm the general distribution pattern of permafrost described by Sharkhuu (2001a, 2001b) for the study area. Permafrost is widespread, about 10 m thick or more in the valley bottoms, and absent on south-facing slopes. Outside the riparian zone in the valley bottoms, the active layer thickness exceeds 3–4 m. The permafrost is close to 0°C, except in the wet grassland, where temperatures are lower and ice-rich permafrost prevails. In a study further south in Mongolia, Ishikawa *et al.* (2005) also emphasised the importance of grass cover and associated organic material, which has a low thermal conductivity during summer and a higher conductivity when frozen. This pattern favours the development of ice-rich, relatively cold permafrost in the riparian zone. The forested areas play an important role because of the shading effects and thus cooling of ground temperatures, which provide a positive feedback mechanism with permafrost. Similar findings have been obtained in other areas of Mongolia, such as the Altai Mountains (Lehmkuhl and Klinge, 2000), where there is a strong relationship between permafrost sites, aspect and vegetation, especially forest cover. A major factor

not considered in detail during this study is the influence of winter temperature inversions on permafrost distribution and characteristics, an effect clearly demonstrated elsewhere (e.g. Lewkowicz and Ednie, 2004). One can expect strong inversions in the study area, even if Lake Hövsgöl may buffer this effect.

CONCLUSIONS

From this study the following conclusions can be drawn:

- Permafrost is widespread in the study area, and the present study confirms the general distribution pattern described in Sharkhuu (1998, 2006).
- *Solar radiation* and topographic *wetness index* in addition to forest cover and vegetation density are the most important factors for predicting permafrost distribution in the area at a local to regional scale.
- The approach used here, utilising multi-criteria analyses with partly statistically-derived score values, gives a valid picture of permafrost distribution at a local scale. The data needed for this analysis—surface temperature measurements, land cover and DEM-derived topographic parameters—can be obtained relatively easily and inexpensively for large areas, making this procedure suitable as an initial modelling approach for areas with little basic quantitative information.
- The study emphasises the importance of DEM-derived parameters for modelling spatial distribution patterns.
- DC resistivity soundings give good indications of the permafrost distribution and active layer thicknesses, and can help validate the results of spatial modelling. The tomography results support the overall permafrost distribution calculated by the empirical model for a major part of the land cover setting in the study area.

ACKNOWLEDGEMENTS

This study was financially supported by the Global Environmental Facility implemented by the World Bank, the Department of Geosciences, University of Oslo, Norway and the Department of Geography, University of Zurich, Switzerland. We thank all the project participants who helped during fieldwork. Special thanks go to Sh. Anarmaa, V. Romanovsky,

Sh. Tumentsetseg and Ya. Jambaljav for help, collaboration and fruitful discussions during the first field campaign in 2002. The comments and suggestion of two anonymous reviewers and the editor Antoni Lewkowicz were highly appreciated and improved the paper considerably.

REFERENCES

- Anisimov OA, Nelson FE. 1996. Permafrost distribution in the Northern Hemisphere under scenarios of climatic change. *Global and Planetary Change* **14**: 59–72.
- Beven KJ, Kirkby MJ. 1979. A physically based, variable contributing area model of basin hydrology. *Hydrological Sciences* **24**: 43–69.
- Bohner J, Lehmkuhl F. 2005. Environmental change modelling for Central and High Asia: Pleistocene, present and future scenarios. *Boreas* **34**: 220–231.
- Brenning A, Gruber S, Hoelzle M. 2005. Sampling and statistical analyses of BTS measurements. *Permafrost and Periglacial Processes* **16**: 383–394. DOI: 10.1002/ppp.541
- Brown J, Ferrians Jr OJ, Heginbottom JA, Melnikov ES. 1995. *Circum-Arctic Map of Permafrost and Ground-ice Conditions*. International Permafrost Association, Woods Hole, MA, USA.
- Burn CR, Smith CAS. 1988. Observations of the ‘thermal offset’ in near-surface mean annual ground temperatures at several sites near Mayo, Yukon Territory Canada. *Arctic* **41**: 99–104.
- Burrough PA, McDonald RA. 1998. *Principles of Geographical Information Systems. Spatial Information Systems and Geostatistics*. Oxford University Press: Oxford.
- Dagvadorj D, Tumurbataar D, Natsagdorj L, Batjargal Z, Mijiddorj R. 2001. Climate change and its impacts on permafrost in Mongolia. In *International Symposium on Mountain and Arid Land Permafrost, Ulaanbaatar, Mongolia*. Urtan Erdem Publishing: Ulaanbaatar, Mongolia; 10–15.
- DeMers MN. 2000. *Fundamentals of Geographic Information Systems*, 2nd edn. Wiley: New York.
- Eastman R. 1999. Multi-criteria evaluation and GIS. In *Geographical Information Systems*, Longley P, Goodchild MF, Maguire DJ, Rhind D (eds). John Wiley and Sons: New York; 493–502.
- Etzelmüller B, Ødegård RS, Berthling I, Sollid JL. 2001. Terrain parameters and remote sensing in the analysis of permafrost distribution and periglacial processes: principles and examples from southern Norway. *Permafrost and Periglacial Processes* **12**: 79–92. DOI: 10.1002/ppp.384
- Etzelmüller B, Berthling I, Sollid JL. 2003. Aspects and Concepts on the Geomorphological Significance of Holocene Permafrost in Southern Norway. *Geomorphology* **52**: 87–104.

- Farbrot H, Etzelmüller B, Gudmundsson A, Schuler TV, Eiken T, Wangenstein B, Humlum O. 2005. Permafrost boreholes in Iceland. *Second European Conference on Permafrost, Potsdam, Germany, 12–16 June*.
- Goulden CE, Etzelmüller B, Ariuntsetseg L, Nandintsetseg B, Avirmed O, Batkhishig O, Sharkhuu A, Sharkhuu N. 2005. Permafrost Thermal Properties and Thaw and its Relationship to Soil and Plant Cover, Lake Hovsgol, Mongolia. *AGU Fall Meeting, San Francisco, USA, 11–15 December*.
- Goulden CE, Tumurtogoo O, Karabanov E, Mongontsetseg A. 2006. The geological history and geography of Lake Hövsgöl, Mongolia. In *The Geology, Biodiversity and Ecology of Lake Hövsgöl (Mongolia)*, Goulden CE, Sitnikova T, Gelhaus J, Boldgiv B (eds). Backhuys Publisher: Leiden, the Netherlands; 1–20.
- Gravis GF. 2001. Permafrost distribution and some indicators of its past changes in Mongolia. In *International Symposium on Mountain and Arid Land Permafrost, Ulaanbaatar, Mongolia*, Uralan Erdem Publishing: Ulaanbaatar, Mongolia; 27–28.
- Gravis GF, Zabolotnik SI, Lisun AM, Sukhodrovskiy VL. 1978. The geocryological characteristics of the Mongolian People's Republic and some characteristics of permafrost development in the past. In *Second International Conference on Permafrost; USSR Contribution*, Sanger FJ, Hyde PJ (eds). National Academy of Science: Washington DC, USA; 81–86.
- Gruber S, Hoelzle M. 2001. Statistical modelling of mountain permafrost distribution: local calibration and incorporation of remotely sensed data. *Permafrost and Periglacial Processes* **12**: 69–78. DOI: 10.1002/ppp.374
- Guzzetti F, Carrara A, Cardinali M, Reichenbach P. 1999. Landslide hazard evaluation: a review of current techniques and their application in a multi-scale study, Central Italy. *Geomorphology* **31**: 181–216.
- Hauck C, Isaksen K, Vonder Mühl D, Sollid JL. 2004. Geophysical surveys designed to delineate the altitudinal limit of mountain permafrost: an example from Jotunheimen, Norway. *Permafrost and Periglacial Processes* **15**: 191–205. DOI: 10.1002/ppp.493
- Heggem ESF. 2005. Mountain permafrost and ground surface temperature variability in Southern Norway and Northern Mongolia—spatial modelling and validation. PhD dissertation, University of Oslo.
- Heggem ESF, Juliussen H, Etzelmüller B. 2005. The permafrost distribution in central-eastern Norway. *Norsk Geografisk Tidsskrift* **59**: 94–108.
- Heginbottom JA. 2002. Permafrost mapping: a review. *Progress Physical Geography* **26**: 623–642.
- Hoelzle M, Wegmann M, Krummenacher B. 1999. Miniature temperature dataloggers for mapping and monitoring of permafrost in high mountain areas: first experience from the Swiss Alps. *Permafrost and Periglacial Processes* **10**: 113–124.
- Hoelzle M, Mittaz C, Etzelmüller B, Haerberli W. 2001. Surface energy fluxes and distribution models relating to permafrost in European Mountain areas: an overview of current developments. *Permafrost and Periglacial Processes* **12**: 53–68. DOI: 10.1002/ppp.385
- Hugget RJ, Cheesman J. 2002. *Topography and the Environment*. Longman: London.
- Hutchinson MF. 1989. A new procedure for gridding elevation and stream line data with automatic removal of spurious pits. *Journal of Hydrology* **106**: 211–232.
- Isaksen K, Hauck C, Gudevang E, Ødegård RS, Sollid JL. 2002. Mountain permafrost distribution on Dovrefjell and Jotunheimen, southern Norway, based on BTS and DC resistivity tomography data. *Norsk Geografisk Tidsskrift* **56**: 122–136.
- Ishikawa M, Sharkhuu N, Zhang Y, Kadota T, Ohata T. 2005. Ground thermal and moisture conditions at the southern boundary of discontinuous permafrost, Mongolia. *Permafrost and Periglacial Processes* **16**: 209–216. DOI: 10.1002/ppp.483
- Janke JR. 2005. The occurrence of alpine permafrost in the Front Range of Colorado. *Geomorphology* **67**: 375–389.
- Jensen JR. 2005. *Introductory Digital Image Processing*, 3rd edn. Pearson Prentice Hall: Upper Saddle River, NJ.
- Keller F. 1992. Automated mapping of mountain permafrost using the program PERMAKART within the geographical information system ARC/INFO. *Permafrost and Periglacial Processes* **3**: 133–138.
- Krivonogov SK. 2006. Late Cenozoic history of the Hövsgöl area. In *The Geology, Biodiversity and Ecology of Lake Hövsgöl (Mongolia)*, Goulden CE, Sitnikova T, Gelhaus J, Boldgiv B (eds). Backhuys Publisher: Leiden, the Netherlands; 21–40.
- Lehmkuhl F, Klinge M. 2000. Bodentemperaturmessungen aus dem Mongolischen Altai als Indikator für periglaziale Geomorphodynamik in hochkontinentalen Gebirgsräumen. *Zeitschrift fuer Geomorphologie* **44**: 75–102.
- Lewkowicz AG, Ednie M. 2004. Probability mapping of mountain permafrost using the BTS method, Wolf Creek, Yukon Territory, Canada. *Permafrost and Periglacial Processes* **15**: 67–80. DOI: 10.1002/ppp.480
- Li X, Cheng G. 1999. A GIS-aided response model of high-altitude permafrost to global change. *Science in China, Series D: Earth Sciences* **42**: 71–79.
- Loke MH, Barker RD. 1995. Rapid least-squares inversion of apparent resistivity pseudosections using a quasi-Newton method. *Geophysical Prospecting* **44**: 131–152.
- Namkhajantsan G. 2006. Climate and climate change of the Hövsgöl region. In *The Geology, Biodiversity and Ecology of Lake Hövsgöl (Mongolia)*, Goulden CE, Sitnikova T, Gelhaus J, Boldgiv B (eds). Backhuys Publisher: Leiden, the Netherlands; 63–76.
- Nelson FE, Outcalt SI. 1987. A computational method for prediction and regionalization of permafrost. *Arctic and Alpine Research* **19**: 279–288.

- Ødegård RS, Isaksen K, Mastervik M, Billdal L, Engler M, Sollid JL. 1999. Comparison of BTS and Landsat TM data from Jotunheimen, southern Norway. *Norsk Geografisk Tidsskrift* **53**: 226–233.
- Reynolds JM. 1997. *An Introduction to Applied and Environmental Geophysics*. John Wiley & Sons: Chichester.
- Sharkhuu N. 1993. Permafrost in the Selenge River Basin. In *Sixth International Conference on Permafrost, Beijing, 5–9 July*. South China University of Technology Press: Beijing, China; 1123–1226.
- Sharkhuu N. 1998. Trends of permafrost development in the Selenge River basin, Mongolia. In *Permafrost; Seventh International Conference, Proceedings*, Lewkowitz AG, Allard M (eds). Centre d'Etudes Nordiques, Université Laval, Quebec, Canada; 979–985.
- Sharkhuu N. 2001a. Permafrost mapping in Mongolia. In *International Symposium on Mountain and Arid Land Permafrost, Ulaanbaatar, Mongolia*. Ulan Erdem Publishing: Ulaanbaatar, Mongolia; 63–67.
- Sharkhuu N. 2001b. Geocryological monitoring in Mongolia. In *International Symposium on Mountain and Arid Land Permafrost, Ulaanbaatar, Mongolia*. Ulan Erdem Publishing: Ulaanbaatar, Mongolia; 59–62.
- Sharkhuu N. 2006. Geocryological conditions of the Hövsgöl mountainous region. In *The Geology, Biodiversity and Ecology of Lake Hövsgöl (Mongolia)*, Goulden CE, Sitnikova T, Gelhaus J, Boldgiv B (eds). Backhuys Publisher: Leiden, the Netherlands; 49–62.
- Starkel L. 1998. Geomorphic response to climatic and environmental changes along a Central Asian transect during the Holocene. *Geomorphology* **23**: 293–305.
- Sulebak JR, Tallaksen LM, Erichsen B. 2000. Estimation of areal soil moisture by use of terrain data. *Geografiska Annaler* **82A**: 89–105.
- Tumurbataar B, Mijiddorj R. 2006. Permafrost and permafrost thaw in Mongolia. In *The Geology, Biodiversity and Ecology of Lake Hövsgöl (Mongolia)*, Goulden CE, Sitnikova T, Gelhaus J, Boldgiv B (eds). Backhuys Publisher: Leiden, the Netherlands; 41–48.
- Vonder Mühl D, Hauck C, Gubler H. 2002. Permafrost mapping—mapping of mountain permafrost using geophysical methods. *Progress Physical Geography* **26**: 643–660.
- Williams PJ, Smith MW. 1989. *The Frozen Earth: Fundamentals of Geocryology*. Cambridge University Press: Cambridge.
- Wilson JP, Gallant JC. 2000. Secondary topographic attributes. In *Terrain Analysis—Principles and Application*, Wilson JP, Gallant JC (eds). Wiley: New York; 87–132.
- Yoshikawa K, Bolton WR, Romanovsky VE, Fukuda M, Hinzman LD. 2002. Impacts of wildfire on the permafrost in the boreal forests of Interior Alaska. *Journal of Geophysical Research-Atmospheres* **108**. DOI: 10.1029/2001JD000438
- Zabolotnik SI. 2001. The development of frozen ground in Mongolia. In *International Symposium on Mountain and Arid Land Permafrost, Ulaanbaatar, Mongolia*. Ulan Erdem Publishing: Ulaanbaatar, Mongolia; 94–95.
- Zevenbergen LW, Thorne CR. 1987. Quantitative analysis of land surface topography. *Earth Surface Processes and Landforms* **12**: 47–56.

Spatial Distribution of Ground Surface Temperatures and Active Layer Depths in the Hövsgöl Area, Northern Mongolia

E. S. F. Heggem,¹ B. Etzelmüller,^{1*} S. Anarmaa,² N. Sharkhuu,² C. E. Goulden³ and B. Nandinsetseg²

¹ Department of Geosciences, University of Oslo, Norway

² Hovsgol GEF Project, Institute of Geo-Ecology, Mongolian Academy of Sciences, Ulaanbaatar, Mongolia

³ Institute of Mongolian Biodiversity and Ecological Studies, Academy of Natural Sciences, Philadelphia, USA

ABSTRACT

Near-surface temperature variations in different topographic settings were obtained from miniature temperature data-loggers at 17 locations over a 2-year period in the Lake Hövsgöl area in northern Mongolia. These measurements were used to analyse the influence of vegetation, solar radiation, surface wetness and snow cover on the ground thermal regime. An empirical modelling approach was applied in order to estimate the spatial distribution of ground surface temperatures, the presence of permafrost and the depth of the active layer. Our study shows that spatial interpolation of ground surface temperature parameters, mainly known from previous research in the Arctic, can be feasible in the arid mountain environments of Central Asia. Copyright © 2006 John Wiley & Sons, Ltd.

KEY WORDS: permafrost; Mongolia; miniature temperature loggers; permafrost distribution modelling; GIS

INTRODUCTION

The mountainous area surrounding Lake Hövsgöl in northern Mongolia is located at the southern edge of the Siberian taiga forest and the continuous permafrost zone (Figure 1). Permafrost in this arid mountain area affects the hydrological cycle and the ecosystem structure, particularly vegetation growth and productivity (e.g. Goulden *et al.*, 2005; Sharkhuu, 2006). Valley bottoms and south-facing slopes are covered by steppe and are used as pasture for the livestock of nomadic herders. This makes the site important for the study of land use, ecosystem vulnerability, and for

understanding permafrost stability under human and climatic impacts.

A permafrost map of the study area based on multi-criteria analyses within a geographical information system (GIS) environment was recently developed (Etzelmüller *et al.*, 2006). This study showed a regional relation between topographic wetness, incoming solar radiation, vegetation cover and elevation. A *favourability index* for permafrost was derived, giving an indication of permafrost distribution over larger areas. This paper focuses on the spatial variability of ground surface temperatures in relation to topographic setting and vegetation cover, monitored by miniature temperature data-loggers (MTDs). The aim is to present a coupling of topography and land cover parameters with ground surface temperatures, and to use this information to estimate ground surface temperature fields and spatial active layer variability at a regional scale. Similar approaches have been used in arctic environments and

* Correspondence to: B. Etzelmüller, Department of Geosciences, Physical Geography, University of Oslo, PO Box 1047, Blindern, N-0316 Oslo, Norway.
E-mail: bernde@geo.uio.no

Contract/grant sponsors: Global Environmental Facility/World Bank; University of Oslo.

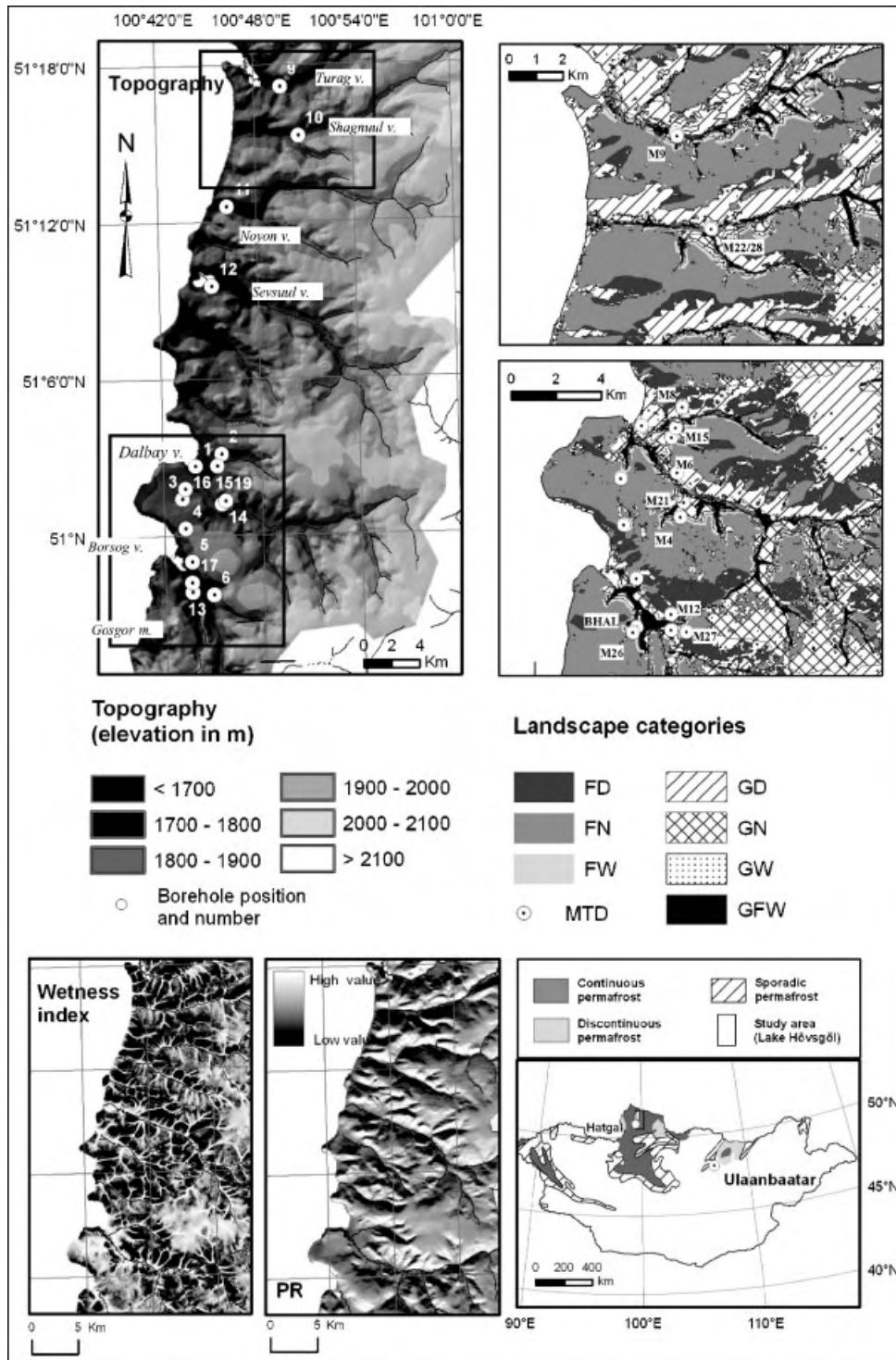


Figure 1 Base maps of the study area. Boreholes are referred to in the text as BH1, BH2, etc. The inset maps show the landscape categories derived for the area, with solid fills for the forest classes. The maps of the *wetness index* (WI) and *potential solar radiation* (PR) are derived from a 50-m digital elevation model (DEM). The key map for Mongolia shows the permafrost distribution based on Brown *et al.* (1995).

allow for additional analyses of potential climate change impacts on permafrost (e.g. Nelson *et al.*, 1997; Klene *et al.*, 2001).

SETTING

Lake Hövsgöl (51°N 100°E) is located at 1645 m a.s.l. in northern Mongolia close to the Russian border (Figure 1). The entire lake watershed has been protected as the Hövsgöl National Park since 1994. There are six west-east oriented valleys opening onto Lake Hövsgöl, spaced out from north to south along the northeastern shore of the lake (Figure 1). The northern valleys are intensely grazed while the two southern valleys have little grazing pressure. The vegetation cover in the valley bottoms is mainly steppe grasses, sedges and forbs. North-facing slopes and ridges are covered by Siberian larch (*Larix sibirica*), and south-facing slopes are sparsely vegetated with dry steppe, or open forest. The mean annual air temperature (MAAT) recorded at the nearest climate station at Hatgal (southern shore of Hövsgöl, Figure 1) is -4.5°C (Namkhajantsan, 2006). The area is semi-arid and the mean annual precipitation is 300–350 mm, increasing to 550 mm in the high mountains. Precipitation occurs mainly in the summer months with a peak of about 100 mm in July. The air temperature has increased over the last 40 years by 1.8°C (Namkhajantsan, 2006). Permafrost exists in the valley bottoms, beneath north-facing forested slopes and in the high mountains, but is absent on south-facing slopes (e.g. Etzelmüller *et al.*, 2006; Sharkhuu, 2006). Permafrost ranges in thickness from 10–20 m in the valley bottoms to hundreds of metres in the high mountains at elevation greater than 2200 m a.s.l. (Sharkhuu, 2006).

METHODS AND APPROACHES

Temperature Measurements

Two years of data (August 2002–July 2004) from 17 near surface UTL1 MTDs were used in the temperature analysis (1.5 h interval, accuracy $\pm 0.25^{\circ}\text{C}$). The loggers were placed in the ground at a depth of 0.05 m to prevent direct irradiation and in different landscape settings: dry south-facing slope, forest, open grassland and north-facing slopes. Altitudinal temperature gradients were not measured systematically except for one profile around the Gozgor Mountain (six MTDs) (Figure 1), which indicated some inversions during the winter. However,

due to differences in snow cover at the sites, trends for inversions or lapse rates are not clear. In the main valleys, the relatively low altitudinal variation of the measurement sites was obscured by other parameters such as irradiation and soil moisture (Etzelmüller *et al.*, 2006).

Air temperature was measured in the Dalbai and Turag valleys, using automatic climate stations. Based on the temperature time series, values for mean ground-surface temperatures (MGST), and thawing (TDD) and freezing (FDD) degree-days were calculated for all the data-loggers. The frost number (FN) was calculated using the following equation (Nelson and Outcalt, 1987):

$$FN = \sqrt{FDD} / \sqrt{FDD + \sqrt{TDD}} \quad (1)$$

A value of FN >0.5 indicates more FDD than TDD, and is an indication of permafrost presence. This is, however, dependent on ground conditions, notably the thermal offset to the top of permafrost (e.g. Smith and Riseborough, 1996) and therefore is not an absolute confirmation of permafrost existence.

Topographic Parameters and Land Cover Classification

The data basis for the digital elevation model (DEM) and land cover classification is the same as used in Etzelmüller *et al.* (2006) and described there in more detail. A 50 m DEM was generated from digitised contour lines (at 20-m intervals) derived from analogue Russian maps published in 1942 and re-printed in 1962, originally at a scale of 1:100000. A gridding algorithm implemented in the GIS software ArcGIS ([®]ESRI, USA) based on Hutchinson's (1989) ANUDEM algorithm was applied (version 4.6.3). The DEM is within the accuracy range of handheld GPS-derived elevations, or some tens of metres. The DEM was used to calculate several topographic parameters (Figure 1). *Slope*, *aspect* and *curvature* were calculated following the procedures described in Zevenbergen and Thorne (1987). The spatial distribution of potential solar radiation (*PR*) was estimated using the 'SRAD' topographic model (cf. Wilson and Gallant, 2000). In our study no adjustment was made for surface characteristics such as albedo or emissivity. The topographic *wetness index* (*WI*) is defined as the quotient of the specific upstream area and the surface slope (Beven and Kirkby, 1979) (Figure 1). For calculating the *specific upstream area*,

an algorithm allowing diverting flow was used (e.g. Wilson and Gallant, 2000).

A Landsat TM mosaic image (ground resolution 30 m) and an ASTER scene (ground resolution 15 m, from 27 August 2001) were used for land cover classification. Both images were subsequently classified using standard supervised maximum likelihood classification routines with the ERDAS Imagine (ver. 8) software. Five classes were selected: forest, open forest, grassland, dry grassland and sand. Scattered clouds or haze and open water were excluded from the classification. Due to a lack of real ground-truthing coverage (aerial photos or updated topographic maps) the classified result was only qualitatively compared to field observations and photographs. The forest classification results were compared to scanned topographic maps containing a forest layer. Deviations were found on small mountain peaks. The topographic map showed forest at these sites whereas the classification results did not. The lower forest border corresponded well with the border displayed on the maps. Considering the simplicity of the land cover classes and the application scale, this classification was considered to be sufficient, and the best obtainable with the available field data.

Landscape Categories and Simple Soil Moisture Content Estimates

The landscape in the study area was classified into categories: we assume that the ground surface temperature variability is more homogenous within a category than among them. Statistical analyses performed in Etzelmüller *et al.* (2006) and recent ground surface measurements in experimental plots (Sharkhuu and Anarmaa, 2005) showed a strong control of permafrost distribution by vegetation cover (forest, grass) and topographic wetness or soil moisture. Consequently, seven landscape categories were established, three for forested areas and four for non-forested sites (Figure 1, Table 1). The categories were generated by parameter overlays, using the classified satellite image and the maps of *PR* and *WI*. As we have no spatially distributed soil moisture measurements in the study area the soil moisture content (*SM*) was roughly estimated by combining the landscape categories with borehole observations within each category zone where available. This resulted in approximate average values for the soil moisture in per cent for each site, based on samples taken during the drilling process and subsequent gravimetric analyses (Table 1).

Empirical Modelling Approach

For spatial modelling of surface temperature fields we developed surface temperature curves for each landscape category. The measured ground surface temperatures were parameterised by assuming that the temperature cycle over the year follows a sine curve. Each curve was manually fitted to temperature amplitude. Approximate values for amplitude and mean values were selected so that the observed number of FDD and TDD were preserved (Figure 2). The temperature of a specific day can then be calculated as:

$$T(\text{day}) = A * \sin(\text{day}) + \text{mean}(z) \quad (2)$$

where, A is the amplitude, and $\text{mean}(z)$ is the mean annual ground surface temperature at elevation z . By integrating the function over the freezing and thawing season, FDD and TDD were estimated as:

$$FDD = \int_{\text{day}=\text{freeze_start}}^{\text{day}=\text{freeze_stop}} T(\text{day}) \quad (3)$$

and

$$TDD = \int_{\text{day}=\text{freeze_stop}}^{\text{day}=\text{freeze_start}} T(\text{day}) \quad (4)$$

where

$$\text{day_freeze_start} = \pi + a \sin\left(\frac{\text{mean}(z)}{A}\right) \quad (5)$$

and

$$\text{day_freeze_stop} = 2 \cdot \pi - a \sin\left(\frac{\text{mean}(z)}{A}\right). \quad (6)$$

The mean temperature within the landscape category was corrected for elevation utilising a fixed temperature lapse rate. The reference elevation for each landscape category mean value ($\text{mean}(z_0)$) was 1650 m. An overall lapse rate of $0.005^\circ\text{Cm}^{-1}$ was selected based on Kozhova *et al.* (1989). The mean temperature was then calculated, following:

$$\text{mean}(z) = \text{mean}(z_0) + (1650 - z) \cdot \text{lapse rate} \quad (6)$$

where z is the elevation in each cell, derived from the DEM. FDD and TDD were then calculated using

Table 1 Definition of the seven categories derived from satellite classification and terrain parameters

Categories	Categories based on satellite classification	Terrain parameter class	Water content*	Sine-based estimates (°C) 2002/2003		Sine-based estimates (°C) 2003/2004	
				Amp	Mean	Amp	Mean
FD	Sunny forest/open forest	$PR > 210 \text{ Wm}^{-2}$	10%	14.0	-1.00	12.0	0.25
FW*	Forest and forest foot slope	$PR < 200 \text{ Wm}^{-2}$ and down-slope distance to grassland $< 150 \text{ m}$	40%	5.0	-1.00	4.25	0.75
FN	Forest/open forest other than FD and FW		15%	12.0	-1.25	10.0	0.00
GD	Dry grassland, sand, sunny grassland	$PR > 210 \text{ Wm}^{-2}$	5%	15.5	0.75	14.5	1.75
GW	Wet grassland	$WI > 12$	35%	13.5	-1.75	11.0	-0.25
GFW	Grassland and open forest incl. forest foot slope	$PR < 200 \text{ Wm}^{-2}$ and slope distance to forest less than 150 m and up-slope length more than 150 m	15%	11.5	-3.50	8.5	-2.00
GN	Grassland other than GD, GW and GFW		15%	15.0	-0.75	12.5	1.00

* Forest foot slope is generated from the terrain parameters and not calculated downslope of dry forest. The water content of the upper soil layer is a constant value for each category based on borehole information. An average elevation of 1700 m is used for all categories shown in this table.

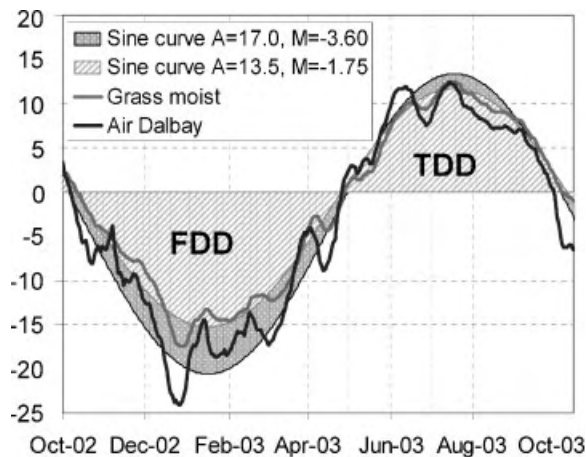


Figure 2 Sine-curve approximation of air and ground surface temperatures estimated from a 15-day moving average. The amplitude is calculated based upon the observed number of freezing (FDD) and thawing degree-days (TDD).

Equations (2), (3) and (4). Finally the FN was calculated for map presentation, following Equation (1). This method assumes an equal amount of snow on each landscape category. The parameterisation of the annual temperatures allows for later climate impact modelling, by altering the mean temperature or the amplitude of the sine curve. Maps of freezing and thawing depths were subsequently calculated based on Stefan's equation:

$$Z = \sqrt{\left[\frac{2\lambda}{\rho_d w L} \right] [S * DD]} \quad (8)$$

where Z is the depth of frost or thaw, λ is the appropriate frozen or thawed thermal conductivity, ρ_d is dry soil density, w is the soil's water content, L is latent heat of fusion, S is a scale factor ($s d^{-1} = 86400$) and DD is the degree-days (e.g. Nelson and Outcalt, 1987). In this study it was assumed that $\lambda = 3.5 \text{ W m}^{-2} \text{ K}^{-1}$ for frozen and $\lambda = 3 \text{ W m}^{-2} \text{ K}^{-1}$ for thawed soils. ρ_d was selected to be 1300 kg m^{-3} . These values were chosen based on borehole information.

Model Validation

DC resistivity tomography (RT) and ground temperature measurements in shallow boreholes were used for initial model validation of the FN fields and the active

layer thickness, respectively. DC RT profiles were generated at 22 sites in the area in August 2002 and 2005. The profiles and methods used and limitations are described in more detail elsewhere (Etzelmüller *et al.*, 2006). The principle of the method is based on the fact that different materials have varying abilities to conduct electricity (e.g. Reynolds, 1997). The application of resistivity soundings in permafrost mapping studies is justified through the large contrast of water resistivity (~ 10 to $100 \Omega\text{m}$) in relation to ground ice ($\sim 10^3$ to $10^6 \Omega\text{m}$). An ABEM Lund ([®]ABEM Sweden) multi-electrode, high-resolution two-dimensional resistivity system was used for the soundings. The system consists of 61 electrodes with a standard spacing of 2 m, giving a maximum penetration depth of approximately 25 m. All profiles were topographically corrected before inversion and then used to validate permafrost existence in relation to modelled MGST, FN averaged over the two seasons and permafrost favourability (f) as defined in Etzelmüller *et al.* (2006). These parameters were correlated against modelled resistivity at a depth of 8 m.

In addition 19 shallow boreholes (< 10 m) drilled as a part of the overall project (see Anarmaa *et al.*, 2005) were available for validation. Most temperatures in the boreholes were read manually two to three times a year, using a movable thermistor string. Seven of these boreholes were equipped with up to three MTDs for continuous reading of ground temperatures. Data from these were used for validation of the active layer estimates.

RESULTS AND DISCUSSION

Ground Surface Temperature Variation

In both seasons, the ground surface temperature amplitude varied with both solar radiation and SM . Summer ground surface temperatures were clearly lower in the wet, riparian zone and higher on the dry sunny slopes (Figure 3a to 3c). The absolute difference in solar radiation between south- and north-facing slopes was not as large during winter as in summer. During winter, the solar radiation reduced snow cover on south-facing slopes, resulting in lower ground surface temperatures. Shading by trees clearly reduced the temperature during the summer in the open forest (Figure 3d). The valleys of Turag and Shagnuul had similar temperatures in open areas during the summer. In winter, air temperatures were colder in Shagnuul than in Turag, but because of thicker snow cover in Shagnuul, the ground surface temperatures were

warmer than in Turag. The difference between the shaded and non-shaded loggers in Shagnuul was absent in winter (Figure 3d).

Ground surface temperatures were warmer in 2003/2004, but air temperatures measured in the Dalbay valley were similar in the 2 years with an almost

identical number of FDD. In contrast, ground surface temperature amplitudes decreased from 2002/2003 to 2003/2004 due to a generally thicker snow cover during the second winter. The highest temperature increase between the two seasons was measured in areas with high amplitude, which during the snowy

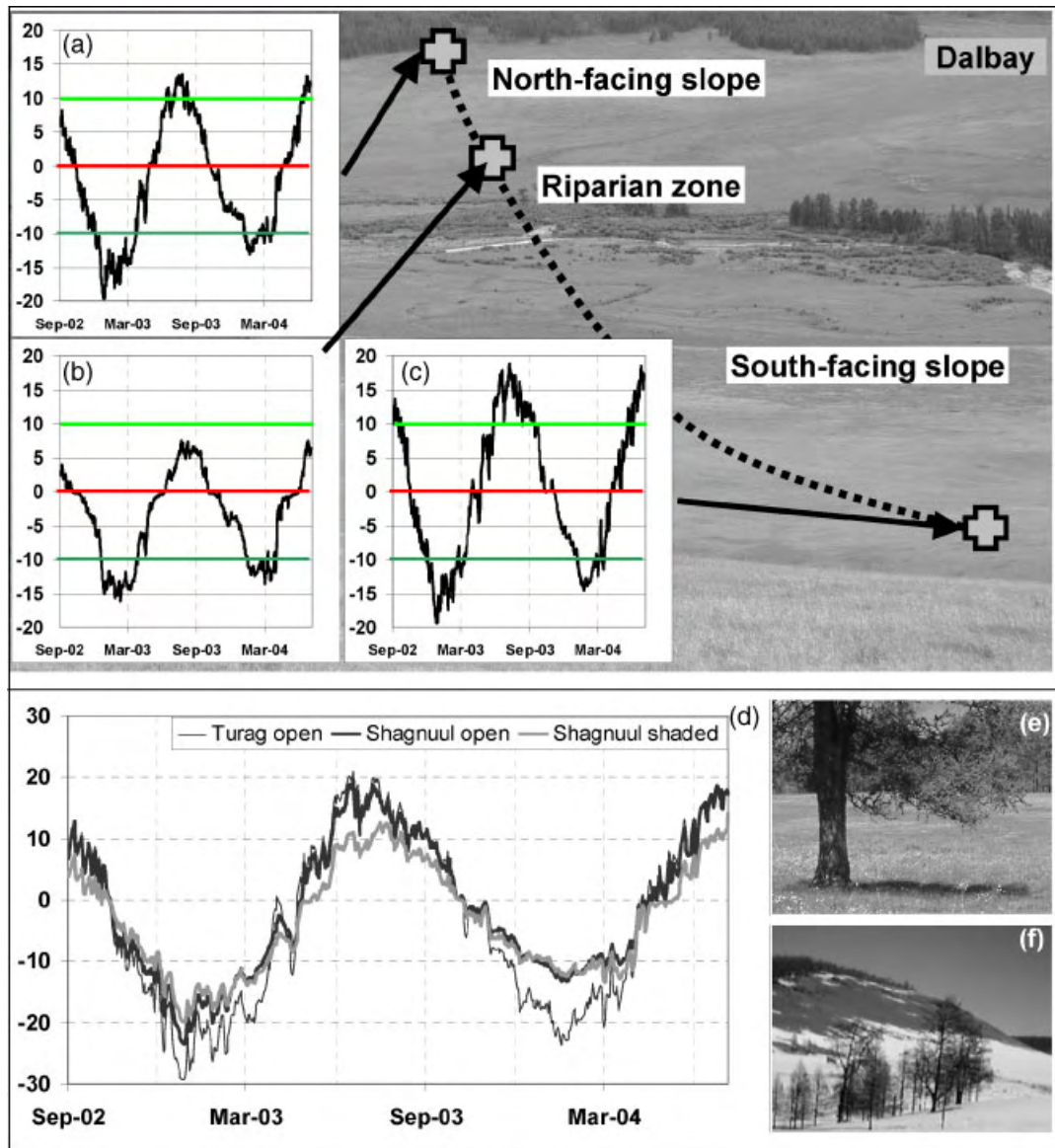


Figure 3 Examples of near-surface daily average temperatures for sites with differing soil moisture contents (*SM*), potential solar radiation (*PR*), shading and snow amounts. (a) Dalbay valley—north-facing slope. (b) The riparian zone. (c) The south-facing slope. Note the differences in temperature amplitude in relation to insolation and moisture content. (d) Shagnuul and Turag valleys—the Shagnuul shaded site has a lower temperature than the open site. In winter, shading has almost no effect. The Turag valley site has less snow and hence the surface is colder than in the Shagnuul valley. (e) The Shagnuul shaded site. (f) Typical south-facing slope winter snow conditions. All temperatures are given in °C.

years had reduced heat loss in winter. In more moist areas at the forest edge, snow cover variations seemed to have less influence on ground surface amplitudes as the temperatures stayed close to 0°C for long periods due to the high water content, even with a shallower snow cover.

Wet areas generally experienced longer zero curtain effects in spring and autumn. For example, a surface icing (*Aufeis*) developed during winter at one logger on a forested slope (surface logger at BH3, Figure 1), where the temperature rose to 0°C for 2 weeks in late December until the water froze again. Thus, there was a decrease in ground surface temperature amplitude with an increase in surface moisture content. The dry grass category (GD) had the highest surface temperature amplitude. The wet grass close to the forest edge (GFW) had the lowest amplitude due to high moisture content and shading from solar radiation in summer (Table 1).

The results show that the insulating and shading effects of vegetation strongly influence ground-surface temperatures and thus permafrost distribution in the study area. A reduction in vegetation cover would raise the ground surface temperature, and thus increase the active layer thickness (Williams and Smith, 1989). A generally thinner snow cover at the dry sites leads to more FDD than areas with thicker snow cover. However, in this area this does not outweigh the cooling effect that vegetation has in summer. Wet vegetation keeps the surface cooler than non-vegetated areas, and if the grassland is dry, temperature amplitudes increase, which in turn leads to a deeper active layer. A thicker active layer reduces the amount of water close to the soil surface, and has an additional drying effect. These processes are important in relation to thermal regime changes due to grazing by nomadic herds or climatic change. The first results of systematic ground surface temperature measurements in small experimental plots with control over vegetation cover and grazing pressure showed significantly higher temperatures for grassed sites than for undisturbed plots nearby (Sharkhuu and Anarmaa, 2005).

Spatial Modelling

Ground Surface Temperatures.

The sine-based model gives a reasonable description of the permafrost distribution in the area, even if the variability within each landscape category is limited (Figure 4). During the first season most of the areas other than the southerly slopes showed MGST values below -1°C , with values of $<-2.5^{\circ}\text{C}$ in the moist valley bottoms. Southerly slopes and dry

settings showed values above 0°C . In contrast the second season was between 1°C and 1.5°C warmer in most sites. A similar pattern is visible for the FN modelling (Figure 4). Larger areas outside the wet valley bottoms show $\text{FN} < 0.5$ during the second season, especially in dry forest and grassland sites. The modelling demonstrates the high inter-annual variability of ground surface temperature, and the need for longer monitoring series to address permafrost occurrence and stability in the region.

The modelling was validated using the DC RT results, assuming that high Ωm values at a depth of 8 m are indicative of permafrost and that low ones are not. Comparison of RT and the temperature parameters produced a trend, but only relatively low R^2 -values of 0.21 ($\rho < 0.06$) and 0.39 ($\rho < 0.006$) for two-season MGST and FN average, respectively (Figure 5a and b). This is not surprising as the temperature parameters were sampled over only 2 years, and the resistivity at 8 m depth is related to longer-term permafrost existence. Moreover, differences in resistivity values are not wholly related to the presence or absence of permafrost. The relation between the temperature parameters and the permafrost favourability (f) is somewhat clearer, with R^2 -values around 0.5 ($\rho < 0.001$) (Figure 5c and 5d). The validation was done for the same locations as the RTs, mostly in or close to the valley systems (Figure 4). Closer inspection indicates that the correspondence between the two approaches was reasonably good in the valleys and the forested areas, but that southerly exposed sites to a higher degree received low favourability values rather than low FN or high MGST values, respectively. Thus, the two approaches are in reasonable overall agreement, but differ locally in certain topographic positions.

Active layer thickness.

The thaw depth estimated for the 2003 thawing season using Equation (7) varied between $<2\text{ m}$ and $>6\text{ m}$, with most areas being between 2 m and 4 m (Figure 6a). The largest thaw values were calculated for dry landscape categories and southerly slopes, while the lowest estimated thaw was for the wet areas. Comparison with observed active layer depth in eight boreholes revealed a root mean square error of 0.6 m for 2003 (Table 2), with wet areas being somewhat overestimated and all others underestimated. However, the general spatial pattern appeared to mimic the borehole observations in the area, and the error is acceptable given the uncertainties relating to the simplified parameterisation and calculation procedure. Estimated freezing depth varied between $<3\text{ m}$ in the valley bottoms to $>6\text{ m}$ on steep dry

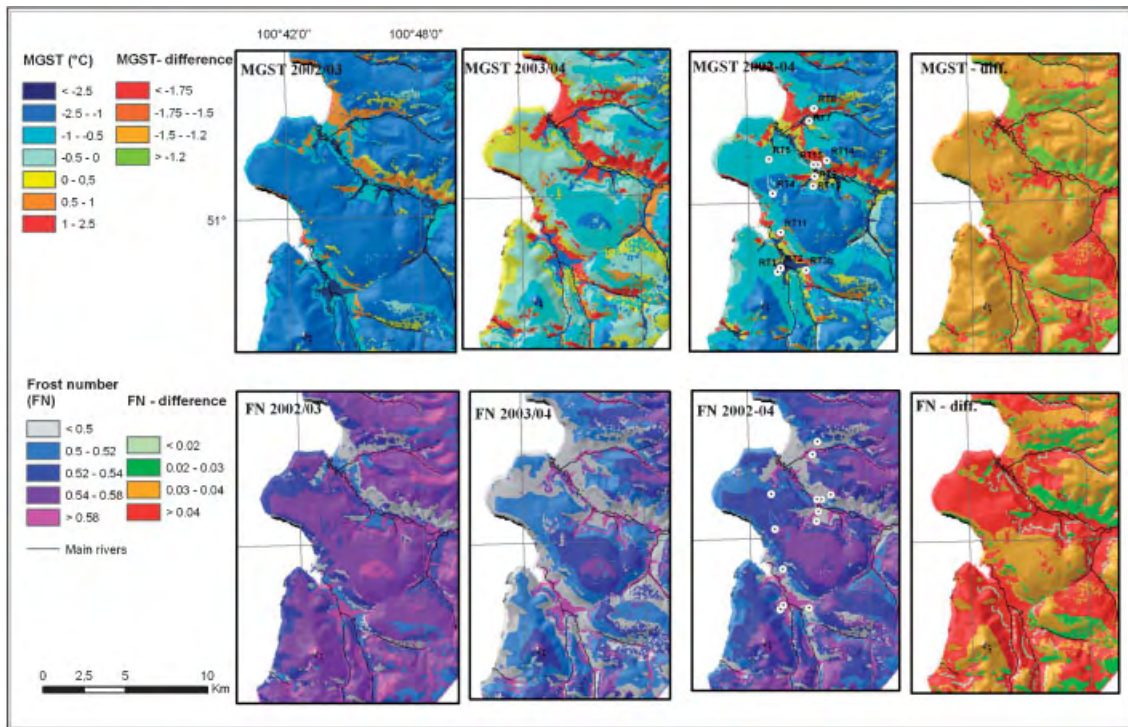


Figure 4 Estimated mean ground-surface temperature (MGST) and frost number (FN) for the 2002/2003 and 2003/2004 seasons in the Borsog and Dalbay valleys. $FN > 0.5$ and $MGST < 0^{\circ}\text{C}$ indicate probable permafrost, depending on ground conditions (thermal offset). The circles denote DC resistivity tomography (RT) sites used for validation. $MGST_{2002-04}$ and $FN_{2002-04}$ are averages of the two seasons. 'Diff.' means the difference between the two seasons, obtained by subtracting the values of the second season from the first on a cell-by-cell basis.

slopes (Figure 6b), and was between 0.2 m and 0.8 m lower during the second winter (Figure 6c). These differences between the two observation years were especially obvious in the open and drier grasslands and forest areas (>0.6 m), but of less importance in the forested (<0.6 m) and especially the wet grassland and forest areas (<0.4 m) (Figure 6d). This shows that the ground thermal characteristics associated with grassland are more sensitive to changes in both snow cover and vegetation thickness. As a consequence, reduced vegetation due to overgrazing is likely to increase surface temperatures and their annual amplitudes, and thus the depth of the active layer.

Map Assessment, Quality and Errors

In general, the modelling results correspond fairly well to borehole observations and estimates based on DC RT. However, several major sources of errors are present.

First, the quality of the DEM was not high since it was based on old contour maps, constructed from old

air photos. Subsequent interpolation could have caused hydrologically inaccurate DEMs, which in turn would have affected the calculation of the topographic parameters. Therefore, the approaches presented can only be used to generate an overview pattern rather than to predict conditions at specific sites.

A second major source of error relates to the satellite image classification and the identification of landscape categories. The model would be improved by the availability of new aerial photos or high-resolution satellite imagery (<10 m), to better identify forest edges, wet sites and forest or general vegetation density. These factors are central to the success of the current approach, especially in an area where vegetation plays a dominant role in ground thermal conditions. The classification used was coarse and therefore had severe limitations.

A third issue is the choice of constant values for soil moisture and thermal conductivities within landscape categories which obviously is a major simplification, but is necessary to allow the calculation of thaw depth

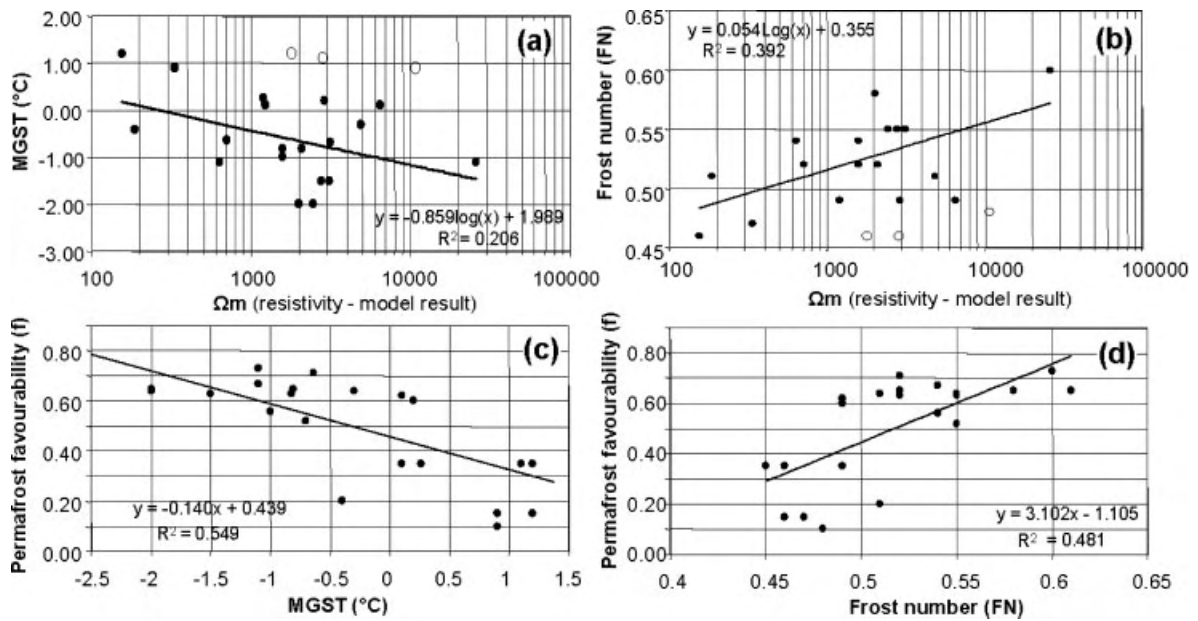


Figure 5 Validation plots. (a) Modelled ground resistivity at 8 m depth vs. estimated MGST and (b) FN, averaged over the two seasons. The open circles are outliers not included in the regression because the sites are within dry bedrock on steep south-facing slopes, and show high resistivities independent of possible permafrost (for more detailed discussion, see Etzelmüller *et al.*, 2006). (c) and (d) Plots of MGST/FN against permafrost favourability (f) as defined in Etzelmüller *et al.* (2006). The data were sampled in exactly the same locations as in (a) and (b).

and freezing depth estimates. Factors like water content and thermal conductivity are highly variable in space and time, but detailed soil and geological maps are not available for the study area. Data on these factors are available along profiles across different valleys (e.g. Batkhisig, 2006), but a comprehensive spatial picture over the study area is lacking. The same

is true for the snow conditions, which were assumed to be constant within a landscape category. However, systematic spatial snow observations are not available for the field area.

Analyses of the thermal offset concept as elaborated by Smith and Riseborough (1996) are not included in this paper. Knowledge of the offsets between the air,

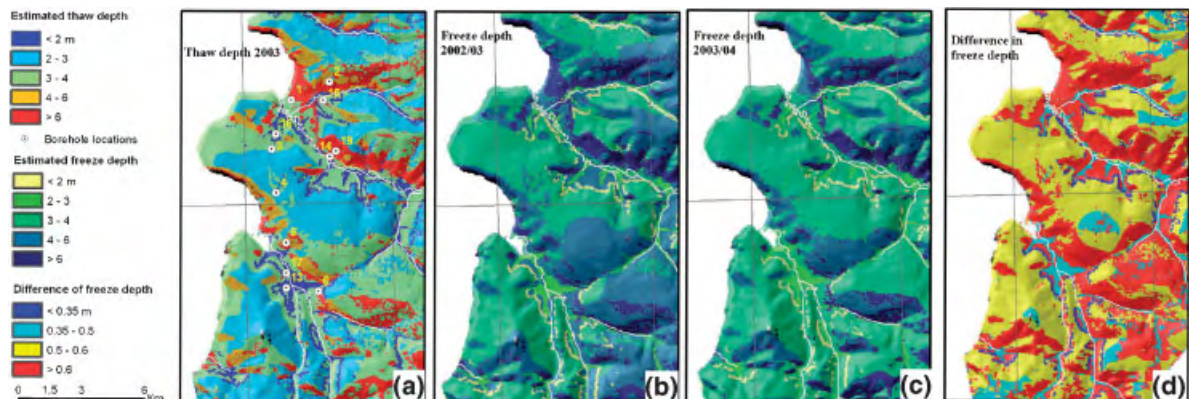


Figure 6 (a) Estimation of thaw depth or active layer thickness in permafrost areas for summer 2003 based on Equation (8). (b) Estimation of freezing depth, winter 2002/2003. (c) Estimation of freezing depth for winter 2003/2004. (d) Difference in freezing depth between the 2 years.

Table 2 Validation table of estimated and observed active layer thickness (m). Thaw depth estimates include minimum, maximum and average values over the entire study site for each landscape category zone. Borehole observations are measurements of active layer depth during autumns 2002 to 2005. For landscape category abbreviations, see Table 1. There was no borehole observation for the wet forest category (FW). The total root mean square error for the eight observation points was 0.61 m. pf = permafrost

Landscape category	Estimated thaw depth min—max (mean) within landscape category 2003 (m)	Sites	Thaw depth model estimate at site 2003 (m)	Observed active layer depth in borehole (m)				Difference between boreholes observations and model estimates for 2003 (m)
				2002	2003	2004	2005	
FD	3.3–4.2 (3.8)	BH2 (Dalb.)	4.1					
FN	2.0–3.1 (2.8)	BH5 (Borsog)	4.2					
		BH3 (Dalb.)	3.0	3.6			+0.2	
		BH4 (Dalb.)	2.9	3.0			+0.6	
		BH11 (Nyon)	3.0	4.0	4.5	3.5	+1.0	
FW	0.0–1.1 (0.7)							
GD	5.3–6.9 (6.3)	BH6 (Borsog)	3.6	>3.7	>3.7	3.0	>+0.4	
		BH12 (Sevs.)	6.8					
		BH19 (Dalbay)	6.8					
		BH1 (Dalb.)	3.6					
GN	2.9–3.6 (3.3)	BH10 (Shagn.)	3.6					
		BH9 (Turag)	4.1	4.2	4.2	4.2	+0.6	
		BH16 (Dalb.)	1.3	4.8	~5.0	4.8	+0.7	
GW	0.0–1.5 (0.9)	BH14 (Dalb.)	2.1	1.0			-0.3	
		BH17 (Borsog)	2.5	1.4			-0.7	

the ground surface and the top of permafrost is essential to fully address permafrost existence and the impact of climate changes on the thermal regime, together with heat flux modelling in borehole sites. As an example, at BH5 (southerly exposed forest, see Figure 1), both resistivity sounding and borehole temperatures clearly indicate that no permafrost is present. However, the surface logger showed below-zero MGST. At BH6 (dry valley bottom, see Figure 1), the MGST was close to +1°C, but shallow permafrost was shown by borehole temperatures and the resistivity soundings (see also Etzelmüller *et al.*, 2006), probably because of the high organic content in the soil. These examples demonstrate the limitation of ground surface temperature-based approaches at sites with varying vegetation cover and snow conditions.

CONCLUDING REMARKS

MGST varied between $\sim -3^{\circ}\text{C}$ and $+2.5^{\circ}\text{C}$ at the measurement sites in the Lake Hövsgöl area. MGST and thus permafrost distribution were largely controlled by solar radiation, ground surface wetness, winter snow cover and tree shading. Based on the continuous temperature measurements an empirical model of ground surface temperatures and FNs was applied. From these results thaw and freeze depths were estimated to vary between $<2\text{ m}$ and $>6\text{ m}$. This type of modelling, developed for arctic areas, appears to work in Central Asian regions, where alternative methods like Basal Temperature of Snow (BTS) or intensive sampling cannot be used. The model results form a realistic distribution pattern of ground surface temperature and active layer thickness variability. However, they should be applied at a regional scale, with ground resolution greater than 50 to 100 m, rather than treated as an expression of small-scale variability. The parameterisation of the annual ground surface temperature cycles should allow for simulation of climate change impacts on the ground thermal regime, which may be helpful as part of a management plan to be developed for the Lake Hövsgöl National Park.

ACKNOWLEDGEMENTS

This study was part of the 'Hövsgöl project', financially supported by the Global Environmental Facility (GEF) and implemented by the World Bank to the Mongolian Academy of Sciences. The Department of

Geosciences, University of Oslo, Norway, gave financial support. The ASTER satellite data were received through the EROS data centre, and are courtesy of NASA/GSFC/METI/ERSDAC/JAROS and the US/Japan ASTER science team. ASTER data processing was done by A. Käab, Department of Geosciences, University of Oslo. We want to thank Regula Frauenfelder, Sh. Tumentsetseg and Vladimir Romanovsky for participating in the fieldwork, and the Lake Hövsgöl Project participants for accompanying and helping us in the field. The paper was heavily improved by the comments of two anonymous reviewers and the editor. All map-based analyses and visualisation were carried out using ArcGIS (©ESRI) or ERDAS IMAGINE at the Laboratory for Geomatics at the Department of Geosciences, University of Oslo, Norway.

REFERENCES

- Anarmaa S, Natsagdorj S, Etzelmüller B, Heggem ESF, Nelson FE, Shiklomanov N, Goulden C. 2005. Monitoring of Permafrost in the Hovsgol Mountain Region, Mongolia. AGU Fall Meeting, 11–15 December, San Francisco.
- Batkhisig O. 2006. Soils of the Lake Hövsgöl area and its watershed. In *The Geology, Biodiversity and Ecology of Lake Hövsgöl (Mongolia)*. Goulden CE, Sitnikova T, Gelhaus J, Boldgiv B (eds). Backhuys Publisher: Leiden, Netherlands; 93–114.
- Beven KJ, Kirkby MJ. 1979. A physically based, variable contributing area model of basin hydrology. *Hydrological Sciences* **24**: 43–69.
- Brown J, Ferrians OJ Jr, Heginbottom JA, Melnikov ES. 1995. *Circum-Arctic map of permafrost and ground-ice conditions*. IPA and USGS: Woods Hole, MA, USA.
- Etzelmüller B, Heggem ESF, Sharkhuu N, Frauenfelder R, Käab A, Goulden CE. 2006. Mountain permafrost distribution modelling using a multi-criteria approach in the Hövsgöl area, Northern Mongolia. *Permafrost and Periglacial Processes* **17**: 91–104. DOI: 10.1002/ppp.554
- Goulden CE, Natsagdorj S, Nandintsetseg A, Etzelmüller B, Ariuntsetseg L, Sharkhuu A, Heggem E, Romanovsky VE. 2005. Recent degradation of permafrost under influence of climate warming and human activities at Lake Hovsgol, Northern Mongolia. Climate and Cryosphere International Science Conference (CLIC), 11–15 April 2005, Beijing, China.
- Hutchinson MF. 1989. A new procedure for gridding elevation and stream line data with automatic removal of spurious pits. *Journal of Hydrology* **106**: 211–232.
- Klone AE, Nelson FE, Shiklomanov NI. 2001. The n-factor as a tool in geocryological mapping: Seasonal thaw in the Kuparuk River basin, Alaska. *Physical Geography* **22**: 449–466.

- Kozhova OM, Shagdarsuren O, Dashdorzh A, Sodnom N (eds). 1989. *Lake Hövsgöl Atlas (in Russian)*. Russian Academy of Sciences: Moscow.
- Namkhajantsan G. 2006. Climate and climate change of the Hövsgöl region. In *The Geology, Biodiversity and Ecology of Lake Hövsgöl (Mongolia)*. Goulden CE, Sitnikova T, Gelhaus J, Boldgiv B (eds). Backhuys Publisher: Leiden: Netherlands; 63–76.
- Nelson FE, Outcalt SI. 1987. A Computational Method for Prediction and Regionalization of Permafrost. *Arctic and Alpine Research* **19**: 279–288.
- Nelson FE, Shiklomanov NI, Mueller GR, Hinkel KM, Walker DA, Bockheim JG. 1997. Estimating active-layer thickness over a large region: Kuparuk River Basin, Alaska, USA. *Arctic and Alpine Research* **29**: 367–378.
- Reynolds JM. 1997. *An Introduction to Applied and environmental geophysics*. John Wiley & Sons: Chichester.
- Sharkhuu N. 2006. Geocryological conditions of the Hövsgöl mountainous region. In *The Geology, Biodiversity and Ecology of Lake Hövsgöl (Mongolia)*. Goulden CE, Sitnikova T, Gelhaus J, Boldgiv B (eds). Backhuys Publisher: Leiden: Netherlands; 49–62.
- Sharkhuu N, Anarmaa S. 2005. Permafrost. In *The Dynamics of Biodiversity Loss and Permafrost Melt in Lake Hövsgöl National Park, Mongolia—Annual Report*. Goulden CE, Tsogtbaatar J, Mendsaikhan B (eds). Geocology Institute of Mongolian Academy of Sciences: Ulaanbaatar, Mongolia.
- Smith MW, Riseborough DW. 1996. Permafrost monitoring and detection of climate change. *Permafrost and Periglacial Processes* **7**: 301–309. DOI: 10.1002/ppp.410
- Williams PJ, Smith MW. 1989. *The Frozen Earth: Fundamentals of Geocryology*. Cambridge University Press: Cambridge.
- Wilson JP, Gallant JC. 2000. Secondary topographic attributes. In *Terrain Analysis - Principles and Application*. Wilson JP, Gallant JC (eds). Wiley: New York, USA; 87–132.
- Zevenbergen LW, Thorne CR. 1987. Quantitative analysis of land surface topography. *Earth Surface Processes and Landforms* **12**: 47–56.

Recent Advances in Permafrost Modelling

Daniel Riseborough,^{1*} Nikolay Shiklomanov,² Bernd Etzelmüller,³ Stephan Gruber⁴ and Sergei Marchenko⁵

¹ Geological Survey of Canada, Ottawa, Canada

² Department of Geography, University of Delaware, Newark, DE, USA

³ Department of Geosciences, Physical Geography, University of Oslo, Oslo, Norway

⁴ Department of Geography, University of Zürich, Zürich, Switzerland

⁵ Geophysical Institute, University of Alaska, Fairbanks, AK, USA

ABSTRACT

This paper provides a review of permafrost modelling advances, primarily since the 2003 permafrost conference in Zürich, Switzerland, with an emphasis on spatial permafrost models, in both arctic and high mountain environments. Models are categorised according to temporal, thermal and spatial criteria, and their approach to defining the relationship between climate, site surface conditions and permafrost status. The most significant recent advances include the expanding application of permafrost thermal models within spatial models, application of transient numerical thermal models within spatial models and incorporation of permafrost directly within global circulation model (GCM) land surface schemes. Future challenges for permafrost modelling will include establishing the appropriate level of integration required for accurate simulation of permafrost-climate interaction within GCMs, the integration of environmental change such as treeline migration into permafrost response to climate change projections, and parameterising the effects of sub-grid scale variability in surface processes and properties on small-scale (large area) spatial models. Copyright © 2008 John Wiley & Sons, Ltd.

KEY WORDS: permafrost; models; geothermal; mountains; spatial models

INTRODUCTION

Permafrost (defined as ground where temperatures have remained at or below 0°C for a period of least two consecutive years) is a key component of the cryosphere through its influence on energy exchanges, hydrological processes, natural hazards and carbon budgets — and hence the global climate system. The climate-permafrost relation has acquired added importance with the increasing awareness and concern that rising temperatures, widely expected throughout the next century, may particularly affect permafrost environments. The Intergovernmental Panel on Climate Change

(1990) has advocated that research should be directed towards addressing the climate-permafrost relation, including the effects of temperature forcing from climatic variation, local environmental factors such as snow and vegetation, and surficial sediments or bedrock types. Permafrost has been identified as one of six cryospheric indicators of global climate change within the international framework of the World Meteorological Organization (WMO) Global Climate Observing System (Brown *et al.*, 2008).

This review gives an overview of permafrost modelling advances, primarily since the 2003 permafrost conference in Zurich, Switzerland, with an emphasis on spatial permafrost models, in both arctic and high mountain environments. Many models have been developed to predict the spatial variation of permafrost thermal response to changing climate

* Correspondence to: Daniel Riseborough, Geological Survey of Canada, 601 Booth Street, Ottawa, Ontario, Canada K1A 0E4. E-mail: drisebor@nrcan.gc.ca

conditions at different scales, including conceptual, empirical and process-based models. The permafrost models considered in this paper are those that define the thermal condition of the ground, based on some combination of climatic conditions and the properties of earth surface and subsurface properties. Particular emphasis is given to models used in spatial applications.

MODELLING BACKGROUND

A model is a conceptual or mathematical representation of a phenomenon, usually conceptualised as a system. It provides an idealised framework for logical reasoning, mathematical or computational evaluation as well as hypothesis testing. Explicit assumptions about or simplifications of the system may be part of model development; how these decisions affect the utility of the model will depend on whether the model serves its intended purpose with satisfactory accuracy. Rykiel (1996) suggests that model ‘validation’ can be separated into evaluations of theory, implementation and data; while some statistical tests can be performed to measure differences between model behaviour and the behaviour of the system, ‘validation’ ultimately depends on whether the model and its behaviour are reasonable in the judgement of knowledgeable people.

The value of a model depends on its usefulness for a given purpose and not its sophistication. Simple models can be more useful than models which incorporate many processes, especially when data are limited. Choosing the appropriate point along the continuum of model complexity depends on data availability, modelling (usually computer) resources and the questions under investigation. The data needed to obtain credible results usually increase with increasing model complexity and with the number of processes that are represented. In mountain environments, lateral variations of surface and subsurface conditions as well as micro-climatology are far greater than in lowland environments.

Process-based permafrost models determine the thermal state of the ground based on principles of heat transfer, and can be categorised using temporal, thermal and spatial criteria. Temporally, models may define equilibrium permafrost conditions for a given annual regime (equilibrium models), or they may capture the transient evolution of permafrost conditions from some initial state to a modelled current or future state (transient models).

Thermally, simple models may define the presence or absence of permafrost, active-layer depth, or mean annual ground temperature, based on empirical and statistical relations or application of so-called equilibrium models utilising transfer functions between

atmosphere and ground. Numerical models (finite-element or finite-difference models) may define the annual and longer term progression of a deep-ground temperature profile (transient models). The influence of surface energy exchange on subsurface conditions may be defined by simplified equations using a few parameters (such as freezing/thawing indices and n factors, or air temperature and snow cover in equilibrium models), or as a fully explicit energy balance, requiring data for atmospheric conditions.

Spatially, models may define conditions at a single location (either as an index or a one-dimensional vertical temperature profile), along a two-dimensional transect, or over a geographic region. Most geographic/spatial permafrost models today are collections of modelled point locations, with no lateral heat flow between adjacent points. Points in such spatial models behave as one-dimensional models, so that small-scale spatial variability in soil properties and snow cover is not considered. This is a central problem for mountain areas where the effects of slope, aspect and elevation must be considered at regional or local scales. Thus, in mountainous regions the scale of variation in these factors requires alternative approaches to spatial modelling.

Heat Flow Theory

Basic heat flow theory is described in some detail in textbooks, such as Carslaw and Jaeger (1959), Williams and Smith (1989) and Lunardini (1981). The equation for heat flow under transient conditions forms the basis of all geothermal models.

$$C \frac{\partial T}{\partial t} = k \frac{\partial^2 T}{\partial z^2} \quad (1)$$

Definitions of equation symbols are given in Table 1.

Two exact analytical models derived for a semi-infinite and isotropic half-space using equation 1 are: the harmonic solution, describing ground temperatures at any time t and depth z below a ground surface experiencing sinusoidal temperature variations:

$$T_{z,t} = \bar{T} + A_s \cdot e^{-z\sqrt{\pi/\alpha P}} \cdot \sin\left(\frac{2\pi t}{P} - z\sqrt{\pi/\alpha P}\right) \quad (2)$$

and the step change solution, describing changes to ground temperatures at any time t and depth z below a ground surface following a step change in ground

Table 1 Symbols used in equations.

A_s	= annual temperature amplitude at soil surface, °C
c	= specific heat, Jkg ⁻¹
C	= volumetric heat capacity, Jm ⁻³
I_{FA}	= seasonal air freezing index, °Cs
I_{FS}	= seasonal ground surface freezing index, °Cs
I_{TA}	= seasonal air thawing index, °Cs
I_{TS}	= seasonal ground surface thawing index, °Cs
L	= volumetric latent heat of fusion, Jm ⁻³
n_F	= surface freezing n-factor
n_T	= surface thawing n-factor
P	= period of the temperature wave, s
P_{sn}	= period of the temperature wave, adjusted for snow melt, s
t	= time, s
\bar{T}	= mean annual temperature, °C
T_0	= initial soil temperature, °C
T_F	= fusion temperature, °C
T_S	= surface temperature, °C
T_{TOP}	= temperature at top of perennially frozen/unfrozen ground, °C
T_z	= mean annual temperature at the depth of seasonal thaw (equivalent to T_{TOP}), °C
$T_{z,t}$	= temperature at depth z at time t , °C
x	= volume fraction
X	= depth of thaw, m
z	= depth, m
θ_U	= volumetric unfrozen water content
ρ	= density, kg m ⁻³
α	= λ/C = thermal diffusivity m ² s ⁻¹
λ	= thermal conductivity, Wm ⁻¹ K ⁻¹

Subscripts for α , λ , ρ , c , C and n :

a	= apparent
i	= subscript identifying component (mineral, ice, water, etc.)
T	= thawed or thawing
F	= frozen or freezing

surface temperature:

$$\Delta T_{z,t} = \Delta T_S \cdot \operatorname{erfc}\left(\frac{z}{2\sqrt{\alpha t}}\right) \quad (3)$$

(*erfc* is the complementary error function)

Permafrost models are a subset of a more general class of geothermal models. In permafrost models, ground freezing and thawing are central in determining the important variables and parameters of which the model is comprised. Equations 2 and 3 form the basis of analyses of ground temperatures outside of permafrost regions, and are most useful where

freezing and thawing of significant amounts of soil moisture do not occur. Exact analytical models of the thermal behaviour of the ground when freezing or thawing occurs are limited to a few idealised conditions (Lunardini, 1981). Real-world conditions such as seasonal variation in the ground surface temperature, accumulation and ablation of snow cover, and temperature dependent thermal properties, are beyond the capacity of these exact models. Two paths move beyond this impasse: approximate analytical models developed by making simplifying assumptions, or numerical techniques employed to solve more complex problems with the acceptance of limited error.

For ground that undergoes freezing and thawing, the release and absorption of the latent heat of fusion of the soil water dominate heat flow, although the temperature-dependence of thermal conductivity is also important. Accounting for latent heat is usually achieved by subsuming its effect in the heat capacity term in equation 1.

$$C_a = \sum x_i \rho_i c_i + L \left(\frac{\partial \theta_u}{\partial T} \right) \quad (4)$$

The Stefan Model

The analytical equation most widely employed in the formulation of permafrost models is the Stefan solution to the moving freezing (or thaw) front. When diffusive effects are small relative to the rate of frost front motion and the initial temperature of the ground is close to 0°C, the exact equation for the moving phase change boundary can be simplified to a form of the Stefan solution using accumulated ground surface degree-day total I (either the freezing index I_F or thawing index I_T) (Lunardini, 1981):

$$X = \sqrt{\frac{2\lambda I}{L}} \quad (5)$$

The form of Stefan solution represented by equation (5) is widely used for spatial active-layer characterisation by estimating soil properties ('edaphic parameters') empirically, using summer air temperature records and active-layer data obtained from representative locations (e.g. Nelson *et al.*, 1997; Shiklomanov and Nelson, 2003; Zhang T. *et al.*, 2005).

Carlson (1952, based on Sumgin *et al.*, 1940) used equation 5 as the origin of a simple model for presence of permafrost, based on the notion that permafrost will

be present where predicted winter season freezing exceeds predicted summer season thaw, so that permafrost exists where $k_F I_{FS} > k_T I_{TS}$. Nelson and Outcalt (1987) derived the Frost Index model on this relationship. While the Frost Index model has been used extensively (e.g. Anisimov and Nelson, 1996), the Kudryavtsev model has become more common in recent studies.

The Kudryavtsev Model

An alternative solution to the Stefan problem was proposed by Kudryavtsev *et al.* (1974) (Figure 1A) for estimating maximum annual depth of thaw propagation and the mean annual temperature at the base of the active layer T_z (equivalent to the temperature at the top of permafrost, or T_{TOP} , described below):

$$Z_{thaw} = \frac{2(A_s - T_z) \cdot \sqrt{\frac{\lambda_T \cdot P_{sn} \cdot C_T}{\pi}} + \frac{(2A_z \cdot C_T \cdot Z_c + L \cdot Z_c) \cdot L \sqrt{\frac{\lambda \cdot P_{sn}}{\pi \cdot C_T}}}{2A_z \cdot C_T \cdot Z_c + L \cdot Z_c + (2A_z \cdot C_T + L) \cdot \sqrt{\frac{\lambda \cdot P_{sn}}{\pi \cdot C_T}}}}{2A_z \cdot C_T + L} \quad (6)$$

where

$$A_z = \frac{A_s - T_z}{\ln \left[\frac{A_s + L/2C_T}{T_z + L/2C_T} \right]} - \frac{L}{2C_T}$$

and

$$Z_c = \frac{2(A_s - T_z) \cdot \sqrt{\frac{\lambda \cdot P_{sn} \cdot C_T}{\pi}}}{2A_z \cdot C_T + L}$$

The mean annual temperature at the depth of seasonal thaw (permafrost surface) can be calculated as:

$$T_z = \frac{0.5T_s \cdot (\lambda_F + \lambda_T) + A_s \frac{\lambda_F - \lambda_T}{\pi} \cdot \left[\frac{T_s}{A_s} \arcsin \frac{T_s}{A_s} + \sqrt{1 - \frac{T_s^2}{A_s^2}} \right]}{\lambda^*} \quad (7)$$

$$\lambda^* = \begin{cases} \lambda_F, & \text{if numerator} < 0 \\ \lambda_T, & \text{if numerator} > 0. \end{cases}$$

Kudryavtsev's equations were derived assuming a periodic steady state with phase change ($L > 0$) (Kudryavtsev *et al.*, 1974). Romanovsky and Osterkamp (1997) indicate that equations 6 and 7 can be applied on an annual basis. Extensive validation of Kudryavtsev's equations using empirical data from the

North Slope of Alaska indicate that they provide more accurate estimates of annual maximum seasonal thaw depth than the Stefan equation (Romanovsky and Osterkamp, 1997; Shiklomanov and Nelson, 1999). Kudryavtsev's model is used extensively at regional (Shiklomanov and Nelson, 1999; Sazonova and Romanovsky, 2003; Stendel *et al.*, 2007) and circum-arctic (Anisimov *et al.*, 1997) scales.

N Factors

Freezing and thawing n factors relate ground surface temperature to air temperature as an empirical alternative to the energy balance (Lunardini, 1978). N factors are applied to seasonal degree-day totals (FDD or I_F for freezing; TDD or I_T for thawing), calculated as the accumulated departure of mean daily

temperature above (or below) 0°C, so that equation 5 can be applied using air temperature data.

$$n_T = \frac{I_{TS}}{I_{TA}}; \quad n_F = \frac{I_{FS}}{I_{FA}} \quad (8)$$

N factors account in a lumped form for the complex processes within the atmosphere-soil system and, as such, n factors will vary for a given location. Shur and Slavin-Borovski (1993) found that site-specific n factors are stable, with interannual changes less than 10 per cent in continental arctic areas. In mountainous regions, however, n factor variations can be much higher, especially during winter due to interannual variation of snow cover (e.g. Juliussen and Humlum, 2007). This variability might be even more accentuated in maritime mountainous areas (e.g. Eitzel-müller *et al.*, 2007, 2008). In low-topography, continental areas n factors can be correlated with surface cover and extrapolated over larger areas (e.g. Duchesne *et al.*, 2008).

The TTOP Model

The TTOP model (Smith and Riseborough, 1996) (Figure 1B) estimates the mean annual temperature at the top of perennial frozen/unfrozen soil by combining a model (Romanovsky and Osterkamp, 1995) of the thermal offset effect (in which the mean annual

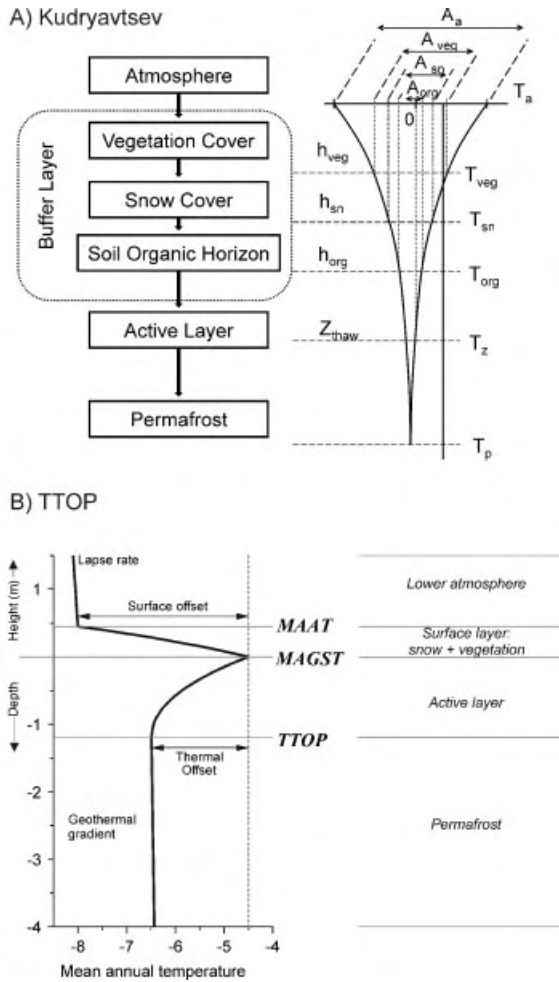


Figure 1 (A) Conceptual drawing of the Kudryavtsev model; (B) temperature at the top of permafrost (TTOP) model conceptual schematic profile of mean annual temperature through the lower atmosphere, active layer and upper permafrost.

temperature shifts to lower values in the active layer because of the difference between frozen and thawed thermal conductivities of the soil) with freezing and thawing indices in the lower atmosphere linked to values at the ground surface using n factors (equation 8):

$$T_{TOP} = \frac{n_T \lambda_T I_{TA} - n_F \lambda_F I_{FA}}{k_F P}, \quad T_{TOP} < 0$$

$$T_{TOP} = \frac{n_T \lambda_T I_{TA} - n_F \lambda_F I_{FA}}{\lambda_T P}, \quad T_{TOP} > 0$$

(9)

Applications of the TTOP model have depended on empirically derived n factors (Wright *et al.*, 2003; Juliussen and Humlum, 2007), although Riseborough

(2004) attempted to develop a physically based n-factor parameterisation of the effect of snow cover.

Statistical-Empirical Models and Multiple-Criteria Analysis

Statistical-empirical permafrost models relate permafrost occurrences to topoclimatic factors (such as altitude, slope and aspect, mean air temperature, or solar radiation), which can easily be measured or computed. This type of model is widely used in mountain permafrost studies (see also Hoelzle *et al.*, 2001), assumes equilibrium conditions and usually relies on basal temperature of the snow cover (BTS), temperatures measured with miniature data loggers, geophysical investigations, or the existence of specific landforms (rock glaciers) as evidence of permafrost occurrence. In the early 1990s, the availability of Geographical Information Systems (GIS) allowed the first estimation and visualisation of the spatial distribution of permafrost in steep mountains. PERMAKART (Keller, 1992) uses an empirical topographic key for permafrost distribution and in the PERMAMAP approach of Hoelzle and Haerberli (1995), BTS measurements, which are associated with the presence or absence of permafrost, are statistically related to mean annual air temperature (MAAT, estimated using nearby climate station records) and potential direct solar radiation during the snow-free season, calculated using digital elevation models (DEMs) (Funk and Hoelzle, 1992). The challenges with these approaches include the often indirect nature of the driving information on permafrost, the strong interannual variability of BTS, and the need to recalibrate for different environments. Statistical-empirical models usually estimate mean ground temperatures or provide measures of permafrost probability.

For small-scale mapping of large mountain areas, MAAT is often used as the sole predictor of permafrost occurrence, using thresholds based on field measurements. This approach involves the spatial interpolation of air temperature patterns from a common reference elevation (usually sea level) and the subsequent calculation of the near-surface MAAT using a DEM and a (sometimes spatially variable) lapse rate. Studies in southern Norway and Iceland have shown that a MAAT of -3 to -4°C is a good estimate for the regional limit of the lower mountain permafrost boundary (Etzelmüller *et al.*, 2003, 2007). These threshold values are normally estimated based on ground surface temperature data from several locations, or other proxy information such as landforms. The resulting mountain permafrost distributions are then compared with more local-scale

observations or maps, confirming the overall spatial pattern for Scandinavia (e.g. Isaksen *et al.*, 2002; Heggem *et al.*, 2005; Etzelmüller *et al.*, 2007; Farbrod *et al.*, 2008).

For more remote areas or regions with sparse data on permafrost indicators, multi-criteria approaches within a GIS framework have been applied to generate maps of 'permafrost favorability'. Here, scores were derived for single factors (elevation, topographic wetness, potential solar radiation, vegetation) based on simple logistic regression or basic process understanding, with the sum of the derived probabilities used as a measure of permafrost favourability in a given location (Etzelmüller *et al.*, 2006).

Numerical Models

The limitations of equilibrium models have spurred the recent adaptation of transient numerical simulation models in spatial applications. Numerical models are flexible enough to accommodate highly variable materials, geometries and boundary conditions. Most thermal models for geoscience applications are implemented by simulating vertical ground temperature profiles in one dimension employing a finite-difference or finite-element form of equation 1, usually following a standard procedure:

1. Define the modelled space: set a starting point in time, and upper and lower boundaries.
2. Divide continuous space into finite pieces (a grid of nodes or elements) and continuous time into finite time steps.
3. Specify the thermal properties of the soil materials.
4. Specify the temperature or heat flow conditions as a function of time (i.e. for each time step) for the upper and lower boundaries.
5. Specify an initial temperature for every point in the profile.
6. For each time step after the starting time, the new temperature profile is calculated, based on the combination of thermal properties, antecedent and boundary conditions.

While the use of numerical models allows the accommodation of heterogeneity in both space and time, it also gives rise to the problem of actually supplying spatial data fields of material properties and initial conditions.

Upper Boundary Conditions

Upper boundary temperature conditions in numerical models can be specified in various ways. Temperatures

may be specified for the ground surface directly or using n factors (e.g. Duchesne *et al.*, 2008); alternately, when snow cover is present the temperature at the snow surface may be specified so that ground surface temperature is determined by heat flow between the snow and the ground (e.g. Oelke and Zhang, 2004). The most elaborate method of establishing the surface boundary temperature is by calculation of the surface energy balance to determine the equilibrium temperature (Budyko, 1958) at the snow or ground surface (e.g. Zhang *et al.*, 2003). Surface energy-balance models generally employ a radiation balance with partitioning of atmospheric sensible and latent heat using aerodynamic theory. The earlier generation of permafrost models generally employed data that were collected locally for site-specific application, including incoming solar radiation, wind speed and air temperature (e.g. Outcalt *et al.*, 1975; Ng and Miller, 1977; Mittaz *et al.*, 2000). Spatial permafrost modelling at regional (Hinzman *et al.*, 1998; Chen *et al.*, 2003) and continental (Anisimov, 1989; Zhang *et al.*, 2007) scales has required a less site-specific approach to the energy balance, with short-wave radiation attenuated through the atmosphere, wind fields modified by local conditions based on satellite-derived leaf area indices, etc., often with climatic conditions obtained from GCM output (e.g. Sushama *et al.*, 2007). In mountain areas, extreme spatial variability requires the parameterisation of the influence of topography on surface micro-climatology for the derivation of spatially distributed information about temperature and snow cover (cf. Stocker-Mittaz *et al.*, 2002; Gruber, 2005).

SPATIAL MODELS

Application of the types of models described in the previous sections to the simulation and prediction of permafrost distribution at continental, regional and local scales is discussed in the following sections. Mountain permafrost models are discussed in a separate section, as is recent work incorporating permafrost into General Circulation Model (GCM) land surface schemes.

Continental/circumpolar

Due to the strong dependence of permafrost conditions on regional climate, geocryological spatial modelling has been dominated by national- to circumpolar-scale (i.e. small scale) studies in which broad spatial patterns can be related to a few readily available

climatic parameters. The empirical methods frequently used to assess permafrost distribution at these scales implicitly assume that the thermal regime of near-surface permafrost is determined by modern climatic conditions. The use of macro-scale patterns of climatic parameters to infer the configuration of permafrost zones was first proposed by G. Wild (Shiklomanov, 2005), who was able to correlate the southern boundary of permafrost with the -2°C isotherm of MAAT (Wild, 1882). Such simple empirical relations were frequently used throughout the twentieth century for permafrost regionalisation (Heginbottom, 2002), although they do not account for the thermal inertia of permafrost.

Equilibrium Models.

The Frost Number model was applied successfully to central Canada (Nelson, 1986) and continental Europe (Nelson and Anisimov, 1993) for modern climatic conditions. Calculated boundaries of continuous and discontinuous permafrost were in satisfactory agreement with existing geocryological maps. The Frost Number was used with an empirical scenario derived from palaeoanalogues and with output from several GCMs to predict the future distribution of 'climatic' permafrost in the northern hemisphere (Anisimov and Nelson, 1996; Anisimov and Nelson, 1997). An alternative approach was used by Smith and Riseborough (2002) to evaluate the conditions controlling the limits and continuity of permafrost in the Canadian Arctic by means of the TTOP model. Using a model derived from the TTOP model, based primarily on the roles of snow and soil thermal properties on the thermal effect of the winter snow cover, Riseborough (2004) produced maps of the southern boundary of permafrost in Canada for a range of substrate conditions.

Several variations of the Kudryavtsev model have been used with GIS technology to calculate both active-layer thickness and mean annual ground temperatures at circum-arctic scales (Anisimov *et al.*, 1997). The thermal and physical properties of snow, vegetation, and organic and mineral soils were fixed both spatially and temporally. These properties were varied stochastically within a range of published data for each grid cell, producing a range of geographically varying active-layer estimates. The final active-layer field was produced by averaging of intermediate results. The model was extensively used to evaluate the potential changes in active-layer thickness under different climate change scenarios at circumpolar (Anisimov *et al.*, 1997) and continental (Anisimov and Reneva, 2006) scales, to assess the hazard potential associated with progressive deepening of the active

layer (Nelson *et al.*, 2001, 2002; Anisimov and Reneva, 2006) and to evaluate the emission of greenhouse gases from the Arctic wetlands under global warming conditions for Russian territory (Anisimov *et al.*, 2005; Anisimov and Reneva, 2006).

Numerical Models.

A one-dimensional finite-difference model for heat conduction with phase change and a snow routine (Goodrich, 1978, 1982) has been adapted at the National Snow and Ice Data Center (NSIDC) to simulate soil freeze/thaw processes at regional or hemispheric scales (Oelke *et al.*, 2003, 2004; Zhang T. *et al.*, 2005). The NSIDC permafrost model requires gridded fields of daily meteorological parameters (air temperature, precipitation), snow depth and soil moisture content, as well as spatial representation of soil properties, land cover categories, and DEMs to evaluate the daily progression of freeze/thaw cycles and soil temperature at specified depth(s) over the modelling domain. Initial soil temperatures are prescribed from available empirical observations associated with permafrost classification from the International Permafrost Association's Circum-Arctic Permafrost Map (Brown, 1997; Zhang *et al.*, 1999), with a grid resolution of $25\text{ km} \times 25\text{ km}$. The numerical model has been shown to provide excellent results for active-layer depth and permafrost temperatures (Zhang *et al.*, 1996; Zhang and Stamnes, 1998) when driven with well-known boundary conditions and forcing parameters at specific locations.

Several numerical models have been developed recently for simulating permafrost evolution at continental scales. The Main Geophysical Observatory (St Petersburg) model was developed for Russian territory, using principles similar to those applied at the NSIDC but differing in computational details and parameterisations. In particular, the model was designed to be driven by GCM output to provide a substitute for unavailable empirical observations (Malevsky-Malevich *et al.*, 2001; Molkentin *et al.*, 2001).

Zhang *et al.* (2006) developed the Northern Ecosystem Soil Temperature (NEST) numeric model to simulate the evolution of the ground thermal regime of the Canadian landmass since the Little Ice Age (1850) (Figure 2). The model explicitly considered the effects of differing ground conditions, including vegetation, snow, forest floor or moss layers, peat layers, mineral soils and bedrock. Soil temperature dynamics were simulated with the upper boundary condition (the ground surface or snow surface when snow is present) determined by the surface energy balance and the lower boundary condition (at a depth of 120 m) defined by the geothermal heat flux (Zhang *et al.*, 2003). The NEST

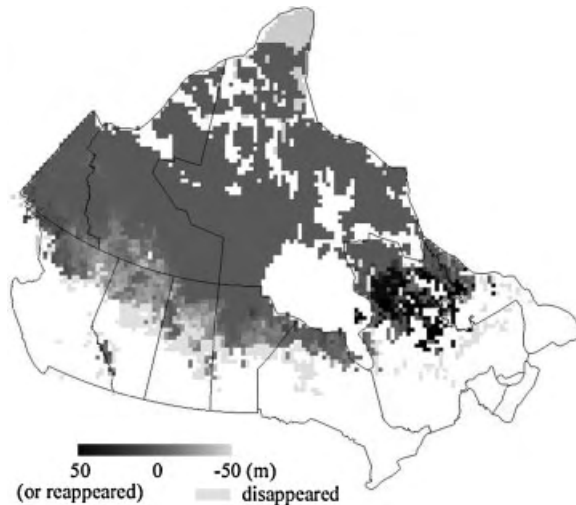


Figure 2 Modelled changes in depth to the permafrost base from the 1850s to the 1990s, simulated using the Northern Ecosystem Soil Temperature numeric model (Zhang *et al.*, 2006).

model operates at half-degree latitude/longitude resolution and requires inputs relating to vegetation (vegetation type and leaf area index), ground conditions (thickness of forest floor and peat, mineral soil texture and organic carbon content, ground ice content, thermal conductivity of bedrock and geothermal heat flux) and atmospheric climate (air temperature, precipitation, solar radiation, vapour pressure and wind speed).

Marchenko *et al.* (2008) developed University of Alaska Fairbanks–Geophysical Institute Permafrost Lab model Version 2 (UAF-GIPL 2.0), an Alaska-specific, implicit finite-difference, numerical model (Tipenko *et al.*, 2004). The formulation of the one-dimensional Stefan problem (Alexiades and Solomon, 1993; Verdi, 1994) makes it possible to use coarse vertical resolution without loss of latent-heat effects in the phase transition zone, even under conditions of rapid or abrupt changes in the temperature fields. Soil freezing and thawing follow the unfrozen water content curve in the model, specified for each grid point and soil layer, down to the depth of constant geothermal heat flux (typically 500 to 1000 m). The model uses gridded fields of monthly air temperature, snow depth, soil moisture, and thermal properties of snow, vegetation and soil at $0.5^\circ \times 0.5^\circ$ resolution. Extensive field observations from representative locations characteristic of the major physiographic units of Alaska were used to develop gridded fields of soil thermal properties and moisture conditions.

Non-linearity of sub-grid scale processes may lead to biased estimation of permafrost parameters when input

data and computational results are averaged at the grid scale. While coarse spatial resolution is sufficient for many small-scale geocryological applications such as permafrost regionalisation, evaluation of spatial variations in near surface permafrost temperature and the active layer should account for more localised spatial variability. This problem is addressed to some extent by regional, spatial permafrost models.

Local/regional

In general the approaches to permafrost modelling at regional scale are similar to those at small geographical scale. However, regional, spatial permafrost models are applied in areas for which significant amounts of data are available, with the underlying principle to ‘stay close to the data’. Available observations allow comprehensive analysis of landscape-specific (vegetation, topography, soil properties and composition) and climatic (air temperature and its amplitude, snow cover, precipitation) characteristics that influence the ground thermal regime and provide realistic parameterisations for high-resolution modelling.

Empirical Models.

Using empirically derived landscape-specific edaphic parameters representing the response of the active layer and permafrost to both climatic forcing and local factors (soil properties, moisture conditions and vegetation), empirical spatial modelling was successfully applied to high-resolution spatial modelling of the annual thaw depth propagation over the 29 000 km² Kuparuk region in north-central Alaska (Nelson *et al.*, 1997; Shiklomanov and Nelson, 2002) and the northern portion of west Siberia (Shiklomanov *et al.*, 2008). Zhang T. *et al.* (2005) used a landscape-sensitivity approach in conjunction with Russian historic ground temperature measurements to evaluate spatial and temporal variability in active-layer thickness over several Russian arctic drainage basins.

Equilibrium Models (Kudryavtsev, Stefan and TTOP).

The Kudryavtsev approach was applied successfully over the Kuparuk region of north-central Alaska by Shiklomanov and Nelson (1999) for high-resolution (1 km²) characterisation of active-layer thickness and was used as the basis for the GIPL 1.0, an interactive GIS model designed to estimate the long-term response of permafrost to changes in climate. The GIPL 1.0 model has been applied to detailed analysis of permafrost conditions over two regional transects in Alaska and eastern Siberia (Sazonova and Romanovsky, 2003). In particular it

was used to simulate the dynamics of active-layer thickness and ground temperature, both retrospectively and prognostically, using climate forcing from six GCMs (Sazonova *et al.*, 2004). To refine its spatial resolution, the GIPL 1.0 model was used in conjunction with a regional climate model (RCM) to provide more realistic trends of permafrost dynamics over the east-Siberian transect (Stendel *et al.*, 2007).

Stefan-based methods range from straightforward computational algorithms requiring deterministic specification of input parameters (gridded fields of thawing indices, thermal properties of soil, moisture/ice content and land cover characteristics, and terrain models) (Klene *et al.*, 2001) to establishing empirical and semi-empirical relationships between variables based on comprehensive field sampling (Nelson *et al.*, 1997; Shiklomanov and Nelson, 2002). These methods were used for high-resolution mapping of the active layer in the Kuparuk region (Klene *et al.*, 2001) and for detailed spatial characterisation of active-layer thickness in an urbanised area in the Arctic (Klene *et al.*, 2003).

Wright *et al.* (2003) used the TTOP formulation for high-resolution (1 km²) characterisation of permafrost distribution and thickness in the broader Mackenzie River valley, north of 60°N. The TTOP model calibrated for the Mackenzie region using observations of permafrost occurrence and thickness at 154 geotechnical borehole sites along the Norman Wells Pipeline provided good general agreement with currently available information. The results indicate that given adequate empirically derived parameterisations, the simple TTOP model is well suited for regional-scale GIS-based mapping applications and investigations of the potential impacts of climate change on permafrost.

Numerical Models.

Although empirical and equilibrium approaches currently dominate spatial permafrost modelling at a regional scale, several numerical models were adopted for regional applications to provide spatial-temporal evolution of permafrost parameters.

A regional, spatial, numerical thermal model was developed by Hinzman *et al.* (1998) and applied to simulate active layer and permafrost processes over the Kuparuk region, the North Slope of Alaska, at 1 km² resolution. The model utilises a surface energy balance and subsurface finite-element formulations to calculate the temperature profile and the depth of thaw. Meteorological data were provided by a local high-density observational network and surface and subsurface characteristics were spatially interpolated

based on measurements collected in typical landform and vegetation units.

Duchesne *et al.* (2008) use a one-dimensional finite-element heat conduction model integrated with a GIS to investigate the transient impact of climate change on permafrost over three areas of intensive human activity in the Mackenzie valley (Figure 3). The model uses extensive field survey data and existing regional maps of surface and subsurface characteristics as input parameters to predict permafrost distribution and temperature characteristics at high resolution (1 km²), and facilitates transient modelling of permafrost evolution over selected time frames. Statistical validation of modelling results indicates a reasonable level of confidence in model performance for applications specific to the Mackenzie River valley.

Mountains

The lateral variability of surface micro-climate and subsurface conditions is far greater in mountains than in lowland environments. The processes that govern the existence and evolution of mountain permafrost can be categorised into the scales and process domains of climate, topography and ground conditions (Figure 4). At the global scale, latitude and global circulation patterns determine the distribution of cold mountain climates. These climatic conditions are modified locally by topography, influencing micro-climate and surface temperature due to differences in ambient air temperature caused by elevation, differences in solar radiation caused by terrain shape and orientation, and differences in snow cover due to transport by wind and avalanches. The influence of topographically altered climate conditions on ground temperatures is further modified locally by the physical and thermal properties of the ground. Substrate materials with high ice content can significantly retard warming and permafrost degradation at depth, while, especially in mountainous terrain, coarse blocky layers promote ground cooling relative to bedrock or fine-grained substrates (Hanson and Hoelzle, 2004; Juliussen and Humlum, 2008). Conceptually, these three scales and process domains are useful in understanding the diverse influences on mountain permafrost characteristics and the differences between modelling approaches, although divisions between scales are not sharply defined. The overall magnitude of the effect of topography on ground temperature conditions can be as high as 15°C within a horizontal distance of 1 km — comparable to the effect of a latitudinal distance of 1000 km in polar lowland areas.

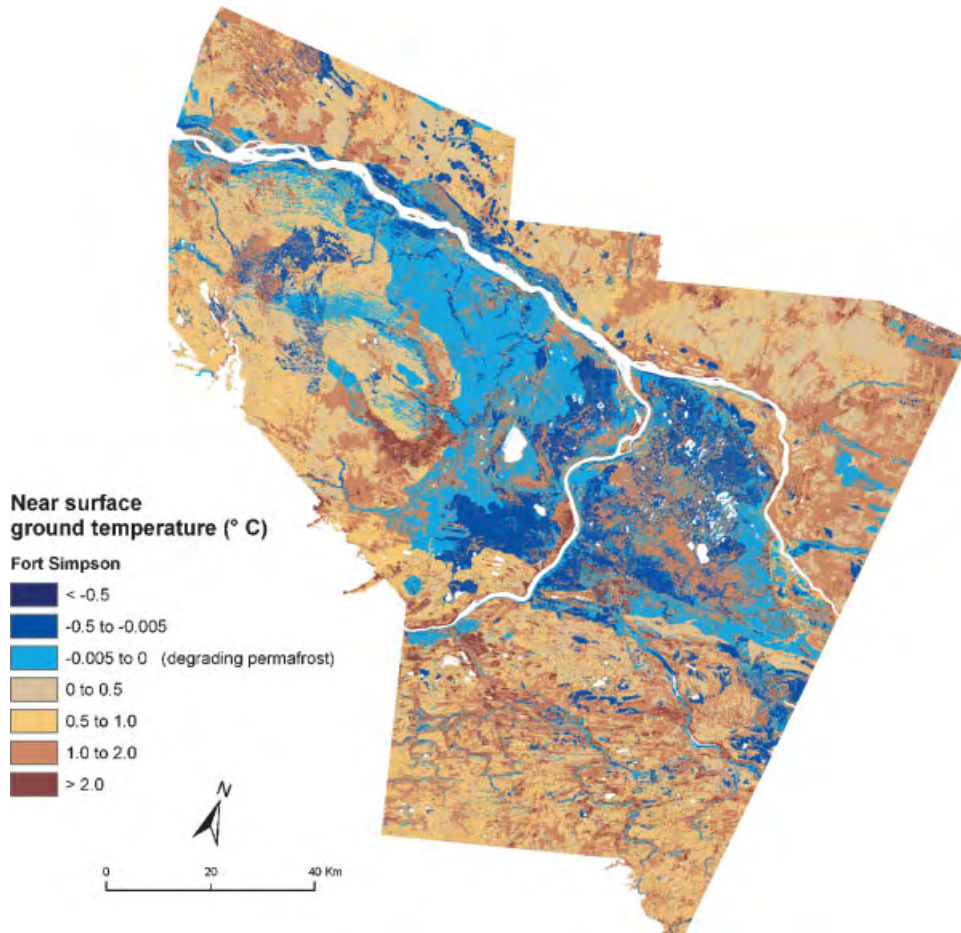


Figure 3 Near-surface permafrost temperature in the Fort Simpson region of Northwest Territories, Canada, simulated using a finite-element model with surface boundary conditions (n factors, subsurface properties) derived from satellite and map-based vegetation characteristics (Duchesne *et al.*, 2008).

Empirical-Statistical and Analytical Distributed Models.

Lewkowicz and Ednie (2004) designed a BTS- and radiation-based statistical model in the Yukon Territory in Canada, using an extensive set of observations in pits

for calibration and validation. Lewkowicz and Bonneventure (2008) examined strategies for transferring BTS-based statistical models to other regions, with the aim of modelling permafrost probabilities over the extensive mountain areas of western Canada. Brenning



Figure 4 Conceptual hierarchy of scales and process domains that influence ground temperature and permafrost conditions in mountain areas. The white disk in the two leftmost images refers to a location that is then depicted in the image to the right — and has its conditions further overprinted by the respective conditions at that scale.

et al. (2005) have outlined statistical techniques for improving the definition of such models, as well as for designing effective measurement campaigns.

A very simple alternative approach is to represent the influence of solar radiation on ground temperatures using a model of the form: $MAGT = MAAT + a + b \cdot PR$, where PR is the potential direct short-wave radiation, MAGT is the mean annual ground temperature, and a, b are model constants. This approach is usually limited by the available data for MAGT but can be a valuable first guess in remote locations (cf. Abramov *et al.*, 2008).

DEM-derived topographic parameters and information derived from satellite images offer the potential for more accurate permafrost distribution modelling in remote mountainous areas. Heggem *et al.* (2006) estimated the spatial distribution of mean annual ground surface temperature and active-layer thickness based on measured ground surface temperatures in different landscape classes defined by topographic parameters (elevation, potential solar radiation, wetness index) and satellite image-derived factors (forest and grass cover). A sine function was fitted to the surface temperature measurements (parameterised as the mean annual temperature and amplitude), providing input for the Stefan equation. Unlike the statistical approaches, this allowed the spatial mapping of simulated ground surface temperature and active-layer thickness fields for changing temperature or snow cover.

Juuliusen and Humlum (2007) proposed a TTOP-type model adapted for mountain areas. Elevation change is described through air temperatures, while slope dependencies are parameterised by potential solar radiation as a multiplicative summer-thaw n factor, including parameterisation for convective flow in blocky material. While there are benefits to this approach (such as a broad base of experience in lowland areas), the multiplicative treatment of solar radiation in the n factors will lead to problems when used over large ranges in elevation and needs further study. For Iceland, Etzelmüller *et al.* (2008) used the TTOP-modelling approach to estimate the influence of snow cover on permafrost existence at four mountain sites. The results were compared against transient heat flow modelling of borehole temperatures. Both studies show a high variability of winter n factors through the years of monitoring.

Transient Models, Energy-balance Modelling and RCM-Coupling.

In Scandinavia, one-dimensional transient models were applied to ground temperatures measured in permafrost boreholes in Iceland (Farbrot *et al.*, 2007; Etzelmüller *et al.*, 2008).

The slope instability associated with the rapid thermal response of permafrost in steep bedrock slopes (cf. Gruber and Haerberli, 2007) has led to increased interest in measurements (Gruber *et al.*, 2003) and models (Gruber *et al.*, 2004a, 2004b) of near-surface rock temperatures in steep terrain. The physics-based modelling (and validation) of temperatures in steep bedrock is an interesting subset of modelling the whole mountain cryosphere, because the influence of topography on micro-climate is maximised, while the influence of all other factors is minimal. The mostly thin snow cover on steep rock walls implies gravitational transport of snow and deposition at the foot of the slope. This is manifested in the occurrence of low-elevation permafrost as well as small glaciers that are entirely below the glacier equilibrium line altitude. A simple and fast algorithm for gravitational redistribution of snow (Gruber, 2007) is currently being tested in distributed energy-balance models (e.g. Strasser *et al.*, 2007).

Terrain geometry and highly variable upper boundary conditions determine the shape of the permafrost body, borehole temperature profiles (cf. Gruber *et al.*, 2004c) and potential rates of permafrost degradation. Noetzli *et al.* (2007) have conducted detailed experiments with two- and three-dimensional thermal models, demonstrating that zones of very high lateral heat flux exist in ridges and peaks, and that these zones are subject to accelerated degradation as warming takes place from several sides (Noetzli *et al.*, 2008).

The one-dimensional model SNOWPACK (Bartelt and Lehning, 2002), originally developed to represent a highly differentiated seasonal snow cover, has been used in several pilot studies to investigate permafrost (Luetsch *et al.*, 2004; Luetsch and Haerberli, 2005). In this model, mass and energy transport as well as phase change processes are treated with equal detail throughout all snow and soil layers, with water transported in a linear reservoir cascade. The distributed model Alpine3D (employing SNOWPACK) can calculate or parameterise wind transport of snow, terrain-reflected radiation and snow structure (Lehning *et al.*, 2006).

Freeze-thaw processes combined with steep slopes produce significant fluctuations in water and ice content in the active layer of mountain permafrost. GEOTop (Zanotti *et al.*, 2004; Bertoldi *et al.*, 2006; Rigon *et al.*, 2006; Endrizzi, 2007) is a distributed hydrological model with coupled water and energy budgets that is specifically designed for use in mountain areas and is currently being adapted to permafrost research. While the parameterisation, initialisation and validation of such complex models are demanding, the initial results of this research are promising.

In contrast to high-latitude mountains and lowlands, the central Asian mid-latitude permafrost of the Tien Shan Mountains can be attributed exclusively to elevation. In the inner and eastern Tien Shan region the high level of solar radiation and high winds in combination with low atmospheric pressure and low humidity promote very intensive evaporation/sublimation in the upper ground and can lead to the formation of unexpectedly thick permafrost, especially within blocky debris (Haerberli *et al.*, 1992; Harris, 1996; Humlum, 1997; Harris and Pedersen, 1998; Delaloye *et al.*, 2003; Gorbunov *et al.*, 2004; Delaloye and Lambiel, 2005; Juliussen and Humlum, 2008; Gruber and Hoelzle, 2008). Spatial modelling of altitudinal permafrost in the Tien Shan and Altai mountains examined both permafrost evolution over time and permafrost dynamics at the local scale for specific sites within selected river basins (Marchenko, 2001; Marchenko *et al.*, 2007) and also at regional scale for the entire Tien Shan permafrost domain. Regional-scale simulation used a multi-layered numerical soil model, including the latent heat of fusion, with snow cover and vegetation having time-dependent thermal properties. The model uses soil extending down to a depth at least of 100 m (without horizontal fluxes), and takes into account convective cooling within coarse debris and underlying soils (Marchenko, 2001). An international team of experts is currently working on a unified permafrost map of Central Asia (Lai *et al.*, 2006), including the Altai Mountain region. Figure 5 shows the first attempt to simulate the Altai's spatially distributed altitudinal permafrost, with a 5-km grid size.

Permafrost in Global/RCMs

Until recently the transient response of permafrost to projected climate change has usually been modelled outside of GCMs, using GCM results only to force surface conditions, in what Nicolsky *et al.* (2007) call a 'post-processing approach', primarily because the coarse subsurface resolution within GCMs did not adequately represent permafrost processes. The representation of the soil column within early GCM land surface schemes did not include freezing and thawing processes, and most recent implementations include few soil layers and a soil column of less than 10 m (e.g. Li and Koike, 2003; Lawrence and Slater, 2005; Saha *et al.*, 2006; Saito *et al.*, 2007; Sushama *et al.*, 2007). Christensen and Kuhry (2000) and Stendel and Christensen (2002) used RCM- and GCM-derived surface temperature indices to model active-layer thickness using the Stefan equation, and permafrost distribution using the Frost Number model,

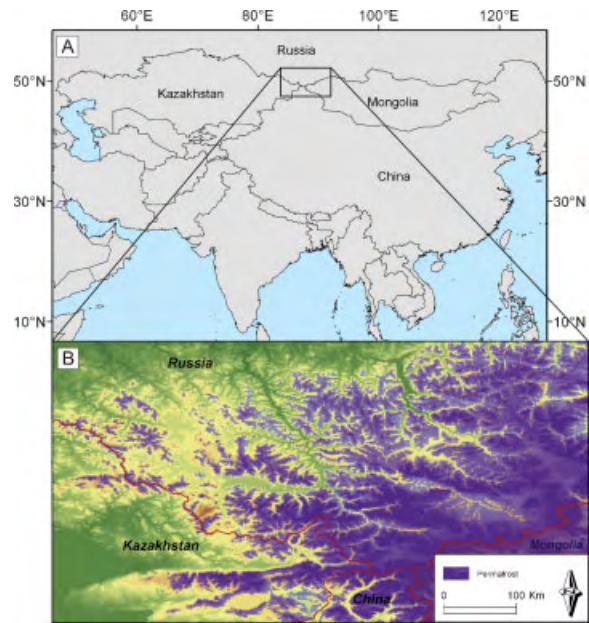


Figure 5 (A) Location map for the Altai Mountains; (B) modelled permafrost distribution within the northwest part of the region.

while Stendel *et al.* (2007) evaluated permafrost conditions by driving the Kudryavtsev model with GCM output downscaled to RCM resolution. Li and Koike (2003) and Yi *et al.* (2006) have developed schemes to improve the accuracy of frost line or active-layer thickness estimates with coarsely layered soils grids using modified forms of the Stefan equation.

Lawrence and Slater (2005) modelled transient permafrost evolution directly within the Community Climate System Model GCM (Collins *et al.*, 2006) and Community Land Model Version 3 (CLM3) (Oleson *et al.*, 2004). Their results generated significant discussion within the permafrost community (Burn and Nelson, 2006; Lawrence and Slater, 2006; Delisle, 2007; Yi *et al.*, 2007) for reasons largely related to the shallow (3.43 m) soil profile (see following section on depth, memory and spin-up), although Yi *et al.* (2007) also demonstrate the importance of the surface organic layer. Subsequent work on the geothermal component of CLM3 (Mölders and Romanovsky, 2006; Alexeev *et al.*, 2007; Nicolsky *et al.*, 2007) has clarified many issues involved in accounting for the annual permafrost regime. While a modified scheme has been evaluated against long-term monitoring data (Mölders and Romanovsky, 2006), spatial results using the modified scheme at global or regional scale have not yet appeared.

At present the most realistic representation of transient permafrost dynamics within spatial models is within externally forced 'post-processed' models which incorporate high-resolution finite-element or finite-difference, numerical heat flow models (e.g. Oelke and Zhang, 2004; Zhang Y. *et al.*, 2005, 2006).

The application of RCM/GCM output to the physics-based modelling of permafrost is especially difficult in mountain areas. Because of the poor representation of steep topography on coarse grids, strong differences between simulated and measured climate in those areas exist. Salzmann *et al.* (2006, 2007) and Noetzli *et al.* (2007) have described a method that allows downscaling RCM/GCM results in mountain areas and their application to energy-balance and three-dimensional temperature modelling in steep bedrock.

DISCUSSION AND FUTURE DIRECTIONS

Model Uncertainty and Data Uncertainty

Permafrost models that operate on broad (circumpolar/continental) geographical scale are the most appropriate tools for providing descriptions of climate-permafrost interactions over the terrestrial Arctic. However, their spatial resolution and accuracy are limited by availability of data characterising the spatial heterogeneity of many important processes controlling the ground thermal regime. Shiklomanov *et al.* (2007) found large differences between spatially modelled active-layer fields produced by various small-scale permafrost models, due primarily to differences in the models' approaches to characterisation of largely unknown spatial distributions of surface (vegetation, snow) and subsurface (soil properties, soil moisture) conditions. Further, Anisimov *et al.* (2007) found the differences in global baseline climate datasets (air temperature, precipitations), widely used for forcing small-scale permafrost models, can translate into uncertainty of up to 20 per cent in estimates of near-surface permafrost area, which is comparable to the extent of changes projected for the current century.

Lower Boundary and Initial Conditions — Depth, Memory and Spin-up

Ground temperature is largely controlled by changes at the surface, with change lagged and damped by diffusion at depth. The depth to which numerical models simulate temperature is limited by the relationship between the thermal properties of the

ground and the size of time step and grid spacing (and as determined by the limitations of the model). One-dimensional permafrost model studies typically specify a modelled soil depth of 20 m or more, in order to capture the annual ground temperature cycle, with deeper profiles specified when the long-term evolution of the ground thermal regime is being evaluated. The medium- and long-term fate of permafrost is determined by changes at depth, such as the development of supra-permafrost taliks. Truncating the ground temperature profile at too shallow a depth will introduce errors as the deep profile influences the thermal regime of the near surface, with errors accumulating as the temperature change at the surface penetrates to the base of the profile.

Alexeev *et al.* (2007) suggest that in general the lower boundary should be specified so that the total soil depth is much greater than the damping length for the timescale of interest. They suggest that the timescale of maximum error is about two years for a 4-m-deep soil layer, or about 200 years for a 30-m-deep grid, although their analysis ignores the effect of latent heat. In a comparison with an equilibrium model (a situation with no memory at all) and a numerical model that accounts for latent heat, Riseborough (2007) showed that the long-term mean annual temperature at the base of the active layer could be accurately predicted under transient conditions except where a talik was present. Applying this result to the analysis of Alexeev *et al.* (2007), they likely underestimate the magnitude of errors due to a shallow base, as thaw to the base does not imply the disappearance of permafrost, but does imply the development of a talik, and that permafrost is no longer sustainable under the changing climate.

The inclusion of a deep temperature profile for the modelled space introduces the additional challenge of estimating a realistic initial condition. While this can be established using field temperature data, this approach is impractical in spatial modelling; where no data are available, an initial temperature profile is usually established by an equilibration or 'spin-up' procedure, running the model through repeated annual cycles with a stationary surface climate, until an equilibrium ground temperature profile develops.

Depending on the profile used to initiate the spin-up procedure, equilibration of deep profiles typically requires hundreds of cycles, although as Lawrence and Slater (2005) and others have noted, the initial profile has little effect if the profile is very shallow. In a regional permafrost model, with a 120-m-deep temperature profile Ednie *et al.* (2008) found that permafrost profiles equilibrated using twentieth century climate data did not adequately reproduce

the essential characteristics of the current regime in the Mackenzie Valley, Northwest Territories, Canada, in particular the presence of deep, nearly isothermal (disequilibrium) permafrost. They initiated their model with a spin-up to equilibrium for the year 1721, followed by a surface history combining local palaeo-climatic reconstructions and the instrumental record. For a national scale model, Zhang Y. *et al.* (2005, 2006) began their long-term simulations assuming equilibrium in 1850, with climate data for the 1850–1900 period estimated by backward linear extrapolation from twentieth century climatic data.

Initial modelling of permafrost distribution in the Mackenzie Valley (Northwest Territories, Canada) used the TTOP model (Wright *et al.*, 2003), predicting mean annual ground temperature and permafrost thickness. The TTOP model was used to improve efficiency when modelling the transient evolution of permafrost in this environment using a one-dimensional finite-element model (Duchesne *et al.*, 2008). First, the accuracy of the TTOP model for estimating equilibrium conditions allowed for a reasonable first estimate of the initial ground temperature profile, minimising the time required for model equilibration. Second, the equilibrium permafrost thickness estimated using the TTOP model was used to establish the depth of the bottom of the grid.

Modelling Permafrost and Environmental Change

Future refinements to modelling of permafrost response to climate change projections will require consideration of the interaction between permafrost, snow cover, vegetation and other environmental factors at timescales ranging from decadal to millennial. To a significant degree, the position of treeline controls the geographic distribution of snow density (Riseborough, 2004), so that changes in permafrost distribution, migration of treeline and changes in snow cover properties in the forest-tundra transition zone will be highly inter-dependent. At much longer timescales, the distribution of peatlands depends on the relative rates of carbon accumulation and depletion in the soil, with the zone of peak soil carbon and peatland distribution close to the position of the 0°C mean annual ground temperature isotherm (Swanson *et al.*, 2000). Changing ground temperatures under climate warming will alter the distribution of peatlands, thereby altering local permafrost distribution. These changes will influence surface and subsurface physical, thermal and hydraulic properties,

which are often currently assumed to remain unchanged, even in a future climate.

N Factors and Parameterisation

N factors expressed as a ratio (equation 8) or the layers of the Kudryavtsev model (which function by diffusive extinction) may not adequately express the empirical relationships among the multitude of processes they subsume and the underlying system behaviour (as opposed to model behaviour). The functional form in which parameters encapsulate complex processes in simple models will influence the behaviour of the model, especially where models are used for predictions beyond the scope in which the parameters were derived. Unless there is a strong theoretical basis for the functional form of the parameterisation, it may be better to express the relationship in a form dictated by empirical results; alternate forms include differences or multi-parameter linear or non-linear relationships.

CONCLUSION

The fate of permafrost under a changing climate has been a concern since the earliest GCM results demonstrated the magnitude of the problem. Current permafrost transient modelling efforts generally follow two approaches: incorporation of permafrost dynamics directly into GCM surface schemes and increasingly sophisticated regional, national and global models forced by GCM output. Although computational cost is becoming less critical as computer technology advances, these two approaches will continue to evolve in tandem, and are unlikely to merge. While Stevens *et al.* (2007) demonstrate the importance of the deep geothermal regime on heat storage under a changing climate, the influence of permafrost conditions on the evolving GCM climate and the computational requirements of a multi-layer ground thermal scheme will likely be balanced with a level of complexity that is less than can be achieved in detailed regional models. Once this balance is achieved, the relationship between GCM-based and post-processed models will be equivalent to the relationship between global and regional climate models.

Historically, spatial models of permafrost in arctic lowlands and mountain terrain have developed following different principles. Permafrost was initially studied in Arctic lowland areas, mainly because of human development in these regions. Both numerical and analytical solutions were developed early, both of

which were easy to apply to spatial models as GIS and computer power developed. Permafrost in mountains was recognised as an engineering and scientific topic much later (1970s), and the spatial heterogeneity of factors influencing permafrost led to the development of empirical concepts. A trend apparent today is the merging of the concepts developed in Arctic lowland regions in mountain environments. This is now possible with the increasing power of computer hardware and software, but the treatment of sub-grid heterogeneity (such as the effect of topography) over continental or hemispheric areas remains a major scientific challenge.

ACKNOWLEDGEMENTS

The authors would like to thank Caroline Duchesne and two anonymous reviewers whose comments were useful in revising the paper. Yu Zhang and Caroline Duchesne provided graphical examples of recent work for inclusion as figures. The forbearance of the journal's editors is gratefully acknowledged.

REFERENCES

- Abramov A, Gruber S, Gilichinsky D. 2008. Mountain permafrost on active volcanoes: field data and statistical mapping, Klyuchevskaya volcano group, Kamchatka, Russia. *Permafrost and Periglacial Processes* (in press).
- Alexeev VA, Nicolsky DJ, Romanovsky VE, Lawrence DM. 2007. An evaluation of deep soil configurations in the CLM3 for improved representation of permafrost. *Geophysical Research Letters* **34**: L09502. DOI:10.1029/2007GL029536.
- Alexiades V, Solomon AD. 1993. *Mathematical modeling of melting and freezing processes*. Hemisphere: Washington.
- Anisimov OA. 1989. Changing climate and permafrost distribution in the Soviet Arctic. *Physical Geography* **10**: 285–293.
- Anisimov OA, Nelson FE. 1996. Permafrost distribution in the Northern Hemisphere under scenarios of climatic change. *Global and Planetary Change* **14**(1–2): 59–72. DOI:10.1016/0921-8181(96)00002-1.
- Anisimov OA, Nelson FE. 1997. Permafrost zonation and climate change in the northern hemisphere: results from transient general circulation models. *Climatic Change*, **35**(2): 241–258. DOI: 10.1023/A:1005315409698.
- Anisimov OA, Reneva SA. 2006. Permafrost and changing climate: the Russian perspective. *Ambio* **35**: 169–175. DOI:10.1579/0044-7447(2006)35[169:PACCTR]2.0.CO;2.
- Anisimov OA, Shiklomanov NI, Nelson FE. 1997. Effects of global warming on permafrost and active-layer thickness: results from transient general circulation models. *Global and Planetary Change*, **15**: 61–77. DOI: 10.1016/S0921-8181(97)00009-X.
- Anisimov OA, Lavrov SA, Reneva SA. 2005. Emission of methane from the Russian frozen wetlands under the conditions of the changing climate. In *Problems of Ecological Modeling and Monitoring of Ecosystems*, Izrael Y (ed.). Hydrometeoizdat: St Petersburg; 124–142 (in Russian).
- Anisimov OA, Lobanov VA, Reneva SA, Shiklomanov NI, Zhang T, Nelson FE. 2007. Uncertainties in gridded air temperature fields and effects on predictive active layer modeling. *Journal Of Geophysical Research*, **112**: F02S14. DOI:10.1029/2006JF000593.
- Bartelt P, Lehning M. 2002. A physical SNOWPACK model for the Swiss avalanche warning. Part I: numerical model. *Cold Regions Science and Technology*. **35**(3): 123–145. DOI: 10.1016/S0165-232X(02)00074-5.
- Bertoldi G, Rigon R, Over TM. 2006. Impact of watershed geomorphic characteristics on the energy and water budgets. *Journal of Hydrometeorology* **7**(3): 389–403. DOI: 10.1175/JHM500.1.
- Brenning A, Gruber S, Hoelzle M. 2005. Sampling and statistical analyses of BTS measurements. *Permafrost and Periglacial Processes* **16**: 383–393. DOI: 10.1002/ppp.541.
- Brown J. 1997. A new permafrost map of the Northern Hemisphere. *Eos Transactions of the American Geophysical Union* **78**: F274.
- Brown J, Smith SL, Romanovsky V, Christiansen HH, Clow G, Nelson FE. 2008. Global Terrestrial Network for Permafrost. In *Terrestrial Essential Climate Variables for Assessment, Mitigation and Adaptation*, WMO Global Climate Observing System report GTOS-52, Sessa, Dolman (eds). Food and Agriculture Organization of the United Nations (UN FAO), Rome; pp. 24–25.
- Budyko MI. 1958. Earth Surface Temperature and its bioclimatic importance. In *Contemporary problems of boundary layer climatology*. Leningrad: Gidrometizdat; 234 pp. (in Russian).
- Burn CR, Nelson FE. 2006. Comment on 'A projection of severe near-surface permafrost degradation during the 21st century' by David M. Lawrence and Andrew G. Slater. *Geophysical Research Letters* **33**: L21503. DOI:10.1029/2006GL027077.
- Carlson H. 1952. Calculation of depth of thaw in frozen ground. Frost action in soils Highway Research Board Special Report Number 2, 192–223.
- Carlslaw HS, Jaeger JC. 1959. *Conduction of Heat in Solids*, 2nd Ed. Oxford University Press: Oxford.
- Chen W, Zhang Y, Cihlar J, Smith SL, Riseborough DW. 2003. Changes in soil temperature and active-layer thickness during the twentieth century in a region in western Canada. *Journal of Geophysical Research*, **108**(D22): 4696. DOI:10.1029/2002JD003355.
- Christensen JH, Kuhry P. 2000. High-resolution regional climate model validation and permafrost simulation for the East European Russian Arctic. *Journal of Geophysical Research-Atmospheres*, **105**: 29647–29658.

- Collins WD, Bitz CM, Blackmon ML, Bonan GB, Bretherton CS, Carton JA, Chang P, Doney SC, Hack JJ, Henderson TB, Kiehl JT, Large WG, Mckenna DS, Santer BD, Smith RD. 2006. The community climate system model: CCSM3. *Journal of Climate* **19**(11): 2122–2143. DOI: 10.1175/JCLI3761.1.
- Delaloye R, Lambiel C. 2005. Evidence of winter ascending air circulation throughout talus slopes and rock glaciers situated in the lower belt of alpine discontinuous permafrost (Swiss Alps). *Norwegian Journal of Geography*, **59**(2): 194–203. DOI: 10.1080/00291950510020673.
- Delaloye R, Reynard E, Lambiel C, Marescot L, Monnet R. 2003. Thermal anomaly in a cold scree slope, Creux du Van, Switzerland. In *Proceedings of the Eighth International Conference on Permafrost*, A. A. Balkema: Lisse; 175–180.
- Delisle G. 2007. Near-surface permafrost degradation: How severe during the 21st century? *Geophysical Research Letters* **34**: L09503. DOI:10.1029/2007GL029323.
- Duchesne C, Ednie M, Wright JF. 2008. High resolution numerical modeling of climate change impacts to permafrost in the vicinities of Inuvik, Norman Wells, and Fort Simpson, NT, Canada. In *Proceedings of the Ninth International Conference on Permafrost*, Fairbanks, Alaska. Institute of Northern Engineering, University of Alaska, Fairbanks.
- Ednie M, Duchesne C, Wright JF. 2008. A paleo-climatic reconstruction for transient ground thermal modeling in the Mackenzie River valley. In *Proceedings of the Ninth International Conference on Permafrost*, Fairbanks, Alaska. Institute of Northern Engineering, University of Alaska, Fairbanks.
- Endrizzi S. 2007. Snow cover modelling at a local and distributed scale over complex terrain PhD dissertation, Department of Environmental Engineering, University of Trento, Italy, 189pp.
- Etzelmüller B, Berthling I, Sollid JL. 2003. Aspects and Concepts on the Geomorphological Significance of Holocene Permafrost in Southern Norway. *Geomorphology*, **52**: 87–104.
- Etzelmüller B, Heggem ESF, Sharkhuu N, Frauenfelder R, Käab A, Goulden C. 2006. Mountain permafrost distribution modeling using a multi-criteria approach in the Hövsgöl area, Northern Mongolia. *Permafrost and Periglacial Processes* **17**: 91–104. DOI: 10.1002/ppp.554.
- Etzelmüller B, Farbroth H, Gudmundsson A, Humlum O, Tveit OE, Björnsson H. 2007. The regional distribution of mountain permafrost in Iceland. *Permafrost and Periglacial Processes* **18**: 185–199. DOI: 10.1002/ppp.583.
- Etzelmüller B, Schuler TV, Farbroth H, Gudmundsson A. 2008. Permafrost in Iceland – distribution, ground temperatures and climate change impact. In *Proceedings of the Ninth International Conference on Permafrost*, 29 June–3 July 2008, University of Fairbanks, Fairbanks, Alaska. Institute of Northern Engineering, University of Alaska, Fairbanks.
- Farbroth H, Etzelmüller B, Gudmundsson A, Schuler TV, Eiken T, Humlum O, Björnsson H. 2007. Thermal characteristics and impact of climate change on mountain permafrost in Iceland. *Journal of Geophysical Research*, **112**: F03S90. DOI:10.1029/2006JF000541.
- Farbroth H, Etzelmüller B, Isaksen K. 2008. Present and past distribution of mountain permafrost in Gaissane Mountains, northern Norway. In *Proceedings of the Ninth International Conference on Permafrost*, 29 June–3 July 2008, University of Fairbanks, Fairbanks, Alaska. Institute of Northern Engineering, University of Alaska, Fairbanks.
- Funk M, Hoelzle M. 1992. A model of potential direct solar radiation for investigating occurrences of mountain permafrost. *Permafrost and Periglacial Processes*, **3**: 139–142.
- Goodrich LE. 1978. Some results of a numerical study of ground thermal regimes. In *Proceedings of the Third International Conference on Permafrost*, Edmonton, Canada. National Research Council of Canada, Ottawa; 30–34.
- Goodrich LE. 1982. The influence of snow cover on the ground thermal regime. *Canadian Geotechnical Journal* **19**: 421–432.
- Gorbunov AP, Marchenko S, Seversky E. 2004. The Thermal Environment of Blocky Materials in the Mountains of Central Asia. *Permafrost and Periglacial Processes* **15**: 95–98. DOI: 10.1002/ppp.478.
- Gruber S. 2005. Mountain permafrost: transient spatial modeling, model verification and the use of remote sensing PhD dissertation, Department of Geography, University of Zurich, Switzerland, 123pp.
- Gruber S. 2007. MTD: a mass-conserving algorithm to parameterize gravitational transport and deposition processes using digital elevation models. *Water Resources Research*, **43**: W06412. DOI:10.1029/2006WR004868.
- Gruber S, Haeberli W. 2007. Permafrost in steep bedrock slopes and its temperature-related destabilization following climate change. *Journal of Geophysical Research*, **112**: F02S18. DOI:10.1029/2006JF000547.
- Gruber S, Hoelzle M. 2008. The cooling effect of coarse blocks revisited. In *Proceedings of the Ninth International Conference on Permafrost*, Fairbanks, Alaska. Institute of Northern Engineering, University of Alaska, Fairbanks.
- Gruber S, Peter M, Hoelzle M, Woodhatch I, Haeberli W. 2003. Surface temperatures in steep alpine rock faces; a strategy for regional-scale measurement and modelling. In *Proceedings of the Eighth International Conference on Permafrost*, Vol. 1, Phillips M, Springman SM, Arenson LU (eds). A.A. Balkema: Lisse; 325–330.
- Gruber S, Hoelzle M, Haeberli W. 2004a. Permafrost thaw and destabilization of Alpine rock walls in the hot summer of 2003. *Geophysical Research Letters* **31**: L13504, 4pp, DOI:10.1029/2006JF000547.
- Gruber S, Hoelzle M, Haeberli W. 2004b. Rock-wall temperatures in the alps: modeling their topographic distribution and regional differences. *Permafrost and*

- Periglacial Processes* **15**: 299–307. DOI: 10.1002/ppp.501.
- Gruber S, King L, Kohl T, Herz T, Haeberli W, Hoelzle M. 2004c. Interpretation of geothermal profiles perturbed by topography: the Alpine permafrost boreholes at Stockhorn Plateau, Switzerland. *Permafrost and Periglacial Processes* **15**(4): 349–357. DOI: 10.1022/ppp.503.
- Haeberli W, Evin M, Tenthorey G, Kensen R, Hoelzle M, Keller F, Vonder Mühl D, Wagner S, Pelfini W, Smiraglia C. 1992. Permafrost research sites in the Alps: excursions of the International Workshop on Permafrost and Periglacial Environments in Mountain Areas. *Permafrost and Periglacial Processes* **3**: 189–202.
- Hanson S, Hoelzle M. 2004. The thermal regime of the active layer at the Murtèl Rock Glacier based on data from 2002. *Permafrost and Periglacial Processes* **15**(3): 273–282. DOI: 10.1002/ppp.499.
- Harris SA. 1996. Lower mean annual ground temperature beneath a block stream in the Kunlun Pass, Qinghai Province, China. In *Proceedings of the Fifth Chinese Permafrost Conference*, Lanzhou. Gansu Culture Press: Lanzhou, China; 227–237.
- Harris SA, Pedersen DE. 1998. Thermal regimes beneath coarse blocky materials. *Permafrost and Periglacial Processes* **9**: 107–120. DOI: 10.1002/(SICI)1099-1530(199804/06)9:2<107::AID-PPP277>3.0.CO;2-G.
- Heggem ESF, Juliussen H, Etzelmüller B. 2005. The permafrost distribution in central-eastern Norway. *Norsk Geografisk Tidsskrift*, **59**: 94–108. DOI:10.1080/00291950510038377.
- Heggem ESF, Etzelmüller B, Sharkhuu N, Goulden CE, Nandinsetseg B. 2006. Spatial empirical modelling of ground surface temperature in the Hövsgöl area, Northern Mongolia. *Permafrost and Periglacial Processes*, **17**: 357–369. DOI: 10.1002/ppp.568.
- Heginbottom JA. 2002. Permafrost mapping: a review. *Progress in Physical Geography*, **26**: 623–642. DOI: 10.1191/0309133302pp355ra.
- Hinzman LD, Goering DJ, Kane DL. 1998. A distributed thermal model for calculating soil temperature profiles and depth of thaw in permafrost. *Journal of Geophysical Research*, **103**: 28975–28991.
- Hoelzle M, Haeberli W. 1995. Simulating the effects of mean annual air temperature changes on permafrost distribution and glacier size: an example from the Upper Engadin, Swiss Alps. *Annals of Glaciology* **21**: 399–405.
- Hoelzle M, Mittaz C, Etzelmüller B, Haeberli W. 2001. Surface energy fluxes and distribution models relating to permafrost in European Mountain areas: an overview of current developments. *Permafrost and Periglacial Processes* **12**: 53–68. DOI: 10.1002/ppp.385.
- Humlum O. 1997. Active layer thermal regime at three rock glaciers in Greenland. *Permafrost and Periglacial Processes* **8**(4): 383–408. DOI: 10.1002/(SICI)1099-1530(199710/12)8:4<383::AID-PPP265> 3.0.CO;2-V.
- Intergovernmental Panel on Climate Change (IPCC). 1990. Seasonal snow cover, ice and permafrost. In *Climate Change: The IPCC Impacts Assessment*, Tegart WJ McG, Sheldon GW, Griffiths DC (eds). Australian Government Publishing Service: Canberra; 7.1–7.45.
- Isaksen K, Hauck C, Gudevang E, Ødegård RS, Sollid JL. 2002. Mountain permafrost distribution on Dovrefjell and Jotunheimen, southern Norway, based on BTS and DC resistivity tomography data. *Norsk Geografisk Tidsskrift*, **56**: 122–136. DOI: 10.1080/002919502760056459.
- Juliussen H, Humlum O. 2007. Towards a TTOP ground temperature model for mountainous terrain in central-eastern Norway. *Permafrost and Periglacial Processes* **18**: 161–184. DOI: 10.1002/ppp.586.
- Juliussen H, Humlum O. 2008. Thermal Regime of Openwork Block Fields on the Mountains Elgåhogna and Sølén, Central-eastern Norway. *Permafrost and Periglacial Processes* **19**: 1–18. DOI: 10.1002/ppp.607.
- Keller F. 1992. Automated mapping of mountain permafrost using the program PERMAKART within the geographical information system ARC/INFO. *Permafrost and Periglacial Processes* **3**: 133–138. DOI: 10.1002/ppp.3430030210.
- Klene AE, Nelson FE, Shiklomanov NI, Hinkel KM. 2001b. The n-factor in natural landscapes: variability of air and soil-surface temperatures, Kuparuk River basin, Alaska. *Arctic, Antarctic, and Alpine Research*, **33**(2): 140–148.
- Klene AE, Hinkel KM, Nelson FE. 2003. The Barrow Urban Heat Island Study: Soil temperatures and active-layer thickness. In *Proceedings of the Eighth International Conference on Permafrost*, vol. 1, Phillips M, Springman SM, and Arenson LU (eds). Lisse: A.A. Balkema, pp. 555–560.
- Kudryavtsev VA, Garagulya LS, Kondrat'yeva KA, Melamed VG. 1974. *Fundamentals of Frost Forecasting in Geological Engineering Investigations*. Cold Regions Research and Engineering Laboratory: Hanover, NH.
- Lai Y, Huijun J, Brown J. 2006. Asian conference on permafrost. *Frozen Ground* **30**: 5–6.
- Lawrence DM, Slater AG. 2005. A projection of severe near-surface permafrost degradation during the 21st century. *Geophysical Research Letters* **32**: L24401. DOI:10.1029/2005GL025080.2005.
- Lawrence DM, Slater AG. 2006. Reply to comment by C.R. Burn and F.E. Nelson on 'A projection of near-surface permafrost degradation during the 21st century'. *Geophysical Research Letters* **33**(21): L21504. DOI: 10.1029/2006GL027955.
- Lehning M, Völksch I, Gustafsson D, Nguyen TA, Stähli M, Zappa M. 2006. ALPINE3D: A detailed model of mountain surface processes and its application to snow hydrology. *Hydrological Processes* **20**: 2111–2128. DOI: 10.1002/hyp.6204.
- Lewkowicz AG, Bonnaventure PP. 2008. Interchangeability of local mountain permafrost probability models, northwest Canada. *Permafrost and Periglacial Processes*, **19**: 49–62. DOI: 10.1002/ppp.612.
- Lewkowicz AG, Ednie M. 2004. Probability mapping of mountain permafrost using the BTS method, Wolf Creek, Yukon Territory, Canada. *Permafrost and Periglacial Processes* **15**: 67–80. DOI: 10.1002/ppp.480.

- Li X, Koike T. 2003. Frozen soil parameterization in SiB2 and its validation with GAME-Tibet observations. *Cold Regions Science and Technology*, **36**: 165–182. DOI: 10.1016/S0165-232X(03)00009-0.
- Ling F, Zhang T. 2004. A numerical model for surface energy balance and thermal regime of the active layer and permafrost containing unfrozen water. *Cold Regions Science and Technology* **38**: 1–15. DOI: 10.1016/S0165-232X(03)00057-0.
- Luetschg M, Haerberli W. 2005. Permafrost evolution in the Swiss Alps in a changing climate and the role of the snow cover. *Norsk Geografisk Tidsskrift–Norwegian Journal of Geography* Vol. **59**: 78–83. Oslo. ISSN 0029-1951 DOI: 10.1080/00291950510020583.
- Luetschg M, Stoeckli V, Lehning M, Haerberli W, Ammann W. 2004. Temperatures in two boreholes at Flüela Pass, Eastern Swiss Alps: the effect of snow redistribution on permafrost distribution patterns in high mountain areas. *Permafrost and Periglacial Processes*, **15**(3): 283–297. DOI: 10.1002/ppp.500.
- Lunardini VJ. 1978. Theory of N-factors and correlation of data. In Proceedings of the Third International Conference on Permafrost, Vol. 1. National Council of Canada: Ottawa; 40–46.
- Lunardini VJ. 1981. *Heat transfer in cold climates*. Van Nostrand Reinhold: New York.
- Malevsky-Malevich SP, Mol Kentin EK, Nadyozhina ED, Shklyarevich OB. 2001. Numerical simulation of permafrost parameters distribution in Russia. *Cold Regions Science and Technology*, **32**: 1–11. DOI: 10.1016/S0165-232X(01)00018-0.
- Marchenko S, Gorbunov A, Romanovsky V. 2007. Permafrost warming in the Tien Shan Mountains, Central Asia. *Global and Planetary Change* **56**: 311–327. DOI: 10.1016/j.gloplacha.2006.07.023.
- Marchenko SS. 2001. A model of permafrost formation and occurrences in the intracontinental mountains. *Norsk Geografisk Tidsskrift–Norwegian Journal of Geography*, **55**: 230–234.
- Marchenko SS, Romanovsky VE, Topenko G. 2008. Numerical modeling of spatial permafrost dynamics in Alaska. In Proceedings of the Ninth International Conference on Permafrost, 29 June–3 July 2008, Fairbanks, Alaska. Institute of Northern Engineering, University of Alaska, Fairbanks.
- Mittaz C, Hoelzle M, Haerberli W. 2000. First results and interpretation of energy-flux measurements of Alpine permafrost. *Annals of Glaciology*, **31**: 275–280.
- Mölders N, Romanovsky VE. 2006. Long-term evaluation of the Hydro-Thermodynamic Soil-Vegetation Scheme's frozen ground/permafrost component using observations at Barrow, Alaska. *Journal of Geophysical Research* **111**: D04105. DOI: 10.1029/2005JD005957.
- Mol Kentin EK, Nadyozhina ED, Shklyarevich OB. 2001. Spatial distribution of modeled permafrost characteristics. *Gidrologia i Meteorologia*, **8**: 89–97 (in Russian).
- Nelson FE. 1986. Permafrost distribution in central Canada: applications of a climate-based predictive model. *Annals of the Association of American Geographers*, **76**(4): 550–569.
- Nelson FE, Anisimov OA. 1993. Permafrost zonation in Russia under anthropogenic climatic change. *Permafrost and Periglacial Processes*, **4**(2): 137–148.
- Nelson FE, Outcalt SI. 1987. A computational method for prediction and regionalization of permafrost. *Arctic and Alpine Research*. **19**(3): 279–288.
- Nelson FE, Shiklomanov NI, Mueller GR, Hinkel KM, Walker DA, Bockheim JG. 1997. Estimating active-layer thickness over a large region: Kuparuk River Basin, Alaska, USA. *Arctic and Alpine Research*, **29**(4): 367–378.
- Nelson FE, Anisimov OA, Shiklomanov NI. 2001. Climate change and hazard potential in northern permafrost regions. *Nature*, **410**: 889–890. DOI: 10.1038/35073746.
- Nelson FE, Anisimov OA, Shiklomanov NI. 2002. Climate change and hazard zonation in the circum-arctic permafrost regions. *Natural Hazards* **26**(3): 203–225.
- Ng E, Miller PC. 1977. Validation of a model of the effect of tundra vegetation on soil temperatures. *Arctic and Alpine Research*, **9**(2): 89–104.
- Nicolosky DJ, Romanovsky VE, Alexeev VA, Lawrence DM. 2007. Improved modeling of permafrost dynamics in a GCM land-surface scheme. *Geophysical Research Letters* **34**: L08501. DOI: 10.1029/2007GL029525.
- Noetzli J, Gruber S, Kohl T, Salzmann N, Haerberli W. 2007. Three-dimensional distribution and evolution of permafrost temperatures in idealized high-mountain topography. *Journal of Geophysical Research* **112**: F02S13. DOI: 10.1029/2006JF000545.
- Noetzli J, Hilbich C, Hoelzle M, Hauck C, Gruber S, Krauer M. 2008. Comparison of transient 2D temperature fields with time-lapse electrical resistivity data at the Schilthorn Crest, Switzerland. In Proceedings of the Ninth International Conference on Permafrost, Fairbanks, Alaska. Institute of Northern Engineering, University of Alaska, Fairbanks.
- Oelke C, Zhang T. 2004. A model study of circum-arctic soil temperatures. *Permafrost and Periglacial Processes* **15**: 103–121. DOI: 10.1002/ppp.485.
- Oelke C, Zhang T, Serreze MC, Armstrong RL. 2003. Regional-scale modeling of soil freeze/thaw over the arctic drainage basin. *Journal of Geophysical Research* **108**(D10): 4314. DOI: 10.1029/2002JD002722.
- Oelke C, Zhang T, Serreze MC. 2004. Modeling evidence for recent warming of the Arctic soil thermal regime. *Geophysical Research Letters* **31**: L07208. DOI: 10.1029/2003GL019300.
- Oleson KW, Dai Y, Bonan GB, Bosilovich M, Dickinson R, Dirmeyer P, Hoffman F, Houser P, Levis S, Niu G-Y, Thornton P, Vertenstein M, Yang ZL, Zeng X. 2004. Technical description of the Community Land Model (CLM) NCAR Technical Note NCAR/TN-461+STR, Boulder, Colorado. 173pp.
- Outcalt SI, Goodwin C, Weller G, Brown J. 1975. Computer simulation of the snowmelt and soil thermal regime at Barrow, Alaska. *Water Resources Research*, **11**(5): 709–715.

- Rigon R, Bertoldi G, Over TM. 2006. GEOTop: A distributed hydrological model with coupled water and energy budgets. *Journal of Hydrometeorology* **7**(3): 371–388. DOI: 10.1175/JHM497.1.
- Riseborough DW. 2004. Exploring the parameters of a simple model of the permafrost – climate relationship PhD dissertation, Department of Geography, Carleton University, Canada, 329 pp.
- Riseborough DW. 2007. The effect of transient conditions on an equilibrium permafrost-climate model. *Permafrost and Periglacial Processes* **18**: 21–32. DOI: 10.1002/ppp.579.
- Romanovsky VE, Osterkamp TE. 1995. Interannual variations of the thermal regime of the active layer and near-surface permafrost in northern Alaska. *Permafrost and Periglacial Processes*, **6**(4): 313–335. DOI: 10.1000/PPP.3430060404.
- Romanovsky VE, Osterkamp TE. 1997. Thawing of the active layer on the coastal plain of the Alaskan Arctic. *Permafrost and Periglacial Processes*, **8**(1): 1–22. DOI: 10.1002/(SICI)1099-1530(199701)8:1<1::AID-PPP243>3.0.CO;2-U.
- Rykiel EJ. 1996. Testing ecological models: the meaning of validation. *Ecological Modelling* **90**: 229–244.
- Saha SK, Rinke A, Dethloff K, Kuhry P. 2006. Influence of a complex land surface scheme on Arctic climate simulations. *Journal Of Geophysical Research* **111**: D22104. DOI:10.1029/2006JD007188.
- Saito K, Kimoto M, Zhang T, Takata K, Emori S. 2007. Evaluating a high-resolution climate model: Simulated hydrothermal regimes in frozen ground regions and their change under the global warming scenario. *Journal Of Geophysical Research*, **112**: F02S11. DOI:10.1029/2006JF000577.
- Salzmann N, Frei C, Vidale P-L, Hoelzle M. 2006. The application of regional climate model output for the simulation of high-mountain permafrost scenarios. *Global and Planetary Change* **56**: 188–202. DOI: 10.1016/j.gloplacha.2006.07.006.
- Salzmann N, Noetzli J, Hauck C, Gruber S, Hoelzle M. 2007. RCM-based ground surface temperature scenarios in high-mountain topography and their uncertainty ranges. *Journal of Geophysical Research*, **112**: F02S12. DOI:10.1029/2006JF000527.
- Sazonova TS, Romanovsky VE. 2003. A model for regional-scale estimation of temporal and spatial variability of active layer thickness and mean annual ground temperatures. *Permafrost and Periglacial Processes* **14**: 125–139. DOI: 10.1002/ppp.449.
- Sazonova TS, Romanovsky VE, Walsh JE, Sergueev DO. 2004. Permafrost dynamics in the 20th and 21st centuries along the East Siberian transect. *Journal of Geophysical Research-Atmos.* **109**(D1): D01108. DOI: 10.1029/2003JD003680.
- Shiklomanov NI. 2005. From exploration to systematic investigation; development of geocryology in 19th- and early-20th-century Russia. *Physical Geography* **26**(4): 249–263. DOI: 10.2747/0272-3646.26.4.249
- Shiklomanov NI, Nelson FE. 1999. Analytic representation of the active layer thickness field, Kuparuk River Basin, Alaska. *Ecological Modeling*, **123**(2-3): 105–125. DOI: 10.1016/S0304-3800(99)00127-1.
- Shiklomanov NI, Nelson FE. 2002. Active-layer mapping at regional scales: A 13-year spatial time series for the Kuparuk region, north-central Alaska. *Permafrost and Periglacial Processes*, **13**: 219–230. DOI: 10.1002/ppp.425.
- Shiklomanov NI, Nelson FE. 2003. Statistical representation of landscape-specific active-layer variability. In: Phillips, M., Springman S.M., and Arenson, L.U. (eds.) Proceedings of the Eighth International Conference on Permafrost, Zurich, Switzerland. Lisse: A.A. Balkema, pp. 1039–1044.
- Shiklomanov NI, Anisimov OA, Zhang T, Marchenko SS, Nelson FE, Oelke C. 2007. Comparison of model-produced active layer fields: Results for northern Alaska. *Journal of Geophysical Research*, **112**: F02S10. DOI:10.1029/2006JF000571.
- Shiklomanov NI, Nelson FE, Streletskiy DA, Hinkel KM, Brown J. 2008. The Circumpolar Active Layer Monitoring (CALM) Program: Data collection, management, and dissemination strategies. In *Proceedings of the Ninth International Conference on Permafrost*, 29 June–3 July 2008, Fairbanks, Alaska. Institute of Northern Engineering, University of Alaska, Fairbanks.
- Shur YL, Slavin-Borovskiy VB. 1993. N-factor maps of Russian permafrost region. In *Proceedings of the Sixth International Conference on Permafrost*, Vol. II. South China University of Technology Press, Wushan, Guangzhou, China; 564–568.
- Smith MW, Riseborough DW. 1996. Ground temperature monitoring and detection of climate change. *Permafrost and Periglacial Processes*, vol 7 no 4, pp. 301–310. DOI: 10.1002/(SICI)1099-1530(199610)7:4<301::AID-PPP231>3.0.CO;2-R.
- Smith MW, Riseborough DW. 2002. Climate and the limits of permafrost: a zonal analysis. *Permafrost and Periglacial Processes*, **13**(1): 1–15. DOI: 10.1002/ppp.410
- Stendel M, Christensen JH. 2002. Impact of global warming on permafrost conditions in a coupled GCM. *Geophysical Research Letters*, **29**: art. no.-1632. DOI: 10.1029/2001GL014345.
- Stendel M, Romanovsky VE, Christensen JH, Sazonova T. 2007. Using dynamical downscaling to close the gap between global change scenarios and local permafrost dynamics. *Global and Planetary Change* **56**: 203–214. DOI:10.1016/j.gloplacha.2006.07.014.
- Stevens MB, Smerdon JE, Gonzalez-Rouco JF, Stieglitz M, Beltrami H. 2007. Effects of bottom boundary placement on subsurface heat storage: Implications for climate model simulations. *Geophysical Research Letters* **34**: L02702. DOI: 10.1029/2006GL028546.
- Stocker-Mittaz C, Hoelzle M, Haerberli W. 2002. Permafrost distribution modeling based on energy-balance data: a first step. *Permafrost and Periglacial Processes*, **13**(4): 271–282. DOI: 10.1002/ppp.426.

- Strasser U, Bernhardt M, Weber M, Liston GE, Mauser W. 2007. Is snow sublimation important in the alpine water balance? *The Cryosphere Discussions* **1**: 303–350.
- Sushama L, Laprise R, Caya D, Versegny D, Allard M. 2007. An RCM projection of soil thermal and moisture regimes for North American permafrost zones. *Geophysical Research Letters*, **34**: L20711, DOI: 10.1029/2007GL031385.
- Swanson DK, Lacelle B, Tarnocai C. 2000. Temperature and the boreal subarctic maximum in soil organic carbon. *Geographie Physique et Quaternaire* **54**(2): 157–167.
- Tipenko G, Marchenko S, Romanovsky S, Groshev V, Sazonova T. 2004. Spatially distributed model of permafrost dynamics in Alaska. *Eos Transactions AGU*, **85**(47): Fall Meet. Suppl., Abstract C12A-02.
- Verdi C. 1994. Numerical aspects of parabolic free boundary and hysteresis problems. In *Lecture Notes in Mathematics*. Springer-Verlag: New York; 213–284.
- Wild GO. 1882. *Air Temperature in the Russian Empire*. Izdatel'stvo Russkogo Geograficheskogo Obshestva: St Petersburg (in Russian).
- Williams PJ, Smith MW. 1989. *The Frozen Earth: Fundamentals of Geocryology*. Cambridge University Press: Cambridge.
- Wright JF, Duchesne C, Côté MM. 2003. Regional-scale permafrost mapping using the TTOP ground temperature model. In *Proceedings of the Eighth International Conference on Permafrost*, Zurich, Switzerland, Phillips M, Springman SM, Arenson LU (eds). A.A. Balkema: Lisse; 1241–1246.
- Yi S, Arain MA, Woo M-K. 2006. Modifications of a land surface scheme for improved simulation of ground freeze-thaw in northern environments. *Geophysical Research Letters* **33**: L13501. DOI:10.1029/2006GL026340.
- Yi S, Woo M-K, Arain MA. 2007. Impacts of peat and vegetation on permafrost degradation under climate warming. *Geophysical Research Letters* **34**: L16504. DOI: 10.1029/2007GL030550.
- Zanotti F, Endrizzi S, Bertoldi G, Rigon R. 2004. The GEOTOP snow module. *Hydrological Processes* **18**: 3667–3679. DOI: 10.1002/hyp.5794.
- Zhang T, Stamnes K. 1998. Impact of climatic factors on the active layer and permafrost at Barrow, Alaska. *Permafrost and Periglacial Processes*, **9**: 229–246. DOI:10.1002/(SICI)1099-1530(199807/09)9:3<229::AID-PPP286>3.0.CO;2-T.
- Zhang T, Osterkamp TE, Stamnes K. 1996. Influence of the depth hoar layer of the seasonal snow cover on the ground thermal regime. *Water Resources Research*, **32**(7): 2075–2086.
- Zhang T, Barry RG, Knowles K, Heginbottom JA, Brown J. 1999. Statistics and characteristics of permafrost and ground ice distribution in the Northern Hemisphere. *Polar Geography*, **23**(2): 147–169.
- Zhang T, Frauenfeld OW, Serreze MC, Etringer A, Oelke C, McCreight J, Barry RG, Gilichinsky D, Yang D, Ye H, Ling F, Chudinova S. 2005. Spatial and temporal variability in active layer thickness over the Russian Arctic drainage basin. *Journal of Geophysical Research-Atmospheres*, **110**: D16101. DOI:10.1029/2004JD005642.
- Zhang T, Nelson FE, Gruber S. 2007. Introduction to special section: Permafrost and seasonally frozen ground under a changing climate. *Journal of Geophysical Research*, **112**: F02S01. DOI:10.1029/2007JF000821.
- Zhang Y, Chen W, Cihlar J. 2003. A process-based model for quantifying the impact of climate change on permafrost thermal regimes. *Journal of Geophysical Research-Atmospheres*, **108**(D22): 4695, DOI:10.1029/2002JD003354.
- Zhang Y, Chen W, Smith SL, Riseborough DW, Cihlar J. 2005. Soil temperature in Canada during the twentieth century: complex responses to the changes in air temperature at high latitudes. *Journal of Geophysical Research*, vol. **110**: D03112. DOI: 10.1029/2004JD004910.
- Zhang Y, Chen W, Riseborough DW. 2006. Temporal and spatial changes of permafrost in Canada since the end of the Little Ice Age. *Journal of Geophysical Research* **111**: D22103. DOI: 10.1029/2006JD007284.

Geological Society, London, Special Publications

Glacier-permafrost interaction in Arctic and alpine mountain environments with examples from southern Norway and Svalbard

Bernd Etzelmüller and Jon Ove Hagen

Geological Society, London, Special Publications 2005; v. 242; p. 11-27
doi:10.1144/GSL.SP.2005.242.01.02

Email alerting service [click here](#) to receive free email alerts when new articles cite this article

Permission request [click here](#) to seek permission to re-use all or part of this article

Subscribe [click here](#) to subscribe to Geological Society, London, Special Publications or the Lyell Collection

Notes

Downloaded by on 18 May 2007

Glacier–permafrost interaction in Arctic and alpine mountain environments with examples from southern Norway and Svalbard

BERND ETZELMÜLLER & JON OVE HAGEN

Department of Geosciences, Section of Physical Geography, University of Oslo,

PO Box 1047, Blindern, N–0316 Oslo, Norway

(e-mail: bernde@geo.uio.no, joh@geo.uio.no)

Abstract: The interaction between glaciers and permafrost was long ago addressed for glaciers in Arctic regions. Analogies from modern environments have been used to understand landform development at the margins of Pleistocene ice sheets. During more recent decades many systematic measurements of permafrost in boreholes, geophysical soundings and temperature monitoring have revealed permafrost to be more abundant in many more high-mountain areas than previously thought. This suggests that permafrost may be a governing factor not only for periglacial landform evolution in these areas, but also, given the potential for glacier–permafrost interaction, for glacial landform generation. This paper presents and discusses observation and study results on the geomorphological significance of the interrelationship between glaciers and permafrost, in relation to geomorphological processes, landform generation and response of the system to climate fluctuations.

In the geo-scientific literature, processes and landforms related to glaciers and permafrost are often treated separately. However, both are part of the cryosphere, they often co-exist and therefore there is a potential for interaction. Thus, knowledge of these interactions promotes better understanding of glacial landform formation, and is crucial when discussing glacial and para-glacial processes and geotechnical hazards (Haeberli 1992). Interaction between glaciers and permafrost has been given only limited attention in scientific literature, even though such relationships have long been recognized, for example the role of permafrost in the development of push moraines in central Europe during the last glaciation (e.g., Gripp 1929) or more recently in the southern fringe of the Wisconsin ice sheet in North America (e.g., Bluemle & Clayton 1984; Clayton *et al.* 2001). Attention has focussed on the co-existence of glaciers in permafrost areas, mainly in the Arctic and/or former Pleistocene cryosphere environments. An exception to this is provided by the work of Liestøl (1977, 1996), who linked ground and glacier thermal regimes to catchment hydrology and pingo development on Svalbard, highlighting the importance of a fundamental understanding of glacier–permafrost interaction. During the last 20 years, it has been apparent that there is extensive permafrost in many high-mountain

environments, even at lower latitudes (e.g., Haeberli *et al.* 1993). Recently, boreholes revealed permafrost up to several hundreds of metres thick across a number of European mountain regions (Harris *et al.* 2003).

This paper presents observations from glaciers and permafrost in mountain environments of southern Norway and Svalbard. The paper focuses on mountainous environments, with cirque, valley or plateau glaciers, with terrestrial glacier tongues. The aim of the paper is to discuss field and laboratory results and certain well-known glaciological and geomorphological relationships conceptionally, emphasizing the role of glacier–permafrost interaction, its relevance to selected geomorphological processes and their response to climate change. Furthermore, we want to draw together some general and hypothetical concepts, which may serve to stimulate further research within this field.

Permafrost definition

According to the International Permafrost Association (1998), permafrost is thermally defined as ‘ground that remains at or below 0°C for at least two consecutive years’. Perennial ground ice or congelation ice is explicitly included in the permafrost definition, while glacier ice (sedimentary ice) is not (see also

Shumskiy 1964). From a purely thermal point of view at least, glacier ice at sub-pressure melting point temperatures would become a part of the permafrost environment. On the other hand, permafrost is not a precondition for the formation of sedimentary ice (in contrast to congelation ice), and thus, being part of the hydrosphere, glaciers are excluded. These definitions and their conceptual boundaries are of geomorphological importance and form the basis for the further discussion and hypotheses presented in this paper.

Glacier–permafrost interaction

Most glaciers present in permafrost regions are characterized by relatively low accumulation rates and a short ablation season, of 2–4 months, during summer. This leads to a smaller mass turnover and lower meltwater discharges compared with temperate regions (Bogen & Bønsnes 2003; Hagen *et al.* 2003). The lower activity is manifested in lower velocities, often resulting in smoother ice surfaces (low crevasse density), which often prevents linkage between supraglacial meltwater and englacial or subglacial drainage systems.

Most glaciers have areas with below-pressure-melting-point temperatures, and are thus connected to the permafrost environment. The distribution of cold ice in glaciers varies however, depending on the thickness of the ice body and the energy exchange processes due to phase transitions of water (Paterson 1994). In general, one can expect cold-based ice in glaciers when the equilibrium line altitude (ELA) is at or well below the lower limit of widespread permafrost in a region (mountain permafrost altitude, MPA; Fig. 1). Thin glaciers in Arctic or high-altitude regions with the MPA well below the glacier terminus are often entirely cold-based (Fig. 1a), while in warmer and wetter areas, where summer melting occurs, the ice in the accumulation area is warmed due to latent heat release by meltwater refreezing, resulting in less extensive (Fig. 1b, c) or even absent below-pressure-melting-point temperatures in the accumulation area (Fig. 1d; Paterson 1994). Glaciers where both temperate (temperatures at the pressure melting point) and cold (below-pressure-melting-point temperatures) ice is present are called *polythermal* glaciers. In such cases the marginal parts of the accumulation area

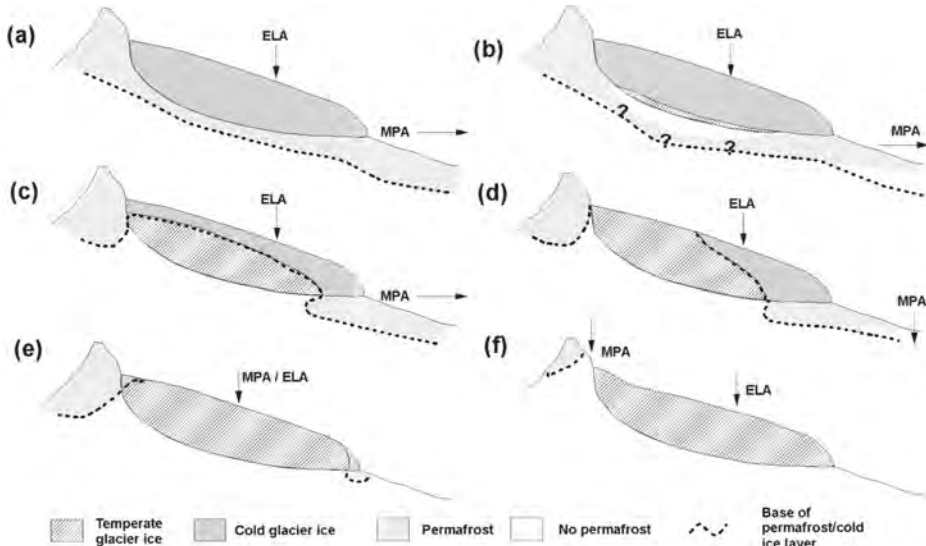


Fig. 1. Schematic illustration of thermal regimes in glaciers related to permafrost in mountain areas. (a) Entire cold glacier in a permafrost environment. $MPA \ll ELA$. (b) Mostly cold-based glacier with temperate layers along the glacier-ground interface (e.g., Austre Brøggerbreen, Midtre Lovénbreen, Svalbard; Björnsson *et al.* 1996). $MPA \ll ELA$. (c,d) Polythermal glacier with temperate glacier ice along most of the bottom and in the accumulation area (e.g., Erikbreen, Finsterwalderbreen, Kongsvegen; Ødegård *et al.* 1992, 1997; Björnsson *et al.* 1996), $MPA < ELA$. This is the typical case described by Liestøl (1977) for most of the terrestrial glaciers on Svalbard. (e) Mostly warm-based glacier with some cold patches, either locally in the frontal areas (e.g., Midtdalsbreen, southern Norway) or in dry, cold accumulation areas (e.g., Alps). $MPA \approx ELA$ or $MPA > ELA$. For entirely temperate glaciers, $MPA \gg ELA$. (f) Åfotbreen, Nigardsbreen, southern Norway

may be frozen to the mountain side and head wall, and the terminal zone of the glacier may be frozen to the ground. Several examples of these glaciers exist in the Arctic, for instance on Svalbard (Björnsson *et al.* 1996) or in Arctic Canada (Blatter 1987). The size of the glacier area that is cold-based varies (Blatter & Hutter 1991). In sub-Arctic regions, there are reported to be glaciers with only very marginal cold areas, such as Midtdalsbreen (Hagen 1978; Liestøl & Sollid 1980) and Leirbreen (Harris & Bothamley 1984) in southern Norway. Where the ice is thin, such as along glacier margins slightly below the MPA, winter cold may penetrate the glacier ice. During the summer, this cold is not removed, leading to temperatures below the pressure melting point temperatures (Fig. 1e). Another thermal type occurs in high-altitude glaciers that start above and end below the MPA. These glaciers may have partly cold accumulation areas (Suter *et al.* 2001) if such areas are situated at altitudes with no or only very limited summer melting, such as for example in certain parts of the Alps. If the ELA is located well below the MPA, temperate glaciers dominate (Fig. 1f).

Glaciers have the ability to advect heat to the ice-bed interface in the accumulation areas, and thus can promote the development of closed or open taliks in the underlying sediments

or bedrock (either totally enclosed by permafrost or connected with the unfrozen sub-permafrost drainage system). Liestøl (1977) (Fig. 2) defined this open talik as the characteristic case for Svalbard, where he described glacier meltwater penetration, subglacially into the ground, feeding sub-permafrost groundwater flow in the valleys, which locally form open-system pingos, pro-glacial winter icings and springs. In addition, thin ice covers and snow-fields or snow patches lying slightly below the MPA preserve subzero temperatures in the ground if they are sufficiently thin that the winter cold penetrates the snow/ice mass.

In summary, glaciers ending in a stable terrestrial permafrost environment will always be polythermal, as at least marginal areas of the glaciers will be cold-based.

Svalbard and southern Norway

Morphological visible interaction of glaciers and permafrost exists, especially in areas where glaciers end in a permafrost environment. As permafrost is thermally defined, climate forcing, the ability of the ground to conduct heat and the local geothermal gradient govern permafrost distribution and thickness.

On Svalbard, the mean annual air temperature (MAAT) at the coast is about -5°C , with low

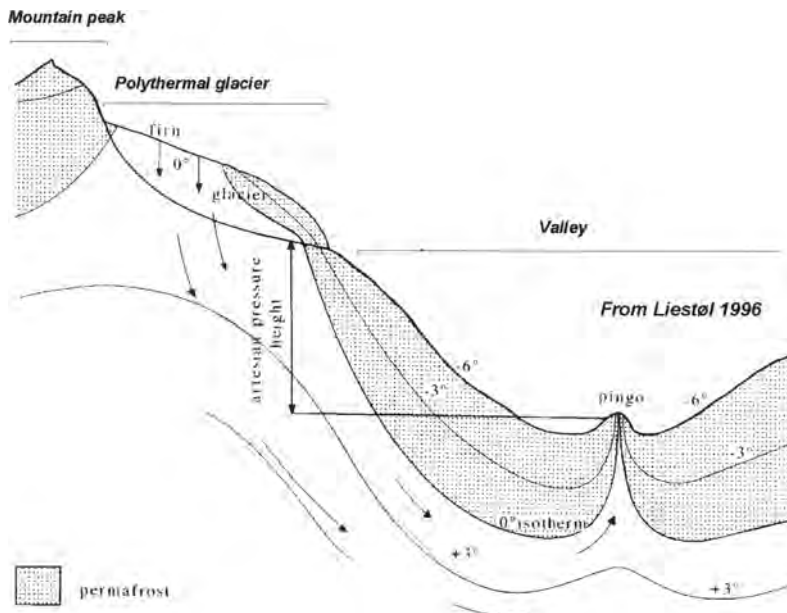


Fig. 2. This profile illustrates the relationship between glacier thermal regime and permafrost distribution in a typical valley setting on Svalbard. Reprinted from Open-system pingos in Spitsbergen by Liestøl from *Norsk Geografisk Tidsskrift*, www.tandf.no/ngeog, 1996, 50, 81–84, by permission of Taylor and Francis AS.

winter temperatures and stable summer temperatures below 10°C. This results in a high number of freezing degree-days (2000–3000°C days) in relation to thawing degree-days (400–550°C days; Humlum *et al.* 2003), and thus continuous permafrost. Permafrost in the non-glacierized central mountains of Svalbard reaches a thickness of more than 450 m, decreasing to below 150 m towards the coast (Liestøl 1977). This means that all glaciers ending on land on Svalbard extend into a permafrost environment. The distribution of surficial material on Svalbard is dominated by *in-situ* weathered material (Kristiansen & Sollid 1987; Sollid & Sørbel 1988b) in the interior parts of the islands. Close to the coast, sediments range from gravelly beach sediments to finer-grained marine deposits, as a consequence of high post-Weichselian marine limits (Mangerud *et al.* 1996). In the marine sediments, saline pore water is common, depressing the freezing point. This results in a considerable amount of unfrozen pore water, generating a relatively weak permafrost layer, as observed in Svea (Gregersen *et al.* 1983; Furuberg & Berggren 1988). The permafrost thins towards the coast. There are no indications of sub-sea permafrost. Recent investigations indicate permafrost aggradation in response to Holocene isostatic uplift (Humlum 2004). The permafrost altitude that defines where permafrost becomes abundant (lower regional MPA) lies below or near sea level on Svalbard.

Permafrost in southern Norway is restricted to high-mountainous areas. At a regional scale, the MAAT of -3.5 to -4°C gives a good estimate of the lower limit of regional, discontinuous permafrost (King 1986; Ødegård *et al.* 1996; Etzelmüller *et al.* 1998). However, snow cover and other local climate effects make permafrost abundant even in warmer or lower settings (e.g. Sollid *et al.* 2003). Based on these boundary conditions, permafrost is mainly concentrated in a 50–100 km-wide zone following the main mountain crest in a southwest-northeast direction (Fig. 3). Only small areas east and west of this zone have permafrost. The regional MPA decreases from above 1600 m above sea level (a.s.l.) in the west to below 1300 m a.s.l. in the east, close to the Swedish border.

On the western side, several glaciers cover high mountain areas, and the landscape is dominated by alpine relief types with high peaks and deeply incised valleys. On the eastern side of this zone, the area is dominated by mountain plateaux situated below the lower regional MPA. However, small mountain areas or single peaks reach altitudes above this limit (Heggem *et al.* 2003). Patchy permafrost is abundant at much

lower altitudes than described above, e.g., in *palsa mires* (Sollid & Sørbel 1998) or in coarse slope deposits in extreme shadow (Liestøl 1965). Surficial material in mountain areas is often thin morainic or *in-situ*-weathered material. In southern Norway, glaciers end both below and above the MPA. In most maritime environments with high mean annual precipitation and MAAT of *c.* 0°C, at the glacier equilibrium line altitude (ELA), temperate glaciers dominate, extending below the lower regional MPA. In these areas the ELA lies at or well below the MPA. Glacier–permafrost interactions are most likely when the ELA lies well above the MPA, especially when the glacier snout terminates at or above the MPA. In dry, cold areas, insufficient precipitation is present for the formation of glaciers. For southern Norway, therefore, a west–east gradient is present with respect to ELA, MPA, and glaciers within the permafrost zone in the central areas (Fig. 3).

For both southern Norway and Svalbard there is strong evidence that the present glacier coverage is a response to late Holocene cooling, which started about 4000–5000 year BP. In southern Norway, it has been shown that there were few glaciers during the Holocene climatic optimum (Dahl & Nesje 1994; Nesje *et al.* 2000), while on Svalbard glacier coverage was certainly considerably less, and many smaller glaciers even disappeared, with permafrost-free areas along the coast and in low-lying valley bottoms. A comprehensive review of Holocene climate change in the northern polar and sub-polar hemisphere is given in Humlum *et al.* (2005) and Humlum (2005).

Geomorphological processes: general observations

General landform type and distribution pattern

Svalbard. For most glaciers ending on land on Svalbard, one or occasionally two prominent arcs of end moraines, often up to 50 m in height, enclose the glacier foreland, indicating the maximum Holocene extension of these glaciers (Figs 4a and 5a). The few dates available for Svalbard indicate that the outermost post-glacial position was reached a couple of times since 2500 years BP, and culminated during the Little Ice Age (LIA) at the turn of the twentieth century (Furrer 1992; Snyder *et al.* 2000; Humlum *et al.* 2005). Between these outermost ridges and the present glacier front, areas with minor glacial mounds, flow tills and outwash

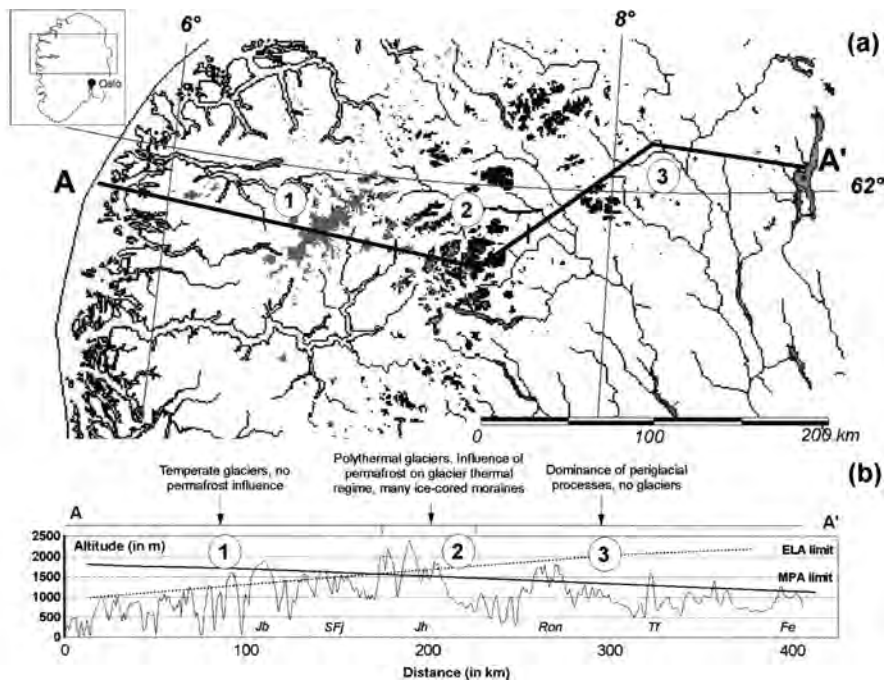


Fig. 3. (a) The distribution of alpine permafrost in southern Norway. Probable permafrost areas are displayed in dark shading, recent glacier coverage in grey shading. The solid line shows the profile line displayed in (b). The method of deriving permafrost areas used for southern Norway is described in Etzelmüller *et al.* (1998, 2003). The inset map denotes the position of the drawing in southern Norway. The numbers correspond to those described in (b). (b) Profile through southern Norway including the lower limit of alpine permafrost and the limits of the ELA. A spatial distribution of the ELA in southern Norway was generated based on an ELA contour map published in Liestøl (1994). The profile is interpreted to distinguish three major morphogenetic zones in relation to glacial and periglacial processes (zones 1–3). *Jb* = Jostedalsbreen glacier; *SFj* = Sognefjellet mountains; *Jh* = Jotunheimen; *Ron* = Rondane mountains. Based on Etzelmüller *et al.* (2003), slightly changed

plains are found. Both the end moraines and much of the flow till areas are cored or underlain by glacier ice (Boulton 1967; Sollid & Sørbel 1988a; Etzelmüller *et al.* 1996; Lyså & Lønne 2001). Fluting and stream-lined ridges in this marginal zone indicate temperate conditions during maximal glacial extension (Glasser & Hambrey 2001). Multi-temporal altitude comparison by air photos for several glacier forelands on Svalbard demonstrated a surface lowering along erosive river channels and along ice-cliffs, displaying the stability of areas with debris-covered ice vs melting of areas with exposed ice over periods of several decades (Etzelmüller 2000). When deposited on steep slopes, some ice-cored terminal or lateral moraines evolve into creeping bodies, commonly termed glacier-derived rock glaciers (Fig. 5b). These forms are abundant in the drier central areas of the Spitsbergen Island (Kristiansen & Sollid 1987),

and their dynamics are often decoupled from the glacier dynamics.

In some Svalbard glaciers, push moraines (Gripp 1929; Stauchendmoränen) or composite ridges (Benn & Evans 1998) are observed outside the main ice-cored moraines. These are normally less than 10 m in height, and occur in distinct zones at the limit of the glacier foreland (Figs. 4a and 5c). The forms may be defined as pro-glacial sediments, pushed into ridges by advance of the glacier margin, and showing thrust structures (Hambrey *et al.* 1996) or other deformation structures (Boulton 1986; Etzelmüller *et al.* 1996). These moraines are, however, not in direct contact with the glacier snout today. Numerous sedimentological studies show folding and thrusting in both coarse-grained and fine-grained pro-glacial sediments on Svalbard (Fig. 5d; Croot 1988; Hart & Watts 1997; Boulton *et al.* 1999).

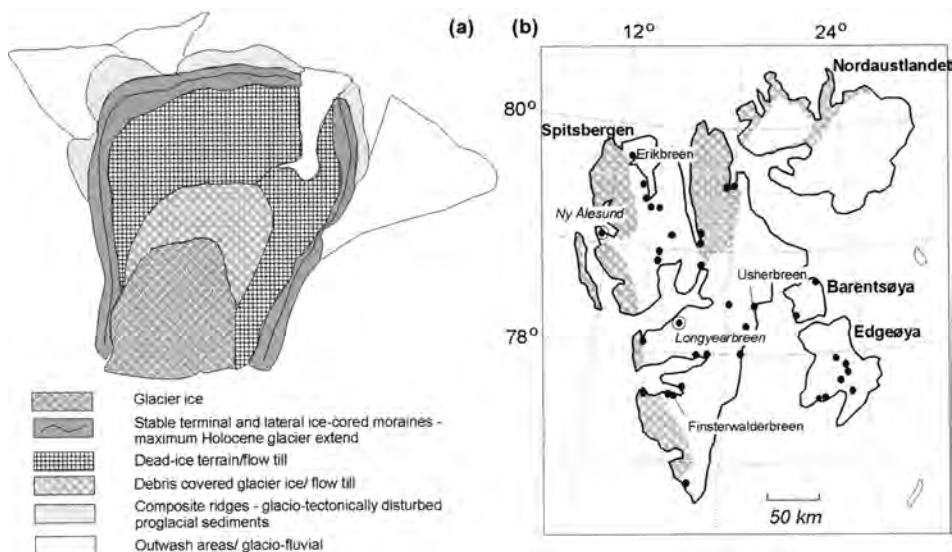


Fig. 4. (a) Schematic draft of a typical terrestrial glacial marginal area on Svalbard. The pro-glacial areas contain one or two prominent arcs of ice-cored moraines and a dead-ice zone with flow tills. An outermost zone of composite ridges is identified on numerous glaciers; however, they are mostly below the marine limit and preferably in areas dominated by sedimentary bedrock. (b) Location of composite ridges in the sense of large-scale deformed and thrust pro-glacial sediments on Svalbard. The shaded area denotes pre-Devonian basement rocks, while the other areas are dominated by sedimentary bedrock. Based on Etzelmüller *et al.* (1996), slightly changed

Both ice-cored and pro-glacial push moraines co-exist in front of numerous Svalbard glaciers (Fig. 4a). The pro-glacial push moraines on, for example, Erikbreen display relict forms, generated during former advances. On Usherbreen, active formation of push moraines was observed and measured during a glacier surge in 1985 (Hagen 1988). O. Liestøl (personal communication) recognized at an early stage that these types of moraine on Svalbard are restricted to areas below the Holocene marine limit. They also seem more abundant in areas dominated by sedimentary rocks. Ice-cored moraines, however, develop practically in all glaciers margins ending on land on Svalbard.

Southern Norway. In southern Norway, stable ice-cored moraines are abundant in the Jotunheimen and Dovrefjell areas (Østrem 1964). These ice-cored moraines are connected mostly to minor cirque glaciers. These glaciers end within environments where regional permafrost modelling confirmed by site investigations suggests widespread permafrost (Ødegård *et al.* 1996; Etzelmüller *et al.* 1998; Isaksen *et al.* 2002). Composite ridges in the sense described in Svalbard have not been observed in southern Norway. Haeberli (1979), however, indicated that moraine features in front of many glaciers in the high mountains of Scandinavia might

partly be a result of sediment deformation in a permafrost environment.

The glacial particulate sediment flux system

Most measurements of fluvial sediment flux have been carried out in relation to temperate glaciers within a non-permafrost environment (Lawson 1993). More recently, however, flux from polythermal glacial settings in Svalbard (Bogen & Bønsnes 2003) has been measured. In general, these studies indicate that, in temperate glacier systems, most of the sediments produced by the glacier are evacuated by meltwater, and sediment flux during summer decreases, despite increasing discharge (Liestøl 1967; Østrem 1975). In permafrost areas with cold or polythermal glaciers, a closer relationship has been observed between discharge and sediment concentrations throughout the melting season (e.g. Vatne *et al.* 1995; Bogen 1996). This observation indicates the more limited ability of the meltwater to exhaust subglacially stored material, and the general availability of sediments for fluvial erosion beneath and in front of these glaciers (Vatne *et al.* 1995; Hodgkins 1997; Hodson *et al.* 1997). Despite the more limited glacier activity, the shorter meltwater season and the lower meltwater production, overall erosion

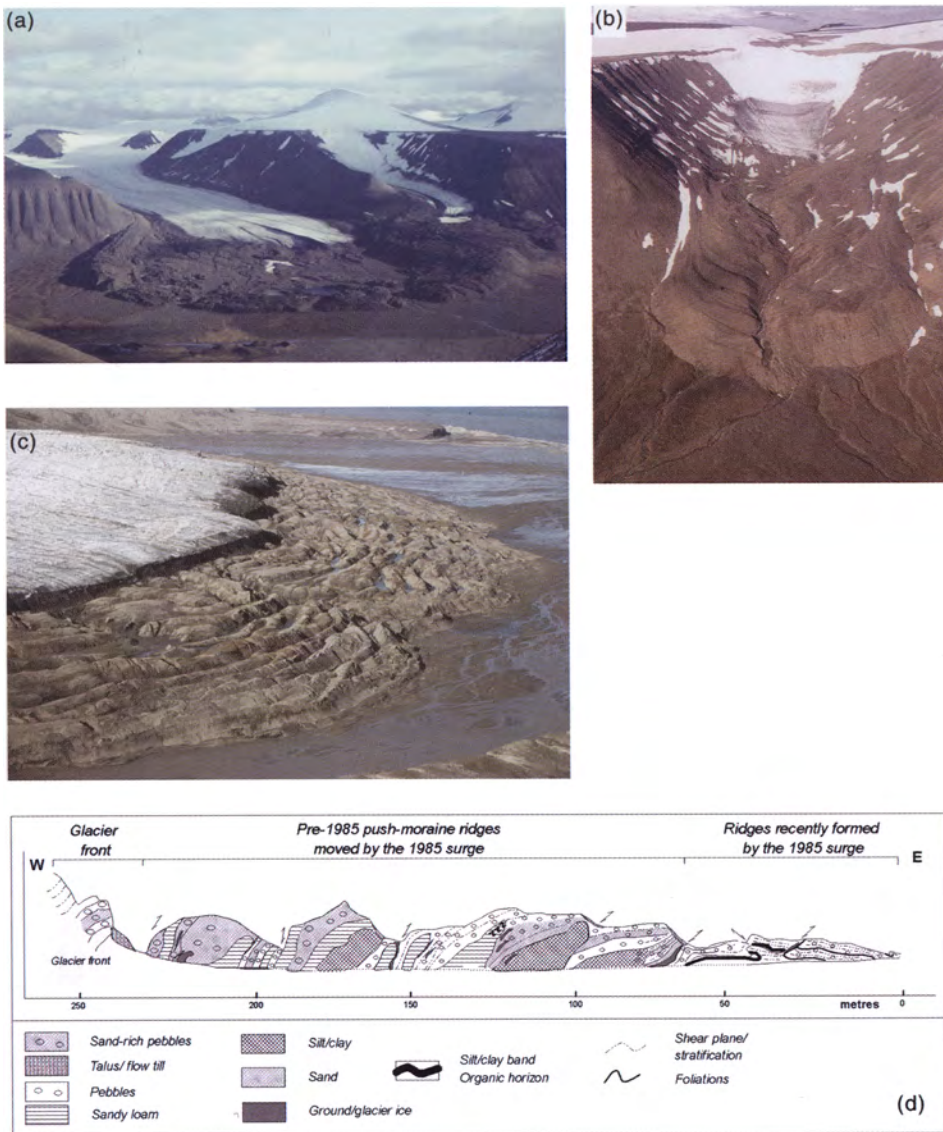


Fig. 5. (a) Moraine area in front of Marthabreen in the Reindalen valley on central Spitsbergen, south of Longyearbyen. Most of the glacier fore-field is underlain by glacier ice, and the outer-most ridges of the area are dominated by ice-cored moraines (photograph: Jon Ove Hagen, 1986, 1994). (b) Marginal zone of a unnamed glacier, Reindalen (photograph Leif Sørbel, 1994). The moraine area is ice-cored, creeping down-slope independently of the glacier dynamics, forming a rock glacier. (c) Glacier marginal zone of Usherbreen, eastern Spitsbergen. The ridges are pushed and moved by a surge advance of the glacier (photo: Jon Ove Hagen, 1985). The white line indicates the location of the profile shown in (d). (d) Section logged in the moraine area of Usherbreen. The structure of the ridge system could be observed in a cross section carved through the ridge system by a water channel. The sediment layers are highly dipped and deformed, folded ice layers are frequently observed (based on Etzelmüller *et al.* 1996, slightly changed)

rates from poly-thermal glacier catchments on Svalbard are remarkably high, with values up to 1 mm per annum (Sollid *et al.* 1994; Hallet *et al.* 1996; Hodgkins *et al.* 2003), even for small, relatively inactive and presumably cold

glacier catchments like Longyearbreen (Etzelmüller *et al.* 2000). These high values are mainly attributed to the easy availability of sediments in the dead-ice and flow till-dominated glacier fore fields.

Geomorphological processes: conceptual models and hypotheses

The distribution of sub pressure-melting point temperatures in glaciers is recognized as a crucial factor for the production, incorporation, transport and sedimentation of glacial material (Weertman 1961; Boulton 1972). This factor has also recently been identified in sedimentological work on small terrestrial Svalbard glaciers (Hambrey *et al.* 1999; Glasser & Hambrey 2001). In the following section, some of these topics are outlined in the framework of glacier–permafrost interaction.

Ice-cored moraines

At the glacier bed the transition zone between temperate and cold ice favours the adfreezing of sediments into basal ice and their transport to englacial and ultimately supraglacial locations. At this thermal transition, the incorporation of sediments due to thrusting and along shear planes is also facilitated by high compressive flow, resulting in a frontal ice-compression zone in which shear zones and folding of ice develops (Hambrey *et al.* 1999; Glasser & Hambrey 2001). This leads to en-glacial transport of sediments towards the ice surface. These processes cause the accumulation of often coarse-grained or even stratified debris in and on the glacier snout. In permafrost environments the thickness of accumulated supraglacial debris may exceed the climate-controlled active-layer thickness, and thus protect the ice below from melting, resulting in the development of ice-cored moraines. This pattern is commonly described from polythermal glaciers in the high-Arctic (Johnson 1971; Souchez 1971; Sollid & Sørbel 1988a; Etzelmüller *et al.* 1996; Lyså & Lønne 2001; Sletten *et al.* 2001). In southern Norway, comparable processes and landform developments are observed on glaciers in the central high-mountain area described earlier (Østrem 1964), where permafrost is widespread.

The survival time of these ice-cored moraines is related to the thickness of the sediment cover. If the temperature under the material cover is below 0°C throughout the year, the ice will not melt, and the ice-core will be stable. In temperate glacier marginal settings, ice-cored moraines are also observed, especially in front of surging glaciers, in areas of high material production and sedimentation and in areas of meltwater flooding events that cover the ice with sediments, e.g., on Iceland (Krüger & Kjær 2000; Kjær & Krüger 2001). However, these ice-cored structures are prone to rapid mass wasting and are not stable,

decaying over decades (Krüger & Kjær 2000). Ice-cored moraines in a permafrost setting are, therefore, prominent features and stable over long time periods. Ice-core decay may first happen during a climatic warming and with resulting increase in of the active-layer thickness. Thus, stable ice-cored moraines are restricted to climatically stable areas and are thus good permafrost indicators.

Close to the fringe of the lower limit of mountain permafrost, adfreezing of material is observed in very marginal areas of glaciers, building asymmetric moraine morphology, often in the form of annual moraines. An example is Midtdalsbreen in the Finse area of southern Norway, a temperate outlet glacier of the Hardangerjøkulen ice cap. Here, thermistor measurements have shown that the lower-most, up to 20 m thick area of the glacier front is cold-based (Hagen 1978; Liestøl & Sollid 1980). Annual moraines built up since the 1960s show clear melt-out of frozen subglacial layers (Andersen & Sollid 1971). Harris & Bothamley (1984) and Matthews *et al.* (1995) describe similar processes in front of Leirbreen and Styggedalsbreen, western Jotunheimen, respectively. These examples discussed above illustrate that the ice-marginal thermal regime is critically important in controlling processes of sedimentation.

Proglacial folding and thrusting

During glacier advances, compressive stresses can be transmitted by the glacier into pro-glacial sediments that may locally result in large-scale deformation and thrusting (Hagen 1988; Bennett 2001). The scale of this process depends on the sub-surface geo-technical conditions (sediment strength and structure), and the magnitude and duration of applied stress. Sediment deformation will occur if glacier-induced stress exceeds the sediment creep strength. The creep strength of the frozen sediment, in a permafrost environment, is highly dependent on liquid water content, ice content and the duration of applied stress (Tsytovich 1975; Williams & Smith 1989). The ratio of liquid water to solid ice within is in turn dependent on sediment type, and fine-grained sediment will contain more liquid water than coarse-grained sediment at the same temperature. In exposed marine sediments, the unfrozen water content also depends on salt content in the pore water, which depresses the freezing point (Tsytovich 1975). Cohesion is the dominant factor controlling the shear strength at sub-zero temperatures. Coarse-grained sediments have no cohesion in the unfrozen state, their strength characteristics depending on effective normal

stress and the internal angle of friction. Once frozen, ice-bonds between grains provide considerable cohesion, and sediment strength increases. In a situation with a high frozen pore water content, contacts between grains can be partly or wholly replaced by ice-bonds (Tsytoich 1975). Frictional strength is then reduced and the creep characteristics of the soil increasingly determine the sediment strength. As ice has low long-term shear strength, layers of supersaturated coarse-grained sediments, e.g., outwash gravels, may then deform plastically under low applied stress. In the case of unfrozen fine-grained cohesive sediments, frictional shear strength is often lower but cohesion higher. In their unfrozen state, such soils are weaker than coarser sediments, and their low permeability allows pore water pressure to rise when compressive stresses are applied. Once frozen, ice-bonds increase the cohesion and sediment strength increases. The sediment then acts more like a rigid mass, allowing the transfer of stresses over longer distances.

In Svalbard, the deformation of frozen proglacial sediments often causes formation of large-scale composite ridges, showing evidence of internal deformation or block-thrusting over large areas across the front of terrestrial glacier snouts (Hagen 1988; Hambrey *et al.* 1996; Hart & Watts 1997; Boulton *et al.* 1999). Such moraines are particularly abundant in fine-grained saline coastal sediments below the marine limit (Fig. 4b). In these areas the strength of the partially frozen sediments is lower than that of the deforming glacier ice. The major décollement plane is often within sub-permafrost unfrozen sediments where porewater pressures are raised and effective stresses therefore are low. This is possible at glaciers near the coast on Svalbard, where permafrost is probably thin and in some cases is still aggrading. Humlum (2004) presents evidence that the permafrost in the major valleys started to aggrade at the present marine limit about 3500–3000 years BP in response to the general Holocene cooling in the Arctic. In the light of this, most of the composite ridges on near-coast Svalbard glaciers were probably developed earlier in the present phase of permafrost formation, when coastal permafrost was thinner than today.

Conceptual relationships between climate, thermal regime and landform generation

The relationship between climate, glacier thermal regime and glacial landform generation is conceptually exemplified in Fig. 6a. Based

on this concept, zones of glacier processes in relation to temperature (presence or absence of permafrost) are outlined (Fig. 6b). A distinction is made between entirely cold glaciers, polythermal glaciers with cold glacier margins, glaciers with patchy zones of marginal adfreezing and glaciers dominated by marginal basal melting. The likely occurrence of a zone of composite ridges in the glacier foreland is suggested to decrease on both ends of the temperature range. If temperatures are low, permafrost becomes thick and stiff, decreasing its ability to deform or thrust the proglacial zone. The deeply frozen ice-cemented sediments have higher shear strengths than the glacier ice and are unlikely to be deformed by it. At the warmer extreme of the thermal continuum permafrost becomes sporadic and large-scale thrusting in the sense described in this paper becomes less likely. Thus, both ice-cored moraines and composite ridges can be recognized as indicators of permafrost conditions during their formation.

Influence of permafrost on the particulate sediment transfer system

In permafrost environments a thick material cover may preserve underlying ice over long time periods. Together with high extra-glacial material production and relatively low meltwater flux, permafrost favours the storage of sediments in the glacier forefields. However, water may locally remove the loose cover material, or mass movement processes may expose ice-cores, accelerating ice-core decay under permafrost conditions, and resulting in the formation of hummocky terrain (e.g. Sollid & Sørbel 1988a). These processes result in a chaotic dead ice terrain, with flow-tills and re-sedimentation processes (Boulton 1968; Etzelmüller 2000; Sletten *et al.* 2001). Thus, in such environments much material is mobilized, and available for erosion. Permafrost and ice-cored glacier marginal areas therefore form an important regulator of the sediment transfer system in which the particulate sediment evacuation is less likely to suffer sediment exhaustion during the summer. Material release depends on the removal of material protecting the ice-core, and this is a process happening through the summer melting season independent of glacial activity. Thus, even with low erosional potential, cirque and valley glacier catchments in permafrost environments have relatively high material transport and long-term erosion rates as measured by meltwater evacuation of solids (e.g. Hallet *et al.* 1996).

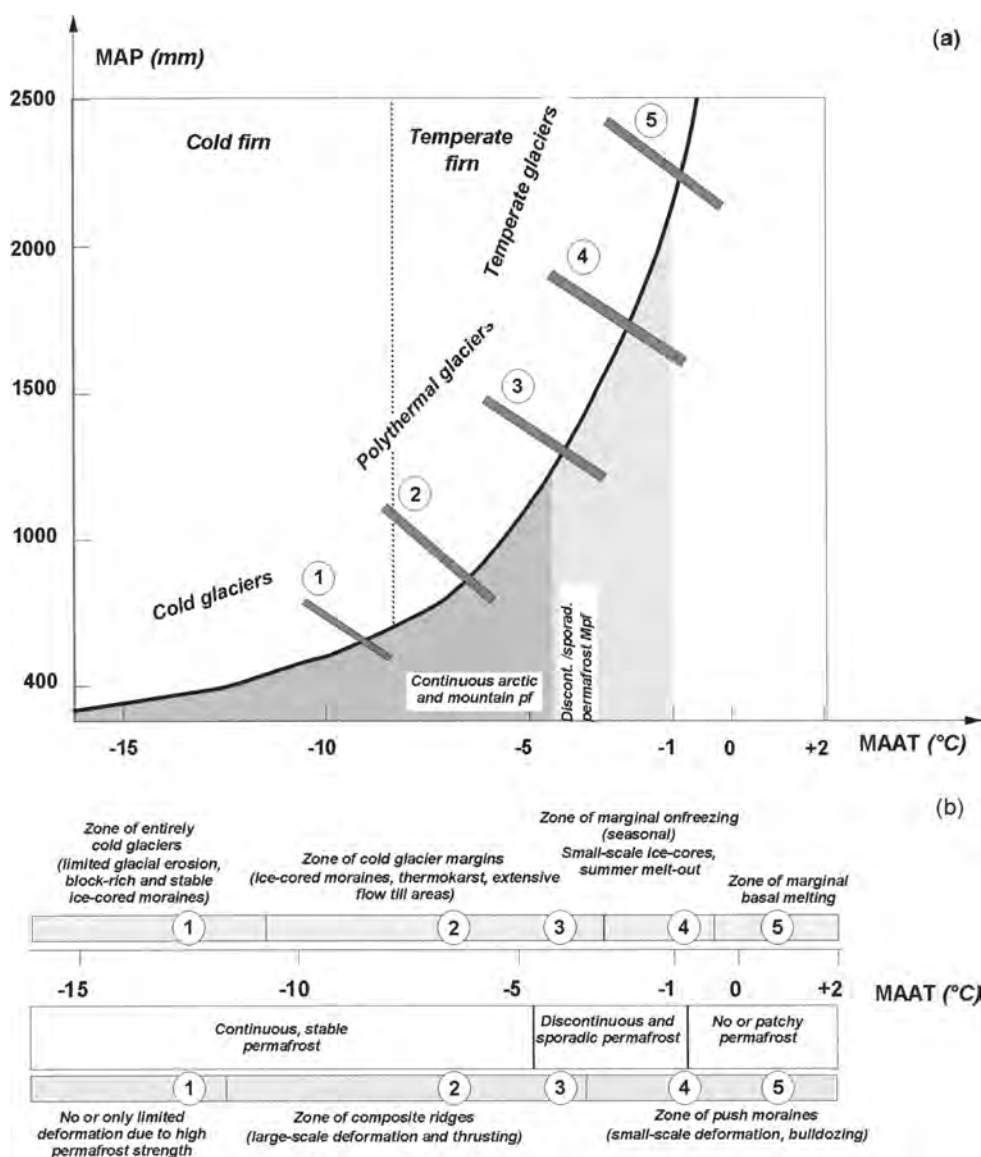


Fig. 6. (a) Schematic illustration of the relationship between MAAT and mean annual precipitation (MAP) at the ELA (solid line), and between (mountain) permafrost and thermal regime of the glaciers (based on Barsch 1996, modified). Above the solid line, glaciers dominate; while below the line permafrost dominates in colder environments due to lower precipitation. The permafrost-dominated regions are delineated into continuous and discontinuous/sporadic. The approximate division was set to MAAT $< -4^{\circ}\text{C}$ and $< -1^{\circ}\text{C}$, respectively. These values may be widely valid in a regional context; however, locally large variations are widely reported due to the varying influence of topographic expositions, surficial material and snow distribution. The rectangles illustrate possible glacier extensions within this diagram. 1, Cold glaciers in continuous permafrost; 2, polythermal glaciers in continuous permafrost (e.g., on Svalbard); 3, polythermal glaciers advancing in discontinuous permafrost (e.g., high mountain areas of Scandinavia or the Alps); 4, temperate glaciers advancing through the discontinuous mountain permafrost zone; marginal permafrost at the front can be observed due to favourable local climatic conditions (topography, snow drift etc. e.g., Midtdalsbreen, Norway); 5, temperate glacier (e.g., Nigardsbreen). (b) Simplified illustration of the relationship between permafrost zones (indicated with MAAT) and marginal glacial-geomorphological processes. The numbers correspond to the glacier positions in (a). Pf = Permafrost

Response of the geomorphological process system to climate change

Both glaciers and permafrost respond to changing thermal boundary conditions that are largely climatically controlled. Glaciers react particularly to changing summer temperature and winter precipitation. Permafrost, being thermally defined, is controlled by the complex energy transfer processes at the boundary between the atmosphere and the earth surface. A geomorphologically important point is that glaciers show a relatively rapid response to climate change (years to tens of years), depending on glacier size and geometry. Permafrost, on the other hand, shows a comparatively slow response (hundreds to thousands of years), due to the dampening of diurnal to annual ground surface temperature variation with depth, which is controlled mainly by snow cover, the water content and the thermal properties of the surface sediments (Lachenbruch & Marshall 1986). This means, following the relationship illustrated in Fig. 1, that the shift of the ELA is normally faster than the shift of the MPA. This leads in turn to a potentially complex system of relationships between the thermal regimes of glaciers and permafrost.

A glacier advance caused by summer cooling or increased winter precipitation over proglacial permafrost leads to a warming of the ground over which the glacier has advanced. Advancing glaciers will introduce a more effective thermal buffer zone between atmosphere and lithosphere, and thus have both an insulating and a warming effect due to the potential advective heat transport of ice masses. This often leads to a warming of the overrun sub-glacial permafrost system despite cooling of the atmosphere. This was probably the case for the advance of glaciers during, for example, the LIA in many mountain and Arctic environments (Glasser & Hambrey 2001; Guglielmin 2004). During the cooler LIA period permafrost was more extensive in Norway, as a result of a lower mean annual ground surface temperature (MAGST). An empirical modelling approach based on distributed air temperatures indicated that the area affected by permafrost in southern Norway would have almost doubled with a 1°C decrease of air temperature (Etzelmüller *et al.* 2003). However, since the LIA, climate cooling has also been associated with glacier advance, and the actual area of permafrost has increased by less than this amount. However, as an advance of a glacier over permafrost results first in a decrease in the ground temperature gradient, meaning that the warming is extremely slow,

permafrost can survive for a very long time even under a temperate glacier.

Glacier retreat led to a cooling of the ground thermal regime in the newly exposed proglacial zone, and thus permafrost aggradation. In addition, initially temperate glaciers retreating into the marginal permafrost zone develop cold glacier snouts (Björnsson *et al.* 1996; Glasser & Hambrey 2001). Thus, in many areas, permafrost may have formed in the glacier marginal zones during glacier retreat, as recently documented by Kneisel (2003). In high mountain areas of southern Norway, where glaciers have been retreating into the permafrost zone since the LIA, this has been the case. Morphologically, this transition from temperate to cold-margin glaciers is evidenced by glacial landforms indicative of temperate glacier beds (e.g., flutings or striae) in areas which at present are underlain by permafrost (e.g. in Jotunheimen; Erikstad & Sollid 1990). Similar observations have also been reported from Svalbard by, for example, Glasser and Hambrey (2001), highlighting the consequences of the thermal regime change on the style of material entrainment and sedimentation.

Thinning of polythermal glaciers may result in their becoming entirely cold-based. Examples of this have been reported from Svalbard (Björnsson *et al.* 1996). A general thinning of the glaciers may therefore lead to a partial or total re-freezing of taliks below the glaciers and thus a restriction in potential sub-permafrost ground water inflow from glaciers. Subglacial erosion then stops in former temperate areas, with an associated increase in the potential for adfreezing of subglacial sediments (Weertman 1961).

As described earlier in this paper, glacial sediments in the permafrost zone are stored in extensive dead-ice terrain and ice-cored moraines over long time periods (decades to centuries), under steady climatic conditions and without erosive disturbance of the surface. During climate warming, a thicker active layer and thus an enhanced differential melting of debris-covered ice can be expected. Therefore, erosion of formerly permafrost-bonded sediment can be expected during warmer climate. These relationships are shown conceptually in Fig. 7.

Climate warming is also generally associated with reduction in glacier size. During such a phase glacial erosion rates will be reduced and meltwater discharge will increase, at least periodically, due to higher ice melting. Owing to lower sub-glacial material production, particulate suspended sediment concentrations in melt water rivers will decrease. This relationship has widely been used in analyses of lacustrine

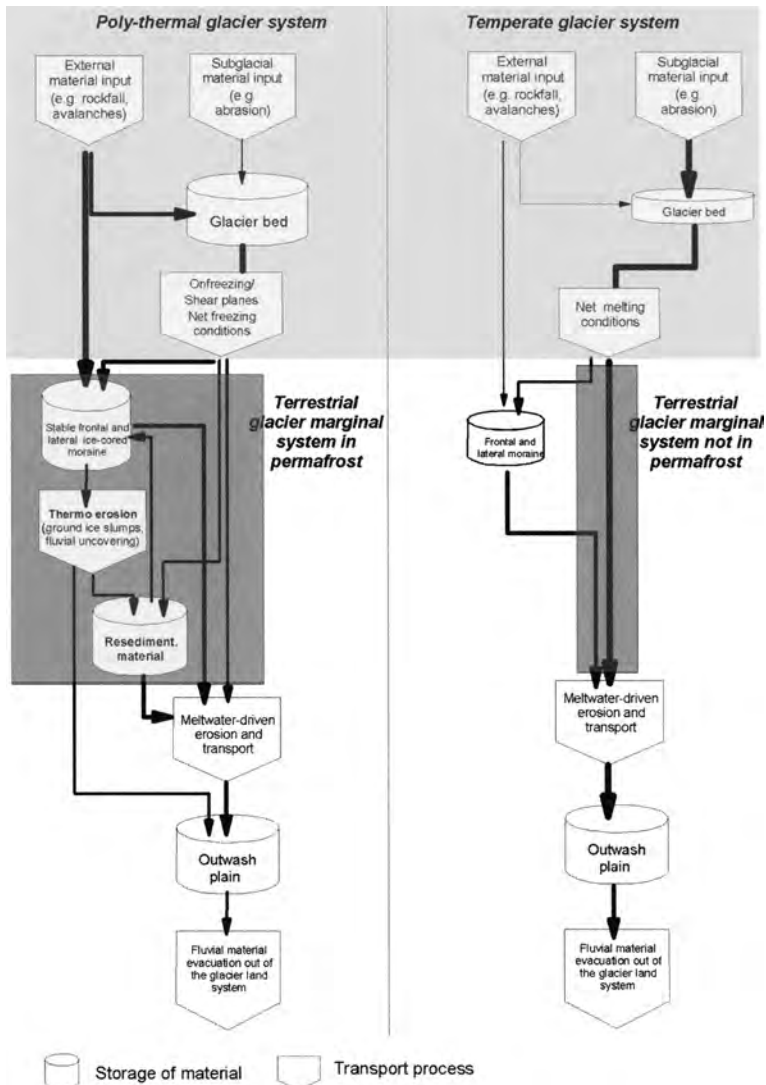


Fig. 7. Idealized schematic flow scheme of particulate material transport in cold/polythermal and temperate glacier environments. The grey shaded area denotes the glacier body, while the non-shaded areas display the terrestrial pro-glacial environment with and without permafrost. The thickness of the lines symbolizes the relative amount of material transported. The flow scheme illustrates that in permafrost environments a relatively larger portion of available material is routed through the ice-cored moraine system, while in the non-permafrost area most of the material is evacuated through the glacio-fluvial system. This affects the relationship between glacier activity and fluvial evacuation of particulate sediments out of glacierized catchments. During climate warming the two systems respond differently. Based on Etzelmüller *et al.* (2000), modified

sediment cores with respect to Holocene climate change (Nesje *et al.* 2001). However, in the permafrost zone, this reduced direct glacier sediment supply may well be compensated for by more rapid release of the sediments stored in the dead ice marginal zones and ice-cored moraines. On some glaciers on Svalbard, for

instance, disintegration of ice-cored moraines has increased in the last 30 years, and the amount of material potentially mobilized by these processes nearly equals the measured suspended sediment yield from the investigated catchments (Etzelmüller 2000). Hodgkins *et al.* (2003) recently demonstrated the absence of a

straightforward relationship between melt water production sediment yield from high-Arctic catchments.

In the context of paraglacial activity in high-alpine environments (Church & Ryder 1972; Ballantyne 2002), permafrost reduces the variability of sediment yield and promotes sediment storage in over longer time periods. Sediment stores are mobilized during permafrost degradation.

Concluding remarks

The distribution of sub-zero temperatures within glacier bodies and in the surrounding landscape is crucial for understanding geomorphological processes with respect to sediment production, transport and deposition in modern arctic and high-alpine glacierized environments. Within the system differing response times to climate change result in a complex ground and glacial thermal regime, influencing landform generation and preservation. There is a close interaction between the glacial and the periglacial system, affecting all chains of the sediment cascade system within landform evolution. In the framework of understanding geomorphological processes and response of the system to climate change, glaciers and permafrost systems must be regarded as an integrated part of the analyses (Fig. 8).

The proposed influence of permafrost on the sediment transfer system also provides constraints on lacustrine sedimentation. In studies on lake sediments, the signal in the lake cores indicates good correlation between glacier

presence, size and the sediment record (Nesje *et al.* 2000). The glaciers referred to in these studies are temperate, and the lake cores allowed a detailed reconstruction of Holocene glaciers and, thus, climate history. Catchments containing cold and polythermal glaciers may also give higher sediment yields signal than those with no glacier at all (Svendsen *et al.* 1989; Barsch *et al.* 1994; Svendsen & Mangerud 1997; Bogen & Bønsnes 2003); however, the relationships between glacier variations, thermal regime and particulate sediment flux from such glacierized basins are likely to be complex and remain to be evaluated in more detail.

The process interrelationships discussed in this paper are crucial for understanding both the modern and former landscape formation in Scandinavia. The recent decades have provided an increased recognition of cold-based ice in both interior and marginal parts of the Scandinavian ice sheets (Sollid & Sørbel 1984, 1994; Kleman 1994), explaining landform preservation, pro-glacial sediment accumulation and deformation. In southern Norway at present, permafrost persist during glaciations or extends over at least twice the area of the glacierized zone. During considerable time spans in the Pleistocene it can be expected that permafrost affected large areas, including the mountainous zones, since it is likely that permafrost developed during glacier build-up, and that permafrost persist during glaciations or again formed during the retreat of the Pleistocene ice sheets. Therefore, it is likely that permafrost–glacier interaction influenced landform development over considerable time spans during the Pleistocene, both at microscales (moraine formation, slope processes) and macroscales (valley formation, strandflats).

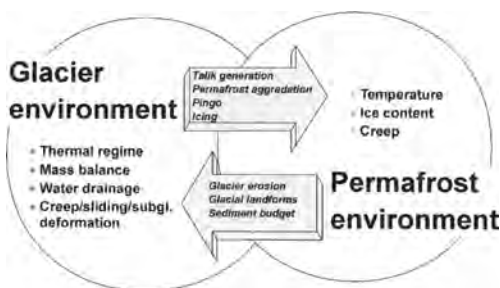


Fig. 8. Simplified diagram illustrating the coupling of cryospheric systems. Glaciers influence on the thermal regime of permafrost areas, resulting in permafrost degradation (talik) or aggradation and specific periglacial landforms such as open-system pingos. Permafrost influences glacial–geomorphological processes in terms of reduced subglacial erosion, specific glacial landform pattern and sediment budgets

This paper is based on a presentation given at the symposium on cryogenic systems held at the Geological Society cryospheric systems. London, in January 2003 by the first author. Most of the examples from Svalbard and southern Norway are based on field studies and observations, partly published in main co-authorships with J. L. Sollid, R. Ødegård, G. Vatne, K. Melvold and I. Berthling. The late Professor Olav Liestøl from the former Department of Physical Geography, University of Oslo, early realized the importance of permafrost on glacial geomorphological processes, and his work as glaciologist at the Norwegian Polar Institute (NPI) and teacher at the former Department of Physical Geography is a fundamental basis for this paper. Professor Emeritus J. L. Sollid, University of Oslo, Norway, over many years focused on the importance of glacial thermal regime in landform generation and deglaciation studies, and initiated the study of mountain permafrost in Norway at the former Department of Physical Geography, University of Oslo. N. Glasser and B. Rea reviewed this

paper, and their numerous comments improved it considerably. O. Humlum gave valuable comments and new input to a later revised version of the paper, which the authors highly appreciate. We want to thank all mentioned persons and institutions.

References

- ANDERSEN, J. L. & SOLLID, J. L. 1971. Glacial chronology and glacial geomorphology in the marginal zones of the glaciers Midtdalsbreen and Nigardsbreen, Southern Norway. *Norsk geografisk Tidsskrift*, **25**, 1–38.
- BALLANTYNE, C. K. 2002. Paraglacial geomorphology. *Quaternary Science Reviews*, **21**, 1935–2017.
- BARSCHE, D. 1996. *Rock glaciers*, Springer, Berlin.
- BARSCHE, D., GUDE, M., MAUSBACHER, R., SCHUKRAFT, G. & SCHULTE, A. 1994. Recent fluvial sediment budgets in glacial and periglacial environments, NW Spitsbergen. *Zeitschrift für Geomorphologie*, **97**(suppl.), 111–122.
- BENN, D. I. & EVANS, D. J. A. 1998. *Glaciers and Glaciations*, Arnold, London.
- BENNETT, M. 2001. The morphology, structural evolution and significance of push moraines. *Earth Science Reviews*, **53**(3–4), 197–236.
- BJÖRNSSON, H., GJESSING, Y., HAMRAN, S.-E., HAGEN, J. O., LIESTØL, O., PALSSON, F. & ERLINGSSON, B. 1996. The thermal regime of sub-polar glaciers mapped by multi-frequency radio-echo sounding. *Journal of Glaciology*, **42**(140), 23–32.
- BLATTER, H. 1987. On the thermal regime of an Arctic valley glacier: A study of White Glacier, Axel Heiberg Island, N.W.T., Canada. *Journal of Glaciology*, **33**(114), 200–211.
- BLATTER, H. & HUTTER, K. 1991. Polythermal conditions in Arctic glaciers. *Journal of Glaciology*, **37**(126), 261–269.
- BLUEMLE, J. P. & CLAYTON, L. 1984. Large-scale glacial thrusting and related processes in North Dakota. *Boreas*, **13**, 279–299.
- BOGEN, J. 1996. Erosion rates and sediment yields of glaciers. *Annals of Glaciology*, **22**, 48–52.
- BOGEN, J. & BØNSNES, T. E. 2003. Erosion and sediment transport in High Arctic rivers, Svalbard. *Polar Research*, **22**(2), 175–189.
- BOULTON, G. S. 1967. The development of a complex supraglacial moraine of the margin of Sørbreen, Ny Friesland, Vestspitsbergen. *Journal of Glaciology*, **6**, 717–735.
- BOULTON, G. S. 1968. Flow tills and related deposits on some Vestspitsbergen glaciers. *Journal of Glaciology*, **7**, 391–412.
- BOULTON, G. S. 1972. *The Role of Thermal Regime in Glacial Sedimentation*. Institute of British Geography Special Publication no 4, 1–19.
- BOULTON, G. S. 1986. Push moraines and glacier contact fans in marine and terrestrial environments. *Sedimentology*, **33**, 677–698.
- BOULTON, G. S., VAN DER MEER, J. J. M., BEETS, D. J., HART, J. K. & RUEGG, G. H. J. 1999. The sedimentary and structural evolution of a recent push moraine complex: Holmstrømbreen, Spitsbergen. *Quaternary Science Reviews*, **18**, 339–371.
- CHURCH, M. & RYDER, J. M. 1972. Paraglacial sedimentation: A consideration of fluvial processes conditioned by glaciation. *Geological Society American Bulletin*, **83**, 3059–3071.
- CLAYTON, L., ATTIG, J. W. & MICKELSON, D. M. 2001. Effects of late Pleistocene permafrost on the landscape of Wisconsin, USA. *Boreas*, **30**, 173–188.
- CROOT, D. G. 1988. Glaciotectonics and surging glaciers: A correlation based on Vestspitsbergen, Svalbard, Norway. In: CROOT, D. G. (ed.), *Glaciotectonics: Forms and Processes*, Balkema, Rotterdam, 49–62.
- DAHL, S. O. & NESJE, A. 1994. Holocene glacier fluctuations at Hardangerjøkulen, central southern Norway: A high-resolution composite chronology from lacustrine and terrestrial deposits. *The Holocene*, **4**, 269–277.
- ERIKSTAD, L. & SOLLID, J. L. 1990. *Memurubreene, Jotunheimen – glacialgeomorfologi 1:6500*, Norsk Institutt for Naturforskning/Geografisk institutt, UiO, Oslo.
- ETZELMÜLLER, B. 2000. Quantification of thermo-erosion in pro-glacial areas – examples from Spitsbergen. *Zeitschrift für Geomorphologie*, **44**(3), 343–361.
- ETZELMÜLLER, B., HAGEN, J. O., VATNE, G., ØDEGÅRD, R. S. & SOLLID, J. L. 1996. Glacier debris accumulation and sediment deformation influenced by permafrost, examples from Svalbard. *Annals of Glaciology*, **22**, 53–62.
- ETZELMÜLLER, B., BERTHLING, I. & SOLLID, J. L. 1998. The distribution of permafrost in Southern Norway; a GIS approach. In: LEWKOWICZ, A. G. & ALLARD, M. (eds), *Seventh International Conference on Permafrost, Proc.*, Collection Nordicana, Centre d'Etudes Nordiques, Université Laval, Quebec, 251–257.
- ETZELMÜLLER, B., ØDEGÅRD, R. S., VATNE, G., MYSTERUD, R. S., TONNING, T. & SOLLID, J. L. 2000. Glacier characteristic and sediment transfer systems of Longyearbyen and Larsbreen, western Spitsbergen. *Norsk geografisk Tidsskrift*, **54**(4), 157–168.
- ETZELMÜLLER, B., BERTHLING, I. & SOLLID, J. L. 2003. Aspects and Concepts on the Geomorphological Significance of Holocene Permafrost in Southern Norway. *Geomorphology*, **52**(1–2), 87–104.
- FURRER, G. 1992. Zur Gletschergeschichte des Liefdefjords. *Stuttgarter Geographische Studien*, **117**, 267–278.
- FURUBERG, T. & BERGGREN, A.-L. 1988. Mechanical properties of frozen saline clays. In: *Proceedings 5th International Conference on Permafrost*, Trondheim, Norway, 1078–1084.
- GLASSER, N. & HAMBREY, M. 2001. Styles of sedimentation beneath Svalbard valley glaciers under changing dynamic and thermal regimes. *Journal of the Geological Society London*, **158**, 697–707.
- GREGENSEN, O., PHUKAN, A. & JOHANSEN, T. 1983. Engineering properties and foundation design

- alternatives in marine Svea Clay, Svalbard. *In: 4th International Conference on Permafrost*, Fairbanks, AK, 384–388.
- GRIPP, K. 1929. Glaziologiske og geologiske Resultater af den danske Spitzbergen Expedition. *Abhandlungen des Naturwissenschaftlichen Vereins zu Hamburg*, **22**, 147–247.
- GUGLIELMIN, M. 2004. Observations on permafrost ground thermal regimes from Antarctica and the Italian Alps, and their relevance to global climate change. *Global and Planetary Change*, **40**, 159–167.
- HAEBERLI, W. 1979. Holocene push-moraines in alpine permafrost. *Geografiska Annaler*, **61A**, 43–48.
- HAEBERLI, W. 1992. Construction, environmental problems and natural hazards in periglacial mountain belts. *Permafrost and Periglacial Processes*, **3**, 111–124.
- HAEBERLI, W., CHENG, G., GORBUNOV, A. P. & HARRIS, S. A. 1993. Mountain permafrost and climatic change. *Permafrost and Periglacial Processes*, **4**(2), 165–174.
- HAGEN, J. O. 1978. Brefrontprosesser ved Hardangerjøkulen [Glacier front processes at Hardangerjøkulen]. Cand. real. Thesis, University of Oslo, Norway, Oslo.
- HAGEN, J. O. 1988. Glacier surge in Svalbard with examples from Usherbreen. *Norsk Geografisk Tidsskrift*, **42**(4), 239–252.
- HAGEN, J. O., KOHLER, J., MELVOLD, K. & WINTHER, J. G. 2003. Glaciers in Svalbard: Mass balance, runoff and freshwater flux. *Polar Research*, **22**(2), 145–160.
- HALLET, B., HUNTER, L. & BOGEN, J. 1996. Rates of erosion and sediment evacuation by glaciers: A review of field data and their implications. *Global and Planetary Change*, **12**, 213–235.
- HAMBREY, M. J., DOWDESWELL, J. A., MURRAY, T. & PORTER, P. R. 1996. Thrusting and debris entrainment in a surging glacier: Bakaninbreen, Svalbard. *Annals of Glaciology*, **22**, 241–248.
- HAMBREY, M. J., BENNETT, M. R., DOWDESWELL, J. A., GLASSER, N. F. & HUDDART, D. 1999. Debris entrainment and transfer in polythermal valley glaciers. *Journal of Glaciology*, **45**(149), 69–86.
- HARRIS, C. & BOTHAMLEY, K. 1984. Englacial deltaic sediments as evidence for basal freezing and marginal shearing, Leirbreen, Southern Norway. *Journal of Glaciology*, **30**(104), 30–34.
- HARRIS, C., VONDER MÜHLL, D., ISAKSEN, K., HAEBERLI, W., SOLLID, J. L., KING, L., HOLMLUND, P., DRAMIS, F., GUGLIELMIN, M. & PALACIOS, D. 2003. Warming permafrost in European mountains. *Global and Planetary Change*, **39**, 215–225.
- HART, J. K. & WATTS, R. J. 1997. A comparison of the styles of deformation associated with two recent push moraines, south Van Keulenfjorden, Svalbard. *Earth Surface Processes and Landforms*, **22**, 1089–1107.
- HEGEM, E. S. F., JULIUSSEN, H. & ETZELMÜLLER, B. 2003. Mountain permafrost in the Sølen massif, Central-Eastern Norway. *In: PHILLIPS, M., SPRINGMAN, S. M. & ARENSEN, L. U. (eds), Eighth International Conference on Permafrost, Proc.*, Balkema, Zurich, 367–372.
- HODGKINS, R. 1997. Glacier hydrology in Svalbard, Norwegian High Arctic. *Quaternary Science Reviews*, **16**, 957–973.
- HODGKINS, R., COOPER, R., WADHAM, J. & TRANTER, M. 2003. Suspended sediment fluxes in a high-Arctic glacierised catchment: Implications for fluvial sediment storage. *Sedimentary Geology*, **162**, 105–117.
- HODSON, A. J., TRANTER, M., DOWDESWELL, J. A., GURNELL, A. M. & HAGEN, J. O. 1997. Glacier thermal regime and suspended-sediment yield: A comparison of two high-Arctic glaciers. *Annals of Glaciology*, **24**, 32–37.
- HUMLUM, O. 2004. *Holocene Permafrost Aggradation in Svalbard*. *In: Harris, C. & Murton, J. (eds.): Cryospheric Systems: Glaciers and Permafrost*. Geological Society, London, Special Publications, **242**, 119–130.
- HUMLUM, O., INSTANES, A. & SOLLID, J. L. 2003. Permafrost in Svalbard: A review of research history, climatic background and engineering challenges. *Polar Research*, **22**(2), 191–215.
- HUMLUM, O., ELBERLING, B., HORMES, A., FIORDHEIM, K., HANSEN, O. H. & HEINEMEIER, J. 2005. Late Holocene glacier growth in Svalbard, documented by subglacial find of old vegetation and still alive soil microbes. *The Holocene* (in press).
- INTERNATIONAL PERMAFROST ASSOCIATION 1998. *Multi-language Glossary of Permafrost and Related Ground-ice Terms*, IPA, The University of Calgary, Calgary.
- ISAKSEN, K., HAUCK, C., GUDEVANG, E., ØDEGÅRD, R. S. & SOLLID, J. L. 2002. Mountain permafrost distribution on Dovrefjell and Jotunheimen, southern Norway, based on BTS and DC resistivity tomography data. *Norsk Geografiska Tidsskrift*, **56**(2), 122–136.
- JOHNSON, P. G. 1971. Ice-cored moraine formation and degradation, Donjek glacier, Yukon Territory, Canada. *Geografiska Annaler*, **53A**, 198–202.
- KING, L. 1986. Zonation and ecology of high mountain permafrost in Scandinavia. *Geografiska Annaler*, **68A**, 131–139.
- KJÆR, K. H. & KRÜGER, J. 2001. The final phase of dead-ice moraine development: Processes and sediment architecture, Kotlujokull, Iceland. *Sedimentology*, **48**(5), 935–952.
- KLEMAN, J. 1994. Preservation of landforms under ice sheets and ice caps. *Geomorphology*, **9**, 19–32.
- KNEISEL, C. 2003. Permafrost in recently deglaciated glacier forefields – measurements and observations in the eastern Swiss Alps and northern Sweden. *Zeitschrift fuer Geomorphologie*, **47**(3), 289–305.
- KRISTIANSEN, K. & SOLLID, J. L. 1987. Svalbard, Glacial geologi og geomorfologi, 1:1000000. Geografisk institutt, Universitetet i Oslo.
- Krüger, J. & Kjær, K. H. 2000. De-icing progression of ice-cored moraines in a humid, subpolar

- climate, Kotlujökull, Iceland. *The Holocene*, **10**(6), 737–747.
- LACHENBRUCH, A. H. & MARSHALL, B. V. 1986. Changing climate: Geothermal evidence from permafrost in the Alaskan Arctic. *Science*, **234**, 689–696.
- LAWSON, D. E. 1993. Glaciohydrologic and glaciohydraulic effects on runoff and sediment yield in glaciated basins. US Army Corps of Engineers, Cold Region Research and Engineering Laboratory (CRREL), 93-2.
- LIESTØL, O. 1965. Lokalt område med permafrost i Gudbrandsdalen. *Norsk Polarinstitutt Aarbok*, **1965**, 129–133.
- LIESTØL, O. 1967. Storbreen glacier in Jotunheimen, Norway. *Norsk Polarinstitutt Skrifter*, **141**, 63.
- LIESTØL, O. 1977. Pingos, springs, and permafrost in Spitsbergen. *Norsk Polarinstitutt Årbok*, **1975**, 7–29.
- LIESTØL, O., 1994. Kompendium i glasiologi, Geografisk institutt, Universitetet i Oslo, Oslo.
- LIESTØL, O. 1996. Open-system pingos in Spitsbergen. *Norsk geografisk Tidsskrifts*, **50**, 81–84.
- LIESTØL, O. & SOLLID, J. L. 1980. Glacier erosion and sedimentation at Hardangerjøkullen and Omnsbreen. In: ORHEIM, O. (ed.), *Symposium on Processes of Glacier Erosion and Sedimentation, Field Guide to Excursion*. Norsk Polarinstitutt, Oslo, Geilo, Norway, 1–22.
- LYSÅ, A. & LØNNE, I. 2001. Moraine development at a small High-Arctic valley glacier: Rieperbreen, Svalbard. *Journal of Quaternary Science*, **16**(6), 519–529.
- MANGERUD, J., JANSEN, E. & LANDVIK, J. Y. 1996. Late Cenozoic history of the Scandinavian and Barents Sea ice sheets. *Global and Planetary Change*, **12**, 11–26.
- MATTHEWS, J. A., MCCARROLL, D. & SHAKESBY, R. A. 1995. Contemporary terminal-moraine ridge formation at a temperate glacier – Styggealsbreen, Jotunheimen, Southern Norway. *Boreas*, **24**(2), 129–139.
- NESJE, A., DAHL, S. O., ANDERSSON, C. & MATTHEWS, J. A. 2000. The lacustrine sedimentary sequence in Sygneskardvatnet, western Norway: A continuous, high-resolution record of the Jostedalbreen ice cap during the Holocene. *Quaternary Science Reviews*, **19**, 1047–1065.
- NESJE, A., MATTHEWS, J. A., DAHL, S. O., BERRISFORD, M. S. & ANDERSSON, C. 2001. Holocene glacier fluctuations and winter precipitation changes in the Jostedalbreen region, western Norway: Evidence from pro-glacial lacustrine sediment records. *The Holocene*, **11**, 267–280.
- ØDEGÅRD, R., HAMRAN, S. E., BØ, P. H., ETZELMÜLLER, B., VATNE, G. & SOLLID, J. L. 1992. Thermal regime of a valley glacier, Erikbreen, northern Spitsbergen. *Polar Research*, **11**, 69–80.
- ØDEGÅRD, R. S., HOELZLE, M., JOHANSEN, K. V. & SOLLID, J. L. 1996. Permafrost mapping and prospecting in southern Norway. *Norsk geografisk Tidsskrift*, **50**, 41–54.
- ØDEGÅRD, R. S., HAGEN, J. O. & HAMRAM, S.-E. 1997. Comparison of radio-echo sounding (30–1000 MHz) and high-resolution borehole-temperature measurements at Finsterwalderbreen, southern Spitsbergen, Svalbard. *Annals of Glaciology*, **24**, 262–271.
- ØSTREM, G. 1964. Ice-cored moraines in Scandinavia. *Geografisk Annaler*, **46A**, 282–337.
- ØSTREM, G. 1975. Sediment transport in glacial meltwater streams. In: JOPLING, A. V. & McDONALD, B. C. (eds) *Glaciofluvial and Glaciolacustrine Sedimentation*, Society of Economic Paleontologists, Tulsa, OK, 101–122.
- PATERSON, W. S. B. 1994. *The Physics of Glaciers*, Pergamon/Elsevier Science, Oxford.
- SHUMSKIY, P. A. 1964. Principles of structural glaciology: The petrography of fresh-water ice as a method of glaciological investigation. Translated from the Russian by KRAUS, D., Dover, New York.
- SLETTEN, K., LYSÅ, A. & LØNNE, I. 2001. Formation and disintegration of a high-arctic ice-cored moraine complex, Scott Turnerbreen, Svalbard. *Boreas*, **30**(4), 272–284.
- SNYDER, J. A., WERNER, A. & MILLER, G. H. 2000. Holocene cirque glacier activity in western Spitsbergen, Svalbard: Sediment records from proglacial Linnevatnet. *The Holocene*, **10**(5), 555–563.
- SOLLID, J. L. & SØRBEL, L. 1984. Distribution and genesis of moraines in Central Norway. *Striae*, **20**, 63–67.
- SOLLID, J. L. & SØRBEL, L. 1988a. Influence of temperature conditions in formation of end moraines in Fennoscandia and Svalbard. *Boreas*, **17**, 553–558.
- SOLLID, J. L. & SØRBEL, L. 1988b. Utbredelsesmønsteret av løsmateriale og landformer på Svalbard – noen hovedtrekk. *Norsk geografisk Tidsskrift*, **42**(4), 265–270.
- SOLLID, J. L. & SØRBEL, L. 1994. Distribution of glacial landforms in southern Norway in relation to the thermal regime of the last continental ice-sheet. *Geografiska Annaler*, **76**(1–2), 25–35.
- SOLLID, J. L. & SØRBEL, L. 1998. Palsa bogs as a climate indicator – examples from Dovrefjell, Southern Norway. *Ambio*, **27**(4), 287–291.
- SOLLID, J. L., ETZELMÜLLER, B., VATNE, G. & ØDEGÅRD, R. 1994. Glacial dynamics, material transfer and sedimentation of Erikbreen and Hannabreen, Liefdefjorden, northern Spitsbergen. *Zeitschrift für Geomorphologie*, Suppl. Bind, **97**, 123–144.
- SOLLID, J. L., ISAKSEN, K., EIKEN, T. & ØDEGÅRD, R. S. 2003. The transition zone of mountain permafrost on Dovrefjell, southern Norway. In: PHILLIPS, M., SPRINGMAN, S. M. & ATENSON, L. U. (eds.), *Eighth International Conference on Permafrost*, Proc., Balkema, Zurich, 1085–1090.
- SOUCHEZ, R. A. 1971. Ice-cored moraines in South-Western Ellesmere Island, N.W.T., Canada. *Journal of Glaciology*, **10**, 245–254.
- SUTER, S., LATERNSE, M., HAEBERLI, W., FRAUENFELDER, R. & HOELZLE, M. 2001. Cold firm and ice of high-altitude glaciers in the Alps:

- Measurements and distribution modelling. *Journal of Glaciology*, **47**(156), 85–96.
- SVENDSEN, J. I. & MANGERUD, J. 1997. Holocene glacial and climate variations on Spitsbergen, Svalbard. *The Holocene*, **7**(1), 45–57.
- SVENDSEN, J. I., MANGERUD, J. & MILLER, G. H. 1989. Denudation rates in the Arctic estimated from lake sediments on Spitsbergen, Svalbard. *Palaeogeography, Palaeoclimatology, Palaeoecology*, **76**(1–2), 153–168.
- TSYTOVICH, N. A. 1975. *The Mechanics of Frozen Ground*, McGraw-Hill, Washington, DC.
- VATNE, G., ETZELMÜLLER, B., ØDEGÅRD, R. & SOLLID, J. L. 1995. Subglacial drainage and sediment evacuation at Erikbreen, northern Spitsbergen. *Nordic Hydrology*, **26**, 169–190.
- WEERTMAN, J. 1961. Mechanism for the formation of inner moraines found near the edge of cold ice caps and ice sheets. *Journal of Glaciology*, **3**, 965–978.
- WILLIAMS, P. J. & SMITH, M. W. 1989. *The Frozen Earth: Fundamentals of Geocryology*, Cambridge University Press, Cambridge.

Glaciological investigations in Norway in 2008

Report No 2

Glaciological investigations in Norway in 2008

Published by: Norwegian Water Resources and Energy Directorate
Editor: Bjarne Kjøllmoen
Authors: Liss M. Andreassen, Hallgeir Elvehøy, Miriam Jackson, Bjarne Kjøllmoen, Rianne H. Giesen* and Arve M. Tvede**
*Utrecht University, the Netherlands
**Statkraft AS

Print: NVE
Number printed: 250
Frontpage photo: Storbreen in Jotunheimen. The photo was taken 29th July 2008 by Liss M. Andreassen.
ISSN: 1502-3540
ISBN: 978-82-410-0686-9

Abstract: Results of glaciological investigations performed at Norwegian glaciers in 2008 are presented in this report. The main part concerns mass balance investigations. Results from investigations of glacier length changes are discussed in a separate chapter.
Subjects: Glaciology, Mass balance, Glacier length change, Glacier velocity, Meteorology, Subglacial laboratory

Norwegian Water Resources and Energy Directorate
Middelthunsgate 29
Post office box 5091 Majorstua
N-0301 OSLO

Telephone: +47 22 95 95 95
Telefax: +47 22 95 90 00
Internet: www.nve.no

April 2009

Contents

Preface	4
Summary	5
Sammendrag	6
1. Glacier investigations in Norway in 2008	7
2. Ålfotbreen	14
3. Folgefonna	20
4. Nigardsbreen	33
5. Austdalsbreen	38
6. Hardangerjøkulen	45
7. Storbreen	52
8. Hellstugubreen	55
9. Gråsubreen	58
10. Engabreen	61
11. Langfjordjøkelen	69
12. Glacier length change	74
13. References	79
Appendix A (Publications published in 2008)	i
Appendix B (Mass balance measurements in Norway - an overview)	ii
Appendix C (Mass balance measurements in Norway - annual results)	iii

Preface

This report is a new volume in the series "Glaciological investigations in Norway", which has been published since 1963.

The report is based on investigations of several Norwegian glaciers. Measurements of mass balance, glacier length change, glacier velocity, meteorology and other glaciological investigations are presented. Most of the investigations were ordered by private companies and have been published previously as reports to the respective companies. The annual results from mass balance and glacier length changes are also reported to the World Glacier Monitoring Service (WGMS) in Switzerland.

The report is published in English with a summary in Norwegian. The purpose of this report is to provide a joint presentation of the investigations and calculations made mainly by NVEs Section for Glaciers and Environmental Hydrology during 2008. The chapters are written by different authors with different objectives, but are presented in a uniform format. The individual authors hold the professional responsibility for the contents of each chapter. The fieldwork and the calculations are mainly the result of co-operative work amongst the personnel at NVE.

Bjarne Kjølmoen was editor and Miriam Jackson made many corrections and improvements to the text.

Oslo, April 2009

Morten Johnsrud
Director,
Hydrology Department

Thomas Skaugen
Head of section,
Section for Glaciers and
Environmental Hydrology

Summary

Mass balance

Mass balance investigations were performed on fourteen glaciers in Norway in 2008. Twelve of these glaciers are in southern Norway and two are in northern Norway.

The winter balance was greater than average for all measured glaciers in southern Norway. In northern Norway the winter balance was lower than average on both Engabreen and Langfjordjøkelen.

The summer balance was approximately average at the glaciers in southern Norway. In northern Norway, Langfjordjøkelen had the lowest summer balance since measurements started in 1989.

In southern Norway the net balance was positive for eight of twelve measured glaciers. Blomstølskardsbreen (+1.3 m) and Nigardsbreen (+1.1 m) had the greatest surplus. In northern Norway, Langfjordjøkelen had the twelfth successive year of deficit.

Glacier length change

Glacier length changes were measured at 24 glaciers in southern Norway and eight glaciers in northern Norway in 2008. Twenty four of the glacier outlets had a retreat in length, five were unchanged and three outlets had an advance. Fåbergstølsbreen and Brenndalsbreen, both outlets from Jostedalbreen, showed retreats of between 50 and 60 metres. Bondhusbreen, an outlet from Folgefonna, had a retreat of 50 metres.

Sammendrag

Massebalanse

I 2008 ble det utført massebalansemålinger på 14 breer i Norge – tolv i Sør-Norge og to i Nord-Norge.

Vinterbalansen ble større enn gjennomsnittet på samtlige målte breer i Sør-Norge. I Nord-Norge ble vinterbalansen mindre enn gjennomsnittet på både Engabreen og Langfjordjøkelen.

Sommerbalansen ble omtrent som gjennomsnittet for breene i Sør-Norge. I Nord-Norge fikk Langfjordjøkelen den minste sommerbalansen som er målt siden målingene startet i 1989.

I Sør-Norge ble det positiv nettobalanse på åtte av tolv målte breer. Størst overskudd fikk Blomstølskardsbreen (1,3 m) og Nigardsbreen (1,1 m). I Nord-Norge fikk Langfjordjøkelen underskudd for tolvte året på rad.

Lengdeendringer

Lengdeendringer ble målt på 24 breer i Sør-Norge og åtte breer i Nord-Norge i 2008. Tjuefire av breutløperne hadde tilbakegang, fem var uendret og tre hadde framgang. Fåbergstølsbreen og Brenndalsbreen, begge utløpere fra Jostedalsbreen, hadde tilbakegang på mellom 50 og 60 m. Bondhusbreen, en utløper fra Folgefonna, smeltet tilbake 50 m.

1. Glacier investigations in Norway in 2008

1.1 Mass balance

Studies of mass balance include measurements of accumulated snow (winter balance) during the winter season, and measurements of snow and ice removed by melting (summer balance) during the summer season. The difference between these two parameters gives the net balance. If the winter balance is greater than the summer balance, the net balance is positive and the glacier increases in volume. Alternatively, if the melting of snow and ice during the summer is larger than the winter balance, the net balance is negative and the ice volume decreases.

Method

The method used to measure mass balance is the same as used in previous years. With the experience gained from many years of measurements, the measurement network was simplified on individual glaciers at the beginning of the 1990s, without affecting the accuracy of the resulting balance calculations or the final results.

Winter balance

The winter balance is normally measured in April or May by probing to the previous year's summer surface along approximately the same profile each year. Stake readings are used to verify the probings where possible. Since the stakes can disappear during particularly snow-rich winters, and since it is often difficult to distinguish the summer surface (S.S.) by probing alone, snow coring is also used to confirm the probing results. Snow density is measured in pits at one or two locations at different elevations on each glacier.

Summer and net balance

Summer and net balances are obtained from stake measurements, usually performed in September or October. Below the glacier's equilibrium line the net balance is negative, meaning that more snow and ice melts during a given summer than accumulates during the winter. Above the equilibrium line, in the accumulation area, the net balance is positive. Based on past experience, snow density of the remaining snow in the accumulation area is typically assumed to be 0.60 g/cm^3 . After especially cold summers, or if there is more snow than usual remaining at the end of the summer, snow density is either measured using snow-cores or is assumed to be 0.65 g/cm^3 . The density of melted firn is, depending on the age, assumed to be between 0.65 and 0.80 g/cm^3 . The density of melted ice is taken as 0.90 g/cm^3 .



Figure 1-1
Ice-covered tower at Engabreen, Svartisen in March 2008. Photo: Hallgeir Elvehøy.

Stratigraphic method

The mass balance is usually calculated using the traditional stratigraphic method (Østrem and Brugman 1991), which means the balance between two successive “summer surfaces” (i.e. surface minima). Consequently, the measurements describe the state of the glacier *after* the end of melting and *before* fresh snow has fallen. On some occasions ablation *after* the final measurements in September/October can occur. Strictly speaking, this ablation should be included in that year’s summer balance. However, measuring and calculating this additional ablation cannot be done until the following winter or spring. Thus, it is counted as a negative contribution to the next year’s winter balance.

Accuracy

The accuracy of the mass balance measurements depends on several factors. The accuracy of the winter balance is influenced mainly by the accuracy of the point measurements (soundings, core drillings, stakes, towers and density pit) and how representative they are. The smoothness of the snow layer is also of importance. The accuracy of soundings and core drillings depends on the number of point measurements, the certainty of identifying the summer surface and the implementation of the measurements (e.g. if the probe penetrates vertically through the snow pack). Overall, the accuracy of winter balance decreases with increasing snow depth.

The accuracy of summer balance is dependent on the number of ablation stakes, the height distribution, how representative they are and on the state of the stakes. Sources of error can be stakes sinking or tilting to one side.

The accuracy of the net balance is dependent on all the factors mentioned above.

As the mass balance is measured and calculated, it is very difficult to quantify the accuracy of the individual factors. The determined values of accuracy are therefore based on a subjective estimate.

Mass balance program

In 2008 mass balance measurements were performed on 14 glaciers in Norway - 12 in southern Norway and 2 in northern Norway. In southern Norway, 6 of the glaciers have been measured for 46 consecutive years or more. They constitute a west-east profile extending from the maritime Ålfotbreen glacier with an average winter balance of 3.7 m water equivalent to the continental Gråsusbreen with an average winter balance of 0.8 m w.e. Storbreen in Jotunheimen has the longest series of all glaciers in Norway with 60 years of measurements, while Engabreen at Svartisen has the longest series (39 years) in northern Norway. The location of the glaciers investigated is shown in Figure 1-2. A comprehensive review of the glacier mass balance and length measurements in Norway is given in Andreassen et al. (2005).

In the following chapters mass balance studies performed on Norwegian glaciers in 2008 are reported.

The mass balance (winter, summer and net balance) is given both in volume (m^3 water) and specific water equivalent for each 50 or 100 m height interval. The results are presented in tables and diagrams. All diagrams have the same ratio between units on the x- and y-axes in order to make comparison straightforward. Finally, histograms showing the complete mass balance results for each glacier are presented.

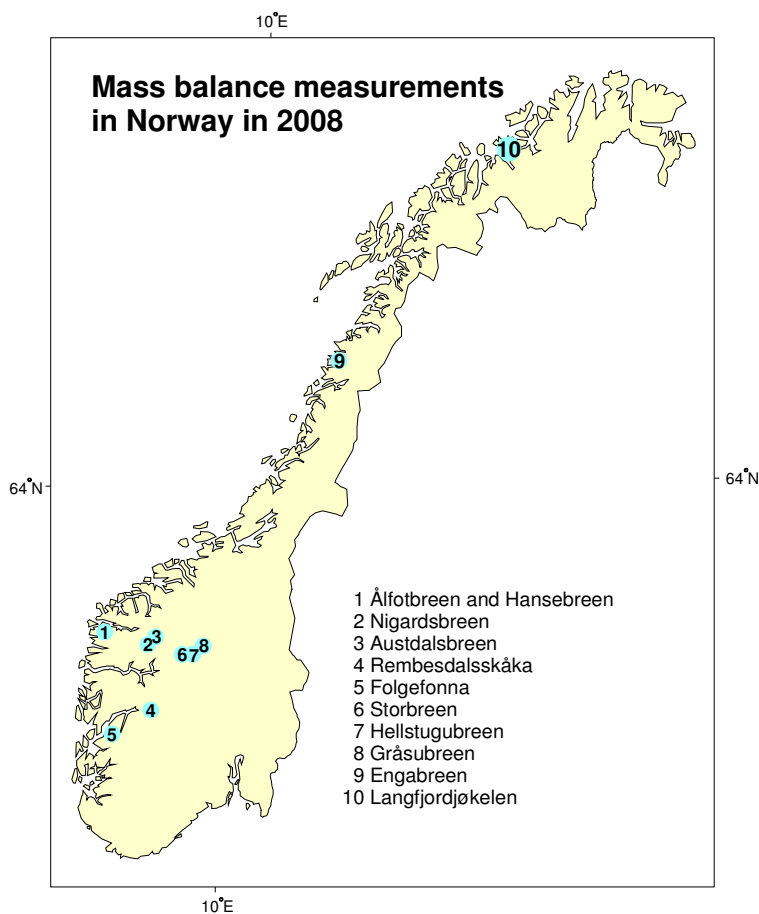


Figure 1-2
Location of the glaciers at which mass balance studies were performed in 2008.

Weather conditions and mass balance results

Wintry weather

The 2007/2008 winter season was mild and snow-rich in southern Norway. In northern Norway the winter was also mild, but snow conditions were normal. However, the winter season in southern Norway started with a dry October and November, but the following winter months were snow-rich, particularly January and February. Some parts of northern Norway had heavy snowfall in December and February.

Snow accumulation and winter balance

The winter balance was greater than average at all measured glaciers in southern Norway. The long-term (20 years of measurements or more) glaciers in western Norway had results of 108 to 126 % of their average winter balance. Nigardsbreen had the greatest relative winter balance with 126 % (3.0 m w.e.). The glaciers in Jotunheimen had between 125 and 139 % of average. In northern Norway, Engabreen had 96 % of average, and Langfjordjøkelen in western Finnmark had the fourth lowest winter balance (78 %) since measurements started in 1989.

Summer weather

The summer season in 2008 was slightly warmer than normal in southern Norway. June was rather cool, but July and August were warmer than normal. In northern Norway, the summer was cooler than normal in the northernmost parts.

Ablation and summer balance

The summer balance was about average at the glaciers in southern Norway. The long-term glaciers in western Norway had summer balances between 92 and 108 % of their average. The glaciers in Jotunheimen had between 77 and 109 % of their average. In northern Norway, Engabreen had summer balance slightly above average, while Langfjordjøkelen had the lowest summer balance ever measured.

Net balance

In southern Norway net balance was positive for eight of twelve measured glaciers in 2008. The greatest surplus was measured at Blomstølskardsbreen (+1.3 m w.e.) and Nigardsbreen (+1.1 m w.e.). The three measured glaciers in Jotunheimen were all approximately in balance. In northern Norway, Engabreen had a slight surplus, while Langfjordjøkelen had the twelfth successive year with deficit.

The results from the mass balance measurements in Norway in 2008 are shown in Table 1-1. Winter (\mathbf{b}_w), summer (\mathbf{b}_s) and net balance (\mathbf{b}_n) are given in metres water equivalent (m w.e.) smoothly distributed over the entire glacier surface. The figures in the **% of average** column show the current results in percent of the average for the previous years (minimum eight years of measurements). The net balance results are compared with the mean net balance in the same way. **ELA** is the equilibrium line altitude (m a.s.l.) and **AAR** is the accumulation area ratio (%).

Table 1-1
Review of the results from mass balance measurements performed in Norway in 2008. The glaciers in southern Norway are listed from west to east.

<i>Glacier</i>	<i>Period</i>	<i>Area (km²)</i>	<i>Altitude (m a.s.l.)</i>	<i>b_w (m)</i>	<i>% of average</i>	<i>b_s (m)</i>	<i>% of average</i>	<i>b_n (m)</i>	<i>b_n middle</i>	<i>ELA</i>	<i>AAR %</i>
Ålftobreen	1963-08	4.5	903-1382	4.04	108	-3.35	94	0.69	0.17	1130	79
Hansebreen	1986-08	3.1	930-1327	3.90	113	-3.65	92	0.25	-0.49	1125	64
Svelgjabreen	2007-08	22.5	832-1636	3.65	-	-2.88	-	0.77	-	1225	75
Blomstølskardsbreen	2007-08	22.8	1013-1636	3.69	-	-2.36	-	1.33	-	1260	86
Breidablikkbrea	1963-68	3.9	1219-1660						-0.19		
	2003-08	3.4	1234-1651	2.71	¹⁾ 117	-2.96	¹⁾ 99	-0.25	¹⁾ -0.65	1505	46
Gråfjellsbrea	1964-68	9.4	1039-1660						0.20		
	1974-75										
	2003-08	8.4	1049-1651	2.72	²⁾ 112	-2.80	²⁾ 102	-0.08	²⁾ -0.33	1580	59
Nigardsbreen	1962-08	47.8	320-1960	3.01	126	-1.92	96	1.09	0.39	1325	91
Austdalsbreen	1988-08	11.8	1200-1757	2.55	116	³⁾ -2.62	105	-0.07	-0.28	1420	71
Rembesdalsskåka	1963-08	17.1	1020-1865	2.61	124	-2.16	108	0.45	0.10	1610	82
Storbreen	1949-08	5.4	1390-2100	1.99	139	-1.88	109	0.11	-0.29	1770	51
Hellstugubreen	1962-08	3.0	1480-2210	1.41	129	-1.47	100	-0.06	-0.38	1880	57
Gråsubreen	1962-08	2.3	1830-2290	0.95	125	-0.86	77	0.09	-0.36	Undef.	-
Engabreen	1970-08	38.7	89-1574	2.81	96	-2.50	107	0.31	0.60	1093	77
Langfjordjøkelen	1989-93										
	1996-08	3.2	280-1050	1.67	⁴⁾ 77	-2.02	⁴⁾ 67	-0.35	⁴⁾ -0.87	835	53

¹⁾ Calculated for the measured periods 1963-68 and 2003-07

²⁾ Calculated for the measured periods 1964-68, 1974-75 and 2003-07

³⁾ Contribution from calving amounts to 0.31 m for b_s

⁴⁾ Calculated for the measured periods 1989-93 and 1996-2007

Figure 1-3 gives a graphical presentation of the mass balance results in southern Norway for 2008. The west-east gradient is evident for both winter and summer balances.

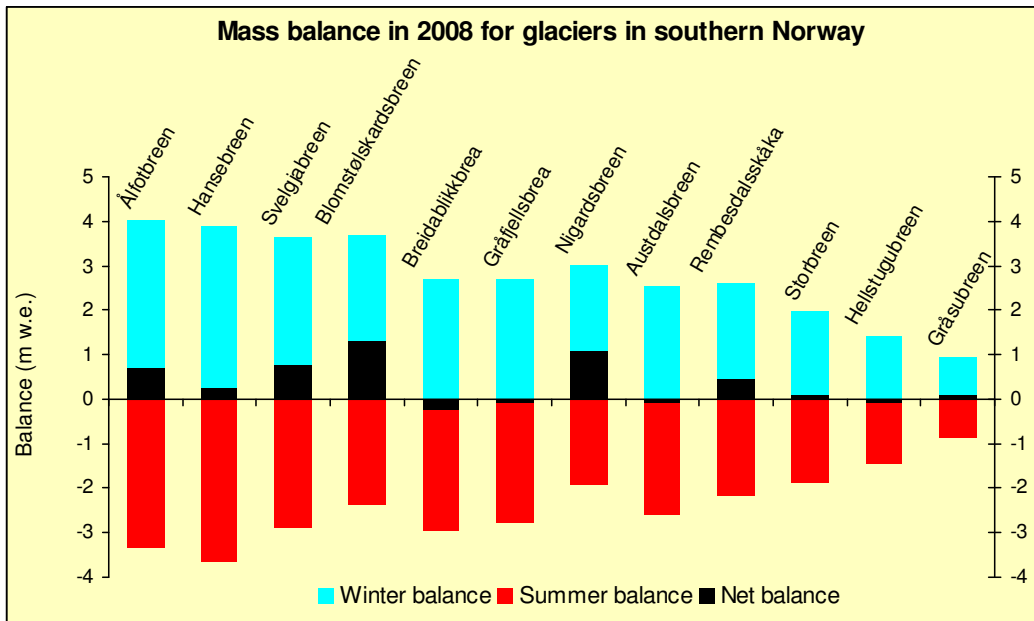


Figure 1-3
Mass balance 2008 in southern Norway. The glaciers are listed from west to east.

The cumulative net balance for glaciers in southern Norway with long-time series during the period 1963-2008 is shown in Figure 1-4. The maritime glaciers – Ålfotbreen, Nigardsbreen and Rembesdalsskåka showed a marked increase in volume during the period 1989-95. The surplus was mainly the result of several winters with heavy snowfall. The results for 2008 also show a positive net balance for seven of twelve measured glaciers in southern Norway.

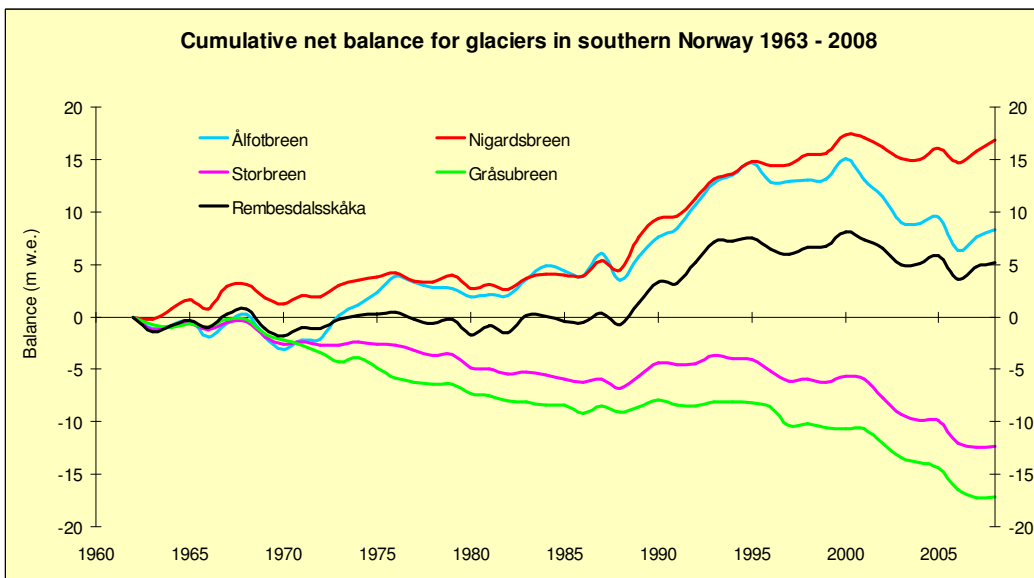


Figure 1-4
Cumulative net balance for Ålfotbreen, Nigardsbreen, Rembesdalsskåka (Hardangerjøkulen), Storbreen and Gråsubreen during the period 1963-2008.

1.2 Other investigations

Glacier length change measurements were performed at 32 glaciers in Norway in 2008. Some of the glaciers have a measurement series going back to about 1900. The length changes are described in a separate chapter (chap. 12).

Glacier dynamics (velocity) have been studied at Austdalsbreen since 1987 (chap. 5). The measurements continued in 2008.

Meteorological observations have been performed at Hardangerjøkulen (chap. 6) and Engabreen (chap. 10).

Svartisen Subglacial Laboratory was initiated in 1992 and has since been used by researchers from several different countries (Jackson 2000). An overview of activities in the laboratory is given in chapter 10.

2. Ålfotbreen (Bjarne Kjøllmoen)

Ålfotbreen ice cap (61°45'N, 5°40'E) has an area of about 17 km², and is both the westernmost and the most maritime glacier in Norway. Mass balance studies have been carried out on two adjacent north-facing outlet glaciers - Ålfotbreen (4.5 km².) and Hansebreen (3.1 km²). The westernmost of these two has been the subject of mass balance investigations since 1963, and has always been reported as Ålfotbreen. The adjacent glacier to the east of Ålfotbreen has been given the name Hansebreen, and has been measured since 1986. None of the outlet glaciers from the icecap are given names on the official maps. Ålfotbreen, including its component parts and surroundings, is shown in Figure 2-1.

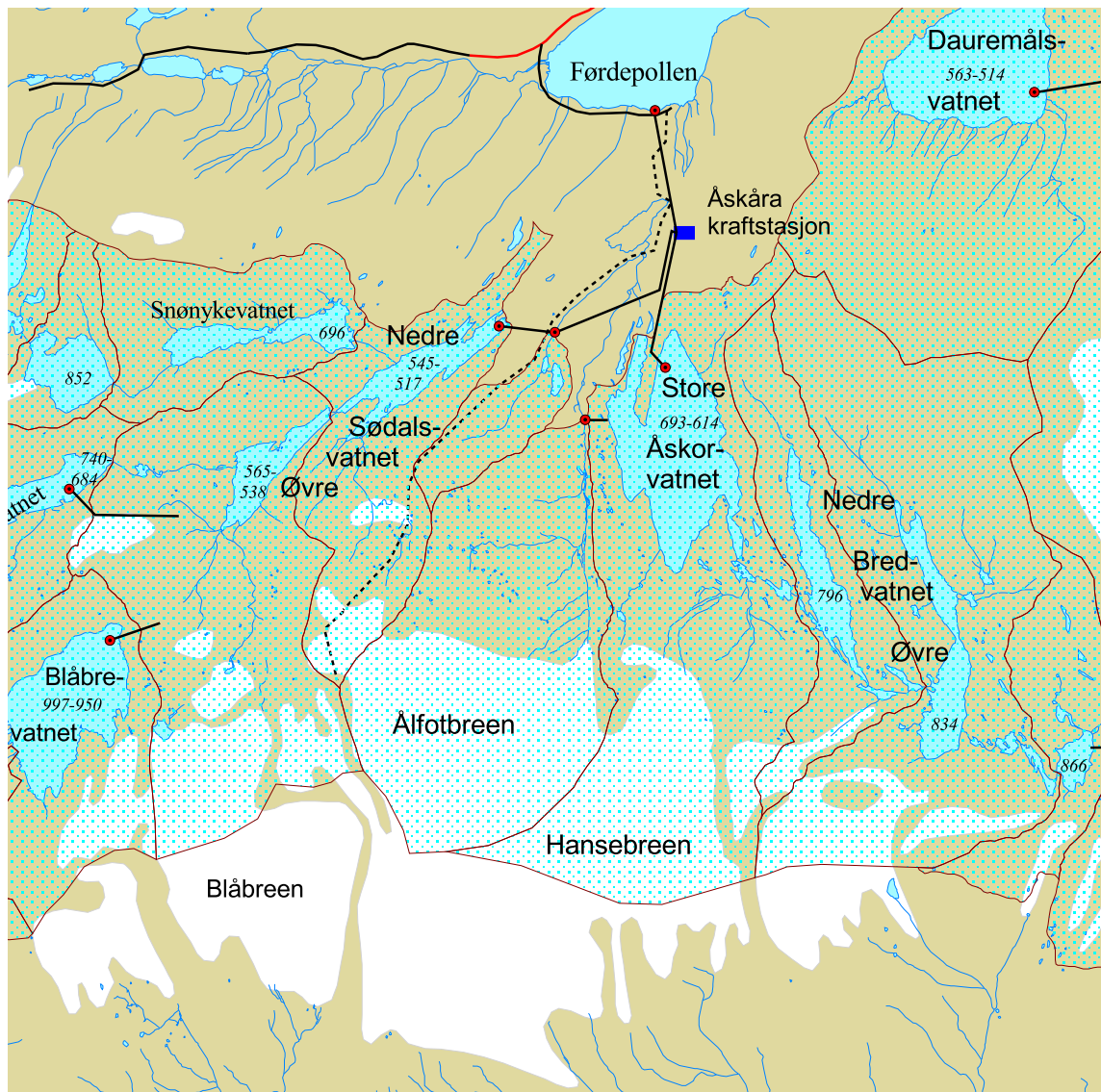


Figure 2-1
Ålfotbreen ice cap and surrounding area, showing the two north-facing glaciers Ålfotbreen and Hansebreen at which mass balance studies are performed.

2.1 Mass balance 2008

Fieldwork

Snow accumulation measurements

Snow accumulation measurements were performed on 21st and 22nd April. The calculation of winter balance at Ålfotbreen and Hansebreen is based on (Fig. 2-2):

- Measurements of stake replacements and older stakes that appeared during the melt season at positions 12 (960 m a.s.l.), 13 (1100 m a.s.l.), 45 (1180 m a.s.l.), 37 (1225 m a.s.l.) and 28 (1240 m a.s.l.) on Ålfotbreen. Measurements of stake replacements and older stakes that appeared during the melt season in positions 50 (1020 m a.s.l.), 60 (1070 m a.s.l.) and 80 (1125 m a.s.l.) on Hansebreen.
- 46 snow depth soundings between 930 and 1380 m elevation on Ålfotbreen, and 43 snow depth soundings between 955 and 1310 m elevation on Hansebreen. The snow depth at Ålfotbreen was generally between 8 and 10 m, while measurements at Hansebreen showed snow depths between 7 and 10 m. In spite of deep snow the summer surface (SS) could be identified easily on both glaciers.
- Snow density was measured down to 6.2 m depth (SS at 7.8 m) at stake position 37.

The location of tower, stakes, snow pit and soundings are shown in Figure 2-2.

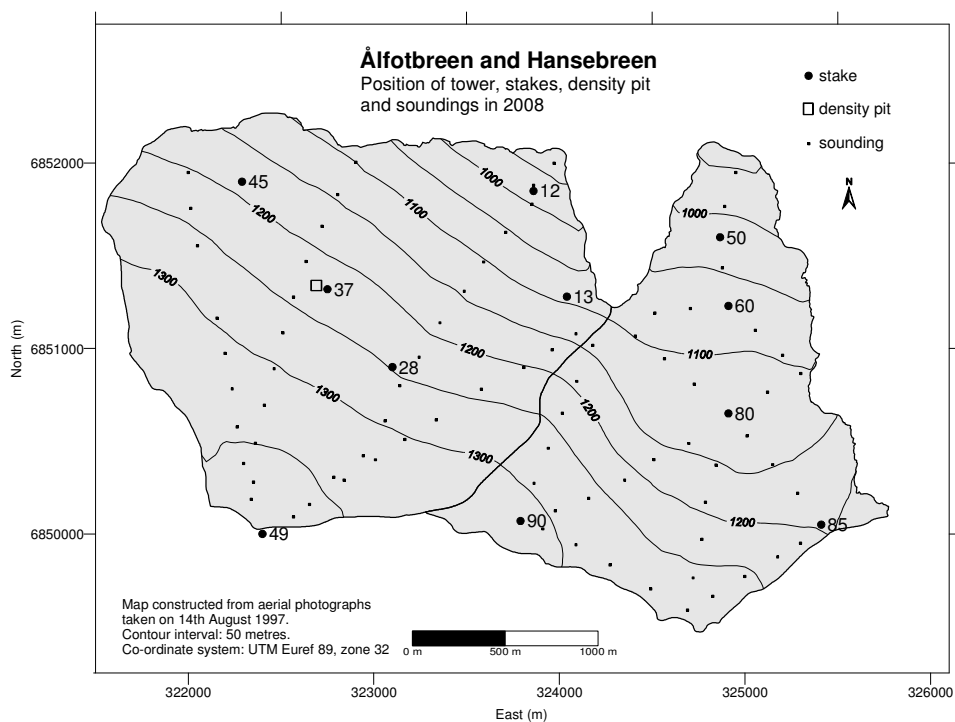


Figure 2-2
Location of stakes, soundings and snow pit at Ålfotbreen (left) and Hansebreen (right) in 2008.

Ablation measurements

Ablation was measured on 31st October. The net balance was measured directly at stakes in six different positions on Ålfotbreen and five positions on Hansebreen. There was

between 2 and 3 m of snow remaining in the upper areas of the glacier. At the time of the ablation measurements between 1 and 1.5 m of fresh snow had fallen.



Figure 2-3
Measurement and maintenance of stake 49 on Ålfotbreen in August. Photo: Hallgeir Elvehøy.

Results

The calculations are based on a glacier map from 1997.

Winter balance

The calculation of winter balance is based on point measurements of snow depth (stakes and probings) and on measurement of snow density in one location. There was no melting after the final measurements in October 2007.

A density profile was modelled from the snow density measured at 1225 m a.s.l. The mean snow density of 7.8 m snow was 0.48 g/cm^3 . The density model was assumed to be representative for both Ålfotbreen and Hansebreen, and all snow depths were converted to water equivalents using this model.

The calculation of winter balance was performed by plotting the point measurements (water equivalents) in a diagram. A curve was drawn based on a visual evaluation (Fig. 2-5) and a mean value for each 50 m height interval was estimated (Tab. 2-1).

Winter balance at Ålfotbreen in 2008 was $4.0 \pm 0.2 \text{ m w.e.}$, corresponding to a volume of $18 \pm 1 \text{ mill. m}^3$ of water. The result is 108 % of the mean winter balance for 1963-2007, and 102 % of the mean for 1986-2007 (same measurement period as Hansebreen).

The winter balance at Hansebreen was $3.9 \pm 0.2 \text{ m w.e.}$, corresponding to a volume of $12 \pm 1 \text{ mill. m}^3$ of water. The result is 113 % of the mean value.

The winter balance was also calculated using a gridding method based on the aerial distribution of the snow depth measurements (Fig. 2-4). Water equivalents for each cell in a $100 \times 100 \text{ m}$ grid were calculated and summarised. Using this method, which is a

control of the traditional method, gave 4.0 m w.e. for Ålfotbreen and 3.8 m w.e. for Hansebreen.

Summer balance

The density of remaining snow was estimated as 0.60 g/cm^3 . The density of one year old melted firn was estimated as 0.65 g/cm^3 , while the density of ice was taken as 0.90 g/cm^3 .

The summer balance at Ålfotbreen was measured and calculated directly at stakes in six different positions. The calculated values increased from 2.3 m w.e. at the glacier summit (1380 m a.s.l.) to 5.2 m on the tongue (960 m a.s.l.). Based on estimated density and stake measurements the summer balance for Ålfotbreen was calculated as $-3.4 \pm 0.3 \text{ m w.e.}$, corresponding to $-15 \pm 1 \text{ mill. m}^3$ of water. This result is 94 % of the average between 1963 and 2007, and 88 % of the average between 1986 and 2007.

The summer balance for Hansebreen was measured and calculated at stakes in five different positions. It increased from -2.8 m w.e. at 1310 m elevation to -4.9 m w.e. at 1020 m elevation. Based on the stake measurements and the estimated density, the summer balance was calculated as $-3.6 \pm 0.3 \text{ m w.e.}$ or $-11 \pm 1 \text{ mill. m}^3$ of water. The result is 92 % of the mean value.

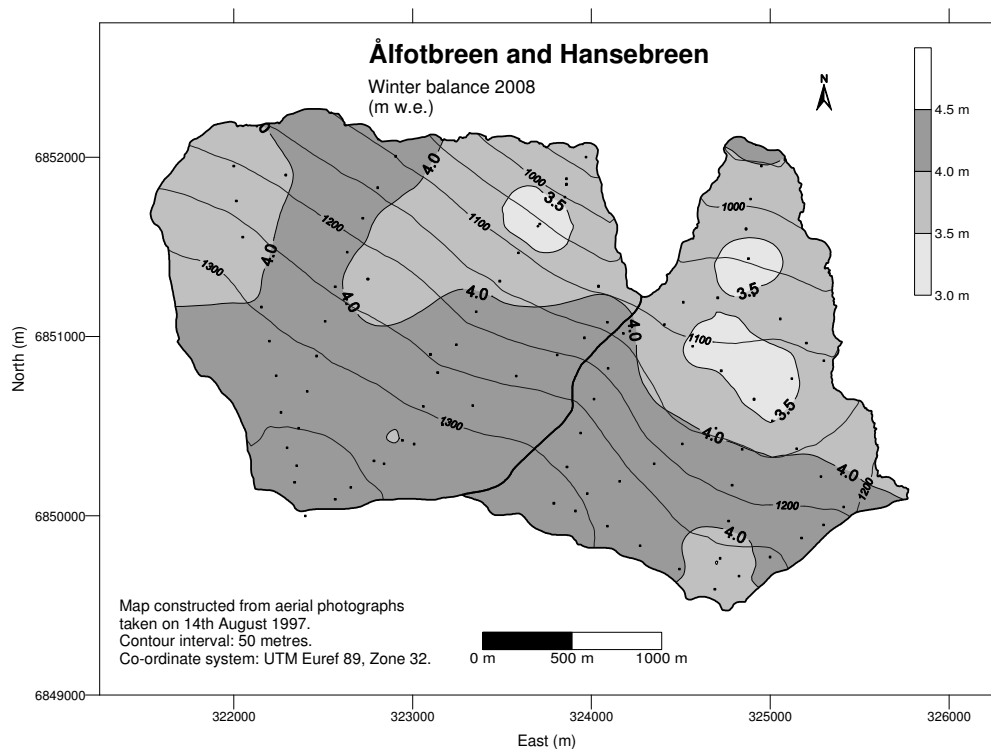


Figure 2-4
Winter balance at Ålfotbreen and Hansebreen in 2008 interpolated from 98 snow depth measurements, shown by (-).

Net balance

The net balance at Ålfotbreen for 2008 was positive, at $+0.7 \pm 0.4 \text{ m w.e.}$, or a surplus of $3 \pm 2 \text{ mill. m}^3$ of water. The mean net balance between 1963 and 2007 is $+0.17 \text{ m w.e.}$, and $+0.15 \text{ m w.e.}$ during 1986-2007. Since measurements started at Ålfotbreen in 1963 the cumulative net balance is $+8.3 \text{ m w.e.}$ Since 1996, however, the net balance shows a deficit of -6.4 m w.e.

The net balance at Hansnebreen was calculated as $+0.3 \pm 0.4$ m w.e., or a surplus of 1 ± 1 mill. m^3 of water. The mean value for the period 1986-2007 is -0.49 m w.e. After six successive years with negative net balance this is the second year with surplus on Hansnebreen since 2000. Since measurements began in 1986 the cumulative net balance is -10.5 m w.e.

According to Figure 2-5 the Equilibrium Line Altitude (ELA) lies at 1130 m a.s.l. on Ålfotbreen and at 1125 m a.s.l. on Hansnebreen. Consequently, the AAR is 79 % and 64 % respectively.

The mass balance results are shown in Table 2-1. The corresponding curves for specific and volume balance are shown in Figure 2-5. The historical mass balance results are presented in Figure 2-6.

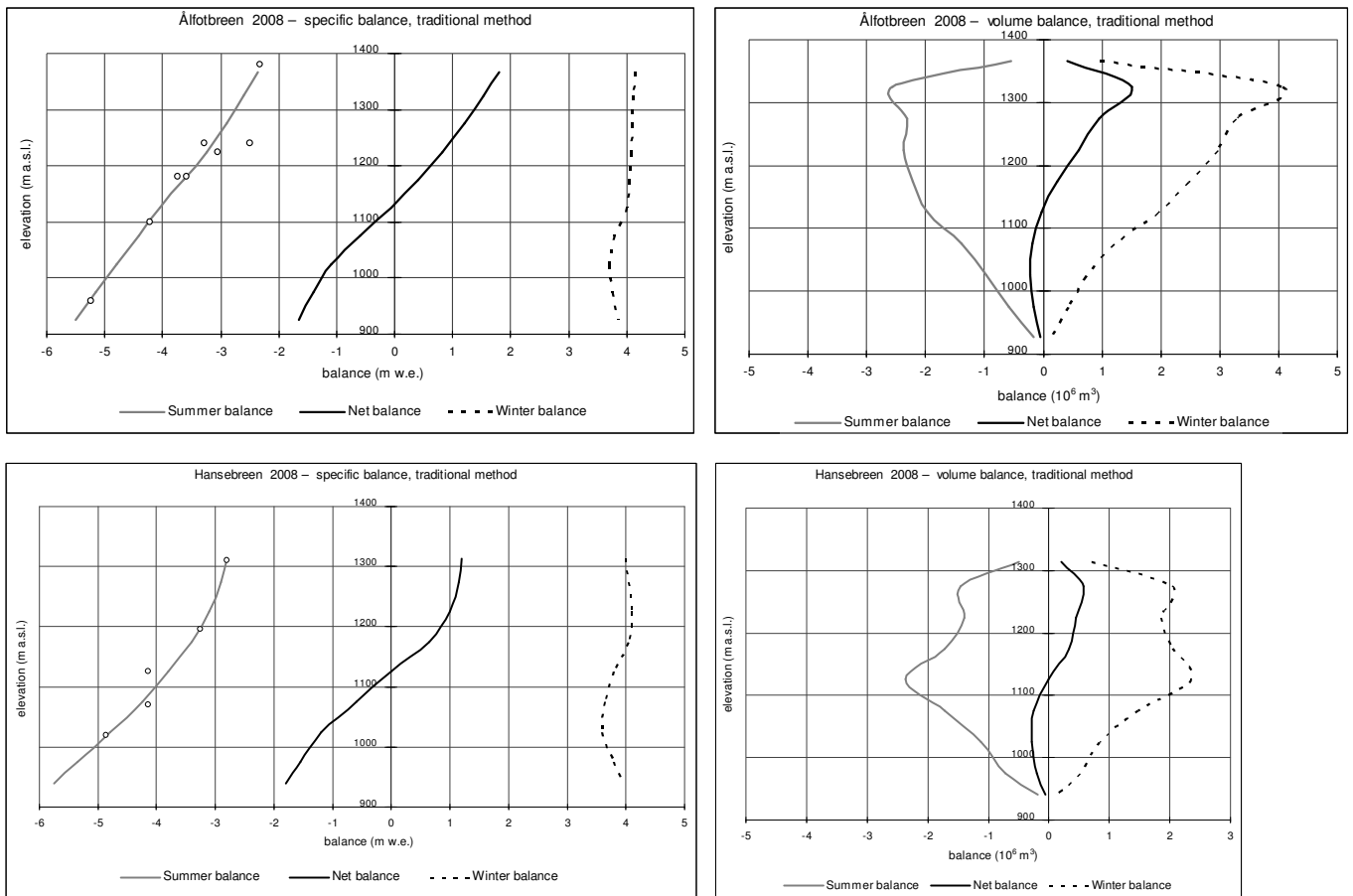


Figure 2-5
Mass balance diagram for Ålfotbreen (upper) and Hansnebreen (lower) in 2008 showing altitudinal distribution of specific (left) and volumetric (right) winter, summer and net balance. Specific summer balance at each stake is shown (○).

Table 2-1
Winter, summer and net balances for Ålfotbreen (upper) and Hansebreen (lower) in 2008.

Mass balance Ålfotbreen 2007/08 – traditional method							
Altitude (m a.s.l.)	Area (km ²)	Winter balance		Summer balance		Net balance	
		Measured 21st Apr 2008		Measured 31st Oct 2008		Summer surfaces 2007 - 2008	
		Specific (m w.e.)	Volume (10 ⁶ m ³)	Specific (m w.e.)	Volume (10 ⁶ m ³)	Specific (m w.e.)	Volume (10 ⁶ m ³)
1350 - 1382	0.23	4.15	1.0	-2.35	-0.5	1.80	0.4
1300 - 1350	0.98	4.13	4.1	-2.60	-2.6	1.53	1.5
1250 - 1300	0.80	4.10	3.3	-2.90	-2.3	1.20	1.0
1200 - 1250	0.73	4.08	3.0	-3.25	-2.4	0.83	0.6
1150 - 1200	0.61	4.05	2.5	-3.65	-2.2	0.40	0.2
1100 - 1150	0.49	4.00	1.9	-4.05	-2.0	-0.05	0.0
1050 - 1100	0.32	3.80	1.2	-4.40	-1.4	-0.60	-0.2
1000 - 1050	0.20	3.70	0.7	-4.80	-1.0	-1.10	-0.2
950 - 1000	0.11	3.75	0.4	-5.15	-0.6	-1.40	-0.2
903 - 950	0.03	3.85	0.1	-5.50	-0.2	-1.65	-0.1
903 - 1382	4.50	4.04	18.2	-3.35	-15.1	0.68	3.1

Mass balance Hansebreen 2007/08 – traditional method							
Altitude (m a.s.l.)	Area (km ²)	Winter balance		Summer balance		Net balance	
		Measured 21st Apr 2008		Measured 31st Oct 2008		Summer surface 2007 - 2008	
		Specific (m w.e.)	Volume (10 ⁶ m ³)	Specific (m w.e.)	Volume (10 ⁶ m ³)	Specific (m w.e.)	Volume (10 ⁶ m ³)
1300 - 1327	0.18	4.00	0.71	-2.80	-0.49	1.20	0.21
1250 - 1300	0.50	4.05	2.03	-2.90	-1.45	1.15	0.58
1200 - 1250	0.45	4.10	1.85	-3.10	-1.40	1.00	0.45
1150 - 1200	0.51	4.05	2.05	-3.40	-1.72	0.65	0.33
1100 - 1150	0.62	3.80	2.36	-3.80	-2.36	0.00	0.00
1050 - 1100	0.40	3.65	1.47	-4.25	-1.71	-0.60	-0.24
1000 - 1050	0.23	3.60	0.84	-4.80	-1.12	-1.20	-0.28
950 - 1000	0.13	3.80	0.51	-5.35	-0.71	-1.55	-0.21
930 - 950	0.03	3.95	0.13	-5.75	-0.19	-1.80	-0.06
930 - 1327	3.06	3.90	11.9	-3.65	-11.2	0.26	0.8

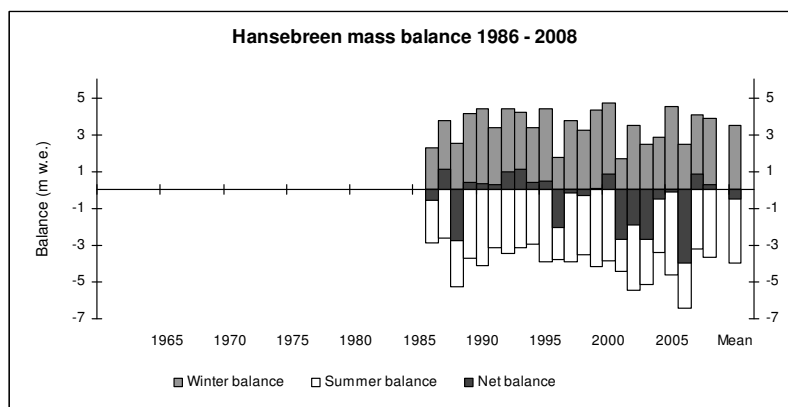
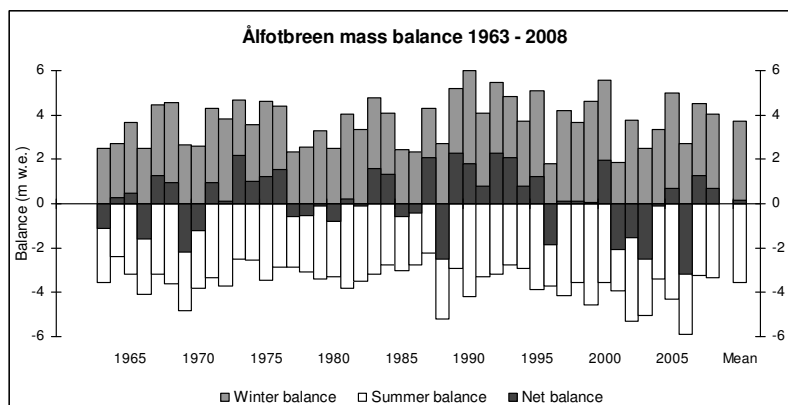


Figure 2-6
Mass balance at Ålfotbreen (upper) 1963-2008 and Hansebreen (lower) 1986-2008.

3. Folgefonna (Bjarne Kjøllmoen)

Folgefonna is situated in the south-western part of Norway between Hardangerfjorden to the west and the mountain plateau Hardangervidda to the east. It is divided into three separate ice caps - Northern, Middle and Southern Folgefonna. Southern Folgefonna is the third largest (161 km² in 2007) ice cap in Norway. In 2003 mass balance measurements began on two adjacent northwestward-facing outlet glaciers of Southern Folgefonna (60°4'N, 6°24'E) – Breidablikkbrea (3.4 km²) and Gråfjellsbrea (8.4 km²) (Fig. 3-1). In 2007 mass balance measurements began on two more outlet glaciers of Southern Folgefonna – the two adjacent southward-facing glaciers Svelgjabreen (22.5 km²) and Blomstølskardsbreen (22.8 km²).

Mass balance measurements were previously carried out at Breidablikkbrea during 1963-68 (Pytte, 1969) and at Gråfjellsbrea during the periods 1964-68 and 1974-75 (Wold and Hagen, 1977). The historical results are presented in Figure 3-4. Mass balance measurements were also carried out at Svelgjabreen/Blomstølskardsbreen (then called Blomsterskardsbreen) in 1971 (Tvede, 1973), and net balance only was measured in the period 1972-77.

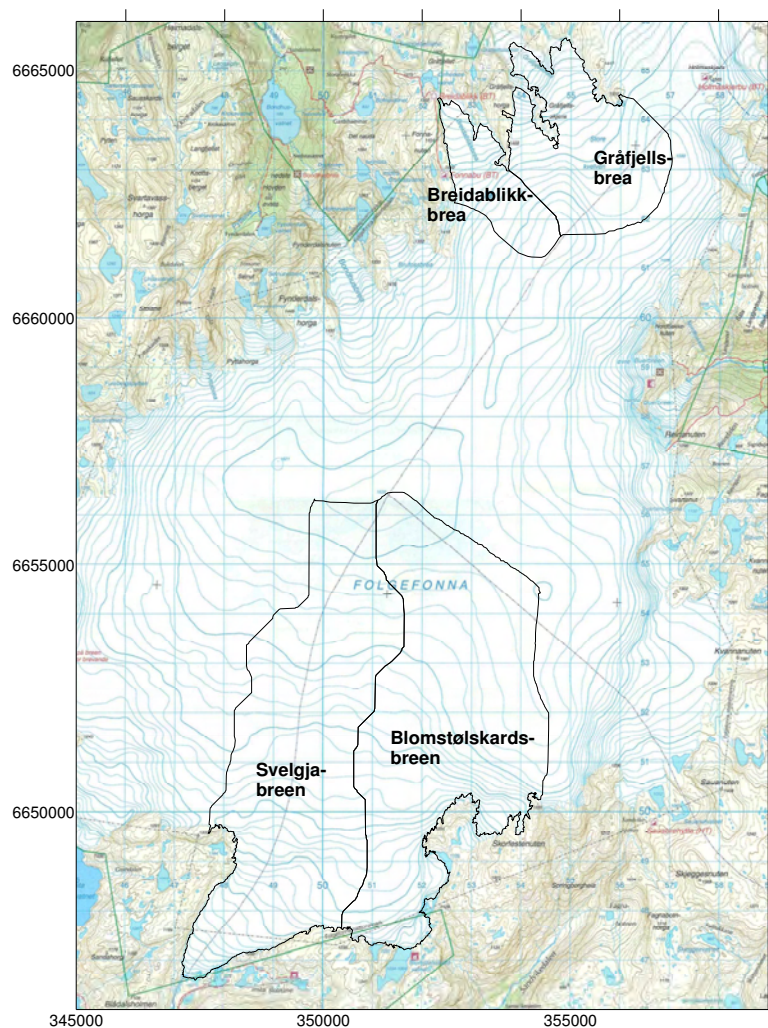


Figure 3-1 Southern Folgefonna with Breidablikkbrea and Gråfjellsbrea in the northwest and Svelgjabreen and Blomstølskardsbreen in the south.

3.1 Mass balance at Gråfjellsbrea and Breidablikkbrea in 2008

Fieldwork

Snow accumulation measurements

Snow accumulation measurements were performed on 22nd and 23rd April. The calculation of winter balance at Breidablikkbrea and Gråfjellsbrea is based on (Fig. 3-2):

- Measurement of stakes at positions 40 (1247 m a.s.l.), 47 (1420 m a.s.l.) and T60 (1641 m a.s.l.) on Breidablikkbrea and measurement of a stake in position 10 (1073 m a.s.l.), 15 (1267 m a.s.l.), 20 (1345 m a.s.l.), 25 (1474 m a.s.l.), 30 (1546 m a.s.l.) and T60 on Gråfjellsbrea. Measurements of stake replacements and older stakes that appeared during the melt season at position 55 and 56 (both 1564 m a.s.l.) on Breidablikkbrea.
- 48 snow depth soundings between 1247 and 1645 m a.s.l. on Breidablikkbrea, and 66 snow depth soundings between 1260 and 1641 m a.s.l. on Gråfjellsbrea. The sounding conditions were reasonable on both glaciers. However, the snow depth may be some uncertain in areas with snow remaining from winter 2007. Generally, the snow depth varied between 5 and 6 m.
- A core sample and snow density was measured down to the summer surface (5.4 m) at position 25 at Gråfjellsbrea.

The locations of stakes, density pit and soundings are shown in Figure 3-2.

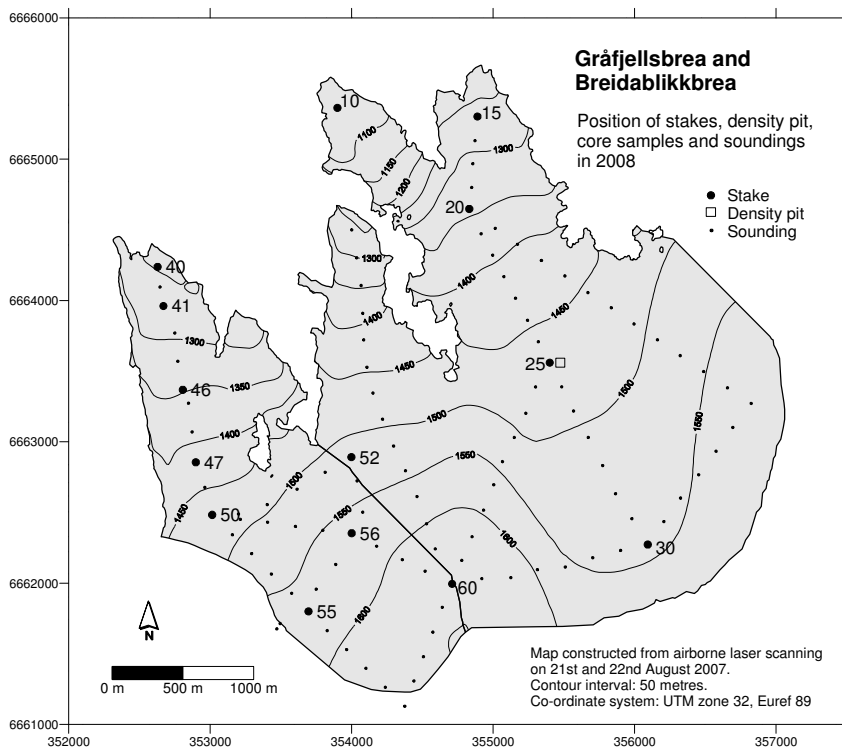


Figure 3-2
Location of stakes, soundings and density pit at Breidablikkbrea and Gråfjellsbrea in 2008.

Ablation measurements

Ablation was measured on 23rd September (Fig. 3-3). The net balance was measured at stakes in nine different positions on Breidablikkbrea and seven positions on Gråfjellsbrea. There was about 1 m of snow remaining in the upper areas of the glacier. No fresh snow had fallen at the time of the ablation measurements.

The glacier was visited again on 4th December. Some of the stakes were extended and the fresh snow layer was sounded. A comparison of the stake measurements and the probings showed that some melting had occurred after the ablation measurements in September. Between 5 and 20 cm melting had occurred at the stakes below 1350 m a.s.l.



Figure 3-3
Gråfjellsbrea photographed on
23rd September 2008.
Photo: Geir Johan Knudsen.

Results

The calculations are based on a glacier map from 2007.

Winter balance

The calculation of winter balance is based on point measurements of snow depth (stakes and soundings) and on measurement of snow density at one representative location. Soundings and stake measurements in December 2007 indicated some melting after the final measurements in September 2007. This melting was included in the 2007 summer balance.

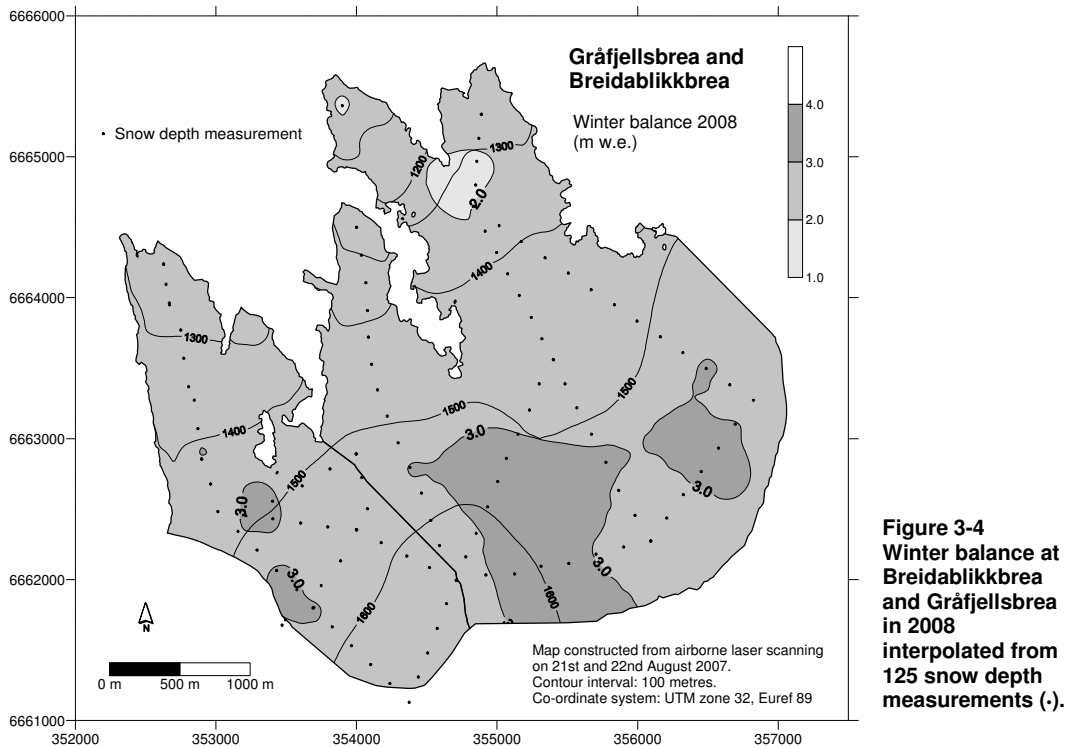
A density profile was modelled from the snow density measured at 1474 m a.s.l. The mean snow density of 5.4 m snow was 0.49 g/cm^3 . The density model was assumed to be representative for both Breidablikkbrea and Gråfjellsbrea, and all snow depths were converted to water equivalent using this model.

The calculation of winter balance was performed by plotting the point measurements (water equivalent) in a diagram. A curve was drawn based on visual evaluation (Fig. 3-5) and a mean value for each 50 m height interval was estimated (Tab. 3-1).

Winter balance at Breidablikkbrea in 2008 was $2.7 \pm 0.2 \text{ m w.e.}$, corresponding to a volume of $9 \pm 1 \text{ mill. m}^3$ of water. The result is 117 % of the average for the periods 1963-68 and 2003-07.

The winter balance at Gråfjellsbrea was 2.7 ± 0.2 m w.e., corresponding to a volume of 23 ± 1 mill. m^3 of water. This result is 112 % of the average for 1964-68, 1974-75 and 2003-07.

As verification, the winter balance was also calculated using a gridding method based on the aerial distribution of the snow depth measurements (Fig. 3-4). Water equivalents for each cell in a 100 x 100 m grid were calculated and summarised. This method gave results of 2.6 m w.e. for Breidablikkbrea and 2.7 m w.e. for Gråfjellsbrea.



Summer balance

When calculating the summer balance the density of remaining snow was estimated as 0.60 g/cm^3 . The density of melted firn was estimated as 0.65 g/cm^3 , and the density of melted ice was assumed to be 0.90 g/cm^3 .

The melting that occurred after the ablation measurement at the end of September 2008 is included in the summer balance for 2008. The additional melting is calculated to be 0.05-0.20 m w.e. at the elevation interval from 1347 to 1073 m a.s.l.

The summer balance at Breidablikkbrea was measured and calculated at nine stakes. The stake values increased from 2.0 m w.e. at the topmost stake to 4.3 m w.e. at the lowest stake position. Based on estimated density and stake measurements the summer balance was calculated as -3.0 ± 0.3 m w.e., corresponding to -10 ± 1 mill. m^3 of water. This is 99 % of the mean value for 1963-68 and 2003-07.

The summer balance for Gråfjellsbrea was measured and calculated at seven stakes. The stake values increased from 2.0 m w.e. at the topmost stake to 5.1 m w.e. at the lowest stake position. Based on the seven stakes and the estimated density the summer balance

was calculated as -2.8 ± 0.3 m w.e. or -24 ± 1 mill. m^3 of water. This is 102 % of the mean value for 1964-68, 1974-75 and 2003-07.

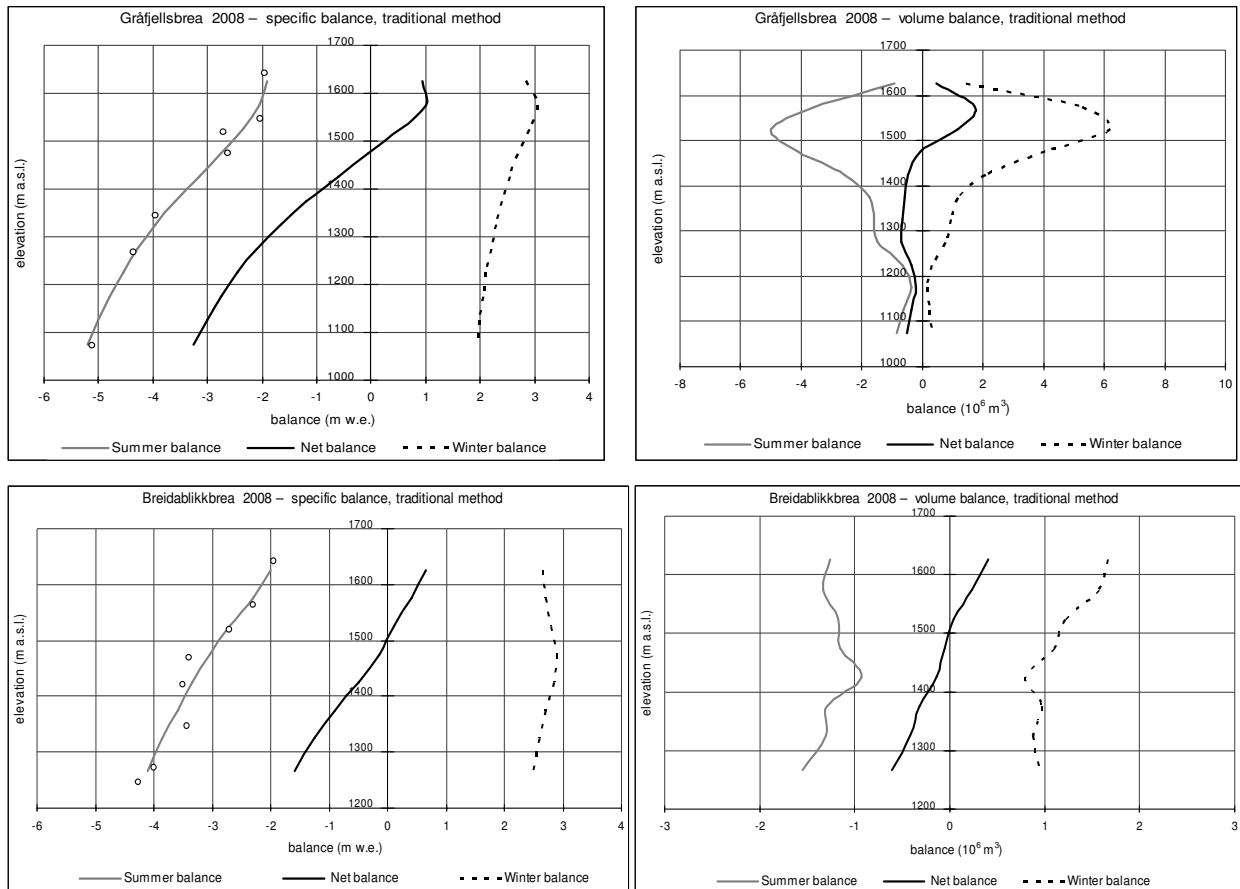


Figure 3-5
Mass balance diagram for Gråfjellsbrea (upper) and Breidablikkbrea (lower) in 2008 showing altitudinal distribution of specific (left) and volumetric (right) winter, summer and net balance. Specific summer balance at each stake is shown (○). Melting after the ablation measurements on 23rd September is included in the summer balance for 2008.

Net balance

The net balance at Breidablikkbrea for 2008 was calculated as -0.3 ± 0.4 m w.e. or a deficit of -1 ± 2 mill. m^3 of water. The mean net balance for 1963-68 and 2003-07 is -0.65 m w.e.

The net balance at Gråfjellsbrea was calculated as -0.1 ± 0.4 m w.e. or a deficit of -1 ± 2 mill. m^3 of water. The mean value for the years 1964-68, 1974-75 and 2003-07 is -0.33 m w.e.

As shown in Figure 3-5, the Equilibrium Line Altitude (ELA) lies at 1505 m a.s.l. on Breidablikkbrea and 1480 m a.s.l. on Gråfjellsbrea. Consequently, the Accumulation Area Ratio (AAR) is 46 % and 59 % respectively.

The mass balance results are shown in Table 3-1. The corresponding curves for specific and volume balance are shown in Figure 3-5. The historical mass balance results are presented in Figure 3-6.

Table 3-1
Winter, summer and net balances for Breidablikkbrea (upper) and Gráfjellsbrea (lower) in 2008.

Mass balance Breidablikkbrea 2007/08 – traditional method							
Altitude (m a.s.l.)	Area (km ²)	Winter balance		Summer balance		Net balance	
		Measured 22nd April 2008		Measured 23rd Sep 2008		Summer surfaces 2007 - 2008	
		Specific (m w.e.)	Volume (10 ⁶ m ³)	Specific (m w.e.)	Volume (10 ⁶ m ³)	Specific (m w.e.)	Volume (10 ⁶ m ³)
1600 - 1651	0.63	2.65	1.7	-2.00	-1.3	0.65	0.4
1550 - 1600	0.58	2.70	1.6	-2.30	-1.3	0.40	0.2
1500 - 1550	0.43	2.80	1.2	-2.70	-1.2	0.10	0.0
1450 - 1500	0.38	2.90	1.1	-3.05	-1.2	-0.15	-0.1
1400 - 1450	0.28	2.85	0.8	-3.35	-0.9	-0.50	-0.1
1350 - 1400	0.36	2.70	1.0	-3.60	-1.3	-0.90	-0.3
1300 - 1350	0.34	2.60	0.9	-3.85	-1.3	-1.25	-0.4
1234 - 1300	0.38	2.50	0.9	-4.10	-1.6	-1.60	-0.6
1234 - 1651	3.37	2.71	9.1	-2.96	-10.0	-0.26	-0.9

Mass balance Gráfjellsbrea 2007/08 – traditional method							
Altitude (m a.s.l.)	Area (km ²)	Winter balance		Summer balance		Net balance	
		Measured 22nd April 2008		Measured 23rd Sep 2008		Summer surfaces 2007 - 2008	
		Specific (m w.e.)	Volume (10 ⁶ m ³)	Specific (m w.e.)	Volume (10 ⁶ m ³)	Specific (m w.e.)	Volume (10 ⁶ m ³)
1600 - 1651	0.50	2.85	1.4	-1.90	-0.9	0.95	0.5
1550 - 1600	1.72	3.05	5.3	-2.05	-3.5	1.00	1.7
1500 - 1550	2.13	2.90	6.2	-2.35	-5.0	0.55	1.2
1450 - 1500	1.49	2.70	4.0	-2.75	-4.1	-0.05	-0.1
1400 - 1450	0.81	2.55	2.1	-3.15	-2.6	-0.60	-0.5
1350 - 1400	0.49	2.40	1.2	-3.60	-1.8	-1.20	-0.6
1300 - 1350	0.41	2.30	0.9	-3.95	-1.6	-1.65	-0.7
1250 - 1300	0.34	2.20	0.8	-4.30	-1.5	-2.10	-0.7
1200 - 1250	0.15	2.10	0.3	-4.55	-0.7	-2.45	-0.4
1150 - 1200	0.08	2.05	0.2	-4.80	-0.4	-2.75	-0.2
1100 - 1150	0.12	2.00	0.2	-5.00	-0.6	-3.00	-0.4
1049 - 1100	0.16	1.95	0.3	-5.20	-0.8	-3.25	-0.5
1049 - 1651	8.41	2.72	22.9	-2.80	-23.5	-0.08	-0.7

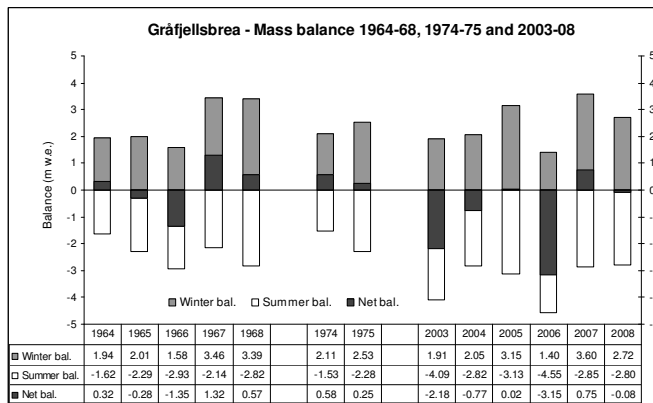
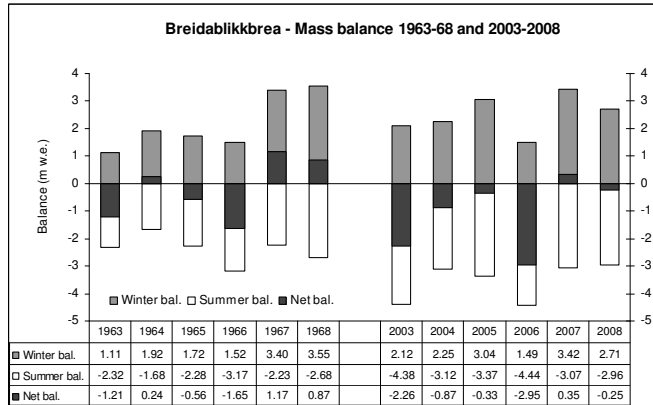


Figure 3-6
Winter, summer and net balance at Breidablikkbrea for the periods 1963-68 and 2003-08 (upper figure), and at Gráfjellsbrea for the periods 1964-68, 1974-75 and 2003-08 (lower figure).

3.2 Mass balance at Svelgjabreen and Blomstølskardsbreen in 2008

Fieldwork

Snow accumulation measurements

Snow accumulation measurements were performed on 21st and 22nd April. The calculation of winter balance at Svelgjabreen and Blomstølskardsbreen is based on (Fig. 3-7):

- Measurement of stakes at positions 10 (978 m a.s.l.), 20 (1156 m a.s.l.) and 30 (1245 m a.s.l.) on Svelgjabreen and measurement of stakes at positions 25 (1232 m a.s.l.) and 45 (1428 m a.s.l.) on Blomstølskardsbreen. Measurements of stake replacements and older stakes that appeared during the melt season at position 40 (1363 m a.s.l.) on Svelgjabreen and positions 35 (1351 m a.s.l.) and 75 (1585 m a.s.l.).
- 26 snow depth soundings between 920 and 1628 m a.s.l. on Svelgjabreen, and 48 snow depth soundings between 1082 and 1624 m a.s.l. on Blomstølskardsbreen. In the lower areas the summer surface (SS) was easy to define. In the upper areas the SS was rather difficult to determine. However, by taking a couple of core samples, the SS was easily defined in these areas too. The snow depth varied between 4 and 9 m at Svelgjabreen, and between 6 and 9 m at Blomstølskardsbreen.
- Snow density was measured down to 7.7 m (SS) at stake position 65 (1530 m a.s.l.) (1530 m a.s.l.) at Blomstølskardsbreen.

The location of stakes, density pit and soundings are shown in Figure 3-7.

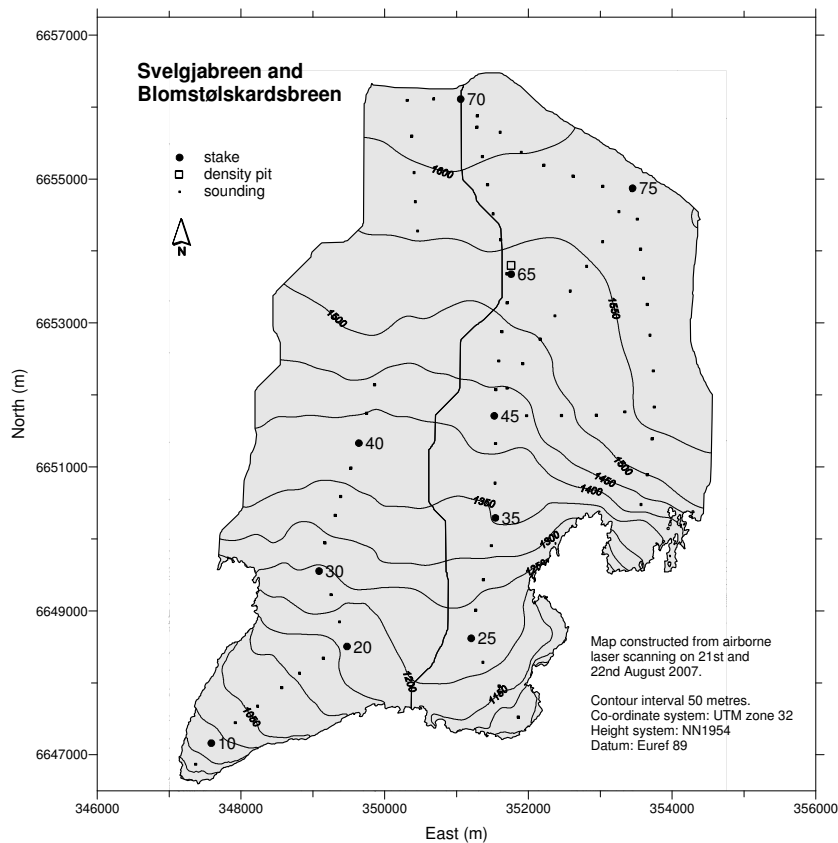


Figure 3-7
Location of stakes,
soundings and
density pit at
Svelgjabreen and
Blomstølskardsbreen
in 2008.

Ablation measurements

Ablation was measured on 23rd September. The net balance was measured at stakes in ten different positions on the two glaciers. There was up to 4.5 m of snow remaining in the upper areas of the glacier. No fresh snow had fallen at the time of the ablation measurements.

Results

The calculations are based on a glacier map from 2007.

Stake measurements in positions 65 and 70 are included in the mass balance calculations for both Svelgjabreen and Blomstølskardsbreen.

Winter balance

The calculation of winter balance is based on point measurements of snow depth (soundings) and on measurement of snow density at one representative location.

A density profile was modelled from the snow density measured at 1530 m a.s.l. The mean snow density of 7.7 m snow was 0.50 g/cm^3 . The density model was assumed to be representative for both Svelgjabreen and Blomstølskardsbreen, and all snow depths were converted to water equivalent using this model.

The calculation of winter balance was performed by plotting the point measurements (water equivalent) in a diagram. A curve was drawn based on visual evaluation (Fig. 3-9) and a mean value for each 50 m height interval was estimated (Tab. 3-2).

Winter balance at Svelgjabreen in 2008 was $3.6 \pm 0.2 \text{ m w.e.}$, corresponding to a volume of $82 \pm 4 \text{ mill. m}^3$ of water. The winter balance at Blomstølskardsbreen was $3.7 \pm 0.2 \text{ m w.e.}$, corresponding to a volume of $84 \pm 1 \text{ mill. m}^3$ of water.

As verification, the winter balance was also calculated using a gridding method based on the aerial distribution of the snow depth measurements (Fig. 3-8). Water equivalents for each cell in a $400 \times 400 \text{ m}$ grid were calculated and summarised. This method gave the same results: 3.6 and 3.7 m w.e., respectively.

The aerial distribution of winter balance for both glaciers is shown in Figure 3-8.

Summer balance

When calculating the summer balance the density of remaining snow was estimated as 0.60 g/cm^3 . The density of melted ice was assumed to be 0.90 g/cm^3 .

The summer balance at Svelgjabreen was measured at six stakes. The stake values increased from 1.3 m w.e. (1632 m a.s.l.) to 5.0 m w.e. (978 m a.s.l.). Based on estimated density and stake measurements the summer balance was calculated as $-2.9 \pm 0.3 \text{ m w.e.}$ corresponding to $-65 \pm 6 \text{ mill. m}^3$ of water.

The summer balance for Blomstølskardsbreen was measured and calculated at six stakes. The stake values increased from 1.3 m w.e. (1632 m a.s.l.) to 2.9 m w.e. (1232 m a.s.l.). Based on the six stakes and the estimated density the summer balance was calculated as $-2.4 \pm 0.3 \text{ m w.e.}$ or $-54 \pm 6 \text{ mill. m}^3$ of water.

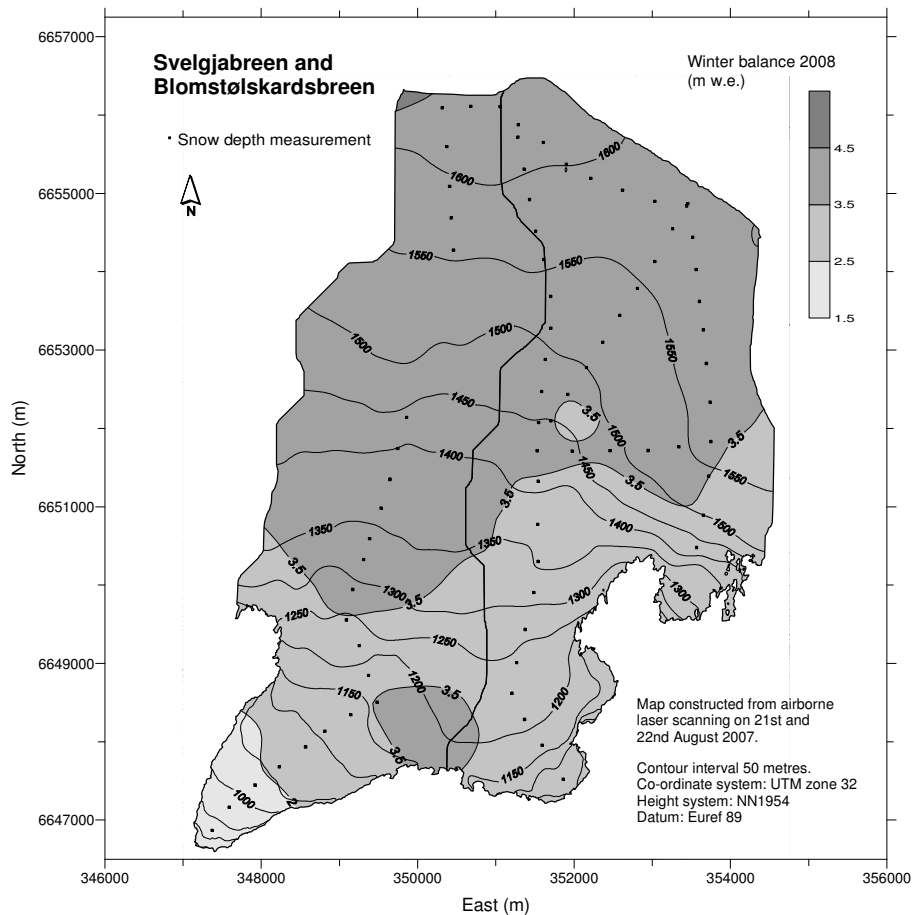


Figure 3-8
Winter balance at Svelgjabreen and Blomstølskardsbreen in 2008 interpolated from 85 snow depth measurements (-).

Net balance

The net balance at Svelgjabreen for 2008 was calculated as $+0.8 \pm 0.4$ m w.e. or a surplus of 17 ± 9 mill. m^3 of water.

The net balance at Blomstølskardsbreen was calculated as $+1.3 \pm 0.4$ m w.e. or a surplus of 30 ± 9 mill. m^3 of water.

As shown in Figure 3-9, the equilibrium line altitude (ELA) lies at 1225 m a.s.l. on Svelgjabreen and 1260 m a.s.l. on Blomstølskardsbreen. Consequently, the Accumulation Area Ratio (AAR) is 75 % and 86 % respectively.

The mass balance results are shown in Table 3-2. The corresponding curves for specific and volume balance are shown in Figure 3-9.

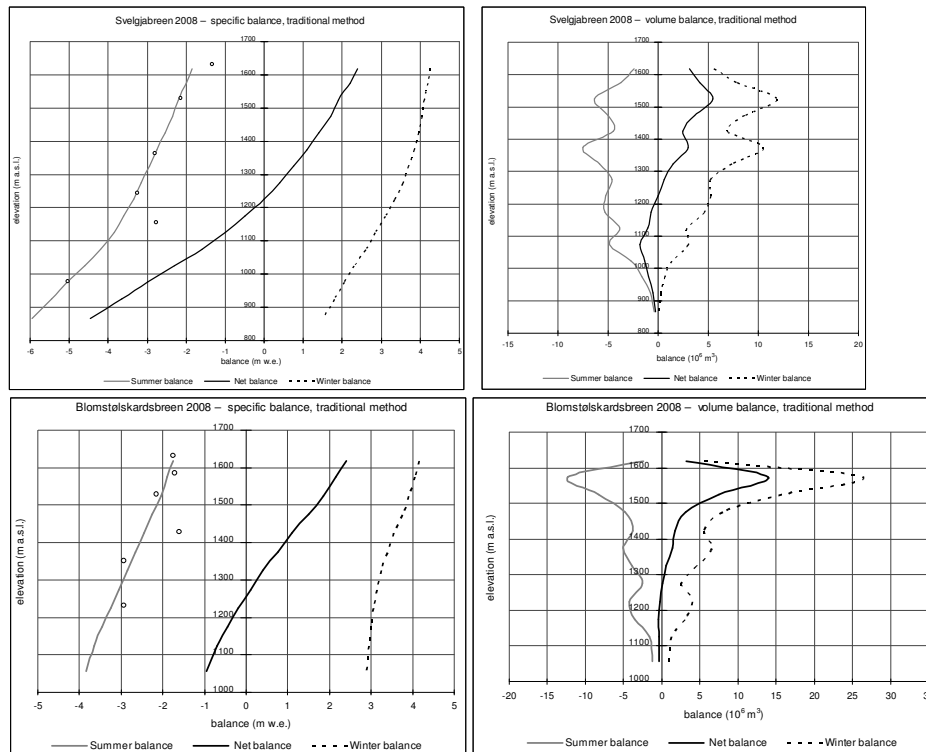


Figure 3-9
Mass balance diagram for Svelgjåbreen (upper) and Blomstølskardsbreen (lower) in 2008 showing altitudinal distribution of specific (left) and volumetric (right) winter, summer and net balance. Specific summer balance at each stake is shown (○).

Mass balance Svelgjåbreen 2007/08 – traditional method							
Altitude (m a.s.l.)	Area (km ²)	Winter balance Measured 21st April 2008		Summer balance Measured 23rd Sep 2008		Net balance Summer surface 2007 - 2008	
		Specific (m w.e.)	Volume (10 ⁶ m ³)	Specific (m w.e.)	Volume (10 ⁶ m ³)	Specific (m w.e.)	Volume (10 ⁶ m ³)
1600 - 1636	1.30	4.25	5.5	-1.85	-2.4	2.40	3.1
1550 - 1600	1.87	4.20	7.8	-2.00	-3.7	2.20	4.1
1500 - 1550	2.89	4.10	11.8	-2.20	-6.4	1.90	5.5
1450 - 1500	2.13	4.05	8.6	-2.35	-5.0	1.70	3.6
1400 - 1450	1.75	3.95	6.9	-2.55	-4.5	1.40	2.4
1350 - 1400	2.73	3.85	10.5	-2.75	-7.5	1.10	3.0
1300 - 1350	1.99	3.70	7.4	-2.95	-5.9	0.75	1.5
1250 - 1300	1.47	3.55	5.2	-3.15	-4.6	0.40	0.6
1200 - 1250	1.57	3.35	5.3	-3.35	-5.3	0.00	0.0
1150 - 1200	1.47	3.10	4.6	-3.60	-5.3	-0.50	-0.7
1100 - 1150	1.00	2.85	2.9	-3.85	-3.9	-1.00	-1.0
1050 - 1100	1.16	2.60	3.0	-4.20	-4.9	-1.60	-1.9
1000 - 1050	0.59	2.30	1.4	-4.60	-2.7	-2.30	-1.4
950 - 1000	0.32	2.05	0.7	-5.05	-1.6	-3.00	-1.0
900 - 950	0.14	1.80	0.3	-5.45	-0.8	-3.65	-0.5
832 - 900	0.06	1.50	0.1	-5.95	-0.4	-4.45	-0.3
832 - 1636	22.45	3.65	81.9	-2.88	-64.8	0.76	17.1

Table 3-2
Winter, summer and net balances for Svelgjåbreen (upper) and Blomstølskardsbreen (lower) in 2008.

Mass balance Blomstølskardsbreen 2007/08 – traditional method							
Altitude (m a.s.l.)	Area (km ²)	Winter balance Measured 21st April 2008		Summer balance Measured 23rd Sep 2008		Net balance Summer surfaces 2007 - 2008	
		Specific (m w.e.)	Volume (10 ⁶ m ³)	Specific (m w.e.)	Volume (10 ⁶ m ³)	Specific (m w.e.)	Volume (10 ⁶ m ³)
1600 - 1636	1.35	4.15	5.6	-1.75	-2.4	2.40	3.2
1550 - 1600	6.49	4.05	26.3	-1.90	-12.3	2.15	14.0
1500 - 1550	4.04	3.90	15.8	-2.05	-8.3	1.85	7.5
1450 - 1500	2.11	3.75	7.9	-2.25	-4.8	1.50	3.2
1400 - 1450	1.56	3.55	5.5	-2.45	-3.8	1.10	1.7
1350 - 1400	1.92	3.40	6.5	-2.65	-5.1	0.75	1.4
1300 - 1350	1.37	3.25	4.5	-2.85	-3.9	0.40	0.5
1250 - 1300	0.81	3.15	2.6	-3.05	-2.5	0.10	0.1
1200 - 1250	1.31	3.05	4.0	-3.25	-4.3	-0.20	-0.3
1150 - 1200	1.02	3.00	3.0	-3.45	-3.5	-0.45	-0.5
1100 - 1150	0.45	2.95	1.3	-3.65	-1.6	-0.70	-0.3
1013 - 1100	0.33	2.90	1.0	-3.85	-1.3	-0.95	-0.3
1013 - 1636	22.77	3.69	84.0	-2.36	-53.7	1.33	30.3

3.3 The changes in areas of the Folgefonna glaciers during historical times (Arve M. Tvede)

Introduction

The Folgefonna glaciers, situated on the Folgefonna Peninsula about 70 km southeast of Bergen, consist of three separate ice caps called Northern, Middle and Southern Folgefonna. The Southern icecap is by far the largest and is ranked as third largest in Scandinavia in terms of area. There are also several small glaciers in the mountains surrounding the ice caps. In connection with an article published by the author in the book “Folgefonna og fjordbygdene” (Folgefonna and the fjord district) (Brekke, 2008), a calculation of the areas of the glaciers was carried out, based on the newest air photos. The results are presented here and will be compared with earlier calculations of the area of the Folgefonna glaciers.

Data and methodology

The area values from August 1981 and July 2006 were found by applying the planimeter tool to the maps and the air photos at www.Zett.no. The air photos from July 2006 were taken during a summer with extreme negative mass balance (see Kjöllmoen, 2007). The photos expose glacier ice along nearly all the edges of the ice caps, so it is straight forward to draw the correct line for the actual glacier border. The areas of the nunataks are subtracted. The corresponding borders from 1981 are from the official M711 maps which were constructed from air photos taken in August 1981. Glacier area values for 1928-53 and 1959 are taken from Liestøl (1962) and Østrem & Ziegler (1969) respectively. Liestøl used the maps available at that time. The publication years vary between 1928 and 1953, and only the southernmost are based on air photos. It is thus assumed that the quality of the maps is quite variable. The Østrem & Ziegler (1969) values are all from excellent air photos taken in 1959, also a summer with little snow on the glaciers in August.

The values for the areas at the largest historical extent are taken from the University thesis of the author (Tvede), see also Figure 3-11. The glacier borders were mapped using a combination of field studies of moraines, lichen growth and scouring marks on rocks in combination with studies of the air photos from 1959. It must be pointed out that the maximum extent was not synchronous at all the Folgefonna glaciers. Field studies revealed that the maximum extent probably was around 1750 at the northern parts of Søndre Folgefonna, around 1890 at Bondhusbrea and Buerbreen and as late as 1940 at Blomstølskardsbreen and Svelgjåbreen (Tvede & Liestøl, 1977).

Results

The results from this and previous studies are presented in table 3-3. It should also be mentioned that the values in the NVE publication “Atlas over breer i Sør-Norge” from 1988, are not included in the table. The area values of Folgefonna in that publication was also based on the air photos from 1981. The value for Southern Folgefonna was presented as 185 km². Evidently some mistakes were made as there is no reason to believe that the glacier had increased its size by 13 km² since 1959.

Table 3-3
Glacier areas in km².

<i>Glacier name</i>	<i>Largest in historical time (Tvede, 1972)</i>	<i>From maps surveyed 1928-53 (Liestøl, 1962)</i>	<i>Air photos August 1959 (*NVE, 1969)</i>	<i>Air photos August 1981 (Tvede, 2008)</i>	<i>Air photos July 2006 (Tvede, 2008)</i>
Northern Folgefonna	35.4	31.1	27.0	27.3	26.5
Middle Folgefonna	19.8	13.5	12.8	12.0	11.4
Southern Folgefonna	189.2	180.6	171.7	167.8	166.5
Total for the ice caps		225.1	211.5	207.1	204.3
Sum small glaciers	**Estimated 5.0	4.5	1.5	4.8	3.2
Total for all glaciers	Estimated 250	229.6	212.2	211.9	207.5

**Østrem, G & T. Ziegler*

***Not surveyed*

Some comments should be made about the small glaciers. In the survey published in 1962 (Liestøl, 1962) and in 1969 (Østrem & Ziegler, 1969), only 6 “small glaciers” are presented. The survey in 2006 found a total of 68 small glaciers on the air photos. These glaciers ranged in size from 0.01 km² to 0.4 km². A typical “small glacier” is shown in Figure 3-10. It is evident that the number must have been higher than actually reported also in 1961 and in 1969. The number of small glaciers has, however, probably grown because larger units have been divided into several units due to downmelting. Some units were also previously connected to the main ice caps. This was the case with the small glacier on Figure 3-10 for example. The number and areas of the small glaciers at the historical maximum is not surveyed, because this will require closer field studies.



Figure 3-10
Photo of an unnamed, small glacier north of the mountain Hundsøyra on 5th September 2003. That summer all the glaciers had a strong negative mass balance and only the glacier ice was left. Field studies indicate that this glacier was connected to the main ice cap (seen in the background) at the maximum historical glacier extent. Photo: Arve M. Tvede.

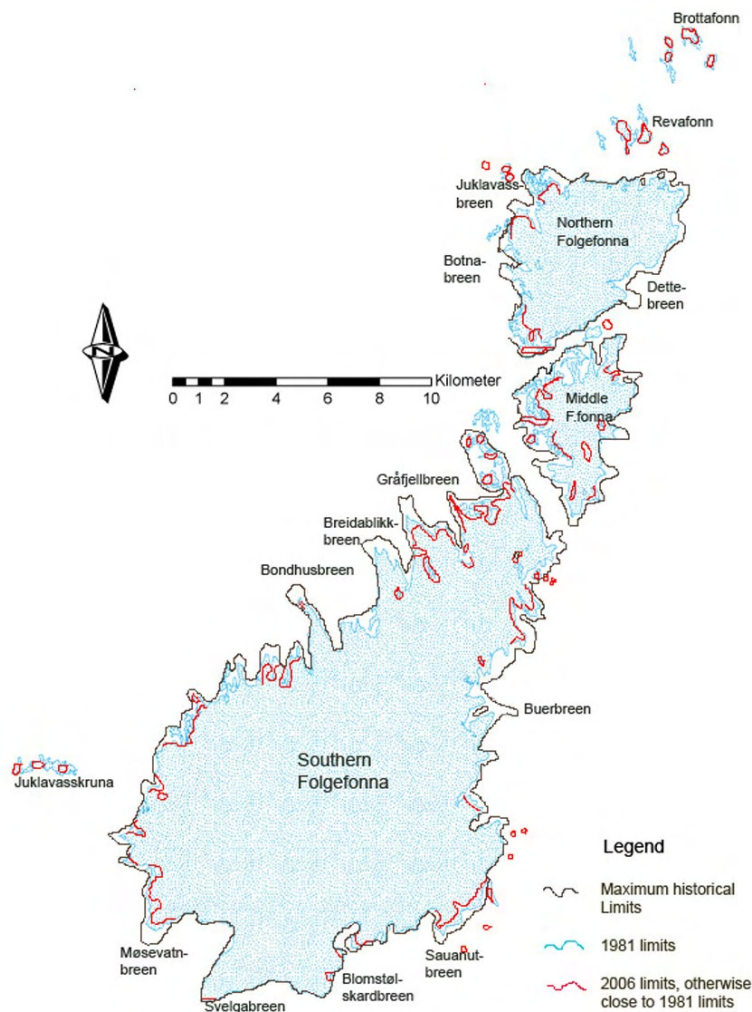


Figure 3-11
Map showing the Folgefonna ice caps at the maximum historical limits, the limits in 1981 and the limits in 2006 for the areas where they differ from the 1981-limits. The maximum historical limits are not mapped for the small isolated glaciers. Map source: Norge digitalt.

Discussion

The glaciers on the Folgefonna peninsula today cover 83 % of their maximum historical extent, giving a mean area loss of 17 %. If one assume that the glaciers were close to this size as late as 1890, it means that the mean reduction rate has been 0.16 % per. year between 1890 and 2006. A similar calculation for the period 1981-2006 gives only 0.08 % per. year. However, it should be mentioned that the western glaciers in southern Norway all had mainly positive mass balances between 1981 and 1995 and most glacier tongues had a net advance. Nearly all the area reduction between 1981 and 2006 probably took place in the last part of this period.

The reduction rate is, however, not uniform as can clearly be seen from Table 3-3 and Figure 3-11. The Southern Folgefonna has lost only 12 % and most of this loss is found on the northern third of that ice cap. Middle Folgefonna has lost 38 % and Northern Folgefonna has lost 25 % of its maximum size.

The volume changes of the glaciers are not dealt with in this study. Some earlier papers have documented recent volume changes within certain drainage basins of Folgefonna, (Østrem & Tvede, 1986), (Smith-Meyer & Tvede, 1996) and (Kjøllmoen, 2008).

4. Nigardsbreen (Bjarne Kjøllmoen)

Nigardsbreen (61°42'N, 7°08'E) is one of the largest and best known outlet glaciers from Jostedalbreen. It has an area of 47.8 km² (measured in 1984) and flows south-east from the centre of the ice cap. Nigardsbreen accounts for approximately 10 % of the total area of Jostedalbreen, and extends from 1960 m a.s.l. down to approximately 320 m a.s.l.

Glaciological investigations in 2008 include mass balance and glacier length change. Nigardsbreen has been the subject of mass balance investigations since 1962.



Figure 4-1
The outlet of Nigardsbreen photographed on 30th October 2008. Photo: Miriam Jackson.

4.1 Mass balance 2008

Fieldwork

Snow accumulation measurements

Snow accumulation measurements were performed on 7th and 8th May and the calculation of winter balance (Fig. 4-2) is based on:

- Uninterrupted measurement of stakes and towers in positions 600 (580 m a.s.l.), 1000 (960 m a.s.l.), T95 (1688 m a.s.l.) and T56 (1799 m a.s.l.). It was also possible to make use of measurements of a substitute stake drilled in May 2008 and an older stake that appeared during the melt season in position 54 (1613 m a.s.l.). The stake measurements on the plateau showed snow depth between 6.8 (54) and 7.8 m (T95). Measured snow depth at position 1000 was 3.7 m and 1.4 m at position 600. Stake readings did not show any indication of melting after the final measurements in September 2007.
- Core sample at position 94 (1705 m a.s.l.) showing snow depth of 6.7 m.

- 124 snow depth soundings on the plateau between 1315 and 1966 m a.s.l. Some few probings at the tongue at 580 and 995 m elevation. Due to hard-packed snow it was relatively difficult to define the snow depth on the plateau. The snow depth soundings on the plateau gave a snow thickness between 6.5 and 7.5 m. Down on the tongue the snow depth was 3.6 m (995 m a.s.l.) and 1.4 m (580 m a.s.l.).
- Snow density was measured down to 6.6 m depth (SS at 6.7 m) at position 94 (Fig. 4-2).

Location of stakes, towers, snow pit, core samples and soundings are shown in Figure 4-2.

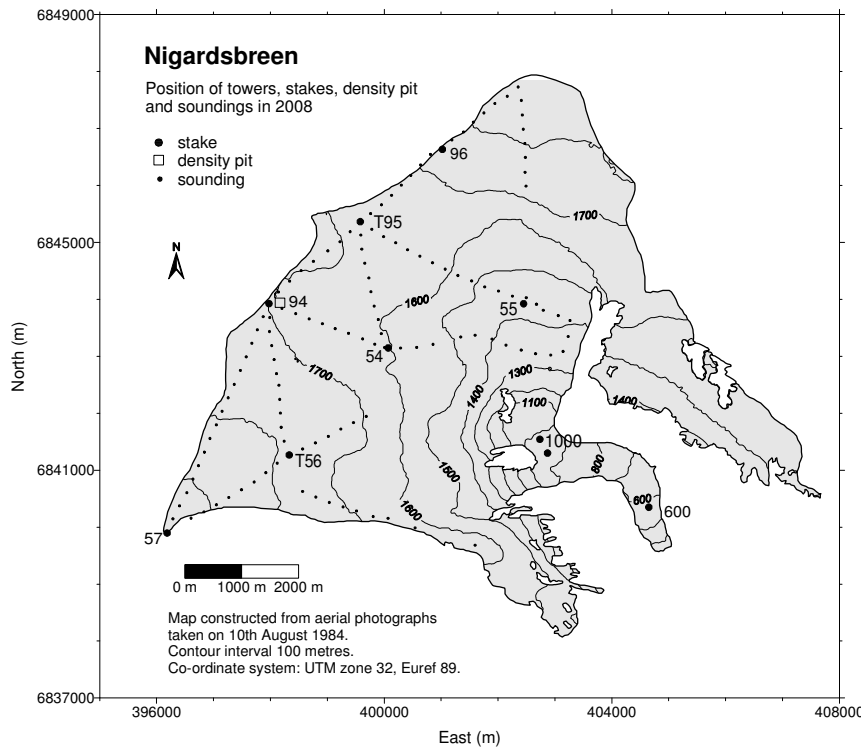


Figure 4-2
Location of towers and stakes, snow pit and soundings on Nigardsbreen in 2008.

Ablation measurements

Ablation measurements were carried out on 30th October. Measurements were made at four stakes and two towers in six different positions. Since snow measurements in May the stakes on the plateau had increased in length between 3.7 and 4.0 m. Hence, there was between 2.5 and 4.0 m of snow remaining from winter 2007/2008. At the time of measurement, approximately 2 m of fresh snow had fallen in the upper areas above 1600 m elevation.

Results

The calculations are based on a glacier map from 1984.

Winter balance

The calculation of winter balance is based on point measurements of snow depth (stakes and towers, probings and core drillings) and on measurement of snow density at one representative location.

There was no melting after the final measurements in September 2007. Consequently, winter *accumulation* and winter *balance* are equal.

A density profile was modelled from the snow density measured at 1705 m altitude (6.6 m depth). Using this model gave a snow density of 0.46 g/cm³. This model was used for all snow depth measurements.

The winter balance calculation was performed by plotting measurements (water equivalent) in a diagram. A curve was drawn based on visual evaluation (Fig. 4-4), and a mean value for each 100 m height interval estimated (Tab. 4-1). The elevations above 1320 m a.s.l. were well represented with point measurements. Below this altitude the curve pattern was based on point measurements at 995, 960 and 580 m altitude.

These calculations give a winter balance of 3.0 ± 0.2 m w.e., corresponding to a water volume of 144 ± 10 mill. m³. This is 126 % of the average for 1962-2007. Nine years have shown a greater winter balance on Nigardsbreen; the greatest was in 1989 with 4.0 m w.e.

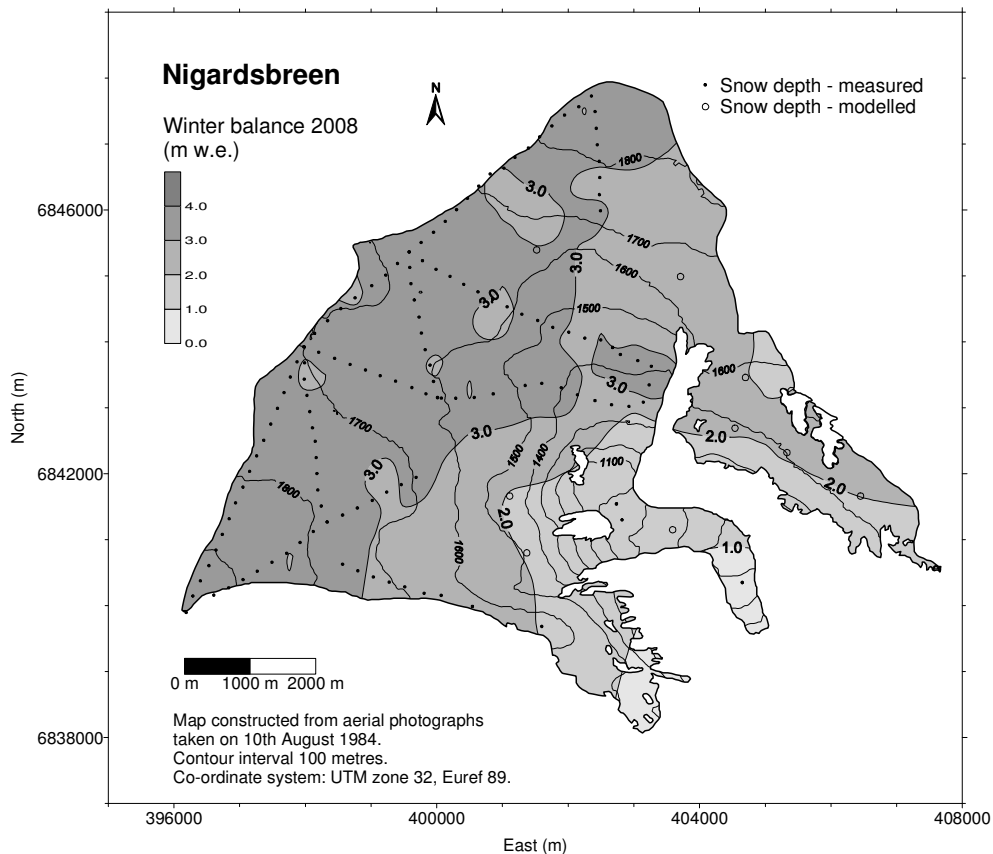


Figure 4-3
 Winter balance at Nigardsbreen in 2008 interpolated from 139 measurements (•) of snow depth. In areas with few or no measurements nine extrapolated points (○) are added.

The winter balance was also calculated using a gridding method (Kriging) based on the aerial distribution of the snow depth measurements (Fig. 4-3). In areas with insufficient measurements some (nine) simulated points were extracted. These point values were calculated based on measurements from the period 1975-81, years with extensive measurements. Water equivalents for each cell in a 250 x 250 m grid were calculated and summarised. The result obtained using this gridding method was 2.7 m w.e.

Summer balance

When calculating the summer balance the density of the remaining snow was estimated as 0.60 g/cm^3 . The density of melted firm was assumed to be 0.65 g/cm^3 , while the density of ice was taken as 0.90 g/cm^3 .

The summer balance was calculated at stakes and towers at seven different elevations. For stakes 57 (1966 m a.s.l.) and 1000 the measurements were supplemented with estimated values based on correlation with other stakes. The summer balance increased (in absolute value) from -1.0 m w.e. at the glacier summit (1966 m a.s.l.) to -8.8 m down on the tongue (580 m a.s.l.). Based on estimated density and stake measurements the summer balance was calculated to be $-1.9 \pm 0.3 \text{ m w.e.}$, which is $-92 \pm 15 \text{ mill. m}^3$ of water. This is 96 % of the average for 1962-2007.

Net balance

The net balance for 2008 was calculated at stakes and towers in eight different positions. The result was a surplus of $+1.1 \text{ m} \pm 0.3 \text{ m w.e.}$, which means a volume increase of $52 \pm 15 \text{ mill.m}^3$ water. The mean value for the period 1962-2007 is $+0.39 \text{ m w.e.}$ (Fig. 4-5), while the average for 1996-2007 is $+0.01 \text{ m w.e.}$

Based on Figure 4-4, the Equilibrium Line Altitude (ELA) was 1325 m a.s.l. Accordingly, the Accumulation Area Ratio (AAR) was 91 %.

The mass balance for Nigardsbreen in 2008 is shown in Table 4-1 and the corresponding curves are shown in Figure 4-4. The historical mass balance results are presented in Figure 4-5.

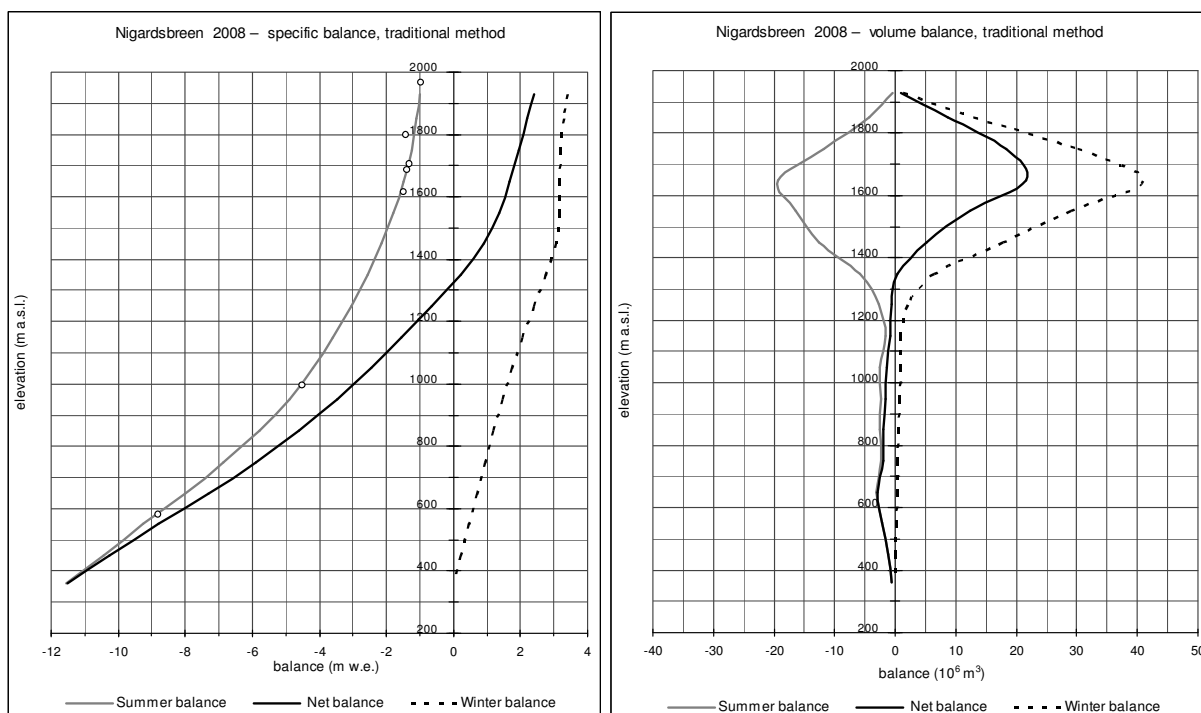


Figure 4-4

Mass balance diagram showing specific balance (left) and volume balance (right) for Nigardsbreen in 2008. Specific summer balance at seven stake positions is shown as dots (o). The net balance curve intersects the y-axis and defines the ELA as 1325 m a.s.l. Thus the AAR was 91 %.

Table 4-1
Winter, summer and net balance for Nigardsbreen in 2008. Mean values for the period 1962-2007 are 2.38 (b_s), -1.99 m (b_s) and +0.39 m (b_n) water equivalent.

Mass balance Nigardsbreen 2007/08 – traditional method							
Altitude (m a.s.l.)	Area (km ²)	Winter balance		Summer balance		Net balance	
		Measured 8th May 2008		Measured 30th Oct 2008		Summer surface 2007 - 2008	
		Specific (m w.e.)	Volume (10 ⁶ m ³)	Specific (m w.e.)	Volume (10 ⁶ m ³)	Specific (m w.e.)	Volume (10 ⁶ m ³)
1900 - 1960	0.38	3.40	1.3	-1.00	-0.4	2.40	0.9
1800 - 1900	3.92	3.30	12.9	-1.10	-4.3	2.20	8.6
1700 - 1800	9.39	3.20	30.0	-1.25	-11.7	1.95	18.3
1600 - 1700	12.88	3.18	40.9	-1.50	-19.3	1.68	21.6
1500 - 1600	9.18	3.15	28.9	-1.80	-16.5	1.35	12.4
1400 - 1500	5.82	3.05	17.8	-2.15	-12.5	0.90	5.2
1300 - 1400	2.28	2.75	6.3	-2.55	-5.8	0.20	0.5
1200 - 1300	0.90	2.40	2.2	-3.05	-2.7	-0.65	-0.6
1100 - 1200	0.45	2.05	0.9	-3.60	-1.6	-1.55	-0.7
1000 - 1100	0.58	1.75	1.0	-4.20	-2.4	-2.45	-1.4
900 - 1000	0.47	1.45	0.7	-4.90	-2.3	-3.45	-1.6
800 - 900	0.44	1.20	0.5	-5.80	-2.6	-4.60	-2.0
700 - 800	0.33	0.95	0.3	-6.85	-2.3	-5.90	-1.9
600 - 700	0.39	0.70	0.3	-8.00	-3.1	-7.30	-2.8
500 - 600	0.24	0.45	0.1	-9.25	-2.2	-8.80	-2.1
400 - 500	0.12	0.20	0.0	-10.45	-1.3	-10.25	-1.2
320 - 400	0.05	0.05	0.0	-11.55	-0.6	-11.50	-0.6
320 - 1960	47.82	3.01	144.1	-1.92	-91.7	1.10	52.4

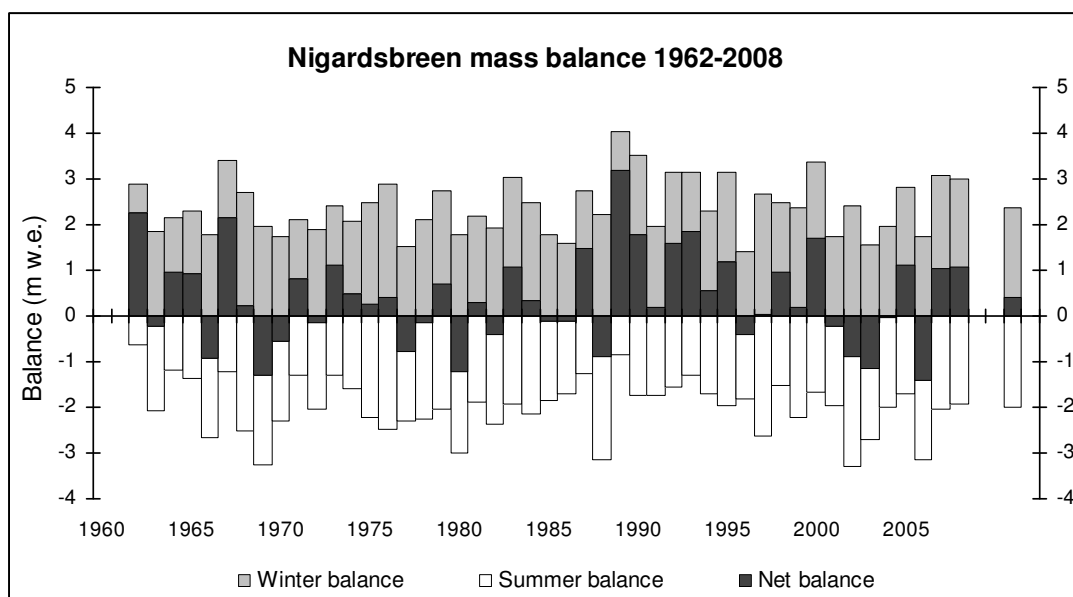


Figure 4-5
Annual mass balance at Nigardsbreen during the period 1962-2008.

5. Austdalsbreen (Hallgeir Elvehøy)

Austdalsbreen (61°45'N, 7°20'E) is an eastern outlet of the northern part of Jostedalsgreen, ranging in altitude from 1200 to 1757 m a.s.l. The glacier terminates in Austdalsvatnet, which has been part of the hydropower reservoir Styggevatnet since 1988.

Glaciological investigations at Austdalsbreen started in 1986 in connection with the construction of the hydropower reservoir.

The glaciological investigations in 2008 included mass balance, front position change and glacier velocity. Mass balance has been measured at Austdalsbreen since 1988.



Figure 5-1
Austdalsbreen seen from AUS100 (see Fig. 5-2 for location) on 30th October 2008. The lake level was close to 1200 m a.s.l. which is the highest possible regulated lake level. Photo: Miriam Jackson.

5.1 Mass balance 2008

Fieldwork

Four mass balance stakes were maintained through out the winter.

The winter balance was measured on 22nd May. The calculation of winter balance was based on the following data (Fig. 5-2):

- Snow depth at stakes A5 (1.15 m), A90 (3.85 m), A24 (4.75 m) and T70 (5.50 m).
- Snow density down to the previous summer surface at 5.0 m depth at stake A60 (1490 m a.s.l.). The mean snow density was 0.53 g/cm³.
- 87 snow depth measurements along 16 km of profiles. At Austdalsnuten above 1600 m a.s.l. the snow depth was 3 to 5 m. Between 1400 and 1600 m a.s.l. the snow was 4 to 6 m deep. Below 1400 m a.s.l. the snow depth was between 3 and 4.5 m at most locations. The summer surface (SS) from 2007 was difficult to detect in the upper areas. A transition to coarser snow was found to correspond with the summer surface at stakes A24, A60 and A70, and this transition was used as the summer surface.

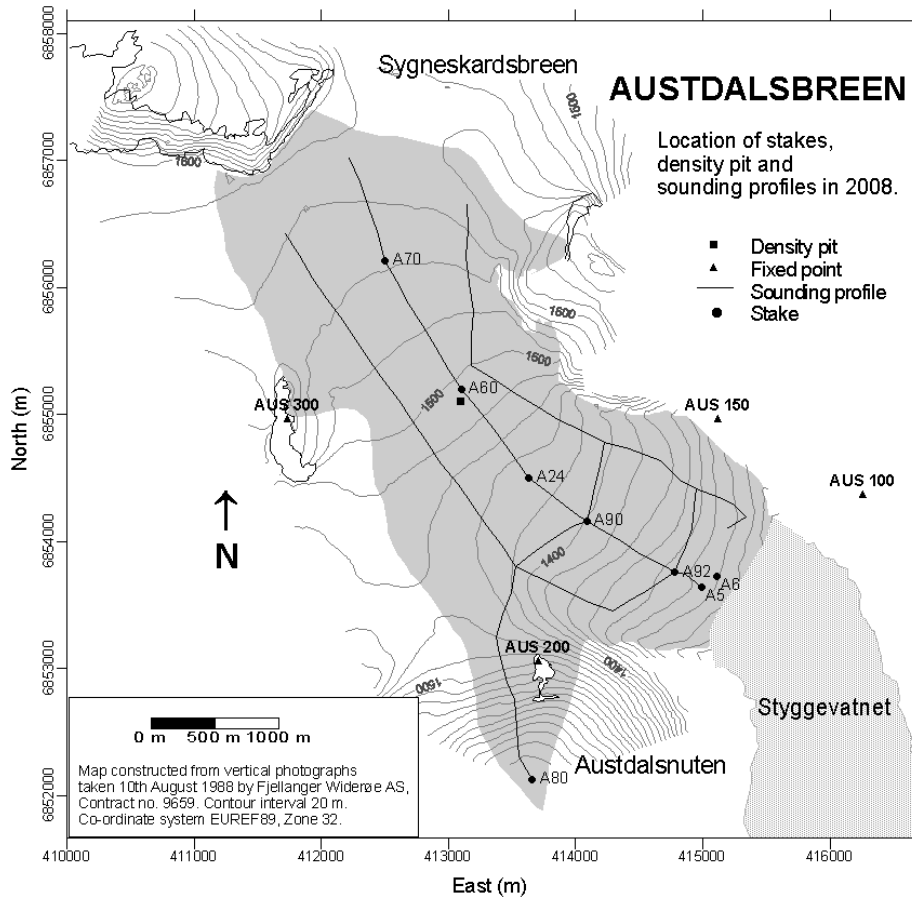


Figure 5-2
Location of stakes, density pit and sounding profiles at Austdalsbreen in 2008.

On 19th August the transient snow line was 1370 m a.s.l.

Summer and net balance measurements were carried out on 30th October. The glacier was covered with up to 1.7 m of new snow. Based on the stake measurements the temporary snow line (TSL) at the end of the summer season was about 1420 m a.s.l. At stakes above 1420 m a.s.l. 3 to 4 m of snow had melted and 1 to 2 m of snow remained. At the TSL around 4 m of snow had melted. At the stakes close to the terminus 4.5 m of ice had melted.

Results

The mass balance was calculated according to the stratigraphic method (see chap.1). The calculations are based on a map from 10th August 1988 reduced for the areas below the highest regulated lake level (below 1200 m a.s.l., 0.11 km²). However, the actual glacier area based on front position measurements (chap. 5-2) has been reduced by 0.44 km², and the surface elevation has been reduced accordingly on the lower part of the glacier.

Winter balance

There is no evidence for significant melting after the stake measurements on 27th September 2007.

The winter balance was calculated from snow depth and snow density measurements on 22nd May. A function correlating snow depth with water equivalent was calculated based on snow density measurements at stake A60 (1490 m a.s.l.).

Snow depth water equivalent values of all snow depth measurements were plotted against altitude. Mean values of altitude and Snow Water Equivalent (SWE) in 50 m altitude intervals were calculated and plotted. An altitudinal winter balance curve was drawn from a visual evaluation of the mean values, and from this a mean value for each 50 m altitude interval was determined. The winter balance was 30 ± 2 mill. m³ water or 2.6 ± 0.2 m w.e., which is 116 % of the 1988-2007 average (2.22 m w.e.).

The winter balance was calculated using a gridding method also, based on the spatial distribution of the snow depth measurements (Fig. 5-3). Water equivalents for each cell in a 50 x 50 m grid were calculated and summarised. The result based on this method, which is a control of the traditional method, showed a winter balance of 2.7 m w.e.

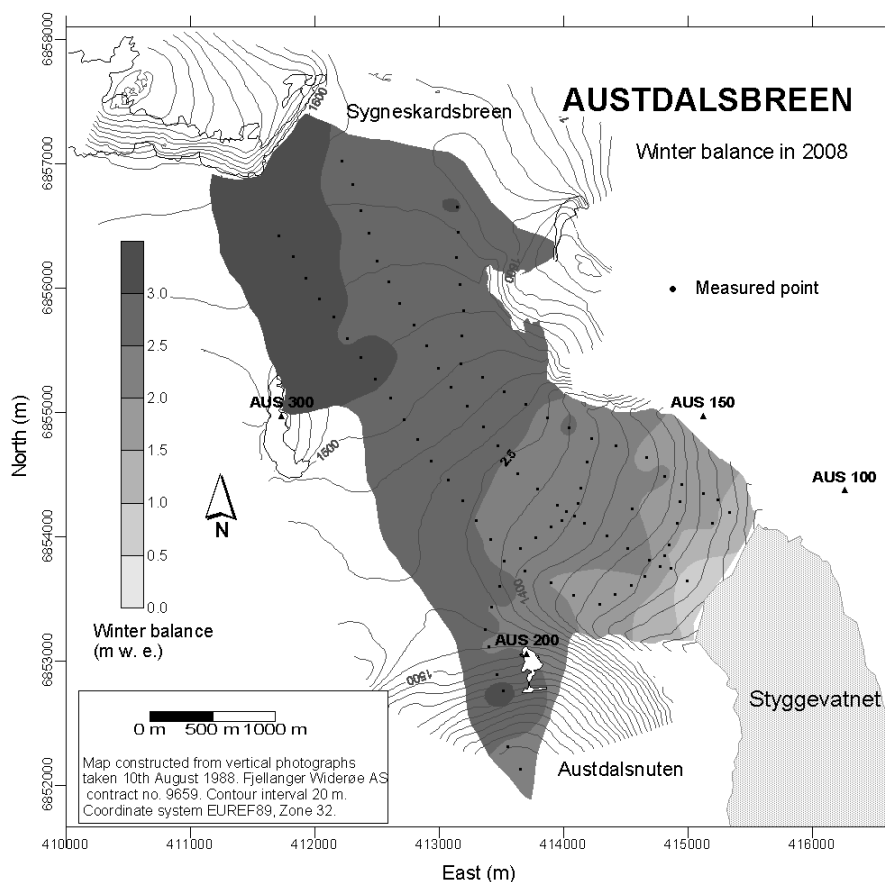


Figure 5-3
Winter balance at Austdalsbreen in 2008 from 92 water equivalent values calculated from snow depth measurements.

Summer balance

The summer balance was calculated for nine stakes in eight positions between 1250 and 1730 m a.s.l. Stake A90 was lost between 19th August and 30th October, and the amount of melted ice was estimated from stakes A92 and A24. The summer balance curve was drawn from these values (Fig. 5-4).

Calving from the glacier terminus was calculated as the annual volume of ice (in water equivalent) transported through a cross section close to the terminus, and adjusted for the volume change related to the annual front position change. This volume is calculated as:

$$Q_k = \rho_{ice} * (u_{ice} - u_f) * W * H$$

where ρ_{ice} is 0.9 g/cm^3 , u_{ice} is annual glacier velocity ($60 \pm 10 \text{ m/a}$, chap. 5.3), u_f is front position change averaged across the terminus ($-33 \pm 5 \text{ m/a}$, chap. 5.2), W is terminus width ($1010 \pm 20 \text{ m}$) and H is mean ice thickness at the terminus ($43 \pm 5 \text{ m}$). The mean ice thickness was calculated from mean surface altitudes along the calving terminus surveyed on 27th September 2007 (1211 m a.s.l.) and 30th October 2008 (1223 m a.s.l.), and mean bottom elevation along the terminus in September 2007 (1173 m a.s.l.) and October 2008 (1174 m a.s.l.) calculated from a bottom topography map compiled from radar ice thickness measurements (1986), hot water drilling (1987) and lake depth surveying (1988 and 1989). The resulting calving volume was $4 \pm 1 \text{ mill. m}^3$ water or $0.3 \pm 0.1 \text{ m w.e.}$ averaged over the glacier area (11.8 km^2).

The summer balance, including calving, was calculated as $-2.6 \pm 0.3 \text{ m w.e.}$, which corresponds to $-31 \pm 3 \text{ mill. m}^3$ of water. The result is 105 % of the 1988-2007 average (-2.48 m w.e.). The calving volume was 13 % of the summer balance.

Net balance

The net balance at Austdalsbreen was calculated as $-0.1 \pm 0.3 \text{ m w.e.}$, corresponding to $-1 \pm 3 \text{ mill. m}^3$ water. The 1988-2007 average is -0.28 m w.e. The equilibrium line altitude (ELA) was 1420 m a.s.l. Correspondingly, the Accumulation Area Ratio (AAR) was 71 % in 2008. The altitudinal distribution of winter, summer and net balances is shown in Figure 5-4 and Table 5-1. Results from 1988-2008 are shown in Figure 5-5.

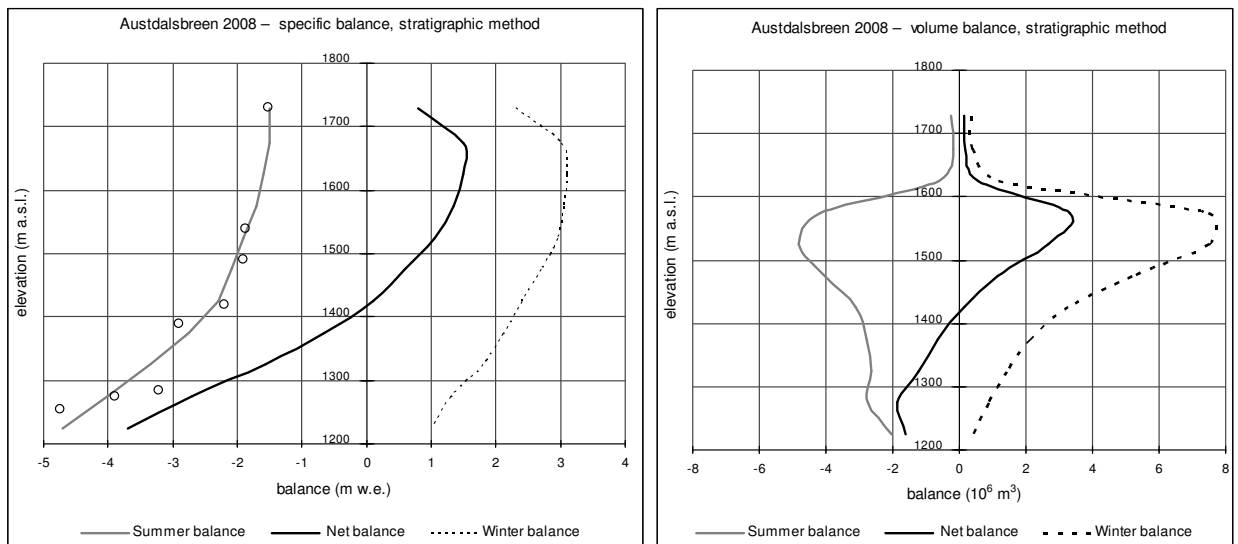


Figure 5-4
Altitudinal distribution of winter, summer and net balances is shown as specific balance (left) and volume balance (right) at Austdalsbreen in 2008. Specific summer balance at eight stake locations is shown (○).

Table 5-1
Altitudinal distribution of winter, summer and net balances at Austdalsbreen in 2008.

Mass balance Austdalsbreen 2007/08 – stratigraphic method							
Altitude (m a.s.l.)	Area (km ²)	Winter balance		Summer balance		Net balance	
		Measured 22nd May 2008		Measured 30th Oct 2008		Summer surface 2007 - 2008	
		Specific (m w.e.)	Volume (10 ⁶ m ³)	Specific (m w.e.)	Volume (10 ⁶ m ³)	Specific (m w.e.)	Volume (10 ⁶ m ³)
1700 - 1757	0.16	2.30	0.36	-1.50	-0.24	0.80	0.13
1650 - 1700	0.13	3.00	0.38	-1.50	-0.19	1.50	0.19
1600 - 1650	0.38	3.10	1.17	-1.60	-0.60	1.50	0.56
1550 - 1600	2.45	3.05	7.47	-1.70	-4.16	1.35	3.30
1500 - 1550	2.54	2.95	7.49	-1.90	-4.82	1.05	2.67
1450 - 1500	1.92	2.70	5.19	-2.10	-4.04	0.60	1.15
1400 - 1450	1.36	2.40	3.25	-2.30	-3.12	0.10	0.14
1350 - 1400	1.01	2.10	2.12	-2.75	-2.78	-0.65	-0.66
1300 - 1350	0.79	1.80	1.42	-3.35	-2.64	-1.55	-1.22
1250 - 1300	0.69	1.30	0.89	-4.00	-2.75	-2.70	-1.85
1200 - 1250	0.44	1.00	0.44	-4.70	-2.04	-3.70	-1.61
Calving					-3.6		-3.6
1200 - 1757	11.84	2.55	30.2	-2.62	-31.0	-0.07	-0.8

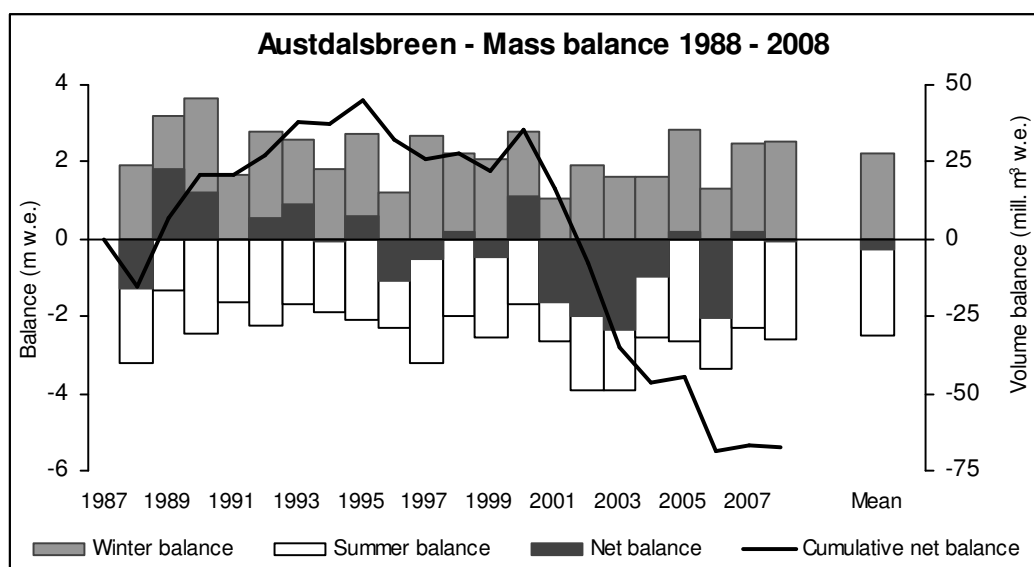


Figure 5-5
Winter, summer and net balances at Austdalsbreen during the period 1988-2008. Mean winter, summer and net balance is 2.22, -2.49 and -0.27 m w.e., respectively.

5.2 Front position change

Eight points along the calving terminus were surveyed on 30th October 2008. The mean front position change was -33 ± 5 m (Fig. 5-6) between 27th September 2007 and 30th October 2008. The width of the calving terminus was 1010 ± 20 metres. Since 1988 the glacier terminus has retreated 459 metres, whilst the glacier area has decreased by approximately 0.48 km^2 (Fig. 5-6).

The terminus position was surveyed on 19th August 2008. A comparison of surveyed front positions and stake positions at stakes A5 and A6 shows that in front of these stakes the ice cliff calved 30 metres between 27th September 2007 and 19th August 2008, and 50 metres between 19th August and 30th October 2008.

Due to large variations in calving, the variation in front position throughout the year is large compared with the net change from year to year. Figure 5-7 illustrates how the front position at a central flow line has varied over the last 20 years. As a consequence of lake regulation it was expected that the glacier terminus would retreat. Modelling predicted a future change in front position that is shown as a broken line in Figure 5-7. The mean annual net balance used in the model was -0.47 m w.e., whilst the measured mean net balance has been -0.27 m w.e. (1988-2008).

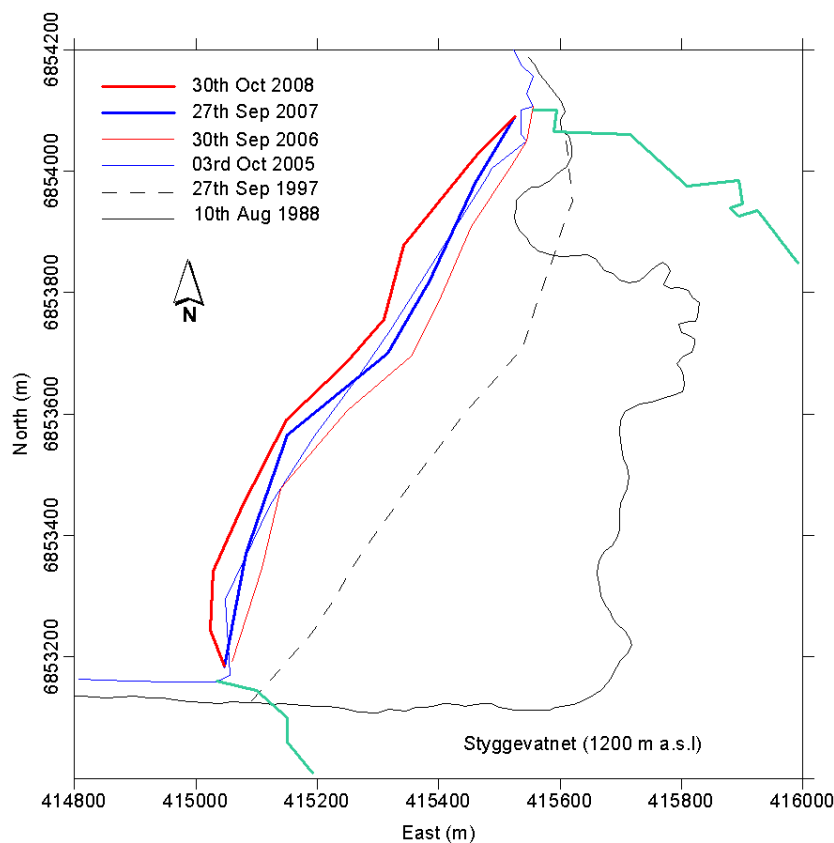


Figure 5-6
Surveyed front position of Austdalsbreen in 1988 when the lake was regulated, in 1997, and in 2005-2008. The mean front position change between 27th September 2007 and 30th October 2008 was -33 metres.

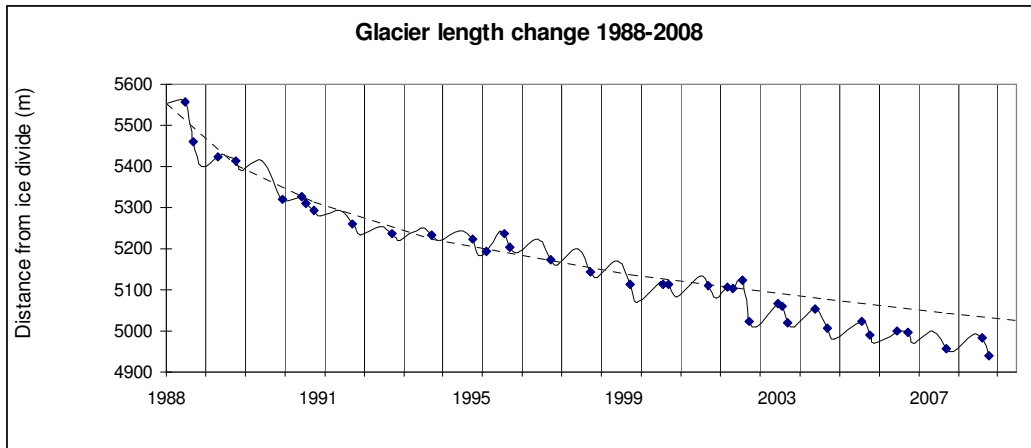


Figure 5-7
 Surveyed glacier front position along a central flow line, shown as change in glacier length along this flow line (dots). The solid line indicates annual variation in front position. The glacier terminus advances from December to July when the lake is frozen, and retreats during July-December due to calving. Lake Austdalsvatnet/Styggevatnet was regulated as a reservoir for the first time in 1988. The dashed line shows predicted glacier length change based on expected annual lake level variations due to regulation and an annual net balance of -0.47 m w.e. (Laumann & Wold, 1992).

5.3 Glacier dynamics

Glacier velocities are calculated from repeated surveys of stakes. The stake network was surveyed on 27th September 2007, and 22nd May, 19th August and 30th October 2008.

Annual velocities were calculated for five stake locations based on surveys on 27th September and 19th August (327 days). The annual velocities at stake locations A5, A6, A92, A90, and A24 were 69 m/a, 63 m/a, 50 m/a, 33 m/a and 23 m/a, respectively. This is similar to velocities calculated for 2006/2007.

The glacier velocity averaged across the front width and thickness must be estimated in order to calculate the calving volume (chap. 5.1). The surface centre line velocity at the terminus was calculated from summer measurements at stake A5 (70 m/a), average distance from the stake to terminus (170 m), and an average strain rate from previous years (0.1 a^{-1}) as 87 m/a. The glacier velocity averaged over the cross-section is estimated to be 70 % of the centre line surface velocity based on earlier measurements and estimates of the amount of glacier sliding at the bed. The resulting terminus cross-sectional averaged glacier velocity for 2007/2008 is 60 ± 10 m/a.

6. Hardangerjøkulen (Hallgeir Elvehøy)

Hardangerjøkulen (60°32'N, 7°22'E) is the sixth largest (73 km²) glacier in Norway. The glacier is situated on the main water divide between Hardangerfjorden and Hallingdalen valley. In 1963 the Norwegian Polar Institute began mass balance measurements on the south-western outlet glacier Rembesdalsskåka (17 km²), which drains towards Simadalen valley and Hardangerfjorden. In the past Simadalen has been flooded by jökulhlaups (outburst floods) from the glacier-dammed lake Demmevatnet, the most recent occurring in 1937 and 1938.

The Norwegian Water Resources and Energy Directorate (NVE) has been responsible for the mass balance investigations at Rembesdalsskåka since 1985. The investigated basin covers the altitudinal range between 1020 and 1865 m a.s.l. At Rembesdalsskåka, glacier length observations were initiated in 1917 by Johan Rekstad at Bergen Museum. Observations were conducted in several periods during the 20th century. Statkraft Energy AS re-initiated the observations at Rembesdalsskåka in 1995. At Midtdalsbreen, glacier length observations were started by Prof. Atle Nesje at the University of Bergen in 1982. Glacier length observations are described in chapter 12. The University of Utrecht, Netherlands, operates an automatic weather station (AWS) close to the terminus of Midtdalsbreen (chap. 6-2).

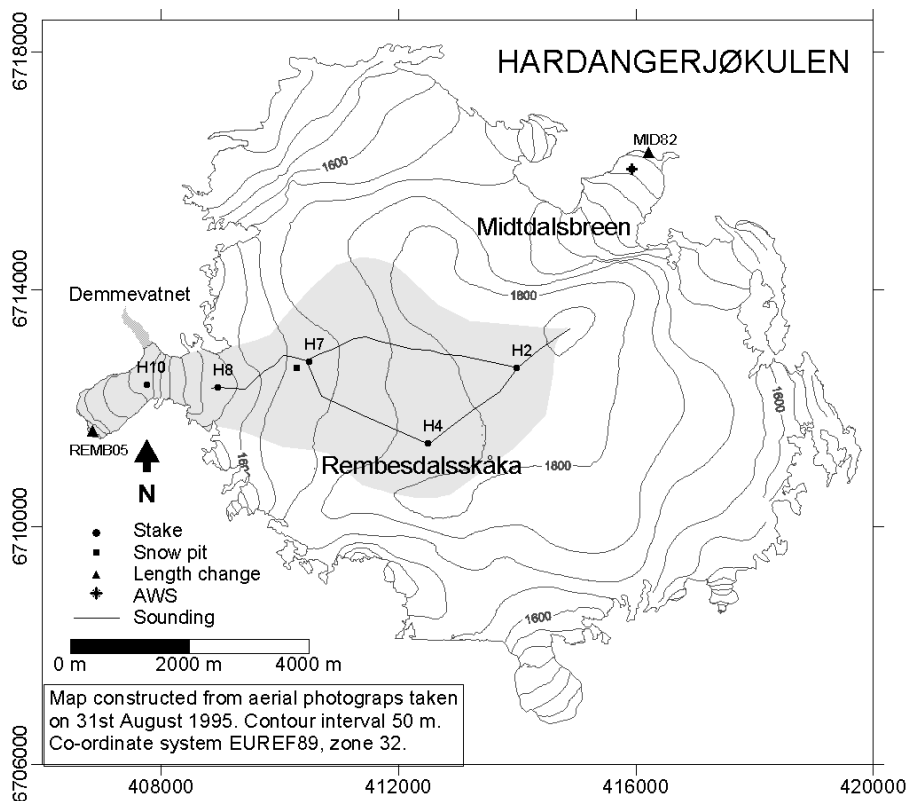


Figure 6-1 Location of sounding profiles, stakes and snow pit at Rembesdalsskåka (shaded), glacier length observations at Rembesdalsskåka and Midtdalsbreen, and an automatic weather station (AWS) at Midtdalsbreen.



Figure 6-2
Stake H4 (1775 m a.s.l.) at Hardangerjøkulen on 14th February 2008. The snow depth was 4.35 metres.
Photo: Hallgeir Elvehøy.

6.1 Mass balance at Rembesdalsskåka in 2008

Fieldwork

The stake network was checked on 11th December 2007, 14th February, 3rd April and 16th April 2008. Stakes were maintained throughout the winter in four positions. Snow depth soundings and stake measurements on 11th December 2007 showed that 0.15 m of ice had melted at stakes H10 after the autumn measurements on 3rd October 2007.

The winter balance measurements were carried out on 21st May with supplementary measurements from 16th April. The calculation of winter balance is based on the following data (see fig. 6-1 for locations):

16th April:

- Snow depth measurements at stakes H8 (1515 m a.s.l.), H706 (1660 m a.s.l.) and H4 (1775 m a.s.l.), showing snow depths of 3.4 – 5.0 and 5.9 m, respectively.
- Snow depth coring at location H4 (1770 m a.s.l.) and H2 (1830 m a.s.l.) showing snow depths of 5.7 and 6.4 m, respectively.
- Snow density down to last years summer surface (SS) at 5.0 m depth at location H7 (1660 m a.s.l.). There was firn below the SS.
- Snow density down to last years summer surface (SS) at 5.3 m depth at location H2 (1830 m a.s.l.). New stake H208. Below the SS there was firn.
- Snow depth soundings along profiles H7 – H4 – H2 and H7 – H2. The snow depth was between 5 and 6 metres.

21st May:

- Snow depth measurements at stakes H10 (1270 m a.s.l.), H8 (1515 m a.s.l.), stake H706 (1660 m a.s.l.), H4 (1775 m a.s.l.) and H208 (1830 m a.s.l.), showing snow depths of 1.9 – 2.85 – 4.65 – 5.85 and 5.2 metres, respectively.
- Snow density down to last years summer surface (SS) at 4.65 m depth at location H7 (1660 m a.s.l.).
- Snow density down to a reference surface from 16th April at 0.48 m depth at location H2 (1830 m a.s.l.).
- Snow depth soundings along profiles H8 – H7 and H2 – summit, plus some additional points between 1650 and 1700 m a.s.l. Between 1500 and 1650 m a.s.l. and above 1830 m a.s.l. the snow depth was 4 to 5 metres. Between 1650 and 1830 m a.s.l. the snow depth was 5 to 6 metres. The SS was difficult to detect. It was defined by a transition to coarse snow.

On 15th August the temporary snow line (TSL) altitude was about 1525 m a.s.l. At the stakes above the TSL, 2.6 to 3.1 m of snow had melted. Below the TSL all the snow and about 0.75 and 2.95 m of ice had melted.

Summer and net balance were measured on 30th and 31st October. Measurements at the stakes showed up to 2 m of new snow at the stakes. The TSL could not be detected due to the new snow cover, but stake readings indicate that the TSL altitude was about 1600 m a.s.l. After 15th August 0.4 to 0.7 m of snow had melted at the stakes above the TSL, while up to 2 m of ice had melted at the stakes below the TSL. The accumulation of new snow probably started late in September. Up to 2.5 m of snow remained from winter 2008 at the plateau. At stake H10 on the glacier tongue more than 5 m of ice had melted.

Results

The mass balance is calculated according to a stratigraphic method relating the net balance to the difference between two successive “summer surfaces”, but including melting after 3rd October 2007 and excluding snow accumulation before 30th October 2008. The calculations are based on a map from 1995.

Winter balance

The winter balance was calculated from the snow depth and snow density measurements on 21st May and the snow depth measurements on 16th April corrected for snow depth change as interpolated from stake measurements at stake H7, H4 and H2.

Stake measurements and snow depth soundings on 11th December 2007 showed that ice melting had occurred after 3rd October 2007 at stake H10 but not at stake H8. As the winter balance curve below 1500 m a.s.l. is inter- and extrapolated based on the winter balance at stake H10, this was calculated as the sum of late autumn melting and snow accumulation at the stake. The density of melted ice was set as 0.90 g/cm³. The late autumn melt was estimated as 0.13 m w.e.

Between 16th April and 21st May the snow depth at stakes H7, H4 and H2 was reduced by 0.35, 0.1 and 0.0 m in a combination of snow compaction and snow accumulation. The snow depth soundings on 16th April were reduced accordingly based on elevation.

A snow depth-water equivalent profile was calculated based on snow density measurements at location H7 (1660 m a.s.l.) on 21st May. Using the calculated profile, the mean density of 5 m of snow was 0.54 g/cm³. The snow depth measurements were transformed to water equivalent values using this profile. From the calculated water equivalent values, averages for 50 m elevation bands were calculated and plotted against altitude. An altitudinal winter balance curve was drawn from these averages, (Fig. 6-3). Below 1500 m a.s.l. the winter balance curve was extrapolated from the measurements at stakes 8 and 10. a mean value for each 50 m elevation interval was then determined from this curve.

The resulting winter balance was 2.6 ±0.2 m w.e. or 45 ±3 mill. m³ water. This is 124 % of the 1963-2007 average of 2.10 m w.e., and 130 % of the 2003-2007 average of 2.00 m w.e. The altitudinal distribution of the winter balance is shown in Figure 6-3 and Table 6-1.

Summer balance

The summer balance was calculated directly at five locations between 1270 and 1830 m a.s.l. The density of the remaining snow at locations H7, H4 and H2 was set as 0.6 g/cm³. The density of the melted ice at stakes H8 and H10 was set as 0.9 g/cm³.

The summer balance curve in Figure 6-2 was drawn from these five point values. The summer balance was calculated as -2.2 ±0.2 m w.e., corresponding to -37 ±3 mill. m³ of water. This is 108 % of the 1963-2007 average, which is -2.00 m w.e., and 93 % of the 2003-2007 average of -2.32 m w.e.

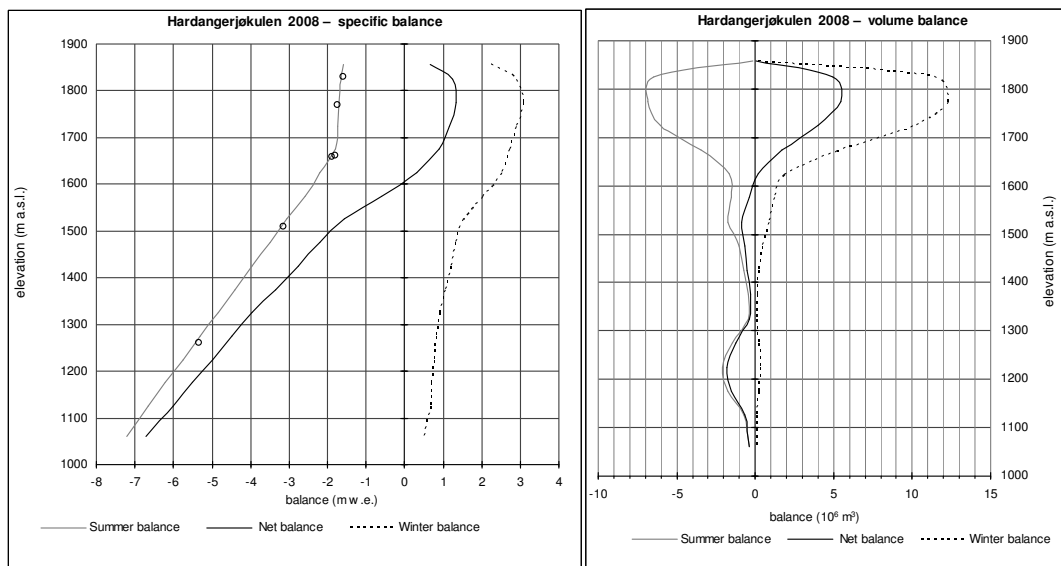


Figure 6-3
Altitudinal distribution of winter-, summer- and net balance shown as specific balance (left) and volume balance (right) at Rembesdalsskåka, Hardangerjøkulen in 2008. Specific summer balance at six stakes is shown (○).

Table 6-1
Altitudinal distribution of winter, summer and net balance at Rembesdalsskåka in 2008.

Mass balance Hardangerjøkulen 2007/08 – traditional method							
Altitude (m a.s.l.)	Area (km ²)	Winter balance		Summer balance		Net balance	
		Measured 21st May 2008		Measured 30th Oct 2008		Summer surface 2007 - 2008	
		Specific (m w.e.)	Volume (10 ⁶ m ³)	Specific (m w.e.)	Volume (10 ⁶ m ³)	Specific (m w.e.)	Volume (10 ⁶ m ³)
1850 - 1865	0.09	2.25	0.2	-1.60	-0.1	0.65	0.1
1800 - 1850	3.93	2.90	11.4	-1.65	-6.5	1.25	4.9
1750 - 1800	4.03	3.05	12.3	-1.70	-6.9	1.35	5.4
1700 - 1750	3.46	2.90	10.0	-1.75	-6.1	1.15	4.0
1650 - 1700	1.94	2.70	5.2	-1.80	-3.5	0.90	1.7
1600 - 1650	0.75	2.50	1.9	-2.20	-1.6	0.30	0.2
1550 - 1600	0.59	2.00	1.2	-2.60	-1.5	-0.60	-0.4
1500 - 1550	0.57	1.50	0.9	-3.05	-1.7	-1.55	-0.9
1450 - 1500	0.29	1.30	0.4	-3.50	-1.0	-2.20	-0.6
1400 - 1450	0.19	1.20	0.2	-3.95	-0.7	-2.75	-0.5
1350 - 1400	0.10	1.05	0.1	-4.40	-0.4	-3.35	-0.3
1300 - 1350	0.10	0.90	0.1	-4.85	-0.5	-3.95	-0.4
1250 - 1300	0.27	0.80	0.2	-5.30	-1.4	-4.50	-1.2
1200 - 1250	0.36	0.75	0.3	-5.75	-2.1	-5.00	-1.8
1150 - 1200	0.28	0.70	0.2	-6.20	-1.7	-5.50	-1.6
1100 - 1150	0.11	0.65	0.1	-6.65	-0.7	-6.00	-0.6
1020 - 1100	0.05	0.50	0.0	-7.20	-0.4	-6.70	-0.4
1020 - 1865	17.1	2.61	44.7	-2.16	-37.0	0.45	7.7

Net balance

The net balance at Rembesdalsskåka was calculated as $+0.5 \pm 0.3$ m w.e. or $+8 \pm 5$ mill. m³ water. The 1963-2007 average is $+0.10$ m w.e., and the 2003-2007 average is -0.32 m w.e. The altitudinal distribution of winter, summer and net balances is shown in Figure 6-3 and Table 6-1. The equilibrium line altitude (ELA) was set to 1610 m a.s.l. from the net balance curve in Figure 6-3. The corresponding accumulation area ratio (AAR) was 82 %. Results from 1963-2008 are shown in Figure 6-4. The cumulative net balance is $+5.1$ m w.e.

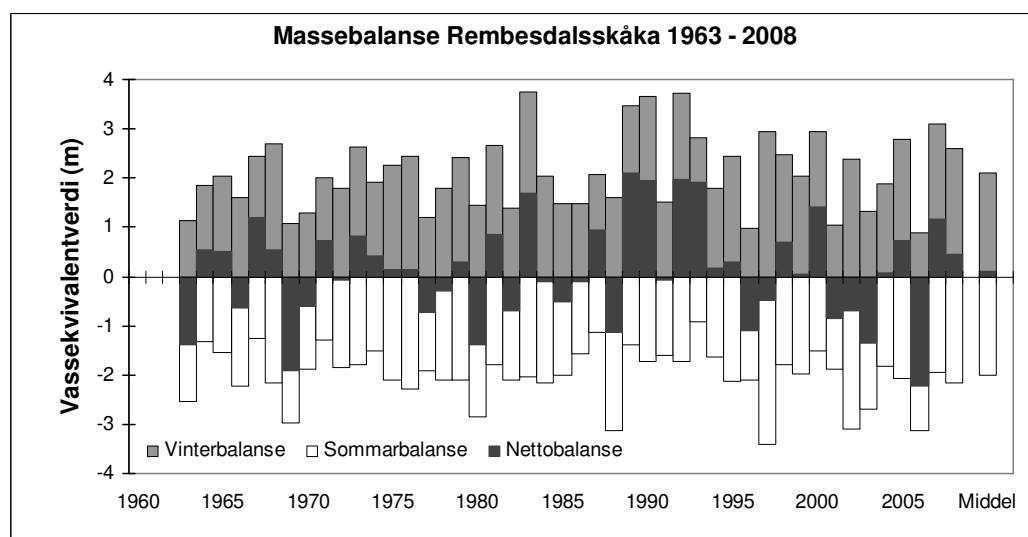


Figure 6-4
Winter-, summer- and net balances at Hardangerjøkulen during the period 1963-2008. Mean values for the period are $b_w=2.12$ m, $b_s=-2.01$ m and $b_n=+0.12$ m water equivalent.

6.2 Meteorological measurements on Midtdalsbreen

(Rianne H. Giesen, Utrecht University)

Since October 2000, an automatic weather station (AWS) has been operating in the ablation area on Midtdalsbreen, a north-easterly outlet glacier of Hardangerjøkulen (Fig. 6-1 for location). The station (Fig. 6-5) is owned and maintained by the Institute of Marine and Atmospheric research Utrecht (IMAU), Utrecht University (contact: J.Oerlemans@uu.nl). The station records air temperature, relative humidity, wind speed and direction, distance to the surface, shortwave and long wave radiation and air pressure. Sampling is done every few minutes (depending on the sensor) and 30-minute averages are stored. The measurements are used to study the local microclimate at Hardangerjøkulen and to calibrate and validate a mass balance model for the glacier. Here, we present the surface energy balance calculated from AWS data collected between 16th September 2007 and 27th August 2008.

The surface energy balance

The surface energy balance at a glacier's surface can be described by:

$$Q = S_{\text{net}} + L_{\text{net}} + H_{\text{sen}} + H_{\text{lat}} + G,$$

where S_{net} and L_{net} are the net shortwave and long wave radiation, H_{sen} and H_{lat} the turbulent fluxes of sensible and latent heat, G the subsurface heat flux and Q the energy available for melt. The shortwave and long wave radiation fluxes are directly measured; the remaining fluxes have been calculated from the AWS measurements with an energy balance model. A description of the model and additional results can be found in Giesen et al., 2008.

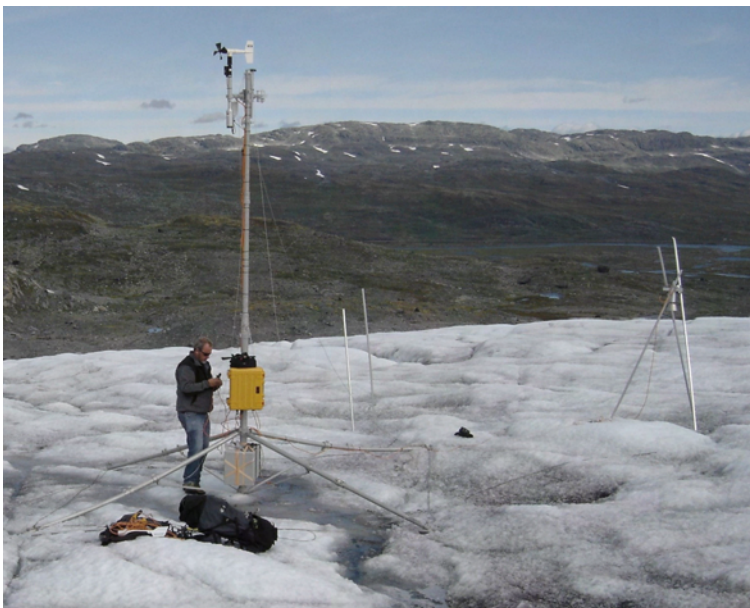


Figure 6-5
The AWS site on Midtdalsbreen on 29th August 2008. The sonic ranger measuring the changing distance to the ice surface is to the right. Photo: Rianne H. Giesen.

Daily mean values of the energy fluxes during the period considered here are shown in Figure 6-6. S_{net} has the largest seasonal cycle of the radiative and turbulent fluxes. From late November to late January, S_{net} is practically zero, because the AWS site does not receive any direct sunlight and the surface albedo is high. The winter snowpack at the AWS site disappeared around 1st July. The associated decrease in surface albedo is leading to a large increase in S_{net} . Changes in cloudiness cause the large fluctuations in

S_{net} and L_{net} , which have opposite signs because clouds reduce S_{net} and enhance L_{net} . In winter, net radiation ($S_{net} + L_{net}$) is negative; between May and September, S_{net} dominates net radiation. In mid-summer L_{net} can become positive on cloudy days with air temperatures well above 0 °C.

The contribution of H_{sen} to the energy balance is almost continuously positive; in summer a significant part of the melt energy is supplied by H_{sen} . High values of H_{sen} in summer occur on days with high air temperatures, while in autumn and winter, peaks in H_{sen} are the combined result of relative high air temperatures and high wind speeds. H_{lat} is small compared to H_{sen} . It is mainly negative in spring, but contributes positively to the surface energy balance in summer, when the air is relatively warm and humid compared to the air just above the glacier surface. Daily mean values of G fluctuate around zero, values are generally positive in spring, when the entire snowpack is at the melting point temperature and cannot be heat further. The calculated melt energy Q shows that some melting occurred until November on days with large turbulent fluxes. After melting started again in the middle of April, the surface was almost continuously melting except for a short cold period in May. The large variations in Q are due to coinciding periods with both high S_{net} and large turbulent fluxes.

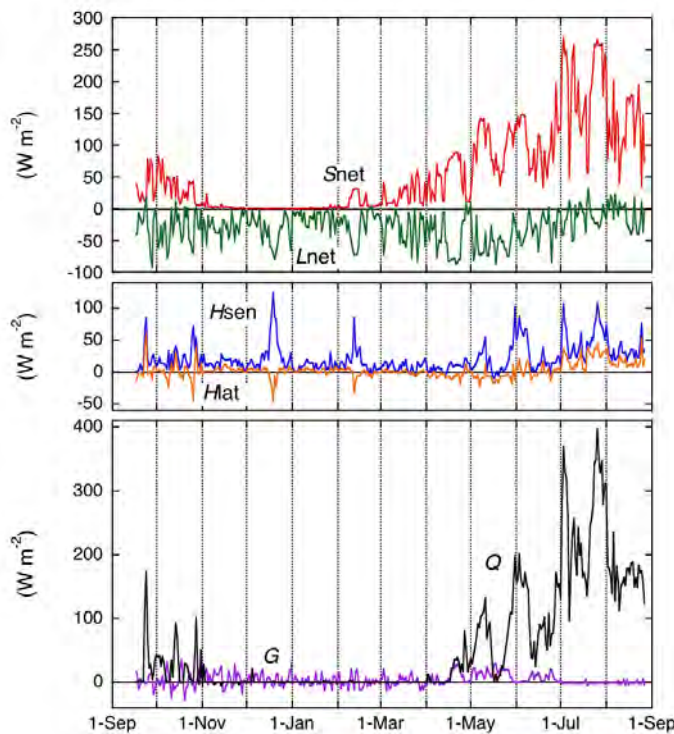


Figure 6-6
Daily mean surface energy fluxes at the AWS site on Middalsbreen. Q is the energy available for melt.

During the 347-day period considered here, the surface was melting 33 % of the time, which is similar to earlier years (2001-2005, Giesen et al., 2008). However, the mean Q during melt is almost 10 % higher than in the same period in earlier years. The primary reason is a larger S_{net} (22 % increase) because the spring and summer of 2008 were sunnier than in the other years. Furthermore, a melt water stream under the AWS mast (Fig. 6-5) lowered the surface albedo, also increasing S_{net} . For the 347-day period, 85 % of the melt energy was supplied by S_{net} , 21 % by H_{sen} and 6 % by H_{lat} , while L_{net} and G were energy sinks of 11 % and 2 %, respectively.

7. Storbreen (Liss M. Andreassen)

Storbreen (61°34' N, 8°8' E) is situated in the Jotunheimen mountain massif in central southern Norway (Fig. 7-1). The glacier has a total area of 5.4 km² and ranges in altitude from 1390 to 2100 m a.s.l. (Fig. 7-1). Mass balance measurements began in 1949 and 2008 is the 60th year of continuous measurements.



Figure 7-1
View of Storbreen taken from northeast (from Sauhøi) on 29th July 2008. Photo: Liss M. Andreassen.

7.1 Mass balance 2008

Fieldwork

Accumulation measurements were performed on 6-7th May and the calculation of winter balance is based on:

- Measurements of stakes in 6 different positions. The stake readings did not indicate any significant additional surface melting after the ablation measurements in the previous mass balance year (19th September 2007).
- Soundings of snow depth in 143 positions between 1458 and 1955 m a.s.l., covering most of the altitudinal range of the glacier. The summer surface was easy to identify over the whole glacier. The snow depth varied between 1.52 and 6.35 m, the mean being 3.84 m.
- Snow density was measured at two positions, at the automatic weather station (AWS) on the glacier at 1570 m a.s.l. and at stake 4 at 1725 m a.s.l.
- Ablation measurements were performed on 1st September on stakes in all positions. The locations of stakes, density pits and soundings are shown in Figure 7-2.

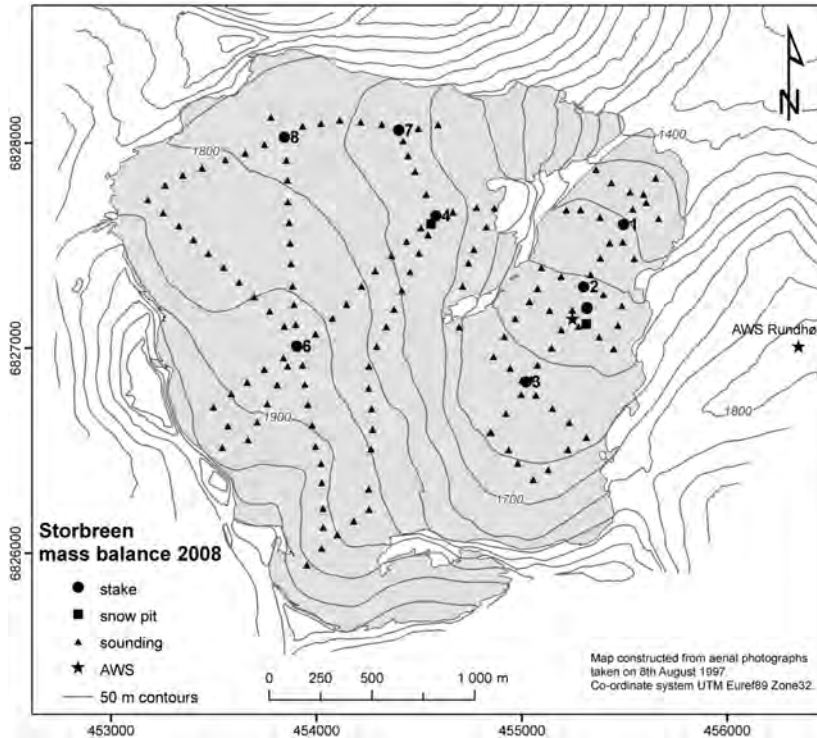


Figure 7-2
Location of stakes, density pits and the automatic weather stations (AWS) at Storbreen in 2008.

Results

The mass balance results are shown in Table 7-1 and Figure 7-3.

Winter balance

Winter accumulation was calculated from soundings and the snow density measurements. The mean measured snow density was 0.495 g/cm^3 (0.51 g/cm^3 at the AWS and 0.48 g/cm^3 at stake 4). The winter accumulation was calculated as the mean of the soundings within each 50-metre height interval. The specific winter balance was calculated to be $2.0 \pm 0.2 \text{ m w.e.}$. This is 130 % of the mean for 1971-2000.

Summer balance

Summer balance was calculated directly from stakes at 7 locations (1, 2, AWS, 3, 4, 6 and 7). The density of the remaining snow was assumed to be 0.6 g/cm^3 . The density of the melted ice was assumed to be 0.9 g/cm^3 . The summer balance was calculated to be $-1.9 \pm 0.3 \text{ m w.e.}$, which is 115 % of the mean for 1971-2000.

Net balance

The net balance of Storbreen was slightly positive in 2008, $0.1 \pm 0.3 \text{ m w.e.}$, which is equivalent to a volume of $\pm 0.59 \text{ mill. m}^3$ of water. The ELA calculated from the net balance diagram (Fig. 7-3) was 1770 m a.s.l. and the accumulation area ratio (AAR) was 51 %. The cumulative balance since 1949 is -17.2 m w.e. , giving a mean annual net balance of -0.29 m w.e. over the 60 years of measurements (Fig. 7-4).

Table 7-1
The distribution of winter, summer and net balance in 50 m altitudinal intervals for Storbreen in 2008.

Mass balance Storbreen 2007/08 – traditional method							
Altitude (m a.s.l.)	Area (km ²)	Winter balance Measured 7 May 2008		Summer balance Measured 1 Sep 2008		Net balance Summer surfaces 2007 - 2008	
		Specific (m w.e.)	Volume (10 ⁶ m ³)	Specific (m w.e.)	Volume (10 ⁶ m ³)	Specific (m w.e.)	Volume (10 ⁶ m ³)
2050 - 2100	0.04	2.60	0.10	-0.50	-0.02	2.10	0.08
2000 - 2050	0.15	2.67	0.40	-0.65	-0.10	2.02	0.30
1950 - 2000	0.23	2.75	0.63	-0.80	-0.18	1.95	0.45
1900 - 1950	0.36	2.83	1.02	-1.00	-0.36	1.83	0.66
1850 - 1900	0.57	2.45	1.40	-1.25	-0.71	1.20	0.69
1800 - 1850	0.92	2.03	1.87	-1.65	-1.52	0.38	0.35
1750 - 1800	0.75	1.97	1.47	-1.90	-1.43	0.07	0.05
1700 - 1750	0.64	1.72	1.10	-2.20	-1.41	-0.48	-0.31
1650 - 1700	0.40	2.00	0.80	-2.30	-0.92	-0.30	-0.12
1600 - 1650	0.49	1.77	0.87	-2.38	-1.17	-0.61	-0.30
1550 - 1600	0.35	1.40	0.49	-2.55	-0.89	-1.15	-0.40
1500 - 1550	0.21	1.08	0.23	-2.80	-0.59	-1.72	-0.36
1450 - 1500	0.18	1.10	0.20	-3.10	-0.56	-2.00	-0.36
1390 - 1450	0.06	1.09	0.07	-3.39	-0.20	-2.30	-0.14
1390 - 2100	5.35	1.99	10.64	-1.88	-10.05	0.11	0.59

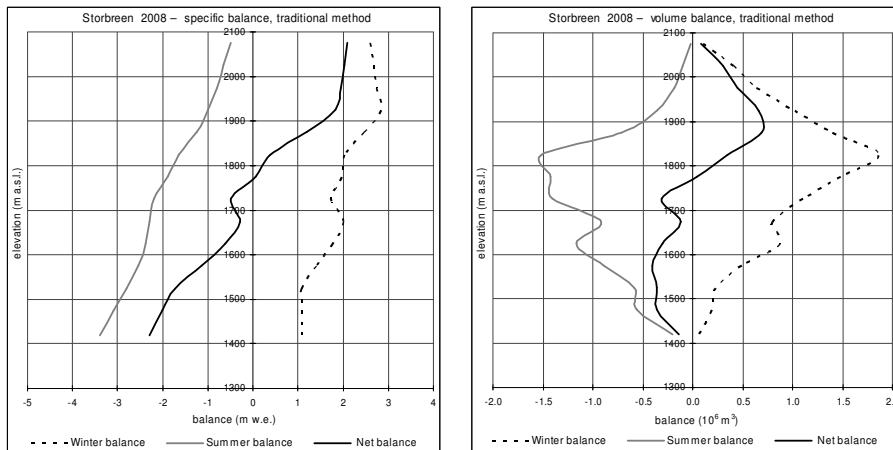


Figure 7-3
Mass balance diagram for Storbreen 2008, showing specific balance on the left and volume balance on the right.

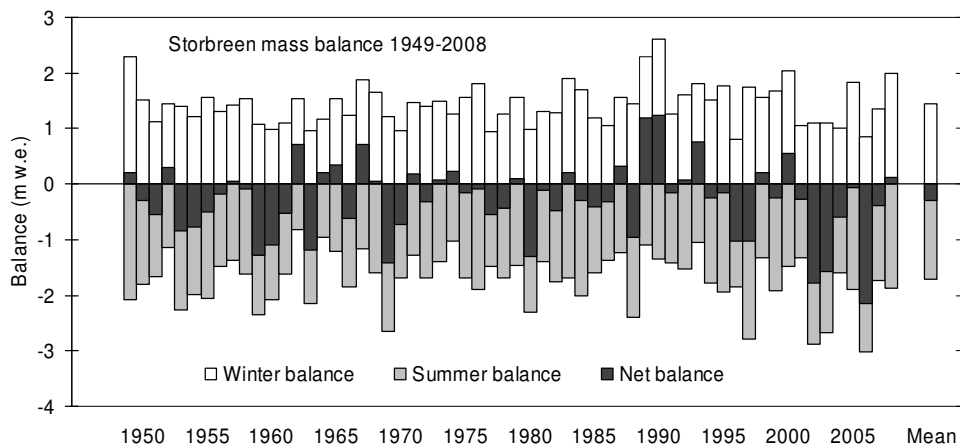


Figure 7-4
Winter, summer and net balance at Storbreen for the period 1949-2008.

8. Hellstugubreen (Liss M. Andreassen)

Hellstugubreen (61°34' N, 8° 26' E) is a north-facing valley glacier situated in central Jotunheimen (Fig. 8-1). The glacier shares a border with Vestre Memurubre and ranges in elevation from 1480 to 2210 m a.s.l. It had an area of 3.0 km² in 1997, and the glacier terminus retreated about 100 m from 1997 to 2007 (Fig. 8-2). Annual mass balance measurements began in 1962 and have continued annually since then.



Figure 8-1
Photograph of Hellstugubreen on 30th July 2008. The temporary snow line was then located at about 1680 m a.s.l. Photo: Liss M. Andreassen.

8.1 Mass balance 2008

Fieldwork

Accumulation measurements were performed on 6th May and the calculation of winter balance is based on:

- Measurements of stakes in 11 different positions. Stake readings indicated that only at the two lowest stakes there had been additional melting after the ablation measurements on 11th September 2007.
- Soundings of snow depth in 100 positions between 1533 and 2145 m a.s.l. covering most of the altitudinal range of the glacier (Fig. 8-2). The snow depth varied between 1.15 and 5.00 m, the mean being 3.2 m.
- The snow density was measured by sampling in a pit at 1960 m a.s.l. where the total snow depth was 3.5 m.

Ablation measurements were carried out on 18th September on all visible stakes. The location of stakes, density pit and sounding profiles are shown in Figure 8-2.

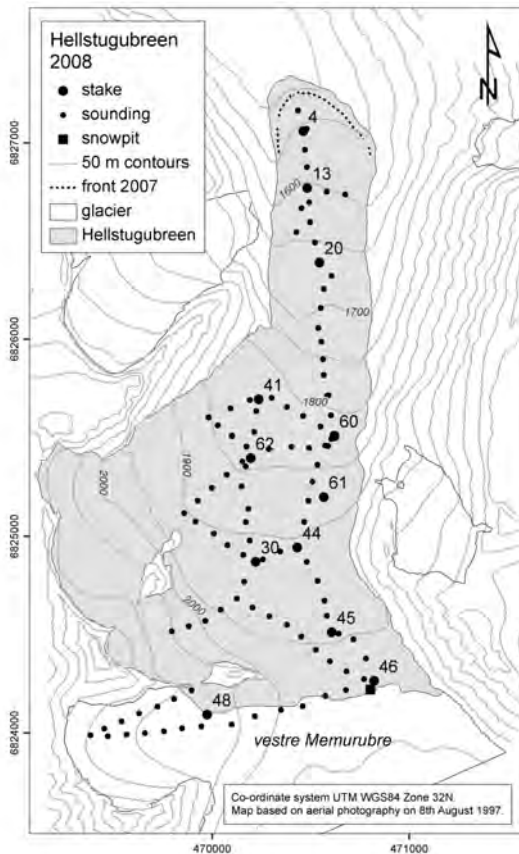


Figure 8-2
Map of Hellstugubreen showing the location of stakes, sounding profiles and snow pit in 2008. The position of the glacier front in 2007 (measured by handheld GPS) is also indicated.

Results

The mass balance results of 2008 are presented in Table 8-1 and Figure 8-3.

Winter balance

The winter balance was calculated from the soundings and the snow density measurement, which was considered to be representative for the whole glacier. The density in the snow pit was 0.45 g/cm^3 . The winter balance was calculated as the mean of the soundings within each 50-metre height interval and was $1.4 \pm 0.2 \text{ m w.e.}$ This is 123 % of the mean for the period 1971-2000.

Summer balance

Direct summer balance was calculated from stakes in 9 locations. The density of the melted ice was assumed to be 0.9 g/cm^3 and the density of remaining snow to be 0.6 g/cm^3 . The summer balance was calculated to be $-1.5 \pm 0.3 \text{ m w.e.}$, which is 104 % of the mean value for the period 1971-2000.

Net balance

The net balance of Hellstugubreen in 2008 was almost in balance, but slightly negative, $-0.1 \pm 0.3 \text{ m w.e.}$, which amounts to a volume loss of $-0.17 \pm 0.9 \text{ mill. m}^3$ water. The equilibrium line altitude (ELA) (calculated from Figure 8-3) was 1880 m a.s.l. resulting in an accumulation area ratio (AAR) of 57 %. The cumulative net balance since 1962 is -17.5 m w.e. , giving a mean annual deficit of 0.37 m w.e. per year (Fig. 8-4). The calculated annual net balance for Hellstugubreen has been negative every year since 2001. The cumulative deficit amounts to 7.2 m w.e. for the period 2001-2008.

Table 8-1
The distribution of winter, summer and net balance in 50 m altitudinal intervals for Hellstugubreen in 2008.

Mass balance Hellstugubreen 2007/08 – traditional method							
Altitude (m a.s.l.)	Area (km ²)	Winter balance Measured 6 May 2008		Summer balance Measured 18 Sep 2008		Net balance Summer surfaces 2007 - 2008	
		Specific (m w.e.)	Volume (10 ⁶ m ³)	Specific (m w.e.)	Volume (10 ⁶ m ³)	Specific (m w.e.)	Volume (10 ⁶ m ³)
2150 - 2210	0.02	1.80	0.04	-0.20	0.00	1.60	0.03
2100 - 2150	0.09	1.72	0.16	-0.41	-0.04	1.31	0.12
2050 - 2150	0.28	1.89	0.53	-0.50	-0.14	1.39	0.39
2000 - 2050	0.18	1.95	0.36	-0.76	-0.14	1.19	0.22
1950 - 2000	0.38	1.57	0.59	-0.98	-0.37	0.59	0.22
1900 - 1950	0.61	1.57	0.96	-1.20	-0.73	0.37	0.23
1850 - 1900	0.35	1.36	0.47	-1.44	-0.50	-0.08	-0.03
1800 - 1850	0.33	1.36	0.45	-1.70	-0.56	-0.34	-0.11
1750 - 1800	0.13	1.24	0.16	-1.94	-0.26	-0.70	-0.09
1700 - 1750	0.10	1.09	0.11	-2.16	-0.23	-1.07	-0.11
1650 - 1700	0.17	1.05	0.18	-2.35	-0.40	-1.30	-0.22
1600 - 1650	0.13	0.90	0.11	-2.60	-0.33	-1.70	-0.21
1550 - 1600	0.16	0.63	0.10	-2.85	-0.45	-2.22	-0.35
1500 - 1550	0.08	0.49	0.04	-3.13	-0.24	-2.64	-0.21
1480 - 1500	0.02	0.43	0.01	-3.30	-0.06	-2.87	-0.05
1480 - 2210	3.03	1.41	4.28	-1.47	-4.45	-0.06	-0.17

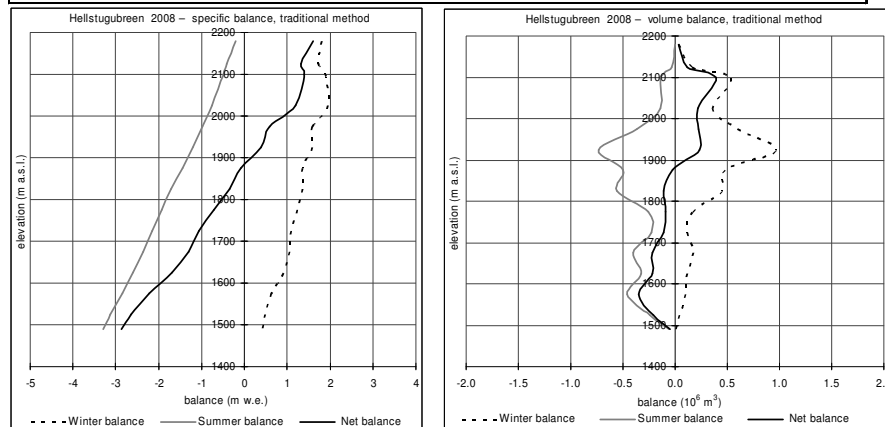


Figure 8-3
Mass balance diagram for Hellstugubreen in 2008, showing specific balance on the left and volume balance on the right.

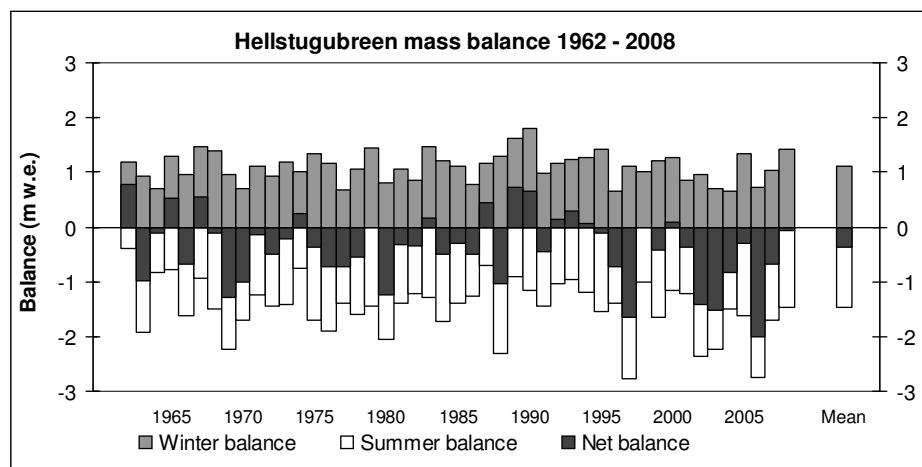


Figure 8-4
Winter, summer and net balance at Hellstugubreen for the period 1962-2008.

9. Gråsubreen (Liss M. Andreassen)

Gråsubreen (61°39' N, 8°37' E) is located in the eastern part of the Jotunheimen mountain area in southern Norway. The glacier covers an area of 2.2 km² and ranges in elevation from 1830 to 2290 m a.s.l. (Fig. 9-1). Mass balance investigations have been carried out annually since 1962 and 2008 is the 47th year of continuous measurements.

Gråsubreen is a polythermal glacier. Superimposed ice occurs in the central parts of the glacier where snowdrift causes a relatively thin snow pack.

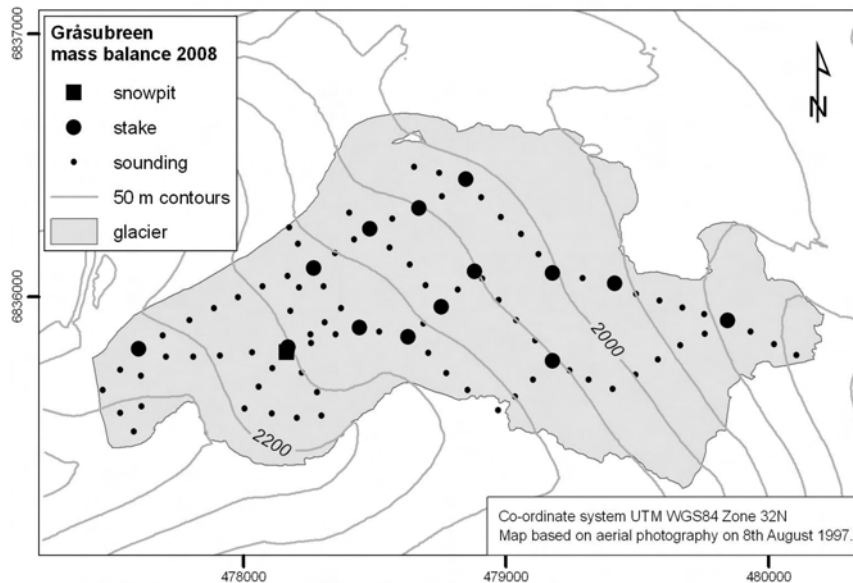


Figure 9-1
Map of Gråsubreen (shaded in grey) showing the location of stakes, snow pit and soundings in 2008.

9.1 Mass balance 2008

Fieldwork

Accumulation measurements were performed on 5th - 6th June 2008. The calculation of winter balance is based on:

- Measurements of stakes in 12 different positions.
- Soundings of snow depth in 93 positions between 1845 and 2275 m a.s.l., covering most of the altitudinal range of the glacier. The summer surface was easy to identify over the whole glacier. The snow depth varied between 0.36 and 3.2 m, the mean being 1.74 m.
- The snow density was measured by sampling in a pit near stake 8 at 2150 m a.s.l. where the total snow depth was 1.9 m.

Ablation measurements were carried out on 16th-17th September, when stakes in all locations were measured. A thin layer of new snow covered most of the glacier at the time of the ablation measurements (Fig. 9-2).



Figure 9-2
Field work at Gråsubreen in September 2008. A fresh layer of snow covered the glacier. View towards southwest to Glittertind. Photo: Jon Endre Hausberg.

Results

The mass balance results are presented in Table 9-1 and Figure 9-3.

Winter balance

Winter accumulation was calculated from the soundings and the snow density measurement, which was considered representative for the whole glacier. The mean measured snow density was 0.51 g/cm^3 . The stake recordings showed neither significant additional melting nor any significant formation of superimposed ice after the previous year's ablation measurements (on 12th September 2007).

The winter balance was calculated as the mean of the soundings within each 50-metre height interval. This gave a winter balance of $1.0 \pm 0.2 \text{ m w.e.}$, which is 121 % of the mean winter balance for the period 1971-2000.

Summer balance

Summer balance was calculated from direct measurements of stakes in eleven locations. The density of the remaining snow was estimated to be 0.60 g/cm^3 and melted ice was estimated to be 0.90 g/cm^3 . The resulting summer balance was $-0.9 \pm 0.3 \text{ m w.e.}$ The specific summer balance is 80 % of the mean for the period 1971-2000.

Net balance

The net balance of Gråsubreen in 2008 was slightly positive, $0.1 \pm 0.3 \text{ m w.e.}$ The mass balance diagram shows that the net balance curve intersects the y-axis at two elevations, at about 2100 and 1985 m a.s.l. due to the low accumulation in the central part of the glacier (Fig. 9-3). The equilibrium line altitude (ELA) and accumulation area ratio (AAR) were therefore not determined in 2008.

Gråsubreen has had a cumulative mass loss of -16.4 m w.e. since 1962, which is an average of -0.35 m w.e. per year. Most of this mass loss occurred in the 1970s and 1980s, and since 2001.

Table 9-1
The distribution of winter, summer and net balance in 50 m altitudinal intervals for Gråsubreen in 2008.

Mass balance Gråsubreen 2007/08 – traditional method							
Altitude (m a.s.l.)	Area (km ²)	Winter balance		Summer balance		Net balance	
		Measured 5 June 2008		Measured 16 Sep 2008		Summer surfaces 2007 - 2008	
		Specific (m w.e.)	Volume (10 ⁶ m ³)	Specific (m w.e.)	Volume (10 ⁶ m ³)	Specific (m w.e.)	Volume (10 ⁶ m ³)
2250 - 2290	0.04	0.85	0.04	-0.30	-0.01	0.55	0.02
2200 - 2250	0.17	0.69	0.11	-0.43	-0.07	0.26	0.04
2150 - 2200	0.26	1.01	0.27	-0.56	-0.15	0.45	0.12
2100 - 2150	0.34	0.79	0.27	-0.67	-0.23	0.12	0.04
2050 - 2100	0.37	0.73	0.27	-0.80	-0.30	-0.07	-0.03
2000 - 2050	0.42	0.86	0.36	-0.97	-0.41	-0.11	-0.04
1950 - 2000	0.36	1.16	0.41	-1.13	-0.40	0.03	0.01
1900 - 1950	0.14	1.36	0.19	-1.23	-0.18	0.13	0.02
1830 - 1900	0.15	1.37	0.21	-1.35	-0.21	0.02	0.00
1830 - 2290	2.25	0.95	2.13	-0.86	-1.95	0.08	0.19

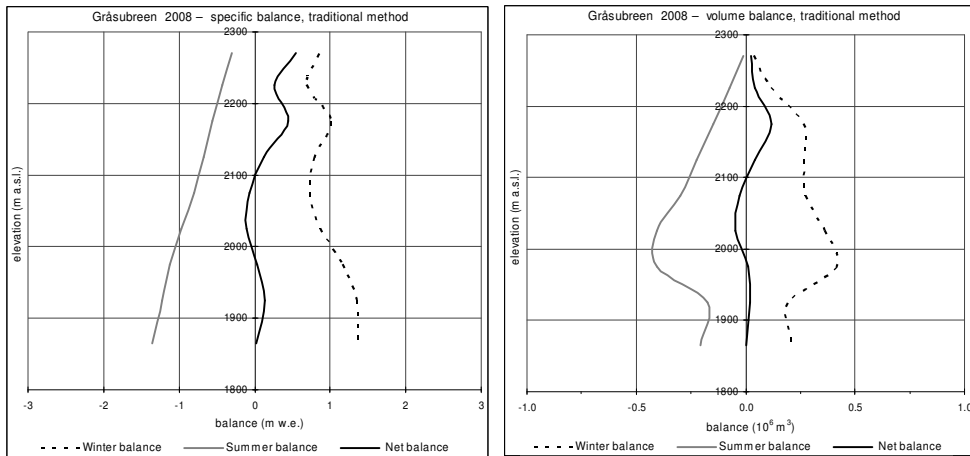


Figure 9-3
Mass balance diagram for Gråsubreen in 2008, showing specific balance on the left and volume balance on the right.

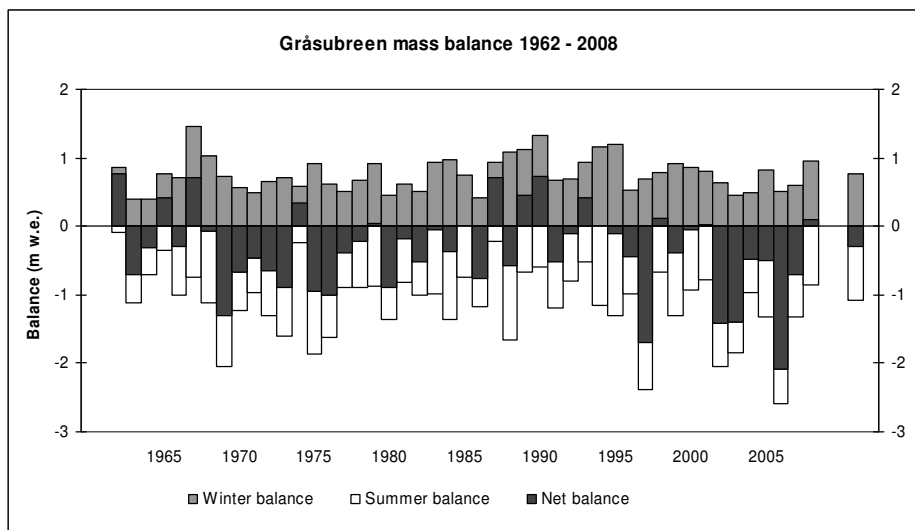


Figure 9-4
Winter, summer and net balance at Gråsubreen during the period 1962-2008.

10. Engabreen (Hallgeir Elvehøy and Miriam Jackson)

Engabreen (66°40'N, 13°45'E) is a 40 km² north-western outlet from the western Svartisen ice cap. It covers an altitude range from 1575 m a.s.l. (at Snøtind) down to 10 m a.s.l. (at Engabrevatnet), as shown in Figure 10-1. Mass balance measurements have been performed annually since 1970, and length change observations started in 1903 (chap. 12). A meteorological station has been operated at the nunatak Skjæret (1364 m a.s.l.) since 1995. In September 2008 this station was upgraded and measures wind speed, wind direction, global radiation, relative humidity and air temperature. In 2008 both Engabreen and Storglombreen was mapped using airborne laser altimetry (Lidar).

10.1 New map of Engabreen

As part of the International Polar Year (IPY) project Glaciodyn a large part of Vestisen (western Svartisen) was mapped on 2nd September 2008 (Blom Geomatics AS, Oslo, Norway). The point density varies between 2.6 and 6 points square metre. A homogeneity check investigating elevation deviations between neighbouring flight lines gave a total RM-error of 0.175 m. The highest deviations are found in steep terrain, as expected. Based on the point elevation data a 5 x 5 m DEM covering Engabreen, Litlebreen and Storglom-breen was constructed. A second quality check was carried out comparing the 5 x 5 m DEM with 438 point elevations measured with differential GPS (dGPS) on the glacier plateau on the same day as the ALS data collection. The dGPS reference station was Holandsfjord, 5 km north of the surveyed area. The difference between dGPS and ALS elevations was less than 0.2 m at 96.5 % of the dGPS points.

The glacier outline was mapped using a combination of laser intensity values and terrain relief. The drainage basin for calculation of the mass balance at Engabreen was updated using the new glacier outline.

The elevation distribution was calculated by counting grid cells within 100 metre elevation bins, each grid cell representing 25 m². The elevation and volume changes will be discussed elsewhere.

10.2 Mass balance 2008

Fieldwork

The glacier was visited on 7th March. Stakes in positions E105, E101 and E17 were measured. The snow depth at the stakes on the plateau was 5.5 to 6 metres.

The locations of stakes and towers, the density pit and the sounding profile are shown in Figure 10-1. The calculation of the winter balance is based on the following measurements on 15th May:

- Direct measurement of snow depth at locations E105 (6.15 m) and E101 (5.75 m).
- Snow depth from coring at stake E5, E38 and E34, showing 6.35, 5.55 and 2.4 m of snow, respectively.

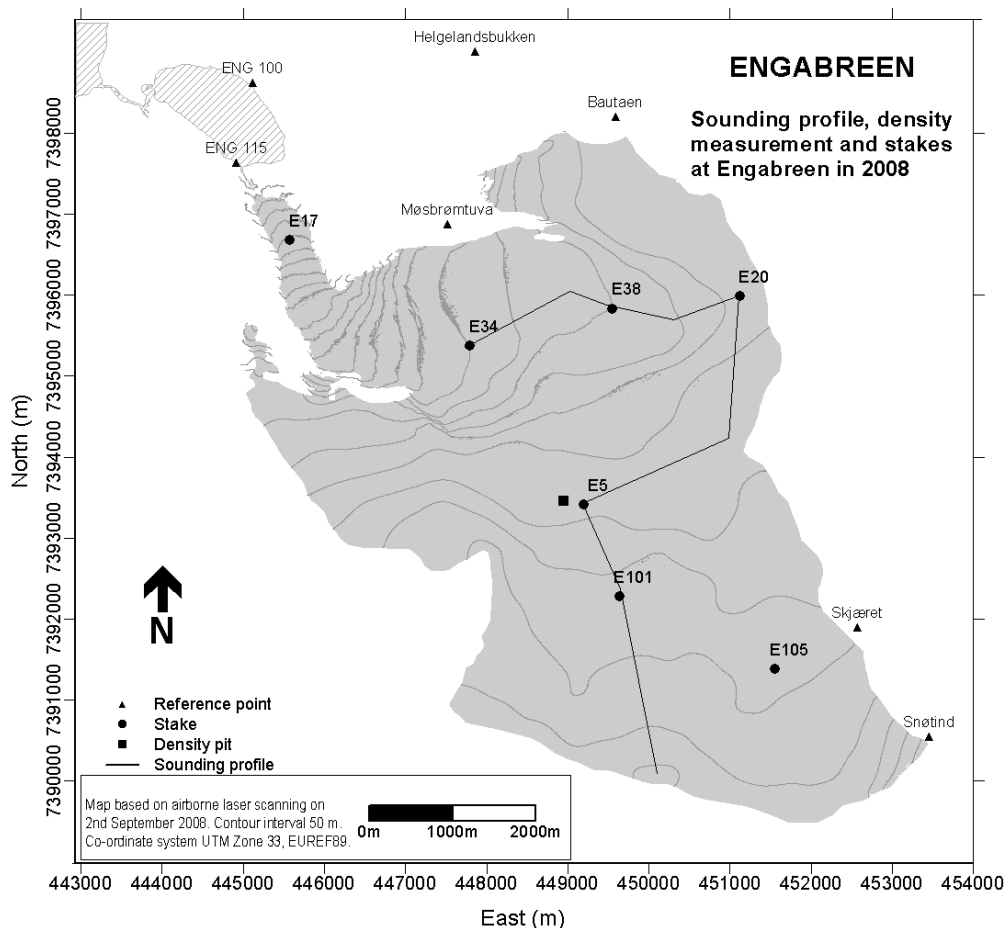


Figure 10-1
Location of stakes, density pit and sounding profiles on Engabreen in 2008.

- Snow depth sounding at 49 locations on a 11 km long profile and 5 extra locations. The snow depth was about 6 m at most of the locations above 1200 m a.s.l., and mainly between 2 and 6 m between 950 and 1200 m a.s.l.
- Direct measurement of 0.5 m of ice melt at location E17.
- Snow density measured down to the summer surface (SS) at 5.55 m depth at stake E5. The mean snow density was 0.54 g/cm^3 .

The stake in position E17 at the tongue melted out around 29th July, and it was replaced on 5th August. About 6 m of ice melted before 5th August, and 2.7 m ice melted between 5th August and 3rd October. At the plateau, between 3.5 and 5 m of snow melted between 15th May and 2nd September. After 2nd September up to 0.7 m snow melted before the winter snow accumulation started.

The net and summer balance measurements were carried out on 3rd October. There was up to 0.5 m of new snow on the glacier plateau. Stakes were found in seven locations (E17, E34, E38, E20, E5, E101 and E105). From stake measurements the TSL altitude was between 960 and 1050 m a.s.l. At stake E34 all the snow and 3 m of ice had melted during summer. At the stakes above the TSL 1 to 2.5 m of snow remained.

Results

The mass balance is calculated using the stratigraphic method, which reports the balance between two successive "summer surfaces", excluding snow accumulation before the date of net balance measurements but also excluding ablation after net balance measurements. The mass balance calculations are based on a map from 2008.

Winter balance

The temperature record at Skjæret (Fig. 10-1 for location) shows that the air temperature on the glacier plateau was at or below zero for most of the period between 25th August and 13th November 2007. This implies that no significant late autumn melting occurred. The winter maximum snow-water-equivalent (SWE) occurred around the date of the snow measurements 15th May 2008. At stake E34 the maximum SWE occurred a little earlier, around 1st May, and at the glacier tongue melting probably occurred in periods through the entire winter season. This run-off volume has not been calculated.

The calculation of the winter balance was based on point measurements of snow depth (stake readings, coring and snow depth soundings) and on snow density measurements. A water equivalent profile was modelled from the snow density measured at stake E5 (1240 m a.s.l.). This model was then used to calculate the water equivalent value of the snow depth measurements.

Point values of the snow water equivalent (SWE) were plotted against altitude, and a curve was drawn based on visual evaluation (Fig. 10-2). Below 960 m a.s.l. the winter balance curve was interpolated based on the observed snow depth at stake E34 and the observed negative winter balance at stake E17. Based on this altitudinal distribution curve, the winter balance was calculated as 2.8 ± 0.2 m w.e., which corresponds to a volume of 109 ± 8 mill. m³ of water. This is 96 % of the mean value for the period 1970-2007 (2.94 m w.e.), and 102 % of the mean value for the 5-year period 2003-2007 (2.77 m w.e.).

Summer balance

The summer balance was measured directly at stakes E105 and E101. It was calculated from snow depth sounding and stake measurements at stakes E34, E38, E20 and E5. At location E17 some of the summer melting had to be estimated. An altitudinal distribution curve was drawn based on the calculated summer balance in seven locations between 300 and 1350 m a.s.l. (Fig. 10-2). The summer balance was calculated as -2.5 ± 0.2 m w.e., which equals a volume of -97 ± 8 mill. m³ water. This is 107 % of the average for the period 1970-2007 (-2.33 m w.e.), but 97 % of the average for the 5-year period 2003-2007 (-2.58 m w.e.).

Net balance

The net balance of Engabreen for 2008 was calculated as 0.3 ± 0.3 m w.e., which corresponds to a mass gain of 10 ± 10 mill. m³ water. The mean value for the period 1970-2007 is $+0.60$ m w.e., but $+0.19$ m w.e. for 2003-2007. The equilibrium line altitude (ELA) was determined as 1093 m a.s.l. from the net balance curve in Figure 10-2. This corresponds to an accumulation area ratio (AAR) of 77 %. The mass balance results are shown in Figure 10-2 and Table 10-1. The results from 2008 are compared with mass balance results for the period 1970-2007 in Figure 10-3.

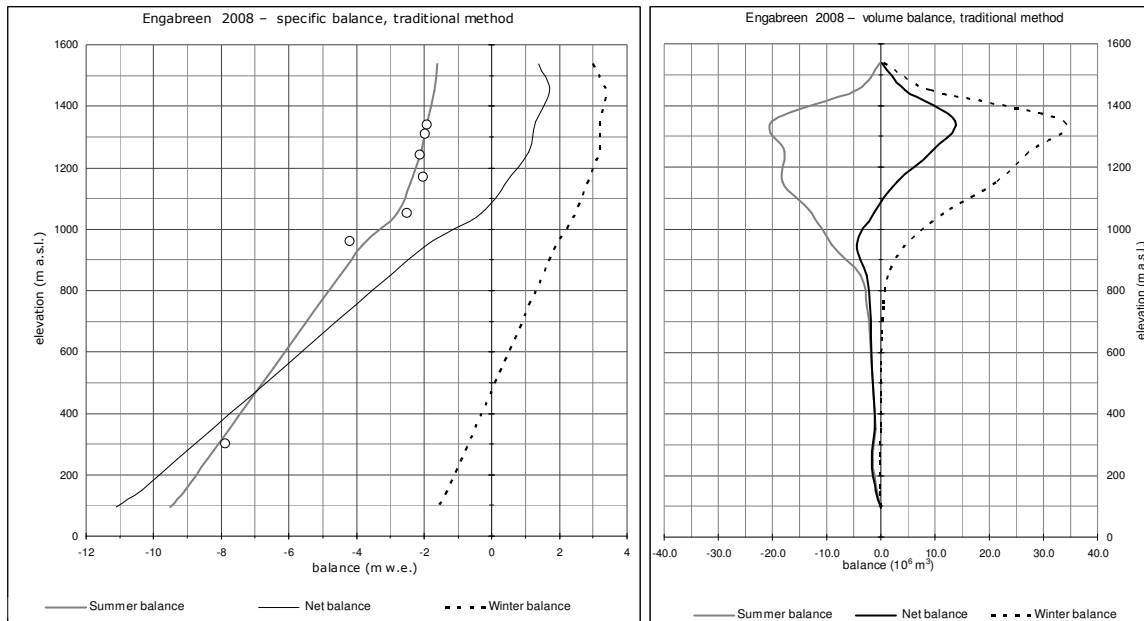


Figure 10-2
Mass balance diagram showing specific balance (left) and volume balance (right) for Engabreen in 2008.
Summer balance at stakes and towers is shown as circles (o).

Table 10-1
Specific and volume winter, summer and net balance calculated for 100 m elevation intervals at Engabreen in 2008, using the map from 2008.

Mass balance Engabreen 2007/08 – traditional method							
Altitude (m a.s.l.)	Area (km ²)	Winter balance		Summer balance		Net balance	
		Measured 15th May 2008		Measured 3rd Oct 2008		Summer surface 2007 - 2008	
		Specific (m w.e.)	Volume (10 ⁶ m ³)	Specific (m w.e.)	Volume (10 ⁶ m ³)	Specific (m w.e.)	Volume (10 ⁶ m ³)
1500 - 1574	0.10	3.00	0.3	-1.60	-0.2	1.40	0.1
1400 - 1500	2.65	3.40	9.0	-1.70	-4.5	1.70	4.5
1300 - 1400	10.49	3.20	33.6	-1.90	-19.9	1.30	13.6
1200 - 1300	8.46	3.20	27.1	-2.10	-17.8	1.10	9.3
1100 - 1200	7.56	2.80	21.2	-2.40	-18.1	0.40	3.0
1000 - 1100	4.57	2.50	11.4	-2.80	-12.8	-0.30	-1.4
900 - 1000	2.38	1.90	4.5	-3.80	-9.1	-1.90	-4.5
800 - 900	0.84	1.50	1.3	-4.50	-3.8	-3.00	-2.5
700 - 800	0.51	1.10	0.6	-5.15	-2.6	-4.05	-2.1
600 - 700	0.35	0.70	0.2	-5.80	-2.0	-5.10	-1.8
500 - 600	0.26	0.30	0.1	-6.45	-1.7	-6.15	-1.6
400 - 500	0.17	-0.10	0.0	-7.10	-1.2	-7.20	-1.2
300 - 400	0.13	-0.50	-0.1	-7.75	-1.0	-8.25	-1.0
200 - 300	0.18	-0.90	-0.2	-8.40	-1.5	-9.30	-1.7
100 - 200	0.09	-1.30	-0.1	-9.05	-0.8	-10.35	-0.9
89 - 100	0.00	-1.60	0.0	-9.50	0.0	-11.10	0.0
85 - 1574	38.74	2.81	108.9	-2.50	-97.0	0.31	11.9

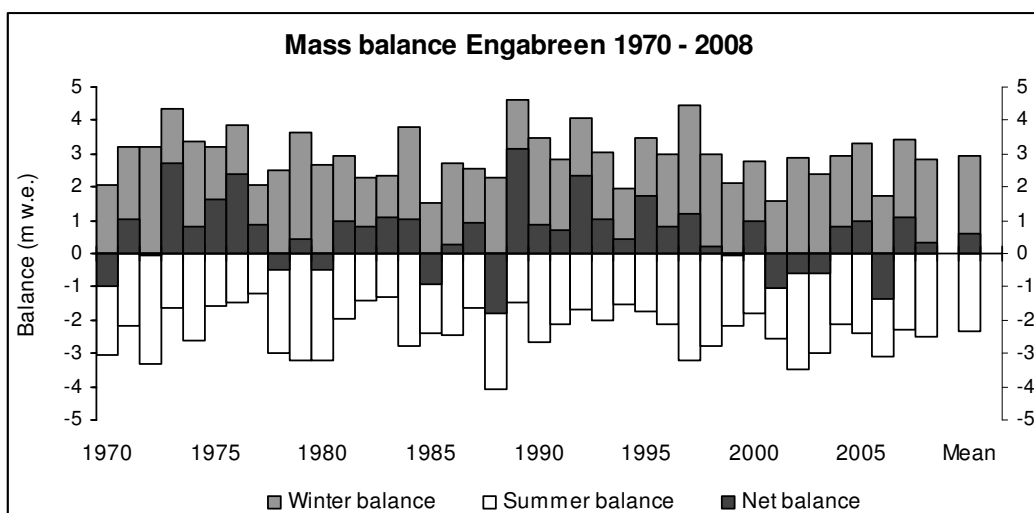


Figure 10-3
Mass balance at Engabreen during the period 1970-2008. The average winter, summer and net balances are $b_w = 2.93$ m w.e., $b_s = -2.34$ m w.e., and $b_n = 0.59$ m w.e.

10.3 Meteorological observations

A meteorological station recording air temperature and global radiation is located on the nunatak Skjæret (1364 m a.s.l.) close to the drainage divide between Engabreen and Storglombreen (Fig. 10-1). The station has recorded data since 1995 with some gaps. In September the station was upgraded to include humidity, wind direction and wind speed. The nearest meteorological station is 80700 Glomfjord (39 m a.s.l.), 19 km north of Skjæret. This station has been operated by the Norwegian Meteorological Institute (DNMI) since 1916. The precipitation record has been incomplete since 2004. The precipitation station 80740 Reipå (9 m a.s.l.) has been operated by the Norwegian Meteorological Institute (DNMI) since 1995. This station is located 28 km north of Engabreen and 19 km north-west of Glomfjord.

In 2008, data was collected at Skjæret with no gaps (Fig. 10-4). When the autumn measurements were carried out on 13th November 2007 up to 2 metres of snow had accumulated on the glacier plateau. The air temperature was mainly close to or above freezing during the first half of October. The coldest period this winter was around 21st March when the daily mean temperature was -17.7 °C. The first period in spring with daily temperatures above 0 °C was 29th April to 3rd May. The temperature was then mainly below 0 °C until 29th May. The snow measurements were performed on 15th May. The temperature stayed above 0 °C even at night from 29th May until 8th June. The maximum daily temperature was measured on 28th July (13.1 °C). Except for cold periods between 9th and 13th June and from 24th to 27th June the air temperature was at or above 0 °C until 26th September. At Skjæret the summer mean temperature was 2.7 °C which is 1.4 °C lower than in the warm summers of 2002 and 2006 but similar to 2001, 2005 and 2007.

In Glomfjord the mean annual temperature in 2008 was 6.1 °C, which is 1.1 °C above the 1961-90 average. The summer temperature in Glomfjord (1st June -30th September, 11.9 °C) was 0.8 °C higher than the 1961-90 average.

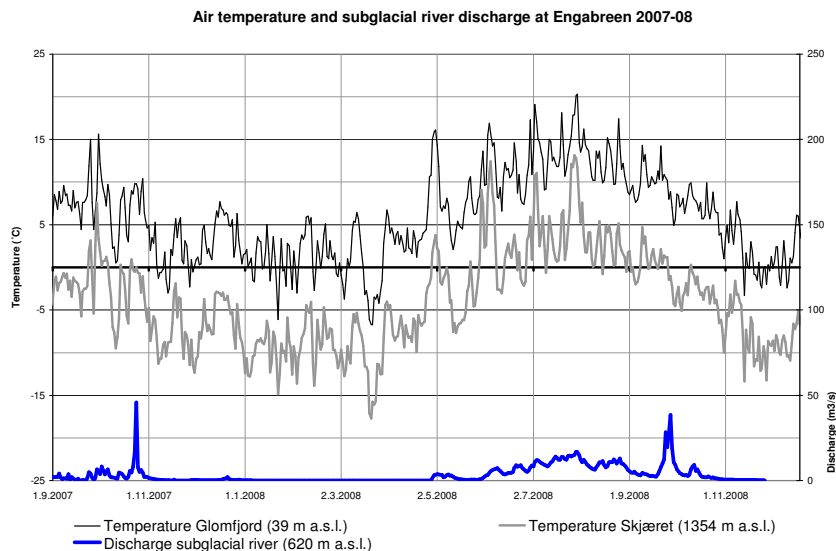


Figure 10-4
Daily mean air temperature at Skjæret (159.20) and Glomfjord (80700), and discharge in the subglacial river intake beneath Engabreen between 1st September 2007 and 31st December 2008.

At the precipitation station Reipå the recorded winter precipitation in 2008 was 877 mm, which is more than in 2001 and 2003, but comparable to 2004. The 1961-90 annual mean is estimated as 1452 mm (71 % of Glomfjord). A comparison of winter precipitation sums (1st October – 31st May) from 1997 to 2002 indicates that Reipå gets 67 % of the winter precipitation in Glomfjord. This suggests that the winter precipitation in Glomfjord in 2008 was a little less than the 1961-1990 average.

10.4 Svartisen subglacial laboratory

Svartisen Subglacial Laboratory is a unique facility situated under Engabreen. It allows direct access to the bed of the glacier for the purposes of measuring sub-glacial parameters and performing experiments on the ice. Further general information about the laboratory is available in report number 14 in NVE's document series for 2000, entitled 'Svartisen Subglacial Laboratory' (Jackson, 2000).

Pressure measurements

Six load cells were installed at the bed of the glacier in December 1992 in order to measure variations in subglacial pressure. The load cells are Geonor P-105 Earth Pressure Cells. Readings are recorded from the load cells at 15 minute intervals (more frequently when experiments are being performed). Four of these load cells were still functioning at the beginning of 2008. A further two load cells were installed in November 1997 and were also still operating into 2008 (Fig. 10-5). One load cell (1e) recorded very little data from mid-March to June, but showed reliable values from July onwards. Another load cell (97-1) registered only error (or nonsense) values for much of August and September. On 11th October the Campbell datalogger suddenly started registering only error values for all load cells. This was due to an electronics problem and has now been fixed, but there were no more data recorded in 2008. There is a break in the data in mid-May, as this was during a field campaign and data was recorded at a different data interval, so is not presented here. A seventh load cell (number 7, Fig 10-5), has recorded intermittently since installation in November 2003, and showed error values for much of 2008, hence

these results are not included here. Note that the graphs of load cell pressure variations have different axes.

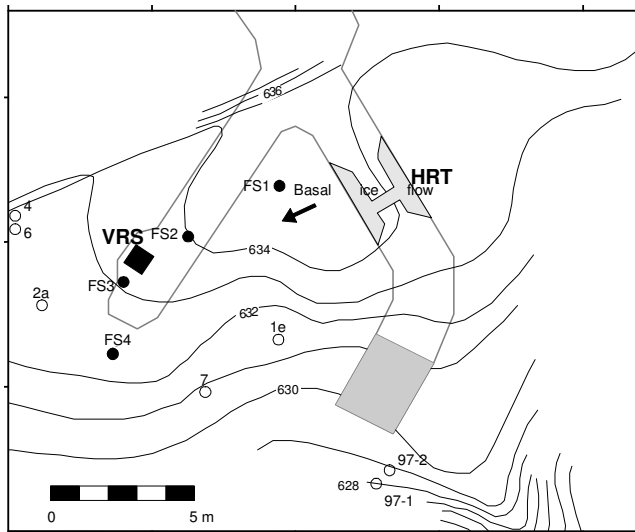


Figure 10-5
Tunnel system showing locations of horizontal research tunnel (HRT) and vertical research shaft (VRS), load cells 1e, 2a, 4, 6, 97-1 and 97-2 and boreholes, marked FS.

Pressure sensor records for winter 2008 from 1st January to 31st March are shown in Figure 10-6. The records are generally typical for the winter period - relatively quiet and stable, corresponding with very low discharge measured in the subglacial tunnel, although somewhat noisier than is usual. Temperatures as measured at the meteorological station (Fig. 10-4) at Skjæret were low (between about -18°C and -4°C) and discharge in the subglacial tunnels was correspondingly low. Values measured at the pressure sensors were generally similar, although 97-1 was noticeably lower (by 2-3 bars) compared with the same period in 2007.

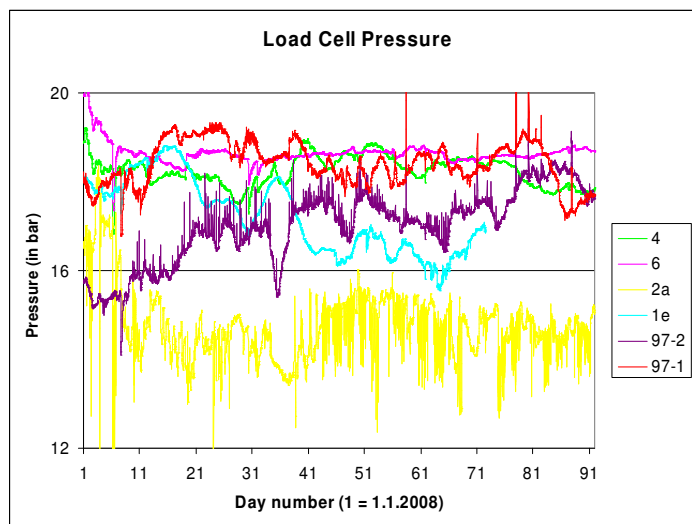


Figure 10-6
Pressure records for 1st January to 31st March.

Pressure sensor records for the late-spring and early-summer, from 1st April to 30th June, are shown in Figure 10-7. There are no data presented here for the period between 9:46 on 9th May and 7:01 on 14th May, because this was during a measurement campaign on the glacier surface and a different recording interval was used at this time. This period is

represented by a break in the graph. The first major melting event occurred between 29th April and 3rd May when temperatures were unseasonably high. Discharge in the subglacial system rose rapidly, and this was quickly reflected at all load cells, which first dropped in value then sharply rose again as there was extensive meltwater under the glacier.

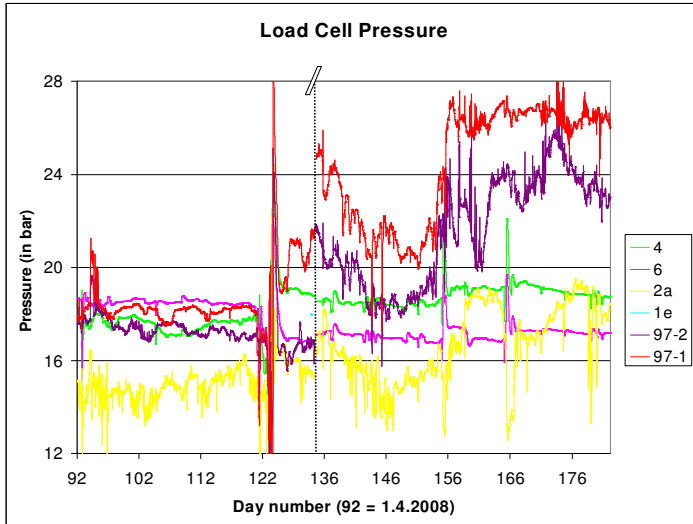


Figure 10-7
Pressure records for 1st April to 30th June. Note the gap in data between 9:46 on 9th May and 7:01 on 14th May.

Pressure sensor records for the summer and autumn, from 1st July to 11th October, are shown in Figure 10-8. These are fairly typical for the summer period. Changes in pressure recorded at the sensors are for the most part well-correlated with each other, although 97-2, shows some unusual variations. There was an unusually high amount of subglacial meltwater at the end of September that corresponds with a rainy period between 19th and 30th September, when there was probably more than 100 mm rain between 25th and 30th September. This is reflected in the pressure records especially at load cells 4 and 6, and also at 2a and 1e.

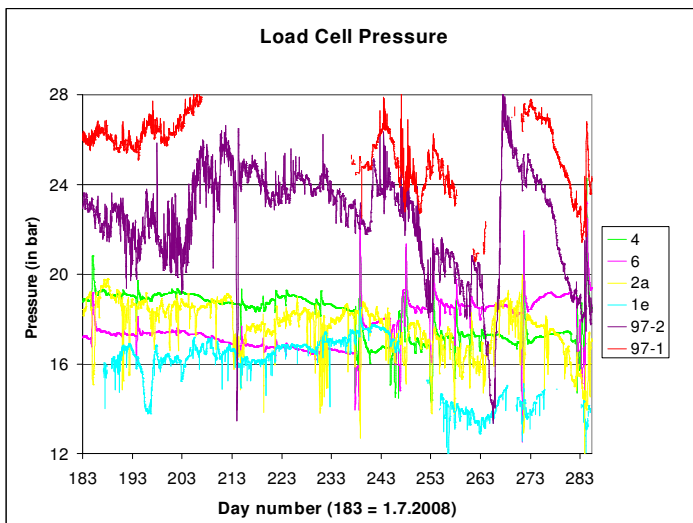


Figure 10-8
Pressure records for 1st July to 11th October.

11. Langfjordjøkelen (Bjarne Kjøllmoen)

Langfjordjøkelen (70°10'N, 21°45'E) is a plateau glacier situated on the border of Troms and Finnmark counties, approximately 60 km northwest of the city of Alta. It has an area of about 7.7 km² (2008), and of this 3.2 km² drains eastward. The investigations are performed on this east-facing part, ranging from 302 to 1050 m a.s.l.

The glaciological investigations in 2008 include mass balance and change in glacier length (chap. 12). Langfjordjøkelen has been the subject of mass balance measurements since 1989 with the exception of 1994 and 1995.

11.1 Mass balance 2008

New mapping of Langfjordjøkelen

The mass balance of Langfjordjøkelen was previously calculated using a map constructed from aerial photographs taken on 1st August 1994. As part of Glaciodyn, an International Polar Year project, NVE has constructed a new Digital Elevation Model (DEM) from airborne laser scanning acquired on 9th September 2008 (Blom Geomatics AS, Norway). This DEM is now used in the mass balance calculations.



Figure 11-1
The outlet of Langfjordjøkelen photographed on 26th May 2008 (left) and 5th August 2008 (right).
Photo: Kjetil Melvold (left) and Bjarne Kjøllmoen (right).

Fieldwork

Snow accumulation measurements

Snow accumulation was measured on 22nd May and the calculation of winter balance is based on (Fig. 11-2):

- Measurements of stakes in positions 10 (470 m a.s.l.), 20 (634 m a.s.l.) and 25 (724 m a.s.l.) showing snow depths of 2.1, 3.2 and 3.7 m respectively.
- 78 snow depth soundings between 309 and 1050 m elevation. Generally, the sounding conditions were reasonable over the whole glacier. However, the summer surface was

more difficult to detect in the upper areas. In general the snow depth varied between 2 and 5 m.

- Snow density was measured down to SS at 3.5 m depth at stake position 30.

Ablation measurements

Ablation was measured on 16th October. The net balance was measured at seven stakes in all five locations between 502 and 1050 m a.s.l. Since the snow measurements in May the stakes had increased in length between 4.2 m (724 m a.s.l.) and 4.8 m (634 m a.s.l.). There was about 1 m of snow remaining at the top of the glacier from the winter season 2007/2008. At the time of measurements up to 15 cm of fresh snow had fallen.

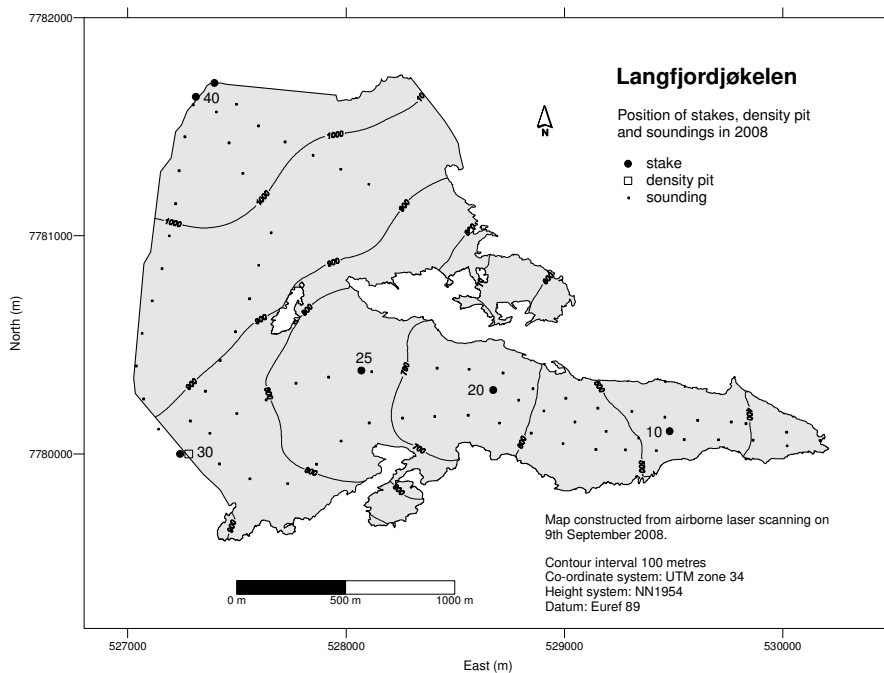


Figure 11-2
Location of stakes, soundings and snow pit at Langfjordjøkelen in 2008.

Results

The calculations are based on a glacier map from 2008.

Winter balance

The calculations of winter balance are based on several point measurements of snow depth (stakes and soundings) and on one snow density measurement.

There was no melting after the final measurements in November 2007. Consequently, winter *accumulation* and winter *balance* are equal.

A density profile was modelled from the snow density measurement at 884 m altitude. The mean density of 3.4 m snow was 0.46 g/cm^3 . The density model was used to convert all measured snow depths to water equivalent.

The winter balance calculations were performed by plotting the measurements (water equivalent) in a diagram. A curve was drawn based on visual evaluation (Fig. 11-4) and a mean value for each 50 m height interval was estimated (Tab. 11-1).

The winter balance was calculated as 1.7 ± 0.2 m w.e., corresponding to a water volume of 5 ± 1 mill. m^3 . The result is 77 % of the mean value for the periods 1989-1993 and 1996-2007. Only three years (2006, 2001 and 1999) have shown a lower winter balance since the measurements began in 1989.

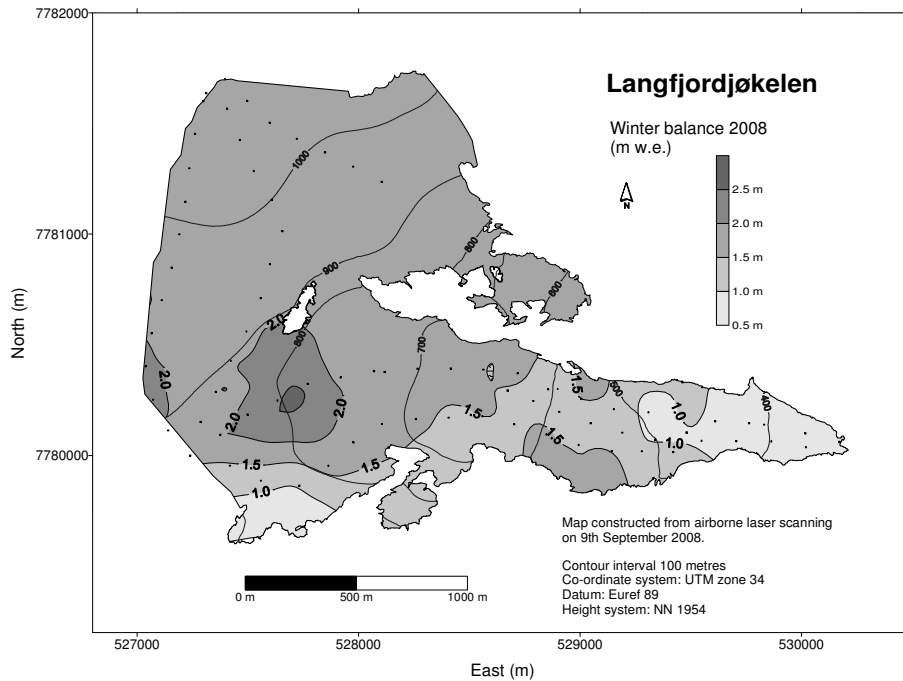


Figure 11-3
Winter balance at Langfjordjøkelen in 2008 interpolated from 82 snow depth measurements (•).

The winter balance was also calculated using a gridding method (Kriging) based on the aerial distribution of the snow depth measurements (Fig. 11-3). Water equivalents for each cell in a 100 x 100 m grid were calculated and summarised. The result obtained using this gridding method was 1.6 m w.e.

Summer balance

When calculating the summer balance the density of melted ice was taken as 0.90 g/cm^3 . The density of the remaining snow was empirically estimated as 0.60 g/cm^3 .

The summer balance was calculated at all five locations. The summer balance increased from -1.1 m w.e. at position 40 (1050 m a.s.l.) to -3.2 m w.e. at position 10 (470 m a.s.l.). Based on estimated density and stake measurements, the summer balance was calculated to be -2.0 ± 0.3 m w.e., which is -6 ± 1 mill. m^3 of water. The result is 67 % of the average for the periods 1989-1993 and 1996-2007. This is the lowest summer balance measured at Langfjordjøkelen.

Net balance

The net balance at Langfjordjøkelen for 2008 was -0.3 ± 0.3 m w.e., which equals a volume loss of -1 ± 1 mill. m^3 of water (Tab. 11-1). The mean value for the measurement periods 1989-93 and 1996-2007 is -0.87 m w.e. (Fig. 11-5), while the average over the 5-year period 2003-2007 is -1.3 m w.e.

Based on Figure 11-4, the Equilibrium Line Altitude (ELA) lies at 835 m a.s.l. Accordingly, the Accumulation Area Ratio is 53 %.

The mass balance results are shown in Table 11-1. The corresponding curves for specific and volume balance are shown in Figure 11-4. The historical mass balance results are presented in Figure 11-5.

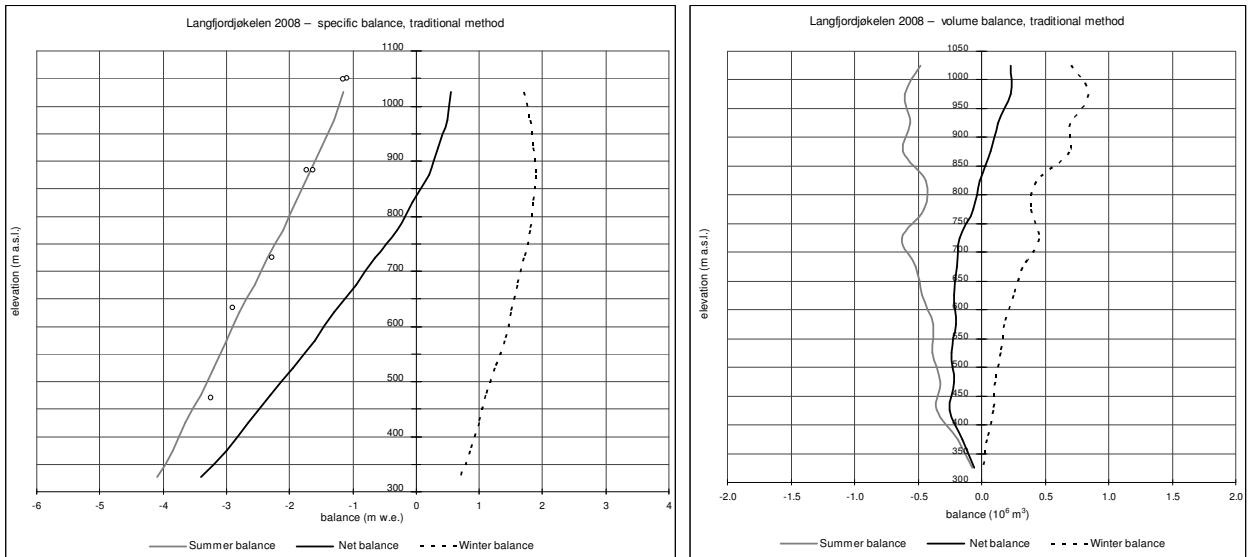


Figure 11-4
Mass balance diagram showing specific balance (left) and volume balance (right) for Langfjordjøkelen in 2008. Summer balance for seven stakes is shown (o).

Table 11-1
Winter, summer and net balance for Langfjordjøkelen in 2008. Mean values for the periods 1989-93 and 1996-2007 are $b_w = 2,16$ m, $b_s = -3,03$ m and $b_n = -0,87$ m w.e.

Mass balance Langfjordjøkelen 2007/08 – traditional method							
Altitude (m a.s.l.)	Area (km ²)	Winter balance		Summer balance		Net balance	
		Measured 22nd May 2008		Measured 16th Oct 2008		Summer surface 2007 - 2008	
		Specific (m w.e.)	Volume (10 ⁶ m ³)	Specific (m w.e.)	Volume (10 ⁶ m ³)	Specific (m w.e.)	Volume (10 ⁶ m ³)
1000 - 1050	0.42	1.70	0.7	-1.15	-0.5	0.55	0.2
950 - 1000	0.47	1.80	0.8	-1.30	-0.6	0.50	0.2
900 - 950	0.38	1.85	0.7	-1.50	-0.6	0.35	0.1
850 - 900	0.36	1.90	0.7	-1.70	-0.6	0.20	0.1
800 - 850	0.23	1.85	0.4	-1.90	-0.4	-0.05	0.0
750 - 800	0.22	1.80	0.4	-2.10	-0.5	-0.30	-0.1
700 - 750	0.27	1.70	0.5	-2.35	-0.6	-0.65	-0.2
650 - 700	0.20	1.60	0.3	-2.55	-0.5	-0.95	-0.2
600 - 650	0.17	1.50	0.3	-2.80	-0.5	-1.30	-0.2
550 - 600	0.13	1.40	0.2	-3.00	-0.4	-1.60	-0.2
500 - 550	0.12	1.25	0.2	-3.20	-0.4	-1.95	-0.2
450 - 500	0.10	1.10	0.1	-3.40	-0.3	-2.30	-0.2
400 - 450	0.10	1.00	0.1	-3.65	-0.3	-2.65	-0.3
350 - 400	0.05	0.85	0.0	-3.85	-0.2	-3.00	-0.1
302 - 350	0.02	0.70	0.0	-4.10	-0.1	-3.40	-0.1
302 - 1050	3.21	1.67	5.4	-2.02	-6.5	-0.35	-1.1

The balance year 2007/2008 is the twelfth successive year with significant negative net balance at Langfjordjøkelen. The cumulative net balance for the period 1989-2008 (estimated values for 1994 and 1995 included) is -16 m w.e.

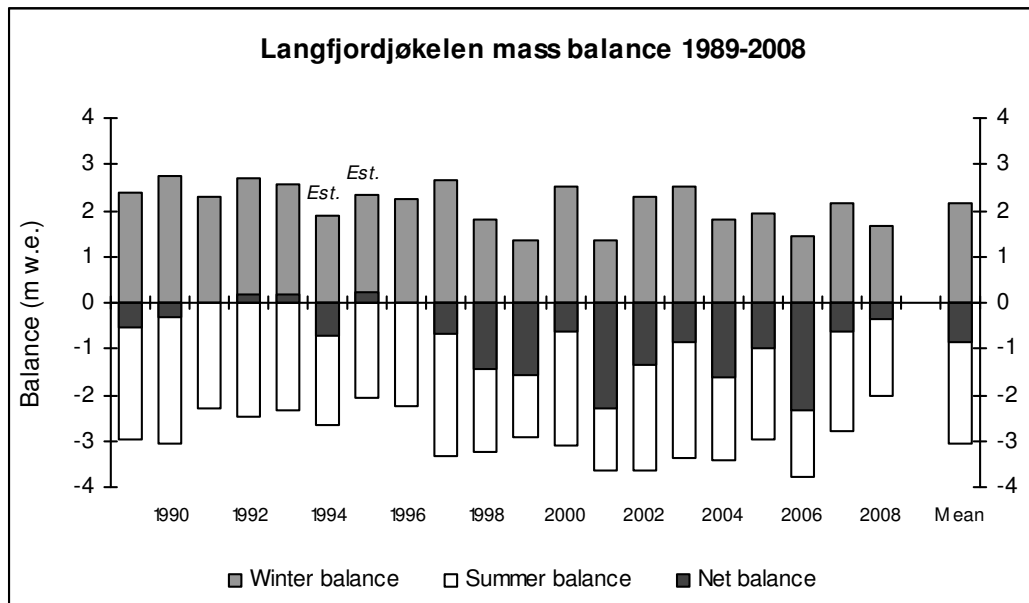


Figure 11-5
Mass balance at Langfjordjøkelen during the period 1989-2008. The total accumulated deficit over 1989-2008 is 15.7 m w.e. (includes estimated values for 1994-2008).

12. Glacier length change (Hallgeir Elvehøy)

Observations of glacier length change at Norwegian glaciers started around 1900. In 2008, glacier length change was measured for 32 glaciers - 24 in southern Norway and eight glaciers in northern Norway (Fig. 12-1). Length change measurements have been resumed at Tunsbergdalsbreen, an outlet glacier from Jostedalbreen (Fig. 12-2), and at Trollkyrkjebreen (Fig. 12-3) and Finnanbreen, two valley/cirque glaciers in Møre & Romsdal.

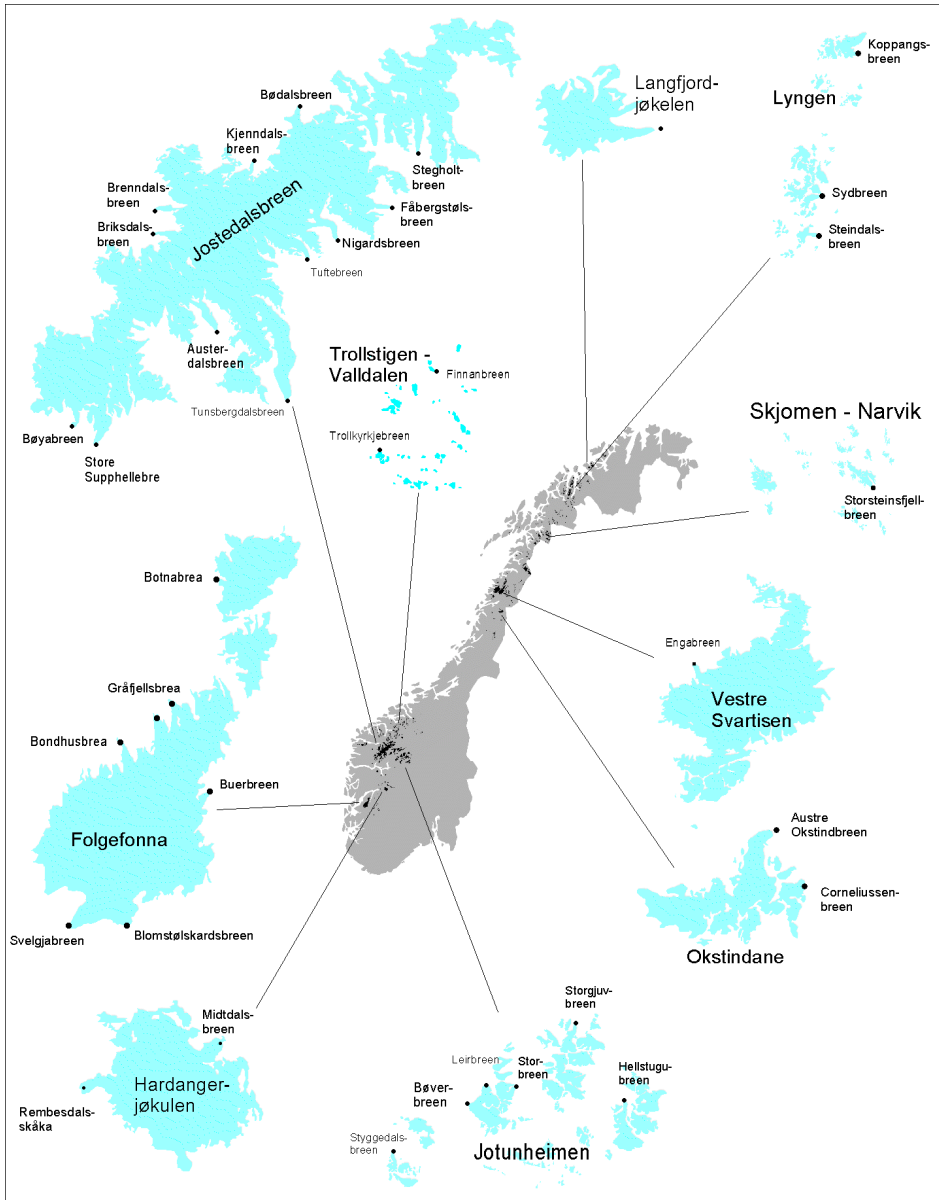


Figure 12-1
Location map showing glaciers where length change observations were performed in 2008. Note that the different glacier areas are not to the same scale.



Figure 12-2
Tunsbergdalsbreen was photographed on 5th July 2007. Glacier length change measurements were initiated in 1900. At that time the glacier terminus was located on the sandur in the lower central part of the photo. The glacier retreated 980 m between 1900 and 1960. Glacier length change measurements were resumed by Norsk bremuseum (Norwegian glacier museum) in 2008 when fixed points were established on the left bank of the proglacial lake. Photo: Miriam Jackson.

Methods

The distance to the glacier terminus is measured from one or several fixed points in defined directions, usually in September or October each year. The change in distance gives a rough estimate of the length change of the glacier. The representativity for the glacier tongue of the annual length change calculated from measurements from one reference point can be questionable. However, when longer time periods are considered the measurements give valuable information about glacier fluctuations, as well as regional tendencies and variations (Andreassen et al., 2005).

Results 2008

In 2008, 32 glaciers were measured, eight in northern Norway and 24 glaciers in southern Norway. The glacier length changes at the observed glaciers are listed in Table 12-1.

At Jostedalsbreen, Fåbergstølsbreen retreated 60 m, and has retreated a total of 166 m since 2000. Brenndalsbreen retreated 56 m, and has retreated 444 m since 2000. The average retreat of eleven outlet glaciers from Jostedalsbreen was 16 metres.

At Folgefonna, Bondhusbrea retreated 50 metres, and has retreated 287 m since 1996 when measurements resumed. At Hardangerjøkulen, Rembesdalskkåka retreated 35 metres, and has retreated 319 m since 1997.

In Jotunheimen, the length change rates are generally slow. Styggedalsbreen, Bøverbreen and Storgjuvbreen advanced slightly in the second half of the 1990s, and at Storbreen and Hellstugubreen the retreat rates were lower than in previous and following periods. After 2000 the rate of retreat has increased, but it is considerably lower than in the 1940s, 1950s and 1960s.

In Nordland, Engabreen retreated 29 m and has retreated 247 m since the last advance ended in 1999. Corneliussenbreen advanced during the 1970s, -80s and -90s, but has retreated 240 metres from its most recent end moraine which was formed late in the 1990s. Austre Okstindbreen has not changed significantly during the last two years, but has retreated from fresh end moraines probably formed in the 1990s, located on the shore of the pro-glacial lake Bretjørna, and terminates completely in this lake. Storsteinsfjellbreen in Skjomen retreated 470 m between 1963 and 2006 (–11 m/a), but retreated only 12 metres during the last two years. The glacier terminus is at present on a rock threshold.

In Troms and Finnmark the retreat at Koppangsbreen has decreased probably because the retreating terminus has reached a narrowing part of the valley. The mean retreat of four glaciers is 14 metres.



Figure 12-3
Photograph showing the terminus of Trollkyrkjebreen, a north-facing valley glacier in Valdalen, Møre & Romsdal, on 24th September 2008. The glacier area was 1.5 km² and covered the altitudinal interval between 1180 and 1570 m a.s.l. Glacier length change measurements were carried out between 1944 and 1974, and was re-initiated in 2008. The length change is measured on the western (right) side of the river. Photo: Tore Klokk.

Table 12-1
Glacier length change between autumn 2007 and autumn 2008. See Figure 12-1 for locations.

Region	Glacier	2007-08 (m)	Observer	Period(s) of length change measurements	Number of obs.	Change since	Length change
Jostedalbreen	Austerdalsbreen	-20	NVE	1905-20, 1933-	88	1933	-1386
	Brenndalsbreen	-56	SW	1900-62, 1996-	72	1900	-1591
	Briksdalsbreen	-12	NVE/AN	1900-	108	1900	-863
	Bødalsbreen	-22	SW	1900-53, 1996-	57	1900	-831
	Fåbergstølsbreen	-60	NVE	1899-	103	1899	-2435
	Kjendalsbreen	-4	SW	1900-52, 1996-	55	1996	-505
	Nigardsbreen	-1	NVE	1899-	97	1899	-2365
	Stegholtbreen	-30	NVE	1903-	102	1903	-1800
	Tuftebreen	-12	NVE	2007-	1		
	Tunsbergdalsbreen	X	NB	1900-1960, 2008-	55		
	Bøyabreen	32	NB	1899-1953, 2003-	52	2003	-106
Store Supphellebreen	9	NB	1899-1958, 1977-83, 1992-	74	1992	-46	
Folgefonna	Bondhusbrea	-50	S	1901-86, 1996-	75	1996	-287
	Botnabrea	-9 ¹	GK	1996-	10	1996	-31
	Blomstølskardsbreen	0	SKL	1994-	11	1994	-6
	Buerbreen	3	NVE	1900-80, 1995-	60	1900	-741
	Gråfjellsbrea	-19	S	2002-	9	1959	-864
	Svelgjåbreen	-1	SKL	2007-	1		
Hardanger- jøkulen	Midtdalsbreen	-31	AN	1982-	26	1982	-80
	Rembesdalsskåka	-35	S	1918-41, 1968-83, 1995-	30	1918	-1123
Jotunheimen	Bøverbreen	-2	SW	1903-12, 1936-63, 1997-	35	1997	-19
	Hellstugubreen	0	NVE	1901-	68	1901	-1071
	Leirbreen	NM	NVE	1909-	50	1909	-713
	Storbreen	-7	NVE	1902-	77	1902	-1088
	Storgjuvbreen	-4	SW	1901-12, 1933-63, 1997-	78	1997	+9
	Styggedalsbreen	9	NVE	1901-	87	1901	-492
Møre & Romsdal	Trollkyrkjebreen	X	NVE	1944-74, 2008-	28	1944	-289
	Finnanbreen	X	NVE	1950-74, 2008-	20	1950	-190
Okstindane	Austre Okstindbreen	2	NVE	1909-44, 2006-	22	2006	+3
	Corneliussenbreen	-24	NVE	2006-	2	2006	-66
Svartisen	Engabreen	-29	S	1903-	74	1903	-2191
Skjomen	Storsteinsfjellbreen	-9	NVE	2006-	2	2006	-12
Lyngen	Koppangsbreen	-4	NVE	1998-	8	1998	-167
	Sydbreen	-14	NVE	2007-	1		
	Steindalsbreen	-24	NVE	1998-	7	1998	-196
Finmark	Langfjordjøkelen	-18	NVE	1998-	10	1966	-1119

X: measurements started or resumed in 2008

NM: not measured in 2008

¹Since 2006 (the terminus of Botnabrea was snow-covered in 2007)

Observers:

AN: Prof. Atle. Nesje, University of Bergen

GK: Geir Knudsen, Tyssedal

NB: Norwegian glacier museum, Fjærland

S: Statkraft

SKL: Sunnhordland Kraftlag

SW: Dr. Stefan Winkler, Germany

Changes since 1982

In the 1980s, most of the observed glaciers retreated slowly (Fig. 12-4). Many outlet glaciers from coastal ice caps started to advance late in the 1980s. This advance ended before the turn of the century. At Stegholtbreen the advance didn't begin until 1996 and lasted four years. After 2000 the steep outlet glaciers have retreated quickly. At Nigardsbreen the retreating phase has been much less dramatic than at most other outlet glaciers. The more continental glaciers such as Hellstugubreen have been retreating slowly for decades.

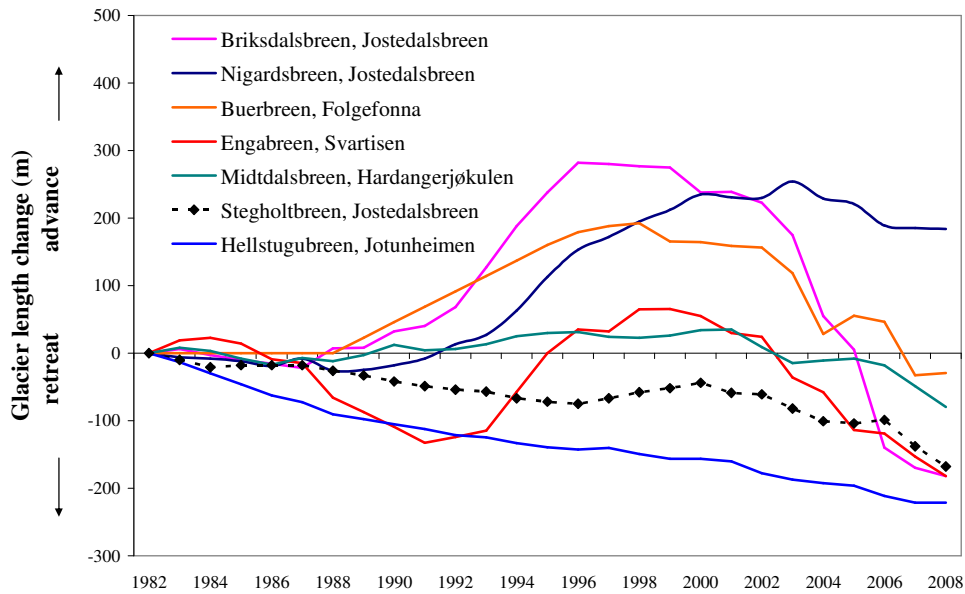


Figure 12-4
Cumulative glacier length change since 1982 at seven glaciers. See Figure 12-1 for locations.

13. References

- Andreassen, L.M., H. Elvehøy, B. Kjøllmoen., R. Engeset & N. Haakensen
2005: Glacier mass balance and length variation in Norway. *Annals of Glaciology*, 42, p. 317-325.
- Andreassen, L.M., M.R. van den Broeke, R.H. Giesen & J. Oerlemans
2008: A five-year record of surface energy and mass balance from the ablation zone of Storbreen, Norway. *Journal of Glaciology*, 54 (185), p. 245-258.
- Giesen, R.H., L.M. Andreassen, M.R. van den Broeke & J. Oerlemans
2009: Comparison of meteorology and surface energy balance at Storbreen, and Midtdalsbreen, two glaciers in southern Norway. *The Cryosphere*, 3, p. 57-74.
- Giesen, R.H., M.R. van den Broeke, J. Oerlemans & L.M. Andreassen
2008: Surface energy balance in the ablation zone of Midtdalsbreen, a glacier in southern Norway: Interannual variability and the effect of clouds, *Journal of Geophysical Research*, 113, D21111, doi:10.1029/2008JD010390.
- Jackson, M.
2000: Svartisen Subglacial Laboratory. *NVE Document 14 2000*, 27 pp.
- Kjøllmoen, B.
2007: Hydrologiske undersøkelser ved Maurangervassdraget. Årsrapport 2006. *NVE Oppdragsrapport 1 2007*, 30 pp.
- Kjøllmoen, B.
2008: Hydrologiske undersøkelser ved Maurangervassdraget. Årsrapport 2007. *NVE Oppdragsrapport 4 2008*, 32 pp.
- Laumann, T. & B. Wold
1992: Reactions of a calving glacier to large changes in water level. *Annals of Glaciology*, 16, p. 158-162.
- Liestøl, O.
1961: Glaciers and snowfields in Norway. In: Hoel, A. & W. Werenskiold (eds.). *Norsk Polarinstitutt Skrifter Nr. 114*.
- Pytte, R. (ed.)
1969: Glasiologiske undersøkelser i Norge 1969. *NVE Rapport 5 1970*, p. 17-25.
- Smith-Meyer, S. & A.M. Tvede
1996: Volumendringer på Søre Folgefonna mellom 1959 og 1995. *NVE Rapport 36 1996*, 12 pp.
- Tvede, A.M.
1972: En glasio-klimatisk undersøkelse av Folgefonna. *Hovedfagsoppgave i geografi, Universitetet i Oslo*.
- Tvede, A.M. (ed.)
1973: Glasiologiske undersøkelser i Norge i 1971. *NVE Rapport 2 1973*, p. 18-20.

Tvede, A.M. & O. Liestøl

1977: Blomstølskardbreen, Folgefonni, mass balance and recent fluctuations. *Norsk Polarinstitutt årsbok 1976*.

Tvede, A.M.

2008: Den store fonna. In: Brekke N.G. (ed.). Folgefonna og fjordbygdene. *Book from the publishing firm Nord 4*, p. 25-35.

Wold, B & J.O. Hagen (ed.)

1977: Glasiologiske undersøkelser i Norge 1975. *NVE Rapport 2 1977*, p. 13-15.

Østrem, G. & M. Brugman

1991: Glacier mass-balance measurements. A manual for field and office work. National Hydrology Research Institute, *Scientific Report, No. 4*. Environment Canada, N.H.R.I., Saskatoon and Norwegian Water Resources and Energy Directorate, Oslo, 224 pp.

Østrem, G. & T. Ziegler

1969: Atlas of glaciers in South Norway. *Meddelelse nr. 20 fra Hydrologisk avdeling, NVE*, 207 pp.

Østrem, G. & A.M. Tvede

1986: Comparison of glacier maps – a source of climatological information? *Geografiska Annaler, Vol. 68A*.

Appendix A

Publications published in 2008

Andreassen, L. M., F. Paul, A. Kääb & J.E. Hausberg

Landsat-derived glacier inventory for Jotunheimen, Norway, and deduced glacier changes since the 1930s. *The Cryosphere*, Vol. 2, No. 3, p 131-145.

Andreassen, L.M., M.R. van den Broeke, R. Giesen & J. Oerlemans

A 5 year record of surface energy and mass balance from the ablation zone of Storbreen, Norway. *Journal of Glaciology*, Vol. 54, No. 185, p 245-258.

Giesen, R.H., M.R. van den Broeke, J. Oerlemans & L.M. Andreassen

Surface energy balance in the ablation zone of Midtdalsbreen, a glacier in southern Norway: Interannual variability and the effect of clouds. *Journal of Geophysical Research*, Vol. 113, D21111, doi:10.1029/2008JD010390.

Giesen, R.H., L.M. Andreassen, M.R. van den Broeke & J. Oerlemans

Comparison of meteorology and surface energy balance at Storbreen, and Midtdalsbreen, two glaciers in southern Norway. *The Cryosphere Discussions Vol. 2, No. 5*, p 873-916.

Kjøllmoen, B. (Ed.)

Glaciological investigations in Norway in 2007. *NVE Report 3 2008*, 91 pp.

Schuler, T.V., P. Crochet, R. Hock, M. Jackson, I. Barstad & T. Jóhannesson

Distribution of snow accumulation on the Svartisen ice cap, Norway, assessed by a model of orographic precipitation. *Hydrological Processes*, Vol. 22, No. 19, p 3998-4008.

Appendix B

Mass balance measurements in Norway – an overview

During the period 1949-2008 there are carried out mass balance measurements at 42 Norwegian glaciers. The table below shows some characteristic data for the individual glaciers.

Area/ No. Glacier	Area (km ²)	Altitude (m a.s.l.)	Mapping year	Period	No. of years
Ålfotbreen					
1 Ålfotbreen	4.5	903-1382	1997	1963-	46
2 Hansebreen	3.1	930-1327	1997	1986-	23
Folgefonna					
3 Blomsterskardsbreen	45.7	850-1640	1959	1970-77	8
3a Svelgjåbreen*	22.5	832-1636	2007	2007-	2
3b Blomstølskardsbreen*	22.8	1013-1636	2007	2007-	2
4 Bondhusbrea	10.7	480-1635	1979	1977-81	5
5 Breidablikkbrea	3.4	1234-1651	2007	1963-68, 2003-	12
6 Gråfjellsbrea	8.4	1049-1651	2007	64-68, 74- 75, 2003-	13
7 Blåbreen and Ruklebreen	4.5	1065-1610	1959	1963-68	6
8 Midtre Folgefonna	8.7	1100-1570	1959	1970-71	2
Jostedalsbreen					
9 Jostefonn	3.8	960-1622	1993	1996-2000	5
10 Vesledalsbreen	4.2	1130-1730	1966	1967-72	6
11 Tunsbergdalsbreen	50.1	540-1930	1964	1966-72	7
12 Nigardsbreen	47.8	320-1960	1984	1962-	47
13 Store Supphellebreen	12.0	80-300/ 720-1740	1966	1964-67, 73- 75, 79-82	11
14 Austdalsbreen	11.8	1200-1757	1988	1988-	21
15 Spørteggubreen	27.9	1260-1770	1988	1988-91	4
16 Harbardsbreen	13.2	1250-1960	1996	1997-2001	5
Hardangerjøkulen					
17 Rembesdalskåka	17.1	1020-1865	1995	1963-	46
18 Midtdalsbreen	6.7	1380-1862	1995	2000-2001	2
19 Omnsbreen	1.5	1460-1570	1969	1966-70	5
Jotunheimen					
20 Tverråbreen	5.9	1415-2200		1962-63	2
21 Blåbreen	3.6	1550-2150	1961	1962-63	2
22 Storbreen	5.4	1390-2100	1997	1949-	60
23 Vestre Memurubre	9.0	1570-2230	1966	1968-72	5
24 Austre Memurubre	8.7	1630-2250	1966	1968-72	5
25 Hellstugubreen	3.0	1480-2210	1997	1962-	47
26 Gråsubreen	2.3	1830-2290	1997	1962-	47
Okstindbreene					
27 Charles Rabot Bre	1.1	1090-1760	1965	1970-73	4
28 Austre Okstindbre	14.0	730-1750	1962	1987-96	10
Svartisen					
29 Høgtuvbreen	2.6	590-1170	1972	1971-77	7
30 Svartisheibreen	5.5	770-1420	1985	1988-94	7
31 Engabreen	38.7	89-1574	2008	1970-	39
32 Storglombreen	59.2	520-1580		1985-88	10
	62.4	520-1580	1968	2000-05	
33 Tretten-null-tobreen	4.3	580-1260	1968	1985-86	2
34 Glombreen	2.2	870-1110	1953	1954-56	3
35 Kjølbreen	3.9	850-1250	1953	1954-56	3
36 Trollbergdalsbreen	1.8	900-1375	1968	1970-75	11
	1.6	900-1300	1985	1990-94	
Blåmannsisen					
37 Rundvassbreen	11.6	788-1537	1998	2002-04	3
Skjomen					
38 Blåisen	2.2	850-1200	1960	1963-68	6
39 Storsteinsfjellbreen	6.1	920-1850	1960	1964-68	10
	5.9	970-1850	1993	1991-95	
40 Cainhavarre	0.7	1210-1540	1960	1965-68	4
Vest-Finnmark					
41 Svartfjelljøkelen	2.7	500-1080	1966	1978-79	2
42 Langfjordjøkelen	3.7	280-1050	1994	1989-93,	18
	3.2	302-1050	2008	1996-	

* Part of Blomsterskardsbreen

Appendix C

Mass balance measurements in Norway – annual results

There are results from 585 years of measurements at Norwegian glaciers. The following tables show winter (bw), summer (bs) and net balance (bn) together with cumulative net balance (Cum. bn) and equilibrium line altitude (ELA) for every single year at each glacier. In front of each table there is a heading containing the name and the area of the glacier. The reported year (in brackets) corresponds to the given area.

1 Ålfotbreen - 4.5 km² (1997)

No. of years	Year	bw (m w.e.)	bs	bn (m w.e.)	Cum. bn	ELA (m a.s.l.)
1	1963	2.48	-3.58	-1.10	-1.10	1300
2	64	2.69	-2.41	0.28	-0.82	1140
3	65	3.64	-3.16	0.48	-0.34	1150
4	66	2.47	-4.08	-1.61	-1.95	>1380
5	67	4.46	-3.18	1.28	-0.67	950
6	68	4.55	-3.60	0.95	0.28	1075
7	69	2.66	-4.83	-2.17	-1.89	>1380
8	1970	2.60	-3.83	-1.23	-3.12	>1380
9	71	4.29	-3.35	0.94	-2.18	1140
10	72	3.81	-3.70	0.11	-2.07	1195
11	73	4.67	-2.49	2.18	0.11	<870
12	74	3.57	-2.54	1.03	1.14	1065
13	75	4.64	-3.43	1.21	2.35	1050
14	76	4.40	-2.87	1.53	3.88	<870
15	77	2.33	-2.89	-0.56	3.32	1280
16	78	2.56	-3.07	-0.51	2.81	1290
17	79	3.28	-3.41	-0.13	2.68	1240
18	1980	2.51	-3.30	-0.79	1.89	1275
19	81	4.04	-3.82	0.22	2.11	1210
20	82	3.35	-3.48	-0.13	1.98	1240
21	83	4.79	-3.19	1.60	3.58	1010
22	84	4.09	-2.77	1.32	4.90	1050
23	85	2.44	-3.00	-0.56	4.34	1290
24	86	2.35	-2.76	-0.41	3.93	1255
25	87	4.29	-2.22	2.07	6.00	<870
26	88	2.73	-5.21	-2.48	3.52	>1380
27	89	5.20	-2.93	2.27	5.79	1030
28	1990	5.98	-4.19	1.79	7.58	995
29	91	4.09	-3.30	0.79	8.37	1035
30	92	5.48	-3.19	2.29	10.66	1050
31	93	4.81	-2.74	2.07	12.73	<870
32	94	3.71	-2.92	0.79	13.52	925
33	95	5.10	-3.90	1.20	14.72	1120
34	96	1.83	-3.71	-1.88	12.84	>1380
35	97	4.22	-4.14	0.08	12.92	1200
36	98	3.66	-3.55	0.11	13.03	1240
37	99	4.61	-4.55	0.06	13.09	1245
38	2000	5.57	-3.58	1.99	15.08	1025
39	01	1.86	-3.95	-2.09	12.99	>1382
40	02	3.78	-5.31	-1.53	11.46	>1382
41	03	2.52	-5.03	-2.51	8.95	>1382
42	04	3.32	-3.42	-0.10	8.85	1225
43	05	4.99	-4.32	0.67	9.52	1135
44	06	2.69	-5.88	-3.19	6.33	>1382
45	07	4.49	-3.22	1.27	7.60	1000
46	08	4.04	-3.35	0.69	8.29	1130
Mean 1963-2008		3.73	-3.55	0.18		

2 Hansebreen - 3.1 km² (1997)

No. of years	Year	bw (m w.e.)	bs	bn (m w.e.)	Cum. bn	ELA (m a.s.l.)
1	1986	2.28	-2.87	-0.59	-0.59	1200
2	87	3.76	-2.63	1.13	0.54	1100
3	88	2.50	-5.24	-2.74	-2.20	>1320
4	89	4.13	-3.71	0.42	-1.78	1140
5	1990	4.42	-4.10	0.32	-1.46	1140
6	91	3.37	-3.11	0.26	-1.20	1125
7	92	4.41	-3.43	0.98	-0.22	1125
8	93	4.23	-3.15	1.08	0.86	<925
9	94	3.39	-2.97	0.42	1.28	1120
10	95	4.38	-3.90	0.48	1.76	1140
11	96	1.74	-3.76	-2.02	-0.26	>1320
12	97	3.77	-3.92	-0.15	-0.41	1160
13	98	3.21	-3.51	-0.30	-0.71	1170
14	99	4.30	-4.19	0.11	-0.60	1155
15	2000	4.69	-3.82	0.87	0.27	1075
16	01	1.71	-4.43	-2.72	-2.45	>1327
17	02	3.51	-5.44	-1.93	-4.38	>1327
18	03	2.45	-5.12	-2.67	-7.05	>1327
19	04	2.87	-3.38	-0.51	-7.56	1220
20	05	4.52	-4.61	-0.09	-7.65	1150
21	06	2.45	-6.43	-3.98	-11.63	>1327
22	07	4.07	-3.23	0.84	-10.79	1042
23	08	3.90	-3.65	0.25	-10.54	1125
Mean 1986-2008		3.48	-3.94	-0.46		

3 Blomsterskardsbreen - 45.7 km² (1959)

No. of years	Year	bw (m w.e.)	bs	bn (m w.e.)	Cum. bn	ELA (m a.s.l.)
1	1970					1370
2	71	2.85	-1.87	0.98	0.98	1240
3	72			0.32	1.30	1340
4	73			1.57	2.87	1180
5	74			0.51	3.38	1325
6	75			1.70	5.08	1170
7	76			1.40	6.48	1210
8	77			-1.40	5.08	>1640
Mean 1971-77				0.73		

3a Svelgjåbreen - 22.5 km² (2007)

No. of years	Year	bw (m w.e.)	bs	bn (m w.e.)	Cum. bn	ELA (m a.s.l.)
1	2007	3.89	-2.54	1.35	1.35	1205
2	08	3.65	-2.88	0.77	2.12	1225
Mean 2007-08		3.77	-2.71	1.06		

3b Blomstølskardsbreen - 22.8 km² (2007)

No. of years	Year	bw (m w.e.)	bs	bn (m w.e.)	Cum. bn	ELA (m a.s.l.)
1	2007	4.17	-2.30	1.87	1.87	1230
2	08	3.69	-2.36	1.33	3.20	1260
Mean 2007-08		3.93	-2.33	1.60		

4 Bondhusbrea - 10.7 km² (1979)

No. of years	Year	bw (m w.e.)	bs	bn (m w.e.)	Cum. bn	ELA (m a.s.l.)
1	77	1.96	-2.96	-1.00	-1.00	1620
2	78	2.37	-2.88	-0.51	-1.51	1540
3	79	2.82	-2.49	0.33	-1.18	1445
4	1980	2.33	-2.78	-0.45	-1.63	1500
5	81	3.32	-2.00	1.32	-0.31	1460
Mean 1977-81		2.56	-2.62	-0.06		

5 Breidablikkbrea - 3.4 km² (2007)

No. of years	Year	bw (m w.e.)	bs	bn (m w.e.)	Cum. bn (m w.e.)	ELA (m a.s.l.)
1	1963	1.11	-2.32	-1.21	-1.21	1635
2	64	1.92	-1.68	0.24	-0.97	1450
3	65	1.72	-2.28	-0.56	-1.53	1525
4	66	1.52	-3.17	-1.65	-3.18	>1660
5	67	3.40	-2.23	1.17	-2.01	1355
6	68	3.55	-2.68	0.87	-1.14	1360
7	2003	2.12	-4.38	-2.26	-2.26	>1659
8	04	2.25	-3.12	-0.87	-3.13	1595
9	05	3.04	-3.37	-0.33	-3.46	1510
10	06	1.49	-4.44	-2.95	-6.41	>1659
11	07	3.42	-3.07	0.35	-6.06	1410
12	08	2.71	-2.96	-0.25	-6.31	1505
Mean 1963-68		2.20	-2.39	-0.19		
Mean 2003-08		2.51	-3.56	-1.05		

6 Gråfjellsbrea - 8.4 km² (2007)

No. of years	Year	bw (m w.e.)	bs	bn (m w.e.)	Cum. bn (m w.e.)	ELA (m a.s.l.)
1	1964	1.94	-1.62	0.32	0.32	1385
2	65	2.01	-2.29	-0.28	0.04	1490
3	66	1.58	-2.93	-1.35	-1.31	>1660
4	67	3.46	-2.14	1.32	0.01	1355
5	68	3.39	-2.82	0.57	0.58	1380
6	1974	2.11	-1.53	0.58	0.58	1370
7	75	2.53	-2.28	0.25	0.83	1420
8	2003	1.91	-4.09	-2.18	-2.18	>1659
9	04	2.05	-2.82	-0.77	-2.95	1565
10	05	3.15	-3.13	0.02	-2.93	1460
11	06	1.40	-4.55	-3.15	-6.08	>1659
12	07	3.60	-2.85	0.75	-5.33	1395
13	08	2.72	-2.80	-0.08	-5.41	1580
Mean 1964-68		2.48	-2.36	0.12		
Mean 1974-75		2.32	-1.91	0.42		
Mean 2003-08		2.47	-3.37	-0.90		

7 Blåbreen and Ruklebreen - 4.5 km² (1959)

No. of years	Year	bw (m w.e.)	bs	bn (m w.e.)	Cum. bn (m w.e.)	ELA (m a.s.l.)
1	1963 ¹⁾	1.30	-3.40	-2.10	-2.10	1620
2	64	2.18	-1.68	0.50	-1.60	1350
3	65	2.53	-2.48	0.05	-1.55	1450
4	66	1.76	-3.26	-1.50	-3.05	>1620
5	67	3.86	-2.56	1.30	-1.75	1300
6	68	3.18	-2.80	0.38	-1.37	1395
Mean 1963-68		2.47	-2.70	-0.23		

¹⁾ Blåbreen only

8 Midtre Folgefonna - 8.7 km² (1959)

No. of years	Year	bw (m w.e.)	bs	bn (m w.e.)	Cum. bn (m w.e.)	ELA (m a.s.l.)
1	1970	2.07	-2.69	-0.62	-0.62	>1580
2	71	2.33	-1.96	0.37	-0.25	1260
Mean 1970-71		2.20	-2.33	-0.13		

9 Jostefonn - 3.8 km² (1993)

No. of years	Year	bw (m w.e.)	bs	bn (m w.e.)	Cum. bn (m w.e.)	ELA (m a.s.l.)
1	1996	1.19	-2.72	-1.53	-1.53	>1620
2	97	3.59	-3.87	-0.28	-1.81	1500
3	98	2.84	-2.54	0.30	-1.51	1250
4	99	2.92	-2.54	0.38	-1.13	1200
5	2000	3.49	-2.47	1.02	-0.11	1050
Mean 1996-2000		2.81	-2.83	-0.02		

10 Vesledalsbreen - 4.2 km² (1966)

No. of years	Year	bw (m w.e.)	bs	bn (m w.e.)	Cum. bn (m w.e.)	ELA (m a.s.l.)
1	1967	2.06	-1.71	0.35	0.35	1400
2	68	3.14	-2.50	0.64	0.99	1320
3	69	1.26	-3.44	-2.18	-1.19	>1730
4	1970	1.52	-2.66	-1.14	-2.33	>1730
5	71	2.21	-1.80	0.41	-1.92	1375
6	72	1.92	-2.27	-0.35	-2.27	1570
Mean 1967-72		2.02	-2.40	-0.38		

11 Tunsbergdalsbreen - 50.1 km² (1964)

No. of years	Year	bw (m w.e.)	bs	bn (m w.e.)	Cum. bn (m w.e.)	ELA (m a.s.l.)
1	1966	1.57	-2.66	-1.09	-1.09	1640
2	67	3.31	-1.52	1.79	0.70	1160
3	68	2.74	-2.70	0.04	0.74	1550
4	69	1.53	-3.22	-1.69	-0.95	1700
5	1970	1.54	-2.38	-0.84	-1.79	1590
6	71	2.36	-1.79	0.57	-1.22	1240
7	72	2.02	-2.52	-0.50	-1.72	1490
Mean 1966-72		2.15	-2.40	-0.25		

12 Nigardsbreen - 47.8 km² (1984)

No. of years	Year	bw (m w.e.)	bs	bn (m w.e.)	Cum. bn (m w.e.)	ELA (m a.s.l.)
1	1962	2.88	-0.63	2.25	2.25	1260
2	63	1.87	-2.09	-0.22	2.03	1550
3	64	2.13	-1.18	0.95	2.98	1400
4	65	2.29	-1.38	0.91	3.89	1395
5	66	1.76	-2.68	-0.92	2.97	1700
6	67	3.40	-1.24	2.16	5.13	1310
7	68	2.72	-2.50	0.22	5.35	1550
8	69	1.95	-3.26	-1.31	4.04	1850
9	1970	1.73	-2.29	-0.56	3.48	1650
10	71	2.11	-1.29	0.82	4.30	1400
11	72	1.88	-2.02	-0.14	4.16	1570
12	73	2.40	-1.30	1.10	5.26	1410
13	74	2.06	-1.58	0.48	5.74	1490
14	75	2.50	-2.23	0.27	6.01	1450
15	76	2.88	-2.48	0.40	6.41	1540
16	77	1.52	-2.29	-0.77	5.64	1650
17	78	2.12	-2.25	-0.13	5.51	1590
18	79	2.75	-2.04	0.71	6.22	1500
19	1980	1.77	-2.99	-1.22	5.00	1730
20	81	2.19	-1.88	0.31	5.31	1560
21	82	1.94	-2.36	-0.42	4.89	1600
22	83	3.02	-1.93	1.09	5.98	1445
23	84	2.49	-2.15	0.34	6.32	1500
24	85	1.77	-1.87	-0.10	6.22	1590
25	86	1.61	-1.71	-0.10	6.12	1590
26	87	2.73	-1.25	1.48	7.60	1350
27	88	2.24	-3.13	-0.89	6.71	1660
28	89	4.05	-0.85	3.20	9.91	1175
29	1990	3.52	-1.75	1.77	11.68	1430
30	91	1.95	-1.75	0.20	11.88	1520
31	92	3.16	-1.56	1.60	13.48	1360
32	93	3.13	-1.28	1.85	15.33	1300
33	94	2.28	-1.72	0.56	15.89	1400
34	95	3.16	-1.97	1.19	17.08	1320
35	96	1.40	-1.81	-0.41	16.67	1660
36	97	2.66	-2.62	0.04	16.71	1500
37	98	2.50	-1.53	0.97	17.68	1350
38	99	2.38	-2.21	0.17	17.85	1470
39	2000	3.38	-1.66	1.72	19.57	1250
40	01	1.75	-1.97	-0.22	19.35	1560
41	02	2.41	-3.30	-0.89	18.46	1715
42	03	1.56	-2.72	-1.16	17.30	>1960
43	04	1.97	-2.01	-0.04	17.26	1530
44	05	2.80	-1.70	1.10	18.36	1395
45	06	1.75	-3.15	-1.40	16.96	1850
46	07	3.09	-2.05	1.04	18.00	1320
47	08	3.01	-1.92	1.09	19.09	1325
Mean 1962-2008		2.40	-1.99	0.41		

13 Store Supphellebreen - 12.0 km² (1966)

No. of years	Year	bw (m w.e.)	bs	bn (m w.e.)	Cum. bn	ELA (m a.s.l.)
1	1964	2.20	-1.50	0.70	0.70	1190
2	65	2.32	-1.76	0.56	1.26	1250
3	66	1.63	-2.40	-0.77	0.49	1590
4	67	2.72	-1.50	1.22	1.71	1190
5	73			1.50	1.50	
6	74			0.80	2.30	
7	75			1.00	3.30	
8	79			1.10	1.10	
9	1980			-1.40	-0.30	
10	81			0.20	-0.10	
11	82			-1.70	-1.80	
Mean 1964-67		2.22	-1.79	0.43		
Mean 1973-75				1.10		
Mean 1979-82				-0.45		

14 Austdalsbreen - 11.8 km² (1988)

No. of years	Year	bw (m w.e.)	bs	bn (m w.e.)	Cum. bn	ELA (m a.s.l.)
1	1988	1.94	-3.22	-1.28	-1.28	1570
2	89	3.18	-1.34	1.84	0.56	1275
3	1990	3.65	-2.45	1.20	1.76	1310
4	91	1.64	-1.64	0.00	1.76	1435
5	92	2.80	-2.26	0.54	2.30	1375
6	93	2.60	-1.69	0.91	3.21	1320
7	94	1.81	-1.88	-0.07	3.14	1425
8	95	2.72	-2.10	0.62	3.76	1360
9	96	1.20	-2.27	-1.07	2.69	1565
10	97	2.67	-3.20	-0.53	2.16	1450
11	98	2.20	-2.01	0.19	2.35	1420
12	99	2.08	-2.56	-0.48	1.87	1435
13	2000	2.77	-1.66	1.11	2.98	1315
14	01	1.04	-2.66	-1.62	1.36	>1757
15	02	1.91	-3.92	-2.01	-0.65	>1757
16	03	1.60	-3.94	-2.34	-2.99	>1757
17	04	1.60	-2.56	-0.96	-3.95	1495
18	05	2.85	-2.66	0.19	-3.76	1385
19	06	1.32	-3.38	-2.06	-5.82	>1757
20	07	2.46	-2.28	0.18	-5.64	1405
21	08	2.55	-2.62	-0.07	-5.71	1420
Mean 1988-2008		2.22	-2.49	-0.27		

15 Spøtteggbreen - 27.9 km² (1988)

No. of years	Year	bw (m w.e.)	bs	bn (m w.e.)	Cum. bn	ELA (m a.s.l.)
1	1988	1.61	-3.15	-1.54	-1.54	>1770
2	89	2.76	-1.62	1.14	-0.40	1410
3	1990	3.34	-2.33	1.01	0.61	1390
4	91	1.40	-1.37	0.03	0.64	1540
Mean 1988-91		2.28	-2.12	0.16		

16 Harbardsbreen - 13.2 km² (1996)

No. of years	Year	bw (m w.e.)	bs	bn (m w.e.)	Cum. bn	ELA (m a.s.l.)
1	1997	2.17	-2.72	-0.55	-0.55	>1960
2	98	1.66	-1.60	0.06	-0.49	1500
3	99	1.81	-2.15	-0.34	-0.83	>1960
4	2000	2.30	-1.52	0.78	-0.05	1250
5	01	0.88	-1.99	-1.11	-1.16	>1960
Mean 1997-2001		1.76	-2.00	-0.23		

17 Rembesdalsskåka - 17.1 km² (1995)

No. of years	Year	bw (m w.e.)	bs	bn (m w.e.)	Cum. bn	ELA (m a.s.l.)
1	1963	1.15	-2.55	-1.40	-1.40	>1860
2	64	1.85	-1.31	0.54	-0.86	1620
3	65	2.05	-1.54	0.51	-0.35	1620
4	66	1.60	-2.24	-0.64	-0.99	1750
5	67	2.44	-1.25	1.19	0.20	1540
6	68	2.68	-2.15	0.53	0.73	1600
7	69	1.07	-2.97	-1.90	-1.17	>1860
8	1970	1.29	-1.89	-0.60	-1.77	1780
9	71	2.02	-1.28	0.74	-1.03	1600
10	72	1.78	-1.86	-0.08	-1.11	1650
11	73	2.62	-1.79	0.83	-0.28	1570
12	74	1.91	-1.50	0.41	0.13	1615
13	75	2.25	-2.10	0.15	0.28	1620
14	76	2.45	-2.30	0.15	0.43	1620
15	77	1.20	-1.92	-0.72	-0.29	>1860
16	78	1.80	-2.10	-0.30	-0.59	
17	79	2.40	-2.10	0.30	-0.29	
18	1980	1.45	-2.85	-1.40	-1.69	>1860
19	81	2.65	-1.80	0.85	-0.84	1590
20	82	1.40	-2.10	-0.70	-1.54	1800
21	83	3.75	-2.05	1.70	0.16	1450
22	84	2.05	-2.15	-0.10	0.06	1675
23	85	1.48	-2.00	-0.52	-0.46	1715
24	86	1.47	-1.57	-0.10	-0.56	1670
25	87	2.08	-1.14	0.94	0.38	1535
26	88	1.61	-3.13	-1.52	-1.14	1860
27	89	3.48	-1.37	2.11	0.97	1420
28	1990	3.65	-1.72	1.93	2.90	1450
29	91	1.52	-1.61	-0.09	2.81	1660
30	92	3.71	-1.72	1.99	4.80	1525
31	93	2.82	-0.91	1.91	6.71	1450
32	94	1.79	-1.63	0.16	6.87	1600
33	95	2.44	-2.14	0.30	7.17	1575
34	96	0.99	-2.10	-1.11	6.06	>1860
35	97	2.94	-3.41	-0.47	5.59	1700
36	98	2.47	-1.78	0.69	6.28	1585
37	99	2.04	-1.99	0.05	6.33	1685
38	2000	2.93	-1.50	1.43	7.76	1425
39	01	1.03	-1.88	-0.85	6.91	1760
40	02	2.39	-3.10	-0.71	6.20	1750
41	03	1.33	-2.69	-1.36	4.84	>1860
42	04	1.89	-1.81	0.08	4.92	1670
43	05	2.79	-2.07	0.72	5.64	1590
44	06	0.90	-3.12	-2.22	3.42	>1860
45	07	3.10	-1.93	1.17	4.59	1570
46	08	2.61	-2.16	0.45	5.04	1610
Mean 1963-2008		2.12	-2.01	0.11		

18 Midtdalsbreen - 6.7 km² (1995)

No. of years	Year	bw (m w.e.)	bs	bn (m w.e.)	Cum. bn	ELA (m a.s.l.)
1	2000	2.89	-1.57	1.32	1.32	1500
2	01	1.26	-1.90	-0.64	0.68	1785
Mean 2000-2001		2.08	-1.74	0.34		

19 Omnsbreen - 1.5 km² (1969)

No. of years	Year	bw (m w.e.)	bs	bn (m w.e.)	Cum. bn	ELA (m a.s.l.)
1	1966	1.44	-2.28	-0.84	-0.84	
2	67	2.21	-1.72	0.49	-0.35	
3	68	2.20	-2.38	-0.18	-0.53	1520
4	69	1.09	-3.68	-2.59	-3.12	
5	1970	1.12	-2.62	-1.50	-4.62	
Mean 1966-70		1.61	-2.54	-0.92		

20 Tverråbreen - 5.9 km² ()

No. of years	Year	bw (m w.e.)	bs	bn (m w.e.)	Cum. bn (m w.e.)	ELA (m a.s.l.)
1	1962	2.03	-1.28	0.75	0.75	
2	63	1.24	-2.46	-1.22	-0.47	
Mean 1962-63		1.64	-1.87	-0.24		

21 Blåbreen - 3.6 km² (1961)

No. of years	Year	bw (m w.e.)	bs	bn (m w.e.)	Cum. bn (m w.e.)	ELA (m a.s.l.)
1	1962	1.15	-0.35	0.80	0.80	<1550
2	63	0.85	-1.71	-0.86	-0.06	1970
Mean 1962-63		1.00	-1.03	-0.03		

22 Storbreen - 5.4 km² (1997)

No. of years	Year	bw (m w.e.)	bs	bn (m w.e.)	Cum. bn (m w.e.)	ELA (m a.s.l.)
1	49	2.28	-2.08	0.20	0.20	1650
2	1950	1.52	-1.81	-0.29	-0.09	1750
3	51	1.13	-1.67	-0.54	-0.63	1770
4	52	1.44	-1.13	0.31	-0.32	1630
5	53	1.40	-2.25	-0.85	-1.17	1850
6	54	1.21	-1.98	-0.77	-1.94	1830
7	55	1.57	-2.06	-0.49	-2.43	1800
8	56	1.31	-1.48	-0.17	-2.60	1705
9	57	1.42	-1.37	0.05	-2.55	1680
10	58	1.54	-1.62	-0.08	-2.63	1700
11	59	1.07	-2.35	-1.28	-3.91	1930
12	1960	0.98	-2.07	-1.09	-5.00	1910
13	61	1.10	-1.62	-0.52	-5.52	1820
14	62	1.54	-0.82	0.72	-4.80	1510
15	63	0.96	-2.14	-1.18	-5.98	1900
16	64	1.16	-0.95	0.21	-5.77	1655
17	65	1.54	-1.20	0.34	-5.43	1650
18	66	1.25	-1.86	-0.61	-6.04	1815
19	67	1.89	-1.17	0.72	-5.32	1570
20	68	1.64	-1.59	0.05	-5.27	1700
21	69	1.22	-2.64	-1.42	-6.69	2020
22	1970	0.97	-1.69	-0.72	-7.41	1840
23	71	1.46	-1.28	0.18	-7.23	1690
24	72	1.39	-1.70	-0.31	-7.54	1770
25	73	1.48	-1.40	0.08	-7.46	1705
26	74	1.26	-1.02	0.24	-7.22	1630
27	75	1.55	-1.70	-0.15	-7.37	1760
28	76	1.81	-1.90	-0.09	-7.46	1740
29	77	0.94	-1.48	-0.54	-8.00	1840
30	78	1.26	-1.70	-0.44	-8.44	1815
31	79	1.55	-1.45	0.10	-8.34	1700
32	1980	0.99	-2.30	-1.31	-9.65	1975
33	81	1.30	-1.40	-0.10	-9.75	1730
34	82	1.28	-1.75	-0.47	-10.22	1785
35	83	1.90	-1.70	0.20	-10.02	1625
36	84	1.70	-2.00	-0.30	-10.32	1765
37	85	1.20	-1.60	-0.40	-10.72	1790
38	86	1.05	-1.37	-0.32	-11.04	1770
39	87	1.55	-1.23	0.32	-10.72	1570
40	88	1.45	-2.40	-0.95	-11.67	1970
41	89	2.30	-1.10	1.20	-10.47	1550
42	1990	2.60	-1.35	1.25	-9.22	1530
43	91	1.26	-1.41	-0.15	-9.37	1740
44	92	1.61	-1.53	0.08	-9.29	1715
45	93	1.81	-1.06	0.75	-8.54	1605
46	94	1.52	-1.77	-0.25	-8.79	1800
47	95	1.77	-1.93	-0.16	-8.95	1810
48	96	0.81	-1.84	-1.03	-9.98	1890
49	97	1.75	-2.78	-1.03	-11.01	1875
50	98	1.55	-1.33	0.22	-10.79	1680
51	99	1.67	-1.91	-0.24	-11.03	1830
52	2000	2.04	-1.49	0.55	-10.48	1650
53	01	1.05	-1.32	-0.27	-10.75	1845
54	02	1.09	-2.87	-1.78	-12.53	2075
55	03	1.11	-2.68	-1.57	-14.10	2025
56	04	1.01	-1.59	-0.58	-14.68	1855
57	05	1.83	-1.89	-0.06	-14.74	1795
58	06	0.86	-3.01	-2.15	-16.89	>2100
59	07	1.35	-1.74	-0.39	-17.28	1835
60	08	1.99	-1.88	0.11	-17.17	1770
Mean 1949-2008		1.44	-1.72	-0.29		

23 Vestre Memurubre - 9.0 km² (1966)

No. of years	Year	bw (m w.e.)	bs	bn (m w.e.)	Cum. bn (m w.e.)	ELA (m a.s.l.)
1	1968	1.70	-1.46	0.24	0.24	1820
2	69	1.05	-2.11	-1.06	-0.82	2170
3	1970	0.84	-1.63	-0.79	-1.61	1990
4	71	1.30	-1.19	0.11	-1.50	1845
5	72	1.19	-1.47	-0.28	-1.78	1885
Mean 1968-72		1.22	-1.57	-0.36		

24 Austre Memurubre - 8.7 km² (1966)

No. of years	Year	bw (m w.e.)	bs	bn (m w.e.)	Cum. bn (m w.e.)	ELA (m a.s.l.)
1	1968	1.77	-1.76	0.01	0.01	1960
2	69	0.99	-2.45	-1.46	-1.45	2130
3	1970	0.81	-1.71	-0.90	-2.35	2090
4	71	1.33	-1.51	-0.18	-2.53	1960
5	72	1.02	-1.42	-0.40	-2.93	1985
Mean 1968-72		1.18	-1.77	-0.59		

25 Hellstugubreen - 3.0 km² (1997)

No. of years	Year	bw (m w.e.)	bs	bn (m w.e.)	Cum. bn (m w.e.)	ELA (m a.s.l.)
1	1962	1.18	-0.40	0.78	0.78	
2	63	0.94	-1.92	-0.98	-0.20	2020
3	64	0.71	-0.83	-0.12	-0.32	1900
4	65	1.29	-0.77	0.52	0.20	1690
5	66	0.95	-1.62	-0.67	-0.47	1940
6	67	1.48	-0.93	0.55	0.08	1800
7	68	1.38	-1.49	-0.11	-0.03	1875
8	69	0.95	-2.23	-1.28	-1.31	2130
9	1970	0.70	-1.70	-1.00	-2.31	2020
10	71	1.12	-1.25	-0.13	-2.44	1860
11	72	0.94	-1.43	-0.49	-2.93	1950
12	73	1.20	-1.41	-0.21	-3.14	1880
13	74	1.00	-0.76	0.24	-2.90	1785
14	75	1.35	-1.71	-0.36	-3.26	1950
15	76	1.16	-1.89	-0.73	-3.99	1970
16	77	0.68	-1.40	-0.72	-4.71	2075
17	78	1.05	-1.59	-0.54	-5.25	1890
18	79	1.43	-1.45	-0.02	-5.27	1820
19	1980	0.81	-2.05	-1.24	-6.51	2050
20	81	1.06	-1.39	-0.33	-6.84	1950
21	82	0.85	-1.20	-0.35	-7.19	1920
22	83	1.47	-1.30	0.17	-7.02	1820
23	84	1.22	-1.73	-0.51	-7.53	1965
24	85	1.11	-1.40	-0.29	-7.82	1840
25	86	0.78	-1.27	-0.49	-8.31	1940
26	87	1.15	-0.70	0.45	-7.86	1690
27	88	1.28	-2.32	-1.04	-8.90	2025
28	89	1.62	-0.90	0.72	-8.18	1660
29	1990	1.81	-1.15	0.66	-7.52	1640
30	91	0.98	-1.43	-0.45	-7.97	1950
31	92	1.17	-1.03	0.14	-7.83	1850
32	93	1.25	-0.95	0.30	-7.53	1670
33	94	1.26	-1.19	0.07	-7.46	1850
34	95	1.42	-1.54	-0.12	-7.58	1885
35	96	0.65	-1.39	-0.74	-8.32	1955
36	97	1.12	-2.77	-1.65	-9.97	2200
37	98	1.00	-1.02	-0.02	-9.99	1870
38	99	1.22	-1.64	-0.42	-10.41	1930
39	2000	1.26	-1.16	0.10	-10.31	1840
40	01	0.85	-1.21	-0.36	-10.67	1910
41	02	0.96	-2.37	-1.41	-12.08	2080
42	03	0.71	-2.23	-1.52	-13.60	2200
43	04	0.65	-1.49	-0.84	-14.44	1980
44	05	1.34	-1.63	-0.29	-14.73	1930
45	06	0.73	-2.74	-2.01	-16.74	>2210
46	07	1.03	-1.7	-0.67	-17.41	1975
47	08	1.41	-1.47	-0.06	-17.47	1880
Mean 1962-2008		1.10	-1.47	-0.37		

26 Gråsubreen - 2.3 km² (1997)

No. of years	Year	bw (m w.e.)	bs	bn (m w.e.)	Cum. bn (m w.e.)	ELA (m a.s.l.)
1	1962	0.86	-0.09	0.77	0.77	1870
2	63	0.40	-1.11	-0.71	0.06	2275
3	64	0.39	-0.71	-0.32	-0.26	2160
4	65	0.77	-0.36	0.41	0.15	1900
5	66	0.72	-1.01	-0.29	-0.14	2150
6	67	1.45	-0.74	0.71	0.57	1870
7	68	1.03	-1.11	-0.08	0.49	2140
8	69	0.74	-2.04	-1.30	-0.81	2275
9	1970	0.57	-1.23	-0.66	-1.47	2200
10	71	0.49	-0.96	-0.47	-1.94	2200
11	72	0.66	-1.30	-0.64	-2.58	2240
12	73	0.72	-1.61	-0.89	-3.47	2275
13	74	0.58	-0.24	0.34	-3.13	1870
14	75	0.91	-1.86	-0.95	-4.08	2275
15	76	0.62	-1.62	-1.00	-5.08	2275
16	77	0.51	-0.90	-0.39	-5.47	2275
17	78	0.67	-0.89	-0.22	-5.69	2140
18	79	0.91	-0.87	0.04	-5.65	2025
19	1980	0.46	-1.35	-0.89	-6.54	2225
20	81	0.62	-0.81	-0.19	-6.73	2180
21	82	0.50	-1.01	-0.51	-7.24	2275
22	83	0.94	-0.99	-0.05	-7.29	2090
23	84	0.98	-1.35	-0.37	-7.66	2275
24	85	0.75	-0.75	0.00	-7.66	2100
25	86	0.42	-1.18	-0.76	-8.42	2275
26	87	0.94	-0.22	0.72	-7.70	1870
27	88	1.08	-1.66	-0.58	-8.28	2195
28	89	1.12	-0.67	0.45	-7.83	1870
29	1990	1.33	-0.60	0.73	-7.10	1870
30	91	0.67	-1.19	-0.52	-7.62	1950
31	92	0.70	-0.80	-0.10	-7.72	
32	93	0.93	-0.51	0.42	-7.30	<1850
33	94	1.16	-1.16	0.00	-7.30	2075
34	95	1.19	-1.30	-0.11	-7.41	2180
35	96	0.53	-0.98	-0.45	-7.86	2205
36	97	0.70	-2.39	-1.69	-9.55	>2290
37	98	0.78	-0.67	0.11	-9.44	Undef.
38	99	0.91	-1.30	-0.39	-9.83	2210
39	2000	0.87	-0.92	-0.05	-9.88	Undef.
40	01	0.80	-0.78	0.02	-9.86	2070
41	02	0.63	-2.05	-1.42	-11.28	>2290
42	03	0.45	-1.84	-1.39	-12.67	>2290
43	04	0.48	-0.97	-0.49	-13.16	2210
44	05	0.83	-1.33	-0.50	-13.66	2180
45	06	0.51	-2.59	-2.08	-15.74	>2290
46	07	0.61	-1.32	-0.71	-16.45	2265
47	08	0.95	-0.86	0.09	-16.36	Undef.
Mean 1962-2008		0.76	-1.11	-0.35		

27 Charles Rabots Bre - 1.1 km² (1965)

No. of years	Year	bw (m w.e.)	bs	bn (m w.e.)	Cum. bn (m w.e.)	ELA (m a.s.l.)
1	1970			-1.90	-1.90	
2	71			0.47	-1.43	
3	72			-1.04	-2.47	
4	73			1.44	-1.03	
Mean 1970-73				-0.26		

28 Austre Okstindbre - 14.0 km² (1962)

No. of years	Year	bw (m w.e.)	bs	bn (m w.e.)	Cum. bn (m w.e.)	ELA (m a.s.l.)
1	1987	2.30	-1.60	0.70	0.70	1280
2	88	1.50	-3.40	-1.90	-1.20	>1750
3	89	3.70	-2.20	1.50	0.30	1275
4	1990	3.00	-2.70	0.30	0.60	1310
5	91	1.80	-2.30	-0.50	0.10	1315
6	92	2.88	-1.65	1.23	1.33	1260
7	93	2.22	-2.01	0.21	1.54	1290
8	94	1.45	-1.62	-0.17	1.37	1310
9	95	2.25	-1.79	0.46	1.83	1280
10	96	1.62	-1.92	-0.30	1.53	1330
Mean 1987-96		2.27	-2.12	0.15		

29 Høgtuvbreen - 2.6 km² (1972)

No. of years	Year	bw (m w.e.)	bs	bn (m w.e.)	Cum. bn (m w.e.)	ELA (m a.s.l.)
1	1971	3.05	-3.78	-0.73	-0.73	950
2	72	3.34	-4.30	-0.96	-1.69	970
3	73	3.90	-2.82	1.08	-0.61	720
4	74	3.46	-3.68	-0.22	-0.83	900
5	75	3.00	-2.27	0.73	-0.10	760
6	76	3.66	-2.75	0.91	0.81	730
7	77	2.20	-2.72	-0.52	0.29	900
Mean 1971-77		3.23	-3.19	0.04		

30 Svartisheibreen - 5.5 km² (1985)

No. of years	Year	bw (m w.e.)	bs	bn (m w.e.)	Cum. bn (m w.e.)	ELA (m a.s.l.)
1	1988	2.42	-4.03	-1.61	-1.61	1180
2	89	3.72	-1.36	2.36	0.75	900
3	1990	3.79	-2.97	0.82	1.57	930
4	91	2.61	-2.44	0.17	1.74	950
5	92	3.89	-2.68	1.21	2.95	890
6	93	3.50	-2.59	0.91	3.86	910
7	94	1.83	-1.85	-0.02	3.84	975
Mean 1988-94		3.11	-2.56	0.55		

31 Engabreen - 38.7 km² (2008)

No. of years	Year	bw (m w.e.)	bs	bn (m w.e.)	Cum. bn (m w.e.)	ELA (m a.s.l.)
1	1970	2.05	-3.04	-0.99	-0.99	1280
2	71	3.20	-2.19	1.01	0.02	1070
3	72	3.22	-3.29	-0.07	-0.05	1150
4	73	4.37	-1.65	2.72	2.67	830
5	74	3.39	-2.59	0.80	3.47	1030
6	75	3.18	-1.57	1.61	5.08	960
7	76	3.86	-1.45	2.41	7.49	910
8	77	2.08	-1.20	0.88	8.37	1000
9	78	2.48	-2.99	-0.51	7.86	1250
10	79	3.64	-3.22	0.42	8.28	1130
11	1980	2.68	-3.18	-0.50	7.78	1270
12	81	2.91	-1.93	0.98	8.76	965
13	82	2.27	-1.43	0.84	9.60	1030
14	83	2.34	-1.28	1.06	10.66	1020
15	84	3.83	-2.78	1.05	11.71	1000
16	85	1.50	-2.40	-0.90	10.81	1375
17	86	2.70	-2.45	0.25	11.06	1170
18	87	2.57	-1.63	0.94	12.00	1000
19	88	2.26	-4.05	-1.79	10.21	1400
20	89	4.62	-1.45	3.17	13.38	890
21	1990	3.49	-2.64	0.85	14.23	1035
22	91	2.83	-2.14	0.69	14.92	1090
23	92	4.05	-1.71	2.34	17.26	875
24	93	3.06	-2.02	1.04	18.30	985
25	94	1.95	-1.53	0.42	18.72	1050
26	95	3.50	-1.76	1.74	20.46	940
27	96	2.97	-2.14	0.83	21.29	970
28	97	4.44	-3.22	1.22	22.51	1010
29	98	2.98	-2.77	0.21	22.72	1100
30	99	2.12	-2.15	-0.03	22.69	1215
31	2000	2.76	-1.27	1.49	24.18	970
32	01	1.05	-2.58	-1.53	22.65	>1594
33	02	2.89	-3.48	-0.59	22.06	1200
34	03	2.41	-3.00	-0.59	21.47	1195
35	04	2.92	-2.10	0.82	22.29	1040
36	05	3.31	-2.42	0.89	23.18	1060
37	06	1.73	-3.16	-1.43	21.75	1325
38	07	3.37	-2.83	0.54	22.29	1100
39	08	2.81	-2.50	0.31	22.60	1093
Mean 1970-2008		2.92	-2.34	0.58		

32 Storglombreen - 62.4 km² (1968)

No. of years	Year	bw (m w.e.)	bs	bn (m w.e.)	Cum. bn (m w.e.)	ELA (m a.s.l.)
1	1985	1.40	-2.59	-1.19	-1.19	1300
2	86	2.45	-2.87	-0.42	-1.61	1100
3	87	2.32	-1.87	0.45	-1.16	1020
4	88	2.06	-3.88	-1.82	-2.98	1350
5	2000	2.66	-1.55	1.11	1.11	1000
6	01	1.15	-2.91	-1.76	-0.65	>1580
7	02	2.33	-3.58	-1.25	-1.90	>1580
8	03	2.18	-3.28	-1.10	-3.00	>1580
9	04	2.26	-2.14	0.12	-2.88	1075
10	05	2.74	-2.41	0.33	-2.55	1060
Mean 1985-88		2.06	-2.80	-0.75		
Mean 2000-05		2.22	-2.65	-0.43		

33 Tretten-null-tobreen - 4.9 km² (1968)

No. of years	Year	bw (m w.e.)	bs	bn (m w.e.)	Cum. bn (m w.e.)	ELA (m a.s.l.)
1	1985	1.47	-3.20	-1.73	-1.73	>1260
2	86	2.40	-2.84	-0.44	-2.17	1100
Mean 1985-86		1.94	-3.02	-1.09		

34 Glombreen - 2.2 km² (1953)

No. of years	Year	bw (m w.e.)	bs	bn (m w.e.)	Cum. bn (m w.e.)	ELA (m a.s.l.)
1	1954	2.30	-3.50	-1.20	-1.20	
2	55	2.60	-2.70	-0.10	-1.30	
3	56	1.50	-2.10	-0.60	-1.90	
Mean 1954-56		2.13	-2.77	-0.63		

35 Kjølbreen - 3.9 km² (1953)

No. of years	Year	bw (m w.e.)	bs	bn (m w.e.)	Cum. bn (m w.e.)	ELA (m a.s.l.)
1	1954	1.90	-2.60	-0.70	-0.70	
2	55	2.10	-2.80	-0.70	-1.40	
3	56	1.10	-1.10	0.00	-1.40	
Mean 1954-56		1.70	-2.17	-0.47		

36 Trollbergdalsbreen - 1.6 km² (1985)

No. of years	Year	bw (m w.e.)	bs	bn (m w.e.)	Cum. bn (m w.e.)	ELA (m a.s.l.)
1	1970	1.74	-4.21	-2.47	-2.47	>1370
2	71	2.14	-2.47	-0.33	-2.80	1100
3	72	2.44	-3.68	-1.24	-4.04	1160
4	73	3.19	-2.43	0.76	-3.28	<900
5	74	2.57	-2.97	-0.40	-3.68	1090
6	75			-0.28	-3.96	1090
7	1990	2.94	-3.23	-0.29	-0.29	1075
8	91	2.29	-2.45	-0.16	-0.45	1070
9	92	2.63	-2.13	0.50	0.05	<900
10	93	2.45	-2.38	0.07	0.12	1045
11	94	1.49	-2.59	-1.10	-0.98	1180
Mean 1970-74(75)		2.42	-3.15	-0.66		
Mean 1990-94		2.36	-2.56	-0.20		

37 Rundvassbreen - 11.6 km² (1998)

No. of years	Year	bw (m w.e.)	bs	bn (m w.e.)	Cum. bn (m w.e.)	ELA (m a.s.l.)
1	2002	2.14	-3.19	-1.05	-1.05	1320
2	03	1.88	-2.95	-1.07	-2.12	1360
3	04	1.95	-2.16	-0.21	-2.33	1260
Mean 2002-04		1.99	-2.77	-0.777		

38 Blåisen - 2.2 km² (1960)

No. of years	Year	bw (m w.e.)	bs	bn (m w.e.)	Cum. bn (m w.e.)	ELA (m a.s.l.)
1	1963	2.60	-2.40	0.20	0.20	1050
2	64	2.30	-1.67	0.63	0.83	980
3	65	2.00	-1.46	0.54	1.37	960
4	66	1.12	-2.39	-1.27	0.10	>1200
5	67	1.38	-2.35	-0.97	-0.87	1175
6	68	1.62	-1.36	0.26	-0.61	1010
Mean 1963-68		1.84	-1.94	-0.10		

39 Storsteinsfjellbreen - 5.9 km² (1993)

No. of years	Year	bw (m w.e.)	bs	bn (m w.e.)	Cum. bn (m w.e.)	ELA (m a.s.l.)
1	1964	1.85	-1.20	0.65	0.65	1220
2	65	1.69	-1.25	0.44	1.09	1270
3	66	1.05	-1.88	-0.83	0.26	1500
4	67	1.37	-1.77	-0.40	-0.14	1450
5	68	1.44	-0.99	0.45	0.31	1275
6	1991	1.59	-1.63	-0.04	-0.04	1395
7	92	2.21	-1.10	1.11	1.07	1250
8	93	2.10	-1.29	0.81	1.88	1260
9	94	1.15	-1.35	-0.20	1.68	1375
10	95	1.81	-1.24	0.57	2.25	1280
Mean 1964-68		1.48	-1.42	0.06		
Mean 1991-95		1.77	-1.32	0.45		

40 Cainhavarre - 0.7 km² (1960)

No. of years	Year	bw (m w.e.)	bs	bn (m w.e.)	Cum. bn (m w.e.)	ELA (m a.s.l.)
1	1965	1.41	-1.20	0.21	0.21	1300
2	66	1.12	-2.07	-0.95	-0.74	>1550
3	67	1.63	-1.79	-0.16	-0.90	1450
4	68	1.31	-1.05	0.26	-0.64	1290
Mean 1965-68		1.37	-1.53	-0.16		

41 Svartfjelljøkelen - 2.7 km² (1966)

No. of years	Year	bw (m w.e.)	bs	bn (m w.e.)	Cum. bn (m w.e.)	ELA (m a.s.l.)
1	1978	2.30	-2.40	-0.10	-0.10	
2	79	2.10				
Mean 1978-79		2.20				

42 Langfjordjøkelen - 3.2 km² (2008)

No. of years	Year	bw (m w.e.)	bs	bn (m w.e.)	Cum. bn (m w.e.)	ELA (m a.s.l.)
1	89	2.40	-2.96	-0.56	-0.56	870
2	1990	2.74	-3.06	-0.32	-0.88	780
3	91	2.31	-2.31	0.00	-0.88	710
4	92	2.68	-2.49	0.19	-0.69	700
5	93	2.55	-2.35	0.20	-0.49	740
6	96	2.25	-2.23	0.02	0.02	700
7	97	2.65	-3.34	-0.69	-0.67	820
8	98	1.80	-3.24	-1.44	-2.11	>1050
9	99	1.33	-2.91	-1.58	-3.69	970
10	2000	2.51	-3.12	-0.61	-4.30	860
11	01	1.36	-3.64	-2.28	-6.58	>1050
12	02	2.19	-3.73	-1.54	-8.12	>1050
13	03	2.44	-3.51	-1.07	-9.19	>1050
14	04	1.69	-3.61	-1.92	-11.11	>1050
15	05	1.88	-3.14	-1.26	-12.37	940
16	06	1.42	-3.83	-2.41	-14.78	>1050
17	07	2.09	-2.90	-0.81	-15.59	870
18	08	1.67	-2.02	-0.35	-15.94	835
Mean 1989-93		2.54	-2.63	-0.10		
Mean 1996-2008		1.94	-3.17	-1.23		



Comparing Traditional Mass Balance Measurements with Long-Term Volume Change Extracted from Topographical Maps: A Case Study of Storbreen Glacier in Jotunheimen, Norway, for the Period 1940–1997

Author(s): Liss M. Andreassen

Source: *Geografiska Annaler. Series A, Physical Geography*, Vol. 81, No. 4, Methods of Mass Balance Measurements and Modelling (1999), pp. 467–476

Published by: Blackwell Publishing on behalf of the Swedish Society for Anthropology and Geography

Stable URL: <http://www.jstor.org/stable/521486>

Accessed: 04/06/2009 08:38

Your use of the JSTOR archive indicates your acceptance of JSTOR's Terms and Conditions of Use, available at <http://www.jstor.org/page/info/about/policies/terms.jsp>. JSTOR's Terms and Conditions of Use provides, in part, that unless you have obtained prior permission, you may not download an entire issue of a journal or multiple copies of articles, and you may use content in the JSTOR archive only for your personal, non-commercial use.

Please contact the publisher regarding any further use of this work. Publisher contact information may be obtained at <http://www.jstor.org/action/showPublisher?publisherCode=black>.

Each copy of any part of a JSTOR transmission must contain the same copyright notice that appears on the screen or printed page of such transmission.

JSTOR is a not-for-profit organization founded in 1995 to build trusted digital archives for scholarship. We work with the scholarly community to preserve their work and the materials they rely upon, and to build a common research platform that promotes the discovery and use of these resources. For more information about JSTOR, please contact support@jstor.org.



Swedish Society for Anthropology and Geography and Blackwell Publishing are collaborating with JSTOR to digitize, preserve and extend access to *Geografiska Annaler. Series A, Physical Geography*.

<http://www.jstor.org>

COMPARING TRADITIONAL MASS BALANCE MEASUREMENTS WITH LONG-TERM VOLUME CHANGE EXTRACTED FROM TOPOGRAPHICAL MAPS: A CASE STUDY OF STORBREEN GLACIER IN JOTUNHEIMEN, NORWAY, FOR THE PERIOD 1940–1997

BY
LISS M. ANDREASSEN

Norwegian Water Resources and Energy Directorate, Oslo, Norway

Andreassen, Liss M., 1999: Comparing traditional mass balance measurements with long-term volume change extracted from topographical maps: A case study of Storbreen glacier in Jotunheimen, Norway, for the period 1940–1997. Geogr. Ann., 81 A (4): 467–476.

ABSTRACT: Storbreen glacier is situated in the western part of Jotunheimen, a mountain area in central southern Norway. Annual mass balance data have been recorded since 1949. In addition, detailed topographical maps at the scale 1:10,000 exist from the years 1940, 1951, 1968, 1984 and 1997. In this paper, volume change calculated from maps is compared with annual mass balance data. The volume change was in reasonable agreement with the measured cumulative mass balance for the periods 1940–1951 and 1968–1984; however, for the periods 1951–1968 and 1984–1997, the mass balance measurements showed larger negative values than obtained from map comparisons. One obvious reason for this is the inaccuracy of the contour lines in the upper areas of the glacier on maps from 1940 and 1951. Other factors influencing the result are tested, and also suggestions are given for improving the techniques for mapping glacier volume changes.

Introduction

The traditional method of mass balance measurements is based on annual measurements of snow density, snow depth along sounding profiles and ablation on a number of stakes on a glacier. This method can be quite expensive and time consuming, even if the monitoring programme is reduced to a minimum. Another method used to calculate volume change is the cartographic method, where the average annual mass balance is calculated by comparison of topographic maps from two different years. This method is far less expensive and time consuming, but gives no information about annual variations in accumulation and ablation. The 49-year-long record of traditional mass bal-

ance data and the five detailed maps on Storbreen provide a unique opportunity to compare the two methods. In this paper the volume change calculated from the maps is compared with the measured cumulative mass balance, obtained during the period between the mappings.

Storbreen was first described in detail by Øyen (1893), who established cairns to measure front fluctuations in 1902 (Øyen 1908). Mass balance measurements were initiated in spring 1949. In addition to mass balance measurements, ice velocity and sediment load in the glacier river have been studied (Liestøl 1967). In the 1970s and 1980s, several studies of the moraine system of Storbreen were carried out (Matthews 1973, 1974, 1975, 1976; Erikstad and Sollid 1986; Darmody *et al.* 1987).

Geographical setting

Storbreen (61°36'N, 8°8'E) is situated in the Leirdalen valley in the western part of Jotunheimen, a mountain area in southern Norway (Fig. 1). The glacier has a total area of 5.4 km² and ranges in altitude from 1390 to 2090 m a.s.l. The length of this east-facing glacier is 3 km, and it has an average slope of 14° (Table 1). Storbreen has fairly well defined borders, and may be characterised as a short valley glacier or a composite cirque glacier (Liestøl 1967). A subglacial ridge divides the glacier into two rather well defined parts. No thickness measurements have been made on Storbreen. The glacier has an uneven surface, indicating thin ice and undulating bottom topography. Distinct end mo-

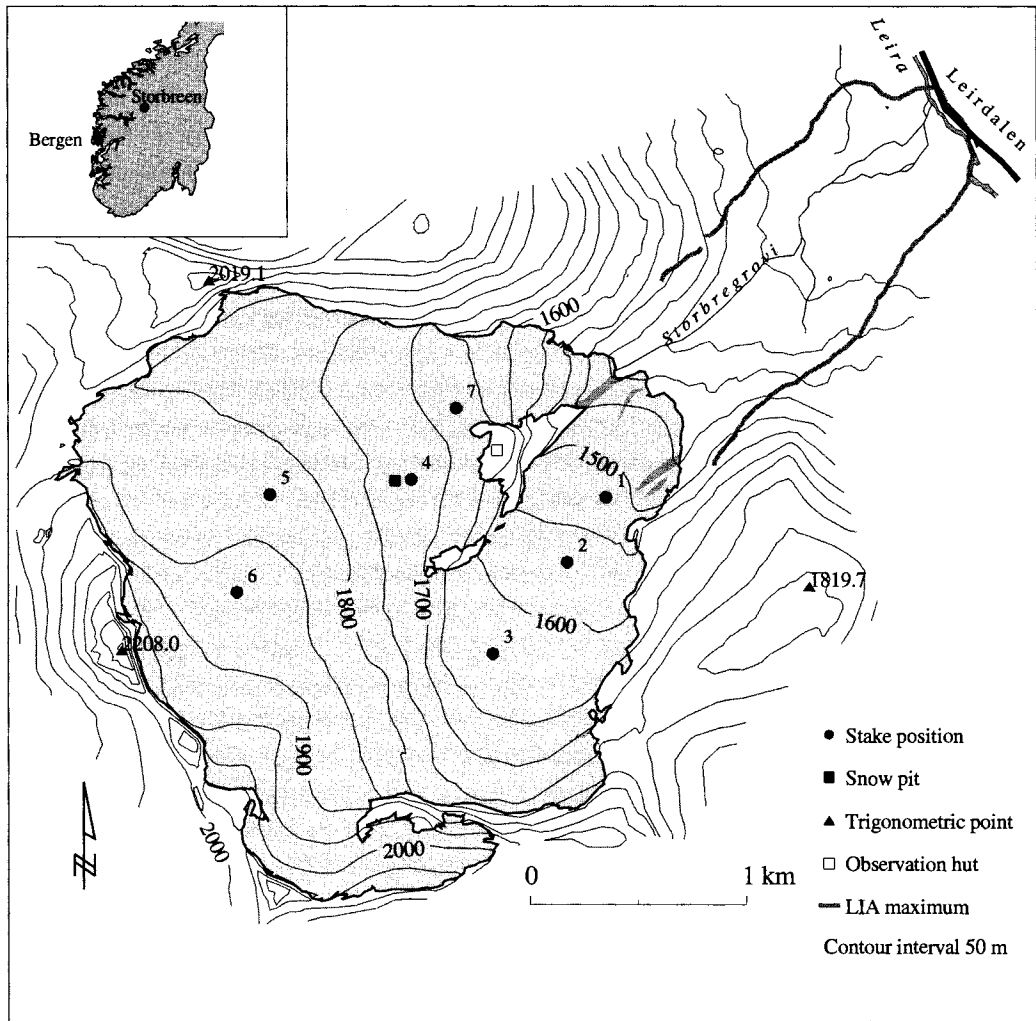


Fig. 1. The location of Storbreen in Leirdalen, West Jotunheimen, Norway. Contour lines and glacier outline are from the 1997 map. Positions of stakes and snow pits used in the present mass balance programme are marked on the map.

raines mark the post-glacial maximum of Storbreen; they reach as far as the Leira river in the valley bottom (Fig. 1). Storbreen probably reached its post-glacial maximum extent somewhere between 1740 and 1770 (Matthews 1976). From its maximum extent the glacier has reduced its area by 25% and the length by almost 40% (Table 1).

Data and methods

Mass balance

Traditional mass balance measurements were initiated in the spring of 1949 by the Norwegian Polar

Institute, and have been carried out every year since (Liestøl 1967; Kjølmoen 1998). Storbreen has the longest series of mass balance measurements in Norway and the second longest series of this kind in the world. NVE (Norwegian Water Resources and Energy Directorate) took over responsibility for the monitoring programme from 1993. The monitoring programme has been greatly reduced over the years. In the first years, more than three snow density pits were dug, snow depth was measured in about 600 points and ablation was measured on 30 stakes evenly distributed on the glacier (Liestøl 1960, 1967). Today, accumulation is

COMPARING MASS BALANCE MEASUREMENTS

Table 1. Length, area, altitude and slope of Storbreen from the post-glacial maximum extent around 1750 (LIA) to 1997.

Year	Length (km)	Area (km ²)	Altituderange (m a.s.l.)	Mean height (m a.s.l.)	Slope (degrees)
LIA	4.85	7.17	1150–2090	-	-
1940	3.84	5.96	1280–2090	1725	11.7
1951	3.66	5.73	1315–2090	1731	12.4
1968	3.38	5.60	1350–2090	1745	13.1
1984	3.04	5.35	1370–2090	1747	13.3
1997	2.99	5.36	1390–2090	1750	13.7

measured in about 100 points, snow density in one pit and ablation on stakes in seven positions (Fig. 1). However, these stakes are regarded as representative for the parts of the glacier where they are located. According to the mass balance records, Storbreen has had an average loss of 11 metres of water equivalents (m w.eq.) between 1949 and 1997, or 0.22 m w.eq. per year. Of these 49 years with data, 18 have had a positive net balance, while the rest of the years were negative, resulting in a thinning of the glacier (see Fig. 3). For the last 10–15 years the glacier have been more or less in balance and both the retreat of the front and the thinning of the glacier have stopped (see Figs 3 and 4).

To compare annual mass balance data with volume change from maps, the cumulative mass balance in the period between the mappings was calculated. However, for the period 1940–1951, annual mass balance data exist only for the years 1948/49, 1949/50 and 1950/51. Hence, other methods were used to calculate annual mass balance between 1940 and 1948. Liestøl (1967) found a good correlation between ablation and accumulation on Storbreen and temperature and precipitation data from a meteorological station in Bergen, western

Norway. Lacking other data, Liestøl's figures from 1940 to 1948 are used to calculate the cumulative net balance for the period 1940–1951 together with the mass balance data for the last three years of the period (Liestøl 1967).

Errors. The undulating surface of Storbreen complicates mass balance measurements. The uneven snow distribution with altitude results in a patchy snow line on the glacier (Fig. 2). In the heavily crevassed areas, no reliable measurements can be made. However, these areas are small compared to the total area of the glacier (about 15%), and will not significantly influence the result. Additional uncertainties arise from the variation of the snow density, which will influence the total result. Estimates of the uncertainty of the total net balance are at best qualified guessing.

Topographic maps

Storbreen has been mapped in detail five times, all at the scale of 1:10,000 with 10 m contour interval (Table 2). The maps were constructed from terrestrial photos taken in 1940 and 1951 and from ver-

Table 2. Detailed maps constructed of Storbreen.

Year	Map			Contract no.	Date	Photos	
	Method	Scale	Contour interval (m)			Scale	Remarks
1940	APT	1:10,000	10	-	-	-	Map: Parts of the firm area are not covered.
1951	APT	1:10,000	10	-	-	-	
1968	APV	1:10,000	10	WF 3207	1968.27.08	1:15,000	Photos: Good contrast.
1984	APV	1:10,000	10	FW 8336	1984.24.08	1:20,000	Photos: Very good contrast.
1997	DPV	1:10,000*	10*	FW 12173	1997.08.08	1:30,000	Photos: Quite good contrast.

* Originally constructed as a DTM.

Explanation: APT: analogue photogrammetry (terr. photos); DPV: digital photogrammetry (scanned vertical aerial photos); FW: Fjellanger Widerøe A/S.

APV: analogue photogrammetry (vertical aerial photos); WF: Widerøe Flyveselskap A/S; * originally constructed as a DTM.

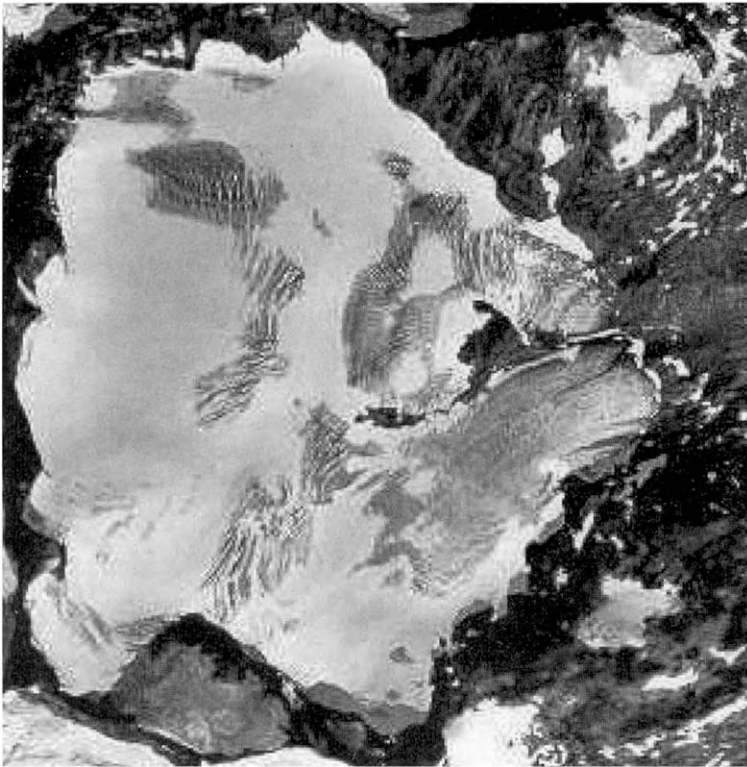


Fig. 2. Vertical aerial photo of Storbreven taken on 8 August 1997 used to construct the 1997 DTM and map. Notice the uneven distribution of the snow-line. Photo: Fjellanger Widerøe A/S.

tical aerial photos taken in 1968, 1984 and 1997. The 1940 map covers most of the glacier, except parts of the upper firn area. The 1951 map covers the whole glacier and was analogue constructed from terrestrial photos and some additional points surveyed by theodolite (Liestøl 1967). The 1968 and 1984, maps were analogue constructed from vertical aerial photos. Verticals taken in 1997 were scanned and used to construct a digital terrain model (DTM) (Fig. 2).

Data processing. All data processing and calculations were performed in a Geographical Information System (GIS) with ARC/Info software (ESRI 1995). The analogue glacier maps from 1940, 1951, 1968 and 1984 were digitised and transformed to the UTM coordinate system. Several interpolation techniques were tested and compared, so as to choose the best method for creating DTMs from contour maps. The different methods gave only small variations, probably due to the detailed original data. This was also found in similar studies (Kjøllmoen 1996; Andreassen 1998). Triangular

interpolation was considered to give the best DTM and was chosen for further calculations. For each of the maps, a triangular network (TIN) was constructed from the contour lines and elevation points. A regular grid was then generated from the TIN for the further overlay operations.

Length, area and volume change. The length of the glacier was determined as the average length along two defined central flow lines on Storbreven. The area–altitude distribution was determined for 50 m altitude intervals (excluding nunatak areas). One of the errors introduced is the difficulty of defining the glacier outline; another is the slope of the ice surface that will underestimate the area in each interval.

The thickness change, ΔG_{xx-yy} , in the periods between the maps is calculated for the periods 1940–1951, 1951–1968, 1968–1984, 1984–1997 and 1940–97 by subtracting the regular grids. This calculation gives a grid with altitude differences in glacier ice, firn and partly snow. To compare the change extracted from maps with the measured cu-

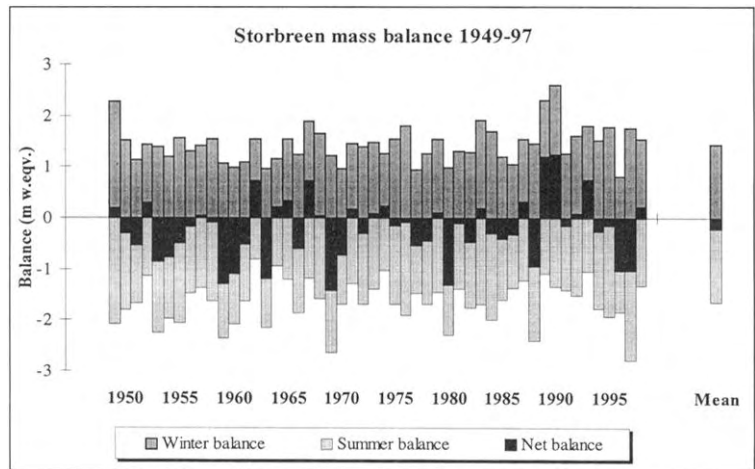


Fig. 3. Annual and cumulative mass balance measured on Storbreen for the period 1949–1997 (Data: Norwegian Polar Institute 1949–1993 and NVE 1994–1997).

mulative mass balance, one needs to convert altitude difference to difference in water equivalents. Ideally, one should know the density and the thickness of the accumulation area at the times of photography. No field data are available, and estimating the density in the snow-covered areas is difficult. Therefore, the density profile from the surface to the firn–ice transition is assumed to be unchanged in the periods between the mapping. The volume change, ΔV_{xx-yy} , can be calculated by multiplying the glacier difference grid by the density of ice, usually 0.9 g/cm^3 (Paterson 1994):

$$\Delta V_{xx-yy} = \Delta G_{xx-yy} \times 0.9$$

The result, the water difference grid, was then used to calculate total volume change and average volume change for Storbreen in the periods 1940–1951, 1951–1968, 1968–1984 and 1984–1997. For the first period, only 70% of the glacier is compared, since contour lines are lacking for the north-western upper part of the glacier on the 1940 map.

Even if it might be misleading, the figures given for volume change in this paper are the average change in water volume (w.eq.) for a given period of time, rather than using the total volume figures. The average figures are considered easier to compare than the total volume change figures.

When comparing volume change from the two different methods one must consider the additional melting that occurs after the time of photographing. The ablation measurements on Storbreen were carried out in September, while all the photographs used for the map/DTM construc-

tions were taken before the end of the ablation season. Thus, this amount was roughly estimated for each year by studying temperature records. For the first three periods no significant differences in additional melting were found and are thus neglected in this paper. However, considering the last period (1984–1997), several factors indicate a difference in additional melting. The 1997 photographs were taken relatively early (8 August), while the air photos from 1984 were taken on 24 August. The temperature data show that a lot of melting must have occurred after 8 August 1997 due to high temperatures. The total ablation in 1997 is the highest that ever measured on Storbreen, 2.8 m w.eq. compared with 2.0 m w.eq. in 1984 (Fig. 3). A simple calculation based on temperature records and the total ablation figures gives an additional melting of approximately 0.8 m w.eq. in 1997 compared with 1984. Thus, the average volume change calculated for the period 1984–1997 from the DTM comparison must be subtracted by this figure before comparing with the measured cumulative mass balance data for the same period.

Errors. One problem when using old glacier maps is that detailed information about the map constructions and estimates of the accuracy is seldom mentioned in publications (if these exist). Hence, it is difficult to give estimates of the accuracy of these maps. Generally, a number of errors will affect the final result. The result will be influenced by errors in the original data, data transformations, interpolations and calculations. One of the

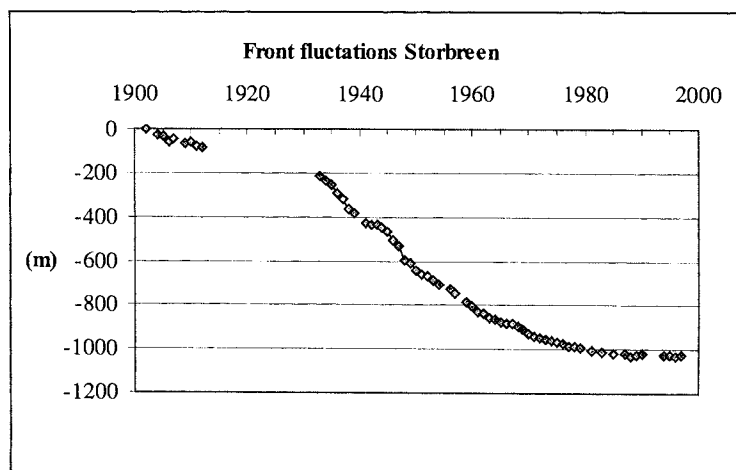


Fig. 4. Cumulative front fluctuations of Storbreen from 1902 to 1997. Due to lack of funding no measurements were carried out between 1912 and 1933. Storbreen had a minor advance in this period, probably at the end of the 1920s (Data: Norwegian Polar Institute 1902–1993 and NVE 1994–1997).

factors determining the accuracy of the contour map is the photo scale of the verticals: a larger scale (lower fly height) gives a smaller standard error. Other factors that have an influence are the accuracy of the geodetic reference network and the precision and the experience of the constructor. The quality of the aerial photos is also crucial and especially the characteristics of the snow surface. Constructing contour lines over snow areas is always difficult due to the poor contrast. The photos used for mapping Storbreen are of good quality, but still it was difficult to construct contour lines in some parts of the firn area (Liestøl and Lytschold, pers. comm.; Table 2). The accuracy of the 1997 DTM is assumed to be ± 0.8 m. The quality of the contour maps was tested by comparing the contour lines outside the glacier. This comparison, combined with judgement of other errors, leads to an estimate of the accuracy of the 1940, 1951, 1968 and 1984 maps in the range of ± 1.0 – 2.0 m, with the highest accuracy for the newest maps. In the white snow parts of the glacier the accuracy is lower.

Digitising procedures introduce horizontal random errors due to the accuracy of the digitiser and the condition of the analogue manuscript. GIS calculations introduce errors when converting data from local coordinate systems, generating DTMs and in the overlay operations (Burrough 1986; Arabia, *et al.* 1998). How the sampling size of the grid influences the result was tested by using 5, 10, 20, 50 and 100 m cell size. The final result showed little variation when using 5, 10 and 20 m intervals; however, when using 50 and 100 m cell size, larger dif-

ferences occurred. Therefore, when using small cell sizes (5–20 m), the sampling size seems to be an unproblematic factor.

Results

Changes in length, area and volume

As previously mentioned, marginal fluctuations have been measured on Storbreen since the beginning of this century. Since 1902, the glacier has had a net retreat of over 1 km (Fig. 4). More than 800 m of this retreat occurred from 1940 to 1997 (Table 1). During this period, the area was also reduced by 0.6 km^2 , from 6.0 to 5.4 km^2 , mainly due to the retreat of the front. The retreat of the front seems to have stopped now. In fact the last years of front measurements show some small advances (Fig. 4). According to the digital terrain models, the mean height (above sea level) of the glacier increased by 25 m since 1940 and the slope of the glacier has increased by 2° resulting in a steeper glacier surface (Table 1).

The area–altitude distribution for each year of mapping shows that the glacier has reduced its area significantly in the lower height intervals since 1940 (Table 3). In contrast, the glacier has increased the area between 1800 and 1950 m a.s.l. from 1984 to 1997, probably as a result of a more positive net balance.

The volume change was in reasonable agreement with the measured cumulative mass balance for two of the four periods (Table 4). In the second and the fourth periods, however, the measured cumulative values were generally more negative than

COMPARING MASS BALANCE MEASUREMENTS

Table 3. Area-altitude distribution of Storbreen in 1940, 1951, 1968, 1984 and 1997.

Altitude (m a.s.l.) interval	Area (km ²)				
	1940	1951	1968	1984	1997
2050–2090	-	0.03	0.05	0.04	0.04
2000–2050	0.14	0.12	0.16	0.15	0.15
1950–2000	0.18	0.22	0.24	0.22	0.23
1900–1950	0.33	0.32	0.34	0.34	0.36
1850–1900	0.47	0.48	0.55	0.51	0.57
1800–1850	0.97	0.93	0.91	0.86	0.92
1750–1800	0.79	0.76	0.78	0.77	0.75
1700–1750	0.71	0.70	0.64	0.65	0.64
1650–1700	0.49	0.45	0.42	0.41	0.40
1600–1650	0.63	0.59	0.53	0.49	0.49
1550–1600	0.36	0.37	0.35	0.36	0.35
1500–1550	0.35	0.33	0.26	0.24	0.21
1450–1500	0.18	0.20	0.22	0.19	0.18
1400–1450	0.15	0.13	0.10	0.08	0.06
1350–1400	0.11	0.09	0.07	0.02	0.00
1300–1350	0.05	0.02	0.00	-	-
1280–1300	0.01	-	-	-	-
1280–2090	5.94	5.73	5.60	5.35	5.36

shown by results of the volume change determined by mapping methods.

Comparison of DTMs from 1940 and 1951 gives a negative net balance of -5.4 m w.eq. in average for the part of the glacier (70%) covered by the 1940 map (Table 4). The water difference grid shows a thinning at the tongue corresponding to 40 m w.eq. In the higher areas of the glacier, the grid shows a thickening of the glacier. The calculated mass balances in the same period also show a pronounced decrease of the glacier, a net result of -6.4 m (Table 4). Both methods show a noticeable thinning of the glacier tongue in this period. This is in good agreement with the front position measure-

Table 4. Comparison of cumulative annual mass balance measurements with volume calculations from digital terrain models (DTM's).

Period	Mass balance (m w.eq.)		DTM (m w.eq.)	
	Total	Annual	Total	Annual
1940–51	-6.4	-0.6	-5.4	-0.4
1951–68	-4.6	-0.3	-1.5	-0.1
1968–84	-5.1	-0.4	-6.4	-0.5
1984–97	-0.7	-0.1	2.4	0.2
1940–97	-16.8	-0.3	-10.9	-0.2

Notice: The DTM figures for 1940–51 and 1951–68 only include 70% of the glacier. The DTM column includes possible differences in additional melting from date of photo.

ments and field observations carried out every year (Liestøl 1967; pers. comm.).

In the period 1951–1968, the DTM calculation gives an unexpected positive net balance of 0.9 m w.eq., i.e. the glacier has increased in volume. According to the DTMs, a thinning of the glacier tongue has occurred, in contrast to a thickening of larger parts of the glacier accumulation area. When removing the problematic upper area in the firm area (the same area that was not mapped in 1940; Fig. 5), the result becomes more negative, -1.5 m w.eq. (Table 4). This is not in very good agreement with the cumulative mass balance data, which show a negative net balance of 4.6 m. The difference is more than 3 m w.eq. between the two methods. There is better agreement between the two methods for the period 1968–1984. The cumulative mass balance was -5.1 m w.eq. while the DTM comparison showed a slightly more negative result, -6.4 m w.eq. Again, the tongue of the glacier is markedly reduced in this period. Most of the glacier has thinned, except small parts in the accumulation area. Finally, the period between 1984 and 1997 gives a positive net balance of 3.2 m w.eq. on average for the whole glacier from the DTM comparison. Subtracting the estimated additional melting of 0.8 m w.eq. in 1997 compared to 1984, the net balance is reduced to 2.4 m (Table 4). The difference grid shows a much smaller thinning of the glacier tongue than the previous three periods, and a positive volume change for the major parts of the glacier. The measured cumulative balance gives a slightly negative value for this period, -0.7 m w.eq. Thus, the difference between the two methods is about 3 m w.eq.

Discussion

The difference between the methods for the period 1951–1968 can be explained by the inaccuracy of the 1951 map, where poor contrast in the upper firm area may have underestimated the altitude of this part of the glacier. Photogrammetric contours tend to float upwards in areas with poor contrast. The mass balance monitoring programme was very detailed in these years; nevertheless, there will always be uncertainties in these data as well. The volume change from the map comparison is still less credible than the more negative measured cumulative mass balance.

The discrepancy for the last period (1984–1997) may be partly explained by inaccurate mapping, or rather by difficulties in comparing the two maps/

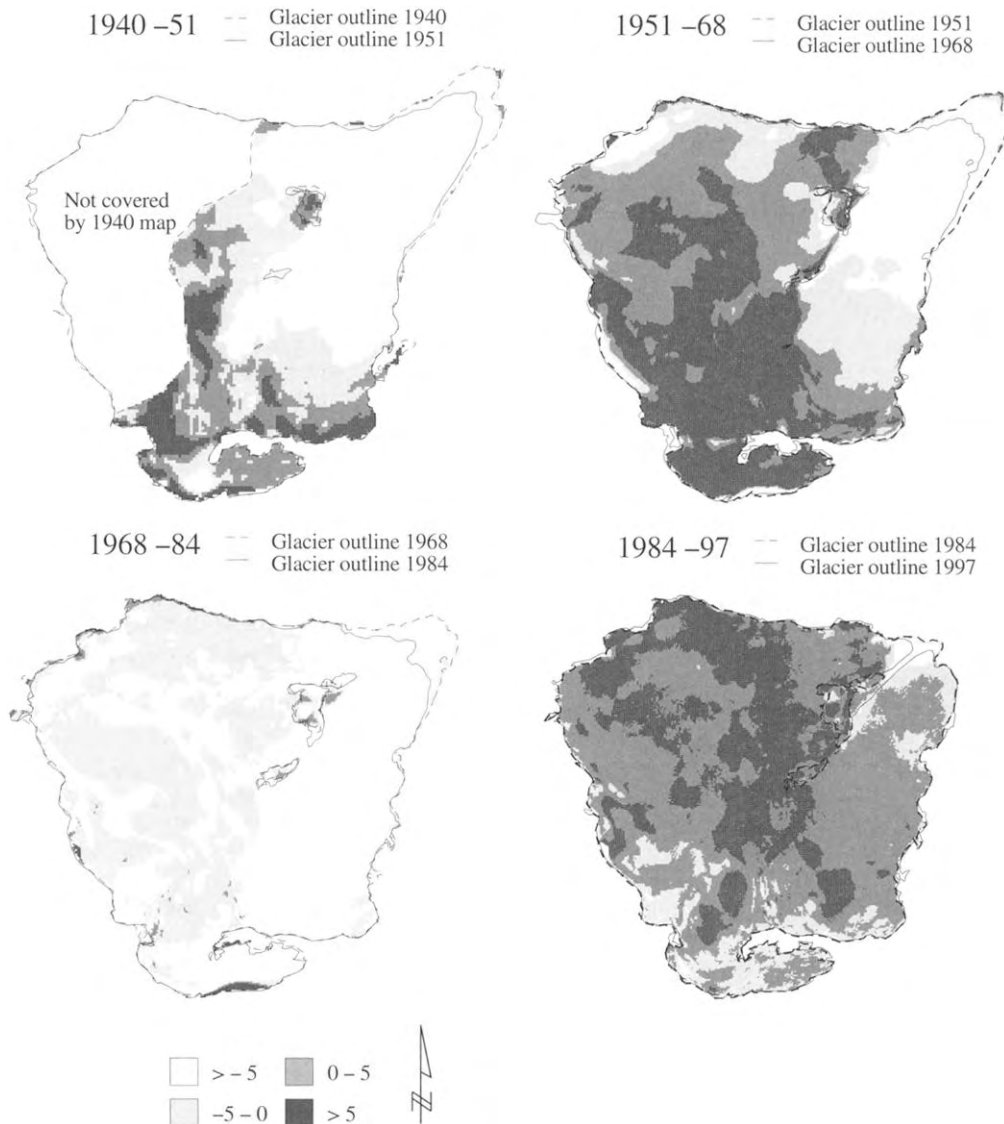


Fig. 5. Volume change (m w.e.) of Storbreenn in the periods: 1940–1951, 1951–1968, 1968–1984 and 1984–1997.

DTMs that were constructed from different triangulation points. The scale of the 1997 map was not as good as in 1984, 1:30,000 versus 1:20,000 (Table 2). This gives a less accurate DTM from 1997. However, another aspect, which certainly deserves attention, is the accuracy of the annual mass balance data. From 1984 to 1994 the monitoring programme was markedly reduced. For instance, in 1992 and 1993 only 12 sounding points of snow

depth were measured. At the end of the 1980s and the beginning of the 1990s, some years with large accumulation occurred in western Norway, and also at Storbreenn (Fig. 3). Storbreenn is located near the watershed (east/west divide) and will receive precipitation from both the west and east. Simple correlation calculations with Nigardsbreen and Hellstugubreen, located west and east of Storbreenn respectively, give reason to believe that the winter

accumulation may have been underestimated in at least some of these years with high accumulation. Years of high accumulation rates followed by years with low ablation leads to difficult snow sounding conditions. Also, when using few points to measure accumulation, the results will have a higher degree of uncertainty.

As for the period 1968–1984, the calculated difference between the two methods of 1.3 m is within the error limit for this type of comparison. Better maps may explain the better agreement here. Both the 1968 and 1984 maps are constructed from vertical aerial photos with good contrast and using the same triangulation points. However, the map comparison cannot verify the annual mass balance measurements or *vice versa*, since the answer (the change of the glacier) is not known. In any case, both methods show that Storbreen had an unquestionable pronounced thinning in this period. The observed and measured retreat of the glacier front confirms this result also.

The volume change calculated from the DTMs assumes an unchanged density profile between the periods of mapping, in other words, a steady-state glacier is assumed (Bader 1954). The geometric and volumetric changes of Storbreen reported in this paper show that Storbreen was not in such a steady state in the investigated periods. Assuming a lower density for the firm area will give a smaller absolute figure of volume change, resulting in a smaller difference between the two methods for the last two periods, and a larger difference for the first two periods. Further focus on this issue might give better methods and results. However, to improve glacier volume change calculations, direct measurements of the density profile in the accumulation area at the time of photographing should be done.

Another crucial factor is the geodetic network. Better ground control before photographing and surveying additional points on the glacier, especially in the accumulation area, would give better control of the final result.

Conclusions

The comparison of volume change on Storbreen extracted from maps gave more positive (or less negative) cumulative mass balance data than annual measurements except for one period. Inaccurate maps, especially in the accumulation areas, can explain this difference, especially when using the maps from 1940 and 1951. However, mass balance measurements cannot be considered as 100% trust-

worthy. There are uncertainties in these data as well, especially after the monitoring programme was reduced on Storbreen. Considering the sources of errors in both methods, one cannot use one method to verify the other or *vice versa*. However, using both methods for one glacier and continually comparing them will hopefully lead to improvements for both methods, and thus more accurate results will be achieved.

Calculating volume change from maps cannot yet be an adequate substitute for traditional measurements, since the method does not give information about seasonal variations in ablation and accumulation. However, the method can be used to monitor long-term changes in glacier volume and to make comparisons with volume change measured by traditional methods.

Acknowledgements

Colleagues at the Glacier and Snow Section have given valuable advice. Espen Gudevang digitised the glacier maps from 1940 and 1984. Comments from my referees improved the manuscript. I am grateful for all the assistance in preparing this paper.

Liss M. Andreassen, Norwegian Water Resources and Energy Directorate, Glacier and Snow Section, PO Box 5091, Maj., NO-0301 Oslo, Norway, E-mail: lma@nve.no.

References

- Andreassen, L.M., 1998: Volumendringer på Jostefonn 1966–93. NVE Rapport No. 3. 10 p.
- Arabia, G., Griffith, D. and Haining, R., 1998: Error propagation modelling in raster GIS: overlay operations. *Int. J. Geogr. Inf. Sci.*, 12:145–167.
- Bader, H. 1954: Sorge's law of densification of snow on high polar glaciers. *J. Glac.*, 2: 319–323.
- Burrough, P.A., 1986: Principles of Geographical Information Systems for Land Resources Assessment. Monograph of soil and resources survey No. 12. 176 p.
- Darmody, R.G., Thorn, C.E. and Rissing, J. M., 1987: Chemical weathering of fine debris from series of Holocene moraines: Storbreen, Jotunheimen, Southern Norway. *Geogr. Ann.*, 69A (3–4): 405–413.
- Erikstad, L. and Sollid, J.L., 1986: Neoglaciation in South Norway using lichenometric methods. *Norsk geogr. Tids.*, 40:85–105.
- ESRI, 1995: Understanding GIS. The ARC/INFO method. Version 7. John Wiley & Sons. New York. 400 p.
- Kjøllmoen, B., 1996: Volumendringer på Harbardsbreen 1966–96. NVE Rapport No. 6. 17 p.
- (ed.), 1998: Glasiologiske undersøkelser i Norge 1996 og 1997. NVE Rapport No. 20. 134 p.

- Liestøl, O.*, 1960: Bremålinger og brevariasjoner. DNT Årbok 1960. 24–34.
- 1967: Storbreen glacier in Jotunheimen, Norway. Norsk Polarinstitutts Skrifter, 141. 63 p.
- Matthews, J.A.*, 1973: Lichen growth on an active medial moraine, Jotunheimen, Norway. *J. Glac.*, 12:305–313.
- 1974: Families of lichenometric dating curves from the Storbreen gletschervorfeld, Jotunheimen, Norway. *Norsk geogr. Tids.*, 28:215–235.
- 1975: Experiments on the reproducibility and reliability of lichenometric dates, Storbreen gletschervorfeld, Jotunheimen, Norway. *Norsk geogr. Tids.*, 29:97–109.
- 1976: A lichenometric test of the 1750 end-moraine hypothesis: Storbreen gletschervorfeld, southern Norway. *Norsk geogr. Tids.*, 31:129–136.
- Paterson, W.B.S.*, 1994: The physics of glaciers. (third edition). Pergamon. Oxford. 480 p.
- Øyen, P.A.*, 1893: Isbræstudier i Jotunheimen. *Nyt Mag. for Naturvid.*, 34:12–72.
- 1908: Bidrag til vore brægnes glacialgeologi. *Nyt Mag. for Naturvid.*, 46:301–379.

Manuscript received August 1998, revised and accepted March 1999.